american society for mass spectrometry

The Thirty-Second Annual Conference on Mass Spectrometry and Allied Topics

Hyatt Regency Hotel, San Antonio, Texas

May 27 - June 1, 1984

TABLE OF CONTENTS

1. INTRODUCTION iii

2. DIRECTORY OF CORPORATE MEMBERS iv

3. PROCEEDINGS OF THE 32nd ANNUAL CONFERENCE viii

4. KEYNOTE ADDRESS 858

5. AUTHOR INDEX 873

6. MEMORIAL PAGE 884

7. MINUTES OF THE 1984 ASMS BUSINESS MEETING 885

8. MINUTES OF THE ASTM BUSINESS MEETING 887

9. WORKSHOP REPORTS
   - Reporting of Data and Statistics 890
   - Internal Energy Effects in Collision-Induced Decompositions . 895
   - Spares and Service 896
   - Offline HPLC Mass Spectrometry 898
   - Hybrid Mass Spectrometers 900
   - Quality Control and Standardization in Metabolic Profiles of Urinary Acids 901
   - Ion Physics and Instrumentation 902
   - Microcomputers in Mass Spectrometry 903
   - LC/MS Standards 905
   - Mass Spectrometers of Yesteryear 907
   - Quantitation Using Desorption Techniques 908
   - Artificial Intelligence in Mass Spectrometry 909
   - Electron Impact Ionization Cross Sections 911
   - Isotope Ratio Measurements Using Multiple Collectors . . . 912

10. COMMITTEE REPORTS
   - Computer Applications 914
   - Education 915
   - Environmental Applications 916
   - Good Laboratory Practices 917
   - Isotope Ratio Measurements 918
   - Qualitative Organic 919
   - High Temperatures and Inorganic Solids 919
   - Nomenclature 920

11. ATTENDEES, 32nd ANNUAL CONFERENCE 941

CITATION NOTICE

This volume contains the abstracts of papers presented at the 32nd Annual Conference on Mass Spectrometry and Allied Topics. It is intended that this volume be distributed only to members of ASMS and conference registrants; therefore, it is not to be considered a publication. Any reference to individual abstracts in this volume should be cited in the following form:

"Title, author(s); presented at the 32nd Annual Conference on Mass Spectrometry and Allied Topics, San Antonio, TX, May 27 - June 1, 1984."

INTRODUCTION

This "Bound Volume is the official record of the Thirty-Second Annual Conference on Mass Spectrometry and Allied Topics, which was held in San Antonio, Texas from May 27th through June 1, 1984. This year we are publishing only extended abstracts of papers presented at the conference; the short abstracts are contained in the conference program. We have also included standing and ad hoc committee reports, workshop reports, minutes of the annual business meeting and other information of interest to the membership.

I would like to express my appreciation to the contributors for the care that went into preparation of their extended abstracts and for their cooperation in meeting deadlines for publication. Special thanks go to Mrs. Judith A. Watson of P.A.M. who compiled the bound volume at the ASMS society office. Printing and distribution was coordinated by Mr. Robert Meltzer of ASTM.

Robert E. Finnigan
Editor and Member-at-Large
ASMS Board of Directors

BOARD OF DIRECTORS
AMERICAN SOCIETY FOR MASS SPECTROMETRY

PRESIDENT
Catherine C. Fenselau
Johns Hopkins University
Pharmacology Department
Baltimore, MD 21205

VICE PRESIDENT FOR PROGRAMS
R. Graham Cooks
Purdue University
Chemistry Department
West Lafayette, IN 47907

VICE PRESIDENT FOR ARRANGEMENTS
Michael A. Grayson
McDonnel Douglas Research
Dept. 222, Bldg. 110
St. Louis, MO 63166

SECRETARY
Harry S. Hertz
Nat'l Bureau of Standards
A309 Chemistry
Washington, DC 20234

TREASURER
James J. DeCorpo
Naval Sea Systems Command
Code 05R32
Washington, DC 20362

CHAIRMAN, ASTM Committee E-14
Ed Emery
Balzers
8 Sagamore Park Road
Hudson, NH 03051

MEMBER-AT-LARGE
Robert E. Finnigan
Finnigan MAT Corp.
355 River Oaks Parkway
San Jose, CA 95134

MEMBER-AT-LARGE
Marvin Vestal
University of Houston
4800 Calhoun
Houston, TX 77005

PAST PRESIDENT
Burnaby Munson
University of Delaware
Chemistry Department
Newark, DE 19711

SOCIETY OFFICE
Judith A. Watson
Post Office Box 1508
East Lansing, MI 48823
517/337-2548

DIRECTORY OF CORPORATE MEMBERS

BALZERS 8 Sagamore Park Road Hudson, NH 03051 603/889-6888	Quadrupole mass spectrometers for wide variety of applications (residual gas analysis, plasma characterization and process gas analysis). Also, turbomolecular and mechanical pumps, as well as instrumentation to produce and monitor vacuum systems.
BIO-ION P. O. Box 15045 Uppsala S-75215 Sweden 018-104440	252Cf-Plasma Desorption Mass Spectrometer.
R. J. BRUNFELDT Co. P. O. Box 2066 Bartlesville, OK 74005 918/336-4467	Design and fabrication of all-glass inlet systems. Repair and fabrication of reentrants and probes.
CAMBRIDGE ISOTOPE LABS 20 Commerce Way Woburn, MA 01801 800/322-1174	Manufacture of stable isotope labelled compounds - environmental contaminant standards, isotopic gases, reagents, drugs, metabolites, biochemicals. Also, complete custom synthetic work with stable isotopes.
COLORADO GROUP 490 Orchard Street Golden, CO 80401 303/442-2141	Laboratory services, repairs and custom-made glassware.
CVC PRODUCTS 525 Lee Road Rochester, NY 14603 716/458-2550	Quadrupole mass spectrometers, RGA's, time-of-flight mass spectrometers.
COMPUCHEM LABORATORIES P. O. Box 12652 Research Triangle Pk, NC 919/549-8263	GC/MS and related chemical analysis of environmental pollutants and body fluids for drugs of abuse. 24 GC/MS instruments as well as GC, ICP, AA, EMIT instrumentation.
DETECTOR TECHNOLOGY P. O. Box K-300 Brookfield, MA 01506 617/867-7156	Manufacturer of new and rebuilt continuous dynode electron multipliers.
EXTRANUCLEAR LABS P. O. Box 11512 Pittsburgh, PA 15238 412/782-3884	Analytical mass spectrometer systems including triple quads - thermospray. Process control mass spectrometer systems and research mass spectrometer systems and components.
FEIN-MARQUART ASSOC. 7215 York Road Baltimore, MD 21212 301/821-5980	Computer software for mass spectrometry.
FINNIGAN MAT 355 River Oaks Pkwy. San Jose, CA 95130 408/946-4848	Inexpensive, universal GC detectors; low-cost GC/MS systems; LC/MS interfaces, high resolution, high mass MS systems, tandem and hybrid MS/MS systems; high-precision isotope ratio intruments.
FINNIGAN MAT INSTITUTE 11 Triangle Park Drive Cincinnati, OH 45246 513/772-5500	Training courses in GC/MS operation and maintenance. Advanced mass spectrometry topics. Analysis of hazardous wastes and priority pollutants. Consultation services in GC/MS and laboratory methodology.

GALILEO ELECTRO-OPTICS Galileo Park Sturbridge, MA 01518 617/347-9191	Channeltron Electron Multiplier Detectors.
HEWLETT PACKARD 1601 California Ave. Palo Alto, CA 94304 415/857-6090	Products include HP5970B Mass Selective Detector used with most capillary GC's; HP5995C GC/MS, a bench-top unit with big system capabilites; HP5987A GC/MS, H-P's largest and most versatile system.
HITACHI LTD 5-1 Marunouchi Chiyoda-ku Tokyo 100, Japan 03/212-111	
INFICON LEYBOLD-HERAEUS 6500 Fly Road East Syracuse, NY 13057 315/437-0377	Quadrex 200 RGA; 1PC-200 Mass spectrometer.
IONSPEC One Longstreet Irvine, CA 92714 714/857-0793	Data systems and components for fourier transform mass spectrometry.
JEOL, Ltd. 11 Dearborn Road Peabody, MA 01960 617/535-5900	DX-300/303 double focussing GC/MS; HX-100/110 ultra high resolution mass spectrometer; DA-5000/5100 data system.
KRATOS ANALYTICAL INST. 170 Williams Drive Ramsey, NJ 07446 201/934-9000	High Resolution and GC/MS mass spectrometers, data systems and surface science instrumentation.
MASSPEC, Inc. 2500 S. Berry Road Norman, OK 73069 405/360-0493	Direct introduction probe systems for mass spectrometers.
MSD ISOTOPES P. O. Box 899 Pointe Claire, Quebec H9R 4P7 Canada 514/697-2823	Stable isotope labelled compounds - custom synthesis.
MERIDIAN INSTRUMENTS 2310 Science Pkwy. Okemos, MI 48864 517/349-7200	GC-DS for metabolic profiling analysis and GC-MS-DS metabolic profiling analysis - single focusing magmetic sector. Diagnostic laboratory service - urine specimens for organic acid profiling.
M&R ANALYTICAL SERVICES 700 Barksdale Road, #1 Newark, DE 19711 302/453-9599	Maintenance, repair and parts supply of mass spectrometry and surface science instruments.
NERMAG 15423 Vantage Pkwy. Houston, TX 77032 713/442-0970	Quadrupole GC/MS systems including "low-cost" routine systems; research instruments including extended mass range and MS/MS. Accessories including negative ions, LC/MS, DCI and FAB.

NICOLET ANALYTICAL INST. 5225 Verona Road Madison, WI 53711 606/271-3333	FTMS - spectrometers; super conducting magnets.
NUCLIDE CORP. 642 E. College Ave. State College, PA 16801 814/238-0541	Magnetic mass spectrometers and spectrographs and automation/data processing systems for same. GC/MS/DS systems; tandem and 3 stage analyzers. Upgrading/updating for CEC/duPont, LKB, RMU, Bendix, Brand X instruments. Magnets, analyzers, HV supplies.
ONEIDA RESEARCH SERVICES 3 Ellinwood Court New Hartford, NY 13413	Routine R & D supporting industry and government using MS/MS, GC/MS/MS, GC/MS, FAB, DCI, pyrolysis, purge and trap, surface SIMS and RGA/MS.
PHRASOR SCIENTIFIC INST. 1536 Highland Avenue Duarte, CA 91010 818/357-3201	Direct insertion probe FAB gun; FAB guns, cesium guns, electronic controllers, Spectrometer upgrading and custom modifications.
SCIENTIFIC GLASS ENGIN. 2007 Kramer Lane Austin, TX 78758 512/837-7190	GC/MS accessories, molecular jet separators, valves, columns, ferrules, open split interfaces, syringes.
SCIEX 55 Glencameron Rd. Thornhill, Ontario Canada L3T 1P2 416/881-4646	TAGA 6000E (triple quadrupole MS/MS system); Mobile TAGA 6000E (van mounted MS/MS system); ELAN 250 (IPC/MS system).
SHIMADZU INSTRUMENTS 7102 Riverwood Drive Columbia, MD 21046 301/997-1227	Shimadzu gas chromatograph-mass spectrometer system (model GCMS-OP1000).
SHRADER ANALYTICAL 3814 Vinewood Detroit, MI 48208 313/894-4440	Analytical services include low resolution mass spectrometry, high resolution mass spectrometry and GC/MS. Manufacturer of MSDC data system.
SPECTROSPIN industriestrasse 26 Fallenden CH-8117 Switzerland 01/825 48 55	High resolution FT-ICR spectrometers and accessories; Super conducting magnets; rugg ed quadrupole mass spectrometers designed for mobility and ease of operation.
TEKNIVENT 10774 Trenton Avenue St. Louis, MO 63132 314/429-7272	Complete research GC/MS, MS/MS data systems based on high speed microcomputers. Also turnkey systems based on the IBM PC for mass spectrometry and chromatography. Custom designed hardware and software systems for H-P mass spectrometers and gas analyzers.
TOFTEC P. O. Box 12877 Gainesville, FL 32604 904/472-2668	Custom velocity compaction time-of-flight mass spectrometer design.
VACUMED 2261 Palma Drive Ventura, CA 93003 805/644-7461	Mass spectrometer accessories including GC/LC/MS interfaces; FAB-SIMS equipment; GC/MS data systems; electron mulitpliers, DCI, solids, liquids, gas probes; FD equipment; software; filaments; inlet systems; 'O' rings.

VESTEC 2524 Sunset Blvd. Houston, TX 77005 713/521-2599	Thermospray LC/MS Interface
VG INSTRUMENTS 300 Broad Street Stamford, CT 06901 203/322-4546	Magnetic deflection and quadrupole mass spectrometers for GC/MS, LC/MS, isotope ratio and ICP/MS. Instruments for very high mass and very high resolution. Data systems for control and data reduction.
VG INORGANIC DIVISION 300 Broad Street Stamford, CT 06901 203/329-8050	Thermal Ionisation MS; gas analysis MS, ICP-MS, glow discharge MS; stable isotope ratio MS.
John Wiley and Sons 605 Third Avenue New York, NY 10158 212/850-6570	Journals and books covering the field of mass spectrometry. Journals include Biomedical Mass Spectrometry, Organic Mass Spectrometry, and Mass Spectrometry Reviews.

32nd ANNUAL CONFERENCE ON MASS SPECTROMETRY AND ALLIED TOPICS

MOA — Dioxins and Pesticides

A COMPARISON OF DIRECT LIQUID INTRODUCTION AND THERMOSPRAY HPLC/MS FOR THE ANALYSIS OF PESTICIDES 3
*BURSEY,J T,VOYKSNER,R D AND PELLIZZARI,E

COMPUTER CONTROLLED HIGH RESOLUTION EXTENDED RANGE MPM RETROFIT OF AEI MS-30 FOR PART-PER-TRILLION ANALYSIS OF CHLORODIBENZODIOXINS AND SIMILAR RESIDUES IN ENVIRONMENTAL SAMPLES 5
*SOLCH,J G,MILLER,D,GARRETT,J H,TIERNAN,T O AND TAYLOR,M L

MOBILE TANDEM MASS SPECTROMETRY RECENT APPLICATIONS OF MS/MS ON WHEELS 7
*SHUSHAN,B,FULFORD,J,THOMSON,B A,TANNER,S D,NGO,A AND DAVIDSON,W R

A SIMULTANEOUS DUAL CAPILLARY COLUMN GC/MS METHOD FOR THE DETERMINATION OF 2,3,7,8-TCDD AND 2,3,7,8-TCDF 9
*PARR,J L,WILLIAMS,C H,GARRETSON,L D AND STEWART,P B

GC/MS CHARACTERIZATION OF PCDD RESIDUES IN FRESHWATER FISH EXPOSED TO MUNICIPAL INCINERATOR FLY ASH 11
*KUEHL,D W,BUTTERWORTH,B C AND LINN,D

DETECTION/IDENTIFICATION OF VOLATILE ORGANIC PHOSPHONATES BY SIMS 12
*GROENEWOLD,G S AND TODD,P J

DETERMINATION OF ALDICARB,ALDICARB NITRILE,AND ALDICARB OXIME IN WATER BY GC/MS 14
*TREHY,M L AND YOST,R A

SCREENING METHODS FOR ORGANOPHOSPHORUS PESTICIDES USING TRIPLE QUADRUPOLE MASS SPECTROMETRY 16
*BAUER,M R AND ENKE,C G

MOB — Photodissociation & Neutral Fragment MS

STUDIES ON ENERGY PARTITIONING ON PHOTODISSOCIATION OF POLYATOMIC SYSTEMS 18
KRAILLER,R E

MASS SPECTROMETRIC STUDIES OF HYPERVALENT MOLECULES 20
*GELLENE,G I AND PORTER,R F

ISOMERIZATION AND DISSOCIATION PROCESSES OF AROMATIC IONS FOUND WITH MULTIPLE TECHNIQUES 22
*WESDEMIOTIS,C,GROTEMEYER,J,DANIS,P O AND MCLAFFERTY,F W

THE CHARACTERIZATION OF NEUTRAL SPECIES FORMED BY ELECTRON IMPACT ON SOME C1-C5 ALKANES AND C2-C4 ALKENES 24
*FLESCH,G D AND SVEC,H J

MOC — **Peptides**

MASS SPECTROMETRIC MEASUREMENT OF BIOLOGIC PEPTIDES 25
*DESIDERIO,D M,ONISHI,H,TAKESHITA,H,TANZER,F S AND WALKER,J

DESORPTION OF INSULIN MOLECULAR IONS FROM POLYMERIC SURFACES 26
*JORDAN,E A,MCNEAL,C J,MARTIN,C R AND MCFARLANE,R D

FAST ATOM BOMBARDMENT MASS SPECTROMETRY OF THE S. AUREUS DIGEST OF HUMAN INSULIN 28
*FETTEROLF,D D,CHABER,J,BYRN,S,PFEIFFER,R AND CHANCE,R

DETECTION OF PTH-DERIVATIVES OF AMINO ACIDS BY SIMS 30
*BENNINGHOVEN,A AND ANDERS,V

252Cf-PLASMA DESORPTION TIME OF FLIGHT MASS SPECTROMETRY OF PEPTIDES AND PROTEINS 32
*ROEPSTORFF,P,SUNDQUIST,B,KAMENSKY,I,HAKONSON,P AND FOHLMAN,J

COMBINED LC/MS OF AMINO ACIDS AND PEPTIDES 34
*GAMES,D E,RAMSEY,E D,CATLOW,D A,WOODHALL,B J AND ROEPSTORFF,P

MOD — **Energy Dependence of Fragmentation**

ENERGY-RESOLVED STUDIES OF IONIC FRAGMENTATION REACTIONS A COMPARISON OF CHARGE EXCHANGE MASS SPECTROMETRY WITH FIELD IONIZATION KINETICS, ANGLE RESOLVED MASS SPECTROMETRY & VARIABLE ENERGY COLLISION-INDUCED DISSOCIATION SPECTROMETRY 36
*HARRISON,A G,NACSON,S AND ZWINSELMAN,J J

SOME COMMENTS ON THE METASTABLE FRAGMENTATION OF INSULIN IONS PRODUCED BY FISSION FRAGMENT BOMBARDMENT 38
*CHAIT,B T,GRACE,L AND FIELD,F H

CHARGE STRIPPING OF MONATOMIC IONS: DEPENDENCE OF THE CROSS-SECTION ON VARIOUS PARAMETERS OF THE COLLISION PARTNERS 40
GUILHAUS,M,*BRENTON,A G AND BEYNON,J H

ULTRA SLOW METASTABLE ION DECOMPOSITIONS 42
*LIFSHITZ,C,MALINOVICH,Y,ARAKAWA,R,GEFEN,S AND HASE,G

THE ANGLE-ENERGY RESOLVED CID OF CS2+ IONS AT LOW INCIDENT ION ENERGIES 44
SHUKLA,A,LARAMEE,J A,HIRST,D M AND *JENNINGS,K R

THE HEAT OF FORMATION OF C3H2+ 46
SMITH,D,ADAMS,N G AND *FERGUSON,E E

ENERGY BARRIERS FOR EXOTHERMIC ION/RADICAL REACTIONS 48
*BURGERS,P C,HOLMES,J L AND TERLOUW,J K

DISSOCIATION OF ENERGY SELECTED IONS FORMED BY PHOTOIONIZATION OF "COLD" MOLECULES 50
*BASS,L M AND BAER,T

MOE — **Negative CI of Pollutants**

POSITIVE ION AND ELCTRON CAPTURE NEGATIVE ION CHEMICAL IONIZATION MASS SPECTROMETRY OF CHLORINATED PHENOXYANISOLES AND BENZENES 52
CAMPBELL,J A,GRIFFIN,D,FREEMAN,P AND *DEINZER,M

THE ROLE OF NCI-MS IN THE DETERMINATION OF CHLORDANE AND TOXAPHENE IN GREAT LAKES SPORT FISH 54
*SCHEEL,R H,PRICE,H A AND WELCH,R L

BETTER NCI MASS SPECTRA OF HEXACHLOROCYCLOPENTADIENE-BASED PESTICIDES 56
*STEMMLER,E A AND HITES,R A

EVALUATION OF NEGATIVE ION CHEMICAL IONIZATION WITH CAPILLARY COLUMN GAS CHROMATOGRAPHY/LOW RESOLUTION MASS SPECTROMETRY FOR THE ANALYSIS OF CHLORINATED DIBENZODIOXINS,FURANS,AND RELATED COMPOUNDS 58
*BUDDE,W L AND EICHELBERGER,J W

ISOMERIC DISTINCTION OF DERIVATIZED AMINOANTHRACENES AND AMINOPHENANTHRENES BY NEGATIVE CHEMICAL IONIZATION MASS SPECTROMETRY 59
*SEARS,L J,GRIMSRUD,E P AND CAMPBELL,J A

MEASUREMENT OF TOXIC ORGANIC COMPOUNDS IN ENVIRONMENTAL SAMPLES USING NEGATIVE CHEMICAL IONIZATION MASS SPECTROMETRY 61
*HILPERT,L R AND BYRD,G D

THE RESPONSE OF ANTHRACENE IN THE ELECTRON CAPTURE DETECTOR: THREE COMPETITIVE PROCESSES 63
*GRIMSRUD,E P AND VALKENBURG,C A

DIFFERENTIATION OF ISOMERIC POLYCYCLIC AROMATICS USING NEGATIVE CHEMICAL IONIZATION 65
*BUCHANAN,M V AND OLERICH,G

MOF — **Leukotrienes; Isotopes in Biological Studies**

GC/MS CHARACTERIZATION OF LIPOXYGENASE METABOLITES OF LINOLEIC ACID FORMED BY PORCINE LEUKOCYTES 67
*CLAEYS,M,KIVITS,G A A,CHRIST-HAZELHOF,E AND NUGTEREN,D H

ISOPROPYL AND METHYL-T-BUTYL ETHERS AS CHEMICAL IONIZATION REAGENT GASES 69
*MENTZER,M,KILLMER,L B AND ROTTSCHAEFER,S

MEASUREMENT OF PLATELET ACTIVATING FACTOR BY GAS CHROMATOGRAPHY-MASS SPECTROMETRY 71
*CLAY,K L AND MURPHY,R C

SIMULTANEOUS MEASUREMENT OF HISTAMINE METABOLITES BY GC-MS 73
*KHANDELWAL,J K,HOUGH,L B,KLINE,T AND GREEN,J P

A CANDIDATE DEFINITIVE METHOD FOR THE DETERMINATION OF SERUM CREATININE BY ISOTOPE DILUTION/MASS SPECTROMETRY 74
*NG,K J,WELCH,M J,COHEN,A,HERTZ,H S,SCHAFFER,R AND WHITE,E

IDENTIFICATION AND QUANTITATIVE ANALYSIS OF ACYLCARNITINES IN HUMAN URINE BY THERMOSPRAY LC/MS 76
*LIBERATO,D J,YERGEY,A L AND MILLINGTON,D S

MEASUREMENT OF PLASMA THROMBOXANE B2 BY GC/MS USING 18O LABELLED THROMBOXANE B2 78
*HEROLD,D A,ROSS,R M,MARQUIS,F,SAVORY,J,WILLS,M R,AYERS,C R AND SMITH,B J

NEGATIVE ION CHEMICAL IONIZATION GC-MS FOR QUANTITATIVE MEASUREMENT OF URINARY OCTOPAMINES AND SYNEPHRINES 80
IBRAHIM,K E,MIDGLEY,J M,COUCH,M W,*WILLIAMS,C M,BUDD,M B AND YOST,R A

THE SEARCH FOR 5-HYDROXYEICOSATETRAENOIC ACID IN RAT PLASMA BY GC/MS AS THE t-BUTYLDIMETHYLSILYL DERIVATIVE 82
*MURPHY,R C AND ANDERSON,F A

MPA — **LC/MS**

THERMOSPRAY IONIZATION OF MIDDLE MOLECULES 84
*LARSEN,B S,HELLER,D N,FENSELAU,C AND COTTER,R J

METABOLIC STUDIES OF EXPLOSIVES. LC/MS OF METABOLITES OF 2,4,6-TRINITROTOLUENE 86
*YINON,J AND HWANG,D -G

MOVING BELT INTERFACE APPLICABILITY WITH MICROBORE LIQUID CHROMATOGRAPHY/ MASS SPECTROMETRY 88
ALAMERCERY,S,EMMELIN,M,*FRAISSE,D AND ROCCA,J L

ANALYSIS OF INTRACTABLE ENDOGENOUS MOLECULES BY THERMOSPRAY LC/MS 90
*YERGEY,A L AND LIBERATO,D J

THE ELCTROSPRAY ION SOURCE (ESPIS) AS AN LC-MS INTERFACE 92
*WHITEHOUSE,C M AND FENN,J B

CROSSED-BEAM TECHNIQUE FOR COUPLING LC/MS 94
*MAHONEY,J F,PEREL,J AND SIEGEL,M

APPLICATION OF A MONODISPERSE AEROSOL GENERATION/LIQUID CHROMATOGRAPHY INTERFACE (MAGIC) TO SAMPLES OF ENVIRONEMNTAL & BIOCHEMICAL IMPORTANCE 96
*ABBEY,L E,BOSTWICK,D E,WINKLER,P C,WILLOUGHBY,R C AND BROWNER,R F

OPTIMIZATION OF SOURCE AND PROBE DESIGN IN A COMMERCIALLY AVAILABLE THERMOSPRAY LC-MS 98
*POEPPEL,F,BUCHNER,J,LO,H H AND DULAK,J

THERMOSPRAY: NEW DEVELOPMENTS AND APPLICATIONS 100
*MCFADDEN,W H AND TUCKER,M G

ANALYSIS OF PHOSPHOLIPIDS BY HPLC-MASS SPECTROMETRY 102
*MCCLUER,R H,JUNGHALWALA,F B AND EVANS,J E

THERMOSPRAY HPLC-MS OF PROSTAGLANDINS AND OXYGENATED METABOLITES OF ARACHIDONIC ACID (C20·4) AND DOCOSAHEXANOIC ACID (C22·6) 104
YERGEY,J AND SALEM,N

DIRECT LIQUID INTRODUCTION AND THERMOSPRAY OPERATION ON A MAGNETIC SECTOR INSTRUMENT 106
CHAPMAN,J R,SAYYID,S AND *EVANS,S

THE ANALYSIS OF MOLECULES OF MOLECULAR WEIGHT GREATER THAN 1500 A M U USING DLI OR THERMOSPRAY 108
*GOODLEY,P C AND KENYON,C N

SELECTED APPLICATIONS OF DLI-LC/MS TO PROBLEMS IN BIOMEDICAL ANALYSIS 110
SMITH,R W,YAMAGUCHI,K,PARKER,C E AND MATTHEWS,H B

IDENTIFICATION OF PLANT CELL CULTURE PRODUCTS BY COMBINED MICRO LIQUID CHROMATOGRAPHY/MASS SPECTROMETRY 111
*BRUINS,A P AND PRAS,N

A SIMPLIFIED MOVING-BELT INTERFACE FOR LIQUID CHROMATOGRAPHY-MASS SPECTROMETRY 113
*STOUT,S J AND DACUNHA,A R

DLI/LC-MS OF NUCLEOSIDES USING A SELF-MADE DISSOLVATION CHAMBER 115
*ESMANS,E L,LUYTEN,Y,GEBOES,P AND ALDERWEIRELDT,F C

ANALYSIS OF CANDIDATE ANTI-CANCER DRUGS BY THERMOSPRAY HPLC/MS 117
VOYKSNER,R D,*BURSEY,J T AND HINES,J

LIQUID CHROMATOGRAPHY/FAST ATOM BOMDARDMENT MASS SPECTROMETRY (LC/FABMS) 119
*STROH,J G,COOK,J C,RINEHART,K L AND LEWIS,I A S

MPB — Metabolic Profiling; Natural Products

METABOLIC PROFILE STUDIES OF A PATIENT WITH CYTOCHROM C OXIDASE DEFICIENCY 121
*MATSUMOTO,I AND KUHARA,T

QUANTIFYING CHOLESTEROL SULFATE IN SERUM BY LIQUID SIMS 123
*CHAI,W AND SHACKLETON,C

LIQUID SECONDARY ION MASS SPECTROMETRY OF BILIRUBIN AND BILIRUBIN ANALOGS 125
*CHAJ,W,WHITNEY,J O,BLANCKAERT,N AND BURLINGAME,A L

ANALYSIS OF ISOMERIC BILE SALTS USING FAB IN COMBINATION WITH CID-MIKE 127
*LIEHR,J G AND KINGSTON,E E

DIRECT DETERMINATION OF ACETYLCHOLINE IN BRAIN TISSUE 129
*WEINTRAUB,S T,LIBERATO,D J AND YERGEY,A L

ANALYSIS OF ACYLCARNITINES FROM BIOLOGICAL SAMPLES BY FAB-MS 131
*HUGHES,H,NOWLIN,J G,SMITH,C V,CARROLL,D I AND HORNING,E C

LSIMS PROFILING OF RAW UNEXTRACTED BILE IN METABOLIC STUDIES OF HEPATOTOXIC BILE ACIDS IN ANIMALS AND HUMANS 133
*WHITNEY,J O,GRUNBERGER,D,ROITMAN,E,YANG,Y-M,ROSENTHAL,P AND BURLINGAME,A L

STRUCTURE OF AN UNUSUAL URINARY COMPOUND FORMED IN A REACTION OF CREATININE AND ETHANOL 135
CHHEDA,G B,FARBER,A,ALDERFER,J L,PARTHASARATHY,R,JENKINS,E, MCCLOSKEY,J A AND *ARAKALI,A

APPLICATION OF MASS SPECTROMETRY TO THE STUDY OF THE BACTERIAL METABOLISM OF ISOMERIC AMINO AND NITRO BIPHENYLS 137
*MASSE,R,AYOTTE,C,MESSIER,F,BADR,M AND MOSHEN,M

BENZOYLALANINE, A NEW METABOLITE IN HYPERAMMONEMIC PATIENTS TREATED WITH SODIUM BENZOATE 139
*SHINKAI,T,INOUE,Y,KUHARA,T,MATSUMOTO,M AND MATSUMOTO,I

EVALUATION OF INFRA-RED HETERODYNE RATIOMETRY AS AN ALTERNATIVE TO GAS ISOTOPE MASS SPECTROMETRY FOR ANALYSIS OF 13CO2 IN BREATH 141
*IRVING,C S,BOUTTON,T W,NAVRATIL,P R AND KLEIN,P D

A MODIFIED BREATH INLET SYSTEM FOR BREATH ANALYSIS BY ALI/MS 143
*BENOIT,F M,CENA,K AND MUIR,D C F

NATURAL PRODUCTS FROM SOIL 144
*WALLER,G R,RITCHEY,C R AND KRENZER,E G

PRODUCTION OF A NEW COMPOUND BY METABOLISM OF THEOPHYLLINE IN COFFEE ARABICA 146
*WALLER,G R AND LUDOVIC,Y

ANALYSIS OF TRAZODONE AND 4H4-TRAZODONE BY CAPILLARY GC/MS/SIM 148
*KERNS,E H,GAMMANS,R E,BULLEN,W W AND RUSSELL,J R

DESORPTION CHEMICAL IONIZATION MASS SPECTRA OF UNDERIVATIZED ABSCISIC ACID-CONJUGATED METABOLITES, A USEFUL AID FOR STRUCTURAL CHARACTERIZATION 150
*TAKEDA,N,HARADA,K -I,SUZUKI,M,TATEMATSU,A,HIRAI,N AND KOSHIMIZU,K

QUANTITATION OF SUCROSE ESTERS IN TOBACCO BY DIRECT CHEMICAL IONIZATION MASS SPECTROMETRY 152
*EINOLF,W N AND CHAN,W G

USING GC/MS TO MONITOR THE EFFECTS OF ACENAPHTHENE ON AQUATIC PLANTS 153
VESTLING,M M

APPLICATION OF 252cf-PDMS TO CHLOROPHYLL LINKED PAIRS 155
*HUNT,J E,MICHALSKI,T J AND KATZ,J J

SIMULTANEOUS DETERMINATION OF ABA AND IAA IN PLANT EXTRACTS USING GC/MS/MPM 156
*JAYASIMHULU,J AND CARUSO,J L

MASS SPECTROMETRY DETERMINATION OF ALTERATIONS IN STRUCTURE AND CONCENTRATIONS OF SELECTED CHEMICAL MUTAGENS INCUBATED IN CULTURE MEDIUM 158
PROCTOR,B L,*DOWD,M A AND GAULDEN,M E

TOA — **Novel Concepts and Determinations**

NEUTRAL PRODUCTS FROM FLUORIDE TRANSFER BETWEEN ALKYL FLUORIDES AND ALKYL CATIONS IN THE GAS PHASE 160
JOHRI,K K,REDMAN,E W,LEE,R W K AND *MORTON,T H

TIME-RESOLVED KINETIC ENERGY RELEASES FOR METASTABLE PHENOL IONS 162
*LIFSHITZ,C,GEFEN,S AND ARAKAWA,R

SUPERSONIC BEAM MASS SPECTROMETRY 164
LUBMAN,D M AND TEMBREULL,R

A NEW APPROACH TO ISOTOPIC ABUNDANCE CALCULATIONS 166
HSU,C S

RECENT APPLICATIONS OF INDUCTIVELY COUPLED PLASMA MASS SPECTROMETRY (ICP MS) TO ELEMENTAL AND ISOTOPIC ANALYSIS 168
*DOUGLAS,D J,BOORN,A AND QUAN,E S K

ON-LINE CHIRAL LC/MS FOR THE IDENTIFICATION OF DL ENANTIOMER PAIRS 170
*HENION,J,CROWTHERS,J AND COVEY,T

EXPERIMENTAL EVIDENCE FOR STABLE CC142+ IONS 172
*STAHL,D,GUENAT,C AND MAQUIN,F

PARALLEL MASS SPECTROMETRY 174
CHANG,C

ULTRAPRECISE MASS SPECTROMETRIC ANALYSIS OF GAS MIXTURES DOWN TO THE TRACE IMPURITIES CONCENTRATION LEVEL 176
*WAGNER,G,LASER,B AND BRUNNEE,C

ELECTRON CAPTURE EFFECT IN CI MS 178
*RUDEWICZ,P AND MUNSON,B

TOB — **Fundamentals of Desorption**

SIMS OF BIOMOLECULES IN THE PICO- AND FEMTOMOL RANGE 180
*BENNINGHOVEN,A,NIEHUIS,E,FRIESE,T,GREIFENDORF,D AND STEFFENS,P

TOTAL PARTICLE YIELDS FROM LIQUID ORGANIC MATRICES UNDER BOMBARDMENT FROM KEV IONS 182
*BAROFSKY,D F,ILIAS,A M,BAROFSKY,E AND MURPHY,J H

SECONDARY ION MULTIPLICITY UNDER BOMBARDMENT WITH keV PRIMARY IONS 184
*BEAVIS,R,ENS,W,MAIN,D E,SCHUELER,B AND STANDING,K G

CLUSTERING PHENOMENA IN FAB MASS SPECTROMETRY 186
WONG,S S,*GIESSMANN,U AND ROLLGEN,F W

AN ELECTROSPRAY ION SOURCE (ESPIS) FOR MASS SPECTROMETRY OF FRAGILE ORGANIC SPECIES 188
WHITEHOUSE,C M,FENN,J B AND YAMASHITA,M

TOC — **LC/MS Interfaces**

ION EMMISSION PROCESSES AT ATMOSPHERIC PRESSURE - A COMPARISON OF THERMOSPRAY AND ION EVAPORATION 190
THOMSON,B A

MONODISPERSE AEROSOL GENERATION INTERFACE FOR COMBINING LIQUID CHROMATOGRAPHY WITH MASS SPECTROMETRY (MAGIC): SOME THEORETICAL CONSIDERATIONS 192
*WILLOUGHBY,R C AND BROWNER,R F

MECHANISTIC STUDIES ON THERMOSPRAY IONIZATION 193
*PILOSOF,D,KIM,H Y AND VESTAL,M L

STUDIES WITH MOVING BELT AND THERMOSPRAY LC/MS 195
*GAMES,D E,ALCOCK,N J,BEATTIE,I G,MCDOWALL,M A,MONCUR,A V, RAMSEY,E D AND SKETT,P W

METHODS TO ENHANCE THE AMOUNT OF INFORMATION OBTAINED BY THERMOSPRAY HPLC/MS 197
*VOYKSNER,R D AND BURSEY,J T

FAST INJECTION OF LIQUID SOLUTIONS INTO A QUADRUPOLE MASS SPECTROMETER USING SHORT FUSED SILICA CAPILLARIES 199
*ARPINO,P J AND BEAUGRAND,C

ANALYSIS OF POTENT METAGENS IN BROILED FISH BY COMBINED LIQUID CHROMATOGRAPHY-THERMOSPRAY MASS SPECTROMETRY 201
*EDMONDS,C G,SETHI,S K,MCCLOSKEY,J A,KASAI,H AND NISHIMURA,S

AN IMPROVED THERMOSPRAY LC/MS SYSTEM FOR DETERMINING DRUGS IN URINE 203
*HENION,J,CROWTHERS,J AND COVEY,T

HIGH PERFORMANCE GRADIENT LC/MS USING MICROBORE COLUMNS WITH A MOVING BELT INTERFACE 205
*HAYES,M J,SCHWARTZ,H E,VOUROS,P,KARGER,B L,THRUSTON,A D AND MCGUIRE,J M

NEW DEVELOPMENTS IN HIGH PERFORMANCE CAPILLARY SUPERCRITICAL FLUID CHROMATOGRAPHY-MASS SPECTROMETRY 207
*SMITH,R D,WRIGHT,B W AND UDSETH,H R

TOD — **Gas Phase Organometallic Chemistry**

STUDIES ON THE CHEMISTRY OF TRANSITION METAL CLUSTERS USING FOURIER TRANSFORM MASS SPECTROMETRY 209
*ANDERSON,D J AND ADAMS,T A

FLOWING AFTERGLOW STUDIES OF OXIDATION AND REDUCTION REACTIONS OF TRANSITION METAL CARBONYLS 211
LANE,K,SALLANS,L AND *SQUIRES,R R

STABLE MOLECULAR IONS ABOVE THE FRAGMENTATION ONSET IN THE BREAKDOWN GRAPH OF HEXACARBONYL CHRONIUM 213
*DAS,P R,NISHIMURA,T AND MEISELS,G G

GAS PHASE ION CHEMISTRY AND PHOTOCHEMISTRY OF GROUP 8(Fe,Co,Ni) MX+ (X=H,O,S,CH2 AND CH3) 215
JACOBSON,D B,CASSADY,C J,JACKSON,T C AND *FREISER,B S

ORGANOMETALLIC CHEMISTRY IN THE GAS PHASE. ION/MOLECULE REACTIONS OF TRANSITION METAL IONS WITH AMINES 217
BABINEC,S,HARRISON,J AND *ALLISON,J

COLLISION-INDUCED DISSOCIATION STUDIES OF ION-MOLECULE PRODUCT IONS USING FOURIER TRANSFORM MASS SPECTROMETRY 219
*BRICKER,D L AND RUSSELL,D H

REACTIONS OF IRON IN THREE OXIDATION STATES WITH ORGANIC MOLECULES 221
SMITH,A AND *RIDGE,D P

REACTIONS OF BARE AND SOLVATED ANIONS WITH TRANSITION METAL COMPLEXES IN THE GAS PHASE 223
LANE,K,SALLANS,L AND *SQUIRES,R R

CHAIN LENGTH EFFECTS IN GAS PHASE ORGANOMETALLIC CHEMISTRY 225
*TSARBOPOULOS,A AND ALLISON,J

TOE — **Cluster Ions; Time of Flight**

ION/MOLECULE REACTIONS OF GROUP VII METAL CARBONYLS 227
*MECKSTROTH,W K,FREAS,R B AND RIDGE,D P

STUDIES OF MIXED CLUSTERS VIA HIGH PRESSURE MASS SPECTROMETRY 229
*UPSCHULTE,B L,SCHELLING,F J,EVANS,D H,KEESEE,R G
AND CASTLEMAN,A W

ION MOLECULE REACTIONS IN THE NEGATIVE ION LASER MASS SPECTRA OF NITRO AROMATIC COMPOUNDS 231
*VISWANADHAM,S K AND HERCULES,D M

MASS SPECTROMETRIC INVESTIGATION OF FRAGMENTATION AND PHASE TRANSITIONS OF CARBON DIOXIDE CLUSTERS GENERATED IN A SUPERSONIC BEAM 233
ROMANOWSKI,G AND *WANCZEK,K P

CLUSTER IONS FROM HETEROCYCLIC NITRAMINES 235
*DOYLE,R J,WYATT,J R AND CAMPANA,J E

A HIGHLY SENSITIVE PULSED ION BOMBARDMENT TIME-OF-FLIGHT MASS SPECTROMETER 237
*CHAIT,B T AND FIELD,F H

A MULTISTOP TIME DIGITIZER FOR THE MANITOBA TIME-OF-FLIGHT MASS SPECTROMETER 239
*ENS,W,BEAVIS,R,MAIN,D E,SCHUELER,B AND STANDING,K G

VELOCITY COMPACTION FOCUSSING IN A TIME-OF-FLIGHT MASS SPECTROMETER 241
MUGA,M L

PERFORMANCE OF A MICROCHANNEL PLATE DETECTOR IN A TIME-OF-FLIGHT MASS SPECTROMETER OPERATION AT HIGH DUTY CYCLE AND HIGH ION CURRENTS 242
LINCOLN,K A

TOF — **Surface and Matrix Effects in Desorption Ionization**

GLYSEROL SOLUTIONS OF SILVER SALTS AS A SOURCE FOR GENERATION OF SILVER- CONTAINING ADDUCT IONS IN FAB-MS 244
*MUSSELMAN,B D AND WATSON,J T

MOLECULAR ION ENHANCEMENT USING SOLID MATRICES IN LDMS AND SIMS 246
*HARDIN,E D,FAN,T P AND VESTAL,M L

GAS PHASE MOLECULAR SIMS 247
*TODD,P J AND GROENEWOLD,G S

SELECTIVE DETECTION OF MIXTURE COMPONENTS BY SIMS 249
*ROSS,M M,KIDWELL,D A AND COLTON,R J

COMPARATIVE SIMS INVESTIGATION OF THERMALLY LABILE ORGANIC MOLECULES ON SILVER SUPPORT AND IN A GLYCEROL MATRIX 251
*BENNINGHOVEN,A,JUNACK,M AND SICHTERMANN W

ENHANCEMENT OF SECONDARY RADICAL CATION EMISSION BY MOLTEN SbCl3 253
*GROENEWOLD,G S AND TODD,P J

ISOMER DIFFERENTIATION IN PARTICLE-INDUCED DESORPTION MASS SPECTROMETRY/ MASS SPECTROMETRY 255
UNGER,S E

INFLUENCE OF THE LASER WAVELENGTH IN LAMMA DESORPTION OF ORGANIC MOLECULES 257
*KARAS,M,BACHMAHN,D AND HILLENKAMP,F

TPA — **Environmental**

QUALITATIVE AND QUANTITATIVE ANALYSIS OF SYNTHETIC ORGANIC POLLUTANTS IN RIVER WATER BY GC/MS 259
*DIETRICH,A M,SEO,Y-H,CUTUGNO,D AND MILLINGTON,D S

ISOMER SEPARATION OF A FLY ASH SAMPLE USING VARIOUS CAPILLARY COLUMNS 261
*SUN,W -F,LAU,B P -Y AND RYAN,J J

LONG-TERM GC/MS PRECISION AND ACCURACY STUDY FOR ENVIRONMENTAL MONITORING 263
VERRET,W J,HEDIN,C M,GARNER,F C AND *DONNELLY,J R

DEVELOPMENT OF ANALYTICAL METHODS FOR RESIDUAL POLYCATIONIC POLYMERS IN DRINKING WATER 265
HSU,K L,TRUSSELL,A R AND *MONCUR,J G

ANALYSIS OF A SOLID SLUDGE MATERIAL BY GC/MS 267
*BYRD,C D AND HILPERT,L R

METHOD FOR THE DETECTION OF BENZOTRIFLUORIDES IN ENVIRONMENTAL SAMPLES 269
PROCTOR,B L

CHARACTERIZATION OF ORGANIC EMISSIONS FROM HAZARDOUS WASTE DISPOSAL SITES BY GC-MS 271
*PRESCOTT,C L,PARR,J L AND HANISCH,R C

INDIVIDUAL AND BULK ANALYSIS OF AEROSOLS COLLECTED FROM ATMOSPHERE BY SIMS 273
*BARIL,M AND ADNOT,A

ANALYSIS OF DIESEL SOOT FOR NITRO-PAHS BY GC-MS 275
*HENDERSON,T R,HANSON,R L,SUN,J D AND BROOKS,A L

HPLC-MS DETERMINATION OF POLYCYCLIC AROMATIC COMPOUNDS IN MARINE SEDIMENTS 277
*QUILLIAM,M A,LANT,M S,JAMIESON,W D,LEWIS,E,GERSHEY,R M AND GERGELY,R J

FRACTIONATION AND IDENTIFICATION OF POLYCYCLIC AROMATIC COMPOUNDS IN MUTAGENIC EXTRACTS OF STEEL FOUNDRY PARTICULATES 279
*QUILLIAM,M A,TASHIRO,C,MCCALLA,D R AND KAISER-FARRELL,C

MULTIMEDIA DETERMINATION OF ORGANIC INDOOR AIR POLLUTANTS AT SUB-PART PER BILLION CONCENTRATIONS 281
*WILLIAMS,C H,MCDEVITT,M A AND PRESCOTT,C L

ANALYSIS OF THE POST DETONATION ENVIRONMENT OF AN EXPLOSIVES TEST FIRING CHAMBER 283
*YELTON,R O,HUGHES,B M AND MAZER,S M

DETERMINATION OF PART PER BILLION LEVELS OF 2,3,7,8-TCDD IN ENVIRONMENTAL SAMPLES AT HIGH PRECISION AND ACCURACY 285
*CARRETSON,L D,WILLIAMS,C H AND PROVOST,L P

RESPONSE FACTOR STUDIES FOR ANALYSIS OF POLYCHLORINATED DIBENZO-P-DIOXINS BY GAS CHROMATOGRAPHY-ELECTRON IMPACT MASS SPECTROMETRY 287
*CLEMENT,R E,TOSINE,H AND ALFIERI,A

VALIDATION BY HIGH RESOLUTION MASS SPECTROMETRY OF A BIOASSAY FOR "TCDD-LIKE" ACTIVITY 289
*HILKER,D R,ALDOUS,K M,O'KEEFE,P W,SMITH,R M,GIERTHY,J,EADON,G, JURUSIK,J AND HIBBINS,S W

GC/MS STUDIES OF SPECIFIC CONGENERS OF POLYCHLORODIBENZOFURANS 291
FUNG,D,*BOYD,R K,SAFE,S AND CHITTIM,B

HRGC/HRMS IDENTIFICATION OF CHLORINATED PHENYL AND PHENOXY SUBSTITUTED DIOXINS, FURANS AND DIPHENYL ETHERS IN COMMERCIAL GRADE PENTACHLOROPHENOL 293
*ONSTOT,J,TIMMONS,L AND JAMESON,C W

COMBINED GC/HRMS FOR THE ANALYSIS OF TCDD,TCDF AND PCB IN COMPLEX SAMPLE MATRICES 295
*WEERASINGHE,N C A,MEEHAN,J L AND BROOKS,H B

A COMPARISON OF TECHNIQUES FOR THE ANALYSIS OF EDB 297
ASHCROFT,A E,KEARNS,M,DENNE,D R AND *COMPSON,K R

MASS SPECTRAL IDENTIFICATION OF CHEMICAL RESIDUES FOUND IN THE TOTAL DIET PROGRAM 299
HEIKES,D L

MS-MS ANALYSIS OF GEOLOGICAL BIO-MARKER COMPOUNDS 301
*BROOKS,P W,PORTER,C J AND BILL,J C

FINGERPRINTING OF OIL SAMPLES BY MULTIPLE METASTABLE ION RECORDING 303
RAPP,U,HOHN,M,*PESCH,R AND BONNER,R

MASS SPECTRAL DETECTION AND CHARACTERIZATION OF PETROLEUM DYES AND TRACERS 305
*YOUNGLESS,T L,DANNER,D A AND SWANSIGER,J T

MOLECULAR BEAM MASS SPECTROMETRIC STUDIES OF THE OXIDATION OF ORGANIC MOLECULES 307
GREENE,F T AND O'DONNELL,J E

QUANTITATIVE TRACE ANALYSIS BY LC/MS/MS 308
*CHRISTENSEN,R G AND WHITE,E

APPLICATION OF CAPILLARY GC/MS TO MONITOR THE EFFECTS OF PRETREATMENT CHLORINATION OF NATURAL WATERS FOR THEIR USE IN DESALINATION FACILITIES 310
*LEIKER,T J AND HOHNHOLT,J M

TPC — **Fundamentals; Peptides**

SOME ION MOLECULE REACTIONS REQUIRING TRANSLATIONAL ENERGY INPUT 312
WHITE,E L,KINTER,M T,*BURSEY,M M AND KENAN,W R

CRITERIA FOR DETECTING INTERMEDIATE ION-NEUTRAL COMPLEXES IN UNIMOLECULAR IONIC DECOMPOSITIONS IN THE GAS PHASE 314
*MCADOO,D J AND HUDSON,C E

REACTIONS OF NEGATIVE CLUSTER IONS IN A TANDEM QUADRUPOLE MASS SPECTROMETER 315
*DALE,F,PAULSON,J F AND VIGGIANO,A A

SOME ION-MOLECULE INTERACTIONS OBSERVED IN A TRIPLE QUADRUPOLE 316
DAWSON,P H

RATE CONSTANTS FOR QUENCHING THE METASTABLE 2A2 STATE OF SO2+ BY ATMOSPHERIC GASES 318
*THOMAS,T F,DALE,F AND PAULSON,J F

LASER DESORPTION. THE THERMAL APPROACH 320
COTTER,R J

ISOTOPIC RATIOS IN FAST ATOM BOMBARDMENT MASS SPECTROMETRY 322
*CERNY,R L AND LAPP,R L

STUDIES OF THE TRAPPING OF POSITIVE IONS IN THE ELECTRON BEAM OF A SOURCE USING LASER RADIATION AS A PROBE 324
MORGAN,T G,MARCH,R E,*BRENTON,A G,HARRIS,F M AND BEYNON,J H

PENETRATION CHARACTERISTICS OF LOW ENERGY ELECTRONS 326
*VAN KALLEVEEN,T H AND MEISELS,G G

BREAKDOWN GRAPH OF DIMETHYL ETHER ION FROM ONSET TO 18 eV USING TPEPICO MASS SPECTROSCOPY 328
*DAS,P R,NISHIMURA,T AND MEISELS,G G

ELECTRON AFFINITIES FROM DISSOCIATIONS OF MIXED NEGATIVE ION DIMERS 330
*FUKUDA,E K,BURINSKY,D J AND CAMPANA,J E

EXPERIMENTAL AND THEORETICAL STUDIES OF PREDISSOCIATION PROCESSES IN DOUBLY CHARGED DIATOMICS 332
CURTIS,J M,WETMORE,R W,LEROY,R J AND *BOYD,R K

AROMATIC HYDROCARBONS IN THE MURCHISON METEORITE 334
*BASILE,B,MIDDLEDITCH,B S AND ORO,J

A COMPILATION OF ANION THERMOCHEMISTRY 336
BARTMESS,J E

PHOTODISSOCIATION OF SMALL PEPTIDE IONS 337
*BOWERS,W D,DELBERT,S S AND MCIVER,R T

FAB MASS SPECTROMETRY OF HUMAN FIBRINOGEN GLYCOPEPTIDES 339
*HELLER,D,FENSELAU,C,TOWNSEND,R AND LEE,Y C

FAST ATOM BOMDARDMENT MASS SPECTROMETRIC CARBOHYDRATE ANALYSIS OF GLYCOPEPTIDE ANTIBIOTICS 341
*ROBERTS,G,ROTTSCHAEFER,S,SITRIN,R AND JEFFS,P

GC/MS CHARACTERIZATION OF DIKETOPIPERAZINES FORMED BY THE ACTION OF DIMETHYLHYDRAZINE ON PEPTIDES 343
*BENNETT,B D,DAY,R A AND JAYASIMHULU,K

PARTIAL HYDRAZINOLYSIS OF PEPTIDES AND GC/MS ANALYSIS 345
*DAY,R A,JAYASIMHULU,K,BENNETT,B D,KELSO,G AND WEBER,L

STRUCTURE DETERMINATION OF A NEW CYCLODEPSIPEPTIDE ANTIBIOTIC FROM FUSARIA FUNGI 347
*CARR,S A,COSTELLO,C E,BLOCK,E,VESONDER,R F AND BURMEISTER,H R

ALGORITHMS USEFUL IN THE CONFIRMATION OR CORRECTION OF DNA-DERIVED AMINO ACID SEQUENCES OF PROTEINS 349
*SCOBLE,H A AND BIEMANN,K

FAST ATOM BOMBARDMENT MASS SPECTROMETRY OF THIOREDOXIN 351
*MATHEWS,W R AND BIEMANN,K

PEPTIDE SEQUENCING BY ON-LINE ENZYMATIC HYDROLYSIS AND THERMOSPRAY LC/MS 353
*KIM,H Y,PILOSOF,D,DYCKES,D F AND VESTAL,M L

MIXTURE ANALYSIS OF PEPTIDES BY FAB MS/MS 355
LIPPSTREU,D L

MECHANISMS OF ANTIOZONANT PROTECTION,ANTIOZONANT-RUBBER REACTIONS DURING OZONE EXPOSURE 257
*LATTIMER,R P,LAYER,R W AND RHEE,C K

QUALITATIVE AND QUANTITATIVE ASPECTS OF HIGH MASS FAB-MS USING SIGNAL AVERAGING TECHNIQUES 359
*TAYLOR,L C E AND GROTJAHN,L

SOLUTION INTRODUCTION MASS SPECTROMETRY. A SIMPLE ALTERNATIVE TO DESORPTION TECHNIQUES 362
*DOUGHERTY,R C AND DE KANEL,J

WOA — Resonance Ionization MS

THE HOLLOW CATHODE AS AN ATOM SOURCE FOR RESONANCE IONIZATION MASS SPECTROMETRY 364
*MARCUS,R K AND HARRISON,W W

SELECTIVE COUNTING OF KRYPTON ATOMS USING RESONANCE IONIZATION MASS SPECTROMETRY 366
*CHEN,C H,KRAMER,S D,ALLMAN,S L AND HURST,G S

ANALYTICAL DEVELOPMENTS IN RESONANCE IONIZATION MASS SPECTROMETRY 368
*MILLER,C M,NOGAR,N S AND DOWNEY,S W

MULTIWAVEKENGTH RESONANCE IONIZATION OF TECHNETIUM 370
*DOWNEY,S W,NOGAR,N S AND MILLER,C M

APPLICATION OF AN ARTIFICIAL INTELLIGENCE EXPERT SYSTEM FOR OPTIMIZATION OF REAL-TIME DATA FROM PYROLYSIS EXPERIMENTS 372
*WONG,C M,CRAWFORD,R W,LANNING,S M AND BRAND,H R

DIRECT DETERMINATION OF RELATIVE IONIZATION CROSS SECTIONS BY TRANSPIRATION MASS SPECTROMETRY 374
*BONNELL,D W AND HASTIE,J W

WOB — New Instruments

FAQQQ,THE TANDEM FLOWING AFTERGLOW-TRIPLE QUADRUPOLE A MARRIAGE OF CONVENIENCE 376
*SQUIRES,R R,LANE,K,LEE,R E,WRIGHT,L G,WOOD,K V AND COOKS,R G

THE BEQQ TANDEM MASS SPECTROMETER 378
*CIUPEK,J D,O'LEAR,J R,COOKS,R G,DOBBERSTEIN,P AND SCHOEN,A E

DESIGN AND PERFORMANCE OF A NEW TANDEM DOUBLE-FOCUSING MASS SPECTROMETER 380
*HASS,J R,GREEN,B N,BATEMAN,R H AND BOTT,P A

A DOUBLE FOCUSSING MASS SPECTROMETER FOR THE STUDY OF HIGH MOLECULAR WEIGHT BIO-MOLECULES 382
COTTRELL,J S,*TAYLOR,L C E AND WILLIAMS,D H

DESIGN ASPECTS IN HYBRID MASS SPECTROMETRY 384
*TAYLOR,L C E,STRADLING,R S,BUSCH,K L AND QUALLS,W C

PLENARY· MOLECULAR COMPUTER GRAPHICS· ,A PICTURE IS WORTH 4000 BYTES 1
SIGLER,P

WOC — **Nucleosides, Nucleotides and Carbohydrates**

OLIGOSACCHARIDE SEQUENCE INFORMATION AND DIRECT CHEMICAL IONIZATION 386
*REINHOLD,V N AND CARR,S A

SEQUENCING OF BIOLOGICAL MOLECULES BY SIMS 388
*KIDWELL,D A,ROSS,M M AND COLTON,R J

EVALUATION OF CYCLIC DI-t-BUTYLSILYL (DTBS) DIETHERS AS DERIVATIVES FOR GC-MS OF DIOLS 390
*BROOKS,C J W,COLE,W J AND BARRETT,G M

FABMS ANALYSIS OF BACTERIAL ANTIGENIC TREHALOSE-CONTAINING LIPOOLIGOSACCHARIDES 392
*JARDINE,I,SCANLAN,G,HUNTER,S W AND BRENNAN,P J

SPECIAL TECHNIQUES OF FAST ATOM BOMBARDMENT (FAB) MASS SPECTROMETRY FOR THE STUDY OF OLIGOSACCHARIDE ANTIBIOTICS: STRUCTURE OF KIJANIMICIN AND EVERNINOMICINS 394
*PRAMANIK,B N,GANGULY,A K,MALLAMS,A K AND SARRE,O

MASS SPECTROMETRIC SEQUENCING OF MODIFIED NUCLEOTIDES AND OLIGONUCLEOTIDES 396
GROTJAHN,L

CHARACTERIZATION AND IDENTIFICATION OF COENZYME A AND ITS ACYL DERIVATIVES BY FAB-MS/MS 398
*MILLINGTON,D S AND MALTBY,D A

SAMPLE PREPARATION AND CAPILLARY GCMS IDENTIFICATION OF MODIFIED NUCLEOSIDES IN HUMAN URINE 400
*TEECE,R G AND SCHRAM,K H

ANALYSIS OF PROTECTED AND UNPROTECTED NUCLEOTIDES BY FABMS 402
*HEMLING,M E,COOK,J C,RINEHART,K L,GUMPORT,R I AND PFLEIDERER,W

IN VITRO ALKYLATION OF CALF THYMUS DNA BY ACRYLONITRILE ISOLATION OF CYANOETHYL-ADDUCTS OF GUANINE AND THYMINE AND CARBOXYETHYL-ADDUCTS OF ADENINE AND CYTOSINE 404
*SOLOMON,J J,COTE,I L,DECKER,K AND SEGAL,A

WOD — **Isotope Ratios and Elemental Analysis**

A NEW METHOD FOR ESTIMATING ISOTOPIC RATIOS FROM PULSE-COUNTING MASS SPECTROMETRIC DATA 406
*BAYNE,C K AND SMITH,D H

CHARACTERIZATION OF A PULSED GLOW DISCHARGE AS A SOLIDS IONIZATION SOURCE 408
SAVICKAS,P J AND *HARRISON,W W

AMERICIUM DETERMINATION USING ISOTOPE DILUTION MASS SPECTROMETRY 410
*CRAWFORD,D W,CACIC,C C AND PEAVY,R D

INDUCTIVELY COUPLED PLASMA MASS SPECTROMETRY (ICP-MS) EFFECTS OF EXPERIMENTAL PARAMETERS ON SIGNAL TO NOISE RATIO 412
*OLIVARES,J A AND HOUK,R S

ELEMENTAL DETECTION BY COMBINED MICROWAVE PLASMA-GC/MS 414
*HEPPNER,R A AND PROCTOR,D W

GLOW DISCHARGE ATOMIZATION SOURCE FOR RESONANCE IONIZATION MASS SPECTROMETRY 416
*HESS,K R AND HARRISON,W W

THE PRODUCTION AND CERTIFICATION OF AN EQUAL ATOM PLUTONIUM ISOTOPIC STANDARD 418
*CACIC,C G,CRAWFORD,D W AND MACHLAN,L A

SEPARATION AND MASS SPECTROMETRY OF Nd,Pu AND U FROM U AND (U,Pu) FUELS 420
*GREEN,L W AND ELLIOTT,N L

DETERMINATION OF CONTAMINANTS IN UF6 SPECIFIC ANALYTICAL IMPLICATIONS 422
*HUBER,W K AND RETTINGHAUS,G

WOE — **Petroleum and Fuels**

MOLECULAR BEAM MASS SPECTROMETRIC STUDIES OF COAL DUST AIR FLAMES 424
*GREENE,F T,BRILL,F W,HUANG,J AND O'DONNELL,J E

ION/MOLECULE REACTIONS OF SMALL HYDROCARBON IONS 425
*BAYKUT,M G,BRILL,F W AND EYLER,J R

SCREENING MIDDLE DISTILLATE FUELS FOR SELECTED SPECIES BY TRIPLE QUADRUPOLE MASS SPECTROMETRY 426
*SCHUBERT,A J AND MYERHOLTZ,C A

A COMBINATION OF CHEMICAL REDUCTION AND TANDEM MASS SPECTROMETRY FOR THE CHARACTERIZATION OF SULFUR-CONTAINING COMPOUNDS 428
*WOOD,K V,LAUGAL,J A AND BENKESER,R A

APPLICATION OF FIELD DESORPTION MASS SPECTROMETRY TO CHARACTERIZATION OF PETROLEUM PRODUCTS AND IDENTIFICATION OF SPILLED OILS 430
*SHEN,J AND SAADEH,N K

MASS SPECTROMETRIC AND CHROMATOGRAPHIC METHODS APPLIED TO THE ISOLATION AND IDENTIFICATION OF TUMORIGENIC POLYCYCLIC AROMATIC HYDROCARBONS IN COAL LIQUEFACTION DISTILLATES 432
*LATER,D W,CHESS,E K,WRIGHT,C W,LUCKE,R B,MAHLUM,D D AND WILSON,B W

ANALYSIS OF JET FUELS BY CAPILLARY COLUMN GC/MS 434
*BLANTON,W E,HEPPNER,R A AND NETZEL,D A

MASS SPECTRAL STUDY OF COMPLEX MODEL COMPOUNDS FOR COAL STRUCTURE ELUCIDATION 436
*ZOELLER,J H,VINDIOLA,A G,ZINGARO,R A AND MACFARLANE,R D

MASS SPECTRAL COMPARISON OF MUTAGENS EXTRACTED FROM FLUIDIZED BED AND PULVERIZED COAL COMBUSTION FLY ASHES 438
*CHESS,E K,LATER,D W,HARRIS,W R,OKOMOTO,D AND WILSON,B W

WOF — **Xenobiotic Metabolism**

RESOLUTION OF THE ENENTIOMERS OF 6-HYDROXY-1-METHYLTETRAHYDRO--CARBOLINE IN URINE BY CAPILLARY COLUMN GC/MS 440
*BECK,O,FAULL,K F AND BARCHAS,J D

GC/NCIMS OF N-N-PROPYLNORAPOMORPHINE AND METABOLITES 441
*TRAINOR,T M,VOUROS,P,MAKSOUD,H AND NEUMEYER,J L

FAST ATOM BOMBARDMENT (FAB) MASS SPECTRA OF ANTINEOPLASTIC AGENTS 443
SUZUKI,R AND *ROBOZ,J

METABOLITE IDENTIFICATION OF CIS- AND TRANS-DECALIN IN KIDNEY AND URINE OF FISCHER RATS BY GC/MS 444
*YU,K O,OLSON,C T AND SERVE,M P

A DLI MICRO LC/MS PROCEDURE FOR DETERMINATION OF DIETHYLSTILBESTROL AND ITS METABOLITES 446
*COVEY,T,CROWTHERS,J,MAYLIN,G AND HENION,J

DESORPTION CHEMICAL IONIZATION (DCI) AND FAST ATOM BOMBARDMENT (FAB) SPECTRA OF DACTINOMYCIN (DACT) 447
*CREAVES,J,MCCAMISH,M AND ROBOZ,J

GC/MS STUDIES ON THE METABOLISM OF TETRAHYDROCANNABINOL HOMOLOGUES 448
HARVEY,D J

DEGRADATION PRODUCTS OF 9-ALKYLTHIO-9,10-DIHYDRO-9-HYDROXYPHENANTHRENES 450
*FEIL,V J,HUWE,J K AND BAKKE,J E

MASS SPECTRAL CHARACTERIZATION OF GLUTATHIONE CONJUGATES 451
*PALLANTE,S L,LISEK,C A AND FENSELAU,C

WPA — **Organic Mass Spectrometry**

ANALYSIS OF KETIMINES BY FAST ATOM BOMBARDMENT MASS SPECTROMETRY 453
*LAY,J O AND CHANG,T T

HIGH PRESSURE COLLISIONAL ACTIVATION MASS SPECTROMETRY OF SOME SUBSTITUTED BENZENES 455
*BLOM,K F AND MUNSON,B

NEUTRAL PRODUCT DISTRIBUTIONS FROM DEPROTONATION OF 1-METHYLCYCLOPENTYL CATION IN THE GAS PHASE 457
*REDMAN,E W AND MORTON,T H

SOME COMPARISONS BETWEEN THE ELECTRON IMPACT MASS SPECTRA OF FLUORINE SUBSTITUTED BETA-DIKETONATE AND MONOTHIO-BETA-DIKETONATE COMPLEXES OF METALS 459
*REIMER,M L J,WESTMORE,J B AND DAS,M

STEREOCHEMICAL EFFECTS IN THE ELECTRON IMPACT MASS SPECTRA OF EPIMERIC STEROID KETONES AND DIOLS 460
*WESTMORE,J B,REIMER,M L J,TEMPLETON,J F AND JACKSON,C-J C

STUDY OF AZA-1 BICYCLO (n,2,0) ALKANE STEREOCHEMISTRY EFFECTS IN OH NCI-MS 462
*TABET,J C,TONDEUR,Y,TROIN,Y,GRAMAIN,J C AND FRAISSE,D

EVIDENCE FOR STEREOSPECIFIC INTRAMOLECULAR HYDRIDE TRANSFER IN OH NCI 464
*TABET,J C,HANNA,I AND FETIZON,M

NITROGEN TRIFLUORIDE (NF3) AS A NEGATIVE CHEMICAL IONIZATION REAGENT GAS 466
*KILLMER,L B,ROTTSCHAEFER,S AND MENTZER,M

IDENTIFICATION OF SUBMICROGRAM QUANTITIES OF POSITIONAL AND GEOMETRICAL ISOMERS OF MULTI-UNSATURATED ALIPHATIC ALCOHOLS USING CAPILLARY COLUMN GC/MS METHOD 468
*HOGGE,L R,UNDERHILL,E W AND WONG,J W

CROSSED BEAM STUDIES OF THE REACTION OF O- WITH HYDROGEN AND THE LOWER HYDROCARBONS 470
*WU,R L C AND TIERNAN,T O

THE THERMOCHEMISTRY AND ION CHEMISTRY OF THE TRIPHENYLMETHYL SPECIES 472
*BARTMESS,J E AND KIPLINGER,J P

THE DECOMPOSITIONS OF METASTABLE C6H10O+ IONS WITH THE OXYGEN ON THE SECOND CARBON 473
*GRIFFIN,L L,HUDSON,C E AND MCADOO,D J

PROVITAMIN D - VITAMIN D INTERCONVERSIONS IN THE MASS SPECTROMETER. TRANSLATIONAL ENERGY RELEASE AND CID MIKE STUDIES 475
*ZARETSKII,Z V I AND KINGSTON,E E

TANDEM MASS SPECTROMETRY FOR THE ANALYSIS OF TRACE LEVELS OF -UNSATURATED SULTONES IN COMPLEX MATRICES 477
*BRAIN,D K,SLAYBACK,J R B AND RAHN,G

MASS SPECTROMETRIC INVESTIGATION OF 10 AND 11 CARBON ATOM CONTAINING ALPHA-OMEGA DIYNES 479
ROBBINS,R C AND *FOSTER,N G

CHEMISTRY AND MASS SPECTROMETRY OF POLYSULFANES. SELECTIVE SULFUR-34 INCORPORATION STUDIES 481
BARANY,G,MOTT,A W AND *LARKA,E A

QUANTITATIVE GC/MS USING NEGATIVE CHEMICAL IONIZATION WITH OH- AS THE REACTANT ION; APPLICATION TO FLAVOUR COMPONENTS 483
*BRUINS,A P,ELEMA,E T AND HENDRIKS,H

SEQUENTIAL ION-MOLECULE REACTIONS IN A FOURIER TRANSFORM MASS SPECTROMETER FOR ION STRUCTURE DETERMINATIONS 485
*DASS,C AND SACK,T M

SELECTIVE SYNTHESIS INSIDE THE COLLISION CELL OF A TANDEM QUADRUPOLE MS/MS 487
*SCHMIT,J P AND DAWSON,P H

ADDITIVITY OF COLLICIONAL ACTIVATION SPECTRA: A COMPARISON USING RESOLVED ISOBARIC MAIN BEAMS AND COLLISIONAL ACTIVATION PRODUCTS 489
HARVAN,D J,*BURSEY,M M AND HASS,J R

SITE OF GAS-PHASE CATION ATTACHMENT. THE PROTONATION AND ALKYLATION OF BIFUNCTIONAL NUCLEOPHILES 490
*BURINSKY,D J AND CAMPANA,J E

CHARGE STRIPPING MASS SPECTROMETRY OF MOLECULAR IONS FROM POLYCYCLIC AROMATIC HYDROCARBONS 492
*STAHL,D AND MAQUIN,F

THE COLLISIONALLY ACTIVATED FRAGMENTATION OF (M-H)- IONS OF POLYHYDROXY COMPOUNDS PRODUCED UNDER OH- NICIMS AND APPLICATIONS TO OLIGOMERS OF POLYMERIC FOOD ADDITIVES 494
BRUMLEY,W C,ANDRZEJEWSKI,D AND *SPHON,J A

NEW MS/MS SOFTWARE TOOLS FOR ELUCIDATION OF FRAGMENTATION MECHANISMS IN DIACETAMIDES 496
*WEINTRAUB,S T AND JOHNSTON,M

THE COLLISION INDUCED DISSOCIATIVE IONISATION OF NEUTRAL SPECIES 498
*BURGERS,P C,MOMMERS,A A,TERLOUW,J K AND HOLMES,J L

NEUTRALIZATION-REIONIZATION MASS SPECTROMETRY 499
*DANIS,P O,WESDEMIOTIS,C,FENG,R,TSO,J AND MCLAFFERTY,F W

WPF — **Instrumentation**

FIELD IONIZATION AND FIELD DESORPTION COMBINED WITH TANDEM MASS SPECTROMETRY 501
CERNY,R L

TANDEM MASS SPECTROMETRY OF HIGH MOLECULAR WEIGHT COMPOUNDS 503
*AMSTER,I J,COHEN,S L,CHAN,K W,ALI,M F,LOO,J A AND MCLAFFERTY,F W

A THEORETICAL MODEL FOR MASS SELECTIVE INSTABILITY AND HIGH PRESSURE OPERATION OF THE ION TRAP 505
*KELLEY,P E,STAFFORD,G C,FIES,W J,SYKA,J E P,MCIVER,R T, HUNTER,R L,TODD,J F J AND BEXON,J J

CONSTRUCTION OF AN INEXPENSIVE POLE BIAS SCANNER FOR QUADRUPOLE MASS SPECTROMETERS OF EARLY DESIGN 507
*BENCSATH,F A,NG,Y T AND FIELD,F H

QUADRUPOLES OPERATING IN THE SECOND STABILITY REGION 509
*DAWSON,P H AND BINGOI,Y

PARALLEL/TANDEM MASS SPECTROMETRY 511
*CHANG,C AND TIERNAN,T O

ISOTROPIC COLLISION INDUCED DISSOCIATION STUDIES WITH A NOVEL HYBRID INSTRUMENT 513
HO,M,HUGHES,R J,KAZDAN,E,MATTHEWS,P J,YOUNG,A B AND *MARCH,R E

A NEW INSTRUMENT FOR HIGH MASS APPLICATIONS 515
BATEMAN,R H,BORDOLI,R S,*GREEN,B N AND BARBER,M

VERSATILE ISOCHRONOUS DETECTOR FOR MASSIVE MOLECULAR IONS 517
*HILL,J C,MCNEAL,C J AND MACFARLANE,R D

ION ENERGY EFFECTS IN TIME-RESOLVED ION MOMENTUM SPECTROMETRY (TRIMS) 519
*STULTS,J T,HOLLAND,J F AND ENKE,C G

TANDEM QUADRUPOLE/TIME-OF-FLIGHT INSTRUMENT FOR MS/MS STUDIES 521
*GOERINGER,D E AND GLISH,G L

A NEW TYPE MS/MS WITH A CROSSED ExB FIELD AS THE SECOND MASS ANALYZER 523
*KUNIHIRO,F,NAITO,Y,KAMMEI,Y,NAITO,M AND ITAGAKI,Y

TANDEM MASS SPECTROMETRY WITH A HYBRID GEOMETRY INSTRUMENT 525
*BUSCH,K L AND QUALLS,W C

APPLICATIONS OF A HYBRID MS/MS INSTRUMENT UTILIZING PARENT IONS SELECTED AT HIGH RESOLUTION 527
FRALEY,D F

A MODERN CONTROL SCHEME FOR DOUBLE-FOCUSING MASS SPECTROMETERS 529
*LINN,W G AND ESKEW,T J

HIGH ACCURACY MASS MEASUREMENT WITH A FOURIER TRANSFORM MASS SPECTROMETER 530
REENTS,W D

ACCURATE MASS MEASUREMENT IN FOURIER TRANSFORM MASS SPECTROMETRY 532
*FRANCL,T J AND MCIVER,R T

MODIFICATION OF A BENDIX 12-101 TIME-OF-FLIGHT MASS SPECTROMETER FOR IMPROVED MASS RESOLUTION 534
*PINKSTON,J D,ALLISON,J AND WATSON,J T

IMPROVEMENT OF MASS RESOLUTION IN THRESHOLD PHOTOELECTRON-PHOTOION COINCIDENCE TOF MASS SPECTROMETER (TPEPICO-MS) 536
*NISHIMURA,T AND CHIARELLI,P

HIGH FLUX PARTICLE BOMBARDMENT TOF MASS SPECTROMETRY 538
*COTTER,R J AND DOLIN,B

QUANTITATIVE DETERMINATION OF RUBBER TRIBLEND COMPONENTS BY CURIE-POINT PYROLYSIS MASS SPECTROMETRY 540
MEUZELAAR,H L C,HARPER,A M,*WINDIG,W,LATTIMER,R P AND SCHUR,K M

STUDIES OF SUPERCRITICAL FLUID EXTRACTION AND FRACTIONATION PROCESSES FOR POLAR AND MIXED FLUIDS BY DFI-MS 542
*UDSETH,H R AND SMITH,R D

A PENNING TRAP MASS SPECTROMETER FOR HIGH PRECISION MASS MEASUREMENTS ON SHORT-LIVED ISOTOPES 544
*DABKIEWICZ,P,KALINOWSKI,H,KERN,F,KLUGE,H -J,SCHWEIKARD,L, SCHNATZ,H AND STUERMER,H

THE CAUSES OF ION CYCLOTRON FREQUENCY SHIFTS IN FTMS AND THEIR RELEVANCE TO EXACT MASS MEASUREMENT 546
*HUANG,S K AND REMPEL,D L

COMPUTER-CONTROLLED PEAK MATCHING 548
*GIBLIN,D E AND LAPP,R L

ROA — Techniques for Ionization and Excitation

FAB ANALYSES OF POLYMERS BY AN OPTIMIZED QUADRUPOLE MASS SPECTROMETER 550
YOUSSEFI,M

THE EFFECT OF POLYMER-SOLVENT INTERACTIONS ON SAMPLING EFFICIENCY IN ELECTROHYDRODYNAMIC IONIZATION MASS SPECTROMETRY 552
*CALLAHAN,J H AND COOK,K D

CHEMICAL IONIZATION/FAST ATOM BOMBARDMENT. A NOVEL IONIZATION METHOD 554
*FREAS,R B AND CAMPANA,J E

A SIMPLE APPROACH TO "IN-BEAM" CHEMICAL IONIZATION 556
*JAMIESON,G C,REUTER,C AND FITCH,W L

LIQUID IONIZATION MASS SPECTROMETRY OF ORGANOMETALLIC COMPOUNDS 558
MUSHA,K,KUWABARA,H AND *TSUCHIYA,M

CHARACTERIZATION OF SUPERCRITICAL FLUIDS USING DIRECT FLUID INJECTION-MASS SPECTROMETRY 560
*SMITH,R D,LUCKE,R B AND UDSETH,H R

A NEW SOURCE FOR STUDIES OF ANGLE-RESOLVED COLLISION-INDUCED DECOMPOSITIONS OF IONS 562
*JENNINGS,K R,MASON,R S AND MOORE,C

FIELD DESORPTION MASS SPECTROMETRY OF ortho,meta and para-TRIMETHYLAMMONIOPHENOLATES 563
WOOD,G W,*OBAL,T AND RAMANA,D V

ROB — **Organic Ion Structures**

MORE CANDIDATES FOR THE BENZYL/TROPYL PROBLEM: BENZOISOTOLUENE AND DIBENZOISOTOLUENE 565
BARTMESS,J E

THE NON-RESONANT MULTIPHOTON IONIZATION AND FRAGMENTATION OF SOME SUBSTITUTED BENZENE MOLECULES 566
*MARTIN,W B AND O'MALLEY,R M

THREE-MEMBERED RING ISOMERIZATIONS IN RADICAL CATIONS 568
*HUDSON,C E AND MCADOO,D J

DEPENDENCE OF FRAGMENTATION ON THE METHOD OF ENERGY DEPOSITION 570
*KENTTAMAA,H I AND COOKS,R G

ROTATIONAL PREDISSOCIATION OF D+2 FORMED FROM CD4 572
*BRENTON,A G,GUILHAUS,M,BEYNON,J H AND FOURNIER,P G

MECHANISM OF ELECTRON IMPACT INDUCED ALCOHOL ELIMINATION FROM DIALKYL MESACONATES. ANOTHER EXAMPLE OF A HIDDEN HYDROGEN TRANSFER 574
*MANDELBAUM,A,BORNSTEIN,D AND WEISZ,A

ROC — **Metabolic Profiling**

HIGH PERFORMANCE CHROMATOGRAPHY AND THE ART OF GC-MS HAVE PRODUCED GC METABOLIC PROFILING 576
*SWEELEY,C C,MUSSELMAN,B,MARTIN,M AND HOLLAND,J

AUTOMATED QUANTITATIVE ROUTINES FOR PROFILING PRIORITY URINARY ORGANIC ACIDS 578
*LIN,S-N AND CAPRIOLI,R M

THE CONTRIBUTION OF BACTERIAL FLORA IN METABOLIC PROFILING 580
*STOBIECKI,M,CARR,S A,SIEVERT,H -J,REINHOLD,V N AND GOLDMAN,P

TRIMETHYLAMINE (FISH ODOR SYNDROME) - THE DEVELOPMENT OF A METHOD FOR SCREENING OF THE INBORN ERROR OF METABOLISM 582
TJOA,S S AND *FENNESSEY,P V

GC/MS ANALYSIS OF FREE SHORT CHAIN CARBOXYLIC ACIDS IN PHYSIOLOGICAL FLUIDS BY ON-COLUMN INJECTION ON A FUSED SILICA CAPILLARY COLUMN 583
*MALTBY,D A,MILLINGTON,D S AND ROE,C R

MUSCLE METABOLISM OF BRANCHED CHAIN AMINO ACIDS IN TRAUMA-SEPSIS 585
*MCREYNOLDS,J H,HASSETT,J M,ROCHE,F R,HO,Y K,PAUL,T D,ANBAR,M AND BORDER,J R

ALTERED METABOLIC PROFILES OF VALPROATE AND ENDOGENOUS ACIDS IN A PATIENT WITH REYEL-LIKE SYNDROME 586
*KUHARA,T,MATSUMOTO,M,INOUE,Y,SHINKA,T AND MATSUMOTO,I

ROD — **Fourier Transform MS**

FTMS FOR ANALYSIS OF HIGH MASS AND INVOLATILE MOLECULES 588
IJAMES,C F AND *WILKINS,C L

FOURIER TRANSFORM ION CYCLOTRON RESONANCE MS ANALYTICAL AND CHEMICAL APPLICATIONS 589
*MARSHALL,A G,WANG,T -C L,MULLEN,S L AND SANTOS,I

GAS CHROMATOGRAPHY/MULTIPHOTON IONIZATION FOURIER TRANSFORM MASS SPECTROMETRY 591
*SACK,T M,MCCRERY,D A AND GROSS,M L

RECENT DEVELOPMENTS WITH THE TANDEM QUADRUPOLE-FOURIER TRANSFORM MASS SPECTROMETER 593
*MCIVER,R T,HUNTER,R L AND BOWERS,W D

QUANTITATION IN FTMS 595
WELLER,R R AND *EYLER,J R

PROBLEMS WITH QUANTITATION OF ION ABUNDANCE IN FTMS AND A PROPOSED SOLUTION 596
*HUANG,S K,REMPEL,D L AND GROSS,M L

MASS SELECTIVE INSTABILITY HIGH PRESSURE OPERATION OF THE ION TRAP 598
*STAFFORD,G C,KELLEY,P E,SYKA,J E P,REYNOLDS,W E,FIES,W J AND TODD,J F J

FOURIER TRANSFORM ION CYCLOTRON RESONANCE MASS SPECTROMETRY NEW THEORETICAL AND INSTRUMENTAL DEVELOPMENTS 600
*MARSHALL,A G,WANG,T-C L AND RICCA,T L

ROE — **Surface Analysis**

A CESIUM SURFACE IONIZATION SOURCE FOR SIMS 602
*NODA,T,OKUTANI,T,TAMURA,H AND WATANABE,H

CHARACTERISTICS OF AN IMMERSION LENS USED WITH A CS+ LIQUID SIMS QUADRUPOLE MASS SPECTROMETER 604
ABERTH,W

A COMPARISON OF WIDE APERTURE AND SHORT RESIDENCE TIME ION LENSES 606
DELMORE,J E

MICROANALYSIS OF INORGANIC MATERIALS BY LASER IONIZATION MASS SPECTROMETRY (LIMS) 608
*ODOM,R W,HITZMAN,C J AND BUTTRILL,S E

EFFECTS OF LASER FOCUS ON ION PRODUCTION DIRECTLY FROM SOLIDS 610
*CONZEMIUS,R J,ZHAO,S,HOUK,R S AND SVEC,H J

EVALUATION OF GALLIUM DIFFUSION IN GOLD FILMS BY MEANS OF SIMS 612
*YAMAGUCHI,H,HONMA,Y AND YASUDA,S

SIMS STUDY OF COMPOSITIONAL CHANGES OBSERVED IN A PuO2 HEAT SOURCE CLADDING ALLOY 614
*CHRISTIE,W H,EBY,R E AND TAYLOR,D H

MOLECULAR BEAM/MS SAMPLING OF SILANE OXIDATION IN A LOW-PRESSURE DISCHARGE FLOW REACTOR 616
*PELLETT,G L AND ADAMS,B R

ROF — **Desorption Methods**

MATRIX EFFECTS ON RELATIVE INTENSITIES OF MOLECULAR IONS,ADDUCTS AND FRAGMENTS IN LSIMS OF BRADYKININ 618
*REGINATO,R,CHAI,W,WALLS,F C,WHITNEY,J O AND BURLINGAME,A L

DEHALOGENATION REACTIONS IN FAST ATOM BOMBARDMENT MASS SPECTROMETRY 620
*SETHI,S K,NELSON,C C AND MCCLOSKEY,J A

PHOTOPLATE RECORDING OF FAB MASS SPECTRA TO m/z 3500 621
COSTELLO,C E

FAST ATOM BOMBARDMENT MASS SPECTROMETRY OF NINE NEUROTOXINS ISOLATED FROM PROTOGONYAULAX 622
*WHITE,K D,BRUMLEY,W C,DREIFUSS,P A,ROACH,J A G,PAGE,S W,HALL,S AND SPHON,J A

EXACT MASS MEASUREMENT BY FAB MASS SPECTROMETRY WITHOUT REFERENCE COMPOUNDS 624
CHANG,T T

ANALYSIS OF CATIONIC SURFACTANTS BY MASS SPECTROMETRY/MASS SPECTROMETRY WITH FAST ATOM BOMBARDMENT 625
*LYON,P A,CROW,F W AND TOMER,K B

A STUDY OF ALKALI CATIONIZATION PROCESSES OCCURRING UNDER FAST ATOM BOMBARDMENT CONDITIONS 627
*KEOUGH,T

TANDEM MASS SPECTROMETRY STUDIES OF IONS FORMED USING FAST-ATOM BOMBARDMENT IONIZATION 629
*BRICKER,D L,KRAILLER,R E AND RUSSELL,D H

RPA — **Computers in MS; Inorganic MS**

BOMB REDUCTION OF H20 OVER ZINC FOR ISOTOPE RATIO ANALYSIS 631
*SCHOELLER,D A,DELFINO,R AND BROWN,C J

EI AND PID/MS ANALYSIS OF SILOXANE POLYMERS 633
*BONE,W,MARASCO,J AND COLTON,R

GC/MS ANALYSIS OF SILANE FOR USE IN GLOW DISCHARGE PRODUCTION OF AMORPHOUS SILICON THIN FILMS 635
BENTZ,B L,*GALE,P J,HARRINGTON,W L,MAGEE,C W AND WEAKLIEM,H A

THERMOCHEMICAL STUDIES ON SmO+ AND SmO+2 637
MURAD,E

MASS SPECTROMETRIC INVESTIGATION OF GERMANIUM-SULFUR 638
*KOGAI,T AND ROLINSKI,E J

CALIFORNIUM PLASMA DESORPTION MASS SPECTROMETRY OF SOME METAL-LIGAND COMPLEXES 640
*PANNELL,L K,FALES,H F,SCOVILL,J P AND WEST,D X

APPLICATION OF ARTIFICIAL INTELLIGENCE PROGRAMMING TECHNIQUES TO THE DEVELOPMENT OF AN EXPERT SYSTEM FOR TUNING A TRIPLE QUADRUPOLE MASS SPECTROMETER 642
WONG,C,*LANNING,S,CRAWFORD,R AND BRAND,H

MULTICOMPONENT ANALYSIS OF MS/MS DATA 644
*GIBLIN,D E,PEAKE,D A AND LAPP,R L

MS/MS MATCHING TECHNIQUES AND THEIR DEPENDENCE ON INSTRUMENTAL PARAMETERS 646
*CROSS,K P AND ENKE,C G

ORGANIC STRUCTURE DETERMINATION USING TRIPLE QUADRUPOLE MASS SPECTROMETRY (TQMS); PROGRESS REPORT 648
*GIORDANI,A B,ENKE,C G,GREGG,H R,HOFFMAN,P A,CROSS,K P AND BECKNER,C F

A FULLY INTEGRATED COMPUTER-CONTROLLED THERMOGRAVIMETRIC ANALYSER - TANDEM MASS SPECTROMETER SYSTEM FOR POLYMER CHARACTERIZATION 650
*SHUSHAN,B,WILLIAMSON,C AND BUCKLEY,P H

A MICROCOMPUTER-BASED DATA SYSTEM FOR HIGH RESOLUTION MULTIPLE ION MONITORING AND MULTIPLE METASTABLE PEAK MONITORING 652
THORNE,G C AND *GASKELL,S J

CORRECTION OF MASS SPECTROMETER DRIFT WHILE USING AN INCOS DATA SYSTEM FOR HIGH RESOLUTION SELECTED ION MONITORING 654
COLLINS,G J

GC/MS SPECTRAL DATA ON NITROGEN-CONTAINING COMPOUNDS PUBLISHED AND ARRANGED INTO A CORRELATION INDEX USING COMPUTER TECHNIQUES 565
*HAMMING,M C,GEARHART,H L,PELL,R J AND FERGUSON,A M

THE USE OF ION ABUNDANCE RATIOS FOR THE CHARACTERIZATION OF GC/MS MIXTURES 657
MCCARTHY,E R

ENHANCED PBM FOR UNKNOWN IDENTIFICATION 658
*SPENCER,R B AND STAUFFER,D B

AIDS FOR BUILDING AND MAINTAINING IN-HOUSE SPECIALTY LIBRARIES ON THE SS-200 DATA SYSTEM 659
*MAGIN,D F AND GOOD,B W

ADDING FORWARD-SEARCHING CAPABILITIES TO A REVERSE SEARCH ALGORITHM FOR UNKNOWN MASS SPECTRA 661
*STAUFFER,D B AND MCLAFFERTY,F W

CONSTRUCTION AND USE OF A MASS SPECTRAL LIBRARY OF TRICHOTHECENES TO ASSIST IN THE IDENTIFICATION OF COMPONENTS OF LABORATORY SAMPLES 663
HEWETSON,D AND MIROCHA,C J

A NEW NON-SUPERVISED NUMERICAL METHOD FOR MIXTURE ANALYSIS OF COMPLEX SPECTRA 665
*WINDIG,W AND MEUZELAAR,H L C

A DATASYSTEM TO COMPLEMENT THE PERFORMANCE OF NEWLY DEVELOPED MASS SPECTROMETERS 667
*BILL,J C AND LYNAUGH,N

APPLICATION OF A LOW COST MICROCOMPUTER FOR DIGITAL M/Z READOUT ON A MAGNETIC SECTOR MASS SPECTROMETER 669
*FREEMAN,J P AND MITCHUM,R K

USE OF AN INCOS DATA SYSTEM VIA A PERSONAL COMPUTER· AN APPLE PERSPECTIVE 671
*JAMIESON,W D,GERSHEY,R M AND GUEVREMONT,R

STRUCTURAL CHARACTERIZATION OF GLYCOSAMINOGLYCANS BY FAB MS: APPLICATIONS TO CHONDROITIN AND HEPARIN SULFATES 673
*CARR,S A AND REINHOLD,V N

POLYSACCHARIDE BRANCHING AND LINKAGE DETERMINATION. DEPOLYMERIZATION BY REDUCTIVE CLEAVAGE AND PRODUCT CHARACTERIZATION BY GC-MS 675
*VAN LANGENHOVE,A AND REINHOLD,V N

ANALYSIS OF CARDIAC GLYCOSIDES BY FAST ATOM BOMBARDMENT MASS SPECTROMETRY 677
*ALLMAIER,G AND SCHMID,E R

STRUCTURAL ANALYSIS OF FLAVONOID OLIGOSIDES BY FAST ATOM BOMBARDMENT/TANDEM MASS SPECTROMETRY 679
*CROW,F W,TOMER,K B AND LOOKER,J H

APPLICATIONS OF LASER DESORPTION MASS SPECTROMETRY 681
*COTTER, R J,TABETT,J-C AND VAN BREEMEN,R

LC/MS ANALYSIS OF UNDERIVATIZED GLYCOSPHINGOLIPIDS FROM TISSUE EXTRACTS 683
*EVANS,J E AND MCCLUER,R H

COMPARATIVE CAPILLARY GC/MS OF STANDARD SOLUTIONS OF CHLORINATED BIPHENYLS 685
*JAMIESON,W D,GERSHEY,R M,GUEVREMONT,R,FUNG,D,BOYD,R K,SAFE,S AND CHITTIM,B G

THE ELIMINATION OF MASS SPECTRAL INTERFERENCES FOR THE DETERMINATION OF POLYCHLORINATED BIPHENYLS IN TRANSFORMER OIL AND WASTE OIL 687
*NERO,V P AND HUDSON,R D

EFFECT OF CHLORDECONE (KEPONE) ON THE RAT BRAIN CONCENTRATION OF 3-METHOXY-4-HYDROXY-PHENYLGLYCOL DETERMINED BY GC/MS/SIM 689
*CHEN,P H,TILSON,H A,MARBURY,G D AND HONG,J S

MS/MS STUDY OF OXYXHLORDANE AND HEPTACHLOR EPOXIDE 691
*BALLARD,J M,DONNELLY,J R AND SOVOCOOL,G W

CHARACTERIZATION OF CARBAMYL MERCAPTURIC ACIDS BY EI AND CI MASS SPECTROMETRY 693
LEHMAN,J P

POST-COLUMN BUFFER ADDITION FOR THERMOSPRAY-HPLC/MS ANALYSIS OF PESTICIDES 695
*VOYKSNER,R D,BURSEY,J T AND PELLIZZARI,E D

QUANTITATION OF 6-KETO-PROSTAGLANDIN-F (6K-PGF) AS THE METHOXIME-METHYL ESTER- -BUTYLDINETHYLSILYL (MOME(BDMS) DERIVATIVE USING A RELATIVELY INEXPENSIVE GC-MS-DS 697
*VRBANAC,J J AND KNAPP,D R

BIOCHEMICAL ANALYSES USING AN INSTRUMENT OF EBQ DESIGN 699
*GASKELL,S J,PORTER,C J AND BROOKS,P W

APPLICATION OF SIM TO DETERMINATION OF PAF 701
SATOUCHI,K AND *SAITO,K

QUANTITATIVE ANALYSIS OF 5-HETE IN THE ISOLATED PERFUSED RAT LUNG BY GC/NCI-MS 703
*STRIFE,R J AND MURPHY,R C

FAST ATOM BOMBARDMENT (FAB) MASS SPECTROMETRY OF LEUKOTRIENE C4 DECOMPOSITION PRODUCTS 705
*WESTCOTT,J Y,CLAY,K L AND MURPHY,R C

THE FT-MS SPECTRA OF CIS-DICHLORODIAMMINE PLATINUM (II) (CIS-PLATIN) AND RELATED ANTINEOPLASTIC DERIVATIVES 707
*WELLER,R R,RILEY,C N AND STERNSON,L A

MS/MS STUDIES ON MACROCYCLIC TRICHOTHECENES 709
*KRISHNAMURTHY,T AND SARVER,E W

IDENTIFICATION OF A CYTOTOXIC METABOLITE OF CIS-DICHLORO-TRANS-DIHYDROXY-BIS -ISOPROPYL-AMINE Pt(IV)(CHIP) 711
*COWENS,J W,PENDYALA,L,PAUL,B,ALDERFER,J,DUTTA,S,CHHEDA,G AND CREAVEN,P J

RPC — **Desorption Ionization; Isotope Ratios; Ion Structures**

AN INVESTIGATION OF THE STRUCTURES OF NEUTRAL FRAGMENTS FORMED WHEN IONS DISSOCIATE IN A ZAB-2F SPECTROMETER 713
MORGAN,T G,MARCH,R E,*BRENTON,A G,HARRIS,F M AND BEYNON,J H

SCATTERING IN DISSOCIATIVE COLLISIONS OF IONIZED ACETONE WITH HELIUM 715
*MCLUCKEY,S A,VAN DER ZANDE,W,DE BRUIJN,D P,LOS,J AND KISTEMAKER,P G

COLLISIONALLY INDUCED FRAGMENTATION REMOTE FROM THE SITE OF IONIZATION 717
*TOMER,K B,CROW,F W,JENSEN,N J,GROSS,M L AND LYON,P A

INTERNAL ENERGY EFFECTS IN LOW ENERGY CID 719
*GLISH,G L AND GOERINGER,D E

ISOTOPE EFFECTS AS A PROBE OF COLLISION-ACTIVATED DISSOCIATION SYSTEMATICS 721
*LEHMAN,T A,CROW,F W AND TOMER,K B

AN UNEXPECTED (C3H5O)+ ION (CH2-C(OH)-CH2)+ 723
BOUCHOUX,G,FLAMENT,J P,FLAMMANG,R,MAQUESTIAU,A,*HOPPILLIARD,Y AND MEYRANT,P

HIDDEN REARRANGEMENT OF IONIZED 3-PENTENE-2 ONE BEFORE METHY ELIMINATION 725
BOUCHOUX,G,*HOPPILLIARD,Y AND JAUDON,P

STABILITIES OF C3H3O+ IONS AB INITIO CALCULATIONS 727
BOUCHOUX,G,FLAMENT,J P AND *HOPPILLIARD,Y

EXCITED STATES AND COLLISIONALLY ACTIVATED DISSOCIATION 729
DAWSON,P H

FOURIER TRANSFORM MASS SPECTROMETRY AS A PROBE INTO TRANSITION METAL ION CHEMISTRY 731
*ADAMS,T A,ANDERSON,D AND BRICKER,D L

MASS SPECTROMETRIC INVESTIGATION OF GASEOUS MOLECULES FROM THE VAPORIZATION OF ZnGa2Se4 732
*GRIMES,L E AND EDWARDS,J G

ANALYSIS OF THE VAPOR PHASE OVER LIQUID InTe AT 1106 K 734
*SRINIVASA,R S AND EDWARDS,J G

CAPILLARY GAS CHROMATOGRAPHY FIELD IONIZATION MASS SPECTROMETRY 736
GALLEGOS,E J

FD-MS,FAB-MS AND ESR OXIDATION STUDIES OF PARTIALLY HINDERED AMINES - 3,3-DIALKYLDECAHDROQUINOXALIN-2-ONES 738
LAYER,R W,LAI,J T,*LATTIMER,R P AND WESTFAHL,J C

FAB/MS ANALYSIS OF HI-6 AND ITS DEGRADATION PRODUCTS 740
*BONE,W,MARASCO,J,KAZYAK,L AND BROWN,N

CALIFORNIUM PLASMA DESORPTION MASS SPECTROMETRY OF SOME DYES 742
*FALES,H M,PANNELL,L K AND SOKOLOSKI,E

IDENTIFICATION OF RUBBER ADDITIVES BY FIELD DESORPTION AND FAST ATOM BOMBARDMENT MASS SPECTROMETRY 743
LATTIMER,R P,*HARRIS,R E,ROSS,D B AND DIEM,H E

ENHANCEMENT OF FAST ATOM BOMBARDMENT SPECTRA BY CHARGE TRANSFER DERIVATIZATION 745
*BUSCH,K L AND QUALLS,W C

FAB-MS DIRECTLY FROM ELECTROPHORETIC PLATES APPLICATIONS TO QUATERNARY ORGANOARSENIC COMPOUNDS 747
*BAROFSKY,D F AND ZIMMERMAN,M L

ALKALI HALIDE CLUSTER IONS OBSERVED BY TIME-OF-FLIGHT SIMS 749
*SCHUELER,B,BEAVIS,R,ENS,W,MAIN,D E AND STANDING,K G

FAST ATOM BOMBARDMENT INDUCED ADDUCT IONS 751
*PANG,H,COSTELLO,C E AND BIEMANN,K

STABLE ISOTOPE ANALYSIS OF COLLAGEN TURNOVER AND PROLINE RECYCLING IN SCAR TISSUE 753
*WOLFE,M H,MOLNAR,J A AND WOLFE,R R

STABLE ISOTOPE RATIO MASS SPECTROMETRY IRON BIOAVAILABILITY STUDIES 755
*EVANS,S AND SELF,R

DETERMINATION OF DEUTERIUM CONTENT OF H20 BY REACTION WITH PHENYLMAGNESIUM BROMIDE AND GC-MS-SIR ANALYSIS OF BENZENE 757
SHARP,T R

GC-MS DETERMINATION OF ISOTOPIC ENRICHMENT IN (6-15NH2)-ADENOSINE-5'-MONOPHOSPHATE: APPLICATION TO HUMAN METABOLIC STUDIES 759
*LEWIS,S AND YUDKOFF,M

A NEW APPROACH FOR THE STUDY OF GLUCOSE METABOLISM USING DUAL STABLE ISOTOPIC TRACER INFUSIONS AND GC-MS ANALYSIS 761
*MARTINEAU,A,LECAVALIER,L,CHIASSON,J L AND FALARDEAU,P

STABLE ISOTOPE EXCHANGE STUDY OF A TRYPTOPHAN TRANSAMINASE ISOLATED FROM STREPTOMYCES FLOCCULUS 763
*VICCHIO,D,SPEEDIE,M K AND CALLERY,P S

FOA — Ion/Molecule Reactions

STATISTICAL PHASE SPACE THEORY OF ION-MOLECULE ASSOCIATION 765
*BASS,L M AND JENNINGS,K R

THREE-BODY ION-MOLECULE ASSOCIATION RATE COEFFICIENTS AS A FUNCTION OF TEMPERATURE AND CLUSTER SIZE 767
*VIGGIANO,A A AND PAULSON,J F

RATE COEFFICIENTS AT 300K FOR THE VIBRATIONAL ENERGY TRANSFER REACTIONS FROM N2(v=1) TO O2+(v=0) AND NO+(v=0) 769
*FERGUSON,E E,ADAMS,N G,SMITH,D AND ALGE,E

STABLE MOLECULAR IONS ABOVE FRAGMENTATION ONSET IN THE BREAKDOWN GRAPH OF FURAN 771
*NISHIMURA,T AND MEISELS,G G

(1 + 2) CYCLOADDITION OF KETENE+ RADICAL CATION AND NEUTRAL ETHYLENE 773
DAS,C

ENTROPY CHANGES DURING PROTON TRANSFER IN SUBSTITUTED HALOTOLUENES 775
FERNANDEZ,M T,MASON,R S AND *JENNINGS,K R

FRAGMENT-MOLECULE ADDUCT ION FORMATION IN METHANE CHEMICAL IONIZATION MASS SPECTROMETRY 777
*CHANG,S Y AND MARYANOFF,C A

BREAKDOWN CURVES FROM ERMS AND ARMS: APPLICATION TO ORGANIC ION STRUCTURES 779
*VERMA,S,CIUPEK,J D AND COOKS,R G

FOB Biological Applications of MS/MS

GC/MS AND MS/MS ANALYSIS OF GAMMA-AMINO-BUTYRIC ACID IN BIOLOGICAL SPECIMENS 781
*NORMAN,E J,WEE,E L,ZIMMERMAN,E F,FRALEY,D F AND LAWRENCE,D L

TANDEM MASS SPECTROMETRY FOR THE TRACE DETERMINATION OF TRYPTOLINES IN CRUDE BRAIN EXTRACT 783
*JOHNSON,J V,YOST,R A,FAULL,K F AND BARCHAS,J D

FAB MS/MS APPLICATIONS TO DRUG METABOLISM 785
*STRAUB,K AND LEVANDOSKI,P

MEASURING BIOLOGICALLY ACTIVE COMPOUNDS IN CRUDE PLANT EXTRACTS BY MS/MS 787
*PLATTNER,R D,GROVE,M D AND POWELL,R G

APPLICATION OF GC/CI/MS/MS IN RAPID SCREENING OF EIGHT UNDERIVATIZED TRICHOTHECENES AND ZEARALENONE IN GRAINS 789
*LAU,B P -Y,SCOTT,P M AND SAKUMA,T

PROGRESS IN RAPID URINE ANALYSIS FOR DRUGS BY ON-LINE LC/MS/MS 791
*HENION,J AND COVEY,T

FOC — Structures and Assays

LOCATION OF DOUBLE BONDS IN OLFEINS BY MS/MS OF Fe(OLEFIN)+ COMPLEXES 793
*PEAKE,D A AND GROSS,M L

FASTER AND MORE SENSITIVE GC/MS BY REDUCING THE CAPILLARY COLUMN INNER DIAMETER 795
*LECLERCQ,P A,SCHUTJES,C P AND CRAMERS,C A

CHARACTERIZATION OF ALKYLAMINE COMPLEXES OF FE,CR,NI AND MO USING FAB AND MS/MS 797
*HOLMES,G A AND RUSSELL,D H

A MICROCOMPUTER-BASED WORKSTATION FOR THE INTERPRETATION OF MS/MS SPECTRA 799
BARBALAS,M P

STRUCTURE AND STABILITY OF (CnH2n-1O)+ IONS PRODUCED IN LOW ENERGY PROCESSES 801
BOUCHOUX,G AND *HOPPILLIARD,Y

THE ANALYSIS OF TRACE QUANTITIES OF THERMALLY LABILE COMPOUNDS BY THERMOSPRAY LIQUID CHROMATOGRAPHY-MASS SPECTROMETRY 803
*LEWIS,I A S,SMITH,D C AND VEARES,M

HIGH SENSITIVITY ASSAY FOR PHENOLIC ACID DERIVATIVES WITH OH- NEGATIVE CHEMICAL IONIZATION 805
*BENCSATH,F A,SCHWEITZER,J S,FRIEDHOFF,A J AND FIELD,F H

MASS SPECTROMETRY OF FIVE KETENE DIMERS 807
*OLIVARES,J A,FLESCH,G D AND SVEC,H J

STUDIES IN NH3 CIMS 809
RUDEWICZ,P AND *MUNSON,B

FPA — **FAB; SIMS**

CHARACTERIZATION OF GLYCOSPHINGOLIPIDS BY FABMS 811
*HEMLING,M E,YU,R K,SEDGWICK,R D AND RINEHART,K L

FAST ATOM BOMBARDMENT MASS SPECTROMETRY OF PROTECTED OLIGONUCLEOTIDES 813
*HINDENLANG,D M,SEDGWICK,R D,AARON,C S AND UNGER,P D

FAST ATOM BOMBARDMENT AND COLLISIONAL ACTIVATION MASS SPECTROMETRY AS PROBES TO IDENTIFY ISOMERIC CARCINOGEN-NUCLEIC ACID ADDUCTS 815
*TONDEUR,Y,MOSCHEL,R C AND DIPPLE,A

POSITIVE ION FABMS OF 2-5A TRIMER CORE AND ITS MONOPHOSPHATE 817
*SLOWIKOWSKI,D L,SCHRAM,K H,TORRENCE,P F AND IMAI,J

TYPE IDENTIFICATION OF INDUSTRIAL SURFACTANTS BY FAB 819
*CHANG,T T AND LAY,J O

PHOTODISSOCIATION OF IONS GENERATED BY SOFT IONIZATION TECHNIQUES 820
*WELCH,M J,HERTZ,H S,SAMS,R L AND WHITE,E

A GENERAL NEW SURFACE ANALYSIS TOOL USING SEPARATE SURFACE PROBE AND IONIZATION BEAMS 822
BECKER,C H,*GILLEN,K T AND BUTTRILL,S E

IN BEAM IONIZATION BY ALKALI ION ATTACHMENT 824
REDEKER,G S,*GIESSMANN,U AND ROLLGEN,F W

ORGANIC-ALKALI SURFACE IONIZATION SOURCE 826
*YOUNG,S E,BUTTRILL,S E AND OGIER,W

FAST ATOM BOMBARDMENT STUDIES OF MOLTEN SALTS 828
*TSARBOPOULOS,A,RHINEBARGER,R,ACKERMANN,B,WATSON,J T,POPOV,A I AND ALLISON,J

DETERMINATION OF BETAINES BY FAST ATOM BOMDARDMENT MASS SPECTROMETRY 830
*JAMIESON,G C,MYERS,A C,FITCH,W L AND RHODES,D

COMPARISON OF FAB,FAB AND MS/MS,AND LASER DESORPTION FTMS FOR DETERMINATION OF PHOSPHONIUM SALTS 832
*MCCRERY,D A AND PEAKE,D A

TRENDS IN SECONDARY ION EMISSION FROM QUATERNARY SALTS 833
KIDWELL,D A,ROSS,M M AND *COLTON,R J

NEW DEVELOPMENTS IN HIGH RESOLUTION FAB IONIZATION MASS SPECTROMETRY 835
*COOK,J C

Au- ION GUN FOR LIQUID SIMS 836
*MCEWEN,C N,HARVAN,D J AND HASS,J R

IMAGING SECONDARY ION MASS SPECTROMETRY OF ORGANIC COMPOUNDS 838
STOLL,R,*HARVAN,D J,COLE,R AND HASS,J R

DIRECT COMPARISON OF SIMS AND LDMS ON BIOMOLECULES IN A MOVING BELT LC-MS SYSTEM 840
*FAN,T P,HARDIN,E D AND VESTAL,M L

EFFECTS OF CS+ PRIMARY ENERGY AND INTENSITY ON LIQUID SIMS SPECTRA 842
*MORITA,Y,ABERTH,W AND BURLINGAME,A L

DETERMINATION OF THE CHARACTERISTICS OF A FABRICATED FAB GUN 844
*MITCHUM,R K,FREEMAN,J P AND DUHART,B I

A NEW METHOD FOR THE PREPARATION OF THIN FILMS FOR PARTICLE-INDUCED DESORPTION STUDIES 845
*MANCILL,V K,MACFARLANE,R D,MCNEAL,C J AND SHELTON,D B

ON-LINE ACCURATE MASS MEASUREMENT IN FABMS 847
GILLIAM,J M,LANDIS,P W AND *OCCOLOWITZ,J L

DETERMINATION OF ENZYME KINETIC CONSTANTS USING FAB 848
*CAPRIOLI,R M AND SMITH,L

DETERMINATION OF METAL-LIGAND BINDING CONSTANTS IN SOLUTION BY FAST ATOM BOMDARDMENT MASS SPECTROMETRY 849
*SEIFERT,W E,FAN,T-Y AND CAPRIOLI,R M

MOLECULAR MICROPROBE 850
*KELNER,L,FALES,H M AND MARKEY,S P

CS+ ION DESORPTION IONIZATION USING FOURIER TRANSFORM MASS SPECTROMETRY 852
*CASTRO,M E AND RUSSELL,D H

ANALYSIS OF NONVOLATILE COMPOUNDS USING AN ALKALI THERMIONIC EMITTER 854
BOMBICK,D

MS/MS ANALYSIS OF NON VOLATILE COMPOUNDS 856
*BEAUGRAND,C,DEVANT,G AND ROLANDO,C

MOLECULAR COMPUTER GRAPHICS: A PICTURE IS WORTH 4000 BYTES

Paul Sigler
Department of Biology
University of Chicago

Chemistry is graphic, biochemistry is even more so. No matter how numerical and analytical our justifications, our intuition and concepts are based on models - more specifically visual images. Tangible physical models are slow to build, especially without errors; once built, they are even harder to correct, especially if they are very large and complicated. They are limited to displaying the distribution of matter (rather than, say, charge or magnetic field strength), and they are invariably static. As they are opaque, the outside obscures the inside. Physical models are cumbersome to store, degrade badly with time, and must be tediously measured to yield numerical values. They are not even that cheap. All these deficiencies are overcome with computer graphics. With the increasing use of dedicated microprocessors and improving raster technologies, the hardware value is steadily improving.

The real gain from computer graphics, however, will not be quantitative but qualitative. Graphics is an interface which links the computer to the mind. We know a fair bit about computers but relatively little about the mind. Although the linguists and psychologists are hard at it, we have much to learn and hence much to explore in conveying numerical information to the scientist in its most intellectually stimulating manner. In this respect, computer graphics is heuristic. As we learn to improve the mode of information transfer there will be enormous parallel improvements in processing speed. Coupled together, computer graphics should help to create a qualitatively new intuition in our understanding of chemistry and indeed the natural sciences.

A COMPARISON OF DIRECT LIQUID INTRODUCTION AND THERMOSPRAY HPLC/MS FOR THE ANALYSIS OF PESTICIDES.

Robert D. Voyksner, Joan T. Bursey, Edo D. Pellizzari, Analytical and Chemical Sciences, Research Triangle Institute, Research Triangle Park, NC 27709.

Analytical procedures applicable to the analysis of a variety of pesticides are limited by the thermal lability of these compounds and the sensitivity which can be attained by spectrophotometric methods. The combination of liquid chromatography with mass spectrometry can provide the sensitivity and specificity required to analyze these compounds successfully in environmental media. Two techniques for the interfacing of HPLC with MS have been explored for the analysis of pesticides, namely, direct liquid introduction and thermospray. Both techniques have advantages: thermospray HPLC/MS showed only molecular ion information with detection limits in the ng range, while DLI exhibited more structural information with higher detection limits.

Thermospray HPLC/MS is a relatively new technique for interfacing HPLC to a mass spectrometer. The interface, developed by Dr. Marvin Vestal and marketed by Finnigan Corp., accepts the 1.5-2 mL/min effluent of a standard HPLC column. A schematic diagram of the interface is shown in Figure 1. The interface does not require use of a filament for successful operation, although use of a filament is an option. The interface prefers operation with a polar solvent (water, methanol), and requires the use of a volatile buffer which can be added post-column if a buffer is not required for a chromatographic separation. In our experience, the interface has been simple to operate, rugged, and quite reliable, allowing the analysis of numerous compounds not amenable to other analytical techniques. The mass spectra obtained are very closely similar to the mass spectra obtained under ammonia chemical ionization conditions, yielding an $(M+1)^+$ species and $(M+NH_4)^+$ in most cases.

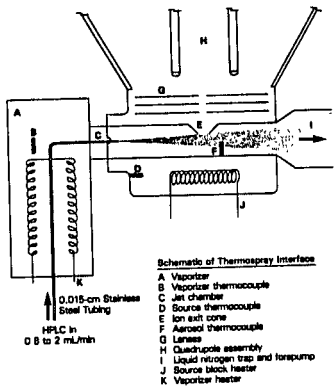

Figure 1. Schematic diagram of the interface

Various system operating parameters affect the sensitivity which can be obtained in thermospray HPLC/MS, among them the operating temperatures used in the vaporizer, aerosol, and jet, solvent composition, nature and concentration of buffer, and mode of detection. The appearance of the mass spectra obtained for the carbaryl by DLI (Figure 2) and thermospray (Figure 3) is quite similar, showing only an $(M+1)^+$ species and an adduct ion. For carbamate pesticides, DLI detection limits were observed to be in the high nanogram-low microgram range, using either positive or negative detection modes. Using the thermospray interface, detection limits for most of the same compounds fell in the low nanogram range using only positive ion detection because negative ion sensitivity was poor, with one detection limits as high as 70-100 ng (see Table 1). Acid pesticides were difficult for both interfaces to handle: DLI detection limits in the positive mode tended to be in the range of 50-75 μg, where the compound could be observed at all. Negative ion detection limits using DLI ranged from 5-60 micrograms injected. Thermospray detection limits, again using only positive ion detection, ranged from 0.3-12 micrograms injected. For oximes, DLI detection limits were in the low microgram range using either positive or negative ion detection. For thermospray, using positive ion detection, detection limits ranged from 70-100 ng. As others have noted, there is no one universal perfect HPLC/MS interface; DLI and thermospray produce comparable data in several areas, with one being superior to the other in certain applications. It would certainly appear that the most desirable option would be to have access to both interfaces and be able to use either according to its utility for a particular application.

This work was supported by EPA Contract No. 68-03-3122.

Class	Compound	Detection Limits DLI, Positive Ion[a]	Ion Monitored	TSP, Positive Ion	Ion Monitored
Carbamates	Carbaryl	0.04 µg	202	3-5 ng	219
	BPMC	0.02 µg	208	3-5 ng	225
	Propoxur	0.05 µg	210	4-8 ng	227
	Chlorpropham	1.0. µg	215	NA[b]	
	Carbofuran	0.05 µg	222	1-4 ng	239
	Phenmedipham	40.0 µg	301	5-8 ng	185
	Desmedipham	12 0 µg	301	70-100 ng	318
	Asulam	30.0 µg	231	20-25 ng	248
	Benomyl	0.5 µg	159	NA	
Acids	Dicamba	50 0 µg	221	300-400 ng	238
	Silvex	---[c]	---	1-3 µg	286
	Chloramben	---[c]	---	8-12 µg	223
	2,4,5-T	75 0 µg	250	800-1000 ng	255
	2,4-D	60.0 µg	216	200-300 ng	238
	Picloram	75.0 µg	241	3-5 µg	258
Oximes	Oxamyl	2.0 µg	220	70-90 ng	237
	Methomyl	1.0 µg	163	80-100 ng	180

[a]Amounts listed are quantities actually injected on-column; only about 1-3% actually enters the mass spectrometer

[b]Not analyzed by TSP HPLC/MS, compound is amenable to gas chromatography.

[c]Not observed in positive ion detection mode

Table 1
Detection Limits for Selected Pesticides Analyzed Using Positive Ion Detection with DLI and the TSP Interface

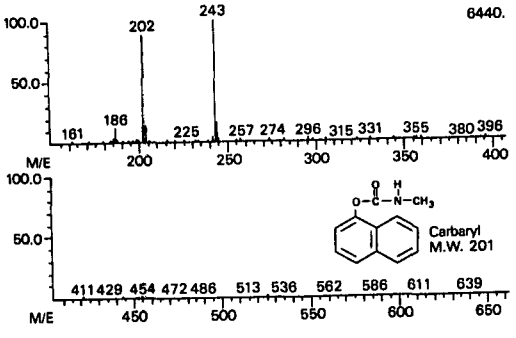

Figure 2
DLI HPLC/MS spectrum of carbaryl: $[M+1]^+$ and $[M+CH_3CNH]^+$

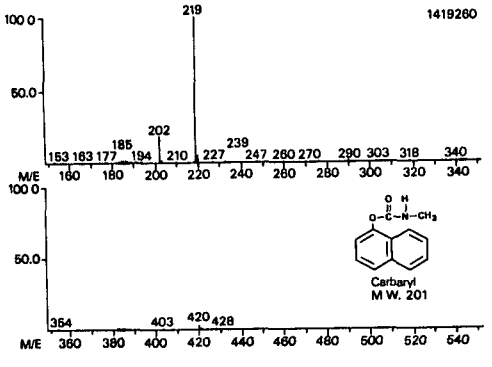

Figure 3
TSP HPLC/MS spectrum of carbaryl: $[M+1]^+$ and $[M+NH_4]^+$

COMPUTER CONTROLLED HIGH RESOLUTION EXTENDED RANGE MPM RETROFIT OF AEI MS-30 FOR PART-PER-TRILLION ANALYSIS OF CHLORODIBENZODIOXINS AND SIMILAR RESIDUES IN ENVIRONMENTAL SAMPLES.

J.G. Solch, D. Miller, J.H. Garrett, T.O. Tiernan and M.L. Taylor
Brehm Laboratory and Depts. of Chemistry and Pharmacology/Toxicology, Wright State University.
Dayton, Ohio 45435

The attainment of mass profile data under high resolution multiple peak monitoring conditions has often been regarded as the ultimate mass spectrometric technique for confirming the presence of certain highly toxic environmental contaminants. The determination of low part-per-trillion (ppt) levels of 2,3,7,8-TCDD has been typical of this type of analysis. Prior to the present work, high resolution peak profiling techniques for ppt level analysis of 2,3,7,8-TCDD on an AEI MS-30 mass spectrometer were reported by this group in 1976, 1979, and 1982. Analysis of ppt levels of TCDD with peak profile data for two mass/energy (m/z) ratios (1976), four m/z ratios (1979), and four m/z ratios under DS-55 data system control (1982) were accomplished using custom-fabricated circuitry and a Nicolet 1074 signal-averaging computer. These methods however, were limited to providing peak profile data for only one TCDD isomer for a given capillary GC/MS analysis.

The presence of multiple TCDD isomers in actual environmental samples has provided the impetus for obtaining mass profile data for all peaks obtained during a typical High Resolution Gas Chromatographic/High Resolution Mass Spectrometric (HRGC/HRMS) analysis. The current system, which will be described in this paper, utilizes a Kratos fast preprocessor equipped with a Nova-4C DS-55 data system, a Kratos MS25/MS80 ERMPM board, and a Kratos 18 bit Programmable Voltage Supply to control, obtain, store, and process mass profile data for all m/z ratios monitored during a HRGC/HRMS analysis. The major components of the system and their basic communication lines are illustrated in Figure 1. The DS-55 data system controls the AEI MS-30 mass spectrometer in the same manner as currently produced MS-25 and MS-80 mass spectrometers. The modifications to the MS-30 which were made in order to arrive at the present configuration were:

1. Installation of a new stand-alone fast preprocessor interface.
2. Modification of the ESA supply according to Kratos Multiple Peak Monitoring (MPM) system retrofit specifications.
3. Installation of the Kratos ERMPM board in the rewired MS-30 timer accessory slot.
4. Modification of the ERMPM board magnet reference to provide correct polarity and connection of this reference in place of the existing MS-30 battery reference.
5. Installation of narrow scan width select, narrow scan speed select, and ERMPM select switches to the MS-30 console.

In addition to the hardware modifications, a number of major changes were made to the Kratos High Resolution Processing Software. These changes included adding:

1. Peak Matching Routine. This routine uses up to two references masses (typically internal standards added to the sample or co-injected external standards) to correct the centroid obtained for the sample peaks by any mass shift that occurred previous to obtaining mass profile data. Since most high resolution mass spectrometers typically have 30-60 minute stabilities (on the order of 5-50 ppm), this routine is invaluable in capillary analysis to provide exact centroids.
2. Three and Five Point Smoothing Routines. These options can significantly improve signal-to-noise ratios in both GC Reports and Peak Profile Reports.
3. Display Enhancements. A number of display enhancements were added which include correcting a baseline zero problem in the GC Report, modifying the GC Report to show all monitored masses with full scale intensities equal to their actual intensities, rather than percentages of the total TIC, and incorporation of a vertical line indicating the theoretical centroid in the Peak Profile Report.

Figure 2 illustrates a typical GC Report obtained for an injection containing 100-400 picograms per isomer of 12 different TCDD isomers. Figure 3 shows a Peak Profile Report obtained at the 2,3,7,8-TCDD retention time for one of the four m/z ratios monitored during the analysis of a crayfish sample. The illustrated peak profile obtained by summing the peak profiles (scans 45-55) that bracket the 2,3,7,8-TCDD retention time and has not been processed by the Peak Matching routine. Figure 4 demonstrates the results obtained when the peak matching routine used the centroids obtained for the $^{13}C_{12}$-2,3,7,8-TCDD internal standard and the $^{37}Cl_4$-2,3,7,8-TCDD co-injected external standard to correct for mass drift. Analyses corrected in this manner typically exhibit centroids less than 5 ppm from the theoretical value.

In conclusion, we have demonstrated the successful retrofitting of a computer controlled HRGC/HRMS peak profile data collection system to an AEI MS-30. In addition, a number of modifications to the post-acquisition processing software have been implemented which signi-

ficantly improve the determination of accurate centroids for low picogram injections of environmental contaminants such as the isomers of TCDD.

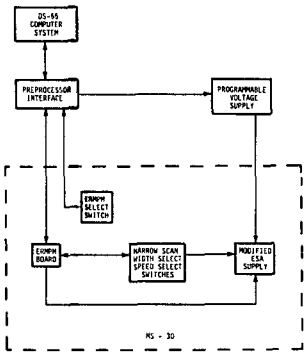

Figure 1

Block Diagram of Extended Range Multiple Peak Monitoring System MS-30

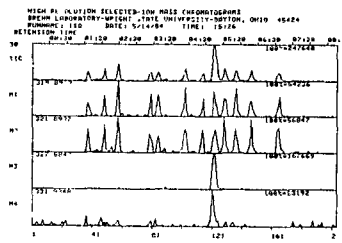

Figure 2

GC Report for 100-400 pg of 12 Separate TCDD Isomers

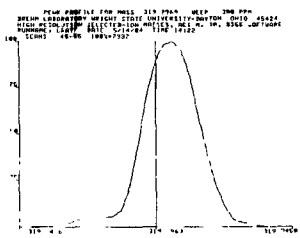

Figure 3

Peak Profile Report Obtained at m/z 319.89F for the Analysis of a Crayfish Sample without Peak Matching

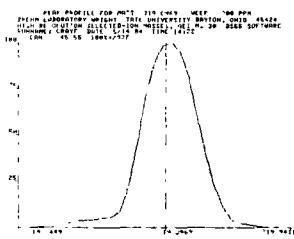

Figure 4

Peak Profile Report Obtained at m/z 319.89F for the Analysis of a Crayfish Sample with Peak Matching

MOBILE TANDEM MASS SPECTROMETRY: RECENT APPLICATIONS OF MS/MS ON WHEELS,

B. I. Shushan, J. E. Fulford, B. A. Thomson, S. D. Tanner, A. Ngo and W. R. Davidson, SCIEX®, 55 Glen Cameron Road, #202, Thornhill, Ontario, Canada, L3T 1P2.

The existence of hundreds of chemical waste dumpsites and the ominous potential for the accidental contamination of the environment by industrial chemicals has prompted the development of a mobile MS/MS system capable of rapid air, water and soil analysis. In emergency situations, analytical answers must be provided on-site and quickly in order to direct remedial action and protect nearby populated areas. Tandem mass spectrometry, as an analytical tool, shows great promise in fulfilling this need due to its proven sensitivity, selectivity and high productivity. Mounted in a mobile configuration, the MS/MS can readily be moved from site-to-site and monitor the ambient air for trace organic pollutants while in motion.

Air monitoring generally has the most severe time constraints since the transport of hazardous chemical vapors in the atmosphere can be rapid. The TAGA® 6000 MS/MS system is capable of direct air monitoring using either an atmospheric pressure chemical ionization source (APCI) or a Townsend/glow discharge CI source. The system, when coupled with air monitoring software, provides real-time qualitative and quantitative data. A typical procedure involves the acquisition of a background subtracted single MS spectrum. The computer then determines which parent ions are "significant" relative to background and directs the system to acquire daughter ion spectra for each of the significant parents. As the spectra are obtained, they are compared to library spectra and the final spectrum is output along with the library search results. Once the parent ions (and thus the chemicals in the air) have been identified, quantitation of the detected chemicals in the areas surrounding the site can take place. Selected parent ions and daughter ions for the determined contaminants are monitored as the mobile laboratory proceeds along a set path. The concentrations of the chemicals are output in real-time to establish concentrating "hot-spots" and highlight the exact source of the vapors. Remedial or emergency action may be required based on the identity of the chemical and its concentration.

To provide the best quantitative data requires that calibration curves are obtained on a routine basis for selected chemicals representative of various chemical classes. Obviously a mobile laboratory is somewhat limited in the amount of ancillary calibration equipment it can carry. One method of calibration which has proven to be of general use is the headspace vapor injection method. In this method, a small amount of liquid is added to the barrel of a gas-tight syringe. The vapors readily equilibrate and are injected into the incoming air stream at various flowrates which relate to various concentrations. The accuracy of the procedure is limited mainly by the accuracy of vapour pressure data and is generally about 10%. The only inventory of chemicals kept on board the mobile system are small vials of standards, as opposed to gas cylinders or permeation devices.

The air monitoring methods described above have been successfully evaluated by the EPA. The evaluation program pointed out two difficulties in direct air sampling MS/MS: the fragmentation of some halohydrocarbons in the source can lead to non-specific parent ions, and some isomers cannot be separated without chromatography. Rapid sample collection followed by "flash" chromatography can alleviate both these limitations.

The major non-air monitoring application of the TAGA® 6000 mobile system has been in the area of soil analysis for chlorinated dibenzodioxins and furans with particular emphasis on TCDD. Since the "regulatory" level for dioxin in Missouri soil was set at 1 ppb, it became apparent that the low detection limit capability of tandem mass spectrometry could be used to simplify sample workup. For example, if 5 grams of soil were extracted with 5 ml of a specific extraction solvent, and the extract were directly analyzed, then 1 ppb corresponds to 1 pg of TCDD in 1-ul injection. In order to ascertain whether such an approach was feasible, several soil samples provided by the EPA were analyzed. The sample workup consisted of adding a sodium sulfate drying agent to the soil along with 5 ml of the extraction solvent. The mixture was shaken for a few minutes and centrifuged. A 1.5-ul aliquot of the extract was injected into the GC/MS/MS following filtering. The total sample workup stage took approximately 8-10 minutes and the elution time for 2,3,7,8-TCDD was approximately four minutes in this procedure. The agreement between GC/MS/MS analysis and the much more time consuming EPA method is extremely good. Based on this work, a further evaluation has taken place on-site using a mobile TAGA® 6000 MS/MS system. One hundred and fifty samples were analyzed at a rate of 25-30 per day

(turnaround time is 15 minutes). Reproducibility was within 6% for a 10 ppb standard and 12% for a 5 ppb soil sample over the two week site evaluation program. Slight modifications to the clean-up procedure are necessary if the soil is highly contaminated with other organics or if lower detection limits are required. A more extensive GC separation is necessary if isomer specificity is required.

The GC/MS/MS and LC/MS/MS techniques developed for water and soil analysis in the stationary lab are slowly being added to the mobile system as the need arises. It is anticipated that within the next few years most of the analytical requirements for hazardous waste sites will be met by mobile tandem mass spectrometry.

Acknowledgement

The authors thank Weston Engineering, TRC Advanced Analytics, EPA-ERT (Edison) and EPA-EMSL (RTP) for their support.

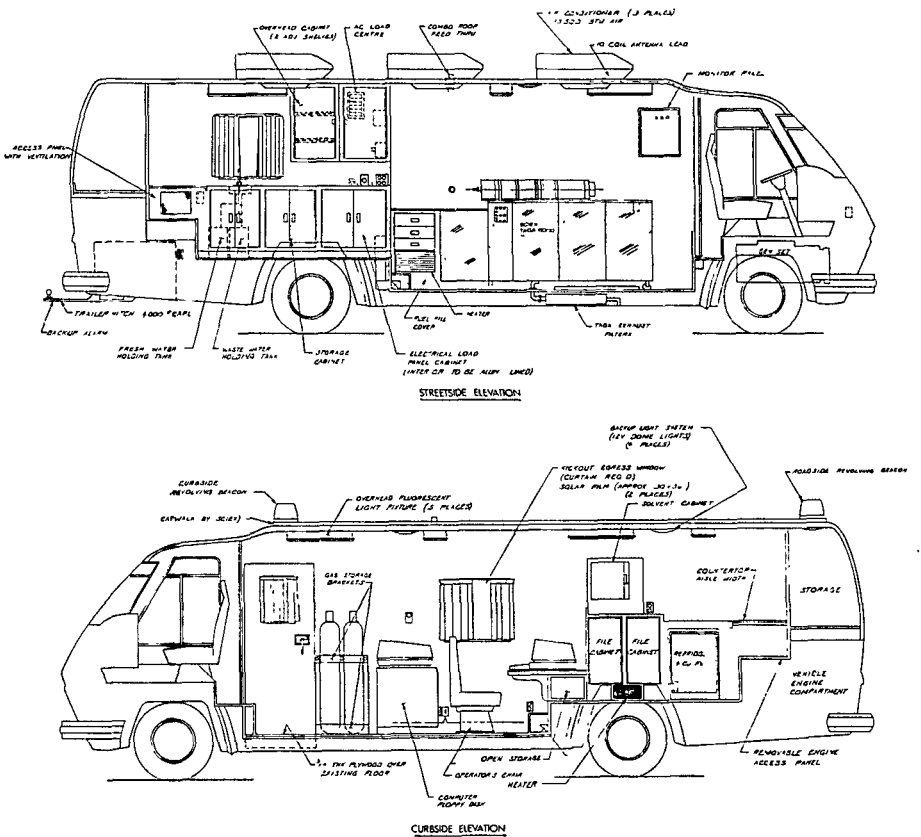

A TYPICAL MOBILE LABORATORY LAYOUT.

IDENTIFICATION OF POLYCHLORINATED DIBENZOFURANS AND OTHER CHLORINATED PYROLYSIS PRODUCTS FORMED IN ACCIDENTAL PCB FIRES

C. Herndon Williams, Jr., Larry D. Garretson, and Pamela B. Stewart, Radian Corporation, 8501 MoPac Blvd., Austin, Texas 78759

The pyrolysis of PCB-contaminated transformer oils in electrical fires is found to form a complex mixture of chlorinated combustion products, including the acutely toxic polychlorinated dibenzofurans (PCDFs), with degrees of chlorination from Cl_1 to Cl_6. In the same samples, only very low or nondetectable levels of the polychlorinated dibenzo-p-dioxins (PCDDs) were found. Other chlorinated species found in even greater abundance than the PCDFs include the polychlorinated biphenylenes (Cl_2 to Cl_6) and polynuclear aromatics (PNAs), such as the polychlorinated pyrenes (Cl_1 to Cl_5), as well as high levels of residual PCBs. Unchlorinated PNAs from anthracene to the benzopyrenes were also detected at levels comparable to the residual PCBs.

Bulk soot and surface wipe samples were collected at the sites of several PCB fires by NIOSH to assess exposure hazards associated with the pyrolysis products. The samples were Soxhlet extracted and analyzed without cleanup in order to characterize the complete sample matrix. Samples were screened by HRGC-MS in the scanning mode, with chromatography performed on a 50 m neutral bonded phase capillary column. Characteristic ions and retention time windows were selected to allow the measurement of all PCDF or PCDD congeners from Cl_1 to Cl_8 substitution in a single analysis. Isomer-specific confirmation of the identities of the 2,3,7,8- and other tetrachloro PCDFs was accomplished by HRGC-MS in the selected ion monitoring (SIM) mode on a 60 m Supelco 2340 capillary column. A detection limit of ~1 ng/sample was achieved. QC procedures made extensive use of labeled internal standards: ^{13}C-2,3,7,8-TCDF, ^{13}C-2,3,7,8-TCDD, ^{13}C-OCDD, d_6-3,4,3',4'-TCBP, d_{10}-anthracene and d_{12}-chrysene.

Up to 26 of the 38 possible isomers of the TCDFs were detected in some soot and wipe samples with the 2,3,7,8-TCDF isomer one of the largest peaks, as seen in Figure 1. The tetrachloro isomer group of the PCDFs was the largest, in concentration up to μg/g in soot and μg/filter in wipes. The other chlorinated pyrolysis products were present at concentrations from 2-20 times that of the PCDFs detected.

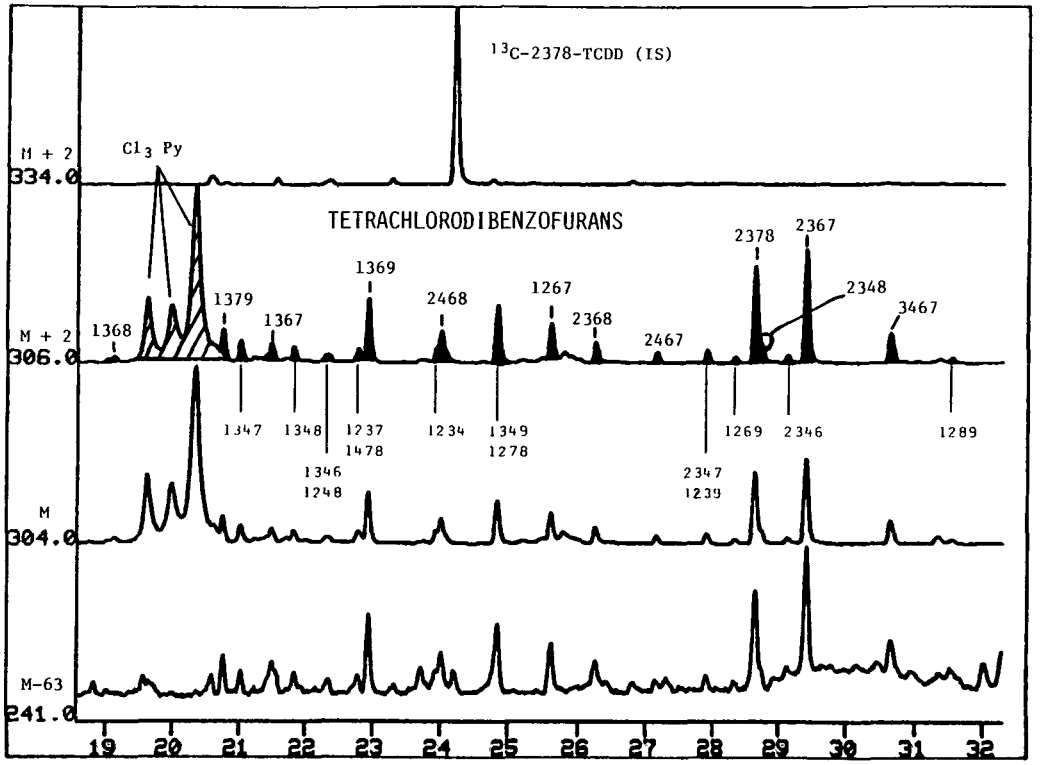

Figure 1. HRGC-MS Chromatogram of Bulk Soot Samples Analyzed for the TCDFs.

GC/MS CHARACTERIZATION OF PCDD RESIDUES IN FRESHWATER FISH EXPOSED TO MUNICIPAL INCINERATOR FLY ASH

D. W. Kuehl, B. C. Butterworth and D. Linn
U.S. Environmental Protection Agency
Environmental Research Laboratory-Duluth, Duluth, MN 55804

Since the discovery that municipal incinerator flyash can contain high levels of PCDDS, the U.S. EPA has been concerned with the potential for their release into the environment. As a result, EPA initiated research with Dow Chemical Company to investigate the potential for PCDDS and PCDFS from municipal incinerator flyash to be bioavailable to freshwater fish. Research efforts at ERL-D included both the bioassay work as well as the development of methodology to analyze small bioassay samples for 1 ppt levels of TCDD and TCDF isomers. Our analyses are based upon a Finnigan-Mat 4500 GM/MS, which has been modified to put 5000 V on the conversion dynode to enhance the signal, operated in the MIS mode; our cleanup procedures are based upon the use of Amaco PX-21 carbon (courtesy of Dr. David Stalling, U.S. FWS) coated on silica gel to isolate planar molecules.

Two flyash samples were collected, one from an incinerator in the Midwest, the other a composite of flyash from five East Coast incinerators. Isomer-specific analysis of the flyash (Dow Chemical Co.) showed that 2378-TCDD comprised only 2% of the total tetra isomers, and was at a level of 160 and 2000 pg/g respectively. Further analysis showed that these flyash contained other polychlorinated compounds such as dibenzofurans, napthalenes, biphenyls and benzenes.

A static bioassay was designed for dosing flyash into 40L aquaria with renewal every other day. Carp were used as the test species. Initial bioassays were done using the East Coast flyash at levels of 2 and 10g doses for 15 and 30 days, and at 250 mg for 90 days. No 2378-TCDD was found above a 1 ppt detection limit in either control or exposure fish. To ensure that 2378-TCDD would be accumulated by the carp under these bioassay conditions, benzene soxhlet extracts of 1 and 5g of East Coast flyash were similarly dosed into bioassay aquaria for a 30-day exposure. Levels of 200 and 1000 pg/g respectively were found in these fish. More interestingly however, only one TCDD isomer was found, 2378. These fish were also analyzed for TCDF isomers; however, none of the samples showed any detectable levels.

An analogous 30-day static bioassay was then conducted using the Midwest flyash. Doses of 2, 5 and 10g were used and resulted in levels of 2378-TCDD in the fish of 20,20; 28,28; and 32,34 pg/g respectively for field duplicates. The control fish were found to be ND (1 pg/g). Again only one isomer was found as a residue. TCDF analysis showed three isomers at 10, 28 and 32 pg/g levels respectively for the major isomer, with no detectable levels in the control.

It appears that TCDD an TCDF may accumulate as a residue in fish that have been exposed to municipal incinerator flyash. Further studies will be done to develop a model to predict when a potential for accumulation occurs.

DETECTION/IDENTIFICATION OF VOLATILE ORGANIC PHOSPHONATES AND PHOSPHATES BY SIMS*

Gary S. Groenewold and Peter J. Todd
Analytical Chemistry Division
Oak Ridge National Laboratory, Oak Ridge, TN 37831

The detection and identification of organophosphonate and organophosphate compounds in the environment is important because many chemical warfare agents and insecticides belong to these classes of compounds. These compounds are unusually biologically active at low concentrations and are generally present as components of complex mixtures. Therefore, sensitive and selective techniques are required for their analyses. A fast analysis is another requirement for the detection of chemical warfare agents because they hydrolyze rapidly. Positive[1] and negative[2] chemical ionization have been successfully used for the detection of picogram levels of phosphate and phosphonate compounds, but these ionization techniques lack specificity and, therefore, are usually used in tandem with the slower technique of gas chromatography.

The goal of this investigation was to find a selective ionization method that is as sensitive as the chemical ionization methods that are referenced above. A selective ionization allows for the elimination of the time-consuming separation presently required before analysis by using mass spectrometry. Molecular secondary ion mass spectrometry (SIMS) and fast atom bombardment mass spectrometry (FABMS) are techniques that have potential for selectivity because the abundances of secondary, analyte ions that are emitted from the bombarded matrix vary dramatically depending on the structure and physical interaction between analyte and matrix.

Dimethylmethylphosphonate (DMMP), diisopropylmethylphosphonate (DIMP) and trimethylphosphate (TMP) were chosen as analytes because they have structural features which are similar to those of chemical warfare agents and because they are not lethal. The three analytes were analyzed as five percent solutions in three matrices (glycerol, concentrated sulfuric acid and polyphosphoric acid) in order to identify the best matrix for the analysis. The solutions were inserted into the mass spectrometer via direct probe and then bombarded by using a 5 keV, 5 $\mu A/cm^2$ Ar^+ beam. The secondary ions that were emitted were analyzed by using a tandem mass spectrometer.

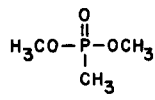

DMMP

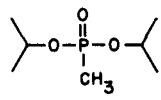

DIMP

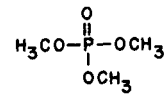

TMP

Abundant DMMP and TMP secondary ions were observed by using polyphosphoric acid (PPA) or concentrated sulfuric acid as a matrix, but not by using glycerol. In contrast, more abundant DIMP secondary ions were observed from glycerol than from sulfuric acid or PPA. Abundant low mass ions were recorded in the DIMP/acid matrix experiments, which may signal condensed phase hydrolysis reactions. PPA was chosen as the best matrix for the analyses based on these data. PPA also has a low background pressure in the mass spectrometer and a low mass spectral background.

An ideal mass spectrometry ionization method has the capability of ionizing the phosphonates and phosphates as they are sampled, i.e., as vapors. There is no a priori reason why SIMS or FABMS could not be used to detect vapor-phase analytes, although these techniques have traditionally been used for the analysis of involatile compounds. In fact, gaseous oxygen is known to influence analyte abundances in static SIMS experiments;[3] therefore, vapor-phase analyte-matrix interaction is a reasonable expectation in molecular SIMS experiments.

*Research sponsored by the U. S. Department of Energy, Office of Basic Energy Sciences, under Contract DE-AC05-84OR21400 with Martin Marietta Energy Systems, Inc., and by the U. S. Department of Energy Postgraduate Research Training Programs administered by Oak Ridge Associated Universities.

By acceptance of this article, the publisher or r cknowledges the U S Gov right to retain a nonexclusive, royalty free license in and to any copyright covering the article

The mass spectrometer was fitted with an all glass heated inlet system in order to analyze vapors by using SIMS. Controlled amounts of analyte were vaporized in the inlet system and subsequently admitted via molecular leak to the source, where PPA was being bombarded by the Ar^+ primary beam. When DMMP was admitted to the source, abundant ions corresponding to DMMP + H^+, loss of CH_3OH and loss of CH_3OCH_3 were immediately observed. The abundance of the DMMP + H^+ ion increased to approximately 50% of its final value after only a few seconds following injection. A slower abundance increase continued over the next two minutes, which may be a consequence of vapor equilibration in the inlet system or of DMMP build-up in the PPA matrix. An analogous decay of DMMP + H^+ abundance was observed when the DMMP was evacuated from the inlet system.

The limit of detection for DMMP was estimated by calculating the rate of DMMP entering the SIMS source and by measuring the S/N ratio obtained from a single DMMP + H^+ (m/z 125) profile acquired at that inlet rate. The rate was calculated by multiplying the amount of DMMP injected into the inlet system by the leak rate constant. The leak rate constant was estimated by monitoring the pressure (baratron) decrease with time. A limit of detection of 10 to 20 pg is estimated by using this method. Furthermore, DMMP + H^+ ion abundance is a linear function of the amount of DMMP injected over two orders of magnitude, i.e., the sensitivity plot is linear. Therefore, quantitative mass spectrometry should be possible by using this ionization technique.

TMP vapor can also be analyzed with high sensitivity by using SIMS. Abundant, secondary ions corresponding to TMP + H^+ and loss of CH_3OH are observed when TMP is admitted to the SIMS source. The limit of detection and the sensitivity plot for TMP are very similar to the analogous DMMP data.

DIMP is not detected as sensitively by using SIMS as are DMMP and TMP. This result may be due to lower analyte solubility in the PPA matrix. Alternatively, the lower sensitivity may be attributable to facile fragmentation and/or hydrolysis reactions, which yield an abundant ion at m/z 97. This ion corresponds to the loss of $2C_3H_6$ from DIMP + H^+, and it was used for the limit of detection determination and the sensitivity plots (rather than DIMP + H^+) because of its greater abundancce. The limit of detection for DIMP (200-300 pg) was approximately 20 times higher than for DMMP and TMP. Similarly, the slope of the sensitivity plot for DIMP was less than one tenth that of DMMP and TMP.

A series of compounds with similar molecular weights and a variety of functional groups were analyzed as vapors by using SIMS with a PPA matrix; this was done to identify other classes of compounds that would be ionized and would therefore interfere with the analysis of the organophosphorous compounds. The vapors of benzyl alcohol, anisole, benzaldehyde, acetone, 10-crown-2, chlorobenzene, toluene, n-nitrotoluene and benzonitrile were not detected and presumably were not ionized. Low abundance protonated molecular ions were observed when acetophenone was admitted to the mass spectrometer. Abundant protonated molecular ions were observed from both benzyl amine and phenylpropyl amine vapors. Phenylpropyl amine was detected with only slightly less sensitivity than was DIMP.

It appears that the ionization of vapor phase organophosphorous compounds by using SIMS with a PPA matrix imparts considerable selectivity to the analysis. Amines are the only major class of compounds that are known to have the potential to interfere with this analysis. For certain analytes, the sensitivity achieved by using this ionization technique is as good as that achieved by using chemical ionization.[1]

References

1. Sass, S.; Fisher, T. L. Org. Mass Spectrom. 1979, 14, 257-264.

2. Busch, K. L.; Bursey, M. M.; Hass, J. R.: Sovocool, G. W. Appl. Spectros. 1978, 32, 388-399.

3. Kloppel, K. D.; Seidel, W. Int. J. Mass Spectrom. Ion Phys. 1979, 31, 151-160.

DETERMINATION OF ALDICARB, ALDICARB NITRILE, AND ALDICARB OXIME IN WATER BY GC/MS

M.L. Trehy, R.A. Yost, Department of Chemistry, J.J. McCreary, Department of Environmental Engineering Science, University of Florida, Gainesville, FL 32611

Aldicarb is a carbamate pesticide manufactured by Union Carbide and sold under the trademark Temik. Analysis for aldicarb and its degradation by-products is of concern since aldicarb has been detected in groundwaters in agricultural areas (1). This report describes a GC/MS method to selectively detect aldicarb, I; aldicarb nitrile, II; and aldicarb oxime, III.

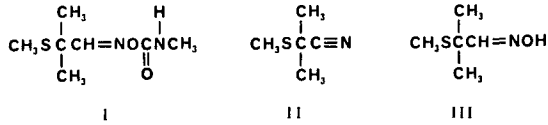

I II III

Aldicarb is thermally labile and rapidly degrades to form aldicarb nitrile in the injection port or on the column in all GC methods previously reported (2,3). A major drawback to the use of GC methods for the analysis of aldicarb is that aldicarb not only degrades during the GC analysis to aldicarb nitrile, but may also chemically degrade to aldicarb nitrile in the environment. The intact aldicarb molecule is detected quantitatively if a 3 m DB5 capillary column is used in place of the standard length columns and cooler injection port and column temperatures are maintained. This results in several major improvements. The presence of aldicarb can unequivocally be determined without derivitization and prior florisil clean up. Aldicarb oxime and aldicarb nitrile can be selectively detected in the presence of aldicarb using a 9 m DB5 capillary column. Using this technique the detection limits for aldicarb, aldicarb nitrile, and aldicarb oxime are 0.3 ng, 0.15 ng, and 1.2 ng, respectively. A representative chromatographic separation using the 3 m DB5 capillary column is shown in Figure 1.

The fate of aldicarb in anaerobic groundwaters was studied with this technique. Aldicarb is found to slowly degrade to aldicarb oxime in sterile anaerobic groundwater at pH 8.2; in the presence of a high concentration of microorganisms, however, aldicarb rapidly degrades to aldicarb nitrile. Aldicarb was spiked into sterile anaerobic well water and stored in septum bottles. At two week intervals samples were extracted with methylene chloride and analyzed using the 3 m DB5 capillary column. As the aldicarb concentration decreased the concentration of aldicarb oxime was observed to rise stoichiometrically as can be seen in Figure 2. The half-life for aldicarb at pH 8.2 due to hydrolysis is 43 days. In another set of spiked anaerobic samples at pH 7, ground limestone was added. In these samples, little degradation was observed after one day but conversion of aldicarb to aldicarb nitrile was nearly complete after 13 days.

The temperature dependence of the intramolecular degradation of aldicarb in the ion source and its unimolecular decomposition was investigated using CI/MS and CI/MS/MS, respectively. The M+1 protonated molecular ion formed in methane CI undergoes a unimolecular decomposition. The rate of decomposition of the M+1 ion is dependent on the source temperature when the pressure is extrapolated to zero. Previous attempts to determine the energy of activation for unimolecular dissociations has relied on the evaluation of CI/MS, in which several reactions are occuring concurrently (4). In our experiments using the MS/MS capabilities of the Finnigan TSQ mass spectrometer, we can determine the effective collision diameter for the CID process from the slope of the plot shown in Figure 3 and the temperature dependence of the unimolecular rate constant from the intercept at zero pressure. The energy of activation for the unimolecular dissociation is calculated to be 2 kcal and the effective collision diameter is 9 and 11 angstroms at 120°C and 160°C, respectively.

The use of GC/MS with short capillary columns has been shown to permit analysis for thermally labile pesticides and offers the advantage of confirmation of identity

and rapid analysis. Up to six samples per hour can be analyzed for aldicarb by this technique. Further, the possibility of misidentification is greatly reduced.

1. Guerrera, A.A; J. Am. Water Works Assoc. 1981, 73(4), 190-199.

2. Metcalf, R.L.; Fukuto, T.R.; Collins, C.; Borch, K.; Burk, J.; Reynolds, H.T.; Osman; M.F. J. Agric. Food Chem., 1966, 14(6), 579-584.

3. Muszkat, L.; Aharonson, Nadav; J. Chromatogr. Sci., 1983, 21, 411-414.

4. Meot-Ner, M.; F.H. Field; J. Amer. Chem. Soc., 1973, 95, 7207-7211.

FIGURE 1

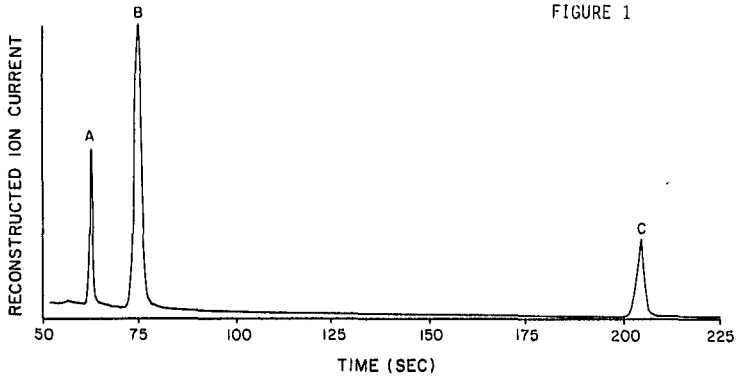

FIGURE 2

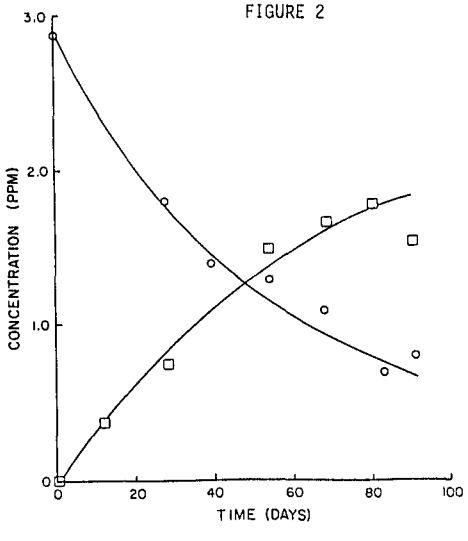

FIGURE 3

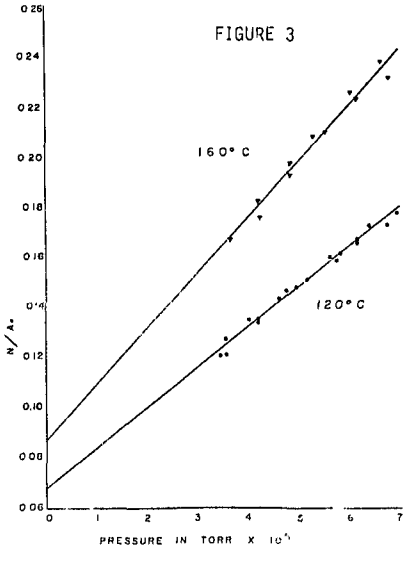

SCREENING METHODS FOR ORGANOPHOSPHORUS PESTICIDES USING TRIPLE QUADRUPOLE MASS SPECTROMETRY.

Mark R. Bauer and C G. Enke;
Department of Chemistry
Michigan State University
East Lansing, Mich. 48824

There is an increasing need for simple and direct detection and identification of trace organophosphorus pesticides in complex environmental matrices. Current detection methods normally require multiple extractions and long chromatographic separation times. The methods described here use characteristic low energy CAD fragmention pathways of organophosphorus compounds to quickly screen samples for pesticides, their metabolites and decomposition products.

The ionization method used can be crucial to the success of mixture analysis with MS/MS. The sensitivity of the analysis is optimized by maximizing the intensity of the molecular ion peak, because the intensity of the daughter ion spectrum is then maximized. Selectivity is increased by creating only molecular ions in the source because this eliminates the possible confusion between fragments formed in the source and molecular ions of the same mass. Electron impact ionization and positive chemical ionization using methane, isobutane, ammonia, methanol and water as reagent gases were used to determine which technique was best able to ionize organophosphorus pesticides for use in MS/MS analysis. The EI spectrum showed no molecular ion peak and numerous fragmentation peaks The isobutane and water spectra contained (M+H)+ base peaks but they also had several other peaks due to fragmet ions. Using ammonia as the CI reagent gas yielded a much lower total ion current as well as both (M+H)+ and (M+NH3)+ ion peaks. Methanol chemical ionization was the only method that gave only (M+H)+ ions and no fragment ions (figure 1). Methanol can hydrogen bond and therefore, at high source pressures, forms protonated clusters which serve as very gentle proton transfer agents.

An examination of the CAD spectra of the (M+H)+ ions of the organophosphorus pesticides revealed several ions and fragmentation mechanisms indicative of the parent compounds, (figure 2) These generally confirm the fragmentation mechanisms infered from EI spectra When the fragment that contains the phosphorus retains the charge, the presence of the phosphate moiety can be detected by using parent ion scans Because the Z moiety is a good leaving group and often contains easily ionized heteroatoms, the CAD spectra of many of the pesticides are dominated by peaks due to the Z group These compounds can be detected using neutral loss scans for the neutral phosphate leaving group. A sequence of eleven different neutral loss and parent scans (figure 3), can be used to detect the presence of over 50 organophosphorus pesticides and other related compounds The TQMS control system can be programed to perform this sequence once or repetivly for general screening analyses Daughter spectra of previously unidentified (M+H)+ masses can be used to provide mass spectral data on these compounds

The method has been used to detect pesticides at the <10 ng level in complex mixtures and to screen for pesticides on fruit and vegetables. Malathion and Azinphos were detected on an apple which had been sprayed with the pesticides The sample was inserted into the mass spectrometer by placing a small piece of the spiked apple on the end of the direct insertion probe which was then heated while the control system automaticaly ran the pesticide screening sequence, (figure 4) The compound specific parent/daughter pairs exploited in this technique, such as 331+ - 127+ for malathion, can also be used for targeted analysis by monitoring specific parent/daughter pairs continiously or sequentially This is called single or multiple reaction monitoring (SRM or MRM) Reaction monitoring limits the the number of compounds that can be detected at one time, but it also lowers detection limits correspondingly

These methods illustrate how MS/MS can, with appropriate ionization and compound class characterization easily detect organophosphorus pesticides and related compounds in complex matrices with no sample work-up

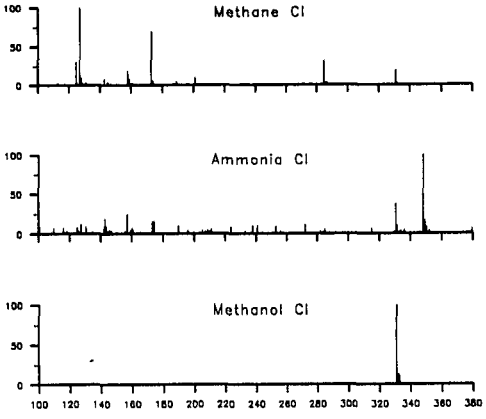

Mass Spectra of Malathion

FIGURE 1

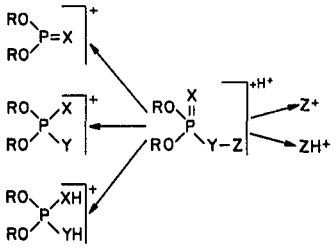

FIGURE 2

SCREENING SCANS

Neutral Loss		**Parent Ion**	
mass selected	# compounds detected	mass selected	# compounds detected
137	2	109	2
142	4	125	8
152	2	127	8
158	3	153	3
170	4	155	2
186	6		

FIGURE 3

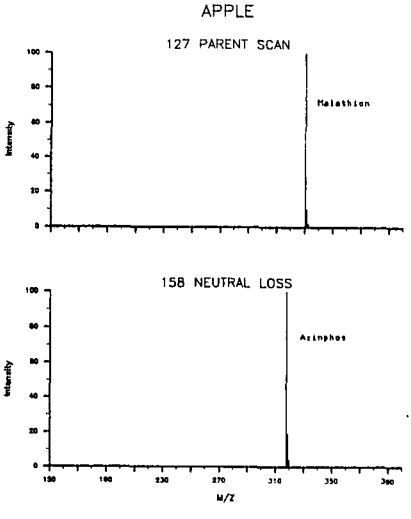

FIGURE 4

This work was supported in part by the Office of Naval Reasearch.

MOB 3 STUDIES ON ENERGY PARTITIONING ON PHOTODISSOCIATION OF POLYATOMIC SYSTEMS

R.E. Krailler

Department of Chemistry
Texas A&M University
College Station, Texas 77843

The 1,3-butadiene system has been extensively studied using a variety of mass spectrometric methods. In a recent paper Farrar has suggested non-statistical dissociation for this system. This disagrees with the results of Baer[2], Bowers[3], and Gross.[4] Farrar reports kinetic energy release values which are not consistent with a statistical model. On the other hand, the PIPECO measurements reported by Baer are consistent with statistical theory. With this controversy in mind, we set out to systematically study various butadiene chromophores and more importantly, to evaluate the utility of kinetic energy release (KER) data for probing dissociation dynamics and/or ion structure.

In terms of dynamics, we are interested in determining the influence of excess internal energy on energy partitioning into translational modes. For an ion population with a fixed internal energy distribution, we can systematically increase the total energy of the dissociating ion by increasing the photon energy. The dependence of KER on varying the internal energy is described by the equation Tav=Te+T*. Thus, as we increase Eint the increase observed for Tav can be attributed to an increase in T*. We assume, based on our understanding of dissociation dynamics, a linear T* vs. Eint relationship.

Although most systems which we have examined show a linear Tab (Te+T*) versus Eint dependence, a substantial number of systems show a non-linear dependence. We must ask what factors other than dynamics (statistical vs. non-statistical behavior) could give rise to nonlinear behavior. One such factor which must be considered is the absolute amount of excess energy. That is, when the amount of excess energy is very large, the ion will be relatively short-lived following internal conversion. For example, the Tav vs. Eint. data for 2,4-hexadiyne is flat i.e., KER is independent of the excess energy. (See Figure 1). This could be interpreted as non-statistical behavior; alternatively, the data can be explained by a lifetime argument. For this system the amount of excess energy is relatively large (.75 to 2.0 eV) and we believe the lifetime of the ion following internal conversion is too short to allow complete energy randomization. Consequently, the excess energy is not distributed into translational modes.

Alternatively, when the total excess energy is small, the ion may be long lived and could possibly isomerize prior to dissociation. This behavior is consistent with the dependence observed for trans-1,3-pentadiene. That is, the KER vs. Eint. seems to be made up of two distinct regions with a threshold at 500nm. (See Figure 2).

A second consideration for the KER dependence is the thermochemistry of the dissociation reaction. For example, the KER for methyl loss from cis-2-trans-4-hexadiene is independent of the photon energy; whereas, the KER for H loss shows the expected linear increase. The photo-induced methyl loss is thermochemically limited, i.e., the energy of the excited state is slightly below (0.2-0.3 eV) the dissociation energy. The photodissociation reaction (methyl loss) is observed only for vibrationally excited ground state precurosr ions, consequently, this system is unique in that the excess energy is zero.

Finally, we must consder the possibility that in systems with a large reverse activation energy, the product ion could be formed in a high energy state (isomeric structure or electronic state). The KER data for halide loss from both propargyl chloride and propargyl bromide are characterized by a dramatic decrease in the absolute KER value upon photodissociation. We believe that for this case we are sampling a high energy product state ($C_3H_3^{+*}$ or X* X=Cl, Br) and that this pathway is a preferred mechanism for energy transfer. A similar result has been postulated for photodissociation of CH_3I.[5]

In conclusion, it is clear that many parameters affect the measured kinetic energy release of a photo-excited ion. Amount these are the absolute amount of excess energy, the lifetime of the ion following internal conversion, the availability of alternate isomeric structures and finally, in systems with large reverse activation energies, the accessibility of high energy product states. At present, we do not have sufficient information on how large amounts of excess energy interact with the reverse activation energy. Clearly, we need to fully consider the nature of the potential energy surface of the ion of interest before we can make statements about the dynamics of the dissociation process based on kinetic energy release data.

The ions are made by electron impact in the source of a double focusing mass spectrometer (AEI MS-902). They are accelerated into the first field-free region where they are photodissociated by the laser beam (Coherent CR-18 Argon-Ion). The laser beam is modulated and the product ions are synchronously detected.

References

1. F.N. Preuninger and J.M. Farrar, J. Chem. Phys., 77, 264 (1982).

2. A.S. Werner and T. Baer, J. Chem. Phys., 62, 2900 (1975).

3. M.F. Jarrold, L.M. Bass, P.R. Kemper, P.A.M. Van Koppen and M.T. Bowers, J. Chem. Phys., 78, 3756 (1983).

4. D.H. Russell, M.H. Gross, J. Van der Greef and N.M.M. Nibbering, J. Am. Chem. Soc., 101, 2086 (1979).

5. E.S. Mukhtar, I.W. Griffiths, F.M. Harris and J.H. Beynon, Int. J. Mass Spectrom. Ion Phys., 42, 77 (1982).

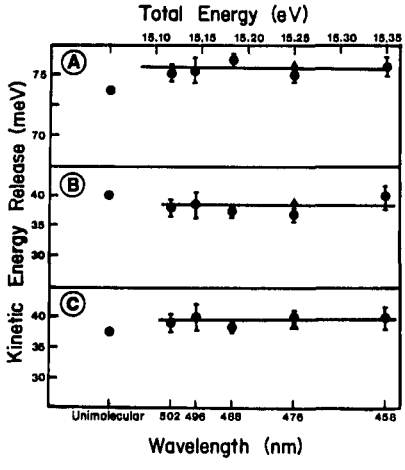

Figure 1: KER vs E_{int} 2,4-Hexadiyne

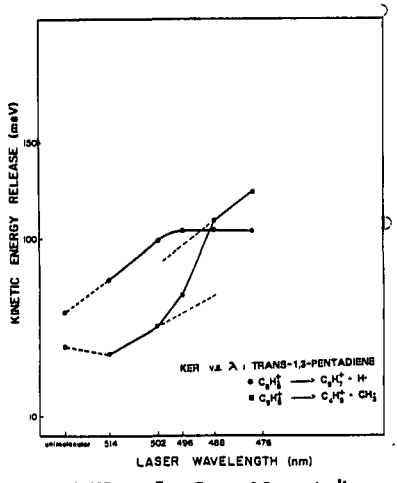

Figure 2: KER vs E_{int} Trans-1,3-pentadiene

MASS SPECTROMETRIC STUDIES OF HYPERVALENT MOLECULES

Gregory I. Gellene and Richard F. Porter
Department of Chemistry, Cornell University, Ithaca, NY 14853

Neutralized ion beam spectroscopy is a technique for generating unusual neutral species when a fast beam of ions is neutralized in an electron transfer reaction:

$$X^+ + M_{(g)} \rightarrow X^* + M^+ \quad (1)$$

where X^+ is any molecular ion and M is the electron donor. The state of X^*, which is dependent on the ionization potential of M can be classified as stable, metastable, dissociative, or radiative by analysis of the observed neutral beam scattering.[1] Additional information can be obtained by reionizing and mass resolving the neutral products of reaction (1). This has been accomplished in the present work by collisions with N_2 gas ($\sigma \sim 10^{-18}$ cm^2).

Previous work in this laboratory[2] has shown that a metastable state of H_3 can be produced by the reaction:

$$H_3^+ + K \rightarrow H_3^* + K^+ \quad (2)$$

This long lived state has been identified as the rotational ground level (N = K = 0) of the electronically excited $2p,A_2''$ Rydberg state. Figure 1 shows reionization spectra obtained for H_3 and D_3 following reaction (2). The decreased amount of D_3^+ relative to H_3^+ can be understood in terms of the effect of the appropriate nuclear statistics (Bose or Fermi respectively) and the Pauli principle in the population of the rotational levels. Thus the reionization spectra lends further support to the identification of the metastable state.

A long lived metastable state of ND_4 was observed in earlier neutral beam work.[3] Figure 3 shows reionization spectra obtained for NH_4, ND_3H, and ND_4 where a parent ion is observed only for the fully deuterated radical. Using a conservative estimate that 1% stable radical would be detected by reionization, an upper limit of 50 ns in the lifetime of ND_3H is calculated. This is almost a factor of 10^3 smaller than the lower bound on the lifetime of ND_4 (20μs).[3] From the ND_3^+/ND_2H^+ intensity ratio observed in the mass spectrum of ND_3H, an H/D kinetic isotope effect for the dissociation of the radical of 8:1 is determined. In this case the reionization spectra has confirmed the unusual stability of the ND_4 radical and allowed a determination of the H/D isotope effect in the dissociation of ND_3H.

We have recently extended our studies to the ammoniated clusters of ammonium, $NH_4(NH_3)_n$, and their deuterated analogs.[4] Figure 3 shows reionization spectra for $ND_4(ND_3)$, N_2D_6H, $NH_4(NH_3)$ where it can be seen that the parent ion is a prominent peak in each spectrum. A comparison of the mass spectral peak intensities indicates that the ammonium ions arise as fragment ions from the collisional ionization of the parent. Further, the ND_4^+/ND_3H^+ ratio observed for N_2D_6H (2:1) is much larger than that predicted from a statistical consideration of static geometric structures (0.75:1) suggesting some fluctional behavior for the radical. Finally a comparison of the (metastable)/(total neutral) intensity ratios for $NH_4(NH_3)$, $ND_4(ND_3)$ strongly suggests that the radical dissociates with loss of a terminal hydrogen atom rather than by rupture of the hydrogen bond.

References:
1) G.I. Gellene and R.F. Porter, Accts. Chem. Res. 16, 200 (1983)
2) G.I. Gellene and R.F. Porter, J. Chem. Phys. 79, 5977 (1983)
3) G.I. Gellene, D.A. Cleary, and R.F. Porter, J. Chem. Phys. 77, 3471 (1982)
4) G.I. Gellene and R.F. Porter, J. Phys. Chem. (submitted)

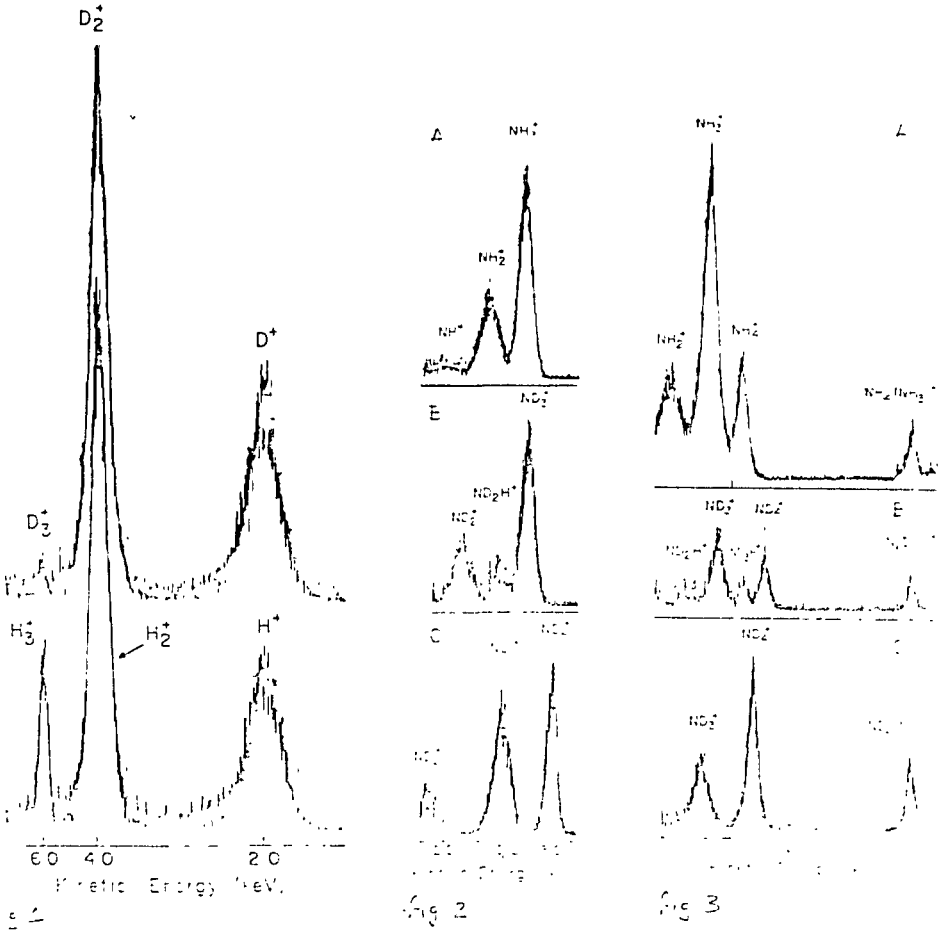

Figure 1 - Mass spectra of collisionally ionized neutrals following electron transfer to H_3^+ and D_3^+.

Figure 2 - Mass spectra of collisionally ionized neutrals following electron transfer to A, NH_4^+; B, ND_3H^+ and C, ND_4^+.

Figure 3 - Mass spectra of collisionally ionized neutrals following electron transfer to A, $NH_4(NH_3^+)$; B, $N_2D_6H^+$ and C, $ND_4(ND_3)^+$.

ISOMERIZATION AND DISSOCIATION PROCESSES OF DISTONIC RADICAL IONS AND AROMATIC IONS FOUND WITH MULTIPLE TECHNIQUES: C. Wesdemiotis, J. Grotemeyer, P. O. Danis, and F. W. McLafferty; Chemistry Department, Cornell University, Ithaca, New York 14853

Distonic radical ions represent species in which the charge and radical sites are separated. Enolic ions, such as $\cdot CH_2C(CH_3)C{=}O^+H$, can be considered as well known examples which can actually be more stable than the keto form, $(CH_3)_2C{=}O^+\cdot$ for this case. The "ion-dipole complex" ions such as $H_2\overset{+}{C}\cdots ClH$ can also be considered as distonic radical ions, $H_2\dot{C}-\overset{+}{Cl}H$. Thermodynamic calculations predict that such ions will be stable for a surprising number of compound types. Confirming such calculations, mass spectra from collisionally-activated dissociation (CAD) and neutralization-reionization (NR) mass spectrometry[1] show $\cdot C_2H_4CH_2CH_2N^+H_3$ to be more stable than $CH_3(CH_2)_3NH_2^+\cdot$.

Figure 1 shows the CAD spectra of n- and i-butylamine. The second major fragment in both spectra is the ammonia loss product; it is formed via

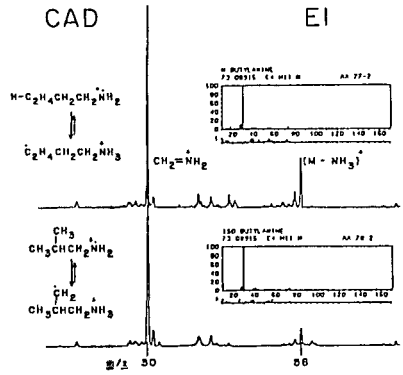

Figure 1. CAD mass spectra of n- (top) and i-butylamine. Inserted are the corresponding 70eV EI mass spectra.

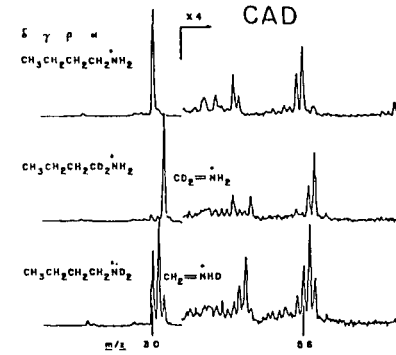

Figure 2. CAD mass spectra of n-butylamine (top) and its α-d_2- (center) and N-d_2-isotopomers.

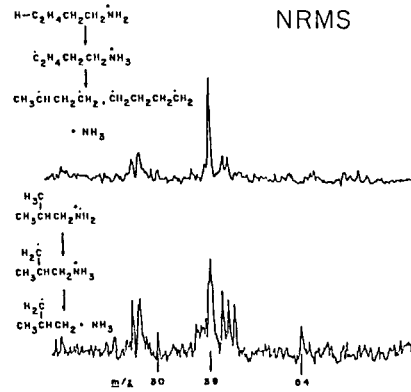

Figure 3. NR mass spectra of n- (top) and i-butylamine.

direct bond cleavage from the distonic isomers shown in the left part of Figure 1. The CAD spectra of deuterated n-butylamines (Figure 2) prove that before fragmentation (e.g., before the $C_3H_7\cdot$ and NH_3 losses which are the major CAD dissociation pathways) the molecular ions equilibrate with their distonic isomers; this equilibration leads to extensive H/D-exchange between the amino hydrogen atoms and at least 5 other hydrogens, the atoms at the γ- and δ-positions of the alkyl chain. As expected, the α-CH_2-group does not participate in this exchange process. Finally, the NR spectra of n- and i-butylamine (Figure 3) prove that the equilibria shown in Figure 1 must be far on the side of the distonic radical ions. Neutralization of the molecular ions should, namely, give NR spectra similar to the EI spectra[2] (see inserts in Figure 1) which is not the case. Obviously, the molecular ions have isomerized to the more stable distonic radical ions before neutralization, as shown in Figure 3. Neutralization of the distonic ions yields hypervalent species which spontaneously lose ammonia forming C_4-diradicals. Reionization of these diradicals (and their neutral dissociation products) gives rise to the observed fragments, with $C_3H_3^+$, m/z 39, being the major product ion.

$\cdot C_2H_4OCH_2-C_6H_6^+$ is also more stable than $C_2H_5OCH_2-C_6H_5^{+\cdot}$ (although $\cdot C_2H_4CH_2CH_2-C_6H_6^+$ is not more stable than $CH_3(CH_2)_3C_6H_5^{+\cdot}$). Thus the rearrangement loss of C_2H_4 must be stepwise, not concerted as postulated by Bowie, et al.[2] Deuterium labeling confirms the reversibly stepwise mechanism.

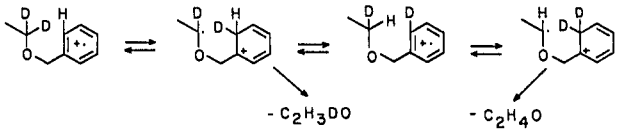

Mass spectra from CAD of alkylbenzenes are relatively independent of the site of protonation, as the loss of an alkyl radical from such even-electron ions is unfavorable. However, such a loss is favored in the odd-electron species formed by neutralization, so that NR mass spectra can provide definitive evidence of the protonation site. Similarly, the NR mass spectra of neutral products formed by dissociation of mass-resolved ions can provide the isomeric identity of the neutral. Supporting the conclusions of Lifshitz, NRMS shows that metastable pyridine ions lose HCN in forming $C_5H_6^+$, but the counterpart reaction of aniline produces the isomer HNC.

A dynamic model of Grotemeyer and Grutzmacher[3] for unimolecular reactions of common $C_8H_{10}^{+\cdot}$ isomers has been extended using C-13 and D-labeled xylenes, ethylbenzenes, and methylcycloheptatrienes utilizing metastable ion dissociations, NR, and CAD, and by varying the ion internal energy. For example, reducing the average ion internal energy of dissociating metastable ions by increasing their lifetime or by lowering the ion source temperature first increases the degree of isotopic scrambling until it becomes statistical; this pathway could involve expansion to an 8-membered ring. However, this is not true at the longest lifetimes and lowest temperatures, where an isomerization reaction of even lower energy requirements is dominant; this appears to involve dissociation of methylcycloheptatriene.

(1) Danis, P. O.; Wesdemiotis, C.; McLafferty, F. W. J. Am. Chem. Soc. **1983**, 105, 7454.

(2) Stone, D. J. M.; Bowie, J. H.; Underwood, D. J.; Donchi, K. F.; Allison, C. E.; Derrick, P. J. J. Am. Chem. Soc. **1983**, 105, 1688.

(3) Grotemeyer, J.; Grützmacher, H.-F. Org. Mass Spectrom. **1982**, 17, 353.

The Characterization of Neutral Species Formed by Electron Impact On Some C_1 - C_5 Alkanes and C_2 - C_4 Alkenes

Gerald D. Flesch and Harry J. Svec
Ames Laboratory-USDOE and Department of Chemistry
Iowa State University, Ames, Iowa 50011

A double-ended neutral fragment mass spectrometer has been used to produce and analyze neutral fragments from hydrocarbon gases. The gases studied are those obtained by systematically replacing the hydrogens of methane with methyl, or the hydrogens of ethylene with methyl.

The most abundant neutral species are M, $(M-H)^{\bullet}$, $(M-H_2)$, $(M-CH_3)^{\bullet}$, $(M-CH_4)$ and $CH_3^{\bullet}$ for the alkanes, and the same fragments and $C_3H_3^{\bullet}$ for the alkenes. These species account for ninety percent or more of the total species produced for each of the gases. The fractional abundances of the M and the fragments $(M-H)^{\bullet}$ and $(M-H_2)$ decrease as the carbon number of the alkane increases, while the fractional abundances of $(M-CH_3)^{\bullet}$, $(M-CH_4)$ and $CH_3^{\bullet}$ decrease. The total abundance of neutral species increases with carbon number for both the alkanes and alkenes.

The fractional abundances of the fragments observed for the alkenes does not vary much within the alkenes studied, except for iso-butene. The neutral fragments spectra for the cis- and trans-butenes are essentially identical, but different from that for iso-butene. There is more $CH_3^{\bullet}$ and $(M-CH_4)$ and less $(M-H_2)$ for the isobutene than the similar fragments from cis- and trans-butene.

The values for the ionization energies of the neutral fragments produced are shown in Table 1. The values shown are the average and standard deviation of the average values obtained for each of the gases studied. The average was calculated from individual values which were weighted inversely according to the value of the standard deviation observed for each gas. A low value of uncertainty, 0.1 - 0.2 eV, indicates that the fragment is in the same energy state regardless of the source of the fragment. An intermediate value of uncertainty, 0.3 - 0.4 eV, indicates that the energy state is probably the same but the statistics are poor. A high value of uncertainty, 0.5 - 0.6 eV, indicates that the energy states are different depending on the source of the fragment.

Table 1. Ionization Energies (eV)
Neutral Products

Mass	Species	Lit	Obs
2	H_2	15.4	14.8 ± 0.2
15	$CH_3^{\bullet}$	9.8	9.5 ± 0.2
26	C_2H_2	11.4	11.1 ± 0.2
28	C_2H_4	10.5	10.6 ± 0.2
39	$CH_2CCH^{\bullet}$	8.7	9.2 ± 0.4
40	CH_2CCH_2	10.0	9.7 ± 0.6
41	$CH_3CHCH_3^{\bullet}$	8.1	8.0 ± 0.2
42	C_3H_6	9.7	9.6 ± 0.3
55	$CH_2C(CH_3)CH_2^{\bullet}$	7.9	7.9 ± 0.1
56	i-C_4H_8	9.2	8.8 ± 0.5

The values for the ionization energy observed for H_2 and $CH_3^{\bullet}$ are less than the literature values. The differences agree well with the first vibrational stretch in H_2 (0.54 eV) and the first symmetrical stretch in $CH_3^{\bullet}$ (0.34 eV).

The appearance energies of the reactions by which the fragments were produced were also determined. The values are nearly equal, 13.5 ± 1 for all the alkanes, and nearly equal, 9.0 ± 2 for all the alkenes. The equality of values for either the alkanes or the alkenes results from the similarity of the number of kinds of bonds broken and rearranged. The inequality between the alkanes and alkenes indicates a basic difference in the reactions occurring. The high alkane value indicates dissociative ionization and the lower alkene value dissociative excitation, but such a simplistic answer is not plausible. A new ion source is being designed which may shed more light on this problem.

ACKNOWLEDGEMENT

Ames Laboratory is operated for the U.S. Department of Energy by Iowa State University under Contract No. W-7405-Eng-82. This research was supported by the Director for Energy Research, Office of Basic Energy Science.

MASS SPECTROMETRIC MEASUREMENTS OF BIOLOGIC PEPTIDES

Dominic M. Desiderio, Hiroshi Onishi, Hisayoshi Takeshita, Francis S. Tanzer, Joann Trimble and Jay Walker, Jr.

Department of Neurology and Charles B. Stout Neuroscience Mass Spectrometry Laboratory-College of Medicine and Departments of Oral Diagnostis and Orthodontics-College of Dentistry; University of Tennessee Center for the Health Sciences; 800 Madison Avenue, Memphis, Tennessee 38163

The overall objective of this research program is to utilize mass spectrometric methods to study the basic molecular reactions of four peptidergic pathways involved in nociception and stress. The pathways include the enkephalinergic, endorphinergic, dynorphinergic and substance P-ergic pathways. Towards that end, data from the following crucial experimental aspects are presented:

1. Perform all animal physiological, neuroantomical and neurosurgical experiments within one research group to maintain maximum quality control over all experimental steps in the analytical process.
2. Collaborate closely with both clinical and dental operation personnel to ensure quality control over sample acquisition and maintain integrity of the molecules which will be quantified.
3. Effectively prepare a peptide-rich fraction which closely represents those endogenous peptides as they exist in the biological tissue.
4. Perform high resolution reverse phase high performance liquid chromatographic separation of peptides.
5. Measure the endogenous amounts of the peptides in several analytical methodologies including:

   a. High performance liquid chromatography with UV absorption at 200 nm;
   b. Radioreceptor assay using a novel canine radioreceptor synaptosomal preparation with a view towards taking advantage of delta, mu, sigma, and kappa receptors;
   c. Use commercial antibodies to measure leucine and methionine enkephalins;
   d. Utilize the novel combination of fast atom bombardment-collision activated dissociation-linked field scanning (B/E,B'/E')-ucom to measure $(M+H)^+$ due to the endogenous peptide and synthetic peptide internal standard.

Preliminary experiments which were performed on a VG ZAB 4F indicate that the highest sensitivity to date which retains optimal molecular specificity is at the one nanogram (corresponding to the two picomole) level. Further experiments are in progress to extend that sensitivity to the femtomole range.

Using human tooth pulp tissue extracts, the analytical data derived from both radioreceptor assay and radioimmunoassay were found to parellel each other.

It is the intent of this research program to calibrate the canine synaptosomal radioreceptors and the commercial antibodies used for radioimmunoassay with the mass spectrometric procedure.

DESORPTION OF INSULIN MOLECULAR IONS FROM POLYMERIC SURFACES

E. A. Jordan, C. R. Martin, C. J. McNeal, R. D. Macfarlane
Department of Chemistry, Texas A&M University, College Station, Texas 77843

Shortly after the first observation of the molecular ions of bovine insulin by the PDMS method[1], similar results were obtained by FAB.[2] Since then, detailed studies have been carried out to increase the yield of molecular ion formation by ^{252}Cf-PDMS and enhance sensitivity of sub-nanomole levels. Good yields of positive and negative ions have been obtained for thick films and some data on fragmentation patterns have been correlated with structure utilizing the small differences in the sequences of bovine, human, and porcine insulin.

It has also been possible to adsorb monolayer films of various species including insulin on the surface (figure 1) of an ion-containing perfluorocarbon polymer (Nafion)[3]. The mass spectrum of insulin desorbed from this matrix shows considerable differences (figure 2): a factor of three higher molecular ion intensity, a lower intensity metastables population and the appearance of doubly-charged molecular ions. These differences are attributed to substrate-adsorbate interactions and demonstrate conclusively that the ionization process is mediated by surface forces.

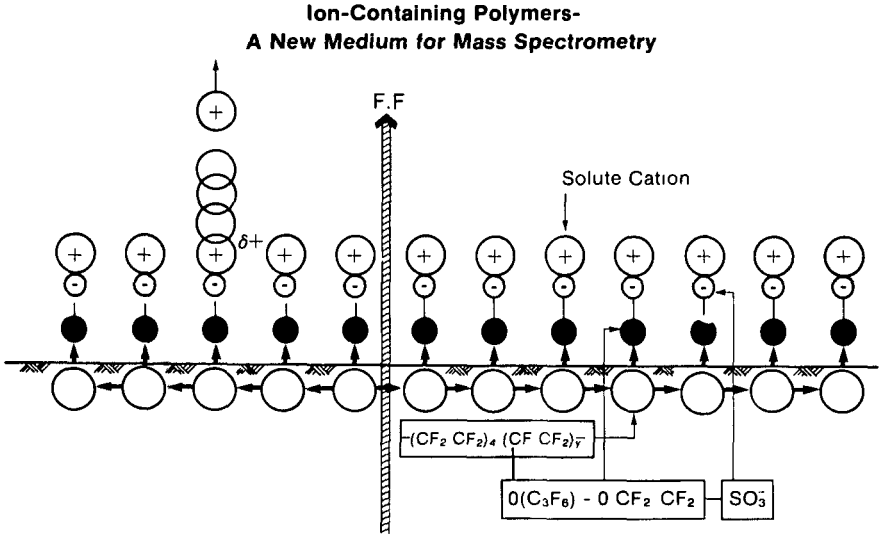

Figure 1. The idealized matrix of insulin adsorbed onto Nafion.

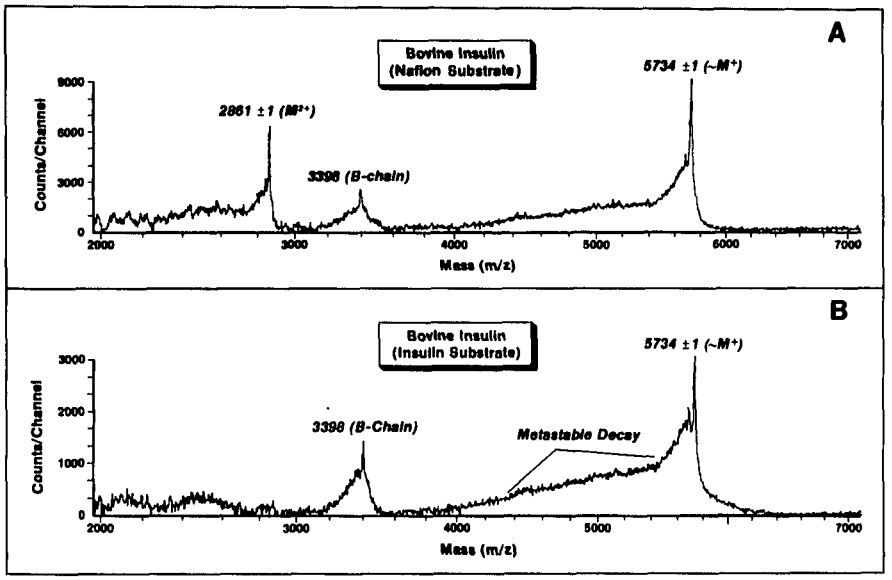

Figure 2. Mass spectral differences between insulin desorbed from a Nafion substrate vs. an insulin substrate.

The fragmentation of insulin was studied by comparing the spectra of human, bovine, and porcine insulins. It was found (figure 3) that human insulin differed from both bovine and porcine insulin in mass, but appeared identicle in pattern. It was then deduced that this fragmentation occurs from the B-chain both from the N and C termini.

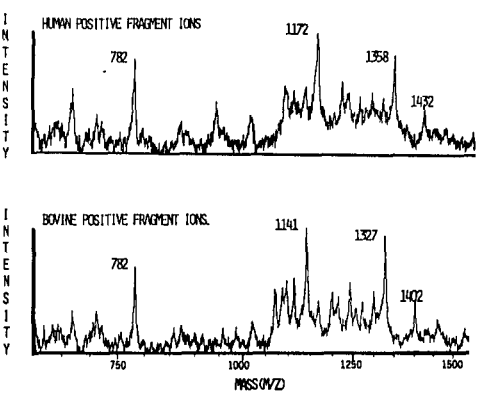

Figure 3. Mass spectra of Human and Bovine insulin fragment ions showing mass shift due to residue changes.

REFERENCES

1. P. Håkansson, et. al., J. Amer. Chem. Soc. 104, 2948 (1982).
2. M. Barber, et. al., J. Chem. Soc. Chem. Commun. 936 (1982).
3. E.A. Jordan, et. al., Inter. J. Mass Spectrom. Ion. Phys. 53, 345 (1983).

FAST ATOM BOMBARDMENT MASS SPECTROMETRY OF THE *S. AUREUS* DIGEST OF HUMAN INSULIN

Dean D. Fetterolf*, John Chaber and Stephen Byrn, Department of Medicinal Chemistry, Purdue University, West Lafayette, IN 47907 and Ralph Pfeiffer and Ron Chance, Lilly Research Laboratories, Eli Lilly and Co., Indianapolis, IN 46206.

In recent years fast atom bombardment (FAB) has been applied to a wide variety of biological molecules including nucleotides and peptides. Although fragmentation can occur from both the C-terminus and N-terminus, the complete sequencing of peptides is not always possible. In addition the mass of many middle molecular weight peptides exceeds the mass range and sensitivity of current instrumentation. The combination of enzymatic digestion with FAB offers one solution to these problems (1).

Insulin degrades upon storage in both the solid state and in solution; however, the chemical nature of these degradation products is not well established (2). As a prelude to our studies of the degradation we have investigated the usefulness of FAB in combination with the enzymatic digestion of human insulin.

Human insulin (monoisotopic mass 5803.6, avg. mass 5807.6) was degraded using *S. aureus* V8 protease following published procedures (3). The digest should contain the fragments shown in Figure 1. The lyopholized digest was dissolved in a mixture of 1N HCl, thioglycerol and glycerol. The mass spectrum (Figure 2) was recorded on a Kratos MS-50 with a high field magnet and post acceleration detector. Xenon was used as the primary beam gas in the FAB gun which was operated at 8 keV at a beam current of 400 μA.

The enzymatic cleavages resulting in the A1-A4, A13-A17 and B14-B21 fragments are confirmed by the protonated molecular ion in the FAB spectrum. Further comparison of the ions observed to those in Figure 1 indicates that a mixture of broken and unbroken disulfide bonds are present. The fragment at m/z 1378 is consistent with an intact disulfide bond linking B14-B21 with A18-A21. In addition the B14-B21 fragment is also observed. However, the fragment A5-A12 which contains an additional disulfide bond is not observed linked to the B chain (B1-B13) or by itself. In addition to the fragments from the enzymatic digestion we have also obtained the molecular ion profile of human insulin (Figure 3). The monoisotopic mass (M+1) of 5804.6 was confirmed by peak matching to CsI clusters.

In conclusion, FAB combined with the *S. aureus* V8 protease digestion appears to be a new and powerful method for the analysis of insulin and its degradation products. The results of this study are completely consistent with those of Chance based on liquid chromatographic and amino acid analysis (3) and provide a rapid method for obtaining the necessary molecular weight and structural information.

References

1. B.W. Gibson and K. Biemann; presented at the 30th Annual Conference on Mass Spectrometry and Allied Topics; Honolulu; June 6-11, 1983.
2. B.V. Fisher and P.B. Porter, J. Pharm. Pharmacol., **33**, 203-206, 1981.
3. R.E. Chance, J.A. Hoffman, E.P. Kroeff, M.G. Johnson, E.W. Schirmer, W.W. Bromer, M.J. Ross, and R. Wetzel; in: Peptides: Synthesis-Structure-Function, Pierce Chemical Company, Rockford, IL, Ed. by D.H. Rich and E. Gross, 1981.

*Current Address: Forensic Science Research Group, Federal Bureau of Investigation, FBI Academy, Quantico, VA 22135.

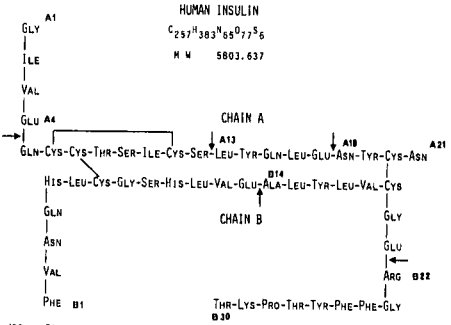

FIGURE 1. S. aureus V8 protease digest of human insulin.

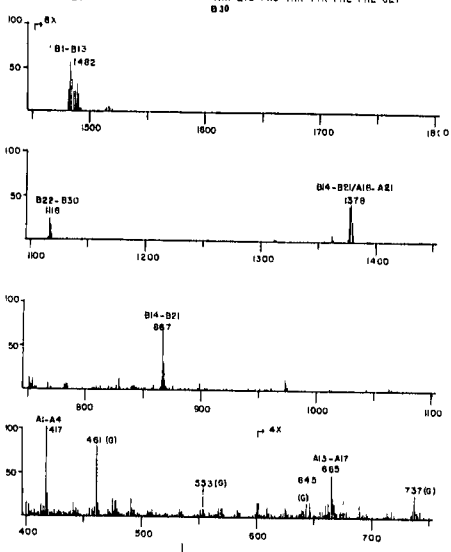

FIGURE 2. FAB mass spectrum of the S. aureus digest of human insulin.

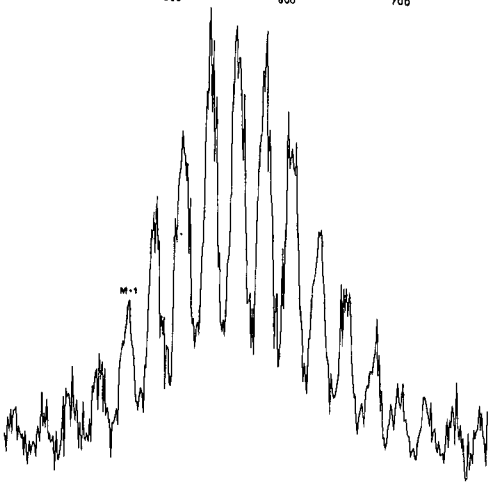

FIGURE 3. Molecular ion profile of human insulin (monoisotopic M+1 = 5804.6).

DETECTION OF PTH-DERIVATIVES OF AMINO ACIDS BY SIMS

A.Benninghoven and V.Anders

Physikalisches Institut der Universität Münster,
D-4400 Münster, Fed. Rep. of Germany

A crucial step in protein sequence analysis by Edman degredation is the detection and identification of phenylthiohydantoine derivatives of amino acids. An important factor determining the minimum sample size of a peptide or a protein required for sequence analysis is the detection limit of these PTH-derivatives.

We have investigated the secondary ion emission behaviour of the PTH-derivatives of a large number of different amino acids. We observed reproducible high intensity parent-ion emission of $(M+H)^+$, $(M-H)^-$, $(M+Au)^+$, and $(2M+Au)^+$ for all PTH-derivatives investigated.

The samples were deposited on gold substrates, which had been cleaned by an etching procedure. For screening experiments, about 1 µl of a 10^{-3} mol solution in methanol was deposited on about 1 cm^2. This ensures a closed monolayer of the sample molecules on the gold substrate. Excess sample molecules form small crystallites on the surface.

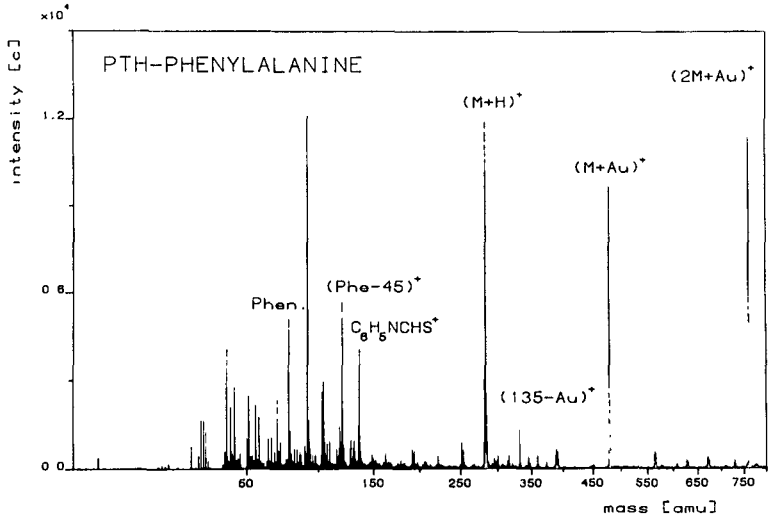

Fig. 1: Positive TOF secondary ion spectrum of PTH-phenylalanine on Au.
Sample: 10 pmol in the bombarded target area of 0.01 cm^2
Primary ion bombardment: $1.9 \cdot 10^8$ Ar^+, 12 keV
For obtaining this spectrum, less than 1 % of the sample has been sputtered.

The samples were investigated in a quadrupole and in a time-of-flight SIMS. Due to the higher transmission and the simultaneous detection of all masses, the sensitivity of a time-of-flight instrument is several orders of magnitude higher than that of the quadrupole SIMS. Useful spectra of all PTH-derivatives can be obtained from samples in the fmol range.

Reference

A.Benninghoven and V.Anders, Org.Mass Spectrom., in press

Positive Parent Ion Emission from PTH-Amino Acids

PTH-amino acid	Molec. Weight	Number of primary ions	Number of detected secondary ions		
			$(M+H)^+$	$(M+Au)^+$	$(2M+Au)^+$
Ala	206	$1.9 \cdot 10^8$	$1.2 \cdot 10^3$	$6.5 \cdot 10^3$	$2.5 \cdot 10^3$
Ser	222	"	8.5	5.0	2.0
Val	234	"	2.5	1.4	9.0
Asn	249	"	2.9	7.3	3.6
Asp	250	"	4.0	6.9	4.0
Gln	263	"	1.2	3.7	2.0
Glu	264	"	4.7	6.0	3.2
Met	266	"	9.5	12.5	9.0
His	272	"	4.3	1.8	0.6
Phe	282	"	11.9	9.7	13.0
Arg	291	"	14.0	4.0	4.0
Trp	321	"	2.0	7.5	2.8
E-PTC-Lys	398	"	3.5	16.5	0.3

Table 1 Positive parent-ion emission from PTH-amino acids. Samples: 10 pmol in the bombarded target area of 1 mm^2

^{252}Cf PLASMA DESORPTION TIME OF FLIGHT MASS SPECTROMETRY OF PEPTIDES AND PROTEINS

P. Roepstorff[+], B. Sundquist[++], J. Fohlmann[+++], P. Håkonsson[++], I. Kamensky[++], M. Lindberg[++], A. Hedin[++] and G. Säve[++]

[+]Department of Molecular Biology, Odense University, DK-5230 Odense M, Denmark.
[++]Tandem Accelerator Laboratory, University of Uppsala, Box 533, S-75122 Uppsala, Sweden.
[+++]Department of Cell Research, The Wallenberg Laboratory, Box 531, S-75121 Uppsala, Sweden.

^{252}Cf plasma desorption mass spectrometry (PDMS) originally develloped by Macfarlane and co-workers[1] allows mass spectrometric analysis of large biomolecules directly from the solid state. We have demonstrated that the molecular weight of proteins up to MW 14.000 can be obtained[2]. In the present study the molecular weight range is extended to approximately MW 25.000. It is further demonstrated that the molecular weight of the individual components in mixtures of peptides and proteins is obtainable. Finally the spectra obtained by fast atom bombardment (FAB) and plasma desorption mass spectrometry of small peptides are compared.

EXPERIMENTAL:
The plasma desorption spectra were obtained on a prototype time-of-flight mass spectrometer constructed in Uppsala. A detailed description of the instrument, the sample preparation and the features of the mass spectra is given in ref. 2. The time spectrum was mass calibrated with the peaks corresponding to H^+ and Na^+:
FAB spectra were obtained with a Finnigan MAT 311A mass spectrometer equipped with an IonTech 11 NF fast atom source. Argon was used as bombardment gas and glycerol as liquid matrix. The proteins analyzed were gifts from Novo Industry, Denmark. The peptides used in the comparative study were synthetic peptides from various sources.

RESULTS AND DISCUSSION
The positive spectrum of porcine trypsin is shown in fig. 1. This is to our knowledge the hitherto largest monomeric protein ion observed in the gas phase. The calculated molecular weight using isotopically averaged atomic weights is 23463. The molecular weights determined from the centroids of the M^+ and M^{2+} peaks is 23406 $\pm$ 140. The peak corresponding to the doubly charged ions is twice as intense as that of the singly charged ions. This is in agreeement with our previous observation, that the ratio of doubly charged ions to singly charged ions increases with the molecular weight[2].

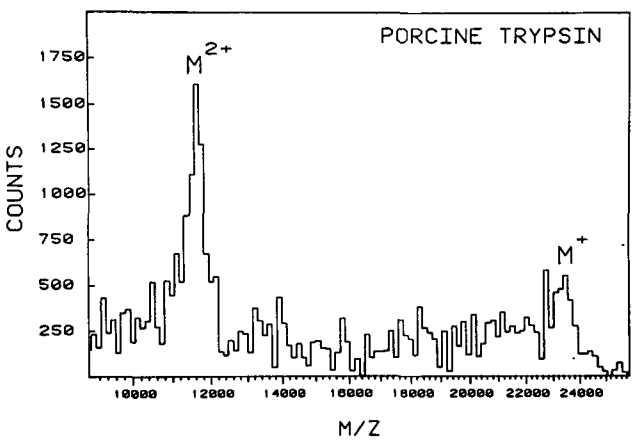

Fig. 1. Positive ion mass spectrum of porcine trypsin.

Molecular weight determination of proteins and peptides in mixtures has been tested on several samples prepared by mixing pure peptides and proteins. Fig. 2 shows the positive ion mass spectrum of a 1:1:1:1 mixture on molar basis of the peptide hormone LH-RH (MW 1182), porcine insulin (MW 5778), pancreatic spasmolytic peptide (PSP) (MW 11711) and phospholipase A2 (MW 13980). The molecular weight, probably MH^+, of the four components in the mixture was experimentally determined to 1183 ± 0.5, 5778 ± 2, 11715 ± 15 and 13963 ± 20 respectively. The same mixtures have been analyzed by SDS-page electrophoresis and high performance gel

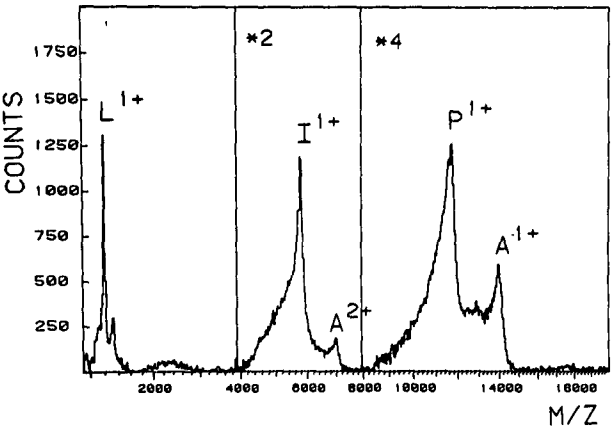

Fig. 2. Positive ion mass spectrum of a mixture of LH-RH (L), porcine insulin (I), pancreatic spasmolytic peptide (P) and phospholipase A2 (A).

permeation chromatography (HP-GPC). PSP and phospholipase A2 could not be separated by either of the techniques and LH-RH was lost in SDS-page electrophoresis. The precision of the molecular weight determination of proteins up to MW 15.000 is better than 0.2%. This is approximately two orders of magnitude better than the precision of SDS-electrophoresis and HP-GPC. Furthermore, the molecular weight determination with the latter two techniques is influenced by properties of the molecule which are irrelevant to the molecular weight such as conformation and hydrophibicity.

^{252}Cf-plasma desorption and fast atom bombardment spectra of eight tri to penta peptides were compared. The main differences in the spectra were observed in the molecular ion region where the PD-MS showed extensive cationization e.g. MNa^+, MNa_2^+-H, whereas MH^+ was the dominating molecular species in FAB. The integrated intensity of the molecular ion region in PDMS is somewhat higher than in FAB-MS. Noticeably the fragmentation patterns obtained with the two techniques were the same although the energy of the incident fission fragments in PD is four orders of magnitude higher than the energy of the bombarding atoms used in FAB.

* the same

References.

1. D.F. Torgerson, R.P. Skowronski and R.D. McFarlane, Biochem. Biophys. Res. Commun. 60 616 (1974).
2. B. Sundquist, P. Håkonsson, I. Kamensky, J. Kjellberg, M. Salehpour, S. Widdiyasehera, J. Fohlmann, P. Peterson and P. Roepstorff, Biomed. Mass Spectrom. In press.

COMBINED LC/MS OF AMINO ACIDS AND PEPTIDES

D.E. Games and E.D. Ramsey, Department of Chemistry, University College, P.O. Box 78, Cardiff CF1 1XL, U.K.

D.A. Catlow and B.J. Woodhall, ICI Pharmaceuticals Division, Hurdsfield Industrial Estate, Macclesfield, Cheshire, SK10 2NA, U.K.

P. Roepstorff, Department of Molecular Biology, Odense University, Campusvej 55, DK 5230 Odense M, Denmark.

Derivatized peptides and derivatized and underivatized amino acids have been studied by high-performance liquid chromatography/mass spectrometry using moving belt interfaces with both electron impact (EI) and chemical ionization (CI).

Amino acids

Ammonia CI was found to be the ionization method of choice for studying a mixture of p-aminophenylalanine, p-hydroxyphenylglycine, phenylglycine, tyrosine, phenylalanine and tryptophan. LC/MS was performed using a gradient system containing varying amounts of water and methanol buffered to pH 2.3 with trifluoracetic acid and ammonium hydroxide. Because of the high percentage aqueous mobile phase at the start of the gradient less than 5% of the mobile phase could be fed to the moving belt interface when conventional LC columns were used. As a result of this and thermal decomposition of the amino acids the limits for obtaining full scan spectra with mol. wt. information were of the order of 5 µg of amino acid injected on the column. Use of 1 mm i.d. microbore columns for LC/MS enabled all the eluent from the liquid chromatograph to be fed to the interface and limits for obtaining full scan spectra with mol. wt. information were of the order of 100 ng of amino acid injected on the LC column. Preliminary studies with p-aminophenylalanine and p-hydroxyphenylglycine using a prototype Finnigan thermospray LC/MS system indicate that considerable improvements in detection limits can be obtained, full scan spectra with mol. wt. information being obtained at the low ng level.

PTH and dansyl amino acids have also been investigated. The dansyl amino acids were not suitable for LC/MS study with moving belt interfaces since we failed to obtain mol. wt. information from most of the compounds studied. PTH amino acids proved to be readily amenable to LC/MS investigation using a moving belt interface. A mixture of eleven PTH amino acids was studied. EI proved to be a suitable ionization method providing both mol. wt. and structurally useful fragment ions. A gradient system using varying amounts of acetonitrile and water with a trace of formic acid proved effective for the separation of all eleven compounds. With conventional LC columns detection limits for full scan spectra containing mol. wt. information are in the high ng range because only 5% of the LC column eluent could be fed to the interface. Using 1 mm i.d. microbore columns, full scan spectra containing mol. wt. information were obtained from solutions containing 10 ng of each of the PTH amino acids.

Protected synthetic peptides

A variety of synthetic di-, tri- and tetrapeptides protected with benzyloxycarbonyl (z), benzyl and t-butyl groups have been studied on a moving belt LC/MS interface. Ammonia CI proved to be the ionization method of choice, however because of the lability of some of the protecting groups it did not always provide mol. wt. information. In cases where mol. wt. information was available LC/MS proved to be useful for the detection of by-products in the synthesis of compounds of this type. For example LC/MS study of the peptide Z-Trp-Ser(OBzl)-Tyr-oMe using a gradient system with methanol and water buffered to pH 7 with ammonium acetate as mobile phase enabled dicyclohexylcarbodimide and a diastereoisomer of the synthetic peptide to be identified as impurities in the sample.

N-Acetyl-N,O-permethylated peptides

The use of N-acetyl-N,O-permethylated peptides for the sequencing of peptides is well established and investigations of the utility of moving belt LC/MS for their study have been reported.[1-3] In our earlier studies[2] problems were encountered in developing suitable chromatographic separations of complex mixtures of these peptides. Using reversed phase gradient systems of methanol and water we have been able to successfully sequence mixtures containing up to seven peptides with from three to five amino acid residues by LC/MS. Ammonia CI has proved to be the ionization method of choice providing both N- and C- terminal sequence ions. The technique has been applied to the sequencing of peptides obtained from locust cuticles. Presently LC/MS using a moving belt interface is not competitive with established peptide sequencing methods since we require of the order of 50nmole of sample. In order to improve the sensitivity of the technique, microbore LC, spray deposition and improvements in permethylation are being investigated.

References
1. T.J. Yu, H. Schwartz, R.W. Giese, B.L. Karger and P. Vouros, J.Chromatogr., 1981, 218, 519.
2. P. Roepstorff, M.A. McDowall, M.P.L. Games and D.E. Games, Int.J. Mass Spectrom. Ion Phys., 1983, 48, 197.
3. T.J. Yu, B.L. Karger and P. Vouros, Biomed. Mass Spectrom., 1983, 10, 633.
4. M.J. Hayes, E.P. Lankmayer, P. Vouros, B.L. Karger and J.M. McGuire, Anal. Chem., 1983, 55, 1745.

ENERGY-RESOLVED STUDIES OF IONIC FRAGMENTATION REACTIONS. A COMPARISON OF CHARGE EXCHANGE WITH FIELD IONIZATION KINETICS, ANGLE RESOLVED MASS SPECTROMETRY AND VARIABLE ENERGY COLLISION-INDUCED DISSOCIATION MASS SPECTROMETRY.

A.G. Harrison, S. Nacson and J.J. Zwinselman, Dept. of Chemistry, University of Toronto, Toronto, Canada M5S 1A1

There is a continuing interest in the energy dependence of ionic fragmentation reactions and in the development of methods which provide such information. Among the methods which have been developed are field ionization kinetics (FIK), angle resolved mass spectrometry (ARMS) and variable low energy collision-induced dissociation (CID). The FIK method provides time-resolved information on fragmentation reactions over the time period from 10^{-12} to 10^{-9}s, while ARMS provides relative product ion intensities as a function of the scattering angle in a high energy activating collision and CID provides product ion distributions as a function of the centre-of-mass collision energy. In all cases, however, it is not possible to correlate the product distribution directly with the internal energy of the fragmenting ion.

We have undertaken a study of a number of systems, previously studied by FIK and ARMS, by charge exchange (CE) mass spectrometry and CID to provide insight as to the internal energy regimes being sampled by the various techniques. In CE the internal energy of the fragmenting $M^{+\cdot}$ ions is given by $RE(R^+)-IE(M)$ and can be varied in a controlled fashion by choosing reagent ions of different recombination energies.

Figure 1 compares results for the competing fragmentation reactions

$$CH_3\text{-}CH{=}CH\text{-}CH(OH)CD_3^{+\cdot} \longrightarrow C_4H_7O^+ + CD_3$$
$$\longrightarrow C_4H_4D_3O^+ + CH_3$$

obtained by FIK[1], ARMS[2] and CE. Allowing that decreasing lifetime corresponds to increasing internal energy in FIK and that increasing angle of observation in ARMS corresponds to increasing deposition of internal energy the agreement between the three methods is quite good. The comparison shows that the FIK and ARMS methods are sampling ions with internal energies in the range ~1 to ~4.5 eV for this system. Figure 2 compares CE, CID and ARMS[3] results for the competing fragmentation reactions

At low internal energies formation of $C_7H_8^{+\cdot}$ dominates but with increasing internal energy simple cleavage to give $C_7H_7^+$ increases rapidly in importance. This behaviour is reflected in the ARMS and CID results, although for the latter the constancy of the ion current ratio beyond E_{CM}=8eV indicates that the average energy converted into internal energy becomes a constant independent of collision energy; the maximum average internal energy in the CID system is ~2.3 eV.

We are indebted to the Sciex Division of MDS for providing access to the TAGA 6000 triple quadrupole mass spectrometer.

1. J.J. Zwinselman, N.M.M. Nibbering, N.E. Middlemiss, J.H. Vajda and A.G. Harrison, Int. J. Mass Spectrom. Ion Phys., 38(1981) 1547.
2. D.J. Burinsky, G.L. Glish, R.G. Cooks, J.J. Zwinselman and N.M.M. Nibbering, J. Am. Chem. Soc., 103 (1981) 465.
3. S.A. McLuckey, S. Verma, R.G. Cooks, M.J. Farncombe, R.S. Mason and K.R. Jennings, Int. J. Mass Spectrom Ion Phys., 48, 423 (1983).

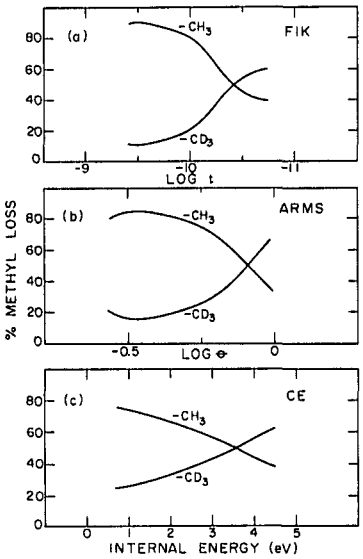

Figure 1: Methyl loss from $CH_3CH{=}CHCH(OH)CD_3$

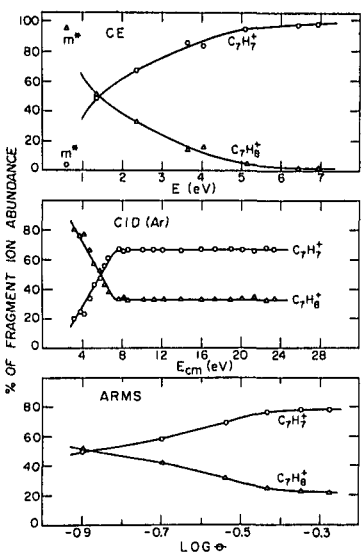

Figure 2: Fragmentation of benzyl methyl ether

SOME COMMENTS ON THE METASTABLE FRAGMENTATION OF INSULIN IONS PRODUCED BY FISSION FRAGMENT BOMBARDMENT, B. T. Chait, L. Grace, F. H. Field, The Rockefeller University, New York, NY 10021

The bombardment of organic ions in the condensed phase by high energy fission fragments gives rise to secondary ions in the gas phase containing appreciable internal energy of excitation. This paper presents the results of time-of-flight mass spectrometric studies of the subsequent metastable decomposition of these excited ions produced from a sample of bovine insulin which is a protein containing 51 amino acid residues and 777 atoms with a molecular weight of 5729.6 u for the ^{12}C containing monoisotopic component. The present work is an extension of our earlier investigations[1-6] of lower molecular weight compounds where we have demonstrated that a large proportion of the secondary ions ejected by massive particle bombardment (at both Mev and Kev energies) are highly excited and fragment extensively both promptly and metastably.

The experimental setup is shown in Figure 1.

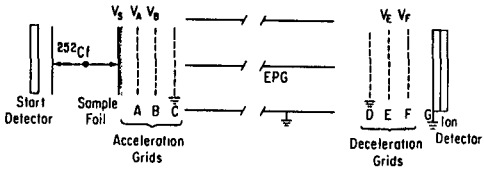

Figure 1

The results of two kinds of experiments are reported. In the first we investigated the integrated metastable fragmentation of ions throughout the whole length of the 3-meter long flight-tube. This corresponds to fragmentations of the molecular ions at times between 400ns and 170μs after ion formation. In these experiments we simply allow the ions to decay in flight and by the application of appropriate retardation potentials[1-3] to grids E and F at the end of the flight-tube, ion fragments with masses less than (retardation potential/acceleration potential)×precurser mass are reflected and thus are not detected.

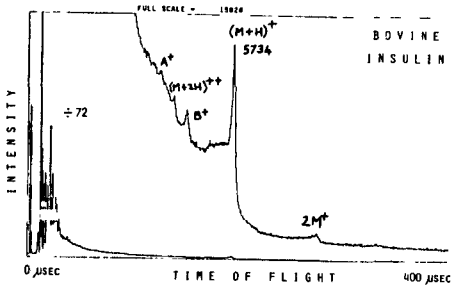

Figure 2

Figure 2 shows the time-of-flight spectrum of bovine insulin with the retardation potential = 0, i.e. no rejection of flight-tube metastables. This spectrum is a snapshot of the distribution of ions a few hundred nanoseconds after ion production. Fig. 3 shows a portion of the same spectral data where the intense continuum has been subtracted.
The 5 ions for which metastable fragmentation data was obtained are indicated. Fig. 4 shows the high mass region of the insulin spectrum where we observe, in addition to the monomer and dimer peaks, small peaks corresponding approximately in mass to the trimer at m/z 17200 and the tetramer at m/z 23000. To increase the detection effeciency for high MW species we coated the front face of the ion detector with a 500Å thick layer of CsI and

also postaccelerated the ions through 4 KV of potential at the end of the flight tube in additional to the initial 10 KV of acceleration potential.

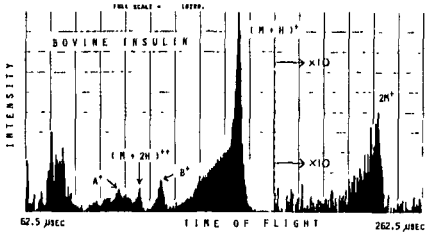

Figure 3

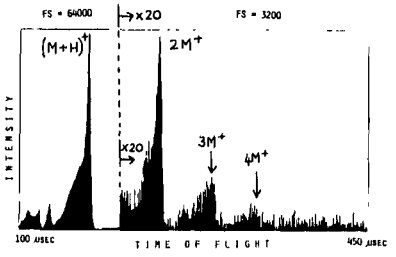

Figure 4

Fig. 5 shows the insulin spectrum taken with a series of different retardation potentials. It can clearly be seen that both the peaks and the continuum get smaller as we apply larger retardation potentials, corresponding to the rejection of increasing amounts of flight-tube fragments and that a high proportion of the ions that survive acceleration subsequently fragment in the flight-tube.

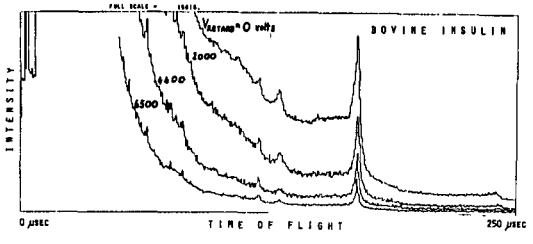

Figure 5

The data shown in Fig. 5 relates to the integrated fragmentation through the whole length of the flight-tube and thus does not yield information on the spatial or temporal distribution of fragmentations within the flight-tube. We thus performed a second set of experiments to investigate the fraction of fragmentations occurring after acceleration and during the first 1 cm of the 300 cm long flight tube. The experimental procedure utilizes appropriate potentials applied to grids A and B (Fig. 1) and is described in Ref. 3. The results indicate clearly that fragmentations are heavily weighted to favour early times and high rate constants.

1. B. T. Chait, F. H. Field, Int. J. Mass Spectrom. Ion Phys. 41 (1981) 17.
2. B. T. Chait, F. H. Field, J. Am. Chem. Soc. 104 (1982) 5157.
3. B. T. Chait, F. H. Field, J. Am. Chem. Soc. 106 (1984) 1931.
4. B. T. Chait, Int. J. Mass Spectrom. Ion Phys. 41 (1983) 227.
5. B. T. Chait, K. G. Standing, Int. J. Mass Spectrom. Ion Phys. 40 (1981) 185.
6. B. T. Chait, W. C. Agosta, F. H. Field, Int. J. Mass Spectom. Ion Phys. 39 (1981) 339.

CHARGE STRIPPING OF MONATOMIC IONS : DEPENDENCE OF CROSS-SECTION ON VARIOUS PARAMETERS OF THE COLLISION PARTNERS

M.Guilhaus, R.G.Kingston, A.G.Brenton and J.H.Beynon.
Royal Society Research Unit, University College of Swansea,
Singleton Park, Swansea SA2 8PP, U.K.

Charge stripping of ions or neutral species, i.e. the removal of one or more of their electrons, is an important reaction channel which is available to most such species involved in keV collisions with gas molecules. Analytical applications of charge stripping in mass spectrometry began to develop in the late sixties. Since that time the process has provided mass spectroscopists with a powerful tool for probing ion structure, determining double-ionization energies of organic molecules and for identifying long-lived electronic states of ions.[1] Little definitive work appears to have been performed on relative efficiencies or cross-sections for charge-stripping processes in mass spectrometry. The efficiency of the process has been observed to vary over a wide range and it has been suggested that this may be due to corresponding differences in Q, the energy defect for the process. This is in qualitative agreement with the adiabatic criterion of Massey which predicts that the cross section for a collisional process involving an electronic transition will maximise when the time required for the electronic transition is equal to the interaction time for the process [2] : $h/Q = a/v$. In this equation a represents the interaction distance and v is the ion velocity.

The aim of the present work is to examine systematically the variation of the efficiency of formation and detection of charge stripped ions as the energy defect, Q and the ion velocity are varied. Monatomic ions comprise the simplest species for such an investigation as their inelastic collisions involve changes only in electronic energy and the relative energies of excited electronic states of monatonic positive ions are very well defined from spectroscopic experiments. The ionization method of fast atom bombardment (FAB) has been chosen because it can be used to generate intense monatomic ion beams from inorganic salts.

Results were obtained with a VG-Analytical ZAB-2F mass spectrometer. The energy of the bombarding neutral argon beam was maintained at 8.0 ± 0.5 keV. The salts used to produce the cations of interest were :$CaCO_3$, $MgSO_4$, $CoSO_4$, CsCl, KCl and NaCl. The ions were selected to cover a range of values of Q from 11.9 eV (Ca^+) to 47.3 eV (Na^+). Monatomic ions produced in the FAB source were accelerated through 2, 4, 6 and 8 kV, mass selected by the magnet and interacted with the collision gas in a cell located at the focal point between the magnetic and electric sectors. The pressure in the 10 mm-length cell was adjusted to allow 80% transmission of the primary ion beam (this corresponded to a number density, in the cell, of 5×10^{14} cm^{-3} at the normal operating temperature of 330 K). The collision gases used were H_2, N_2, He, Ne and Ar. The product m^{2+} ions were energy analyzed by scanning the electric sector and the spectra were signal averaged. Each spectrum was checked to confirm that only the ground-state to ground-state process was being observed. The efficiency for the process was expressed as : $\eta = I_{2+}/I_+$ where I_+ and I_{2+} are the ion currents in the transmitted primary and product ion beams respectively.

Initially, the logarithm (base 10) of η was plotted against Q and v on three orthogonal axes for each collision gas. The values of η were found to decrease with increasing Q and decreasing v. However, the value of η for Cs, the heaviest and largest ion in the series, were found to be significantly higher than the values for adjacent ions. This irregularity was reduced when the 'sizes' of the ions were taken into account and the data were replotted against Q and vb where b is the ionic size from lattice measurements. A typical surface is depicted in Figure 1. The apparently smooth surfaces given by the η values allowed an empirical relationship to be fitted to them. A good fit is obtained up to $Q \simeq 30$ eV with a relationship having the form $\eta = Ce^{-(KQ)/(vb)}$. The values obtained for the constants C and K are given in Table 1. The physical significance of the constants cannot be interpreted without a clear understanding of what the measurement of η encompasses. η is not a direct assessment of the cross-section for the charge-stripping process. Detection systems give responses which depend on the types of ions monitored, (e.g. mass, velocity and charge of an impacting ion) and most mass spectrometers will accept only those ions scattered through angles less than certain critical angles. In the present work the most probable scattering angles have been calculated [3] for all combinations of collision parameters to predict a minimum of 0.5° for Ca^+ on H_2 at 8 kV and a maximum of 11.6° for Na^+ on Ar at 2 kV. The instrumental acceptance angles in z and y are, for our instrument, about 0.3° and 0.7° respectively. Therefore, only a small fraction of the product ions are collected.

The cross-section for the charge-stripping process would be expected to maximise according to Massey's adiabatic criterion. With most mass spectrometers the keV ion energy range does not allow a close approach to optimum conditions (in this work the ion velocity was at best only 10% of that predicted for maximum cross-section). Equations have been proposed to describe the fall-off of cross-section for collisional processes towards lower velocities. For example, Hasted has suggested an exponential decrease in efficiency for charge-exchange processes in which the energy defect is ΔE [4] $\sigma = Ae^{-(B\Delta E)/(hv)}$. In this equation A and B are constants, v is the ion velocity and h is Planck's constant. It is almost identical in form to the empirical relationship derived in our work and the agreement suggests that variations in detection and collection efficiencies contribute to pre-exponential and exponential terms in our empirical relationship. The deviation of the observed efficiency, at Q > 30 eV, from that predicted by the empirical relationship is probably a reflection of the extent to which Massey's adiabatic criterion is not satisfied, i.e. $\sigma/v \gg h/Q$.

Table 1 : Constants C and K determined for the relationship $\eta = Ce^{-KQ/vb}$ for each of the collision gases used in this study. [a,b].

Gas	$\log_{10}C$	K
He	-4.2 ± 0.1	$(3.0 \pm 0.2) \times 10^{-6}$
Ne	-3.0 ± 0.1	$(3.9 \pm 0.2) \times 10^{-6}$
Ar	-2.8 ± 0.1	$(5.3 \pm 0.5) \times 10^{-6}$
H_2	-2.9 ± 0.1	$(5.1 \pm 0.2) \times 10^{-6}$
N_2	0.3 ± 0.7	$(8 \pm 2) \times 10^{-6}$

[a] From results obtained with a gas number density of 5×10^{14} cm^{-3} in the 10 mm collision cell

[b] Q in units of eV; v in ms^{-1}; b in m.

References

1. K.Levsen and H.Schwarz, Mass Spectrom. Rev. 2, (1983) 77.
2. H.S.W.Massey, Rep.Prog.Phys. 12 (1949) 248.
3. R.K.Boyd, E.E.Kingston, A.G.Brenton and J.H.Beynon, Proc.R.Soc.Lond. A.392 (1984) 59.
4. J.B.Hasted, Physics of Atomic Collisions, 2nd Edition, American Elsevier, New York, 1972. p.624.

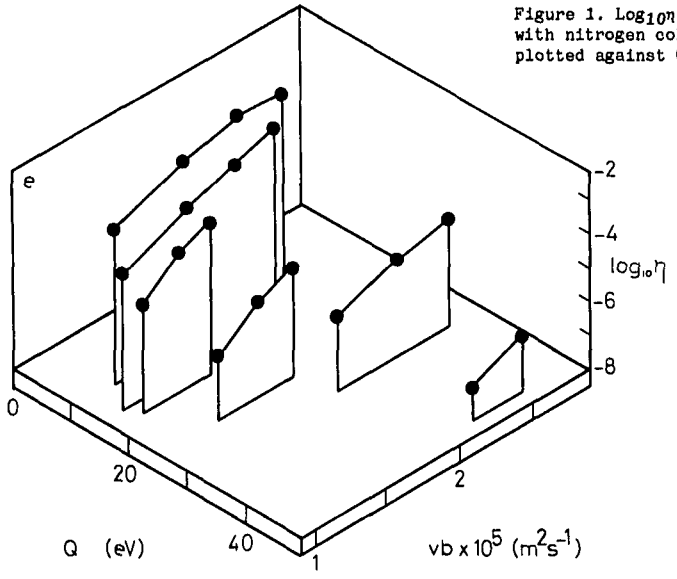

Figure 1. $\text{Log}_{10}\eta$ values obtained with nitrogen collision gas and plotted against Q and vb.

ULTRA SLOW METASTABLE ION DECOMPOSITIONS

C. Lifshitz, Y. Malinovich, R. Arakawa*, S. Gefen and G. Haase

Department of Physical Chemistry

The Hebrew University of Jerusalem, Jerusalem 91904, Israel

We have recently combined[1] a cylindrical ion trapping device (CIT) with photoionization mass spectrometry. The experiment enables determination of time-resolved photoionization efficiency (PIE) curves and breakdown curves from the microsecond to the millisecond range. Two systems were studied by us carefully recently: (1) The reaction $C_6H_5Br^{+\cdot} \rightarrow C_6H_5^{+} + Br\cdot$ in bromobenzene whose kinetics and dynamics are quite well understood from previous coincidence experiments and QET modelling[2] and (2) The reaction $C_6H_5OH^{+\cdot} \rightarrow C_5H_6^{+\cdot} + CO$ which has been the subject of considerable controversy.[3] Both reactions are predicted to have very low dissociation rate constants near threshold, $k_{Diss} \lesssim 1\ s^{-1}$. The question arises whether such slow dissociations are observable. Dunbar[4] has demonstrated that an upper limit on the lifetime of a metastable-ion decomposition is imposed by the competing relaxation of internal excitation by IR radiative cooling. This upper limit lies in the range of $\sim$15-60 s^{-1}.

Figure 1 represents two PIE curves for the $C_6H_5^{+}$ ion from bromobenzene at ion storage

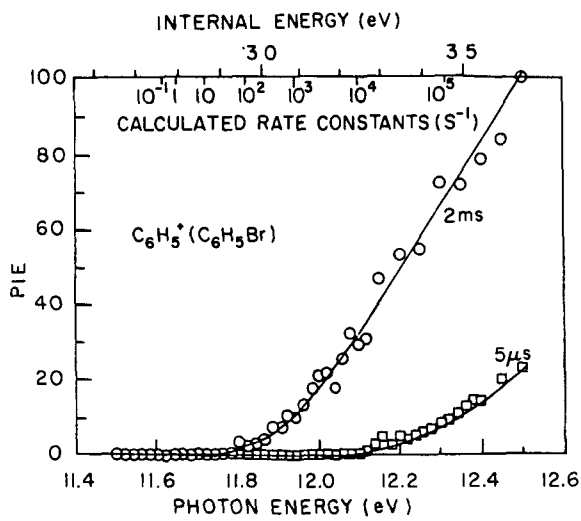

Figure 1: Time-resolved PIE curves for $C_6H_5^{+}$ from bromobenzene; the circles and rectangles are experimental, the smooth curves are QET calculations. The internal energy includes the average thermal energy.

times of 5 μs and 2 ms, respectively. The agreement between experiment and calculation is excellent. Dissociation of the phenol cation is observed at the predicted 298°K threshold, which is quite surprising, in view of the very low predicted rate coefficient at threshold (10^{-3} s^{-1}).[5]

Slow fragmentations are observable and are unperturbed by radiative decay if only low extents of overall (radiative and dissociative) decay of the metastable ion are allowed. Thus, the calculated breakdown curve for $C_6H_5^+(C_6H_5Br)$ at t = 2 ms remains almost unchanged with or without radiative decay. This is easily understood since the fractional abundance is:

$$Fr(C_6H_5^+) = \frac{k_{Diss}}{k_{Diss}+k_{Rad}} \times [1-e^{-(k_{Diss}+k_{Rad})t}]$$

$$\simeq \frac{k_{Diss}}{k_{Diss}+k_{Rad}} \times (k_{Diss}+k_{Rad})t = k_{Diss}\cdot t \simeq 1-e^{-k_{Diss}\cdot t}$$

At higher extents of decay, e.g., at t = 1 s, the calculated breakdown curves with and without radiative decay are quite different

We have demonstrated that appearance energies of daughter ions shift to lower values upon increasing storage time, as expected.[6] It remains for us to explore the limits of detection in terms of slow metastable ion decay.

* *Permanent address: Institute of Chemistry, College of General Education, Osaka University,* Osaka, Japan.

[1] C. Lifshitz, M. Goldenberg, Y. Malinovich and M. Peres, Org. Mass Spectrom. 17, 453 (1982).

[2] H.M. Rosenstock, R. Stockbauer and A.C. Parr, J. Chem. Phys. 73, 773 (1980).

[3] D.H. Russell, M.L. Gross and N.M.M. Nibbering, J. Am. Chem. Soc. 100, 6133 (1978); A. Maquestiau, R. Flammang, G.L. Glish, J.A. Laramée and R.G. Cooks, Org. Mass Spectrom. 15, 131 (1980).

[4] R.C. Dunbar, Int. J. Mass Spectrom. Ion Processes 54, 109 (1983).

[5] M.L. Fraser-Monteiro, L. Fraser-Monteiro, J. de Wit and T. Baer, J. Phys. Chem., in press.

[6] C. Lifshitz, Mass Spectrom. Rev. 1, 309 (1982).

A CROSSED BEAM STUDY OF THE COLLISION INDUCED DISSOCIATION OF CS_2^+

D. M. Hirst, K. R. Jennings, J. A. Laramee and A. K. Shukla

Department of Chemistry, University of Warwick,
Coventry, CV4 7AL, U.K.

CS_2^+ ions are produced by electron impact mass selected by a quadrupole mass spectrometer and focused by an electrostatic octopole lens to yield a beam with an angular spread of less than 2^o(FWHM). The ion beam is intersected at right angles by a beam of target molecules (usually a rare gas) from a differentially pumped effusive capillary array. The detector, which can be rotated about the crossing point, consists of a quadrupole mass spectrometer and a channeltron electron mulitplier operated in pulse counting mode.

In a series of experiments at zero scattering angle, the relative abundances of fragment ions CS^+ and S^+ were measured as functions of ion kinetic energy for target gases He, Ar, Kr, Xe. For low centre of mass energies S^+ is the dominant product but as the initial relative energy is increased the $[CS^+]/[S^+]$ ratio increases and at the higher energies CS^+ is the major product. Some of these results are shown in figure 1. The formation of S^+ is the least endothermic dissociation channel and these data are interpreted in terms of the vibrational excitation of CS_2^+ increasing with the centre of mass collision energy. This is in contrast with the results at high energies where helium is found to be the most effective rare gas target for promoting collision induced dissociation. Polyatomic targets are found to be less effective than monatomic targets for a given centre of mass energy.

The variation of the ratio of the relative abundances of S^+ and CS^+ with scattering angle, for a given ion kinetic energy, has been measured. For the heavier targets (Ar, Kr, Xe), the $[CS^+]/[S^+]$ ratio decreases as the angle increases. It is assumed that the amount of energy transferred to internal modes increases with increasing scattering angle. The increase in the relative abundance of S^+ with respect to that of CS^+ is interpreted in terms of a second dissociation channel leading to $S^+ + CS$ which is more endothermic than the lowest CS^+ channel. This is supported by measurements of the relative abundances as functions of ion energy taken at an angle of 25° (figure 2) in which S^+ becomes the dominant product at large energies.

In the case of the xenon target, the relative abundances of S^+ *and* CS^+ have been measured as functions of angle for a range of centre of mass collision energies from 26 to 37 eV. For a given value of the energy E_{CM}, the value of Θ_{CM} for which the ratio $[CS^+]/[S^+]$ equalled unity was determined and the product $E_{CM}\Theta_{CM}$ was found to be approximately constant over the range of energies considered.

FIGURE 1

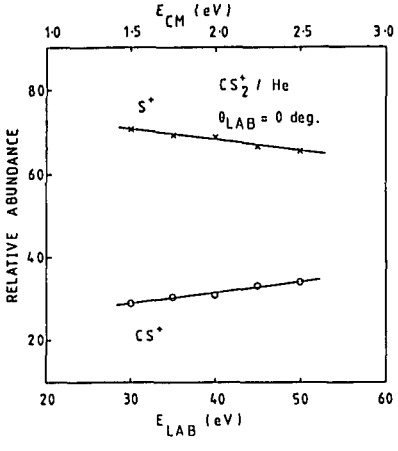

FIGURE 2

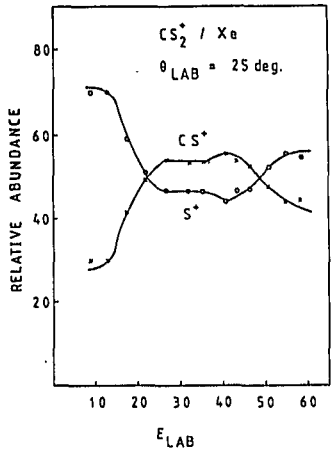

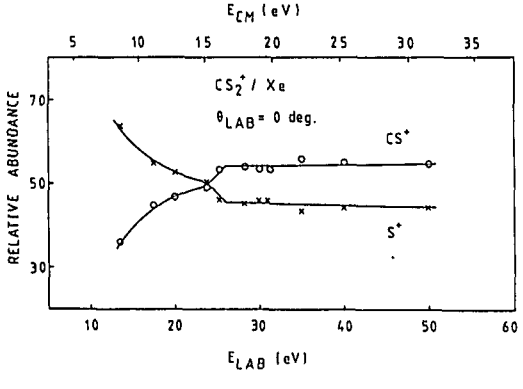

The Heat of Formation of $C_3H_2^+$

D. Smith and N.G. Adams
Department of Space Research,
University of Birmingham
Birmingham B15, 2TT, United Kingdom
E.E. Ferguson
Aeronomy Laboratory, NOAA, Boulder, CO 80303

In the case of slightly endothermic reactions, the temperature dependence of the reaction rate coefficient can be used to determine the endothermicity rather precisely. In the present case the binary reaction of C_3H^+ with H_2 was observed to produce $C_3H_2^+$ with an endothermicity of ~ 1 kcal mol^{-1}. This reaction is calculated to be ~25 kcal mol^{-1} endothermic using literature values of $\Delta Hf(C_3H^+)$ and $\Delta Hf(C_3H_2^+)$, implying a large error in one of these values. The present investigation was carried out to address this problem.

Experimental

The Birmingham selected ion flow tube (SIFT) experiment has been extensively used to study ion-molecule reactions and has been described in the literature[1,2]. Recently, a drift tube has been included in this SIFT thus converting it to a variable temperature selected ion flow drift tube (VT-SIFDT). The C_3H^+ ions were generated in an electron impact ion source from propyne (methyl acetylene) and injected into helium buffer gas. The reactant neutral H_2 was added to the helium carrier gas downstream from the reactant ion entry port, and the primary ion count rates were measured as a function of H_2 flow rate by a downstream mass spectrometer detection system. Rate coefficients were obtained in the usual manner.

Results

The reaction

$$C_3H^+ + H_2 \rightarrow C_3H_2^+ + H \qquad (1)$$

competed with a fast three-body association,

$$C_3H^+ + H_2 + He \rightarrow C_3H_3^+ + He \qquad (2)$$

At 80K, only reaction (2) is observed at zero E/N, but reaction (1) appears when a weak electric field is applied. At 300K reaction (1) is a minor channel and $k_2 = 2.6 \times 10^{-27}$ cm^6 s^{-1}. At 550K, the binary channel accounts for over half the reaction. From these data an endothermicity of ~ 1 kcal mol^{-1} is inferred. This in turn implies that $\Delta Hf(C_3H^+)-\Delta Hf(C_3H_2^+) = \Delta Hf(H)-1 = 51$ kcal mol^{-1}. However, the literature values for these heats of formation, give an average value $\Delta Hf(C_3H^+) - \Delta Hf(C_3H_2^+)$ of 29 kcal mol^{-1} with values ranging from 24 kcal mol^{-1} for allene to 30 kcal mol^{-1} for cyclopropene sources of both ions (from the NBS group[3]). Since the value $\Delta Hf(C_3H^+)$ is supported by theoretical calculations[4] as well as a recent C_3 proton affinity determination[5], we assume the error lies in the value of $\Delta Hf(C_3H_2^+)$ and accordingly deduce that the value of $\Delta Hf(C_3H_2^+) = 332$ kcal mol^{-1}, with the same uncertainty as applies to $\Delta Hf(C_3H^+)$ which seems to be about 5 kcal mol^{-1}. This uncertainty is large compared to the uncertainty in the endothermicity of reaction (1).

The stable form of C_3H^+ is the linear $HC{\equiv}C\text{-}C^+$ ion which lies 52.7 kcal mol^{-1} below an excited non-linear form[4]. In view of the fact that the results of the present studies of reactions (1) and (2) are the same for C_3H^+ ions produced by electron impact on propyne and via the reaction of C_3^+ with H_2, then it seems unlikely that the ions generated in the electron impact ion source are excited. The C_3H^+ ions were also produced from propyne in the NBS measurement[3] and it seems equally unlikely that these ions were excited.

In addition to rationalizing the occurrence of reaction (1), the lower value for $\Delta Hf(C_3H_2^+)$ also rationalizes another observation, namely the failure of the reaction

$$C_3H_2^+ + H_2 \rightarrow C_3H_3^+ + H \qquad (3)$$

to occur, $k_3 < 5 \times 10^{-14}$ cm^3 s^{-1} at 298K, in spite of the large exothermicity of the reaction. This is an exceptional circumstance, since a large number of exothermic ion reactions with H_2 occur very rapidly by H atom abstraction, essentially a reaction per collision. This includes[6] the ions Ar^+, Ar_2^+, CH^+, CH_2^+, CHN^+, CO^+, CO_2^+, C_2^+, C_2H^+, NH^+, O^+, OH^+, H_2O^+, N^+, and N_2^+. Exceptions to fast exothermic H atom abstraction from H_2 are rare if any. Presumably the problem here is essentially a steric one, the most stable form of $C_3H_3^+$ is the cyclic ring structure. Apparently the $C_3H_2^+$ ion does not abstract an H atom from H_2 and close the ring, even though this is exothermic. This does not seem too surprising if $C_3H_2^+$ is linear. However a linear form of $C_3H_3^+$ lies 24 kcal mol^{-1} above the stable ring form[7] (A theoretical value[3] for the energy difference between the ring and linear configurations of $C_3H_3^+$ is 34 kcal mol^{-1}). If $\Delta Hf(C_3H_2^+)$ were as high as 357 kcal mol^{-1}, reaction (3) to produce linear $C_3H_3^+$ would be exothermic by 24 kcal mol^{-1} and so it would be difficult to explain the lack of reactivity since the geometrical constraint would not apply. With the present value $\Delta Hf(C_3H_2^+)$ = 332 kcal mol^{-1}, reaction (3) to form linear $C_3H_3^+$ is 1 kcal mol^{-1} endothermic. Reaction (3) was also studied in the presence of a drift field. Only modest values of E/N were required to drive the reaction and an endothermicity of ~ 4 kcal mol^{-1} was deduced. Accordingly we recommend a value $\Delta Hf(C_3H_2^+)$ of 329 ± 5 kcal mol^{-1}. Since the 4 kcal mol^{-1} endothermicity of reaction (3) corresponds to the endothermicity to produce the linear propargyl ion, $CH_2C \equiv CH^+$ (ΔHf = 281 kcal mol^{-1}) this strongly implies that a linear $C_3H_2^+$ ion reacts with H_2 to form a linear $C_3H_3^+$ ion at threshold. There is therefore little doubt that the most stable form of $C_3H_2^+$ is linear. Detailed results are in press[9].

Curiously, the present value of $\Delta Hf(C_3H_2^+)$ leads to a precisely linear plot of $\Delta Hf(C_3H_n^+)$ vs n. If a similar plot of $\Delta Hf(C_3H_n^+)$ vs n were linear for the cyclic configuration, it would imply $\Delta Hf(C_3H_2^+) \approx 345$ kcal mol^{-1} for the cyclic $C_3H_2^+$ form.

References

1. N.G. Adams and D. Smith, Int. J. Mass Spectrom. Ion Phys., 21, (1970) 349.
2. D. Smith and N.G. Adams, in "Gas Phase Ion Chemistry", Vol. 1, ed. M.T. Bowers (New York: Academic Press), (1979) p. 1.
3. A.C. Parr, A.J. Jason and R. Stockbauer, Int. J. Mass Spectrom. Ion Phys., 33, (1980) 243.
4. K. Raghavachari, R.A. Whiteside, J.A. Pople and P.v.R. Schleyer, J. Am. Chem. Soc., 103, (1981) 5649.
5. A.B. Rakshit and D.K. Bohme, Int. J. Mass Spectrom. Ion Phys., 49, (1983) 275.
6. D.L. Albritton, Atomic Data and Nuclear Tables, 22, (1978) 1.
7. H.M. Rosenstock, K. Draxl, B.W. Steiner and J.T. Herron, J. Phys. and Chem. Ref. Data, 6, 1977 Supplement No. 1
8. L. Radom, P.C. Hariharan, J.A. Pople and P.v.R. Schleyer, J. Am. Chem. Soc., 98, (1976) 10.
9. D. Smith, N.G. Adams and E.E. Ferguson, Int. J. Mass Spectrom. Ion Processes (1984).

ENERGY BARRIERS FOR EXOTHERMIC ION/RADICAL RECOMBINATIONS

P.C. Burgers, Université Laval, Québec, P.Q. Canada
J.L. Holmes, University of Ottawa, Ontario, Canada
J.K. Terlouw, University of Utrecht, The Netherlands.

Unimolecular dissociations of molecules into pairs of radicals generally proceed such that the reverse exothermic radical/radical recombination does not require an activation energy(1). Similarly, the exothermic recombination of an ion and a free radical proceeds with zero or a very small activation energy(2): direct bond cleavage reactions are therefore often used to derive ionic heats of formation. We have generated in the gas phase 8 radical-cations which undergo a dissociation into an ion and a radical with a minimum energy requirement substantially above (c. 1eV) that calculated from the product enthalpies. These cations are: $HCOH^{+\cdot}$ (3), $CH_3COH^{+\cdot}$ (4), $HOCOH^{+\cdot}$ (3), $HOCOCH_3^{+\cdot}$ (4), $HCNH_2^{+\cdot}$ (5), $CH_2NH_3^{+\cdot}$ (6), $CH_3CHOH_2^{+\cdot}$ (7) and $CH_2O(H)CH_3^{+\cdot}$ (7). They were generated by appropriate dissociative ionisations and identified by their collisional activation (CA) mass spectra, appearance energy (AE) measurements and by their metastable ion characteristics. The above ions undergo a direct cleavage reaction in the micro second time frame (in some cases labelling experiments were necessary to establish that the unimolecular reaction is indeed a direct cleavage reaction); the structure of the daughter ions was determined by CA mass spectrometry. The AE (AEm) of these metastable peaks were measured by a comparative method(8) and they were found to be substantially greater than those calculated (AEc) from the known product and reactant enthalpies. The energy barriers for the reverse reactions (exothermic ion/radical recombinations) are given by AEm-AEc and are listed below. Note that the radical attacks the hetero atom; if the radical attacks the carbon atom the energy barrier is zero or small.

$H\overset{+}{C}O + H^{\cdot} \longrightarrow$	$HCOH^{+\cdot}$	1.1eV
$CH_3\overset{+}{C}O + H^{\cdot} \longrightarrow$	$CH_3COH^{+\cdot}$	1.35
$HOCO^{+} + H^{\cdot} \longrightarrow$	$HOCOH^{+\cdot}$	0.7
$HOCO^{+} + CH_3^{\cdot} \longrightarrow$	$HOCOCH_3^{+\cdot}$	1.0
$HCNH^{+} + H^{\cdot} \longrightarrow$	$HCNH_2^{+\cdot}$	1.5
$CH_2NH_2^{+} + H^{\cdot} \longrightarrow$	$CH_2NH_3^{+\cdot}$	0.95
$\overset{+}{C}H_2OH + CH_3^{\cdot} \longrightarrow$	$CH_2O(H)CH_3^{+\cdot}$	1.4
$CH_3\overset{+}{C}HOH + H^{\cdot} \longrightarrow$	$CH_3CHOH_2^{+\cdot}$	1.0

We propose that these observations reflect the different electron densities at the attacked sites, with low electron density giving rise to a low energy barrier. It thus appears that attack of a small radical at the C atom requires little or no energy wheeas reaction at the lone pair possessing heteroatom has a substantial energy requirement.

References:

1. P.J.Robinson and K.A.Holbrook, "Unimolecular reactions", Wiley-Interscience, London, 1972, p. 155.
2. R.G.Cooks, J.H.Beynon, R.M.Capriole and G.R. Lester, "Metastable ions", Elsevier, Amsterdam, 1973, p. 106.
3. C.Wesdemiotis and F.W.McLafferty, Tetrahedron Lett. 22, 3479,(1981).
P.C.Burgers, A.A.Mommers and J.L.Holmes, J.Am.Chem.Soc. 105, 5976,(1983).
4. J.K.Terlouw, J.Wezenberg, P.C.Burgers and J.L.Holmes, J.Chem.Soc. Chem.Commun.

(1983),1121.
5.P.C.Burgers, J.L.Holmes and J.K.Terlouw, J.Am.Chem.Soc., (1984), in press
6.J.L.Holmes, F.P.Lossing, J.K.Terlouw and P.C.Burgers, Can. J. Chem., 61, 2305,(1983)
7.P.C.Burgers, J.L.Holmes, J.K.Terlouw and B. van Baar, Org. Mass. Spectrom. (1984), in press.
8.P.C.Burgers and J.L.Holmes, Org. Mass Spectrom., 18, 123, (1982).

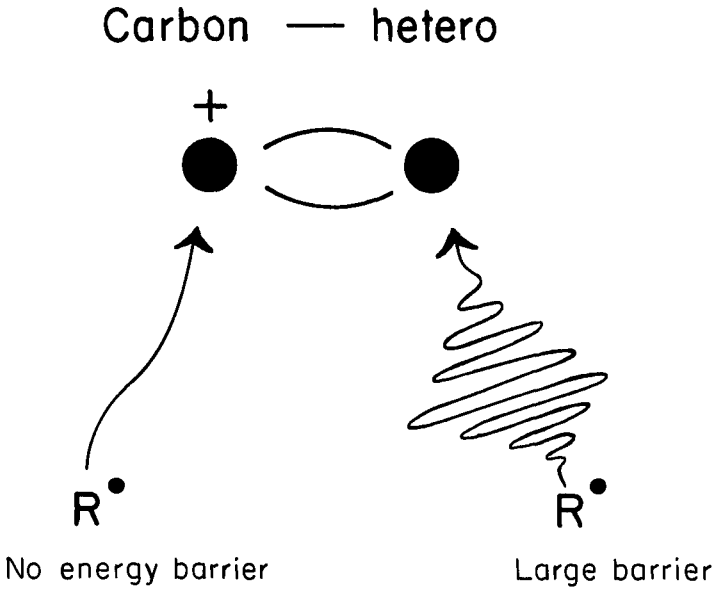

DISSOCIATION OF ENERGY SELECTED IONS
FORMED BY PHOTOIONIZATION OF "COLD" MOLECULES:
APPLICATION TO $C_4H_6^+$

Lewis M. Bass and Tomas Baer
University of North Carolina
Chapel Hill, North Carolina 27514

The $C_4H_6^+$ system was recently used as a test case for the application of the transition state switching model of statistical reaction rate theory[1]. The switching model is based on the premise that the rate determining point along the reaction coordinate may change from an orbiting transition state at low E (energy) and J (angular momentum) to a tight transition state at high E and J. Although the experimental data do not show any clear switching point from one rate determining transition state to the other, the predictions of the transition state switching model were found to be in reasonable agreement with the experimental data[2]. We are presently in the initial stages of a study aimed at obtaining more detailed experimental data on the $C_4H_6^+$ system in order to provide a more complete test of the transition state switching model.

The main thrust of this work is the incorporation of a supersonic nozzle into the standard PEPICO apparatus used for the determination of dissociation rates and breakdown diagrams. By cooling the neutral gas prior to photoionization the thermal spread of internal energy and angular momentum in the resulting ion can be reduced. Thus, each nominal ion internal energy (as determined from the photon energy and ionization potential) will correspond to a much narrower distribution of energy and angular momentum than in the previous experiments. Preliminary results, obtained using a jet of pure C_4H_6 (1,3-butadiene) at nozzle pressures of 50 - 400 Torr, show a small shift (ca. 25 meV) in the k(E) vs E curve measured with the jet as compared with that obtained using thermal C_4H_6, but there is no change in the shape of the curve. Although the translational temperature of the jet is roughly 20 K (as estimated from the width of the parent ion TOF peak), it is likely that rotational and vibrational cooling is much less efficient than translational cooling in a beam of pure butadiene. The next stage of this work will involve the use of various inert carrier gases to optimize the rotational and vibrational cooling. In this case we would expect to see a more substantial change in the k(E) vs E curve.

A second point of concern in comparing theory and experiment is that the PEPICO TOF mass analysis does not have sufficient resolution to distinguish the $C_4H_5^+$ fragment ion from the $C_4H_6^+$ parent ion. Thus, breakdown graphs have been reported previously by treating the sum of the $C_4H_5^+$ and $C_4H_6^+$ intensities as a single channel[2]. In the present work the TOF scale has been expanded in the region of these two peaks and simple Gaussian functions have been used to deconvolute the contributions from the separate ions.

With the help of this deconvolution procedure it is possible to construct a breakdown diagram comparing the parent ion intensity with the total fragment ion intensity. The crossover point in this case represents the energy at which 50% of the $C_4H_6^+$ ions are formed with energy above the appearance potential for the lowest energy fragmentation path. Comparison of this energy with the observed appearance potential can provide information about the width of the thermal energy spread in the neutral precursor prior to ionization. Hence, this approach may prove useful in comparing the neutral internal energy spread for the supersonic beam with that for thermalized molecules.

---

[1] M.F.Jarrold, L.M.Bass, P.R.Kemper, P.A.M.van Koppen and M.T.Bowers, J. Chem. Phys., 78, 3756 (1983).

[2] A.S.Werner and T.Baer, J. Chem. Phys., 62, 2900 (1975).

POSITIVE ION AND ELECTRON CAPTURE NEGATIVE ION CHEMICAL IONIZATION MASS SPECTROMETRY OF CHLORINATED PHENOXYANISOLES AND BENZENES

J.-A. B. Campbell, D. A. Griffin and M. L. Deinzer
Dept. of Agricultural Chemistry, Oregon State University, Corvallis, OR 97331

P. K. Freeman
Dept. of Chemistry, Oregon State University, Corvallis, OR 97331

Polychlorophenoxyphenols with three to nine chlorine atoms were examined as their methyl ethers by electron capture negative ion chemical ionization and positive ion mass spectrometry. Utilization of positive and negative chemical ionization in conjunction with electron impact provides substantial structural information about these compounds.

Loss of hydrogen chloride $[M-36]^-$ by some polychlorophenoxyanisoles to form methoxypolychlorodibenzofuran anions indicates the presence of at least one hydrogen atom ortho to the phenoxy linkage in one ring and at least one chlorine atom ortho to the phenoxy linkage in the other ring. However, some polychlorophenoxyanisoles, fitting these criteria, show no apparent $[M-36]^-$ but instead show an $[M-36-15]^-$. This is consistent with previous observations (1) that opportunity for formation of a resonance stabilized ion of type A would preclude appearance of an intense $[M-36]^-$ in the spectrum. These fragmentations are useful in distinguishing between some polychlorinated 2- or 4-phenoxyanisoles which would give semi-resonance stabilized ions of type B and, thus, an intense precursor $[M-36]^-$ ion, and the polychlorinated 3-phenoxyanisole which would not show an $[M-36]^-$ but go directly to product ion A.

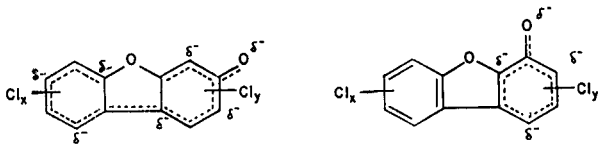

A B

The 2 and 4 isomers may be distinguished further under electron capture negative ion chemical ionization mass spectrometry. Methylated polychloro-2-phenoxyphenols lose chlorinated phenol, through an interannular hydrogen atom transfer to the departing phenoxide radical leaving a methylene derivative of a radical anion. Analysis of deuteriomethyl o-chloroanisoles has confirmed that the hydrogen atom source is the methyl group (2).

In view of the limited methodology available for halogen positional isomer identification by mass spectrometry in the chloroaromatic series, we elected to investigate some theoretical aspects of fragmentation by electron capture negative ion chemical ionization. The log ratios of the intensities of the peaks arising from chloride ion and $[P-35]^-$ versus the sum of the polarity constants $[\Sigma_\sigma = a\Sigma_o + b\Sigma_m + c\Sigma_p]$ were found to be linearly related with $r^2 = 0.977$ (Fig. 1). A Hammett sigma-rho relationship of this type suggests that substituent group effects on fragment ion intensities may be useful in locating halogen atom positions in a given series of haloaromatics.

While electron capture negative ion chemical ionization spectra of polychlorophenoxyanisoles show relatively little sensitivity towards the reagent gas used with respect to fragmentation, positive ion chemical ionization spectra show evidence of charge exchange in nitrogen, argon and helium and produce spectra essentially the same as observed in electron impact. Ionization takes place, resulting in typical positive ion CI spectra in methane and ammonia, while hydrogen as reagent gas gives spectra characteristic of both processes. Under methane and ammonia CI conditions, ion molecule reactions may take place. Chlorinated phenoxonium ions, possibly formed from charge stripping of chlorinated phenoxide anions, are observed particularly with hydrogen as reagent gas and these ions allow determination of the chlorine atom distribution between the rings in the positive ion mode.

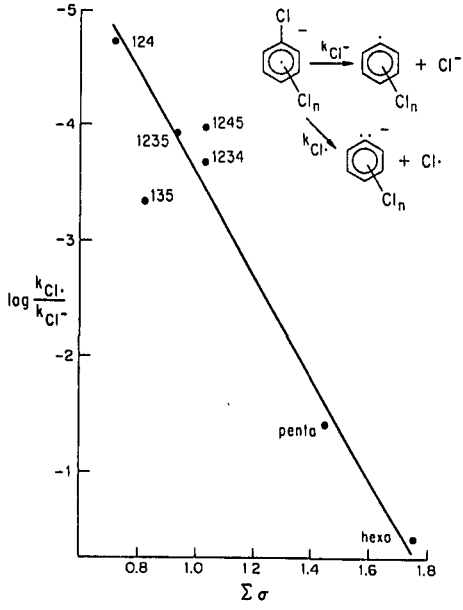

Fig. 1. Correlation of log $[P\text{-}Cl]^-/[Cl]^-$ from electron capture negative ion chemical ionization spectra of chlorinated benzene with σ substituent constants.

1. Deinzer, M., Griffin, D., Miller, T., Lamberton, J., Freeman, P. and Jonas, V. Biomed. Mass Spectrom. 9, 85, (1982).

2. Busch, K. L., Hass, J. R. and Bursey, M. M. Org. Mass Spectrom. 13, 604, (1978).

Acknowledgement

This work was supported by NIEHS grants ES-00040 and ES-00210.

THE ROLE OF NCI-MS IN THE DETERMINATION OF CHLORDANE AND TOXAPHENE IN GREAT LAKES SPORT FISH.

H.A. Price, R.H. Scheel, R.L. Welch, Center for Environmental Health Sciences, Michigan Department of Public Health, Lansing, Michigan 48909

Michigan Department of Public Health was awarded an EPA-TSCA grant to develop a risk assessment protocol for evaluating chemical exposure situations. This protocol included various stages such as identification of the problem, determination of exposure, evaluation of toxicity and, if necessary, removal of exposure. As an extension of this grant, we elected to test a part of this protocol by studying chlordane and toxaphene contamination of Great Lakes sport fish and by determining risk level of people who consume these fish.

Toxaphene is used as a broad-spectrum pesticide and is one of the most extensively used insecticides in the United States. Toxaphene is also an extremely effective pisicide and became of some concern to the U.S. Fish and Wildlife Service in 1973 with respect to Great Lakes fish.[1] Chlordane has been used in the past as a broad-spectrum insecticide but now is regulated for use mainly as a termiticide.

Although gas chromatography with electron capture detection (GC-ECD) is used for the quantitative determinations of chlordane and toxaphene in fish and human blood serum extracts, gas chromatography/mass spectrometry (GC/MS) is used to confirm the presence or absence of these contaminants. Standards of chlordane and toxaphene in iso-octane are easily detected by GC/MS using positive ion chemical ionization (PCI) with iso-butane as the reagent gas. However, at the concentration levels that are anticipated, detection of these compounds in fish and blood serum extracts by GC/PCI-MS is virtually impossible due to the sample matrix effects (See figure 1). This problem has been eliminated by the use of negative ion chemical ionization (NCI) MS with methane as the reagent gas. With GC/NCI-MS, interference from the sample matrix does not appear to be a problem with the detection of chlordane and toxaphene, even at the lower limits of detection (1 ppb for blood sera and 20 ppb for fish.) Figure 2 is an example of a fish extract (lake trout from southern Lake Michigan) done by GC/NCI-MS.

Chlordane (technical grade) is a mixture of chlordane itself, oxychlordane, nonachlor as well as other chlorinated methano-indane species. Toxaphene is made up of a complex mixture of chlorinated camphenes. Figures 3 and 4 show the NCI mass spectra for chlordane and for one of the chromatographic peaks for toxaphene, respectively.

It has been observed that for chlordane, as well as for all of the various chlorinated methano-indane compounds studied, a parent molecular anion (odd electron anion resulting from a resonance capture ionization mechanism[2]) is produced with very little, if any, fragmentation. Toxaphene on the other hand appears to undergo dissociative reasonance capture ionization to produce an $(M-Cl)^-$ ion (even electron anion) species. Because of the difference in anion formation, it is easy to distinguish between the two different compound types in a mixture based on their NCI mass spectra.

From our present work, we have concluded that negative ion chemical ionization is a necessary instrumental tool for confirming the presence of chlordane and toxaphene in biological samples.

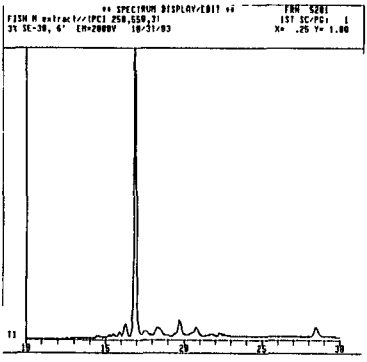

Figure 1. PCI-TIC chromatogram for fish extract.

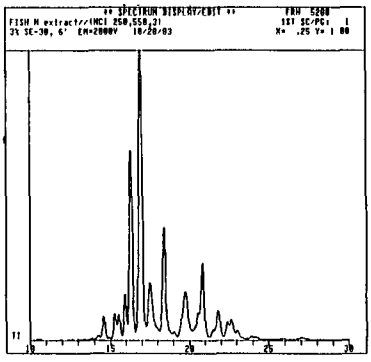

Figure 2. NCI-TIC chromatogram for fish extract.

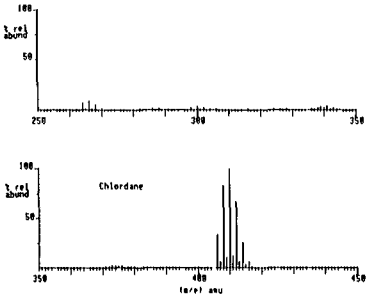

Figure 3. NCI mass spectrum for chlordane.

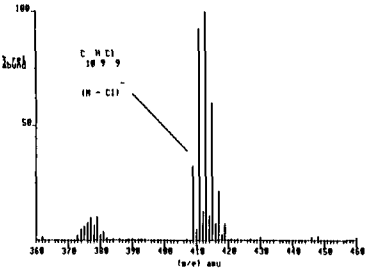

Figure 4. NCI mass spectrum for a component of toxaphene.

Acknowledgment This work was supported by an EPA-TSCA Grant No. CS807912010

Reference

1. M.A. Ribick, G.R. Dubay, J.D. Petty, D.L. Stalling, and C.J. Schmitt; Environ. Sci. Technol. 1982, 16: 310-318

2. M.A. Saleh; J. Agric. Food Chem. 1983, 31: 748-751

BETTER NCI MASS SPECTRA OF HEXACHLOROCYCLOPENTADIENE - BASED PESTICIDES

Elizabeth A. Stemmler and Ronald A. Hites
School of Public and Environmental Affairs
and Department of Chemistry
Indiana University
Bloomington, IN 47405

The electron capture, negative ion mass spectra of twenty polychlorinated pesticides derived from hexachlorocyclopentadiene have been examined using methane reagent gas. The spectra consist of molecular ions, $[M+H-Cl]^-$ ions, and fragment ions including a series of ions with the general formula $[C_{10}Cl_{8-x}H_x]^-$ which were observed for compounds with a ten carbon structure (see Figure 1). The ion source temperature affects the relative intensities of the ions. Lower temperatures enhance molecular ion formation while the relative intensity of fragment ions increases with increasing temperature.

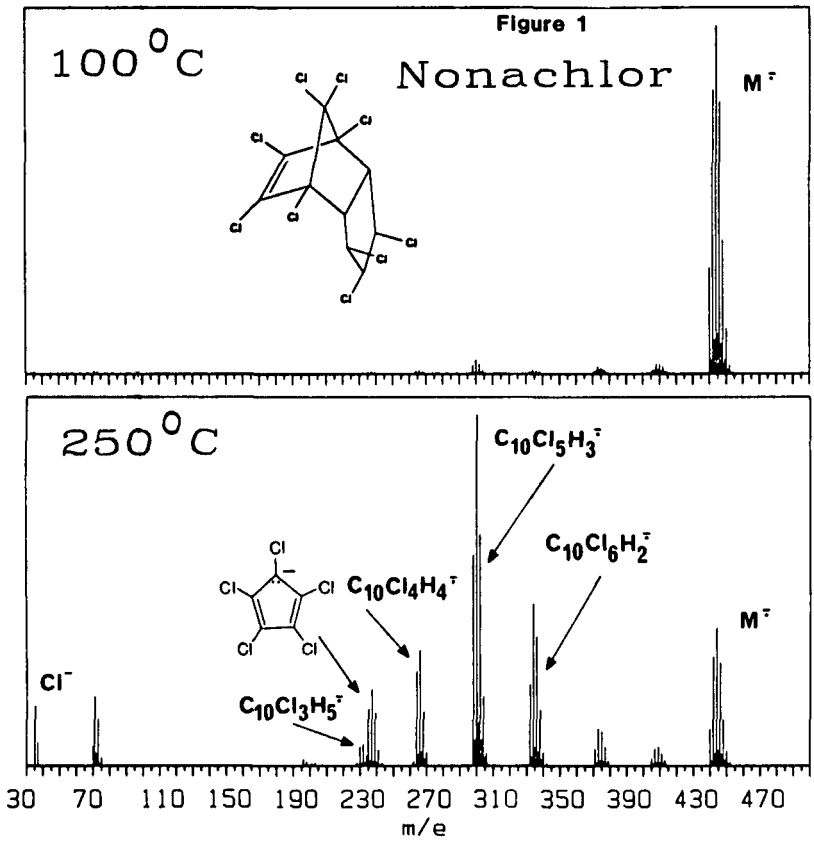

Our spectra differ from the spectra of these compounds which had previously appeared in the literature [R. C. Dougherty, J. Dalton, and F. J. Biros, Org. Mass Spectrom. 6, 1171 (1972)]. In contrast with the spectra we observe, the previous spectra were dominated by $[M+Cl]^-$ ions. It was found that, in our system, sample concentration affects the

relative abundance of $[M+Cl]^-$ and M^- ions. As saturation of the molecular ion current is approached with larger sample concentrations (see Figure 2) adduct ion formation becomes increasingly favored (see Figure 3), possibly because an increasing larger percentage of the sample is available for ionization via chloride attachment. The electron attachment spectra are interpretively useful and favored when working with the low sample concentrations encountered with capillary column GCMS.

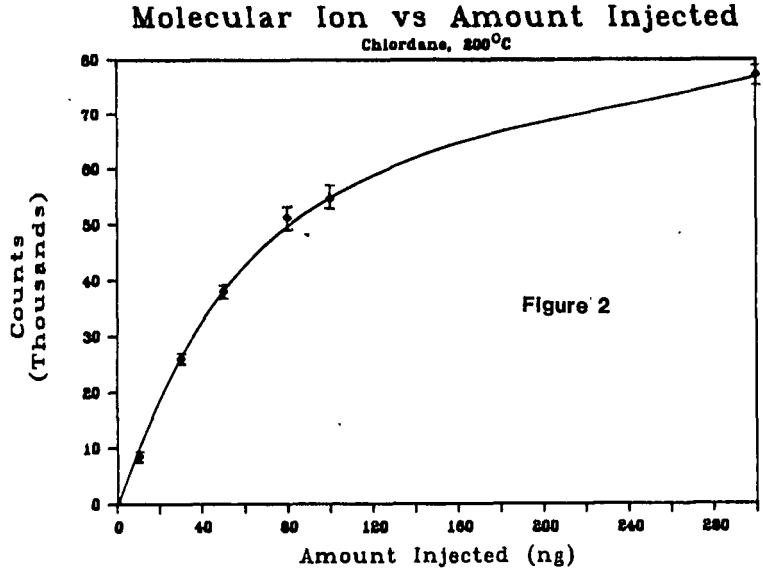

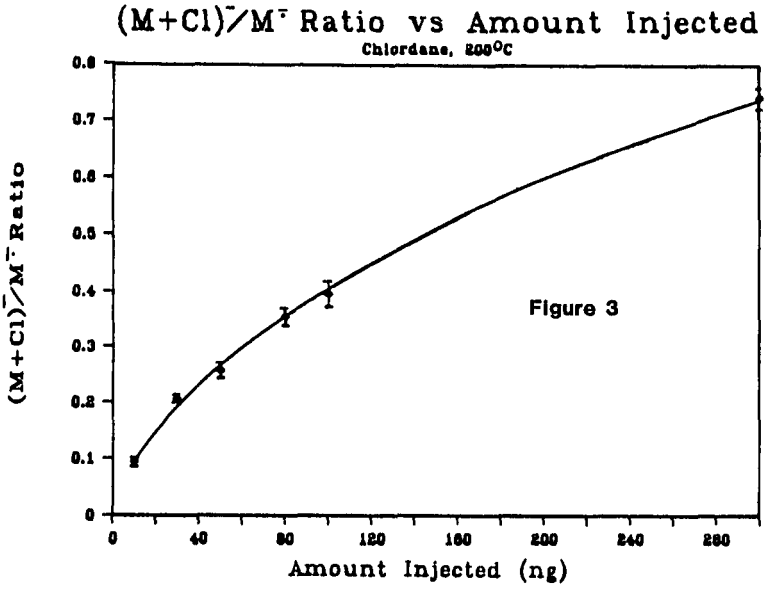

Evaluation of Negative Ion Chemical Ionization with Capillary Column Gas Chromatography/Low Resolution Mass Spectrometry for the Analysis of Chlorinated Dibenzodioxins, Furans, and Related Compounds

by

William L. Budde, and James W. Eichelberger

U. S. Environmental Protection Agency
Office of Research and Development
Cincinnati, Ohio 45268

Between 1984 and 1987 the USEPA will collect 10,000 - 20,000 samples for measurements of 2,3,7,8-tetrachlorodibenzodioxin (2378-TCDD) and related compounds. Most samples will be extracted with an organic solvent and the extracts will be analyzed using high resolution gas chromatography (HRGC), either low or high resolution mass spectrometry (LRMS or HRMS), electron impact (EI) ionization, and selected ion monitoring (SIM) data acquisition. This usually works well, but those ubiquitous environmental contaminants, the polychlorinated biphenyl mixtures, are potential interferences in all these analyses. For example, several heptachlorobiphenyl isomers coelute from the capillary column with 2378-TCDD. A pentachlorobiphenyl fragment ion and the 2378-TCDD M+ ion form an 80 ppm doublet at m/e = 322. Since the 322 ion is widely used for selected ion monitoring measurements of 2378-TCDD, the potential for interference in low and high resolution mass spectrometry is clear.

Several approaches are either routinely used or have been suggested to resolve this problem:

- Extensive sample preparation (clean-up)
- Better gas chromatography
- Higher resolution mass spectrometry
- Tandem mass spectrometry
- Other ionization modes

Methane negative chemical ionization (MNCI) has the advantage of producing fewer chlorinated biphenyl fragment ions. Another advantage is that it is available at relatively low cost on a larger number of low resolution gas chromatography/mass spectrometry systems. Responses of a number of compounds in the positive ion EI and MNCI modes were measured. The conclusion was that MNCI is about 20% as responsive as positive ion EI for 2378-TCDD. However for other chlorinated dioxins, furans, chlorinated biphenyls, diphenyl ethers, and related compounds, MNCI gave the superior response.

ISOMERIC DISTINCTION OF DERIVATIZED AMINOANTHRACENES AND AMINOPHENANTHRENES BY NEGATIVE CHEMICAL IONIZATION MASS SPECTROMETRY

L.J. Sears, J.A. Campbell and E.P. Grimsrud
Department of Chemistry, Montana State, University, Bozeman, Montana 59717

In the trace analysis of environmentally important organic compounds, it is often necessary to be able to distinguish between positional isomers. This is especially true when the position of a substituent is important in the determination of carcinogenic or physicological activity. The amines of anthracene and phenanthrene provide a challenging group of structrally similar isomers for study due to their mutagenic activity, and their presence in the environment as a result of coal related processes.[1]

Previous work with these compounds utilized trifluoroacetic anhydride (TFAA) derivatization of the amines[2] in order to increase their response in analysis by gas chromatography with electron capture detection. Also, oxygen doping of the electron capture detector has been shown to provide response enhancements which are indicative of the individual isomers. In this report analysis by negative chemical ionization (NCI) mass spectrometry of the TFAA-derivatized amines of anthracene and phenanthrene are reported. The spectra were obtained with a VG 7070 double-focusing mass spectrometer with sample introduction by packed and capillary column gas chromatography. GC conditions were intentionally adjusted so that the isomer under study is delivered to the ion source in a broad peak of at least 30 seconds so that numerous spectra at many instantaneous analyte concentrations could be recorded. In each case the total amount of analyte injected was about 10 ng.

Table 1. NCI/Methane Source Temperature 260°C

Derivative	m/z 113	203	269	271	273	289	303
	Percent Height of the Base Peak						
1-Aminoanthracene	1.9	2.6	2.8	–	23.7	100	3.3
2-Aminoanthracene	2.7	25.4	23.6	–	45.9	100	4.1
9-Aminoanthracene	22.6	7.2	9.2	–	55.0	100	36.6
1-Aminophenanthrene	2.6	2.5	20.1	–	100	12.1	2.4
2-Aminophenanthrene	3.4	1.2	72.8	–	100	20.6	2.9
3-Aminophenanthrene	3.0	1.0	56.5	–	100	16.2	2.3
4-Aminophenanthrene	1.2	–	10.0	100	95.6	4.8	5.7
9-Aminophenanthrene	–	1.2	4.7	–	100	4.1	1.8
Composition	$C_2H_2ONF_3$	$C_{15}H_9N$	$C_{16}H_9ONF_2$	$C_{16}H_8NF_3$	$C_{16}H_{10}NF_3$	$C_{16}H_{10}ONF_3$	$C_{17}H_{12}ONF_3$
Origin	$M-C_{14}H_8$	$M-CHOF_3$	M-HF	$M-H_2O$	M-O	M	$M+CH_2$

The intensities of the major ions observed in the NCI/CH_4 spectrum of each isomer are shown in Table I. All assignments of origin indicated in this table were confirmed by accurate mass measurements to within ±2 millimass units of the known values. The spectra indicates that in addition to simple electron capture to form the ion at m/e = 289, other, more complex, processes are occuring which result in unexpected ions. For example, the loss of oxygen atom to formthe ion at m/e = 273 is very favorable for all of the isomers, yet might not have been expected from these molecules in which the oxygen is doubly bonded to carbon. Also, the ion at m/e = 303 is due to the addition of CH_2 to the parent negative ion. Others[4] have also reported this adduct ion to be prominent in the NCI of polycyclic aromatic hydrocarbons and suggest that reactive species such as CH_2 and C_2H_4 are continuously formed in CI ion sources presumably by the interaction of the electron beam with methane. Perhaps the ion corresponding to $(M-O)^-$ is formed first by attachment of CH_2 on the carbonyl oxygen of an M^- species followed by rupture of the skeletal carbon-to-oxygen bond. While it is interesting to speculate on the origin of these and the other ions observed, we will instead turn our attention to the question of whether or not these spectra are dependent on isomeric differences.

Upon first consideration, the spectra in Table I suggest that NCI is indeed useful for the distinction of these isomers. In each case a unique ratio of ion intensities appears to exist which distinguishes it from all the others. The anthracenes are clearly indicated by an M^- base peak and the phenanthrenes by their dominant $(M-O)^-$ peak. Within the anthracene and phenanthrene groups other distinguishing features appear to allow individual distinctions. For some isomers a single ion suggests its presence: for examples, m/e = 113 and 303 for 9-aminoanthracene, m/e = 203 for 2-aminoanthracene and m/e = 271 for 4-aminoanthracene.

Upon closer inspection of the NCI spectra recorded for all isomers, a potential problem is noted which must temper some of the optimistic conclusions suggested by the data in Table I. That is, we have observed the NCI spectra to be somewhat dependent on the instantaineous concentration of analyte in the source. This point is illustrated for one of the isomers in Figure 1 where the normalized intensities of the major ions of the 3-aminophenanthrene derivative are recorded throughout the elution of this isomer from the GC column. The fact that these single-ion reconstructed chromatograms are not precisely superimposed on one another indicates that the relative production rates of the ions shown vary with the instantaneous analyte concentration in the source. All isomers under NCI/CH_4 conditions exhibited a similar degree of concentration dependence. Similar experiments using sample ionization by electron impact and by positive ion CI did not exhibit such concentration dependence. Recalling the discussion above of the unusual ions observed and NCI mechanisms which must be operative here, it is perhaps not entirely surprising that a concentration dependence of the NCI spectra of these compounds is observed.

Figure 1. Reconstructed single-ion chromatograms for NCI/CH_4 mass spectra of the TFAA derivative of 3-aminophenanthrene. Each ion signal is normalized relative to its point of greatest intensity.

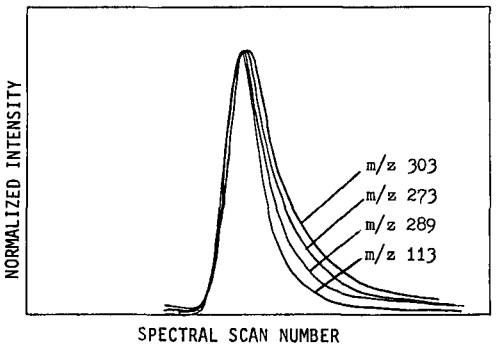

We have also recorded the NCI/CH_4-N_2O spectra of these compounds. As expected of the OH^- reagent ion which is then present, an intense $(M-1)^-$ ion is also observed along with several other ions previously noted in pure CH_4. Again, the spectra varied strongly with isomeric changes, but was again observed to be dependent on analyte concentration.

In an attempt to eliminate any unusual source chemistry associated with methane, nitrogen was also used as the moderating gas. The spectrum produced by use of nitrogen was considerably different than that of methane, but was even more dependent upon the concentration of analyte. Mass 302, having an origin of $(M-H+N)^-$, was then prominent for all eight isomers. Since no N^- or N_2^- ions were observed in the CI plasma, the presence of reactive nitrogen species appears to be indicated. Additional prominent ions were m/e = 178, $(M+N-C_7H_3F_2)^-$; m/e = 204, $(M+N-C_9H_5F_2)^-$; and m/e = 269, $(M-HF)^-$; all which varied considerably with respect to each other with changes in concentration.

In summary, this study indicates that NCI mass spectrometry offers considerable potential for the identification of substitution isomers. However, in our hands, at least, a serious problem has been noted: the ratio of intensities within a given spectrum are somewhat dependent on analyte concentration.

1. B.W. Wilson, R.A. Pelroy and J.T. Cresto, Mutat. Res., 79 (1980) 193.
2. D.W. Later, M.L. Lee and B.W. Wilson, Anal. Chem., 54, (1982) 117.
3. J.A. Campbell, E.P. Grimsrud and L.R. Hageman, Anal. Chem., 55 (1983) 1355.
4. D. Stockly and H. Budzikilewicz, Org. Mass. Spec., 17, (1982) 376.

MEASUREMENT OF TOXIC ORGANIC COMPOUNDS IN ENVIRONMENTAL SAMPLES USING NEGATIVE ION CHEMICAL IONIZATION MASS SPECTROMETRY

L. R. Hilpert and G. D. Byrd, Center for Analytical Chemistry, National Bureau of Standards, Washington, DC 20234

Negative ion chemical ionization (NICI) mass spectra can be obtained from certain organic compounds by resonance capture of thermal electrons if the molecules have positive electron affinities and if the internal energy of the molecular anion is less than the electron affinity of the neutral species. Usually, the major species formed is the molecular anion, $M^{-}\cdot$, which often yields relatively large ion currents and little fragmentation. The selectivity of NICI over electron impact (EI) has been well established, and this feature has permitted NICI to have wide applications over the past few years in the analysis of compounds such as polychlorinated biphenyls, dioxins, pesticides, and nitrated polycyclic aromatic hydrocarbons.

We have used NICI mass spectrometry as a sensitive and selective technique for the quantitative determination of several polycyclic aromatic hydrocarbons (PAH) in a sample of petroleum crude oil which is being certified as a Standard Reference Material (SRM). During the course of preliminary studies, we have confirmed the large degree of selectivity for the detection of benzo[a]pyrene (BaP) over benzo[e]pyrene (BeP) noted by others. We have observed the molecular anion of BaP to be more than 1000 times more abundant than that of BeP under selected source conditions in the NICI mode using methane as the reagent gas. Our observations, reported here, show that the ion source pressure and temperature play an important role in the selectivity of detection for BaP. We have also observed excellent absolute sensitivity for the detection of BaP and are able to detect quantities as low as 1 picogram in the selected ion monitoring mode.

The variation in the selectivity of detection of BaP and BeP was measured as a function of both the ion source pressure and the ion source temperature. In the first series of experiments, a solution of BaP and BeP was analyzed in the NICI mode over a range of ion source manifold pressures from 0.8 to 8.0×10^{-4} Torr (corresponding to a range of ion source pressures from 0.2 to 1.3 Torr) at a constant source temperature of 200 °C. The molecular anions (m/z 252) for BaP and BeP were monitored as a function of pressure and the results of these experiments are illustrated in Figure 1. The selectivity of detection, defined as (peak area BaP/ng BaP)/(peak area BeP/ng BeP), decreases by an order of magnitude in going from low to high pressure. The absolute sensitivity for the detection of BaP was also measured as a function of the ion source pressure and is shown in Figure 1b.

The variation in the selectivity of BaP to BeP in NICI was measured as a function of the ion source temperature at a constant ion source manifold pressure of 3.0×10^{-4} Torr. The results of these experiments are shown in Figure 2. The selectivity of detection for BaP (as defined above) is a maximum at a source temperature of 200 °C. The absolute sensitivity for the detection of BaP is maximized at a lower source temperature of 150 °C as shown in Figure 2b.

Gas chromatography/mass spectrometry using methane negative ion chemical ionization was used for the determination of BaP, indeno[1,2,3-cd]pyrene, and benzo[ghi]perylene in a sample of petroleum crude oil as part of the process of certifying the material as a Standard Reference Material. Figure 3 shows the selected ion monitoring analysis of the petroleum crude oil using EI, PICI, and NICI techniques. The low concentration of BaP in the oil and the presence of co-eluting interferences made accurate quantitation using EI or PICI techniques difficult.

Quantitation of BaP in the NICI mode, Figure 3C, was facilitated by the selectivity of detection for BaP. The BaP peak was free of interferences and was easily integrated, as was the BaP-d_{12} internal standard shown by the single ion record at m/z 264. Note that there was essentially no signal observed for BeP which was present at approximately three times the BaP concentration.

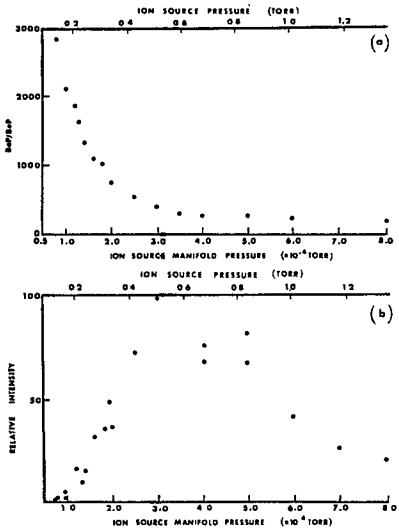

Figure 1

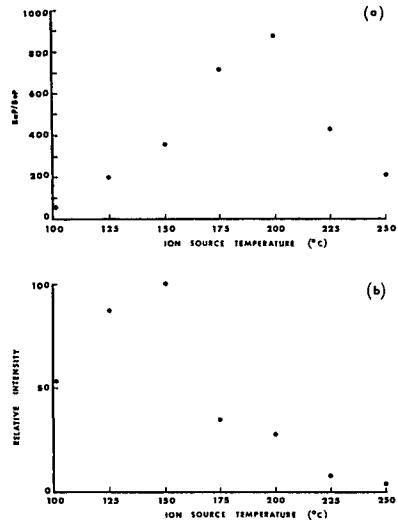

Figure 2

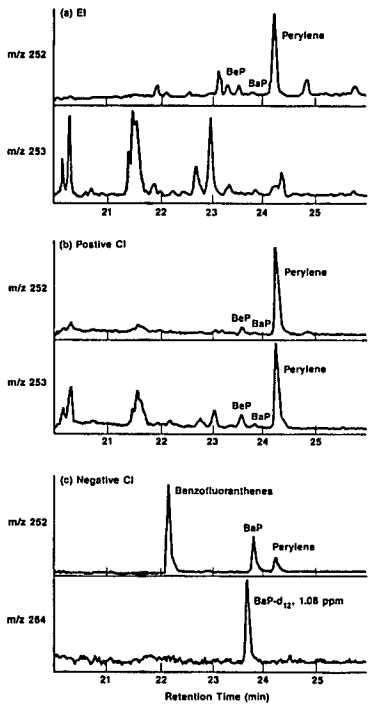

Figure 3

FIGURE CAPTIONS

Figure 1 (Upper Left): Variation of (a) selectivity of BaP to BeP and (b) sensitivity of detection of BaP as a function of ion source pressure.

Figure 2 (Upper Right): Variation of (a) selectivity of BaP to BeP and (b) sensitivity of detection of BaP as a function of ion source temperature.

Figure 3 (Left): Single ion records for GC/MS analysis of Wilmington crude oil sample using (a) electron impact, (b) positive ion chemical ionization, and (c) negative ion chemical ionization.

THE RESPONSE OF ANTHRACENE IN THE ELECTRON CAPTURE DETECTOR: THREE COMPETITIVE PROCESSES

E. P. Grimsrud and C. A. Valkenburg
Department of Chemistry, Montana State University, Bozeman, MT 59717

Of all the transducers which depend on ion-molecule-electron interactions for the generation of their responses to organic compounds, the electron capture detector (ECD) for gas chromatography (GC) is probably the most frequently used. The detailed chemical basis of ECD responses, however, is generally less well understood than those observed by high-pressure mass spectrometers. This is understandable since the ECD provides only a measure of a single variable, electron population, while a high-pressure mass spectrometer often allows the observation of all the ions involved. We wish to report here a study of the EC response of anthracene where simultaneous measurements of positive and negative ions have been made by a specialized atmospheric pressure ionization mass spectrometer (APIMS), the source of which also serves as an ECD.[1] It will be shown that the overall response of an ECD to anthracene can be dependent on three competitive processes, only one of which is simple electron capture. The other two are ion-molecule processes which can be tailored to cause a greatly improved ECD signal.

The results of three experiments performed in this study are shown in the figures below. In each of these experiments, the ECD current response (fixed pulse frequency of 200 μsec), and the APIMS single-ion response of the $(M + 1)^+$ ion of anthracene have been monitored for three samples of anthracene. The GC column used is a simple 2-ft packed column held at 140°C. The temperature of the source is 250°C.

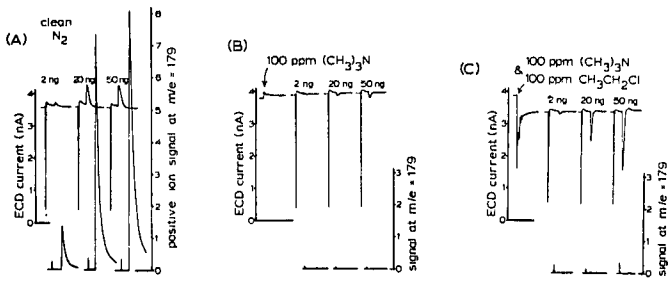

In figure A the ECD response to anthracene in clean N_2 carrier gas is shown to be inverted in that an increase in electron density appears to occur as anthracene enters the detector. The APIMS monitor of the protonated anthracene ion indicates a similar pattern of response. With the 20-ng sample, both the inverted ECD and APIMS signals appear to be saturated.

Upon addition of trimethylamine to the nitrogen carrier gas, both the ECD and the APIMS responses are altered dramatically as shown in figure B. The ECD responses are now weak, but normal in that a loss of electrons is indicated as anthracene passes through the detector. Also, absolutely no positive ionization of anthracene is now indicated by the APIMS signal at m/e = 179. Additional experiments indicated that with changes in the $(CH_3)_3N$ concentration from 25 ppm to 200 ppm, the results as shown in figure B are unchanged.

Upon addition of ethyl chloride, however, to the $(CH_3)_3N$-doped carrier gas, an additional effect on the ECD responses is caused. As shown in figure C, the magnitude of the EC responses is then increased about four times. Again, a variation of the concentration of ethyl chloride used from about 25 to 200 ppm caused little change in the responses from those shown in figure C.

In an attempt to explain the results shown above, the following model is proposed.

$$N_2 \xrightarrow{\beta} P_i^+ + e \xrightarrow[\text{analyte dopants}]{\text{impurities solvent}} P^+ + e \qquad (1)$$

$$e + A \underset{k_{-1}}{\overset{k_1}{\rightleftharpoons}} A^- \qquad (2)$$

$$A^- + EtCl \xrightarrow{k_2} Cl^- + \text{neutrals} \qquad (3)$$

$$e + P^+ \xrightarrow{R} \text{neutrals} \qquad (4)$$

Reaction 1 shows the ionization of the carrier gas by the beta radiation of the ^{63}Ni source. The positive ions which are ultimately formed, P^+, by reaction with the initially formed nitrogen ions, P_i^+, will depend on the minor components of the carrier gas.[2] In "clean" N_2 carrier gas, the impurities which will be observed in the P^+ ions will be water and "column bleed" molecules. With trimethylamine present the terminal positive ions are the $(M-1)^+$ and $(M+1)^+$ ions of $(CH_3)_3N$. The experiments indicate that in clean N_2 gas, the protonation of anthracene occurs readily so that the $(M+1)^+$ ion of anthracene becomes the dominant ion as anthracene passes through the detector. This change in positive ions could cause an increase in electron population if the rate of the recombination reaction 4 is thereby slowed. Due to the large π-resonance system of protonated anthracene, it seems possible that its electron recombination coefficient, R, is lower than that of the positive ions it replaced in clean carrier gas. With trimethylamine present the protonation of anthracene does not occur due to the high proton affinity of $(CH_3)_3N$. Therefore, a stable, unreactive set of ammonium positive ions is continuously maintained in the detector and, of course, the rate of the recombination reaction 4 is never altered. The weak EC reaction 2 can then be observed.

When ethyl chloride is also added to the carrier gas, it is proposed that reaction 3 then occurs. By negative ion APIMS, the production of Cl^- is actually observed during the elution of anthracene. This reaction causes an increase in the ECD response because it prevents the auto-detachment reaction, the reverse of reaction 2, by "trapping" the negative charge of the anthracene anion and irreversibly converting it to chloride anion. Because k_{-1} for anthracene is known to be quite high,[3] this addition to its electron capture sequence provides a useful means of improving its normally weak response.

Two types of ion-molecule reactions, one positive and one negative, have been shown here to have a very significant affect on the normal ECD response of a molecule. Continued studies in our laboratory indicate that these new considerations are operative in the ECD responses of numerous other compounds which have extended π-electron systems. The intentional use of dopants such as trimethylamine and ethylchloride offers a means for the control and optimization of these effects in order to cause improved ECD responses.

1. E. P. Grimsrud, S. H. Kim, and P. L. Gobby, Anal. Chem., 51 (1979) 223.
2. M. W. Siegel and W. L. Fite, J. Phys. Chem., 80 (1976) 2871.
3. L. Wojnarovits and G. Foldiak, J. Chromatogr., 206 (1981) 511.

DIFFERENTIATION OF ISOMERIC POLYCYCLIC AROMATICS
USING NEGATIVE CHEMICAL IONIZATION

M. V. Buchanan and G. Olerich
Oak Ridge National Laboratory
Oak Ridge, Tennessee 37831

Electron impact ionization mass spectrometry is of limited use in the unambiguous identification of isomeric polycyclic aromatic hydrocarbons (PAH). Even PAH with very different structures, such as fluoranthene, I, and pyrene, II, exhibit virtually identical mass spectra.

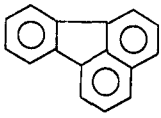

I

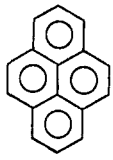

II

Although a number of mass spectral techniques have been devised to distinguish isomeric PAH, all have relied upon the comparison of the ratios of observed ion intensities. This would limit the usefulness of these techniques to compounds for which standards are available.

Negative chemical ionization (NCI) techniques have been investigated as a means of differentiating isomeric PAH without the use of standards. Using methane as a buffer gas, it was initially observed that PAH containing a fully unsaturated five-membered ring, such as fluoranthene, produced intense molecular anions, M^-. On the other hand, pyrene, which contains only six-membered rings, was not observed to ionize. This finding was supported by the fact that PAH containing a fully unsaturated five-membered ring generally have higher electron affinities (EA) than those composed solely of six-membered rings (1). In a study of over thirty PAH, it was determined that a number of PAH may be distinguished on the basis of their EA values. Compounds with EA values greater than about 0.5 eV produced molecular anions, while those with EA values less than 0.5 eV were not observed to ionize. A number of isomeric compounds may be distinguished using this technique, including two important benzopyrene isomers, benzo(a)pyrene, a potent carcinogen, and benzo(e)pyrene, which is not particularly carcinogenic. Benzo(a)pyrene has an EA of 0.64 eV (2) and produces molecular anions at 252. On the other hand, benz(e)pyrene, with an EA of 0.35 eV (2), is not observed to ionize. By comparison of the NCI spectra with either electron impact or positive chemical ionization spectra, these and other isomeric PAH may be readily distinguished on the basis of their EA values.

Unfortunately, EA values are difficult to measure experimentally and few EA values for PAH are available. EA values may be estimated using molecular orbital

calculations because they are directly related to the energy of the lowest unoccupied molecular orbital, ε_{LUMO} (3). The value of ε_{LUMO} is defined as

$$\varepsilon_{LUMO} = \alpha + m_{m+1}\beta$$

where α and β are the Coulomb and resonance integrals, respectively and m_{m+1} is the coefficient of energy for the LUMO. From this equation it may be observed that ε_{LUMO}, and thus EA, is directly proportional to m_{m+1}. The values of m_{m+1} have been calculated for a large number of PAH and are readily available in a number of compilations (for example, ref. 4). Thus, the m_{m+1} values can be used to predict the ionization behavior of PAH under NCI conditions. Using m_{m+1} values, the threshold for ionization is about -0.42. Additionally, theory predicts that ε_{LUMO} and thus, the EA value for a PAH should not be affected greatly by the addition of an alkyl group to the PAH (3). Experiments have shown that alkyl substituted PAH do follow the ionization behavior of the parent PAH, allowing these compounds to be identified without the use of standards as well.

---

(1) M. Zander, in Handbook of Polycyclic Aromatic Hydrocarbons, A. Bjørseth, Ed., Marcel Dekker, Inc., New York, 1983, pp. 1-26.

(2) J. M. Younkin, L. J. Smith, and R. N. Compton, Theoret. Chim. Acta (Berl.) 41, 157 (1976).

(3) A. Streitwieser, Jr., Molecular Orbital Theory for Organic Chemists, John Wiley & Sons, New York, 1961, pp. 175-185.

(4) E. Heibronner-Straub, Huckel Molecular Orbitals, Springer-Verlag, Berlin (1966).

GC/MS CHARACTERIZATION OF LIPOXYGENASE METABOLITES OF LINOLEIC ACID FORMED BY PORCINE LEUKOCYTES.

M.Claeys[1], G.A.A. Kivits[2], E. Christ-Hazelhof[2] and D.H. Nugteren[2]. [1]Department of Pharmaceutical Sciences, University of Antwerp, Universiteitsplein 1, B-2610 Wilrijk, Belgium and [2]Unilever Research Laboratory, P.O. Box 114, NL-3130 AC Vlaardingen, The Netherlands.

Lipoxygenase activity has been well documented in polymorphonuclear leukocytes using arachidonic acid as a substrate (1, 2). The main oxidative metabolites of arachidonic acid in these cells are formed through the action of the enzyme 5-lipoxygenase and include 5-hydroxyeicosatetraenoic acid and leukotriene B_4, which are implicated as mediators of the inflammatory reaction and show potent chemotactic and chemokinetic properties toward the polymorphonuclear leukocyte. We have studied the biotransformation of linoleic acid in polymorphonuclear leukocytes because, linoleic acid is quantitatively an important essential fatty acid of leukocyte cell membrane phospholipids from some animals, e.g. from pigs and rabbits, and is a known substrate for lipoxygenase(s), especially in plant systems. For this investigation, the linoleic acid metabolites were prepared in microgram quantities by incubating linoleic acid with porcine leukocytes and GC/MS was employed to identify the products after conversion into suitable volatile derivatives.

Porcine leukocytes were isolated from whole blood by dextrane precipitation of the erythrocytes and by centrifugation. Incubation of broken cells with added linoleic acid resulted in four major biotransformation products, X_1, X_2, X_3 and X_4, showing R_f-values of respectively, 0.65, 0.57, 0.27 and 0.23 upon thin layer chromatography on a silicagel plate, which was developed with the organic phase of ethyl acetate/2,2,4-trimethylpentane/acetic acid/water (100/60/20/100, by volume). Following isolation by silicagel column chromatography and thin layer chromatography, the products were derivatized and analyzed by GC/electron-impact MS on a 2m x 2mm i.d. 1 % OV.1 column. Derivatization included methyl ester formation, hydrogenation, n-butyl boronate formation and trimethylsilylation and various types of derivatives were made in order to facilitate the structure elucidation.

The major product X_1, which represented 60.5 % of the total metabolites formed, was identified as 13-hydroxy-9,11-octadecadienoic acid. This metabolite has previously been characterized as a biotransformation product of endogenous linoleic acid in rabbit peritoneal tissue (3). Product X_2 (16.2 %) was shown to be 11-hydroxy-12,13-epoxy-9-octadecenoic acid, which is formed through rearrangement of 13-hydroperoxy-9,11-octadecadienoic acid (4). Products X_3 and X_4 (respectively 5.2 and 7.5 %) resulted in identical mass spectra, indicating that these products are stereoisomeric. Furthermore, each of the products X_3 and X_4 was shown to be a mixture of two positional isomers, i.e. of 9,12,13-trihydroxy-10-octadecenoic acid (70 %) and 9,10,13-trihydroxy-12-octadecenoic acid (30 %). Mixtures of the latter isomers have been described in wheat flour incubates as enzymatic oxidation products of linoleic acid (5). With regard to the structure elucidation of mixtures X_3 and X_4, the mixed hydrogenated, n-butylboronate, methyl ester, TMS-ether derivatives were of particular value for the determination of the vicinal diol position. In these derivatives, the lone-standing TMS-ated hydroxyl group directs the fragmentation and yields fragment ions, which are characteristic for each of the positional isomers (Figure 1).

The possible formation of the four identified products is presented in Scheme 1 and is analogous to the metabolism of linoleic acid by cereal lipoxygenases. A major difference however is that porcine leukocyte lipoxygenase predominantly yields products, which arise through 13-lipoxygenation, whereas, in cereals, transformation products of 9-hydroperoxy-10,12-octadecadienoic acid are formed to the same extent as metabolites of 13-hydroperoxy-9,11-octadecadienoic acid.

References.

1. Borgeat, P., Hamberg, M. and Samuelsson, B. (1976). J. Biol. Chem. 251, 7816-7820 and correction 252, 8772.
2. Borgeat, P. and Samuelsson, B. (1979). J. Biol. Chem. 254, 2643-2646.
3. Claeys, M., Coene, M.-C., Herman, A.G., Jouvenaz, G.H. and Nugteren, D.H. (1982). Biochim. Biophys. Acta 713, 160-169 .
4. Hamberg, M. and Gotthammar, B. (1973) Lipids 8, 737-744.
5. Graveland, A. (1970) J. Am. Oil Chem. Soc. 47, 352-361.

Acknowledgements.

M. Claeys is a research associate of the Belgian National Fund for Scientific Research (N.F.S.R.). Work at the University of Antwerp was supported by grant n° 3.9001.79 from the N.F.S.R.

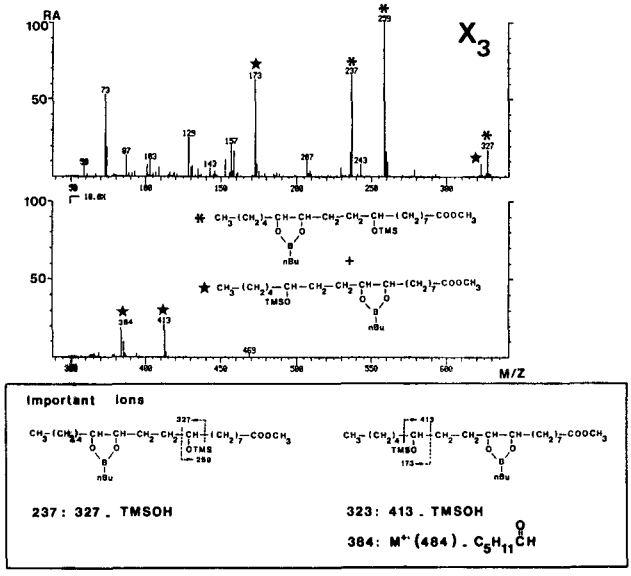

Fig. 1. EI mass spectrum of product X_3 after conversion into the hydrogenated n-butylboronate, methyl ester, TMS-ether derivatives and characteristic fragmentation patterns for the two derivatized positional isomers.

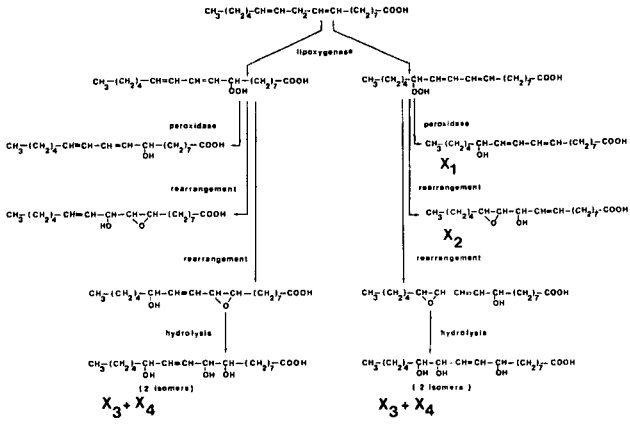

Scheme 1. Biotransformation of linoleic acid by porcine leukocytes.

ISOPROPYL AND METHYL-t-BUTYL ETHERS AS CHEMICAL IONIZATION REAGENT GASES

M. Mentzer, L. B. Killmer, Jr., S. Rottschaefer

Smith Kline and French Laboratories
Philadelphia, PA 19101

Isopropyl and methyl-t-butyl ethers can be used as CI reagent gases to provide molecular weight information and also to yield fragment ions which are useful for structural elucidation. With a proton affinity of 206 and 204 kcal/mole[1] respectively, the ionization is "softer" than with methane (127 kcal/mole). This higher proton affinity enhances the formation of protonated molecular ions for certain compounds.

A simple hardware modification can be made to implement the use of these ethers on a routine basis. This involves the addition of a Swagelok stainless steel tee into the direct probe CI reagent gas line.

Variations of both source pressure and source temperature affect the mass spectrum of the reagent gas. The optimal pressure for isopropyl and methyl-t-butyl ether is approximately 30 microns and 70 microns respectively. The source temperature is optimal between 160°C and 190°C. Operation within the optimal parameters reduces dimer formation of the reagent gas and maintains good sensitivity.

Table 1 outlines the response of three compounds to methane, isopropyl ether and methyl-t-butyl ether. The same quantity of the mixture of compounds A, B and C is introduced for each reagent gas through the GC inlet. The ethers yield the protonated molecular ion as the base peak for each of these compounds. When methane is used, however, a fragment ion is the base peak for compounds A and B. For all three compounds, the absolute intensities of the protonated molecular ion species generated by the ethers are comparable to or greater than the intensities generated by methane.

The total ion current of each compound is due to both fragment ions and protonated molecular ions. The methane mass spectra yield a greater number of fragment ions, and therefore the total ion current is greater with methane. Nevertheless, the relative response of the ethers is still at a useful level, ranging from 26% to 55% of the total ion current measured with methane.

We find that the ethers enhance the formation of protonated molecular ions with several types of compounds. Compounds with multiple t-butyl or benzyl groups, acetals and alcohols are examples which respond well. For these types of compounds, isopropyl and methyl-t-butyl ether are useful additions to the spectrum of reagent gases.

(1) D.H. Aue and M.T. Bowers in "Gas-Phase Ion Chemistry", M.T. Bowers, Ed., Academic Press, New York, 1979, Chapter 9.

TABLE 1

Ethers vs. Methane:
Comparison of the Intensity of the Base Peak

Compound	Intensity of Base Peak (Ion Count)		
	CH_4	IPE	MTBE
A. 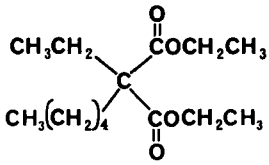 mol. wt. 258	m/z 185 26912	m/z 259 28768	m/z 259 20448
	CH_4	IPE	MTBE
B. 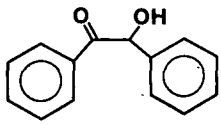 mol. wt. 212	m/z 195 32000	m/z 213 17728	m/z 213 21152
	CH_4	IPE	MTBE
C. $CH_3(CH_2)_7CH{=}CH(CH_2)_7\overset{O}{\overset{\|\|}{C}}OCH_3$ mol. wt. 296	m/z 297 2240	m/z 297 2372	m/z 297 4720

Structure Elucidation of Human Neutrophil
Platelet Activating Factor

K.L. Clay, R.C. Murphy, J. Andres,
J. Lynch and P.M. Henson
Department of Pharmacology
University of Colorado
Health Sciences Center
and
National Jewish Hospital and
Research Center
Denver, Colorado

Platelet activating factor (PAF) is a phospholipid which is produced by a variety of cells after appropriate stimulus. Its structure from animal sources has been determined to be 1-O-alkyl-2-O-acetyl glycero-3-phosphocholine (1,2). When this study was undertaken, no analysis of human PAF had been reported. Two recent studies (3,4) have used widely varying methods to anlayze PAF from human neutrophils and report that human PAF is a mixture of species. Neither study, however, assessed biological activity of isolated fractions, nor was there any analysis of the intact molecule.

With the use of HPLC separation, bioassay for determination of PAF activity and fast atom bombardment of isolated phospholipid molecular species, we have demonstrated that PAF from human neutrophils stimulated with opsonized zymosan or the calcium ionophore A23187 produce the single molecular species of PAF, 1-O-hexadecyl-2-O-acetyl-glycero-3-phosphocholine. A GC/MS procedure was developed for quantitative analysis of PAF, and its use confirmed the unexpected result of production of a single molecular species.

Human neutrophils were prepared by plasma percoll density gradient centrifugation of a leukocyte fraction obtained from healthy volunteers. They were then incubated for 20 minutes in the presence of a phagocytic stimulus, opsonized zymosan, or for two minutes in the presence of calcium ionophore, A23187. At the end of the incubation, the buffer and cells were poured into two volumes of chilled methanol containing ^{3}H-PAF (New England Nuclear). After Bligh & Dyer extraction, TLC separation was used to isolate a purified phosphatidylcholine fraction. The biologically active fraction was then used directly for GC/MS analysis, or it was subjected to HPLC purification prior to FABMS. Each fraction from TLC and HPLC separations was assayed for platelet activating biological activity and for radioactivity. All of the bioactivity was recovered in TLC fractions which were also radioactive. HPLC, however, could separate radioactivity into three distinct species, but only one zone of biological activity.

As shown in Figure 1, the ^{3}H-PAF was a mixture of species with C14, C16, and C18 alkyl ether chains in the sn-1 position and HPLC was effective in resolving those species. Biological activity, however, was never observed in any HPLC fraction except that corresponding to the hexadecyl ether species. FABMS of the HPLC fraction at the C16 ether retention time gave a mass spectrum which has a protonated molecular ion at m/z 524 and which was identical with a spectrum of synthetic hexadecyl PAF. HPLC fractions were examined for the presence of ions at m/z 550 and m/z 552, indicative of mono-unsaturated C18 and saturated C18 ether PAF, respectively, but no such ions were observed in any experiment. When a mixture of standard PAF with those species present was added to a neutrophil preparation, however, all of the added species were recovered in the expected HPLC fractions and easily seen by FABMS.

The GC/MS procedure (which used HF hydrolysis of PAF to yield the ether, acetyl diglyceride followed by trimethylsilylation of the diglyceride) confirmed the FABMS result. Figure 2 illustrates the ion currents obtained from analysis of PAF isolated from stimulated neutrophils and purified by TLC. Prior to extractions, PAF which had been synthesized with three deuterium atoms in the sn-2 acetyl group was added to the cell suspension.

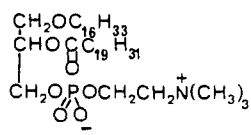

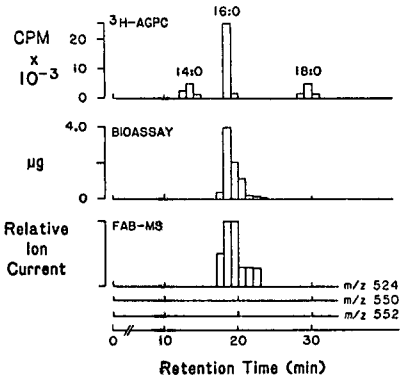

Fig. 1. Assay of HPLC fractions collected at one minute intervals for radioactivity, biological activity and FAB ion currents for C16 and C18 PAF.

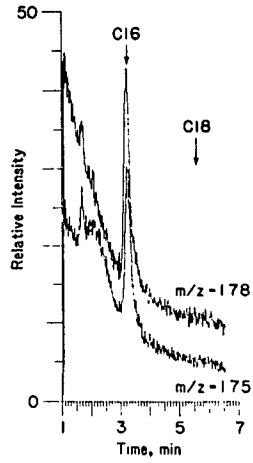

Fig. 2. Selected ion monitoring traces for ions characteristic of TMS diglycerides containing an acetyl moiety at the sn-2 carbon.

TMS diglycerides fragment between the sn-1 and sn-2 carbon atoms of the glycerol backbone to give an ion common to each ether, acetyl diglyceride specie at m/z 175 (m/z 178 for the deuterated analog). Using this ion to monitor for the presence of sn-2 acetyl-containing *diglycerides, GC retention time is a good indication of ether chain length. As shown in Figure 2,* GC/MS analysis of the biologically active TLC fraction produced an ion current indicative of hexadecyl PAF, but no ion current to indicate any species of octadecyl PAF These results suggest a high degree of regulation in the biosynthesis of PAF.

Acknowledgements: This work was supported in part by grant AI20774 from the National Institute of Health.

References

1. Hanahan, D.J., Demopoulos, C.A., Liehr, J. and Pinckard, R.N. J. Biol. Chem. 255:5514-5516 (1980).
2. Polonsky, J., Tence, M., Varenne, P., Das, B., Lunel, J. and Benveniste, J. Proc. Nat. Acad. Sci. 77:7019-7023 (1980).
3. Mueller, H.W., O'Flaherty, J.T. and Wykle, R.L. Fed. Proc. 43:1656-1984.
4. Satouchi, K., Oda, M., Yasunaga, K. and Saito, K. J. Biochem. 94:2067-2070, (1983).

SIMULTANEOUS MEASUREMENT OF HISTAMINE METABOLITES BY GC-MS:

J.K.Khandelwal, L.B.Hough, T.Kline and J.P.Green

Department of Pharmacology, Mount Sinai School of Medicine of the City University of New York, New York, NY , USA

Histamine (HA) is a biogenic amine which undergoes two major metabolic pathways. In one pathway , HA is methylated to tele-methylhistamine (t-MH) followed by its oxidative deamination to tele-methylimidazoleacetic acid (t-MIAA). In the other pathway, HA undergoes direct oxidative deamination to form imidazoleacetic acid (IAA). We describe a sensitive and specific GC-MS method that simultaneously assays HA metabolites, t-MH, t-MIAA and IAA, in the same biological sample . The method has been applied to rat brain tissue and human body fluids[1].

The tissue was homogenized in water,heated for 10 min in a boiling water bath,cooled and centrifuged at 49,500 x g at 4°C for 20 min. To the resulting tissue supernatant or the body fluid was added 10 ng each of d3-t-MH and d3-t-MIAA as internal standards to measure t-MH and t-MIAA,respectively. Appropriate amounts of authentic t-MH and t-MIAA,mixed with the same amounts of both internal standards were assayed in parallel to obtain standard curves. The samples were made alkaline with 1N NaOH (0.012 ul/ml) and 50 mM Tris-acetate buffer, pH 9.0 (100 ul/ml), mixed,and shaken for 30 min with 4 ml of a mixture of n-butanol-chloroform(1:1) to extract t-MH into the organic phase. Following centrifugation (10 min), the aqueous phase was transferred to a fresh tube and shaken again with another aliquot of 4 ml of butanol-chloroform mixture. The organic extracts containing t-MH were pooled whereas the aqueous phase was kept for t-MIAA analysis.

To the organic phase of butanol-chloroform was added approx. 0.5 g of anh.Na2SO4 power, vortexed and centrifuged for 5 min. The upper organic phase was transferred to a conical polypropylene tube containing 0.5 ml of 0.01N HCl and 4 ml of heptane. Following mechanical shaking for 15 min and centrifugation for 5 min,the organic phase was discarded by aspiration.The acidic aqueous phase was transferred to a silanized 1 ml Reactivial and dried by vacuum centrifugation. The residue was derivatized as bis-HFBA derivative for analysis of t-MH by SIM of ions m/e 304 and 307 (internal standard)[2].

Acid metabolites left in the aqueous phase were separated by ion-exchange chromatography on Bio-Rad AG 1-X4,100-200 mesh,in the acetate form; the eluate was dried by vacuum centrifugation and derivatized as n-butyl ester by heating with BF3-BuOH at 90°C for 90 min . t-MIAA was assayed by SIM of ions m/e 95 and m/e 98 (internal standard). pros-methylimidazoleacetic acid,an isomer of t-MIAA, was also measured by SIM of ion m/e 95 at a retention time different from that of t-MIAA[3] IAA is also extracted and derivatized similar to t-MIAA. The butyl ester exhibits base peak at m/e 81 and a small molecular ion at m/e 182.The method measured as little as 4 pmol and 7 pmol respectively of t-MH and t-MIAA , enabling it to be applied to the studies of rat brain regions.The identity of these metabolites in biological samples was rigorously established by retention time, ion abundance ratios, peak shape and isobutane chemical ionization mass-spectrometry.

This work was supported by Grant MH-31805 from the National Institute of Mental Health.

REFERENCES

1. Khandelwal, J.K., Hough , L.B., and Green, J.P. (1984) J. Neurochem. 42, 519-522.

2. Hough, L.B., Khandelwal, J.K., Morrishow, A.M., and Green, J.P. (1981) J. Pharmacol. Methods 5, 143-148.

3. Khandelwal, J.K., Hough, L.B., Pazhenchevsky, B., Morrishow, A.M., and Green, J.P. (1982) J. Biol. Chem. 257, 12815-12819.

A CANDIDATE DEFINITIVE METHOD FOR THE DETERMINATION OF SERUM CREATININE BY ISOTOPE DILUTION/MASS SPECTROMETRY

K. J. Ng, M. J. Welch, A. Cohen, H. S. Hertz, R. Schaffer, and E. White V

Organic Analytical Research Division
Center for Analytical Chemistry
National Bureau of Standards
Washington, DC 20234

Introduction

Serum creatinine levels are frequently measured to evaluate renal function (1). An accurate and precise method for the determination of creatinine in serum has been developed for use as a definitive method for the National Reference System in Clinical Chemistry. This is part of a program to develop highly accurate (definitive) methods for serum analytes(2-5).

Methods

A labeled internal standard, creatinine-$^{13}C_2$, was synthesized from glycine-^{13}C and methyl iodide-^{13}C. A weighed amount of creatinine-$^{13}C_2$ was added to a known weight of serum such that the labeled/unlabeled ratio was approximately 4:1 and the mixture was equilibrated overnight. Creatinine was separated from creatine, a potential interference, on a weak acid ion exchange column. Creatinine was derivatized by heating for three days at 85-86°C in the presence of 2,4-pentanedione, acetic acid and ethanol to form the ethyl ester of N-(4,6-dimethyl-2-pyrimidinyl)-N-methylglycine. Excess reagents were evaporated and the derivative was dissolved in distilled heptane for analysis.

ID/MS measurements were made by GC/MS on a single focusing magnetic instrument. Samples were analyzed using a glass capillary (SCOT) column with a nonpolar liquid phase and electron impact ionization at 70 eV. The base peaks, m/z 150 and 152, for the unlabeled and labeled creatinine derivatives, respectively, were monitored by magnetic switching and a ratio between the two isotopic forms obtained. Two sets of standards containing known weights of unlabeled and labeled creatinine were prepared independently and crosschecked against each other. Each sample was bracketed, both in time and ratio, between two chosen standards which had the ratios of unlabeled to labeled creatinine closest to that of the sample. The sample was remeasured on a separate day with the order of the bracketing standards reversed. The mean of two measurements was reported as a valid measurement. The quantity of creatinine in the sample was determined by linear interpolation between the bracketing standards. This method was applied to three sets of samples. Each set consisted of two aliquots from each of three vials of human serum, Standard Reference Material 909.

As a check for measurement bias a subset consisting of eight samples from the three sets was remeasured and then further measured by two additional methods: (1) chemical ionization with ammonia as a reagent gas monitoring the $(M+H)^+$ ions, and (2) electron impact ionization with a polar bonded phase fused silica column monitoring the $M^{+\cdot}$ ions.

Results

The ID/MS method, using creatinine-$^{13}C_2$, has been used to determine and certify creatinine levels in lyophilyzed serum pools. The results, shown in Table 1, illustrate the excellent precision attainable with this method. The range of measured creatinine concentrations across all three sets was 0.72 percent with a CV of 0.18 percent for a single measurement. The measurements made to confirm the absence of bias are shown in Table II. The range of the mean values measured by the three procedures is 0.05 percent. Therefore, the accuracy and precision required of a definite method has been met (6).

Table I

Creatinine in Human Serum SRM 909 by Isotope Dilution/Mass Spectrometry--
Three Independently Prepared Sets

(Each Sample is Measured Twice)

	Mean Values (mmole x L^{-1} g^{-1})		
Sample	Set 1	Set 2	Set 3
1	0.1798	0.1799	0.1793
2	0.1797	0.1798	0.1797
3	0.1797	0.1794	0.1793
4	0.1800	0.1797	0.1798
5	0.1799	0.1797	0.1792
6		0.1797	0.1796
Mean	0.1798	0.1797	0.1795
CV (%)	0.06	0.08	0.14

Overall Mean = 0.1796
Range of Set Means = 0.17 %

Table II

Confirmatory Measurements on a Sample from the Three Sets
Used for Certification

		Mean Values (mmoles x L^{-1} g^{-1})		
Set	Sample	EI 150/152	CI $(M+H)^+$ 224/226	EI (M^+) 223/225
I	1	0.1794	0.1795	0.1796
	5	0.1800	0.1804	0.1798
II	2	0.1799	0.1793	0.1793
	5	0.1797	0.1798	0.1800
III	2	0.1798	0.1799	0.1798
	3	0.1798	0.1798	0.1795
	5	0.1794	0.1798	0.1804
	6	0.1800	0.1797	0.1796
	Mean	0.1797	0.1798	0.1797
	CV	0.13 %	0.18 %	0.19 %

References

1. S. Narayanan and H. D. Appleton, Clin. Chem. 26, 1119 (1980).
2. A Cohen, H. S. Hertz, J. Mandel, R. C. Paule, R. Schaffer, L. T. Sniegoski, T. Sun, M. J. Welch, and E. White V, Clin. Chem. 26, 854 (1980).
3. E. White V, M. J. Welch, T. Sun, L. T. Sniegoski, R. Schaffer, H. S. Hertz, and A. Cohen, Biomed. Mass Spectrom. 9, 395 (1982).
4. A. Cohen, H. S. Hertz, R. Schaffer, L. T. Sniegoski, M. J. Welch, and E. White V, presented at the 27th Annual Conference on Mass Spectrometry and Allied Topics, Seattle, Washington, June 3-8, 1979.
5. M. J. Welch, A. Cohen, H. S. Hertz, F. C. Ruegg, R. Schaffer, L. T. Sniegoski, and E. White V, Anal. Chem. 56, 713 (1984).
6. "Guidelines for the Development of Definitive Methods for Use in Clinical Chemistry for the National Reference System in Clinical Chemistry," NRSCC 1, National Committee for Clinical Laboratory Standards, Villanova, PA. 1979.

Acknowledgement

Sponsorship of K. J. Ng by the College of American Pathologists is gratefully acknowledged.

IDENTIFICATION AND QUANTITATIVE ANALYSIS OF ACYLCARNITINES IN HUMAN URINE BY THERMOSPRAY HPLC/MS. D.J. LIBERATO, A.L. Yergey, NIH, NICHD, Bethesda, MD and D.S. Millington, Box 3028, Duke University Medical Center, Durham, NC 27710.

Recent studies have indicated that children with disorders of amino acid and fat metabolism ("organic acidurias") excrete elevated concentrations of short-chain acylcarnitine. Preliminary identification and quantitation of specific acylcarnitines in human urine has been accomplished using FAB and MS/MS[1], but the lack of an on-line chromatographic procedure compromises the analytical specificity and sensitivity, thus restricting the application of the method.

Acylcarnitines are not directly amenable to analysis by HPLC using conventional detectors or to GC/MS, owing to their high polarity and lack of a chromophore suitable for UV detection. Thermospray HPLC-MS overcomes these problems by the embodiment of a "soft" ionization process with demonstrated applicability to the qualitative and quantitative analysis of acylcarnitines at physiological levels[2]. Separation was accomplished by reverse phase chromatography (Altex 5μm ODS column: 15cm x 4.6mm) using 0.05M NH_4OAc buffer with methanol (5-50%, depending on the application) as the mobile phase. For pure acylcarnitines, good quality full-scan spectra were obtained from 1 nmole injected on-column. By selected ion monitoring (SIM), 0.1 nmol was easily detectable. Ions at m/z 102 and 130 were monitored to detect acylcarnitines in general, and the MH^+ or $(MH-42)^+$ ions were employed to detect specific acylcarnitines.

Urine samples were passed over Dowex-50 (H^+ form) and, after washing with 0.01 N HCl and water, the acylcarnitine fraction was eluted with 1M NH_4OH in water: ethanol (4:1). After lyophilization, samples were dissolved in HPLC buffer prior to analysis.

The HPLC/MS technique was used to show that the major acylcarnitines excreted in medium-chain acyl-CoA dehydrogenase deficiency (MCAD), a disorder of fat metabolism, are octanoylcarnitine (mostly) and hexanoylcarnitine (Figure 1). This contrasts with true Reye's syndrome, with which the disease may be confused, where high concentrations of acetylcarnitine are excreted.

In isovaleric acidemia, isovalerylcarnitine was shown to be the major excreted acylcarnitine (Figure 2). Quantitative analysis of this newly discovered metabolite was accomplished by isotope dilution and results on selected samples (Table 1) compare well with those obtained by high resolution FAB analysis.

Another new metabolite discovered by thermospray HPLC-MS is valproylcarnitine, an isomer of octanoylcarnitine. The isomers were resolved by HPLC using 50% MeOH with the buffer as elutant. Valproylcarnitine is excreted in small amounts by patients undergoing chronic valproic acid therapy for control of seizures. It represents the first example of drug conjugation with carnitine and may help to account for the development of carnitine deficiency in these patients.

1. D.S. Millington, C.R. Roe and D.A. Maltby, Biomed. Mass. Spectrom. 11, 236 (1984).
2. A.L. Yergey, D. Liberato and D.S. Millington, Analyt. Biochem. 139 (1984), in press.

Figure 1

DETECTION OF HEXANOYL-AND OCTANOYLCARNITINES IN MEDIUM-CHAIN ACYL-CoA DEHYDROGENASE DEFICIENCY (MCAD)

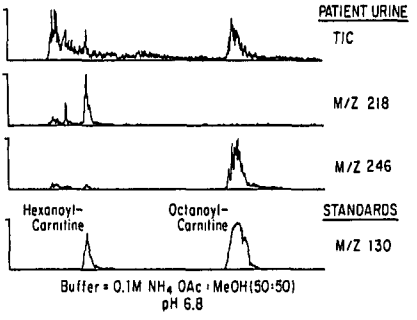

Figure 2

ANALYSIS OF ISOVALERYLCARNITINE IN ISOVALERIC ACIDEMIA BY THERMOSPRAY HPLC-MS WITH ISOTOPE DILUTION

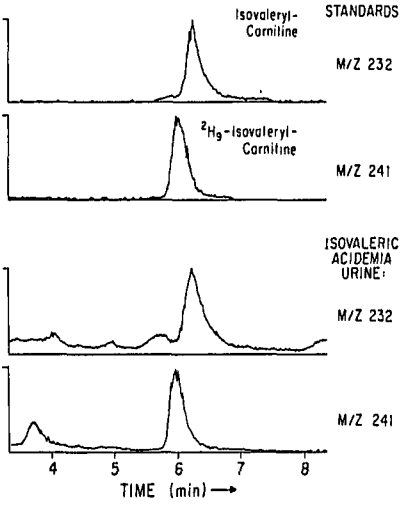

Table

Comparison of FAB with Thermospray HPLC/MS for Analysis of Isovalerylcarnitine in Isovaleric Acidemia by Isotope Dilution

	nmol/ml isovalerylcarnitine:		
Sample:	HPLC MS	FAB	(REA)*
DM F2	258	284	(270)
DM G4	67	66	(90)
DM D9	1320	1328	(1270)

* Radioenzymatic Assay for Acylcarnitine Totals.

MEASUREMENT OF PLASMA THROMBOXANE B_2 BY GC/MS USING ^{18}O-LABELLED THROMBOXANE B_2

David A. Herold, B. Jane Smith, Richard M. Ross, Fiona Marquis, John Savory, Michael R. Wills, and Carlos R. Ayers; Departments of Pathology, Biochemistry and Internal Medicine, University of Virginia Medical Center, Charlottesville, VA 22908.

INTRODUCTION

Stable isotope-labelled compounds used as internal standards are an integral part of the precise and accurate measurement of picogram quantities of prostaglandins in biological matrices by gas chromatography/mass spectrometry. One serious limitation of this technique is the availability of the stable isotope-labelled species and, at the present time, PGE_2, $PGF_{1\alpha}$, $PGF_{2\alpha}$, and 6-keto-$PGF_{1\alpha}$ are the only labelled species commercially available. In an effort to identify a simple and inexpensive procedure for preparing an internal standard for TxB_2, we investigated the esterase-catalyzed carboxylic acid oxygen exchange method of Pickett and Murphy (1).

METHODS

Preparation of [^{18}O]-TxB_2. One hundred and fifty units of esterase solution were transferred to a 5-ml reacti-vial and lyophilized. To the lyophilized esterase 100 ul of $H_2{}^{18}O$ was added, the solution was mixed well and lyophilized again. A second 100 ul aliquot of $H_2{}^{18}O$ was added, the reaction initiated by the addition of 100 ug of TxB_2 in 10 ul of methanol, and the mixture incubated for 2 h at 37°C. The exchange reaction was terminated by the sequential addition of 0.5 ml of methanol, 1.5 ml of anhydrous ethyl ether, and 1.0 ml of H_2O. The ether layer was discarded and the aqueous layer re-extracted with a second 1.5 ml aliquot of ether. The remaining aqueous solution was acidified with 10% formic acid to pH 3.0, and [$^{18}O_2$]-TxB_2 was extracted with 1 ml of chloroform. Solvent was evaporated and the dried residue resuspended in 0.5 ml of acetone and stored at -70°C. The overall recovery of [$^{18}O_2$]-TxB_2 was approximately 65% for 100 ug reaction.

Extraction, Separation, and Analysis of TxB_2 From Plasma. Thromboxane B_2 was extracted from plasma using a modification of the procedure for PGE_2 developed in the authors' laboratory (2). Forty milliliters of blood was collected from each of 11 normal adult volunteers. The volume of each plasma sample was measured, then acidified to pH 3.5-4.0 with formic acid, and 3.1 ng of [$^{18}O_2$]-TxB_2 was added. The treated sample was applied to a C_{18} reverse-phase SEP-PAK cartridge preconditioned with acetonitrile (10 ml) and HPLC-grade water (20 ml). The SEP-PAK was washed sequentially with 10 ml of water, 4 ml of 15% acetonitrile, and 10 ml of petroleum ether, and the prostaglandins eluted with 10 ml of acetonitrile. The plasma extract was converted to its methoxime derivative by dissolution in 50 ul of 2% methoxylamine hydrochloride in pyridine and heating at 70°C for 1 hr. The methoximated extract was separated by thin layer chromatography (TLC). Samples were chromatographed for 20 minutes and after drying, were scraped off the plate and eluted with 3 ml of acidified methanol (100 parts methanol/1 part acetic acid). The TLC extra was dissolved in 30 ul of acetonitrile and 10 ul of 35% pentafluorobenzyl bromide in acetonitrile and 10 ul of 10% diisopropylethylamine in acetonitrile, were added. Vials were heated at 40°C for 15 minutes and solvent evaporated and dried. The trimethylsilyl ether derivative was prepared by treating the residue with 50 ul of acetonitrile and 40 ul of BSTFA, and heating at 40°C for 1 hour.

Gas Chromatography-Mass Spectrometric Analysis. A Finnigan 4021 quadrupole mass spectrometer equipped with the INCOS data system and the pulsed positive ion negative ion chemical ionization (PPINICI) accessory (Finnigan, MAT, Sunnyvale, CA 94086) was used. The gas chromatograph (GC) was equipped with a DB-1 methyl silicone bonded phase fused silica capillary column 0.32 mm I.D. x 30 m (J & W Scientific, Ranch Cordova, CA 95670). The mass spectrometer was operated in the negative ion mode with the electron multiplier at 1200-1500 V and the conversion dynode at 3000 V. The source was maintained at 250°C and pressurized to approximately 0.24 torr with methane gas. Methane gas was also used as the GC carrier. The GC injector and separator oven were maintained at 270°C. Derivatized samples dissolved in tetradecane were injected using an on-column injector (OCI-3, Scientific Glass Engineering, Austin, TX 78759). Injections were made at 200°C and increased to 300° at 20° per minute. Thromboxane B_2 was quantitated by selective ion monitoring using

fragment ions at m/z 614 (TxB_2) and m/z 618 ($[^{18}O_2]$-TxB_2) which correspond to the loss of pentafluorobenzyl radical. Standard curves for TxB_2 were constructed from a plot of peak height ratios (614/618) versus the concentration of prostaglandin added. Plasma concentrations of TxB_2 were calculated from the amount of $[^{18}O_2]$-TxB_2 internal standard added to the sample. The contribution at m/z 614 from $[^{18}O_2]$-TxB_2 relative to the intensity of m/z 618 is demonstrated in Fig. 1. Standardization of the $[^{18}O_2]$-TxB_2 was accomplished by comparison to a known concentration of TxB_2 using ion masses at 618 and 614, respectively.

RESULTS

Quantitation of TxB_2 in Plasma. Endogenous plasma concentrations of TxB_2 were determined in 11 normal adults. A limited mass chromatogram obtained from the analysis of one plasma sample is presented in Fig. 2. After subtraction of the blank, the TxB_2 concentration calculated was 10.6 pg/ml. The mean plasma TxB_2 concentration for all 11 individuals was 7.1 ± 1.7 pg/ml with a range of 5.1-10.6 pg/ml. The limit of detection of TxB_2 in plasma was 3 pg/ml with a signal to noise level of 2:1.

DISCUSSION

In an effort to identify a simple and inexpensive method for preparing an internal standard for TxB_2, we initially investigated the use of deuterated O-methoxylamine hydrochloride for the preparation of the tri-deutero analog (d_3-TxB_2) (4). The method, originally described for $PGF_{2\alpha}$ and its metabolites, was reported to be applicable to the preparation of deuterated internal standards of all prostaglandins containing a keto group. The procedure yielded an internal standard with a high level of isotope incorporation. However, when the newly synthesized d_3-TxB_2 was used to quantitate endogenous TxB_2 in a plasma sample, preparation of the methoxime derivative led to considerable exchange of the d_3-methoxime group, thus making it unsuitable for use as an internal standard. The oxygen exchange method described yielded a product which provides characteristics desired in an internal standard: 1) a high level of isotope incorporation; 2) significant mass difference from the naturally occurring isotope; 3) chemically identical properties as the material being measured; and 4) no isotope exchange under the conditions of extraction, derivatization and analysis. The ease, relative inexpensive nature and general applicability of the procedure make it an attractive way of preparing internal standards.

REFERENCES

1. WC Pickett and RC Murphy. Anal Biochem 111, 115 (1981).
2. BJ Smith, DA Herold, RM Ross et al. Res Comm Chem Pathol Pharmacol 40, 73 (1983).
3. BJ Smith, RM Ross, CR Ayers et al. J Liq Chromatog 6, 1265 (1983).
4. CR Pace-Asciak and NS Edwards. Meth Enzy 86, 552 (1982).

FIGURE 1

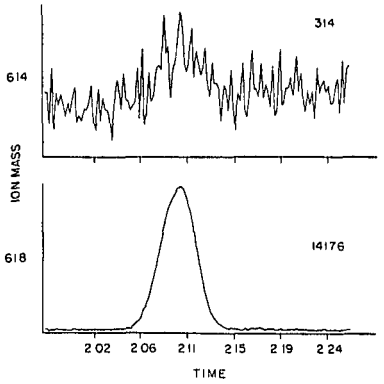

FIGURE 2

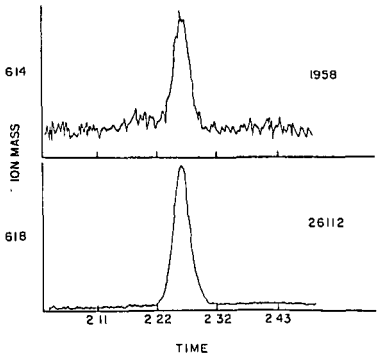

NEGATIVE ION CHEMICAL IONIZATION GC-MS FOR QUANTITATIVE MEASUREMENT OF URINARY OCTOPAMINES AND SYNEPHRINES

K. E. Ibrahim, M. W. Couch and C. M. Williams, Veterans Administration Medical Center and Department of Radiology, University of Florida, Gainesville, Florida, 32610

M. B. Budd and R. A. Yost, Chemistry Department, University of Florida, Gainesville, Florida

J. M. Midgley, Department of Pharmacy, University of Strathclyde, Glasgow, Scotland G1 1XW

The development of a radiochemical enzyme assay for the quantitative determination of p-octopamine led to its discovery in several invertebrate nerve systems and in sympathetically innervated mammalian organs. It was subsequently discovered that this assay would not differentiate between the o-, m- and p-octopamine isomers nor between their N-methyl analogs, the synephrines.

Electron impact gas chromatography mass spectrometry techniques permit the unequivocal identification and quantitative determination of the three isomeric octopamines and synephrines and there is now conclusive evidence for the natural occurrence in mammalian tissue of o- and m-octopamine and m- and p-synephrine. Previous attempts to analyze these compounds in mammalian urine by electron impact gas chromatography-mass spectrometry were unsuccessful because they are present in amounts below the lower limits of detection (50-100 ng/mg creatinine) by this technique. We have developed a new assay which combines ion exchange chromatography, capillary column gas chromatography and electron capture negative ion chemical ionization mass spectrometry.

This work was performed on a Hewlett-Packard 5985 GC-MS system equipped with an EI/CI source with negative chemical ionization capability. The end of the fused silica capillary column ("ultrabond" cross-linked methyl silicone, 25 m x 0.2 mm ID, 0.33 μm film) was inserted into the source of the mass spectrometer where a pressure of 1 Torr was maintained by adding methane. The GC injection port and interfacial region between the GC and the MS were maintained at 250 °C. The GC oven was maintained at 80 °C for 0.5 min following injection and then raised to 250 °C at a rate of 30 °C/min. The electron multiplier voltage was 2400V; source temperature, 100 °C; electron beam current, 300μA.

In a typical analysis, a standard containing 10 ng each o- and m-octopamine-d_3 and 100 ng each of p-octopamine-d_4, o-, m- and p-synephrine-d_3 was added to a volume of urine containing 1 mg creatinine. The urine was acid hydrolyzed, neutralized, passed through an AG 50W-X2 cation exchange column which was subsequently washed with water, sodium acetate, water, 70% ethanol. The amines were eluted with ammoniacal ethanol and the eluate blown to dryness under nitrogen. The residue was reconstituted in water and subjected to a second elution through AG 50W-X2. The resultant amine fraction was derivatized with pentafluoropropionic anhydride and, under electron capture negative chemical ionization conditions, the PFP derivatives gave M^- and $(M-HF)^-$ ions which were suitable for selected ion monitoring.

Detection limits for pure compounds were 100 fg (octopamines) and 500 fg (synephrines). This sensitivity could not be achieved with urinary extracts because the finite population of electrons in the ion source is depleted by other compounds which are derivatized by PFPA and elute shortly before or simultaneously with the compound of interest. This loss of sensitivity ("quenching") ranged from 46-75%, and observed recoveries ranged from 4-12%. As a result, the limit of detection in human urine is about 100 pg/mg creatinine.

The concentrations of o-, m- and p-octopamine and m- and p-synephrine were determined in the urine of 10 normal humans as both the unconjugated and the acid hydrolyzable conjugates. (See Figures 1, 2 and 3 and the table). o-Synephrine was not detected (< 100 pg/mg creatinine). The occurrence of o- and m-octopamine and m-synephrine in human urine has not been reported previously.

Figure 1

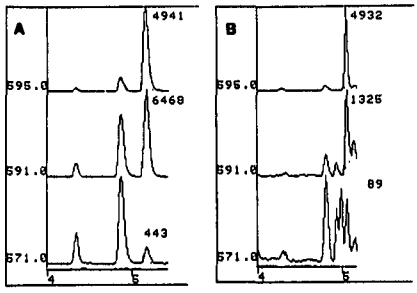

Figure 2

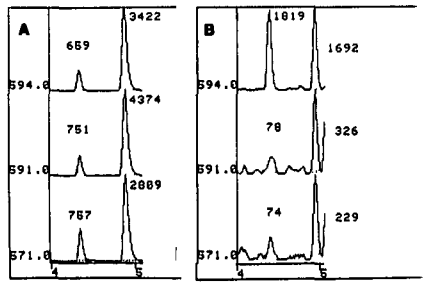

Figure 3

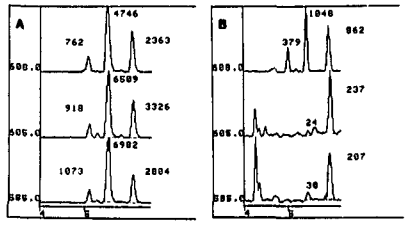

A.1, 2 and 3: The PFP derivatives of p-octopamine-d_0 and -d_4, o- and m-octopamine-d_0 and -d_3 and o-, m- and p-synephrine-d_0 and -d_3, respectively, in the 1:1 standard of undeuterated and deuterated amines.

B.1, 2 and 3: The corresponding derivatives in an aliquot of derivatized urinary extract in hexane from urine containing 1 mg creatinine and 100 ng p-octopamine-d_4, 10 ng each o- and m-octopamine-d_3 and o-, m- and p-synephrine-d_3.

URINARY CONCENTRATION OF OCTOPAMINES AND SYNEPHRINES
IN TEN NORMAL ADULTS

NG MG^{-1} CREATININE

	FREE	TOTAL
o-Octopamine	0.3 (± 0.1)	0.6 (± 0.2)
m-Octopamine	1.0 (± 0.5)	2.1 (± 0.8)
p-Octopamine	0.9 (± 1.2)	2.5 (± 19)
o-Synephrine	ND*	ND
m-Synephrine	1.6 (± 0.5)	1.8 (± 0.7)
p-Synephrine	1.8 (± 1.0)	16 (± 10)

*Not Detected (<0.1).

The Search for LTB_4 in Biological Fluids
by GC/MS as the t-Butyldimethylsilyl Derivative

R.C. Murphy and F.A. Anderson
Department of Pharmacology
University of Colorado School of Medicine
Denver, CO 80262

Recent investigations have suggested that metabolism of arachidonic acid by a specific enzyme, 5-lipoxygenase, can lead to the formation of leukotrienes which are putative chemical mediators of acute hypersensitivity reactions and the inflammatory response (1). Leukotriene B_4 (LTB_4), I, is of particular interest due to its unique and potent biological activity as a chemotactic and chemokinetic factor (2). Therefore, it would be of interest to have available a specific and sensitive means to detect LTB_4 by quantitative mass spectrometric techniques. The TMS, methyl ester (3) and TMS, pentafluorobenzyl esters (4) have been used as derivatives for GC/MS. Previous work with t-butyldimethylsilyl derivatives (5) suggested that these might be useful derivatives.

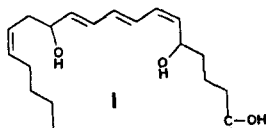

The EI mass spectrum of the tri(t-butyldimethylsilyl) derivative is shown in Figure 1 and has the second most abundant ion at m/z 435 (M - 111 + 132). This ion appears at m/z 439 in the 1,1,12-[$^{18}O_3$]-LTB_4 derivative. It was found that on-column injection was necessary for proper capillary gas chromatographic behavior of this derivative even though it elutes in 5 minutes on a DB-1 column at 260°.

An even more favorable TBDMS derivative investigated was the saturated LTB_4 seen in Figure 2. The base peak corresponded to loss of t-butyl radical and the ion at m/z 629. This derivative was made by catalytic reduction using Rh on alumina (0.5 to 1 mg per sample) suspended in methanol and bubbled with hydrogen for 10 minutes. This catalyst was used to reduce hydrogenolysis as a side reaction. The 5,12-eicosanoic acid was then treated with a solution comprised of MTBSTFA (10%) and Coreys reagent (2%) (t-butyldimethylsilyl chloride (1 M) plus imidazole (2.5 M) in DMF) in acetonitrile for 1 hour at 60°.

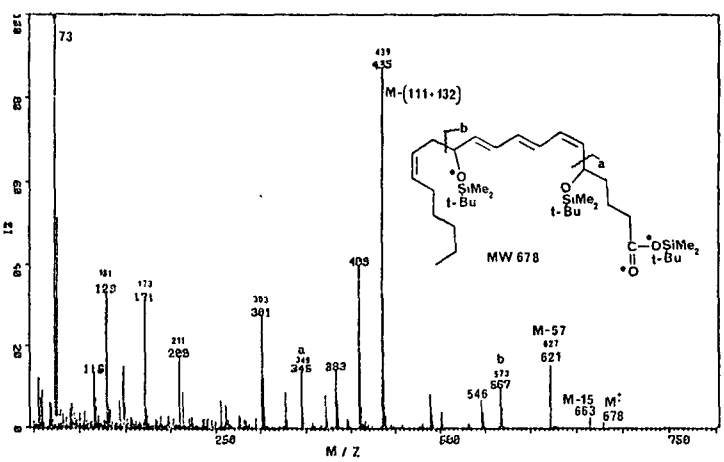

Figure 1: EI mass spectrum of tri-TBDMS derivative of LTB_4.

One unique feature of the oxygen-18 isotopic variants, whose use we have advocated for internal standards, is that they are stable to catalytic hydrogenation as seen in Table 1. [^{3}H]-LTB$_4$ readily loses tritium during the reduction process. Therefore, we feel that the saturated LTB$_4$ as the tri-TBDMS derivative displays considerable promise as a target in the quantitative analysis of LTB$_4$ in biological fluids.

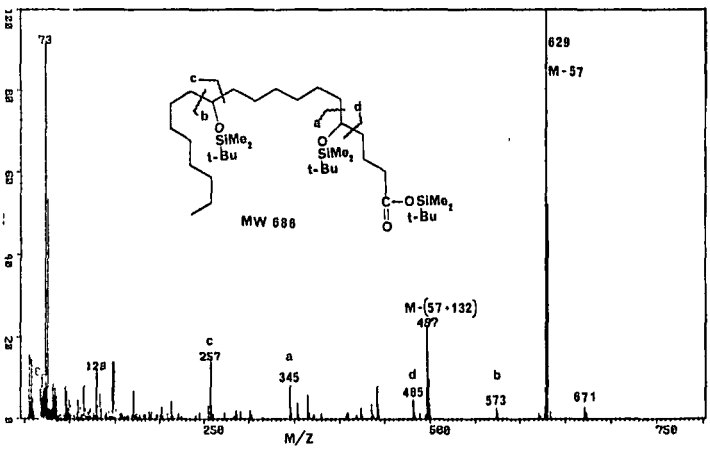

Figure 2: EI mass spectrum of reduced LTB$_4$ as the TBDMS derivative.

Table 1: Catalytic hydrogenation of ^{3}H-LTB4 using Rh/Al$_2$O$_3$ with formation and loss of volatile tritium atoms.

	DPM	
CONTROL	1 Min, H_2	10 Min, H_2
Solution	4000	4180
Residue	3900	4050
Rh/Al$_2$O$_3$		
Solution	2400	2300
Residue	2200	1400

1. 4000 dpm ^{3}H-LTB4 added to each vial
2. Identical aliquots lyophilized to dryness
3. 500 micrograms catalyst added to methanol solution of LTB4
4. H2 gas bubbled at indicated time at 22°

Acknowledgments: This work was supported in part by grant HL 25785 from the National Institutes of Health.

References

1. J.T. O'Flaherty. Lab. Invest. 47:314-329 (1982).

2. A.W. Ford-Hutchinson, et al. Nature 286:264-265 (1980)

3. P. Borgeat and B. Samuelsson. J. Biol. Chem. 254:7865-7869 (1979).

4. R.J. Strife and R.C. Murphy. J. Chromatog. 305:3-12 (1984).

5. M. Mai, B. German and J.E. Kinsilla. J. Chromatog. 254:91-107 (1983).

A THERMOSPRAY IONIZATION ON A SECTOR INSTRUMENT. B. S. Larsen, R. J. Cotter and C. Fenselau, Middle Atlantic Mass Spectrometry Facility, Dept. of Pharmacology, Johns Hopkins University, Baltimore, MD 21205

The thermospray ionization technique has been successfully demonstrated on quadrupole mass spectrometers. However, interfacing the thermospray source to a magnetic sector instrument presents some especially challenging problems because of the high voltages applied to the ion source. Unlike other methods which utilize an electron beam or a reagent gas (i.e., direct liquid injection) to ionize the neutral species, the thermospray technique uses no auxiliary form of ionization. The ions observed by the thermospray method are those ions that are ejected from the solution during the vaporization process. This means that the solution must be carried directly into the source from the grounded LC prior to ion formation; otherwise the ions that are formed would be repelled by the source. Special provisions must be made at the inlet and pump-out line. A configuration which meets the requirement for the magnetic instruments, developed by Vestec, Inc., is currently being tested in this laboratory, and we report some initial results.

APPARATUS - A Kratos MS-50 was fitted with a Vestec thermospray interface which was coupled to a Beckman 110A LC pump fitted with a Rheodyne 7125 injector with a 500 uL sample loop. A schematic is shown in Figure 1.

A supersonic stream of fine particles and droplets is produced by the vaporizer. These particles traverse the source towards the additional pump out line. The ions exit to the analyzer through a conical ion exit aperture.

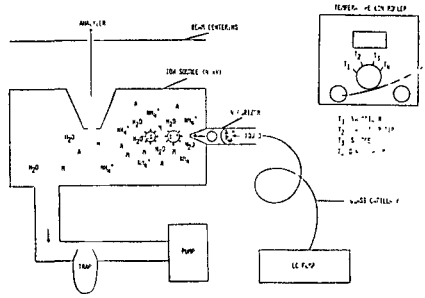

FIGURE 1.

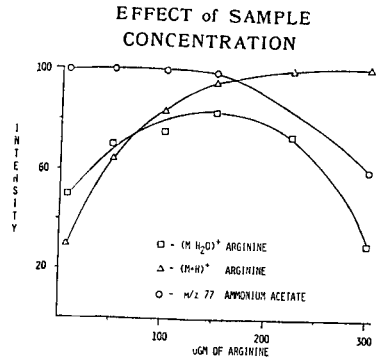

FIGURE 2.

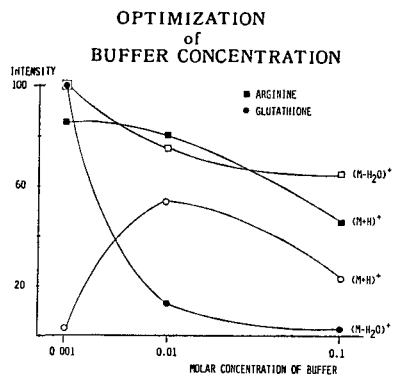

FIGURE 3.

With no electron beam present, the ions sampled are those present in the solution phase as well as those formed as a result of the evaporation process.

It should be noted that for these experiments, no column was present between the LC system and the vaporizer; samples were injected directly into the mobile phase.

The experimental parameters have been optimized. It has been shown that these parameters may not necessarily be the same for a high voltage and low voltage source because of field penetration. Figure 2 shows the optimization of the vaporizer temperature to obtain the best sensitivity for the MH+ ion for a sample or a class of samples. Likewise, Figure 3 represents the effect of the ammonium acetate concentration on a sample spectrum.

Mass spectra for a variety of samples were obtained using 0.01M ammonium acetate buffer at pH 5.5. Shown below are spectra for glutathione and methionine-arginine-phenylalanine. These initial experiments show that the thermospray method can be applied to a magnetic sector instrument and that the interface is stable to 4 kV.

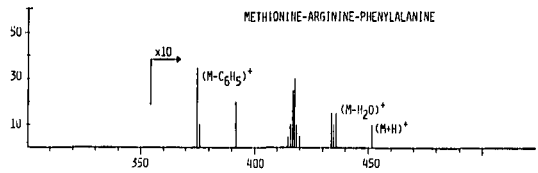

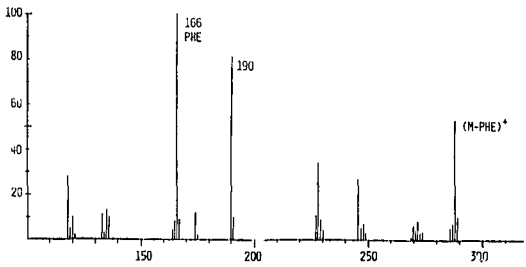

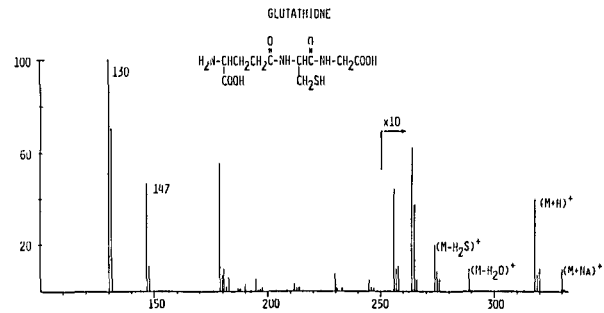

METABOLIC STUDIES OF EXPLOSIVES. LC/MS OF METABOLITES OF 2,4,6-TRINITROTOLUENE

J. Yinon and D.-G. Hwang

Department of Isotope Research
The Weizmann Institute of Science
76100 Rehovot, Israel

The metabolism of explosives in the human body and the analysis of explosives and their metabolites in body fluids are of great importance in several applications:

1. Biomedical field: Many explosives are toxic, therefore inhalation of their vapor presents a major health hazard. Periodical analysis of the body fluids of personnel working in explosives manufacturing plants have to be made for the detection of traces of explosives and their metabolites.

2. Environmental analysis: Improper disposal of obsolete explosives in the environment may cause serious contamination problems. Trace detection of explosives and their metabolites in blood and urine of animals and humans in the disposal area may reveal its contamination state.

3. Forensic application: Trace amounts of explosives absorbed through the pores of a suspect's hands could be detected as metabolites in the blood and urine.

The purpose of this research was to investigate the use of LC/MS as a method for the separation and specification of explosives and their metabolites. The first compounds to be studied were 2,4,6-trinitrotoluene (TNT) and its metabolites (1). The LC/MS system used consisted of an HPLC interfaced to a magnetic sector mass spectrometer by a Direct Liquid Insertion Probe Interface (2). The HPLC column used was an RP-8 reversed-phase column and the mobile phases were acetonitrile:water at various relative concentrations. The investigated metabolites of TNT included 2-amino-4,6-dinitrotoluene (2-A), 4-amino-2,6-dinitrotoluene (4-A), 4-hydroxylamino-2,6-dinitrotoluene (4-OHA), 2,4-diamino-6-nitrotoluene (2,4-DA), 2,6-diamino-4-nitrotoluene (2,6-DA), 2,4,6-trinitrobenzoic acid (TNBAcid), 2,4,6-trinitrobenzyl alcohol (TNBAlcohol), 2,2',6,6'-tetranitro-4,4'-azoxytoluene (4,4'Az) and 4,4',6,6'-tetranitro-2,2'-azoxytoluene (2,2'-Az).
As it is difficult to find one single procedure for the total separation of all these compounds (3) we used several separate isocratic separations with various mobile phases: 20% acetonitrile was used to separate TNBAcid, 2,6-DA, 2,4-DA and TNBAlcohol. 28% Acetonitrile was used to separate TNBAcid, TNBAlcohol, 4-OHA, 2-A, 4-A and TNT; 2,4-DA and 2,6-DA were not separated. 60% Acetonitrile was used to separate TNT, 2,2'-Az and 4,4'-Az. Flow rate was 1 ml/min in all experiments. Figures 1 to 4 show the HPLC chromatogram and the LC/MS mass spectra of TNT, 2,2'-Az and 4,4'-Az respectively, with acetonitrile:water (60:40) as mobile phase.

LC/MS was found to be suitable for the analysis of TNT and its metabolites. The sensitivity of the HPLC measurements was 1 to 10 ng per injected µl, while the sensitivity of the LC/MS system was 100 ng to 1 µg per injected µl. This reduced sensitivity is caused by the low splitting ratio of the LC/MS interface. The use of microbore LC/MS is planned, which is due to increase the sensitivity by two orders of magnitude.

References

1. J. Yinon and D.-G. Hwang, Submitted for publication.

2. J. Yinon and D.-G. Hwang, J. Chromatogr. 268, 45 (1983).

3. D.L. Kaplan and A.M. Kaplan, Anal. Chim. Acta 136, 425 (1982).

COLUMN: RP-8
ACETONITRILE: WATER (60:40)
1 ml/min
UV WAVELENGTH: 214 nm

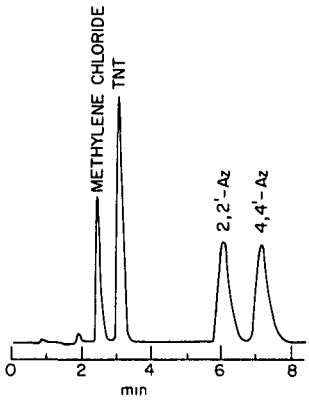

Figure 1

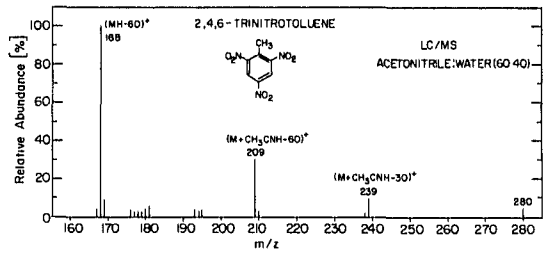

Figure 2

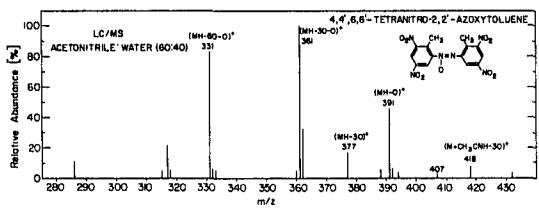

Figure 3

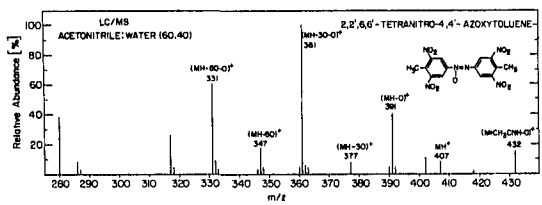

Figure 4

MOVING BELT INTERFACE APPLICABILITY WITH MICROBORE LIQUID CHROMATOGRAPHY/MASS SPECTROMETRY.

D. FRAISSE [1], M. EMMELIN[2], J.L. ROCCA[2], S. ALAMERCERY[1]

(1) Centre de Spectrometrie de Masse du S.C.A.- C.N.R.S.
B.P. 22 - 69390 VERNAISON - FRANCE

(2) Chimie Analytique - Université de LYON I - 43 Bd du 11 Novembre 1918
69621 VILLEURBANNE - FRANCE

The large number of publications published during the last decade shows the interest in on-line liquid chromatography/mass spectrometry technique, but very few papers have been dedicated to the use of microbore columns. The main reason is the very poor efficiency of the commercially available microbore columns. This paper deals with the use of microbore columns with a moving belt interface.

ADVANTAGES OF MICROBORE COLUMNS.

In addition to their advantages for liquid chromatography, i.e low flow rates, smaller amounts of packing materials, higher efficiency and higher mass sensitivity, the packed microbore columns make their coupling with the mass spectrometer much easier.
The major limitation of the moving belt interface with conventional column (i.d 4.6 mm) is the difficulty in using solvent system containing more than 50 % of water. This problem is overcome with microbore columns which make it possible the use of 100 % of water as mobile phase. Even with this percentage of water the reproducibility of repetitive injections of anthracene has proved to be quite good.
Fig. 1 shows the molecular peak ion current of repetitive injections of anthracene with 100 % of water. At flow rates of 20-80µl min^{-1} the infrared heater of the interface is required to get rid of all the water but the temperature can be set much lower than the one necessary at a flow rate of 1 ml min^{-1} with conventional columns. Thus the possible loss of volatile compounds is reduced.
A further advantage of microbore columns is the peak shape which is well improved in comparison with the distorted peak shape obtained with conventional column which involves deposition of large volume of liquid on the belt.
An homemade column developed by ROCCA and EMMELIN permits to obtain 72000 theoretical plates per meter.

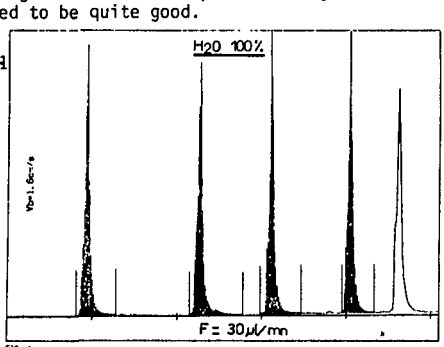

FIG. 1 - REPRODUCIBILITY OF REPETITIVE INJECTIONS OF ANTHRACENE

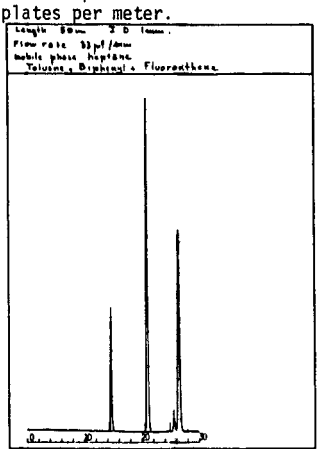

FIG 2 UV TRACES OF A MIXTURE OF TOLUENE / BIPHENYL AND FLUORANTHENE A (500 x 1 MM COLUMN, PACKED WITH 5µ LICHROSORB SI 60 WAS USED WITH HEPTANE AT 33µl MIN^{-1} AS MOBILE PHASE.

This efficiency is illustrated in fig. 2 which shows the UV traces obtained with a mixture of toluene, biphenyl and fluoranthene (200ng of each component) injected into a microbore column (500 x 1 mm)

MICROBORE COLUMN LC/MS:LOSS OF COLUMN EFFICIENCY

For the study of the compatibility of microbore columns the contribution of the moving belt interface and the mass spectrometer on MS peak variance (μl^2) was determined by repetitive injections of anthracene in reversed-phase (methanol / water) and normal phase liquid chromatography at different flow rates (10 to 80 µl min^{-1}). The variance was calculated by using statistical central moment. Fig. 3 and 4 show a plot of MS peak variance against the flow rates. The variance increases faster than the reference variance from an UV detection signal. Fig. 5 shows a plot of efficiency loss against the flow rates. It gives an approach of the value at the capacity factor K' to limit the efficiency loss of the column. In order to reduce at 10 % the loss of efficiency of the column at 50 µl min^{-1} it is recommended to work with a capacity factor $K' \geqslant 6$.

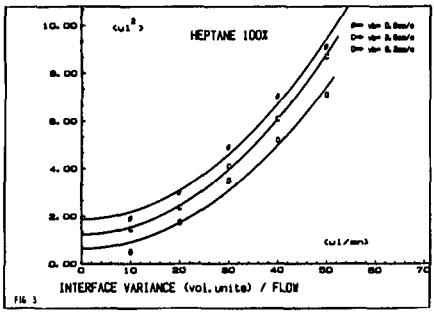

FIG 3

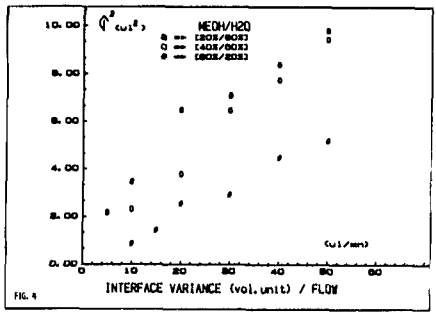

FIG. 4

In conclusion the curve shows that the peak variance and thus the moving belt interface is compatible with microbore columns. It is also advised to have a flow rate as low as possible to limit the loss of efficiency.

ANALYSIS OF BILE ACIDS

To illustrate the utility of the microbore columns for LC/MS a mixture of 7 bile acids (isomers) was analysed (7,12-dioxo-3α-hydroxy, 5β-cholanic acid ; 7-oxo-3,12-dihydroxy cholanic acid ; 3,12-dioxo- 5β-cholanic acid ; 3α- 7β -dihydroxy-5β cholanic acid ; 3α- 7α-dihydroxy-5β-cholanic acid). The seven components are resolved using a 5μ hypersil C18 microbore column (220x1mm) in reversed phase with CH_3OH/H_2O (70:30) as mobile phase. Fig. 6 shows the total ion current trace obtained under EI condition. A flow rate of 80 μl min^{-1} was used to elute the 7 bile acids in a reasonable time. The EI spectra allow the identification of the 7 bile acids isomers but the sensitivity is poor (detection limit 200 ng injected). This is likely due to the partial decomposition of bile acids wich require a high temperature to vaporize.

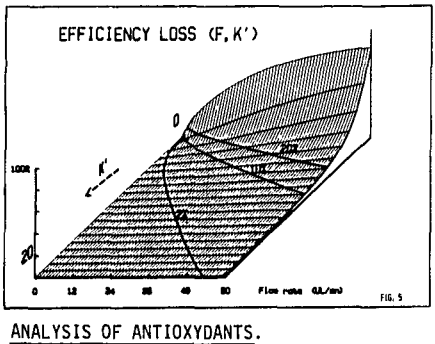

FIG. 5

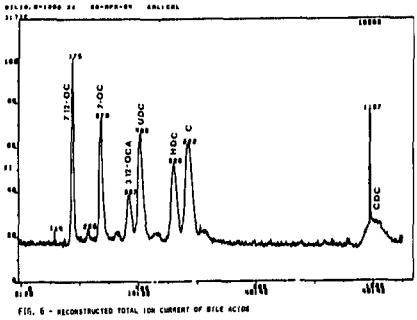

FIG. 6 - RECONSTRUCTED TOTAL ION CURRENT OF BILE ACIDS

ANALYSIS OF ANTIOXYDANTS.

Quantitative analysis of 2 antioxydants, DBPCand Ethyl 702, was investigated in normal phase LC with heptane/ethyl acetate as mobile phase. A 5μ-lichrosorb Si 60 microbore column (220 x 1mm) was chosen. Using selected ion monitoring of the ions m/z 220 (DBPC) and m/z 424 (ethyl 702) quantitative measurements were performed with a good sensitivity : 5 ng for DPBC and better than 800 pg for Ethyl 702. Linear calibration curves (Fig. 7) were obtained in the range of 5 to 100 ng for DBPC and 0.5 to 100 ng for Ethyl 702 with a reproducibility ⩽ 5 %.

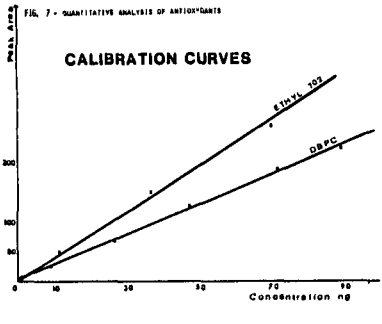

FIG. 7 - QUANTITATIVE ANALYSIS OF ANTIOXYDANTS

ANALYSIS OF INTRACTABLE ENDOGENOUS MOLECULES
BY THERMOSPRAY LC/MS

A.L.Yergey, D.J.Liberato; LTPB, NICHD, NIH, Bethesda, MD 20205

Recent studies continue to show that thermospray LC/MS is a powerful tool for the detection of molecules that are difficult or impossible to analyze by other means. The combination of liquid chromatographic separation and soft ionization lends itself to producing both qualitative and quantitative identification of molecules that have no chromophores, are labile, non-volatile, exist as pre-charged species and/or are isomeric with other components of a mixture.

Two configurations of a thermospray source have been used simultaneously in the last 8 months. The first uses a solid copper block vaporizer described previously (1) in a Biospect mass spectrometer. The second is a Vestec source using a directly heated probe vaporizer (2) in a Finnigan 4000. In general, the two instruments give essentially the same results for mass spectra. The directly heated probe gave an absolute sensitivity of $3x10^{-13}$ coul/ug from a 1 ug direct injection of adenosine with the protonated molecular ion being about 3 times larger than the m/z 136 ion resulting from the sugar loss. The solid block vaporizer gave an absolute sensitivity of about $8x10^{-12}$ coul/ug for a 3.6 ug injection where the molecular ion was about one-third of the m/z 136 ion. Detection limits for acetylcholine are about 0.1 pmoles for the copper block vaporizer and about 80 pmoles for the directly heated probe.The somewhat greater apparent sensitivity of the solid block heater may not be significant in the light of the differences in configuration, and our greater experience in the use of the copper block vaporizer. Certainly one would expect the sensitivities with the two vaporizers to be more nearly the same.

The chromatographic separation and spectra obtained from a study elucidating the biosynthesis of hypusine (3), an amino acid synthesized for a single protein of mammalian cells from spermidine and lysine, by using ^{15}N labelled precursors are shown below. The chromatogram shows the basic amino acids lysine and hypusine and the polyamine spermidine separated using a C-18 column and a 50/50 mixture of .05M ammonium acetate (pH 3.5) and methanol at 1 ml/min. The spectra show incorporation into the secondary nitrogen only in the case where the ^{15}N was used in the synthesis.

In the course of developing a separation for phosphtidylcholines (PC's)we have found an interesting phenomenon in the composition of potential solvent systems. When a methanol/ammonium acetate mobile phase is employed for PC separation, 95% MeOH/5% AmAc (by volume) is required. Very littles ionization is observed with this high organic concentration. The organic modifier could be reduced to 50% by substituting 2-propanol, a separation could still be effected, but again little direct ionization was observed. When several other common organic solvents were studied for their ability to produce direct ionization under thermospray conditions, we noted that there was a very good correlation between the dielectric constant of the mobil phase, as estimated by interpolating between the dielectric constants of the pure solvents, and the ability of the of the solvent to produce ions of either itself or of solute. The limits appear to be about 90% for methanol, 80% for acetonitrile and less for other solvents such as acetone, ethanol, etc. Solvents such as THF and DMSO do not give any ions at 50/50 ratios. It appears that when these solvent mixtures are required for separations, it will be necessary to use filament assisted ionization or to use post column addition of

a solvent with a high dielectric constant such as water or N-methylformamide.

1) Liberato, D.J.; Fenselau, C.C.; Vestal, M.L.; Yergey, A.L. Anal. Chem., 55,1741 (1983).

2) Vestal, M.L.; Fergusson, G.J., submitted.

3) Park, M.H.; Liberato, D.J., Yergey, A.L.; Folk, J.E., submitted.

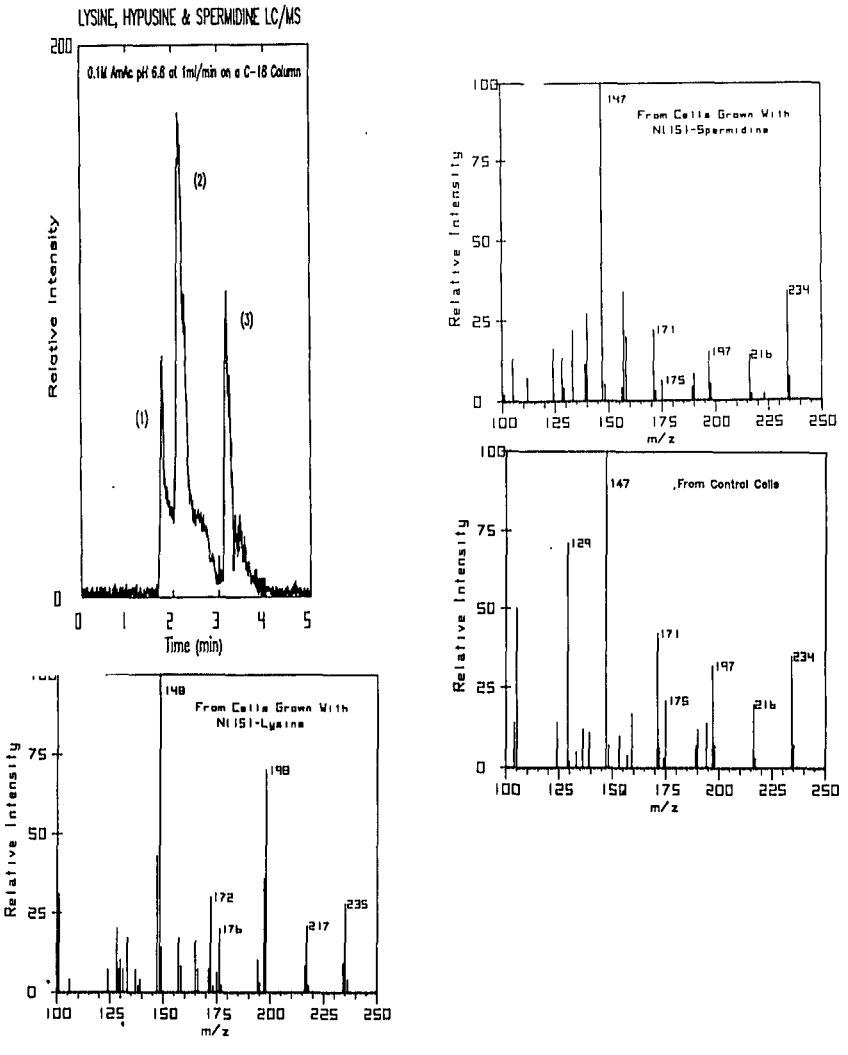

THE ELECTROSPRAY ION (ESPI) SOURCE AS AN LC-MS INTERFACE: C. M. Whitehouse and J. B. Fenn, Department of Chemical Engineering, Yale University, New Haven, CT 06520; R. N. Dreyer, Department of Pharmacology, Yale University, New Haven, CT 06520

We have been investigating the use of the Electrospray Ion (ESPI) source as an on-line interface between a liquid chromatograph and a mass spectrometer. The ESPI source has been described in some detail in our companion paper. We will here simply note that the effluent from the LC is electrosprayed into a bath gas of pure nitrogen at near atmospheric pressure to produce a fine spray of charged droplets that evaporate as they are driven by an electric field toward an orifice or channel that leads into the first stage of the vacuum system housing the MS. As the droplets decrease in size the charge density at the surface increases and their radius of curvature decreases until the resulting field becomes high enough to desorb ions from the liqiud surface. The countercurrent flow of bath gas sweeps away the solvent vapor and any other uncharged material so that what enters the orifice is a dipersion of desorbed and usually desolvated ions in dry bath gas. A core portion of the supersonic free jet on the downstream side of the orifice or channel passes through a skimmer into the vacuum chamber housing and carries ions to the inlet of a quadrupole mass filter (VG Micromass 1212). The LC in these experiments is based on a microbore column (ID 1 mm, LOA 250 mm) kindly provided by Whatman, Ltd. We have not yet obtained appropriately sized injection valves so the samples we introduce have been too large to give rise to "normal" peaks.

Most of our experiments have been carried out with the peptide Cyclosporin A which gives rise to a protonated parent molecule peak having mass of 1203 daltons. The results thus far seem to support the following observations:

1. The shapes of the leading and trailing edges on time-signal are sharp and show little or not tailing. Thus the ESPI source introduces no "dead volume" and does not degrade the LC separation.

2. We have found no evidence to suggest that sensitivity depends on molecular weight of the analyte beyond that expected for decreases in quadrupole trans-

mission and multiplier response for ions of increasing mass. That is, the ionization efficiency seems to be relatively constant over the mass range for the relatively few compounds we have thus far investigated.

3. The system is inherently stable, small fluctuations in liquid flow rate do not cause ripples in the MS output signal. Indeed, for changes in flow rate from about 5 μl/min to 15 μl/min the output changed only a few percent. Modest changes in temperature and flow rate of bath gas do not modify the signal appreciably. Consequently, these variables do not need careful control. The main factors determining the output are the concentration of analyte in the sample liquid flow and the voltage applied to the liquid injection needle. Dependence on the former is not always linear but has a wide dynamic range as one would like for analytical purposes. Dependence on the latter means that a reasonably well stabilized power supply is needed. For a variety of solvents the optimum combination of voltage, bath gas flow rate and temperature settings seem to be identical for all compounds run thus far. Consequently, there is little or no need to adjust these parameters in between peaks.

4. The system is not prone to fouling. The counter-current flow of bath gas sweeps away all the solvent vapor and other uncharged material. In effect, only gaseous ions are carried into the vacuum system by the free jet of bath gas. We have run pretty continuously for as much as a month without any decrease in performance. There was no apparent fouling of surface in the MS chamber. The major problem was a slight accumulation of solid deposit at the end of the hypodermic injection needle and on the side walls of the electrospray chamber. Both of these elements are in the high pressure section of the system and are thus readily accessible for cleaning.

CROSSED-BEAM TECHNIQUE FOR COUPLING LC/MS*

John F. Mahoney, Julius Perel, Phrasor Scientific, Inc., 1536 Highland Ave.,Duarte, CA 91010
Mel Siegel, Carnegie-Mellon University, Schenley Park, Pittsburgh, PA 15213

A crossed-beam technique for coupling LC/MS was investigated under a six month Phase I Small Business Innovation Research (SBIR) Program. The primary objective of this program was to demonstrate the feasibility of combining LC/MS by crossing a liquid jet with a high energy primary ion beam for producing secondary molecular ion signals. The approach adopted for this study comprised the following experimental strategies: (1) minimize evaporation of LC effluent, (2) bombard the liquid jet with an ion beam (particle-induced-desorption) and (3) cryo-collect the non-vaporized mobile phase.

The experimental apparatus used to investigate the crossed-beam LC/MS interface concept is illustrated in Fig. 1.

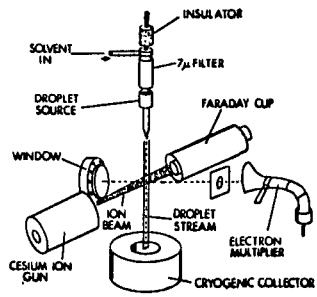

Fig. 1. Crossed-Beam LC/MS Interface Concept.

A Cs^+ primary ion beam was used to bombard a cylindrical liquid jet issuing from a simulated LC column outlet-similar to fast atom bombardment (FAB) where stationary targets are employed. Jet evaporation is minimized by directing the liquid stream into a cryo-collector located 2-3 cm from the injection (droplet source) orifice. The liquid stream, bombarded by primary ions in the exposed transit region, desorb ions by sputtering from the surface. Ions formed in the collision region were detected using a channel electron multiplier. The cryo-collector had a retention capacity of 50 ml - sufficient for conducting tests at flowrates of 1 ml/min for nearly an hour. Preliminary vacuum studies using methanol and acetonitrile jets with flowrates ranging from 0.4 to 2 mil/min demonstrated that the background pressure is independent of the solvent flowrate after the jet starts. System pressures in the 10^{-5} Torr range were maintained at solvent flowrates exceeding 2 ml/min.

Three types of liquid jets were investigated in collision experiments: methanol, 0.1M ammonium acetate buffered methanol and acetonitrile. The Cs^+ ion beam (4kV, 20μA) was scanned across the jets to measure the secondary ion current yield as a function of deflection voltage. A typical result is shown in Fig. 2 for a pure methanol jet at a flowrate of 1.5 ml/min. The secondary ion signal reached a maximum where the primary ion beam directly intercepts the liquid jet. This peak ion current rose two orders of magnitude over the background current measured with the liquid jet off. Secondary ions formed in the collision zone increases with increasing primary ion source voltage or emission current but shows little dependence on the liquid jet flowrate. Substantial gas phase ionization is evident from the signals detected when the primary ion beam is deflected off the jet surface.

Potential advantages of the crossed-beam LC/MS interface concept include:

1. Elimination of the pumping incompatibility of MS systems subjected to complete vaporization of LC effluent.

2. Removal of flowrate restrictions on LC/MS interfaces.

3. Minimal restrictions on LC solvent or buffers.

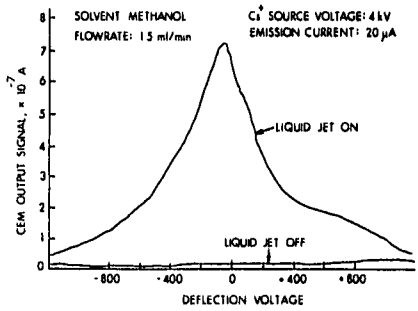

Fig. 2. Secondary Ion Intensity as a Function of Primary Ion Beam Deflection Voltage.

Phase II experimental plans include further characterization of the crossed-beam concept and integration of the interface with a mass spectrometer to study spectra from biological sample molecules. A working prototype LC/MS interface is expected at the completion of Phase II development.

* Supported by NIH-SBIR Grant No. 1 R43 GM 33587-01.

Application of a Monodisperse Aerosol Generation/Liquid Chromatography Interface to Samples of Environmental and Biochemical Importance

L. E. Abbey, D. E. Bostwick, P. C. Winkler,
R. C. Willoughby, and R. F. Browner

School of Chemistry
Georgia Institute of Technology
Atlanta, Georgia 30332

A new liquid chromatograph/mass spectrometer interface has been developed. The design objectives of this new interface include the following: 1) Electron impact (EI) and chemical ionization (CI) operation; 2) Choice of CI reagent gas; 3) No modification of the mass spectrometer; 4) No significant sample heating during transport; 5) No effect on chromatographic resolution; 6) Normal and reverse phase chromatography at solvent flow rates compatible with standard analytical columns.

The interface developed to achieve these objectives features a monodispersed aerosol generator for nebulization of the solvent stream, an atmospheric pressure desolvation chamber, and a two-stage momentum separator to remove solvent vapor from the interface.

The solvent stream from the chromatographic column is nebulized to form a monodispersed aerosol. The aerosol is formed when the solvent stream is forced through a very small glass jet (30 μm i.d.). Droplets of solvent are formed with a regular size and spacing. Before coagulation of adjacent droplets can occur, the jet is dispersed into the desolvation chamber by a helium stream. The aerosol formed by the monodispersed aerosol generator is much more uniform and the flow less turbulent than the more common coaxial pneumatic nebulizer.

The monodispersed aerosol of column eluent is directed by the helium stream through a cylindrical glass chamber. As the droplets travel the length of the chamber, the solvent evaporates, forming a beam of solute particles and solvent vapor entering the momentum separator. Because the evaporation process is carried out at atmospheric pressure, complete desolvation of the solute particles is achieved even using polar solvents (e.g., Methanol, 1 mL/min; Water, 0.5 mL/min).

The beam of solvent particles is separated from the solvent vapor and helium by a two-stage momentum separator. Each stage combines a nozzle and a skimmer, configured to minimize scattering of the particle beam, and a rotary pump. The separator is connected to the mass spectrometer, in this case a Finnigan MAT 112S, using a standard MAT line-of-sight tube in the normal gas chromatographic configuration. The ion source pressure is maintained at 1×10^{-5} Torr for all solvents.

The accompanying chromatogram was obtained using a Finnigan MAT 112S reverse geometry mass spectrometer. The ion source temperature was 240°C, and the resolution (10% valley) was 600. The 112S has an accelerating voltage of 830 eV. In the electron impact mode, the electron energy was 70 eV and the electron current was 1 mA. For chemical ionization, isobutane was used as the

reagent gas. The spectra were obtained using a Finnigah MAT SS200 data system.

The chromatograph was produced using a Kratos Spectroflow 400 pump and an Alltech Econosphere C18 column (25 cm x 4.6 mm, 5 m particle size). The solvent system was 90:10 Methanol:Water; no buffer was used. The chromatography was optimized using a Kratos UV detector set at 254 nm. The pump, column, and detector were supplied to us by Kratos Analytical Instruments.

The monodispersed aerosol generator LC/MS interface produces either EI or CI spectra in an unmodified mass spectrometer. The ionization mode is selected in the same manner as for GC/MS. The choice of CI reagent gas is independent of the LC/MS interface. A wide range of compounds have been run using the interface; no chemical activity has been noted.

Future work will focus on the improvement of the interface transmission efficiency.

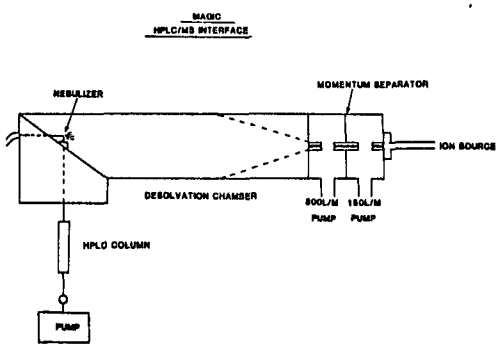

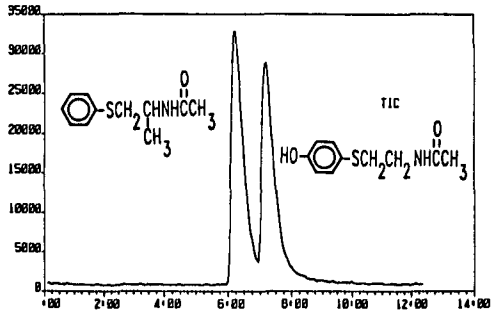

250 x 4.6 mm, 5μm Econosphere Column
Solvent: 90% methanol, 10% water; 0.45 mL/min

OPTIMIZATION OF ION SOURCE IN THERMOSPRAY LC-MS:

F. Poeppel, J. Buchner, H. H. Lo, and J. Dulak,
Extranuclear, Inc. Box 11512, Pittsburgh, PA 15238

INTRODUCTION:

During the last 12-18 months Thermospray LC-MS has become one of the hottest topics in the mass spectrometry community. Pioneering work by Dr. Marvin Vestal has led to commercially available offerings from all major manufacturers. Thermospray can be viewed as both an ionization technique (no filament), and a nebulization technique. An ionizer that doesn't include some means of external ionization will be limited to the analysis of readily ionizable compounds. Unfortunately, due to the high pressures in the thermospray source (10 torr), the inclusion of an electron entrance slit may necessitate the addition of a supplementary LN_2 trap to properly pump the vacuum chamber. This paper will present results of research at thermospray operation as well as thermospray nebulization with supplementary discharge ionization.

OBJECTIVES:

A. Investigate Thermospray Ionization

Probe temperature
Probe position
Vapor stream I.D.

B. Investigate Discharge Ionization (Thermal Nebulization)

Probe temperature
Discharge voltage
Discharge position

RESULTS:

A. Original Design Observations

1. Sample delivery was much more trouble free than DLI
2. Significant thermal fragmentation of Albendazole at optimum temp. for sensitivity
3. Sensitivity for Albendazole by thermospray ionization was about 10x less than by filament generated CI.

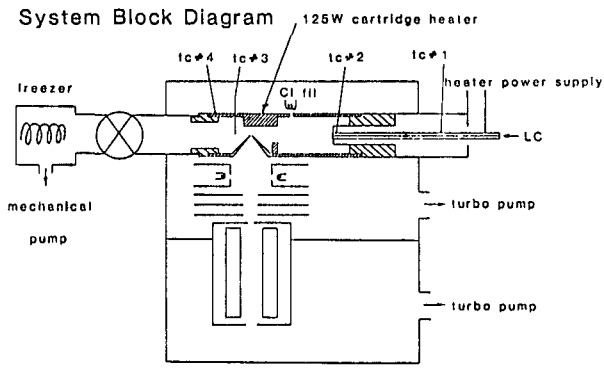

B. Prototype Source Observations

1. Straight through source design didn't work at all for thermospray ionization
2. Presence of a "second ion region" was observed in molecular flow region of the ionizer.
   a. Charged species highly solvated in viscous flow region/or
   b. Gas phase ion paired NH_4OAc

3. Good sensitivity and chromatographic integrity were maintained using discharge ionization at various positions within the source.

4. More ion-molecule reactions were observed from the upstream discharge position as well as higher analyte sensitivities.

Prototype Source

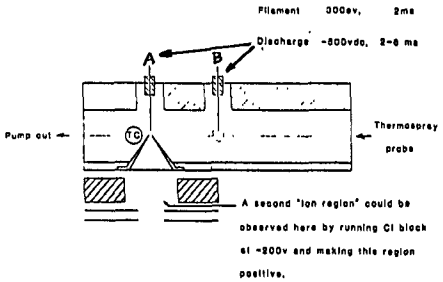

Modified Original Source

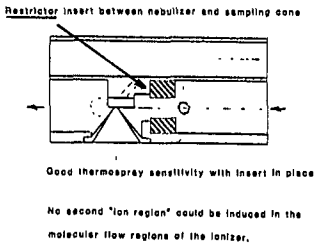

Chromatography

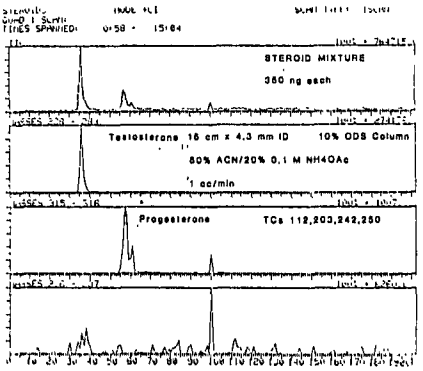

Sensitivity

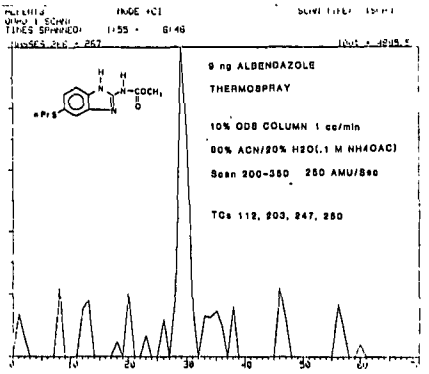

CONCLUSIONS:

1. For Thermospray ionization, heat transfer from the source near the sampling cone is very important.

2. Discharge chemical ionization optimizes at higher nebulizer temperatures but lower source temperatures.

3. For very labile analytes, optimum probe and source temperature is a question of minimizing thermal degradation while maximizing (M+H) + signal.

4. Full scan sensitivities below 10 ng are achievable by either ionization mode.

5. Extranuclear thermospray LC/MS interface includes:
   a. Nebulizer removable for cleaning
   b. 3 different ionization modes: Thermospray, filament, discharge
   c. Pumping via easily regenerated freon refrigerator trapped mechanical pump
   d. Easy changeover from GC to LC via plug in ionizers

ACKNOWLEDGEMENTS:
Dr. Marvin Vestal, Vestec Corporation - Dr. James Yergey, NIH

Thermospray: New Developments and Applications

W.H. McFadden & M.G. Tucker
Finnigan MAT, San Jose, CA

Thermospray is becoming a widely used technique for ionization of sensitive samples and for LCMS studies. The thermospray process involves careful heating of an electrolytic solvent so that the liquid is sprayed out as a fine mist into a jet chamber (the equivalent of the ion chamber). By careful control of the vaporizer temperature, the electrolyte ions can be preserved in the vapor form and interact with the solute to provide gentle sample ionization. Ions are sampled to the mass spectrometer by lateral expansion of the jet stream through a small orifice (nominally 0.02" dia.).

Early models of thermospray utilized a heated copper block to provide vaporization of the solution. The method works well when proper thermal equilibrium has been achieved but suffers an annoying time lag of as much as 30 secs. between sensor, heaters, copperblock, and liquid when temperature adjustments are necessary. Use of direct heating on a hypodermic capillary eliminates the thermal lag and provides more accurate and rapid temperature control of the vaporizer (Figure 1).

The process of sampling ions by lateral expansion of the jet inherently discriminates against higher mass ions. By use of a small repeller electrode (Figure 1) ion extraction can be enhanced 1 to 2 orders of magnitude depending upon the sample and upon other thermospray conditions.

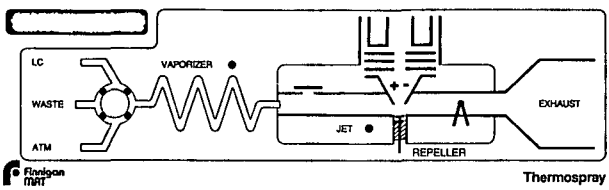

- **Direct Heating of Vaporizer Provides Rapid Response and Improved Control of Vaporizer Temperature**
- **Repeller Voltage Increases Ion Extraction Particularly for High Mass Ions**

Figure 1

A microprocessor control unit is used to provide temperature control of the vaporizer and jet chamber. The program includes a ramp function that permits the vaporizer to be temperature programmed for optimization during gradient elution. In addition the microprocessor provides a diagnostic monitor that checks temperature, vacuum, and component status. In the event of failure, a pneumatic valve in the flow controller is activated to divert the LC flow from the mass spectrometer.

Figure 2 shows the total ion current observed for multiple injections of a polypropylene glycol solution, Av MW 550, as a function of varying repeller voltage. For each duplicate injection, the repeller voltage was reduced 20 volts. The dramatic effect of reducing the repeller voltage is quite evident. Figure 3 shows a plot of base peak intensity (mass 482, n=8 or mass 540, n=9) as a function of repeller voltage. In this specific case, approximately 2 orders of magnitude increased sensitivity were realized by varying the repeller from 0 to 200 volts. The repeller voltage cannot be increased further since discharge will occur in the pressure realm of the thermospray source (ca 10^3 Pascals).

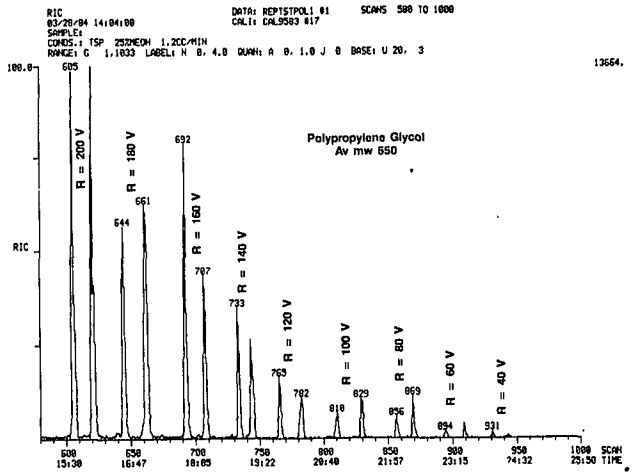

Figure 2

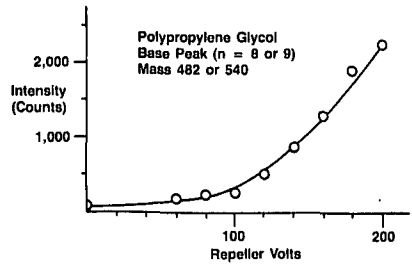

Figure 3

ANALYSIS OF PHOSPHOLIPIDS BY HPLC-MASS SPECTROMETRY

Robert H. McCluer, Firoze B. Jungalwala and James E. Evans
Eunice Kennedy Shriver Center, Waltham, MA 02254

Phospholipids are important constituents of all cell membranes. Phospholipid composition and molecular species of individual phospholipids vary considerably in different cellular and subcellular membranes. Considerable evidence is accumulating to indicate that subtle changes in either the phospholipid composition or molecular species may be responsible for altered biological properties of membranes such as ion transport, enzymic activity, action potential, receptor function or cell-membrane integrity. It is therefore evident that a rapid and sensitive method for the separation and analysis of phospholipids and their molecular species should be useful in understanding cell-surface phenomena. High performance liquid chromatography (HPLC) coupled with mass spectrometry (MS) was employed for the compositional and molecular species analysis of phospholipids. A moving-belt transport type interface was used for the coupling. Chemical ionization mass spectra of various intact phospholipids were obtained after HPLC. By this method extensive information can be directly obtained regarding the composition and relative abundance of molecular species of naturally occurring phospholipids in a short time interval with high sensitivity. We have also used the HPLC-CIMS method for the direct analysis of total lipid extracts from less than 100 ug of tissue samples such as human sural nerve. Cholesterol, cerebrosides, sulfatides and various phospholipids were resolved and analyzed by HPLC-CIMS. The relative abundance of the molecular species of individual lipids was also determined simultaneously by this method.

Experimental

HPLC was performed with a Spectra Physics (model 8700) gradient pump and Brownlee cartridge, 6 cm x 2.0 mm spherical silica (5 μm) column. The colum was eluted with a linear gradient of solvent A, dichloromethane-methanol-water 93:6.5:0.5 (by volume) and solvent B, dichloromethane-methanol-water-15 M NH_4OH 65:31:4:0.1 (by volume), from 12% B to 45% B in 10 min and programming to 100% B in 2 min, at a flow rate of 0.8 ml/min. The sample to be injected was dissolved in dichloromethane-methanol-15 M ammonia 1:1:0.01 (by volume) at a concentration of about 1 μg phospholipid per 1 μl. The HPLC solvent was applied as a fine stream to the moving belt of a Finnigan HPLC-MS interface to achieve an even coating. The stream was formed by inserting a 10-cm section of polyimide-coated fused silica capillary GLC column (0.25 mm i.d.), pulled to a fine orifice. The sample evaporator heater was at 330° C and the cleanup heater was at 210° C. A Finnigan model 4500 mass spectrometer was used with ammonia (0.75 torr) or methane (0.6 torr) as the CI reagent gas. The ion source was at 150° C. Positive and/or negative ion spectra were obtained by the system under the control of a Teknivent model 56K MS data system. MS data were collected from m/z 100-900 with 5-7 second scans.

Results

Positive and negative CIMS of various synthetic and naturally occurring phospholipids were obtained with ammonia and methane as the reagent gases. Major characteristic fragment ions in the positive ammonia CIMS of various phospholipids are listed in Table 1. Each phospholipid had characteristic "base" related ions. These ions were used in monitoring the appropriate phospholipid after HPLC. The major ions in the high mass range of each phospholipid were the diglyceride or ceramide ions, [M+-phosphobase] and the ammonia adduct ions, $[M+35]^+$-phosphobase. It appears from the analysis of relative intensity of the diglyceride-related ions one can directly calculate the percentage composition of molecular species with different fatty acids in each phospholipid. The percent distribution of fatty acid in different phospholipids as analyzed by GLC was very similar to that calculated from the MS data.

HPLC-CIMS of total lipids of a pathological sample of human sural nerve is given in Fig. 1. All major lipids of the nerve were resolved by HPLC-MS. The reconstructed specific ion plots for each lipid are given in Fig. 1, M/z 141 was mostly specific for phosphatidylethanolamine, Pe, Fig. 1b; m/z 142 for phosphatidylcholine, Pc and sphingomyelin, Sp Fig. 1c; m/z 180 for sugar containing lipids, nonhydroxy and hydroxy fatty acid (NFA and HFA) containing cerebrosides, Cer, sulfatides Su, and phosphatidylinositol, Pi, Fig. 1d; m/z 369 for cholesterol, Ch, Fig. 1e; m/z 548 for ceramide with 18:0 and d18:1-sphingenine, Fig. 1f; m/z 551 for diglyceride with 16:0-16:0 Fig. 1g and m/z 648 for ceramide with 18:0 hydroxy fatty acid and d18:1-sphingenine, Fig. 1h.

In summary major complex-lipids of cellular membranes were directly analyzed by HPLC-CIMS method and information on their fatty acid molecular species was derived from the MS data (1).

Reference:

(1) Jungalwala, F.B., Evans, J.E. and McCluer, R.H. (1984) J. Lipid Res. 25:738-749.

TABLE 1. Major characteristic fragment ions in the positive ammonia CIMS of various phospholipids

Phospholipid	m/z	Phospholipid	m/z
PC	142 (from phosphocholine) $[M + 1]^+$ $M^+ - 41$ $M^+ - 182$ $[M + 35]^+ - 182$	SP	142 (from phosphocholine) $M^+ - 182$ $M^+ - 182 - 18$
		Lyso PE	141 (ethanolamine phosphate) $M^+ - 140$
PE	141 (ethanolamine phosphate) $M^+ - 140$ $[M + 35]^+ - 140$ $[M + 17]^+ - 140$		$[M + 35]^+ - 140$ $M^+ - 43$ $M^+ - 17$
		Lyso PC	142 (from phosphocholine) $M^+ - 182$ $[M + 35]^+ - 182$ $M^+ - 31$
PS	105 (serine) $M^+ - 184$ $[M + 35]^+ - 184$		
PI	180 (inositol) 198 (inositol + 18) $M^+ - 259$ $[M + 35]^+ - 259$		$M^+ - 41$
		PG	172 (glycerol phosphate) $M^+ - 171$ $[M + 35]^+ - 171$

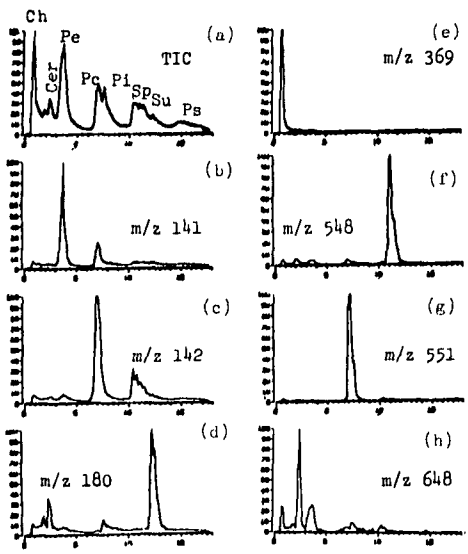

Fig. 1. HPLC-CIMS of complex-lipids from human sural nerve equivalent to 64 μg protein. Reconstructed plots of total ion current (TIC) and specific ions indicated are given.

THERMOSPRAY HPLC-MS OF PROSTAGLANDINS AND OXYGENATED METABOLITES OF ARACHIDONIC ACID (C20:4) AND DOCOSAHEXAENOIC ACID (C22:6).

James Yergey, Norman Salem, Jr.; Laboratory of Clinical Studies, National Institute of Alcohol Abuse and Alcoholism, Room 3C-218, Building 10, NIH, Bethesda, MD, 20205.

INTRODUCTION: Ethanol produces a variety of physiological effects including alteration in membrane physical properties and alteration of the metabolism of unsaturated fatty acids. Reported effects of ethanol on the production of prostaglandins and other oxygenated products of arachidonic acid have been somewhat inconsistent. In addition to clarifying the effects of ethanol and alcoholism on the metabolism of arachidonic acid, our laboratory has initiated investigations into the oxygenated metabolites of docosahexaenoic acid (C22:6), the major polyunsaturated fatty acid in aminophospholipids of brain and retina. Recently, the conversion of C22:6 to a trihydroxylated fatty acid by trout gill homogenate was described, however, this product has never been observed in mammalian tissue nor have the effects of ethanol on this enzymatic system been described.

METHODS: Analysis of the oxygenated metabolites of fatty acids in biological systems has typically involved class separation on a short LC column, followed by one or more HPLC separations, derivitization and final analysis by GC-MS. Reducing the analysis to a single class separation, followed by HPLC-MS analysis should be a more effective method for the investigation of this system of compounds. A thermospray HPLC-MS interface (Vestec Corporation, Houston TX) has been coupled to an Extranuclear ELQ-400-2 quadrupole mass spectrometer. *In vitro* studies of docosahexaenoic acid metabolism were conducted by incubating rat brain homogenate with the C22:6 fatty acid. Supernate from centrifuged samples were separated on Sep-Pak cartridges using 15% ethanol, benzene, and ethyl acetate as eluants. Reverse phase HPLC with 0.1M ammonium acetate as mobile phase and a gradient from 30 to 70% acetonitrile was used to separate the components of the ethyl acetate fraction. Standard prostaglandins and HETE's were used to establish HPLC and interface conditions. Interface and ion source temperatures were optimized at 230°C and 250°C, respectively, and mass spectra were recorded from m/z 110-510 at 500 amu/sec.

RESULTS AND DISCUSSION: Mixtures of standards gave good chromatographic separation with the exception of the twenty carbon prostaglandins, which could be distinguished by examining individual ion chromatograms (Figure 1). Spectra for standards were dominated by molecular species, including ammoniated and natriated molecules and simple losses of water from ammoniated and protonated molecules. An example for leukotriene B_4 is given in Figure 2. Rat brain ethyl acetate fractions yeilded a number of coeluting peaks in the region where hydroxylated arachidonic acid standards eluted (Figure 3). Peaks in the rat brain ethyl acetate fractions were not observed in a boiled control incubation indicating enzymatic formation. Examination of the mass spectra indicated that two distinct groups of metabolites exist (Figures 4 & 5). The later eluting peaks are postulated to be monohydroxylated-C22:6 metabolites based on their spectra, which are analogous to monohydroxylated arachidonic acid with a base peak at $[M+H-H_2O]^+$. The first group of metabolite peaks yielded spectra which were not completely analogous with the standard compounds analyzed. If they are assumed to be trihydroxylated metabolites the spectra are analogous to standard compounds with the exception of a peak at m/z 385, since it might correspond to a natriated dihydroxy metabolite. The possibility that a dihydroxy metabolite is being formed would also seem likely, however, the large peak at m/z 363 would then correspond to an $[M+H]^+$ ion which was not observed for any oxygenated fatty acid examined.

CONCLUSIONS: HPLC/Thermospray mass spectrometry has been successfully demonstrated for a wide variety of oxygenated fatty acid derivatives. Gradient elutions seemed not to effect the sensitivity of the mass spectra in the range neccessary to elute both prostaglandins and hydroxylated derivatives. The spectra of standard compounds are dominated by molecular species, including ammoniated and natriated molecules, and simple losses of water from ammoniated and protonated molecules. Protonated molecules were not observed in comparable intensity, possibly due to the greater energy imparted to the molecule from protonation versus ammoniation. The technique was also successfully applied to the separation and tenative identification of a number of novel oxygenated metabolites of docosahexaenoic acid. Two distinct groups of metabolites were discovered based on the thermospray mass spectra. The later eluting peak envelope appear to be monohydroxylated C22:6, since the spectra were completely analogous to those found for monohydroxyarachidonic acid. However, the other set of peaks produced spectra which could not be completely assigned. Further studies are in progress to establish the identities of the metabolites revealed in this investigation.

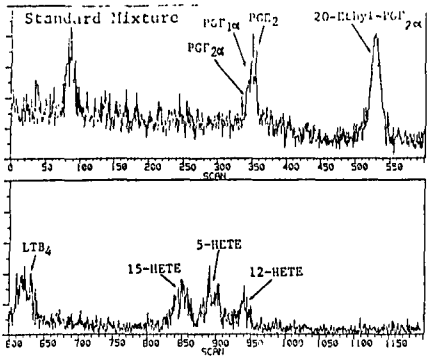

FIGURE 1

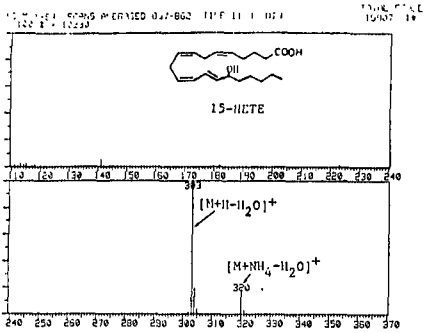

FIGURE 2

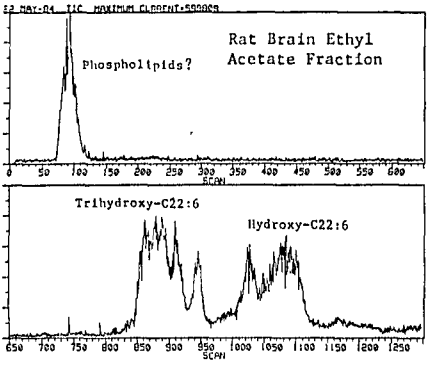

FIGURE 3

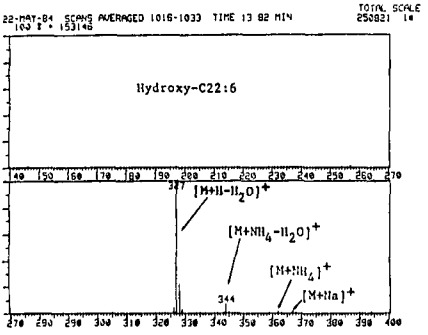

FIGURE 4

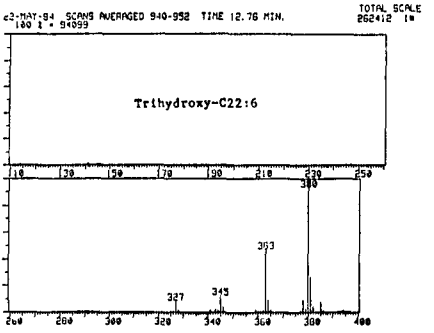

FIGURE 5

LCMS: Direct Liquid Introduction and Thermospray Operation on a Magnetic Sector Instrument

J.R. Chapman, S. Sayyid, S. Evans
Kratos Analytical Instruments, Ramsey, New Jersey, U.S.A.

The thermospray process (1) offers a means of vapourizing high flow rates of solvents and of ionizing labile samples while these are in solution. It is therefore an important method for interfacing a liquid chromatograph and mass spectrometer. This abstract describes an LCMS interface for thermospray operation on a magnetic sector instrument.

Liquid flow from the LC is rapidly vapourized by spraying from the end of a resistively heated stainless steel capillary. This capillary is mounted in a vapourizer probe which is introduced through the standard vacuum lock into a specially designed ion source. Vapourized solvent is removed via a pumping line attached directly to the source. Electrical leakage from the ion source which is operated under conventional high voltage conditions is prevented by a length of fused silica capillary which connects the LC column to the vapourizer probe and by the use of a cold trap in the source pumping line.

During the spraying process, the liquid stream is converted into a directed jet of tiny droplets which themselves evaporate in a short period of time. In the presence of an added electrolyte, such as ammonium acetate, each droplet acquires an excess charge which may be transferred to a dissolved sample molecule during the subsequent evaporation process. Thus, sample ions may now be formed from the most labile molecules by a mild process in the absence of an energetic, external ionization source.

Spectrum quality with thermospray ionization is influenced by operating temperatures particularly that of the capillary. Precise regulation of heat input via the capillary and via the ion source block is therefore an important requirement with this method of LCMS interfacing. A filament may also be used with the same ion source to provide more conventional chemical ionization conditions for compounds that are weakly ionized in solution or when an additional electrolyte is not present.

Thermospray ionization provides strong quasimolecular ions from a wide range of labile compounds. In the case of compounds which contain a quaternary nitrogen a major peak in the mass spectrum corresponds to the intact cation. Under appropriate conditions thermospray ionization also provides structurally informative fragment ions. For example a number of peptides show a virtually complete set of sequencing ions as well as a quasimolecular ion.

(1) Blakley, C.R., Vestal, M.L., Anal. Chem., 55 (1983) 750

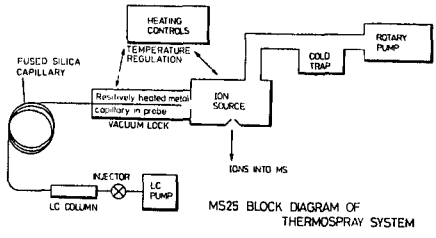

MS25 BLOCK DIAGRAM OF THERMOSPRAY SYSTEM

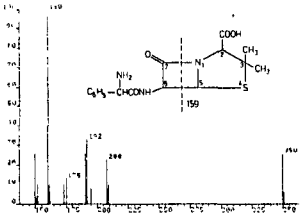

MS25 Thermospray LCMS ampicillin (M wt=349)

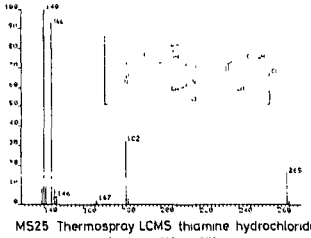

MS25 Thermospray LCMS thiamine hydrochloride (cation – HCl = 265)

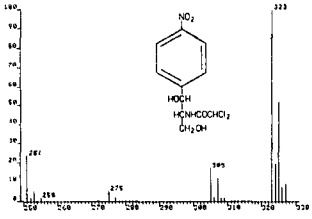

MS25 Filament-on LCMS chloramphenicol (M.wt 322)

MASS ANALYSIS OF MOLECULES OF MOLECULAR WEIGHT GREATER THAN 1500 DALTONS USING A THERMOSPRAY ION SOURCE

Paul C. Goodley and Christine N. Kenyon
Hewlett-Packard Company, 1601 California Avenue, Palo Alto, CA 94304

A powerful new capability of expanded mass range combined with either direct liquid introduction (DLI) or thermospray (TS) liquid chromatography-mass spectrometry (LCMS) can yield important molecular structural information to the synthetic chemist, biochemist, and/or life scientist.

The technique of DLI-LCMS (1) has been shown to be extremely useful for a wide variety of thermally labile and/or non-volatile compounds. Also, TS-LCMS has been shown to be a powerful technique (2-4) for selected synthetic and naturally occurring compounds.

When combining the two techniques or TS-LCMS with expanded mass range on a quadrupole spectrometer, it is necessary to calibrate the mass axis and to obtain optimum resolution. In this study it was found that synthetic polymers of polyethylene glycol and polypropylene glycol could be used to accurately obtain the mass axis calibration. The ease in calibrating the mass axis is enhanced due to the repeating regular polymer units. For polypropylene glycol the unit is 58.04 Daltons, and for polyethylene glycol the unit is 44.03. The calculated masses for the two glycols are shown in Table I. The calculated mass includes the molecular weight plus an H_3O adduct. All the polyglycols examined exhibited the H_3O adduct formation without exception under TS conditions.

Figure 1 shows a mixture of polypropylene glycols having average molecular weights of 1000 and 2000 injected through the vaporizer of a TS-LCMS ion source at 1.8 ml/min. The repeating 58 Dalton separation is depicted along with the isotope distribution.

Figure 2 shows the same PPG mixture scanned from 800-2000 Daltons and two separate distribution patterns. The distribution pattern shown in Figure 2 for the molecular entities of PPG could also be utilized to characterize and/or calculate the average molecular weights of the synthetic polymer reactions, thus eliminating some laborious chromatographic analysis for the synthetic chemist and may offer a new method for the polymer industry.

TABLE I
CALCULATED MASSES OF POLYGLYCOLS

Polymer Units (N)*	PEG Calculated Molecular Weight	PPG Calculated Molecular Weight	Polymer Units (N)*	PEG Calculated Molecular Weight	PPG Calculated Molecular Weight
2	125.1	153.1	19	873.5	1139.8
3	169.1	211.2	20	919.5	1197.9
4	213.1	269.2	21	961.6	1255.9
5	257.2	327.2	22	1005.6	1313.9
6	301.2	385.3	23	1049.6	1372.0
7	345.2	443.3	24	1093.7	1430.0
8	389.2	501.4	25	1137.7	1488.1
9	433.3	559.4	26	1181.7	1546.1
10	477.3	617.4	27	1225.7	1604.2
11	521.3	675.5	28	1269.8	1662.2
12	565.3	733.5	29	1313.8	1720.2
13	609.4	791.6	30	1357.8	1778.3
14	653.4	849.6	31	1401.8	1836.3
15	697.4	907.7	32	1445.9	1894.4
16	741.4	965.7	33	1489.9	1952.4
17	785.5	1023.7	34	1533.9	2010.5
18	829.5	1081.8			

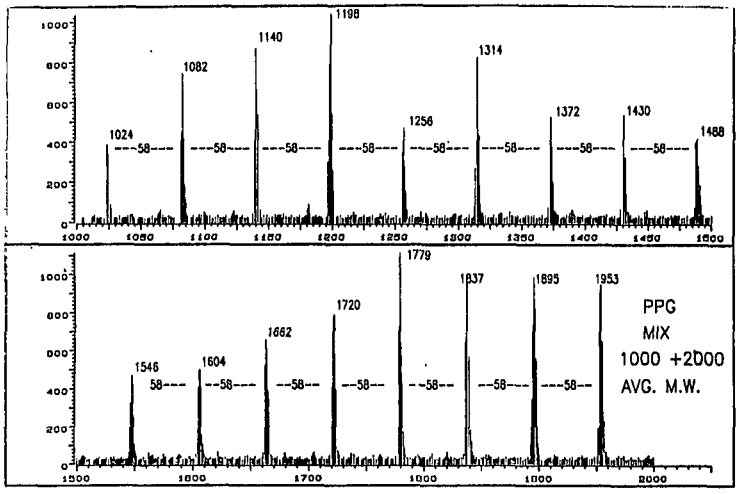

Figure 1. PPG mixture scanned from 1000-2000 Daltons showing the repeating units obtained using a TS ion source.

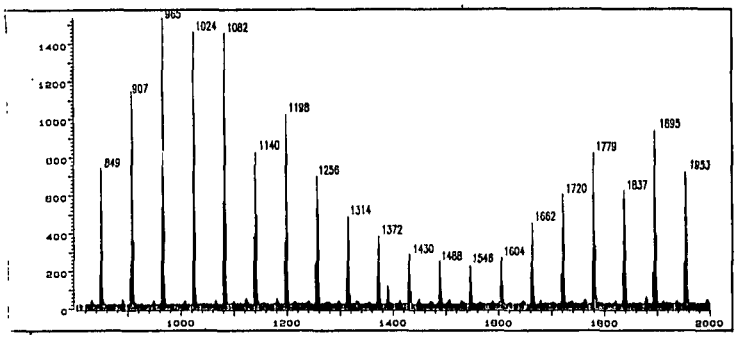

Figure 2. PPG mixture scanned from 800-2000 Daltons using a thermospray ion source and depicting the two distribution patterns.

1. Kenyon, C. N., Biomed. Mass Spec., 10, 10 (1983).
2. Blakley, C. R., M. J. McAdams, and M. L. Vestal, J. Chromatog., 158, 261 (1978).
3. Blakley, C. R., and M. L. Vestal, Anal. Chem., 55, 75 (1983).
4. Blakley, C. R., J. J. Carmody, and M. L. Vestal, J. Am. Chem. Soc., 102, 5931 (1980).

SELECTED APPLICATIONS OF LC/MS TO PROBLEMS IN BIOMEDICAL ANALYSIS:

R.W. Smith, K. Yamaguchi, C.E. Parker, H.B. Matthews, J.R. Hass, T. Nagano, I. Fridovich, I.P. Lee, I.A.S. Lewis and I. Parr. LMB, LRDT, and TRTP, NIEHS, Research Triangle Park, N.C. 27709; Biochemistry Dept., Duke University Medical School, Durham, N.C. 27710; VG Analytical, Manchester, England.

This paper describes the application of LC/MS to four biomedical problems.

The first project involved the identification of the major metabolite of TBBC (4,4'-thio-bis(6-t-butyl-m-cresol)), an antioxidant used in the rubber and plastics industries. The LC/MS technique used for this project involved reversed phase chromatography and negative chemical ionization. Comparisons of LC/MS data for the in vivo metabolite and a synthetic reference compound showed the metabolite to be the glucuronide acid conjugate of TBBC. The LC/MS results confirmed earlier negative ion SIMS MS/MS experiments.

The second project involved the characterization and tentative identification of the metabolites of 2,4-dinitroaniline (2,4-DNA), a compound used widely in the dyestuffs industry. The LC/MS technique used for this project involved reversed phase chromatography and negative chemical ionization. Enzymatic hydrolysis reactions and LC/MS results showed the major metabolite of 2,4-DNA to be the sulphate ester of 2,4-dinitrohydroxylamine.

The third project described in this paper involved the xanthine oxidase-acetaldehyde system which generates superoxide ($O_2^{\cdot -}$) and H_2O_2. The objective was the identification of singlet oxygen ($^1O_2$) generated either in the disproportionation process or in the Fe-catalyzed reaction of $O_2^{\cdot -}$ and H_2O_2 following this reaction. Unstable substituted furan hydroperoxide, the product of the reaction of $^1O_2$ with the dimethyl furan which had been added to the enzymatic system, was detected by DLI (LC/MS. This substituted furan hydroperoxide, which show no UV absorbance, was well-resolved from its degradation products in a normal-phase chromatographic system with CH_2Cl_2/hexane as the solvent. Negative chemical ionization LC/MS of authentic material gave distinct chloride attachment peaks corresponding to $(M+Cl)^-$.

The fourth project involved the use of LC/MS for the detection of procarbazine-induced changes in nucleosides from mammalian tissues in order to relate these DNA modifications to altered gene expression. A DLI LC/MS technique involving micro-LC with reversed-phase chromatography and positive chemical ionization was developed for this project. Nucleosides and bases were also analyzed by thermospray positive ionization LC/MS. Certain nucleosides and bases gave $(M+Na)^+$ and $(M+K)^+$ in the thermospray mode.

ISOLATION OF A PLANT CELL CULTURE PRODUCT AND ITS IDENTIFICATION BY COMBINED LC/MS

A.P. Bruins and N. Pras

State University, Departments of Pharmacy and Pharmaceutical Biotechnology,

A. Deusinglaan 2, 9713 AW Groningen, The Netherlands

In-vitro grown cells of Mucuna Pruriens, immobilized in calcium alginate beads, are able to transform L-tyrosine into dihydroxyphenyl-L-alanine (L-DOPA) (1). Expressed more generally: a para substituted phenol is transformed into a catecholic compound. On the enzymatic level, this biotransformation is conducted by a tyrosinase (Figure 1). Concentrations of substrate (p-hydroxyphenylacetic acid) and product (DOPAC) are routinely monitored by HPLC with UV and electrochemical detection. The identity of DOPAC can be confirmed by LC/MS.

The LC/MS system is a Jasco Familic 100N micro LC coupled to a Finnigan 3300 chemical ionization MS via a home made direct liquid introduction interface (2). The total effluent from the micro LC is transported into the ion source via a 50 µm i.d. fused silica capillary. Solvent and sample are evaporated together inside the last few millimeters of the capillary. Non volatile contaminants, proteins, salts or buffer components will block the capillary.

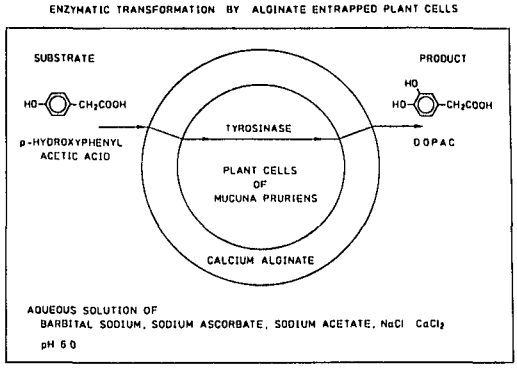

Figure 1

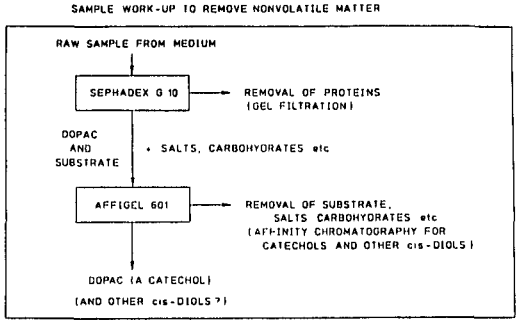

Figure 2

Figure 2 shows the sample preparation scheme for removal of nonvolatile matter and salts. Retention on and elution from Affigel 601 is strongly pH dependent. Final elution with 1 M acetic acid afforded a DOPAC fraction, suitable for LC/MS (3).
LC/MS was performed both in the positive and in the negative ion chemical ionization modes. Additional reactant gases were methane/NH_3 and methane/CF_2Cl_2 for generation of NH_4^+ and CL^- respectively. The micro LC eluent was 80% aqueous ammonium acetate/acetic acid buffer and 20% acetonitrile at 5 µl/min. Figure 3 shows micro liquid chromatography combined with negative chemical ionization using Cl^- as the reactant ion. The extracted ion current profiles in Figure 3 and the positive and negative ion Cl spectra in Figure 4 indicate that the biotransformation product is indeed DOPAC. Figure 3 also demonstrates that the MS has detected and unknown not observable by UV (and electrochemical) detection. The molecular weight of this unknown compound is 148, as derived from the $M.NH_4^+$ and $M.Cl^-$ ions at m/z 166 and m/z 183/185 respectively.

References

1. H.J. Wichers, Th.M. Malingré and H.J. Huizing, Planta 158, 482-486 (1983)
2. A.P. Bruins and B.F.H. Drenth, J. Chromatogr. 271, 71-82 (1983)
3. A.P. Bruins and N. Pras, submitted to Anal. Chim. Acta

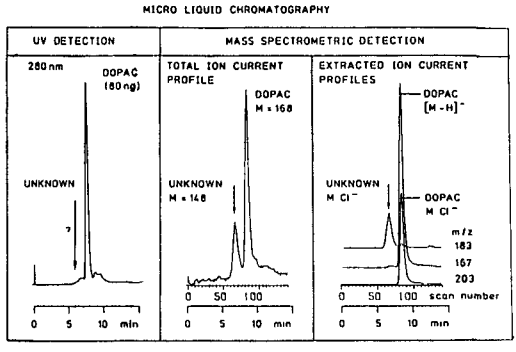

Figure 3

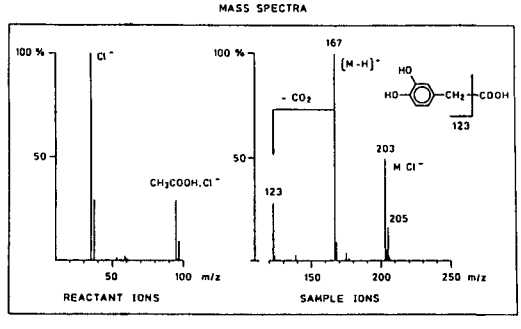

Figure 4

A SIMPLIFIED MOVING-BELT INTERFACE FOR LIQUID CHROMATOGRAPHY-MASS SPECTROMETRY

S. J. Stout and A. R. daCunha

American Cyanamid Company, Agricultural Research Division, P. O. Box 400, Princeton, New Jersey 08540

Introduction

Existing LC-MS interfaces of the moving-belt design rely upon application of the liquid eluate to the belt in a chamber maintained at approximately atmospheric pressure. While atmospheric pressure at the point of solvent application simplifies the process of applying a liquid to a moving belt, it also necessitates the use of two vacuum locks to reduce the pressure to the much lower operating pressures required in the ion source of the mass spectrometer. Each vacuum lock consists of a set of machined slits and an evacuated chamber pumped by its own mechanical vacuum pump. Because of the required machined slits and evacuated chambers, existing moving-belt LC-MS interfaces are rather large and cumbersome and are mounted to the mass spectrometer on a separate flange.

Objective

To design and construct a simplified moving-belt LC-MS interface which can be inserted into the mass spectrometer via the conventional solid probe inlet.

Approach

Apply the liquid eluate to the moving belt inside a single evacuated chamber pumped by a single 200 liter/minute mechanical vacuum pump. Run the belt to the ion source through 1/2-inch OD tubing in order to allow insertion of the interface through a conventional solid probe inlet.

Operating Pressures and Principal Ions

CH_3OH Flow Rate (μL/minute)	Source Pressure (torr)	Interface RP Pressure (torr)	Principal Ions (m/z)
0	0.40 (CH_4)	0.26	17^+ (CH_5^+)
			29^+ ($C_2H_5^+$)
			41^+ ($C_3H_5^+$)
100	0.25	0.35	65^+ $(CH_3OH)_2H^+$
			97^+ $(CH_3OH)_3H^+$
200	0.40	0.70	
100	0.40[a]		33^+ $(CH_3OH)H^+$
			57^+ ($C_4H_9^+$)
100	0.45[a]		57^+ ($C_4H_9^+$)

[a] Balance from isobutane

Conclusions

A simplified moving-belt LC-MS interface has been constructed and has demonstrated applicability to the analyses of organic compounds amenable to mass spectrometric analysis from a conventional solid probe but not from a gas chromatograph. Full scan analyses have been accomplished in the 50 to 100 ng range and selected ion monitoring has been demonstrated at the 1 ng level.

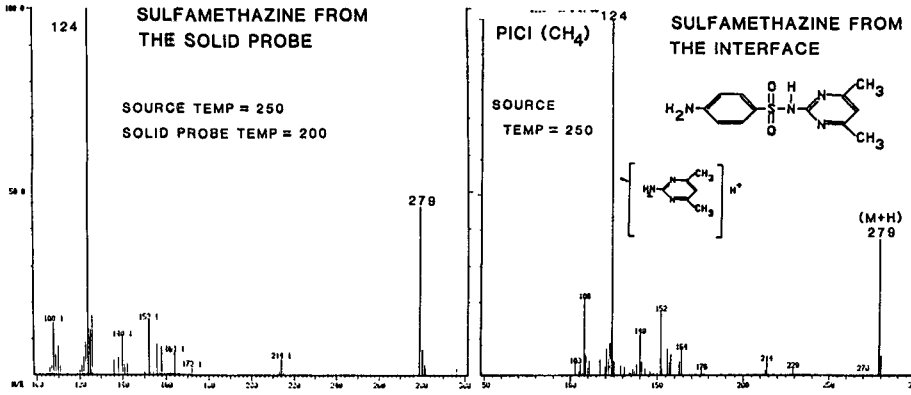

DLI/LC-MS OF NUCLEOSIDES USING A SELF-MADE DESOLVATION CHAMBER.

E. L. Esmans, P. Geboes, Y. Luyten and F.C.Alderweireldt,
University of Antwerp (R.U.C.A.), Laboratory for organic chemistry,
Groenenborgerlaan 171, B-2020 ANTWERP (Belgium).

Nucleosides have been analysed by us by LC-MS, using an early designed DLI-probe, equipped with a nickel diaphragm (1,2). Although promising results were obtained we felt that the system should be improved due to the following draw-backs :

- solvent cluster ion formation in the lower mass region prevented the detection of ions below m/z = 130. Therefore, analysis of structural important sugar and/or base containing fragments was limited in both purine and pyrimidine (deoxy)-nucleosides.
- experimental results were highly dependent upon the spray eluting from the DLI-probe. Slight changes in optimal conditions (spray direction, shape, length, etc...) lead to an immediate deterioration of the system.
- high mass spectral amplification conditions were used (EMP = 2 kV ; preamplifier 10^4), sometimes leading to noisy TIC's.
- if high % of water containing effluents were needed for the sake of chromatographic separation of mixtures, high source temperatures had to be used, with an increasing risk of thermal degradation as a consequence.
- connection of standard 25 cm x 4.6 mm HPLC columns to the interface and used at a flow rate of 1 cc/min implied a serious draw-back in terms of sensitivity especially if one should tend to analyze biological samples.

Taking these considerations into account, we improved the existing system by :

- insertion of a temperature controlled desolvation chamber between the DLI-probe and the ion source.
- mounting of a microbore HPLC column onto the DLI-interface.

The self-built desolvation chamber was based upon the concept of Dedieu et al. (3) and its advantages have been described (4). However, the heating cartridge in the original concept was replaced by a thermocoaxial wire, which was brased around the chamber. This assures a rapid and uniform heat supply. Serious contamination of the ion source was caused by reaction of salt solutions with the silver braze. This forced us to plate the outside of the chamber with gold after which no more problems occurred. Originally our RIBER 10-10 mass spectrometer was not equipped with the necessary electrical connections to accomodate the chamber. Therefore a new ion source housing cover was made equipped with these connections. The available direct probe power supply unit was used for heating up the desolvation chamber.

The influence of the insertion of this chamber upon the analysis of (deoxy)-nucleosides was checked by introducing pure compounds in CH_3OH/H_2O (80/20) on a μ-Bondapack C18 column (1cc/min). The following observations were made :

- suitable chamber temperature ± 180°C.
- source block temperature ± 170°C.

- good spectra were now obtained at much lower amplification (EMP = 1.72 kV ; pre-amplifier 10^3), leading to less noisy TIC's.
- enlarged scan range (from m/z = 115) enabling the detection of the following ions :
  a) deoxynucleosides : $[MH]^+$, $[S]^+$, $[BH+H]^+$, $[B+30]^+$ and $[B+44(-16)]^+$.
  b) nucleosides : $[MH]^+$, $[S]^+$, $[BH+H]^+$, $[B+30]^+$ and $[B+44]^+$.

Remarkable in these results was, in contrast to the observations in E.I. and C.I., the intensities of the $[B+30]^+$ ion to be more pronounced in the 2'-deoxyseries.

Once these conditions were established, a microbore column (Chrompack, C18 ID = 1mm, l = 50cm) was connected to the DLI-interface. The same results were obtained, but now at concentrations of 1.5 µg instead of 30 µg injected on column. Spectra for thymidine were obtained for concentrations as low as 0.25 µg (CH_3OH/H_2O 80/20, 70 µl/min).

Analysis of a synthetic mixture of (deoxy)-nucleosides was performed using 97% 0.01 M NH_4OOCH/3% H_2O. For this system somewhat higher source (190°C) and desolvation chamber temperatures (210°C) were used. However, in such a system the probe had to be cooled to -6°C. Since no water cooling was available in the DLI-interface, this was done by introducing cold CO_2-gas as close to the probe tip as possible. If this is not done, the nickel diaphragm desolves after 1 or 2 minutes. This is due to a reaction of the latter with the NH_4OOCH solution in combination with a too high probe tip temperature. This was never observed when 4.6mm I.D. columns were used. Probably at flow rates of 1cc/min, the effluent itself was able to provide additional cooling to the diaphragm. This was impossible at flow-rates of 70µl/min.

With this knowledge 20cc of urine was brought on an Affigel-boronate column according to the procedure described by Gehrke (5). The retained fraction, containing nucleosides from t-RNA, was analyzed for pseudouridine on the microbore column (isocratic run : 97% 0.01M NH_4OOCH/3% CH_3OH ; 70 µl/min). The desolvation chamber temperature was 210°C, the source block temperature was 190°C and the DLI-interface was again cooled to -6°C. In such a way pseudouridine could be identified.

References.

1. E.L.Esmans, Y.Luyten, F.C.Alderweireldt, Biomed.Mass Spectrom., 10, 347 (1983).
2. E.L.Esmans, Y.Luyten, F.C.Alderweireldt, P.Krien, G.Devant, presented at the 30th Annual Conference on Mass Spectrometry and Allied Topics, Honolulu, Hawaii, 1982, Abstracts p.608.
3. M.Dedieu, C.Juin, P.J.Arpino, G.Guiochon, Anal.Chem., 54, 2372 (1982).
4. M.Dedieu, C.Juin, P.J.Arpino, J.P.Bounine, G.Guiochon, Journ.Chrom., 251, 203 (1983).
5. C.W.Gehrke, K.C.Kuo, G.E.Davis, R.D.Suits, T.P.Waalkes, E.Borek, Journ.Chrom., 150, 455 (1978).

Acknowledgements

We thank the N.F.W.O. for financial support and Mr.J.Schrooten for technical assistance.

ANALYSIS OF CANDIDATE ANTI-CANCER DRUGS BY THERMOSPRAY HPLC/MS. Robert D. Voyksner, Joan T. Bursey, and John Hines, Research Triangle Institute, P.O. Box 12194, Research Triangle Park, North Carolina 27709.

The National Cancer Institute (NCI) is in the advance stages of anti-tumor screening, toxicological studies and clinical trials of candidate anti-cancer drugs. NCI is interested in developing appropriate characterization and analytical methodology for candidate anti-cancer drugs to provide support for IND filings and technical drug specifications. Specifically, the analytical support must develop and apply analytical methodology to qualitatively and quantitatively identify the pharmaceutical drug impurities as well as validate the assay as stability-indicating. The analytical options are sometimes limited since the compounds are generally not amenable to GC analysis. HPLC is an ideal separation technique but lacks detectors of sufficient specificity to validate the identity of the parent drug or to identify impurities. HPLC/MS can provide both the specificity and capability for direct identification needed for the analysis. Of the HPLC/MS techniques available, thermospray (TSP) seems the best choice because there is no splitting of the HPLC flow which would make the detection of minor impurities impossible. TSP can operate with high quantities of water and buffer, necessary for the HPLC separation of these polar, ionic compounds. Also, TSP ionization is very soft, providing molecular weight information from these thermally labile drugs. Off-line HPLC, followed by MS analysis or HPLC/MS techniques requiring thermal desorption, cannot provide such information.

TSP-HPLC/MS analysis has been performed on four anti-cancer drugs. The first was a triazone in which the TSP spectrum (Fig. 1) matched the proposed structure, exhibiting an $[M+H]^+$ and an $[M+NH_4]^+$ signal, as well as fragment ions corresponding to $[M+H-2H_2O]^+$, $[M+H-CNO]^+$, $[M+H-C_2HN_2O]^+$ and $[Ribose+NH_4]^+$. The TSP total ion chromatogram for this compound showed no impurities in the standard.

Another anti-cancer drug similar to triazone, tetrahydrouriden (THU), was also analyzed by TSP-HPLC/MS. The TSP total ion chromatogram for THU exhibited a single major peak, identified as THU, and three impurity peaks (<3% of THU). The TSP spectrum of THU (Fig. 2) exhibited a number of adduct and fragment ions including $[M+H]^+$, $[M+Acetate-H_2O]^+$, $[M+Acetate]^+$, $[2M+H-H_2O]^+$, $[2M+H-2H_2O]^+$, and $[2M+H-Ribose]^+$. The fragment ions consisted of losses of $3H_2O$, $2H_2O$, and H_2O from the protonated molecular ion. One of the chromatographic impurities was identified as ribose; the identification was confirmed by analysis of an authentic ribose standard which exhibited the same retention time and TSP spectrum as the sample impurity. The tentative identification of the other two impurities has not been validated at this time.

The TSP-HPLC/MS analysis of azolastone was used to validate the specificity of the HPLC assay (no degradation products coelute with the drug) which resulted in false positives using HPLC/UV or HPLC/refractive index (RI) detection. Table I summarizes the different forced degradation conditions to which azolastone was exposed for 24 hours. The HPLC/UV and HPLC/RI chromatograms shown in Fig. 3 for condition 1 (control), and 4 indicated that for condition 4, azolastone degraded into a component which elutes 1.2 minutes earlier. Condition 5 indicated that azolastone did not decompose since the retention time (RT) matches the control. However, upon analysis of these six samples (conditions) by TSP-HPLC/MS it was found that condition 5 (Fig. 3) was a degradation product eluting at the same RT as azolastone. Conditions 1, 2, 3, and 6 were correctly identified and validated by TSP to contain azolastone. TSP and HPLC/UV or RI did not detect azolastone under condition 4. The TSP spectrum for azolastone (Fig. 4) consisted of the following ions: $[M+NH_4]^+$, $[M+H]^+$, $[M-H_2O]^+$, $[M-CONH_2]^+$, and $[M+H-CONH_2-Cl]^+$, all of which are indicative of the assigned structure.

The TSP analysis of aphidicolin glycinate HCl (MW431) verified the HPLC retention time and identification. An impurity found in the formulation which affected the drug's activity was aphidicolin. The TSP spectrum (Fig. 5) exhibited an $[M+NH_4]^+$ and $[M+Acetate]^+$ signal for aphidicolin. The HPLC/MS analysis of aphidicolin was impaired by anphicolin, the Aphidicolin glycinate, which appears at a concentration two orders of magnitude greater than aphidicolin. The glycinate's RT is 30 seconds earlier than aphidicolin, but the quantity of glycinate present results in a broad, overloaded HPLC peak which interferes with aphidicolin (Fig. 6). This overlapping interference poses a problem to the TSP-MS analysis since the glycinate exhibits fragment ions at the same masses as the aphidicolin signal. Obviously, a different HPLC separation is needed for quantitation of the aphidicolin impurity.

TSP-HPLC/MS has proved useful in the analysis of anti-cancer drugs. TSP provided information to qualitatively identify the parent drug, identify impurities, and validate HPLC separations.

This work was supported by The Pharmaceutical Resources Branch, Division of Cancer Treatment, National Cancer Institute, under Contract No. 1-CM-37619.

Thermospray HPLC/MS Spectrum of Triazinone

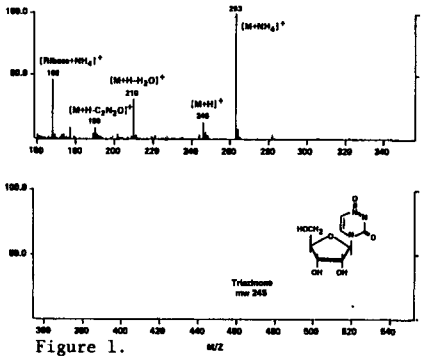

Figure 1.

Thermospray HPLC/MS Spectrum of Tetrahydrouridine

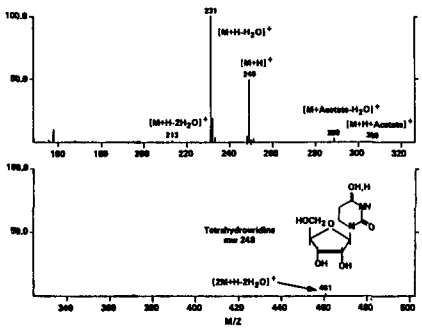

Figure 2.

Thermospray HPLC/MS Spectrum of Azolastone

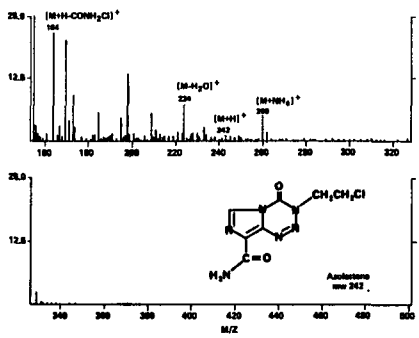

Figure 4.

Table I.

Determination of Possible Interferences in the Azolastone Analysis

Sample No.	Temperature	hv	Solvent
1	25°	dark	dry
2	25°	dark	H_2O (2.0 mL)
3	25°	room light	H_2O (2.0 mL)
4	90°	dark	H_2O (2.0 mL)
5	25°	dark	1N NaOH (2.0 mL)
6	25°	dark	1N H_3PO_4 (2.0 mL)

HPLC Analysis of Azolastone

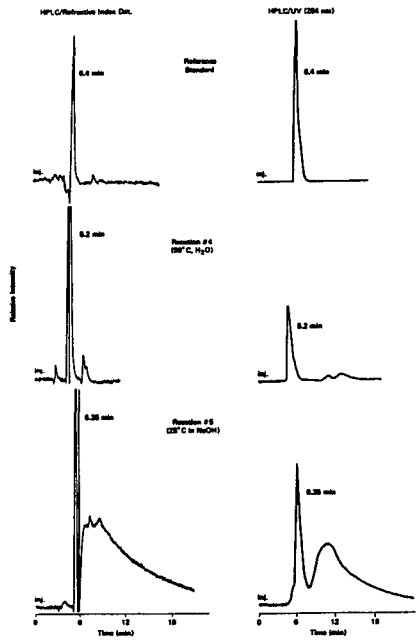

Figure 3.

Thermospray HPLC/MS Spectrum of Aphidicoin

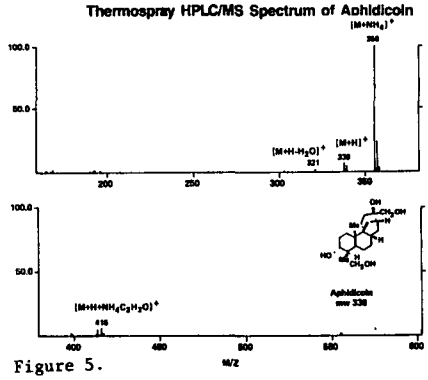

Figure 5.

LIQUID CHROMATOGRAPHY/FAST ATOM BOMBARDMENT MASS SPECTROMETRY (LC/FABMS)

Justin G. Stroh, J. Carter Cook, and Kenneth L. Rinehart, Jr.
University of Illinois at Urbana-Champaign, Urbana, IL 61801
and
Ivor A. S. Lewis
VG Analytical, Ltd., Wythenshawe, Manchester, M23 9LE, England

Since its introduction in 1981, fast atom bombardment mass spectrometry (FABMS) (1,2) has proved to be a powerful tool for the analysis of underivatized peptides. In many cases, however, peptides are obtained as mixtures of compounds and must be separated by high performance liquid chromatography (HPLC) prior to FABMS analysis. In order to analyze mixtures of peptides using this technique we have developed an on-line LC/FABMS system using a modified VG moving belt interface.

We have been able to obtain easily interpretable spectra from the partial hydrolysis of antiamoebin I (3), which yielded peptides in the mass range 500-1000 amu. The spectra were rich in structural information, supporting the amino acid sequence of all the major components observed. A peptide was also observed corresponding to the partial sequence of antiamoebin III, indicating that that component was present as an impurity in the starting material. Furthermore, two new peptides were observed which did not correspond to either antiamoebin I, III or II, assigning the partial sequence of two new antiamoebins as shown in Figures 1 and 2.

Since FABMS is the method of choice for analysis of high molecular weight underivatized peptides, we used LC/FABMS to analyze a mixture of the hexadecapeptides emerimicin IIA (molecular weight 1823) and emerimicin IIB (molecular weight 1837). Although the spectra were weak in intensity, sodiated molecular ions were observed along with useful sequence information. A mixture of intact antiamoebins was also run. Antiamoebin I was the major component of this mixture and only the spectra of this hexadecapeptide yielded molecular weight and sequence information.

We therefore believe that LC/FABMS will be used extensively in the future for analysis of mixtures of both natural and synthetic origin which are amenable to FABMS.

Antiamoebin	I (4):	Ac-Phe-Aib-Aib-Aib-Iva-Gly-Leu-Aib-Aib-Hyp-Gln-Iva-Hyp-Aib-Pro-Phol
Antiamoebin	II (5):	Ac-Phe-Aib-Aib-Aib-Iva-Gly-Leu-Aib-Aib-Hyp-Gln-Iva-Pro-Aib-Pro-Phol
Antiamoebin	III (6):	Ac-Phe-Aib-Aib-Aib-Aib-Gly-Leu-Aib-Aib-Hyp-Gln-Iva-Hyp-Aib-Pro-Phol
Emerimicin	IIA (7):	Ac-Trp-Ile-Gln-Aib-Ile-Thr-Aib-Leu-Aib-Hyp-Gln-Aib-Hyp-Aib-Pro-Phol
Emerimicin	IIB (7):	Ac-Trp-Ile-Gln-Iva-Ile-Thr-Aib-Leu-Aib-Hyp-Gln-Aib-Hyp-Aib-Pro-Phol

References:

1. Barber, M.; Bordoli, R. S.; Sedgwick, R. D.; Tyler, A. N. J. Chem. Soc. Chem. Commun. 1981, 325-327.

2. Surman, D. S.; Vickerman, J. C. J. Chem. Soc. Chem. Commun. 1981, 324-325.

3. Meng, H. Ph.D. Thesis, University of Illinois at Urbana-Champaign, Urbana, IL, 1979.

4. Pandey, R. C.; Meng, H.; Cook, Jr., J. C.; Rinehart, Jr., K. L. J. Am. Chem. Soc. 1977, 99, 5203-5205.

5. Pandey, R. C.; Cook, Jr., J. C.; Rinehart, Jr., K. L. J. Antibiot. 1978, 31, 241-243.

6. Rinehart, Jr., K. L. Trends Anal. Chem. 1983, 2, 10-13.

7. Rinehart, Jr., K. L.; Cook, Jr., J. C.; Pandey, R. C.; Gaudioso, L. A.; Meng, H.; Moore, M. L.; Gloer, J. B.; Wilson, G. R.; Gutowsky, R. E.; Zierath, P. D.; Shield, L. S.; Li, L. H.; Renis, H. E.; McGovren, J. P.; Canonico, P. G. Pure Appl. Chem. 1982, 54, 2409-2424.

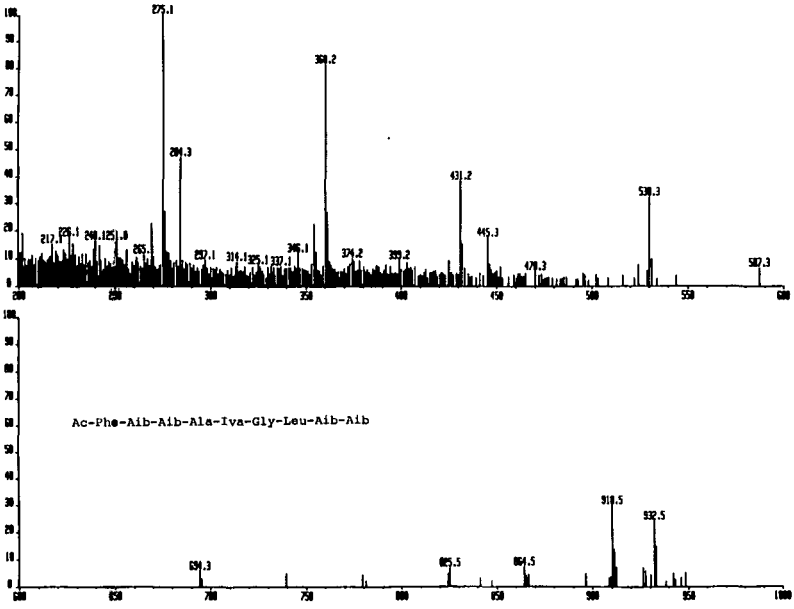

Figure 1.

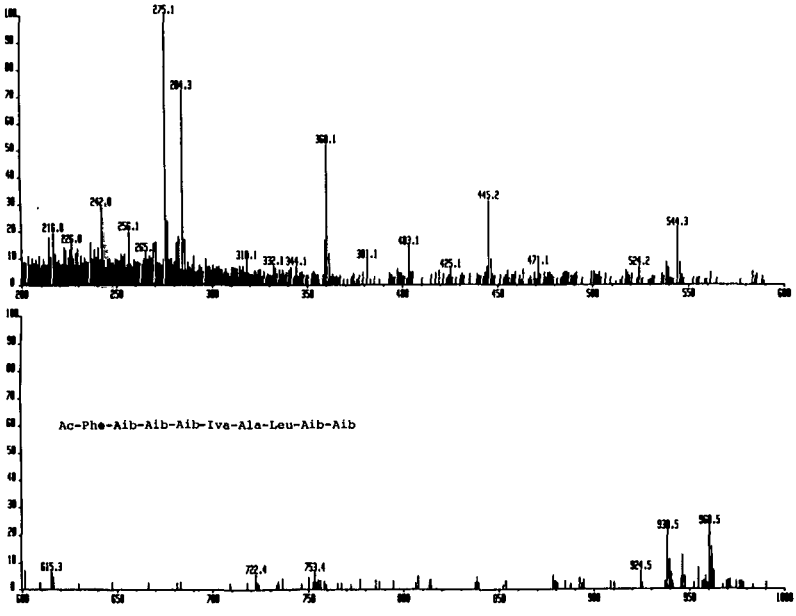

Figure 2.

METABOLIC PROFILE STUDIES OF A PATIENT WITH CYTOCHROME C OXIDASE DEFICIENCY

I. Matsumoto and T. Kuhara

Department of Biochemistry, Institute of Human Genetics,
Kanazawa Medical University, Uchinada, 920-02 Japan

There are many causes of congenital lactic acidosis including the abnormalities of the respiratory chain, the pyruvate dehydrogenase complex, gluconeogenesis and others. Diagnosis of cytochrome C oxidase deficiency, a disorder in the respiratory chain, generally takes time because biochemical information strongly suggestive for this disorder is not easily available. Onlya few reports described detailed organic acid profiles of body fluids of the patients. The urinary organic acid profiles of a 4-month-old floppy baby with profound hypotonia, lactic acidemia and failure to thrive were studied using gas chromatography-mass spectrometry. The patient, a girl, was the first child of healthy unrelated Japanese parents. During the first month she sucked well. At 3 months of age, however, she was referred to Kanazawa Medical University Hospital because of progressive hypotonia and renal glucosuria found since one month of life. On admission her general status was poor and autonomic movement was lost. On the third hospital day, the patient suddenly became dyspnoic and thus was kept under respiratory control. Histopathological examination of her muscle revealed a lipid storage myopathy suggesting either carnitine deficiency or abnormality of cytochromes. Pneumonia recurred to her repeatedly and she died at the age of 9 months.

The urinary organic acid profiles of the girl at 19 and 20 weeks of life were examined as their trimethylsilyl derivatives after extraction with ether using n-heptadecanoate as an internal standard. For gas chromatographic separation a 2 m long glass column packed with 3 % OV-17 was used and the oven temparature programming at a rate of 6 °C/min from 80 °C to 290 °C. The quantitation was carried out either by gas chromatography or by mass chromatography. The serum and urinary amino acid levels were also determined by an JLC 200 A automatic amino acid analyzer.

Gross lactic aciduria was noted, the urinary lactate level was increased (254-456 μmole/mg creatinine, normal value; 0.9 ± 1.4). Different from a deficiency of dihydrolipoyl dehydrogenase (E3) of the 2-oxo acids dehydrogenase complexes, the branched chain keto- and hydroxy- acids in the urine were not increased. The urinary 2-oxoglutarate levels were only moderately increased. In most lactic acidosis lactate accumulates secondarily due to the marked increase of ketone bodies. However, in this case gross lactic aciduria with only a modereate ketosis was found suggesting a primary lactic acidosis. In carnitine deficiency lactic

acidosis is often found. However, such a severe lactic aciduria can not be explained by carnitine deficiency. A marked increase of urinary 2-hydroxybutyrate was found (0.8 and 0.4 μmole/mg creatinine, normal value; 0.01± 0.04). 2-Hydroxybutyrate is formed by reduction of 2-oxobutyrate derived from methionine, threonine and serine, and almost always accumulates in massive lactic aciduria reflecting the $NADH/NAD^+$ ratio in the cell. These data strongly suggested that the patient had a disorder in the electron transport system. In addition we found significantly elevated urinary concentrations of p-hydroxyphenyllactate (0.05 and 0.13 μmole/mg creatinine; normal value < 0.014). p-Hydroxyphenylpyruvate is formed by transamination of tyrosine and is oxidized to homogentisate by p-hydroxyphenylpyruvate oxidase. We suggest that in the presence of high $NADH/NAD^+$ ratio p-hydroxyphenylpyruvate readily undergo reduction to p-hydroxyphenyllactate. In fact we often found increased p-hydroxyphenyllactate without any increase of p-hydroxyphenylpyruvate in the urine of patients with massive lactic aciduria.

The patient had significantly elevated levels of serum alanine (1.2 μmole/ml). However the other amino acids were almost within the normal range. On the other hand, urinary amino acid analysis on two different occasion revealed marked hyperamino aciduria. The feature of this amino aciduria was different from that of hartnup disease nor immature baby, but exactly identical to that of a patient with cytochrome C oxidase deficiency with renal dysfunction reported by Van Biervliet et al. in 1977. The generalized hyperamino aciduria indicating a lack of a common factor, energy, required for the reabsorption of amino acid in proximal tubule. In some cases of cytochrome C oxidase deficiency, decreased carnitine content was reported. However carnitine deficiency found in patients with cytochrome C oxidase deficiency appears a secondary phenomenon since the uptake of carnitine in muscle also requires energy. The clinical and other findings in our patient were almost identical to those with fatal infantile mitochondrial myopathy and renal dysfunction described by DiMauro et al. (1980), Van Biervliet et al (1977) and Stansbie et al (1982). All the three were proved to have cytochrome aa3 and b deficiency. The muscle specimens from our patient was completely devoid of cytochrome C oxidase staining.

In summary, the typical cytochrome C oxidase deficiency can be readily predicted with the highest probability by these metabolic profiles, clinical symptoms and pathological examination.

References

1. J.P.G.M. Van Biervliet, L. Bruinvis, D. Jeeting, P. K. De Bree, C. Van Der Heiden, and S. K. Wadman, J. L. Willems, H. Bookelman, U. Van Haelst, and L. A. H. Monnens, Pediatr. Res. 11, 1088-1093 (1977)

2. S. DiMauro, J. R. Mendell, Z. Sahenk, D. Bachman, A. Scarpa, R. M. Scofield, C. Reiner. Neurology 30, 795-804 (1980)

QUANTIFYING CHOLESTEROL SULFATE IN PLASMA BY LIQUID SIMS

Wengang Chai and Cedric Shackleton, Mass Spectrometry Resource, Dept of Pharmaceutical Chemistry, UCSF, and Children's Hospital Medical Center of Northern California, Oakland, California 94609.

Elevated plasma concentrations of cholesterol sulfate are diagnostic of a dermatological condition Recessive X-linked Ichthyosis (RXLI). In this disorder inefficient shedding of the upper skin layer results in scaly skin. Until now cholesterol sulfate has been determined by gas chromatography following purification and solvolysis (Epstein, Krauss, & Shackleton, Science 214:659, 1981). The current investigation was undertaken to determine if FAB or liquid SIMS mass spectrometry could be used to assay cholesterol sulfate with minimal sample work-up.

Two types of internal standards were investigated (a) ^{13}C labeled cholesterol sulfate and (b) stigmasterol sulfate, a homologue of cholesterol sulfate not found in serum. Cholesterol 3,4-$^{13}C_2$ and stigmasterol were purchased from Merck, Sharp & Dohme Isotopes, and Sigma Chemical Company, respectively. The sterol sulfates were prepared as follows: 10 mg sterol and triethylamine-sulfate trioxide were disolved in 100 µl pyridine. After standing at room temperature for 2 hours, the solvent was evaporated. The residue was redisolved in about 100µl methanol. The sterol sodium sulfate precipitates following addition of an equal volume of 0.2 M NaOH in methanol.

Mass spectrometry was carried out on a Kratos MS 50S mass spectrometer. A primary ionization beam of Cs^+ was used. Samples were prepared for mass spectrometry by applying 1µl of a methanol: water solution of the sample (< 1µg/µl) into a thin layer of glycerol (1 µl, volume) on the copper probe tip. Typical operating conditions were: Scan range 435-505, scan rate 100 seconds /decade, dynamic resolution M/ΔM 3000. Data were acquired and processed by a Logos II computer system. Portions of negative ion mass spectra for the individual compounds and mixture are illustrated in Figure 1. Cholesterol sulfate (CS) has a 'molecular ion' $[M-H]^-$ at m/z 465; 3,4 $^{13}C_2$ cholesterol sulfate (^{13}CCS) a molecular ion at m/z 467 and stigmasterol sulfate a molecular ion at m/z 491. The standard mixtures are approximately 1:1 and the RXLI plasma contains both internal standards.

The following standard mixtures were applied to the probe (a) 0.2µg ^{13}C cholesterol sulfate (CS) with 0.01, 0.02, 0.05, 0.10, 0.20, 0.40 and 0.66 unlabeled cholesterol sulfate and (b) 0.2µg stigmasterol sulfate with 0.01, 0.02, 0.05, 0.10, 0.20, 0.40 and 0.66 µg cholesterol sulfate. Mass spectra (15-20 scans) were acquired for each concentration and mean relative intensities for m/z 465,467 and 491 were determined. For standard mixture (a) the ion intensities for m/z 465 (^{12}C) and 467 (^{13}C) were corrected for their contributions to each others intensities. The standard curve obtained is illustrated in Fig. 2. Reasonable linearity was achieved for mixtures up to 2:1 (unlabeled to labeled). Although structurally similar, cholesterol sulfate and stigmasterol sulfate were not desorbed and ionized at the same rate so a less satisfactory standard curve was obtained with stigmasterol sulfate as internal standard. Therefore, the use of stigmasterol sulfate for quantification of cholesterol sulfate was not pursued further.

Plasma samples from patients with RXLI were analysed as follows: (a) 5 µg of ^{13}C cholesterol sulfate was added to 0.15 ml serum; (b) proteins were precipitated by addition of 15 ml acetone: ethanol (1:1) with sonication; (c) the supernatent was dried and the extract fractionated on a Sephadex LH-20 column using methanol: Chloroform (1:1) as mobile phase (Janne et al, Clin. Chim. Acta 23:405, 1969); (d) the monosulfate fraction was dried, desalted on a Sep-pak cartridge (Waters Associates) and analyzed by mass spectrometry; (e) approximately 1/20 of the extract was applied to the glycerol layer on the copper probe tip. 8 to 15 scans were obtained for each analysis. Reproducibility was acceptable. Figure 3 illustrates the analysis of a patient sample three times using both internal standards. The graphs represent the ratio in individual scans of the intensity of the 'molecular' ion for cholesterol sulfate (m/z 465) to the respective 'molecular' ions for labeled cholesterol sulfate (m/z 467) and stigmasterol sulfate (m/z 491). The stable labeled standard provided good reproducibility but the use of stigmasterol sulfate as internal standard showed much more variability. Using the technique cholesterol sulfate has been determined in 11 patients with RXLI. The mean concentration was 4601 µg/100 ml with a range of 1022-6643 µg/100 ml. Normal individuals have cholesterol sulfate concentrations between 90 and 300 µg /100 ml.

This work was supported by PHS grants RR01614 and AM 33459.

LEGENDS to FIGURES

Figure 1 Partial negative ion mass spectra of unlabeled cholesterol sulfate (CS); labeled cholesterol sulfate (^{13}CCS); stigmasterol sulfate (SS); CS + ^{13}CCS; CS and SS and RXLI plasma containing SS and ^{13}CCS.

Figure 2 Analysis of CS using ^{13}CCS as internal standard. Demonstration of linearity for ratios up to 2:1 (CS: ^{13}CCS).

Figure 3 Reproducibility of CS/^{13}CCS and CS/SS ratios between scans and between separate analyses.

Figure 4 Quantitative measurement of cholesterol sulfate in RXLI plasma.

FIGURE 1

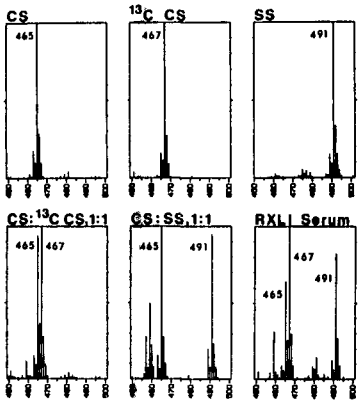

FIGURE 2

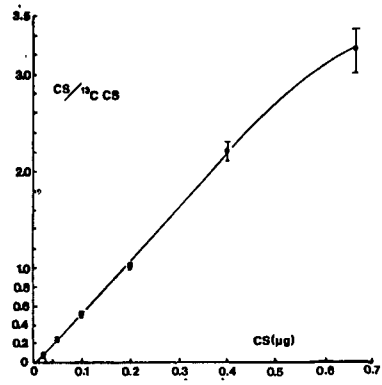

FIGURE 3

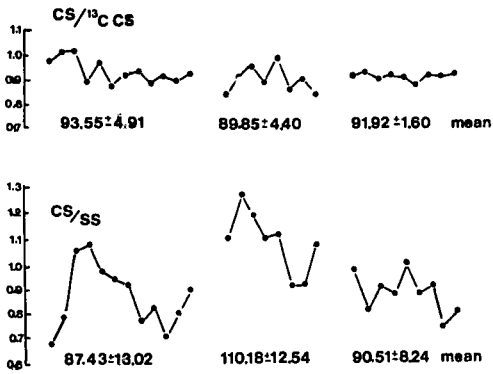

FIGURE 4

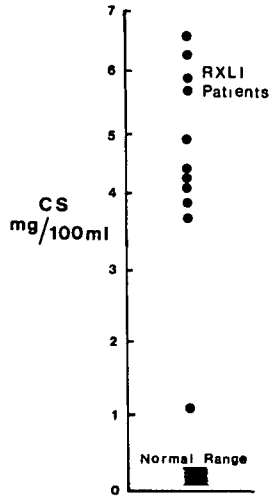

Diethanolamine Assisted Liquid Secondary Ion Mass Spectrometry of Bilirubin and Its Analogs

W. Chai[1], J.O. Whitney,[1,2] N. Blankaert,[2,3] and A.L. Burlingame[1,2];
[1]Dept. of Pharm. Chemistry, School of Pharmacy, [2]Liver Center and
[3]Dept. of Laboratory Medicine, University of California
San Francisco, CA 94143.

Bilirubin (BR, Fig. 1) the major waste product of heme catabolism, is an open chain tetrapyrrole with two vinyl, four methyl and two propionic acid side chains. Because of its low volatility and chemical instability, bilirubin is extremely difficult to analyze by conventional ionization methods (1). In the course of preparing an affinity column in which bilirubin is linked to agarose gel through a suitable intermediate (dithiothreitol or acetylcystein), we needed a method by which we could follow generation of the bilirubin-intermediate covalent products. Successful identification of bilirubin and its analogs and adducts was accomplished using diethanolamine (DEA) assisted liquid secondary ion mass spectrometry (LSIMS) (2) in both negative and positive modes.

All polar groups of bilirubin are involved in extensive intramolecular hydrogen binding so that the carboxyl groups are not available for solvation in most polar solvents such as glycerol. For glycerol assisted SIMS, good spectra could only be obtained by first dissolving bilirubin in aqueous NaOH. The resulting spectrum showed only sodium attachment ions for both molecular ions and fragments (Fig. 2). In the molecular ion region, attachment of up to five sodium ions could be seen at m/z 605, 627, 649, 671 and 693, corresponding to $[M-Na_n-H_{n+1}]^-$ where n=1-5.

DEA, in contrast, is an ideal matrix for bilirubin and its analogs not only because it possesses the low volatility and high viscosity necessary for LSIMS, also because it is basic and bilirubin dissolves well in alkaline solution. Background spectrum of DEA alone showed oligomer ions of $[n\ DEA-H]^-$, $[n\ DEA+44-H]^-$ in negative mode and $[n\ DEA+H]^+$, $[n\ DEA+44+H]^+$ for positive mode.

Positive and negative DEA assisted spectra (Fig. 3) were characterized by intense ions related to the molecular weight, and by the presence of DEA attachment ions. In positive ion spectra, cleavage of bilirubin occurred at the central methylenic portion of the molecule between C_{10} and C_{11}. In contrast, the dominant cleavage was between C_9-C_{10} in negative ion spectra.

Figure 4 is a negative ion spectrum of the covalent adduct of bilirubin and dithiothreitol (DTT). The molecular anion is at m/z 737 and m/z 842 represents an attachment ion of bilirubin-dithiothreitol with DEA. Clearly, the DEA attachment ion is useful in establishing the identity of the molecular ion and thus the molecular weight of the adduct. Fragmentation of the bilirubin-DTT adduct occurred at the linkage of bilirubin with DTT resulting in the formation of a prominent ion at m/z 584. C_9-C_{10} cleavage was also evident. Positive ion spectra were similar but again distinguished by cleavage at C_{10-11} rather than C_9-C_{10}.

Useful spectra with the acetylcysteine bilirubin adduct were also obtained using these procedures. Monitoring bilirubin-DTT or-acetylcysteine intermediates by LSIMS aided considerably in the preparation of bilirubin affinity columns.

This work was supported by NIH Grants RR01614 and HD 13787, and by UCSF Liver Center.

References:

(1) M. Salmon and C. Fenselau, Biomed. Mass Spectrom., 1, 219 (1974).
(2) W. Aberth, K.M. Straub and A.L. Burlingame, Anal. Chem., 54, 2029 (1982).

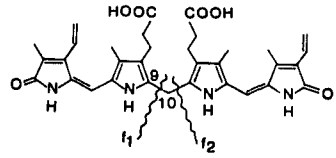

Fig. 1 Bilirubin IX-α MW 584

Fig. 2 Glycerol-NaOH assisted SIM spectrum of BR

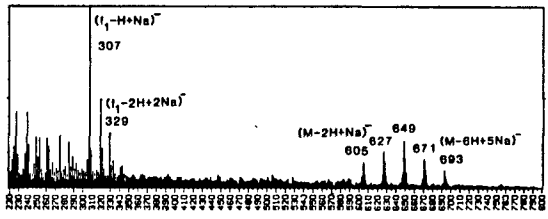

Fig. 3 DEA assisted SIM spectra of BR

(a)

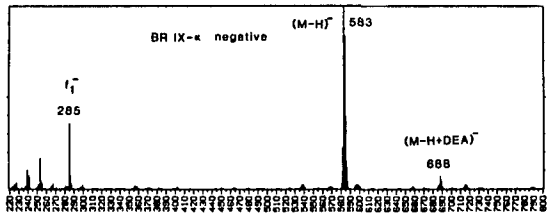

(b)

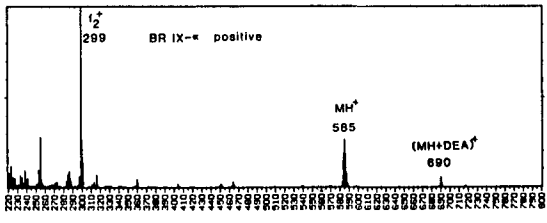

Fig. 4 DEA assisted negative SIM spectrum of BR-DTT

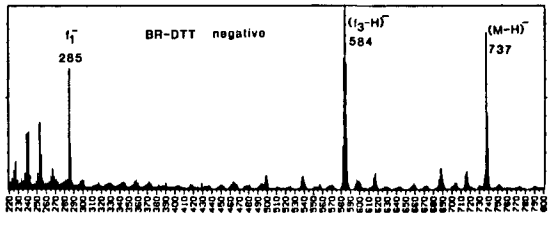

ANALYSIS OF ISOMERIC BILE SALTS USING FAB IN COMBINATION WITH CID-MIKE:

Joachim G. Liehr, Univ. of Texas Medical School at Houston, Texas 77225, Eric E. Kingston and John H. Beynon, Royal Society Research Unit, University College of Swansea, Swansea SA2 8PP, UK.

FAB ionization is a commonly applied technique for the analysis of polar substances. FAB spectra are usually dominated by abundant MH^+, $[M + Na]^+$ or $[M + K]^+$ ions. The spectra characteristically contain little fragmentation, which aids in the recognition of molecular weights of analyzed substances, but represents a lack of structural information. CID-MIKE analysis of FAB-generated molecular parent ions was expected to provide characteristic fragmentation and thus structural information on polar substances which could not be analyzed by more informative methods.

The combination of FAB ionization with CID-MIKE analysis was tested using a series of isomeric bile salts. Sodium tauroursodeoxycholate (I), taurochenodeoxycholate (II), taurodeoxycholate (III), and taurohydeoxycholate (IV) all gave abundant $[M + Na]^+$ ions m/z 544. CID-MIKE spectra generated from the $[M + Na]^+$ ions in this series were similar but showed subtle differences in the middle mass region. The spectrum of sodium tauroursodeoxycholate is shown in Fig. 1. The spectra obtained with the two glycoconjugates, sodium glycodeoxycholate (V) and sodium glycochenodeoxycholate (VI) are shown in Fig.2.

In all spectra, the positive charge was found to reside on the sulfonate or carboxylate moiety, respectively, and did not appear to migrate to other functional groups. In all spectra, the lower mass region was dominated by fragmentation of the side chain. These ions are listed in Table 1.

Table 1: Ions formed by fragmentation of the side chains of bile salts

Ion structure	Tauroconjugates (Salts I,II,III,IV)	Glycoconjugates (Salts V, VI)
CH_3-CH=CH-CH_2-CO-NH-CH_2-R	252	202
CH_2=CH-CO-NH-CH_2-R	224	174
CH_2-CO-NH-CH_2-R	211	161
O=C=N-CH_2R	196	146
HN=CH-R		118
CH_2-R		104
R	140	90

R = CH_2-$SO_3Na^+_2$ (Tauroconjugates) or $CO_2Na^+_2$ (Glycoconjugates)

In the upper mass region, the most intense ion was generated by elimination of H_2O, m/z 526 (tauroconjugates) or m/z 476 (glycoconjugates), respectively. Other ions were formed by fragmentation of the steroid ring system according to the general scheme 1 (Table 2).

Table 2: Ions formed by fragmentation of the steroid ring system (Scheme 1).

Salt	Ions (m/z) a-H	b-H	c-H	d-H
I (R_3 = OH)	471	387	333	279
II (R_1 = OH)	471	387	333	279
III (R_2 = OH)	471	403	333	279
IV (R_4 = OH)	471	387	333	279
V (R_2 = OH)	421	353	283	229
VI (R_1 = OH)	421	337	283	229

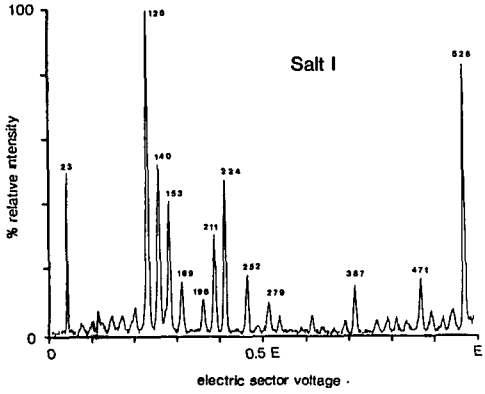

Fig. 1: CID-MIKE spectrum of m/z 544, generated by FAB ionization of sodium tauroursodeoxycholate (I). m/z values of major ions are indicated.

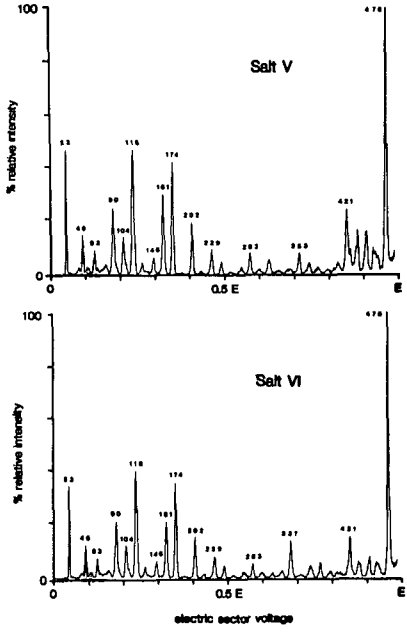

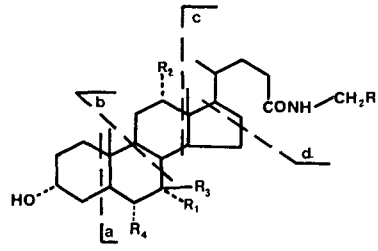

Scheme 1: Fragmentation of the steroid ring system (see Table 2).

Fig 2: CID-MIKE spectra of m/a 494, generated by FAB ionization of sodium glycodeoxycholate (V) and sodium glycochenodeoxycholate (VI). m/z values of major ions are indicated.

DIRECT DETERMINATION OF ACETYLCHOLINE IN MOUSE BRAIN BY THERMOSPRAY-MASS SPECTROMETRY

Susan T. Weintraub
The University of Texas Health Science Center at San Antonio
San Antonio, Texas 78284

Daniel J. Liberato and Alfred L. Yergey
National Institute for Child Health and Human Development
Bethesda, Maryland 20205

Measurement of tissue levels of acetylcholine and choline have long been employed as a means of characterizing the cholinergic nature of a system of interest. Early analyses were performed mainly by bioassay techniques such as those utilizing the clam heart, the dorsal muscle of the leech and the frog rectus abdominus. These obviously indirect and non-specific procedures were replaced in the early 1970's by GC and GC-MS methods which require removal of one of the quaternary methyl groups to provide a volatile product. This can be accomplished by chemical (1) or thermal (2,3) means. The EI mass spectra of the resulting dimethylaminoethanol and its acetate ester are dominated by the m/z 58 base peak and exhibit only a small molecular ion of the demethylated species. Ammonia chemical ionization of these compounds produces a large pseudo-molecular ion but still requires prior demethylation for the analysis (4). Even with the use of direct insertion CI or belt HPLC interface techniques, thermal loss of a methyl group precedes ionization and detection. With the added complication that thermally-induced ester exchange also occurs, these methods are not ideal for evaluation of samples with stable isotopes as biological tracers or internal standards. The use of thermospray HPLC-mass spectrometry for this purpose has overcome these obstacles. By this method the analysis is performed on the intact acetylcholine or choline molecule with no derivatization or pre-treatment needed. To date a realistic limit of detection of standard acetylcholine is less than 8 pmole. With biological samples as low as 100 pmole of acetylcholine has easily been detected. Combining the thermospray-MS technique with the use of microwave radiation to rapidly inactivate brain enzymes prior to analysis (5), greater accuracy and reliability in the measurement is obtained.

In preparation for thermospray-MS analysis, mouse brain samples were placed in 4 ml of acetonitrile containing 15 nmole each of d_0-choline and d_4-acetylcholine and 100 mg of anhydrous magnesium sulfate (6). After homogenization on ice for 30 sec by means of a Polytron, each sample was centrifuged at 3000 rpm for 30 min at 0 °C. The resulting supernatants were extracted 2 times with 1.5 ml portions of n-heptane and evaporated to dryness by a stream of argon. 200 µl of mobile phase was added to each sample prior to HPLC injection. The mobile phase for LC was 0.1 M aqueous ammonium acetate containing 2 mM pyridine and 20 mg/l octanesulfonic acid at a final pH of 5. An LKB pump was employed at a flow rate of 1.25 ml/min in conjunction with a 5 micron, 15 cm Altex Ultrasphere C-18IP column. The retention time was 4.7 min for choline and approximately 14 min for acetylcholine. For multiple ion detection measurements the following ions were monitored: d_0-choline, m/z 104; d_9-choline, m/z 113; d_0-acetylcholine, m/z 146; d_4-acetylcholine, m/z 150. When determination of choline levels was not required, the octanesulfonic acid was omitted from the mobile phase, allowing the acetylcholine to elute with a retention time of 3.5 min (not shown).

1. Jenden, D. J., Roch, M. A. and Booth, K. Anal. Biochem. 55:438 (1973).

2. Szilagyi, P. I. A., Schmidt, D. E. and Green, J. P. Anal. Chem. 40:2009 (1968).

3. Stavinoha, W. B. and Weintraub, S. T. Anal. Chem. 46:757 (1974).

4. Hasegawa, Y., Maruyama, Y. and Weintraub, S. T. Biomed. Mass Spectrom., in press.

5. Stavinoha, W. B., Weintraub, S. T. and Modak, A. T. J. Neurochem. 20:361 (1973).

6. Khandelwal, J. K., Szilagyi, P. I. A., Barker, L. A. and Green, J. P. Eur. J. Pharmacol. 76:145 (1981).

ACETYLCHOLINE CONTENT OF MOUSE BRAIN

METHOD OF SACRIFICE	ANALYTICAL TECHNIQUE	ACETYLCHOLINE CONTENT (NMOLE/GM)
DECAPITATION	THERMOSPRAY-MS	17.0 ± 0.9
DECAPITATION	PYROLYSIS-GCMS[a]	13.7 ± 1.7
MICROWAVE (3 SEC, 1.4 kW)	THERMOSPRAY-MS	34.8 ± 1.6
MICROWAVE (3 SEC, 1.2 kW)	PYROLYSIS-GCMS[a]	25.5 ± 2.6

[a]Determined by the method of Stavinoha and Weintraub (3) as reported by Stavinoha *et al.* (5).

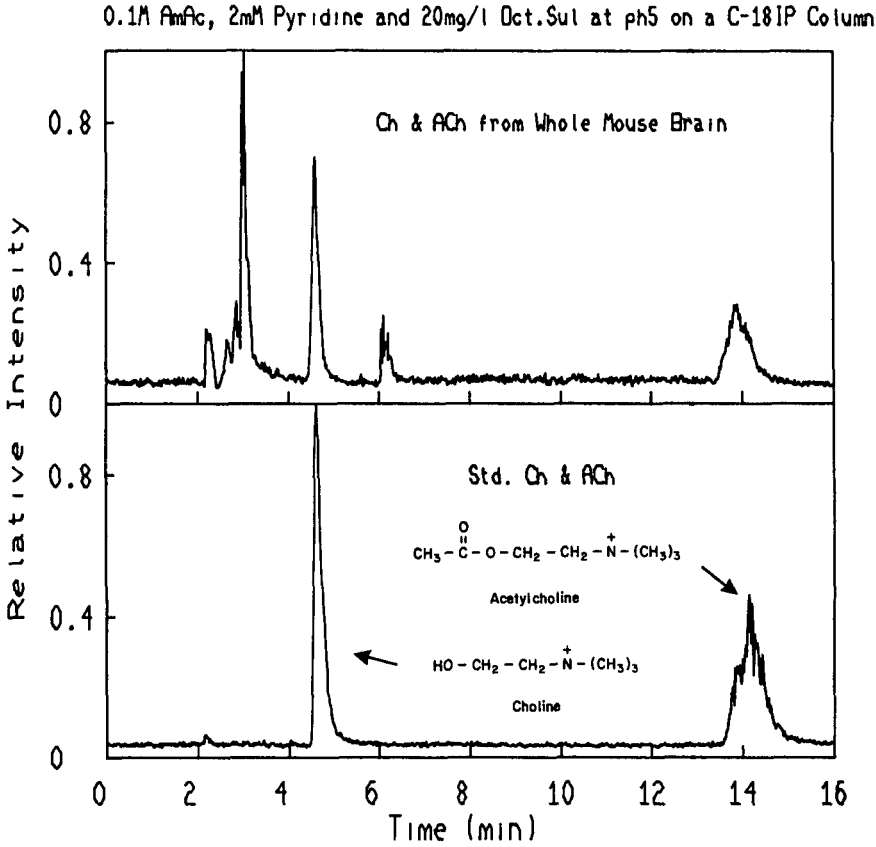

ANALYSIS OF ACYLCARNITINES FROM BIOLOGICAL SAMPLES BY FAB-MS

H. Hughes, Nowlin J.G., Smith C.V., Mitchell J.R. and Horning E.C. Dept. of Medicine and Institute for Lipid Research, Baylor College of Medicine, Houston, Texas 77030.

Carnitines and acylcarnitines are important in many metabolic disorders. Levels of long chain acylcarnitines have also been shown to increase in myocardial ischemia and have been proposed as possible endogenous toxins due to their ionophoretic properties (1). The current method preferred for the analysis and quantitation of acylcarnitines involves a radioenzymatic procedure for the determination of free carnitine (2). Since only free carnitine is measured in this procedure, prior isolation and hydrolysis of long and short chain acylcarnitines is necessary and the specific acylcarnitines are not identified.

We have developed a method for the analysis and quantitation of specific acylcarnitines by Fast Atom Bombardment - Mass Spectrometry (FAB-MS). These quaternary ammonium salts give high intensity molecular ions by FAB-MS and the sensitivity of detection for these compounds is currently at the 0.1 nmole (about 20-50 ng) level. This methodology has been applied to the analysis of urine from patients with Reye's syndrome. Fig. 1 illustrates the FAB spectrum of 3 ul of neat urine from a Reye's syndrome patient. Acetyl- and propionylcarnitine exhibit molecular species at m/z 204 and 218 respectively. These ions were not observed in control urine samples.

Experiments were carried out to determine whether FAB-MS could be used in quantitative studies for the analysis of long chain acylcarnitines, particularly palmitoylcarnitine, in ischemic tissue. For this work heptadecanoylcarnitine was prepared from carnitine and the acid chloride for use as an internal standard. Ions at m/z 400 (palmitoylcarnitine) and m/z 414 (heptadecanoylcarnitine) were monitored. The standard curve obtained is illustrated in Figure 2 showing a linear response from 0.1 to 2.5 nmole palmitoylcarnitine.

1. Idell-Winger, J.A., Crotyohann, L.W. and Neely, J.R.: J. Biol. Chem. 253: 4310-4318, 1978.

2. McGarry, J.D. and Foster, D.W.: J. Lipid Res. 17: 277-281, 1976.

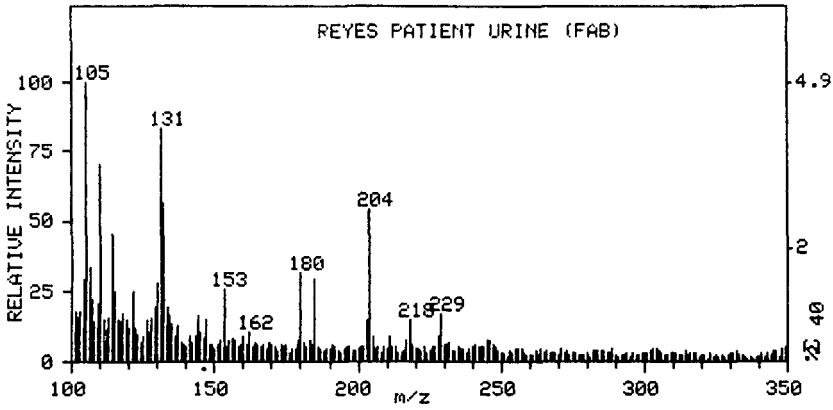

Figure 1: Analysis of urine from a patient with Reye's syndrome. Acetyl- and propionylcarnitines exhibit molecular species at m/z 204 and 218 respectively.

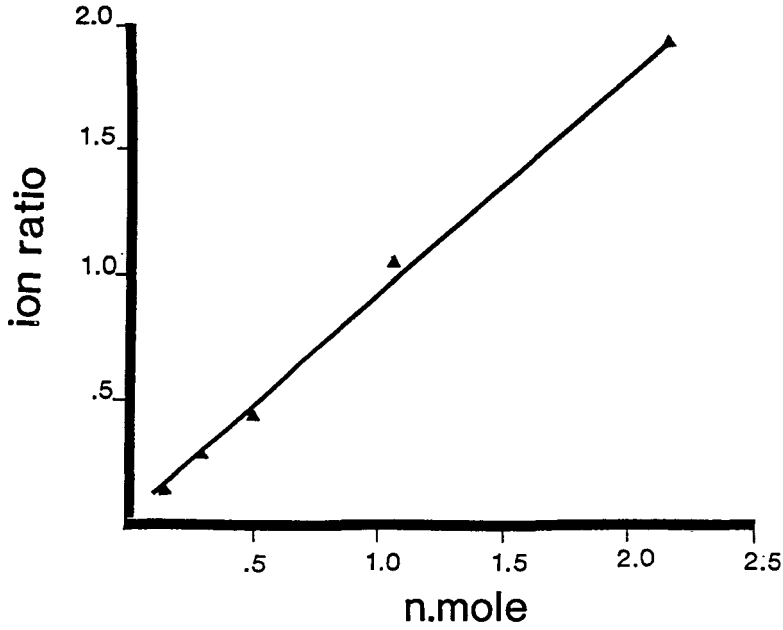

Figure 2: Standard curve for palmitoylcarnitine relative to heptadecanoylcarnitine ion ratio m/z 400/414 were monitored.

LSIMS PROFILING OF RAW UNEXTRACTED BILE IN METABOLIC STUDIES OF HEPATOTOXIC BILE ACIDS IN ANIMALS AND HUMANS:

J.O. Whitney[1,2], D. Grunberger[1,2], E. Roitman[1,2], V. Ling, Y-M. Yang[1], P. Rosenthal[3] and A.L. Burlingame[1,2]. [1]Department of Pharmaceutical Chemistry and [2]Liver Center, University of California, San Francisco, CA 94143; [3]Children's Hospital of Los Angeles, Los Angeles, CA 90027

In a recent series of papers (1,2,3) we have described mass spectral characteristics resulting from both positive and negative liquid secondary ion mass spectrometry (LSIMS) of free, amidated and sulfated bile salts, and have demonstrated the utility of LSIMS in quantitative metabolic studies of bile salt secretion and conjugation. We now report that initial screening of "raw", unextracted bile obtained in animal experiments using an isolated rat liver perfusion system and in duodenal fluid obtained in human studies through a non-invasive Enterotest is invaluable in the elucidation of detoxification pathways of hepatotoxins and in the clinical diagnosis of liver disease.

Fig. 1 is a negative ion LSIMS spectrum of 1 ul of unextracted bile obtained in a rat liver perfusion 5 min before a hepatotoxic bile acid was added to the perfusion fluid. The base peak, m/z 514, represents $(M-H)^-$ for taurocholic acid (TC) with m/z 536 being the sodium salt of taurocholate $(MNa-H)^-$. The strong ion at m/z 498 is $(M-H)^-$ for taurochenodeoxycholate (TCD). Twenty min after the addition of lithocholic acid to the perfusion fluid, the spectrum shown in Fig. 2 was obtained. Both TC and TCD are still present but very strong ions now appear at m/z 482 and m/z 584 which represent taurolithocholate (TL) and sodium taurolithocholate-3-sulfate (TLS), respectively, providing definitive evidence that both taurine conjugation and sulfation of lithocholic acid have occurred. A LSIMS spectrum taken 20 min after 5-cholenoic acid-3β-ol was added to the perfusion fluid (Fig. 3) shows strong ions at m/z 453 and 475, the quasimolecular ions of free 5-cholenoic acid-3-sulfate and the sodium salt of free 5-cholenoic acid-3-sulfate, respectively. A less intense ion at m/z 480 is unsulfated tauro-5-cholenoic-3β-ol, while the sodium salt of sulfated tauro-5-cholenoic acid is represented by a stronger ion at m/z 582. Clearly, sulfation of both free and taurine conjugated 5-cholenoic acid-3β-ol is a major mode of metabolism. The ion at m/z 598 suggests the possibility that 5-cholenoic acid-3β-ol is further metabolized to a dihydroxy bile acid (retaining the double bond) which is then conjugated with both taurine and sulfate.

Fig. 4 and 5 show spectra of raw duodenal fluid obtained by sampling duodenal contents with a string device (Enterotest) normally used in testing for the presence of intestinal parasites. Fig. 4, a sample from a normal child, contains strong ions at m/z 448, 464, 498 and 514, the major bile acid conjugates (found in human bile).

Fig. 5 is a spectrum from a child with diagnosed biliary atresia (congenital absence of bile ducts). The only significant ion present is at m/z 469 and corresponds to an internal standard added for the purpose of quantitation. The spectrum thus confirms the absence of bile ducts since no bile acids are present in duodenal fluid.

Standard curves obtained for the major bile acids in bile, using deuterated and ^{13}C labelled glycholate as an internal standard (1ug) are depicted in Fig. 6 and show the feasibility of bile acid quantitation by LSIMS. Preliminary quantitation of bile acids in duodenal fluid (obtained by the string test) are shown in Table I. Total concentration and glycine/taurine conjugate ratios compare favorably to conventional enzyme assays and HPLC, respectively. Discrepancies in trihydroxy/dihydroxy ratios can probably be accounted for by the fact that LSIMS measures all tri- and dihydroxy bile salts while the HPLC method does not account for bile salts other than cholate and chenodeoxycholate. This work was supported by NIH grants HD13787 and RR01614.

1) Whitney, J.O. et al., Koenshu-Iyo Masu Kenkyukai 6, 33 (1981).
2) Whitney, J.O. et al., Koenshu-Iyo Masu Kenkyukai 7, 3 (1982).
3) Whitney, J.O. et al., Koenshu-Iyo Masu Kenkyukai 8, 47 (1983).

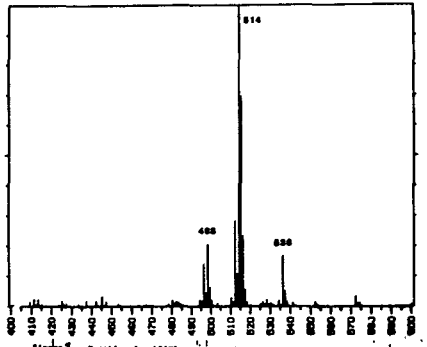

Figure 1. Negative ion LSIMS spectrum of unextracted bile (1 µl), before introduction of deoxycholic bile acid test solution into perfusion fluid.

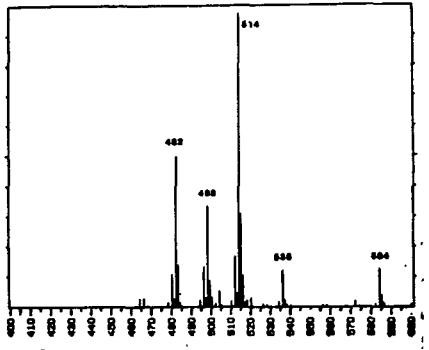

Figure 2. Negative ion LSIMS spectrum of unextracted bile (1 µl), 20 min following introduction of lithocholic acid into perfusion

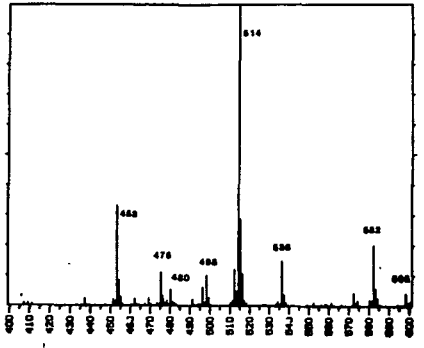

Figure 3. Negative ion LSIMS spectrum of unextracted bile (1 µl), 25 min following introduction of 5-cholenoic-3β-ol acid into perfusion fluid.

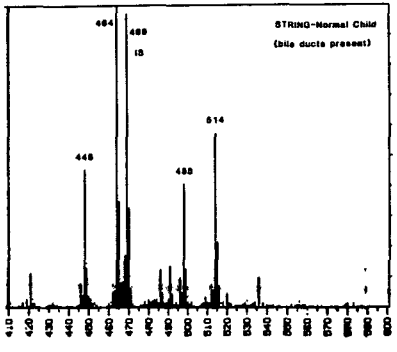

Fig.4

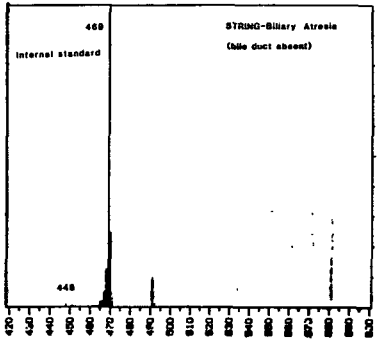

Fig.5

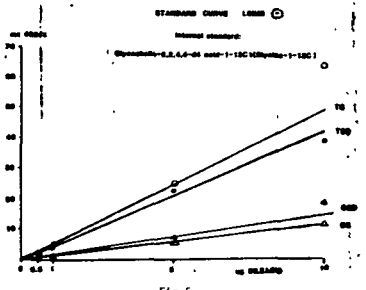

Fig.6
HUMAN ENTEROGESI-LSIMS VERSUS ENZYME ASSAY AND HPLC

Table 1

STRING#	TOTAL CONCENTRATION % LSIMS-ENZYME ASSAY	GLYCINE/TAURINE HPLC	GLYCINE/TAURINE LSIMS	DIHYDROXY/TRIHYDROXY HPLC	DIHYDROXY/TRIHYDROXY LSIMS
43	16	1.4	1.9	1.8	0.7
44	0	3.2	4.4	2.7	1.0
45	0	5.3	6.3	2.9	1.2
46	18	5.2	5.8	2.3	1.9

STRUCTURE OF AN UNUSUAL URINARY COMPOUND FORMED IN A REACTION OF CREATININE WITH ETHANOL.

G.B. Chheda*, A. Farber*, J.L. Alderfer*, R. Parthasarathy*, E. Jenkins†, J.A. McCloskey† and A. Arakali*. *Dept. of Biophysics, Roswell Park Memorial Institute, Buffalo, NY 14263, and †Depts. of Medicinal Chemistry and Biochemistry, University of Utah, Salt Lake City, UT 84112.

Creatinine is an imidazole derivative (2-amino-1,5-dihydro-1-methyl-4-imidazolone) which occurs in mammalian urine and tissues. It has been used as a reference measure to which a number of clinical tests are related. It is a by-product of cellular metabolism related to muscle mass. It is known to produce mutagens when heated with sugars. The purpose of this project was to elucidate the structure and investigate the origin of an unusual creatinine derivative (Compound I) encountered during the isolation of novel substances from the urines of cancer patients.

One liter of urine from a colon carcinoma patient was passed through a column of charcoal celite (2.54 x 45 cm) (1). Salts and urea were removed by washing the column with one liter of water and the column bound material was eluted with 2N ethanolic ammonia in 50% ethanol (1000 ml). The ammonia eluate was concentrated to about 50 ml and centrifuged to remove the insoluble precipitate. The clear solution was then passed through a column of Ag-1-X8-formate (2.54 x 35 cm) and the desired neutral compounds were eluted with water (1000 ml). The water wash was evaporated to dryness and the residue was fractionated into cis-diol and non cis-diol fractions on a DEAE cellulose column equilibrated with boric acid as described previously (2). The compound I was separated from 0.14 M boric acid fraction by successive purification with paper chromatography in seven different solvents (2). The compound I had an Rf of 0.75 in solvent A (isopropanol:NH_4OH: water, 7:1:2). A liter of urine gave 11.0 mg of the compound I (13.2 mg/24 hr urine). The structure of this compound was determined by mass spectrometry, nmr and uv spectrophotometry.

The ultraviolet spectra of compound I exhibited maxima at 242 nm (pH 6.5) with an ϵ_{max} of 4900, while in acid the compound absorbed at λ_{max} 220 nm. In alkaline solution the compound gave an end absorption suggesting degradation with ring opening to give presumably a creatine derivative. The EI mass spectra of the compound I in free form gave a molecular ion at 157 with fragment ions at 129 (M^{+}-CO) and at 112 (creatinine^{+}-H) (Fig. 1). The high resolution mass spectrometry of the trimethylsilylated compound I gave molecular ion at m/z 301.1635 corresponding to $C_{12}H_{27}N_3O_2Si_2$ leading to the molecular composition of $C_6H_{11}N_3O_2$ for the underivatized compound. Study of the collision activation mass spectra produced from m/z 112 and from 113 were indistinguishable from the spectra generated in the same fashion from creatinine, thus demonstrating the presence of creatinine moiety in the compound I (Fig. 2a and 2b).

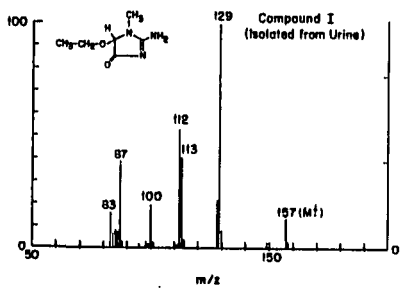

Fig. 1

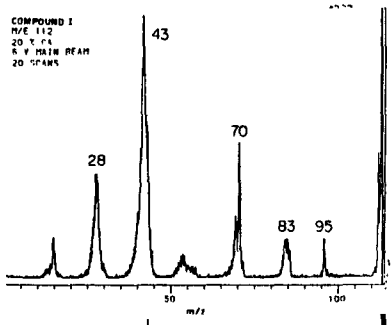

Fig. 2a

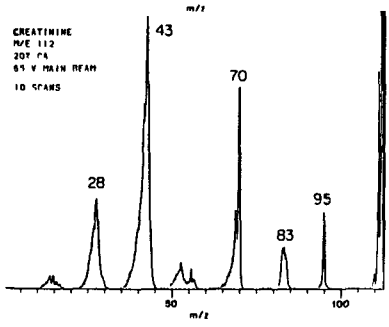

Fig. 2b

In proton nmr spectra, the compound I exhibited resonances at 1.23 (t) for CH_3, 3.02 (s) for N-CH_3, 5.13 (s) for C^5-H and 3.57-3.42 δ (m) for CH_2. Irradiation of the triplet for CH_3 at 1.23 led to a collapse of multiplet to a quartet with a distinct AB pattern, suggesting a non-equivalence of CH_2 protons. Comparative study of the proton and ^{13}C nmr spectra of authentic creatinine suggested that the compound I was 5-substituted creatinine. Thus, the mass spectral as well as nmr and uv data established the structure of the compound I as 5-ethoxycreatinine. Since the compound I was optically inactive and the fact that the occurrence of ethyl groups in nature is rare, it was suspected that the material was formed on the charcoal column during the ethanolic ammonia elution. Thus when creatinine was allowed to react with ethanol at 37° for 96 hours in presence of charcoal and air in a reaction flask it gave the 5-ethoxycreatinine (I) in 58% yield (Fig. 3). This compound was confirmed by elemental analysis. The uv spetra, the mass spectra, and the nmr spectra of this chemically prepared material were identical to those of the material isolated from the processed urine. In paper chromatography the mobilities of the two samples were identical in three solvents.

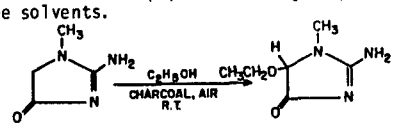

Fig. 3

It appears that this novel reaction of creatinine with ethanol in presence of charcoal and air takes place through a free radical mechanism to give 5-ethoxycreatinine. The reaction is applicable to other alcohols as well. It is not unreasonable to suggest that, 5-substituted creatinines may be generated *in vivo* under suitable oxidizing conditions.

References

1. Chheda, G.B., Nucleic Acids Research 4, 739 (1977).
2. Dutta, S.P., Crain, P.F., McCloskey, J.A. and Chheda, G.B., Life Sciences 24, 1381 (1979).

APPLICATION OF MASS SPECTROMETRY TO THE STUDY OF THE BACTERIAL METABOLISM OF ISOMERIC AMINO AND NITROBIPHENYLS.

Robert Massé, Christiane Ayotte, François Messier, Mohamed Badr and Mohammad Mohsen, Institut National de la Recherche Scientifique, INRS-Santé, Montréal, Québec, H1N 3M5 and Michel Sylvestre, Institut Armand Frappier, Ville de Laval, Québec, H7N 4Z3

INTRODUCTION

The environmental fate of amino and nitrobiphenyls has been very little studied, although they have been recognized as carcinogenic and mutagenic compounds in animal. Aminobiphenyls are used in the synthesis of dyes which are widely employed in the dye manufacturing textile dyeing and paper printing. Epidemiological data indicates that industrial workers exposed to these compounds have a higher incidence of urinary bladder cancer than that of the general population. On the other hand, nitrobiphenyls are used in the preparation of pesticides, explosives, dyes and industrial solvants. In the study reported here, we have investigated the biotransformation of isomeric amino and nitrobiphenyls in gram negative strain B-206 which has the capability to degrade biphenyl. We demonstrate that the biodegradation pathways of the model substrates are highly dependant on the nature as well as on the position of the NH_2 and NO_2 substituants on the biphenyl skeleton.

EXPERIMENTAL

2,3 and 4-aminobiphenyl and 2,3 and 4-nitrobiphenyl were used as substrates. Bacterial strain B-206 was grown in the presence of the substrates as the sole carbon source for periods of time varying for one to 10 days as previously described (1). The broths were successively extracted at pH 7 and pH 3 with ethylacetate. The organic extracts were evaporated under a nitrogen stream at 40°C. The residues were trimethylsilylated with a mixture of BSTFA/acetonitrine (1:4,v/v) and analyzed by HRGC/MS. The gas chromatographic analysis were carried out using a Perkin Elmer Sigma 3 gas chromatograph, equiped with a 30 m DB-1 fused silica capillary column. Electron impact mass spectra were recorded at 70 eV with a Kratos MS-25 mass spectrometer. The scanning speed was 1 sec./decade, source temperature 250°C and trap current was set a 100 A.

RESULTS AND DISCUSSION

Figures 1 and 2 show total ion chromatograms of ethylacetate extracts of incubation broths. Peaks 1, 2 and 3 were identified as the TMS derivatives of 4-nitrobenzoïc acid (M.W. 239), 4-aminobenzoïc acid (M.W. 281) and 4-nitrocinnamic acid (M.W. 265) respectively. The mass spectrum of compound 4 TMS derivative gave a molecular ion at m/z 316 ($M^{+\cdot}$ at m/z 325, d_9 TMS) and ions at m/z 301 (M-15), m/z 271 (M-15-30), m/z 255 (M-15-46). The metabolite was identified as 4-nitro, 2 -hydroxy-3 -nitrosobiphenyl by comparison with the corresponding 4-chloro analog, and with 2-hydroxy-3-nitrosobiphenyl which structures were fully characterized and synthetized. Compound 5 and 6 were easily identified as the 2 -hydroxy and 4 -hydroxy derivatives of 4-nitrobiphenyl. Their mass spectra gave abundant molecular ions (M^+ 287) and structurally informative ions at m/z 226 (M-15-46) and m/z 211. These metabolites arise most probably from the corresponding 2,3 and 3,4 -dihydrodiols 7 and 8 (fig. 4), by elimination of one molecule of water. The dihydrodiols TMS derivative showed a molecular ion at m/z 377 (M^+, 395, d_9-TMS) and other ions at m/z 287 (loss of TMSOH); m/z 272 (M-15-TMSOH). Enzymatic dehydrogenation of the dihydrodiols 7 and 8 leads to the corresponding 4-nitro, 2 , 3 -dihydroxy biphenyl and 4-nitro-3,4 -dihydroxybiphenyl 9. Only the 3,4-dihydroxy metabolite 9 was chromatographically resolved from metabolites 7 and 8 (Fig. 1) its 2 , 3 -dihydroxy analog elutes with peak 8. Finally, peak 10 was identified as the TMS derivative of 2-hydroxy-6-oxo-6-(4-nitrophenyl) hexanoïc acid (M^+, 411). Its mass spectra gave ions at m/z 396 (M-15), m/z 294 (M-COOTMS), m/z 203, 147 and 129. Peak 11 was identified as the corresponding TMS-enol derivative of metabolite 10. Its mass spectrum gave a molecular ion at m/z 483 ($M^{+\cdot}$ 510, d_9-TMS) and structurally informative ions at m/z 393 (M-TMSOH) m/z 250 and 220. On the basis of the data presented above, a metabolic pathway is proposed for the biotransformation of 4-nitrobiphenyl by strain B-206 (Fig. 4). 3-nitrobiphenyl was metabolized following similar pathways, but 2-nitrobiphenyl was shown to be highly resistant to bacterial degradation in the presence of strain B-206. On the other hand, 4-aminobiphenyl and benzidine were degrated buy the bacterium following similar biodegradation pathways to 3,4-dihydroxybenzoïc acid 13 (Fig. 3). 4-hydroxyben-

zoïc acid (peak 12) was also detected in the bacterial extracts. The metabolic pathways by which these metabolites are produced from the parent substrate are being investigated. As observed for 2-nitrobiphenyl, 2-aminobiphenyl is also highly resistant to strain B-206 metabolism.

In this study we have provided evidence strain B-206 have the ability to metabolize 4-nitrobiphenyl to potentially carcinogenic and mutagenic hydroxy-nitroso derivative and to degrade this substrate by oxydative cleavage of its unsubstituted aromatic ring to 4-nitrobenzoïc acid. Furthermore, the bacterium has the ability to degrade the highly carcinogenic 4-aminobiphenyl and benzidine mainly into 3, 4 -dihydroxybenzoïc acid. From and environmental standpoint, the transformation of these aromatic amines by strain B-206 to detoxified products could be very important in their biodegradation in natural habitats.

REFERENCE

1. M. Sylvestre, R. Massé, F. Messier, J. Fauteux, J.G. Bisaillon and R. Beaudet,, Applied Environmental Microbiology, 60, 556-563 (1982).

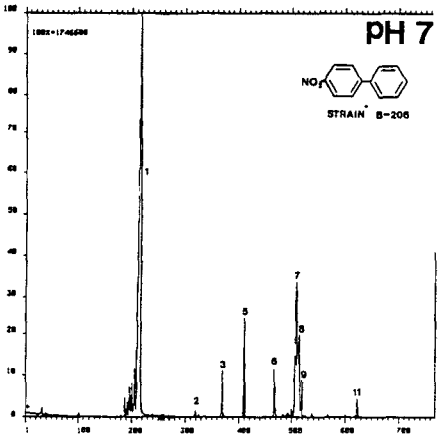

FIGURE I.

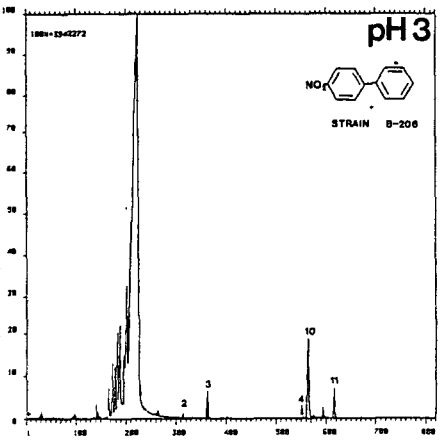

FIGURE 2.

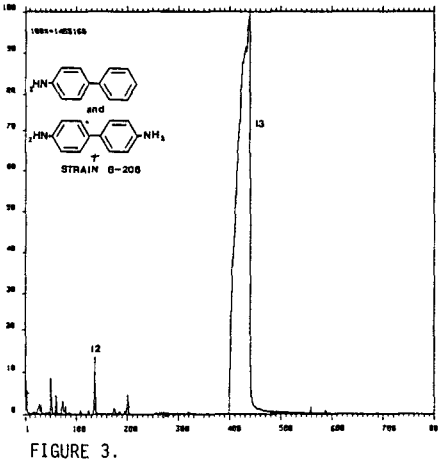

FIGURE 3.

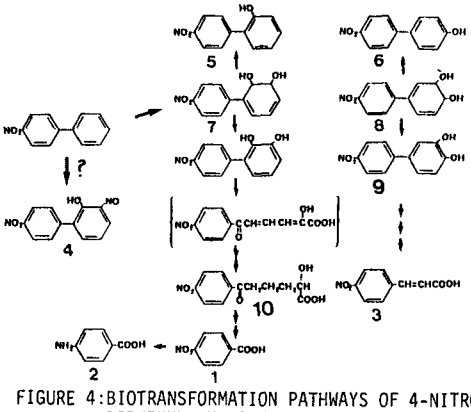

FIGURE 4:BIOTRANSFORMATION PATHWAYS OF 4-NITRO BIPHENYL BY BACTERIAL STRAIN B-206.

BENZOYLALANINE; A NEW METABOLITE IN HYPERAMMONEMIC PATIENTS TREATED WITH SODIUM BENZOATE

T.Shinka, Y.Inoue, T.Kuhara, M.Matsumoto and I.Matsumoto

Department of Biochemistry, Institute of Human Genetics, Kanazawa Medical University, Ishikawa 920-02, Japan

Hyperammonemia is caused mainly by the deficiency of urea cycle enzymes and secondarily accompanied by some organic aciduria, such as methylmalonic aciduria, propionic acidemia and 2-methyl-3-oxobutyric aciduria. Oral or intravenous administration of sodium benzoate is often used for the treatment of the acute hyperammonemia infants to reduce blood ammonia rapidly by conjugate with glycine to form hippuric acid which easily leads to the excretion of nitrogen into the urine. In the urine of two patients with carbamoylphosphate synthetase I (CPS-I) deficiency, one with hyperargininemia and the other with citrullinemia who were treated with large amounts of sodium benzoate, we have found an unusual metabolite and identified by gas chromatography-mass spectrometry as benzoylalanine. In this report, the identification and significance of the formation of benzoylalanie are discussed.

Organic acids in urine were extracted with two volum of diethylether for three times in acidic condition. The extract was dried over anhydrous sodium sulfate and evaporated to dryness under nightrogen gas. The residue was trimethylsilylated with BSTFA. Gas chromatography-mass spectrometry was performed by combination of a HP 5710A gas chromatograph, JEOL JMS DX 300 mass spectrometer and JEOL JMA 3500 acquisition system. The separation of organic acids was carried out on a 2mm x 3m glass column packed with 3% OV-17. The oven temperature was maintained at 105 °C for 4 min, then programmed at a rate of 8 °C per min from 105 °C to 290 °C. Electron impact mass spectra was obtained using an ionizing voltage of 70 eV. The ion source was maintained at 200 °C and the separator at 280 °C. Two minutes after the sample injection, repetitive scanning was started from m/z 50 to m/z 600 in a 5-s cycle.

The urinary organic acid profile of the patient Y.H.(CPS-I deficiency) on the 34th day is shown in Fig. 1. Lactic acid (peak 1), methylsuccinic acid (peak 2), mesaconic acid (peak 3), 5-oxoproline (peak 4) and hippuric acid (peak 7 and 9) were detected as prominant peaks in Fig. 1. In addition to these compounds, previously unidentified metabolites were also detected (peak 6 and 8). The electron impact mass spectrum of peak 6 showed the predominante ions at m/z 337, 322, 294, 247, 220, 105 and 73. These fragment ions indicate that this compound has a molecular weight of 337 with an odd number of nitrogen atoms, and the fragment ions at m/z 322, 294, 247 and 220 correspond to (M-15), (M-43), (M-90) and (M-117) respectively. This fragment pattern is very similar to the mass spectrum observed in hippuric acid-2TMS derivative, but the molecular ion is 14 mass larger than it. The fragment ion m/z 105 detected in hippuric acid-2TMS is also found in peak 6 and this ion corresponds to the benzoylcarbonium ion. So benzoylalanine-2TMS was presumed for the structure of peak 6. Fig. 2 shows the mass spectra of peak 6 and hippuric acid-2TMS. The identification of benzoylalanine was established by the comparison with an authentic compound using GC/MS as well as gas chromatographic retention time. Similarly peak 8 was identified as benzoylalanine-1TMS delivative.

The formation of benzoylalanine may be explained by the condensation of accumulated alanine with benzoyl CoA in the hyperammonemic patient, which is analogous to the formation of hippuric acid from glycine and benzoyl CoA, although Schachter et al.(1) have reported that the catalitic enzyme glycine-N acylase was completely specific for glycine when benzoyl CoA was used as the acyl doner. Batshaw and Brusilow (2) reported the decrease in the levels of ammonia after administration of sodium benzoate to the

patients with urea cycle disorders. This suggests that nitrogenous precursors of urea were used for synthesis of glycine. Simkin et al.(3) have reported that the source of glycine for hippuric acid conjugation was the liver free glycine and that the loading of large amounts of sodium benzoate reduced the free glycine level. From these facts, when the supplementation of glycine is not sufficient for hippuric acid synthesis and free glycine level is reduced, it is suspected that not only glycine but also alanine are used as amino acid doner for conjugation reaction to excrete the waste nitrogen and accumulated a large amount of benzoate.

The lowering of glycine level was also supported from following result. A large amount of 5-oxoproline was detected in both blood and urine of the patient Y.H.. The accumulation of 5-oxoproline was reported in a patient with glutathione synthase deficiency. This enzyme is also mitochondrial enzyme and catalyzes the condensation reaction of gamma-glutamylcysteine and glycine. If the glycine level is reduced, it is expected that the synthesis of glutathione is also reduced and the precursor 5-oxoproline accumulates. In patient Y.H., the accumulation of 5-oxoproline was parallel with that of benzoylalanine. So, it seems that the reduce of free glycine level causes the excretion of the unusual metabolites, benzoylalanine and 5-oxoproline. But it is not known whether the alanine conjugation is catalyzed by the glycine-N acylase.

The toxicity of benzoate at the usual dose employed is thought to be low, but recently, undesirable effects of sodium benzoate are now being recognized. The effect of benzoate on fatty acid and urea cycle metabolism and the resulting metabolic abnormalities are currently under investigation.

1) Schachter,D. and Taggart,J.V. (1954) J.Biol.Chem. 208, 263-275
2) Batshaw,M.L. and Brusilow,S.W. (1980) J.Pediatr. 97, 893-900
3) Simkin,J.L. and White,K. (1957) Biochem.J. 65, 574-582

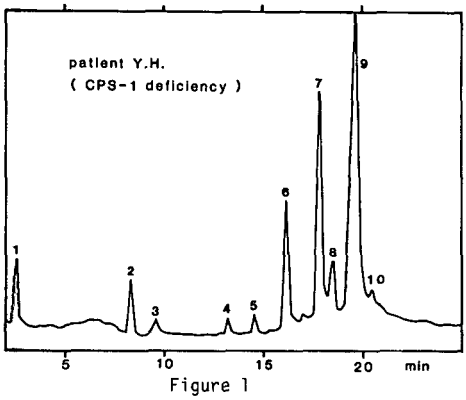

Figure 1

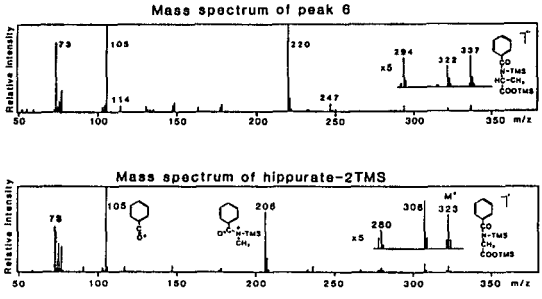

Figure 2

EVALUATION OF INFRARED HETERODYNE RATIOMETRY AS AN ALTERNATIVE TO GAS ISOTOPE MASS SPECTROMETRY FOR ANALYSIS OF $^{13}CO_2$ IN BREATH

C.S. Irving, T.W. Boutton, P.R. Navratil, and P.D. Klein

USDA/ARS Children's Nutrition Research Center, Department of Pediatrics, Baylor College of Medicine, Houston, TX 77030

Background

Measurements of excess $^{13}CO_2$ in breath following the administration of carbon-13-labeled substances have biomedical applications ranging from the monitoring of energy metabolism to the assessment of organ function. Data requirements for ^{13}C isotope ratiometric analysis of breath CO_2 in biomedical applications differ in two important respects from geochemical isotopic measurements. First, less precision is required due to the naturally occurring variations in the isotopic enrichment of respiratory CO_2. These result from changes in the proportions of protein, carbohydrate, and fat undergoing oxidation. Second, sample through-put requirements are greater. Ideal performance characteristics of ^{13}C isotope ratiometers used in biomedical settings also differ from those used in analytical laboratories. Cost-effectiveness in biomedical applications requires that there be a low level of daily and periodic maintenance, a higher level of reliability, less down-time, and operation by nonmass spectrometrists. In 1975, the NIGMS contracted with Andros, Inc. to develop an instrument based upon a new infrared technology that would be better suited to biomedical ^{13}C isotope ratiometry of breath CO_2 than gas isotope ratio mass spectrometry. In 1981, the instrument was awarded to our laboratory and in July 1983, the instrument was shipped to Baylor College of Medicine, where it was fitted with a new operating and data acquisition system based upon an IBM-type personal computer. We present a description of the technique and report the preliminary results of a performance evaluation of the heterodyne nondispersive infrared ratiometer, termed the Metabolic Carbon Analyzer or MCA.

Principle of Heterodyne Nondisperse Infrared Ratiometry

Nondispersed infrared radiation from a heated source passes serially through two gas cells (Fig. 1). Loudspeakers modulate the pressure in each cell in a sinusoidal fashion with frequency **f** and amplitude **A**. As the density of the gas in the light path varies, so does the intensity of the transmitted light at the characteristic absorption frequency of the gas sample. After passing through two cells, the transmitted light will have two AC components at f_1 and f_2, as seen in Eq. 1, where the AC signal at f_1 is given by:

$$I_{2\nu}(f_1) = I_{o\nu}\,[-\sigma_1\ A_1 l_1 \sin f_1 \cdot t] \qquad \text{(Eq. 1)}$$

where $I_{o\nu}$ is the incident light, σ is the absorption cross section per molecule at frequency ν, A_1 is the amplitude of the pressure fluctuation, l_1 is the length of the cell. When the absorption spectra of gases in the two cells overlap, transmitted radiation will possess additional AC components, termed heterodyne signals, at $f_1 + f_2$ and $f_1 - f_2$. The intensities of the heterodyne signals are proportional to the concentrations of the like-absorbing molecules in the two cells. The AC heterodyne signal at $f_1 - f_2$ as a fraction of the DC signal is given by:

$$\frac{I_{2\nu}}{I_{o\nu}} = 1/2\ \sigma_1 \sigma_2 A_1 A_2 l_1 l_2 \qquad \text{(Eq. 2)}$$

When one cell contains a known amount of reference gas and another cell contains the sample gas, the intensity of the heterodyne signal can be used to determine the concentration of the reference gas in the sample cell. The principle can be expanded with multiple reference cells containing $^{12}CO_2$ and $^{13}CO_2$ to carry out isotope ratiometry.

Performance Evaluation Methods

Standard Reference Gases: $^{13}CO_2$ (90 atom% excess), depleted CO_2 (99.9% $^{12}CO_2$), and 2.5% CO_2 (-31.3 δ ‰ vs PDB) in air were mixed to give ten reference gas mixtures of about 2.5% CO_2 in air with ^{13}C enrichments ranging from -111 to 372 δ ‰ vs PDB. The composition of the mixtures was confirmed by gas chromatography and by triplicate gas isotope ratio mass spectrometry of purified CO_2.

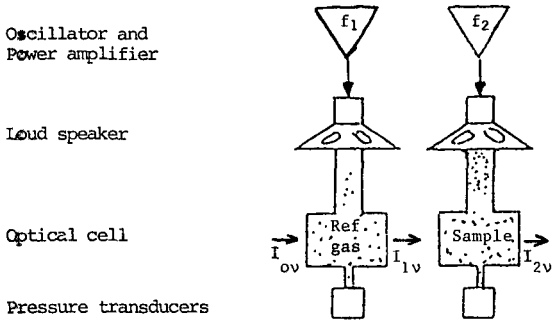

Figure 1

MCA Measurements: The sample cell was evacuated, purged with air, re-evacuated, and filled with 375 ml of a reference gas mixture. Six instrument analog voltages were measured using a 12 bit D/A converter operating over the range of -10 to +10V and an instrument response was calculated. Instrument response, which varied over the range of -.6 to +1.4, was measured once every 1 sec and averaged until a standard deviation of .002 was achieved. Four measurements were carried out on each reference gas mixture.

Data Analysis: Standard statistical methods were used in a linear regression analysis of MCA instrument response vs δ ‰ vs PDB to obtain standard error, slope, and intercept, along with standard deviations for the regression line. These were used to calculate the confidence limits for estimation of absolute ^{13}C enrichments in units of δ ‰ vs PDB for a mean MCA response obtained over a fixed period of time. Intra-sample precision was estimated from the 2nd, 3rd, and 4th measurements. Memory effect was estimated from the difference between the 1st measurement and the mean of the 2nd, 3rd, and 4th measurements.

Performance Evaluation Results

The MCA was evaluated with 10 reference samples containing 2.5% CO_2 in air and ^{13}C abundances from -111 to 372 delta per mil vs PDB (δ) as measured by GIRMS. The 375 mL cell required 60 s for evacuation, purging, and introduction of the sample. The instrument response varied from -.63 to 1.34 MCA units over the range -110 to 372 δ. A mean instrument response with .002 standard deviation required 40-120 sec at a 1-sec sampling rate. Greater precision can be achieved by extension of the counting time. The calibration curve of MCA units vs δ was linear over the entire range and had a slope of .00407 $\pm$ .00002 (SD), an intercept of -.189 $\pm$ .003, and standard error of .016. Using this curve, a mean value of -.300 MCA units, obtained from 60 sec of data acquisition, represents a value of -27.3 + 0.9δ (SD). A cycle of 3.5 min could be achieved in most breath tests, permitting repetitive on-line measurements.

SUMMARY

The performance of the MCA equals that of a GIRMS equipped with an automatic sample purification system with respect to precision and accuracy. The MCA surpasses the GIRMS in the number of samples that can be analyzed per day. The absence of high vacuum and high voltage components, as well as sample purification requirements, allows the instrument to be operated and maintained by non-mass spectrometrists. The MCA appears to be better suited for clinical $^{13}CO_2$ applications than the GIRMS.

Acknowledgments

This work is a publication of the USDA/ARS Children's Nutrition Research Center, Department of Pediatrics, Baylor College of Medicine and Texas Children's Hospital, Houston, TX, and was supported in part by NIH grant GM-28783-01.

A Modified Breath Inlet System For Breath Analysis by API/MS

F.M. Benoit, Environmental Health Directorate,
Health and Welfare Canada, Ottawa, Canada, K1A OL2.
K. Cena and D.C F. Muir, Health Science Centre,
McMaster University, Hamilton, Canada, L8S 4J9.

We have reported[1] previously on the design of a breath inlet system attached to a API/MS (TAGA 3000) which allowed the direct analysis of expired human breath. The specially designed inlet was required to dilute the breath prior to introduction to the ion chamber of the mass spectrometer. Dilution was achieved by bleeding a portion of the exhaled breath through a capillary tube (r = 0.25 mm, ℓ = 5 cm) into a stream of cylinder air. In operation, subjects were required to maintain a fixed pressure differential across the length of the capillary for the duration of the analysis in order to maintain a constant dilution factor. In practice, a number of difficulties were encountered:

1. The slow mass scanning speed of the TAGA 3000 required multiple exhalations for a complete mass spectrum.

2. The ability of the subject to maintain the fixed inlet pressure constant was varied and rendered quantitative estimations difficult.

3. In the selected ion mode, large spikes at the start of an exhalation caused by the rapid pressure increase from 0 to 0.5" H_2O were often observed and rendered quantitative estimations difficult.

4. Water condensation within the unheated inlet retained exhaled organics and contributed to contamination of the system.

5. The system was unable to distinguish alveolar and dead space airs.

To eliminate the above problems the breath inlet was modified by insertion of an air sampling bag (Calibrated Instruments, Inc.) in the system and by heating the sample containment volume to 40^{0}C. When using the modified breath inlet, the subject was required simply to fill the sampling bag; the pressure differential across the length of the capillary required during the analysis of the breath sample was achieved by the instrument operator squeezing the bag.

The advantages of the modified inlet were:

1. Control of the inlet pressure was easier and in the hands of a trained operator.

2. A complete mass spectrum could be obtained from one exhalation.

3. Water condensation problems were eliminated.

4. The system permitted more versatile sampling protocols.

The last feature was important when it was considered that all expired airs were not created equal. Dead space air which remained in the upper respiratory tract was exposed to the mucous lining therein whereas alveolar air entered the alveoli of the lungs and was exposed to venous blood leading to different chemical compositions for the two types of expired airs. The modified inlet permitted the sampling of selected portions of exhaled breath, as required. Indeed, in preliminary experiments where the levels of endogenous acetone and methanol in alveolar (A) and dead space (DS) airs were compared, the levels were higher in alveolar air than in dead space air (ratio A/DS=1.5 and 1.3 for acetone and methanol, respectively).

[1] F.M. Benoit, W.R. Davidson, A.M. Lovett, S. Nacson and A. Ngo, Anal. Chem. 55, 805 (1983).

Waller, G. R.*, Charles R. Ritchey*, Eugene E. Krenzer+
Departments of Biochemistry* and Agronomy+,
Oklahoma Agricultural Experiment Station
Oklahoma State University
Stillwater, Oklahoma 74078

Garmon Smith
Robert S. Kerr Water Laboratory
U. S. Environmental Protection Agency
Ada, Oklahoma 74820

Mynard Hamming
Petroleum Research and Development Department
Conoco, Inc.
Ponca City, Oklahoma 74603

Soils contain a heterogeneous collection of organic matter of various origins. The relative proportion of the different fractions depends upon the biological activity of the individual soils. We report here the results of steam distillation of an Oklahoma soil, collected from Altus, Oklahoma. The soil type is Tillman, clayloam (fine, mixed, thermic Typic paleustolls). Wheat had been grown on the soil for the past decade. A 2-kg sample was subjected to successive steam distillations at pH 5.9(initial conditions-fraction I) 1.0 (fraction A), 11.0 (fraction B), 13.5 (fraction BH), 7.0 (fraction N) and 0.35 (fraction AA), and organic compounds were extracted from each distillate with ethyl ether and subsequently with CH_2Cl_2 or toluene in some cases. Reagent grade solvents were used. These organics were analyzed by glc using a 30 m x 0.32 mm I.D. DB-5 J&W Durabond column with a 1μ- film thickness held at 40°C for 4 min and then programmed to 300°C at 8°C/min and held at 300°C. The compounds were identified tentatively with a GC/MS/DA (Finnigan Model 4500). Those peaks not identified were presumed to be degradation products of pesticides or were present in the diethylether or other extraction solvents.

The mass spectral data were very distinctive, providing the possibility of establishing identifications of a large number of individual compounds. A database on a TSO file served to store compound identifications from the difference fractions. The SAS program SORT was then run to group compounds into various classes such as: n-saturated fatty acids from C_4 to C_{18}; alcohols (aromatic and aliphatic); phenols; amines (aromatic and aliphatic); hydrocarbons (polyaromaics); and compounds having the following general formulas of CHNO, CHNS, CHS, and CHN_2. Some of these are shown in Figures 1-3. SAS PLOT procedures were used to plot scans (retention times) against carbon numbers for a given class of compounds (Figure 4) as a support to identifications. Additional support to identifications is planned.

Our interest is in isolating soil allelochemicals. Allelochemicals are compounds produced by plants which are given off into the soil, water, or air which affect the growth of adjacent plants, even of the same species. Allelochemicals include a variety of compounds such as phenolics, fatty acids, non-protein amino acids, flavanoids, alkaloids, terpenes, terpenoids and cyanogenic glucosides. Some of these molecules may be natural herbicides, insecticides, fungicides or antibiotics. Of the classes of compounds that have known toxicity to plants the phenolic compounds are of most important. Less has been done on the plant toxicity of fatty acids and other classes of compounds.

[1]SAS (Statistical Analysis System) is a computer software system, SAS Institute Inc., Box 8000, Cary, NC 27511.

Figure 1 Occurrence of CHNO Compounds from STEAM DISTILLATES OF A TILLMAN CLAY-LOAM SOIL

FORMULA	C H N O COMPOUNDS MOL	BPK	NAME OF COMPONENT	OCCURRENCE
C 2 H 5 N 1 O 4	107	45	ETHANEDIOL,MONONITRATE	BH1
C 5 H 4 N 2 O 1	118	95	ETHANONE,PYRAZOL-YL	A-1 B-1
C 5 H11 N 1 O 1	101	58	FORMAMIDE,DIMETHYLETHYL	BH3
C 5 H12 N 2 O 1	116	116	TETRAMETHYLUREA	BH3
C 6 H 5 N 1 O 3	139	39	NITROPHENOL	AA1
C 7 H 7 N 1 O 1	121	105	BENZAMIDE	BH5
C 7 H15 N 1 O 1	129	87	PENTANAMIDE,ETHYL	B-1
C 8 H 5 N 1 O 2	147	147	1SOINDOLE,DIONE	BH1
C 8 H15 N 3 O 1	169	169	HYDRAZINECARBOXAMIDE,MECYHEX-	AA1
C 9 H 7 N 1 O 3	177	147	1SOINDOLE	BH2
C 9 H11 N 1 O 1	149	105	BENZAMIDE,ETHYL	BH5
C10 H21 N 1 O 1	171	86	ACETAMIDE,DIBUTYL	B-1
C12 H13 N 3 O 4	263	219	OXADIAZOLINONE,1%BUTYLNITROPH	B-1
C13 H13 N 3 O 1	227	169	HYDRAZINECARBOXAMIDE,DIPHENYL	B-1
C13 H27 N 1 O 2	229	73	HEXANAMIDE	B-1
C18 H18 N 2 O 1	278	219	QUINOXALINE	B-1
C18 H35 N 1 O 1	281	59	OCTADECENAMIDE	AA1
C18 H35 N 1 O 1	281	59	OCTADECENAMIDE	B-1
C18 H37 N 1 O 1	283	59	OCTADECENAMIDE	B-2

Figure 2. Occurrence of Phenols from STEAM DISTILLATES OF A TILLMAN CLAY-LOAM SOIL.

FORMULA	PHENOLS MOL	BPK	NAME OF COMPONENT	OCCURRENCE
C 6 H 6 O 1	94	94	PHENOL	B-1 H-1
C 7 H 8 O 1	108	108	PHENOL,METHYL	H-1
C 8 H10 O 1	122	107	PHENOL,ETHYL	H-1
C 9 H10 O 3	166	124	PHENOL,METHOXY-ACETATE	B-1

Figure 3. Occurrence of PolyNuclear Hydrocarbons from Steam Distillates of a Tillman Clay-Loam Soil.

FORMULA	HYDROCARBONS - POLY-AROMATICS MOL	BPK	NAME OF COMPONENT	OCCURRENCE
C16 H10	202	202	PYRENE	A-1
C16 H10	202	202	FLUORANTHRANE	A-1
C14 H10	246	191	ANTHRACENE	AA1
C20 H12	360	191	PHENANTHRENE	AA1

Figure 4. Plot of Scans (GLC Retention Times) vs Carbon Numbers for Fatty Acids Distribution in Steam Distillates of a Tillman Clay-Loam Soil.

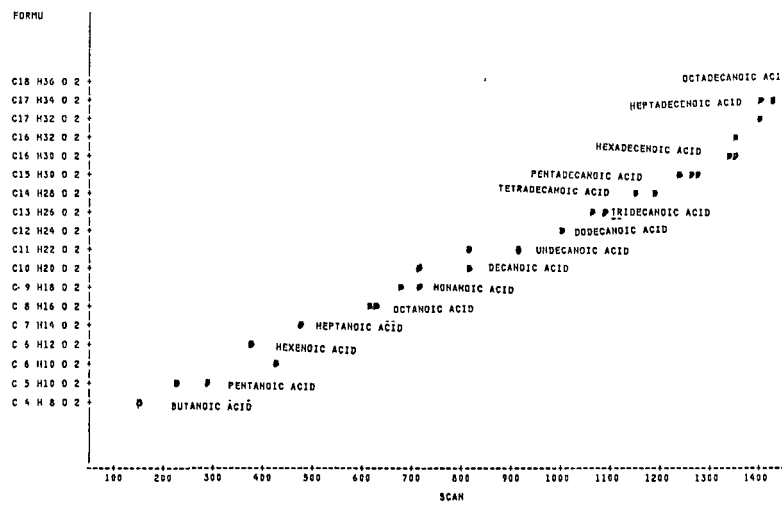

PRODUCTION OF A NEW COMPOUND BY METABOLISM OF THEOPHYLLINE IN COFFEA ARABICA L., MPB 15

Waller, G. R. and Ludovic, Yvonne,
Deparment of Biochemistry
Oklahoma Agricultural Experiment Station
Oklahoma State University
Stillwater, Oklahoma 74078

Biodegradation of caffeine (1,3,7-trimethylxanthine) occurs in Coffea arabica L. plants through theophylline (1,3-dimethylxanthine) and theobromine (3,7-dimethylxanthine) as the first biodegradation products. Theophylline is associated primarily with caffeine biodegradation whereas theobromine is involved in both biosynthesis and biodegradation of caffeine. Theophylline and theobromine are found as minor components whereas the caffeine is the major purine alkaloid produced. Xanthine is produced by removal of the N^1-, N^3- and N^7-methyl groups of the dimethylated xanthine and converted to uric acid which undergoes hydrolytic cleavage to urea and glyoxylic acid in the coffee plant.

One hundred thirty millicuries of the [8-^{14}C]theophylline compound was injected slowly in the branch point of the stems from the main trunk of a coffee plant (Plant Introduction Number 435156) in Stillwater. The chloroform extract was applied to analytical thin layer chromatography plates, and developed using $CHCl_3$:EtOH (9:1). The compounds were detected on the chromatograms by observing their fluorescence at 254 nm; sections of cm 2 width were cut from the plates and used for radioactivty measurements. The zones on the thin layer chromatography plates corresponding to the radioactivity were scraped off into a glass Buchner funnel medium porosity and eluted with chloroform and used for low resolution mass spectrometry (LKB-9000).

The aqueous extract (0.4 ml) was spotted on thin layer chromatography plates, and developed using EtOH:HOAc:H_2O (81:5:4). The plate was observed under UV_{254} nm, and each fraction was scraped and eluted with water. The extracted compounds were evaporated to dryness and 2-ml solutions were prepared. From these solutions 0.5 ml were used for radioactivity measurements, and the solution which contained the radioactive compound was used for HPLC. An ODS-reversed phase column packed with C-18 (250 x 4.6 mm I.D.) was used and the effuent was monitored by UV detectors operated at 214 nm, 254 nm, and 280 nm. The peak which corresponded to the radioactivity had absorbance only at 214 mm.

The collected compound(s) in the peaks from the HPLC were sent to MIT (NIH Division of Research Resources, Grant No. RR00317 to K. Biemann) for high resolution mass spectrometry (EI mode). The results are shown in Table I.

The nomenclature of this class of compounds is based on a personal communication with Kurt L. Loening, Director of Nomenclature, Chemical Abstracts Service, Americn Chemical Society, Columbus, Ohio. A survey of the chemical literature was made and no such structure corresponding to $C_5H_7N_3O_3$ with the imadazolidine ring could be found. The compound is named with the IUPAC rules or organic nomenclature as well as CA practice. Since the radioactivity was retained at position 2 of the imidazolidine ring, it was concluded that the coffee plant modified the pyrimidine ring.

We conclude that the compound, $C_5H_7N_3O_3$, is a new metabolite of theophylline. Its location in the metabolic pathway of theophylline is based on structures proposed in Figure 1 which places it following uric acid. It is likely that this compound is the beginning of a new pathway for the biodegradation of theophylline and caffeine. The possibility exists that this compound is translocated from the stems into the leaves and fruit; however, none of the other samples taken from 96 to 332 hr showed the presence of such a compound. The fact that it is present only at the 72 hr after feeding the radioactive theophylline suggests that it may be an intermediate which occurs early (before 72 hr) in the biodegradation of theophyllne.

TABLE 1
ELEMENTARY FRAGMENTATION OF UNKNOWN BY ELECTRON IMPACT MASS SPECTROMETRY
MOLECULAR FORMULA: $C_5H_7N_3O_3$

Abundance	m/z	Elementary Composition C	H	N	O	Ion Peak	Fragment Lost
405	157	5	7	3	3	$M^{+\cdot}$	
24	156	5	6	3	3	$M^{+\cdot}-1$	-H
179	143	4	5	3	3	$M^{+\cdot}-14$	$-CH_2$
236	140	5	6	3	2	$M^{+\cdot}-17$	-OH
21	129	4	7	3	2	$M^{+\cdot}-28$	-CO
260	127	4	5	3	2	$M^{+\cdot}-30$	$-CH_2O$
551	126	4	4	3	2	$M^{+\cdot}-31$	$-CH_2OH$
609	115	3	5	3	2	$M^{+\cdot}-42$	$-CH_2H_2O$
643	99	3	5	3	1	$M^{+\cdot}-30-28$	$-[CH_2O+CO]$
808	98	3	4	3	1	$M^{+\cdot}-30-28-1$	$-[CH_2O-CHO]$
553	85	2	3	3	1	$M^{+\cdot}-(C_3H_4O_2)$	---

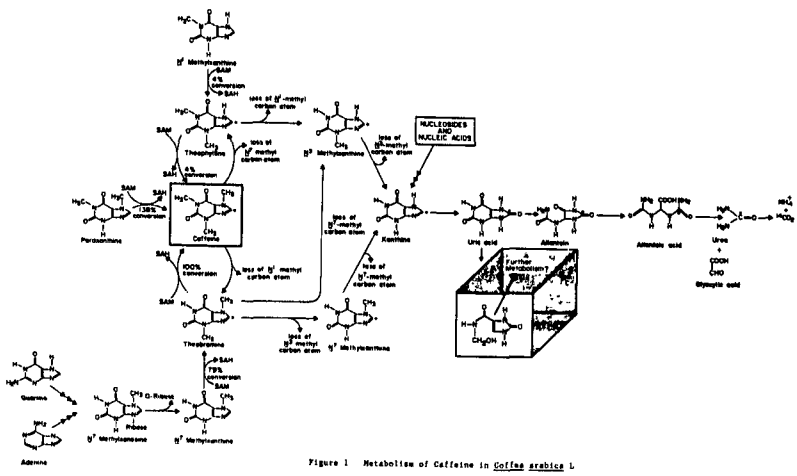

Figure 1 Metabolism of Caffeine in *Coffea arabica* L

ANALYSIS OF TRAZODONE AND $^2H_4$ - TRAZODONE BY CAPILLARY GC/MS/SIM. E. H. Kerns, R. E. Gammans, W. W. Bullen, Bristol-Myers Pharmaceutical Research Development Division, Evansville, Indiana, 47721, and J. W. Russell, Mead Compuchem, Research Triangle Park, North Carolina, 27709.

Introduction

Trazodone HCl is a widely used antidepressant under the trade name Desyrel. During planning for a bioavailability study of tablet formulations the technique of stable-label coadministration with GC/MS determination was chosen because of the superior statistical and financial benefits obtainable. Therefore, a specific, internal standard GC/MS assay was required to quantify trazodone (TZ) and an $^2H_4$ analog (D_4-TZ) in plasma. This procedure has been developed, validated in two independent laboratories and successfully applied to a bioavailability study.

Experimental

Extraction of plasma samples proceeded as follows. One ml of plasma was spiked with 400 ng of etoperidone (IS) internal standard, made basic, and vortex extracted with 9 ml of n-butyl chloride. The organic phase was extracted with aqueous acid, which was made basic and extracted with n-butyl chloride. Following volume reduction under N_2 the extract was dissolved in 20 µl toluene.

Finnigan MAT 4000 series instruments with INCOS data systems were operated at 70 eV for EI. Selected ions were sequentially monitored at 231 (TZ), 235 (D_4-TZ) and 225 (IS) over a unit mass window for 0.21 sec each. Chromatography was performed with a 4 m long x 0.25 mm ID DB-1 fused silica capillary column. The helium carrier gas was at 2 psi. The temperature was 170°C for 1 min then increased at 15°C/min to 225°C. Two µl of extract was injected by splitless technique.

Clinical bioequivalence of TZ and D4-TZ was evaluated by giving a subject a solution containing 50 mg of both compounds in solution. Clinical bioavailability studies were conducted by administering D_4-TZ in solution simultaneously with TZ in a tablet formulation.

Results and Discussion

The EI mass spectrum of TZ and its interpretation are indicated in the figures. D_4-TZ and etoperidone fragment similarly. The base peaks could not be used for SIM because a BP+4 amu ion in TZ would interfer with D_4-TZ. The 22% RA ion chosen was adequate for the sensitivity range required.

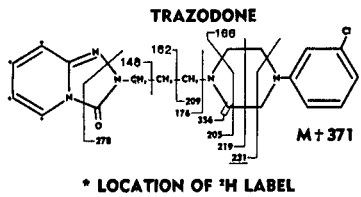

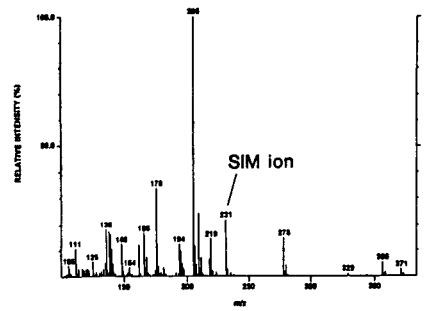

Electron impact mass spectrum of trazodone

The chromatograms depict a blank and a spiked plasma extract at the lowest level of quantification. No endogenous plasma interferences were observed.

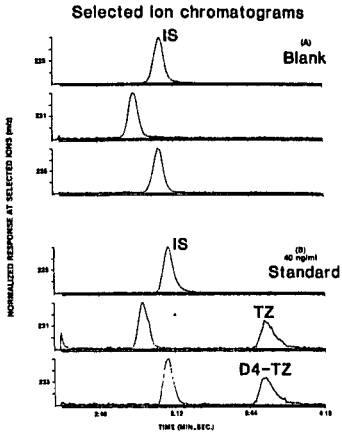

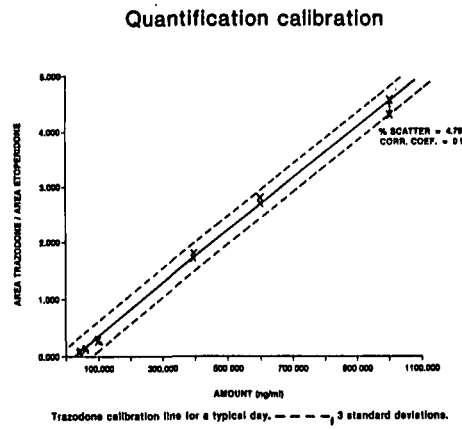

The method was linear over the range of 40-1000 ng/ml which encompassed the range of concentrations in plasma for 34 hours following administration of 50 mg of TZ.

In two independent labs the precision and accuracy of the method was similarly good.

ACCURACY AND PRECISION OF THE ASSAY DEMONSTRATED IN TWO LABS

	TRAZODONE				$^2H_4$–TRAZODONE			
Test	Lab	ng/ml Added	ng/ml Mean Observed	% CV	Lab	ng/ml Added	ng/ml Mean Observed	% CV
Inter-Assay[a]	A	60	60	5.0	A	60	61	4.9
Inter-Assay	A	600	604	3 1	A	600	606	4 5
Inter-Assay	B	60	66	6 0	B	60	63	4 8
Inter-Assay	B	600	594	5 2	B	600	591	5.1
Intra-Assay[b]	B	60	59	5.1	B	60	59	4 2
Intra-Assay	B	600	616	3.4	B	600	619	3 2
Blinded[c]	A	0-600	--	16	A	0 600	--	17
Blinded	B	0 600	--	8 0	B	0-600	--	9 0
QC-Controls[d]	B	60	63	7 9	B	60	64	9 4
QC-Controls	B	600	600	4.0	B	600	601	4.7

[a] Five control plasmas spiked and analyzed each day for 5 days
[b] Ten control plasmas spiked and analyzed on one day.
[c] Spiked controls on one day. Lab A analyzed 12 samples, lab B analyzed 20 samples
[d] Nine control plasmas spiked and analyzed over several days of bioavailability study

DESORPTION CHEMICAL IONIZATION MASS SPECTRA OF UNDERIVATIZED ABSCISIC ACID-CONJUGATED METABOLITES, A USEFUL AID FOR STRUCTURAL CHARACTERIZATION

Naohito TAKEDA, Ken-ichi HARADA, Makoto SUZUKI and Akira TATEMATSU
Faculty of Pharmacy, Meijo University, Nagoya 468, Japan
Nobuhiro HIRAI and Koichi KOSHIMIZU
Faculty of Agriculture, Kyoto University, Kyoto 606, Japan

Plant hormone abscisic acid (ABA) is metabolized to phaseic acid (PA) via a very unstable metabolite, hydroxy ABA (HOABA). This metabolite has been shown to occur in the seeds of Robinia pseudacacia as a stable conjugate, β-hydroxy-β-methylglutaryl-hydroxyabscisic acid (HMG-HOABA) (Scheme 1). The levels of free ABA and HMG-HOABA in plant organs must be closely related to the physiological processes (1). Therefore, the detection, characterization and quantitation of HMG-HOABA in the seeds are very important for the study on the feature of ABA metabolism.

The purpose of our present study is 1) to establish a rapid and specific means for screening of trace amount of HMG-HOABA and related conjugate in the seeds of Robinia pseudacacia and 2) to characterize the structures of individual components in the crude plant extract by the use of mass spectrometry.

1) Screening

Applying desorption CI (D/CI) technique to the screening was found to be the most practical procedure with high sensitivity and reproducibility. The D/CI(NH_3) mass spectrum of the 80% acetone eluate, partially purified extract, clearly showed the $[M \cdot NH_4]^+$ ion of HMG-HOABA at m/z 442 (Fig. 1). The presence of the ion at m/z 456 in the spectrum is very interesting, because this ion can be estimated as the $[M \cdot NH_4]^+$ ion of a monomethyl ester of HMG-HOABA; the spectrum shows the monomethyl ester as a new conjugate occurs in the seeds along with HMG-HOABA. However, there are two possibilities for the structure of the monomethyl ester, MeHMG-HOABA or HMG-MeHOABA (mol.wt. 438) (Scheme 1).

2) Characterization

In order to solve the structural problem mentioned above, linked scan at constant B/E of $[MH]^+$ ion of authentic MeHMG-HOABA was attempted under SIMS conditions (Fig. 2); SIMS is adapted to facilitate the B/E scans due to its ability of yielding long-lived molecular ion species. The ions at m/z 263 and 245 observed in the metastable ion (MI) spectrum are diagnostic species only for MeHMG-HOABA (Fig. 3). The same analysis was made on the 80% acetone eluate and the resultant MI spectrum provided both the fragment ions characteristic of MeHMG-HOABA.

These results demonstrate that the combination of D/CI technique and B/E linked scanning technique under SIMS conditions is capable of characterizing a new conjugated metabolite, MeHMG-HOABA even in the crude extract.

Reference

(1) W. J. Davies and T. A. Mansfield, "Abscisic Acid," ed. by F. T. Addicott, Praegar, New York, N. Y., 1983, p. 237.

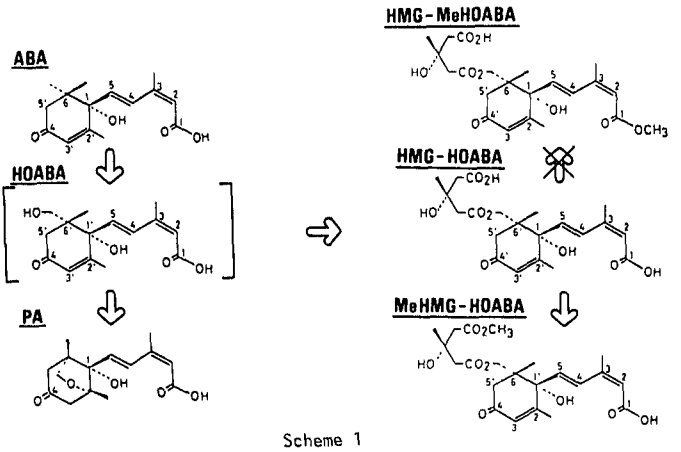

Scheme 1

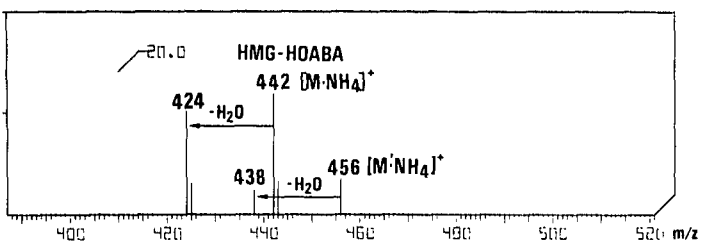

Fig. 1

Metastable ion spectrum of protonated MeHMG-HOABA (m/z 439) produced under SIMS: authentic

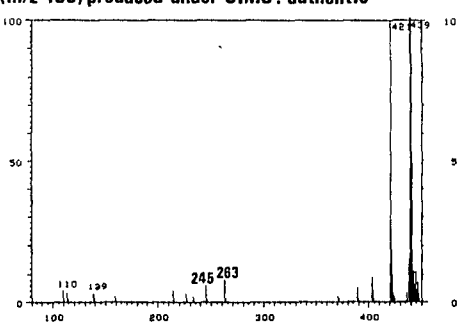

Fig. 2

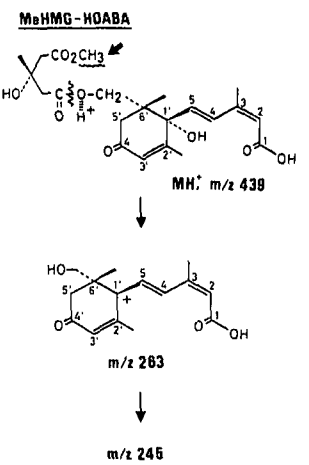

Fig. 3

QUANTITATION OF SUCROSE ESTERS IN TOBACCO BY DIRECT CHEMICAL IONIZATION MASS SPECTROMETRY,

W. N. Einolf and W. G. Chan, Philip Morris Research Center, P. O. Box 26583, Richmond, VA 23261

A direct chemical ionization (DCI) mass spectrometry method for determining underivatized sucrose esters in tobacco has been developed in our laboratory and applied to a growth study involving three tobacco varieties. The method uses a synthetic internal standard, sucrose tetra-ß-methylvalerate. DCI mass spectrometry using ammonia as reagent gas gives abundant $(M+NH_4)^+$ ions for the internal standard (IS) and the sucrose esters in the tobacco extract.

The freeze-dried tobacco sample was extracted with dichloromethane, and the extract was chromatographed on a C_{18} SEP-PAK cartridge, to which a known amount of the IS had been added. An aliquot of the eluate containing both the IS and the sucrose esters was then placed on a Vespel[R] DCI probe tip and analyzed on a MAT 112S instrument under magnetic scanning conditions. The data were processed to give peak area integration of both the IS and selected sample ion peaks, and comparison of the two peak areas resulted in quantitation of individual sucrose esters. Although not fully characterized, the natural sucrose esters were shown by their DCI spectra to be substituted on only one of the saccharide groups, while the synthetic ester was substituted on both groups. Use of the sucrose tetra-ß-methylvalerate placed the $(M+NH_4)^+$ ion at a m/z value which does not interfere with the analysis of the natural sucrose ester components. This is shown in Figure 1, where the peak at m/z 752 corresponds to $(M+NH_4)^+$ for the IS, and the peaks at m/z 640, 654, 668, 682, 696, 710, 724 and 738 correspond to $(M+NH_4)^+$ for the tobacco sucrose esters with side chains of varying carbon numbers. Note the presence of the solanesol (MW 630) peak at m/z 648 $(M+NH_4)^+$ and that of an unknown at m/z 664. Otherwise, the spectra are quite clean due to the selectivity of ammonia as reagent gas.

The growth study was conducted to determine the effect of growth time on the level of sucrose esters in tobacco. As shown in Figure 2, there is an overall increase in the total sucrose ester content of tobacco leaves as a function of plant growth time for these greenhouse-grown plants. In most cases, the esters were observed to maximize after 40 days from transplant, decrease somewhat, and again maximize to a higher value as the plant reached maturity.

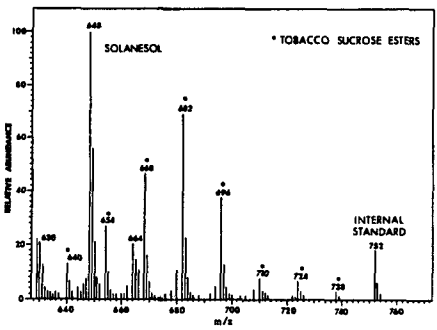

Fig. 1 Partial DCI Mass Spectrum of an Extract of Freeze-Dried Green Oriental Tobacco Leaves Using Ammonia as Reagent Gas

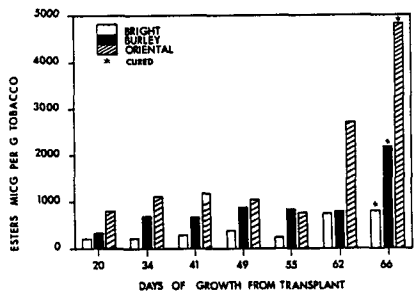

Fig. 2 Total Sucrose Esters in Three Tobacco Varieties as a Function of Plant Growth Time

USING GC/MS TO MONITOR THE EFFECTS OF ACENAPHTHENE ON AQUATIC PLANTS

Martha M. Vestling, Chemistry Department
SUNY College at Brockport, Brockport, NY 14420

Our goal is to develop and use procedures for monitoring the effect of specific chemicals on aquatic plants and for monitoring the effect of aquatic plants on specific chemicals. The plan is to grow aquatic plants in the laboratory under reproducible conditions. After systematically polluting the growth medium, we should be able to monitor both the growth medium and the plants for pollutant and metabolites. We plan to follow any changes in the growth of the plants with a battery of enzyme assays.

We chose acenaphthene as our first pollutant and are currently culturing three plants. They are Nitella clavata (a freshwater giant green alga), Lemna minor (common duckweed) and Spirodela polyrhiza (greater duckweed). The culture medium for Nitella was developed by C. E. Barr of Brockport's Biology Department. It contains humic acid. The duckweeds grow on a completely defined medium of inorganic compounds with potassium nitrate as the nitrogen source. The formulation we use is that of G. Stewart, J. Expt. Bot. 23, 171 (1972).

The literature does not contain any references to plant metabolism of acenaphthene. However, acenaphthene has been studied in rats. See C.J. Simmons, R.P. Hopkins and P. Callagan, Biochem. J. 1971, 124 (2), 26P.

We dosed our plants with 3 mg/ L acenaphthene. Extraction with methylene chloride worked well except that the methylene chloride caused excessive bleed from our gas capillary column (methyl silicone) and lots of ghosts from our reverse phase C-18 HPLC column. So just before chromatographic analysis, we exchanged the methylene chloride for either benzene or hexanes.

Our gc/ms results are qualitative. Nitella incubated five days with acenaphthene gave a medium containing acenaphthene and 1-acenaphthenol. Incubation for 14 days, gave acenaphthene and 1-acenaphthenone. The culture medium with no plants was incubated too, and it gave only a trace of acenaphthene. In contrast, the duckweed medium without plants gave acenaphthene, 1-acenaphthenol, and 1-acenaphthenone. However, Spirodela after five days gave only acenaphthene and 1-acenaphthenone while Lemna gave all three compounds. Both the medium and the plant extractions for Spirodela gave the same two compounds.

We observed also that acenaphthene disolved in water and exposed to light and air, produced a gc/ms run with acenaphthene, 1-acenaphthenol, 1-acenaphthenone and 1,8-naphthalic anhydride clearly present.

The enzyme battery tested consisted of peroxidase, alkaline phosphatase and glutamine synthetase - all activities determined colorimetrically. Total protein in the plant extracts was measured as wet plants are hard to weigh accurately.

Based on the data we have collected so far, we conclude:

1. Nitella clavata, Lemna minor and Spirodela polyrhiza grow in the presence of acenaphthene (3 mg/L).
2. Acenaphthene can be found both in (on?) the plants as well as in the culture medium.
3. Capillary gas chromatography with mass selective detection can separate and identify acenaphthene, acenaphthylene, 1-acenaphthenol, 1-acenaphthenone, 1,2-acenaphthenequinone and 1,8-naphthalic anhydride.
4. Under the culture conditions, photodecomposition of acenaphthene occurs. Acenaphthene is changed to 1-acenaphthenol and 1-acenaphthenone in the presence of water and light as well as in the presence of plants.
5. Acenaphthene changes the enzyme activity of peroxidase, glutamine synthetase and alkaline phosphatase.
6. Using a 10/1 split and 1 μL injection, the mass selective detector in scanning mode gives useful (nice!) spectra with 1-10 ng of compound (injecting 10-100 ng). This is not pushing the detector to its limits.
7. HPLC traces appear to confirm the gc/ms data gathered. Fluorescent detection coupled with a 254 nm detector significantly simplifies data interpretation.
8. Bluegreen algae are difficult to remove from aquatic plant cultures. Use of appropriate controls is therefore quite important in this work.

Six undergraduates have worked on various parts of this project. They are Kenneth Hart '83, Walter Kehoe '83, John Punzi '83, Lynne Fullerton '84, Joseph Sinegra '84 and Patricia Thompson '84.

Application of ^{252}Cf-PDMS to Chlorophylls*

J.E. Hunt, T.J. Michalski, and J.J. Katz

Chemistry Division
Argonne National Laboratory
Argonne, IL 60439

Our research program is involved in the synthesis and photophysical properties of model compounds designed to mimic the in vivo reaction center of photosynthesis. Our primary concern is chlorophyll function in photosynthesis. Although the chlorophylls have been studied for 150 years, astonishingly little is known about many of their physical and chemical properties that are likely to be pertinent to the interpretation of in vivo phenomena. Methods of characterizing these properties have generally been limited to optical measurements which provide little, if any, information about its structure. We have synthesized several new synthetic chlorophylls and have confirmed their structure by ^{252}Cf-PDMS in conjunction with nuclear magnetic resonance measurements and microanalysis by high performance liquid chromatography.

Mass spectra of the chlorophylls are very difficult to obtain because the chlorophylls readily oxidize to form allomers and decompose to pheophytins (loss of the central magnesium atom). In addition, as a class of compounds, the chlorophylls are very involatile. The use of ^{252}Cf-PDMS for analysis considerably simplifies obtaining good mass spectra of the chlorophylls. Our synthetic program for covalently linking two chlorophyll macrocycles has been aided by the rapid feedback given by routine mass analysis of intermediates in the synthesis. ^{252}Cf-PDMS provides a focal point for further reaction steps, and separations and purifications of the products.

The practical use of ^{252}Cf-PDMS is demonstrated in mass measurements to identify intermediates in the formation of a chlorophyll pair covalently linked by a thio-ethoxy bond (Table 1).

TABLE 1

Compound	M^+	$(M\text{-phytyl})^+$	$(M\text{-thioethoxy group})^+$
Chl a-O-$(CH_2)_2$-S-S-$(CH_2)_2$-O-Chl a	1937.2	1659.2	--
Chl a-O-$(CH_2)_2$-S-S-$(CH_2)_2$-OH	1045.5	767.5	968.0
Chl a-O-$(CH_2)_2$-SH	969.5	691.5	892.5
Chl a	892.5	615.5	--

The data acquisition time of each of the samples was generally less than thirty minutes. Analysis of the mass spectra of the covalently linked chlorophyll compound (molecular weight 1937.2 amu) at ten minutes reveals the molecular weight of the compound to within two mass units; and analysis at thirty minutes reveals the molecular weight of the compound to an error of 0.5 amu. This accuracy combined with the fragmentation information in the mass spectrum is sufficient to establish the identify of the compound. Because so little of the sample is probed by ^{252}Cf-PDMS, the sample is easily returned for additional reaction, separation, or purification steps.

In summary, we have found ^{252}Cf-PDMS to be a most useful technique for molecular weight determination of synthetic intermediates and final products of new synthetic chlorophylls. ^{252}Cf-PDMS is expected to continue to contribute to this important area of photosynthesis research.

*Work performed under the auspices of the Office of Basic Energy Sciences, Division of Chemical Sciences, U.S. Department of Energy under contract W-31-109-ENG-38.

SIMULTANEOUS DETERMINATION OF ABA AND IAA IN PLANT EXTRACTS USING GC/MS/MPM

. K. Jayasimhulu and J. L. Caruso

Department of Environmental Health and
Department of Biological Sciences
University of Cincinnati
Ohio 45267

Simultaneous determination of abscisic acid (ABA) and indole-3-acetic acid (IAA) by gas chromatography-mass spectrometry-multiple peak monitoring allows the investigator to gain more information on these plant hormones from each extract. Acetone extracts of Douglas fir seedlings[1] received known amounts of d_6-ABA and d_5-IAA as internal standards (Fig. 1). The ABA analog was synthesized in the laboratory. Good separation was observed with a 2 mm i.d., 6 ft. long glass column packed with 3% OV-101 on gaschrome Q. Quantitation was achieved by multiple peak monitoring of $M^{+\cdot}$ of methylated, trifluoroacetylated IAA (m/z 285.0613), d_5-IAA (m/z 290.0921) and base peaks of methylated ABA (m/z 190.0630) and d_4-ABA (m/z 194.0877). A four carbon fragment containing two deuteriums is lost from the parent ion of hexadeuterated ABA giving rise to the base peak, under EI conditions.

Shoots of two month old Douglas fir seedlings revealed averages (with standard error) of 3 $\pm$ 0.753μg ABA and 0.707 $\pm$ 0.270μg IAA, both on a per gram dry weight basis. Roots usually gave comparable levels of IAA (0.632 $\pm$ 0.13). ABA content, however, varied from 200 ng to 7μg per gram, dry weight.

Supported by NSF grant PCM-83-09132 and the Dieckmann Forestry Fund, University of Cincinnati.

1. Caruso, JL and Zeisler CS, Phytochemistry 22, 589 (1983)

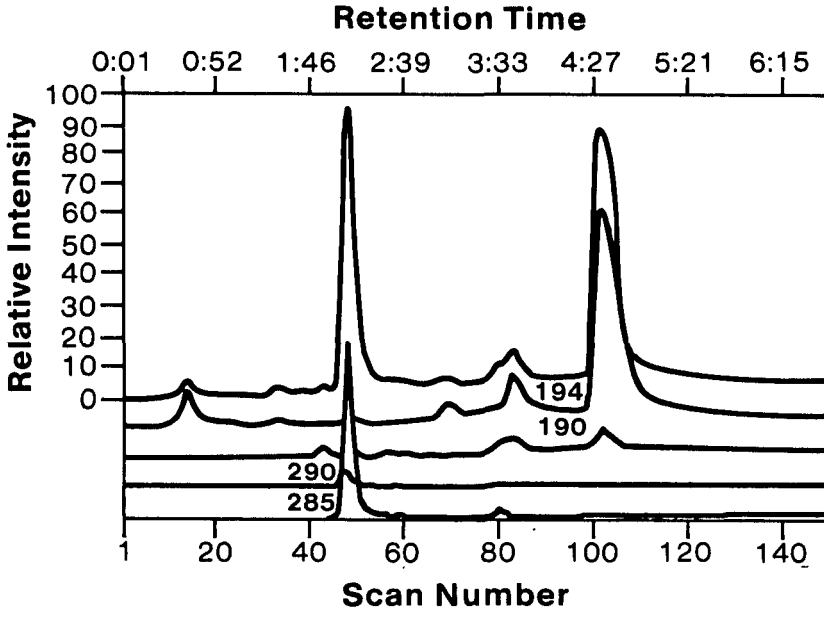

Fig. 1. Multiple peak monitoring of molecular ions of methylated and trifluoroacetylated IAA (m/z 285.0613), d_5-IAA (m/z 290.0921), and base peaks of methylated ABA (m/z 190.0630) and d_4-ABA (m/z 194.0877), obtained using the Kratos MS80.

MASS SPECTROMETRY DETERMINATION OF ALTERATIONS IN STRUCTURE AND CONCENTRATION OF SELECTED CHEMICAL MUTAGENS INCUBATED IN CULTURE MEDIUM.

Bertha L. Proctor
Mary Ann Dowd, Mary Esther Gaulden, University of Texas-Dallas, Richardson, TX

Relatively little attention has been given to the fates of test compounds during mutagenic testing. We have used high resolution gas chromatography mass spectrometry and direct insertion probe mass spectrometry techniques to determine the purity and fates of several known or suspected mutagens in culture medium (Mark's 20M) with 7.5% fetal calf serum incubated at 24°C or 38°C. The test compounds include benzene, formaldehyde as 37%formalin and mitomycin-C.

After purity of the compound was determined, the compound was spiked into the Mark's complete medium and incubated at 24°C (Benzene) or 38°C . Triplicate 6 ml aliquots were removed at 15 minute intervals for microextraction and mass spectrometry analysis. A Nermag R-10-10 Mass Spectrometer equipped with a Carlo Erba Gas Chromatograph and Direct Insertion Probe were used for all analyses. Instrument conditions for each compound is listed below:

Benzene:	Electron Impact MS	Filiment = 70ev Temp.= 200C
	Mass Range	70-400 amu
	Scan Rate	2 msec/amu
	Column	30M DB5 (J&W)
	Program	30C(5 min)- 10C/min-280C(10 min)
	solvent	isopropylether
Formaldehyde:	Electron Impact MS	Filiment = 70ev Temp. = 200C
	Mass Ranges	30-31, 33-43,45-400 amu
	scan rate	2 msec/amu
	column	30M DB5 (J&W)
	program	30C(5min)- 10C/min- 280C(10 min)
	solvent	isopropylether
Mitomycin-C	Purity	
	Direct Insertion Probe Mass Spectrometry	
	mass range	100-400 amu
	scan rate	2 msec/amu
	program	50C-115C/min-165C(1 min)
		165C-135C/min-300C (1min)
		300C -100c/min-500C(1 min)
	Interaction	
	Electron Impact	filiment = 70ev temp.=200c
	mass range	100-400 amu
	scan rate	2 msec/amu
	program	30C(5)-10C/min-280C(10 min)
	solvents	butylacetate, isopropylether

Benzene was unreactive with medium components but was highly volatile, resulting in rapid loss of benzene from the medium. Changes in the protocol (reduction of headspace volume and use of closed vials) dramatically decreased loss of benzene from culture medium. Benzene induced chromosome aberrations in the Grasshopper Neuroblast Assay at 10^{-5}M including fragments, retarded prophases, and 10^{-3}M induced lagging chromosomes and chromosomes off the spindle.

Formaldehyde as 37% formalin is complex mixture of chemicals. A microextraction of 3 mls of formalin with isopropylether followed by GC-MS analysis indicates the presence of 18 compounds. Most of these were hydrated formaldehyde or dimerized formaldehyde species. This mixture was extremely reactive with culture medium. Figure I shows the extreme reactivity of this mixture with culture medium and how the medium composition shifts over the exposure time. Chemical analyses of these mixtures indicate volatilization, degradation and reaction of the test mixture with medium. There is a pronounced shifting from lower molecular weight species to higher molecular weight species over time.

Chromosome aberrations induced by formaldehyde as formalin include ,extreme stickness (10^{-6} to 10^{-3}M), chromosome breaks and constrictions.

Mitomycin-C is often used as a positive control in several bioassays including sister chromatid exchange. Purity of the Mitomycin-C (MMC) was determined by direct insertion probe Mass Spectrometry. Two different lot of MMC (SIGMA) were analyzed. One lot of MMC had a large quanity of unknown compound, the other lot was relatively pure. Mass Spectrometry analyses indicate that the MMC is reactive with medium components but the new products are formed much later in the incubation period (at least 30 minutes at 38C).

FIGURE I Changes in medium composition after addition of Formaldehyde & incubation at 38C

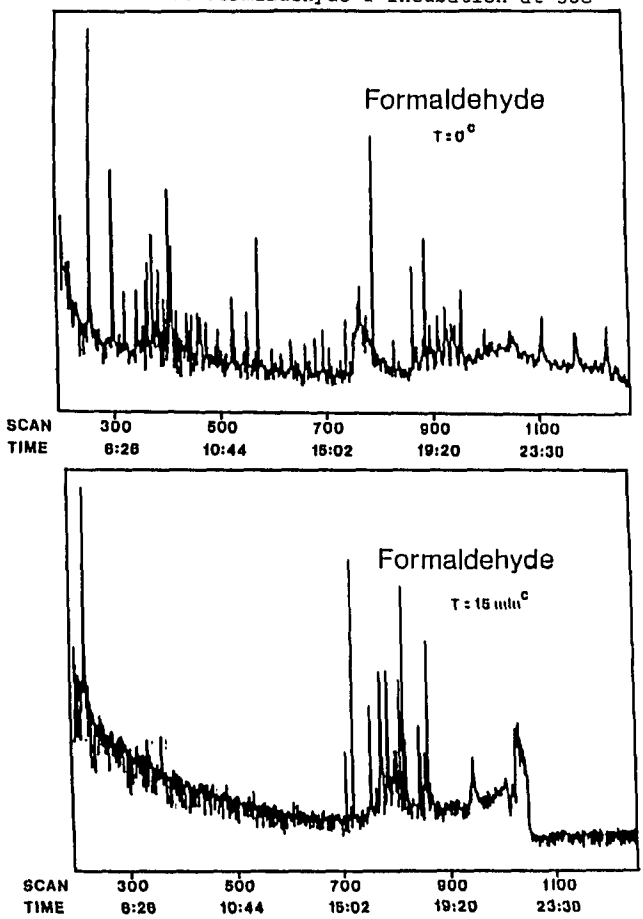

NEUTRAL PRODUCTS FROM FLUORIDE TRANSFER BETWEEN ALKYL FLUORIDES AND ALKYL CATIONS IN THE GAS PHASE.

K.K. Jóhri, Eric W. Redman, Robert W.K. Lee, and Thomas Hellman Morton
Department of Chemistry, Univeristy of California, Riverside, CA 92521

As we have previously shown, examination of the neutral products from gas phase ion-molecule reactions yields important information regarding reaction pathways and ion structure that cannot be obtained through mass spectometry alone.[1,2] In the present study, we have examined the reactions of the 2-fluoroisopropyl cation and the 2-propenyl cation in our EBFlow reactor. The reactions studied yield fluorine-containing products, which we can examine by ^{19}F and proton NMR of the recovered product mixture. We have looked at the products from acid-base reactions of the deuterated ions shown in reaction 1. The d_3, d_2, and d_5 products are well resolved from one another in the high field NMR, as Figure 1 shows, as well as from unreacted starting material, which represents >99% of the reaction mixture.

$$CH_3(CD_3)_2CF \xrightarrow[\text{electron impact}]{70\ \text{eV}} (CD_3)_2\overset{+}{C}F + CH_3\overset{+}{C}FCD_3 \xrightarrow{\text{Ether}} \text{Deuterated 2-Fluoropropenes} \quad (1)$$

Of major importance in Figure 1 is the absence of any NMR peaks corresponding to $CD_2HCF{=}CDH$ or $CDH_2CF{=}CD_2$, which would have been formed by proton abstraction from $CD_2H\overset{+}{C}FCDH_2$. Therefore we infer that the 2-fluoroisopropyl cation does not rearrange on the millisecond timescale (as does the isopropyl cation).

Figure 1

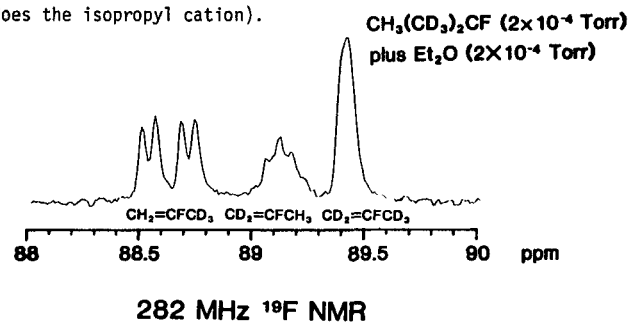

282 MHz ^{19}F NMR

We confirm this inference by studying neutral products from fluoride transfer reactions, as represented by reaction 2. Examination of the proton NMR of the recovered 2,2-difluoropropane exhibits peaks only from $CD_3CF_2CH_3$ (shown relative to $CH_3CF_2CH_3$ in Figure 2).

$$R^+ + R'F \rightarrow R'^+ + RF \quad (2)$$

In this case, the ion-molecule reaction of the parent neutral, t-butyl fluoride-d_6, quenches the cations by fluoride transfer to form t-butyl cations, an ion-molecule reaction that is easily observed by FTMS. We have explored the use of t-butyl fluoride to quench gaseous cations as a method of determining cation structures. We have been especially intrigued by the report of Speranza, Cacace, et al. that gas phase protonation of allene and methylacetylene yields stable 2-propenyl cations that react via bromide abstraction.[3] Bowers et al.

have reported that the same cation is formed by electron impact on 2-bromopropene,[4] as drawn in reaction 3. We have confirmed its structure by quenching the ion as shown in reaction 4. Use of undeuterated t-butyl fluoride to achieve this, however, was not practical, since we find the EBFlow radiolysis of neat t-butyl fluoride yields 2-fluoropropene, the very product we expect from reaction 4. Use of the d_6-compound allows us to circumvent this problem, since all of the 2-fluoropropenes from the deuterated starting material contain deuterium, as shown by the NMR at the top of Figure 3. When equal amounts (2×10^{-4} Torr each) of 2-bromopropene and t-butyl fluoride-d_6 are bombarded with 70 eV electrons, however,

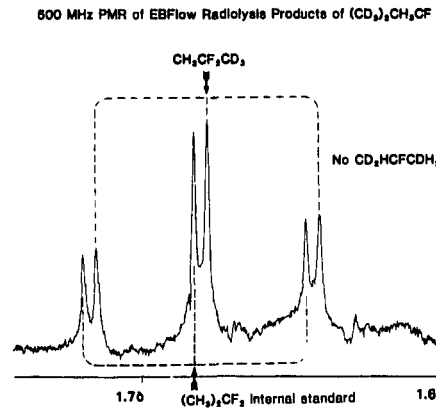

Figure 2

$$CH_3CBr{=}CH_2 \xrightarrow{\text{electron impact}} CH_3\overset{+}{C}{=}CH_2 \not\rightarrow CH_2{=}CHCH_2^{+} \qquad (3)$$

$$CH_3\overset{+}{C}{=}CCH_2 + CH_3(CD_3)_2CF \rightarrow CH_3CF{=}CH_2 \qquad (4)$$

the product mixture exhibits the NMR shown at the bottom of Figure 3. The substantial isotope shift of ^{19}F NMR resonances means that we can identify different isomers and extents of deuteration in neutral products collected from gas phase ion-molecule reactions in the EBFlow reactor.

Acknowledgment. This work was supported by NSF grant CHE 83-06081.

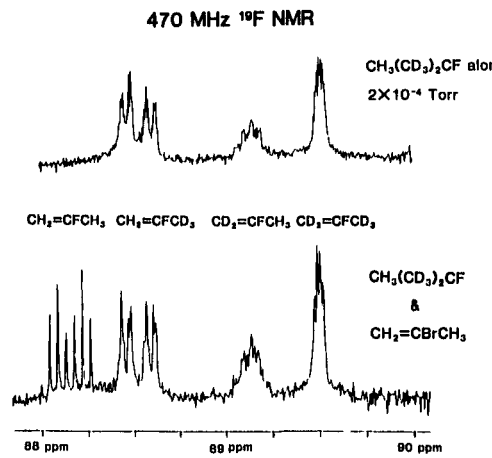

Figure 3

1. D.G. Hall, C.V. Gupta, and T.H. Morton, J. Am. Chem. Soc. 1981, 103, 2416-2417.
2. T.H. Morton, Tetrahedron (Report #137) 1982, 38, 3195-3243.
3. S. Fornari, M. Speranza, M. Attina, F. Cacace, and P. Giacomello, J. Am. Chem. Soc. 1984, 106, 2498-2501.
4. M.T. Bowers, L. Shuying, P. Kemper, R. Stradling, H. Webb, D.H. Aue, J.R. Gilbert, and K.R. Jennings, J. Am. Chem. Soc. 1980, 102, 4830-4832.

TIME-RESOLVED KINETIC ENERGY RELEASES FOR METASTABLE PHENOL IONS

C. Lifshitz, S. Gefen and R. Arakawa*

Department of Physical Chemistry

The Hebrew University of Jerusalem

Jerusalem 91904, Israel

The phenol ion undergoes unimolecular dissociation in the gas phase to $c\text{-}C_5H_6^+$ and CO, a reaction which has been the subject of considerable controversy.[1,2] We have determined for it time-resolved kinetic energy releases (KERs) by employing a new technique, which combines an ion trapping device[3] with MS/MS by time resolved magnetic dispersion.[4] Ionization by electron impact and ion withdrawal are pulsed. Positive ions are trapped for variable delay times in a negative potential well produced by an electron space-charge. Time-resolved detection achieved through a digitizer and transient-recorder is employed in a magnetic sector mass spectrometer (a MAT CH4). Simultaneous momentum and velocity analysis of the ions is achieved and allows the separation, in a single-focussing magnetic instrument, of normal fragment ions from metastable ions having the same nominal mass m*, due to their different flight times. The magnetic field strength is selected and the recorder is triggered by the ion repeller pulse. Ion time-of-flight distributions are accumulated for a pre-selected number of scans and the intensity of the peak maximum is read off. The field strength B is advanced and the whole process is repeated until a complete metastable ion peak shape is obtained for one ion storage time. Time-resolved KERs are obtained by determining the metastable ion peak shapes for several storage times. Since the accelerating potential is held constant there is no problem of variable instrumental discrimination against off-axis ions. Results for phenol are shown in Fig. 1.

The phenol ion data are interpreted by a conical intersection[5] between the $^2B_1$ and $^2A_2$ states of phenol. At higher energies, most of the reactive trajectories prefer to follow a curved path around the apex of the cone. As a result, the minimum fraction of back-activation energy which is deposited into translation decreases with decreasing ion lifetime and with increasing non-fixed energy along the reaction path from about 12% for a most probable rate constant of $k = 4\times10^4\ sec^{-1}$ to about 4% for $k \gtrsim 4\times10^6\ s^{-1}$ (see also reference 6).

---

* Permanent address: Institute of Chemistry, College of General Education, Osaka University, Osaka, Japan

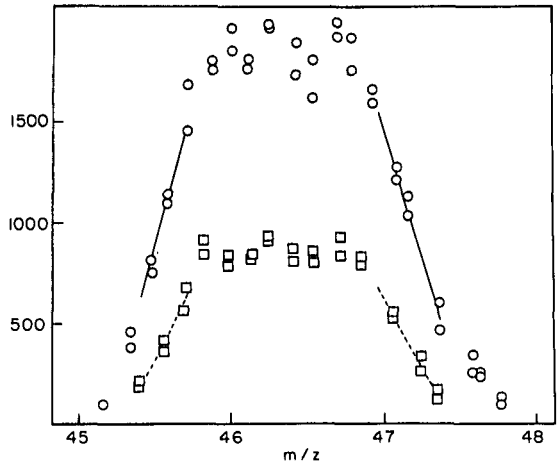

Figure 1. Metastable ion peak shapes for the reaction $C_6H_5OH^+ \rightarrow c\text{-}C_5H_6^+ + CO$ in phenol *at two storage times:* ○ = *10* μs, □ = *20* μs.

1 D.H. Russell, M.L. Gross and N.M.M. Nibbering, J. Am. Chem. Soc. 100, 6133 (1978).

2 A. Maquestiau, R. Flammang, G.L. Glish, J.A. Laramée and R.G. Cooks, Org. Mass Spectrom. 15, 131 (1980).

3 C. Lifshitz, Mass Spectrom. Rev. 1, 309 (1982).

4 J.T. Stults, C.G. Enke and J.F. Holland, Anal. Chem. 55, 1323 (1983).

5 M. Vaz Pires, C. Galloy and J.C. Lorquet, J. Chem. Phys. 69, 3242 (1978).

6 M.L. Fraser-Monteiro, L. Fraser-Monteiro, J. de Wit and T. Baer, "Dissociation Dynamics of Energy Selected Phenol Ions", J. Phys. Chem., in press.

SUPERSONIC BEAM MASS SPECTROMETRY

D. M. Lubman, R. Tembreull and J. Sin

Department of Chemistry
The University of Michigan
Ann Arbor, Michigan 48109

Supersonic beam spectroscopy has the potential of providing great selectivity in analysis. The gas phase UV-Visible spectra of polyaromatic molecules of interest are rather broad and structureless at room temperature thus providing little information for chemical analysis by optical techniques. This broad structure results from thermal population of a wide range of internal states, i.e., rotation and vibrations, of a molecule thus causing congestion in the spectrum. However, using supersonic beam techniques which involve expanding a small amount of the molecule of interest in a large bath of a light carrier gas such as Ar or He into vacuum, one can obtain rapid "cooling" of the molecules by conversion of the energy of the internal degrees of freedom into the translational energy of the carrier gas via two-body collisions. The adiabatic expansion process thus converts a spectrum with either broad features (>100 cm^{-1}) or no discernable structure at all to a spectrum with sharp discrete structure (<6 cm^{-1}). Thus, the unique spectrum of each molecule may serve as an unambiguous means of identification and further as a means of selectivity discriminating one molecule from another in a mixture.

Supersonic beam techniques can be combined with laser multiphoton ionization spectroscopy in order to accomplish sensitive detection and selectivity. In particular, in this work we use (R2PI) resonant two-photon ionization as a means of ionization. R2PI is a two photon ionization process whereby the first photon absorbed pumps a molecule to a real intermediate electronic state of interest, followed by a second photon which excites the molecule above its ionization limit resulting in ionization. The ionization spectrum produced by collecting the ions generated as a function of wavelength reflects the absorption spectrum of the intermediate excited state in resonance with the first photon. The second photon only serves to ionize the molecule. The beauty of this technique is that it provides a wavelength selective ionization source for mass spectrometry. In effect, the sharp, discrete structure obtained in ionization spectroscopy in combination with the use of supersonic beams affords a means of preselecting ions for analysis in a mass spectrometer, thus enhancing the discrimination capability of this device. This technique is analogous to GC:MS where the laser ionization serves as a real-time separation technique by the production of "color" selective ions. The selectivity of this technique can in principle allow for high discrimination even in an inexpensive, low resolution mass spectrometer such as a simple residual gas analyzer device.

In addition to the wavelength selective capability R2PI exhibits many advantages that should be pointed out. In particular, R2PI allows a means of interrogating the spectroscopy of molecules that do not fluoresce due to rapid radiationless processes. However, these "dark" molecules will ionize provided the second photon can ionize the molecule before relaxation from the excited state can occur. This point is of significance because many substituted aromatic molecules with floppy groups such as CH_3, NH_2, etc. have very low or essentially no quantum yield since the added rotations in space open up third channel pathways through which radiationless processes can occur. Fluorescence techniques have been shown to provide very sensitive detection for molecules that do fluoresce; however, they cannot provide ions for mass analysis in a mass spectrometer. Thus, an extra dimensionality is added to spectroscopic analysis where the new axis monitors the mass of the molecule for exact identification.

The use of laser photoionization in mass spectrometry can potentially provide not only a very selective, but also a very sensitive technique for chemical analysis. The R2PI technique provides a very efficient means of soft ionization where typically several percent of the molecules in the laser beam may be ionized. In electron beam ionization typically only $1:10^4$ of the molecules are ionized. The efficiency of the ionization process is further enhanced by the use of the supersonic beam technique, since the number of states populated is now reduced, these states can be more selectively pumped in an electronic transition than in a thermal beam. In addition, R2PI enables one to obtain soft ionization

with high efficiency at modest laser energies. Electron beam ionization can provide soft ionization only with a significant decrease in ionization efficiency. In this study we demonstrate the use of supersonic beams and laser photoionization as a pre-selective technique for producing ions for mass spectrometry. In particular, we have investigated the use of this technique for detecting and discriminating among the isomers of cresol and have examined several disubstituted benzene compounds which have very similar (±4 AMU) molecular weights. These compounds have essentially no quantum yield in fluorescence so that ionization methods are the most appropriate method for their study. A time-of-flight mass spectrometer is used to monitor the product ions of the R2PI process. We demonstrate that using the laser selective technique in combination with a supersonic expansion that a significant discrimination is achieved between the isomers of cresol and that a further enhancement discrimination is obtained between the disubstituted benzenes over using the TOF device alone. In addition, very sensitive detection down to on the order of 20 ppb in air samples is attainable with this technique.

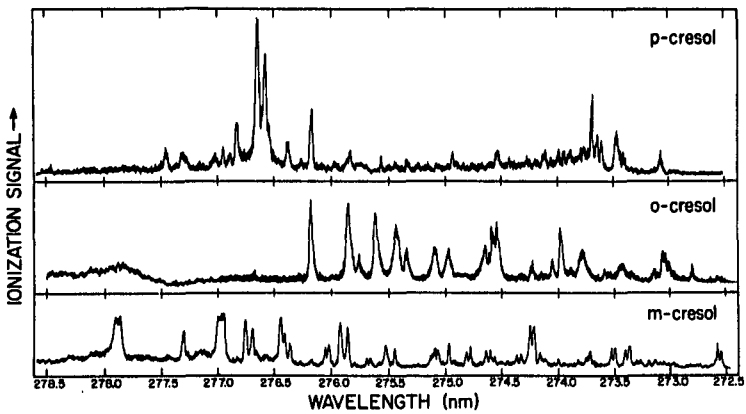

Figure 1. R2PI spectra of the isomers of cresol expanded in a supersonic jet of Ar. The parent peak only was monitored in a TOF mass spectrometer.

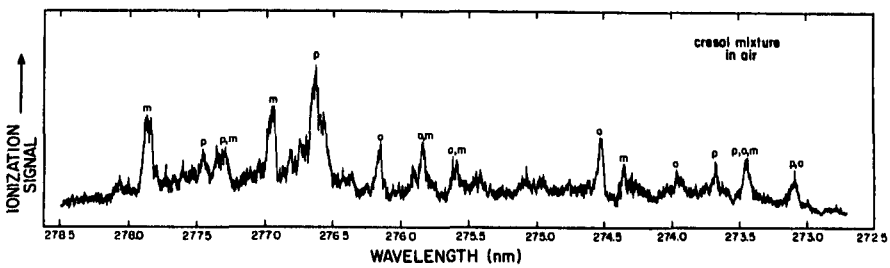

Figure 2. R2PI spectrum of a mixture of cresol isomers in laboratory air at 1 atm. reservoir pressure.

A NEW APPROACH TO ISOTOPIC ABUNDANCE CALCULATIONS:

C. S. HSU, EXXON RESEARCH AND ENGINEERING CO., CLINTON TOWNSHIP ANNANDALE, NJ 08801

Isotopic abundance calculations have been studied by mass spectrometrists for some time. All the approaches appearing in the literature are polynomial approaches. An alternative approach using a Diophantine algorithm for searching all of the possible combinations among the isotopes has been developed to provide simplicity and flexibility of the calculations.

Diophantine equations can be defined generally as a set of algebraic equations with integer coefficients for which integer solutions are desired. The number of solutions in a specific form of a Diophantine equation is varied depending on the values of parameters (other than the variables) in the equation. The Diophantine restraint equation used in the calculations is expressed by

$$\sum_{i=1}^{k} m_i = n, \qquad (1)$$

where n is the number of atoms (occurrences) of one element in a formula, k is the number of isotopes of that element, and m_i is the number of occurrences of the i-th isotope of the element. All of the possible isotopic combinations which satisfy this restraint equation are calculated. For each combination, its fractional abundance is computed by eq 2:

$$\log(F_i) = \sum_{\sigma=1}^{n} \log(\sigma) - \sum_{j=1}^{k} \left[\sum_{i=1}^{m_j} \log(i) \right] + \sum_{j=1}^{k} \left[m_j \cdot \log(f_j) \right] \qquad (2)$$

The fractional abundances among the combinations with the same nominal mass are summed, this yields a mass spectrum of the element. For a molecule or a fragment, the isotopes of all of the elements are convoluted to obtain the fractional abundance of each nominal mass.

The program is written in FORTRAN V and is designed to handle all the elements from hydrogen to uranium with naturally-occurring isotopes. The only input needed is the chemical formula for either a molecule or a fragment. With the Diophantine approach, it is free of limitations in the number of elements, mass numbers, and number of occurrences of each element in the chemical formula being calculated.

The original uses of the isotopic abundance calculations were for organometallics and coordination compounds which contain multiple polyisotopic transition-metal elements. With the improvements in mass spectrometric instrumentation, complex isotopic patterns for ions of organic molecules greater than 1000 amu can also be detected. To reduce computation time and error, the following equations are used for calculating fractional abundances of heavy isotopic clusters:

For the first combination, F_1, of each element,

$$\log(F_1) = n \log(f_1) \qquad (3)$$

where F_1 is the fractional abundance of the lightest isotope.

Fractional abundances for the remaining combinations of the same element can be calculated by a recursive equation,

$$F_{i+1} = F_i \left(\prod_{j=1}^{k} \rho_j \right) \tag{4}$$

where $\rho_j = \dfrac{(m_j)!(f_j')^{m_j'}}{(f_j)^{m_j}(m_j')!}$ and $f_j = f_j'$ for each isotope.

The values of ρ_j where $j = 1,2,\ldots,k$, can be obtained by one of the following equations:

$$\log \rho_j = \sum_{\sigma=m_j'+1}^{m_j} \log(\sigma) - (m_j - m_j') \log(f_j) \qquad \text{if } m_j > m_j'$$

$$\log \rho_j = 0 \qquad \text{if } m_j = m_j'$$

$$\log \rho_j = (m_j' - m_j) \log(f_j) - \sum_{\sigma=m_j+1}^{m_j'} \log(\sigma) \qquad \text{if } m_j < m_j'$$

Further extensions of this computer program can be used for the deconvolution of overlapped isotopic clusters, the analysis of isotopic labeling and the calculations of isotopic distributions in mass spectrometry/mass spectrometry (MS/MS) spectra.

RECENT APPLICATIONS OF INDUCTIVELY COUPLED PLASMA MASS SPECTROMETRY (ICP-MS) TO ELEMENTAL AND ISOTOPIC ANALYSIS, D.J. Douglas, A. Boorn and E.S.K. Quan, SCIEX®, 55 Glen Cameron Road, #202, Thornhill, Ontario, Canada, L3T 1P2.

In ICP-MS instruments, solutions are sprayed into a hot (7000°K) atmospheric pressure argon plasma where the dissolved solids are vapourized and ionized. A small fraction of these ions is sampled through a differentially pumped interface for elemental and isotopic analysis by quadrupole mass spectrometry.

Since the first introduction of a commercial ICP-MS system in early 1983 by SCIEX®, the basic performance features have been refined. Sensitivity is now 10^4 to 10^5 counts s^{-1} per ug ml^{-1} with a background noise of 20 counts s^{-1} through the mass range. Correspondingly detection limits are 0.1 to 1 ng ml^{-1} for a large fraction of the periodic table. In special cases, with an ultrasonic nebuliser or by simply increasing the aerosol flowrate to the plasma with a conventional nebuliser, detection limits as low as 1 pg ml^{-1} can be obtained, although the increased aerosol loading can lead to matrix effects. The abundance sensitivity of the instrument was initially reported to be $1:10^5$ on the low mass side of a peak and $1:10^7$ on the high mass side, measured at mass 88. This has now been achieved at higher mass. Tailing of the 208 peak from Pb to lower mass is $1:10^4$ between peaks and less than $1:10^5$ at mass 207. Oxides of refractory elements can also be reduced to comparatively low levels even for very refractory elements. Figure 1 shows the spectrum of a 1 ug ml^{-1} La solution. LaO at mass 155 is <5% of La at mass 139. Doubly charged ions remain present at lows levels (Ba^{+2}/Ba<2%) over the power range 1.0 to 1.6kw.

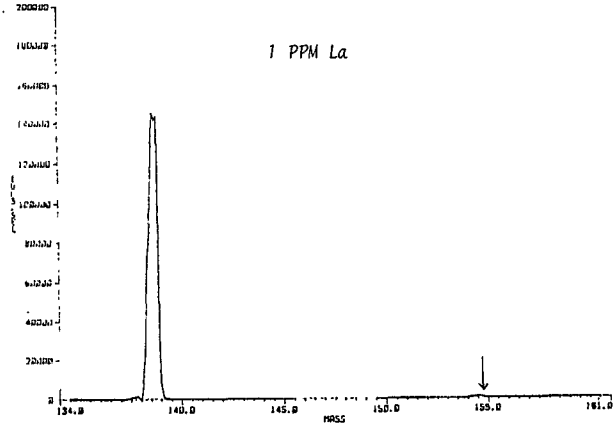

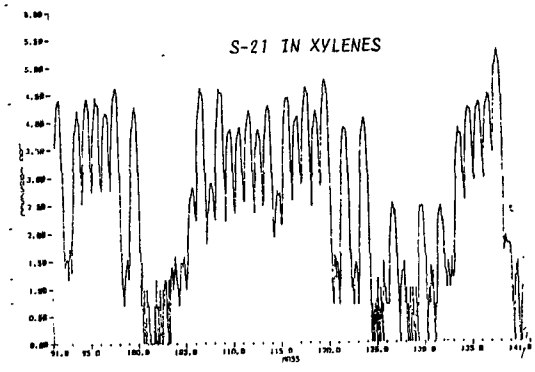

All previous development of ICP-MS has been directed to the analysis of aqueous solution. The analysis of organic solvents by ICP-MS has proved more difficult. In first attempts to use xylene as a solvent at SCIEX®, it was found that the sampling orifice (.027" diameter) was rapidly plugged with a carbon deposit. This has now been overcome by mixing a small flow (2 L min^{-1}) of oxygen in the plasma to burn off the excess carbon. Under these conditions no soot deposits on the sampler, and mass spectra of oils may be obtained. Figure 2 shows on a log scale, a preliminary spectra of Zr, Mo, Ag, Cd, Sn and Ba in a 10 ug gm solution of trace metals in xylene (Conostan standard S-21 diluted). The sensitivity is ca X10 less than with aqueous solutions but this result was obtained under unoptimized conditions.

In parallel with these improvements in the technique, a wide range of application studies have been carried out, including the determination of trace metals in water, impurities in boron indium and lead, analysis of battery acids and determination of elements by isotope dilution. One result is shown in Table 1 which documents the determination of trace metals in EPA standard water. Under software control the count rate for each element was determined with a 1 second measurement time. This was repeated 5 times and the results averaged. Concentration calibration files were then used to determine elemental concentrations from the background subtracted count rates. The total measurement time was 3 minutes for this sample. Agreement with accepted values is fair to good.

Isotope ratios of elements in solution can be determined with moderate precision and accuracy and high sample throughput. Table 2 shows the determination of Pt isotope ratios of a sample spiked with ^{198}Pt. Each peak was measured with a dwell time of 1 second and 30 repeats. The average and standard deviation (σ) of 4 such runs are shown. (Total measurement time 10 minutes.) RSD's of 0.4 to 1.0% are evident. These could be reduced with longer signal averaging times or by measuring only the 198/195 ratio to increase the duty cycle on the two peaks of interest.

EPA No. 1 (WP475) ANALYSIS

ELEMENTS	ICP / MS$^{\sigma}$ (ppb)	ICP / AES' (ppb)	TRUE VALUES (ppb)
Pb	75 ± 6	79	80 ± 4
Cr	62 ± 6	64	59 ± 3
V	197 ± 15	202	199 ± 13
Mn	56 ± 5	56	55 ± 3
Fe	47 ± 13	55	52 ± 4
Ni	71 ± 12	75	69 ± 4
Co	67 ± 9	71	70 ± 2
Cu	33 ± 5	45	40 ± 2
Zn	58 ± 4	62	60 ± 3
Cd	12 ± 4	11	9 ± 1
As	40 ± 6	—	39 ± 3
Se	16 ± 3	—	19 ± 2

TABLE 2

RATIO	192/195	194/195	196/195	198/195
x	0.0235	0.971	0.844	4.328
σ	0.0001	0.0073	0.0048	0.040
RSD	0.43%	0.75%	0.57%	0.91%

ON-LINE CHIRAL LC/MS FOR THE IDENTIFICATION OF DL ENANTIOMER PAIRS, Jack Henion, Jonathan Crowther and Thomas Covey, Equine Drug Testing and Toxicology, Cornell University, 925 Warren Drive, Ithaca, NY 14850

Stereoselectivity is an important phenominon in biological systems. In most cases optical enantiomers exhibit different biological activities due to differences in strength of interaction with corresponding receptors, different transport mechanisms and metabolism along different pathways. Drugs which are characterized by these biological differences include ephedrine, epinephrin, phenylephrine and others. For example, it is the d-enantiomer of penicillamine that is used in cases of cystinuria and mercury poisoning but the l-enantiomer is toxic. Popular nonsteroidal anti-inflammatory agents such as ibuprofen and naproxen show significant differences in potency and metabolism between their stereoisomeric forms. These and many other examples of enantiomeric preference make it important to be able to distinguish and identify optical isomers.

The classical method of measuring the specific rotation of a solution of one enantiomer of the racemic mixture is not appropriate for modern drug metabolism studies. Typically the level of isolated drug metabolite is far too low and exists in the presence of high levels of interfering components. Thus sensitive detection methods and highly efficient chromatographic capability are needed to deal with such analytical problems. Recent advances in the resolution of stereoisomers by HPLC on chiral stationary phases (HPLC-CSPs) have provided capabilities for analysis of enantiomeric compounds using conventional chromatographic technique (1). In particular, application of HPLC-CSPs to pharmaceutical analysis of amide derivatives of 1-phenyl-2-aminopropane has shown impressive success.

The simplist mode of distinguishing enantiomers would be the direct determination of the underivatized compounds by a chromatographic process coupled to a specific detector. Wainer and Doyle have stressed the value of preparing suitable enantiomeric derivatives from achiral reagents (2). The latter form simple amide derivatives, for example, which precludes enantiomeric contamination, differing reaction rates and/or equilibrium constants, and unsatisfactory chromatographic performance. The commercial availability of chiral columns and facile amide forming derivatization techniques make HPLC-CSP a convenient method of resolving and distinguishing biologically important enantiomers. Unfortunately, simply comparing HPLC retention times of resolved standards and unknown enantiomer derivatives does not provide unequivocal identification. A detection system with much more specificity than an UV or fluorescence detector is required to distinguish enantiomeric derivatives from unknown interfering components. This need is particularly important in "real world" biological samples such as plasma and urine extracts.

We have applied combined high performance liquid chromatography/mass spectrometry (LC/MS) with the need to distinguish in certain cases between the enantiomers of administered drugs in race horses. The direct liquid introduction (DLI) technique of LC/MS is readily amenable to HPLCCSP analyses as reported by Pirkle and Wainer. This paper reports our results of on-line LC/MS using a chiral stationary phase (HPLC-CSP/MS) on a series of enaniomeric carboxylic acids and, in particular, the detection and identification of (S)-(+)-ibuprofen in equine urine after administration of dl-ibuprofen.

Experimental

Materials. HPLC grade hexane and isopropyl alcohol were purchased from Burdick and Jackson (Muskegin, MI). Thionyl chloride and benzylamine were purchased from Aldrich Chemical Co. (Milwaukee, WI) and used without further purification. Ibuprofen was administered orally.

HPLC Apparatus and Conditions

The HPLC equipment consisted of two Waters M-6000A pumps and a M-660 solvent programmer (Waters Assoc, Milford, MA). The injector was a Rheodyne Model 7520 micro loop injector with a five microliter loop (Rheodyne, Cotati, CA). The CSP columns were Pirkle type-covalent bound (R)N - (3,5 - dinitrobenzoyl) phenylglycine Pirkle type 1A chiral stationary phase purchased from Regis Chemical Co. and J.T. Baker Chemical Co. The CSP columns were both stainless steel 4.6 mm x 25 cm which were connected to a Waters Model 440 UV detector equipped with a standard flow cell and operated at 254 mm. The eluent was 97/3 hexane/isopropanol maintained at an isocratic flow rate of 2.0 mL/min. All experiments were conducted with the CSP column at ambient temperature. The UV chromatographic trace was recorded on a Fischer Recordall recorder operated at 10 mV and a chart speed of 30 cm/hr.

Mass spectrometer

A Hewlett Packard 5985B GC/MS equipped with a liquid nitrogen cryopump and the Hewlett Packard split effluent DLI LC/MS interface was used in this work. The exit of the UV detector was connected to the DLI LC/MS interface via a Valco 0.5 micron in-line filter

union (Valco Instrument Co., Houston, TX). At the operating HPLC eluent flow rate of 2.0 mL/min the fine metering valve on the LC/MS interface was adjusted to provide about 40 microliters/min effluent introduction into the MS. This amounts to about two percent of the total LC effluent introduction into the MS and of course results in reduced overall LC/MS sensitivity.

Results and Discussion

After optimizing chromatographic conditions for authentic dl ibuprofen benzylamide, the exit of the UV detector was connected to the DLI split effluent LC/MS interface. On-line DLI LC/MS analysis of the standard provided a PCI total ion current profile from one microgram levels with baseline separation of the enantiomers within six minutes of injection. A two hour post ibuprofen administration equine urine extract was obtained and the TLC spot observed at the Rf region of authentic ibuprofen preparatively scraped and eluted. The residue from this TLC scrape was converted to the benzyl amide according to Wainer's procedure and analyzed by chiral DLI LC/MS. By carefully timing sample injection with MS acquisition the retention time for each enantiomer could be reproduced between runs and the PCI chiral LC/MS mass spectrum of each enantiomer obtained. Analysis of the TLC scrape by chiral DLI LC/MS clearly showed that the TLC scrape of equine urine extract contained the (S) - (+) enantiomer of ibuprofen. This corroborates the finding of Brooks (3) in human urine.

The preparative TLC step may be bypassed and the above procedures utilized with the crude two hour equine extract. Chiral DLI LC/MS of this extract produced a complex TIC, but an extracted ion current profile for m/z 296 $(M+1)^+$ clearly indicated which chromatographic peak was the (S) - (+) ibuprofen benzylamide enantiomer, Figure 1. The mass spectrum of the small, resolved chromatographic peak at the 49 minute retention time of the (R) - (-) - enantiomer precluded the presence of the latter by its abundant m/z 294 and different fragmentation pattern. This example demonstrates the practical and analytical utility of chiral LC/MS. Recent chiral micro LC/MS results offer the possibility of increased sensitivity and these results will be reported subsequently.

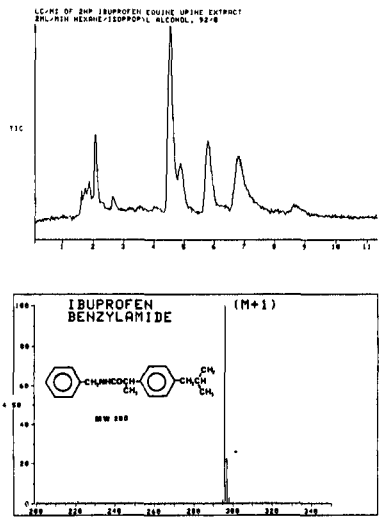

Figure 1

References

1. W.H. Pirkle, D.W. House and J.M. Finn, J. Chromatogr., 1980, 192, 143.
2. I.W. Wainer and T.D. Doyle, LC, 1984, 2, 88.
3. C.J.W. Brooks and M.T. Gilbert, J. Chromatogr., 1974, 99, 541.

EXPERIMENTAL EVIDENCE FOR STABLE CCl_4^{2+} IONS

D.Stahl,C.Guenat and F.Maquin,Institut de Chimie-Physique,Ecole Polytechnique Federale de Lausanne,1015 LAUSANNE,Switzerland
H.Schwarz and W.Koch,Institut fur Organische Chemie,Technische Universitat Berlin,Strasse des 17.Juni,D-1000 BERLIN,West-Germany.

Two techniques are efficient for studying doubly charged ions:2E mass spectrometry based on electron transfer reaction $m^{2+} + N \rightarrow m^{+} + N^{+}$ for dications formed in the ion source and charge stripping mass spectrometry $m^{+} + N \rightarrow m^{2+} + N + e$ which allows measurement of the energetics of formation of the doubly charged species.These two methods are unapplicable for carbon tetrachloride because of the gas phase unstability of $CCl_4^{+\cdot}$ .The source spectrum (ZAB-2F instrument,90 eV electrons , 200 C source tmeperature ,8 kV accelerating voltage) shows very weak signals in the mass range 76-80 (m/z of hypothetical CCl_4^{2+} dications). Their low intensities ,which do not correspond to a 4 chlorine isotopic cluster,do not permit increase of the resolution and exact mass measurement.In order to determine the nature of these ions we performed 0-2E MIKE and CAD/MIKE experiments.Fig.1 shows the section of interest of ions at m/z 76 (0.840E - 1.143E).Two dished peaks centered around 0.921E and 1.079E,

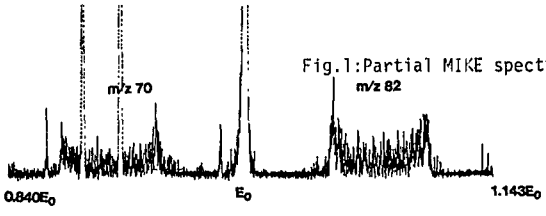

Fig.1:Partial MIKE spectrum of m/z 76

respectively,give the first insight that ions at m/z 76 are partly CCl_4^{2+} dications;they correspond to the fragments of the reaction $C^{35}Cl_4^{2+} \rightarrow C^{35}Cl_2^{+} + {}^{35}Cl_2^{+}$. Mass selection of ions with m/z 77 leads to a MIKE spectrum with composite dished peaks corresponding to the 2 alternative fragmentations of $C^{35}Cl_3{}^{37}Cl^{2+}$ ions into $C^{35}Cl_2^{+} + {}^{35}Cl^{37}Cl^{+}$ and $C^{35}Cl^{37}Cl^{+} + {}^{35}Cl_2^{+}$. Fig.2 represents the CAD/MIKE spectrum (0.82E - 1.62E) obtained with He as the collision gas.The presence of CCl_4^{2+}ions at m/z 76 is confirmed by the observation of an other fragmentation reaction $C^{35}Cl_4^{2+} \rightarrow C^{35}Cl_3^{+} + {}^{35}Cl^{+}$.

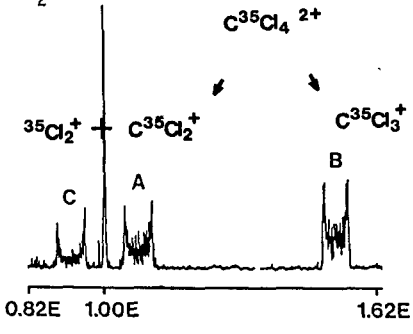

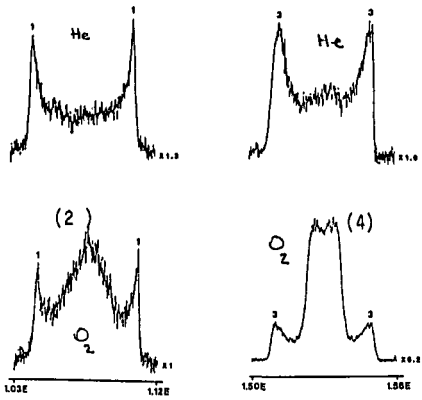

Fig.3 : collision gas O_2

As shown on Fig.3 for m/z 76 , the use of O_2 as the collision gas leads to the observation of two additional decomposition channels:

(2) $CCl_4^{2+} + O_2 \rightarrow CCl_2^{+} + Cl_2 + O_2^{+}$

(4) $CCl_4^{2+} + O_2 \rightarrow CCl_3^{+} + Cl + O_2^{+}$

To support these experimental finfindings ,we performed ab initio calculations on CCl_4 dications and possible decomposition products.Due to the complexity of this system , it was not possible to include polarisation functions and electron correlation energy in the calculations.

Table 1 presents the energies , geometries and relative energies for dissociation processes obtained at the 4-31G level.

Structure	Energy hartrees	E_{rel} Kcal.mol^{-1}	Bond length Å	Angle degrees
CCl_4^{2+} (C_{2v})	-1872.6479	0	Cl(1)-C: 1.64 Cl(2)-C: 2.32 Cl(2)-Cl(2):2.24	Cl(1)-C-Cl(1) 135.9 Cl(2)-C-Cl(2) 57.7
CCl_4^{2+} (D_{4h})	-1872.5143	83.9	Cl-C : 2.02	Cl-C-Cl : 90
CCl_2^{2+} (D_h)	- 954.6896		Cl-C : 1.548	
CCl_3^{2+} (C_{2v}) Cl	-1413.7047 - 458.9715	-17.8		
CCl_3^{+} (D_{3h}) Cl^{+} t	-1414.3593 - 458.4455	-158.6		
CCl_2^{+} (C_{2v}) Cl_2^{+}	- 955.3169 - 917.4994	-105.9		

It is seen that the most stable CCl_4^{2+} dication has the C_{2v} geomerty.

Conclusion : This work illustrates a very seldom situation where the doubly charged ion is shown to be stable in the gas phase while the corresponding monocation is not.Ab initio calculations support this experimental finding.

PARALLEL MASS SPECTROMETRY

C. Chang
Brehm Laboratory and Department of Chemistry
Wright State University, Dayton, Ohio 45435

A parallel mass spectrometer (PMS) is defined as a mass spectrometer equipped with two or more sets of ion resolution devices and detectors connected in parallel. It allows two identical or different ion beams of the sample to be extracted and mass resolved simultaneously and separately for analysis. The concept of PMS was first applied[1] in a magnetic sector instrument for obtaining positive ion electron impact (PIEI) and negative ion electron impact (NIEI) spectra simultaneously. One other known example[2] is the addition of a RF-only quadrupole to a magnetic MS for obtaining real time total ion current (TIC) chromatogram during a normal GC-MS operation.

With the advancement of mass spectrometry, several new types of PMS operations[3] can be added such as simultaneous CI/EI (SCE), simultaneous positive ion and negative ion CI (SPINICI), and simultaneous positive ion EI and negative ion CI. Compared with conventional MS operations such as alternate CI/EI (ACE) and alternate positive ion and negative ion CI (PPINICI), these newer techniques are more suitable for interfaced GC operation. This is especially true for the case of high performance capillary column GC in which the preservation of the GC resolution is often a main concern.

Described in the following is another new technique termed "real time TIC (or SIM) - synchronized mass spectrum" operation[3] with a GC-PMS system. In one version of such operation the first ion beam is continuously monitored under TIC or SIM mode in real time. Once the on-set of a GC peak is sensed, a full mass scan is activated on the second beam in synchronization. An example of this operation is illustrated by Fig. 1 which employs a combined quadrupole magnetic sector mass spectrometer. Discussed below are several highlights of this novel operation:

1. Quantitative Analysis: It is well known that real time SIM operation provides higher sensitivity than that with a re-constructed SIM chromatogram resulted from repetitive mass scan GC-MS operation. However, the fact that the real time TIC operation with a RF only quadrupole could deliver sensitivity two to three orders of magnitude higher than that of a computer re-constructed or electrically integrated TIC based on repetitive mass scan operation has not been widely appreciated. With a RF-only quadrupole all sample ions above an adjustable mass threshold are detected simultaneously and continuously without high-mass-ion discrimination. The results: the GC resolution fidelity is retained; excellent sample detection sensitivity is achieved; low mass background and interference ions are eliminated; and detection of high mass ions is facilitated.

2. Qualitative Analysis: In principle each GC peak is only needed to be covered by one mass scan for the purpose of GC peak identification. This greatly eases the incompatibility problem which previously occurred when a quadrupole or magnetic sector MS is interfaced with an advanced capillary GC column yielding GC peaks as narrow as a few seconds or less. Compared with the conventional repetitive mass scan operation, the requirement on the mass scan speed is much relaxed in the present operation. The duration of each mass scan can often be increased which would allow more ions to be collected for each mass for achieving better spectrum quality. The distortion in the obtained mass spectrum caused by the change of the source sample pressure can be easily corrected based on the TIC or SIM peak profile which closely follows this change.

3. Screening: The first ion beam can be screened such that only the GC peaks of interest are mass scanned and analyzed. The possible screening methods may include ion types by SIM, GC peak intensity by adjusting the peak sensing threshold, cut-off ion mass by adjusting the RF voltage for a RF-only quadrupole, and exact ion mass using a high resolution magnetic sector. With the use of computer more screening criteria (such as isotop ratio, etc.) can be included. Full flexibility ranged from all-GC-peak survey down to single target compound analysis is achievable with ease.

4. Computer: Because of the items 2 and 3 the waste on unnecessary data acquisition, storage and processing is minimized. Consequently, the required load in both the memory storage and data processing can be substantially reduced. This may facilitate the real time library search, GC peak quantitation, and final report preparation, etc.

5. Versatility: At least in principle the first and second ion beams are independent of each other, and can be of either identical or different (PIEI, PICI, NICI, etc.) origins. These, as well as the operations of those two beams can be judiciously selected in order to achieve the best result for sample qualitative and quantitative analysis.

6. Other Application: The principle of the present technique is also applicable for on-line LC-PMS operation. The introduction of high speed LC with narrow peak width and the needs for wide mass scan range for large molecules will also make the present technique very appealing.

In this presentation, the general concept of PMS will be further discussed, while in the companion paper (WPB8) the construction of a novel mass spectrometer capable of switching between the PMS and tandem MS operations will be described.

REFERENCES:

1. H. J. Svec and G. O. Flesch, Int. J. Mass Spect. Ion Phys. 1, 41, (1968).

2. D. Henneberg, U. Henrichs and G. Schomburg, J. Chroma. 112, 343, (1975).

3. C. Chang, U.S. Patents (4,266,127 and 4,377,745) and patent pending.

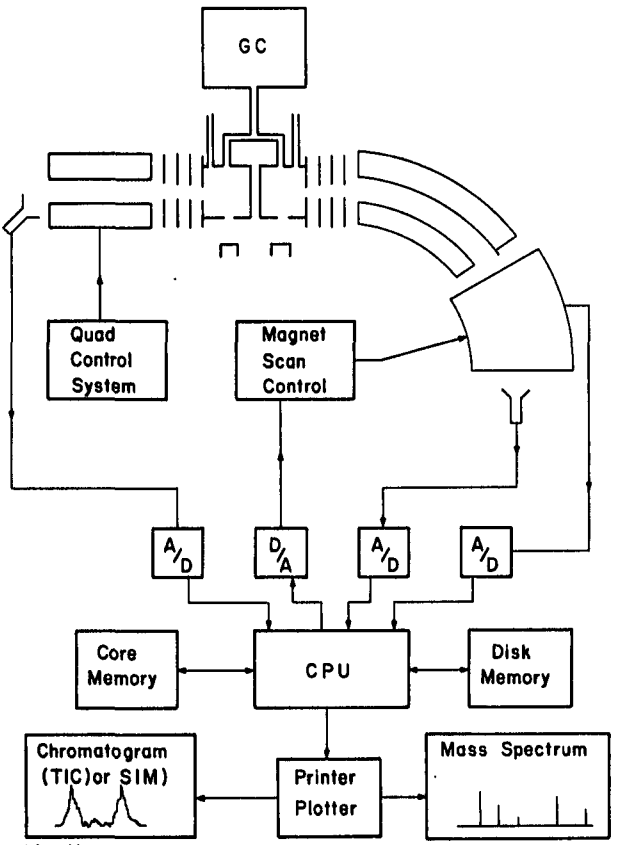

Fig. 1 Schematic diagram of a GC-PMS system for the "real-time TIC (or SIM) - synchronized mass spectrum" operation.

ULTRAPRECISE MASS SPECTROMETRIC ANALYSIS OF GAS MIXTURES DOWN TO THE TRACE IMPURITIES CONCENTRATION LEVEL

G. Wagner, B. Laser, C. Brunnée, Finnigan MAT GmbH,
Barkhausenstr. 2, 2800 Bremen, W. Germany

For fast, accurate and cost effective gas analysis, covering the complete range of elemental and molecular gases over wide ranges of their concentrations, a mass spectrometer system must provide

- extreme stability of mass spectral patterns and sensitivities,
- linearity of spectral signal with the sample's pressure and components partial pressure,
- fast resolution adjustment for mass multiplet separation, with flat top peaks up to a resolution of $m/\Delta m = 1500$,
- reproduction of spectral patterns and sensitivities after resolution changes to better than 0.1 %, to use resolution specific calibration libraries without any recalibration,
- very low peak tail contributions to adjacent mass peaks, even within mass multiplets,
- safe peak detection and very linear digitization over a wide dynamic range of ion signal intensities,
- safe mass calibration, accurate to a few millimass units, for multiplet resolved data acquisition with unambiguous mass peak identification,
- a low and very stable background, even with fast changing sample characteristics.

The mass spectrometer hardware of the Finnigan MAT model 271/45 system does provide these features at a high level of quality and reliability. A differentially turbomolecular-pumped, stigmatic focusing magnetic analyzer with 46 cm effective radius, an electron impact ion source thermostated to 0.1 °C and operated at 10 kV ion accelerating voltage, and an IEEE BUS oriented electronics accessible to direct computer interaction support these features.

Therefore, the acquired mass spectral data are of very high analytical quality. For their evaluation, the function key operated HP 9845 B data system employs data reduction procedures including

- the subtraction of an automatically updated spectral background,
- the compensation of fragment contributions at resolutions insufficient for multiplet resolution,
- the consideration of sample fractionation by molecular flow from a batch inlet system,
- the automated determination of leak rate and sensitivity calibrations,
- the automated selection of calibration data according to the system's actual spectral resolution,
- the direct determination of mole fraction results, and
- the automated closure of accumulated partial pressures versus total sample pressure read by the membrane type manometer attached to the batch inlet system.

As an example, a "pure" argon, specified to 99.995 % argon content, was analyzed. For quantitative evaluation down to the 0.3 ppm concentration level, the ^{36}Ar isotope (0.3 % natural abundance) was used to represent the matrix, spanning the 10^5:1 range of peak dynamics from 0.3 % ^{36}Ar to 0.3 ppm traces. With 99.94 % argon this sample contained a factor of 10 more trace impurities than specified. Air (228 ppm) and hydrogen (256 ppm) amount to about 0.05 Mol %, plus some lower traces of methane, water and ethylene.

E X P E R I M E N T L I S T I N G
25-MAY-83 15:41

Experiment No.: 9
Title: Argon (36Ar)
Channel: FARIV
Resolution: 1400
High Voltage: 10kV
Recorder Range: 10000mV

Line	Masses	Step	Window	(Samples/Peak)
1	2		H2	(20)
2	16		C H4	(20)
3	18		H2 O	(20)
4	28		H2 - C2 H4	(20)
5	32		O2	(20)
6	36		36Ar	(20)
7	44		C O2	(20)

Fig. 1: Experiment set for data acquisition of trace impurities in argon.

S E N S I T I V I T Y - & L E A K R A T E - T A B L E of FARIV
25-MAY-83 15:41

No.	Species	Mass[m/e]	Purity[%]	Sens.[V/Torr]	Leakr.[l/sec]	Molep.[%]
1	H2	2.015650	99.600	173.0248	1.703E-04	100.000
2	C H4	16.031300	99.995	267.5715	7.387E-05	100.000
3	H2 O	18.010565	100.000	298.8630	5.551E-05	100.000
4	N2	28.006148	100.000	373.5787	5.551E-05	100.000
5	C2 H4	28.031300	99.950	363.0863	5.131E-05	100.000
6	O2	31.989830	99.971	317.1260	5.042E-05	100.000
7	36Ar	35.976548	99.996	1.4900	4.204E-05	100.000
8	Ar	39.962384	99.996	540.1367	4.597E-05	100.000
9	C O2	43.989830	100.000	459.3631	4.054E-05	100.000

Fig. 2: Sensitivity and leak rate calibration for trace impurities in argon.
^{36}Ar isotope set to represent argon matrix.

Peak#	Mass	Backgr. (mV)	Gross Peak (mV)	Corr Peak (mV)	Correction (mV)	Net Peak[101] (mV)	Sens. [V/Torr]
1	2 H2	5.69	40.27	34.59	A=0.00E+00 B=0.00E+00 J=0.00E+00	34.94	173.02
2	16	0.00	0.50	0.50		0.50	267.57
3	18 H2O	7.00	12.83	5.83	E=0.00E+00	5.97	298.86
4	28 N2	1.21	49.94	48.72	H=1.97E+00	48.12	373.58
5	28	0.00	0.93	0.93		0.94	363.09
6	32 O2	0.00	15.61	15.61		15.89	317.13
7	36	0.00	1147.95	1147.95		1168.00	1.49
8	44 CO2	0.69	13.77	13.08		13.33	459.36

Peak#	Mass	Part Pres. [m Torr]	Mole Fraction [%]
1	2 H2	0.201	0.025630
2	16	0.002	0.000239
3	18 H2O	0.020	0.002547
4	28 N2	0.129	0.016422
5	28	0.003	0.000331
6	32 O2	0.050	0.006367
7	36	783.883	99.944745
8	44 CO2	0.029	0.003780
	Total:	784.317	100.000000

Total Hr 0.026 %

Closure: 0.053 %

Fig. 3: Data evaluation for analysis of trace impurities in argon.

EFFECT OF ELECTRON CAPTURE AGENTS IN CHEMICAL IONIZATION MASS SPECTROMETRY

Patrick Rudewicz and Burnaby Munson
Department of Chemistry, University of Delaware, Newark, DE 19716

During some of our work with ammonia as a reagent gas in GC/CIMS experiments (1), it was observed that when certain compounds with large electron capture cross sections passed through the source of the mass spectrometer, the relative abundances of the more highly solvated reactant ions increased. The total ion current also increased when these electron capture agents passed through the source. In additional experiments with constant amounts of polar samples introduced from the probe or oven, an increase in the sample ion current, $(M+NH_4)^+$, was noted as these electron capture species were eluted from the gas chromatograph. Fig. 1 shows the effects of certain compounds on the ion currents (and therefore, the relative distributions) of the reactant ions at a pressure of 0.5 torr NH_3 at 100°C. When CCl_4, iodobenzene, and nitrobenzene pass through the source of the mass spectrometer, one sees significant decreases in the ion current of NH_4^+ and significant increases in the ion currents of the solvated ions, $NH_4(NH_3)^+$ and $NH_4(NH_3)_2^+$. No effects are observed when equal amounts of toluene and bromobenzene enter the source. No $(M+H)^+$, $(M+NH_4)^+$, or any other sample-containing ions are observed for these compounds, except for nitrobenzene, which gives $(M+NH_4)^+$ at m/z = 141. The change in pressure as the samples pass through the source of the mass spectrometer is less than 0.005 torr at a total pressure of 0.500 torr. The electron capture coefficients (relative to chlorobenzene = 1) for carbon tetrachloride, iodobenzene, and nitrobenzene are 7000, 370, and 390, and for bromobenzene and toluene, 6 and 0.003.

We attribute these changes in the distributions of the reactant ions to changes in the ionic residence times as these electron capture agents elute through the mass spectrometer. Under the conditions of high pressure and high electron current in CIMS, the positive ions and the negative particles are not independent of each other. At high concentrations of charged species, the positive ions and the negative particles diffuse together at the ambipolar diffision rate which is the composition average of the ordinary or "free" diffusion rates of all of the charged species (2). When the electron capture compounds enter the source of the mass spectrometer, the rapidly moving electrons are converted into much more slowly moving negative ions. Consequently, the ambipolar diffusion rate decreases, and there is an increase in the residence time of ions within the source of the mass spectrometer. This increase in ionic residence time causes an increase in the extent of conversion of the ammonium ions to the more highly solvated species and also an increase in the extent of conversion of reactant ions to sample ions. If the major loss process for positive ions is ambipolar diffusion to the source walls, then a decrease in this diffusion could account for the observed increase in total ion current.

An alternative mechanism may be proposed if ion/ion or ion/electron recombination, rather than lateral diffusion, is the major ionic loss process. If the neutralization rate constants for positive ions with negative ions are significantly smaller than those for positive ions with thermal electrons, replacing electrons by negative ions from the electron capture reagents will decrease the loss of positive ions and increase the total ion current. In addition, if the rate constants for neutralization of the solvated ammonium ions are larger than the rate constant for neutralization of NH_4^+, then this reduction in the loss of positive ions will give a larger increase in the ion current for the solvated species than for NH_4^+, but will not cause a decrease in ion current for NH_4^+. The interpretation of these observations is not clearcut and additional experiments are underway in our laboratory to investigate the mechanism of this electron capture effect in more detail.

The analytical utility of this phenomenon is illustrated in Figure 2. Two sets of experiments were done: one with a small amount of CCl_4 in the source of the mass spectrometer at 0.5 torr NH_3 and 155°C and the other, without this electron capture agent. Different amounts of testosterone, 17β-hydroxy-4-androsten-3-one, were completely vaporized from a probe into the mass spectrometer. The total sample ion current of the $(M+NH_4)^+$ ion was measured for each experiment. As indicated in Fig. 2, the integrated area for the adduct ion is greater by at least a factor of 2 when CCl_4 was present in the source than for pure NH_3. Similar experiments have been reported recently which show an even larger enhancement of sensitivity for other electron capture reagents (3).

Preliminary experiments indicate that this enhancement by electron capture reagents is general, since we observed increases in sample ion current upon the addition of electron capture reagents to CH_4, CH_4/NH_3, and i-C_4H_{10} as CI reagent gases.

Literature Cited

(1) Feng, T.; Rudewicz, P.; Munson, B. Presented at the 30th Annual Conference on Mass Spectrometry and Allied Topics, Honolulu, HI, June 6-11, 1982.

(2) Seigel, M.W. In "Mass Spectrometry, Part B"; Merritt, C., McEwen, C.N., Eds.; Marcel Deker, Inc.: New York, 1980; Chapter 4.

(3) Foltz, R.L. Presented at the 31st Annual Conference on Mass Spectrometry and Allied Topics, Boston, MA, May 8-13, 1983.

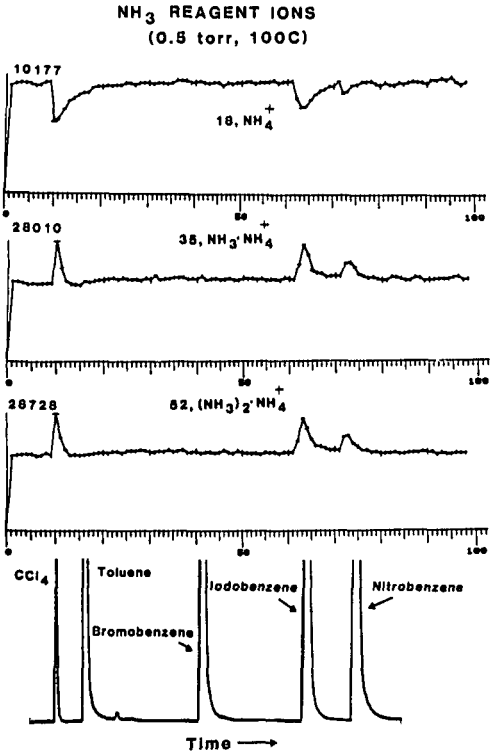

Figure 1. Effect of equimolar quantities of CCl_4, toluene, bromobenzene, iodobenzene, and nitrobenzene eluting from the GC on the relative abundances of the reactant ions in ammonia at 0.5 torr, 100°C.

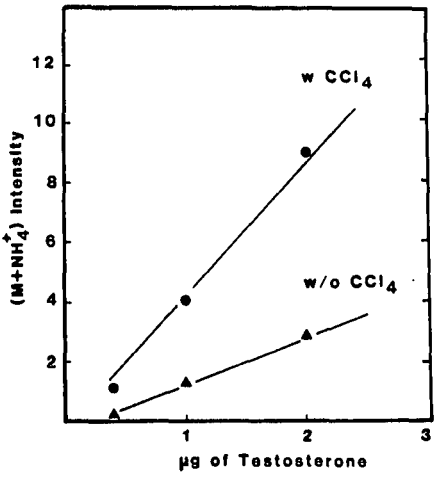

Figure 2. Effect of CCl_4 on NH_3 CI sensitivity for testosterone. Pressure: 0.5 torr, 155°C.

SIMS OF BIOMOLECULES IN THE PICO- AND FEMTOMOL RANGE

A.Benninghoven, E.Niehuis, T.Friese, D.Greifendorf, and P.Steffens

Physikalisches Institut der Universität Münster,
D-4400 Münster, Fed. Rep. of Germany

SIMS can be performed with solid or liquid samples bombarded by positively or negatively charged ions or by neutral atoms or molecules. All resulting SIMS modes, however, are variations of the same theme: the emission of parent and characteristic fragment ions during sputtering of even fragile and thermally labile molecules.

The application of SIMS in standard high resolution magnetic mass spectrometers became feasable by compensation of the low transmission of the instruments through a regenerating liquid matrix. For this SIMS mode, in general labelled as "FAB", the typical sample consumption is in the 10^{-9} mol range. This is too high for many applications, especially in the life sciences.

Much higher sensitivities - at lower mass resolutions, however, - are expected and obtained with time-of-flight (TOF) instruments. Compared with quadrupole and double focussing sector field instruments, time-of-flight instruments have some convincing advantages in SIMS-applications:

- an unlimited mass range
- a very high transmission which is constant over the whole mass range
- a quasisimultaneous detection of all masses of the same charge sign.

The simultaneous ion detection in combination with a high transmission results in very high sensitivity of a well designed TOF-SIMS, which exceeds that of a double focussing sector field instrument by several orders of magnitude.

We have designed and built such a time-of-flight mass spectrometer which is equipped with a mass separating pulsed primary ion source. A high average current density on the target allows sputtering of 1 monolayer in about 15 minutes. The design of the flight path considers the specific angular and energy distribution of the secondary ions. The ion detection system guarantees a high and stable detection probability.

We have investigated the performance of this instrument with a number of biomolecules, such as peptides, oligonucleotides and oligosaccharides. For noble metal substrates, cleaned by ion bombardment or by an etching procedure, reproducible and stable ($>$ 24 hours) targets giving high molecular and fragment ion yields are obtained for all biomolecules investigated. For the standard sample preparation, about 5 picomol of the sample material is in the target area bombarded by the primary ion beam. By dilution series, detection limits are determined.

Reference

A.Benninghoven, E.Niehuis, T.Friese, D.Greifendorf, and P.Steffens, Org.Mass Spectrom., in press

Figures: see following page

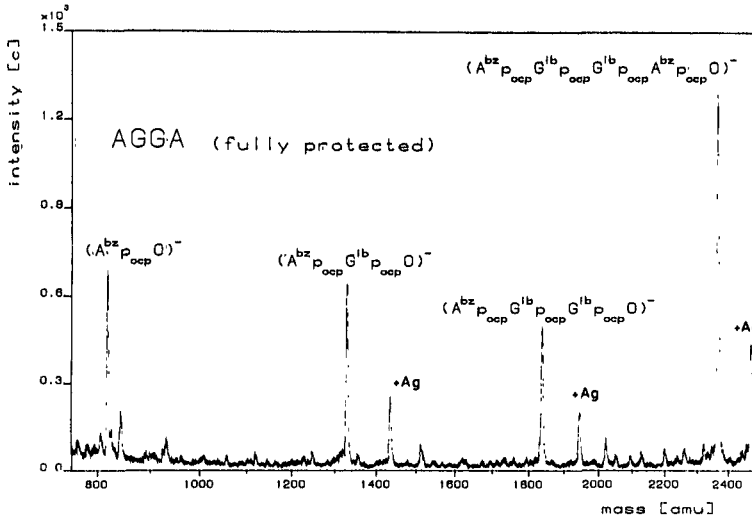

Fig. 1: High mass region of the negative TOF-SIMS spectrum of a fully protected nucleotide. Besides the sequence information, the low mass range spectrum supplies information on the bases and the protection groups.
Sample: 100 picomol deposited on 0.1 cm^2
Bombarded target area: 0.01 cm^2
Primary ions: $3 \cdot 10^8$ Ar^+, 12 keV

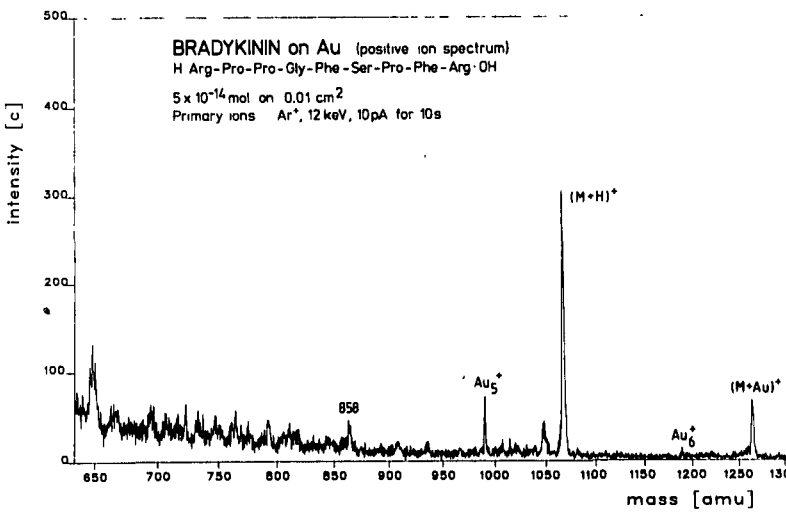

Fig. 2: Trace sensitivity of TOF-SIMS for peptides.
Sample: 40 femtomol bradykinin, deposited on 0.01 cm^2.
Primary ions: 10^9 Ar^+, 12 keV
For obtaining this spectrum, about 1 % of the sample material has been sputtered.

TOTAL PARTICLE YIELDS FROM LIQUID ORGANIC MATRICES UNDER BOMBARDMENT FROM KEV IONS

D. F. Barofsky, A. M. Ilias, E. Barofsky, and J. H. Murphy
Oregon Graduate Center
19600 N. W. Walker Road
Beaverton, OR 97006

Accurate measurements of secondary particle yields are necessary for understanding the mechanisms of secondary ion emission from organic liquids. Total particle yields reflect directly the dynamical aspects of emission processes; variation in primary beam energy, incident flux density, or primary particle mass, for example, are all manifested in changes in total particle yields. The ratio of secondary ion yield to total particle yield and the ratio of secondary ion yields from two different species can be sensitive, quantitative monitors of the chemistry and kinetics respectively of ionization processes.

The secondary particle yield in a given sputtering experiment is given by the simple expression

$$\text{Yield} = (\text{sputtering loss})/(\text{primary particle dose}).$$

The dose can be determined from measurement of the primary beam current, the bombardment time, and the system's geometry. For a single component system the sputtering loss can be simply computed as the difference between the initial and final masses of the sample. If the sample is a liquid with an appreciable vapor pressure, e.g. glycerol, this procedure results in the total loss of material due to both sputtering and evaporation. The amount of sample lost through evaportation can be estimated by multiplying a gravimetrically predetermined evaporation rate by the time the sample spent in vacuum.

In the case of a two component system, e.g. a glycerol solution of a single compound, weight loss measurements alone are insufficient to determine the sample yields. However, by doping the liquid matrix with ^{14}C molecules of the solute, independent measurements of the decrease in both weight and radioactivity of the matrix can be used to determine the specific yields of each of the components. In this method the initial amount of solute is computed from its known concentration and a gravimetric determination of the mass of the solution aliquot prior to sputtering. The final amount of solute is estimated by multiplying the predetermined value of the sample's specific radioactivity by its radioactivity as measured by scintillation counting. The difference between these two quantities is the amount of solute lost during irradiation.

Simple theoretical considerations which take into account the relationship between solute yield and total yield, predict that a counting precision on the order of 1% or less should be sufficient to measure total secondary yields of the solute molecules. This is easily obtainable in scintillation counting by adjusting the disintegration activities of the sample aliquots with the concentration of the radiolabeled material.

Establishment of a standard sample state with known concentration, rate of evaporation, and surface geometry is a difficult experimental problem in the measurement of secondary particle yields from liquids. The hydroscopic character of matrix liquids, like glycerol, and the rapid evaporation of solvents, like ethanol, used to introduce sample into the matrix-liquid are the primary causes for this obstacle. Consequently, we prepared and sealed standard sample solutions in vials fitted with septums for sample withdrawal. Special recepticles with a sample capacity of 8×10^{-4} cm^3 were used to obtain reproducible surface geometries. Once deposited in recepticles, samples were quickly weighed and then equilibrated for several hours in a desiccator which had been pumped with an aspirator. This equilibration step rids the solutions of most of their volatile solvents and, thus, eliminates the bumping or splattering often observed when freshly prepared samples are introduced into vacuum. Time required for handling and transporting samples in air was kept to a minimum.

Evaporation rates were determined for pure glycerol and a few sucrose/glycerol solutions. The values obtained ranged from 0.30 $mg/m \cdot cm^2$ for the pure material to 0.15 $mg/m \cdot cm^2$ for a 2.5×10^{-2}M sucrose solution.

All samples in this study were bombarded with indium ions produced by a liquid metal ion source. The energy of the primary ions was varied from 3 keV to 5 keV. Figure 1 shows the variation in the yield of glycerol as a function of energy. Two curves, one for pure glycerol and one for a 2.5 X 10^{-2}M sucrose/glycerol solution, are shown. Three noteworthy features are readily apparent: (i) the yields are two to three orders of magnitude higher than those generally observed for metals in this energy range; (ii) the yields for the moderately concentrated sugar solution are approximately twice as large as those for the pure glycerol; and (iii) the yields for both the pure material and the solution are nonlinearly increasing functions of energy over the range investigated. The first of these presumably reflects to some degree the difference in binding energies between metals and liquids; the second points to a reduction in the cohesive forces in the solution relative to those in the pure liquid; and the third suggests the initiation of nonlinear collision cascades in the liquid matrix by the bombarding primary particles.

Sucrose yields have been determined at three concentrations; Figure 2 shows a plot of the results. The ratio of yield to concentration on a logarithmic scale is clearly seen to be essentially constant over the range studied, a feature which could have favorable implications for certain forms of quantitative measurements. On a finer scale the discrepancy observed in the values of the yields for the two pairs with the same concentrations is attributable to different primary ion energies. Comparison of the observed particle yields of sucrose with those based on stoichiometric sputtering of the solution indicates that the yield of sucrose is less than that expected by a factor of about 0.4. This result could imply that sucrose has a negative surface activity. Ion count rates for the molecular ion of sucrose (m/z 343 positive ion mode, m/z 341 negative ion mode) combined with an assumed transmission of 10^{-5} for the mass spectrometer (Hitachi RMU-6E) yield values on the order of 1 X 10^{-5} and 4 X 10^{-4} respectively for the positive and negative secondary ionization efficiencies of sucrose.

The yield of adenosine from a 1.7 X 10^{-4}M glycerol solution was measured to be 6.8 X 10^{-3}. This value deviates from a stoichiometric value by a factor of approximately 0.4, essentially the same as in the case of sucrose.

The techniques for total particle yields describe here will continue to be refined in the future; at the same time our measurements will be expanded to include ion yields. The results of these studies are expected to elucidate many of the processes governing secondary ionization from organic liquids.

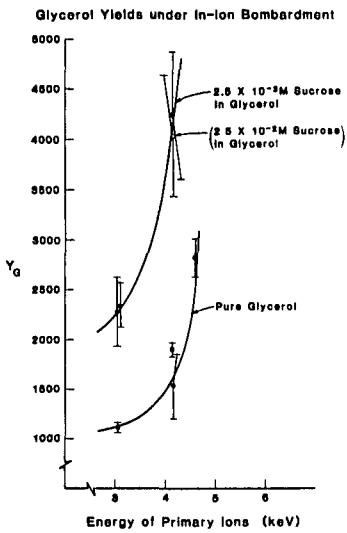

Figure 1

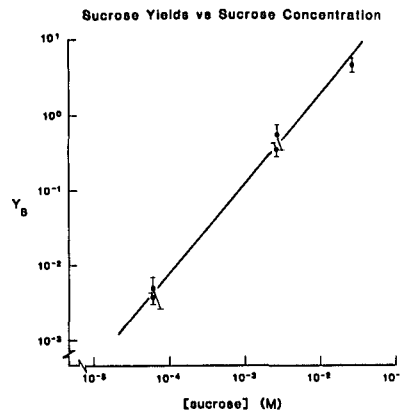

Figure 2

SECONDARY ION MULTIPLICITY
UNDER BOMBARDMENT WITH keV PRIMARY IONS

R. Beavis, W. Ens, D.E. Main, B. Schueler, and K.G. Standing
Physics Department, University of Manitoba
Winnipeg, Canada R3T 2N2

Observations of secondary ion multiplicity have been reported for high energy (~MeV/u) bombardment of large organic molecules (1,2) and CsI (2). The average number of secondary ions detected per primary projectile was $\gtrsim 4$, and some incident particles ejected more than 32 secondary ions. Significant correlations among ions desorbed from thiamine by ^{252}Cf fission fragments have also been observed (3).

We have made similar measurements with low energy primary ions using a multistop time digitizer (4) with the Manitoba time-of-flight mass spectrometer (5). Fig. 1 shows the multiplicity measured for CsI and thiamine with 10 and 13 keV primary Cs^+ ions. In both cases events yielding more than one secondary ion are only a few per cent as intense as those yielding a single secondary ion. The shaded area represents the expected distribution from superposition of independent events based on the probability of detecting at least one ion per pulse. These independent events may be caused by the same primary ion or by different ions in the same primary pulse; ~ 10 ions/pulse for CsI and ~ 70 ions/pulse for thiamine were used. This accounts for all but ~ 1% of the multiple events in CsI and all the multiple events in thiamine.

Much of the multiplicity observed with fission fragments can also be explained by a superposition of independent events in a single track (fig. 2, ref. 2); higher multiplicity with fission fragments than with keV ions reflects the much higher probability of ion production with fission fragments. However, as shown in fig. 2 for an organic compound, much of the tail of the measured distribution is not accounted for by independent events which would result in a Poisson distribution. Thus the correlated multiplicity is also much higher for fission fragments than for low energy ions (note the log scale in fig. 1). Neither measurement was corrected for spectrometer efficiency but these corrections are expected to have the same approximate magnitude.

We have also looked for correlations among specific ions from thiamine and CsI. Fig. 3 shows the normal spectrum of thiamine and the spectrum taken in coincidence with the fragment ion at m/z 144; i.e. only the data from pulses that produced an ion detected at m/z 144 are recorded. The lines shown on the expanded scale are completely accounted for by independent events; the primary current was kept low to reduce this effect. Taking account of the statistical error and the spectrometer efficiency (44% transmission of the grids was assumed) an upper limit of ~ 1% correlation between m/z 144 and 256 is found. Similar results are found for thiamine spectra taken in coincidence with m/z 122 and 256, and for CsI spectra in coincidence with Cs^+ cation. This is in sharp contrast to the results reported for fission fragments. In particular, 100% correlation was found between the thiamine fragment at m/z 144 and the parent ion at m/z 256; i.e. if the fragment ion is desorbed, the parent ion is also desorbed with 100% probability (3). This is surprising since the relative intensities of the 3 peaks (m/z 122, 144, 256) in our case are the same within 5% of those reported for fission fragments (2) (when the TAC start in that experiment is delayed successively to include each peak as the first one).

The absence of multiplicity with low energy ions may explain the fact that the ratio of the yield from fission fragments to that from low energy ions increases with mass (6). It may also explain our difficulty in observing molecular ions from insulin; higher multiplicity has been found to be correlated to events in which these large molecular ions are detected (2). It has been suggested that fission fragments activate a larger volume and this should favor the production of such high multiplicity events.

References

1) B. Sundqvist, P. Håkansson, I. Kamensky, and J. Kjellberg, in A. Benninghoven (Ed.), Ion Formation From Organic Solids, Springer-Verlag, Heidelberg, 1983, pp.52-57.
2) S. Della Negra, D. Jacquet, I. Lorthiois, Y. Le Beyec, O. Becker, and K. Wien, Int. J. Mass Spec. Ion Phys., 53, (1983) 215, and private communication from Y. Le Beyec.
3) N. Fürstenau, W. Knippelberg, F.R. Krueger, G. Weisz, and K. Wien, Z. Naturforsch, 32a, (1977) 71; N. Furstenau, Z. Naturforsch, 32a, (1978) 563.
4) W. Ens, R. Beavis, D.E. Main, B. Schueler, and K.G. Standing, these proceedings.
5) B.T. Chait and K.G. Standing, Int. J. Mass Spectrom. Ion Phys., 40, (1981) 185.
6) I. Kamensky, P. Håkansson, B. Sundqvist, C.J. McNeal, and R. MacFarlane, Nucl. Inst. and Meth. 198 (1982) 65.

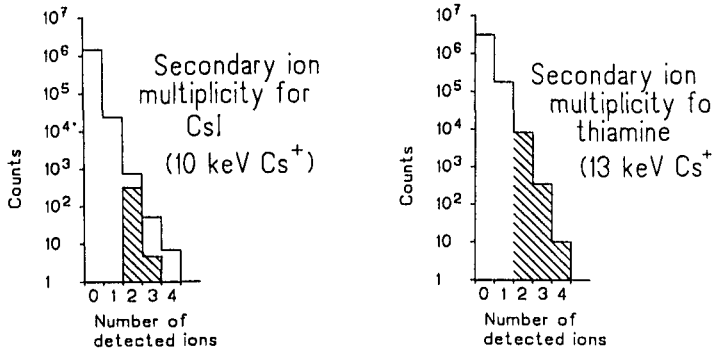

Figure 1 Secondary ion multiplicity for CsI and thiamine for incident Cs^+ ions. The shaded area represents the contribution from independent events based on the probability for detecting one ion per pulse.

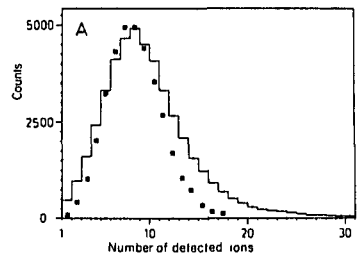

Figure 2 Multiplicity distribution of detected ions desorbed from an organic compound by fission fragments. The points are calculated values assuming a Poisson distribution with an average value of 8. Taken from ref. 2.

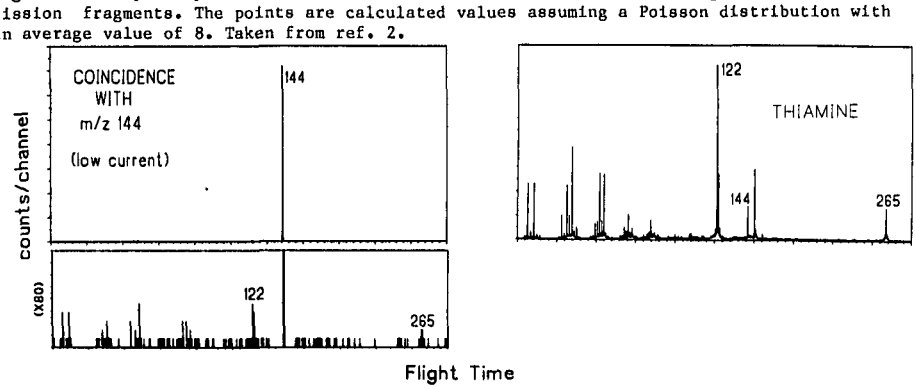

Figure 3 Positive ion spectra of thiamine. The left spectrum was taken in coinicidence with the peak at m/z 144; i.e. only those events that yielded this fragment were stored. The lower left trace is magnified × 80.

CLUSTERING PHENOMENA IN FAB MASS SPECTROMETRY

S.S. Wong, U. Giessmann and F.W. Röllgen

Institute of Physical Chemistry, University of Bonn, D-5300 Bonn, FRG

The relative stability of cluster ions as a function of the number of molecules or atoms forming the clusters, is of current interest. For alkali halides the formation of cluster ions by particle bombardment of salt layers has been extensively studied /1/. Anomalies in the intensity distributions were found to result from the unimolecular decomposition of cluster ions of different thermodynamic stability which form a nearly structureless distribution when leaving the surface /2/.

We applied a double focusing mass spectrometer, equipped with a fast Xe atom gun, for the study of cluster ion emission from various inorganic and organic samples. Some results of this work are the following:

1. The mass spectra of cluster ions formed from NH_4Cl and NH_4Br exhibit the same magic numbers as already reported for the alkali halides. However, in addition the anomaly $(NH_4X)_2NH_4^+ < (NH_4X)_3NH_4^+$ was observed (Fig.1). In the figures the quantity $I_n^2/I_{n-1} \cdot I_{n+1}$ is used for scaling the anomalies in the distribution.
2. In a mixture of NH_4Cl, stachyose and glycerol the above anomaly is reflected in the intensities of quasimolecular ions of stachyose and glycerol formed by clustering with $(NH_4X)_nNH_4^+$ ions.
3. For the quaternary salts and a number of other organic compounds examined, the use of glycerol as matrix was found to promote the formation of cluster ions.
4. Higher glycerol concentration causes a smoothing out of the anomalies (Fig.2). This provides evidence for a reduction of energy transfer to desorbing ions by the glycerol matrix.
5. The magic number n = 4 was observed for the quarternary salts examined. A large cation radius is probably in favour of a stable tetrahedral configuration of the cluster.
6. For sodium acetate more stable clusters are obtained for n = 3 and n = 13 (Fig.3).
7. The distribution of G_nH^+-glycerol cluster ions formed from pure glycerol shows no significant anomalies. However, anomalies are observed for G_nH^+ and G_nNa^+ sputtered from a mixture with tartaric acid and NaI respectively (Fig.4).

/1/ T.M. Barlak, J.E. Campana, R.J. Colton, J.J. DeCorpo and J.R. Wyatt, J. Phys. Chem. 85, 3840 (1981), and following papers of this group.
/2/ W. Ens, R. Beavis and K. Standing, Phys. Rev. Lett., 50, 27 (1983).

fig 1

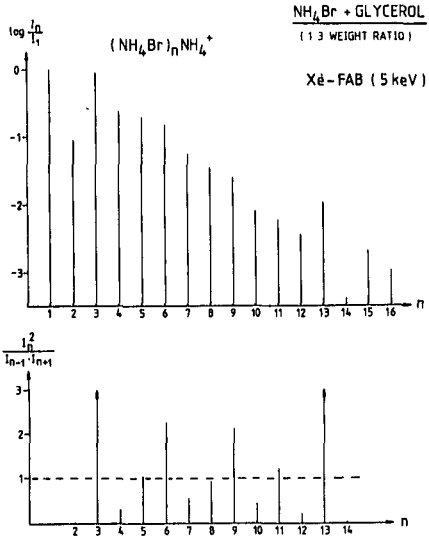

fig 2

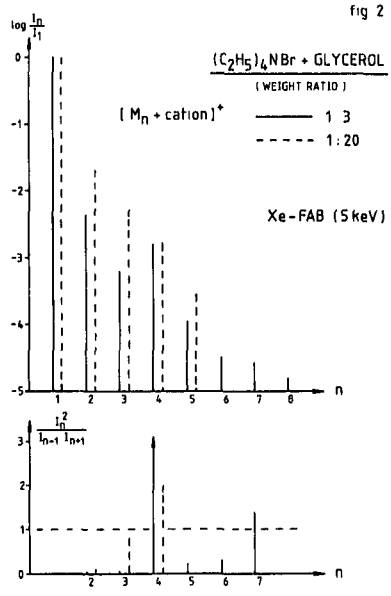

fig 3

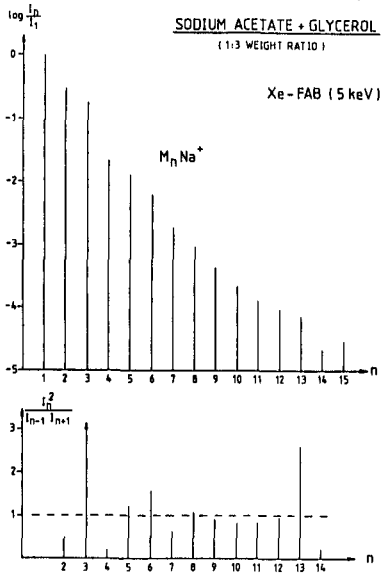

fig 4

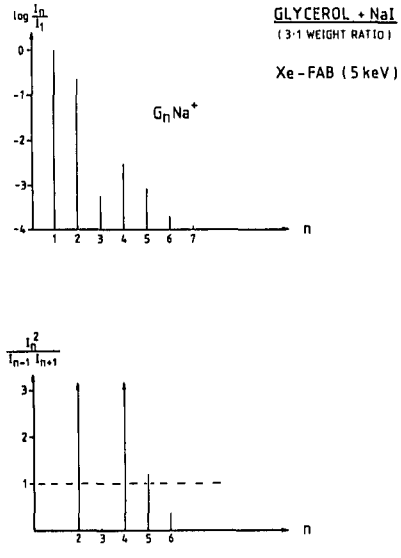

AN ELECTROSPRAY ION (ESPI) SOURCE FOR MASS SPECTROMETRY OF FRAGILE ORGANIC SPECIES:

C. M. Whitehouse and J. B. Fenn, Department of Chemical Engineering, Yale University, New Haven, CT 06520; M. Yamashita, Institute of Space and Astronautical Science, Tokyo 153, Japan

In the past few years there has emerged a method for producing ions in vacuo from solutes in liquid solution for which the underlying mechanism seems to be the desorption of ions by high electrostatic fields at the liquid surface. The required fields are achieved by evaporating charged droplets in an ambient gas. Two approaches to generating charged droplets are embodied in the Atmospheric Pressure Ion Evaporation (APIE) source of Iribarne and Thomson and the Thermospray (TS) source of Vestal and his collaborators. (1,2) A third approach, at once younger and older, is the Electrospray Ion (ESPI) source that we have recently described and is the subject of this report. The application of electrospray techniques to the preparation of ions in vacuo was first carried out by Dole and his collaborators in their attempts over 15 years ago to produce beams of polystyrene macroions in vacuo. (3) In the last three years, we have been exploring the application of electrospray to mass analysis of smaller solute species. (4)

Solution passes through a metal capillary tube with a sharp chamfered tip on the axis of a cylindrical metal chamber through which flows a counter-current of bath gas (dry N_2) at approximately atmospheric pressure. An electrostatic potential of several kilovolts is maintained between the capillary and the end wall of the chamber in which there is a small aperture leading into a second chamber maintained at a pressure of a few millitorr. The potential difference between the tube and end wall charges the surface of the emerging liquid. The resulting coulomb repulsion forces overcome surface tension and the liquid becomes dispersed into a fine spray of charged droplets by the so-called electrospray phenomenon. As evaporation occurs, the field at the droplet surface becomes high enough to desorb solute ions from the droplet surface. The desorbed ions are driven by the field against the flow of bath gas and become desolvated. Arriving at the end wall, some of them are entrained in the flow of bath gas that emerges as a supersonic free jet on the downstream side of the orifice in the low pressure chamber. Observed ions are usually the cations or anions originally in the solution. However, even species that are not ionized in solution can be detected as adducts to solute ions, e.g. as $M-H^+$ or $M-Cl^-$. A core portion of the free jet flow passes through a small orifice at the tip of a conical diaphragm (skimmer) carrying ions to a quadrupole mass spectrometer (VG Micromass 1212) in a third chamber maintained at 10^{-6} or so torr. At electrostatic potentials below a critical value that depends upon solution composition, bath gas pressure and tube-end wall distance, the ionization is very gentle and is accompanied by little or no fragmentation.

ESPI's need for several keV of electric potential difference to produce charged droplets raises the spectre of floating the sample inlet system or the mass spectrometer at high voltage with respect to ground. We find that viscous forces are such that the flow of bath gas through a 6 cm length of 0.2 mm ID glass capillary used as the free jet source can pump ions through potential differences as high as 15 keV. Consequently, we now obtain the potential difference needed for electrospraying by maintaining the inlet face (metallized) of the capillary at the required voltage <u>below</u> the incoming liquid sample flow that is at ground. The gas flowing through the capillary lifts the ions back up to ground potential at the exit where the free jet expansion starts. Thus the only elements at high voltage are inside the apparatus, out of reach of an operator. It turns out that for given conditions at the inlet the flux of ions and gas through the capillary (0.2 mm ID) is almost exactly the same as the flux through the thin plate orifice (0.1 mm) it replaces. With a 9.6 keV potential drop through the capillary we lose about half the ions with masses below 100 daltons and about a quarter of the ions with masses in the 300 to 500 dalton range. These loss observations are from preliminary experiments and should not be construed as characteristic or inevitable, but only as indicative. The ability to pump ions through substantial voltage differences is particularly inviting <u>vis-a-vis</u> the problem of coupling an ion source with a magnetic sector instrument that can require ion injection energies up to 10 keV.

Using the capillary ion-pumping configuration, we have recently obtained mass spectra for several peptides whose masses are substantially higher than we have tried in previous experiments: gramicidin S (1140), cyclosporin A (1202), bleomycin (1375) and its copper complex (1440) and Substance P (1348). It is interesting that for all of these materials except cyclosporin the predominant peak was the doubly protonated ion. This observation invites the possibility of promoting multiple charging in order to extend the effective mass range of both the ESPI source and any mass analyzers with which it might be used. With respect to sensitivity we can say that with gramicidin S if we assume that S/N of 2 is tantamount to "detectability" we can "see" this substance at concentrations as low as 4×10^{-7} molar (in 50-50 methanol-water). The amount of material in a discernible peak is about 10^{-13} g when the concentration is 10^{-5} molar in the same solvent.

References

1. J. B. Iribarne and B. A. Thomson, J. Chem. Phys. 64 (1976) 2287; ibid. 71 (1979) 4451; J. B. Iribarne, P. J. Dziedzic and B. A. Thomson, Int. J. Mass Spect. Ion Phys. 50 (1983) 331.

2. C. R. Blakley, J. J. Carmody and M. L. Vestal, J. Am. Chem. Soc. 102 (1980) 5931; Clin. Chem. 26 (1980) 1467; Anal. Chem. 52 (1980) 1636; C. R. Blakley and M. L. Vestal, Anal. Chem. 55 (1983) 750.

3. M. Dole, L. L. Mack, R. L. Hines, R. C. Mobley, L. D. Ferguson and M. B. Alice, J. Chem. Phys. 49 (1968) 2240; ibid. 52 (1970) 4977; M. Dole, H. L. Cos, Jr. and J. Gieniec, Adv. Chem. Ser. 125 (1973) 73.

4. M. Yamashita and J. B. Fenn, J. Phys. Chem. (in press).

ION EMISSION PROCESSES AT ATMOSPHERIC PRESSURE - A COMPARISON OF THERMOSPRAY AND ION EVAPORATION, Bruce A. Thomson, SCIEX®, 55 Glen Cameron Road, Thornhill, Ontario, Canada, L3T 1P2.

Ion evaporation was first described several years ago (1,2) as a process in which organic ions in aqueous solution may be emitted into the air simply through the action of selfinduced fields at the surface of small charged droplets created by a sprayer. Although the initial discovery of the process arose from an investigation of charged atmospheric aerosols, it became apparent that the technique had application to the chemical analysis of ionic compounds in solution which are otherwise difficult to introduce into a mass spectrometer without thermal degration. Theoretical considerations revealed that the energy barrier faced by an ion at the surface of a charged liquid drop could be expressed as:

$$G = - G_S - \frac{eQ(x_m+d)}{(R-d)(R+x_m)} - \frac{e^2}{4x_m}$$

where G_S=standard free enthalpy of solvation, Q=drop charge, R=drop radius, d= location of the ion beneath the surface of the liquid, x_m=position of the energy barrier maximum above the surface. Experimentally, emission of ions from evaporating droplets was observed at atmospheric pressure, allowing mass spectrometric measurements of the ions in solution by sampling the ions through a small orifice into vacuum.

Several parameters affect the rate of evaporation, and thus the ion signal. These include G_S (energy of solvation, dependent upon the type of ion), Q (net drop charge), R (drop radius) and C_A (concentration of analyte ions in the liquid). In practice, the net droplet charge is enhanced by placing a small electrode close to the head of the sprayer, and applying a high voltage of polarity opposite to that of the ions to be analyzed. This induction electrode thus aids the natural charging process associated with the sprayer.

Thermospray is a process developed specifically as a technique for introducing ionic and labile compounds in a liquid stream into a mass spectrometer(3). The liquid is sprayed into vacuum by passing it through heated microbore tubing. With the liquid flow and temperature correctly adjusted, a hot jet of nebulized and desolvated particles is obtained. This jet is observed to contain evaporated ions which cannot be thermally produced, leading to speculation that the process of ion evaporation is also operative in the jet of the thermosprayer. The addition of an ammonium acetate buffer appears to produce an additional ionization mechanism through the chemical ionization reaction of evaporated ammonium ions with neutral molecules of semi-volatile compounds which are vaporized during the thermospray process. Thus ion evaporation, acting at atmospheric pressure and without the introduction of any heat, allows the analysis of ionic compounds only. Thermospray, which has to date only been used at low pressure, generates a charged mist via a different spraying process, resulting both in ion evaporation as well as chemical ionization of compounds vaporized in the heated sprayer.

In an effort to clarify the details of the ion evaporation process, this study has focussed upon the characteristics of Ion Evaporation (IE) and Thermospray (TS) (here operated at atmospheric pressure). Unfortunately, most of the parameters which directly affect the size of the energy barrier (and thus the ion emission rate) cannot be accurately controlled and measured. Instead, the investigation focussed on how the ion signal is affected by induction electrode voltage, presence of an ionic modifier in solution, type of analyte, and concentration of analyte. The data was obtained separately by Ion Evaporation and by Thermospray, although only preliminary results are available for the latter. It should be recognized that the behavior of Thermospray in the atmospheric pressure configuration does not necessarily reflect its optimum performance as normally enacted in a low pressure configuration.

1. Type of Analyte. Arginine (MW 174), glutamine (MW 146), pancuronium bromide ($C_{35}H_{60}Br_2N_2O_4$, MW 732.7, a divalent quaternary ammonium salt) and NC-45 ($C_{34}H_{57}BrN_3O_4$ MW 637.73, a monovalent quaternary ammonium salt closely related in structure to P.C. Bromide) were used as model compounds. Ion evaporation spectra showed only MH^+ from the first two (m/z 175 and 147), $[M-2Br]^{2+}$ at m/z 286 from P.C. Bromide, and both $[M-Br]^+$ and $[M-Br+H]^{2+}$ at m/z 557 and 279 from NC-45. Thermospray spectra of arginine and glutamine in a mobile phase of 0.1M ammonium acetate were essentially identical to those produced by IE; however, no ion signal was observed for P.C. Bromide and NC-45 by Thermospray. (The thermosprayer consisted of 0.010" ID tubing imbedded in a heated copper cylinder, and produced an optimum ion signal for arginine at a flow of 1.3 ml/min and a temperature or 475°C).

These results for IE are consistent with the fact that ions present in solution are observed without fragmentation in the mass spectrometer. The thermospray results are puzzling, since both P.C. Bromide and NC-45 should have been observed. More investigation is required to determine whether these compounds are observable by TS.

2. Addition of Ionic Modifier. IE spectra were obtained for all four model compounds in distilled, deionized water, 0.1M acetic acid, and 0.1M ammonium acetate. TS spectra were obtained only in the latter (the others were not tried). Ionic strength and pH are expected to affect the drop charge and the ion chemistry in solution. In fact, the ion intensities by IE were nearly identical in 0.1M acetic acid and distilled water, but were all significantly lower (by factors of 3 to 5) in ammonium acetate, perhaps because of competition, or perhaps because this less volatile modifier increased the limit at which the droplets solidified into salt particles, halting the evaporate process. In ammonium acetate, only m/z 557 from NC-45 was observed, apparently due to the absence of H^+ in solution which in acetic acid and distilled water contribute to the formation of $[M-Br+H]^{2+}$.

   Ion evaporation spectra of all four compounds were also obtained in mixtures of acetonitrile/water, with compositions ranging from 50% MeCN up to 100% MeCN. The spectra were essentially the same as those obtained with aqueous mobile phase, except that in 100% MeCN, the m/z 557 ion dominated the NC-45 spectrum. Sensitivities in 100% MeCN were about a factor of 3 lower than in distilled water. Thermospray was not attempted with the acetonitrile/water mixtures.

3. Induction Electrode Voltage. *The IE ion signal as a function of induction electrode* voltage exhibits a threshold below which no ion signal is observed. This suggests that the spray electrification process (in the absence of induction) produces droplet charges insufficient to produce ion evaporation at a significant rate. This threshold voltage is higher for distilled water (700V) than it is for either acetic acid or ammonium acetate (about 500V) due no doubt to the higher conductivitiy of the latter solutions. The signal rises sharply with electrode voltage, and saturates at about 2KV, reflecting a saturation of droplet charge. This saturation voltage is approximately independent of the type of analyte or the concentration, or the type of ionic modifier.

4. Analyte Concentration. Calibration curves for arginine and glutamine were obtained by IE. The ion signal initially increases linearity as a function of concentration, but becomes non-linear at higher concentration. This non-linearity and ultimate saturation (at a level of about 1 ug) is typical of IE calibration curves, and has been explained previously as due to a combination of two effects: 1) the ion concentration in each drop increases linearily with analyte concentration; 2) the solid residue limit also increases with concentration. Thus as the analyte concentration is increased, more ions are present in each drop to evaporate, but more and more drops reach the solid residue (dry particle) limit before all of the net charge has been emitted. The latter effect ultimately results in saturation of the ion signal, and even eventually in depletion of the signal. This effect has not been previously reported for TS, where linear calibration curves have been obtained. However, TS at atmospheric pressure does show precisely the same effect as IE (at least for arginine).

5. Sensitivity. A direct comparison cannot be properly made until TS at atmospheric pressure has been properly explored and optimized. TS was observed readily at temperatures of between 350° and 500°C with little variation in ion signal over the range (at a flowrate of 1.3 ml/min). Detection limits for arginine were about 1 ng (SIM) by IE, and were about a factor of 10 higher by TS. The quaternary ammonium bromide salts gave detection limits of about 10 ng (SIM) by IE, but could not be observed at the 1 ug level by TS. More investigation is required to determine the reason for this.

Conclusion

IE and TS at atmospheric pressure appear to be closely related processes, but may differ in the droplet size and charge. Both processes behave approximately the same as a function of induction electrode voltage and analyte concentration. Further experiments employing a wider range of compounds and ionic modifiers are required in order to provide a more clear comparison.

References

1. J. V. Iribarne and B. A. Thomson, J. Chem. Phys., 64, 6, 2287-2294 (1976).
2. B. A. Thomson and J. V. Iribarne, J. Chem. Phys., 71, 11, 4451-4463 (1979).
3. C. R. Blakley and M. L. Vestal, Anal. Chem., 55, 4, 750-754 (1983).

MONODISPERSE AEROSOL GENERATION INTERFACE FOR COMBINING LIQUID CHROMATOGRAPHY WITH MASS SPECTROMETRY (MAGIC): SOME THEORETICAL CONSIDERATIONS

R.C. WILLOUGHBY, Stuart Pharmaceuticals, Div. of ICI Americas Inc., Wilmington, DE 19897
R.F. BROWNER, Georgia Institute of Technology, School of Chemistry, Atlanta, GA 30332

A working interface for combining a high-performance liquid chromatograph with an electron impact ionization mass spectrometer has been developed using a monodisperse aerosol generation approach (1). The interface can accommodate a wide range of solutes as well as solvents with varying ranges in polarity and volatility, including reversed-phase solvents. Solutes have been detected in the nanogram range. Both electron impact and chemical ionization have been observed. The dynamic range was linear over three orders of magnitude. Under optimum conditions, the interface contributed little to band spreading of the chromatographic peaks. This interface has demonstrated the potential for wide application in the study of involatile and thermally labile molecules. A schematic diagram of the interface is seen in Figure 1.

The development of MAGIC required some experimentation in the fundamental study of nebulization, desolvation, and pressure reduction. This paper will discuss the results of these fundamental studies and the theoretical principles associated with the operation of the interface.

(1) Willoughby, R.C.,"Studies with an Aerosol Generation Interface for Liquid Chromatography - Mass Spectrometry," Ph.D. Thesis, School of Chemistry, Georgia Institute of Technology, July 1983.

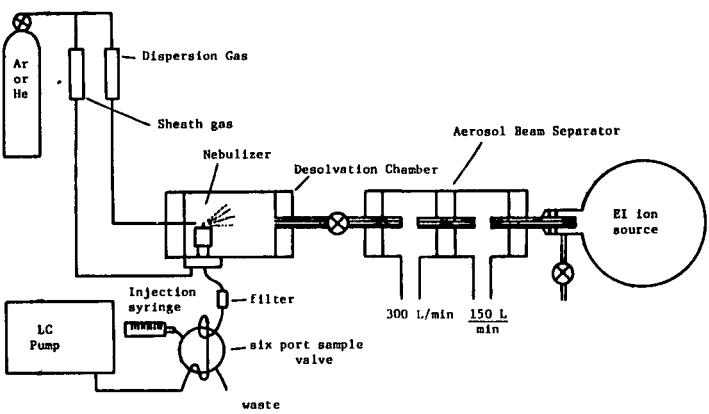

Figure 1. Schematic Diagram of MAGIC LC-MS.

MECHANISTIC STUDIES ON THERMOSPRAY IONIZATION.

D. Pilosof*, H. Y. Kim, M. L. Vestal,
Department of Chemistry, University of Houston, Houston, TX 77004, USA.

Thermospray is broadly defined as a liquid chromatography/mass spectrometry (LC/MS) interface in which a liquid stream flowing through a capillary is completely or partially vaporized by applying heat. Thermospray ionization was discovered as a result of a fortuitous experimental accident (1). During the development of an LC/MS interface, the filament used as a primary source for chemical ionization (CI) burned out, but ionization was nevertheless detectable. Even though current thermospray interfaces include an optional filament for compounds that undergo CI more efficiently (2), most thermospray interfaces are operated in the "filament-off" mode and therefore monitor ions produced solely by thermospray ionization. The purpose of our studies is to investigate such mechanism and its dependence on various experimental parameters.

In the absence of an external primary source, thermospray ionization requires the use of an electrolyte which in the rapidly desolvating charged droplets generated in the heated capillary, produces surface fields that enhance the ejection of ions from the liquid phase (3). The signals observed for ions preformed in solution, such as quaternary ammonium salts and metal complexes, do increase upon addition of an electrolyte. The most widely used electrolyte, ammonium acetate, is advantageous since it is volatile and also provides an efficient gas-phase proton donor (NH_4^+) and acceptor (CH_3COO^-). The results obtained in our studies indicate that in addition to the field effect created by the presence of the electrolyte, the relatively high localized pressure produced by the thermospray (ca. 10 torr) causes a large number of gas-phase collisions in which processes such as proton transfer will invariably occur. The results in Figure 1 show that several amino acids, negatively, positively charged, and neutral in solution, gave comparable signals over the pH 1.85 - 8.0 range when monitoring the MH^+ ion. Taking into consideration the solution pK_a values, ASP and GLU would only be protonated below pH 2 and therefore if the process was dominated by the solution chemistry, their signal would only be detectable below that pH value. From these results it appears that as long as there is an excess of a gas-phase protonating agent, these molecules will protonate by gas collisions regardless of their solution pK_a. When the pH goes above the NH_4^+ pK_a 9.7, thre are neither enough ions in solution to generate electric fields nor enough ammonium ions to produce gas-phase protonation and consequently the signal drops drasticaly.

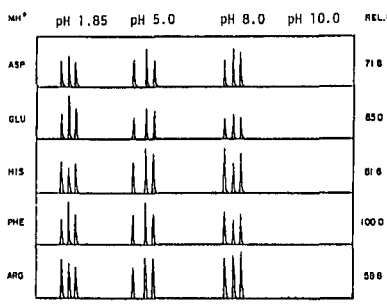

Figure 1

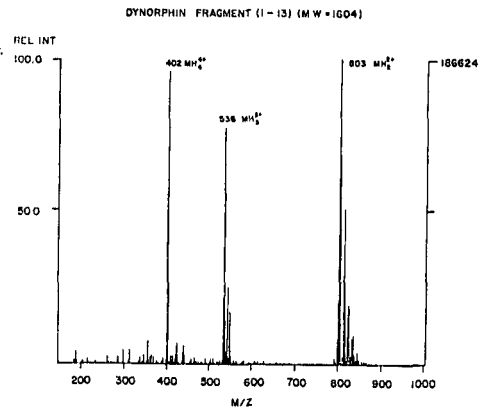

Figure 2

Peptides that produce multiply charged ions (4) such as dynorphin fragment 1-13, shown in Figure 2, have a similar behavior, with the ratio of the multiply charged peaks remaining constant even when the solution pH is varied over a wide range. From solution chemistry considerations the highly protonated forms should be favored by decreasing the pH.

One important parameter to determine in the operation of thermospray interfaces is the temperature of the capillary. In the most recent thermospray version, the flowing solution is vaporized by resistive heating between two points of the capillary tube (2). For most applications the optimal temperature range is that in which the vaporization is almost but not entirely complete before the exit of the capillary. Going above that range results in more fragmentation, significant degradation of the chromatographic peak profile, less reproducible temperature control and deposit of solid particles inside the capillary. The actual experimental value for optimal temperature performance is a function of the solvent composition, the capillary inner diameter and the flow rate. Figure 3 shows repetitive injections for three amino acids at two different capillary tip temperatures. Using a 0.15 mm id capillary at 1.0 mL/min of aqueous buffer, the best temperature range for amino acids is 190-205°C. In this range the signal obtained maintains good peak shape and fragmentation is minimal. Raising the tip temperature to 220°C results in a noisy peak shape, extensive broadening probably due to a capillary GC-like effect, and a larger degree of pyrolytic fragmentation.

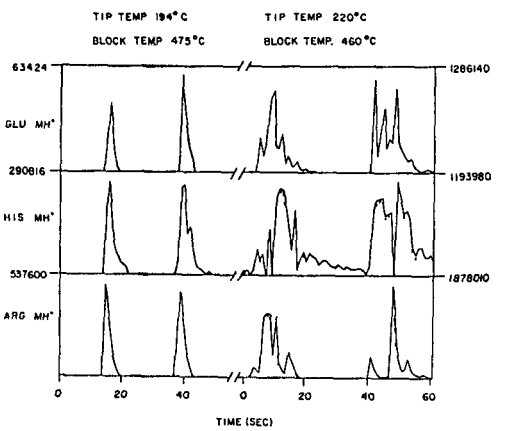

Figure 3

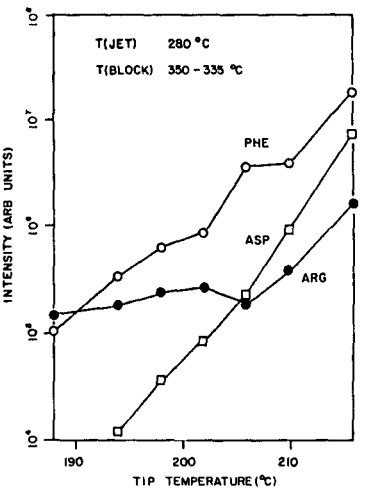

Figure 4

Figure 4 shows the dependence of the signal intensity on the tip temperature. ARG is protonated at pH 5.5 and is observed as MH^+ at much lower temperatures that the amino acids that have to be protonated in the gas phase. ASP and GLU normally show a lower signal since they must be protonated twice to give MH^+. By increasing the tip temperature desolvation is moved upstream and the conditions for gas-phase protonation are preferentially created. However, when reaching the region where vaporization is complete inside the capillary, inspite the higher signal, the limitations shown in Figure 3 become significant and make the mode of operation less analytically useful. In general the optimal temperature range is determined experimentally. Using the resistive heating interface (2), temperature optimization is simple and reliable.

(1) C.R. Blakley, J.J. Carmody, M.L. Vestal, J.Am.Chem.Soc. (1980), 102, 5931

(2) G.J. Fergusson, M.L. Vestal, submitted to Anal.Chem.

(3) B.A. Thomson, J.V. Iribarne, P.J. Dziedic, Anal.Chem (1982), 54, 2219

(4) D. Pilosof, H.Y. Kim, D.F. Dyckes, M.L. Vestal, Anal.Chem. (1984) in print.

STUDIES WITH MOVING BELT AND THERMOSPRAY LC/MS

D. E. Games, N. J. Alcock, I. G. Beattie, M. A. McDowall, A. V. Moncur, E. D. Ramsey and P. W. Skett.
Department of Chemistry, University College, PO Box 78, Cardiff, CFI IXL, U. K.

Three liquid chromatographic/mass spectrometric interfaces of the moving belt type and a prototype Finnigan MAT thermospray interface have been used for studies of a range of organic compounds. Two of the moving belt interfaces we have used enter directly into the ion source of the mass spectrometer,[1,2] whilst the other is interfaced to the ion source block.[3]

Moving belt interfaces for LC/MS have the advantages of providing both EI and CI spectra. This can be of considerable utility in studies aimed at identification of compounds in complex matrices. Our studies[4] of the oleoresins of black pepper illustrate the advantages of this approach. Using a combination of the data obtained from both ionization techniques together with field desorption and EI accurate mass measurements, we have identified a series of N-isobutyltrienamides and dienamides together with piperolein A and B, piperanine, piperylin and piperettin and piperine isomers. In this study EI gave readily interpretable spectra containing molecular ions. The CI spectra served to confirm mol. wt. assignments and assisted in the identification of the constituents of multicomponent peaks. Macrotetrolide ionophores of the actin type have also been studied. These compounds failed to provide molecular ions by EI. Ammonia CI gave abundant $(M + NH_4)^+$ ions together with fragment ions characteristic of three quarters, half and a quarter of the molecule. Comparison of the on-line LC/MS spectra obtained with those obtained using a direct insertion probe indicated that some thermal decomposition occurs on the interface. Preliminary studies of these compounds have been conducted with a thermospray system. Under optimal conditions the thermospray spectra consist of $(M + NH_4)^+$ ions and no fragmentions.

Comparative studies[5] of a range of compound types have been conducted with three moving belt interfaces. The two older interfaces[1,3] proved to be the least effective in providing molecular weight information from mass spectrometrically difficult molecules. For example with ammonia CI a $(M + NH_4)^+$ ion was obtained from raffinose with the latest interface[2], whilst the earlier interfaces failed to give mol. wt. information. Mixtures of pseudomonic acids A, B and C have been studied using ammonia CI on all three interfaces and only the most recent one[2] consistently provides mol. wt. information in the form of $(M + 1)^+$ ions. These compounds have also been investigated on-line with a thermospray system. Spectra similar to those obtained with the best belt system were obtained.

The best moving belt system for LC/MS has a limitation in its ability to provide mol. wt. information, which is similar to that of desorption chemical ionization. Thermospray ionization considerably extends the range of compounds from which mol. wt. information can be obtained. In addition because it works best at high flow rates (1.5 ml min^{-1}) of aqueous mobile phases detection limits for many polar compounds are much lower than can be achieved with moving belt systems. We have made intensive efforts to obtain mol. wt. information from penicillins using moving belt interfaces, but have failed to consistently obtain such data. Using the thermospray system, a mixture of methicillin, benzylpenicillin and phenoxypenicillin gave an acceptable TIC trace and yielded both $(M + 1)^+$ and $(M + NH_4)^+$ ions for each of the compounds together with structurally useful fragmentions. Sensitivity studies with a prototype interface gave detection limits in the low ng. range.

Conclusions

The most recent[2] commercially available moving belt interface for LC/MS considerably extends the range of compounds amenable to study. Moving belt systems have the advantage of providing conventional EI and CI spectra, which is of considerable utility in structural studies. Problems include the handling of high flow rates of high percentage aqueous mobile phases and thermal decomposition of labile compounds. Thermospray LC/MS in contrast can handle mass spectrometrically more difficult molecules and operates best at high flow rates of aqueous mobile phases. However spectra can in many cases contain little structural information apart from mol. wt. Since water and a buffer appear to be necessary to effect ionization, normal phase chromatography and reversed phase chromatography, where a buffer system is not used will require addition of water and an appropriate buffer before introduction into the ion source. The technique may also have difficulties in handling complex mixtures containing a variety of structural types particularly if unknowns are present, since the temperatures of the vaporizer, jet and aerosol may not be optimal for their detection.

We believe that moving belt and thermospray interfaces are complimentary in their ability to assist in the solution of problems.

References

1. D. S. Millington, D. A. Yorke and P. Burns. Adv. Mass Spectrom., 1980, 8B, 1819.

2. P. Dobberstein, E. Korte, G. Meyerhoff and R. Pesch, Int. J. Mass Spectrom. Ion Phys., 1983, 46, 185.

3. W. H. McFadden, H. L. Schwartz and S. Evans, J. Chromatogr., 1976, 122, 389.

4. D. E. Games, N. J. Alcock, J. Van der Greef, L. M. Nyssen, H. Maarse and M. Ten Noever de Brauw, J. Chromatogr., 1984, in press.

5. D. E. Games, M. A. McDowall, K. Levsen, K. H. Schafer, P. Dobberstein and J. L. Gower, Biomed. Mass Spectrom., 1984, 11, 87.

ENHANCEMENT OF THE AMOUNT OF INFORMATION OBTAINED BY THERMOSPRAY HPLC/MS. Robert D. Voyksner, Joan T. Bursey, Analytical and Chemical Sciences, Research Triangle Institute, P. O. Box 12194, Research Triangle Park, NC 27709, and Carol A. Haney, Office of the Vice Chancellor for Research, North Carolina State University, Raleigh, NC 27695.

Thermospray (TSP) HPLC/MS is a method that shows promise for the analysis of thermally labile and nonvolatile compounds. Ions formed by thermospray usually indicate molecular weight ($[M+H]^+$ and/or $[M+NH_4]^+$). However, this soft ionization technique yields few fragment ions making characterization of an unknown compound very difficult. We have investigated various methods to increase the amount of structural information by evaluating the effects of various HPLC mobile phases and buffers. Also, we have investigated means to induce fragmentation by use of a filament and a collision cell in the lens region of the source.

The initial studies evaluated the effect of various solvent on the character of the TSP spectra. Various percentages of acetonitrile/water and methanol/water were used to analyze carbamate pesticides and triazine herbicides. While no new ions were detected or fragment ions formed, the relative abundances of the $[M+H]^+$ and $[M+NH_4]^+$ ions changed. High percentages of water favored the formation of $[M+H]^+$ ions while low percentages of water favored $[M+NH_4]^+$ formation. Acetonitrile produced more adduct ion formation than methanol.

Several volatile buffers were also evaluated to determine if a change of buffer would promote fragmentation. Buffers included ammonium acetate, ammonium formate, ammonium carbonate, ammonium bicarbonate, triethylamine, and H_2SO_4. While the sensitivity of TSP was strongly dependent on buffer choice (sensitivity ranged over three orders of magnitude with ammonium acetate exhibiting the best sensitivity), the spectra contained no new qualitative information. Only triethylamine exhibited a different ion $[M+triethylamine]^+$ although the intensity was too low to be analytically significant.

Replacement of H_2O with D_2O in the HPLC solvent system proved useful in the characterization of compounds analyzed by thermospray by determination of the number of active hydrogens in a compound. Functional groups that undergo hydrogen/deuterium exchange in thermospray HPLC/MS include -OH, $-NH_2$, and -NHR. The types of ions typically observed with D_2O/CH_3CN HPLC solvent include $[MD_x+D]^+$, $[MD_x+ND_4]^+$, $[MD_x+DC_2H_3O_2]^+$, and $[MD_x+DCH_3CN]^+$ where x = the number of active hydrogens in the analyte structure. An example of thermospray HPLC/MS analysis using a D_2O mobile phase is shown in Figure 1. Benzidine, which contains four active hydrogens, exhibited $[MD_4+D]^+$ (m/z 190) and $[MD_4+DCH_3CN]^+$ (m/z 231) ions. Analysis of benzidine in an H_2O mobile phase resulted in an $[M+H]^+$ ion at m/z 185. Thus, the use of D_2O can aid the analyst in determining the number of alcoholic or amine functional groups and can be further used to determine the degree of substitution for amines.

Use of filament ionization combined with TSP ionization was also evaluated. With normal chemical ionization, the use of a filament results in formation of a reagent plasma from the HPLC solvent which then protonates the analyte. The solvent CI process is more energetic than TSP ionization, with more fragment ion formation. For the few compounds analyzed by filament-on thermospray (carbamates, LSD, dyes, triazine herbicides), no new fragment ions were formed, but the ratio of $[M+H]^+/[M+NH_4]^+$ increased with filament ionization (Figure 2).

The final method evaluated involved building a collision chamber in the lens region of the source block to collisionally activate the ions formed by TSP and induce their decomposition. The ion fragment yield was maximized using nitrogen collision gas at an analyzer pressure of 3.5×10^{-5} torr with an extractor voltage of -30V, a lens voltage of -130V, and an quadrupole entrance voltage of -45V. For the compounds analyzed, including LSD, carbamates, and triazines, little gain in fragment ion yield was observed. The TSP spectrum for adenosine (MW 267) exhibited an increase of a factor of 2 in the fragment ion intensity at m/z 136 using the nitrogen collision cell (Figure 3). However, the collision cell effectively dissociated cluster ions such as $[M+NH_4]^+$ and $[M+Acetate]^+$ to form $[M+H]^+$ ions. Figure 4 illustrates this point for the pesticide linuron. The base peak for this pesticide in the TSP spectrum is $[M+NH_4]^+$ (m/z 266). When nitrogen collision gas is introduced, the $[M+H]^+$ becomes the base peak. The $[M+NH_4]^+$ signal level decreased to a relative abundance of 10%.

In conclusion, none of the methods evaluated actually produced new TSP fragment ions. While the collision process increased the relative intensity of an existing fragment ion, no new information was obtained. While this makes the characterization of a complete unknown impossible, it is comforting to know the TSP spectrum of a compound is repeatable over a variety of analysis conditions. In characterizing a complete unknown, D_2O seems to offer the most new information for the TSP-HPLC/MS analysis, indicating the number and, in

most cases, type of functional groups in a molecule. Filament ionization can be used to ionize compounds not amenable to TSP ionization. However, if a compound is sensitive to TSP ionization, filament ionization will usually not produce any extra structural information. The use of a collision region to generate structurally significant ions from the one or two ion TSP spectra appears to be the most promising technique for compound characterization. The collision region effectivelly broke cluster ions and increased TSP fragment ion abundances. The ion energies or focusing characteristics of this collision region were not suitable for the detection of new fragment ions. It is believed that TSP-HPLC/MS/MS will be the best way to obtain structurally relevant information on the molecular ions observed in TSP.

ACKNOWLEDGMENT

This work was partly supported by EPA, Office Research and Development, Environmental Monitoring and Support Laboratory, Cincinnati, Ohio, under Contract No. 68-03-3122.

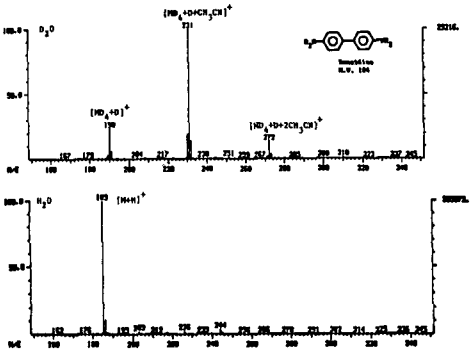

Figure 1. TSP spectrum of benzidine in H_2O and D_2O solutions. Not that all four of the amine hydrogens are exchanged for deutrium.

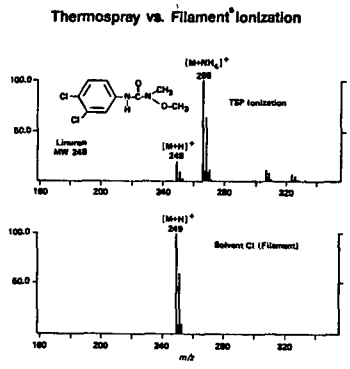

Figure 2. Filament-assisted thermospray spectrum and the thermospray spectrum for the pesticide linuron.

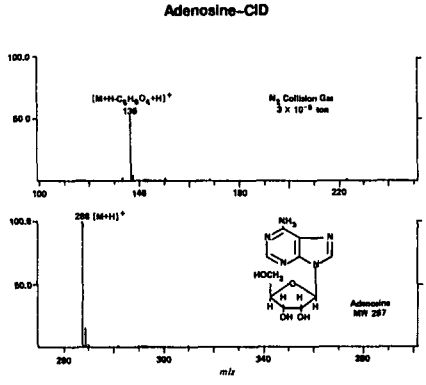

Figure 3. The CID thermospray spectrum for adenosine

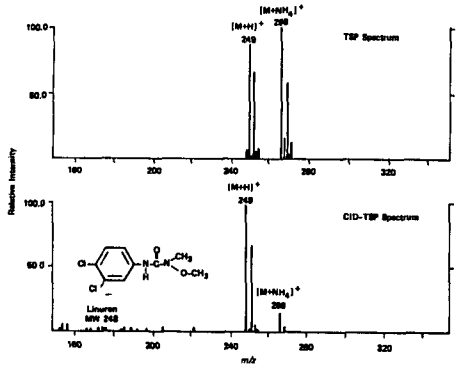

Figure 4. The CID thermospray spectrum of linuron along with the thermospray reference spectrum.

FAST INJECTION OF LIQUID SOLUTIONS INTO A QUADRUPOLE MASS SPECTROMETER USING SHORT FUSED SILICA CAPILLARIES.

Patrick J. Arpino, Ecole Polytechnique, Laboratoire de Chimie Analytique Physique, 91128 Palaiseau, France.
and
Claude Beaugrand, S.N. Nermag, Departement Recherches, 92500 Rueil-Malmaison, France.

One of the most irritating problems that occur when utilizing a Direct Liquid Inlet interface for LC/MS is the frequent plugging of the diaphragm nebulizer. The size of the pinhole in the stainless steel or nickel disk which is in most DLI interfaces depends on the vacuum pumping capacity of the vacuum equipment attached to the mass spectrometer and is 2-5 µm for most chemical ionization mass spectrometers (1). A cryopump located above the ion source is a convenience since it improves the vacuum, but it does not allow the injection of liquid flow rates greater than 50 µL/min because the surface of the cryopump then is saturated rapidly and the action of the pump stops after ca. 30 min of liquid introduction.

One of the many fallouts of the thermospray investigation by Vestal and co-workers (2) is the demonstration that by connecting an auxiliary mechanical pump directly to the ion source and opposite the nebulizer, flow rates up to 1 mL/min can be introduced continuously. This modification was performed on our LC/MS instrument. As a consequence, a 10 µm stainless steel diaphragm could be substituted to the previous 2 µm nickel diaphragm. Solvent flow rates in the 70-100 µL/min range were easily nebulized under a vacuum and the plugging problem was reduced dramatically. Higher flow rates were mainly prevented by the insufficient energy, 100 eV, of the electron beam entering the ion source for inducing CI reactions.

Because of the increase of the acceptable liquid flow rates, capillary tubes were reinvestigated for vacuum nebulization. Theoretical calculations showed that the only parameters of importance for producing a jet are the diameter of the orifice, the liquid flow rate and the liquid temperature. A diaphragm or a capillary tube of the same internal diameter as the diaphragm pinhole produces the same jet. The difference is the pressure drop across the nebulizer and is unacceptable for a 2-5 µm capillary, but it becomes reasonable for a 10 µm tube.

Results obtained when utilizing a special probe holding ca. 1 cm of a 10 µm fused silica capillary tubing confirmed the calculations. The pressure drop was 50-80 bars for aqueous solutions at 100°C in the 80-100 µL/min range. Higher temperatures would produce a thermospray, but this is not recommended because plugging problems reappear due to the partial inside capillary evaporation process involved in thermospray nebulization. The pressure drop across the capillary

tubing is roughly ten times that across a 10 μm commercial diaphragm, however, it is low enough to allow the coupling of most HPLC system delivering a solution at ca. 100 μL/min, and the cost of the tubing is negligible.

An other modification to the Nermag ion source was the replacement of the repeller assembly, which is never used for LC/MS operations, and the insertion in its place of a small volume which can be easily changed for removal of source contaminations.

The new LC/MS interface provides the same basic analytical performance as our previous system, but with added reliability and full sample utilization, as tested when running thermally labile samples including ampicillin and penicillamin. A mass spectrum of 5 μg of tetrabutyl ammonium bromide was recorded with the filament turned off, and only showed the signal for the intact cation. The sample was in solution in a 50:50 acetonitrile : 10^{-2}M ammonium acetate buffer at 120°C, i.e. well below the temperature of the thermospray onset. We assume that the recording was made possible by the volatility of the salt, which we presume to be higher than generally estimated.

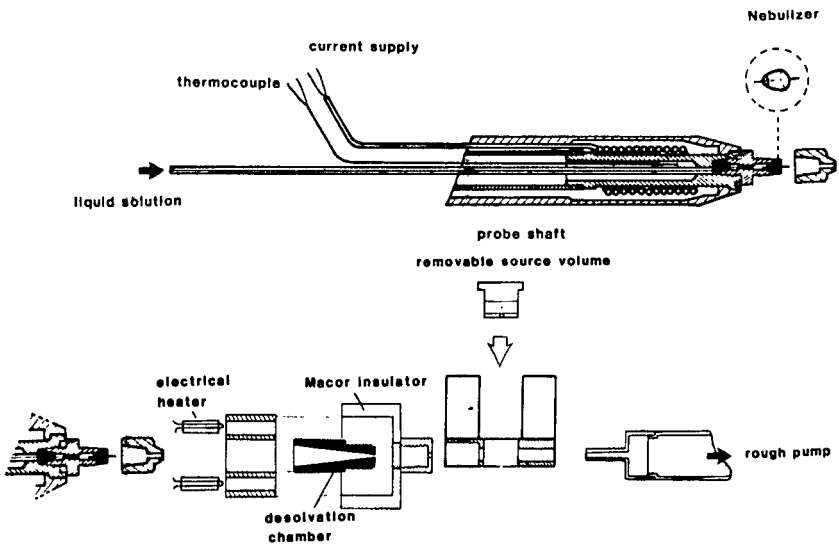

Schematic Diagram of The DLI interface

1) Arpino, P.J. ; Krien, P. ; Vajta, S. ; Devant, G. J. Chromatogr. 1981, 203, 117.
2) Blakley, C.R. ; Vestal, M.L. Anal. Chem. 1983, 55, 750.

ANALYSIS OF POTENT MUTAGENS IN BROILED FISH BY COMBINED LIQUID CHROMATOGRAPHY-THERMOSPRAY MASS SPECTROMETRY. C. G. Edmonds, S. K. Sethi, J. A. McCloskey, Departments of Medicinal Chemistry and Biochemistry, University of Utah, Salt Lake City, Utah, U.S.A.; Z. Yamaizumi, H. Kasai and S. Nishimura, National Cancer Center Research Institute, Tokyo, Japan.

Since the report in 1979 by Sugimura and co-workers (1) of bacterial mutagenic activity in the charred surface of cooked fish and meat in excess of what may be accounted for by benzo[a]pyrene content, some 15 heterocyclic amines responsible for this activity have been identified (2,3). These compounds arise from the pyrolysis of amino acids and proteins during the browning process at high and also at more moderate temperatures in cooking. The assessment of risk of the chronic ingestion of such compounds of high biological activity is a topic of major scientific and public health interest.

Figure 1 summarizes the structures, molecular weights and mutagenic activities of a collection of nine mutagenic heterocyclic amines examined by combined liquid chromatography-thermospray mass spectrometry.

ACRONYM	STRUCTURE	R	MW	REV/µg *
TRP-P-1	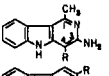	CH_3	211	3.9×10^4
TRP-P-2		H	197	104×10^6
A-α-C	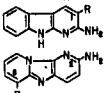	H	183	3×10^2
ME-A-α-C		R	197	2×10^2
GLU-P-1		CH_3	198	4.9×10^4
GLU-P-2		H	184	19×10^3
		R_1 R_2 X		
IQ	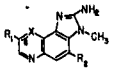	H H CH	198	4.33×10^5
ME-IQ		H CH_3 CH	212	6.6×10^5
ME-IQ_x		CH_3 H N	213	145×10^5

Figure 1. Mutagenic heterocyclic amines from cooked foods.

* Mutagenicity in S. typhimurium TA98 assay.

Table 1 presents the liquid chromatographic, UV absorbance and mass spectrometric behavior of these compounds. Separations are carried out on 4 x 300 mm 10µ µBondapak C-18 or 4.6 x 70 mm 3µ Ultrasphere ODS columns employing 0.1 ammonium formate or acetate (pH 4.8-5.6) buffers in the mobile phase. Peak shapes of these strong bases are improved by the use of 0.02 M diethylamine or triethylamine as competing base in the mobile phase and useful selectivity is obtained using a mixed organic modifier of 4/1 CH_3CN and MeOH (20-40%, isocratic conditions). Thermospray mass spectra under all conditions examined consist exclusively of protonated molecular ions.

COMPOUND	MOL. WT.	k'[a]	RA[b]	MH^+(%)[c]	OTHER IONS, m/z(%)
IQ	198	1.30	83.3	199(100)	
ME-IQ	212	1.37	48.9	213(100)	
GLU-P-2	184	1.37	45.4	185(100)	64(1.5)
GLU-P-1	198	1.48	32.5	199(100)	88(1)
TRP-P-2	197	1.82	147.6	198(100)	
TRP-P-1	211	1.96	180.7	212(100)	
A-α-C	183	2.41	38.3	184(100)	
ME-A-α-C	197	3.22	32.5	198(100)	

[a] LC CONDITIONS 300 x 4.0 cm WATERS µBONDAPAK C-18, A:D 1M AMMONIUM FORMATE, 0.01M DIETHYLAMINE, pH 4.85, B: CH_3CN/CH_3OH (4:1), ISOCRATIC A/B (3:2); FLOWRATE 1.5 ml/min; t_D = 1.06 min.

[b] RATIO OF ABSORBANCE AT 254 AND 280 NM.

[c] THERMOSPRAY IONIZATION WITH ABOVE MOBILE PHASE, VAPORIZER TEMP. 275°C

Table 1. LC, UV absorbance and thermospray MS data for eight mutagenic heterocyclic amines.

The quantification of three of these compounds 2-amino-3-methylimidazo-[4,5-f]quinoline (IQ), 2-amino-3,4-dimethyl-imidazo[4,5-f]quinoline (Me-IQ), and 2-amino-3,8-dimethylimidazo[4,5-4]quinoxaline (Me-IQ_x) in broiled fish is of particular interest. A preliminary experiment on sardine is shown in Figure 2. Acid-base partition of an MeOH extract of whole cooked flesh yields a mutagenically active basic fraction. A SIM experiment on 100µg of extract broiled sardine extract (A) and standard addition experiment for 100µg of extract with 1ng IQ (B) are shown. Point of elution of IQ is marked by arrows. In Figure 2-A, no significant responses are observed for IQ or Me-IQ (4.5 and 6.6 min, resp., Figure 2-A). As both compounds show comparable limits of detection, this standard addition experiment allows us to set an upper limit on the amount of mutagens of a few tenths of a nanogram per 100 µg; this result is significant in being nearly two orders lower than that suggested by mutagenicity assays.

A second experiment employing 3-[$^2H_3$]methyl-analogs of IQ and Me-IQ as internal standards is shown in Figure 3; 3.8mg of an extract of broiled salmon is spiked with internal standards and subjected to preliminary chromatography on trisulfo-Cu-phthalocyanine/cellulose. 115µg of the extract is injected and ions for natural and labeled IQ (m/z 199 and 202) and Me-IQ (m/z 213 and 216) are monitored. Ratios of responses are seen, which indicate levels of 48ng and 92ng of IQ and Me-IQ in the original extract. Yamaizumi and Nishimura have already demonstrated the utility of EI-MS and GC/MS in the analysis of these underiva-

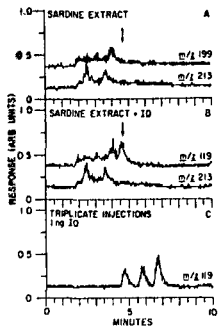

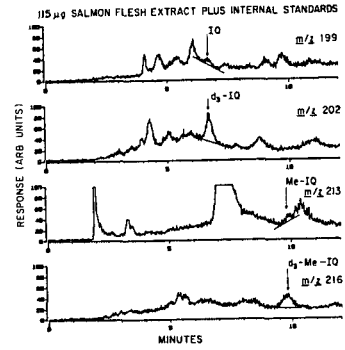

Figure 2. (upper left) SIM experiment on 100µg of extract of broiled sardine extract (A) and standard addition experiment for 100µg of extract with 1ng IQ (B). Triplicate injections of 1ng IQ at one minute intervals shown in C. LC conditions: Waters µBondapak C-18, 1.5ml/min, 0.1M NH_4OAc, 0.02M DEA (pH 5.6) 20% 4/1 CH_3CN:MeOH.

Figure 3. (upper right) Stable isotope dilution experiment on basic extract of broiled salmon flesh. LC conditions: as Figure 2, TEA in mobile phase.

tized compounds from similar sources (2). However, these and quantitative methods of other workers (4) require laborious multi-step purification to separate the compounds of interest from large quantities of interfering sample matrix. The sensitivity and selectivity of combined liquid chromatography-thermospray mass spectrometry offer the prospect of significant simplification and expedition of the analysis of these materials in crude samples.

A schematic of the vaporizer and ion source configuration currently in use is shown in Figure 4. Vaporization is by a direct heating of the interface capillary using an appropriate controlled AC power supply (4) according to a principle first described by Ferguson and Vestal (5). Additionally, a probe assembly formerly employed to close the side port of the ion source has been altered to a geometry which optimizes velocity and pressure of the flowing stream at the point of ion sampling. The application of potentials of 30-60v to this isolated assembly serves to improve the transmission of ions through the sampling aperture for analysis. The effect of these elaborations has been to improve sensitivity, controllability and stability of instrument operation.

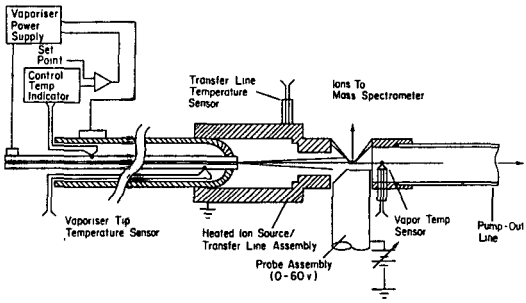

Figure 4. Vaporizer/ion source configuration of combined liquid chromatography-thermospray mass spectrometer.

(1) T. Sugimura, et al., in Origins of Human Cancer, H. H. Hiatt, J. D. Watson and J. A. Winsten, eds., Cold Spring Harbor Laboratory, 1977, pp. 1561-1577.
(2) S. Nishimura and Z. Yamaizumi, Shitsuryo Bunseki, 29(2) (1981) 151-60 and references therein.
(3) M. W. Pariza, Food Technol., 36 (1982) 53-56 and references therein.
(4) For example, W. A. Hargraves and M. W. Pariza, Cancer Res., 43 (1983) 1467-1472.
(5) G. J. Ferguson, unpublished design.
(6) G. J. Ferguson and M. L. Vestal, 31st Ann. Conf. Mass Spectrom. and Allied Topics, Boston, 1983, pp. 609-610.

An Improved Thermospray LC/MS System for Determining Drugs in Urine, Jack Henion, Jonathan Crowthers and Thomas Covey, Equine Drug Testing and Toxicology, Cornell University, 925 Warren Drive, Ithaca, NY 14850

Thermospray LC/MS continues to elicit considerable interest due to the progress reported by Vestal (1). Commercial availability and the reported ease (1) of carrying out thermospray LC/MS has generated a lot of excitement in potential LC/MS markets including the pharmaceutical industry, drug metabolism research, environmental toxicology and industrial chemicals. We have explored the realistic capabilities of thermospray LC/MS by integrating the technique into our existing DLI LC/MS research program. Several changes have been made from our earlier report (2) and these improvements are described in this work.

Experimental

The commerical GC/MS instrument utilized in this work was a Hewlett-Packard Model 5985B. A half inch od. stainless steel pump out line was connected to a 300 L/min Alcatel rough pump with an in-line isolation valve. This thermospray pump out line was equipped with a one-eighth in. stainless steel thermocouple tube which reached through the pumpout line to the ion source chamber to facilitate monitoring the source pressure. An in line liquid nitrogen cryotrap of approximately three liter capacity was installed in series between the thermospray ion source and the thermospray rotary pump. This cryotrap is very useful for protecting the rotary pump from the excess solvent pumped through the thermospray ion source.

The thermospray LC/MS interface developed for this work was similar to our previous design(2). It consists of a ½ in. od. x 3/8 in. id. stainless tube threaded to a heated, copper vaporizer through which a 0.004 in. id. x 0.062 in. od microbore stainless steel tube is silver soldered. The vaporizer was equipped with two 50 watt 1/8 in. x 1 in. cartridge heaters and a 1/16 in diameter iron-constantine thermocouple. The microbore throughput tube of the thermospray probe was connected to the HPLC column via an in-line Valco 0.2 micron filter union. The ion source end of the vaporizor did not contain the removeable threaded end - cap and diaphragm reported earlier, Figure 1 shows the construction details of the new version direct insertion thermospray probe LC/MS interface.

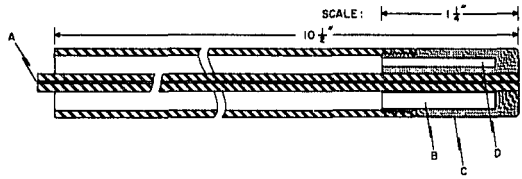

FIGURE I

The biggest change in this thermospray system from our earlier report is the construction of an independent thermospray ion source. Rather than modify the standard HP CI source, a standard HP 5985B source block was drilled out in the solid probe-GC axis to 0.500 in. A removable cylindrical tube of 0.375 in id was inserted through this half-inch hole. This cylindrical "thermospray ion source" was equipped with an ion exit cone as described by Vestal (1) and a 0.500 in id extended desolvation chamber to accommodate the removeable thermospray probe. The thermospray pump out line on the exit side of the source was retained to remove the excess LC solvent vapors. Because this arrangement precluded excessive solvent vapors entering the analyzer region of the quadrupole, the standard DLI cryopump positioned above the ion source was not required. This system produced thermospray ionization the first time it was used and has been operating routinely for several months.

Results and Discussion

This revision of our original thermospray system was a significant improvement with regard to routine operation and sensitivity. It was operated in most cases at 1.4 mL/min with 50/50 methanol/0.1M ammonium acetate and never failed to produce ions from adenosine or 1-methylcystosine in the thermospray ionization (filament off) mode. Sensitivity occasionally deteriated with use, but could be regained by simple electropolishing or cleaning of the thermospray ion exit cone.

A wide variety of drugs and biological extracts have been analyzed. These include studies of pesticides, ibuprofen, phenothiazine tranquilizers, bumetanide, antibiotics and corticosteroids . Figure 2 shows, for example, the LC UV (upper) and thermospray LC/MS (lower) traces for the analysis of a crude equine urine extract resulting from the enzyme hydrolysis of a urine collected four hours post administration of the recommended dose of

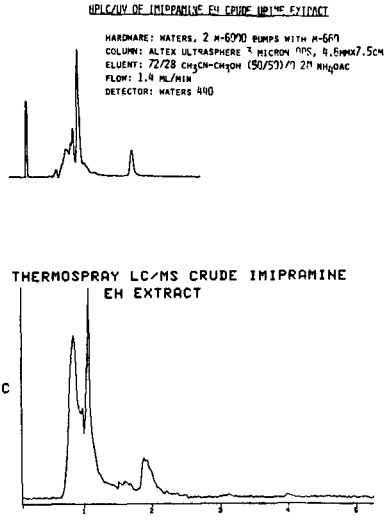

FIGURE II

imipramine. Two polar metabolites are observed in both sets of data which elute at 1.1 and 1.9 min respectively under the LC conditions denoted in Figure II. Control experiments indicated that the five microliter injection of organic extract contained about 25 ng of the minor metabolite observed at the 1.9 min retention time. Thus one can see that the thermospray TIC nicely duplicates the UV chromatogram and, in addition, provides a positive ion chemical ionization (PCI) mass spectrum for each imipramine metabolite in less than three minutes. Unfortunatley, the thermospray PCI mass spectra show only the (M+1) ions with little or no structurally useful fragment ions.

1. C.R. Blakely and M.L. Vestal, Anal. Chem., 1983, 55, 750-754.

2. T. Covey and J.D. Henion, Anal. Chem., 1983, 55, 2275-2280.

High Performance Gradient LC/MS Using Microbore Columns With A Moving Belt Interface

M. J. Hayes, H. E. Schwartz, Paul Vouros, R. L. Karger, Barnett Inst. of Chemical Analysis, and Dept. of Chemistry, Northeastern Univ., Boston MA, 02115
A. D. Thruston Jr., and J. M. McGuire, Athens Environmental Research Laboratory, U. S. EPA Athens GA 30613

Introduction

Recently we published an extensive study on the use of spray deposition, first reported by Smith and Johnson (1), for the optimization of the chromatographic performance of the moving belt LC/MS interface (2). It was shown that it is possible to perform on-line LC/MS with normal bore columns (4.6 mm i.d.). However, some difficulties remained in the handling of high water content mobile phases at flow rates commonly encountered for normal bore columns. In this work we have extended the moving belt spray deposition approach for use with microbore columns.

Experimental

For microbore HPLC/MS, our previously developed nebulizer was modified by the addition of a new transfer line assembly and spray tip (see Figure 1). The transfer line (A in Figure 1), made from a 0.009 in. o.d. by 0.0045 in. i.d. stainless steel tube (Hamilton, Reno NV), was connected to the outlet of the LC column via a modified capillary column butt connector (Supelco, Bellefonte, PA). The gas orifice was made by fusing two pieces of glass together, one of 1.5 mm o.d. by .75 mm i.d. tubing (E in Figure 1) and the other, which served simply as a holder, of 1/4 in. o.d. by 1/8 in. i.d. glass tubing (H in Figure 1). Other details were as found in reference (2).

Results and Conclusions

We have found that using this nebulizer, LC/MS can be performed with high performance microbore columns over a wide range of flow rates and gradient conditions. The use of microbore flow rates allows for a much simpler operation of the spray deposition method than was possible with our previous design for conventional columns. Extracolumn variance can be reduced to below the level of a typical UV detector equipped with a microbore flow cell, thus allowing the use of relatively short 5-um and 7.5-um microbore columns. Figure 2 shows a comparison of an LC/UV chromatogram (Kratos 773 detector with a 0.5 uL cell) with the corresponding LC/MS trace. It can be seen that the LC/MS trace demonstrates excellent chromatographic performance. Accurate determination of efficiency shows that the LC/MS trace yields a 35% greater theoretical plate count for the first peak. It was possible to run full range gradients (0-100% acetonitrile in water) at flow rates up to 40 uL/min without having to alter the nebulization conditions during the course of the run. During the course of the gradient no measurable changes were seen in the extracolumn variance determined for the interface. At higher flow rates small changes in the nebulization conditions must be made in order to minimize extracolumn effects when performing full range gradients. The transfer efficiency to the belt was found to be high under a variety of mobile phase conditions. This is an important consideration when gradient chromatography is being conducted. Spray deposition allows the use of microbore columns either at optimum flow rates for maximum resolution or at higher flow rates for fast analysis times and improved sensitivity. While direct deposition onto the belt without nebulization is possible, the wider flow rate and solvent composition ranges available with spray deposition make the latter approach one of greater flexibility and ease of operation.

The utility of this LC/MS approach was demonstrated by the analysis of phenols in a coal gassifier condensate sample. Detection limits at the low nanogram level were obtained for full scan, on line LC/MS. The importance of the availability of LC/EI-MS was shown since this technique was necessary in elucidating the structure of the unknown species present in the sample.

This work has shown that microbore LC can be utilized with the moving belt interface by using spray deposition. It allows high resolution chromatographic conditions to be effectively used in conjunction with on line MS detection.

References

1) Smith R. D., Johnson, A., Anal. Chem. 1981, 53, 739
2) Hayes, M. J., E. P. Lankmayr, Paul Vouros, B. L. Karger, J. M. McGuire, Anal. Chem. 1983, 55, 1745

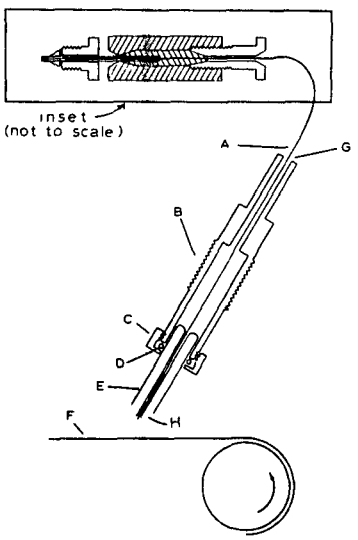

Figure 1. Diagram of spray deposition device A) transfer line; B) body of spray device; C) retaining cap; D) O-ring; E) nebulizer holder; F) moving belt; G) gas inlet; H) nebulizer tip. Inset shows zero volume connector.

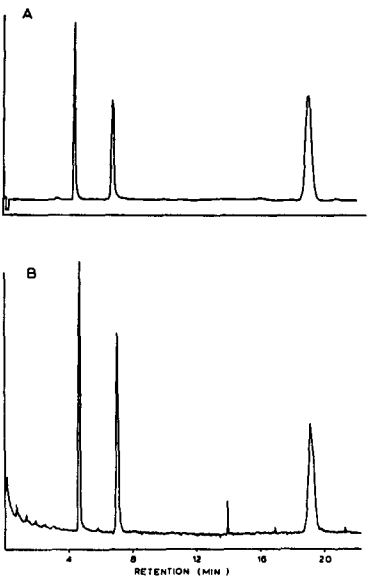

Figure 2. Comparison of UV and MS chromatograms using a 5um microbore column: 250 x 1 mm, Supelcosil C18; Solutes: resorcinol, 1,5-dihydroxynapthol, and 2-methylphenol; flow rate 40 uL/min; mobile phase, 41% acetonitrile, 59% water, 0.1%trifluoroacetic acid added. A) LC/UV B) LC/MS

NEW DEVELOPMENTS IN HIGH PERFORMANCE CAPILLARY SUPERCRITICAL FLUID CHROMATOGRAPHY - MASS SPECTROMETRY[a]

R. D. Smith, B. W. Wright and H. R. Udseth
Chemical Methods and Kinetics Section
Pacific Northwest Laboratory
(Operated by Battelle Memorial Institute)
Richland, WA 99352

The advantages of supercritical fluid chromatography (SFC) accrue from the nature of supercritical fluids. The solvating properties of supercritical fluid mobile phases approach those of liquid phases, yet solute diffusivity typically remains one to two orders of magnitude higher. These properties allow high separation efficiencies to be realized while exploiting the variable and sometimes high solvating power of the supercritical fluid. Consequently, SFC has the capability of separating thermally labile and nonvolatile solutes not possible with gas chromatography and with higher efficiencies than liquid chromatography.

With the development of small diameter (~ 50 μm) fused silica capillary columns coated with crosslinked and nonextractable stationary phases, high resolution separations with efficiencies approaching those of conventional capillary gas chromatography have been obtained. In capillary SFC the solvating power of the fluid can be accurately controlled allowing samples of a wide molecular weight or polarity range to be eluted in a similar fashion to temperature programming in gas chromatography or gradient elution in liquid chromatography.

The introduction of the total chromatographic effluent into the mass spectrometer can be accomplished through the direct fluid injection (DFI) interface. The coupling of capillary SFC with mass spectrometry offers significant advantages over existing HPLC-MS combinations. Supercritical fluids also offer advantages for transport of thermally labile compounds to the ion source since heating is not required for volatilization. Most SFC mobile phases also exhibit higher volatility than liquids which provides a significant advantage in the design of the SFC-MS interface. The DFI process provides for transfer of solutes in the supercritical fluid to the gas phase, so that conventional ionization methods can be used while also avoiding the matrix effects and uncertainties associated with desorption from surfaces. Additionally, ion clustering effects are minimized with spectra showing no evidence of clusters other than that typically observed for chemical ionization.

Three major developments in capillary SFC-MS serve to provide significant advantages compared to HPLC-MS techniques. These include:

1. The development of nonextractable deactivated, bonded, and crosslinked stationary phases for very small diameter fused silica capillary columns (~ 50 μm). These columns are useful for many nonpolar or less polar fluids and provide more than 3000 plates per meter. Nearly 100,000 effective plates can be generated in less than one hour. This high efficiency is enhanced further by the pressure programming capability of capillary SFC-MS.

2. The development of new rapid pressure programming methods for capillary SFC-MS allows high speed separations with enhanced sensitivity for mass spectrometric analysis.

3. The development of a DFI interface for electron impact ionization now allows total flexibility in selection of ionization method for SFC-MS. Nearly comparable detection limits can often be obtained using a new interface design allowing electron impact ionization.

The high resolution and fast separation methods are compared in the Figure on the next page which shows separations obtained for a coal tar extract on (A) 15m x 50 μm column and (B) a fast separation on a short 1.75m x 50 μm column with a rapid pressure program rate of 50 bar/min. This work serves to demonstrate the versatility of the capillary SFC-MS approach.

a. Work supported by the U.S. Department of Energy Office of Health and Environmental Research under Contract DE-AC06-76RLO-1830.

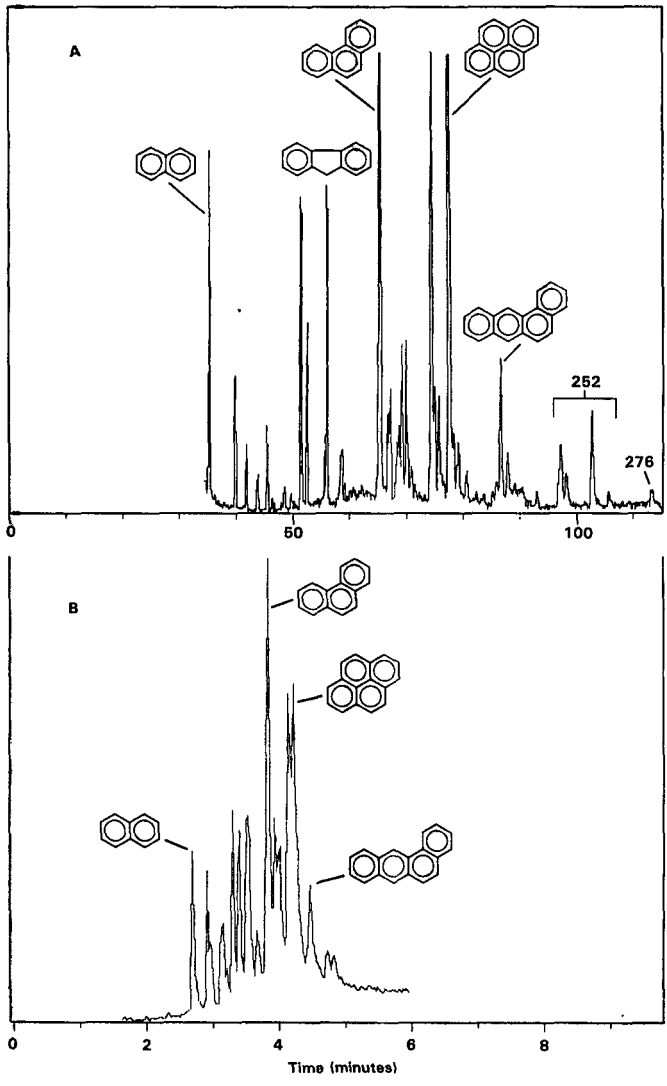
A
252
276
0
50
100
B
0
2
4
6
8
Time (minutes)

TOD 1 STUIDES ON THE CHEMISTRY OF TRANSITION METAL CLUSTERS USING FOURIER TRANSFORM MASS SPECTROMETRY

DONNAJEAN ANDERSON

DEPARTMENT OF CHEMISTRY

TEXAS A&M UNIVERSITY

COLLEGE STATION, TX 77843

Transition metal clusters have long been considered an important key in the understanding of surface catalysts. However, the mechanistic aspect of these reactions have proven elusive. More detailed characterization of the chemical and physical properties of transition metal clusters is due, in part, to the development of new experimental techniques which permit studies at the molecular level. A major emphasis of our research program involves the ion-molecule chemistry of gas-phase transition metal clusters using Fourier transform mass spectrometry (FTMS). The FTMS technique is highly useful for studies on the chemical reactivity of the clusters because (1) reaction sequences can be followed unambiguously using ion ejection techniques; and (2) interferring ion-molecule reactions can be minimized by using pulsed valve sample introduction.

Ion ejection, coupled with temporal plots, has been used to determine reaction sequences of the chromium, iron, cobalt, and nickel carbonyl systems. For the reaction of Co^+ with $Co(CO)_3(NO)$, the experimental sequence is as follows: 1) ionization of $Co(CO)_3(NO)$ by electron impact, 2) ejection of all ions except Co^+, and 3) introduction of a time-delay between 25 and 800 msecs allowing ion-molecule reactions to occur. The reaction sequence for the $Co^+/Co(CO)_3(NO)$ is given in Scheme I. The reaction of the $Co(CO)^+$, $Co(CO)_2^+$, and $Co(CO)_2(NO)^+$ ions with $Co(CO)_3(NO)$ were also studied in a similar manner.[1]

A highly interesting aspect of the data is the product ions are formed by a specific reaction sequence, i.e., the products formed by Co^+ differ from those formed by $Co(CO)_x^+$. In particular, the different reactant ions give rise to product ions of different coordination unsaturation; that is, the metal-to-ligand (M/L) ratio is relatively large, in some cases, M/L = 1. (According to Muetterties, to mimic a metal surface, a metal cluster should have a M/L ratio of 1.[2]) The difference in the product ions produced, coordination unsaturation of the cluster fragment ions, is illustrated in Figure 1. We then selected the most unsaturation cluster ions for further study.

Owing to the reactivity of the metal ionic systems with the neutral metal carbonyl, pulsed valve sample introduction of the non-metal reactant is essential to these studies.

Using the methods described, the reaction of $Co_2(CO)_3(NO)^+$ with H_2/D_2 was studied. After ionization of $Co(CO)_3(NO)$, the $Co(CO)^+$ ion was mass-selected by ion ejection, and the allowed delay introduced to react this ion with $Co(CO)_3(NO)$ to produce $Co_2(CO)_3(NO)^+$. The $Co_2(CO)_3(NO)^+$ ion was then mass-selected , again by ion ejection, followed by hydrogen introduction into the analyzer. A reaction time of 100 msecs was employed for the reaction of $Co_2(CO)_3(NO)^+$ with H_2. The data from this experiment is consistent with elimination of C_2H_2 from the collision complex, e.g., $[Co_2(CO)_3(NO)\cdot H_2]^*$ (m/z = 234). This proposed reaction is further supported by the observed peak at m/z = 208 in the mass spectrum corresponding to a loss of 26 (C_2H_2) from the collision complex. A proposed mechanism for this reaction is given in Figure 2.[3] A similar reaction is observed for the $Co_3(CO)_2(NO)_3^+$ ion, however, the results are more speculative and further studies are required.

[1]DJ. Anderson and D. H. Russell, unpublished results.

[2]E. L. Muetterties, T. N. Rhodin, E. Bond, C. F. Brucker, and W. R. Pretzer. Chem. Rev., 79, 91, (1979).

[3]This reaction mechanism was formulated by information obtained in "Some Reactions of Metal Clusters", A. J. Deeming, Chapter VI, Transition Metal Clusters, B. F. G. Johnson, ed.

SCHEME I

$$Co^+ + Co(CO)_3(NO) \longrightarrow Co_2(CO)_2(NO)^+$$

$$Co_2(CO)_2(NO)^+ + Co(CO)_3(NO) \longrightarrow Co_3(CO)_2(NO)_2^+$$

$$Co_3(CO)_2(NO)_2^+ + Co(CO)_3(NO) \longrightarrow Co_4(CO)_3(NO)_3^+$$

$$Co_4(CO)_3(NO)_3^+ + Co(CO)_3(NO) \longrightarrow Co_5(CO)_4(NO)_4^+$$

$$Co_5(CO)_4(NO)_4^+ + Co(CO)_3(NO) \longrightarrow Co_6(CO)_6(NO)_5^+$$

$$Co_6(CO)_6(NO)_5^+ + Co(CO)_3(NO) \longrightarrow Co_7(CO)_7(NO)_5^+$$

$$Co_7(CO)_7(NO)_5^+ + Co(CO)_3(NO) \longrightarrow Co_8(CO)_8(NO)_6^+$$

FIGURE 1

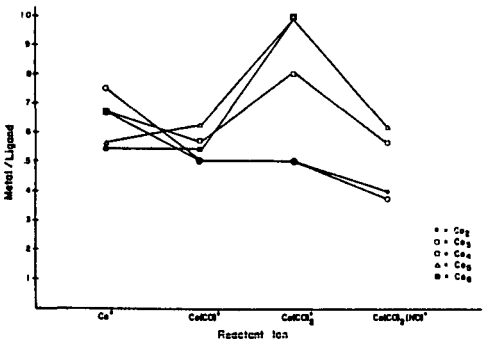

FIGURE 2

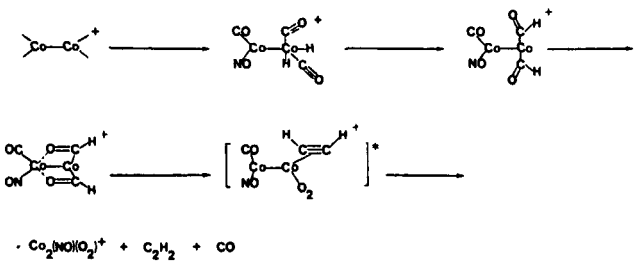

FLOWING AFTERGLOW STUDIES OF OXIDATION AND REDUCTION REACTIONS OF TRANSITION METAL CARBONYLS

Kelley Lane, Larry Sallans and Robert R. Squires
Department of Chemistry
Purdue University
West Lafayette, IN 47907

As part of a general program of study of gas phase transition metal ion chemistry using the flowing afterglow technique, we have recently investigated the reactions of dioxygen with a series of mononuclear metal carbonyl anions along with several binary hydride transfer reactions of neutral metal complexes.

Our experiments were carried out at 300K in a flowing afterglow apparatus recently constructed in our laboratories at Purdue[1]. Briefly, primary reactant ions produced by electron impact are carried the length of a 1 m x 7.3 cm i.d. flow reactor by a fast flow of helium buffer gas ($\bar{v}$(He) = 90 m/s) maintained at a variable pressure of 0.1 - 1.0 torr by a Roots blower. Ion-molecule reactions are initiated by introducing reactant gases into the flowing plasma through any of six fixed inlets located along the flow tube or via a moveable neutral injector. Either positive or negative ions are sampled from the reactor through a small orifice for analysis and detection by a quadrupole mass spectrometer. Binary rate coefficients and branching ratios for ion-molecule reactions are determined by standard techniques with an estimated accuracy of ±20% and ±5%, respectively.

Oxidation of Transition Metal Carbonyl Anions[2]

Molecular metal oxides have provided a key source of fundamental information on oxidation state stabilities, metal-oxygen bonding and catalytic oxidation mechanisms. We have observed the formation of several novel examples of molecular metal oxide anions from reactions between metal carbonyl anions and $^3\Sigma_g O_2$ (eq. 1)

$$(1) \qquad M(CO)_n^- \xrightarrow{O_2} M(CO)_x O_y^- \qquad M = Fe, Cr, Mo, W, Mn, Co;\ n = 4, 5;\ x = 0\text{-}4;\ y = 1\text{-}5$$

Extensive, albeit slow, oxidation of the 17-electron anions $Fe(CO)_4^-$, $Cr(CO)_5^-$, $Mo(CO)_5^-$ and $W(CO)_5^-$ occurs to yield an interesting array of mononuclear metal carbonyl oxides and polyoxide anion products. The measured primary product distributions expose marked differences among these anions with respect to product selection. For example, while $Fe(CO)_4^-$, $Cr(CO)_5^-$ and $W(CO)_5^-$ each yield mainly a monoxide anion by O_2 addition followed by loss of CO_2 and one CO, $Mo(CO)_5^-$ produces a roughly equal mixture of dioxides $Mo(CO)_3O_2^-$ and $Mo(CO)_4O_2^-$. At higher O_2 flow rates, most of the primary products react further to give sets of less reactive polyoxides, MO_x^-, x = 2-5. Noteable exceptions are $Fe(CO)_3O_2^-$, $Cr(CO)_3O_2^-$ and $W(CO)_4O_2^-$ which appear to be relatively inert towards further reaction with O_2. The radical nature of the primary oxidation mechanism is illustrated by lack of reactivity exhibited by the closed-shell, 18-electron species $Mn(CO)_5^-$ and $Co(CO)_4^-$. Preliminary results indicate that several of the metal oxide anions are remarkably reactive. For example PF_3 undergoes extensive oxidation and ligand transfer in the presence of the iron polyoxide anions (eq. 2)

$$(2) \qquad FeO_{2,3,4}^-;\ Fe(CO)_3O_2^- \xrightarrow{PF_3} PO_2^-,\ PO_3^-,\ F_2PO_2^-,\ FeF_3^-,\ FeF_4^-$$

Hydride Addition to Transition Metal Carbonyls[3]

Metal hydrides and formyls are key intermediates in industrially important catalytic processes for CO reduction and hydrocarbon synthesis. We have generated several simple examples of these species in the gas phase by direct H^- addition and binary hydride transfer reactions with $Fe(CO)_5$ and other metal carbonyls. Hydride undergoes an exceedingly rapid reaction with $Fe(CO)_5$ at 0.4 torr reactor pressure to yield hydridoiron carbonyl anion products in which one and two CO ligands have been expelled (eq. 3).

$$(3) \qquad H^- + Fe(CO)_5 \xrightarrow{k = 1.8 \times 10^{-8}\ cc/s} \begin{cases} \xrightarrow{50\%} HFe(CO)_4^- + CO \\ \xrightarrow{50\%} HFe(CO)_3^- + 2CO \end{cases}$$

Subsequent reactions of the hydrides with additional $Fe(CO)_5$ are observed to produce the dinuclear anions $Fe_2(CO)_nH^-$, n = 6-8.

Transfer of H^- to $Fe(CO)_5$ from a variety of anionic reagents is observed to produce the metal formyl and, in some instances, the tetracarbonyl hydride (eq. 4)

$$XH^- + Fe(CO)_5 \longrightarrow \begin{cases} (CO)_4FeCHO^- + X \\ (CO)_4FeH^- + X + CO \end{cases} \qquad (4)$$

By examining the reaction of $Fe(CO)_5$ with a series of hydride donor anions with known heats of formation, we have been able to establish the hydride affinity of $Fe(CO)_5$ as 56.8 ± 3 kcal/mol. From this a heat of formation for $Fe(CO)_4CHO^-$ of -196.6 ± 3.4 kcal/mol may be derived. The observed threshold for appearance of $Fe(CO)_4H^-$ from some of the more exothermic hydride transfers to $Fe(CO)_5$ is in accord with the known heat of formation of $Fe(CO)_4H^-$ of -180 ± 6 kcal/mol.[4]

Qualitative experiments have been performed to determine the reactivity of the metal hydrides and formyls with industrially important small molecules. Most notable is the observation that $Fe(CO)_3H^-$ forms an adduct with CO_2 while $Fe(CO)_4H^-$ does not react. The relationship of these findings to current interests in homogeneous CO_2 activation is also discussed.

References

1. Lane, K.R.; Lee, R.E.; Sallans, L.; Squires, R.R. J. Amer. Chem. Soc. 1984,106,0000.
2. Lane, K. R.; Sallans, L.; Squires, R.R. J. Amer. Chem. Soc. 1984, 106, 2719.
3. Lane. K.R.; Sallans, L.; Squires, R.R. J. Amer. Chem. Soc. submitted.
4. Stevens, A.E.; Beauchamp, J.L. J. Amer. Chem. Soc. in press.

STABLE MOLECULAR IONS ABOVE THE FRAGMENTATION ONSET IN THE BREAKDOWN GRAPH OF HEXACARBONYL CHROMIUM ION.

Pradip R. Das, Toshihide Nishimura and G. G. Meisels,* Department of Chemistry, University of Nebraska, Lincoln, Nebraska, 68588-0304 and Y. Niwa, National Chemical Laboratory for Industry, Tsukuba Research Centre, Yatabe, Ibaraki, 305 (Japan).

The unimolecular dissociation of energetic gaseous ions is usually well described by statistical theories (viz, QET) which assume that ions initially produced in excited electronic states undergo rapid radiationless internal conversion to the ground electronic state from which fragmentation occurs after complete energy randomization. Exceptions have been suggested for some molecules containing a heteroatom (1), and ascribed to non-interconverting states. Most of the work to date has concerned itself with organic molecules. We have chosen hexacarbonyl chromium, $Cr(CO)_6$, for this investigation as an example of an organometallic compound. The onsets of several fragmentation processes of this compound (2) fall in a region between the first and second bands where the HeI PES (Fig. 1) shows very little intensity.

The fragmentation of hexacarbonyl chromium ion, $Cr(CO)_6^{\cdot+}$, was studied by threshold photoelectron-photoion coincidence (TPEPICO) (3) time-of-flight mass spectrometry. Detailed breakdown curves were obtained as a function of ion internal energy from onset to ca. 13 eV above threshold. Fragmentation at photon energies below 12 eV is characterized by 4 fragments, $Cr(CO)_5^+$(m/z 192), $Cr(CO)_4^+$ (m/z 164), $Cr(CO)_3^+$ (m/z 136), and $Cr(CO)_2^+$ (m/z 108) representing 1,2,3 and 4 CO losses from the parent ion, $Cr(CO)_6^{\cdot+}$ (m/z 220). At higher energies (>17 eV), Cr^+ (m/z 52) is the major fragment followed by $Cr(CO)^+$ (m/z 80).

The experimental TOF data at three consecutive photon energies, (Fig. 2) show clearly a substantial increase in parent ion intensity at ~ 11.40 eV which results in a sharp peak of the parent ion abundance in the breakdown graph (Fig. 3). This occurs in the valley between 9 - 13 eV in the PES. In this region fragmentation of the molecular ion occurs also suggesting the involvement of indirect ionization processes and dissociation. We suggest that possibly autoionization occurs in this region. This process produces neutral excited molecules with an energy above the ionization limit which crosses over into the ionization continuum above the dissociation limit of the ground electronic state of the ion with the smallest possible change in vibrational quantum number; therefore the ejected electrons are of almost zero energy. Statistical (QET) dissociation then follows from the ground electronic state. However, at ~ 11.40 eV, over a very narrow energy range, it appears that a more complex process, possibly fluorescence autoionization such as:

$$M + h\nu \longrightarrow M^{**} \longrightarrow M^{*} + h\nu_{fluor.}$$

$$M^{*} \longrightarrow M^{+} + e$$

takes place. In this process, the neutral excited state (Fig. 4) formed initially fluoresces to a level which still retains enough excitation energy to autoionize. But due to the energy lost in fluorescence, $h\nu_{fluor.}$, the internal energy of the molecular ion formed is no longer sufficient for it to dissociate. Since fluorescence is relatively slower ($k_{fluor.} > 10^9$ sec^{-1}) the precursor state must be separated (non-interconverting). Alternate explanations based on ion fluorescence are less probable because neither the HeI PES nor the TPES indicate the presence of a state near 11.40 eV.

Successive losses of CO groups appear to be the main fragmentation routes to ions of lower masses as is apparent from our breakdown graph; metastable studies (V-scan) indicate that Cr^+ is formed primarily from $Cr(CO)^+$ and also direct dissociation from $Cr(CO)_2^+$ makes a minor contribution. This notion is supported by the nature of the increase of Cr^+ in the breakdown graph and the photoionization yield curve of Cr^+ (Fig. 5).

REFERENCES:

1. (a) G. G. Meisels, T. Hsieh and J. P. Gilman, J. Chem. Phys., 73, 4126 (1980)
(b) J. P. Gilman, T. Hsieh and G. G. Meisels, ibid., 78, 1174 (1983).
(c) T. Nishimura, Y. Niwa, T. Tsuchiya and H. Nozoye, ibid., 72, 2222 (1980).
2. (a) R. E. Winters and R. W. Kiser, Inorg. Chem., 4, 157 (1967) (b) D. R. Bidinosti and N. S. McIntyre, Can. J. Chem., 45, 641 (1967).
3. C. Batten, J. Taylor and G. G. Meisels, J. Chem. Phys., 65, 3316 (1976).

PHOTOELECTRON SPECTRUM OF $Cr(CO)_6$ AND BAND ASSIGNMENT

1

Hillier and Saunders, Mol. Phys., 22, 1025 (1971)

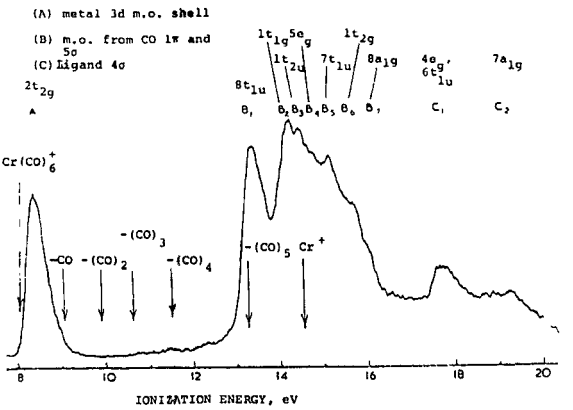

4

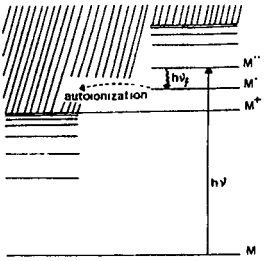

$M + h\nu \longrightarrow M'' \longrightarrow M' + h\nu_{fluor}$

$M' \longrightarrow M^+ + e$

2

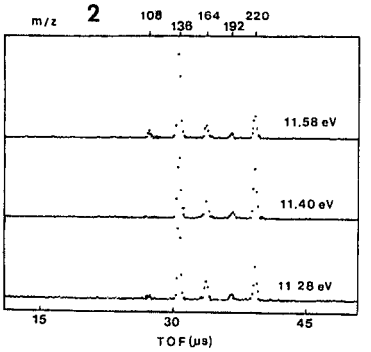

3a

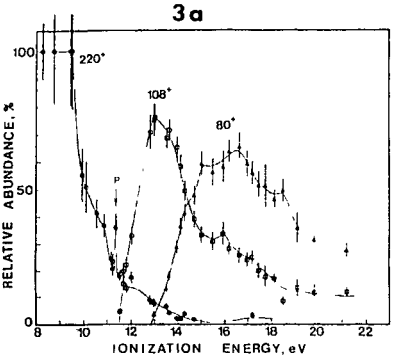

5

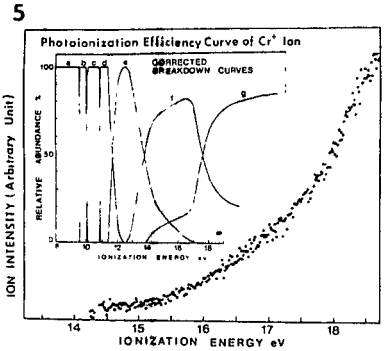

3b

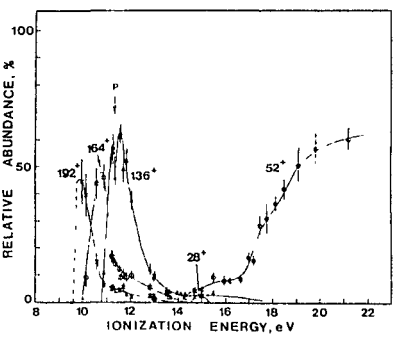

GAS PHASE ION CHEMISTRY AND PHOTOCHEMISTRY OF

GROUP 8 (Fe, Co, Ni) MX^+(X=H, O, S, CH_2, and CH_3)

D. B. Jacobson, C. J. Cassady, T. C. Jackson, and B. S. Freiser, Purdue University, Department of Chemistry, West Lafayette, Indiana USA 47907

Recent developments in our group involving both software and hardware modifications of the Nicolet FTMS-1000 Fourier transform mass spectrometer now enable us to conduct research in what can be properly termed a "complete gas phase chemical laboratory." Selected ions of interest can be mixed with various reagents and their detailed chemistries monitored through a series of as many as eight reaction sequences. At any point in these sequences, ion structures can be elucidated and fundamental kinetic and thermodynamic parameters of the reactions can be determined. One of the areas we are currently examining involves the gas phase chemistry and photochemistry of metal ions, metal clusters, and metal complexes, all of which have a bearing on the fundamentals of catalysis.

Understanding the activation of C-H and C-C bonds by transition metals continues to be one of the most challenging problems in the field of catalysis. Our recent gas phase studies of the reactions of atomic metal ions generated by laser desorption with hydrocarbons represent a method to obtain the inherent reactivity of these ions in the absence of solvent or ligand interferences. Our findings for the group 8 metals, for example, indicate that the order of reactivity is $Fe^+ > Co^+ > Ni^+$ and that, in direct contrast to solution behavior, oxidative insertion into C-C bonds not only occurs but is often the dominant mode of reaction.

A logical extension of this research is to study the effects of small ligands on metal ion reactivity. Thus, we have begun a systematic study on the chemistry of MX^+ where X = H, CH_2, CH_3, C_3H_5, O, S, etc. Illustrative of this work is our study on group 8 hydride ions.

A problem that has delayed the study of gas phase metal hydride reactions is the general difficulty in preparing the metal hydride ion. Metal hydrides can now be formed readily, however, using the complete gas phase chemical laboratory. Reaction of laser desorbed Fe^+, Co^+, and Ni^+ with methyl nitrite yields a methoxy-metal moiety which decomposes by loss of formaldehyde under collisional activation to form the corresponding metal hydride, reaction 1. Using the pulsed valve approach developed in our laboratory, the pressure of reagent gases

$$M^+ + CD_3ONO \xrightarrow{-NO} MOCD_3^+ \xrightarrow[-CD_2O]{CID} MD^+ \qquad (1)$$

can be temporally controlled to eliminate chemical interferences. By combining the remarkable capability to control the ion population in FTMS with this new capacity to control the neutral background, FeD^+, CoD^+, and NiD^+ were synthesized in good yields for gas phase study as shown in the accompanying Figure 1. Spectrum (a) shows the products of the reaction of laser desorbed Ni^+ with methyl nitrite added via the pulsed valve. Argon and 2-methylpropane were present at a constant pressure. $^{60}Ni^+$ was completely ejected immediately after the laser pulse. Ions detected in spectrum (a) are several generations of product ions from the reaction of $^{58}Ni^+$ with methyl nitrite. In spectrum (b) the region from M/z 85-95 has been selected. The resulting mass spectrum after collisional activation of $NiOCD_3^+$ (M/z 92) is shown in spectrum (c). The NiD^+ is isolated (spectrum d) and then reacts with 2-methylpropane for 500 msec to produce the charged products in spectrum (e). Note that there is still sufficient intensity in spectrum (e) for subsequent experiments to be performed. The results from these studies indicate that metal hydrides activate C-H bonds in contrast to the bare metal ions which activate C-C bonds. Furthermore the order of reactivity, $NiD^+ > CoD^+ > FeD^+$ contrasts sharply with the bare metal ion reactivity and emphasizes the complexity of the nature of catalysis and underlines the possibility of fine tuning catalytic processes through an improved understanding of the fundamentals.

Using the techniques described above to generate and isolate MX^+, we have also begun to study the totally unexplored area of photodissociation spectroscopy on MX^+. Using photodissociation, information about the geometric and electronic structure of these species may be obtained as well as useful upper limits on metal-ligand bond energies. Figure 2 shows some of our first results on FeX^+ ions. As can be seen from the figure, the spectra of the ions are remarkably similar with each having absorption maxima at 290 ± 10 nm and 335 ± 10 nm. Both $FeCO^+$ and $FeC_2H_4^+$ absorb at longer wavelengths, however, while $FeOH^+$ cuts off at 390 nm. The results suggest an upper limit of $D(Fe^+-CO)<43$ kcal/mol and $D(Fe^+-C_2H_4)< 43$

kcal/mol, and an absolute value of $D(Fe^+ - OH) = 73 \pm 3$ kcal/mol.

Finally, we have also recently developed methods for generating subtituted metal cluster ions, M_nX^+ (n = 2-5). We believe these techniques will be extended to higher order clusters.

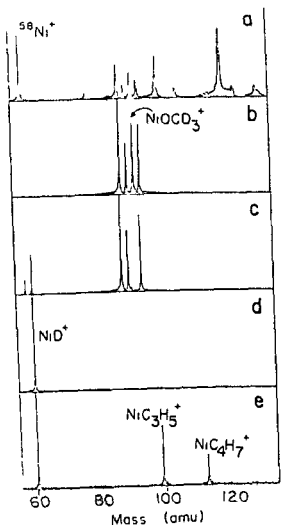

Figure 1

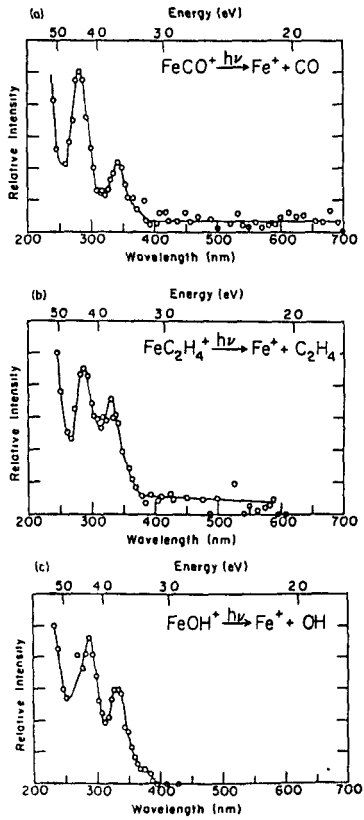

Figure 2

1. T. J. Carlin, L. Sallans, C. J. Cassady, D. B. Jacobson, and B. S. Freiser, J. Am. Chem. Soc., 105, 6320 (1983).

2. T. Jackson, D. B. Jacobson, and B. S. Freiser, J. Am. Chem. Soc., 106, 1252 (1984).

3. T. J. Carlin and B. S. Freiser, Anal. Chem., 55, 571 (1983).

ORGANOMETALLIC CHEMISTRY IN THE GAS PHASE: ION/MOLECULE REACTIONS OF TRANSITION METAL IONS WITH AMINES. S. Babinec*, J. Harrison, J.Allison, Department of Chemistry, Michigan State University, East Lansing, MI 48824

In the past several years, a number of papers in the area of gas phase organometallic chemistry have appeared. A prominent mechanism has been the (i) metal insertion, (ii) β-H shift, (iii) competitive ligand loss sequence, reaction (1).

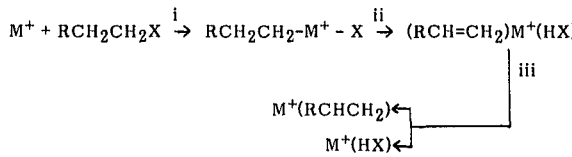

One goal of such work is to sufficiently understand the three mechanistic steps such that product distributions could be predicted. Currently, the relative amounts of products in step (iii), the competition ligand loss, can be "predicted" based on the relative metal ion affinities for the species HX and $RCHCH_2$. These parallel proton affinities. In cases leading to an insertion intermediate of the type $R\text{-}M^+\text{-}R'$, where both R- and R' contain H atoms on C which are β- to the metal, there are also trends concerning which β-H shift is more probable. For example, an examination of the work done to date suggests that a β-H shift from a propyl group is more likely than that from an ethyl group, etc. That is, we can predict what will happen following metal insertion, however, in compounds in which an ion such as Co^+ can insert into a number of skeletal bonds (e.g., alkanes), no attempt has been made to understand when and why certain bonds are selected for attack. This paper discusses the metal insertion step.

One can provide insights into the metal insertion process by identifying reactivity trends for the first row transition metal ions. It has been pointed out that, in the case of alkanes, Fe^+ is indiscrimate in inserting into C-H or C-C bonds, Ni^+ is more selective and Co^+ is intermediate. Mn^+ and Cr^+ are unreactive with alkanes. We observe similar behavior with amines. In the reactions of transition metal ions with n-propylamine, Fe^+ inserts into C-C and C-H bonds, and is the only first row transtion metal ion to insert into the C-N bond. Co^+ is less reactive, followed by Cr^+ and Ni^+. Mn^+ is unreactive with n-propylamine.

It has been suggested that ionic species such as Co^+CH_3 do not correlate to the ground state fragments $[Co^+(3d^8) + CH_3]$, but to $[Co^+(3d^74s^1) + CH_3]$. In reactions leading to the formation of $CoCH_3^+$, the $3d^8 \rightarrow 3d^74s^1$ promotion energy must be accounted for. These results further suggest that the $M^+(s^1d^n)\text{-}CH_3$ bondstrengths are approximately the same, and the "apparent" bondstrengths (relative to the ground state fragments) differ due to the differing promotion energies.

If we extend these concepts to insertion, and assume that a promotion energy (PE) is required to get M^+ to a configuration conducive to 2 bond formation, M^{+*}, and assume that the $M^{+*}\text{-}X$ and the $XM^{+*}\text{-}CH_2CH_2R$ bondstrengths are approximately independent of M (M = first row transition metal), we can suggest a dependence on PE. For the metal insertion to be an exothermic process, the following would hold:

$$D(M^{+*}\text{-}X) + D(XM^{+*}\text{-}CH_2CH_2R) > D(CH_2RCH_2\text{-}X) + PE(M^+ \rightarrow M^{+*})$$

For cases where either the bond being broken is strong, or one or more of the bonds being formed is weak, the PE term could limit the sites thermodynamically accessible for attack. Ab initio calculations suggest that transition metal dihydrides and dihalides are linear due to sp-hybridized orbitals on the metal. Thus the PE's related to achieving an $s^1p^1d^n$ configuration may correlate with M^+ reactivity. A Generalized Valence Bond approach would suggest that PE's related to achieving an s^2d^n configuration would be more useful. Both $PE(s^1p^1d^n)$ and $PE(s^2d^n)$ suggest that $PE(M^+ \rightarrow M^{+*})$ would follow the order:

$$Fe^+ < Co^+ < Cr^+ \approx Ni^+ < Mn^+ < Zn^+ < Cu^+$$

We believe that this ordering correlates with the reactivity which has been observed for these metal ions. Thus, metal ions with sufficiently high promotion energies may not be able to form metal insertion intermediates in an exothermic process.

COLLISION-INDUCED DISSOCIATION STUDIES OF ION-MOLECULE PRODUCT IONS USING FOURIER TRANSFORM MASS SPECTROMETRY

D.L. Bricker and D.H. Russell

Department of Chemistry
Texas A&M University
College Station, Texas 77843

Collision-induced dissociation using Fourier transform mass spectrometry (CID-FTMS) has been used for structural characterization of ionic systems in the same manner as other CID experiments.[1,2,3,4] This method has been particularly useful for structural characterization of ion-molecule product ions.[5,6,7] In our studies on the ion-molecule reactions of transition metal ions and transition metal cluster ions with organics we frequently use CID-FTMS for the characterization of the ion-molecule product ions. However, we find that the CID spectra of the ion-molecule product ions differ markedly from the CID spectra of the ion formed by direct electron impact ionization. The question then arises: are the different CID spectra due to different ion structures or is CID by FTMS sensitive to the initial internal energy of the ion prior to collisional activation (CA). To probe this question we have studied the CID reactions of a number of C_6H_6 radical cations formed by ion-molecule reactions, fragmentation of substituted benzenes, and by direct ionization of benzene and 2,4-hexadiyne.

The C_6H_6 radical cations formed by direct ionization of benzene and 2,4-hexadiyne give similar CID spectra; however, the absolute cross-section for CID of 2,4-hexadiyne C_6H_6+ is substantially greater than that for benzene C_6H_6+. Owing to the lower energy requirements for fragmentation of 2,4-hexadiyne C_6H_6+, the different CID cross-sections are not surprizing. An interesting trend is observed for the CID of 2,4-hexadiyne C_6H_6+ as the ionizing evergy is increased from near threshold to ca. 18 eV. For example, the ratio C_4H_3+/C_5H_3+ increases smoothly as the ionizing energy is increased (see Figure 1). A similar trend is also observed for benzene C_6H_6+. These results suggest that the FTMS CID spectra are sensitive to the internal energy of the ion prior to CA. These experiments were performed at both low (<500 eV) and high (>1000 eV) translational energy, and the ratios are insensitive to the translational energy at which CID is performed.

We have also examined the CID of C_6H_6+ formed by dissociation of anisole and tropone--where the dissociation was a result of EI and CID of the parent molecule. In both of these systems the ratio C_4H_3+/C_5H_3+ shows the same behavior as that observed for 2,4-hexadiyne C_6H_6+. For example, the C_4H_3+/C_5H_3+ ratio for anisole C_6H_6+ formed by CID of the parent ion is significantly larger than for C_6H_6+ formed by EI. The CID spectra of anisole C_6H_6+ also differs significantly from the CID spectra of benzene and 2,4-hexadiyne C H +, viz. the dominant CID fragments are C_4H_3+ and C_3H_3+ and the intensity of C_4H_4+, C_4H_2+, C_3H_2+, C_2H_3+, and C_2H_2+ are very low. This same behavior is observed for tropone C_6H_6+. We attribute these differences in the CID spectra to internal energy effects.

It is interesting to compare the CID spectra of C_6H_6+ formed by reaction 1 with the CID spectra of benzene and anisole C_6H_6+. The C_6H_6+ ion formed by reaction 1 exhibits the same CID spectra as the anisole C_6H_6+. In these studies both Fe^+ and Ni^+ were used as the reactant ion. In both cases the same general behavior is observed; however, the ratio

$$M^+ + C_6H_6 \text{ ----- } [M\ C_6H_6]^+ \text{ ----- } M + C_6H_6^+ \qquad 1$$

C_4H_3+/C_5H_3+ shows a strong dependence on the reactant metal ion. For example, the C_4H_3+/C_5H_3+ ratio for benzene/Ni is 0.83 and the benzene/Fe is 0.93; similarily, the 2,4-hexadiyne/Ni and 2,4-hexadiyne/Fe ratios are 0.76 and 0.85, respectively. The energetics of the ion molecule reactions differ by less than 3 kcal/mole, thus it is very surprizing that the CID ratios are so much different. This could arise from the different binding energies for the benzene-Fe and benzene-Ni complexes. This could also explain the observed differences for the benzene and 2,4-hexadiyne metal systems, i.e., the binding energy of benzene is greater than the binding energy of 2,4-hexadiyne. Additional studies are underway to probe this question.

The FTMS-CID studies reported here indicate that the CID spectra of ion-molecule product ions are sensitive to the internal energies of the ion prior to CA. These results point out potential problems associated with structural characterization of ion-molecule

product ions using CID---in particular assigning structural differences based on small differences in the CID spectra.

1. Cody, R.B.; Burnier, R.C.; Freiser, B.S.; Anal. Chem., 54, 96 (1982)
2. White, R.L.; Withins, C.C.; Anal. Chem., 54, 2211 (1982)
3. Cody, R.B.; Freiser, B.S.; Anal. Chem., 54, 1431 (1982)
4. Bricker, D.L.; Adams, T.A.; Russell, D.H.; Anal. Chem., 55, 2417 (1983)
5. Freiser, B.S.; Jacobson, D.B.; J. Am. Chem. Soc. 105, 736 (1983)
6. Cody, R.B.; Burnier, R.C.; Freiser, B.S.; J. Am. Chem. Soc. 104, 7436 (1982)
7. Carlin, T.J.; Freiser, B.S.; Anal. Chem. 55, 571 (1983)

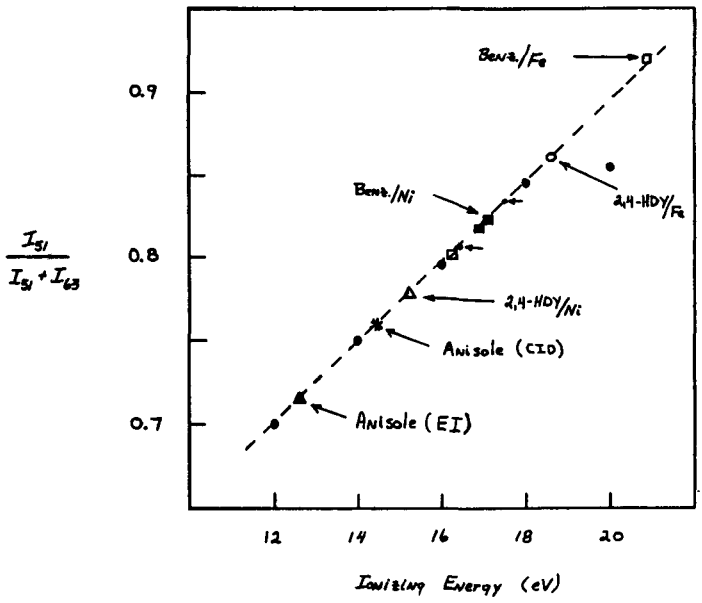

REACTIONS OF IRON IN THREE OXIDATION STATES WITH ORGANIC MOLECULES

A. Smith and D.P. Ridge
University of Delaware, Newark, Delaware 19716

Fe^+, FeI^+, and FeI_2^+ were formed by electron impact on $FeI_2(CO)_4$. These ions represent three different formal oxidation states of iron. Their chemistry was investigated to determine whether elementary concepts regarding metal oxidation states would pertain. It was expected that $^{I}Fe^+$ would react by oxidative addition mechanisms since the second and third oxidation states of Fe are available. $^{III}FeI_2^+$, on the other hand, was not expected to react by oxidative addition since the fourth and fifth oxidation states of iron are relatively inaccessible. FeI_2^+ was expected to react mainly as a Lewis acid accepting charge density from the neutral. The charge should move to some site in the neutral and rearrangements ensue. Chemistry of this kind is exhibited by other ions containing metals in high oxidation states such as $TiCl_3^+$ in its reactions with olefins, ketones, and ethers. It is also expected that the observed chemistry might reflect the fact that ^{I}Fe should be a "soft" acid and ^{III}Fe should be a "hard" acid. Fe^+ should form stronger bonds to "soft" bases such as olefins and CO, while FeI_2^+ might be expected to form stronger bonds to a "hard" base such as H_2O.

The distinction between "hard" and "soft" acids shows itself in the chemistry of isopropanol.

	Fe^+	FeI^+	FeI_2^+
$M^+ + i\text{-}C_3H_7OH \longrightarrow MH_2O^+ + C_3H_6$	0.39	0.64	0.83
$M^+ + i\text{-}C_3H_7OH \longrightarrow MC_3H_6^+ + H_2O$	0.61	0.36	0.17

Both the oxidative addition chemistry expected of Fe^+ and the Lewis acid chemistry expected of FeI_2^+ are consistent with the observed dehydration products. Both mechanisms should involve competition between H_2O and C_3H_6 for the metal center. Note the growing preference for H_2O on going from Fe^+ to FeI^+ to FeI_2^+ reflecting the increasing hardness of the metal.

Fe^+ reacts by oxidative addition to C-C bonds with alkanes. The oxidative addition is followed by shift of a β H atom to the metal and reductive elimination of a small alkane. Pentane, for example, reacts readily with Fe^+ to form $FeC_2H_4^+$ and $FeC_3H_6^+$. Pentane is not observed to react at all with FeI^+ and FeI_2^+ suggesting that the ^{II}Fe

and ^{III}Fe centers in these ions are less subject to oxidative addition than $^{I}Fe^{+}$.

Fe^{+} reacts with a ketone, 2-pentanone, by an oxidative addition mechanism to produce $FeC_5H_8O^{+}$ and $FeC_3H_6O^{+}$. FeI_2^{+} produces $FeI_2(CH_3CHO)^{+}$ and $FeIC_5H_9O^{+}$ which are expected products of Lewis acid chemistry and reminiscent of the chemistry of $TiCl_3^{+}$ with ketones. FeI^{+} produces predominately Lewis acid type products, but there is a small amount of $FeIC_5H_8O^{+}$ which might be the result of oxidative addition.

Fe^{+} reacts with 1-pentene by oxidative addition mechanisms. The major product, $FeC_3H_6^{+}$ corresponds to insertion into the allylic bond. FeI_2^{+} is unreactive. Apparently FeI_2^{+} is not a sufficiently strong Lewis acid to attack the olefin in the manner of $TiCl_3^{+}$. Neither is oxidative addition possible. FeI^{+} does react producing mainly $FeIC_5H_8^{+}$. A Lewis acid mechanism beginning with extraction of an allylic hydride might explain this result. This would produce a metal allyl complex as an intermediate. Such an intermediate would be more favorable for FeI^{+} than FeI_2^{+} since an allylic ligand would be a relatively "soft" ligand. This may help account for the difference between the reactivity of FeI^{+} and FeI_2^{+}. FeI^{+} may also react by oxidative addition in this particular case where activated allylic bonds are available.

In conclusion, results obtained thus far can be interpreted in terms of the elementary concepts regarding formal metal oxidation states outlined in the introductory paragraph.

Finally we note that the product distributions for Fe^{+} reacting with pentane, 2-pentanone, and 1-pentene agree very well with product distributions observed for Fe^{+} obtained by laser vaporization. The agreement is within 5% of the total product for every observed reaction channel. This suggests that neither method produces ions in states with a chemistry significantly different from the ground state.

REACTIONS OF BARE AND SOLVATED ANIONS WITH
TRANSITION METAL COMPLEXES IN THE GAS PHASE

Kelley Lane, Larry Sallans and Robert R. Squires
Department of Chemistry
Purdue University
West Lafayette, IN 47907

Nucleophilic addition to transition metal carbonyls represents a broad class of reactions of synthetic and industrial importance. Using the flowing afterglow technique, we have surveyed the gas phase reactions of a wide variety of anionic nucleophiles and negative ion clusters with several first-row mononuclear metal carbonyls.

The reactions were studied in a flowing afterglow apparatus at 300K.[1] Reactant ions produced by electron impact are entrained in a fast flow of helium buffer gas held at 0.1 to 1.0 torr in a 1 m long flow reactor. The steady-state in composition in the flow tube is continuously monitored by a quadrupole mass spectrometer located behind a small sampling orifice in a downstream nose cone. Multistep ion-molecule reactions are initiated by adding reactive gases to the ion stream through fixed or moveable inlets and rate coefficients may be determined from the observed reactant ion decay as a function of reaction distance or neutral flow rate.

Negative Ion Reactions with $Fe(CO)_5$

Beauchamp and Foster first described the reactions of a few negative ions with $Fe(CO)_5$ at low pressure in an ICR (ca. 10^{-6} torr).[2] Ethoxide and fluoride were observed to react according to eq. 1, n=3, while Cl^- and CN^- were reported to be unreactive.

$$(1) \qquad A^- + Fe(CO)_5 \longrightarrow Fe(CO)_nA^- + (5-n)CO$$

At higher pressure in the flowing afterglow (~0.5 torr), virtually every anion we can generate undergoes reaction with $Fe(CO)_5$; in many cases metal ion products exhibiting losses of either 0, 1 or 2 CO ligands can be observed. For example, while OH^- reacts exclusively via eq. 1, n=3, allyl anion, $CH_2CHCH_2^-$ yields, an adduct, an adduct minus one CO and $Fe(CO)_4^-$ by dissociative charge transfer to $Fe(CO)_5$. Studies with an extensive series of anion reactants possessing a wide range of basicities, heteroatoms and molecular sizes have led to the mechanistic picture summarized below.

Scheme 1

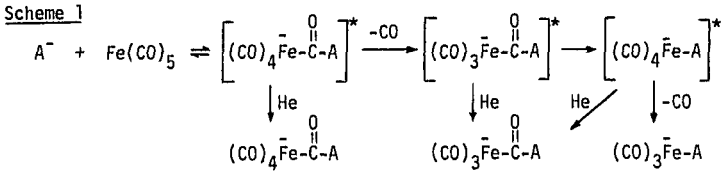

Addition of the anion at carbon initially gives rise to an iron acyl which may possess excess internal energy. Loss of CO competes with collisional stabilization by He at 0.5 torr. The tricarbonyl acyl anion subsequently undergoes a migratory deinsertion of A to yield an Fe—A species. If rearrangement is sufficiently exothermic, loss of a second CO may occur, again in competition with termolecular stabilization. Appearance of the tricarbonyl product, $(CO)_3FeA^-$, generally correlates with high anion basicity, small anion size and heteroatomic substitution. For example, NH_2^- (PA = 404 kcal/mole)[3]; $C_6H_5^-$ (PA = 398 kcal/mole); CH_3O^- (PA = 379 kcal/mole) and HC_2^- (PA = 375 kcal/mole) each produce iron tricarbonyl anion products (among others) while $C_6H_5CH_2^-$ (PA = 379); CH_2CN^- (PA = 372) and most all anions of any size with proton affinities less than 365 kcal/mole yield mainly the metal acyl adduct. The basicity dependence is most likely a reflection of the exothermicity of initial nucleophile attachment at carbon and/or the subsequent attachment at iron. Large or delocalized anions such as $C_6H_5CH_2^-$, $CH_2CHCH_2^-$ and $C_6H_{13}O^-$ may endow the $Fe(CO)_5$ collision complex with a relatively longer lifetime by providing additional modes for energy dispersal; thereby facilitating three body stabilization and production of $(CO)_4\bar{F}eA$ and $(CO)_4\bar{F}e-\overset{O}{\overset{\|}{C}}-A$.

Cluster Ions

The presence of solvent molecules alters the course of gas phase nucleophilic addition to $Fe(CO)_5$ in a striking fashion. For example, the hydrated hydroxide ions $OH(H_2O)_n^-$ n = 1-4 all react with $Fe(CO)_5$ to yield exclusively the iron hydroxycarbonyl:[4] (eq. 2)

(2) $$HO(H_2O)_n^- + Fe(CO)_5 \longrightarrow \underset{\underset{1}{\sim}}{(CO)_4\bar{Fe}-\overset{O}{\overset{\|}{C}}-OH} + nH_2O$$
n = 1-4

Subsequent ion-molecule reactions of the metal ion product $\underset{\sim}{1}$ support a formulation as a bona fide metallocarboxylic acid. The appearance of this ion from a rapid reaction with $HO(H_2O)_4^-$ leads to limits of $D°[(CO_4Fe-\overset{O}{\overset{\|}{C}}-OH] \geq 50$ kcal/mole and $\Delta H_f[(CO)_4FeCO_2H^-] \leq -257$ kcal/mole. An analogous set of reactions are observed for $CH_3O(CH_3OH)_n^-$, n = 1-3 clusters; in this case the corresponding metallocarboxylic ester is produced. Moreover, while acetate ion, $CH_3CO_2^-$, reacts with $Fe(CO)_5$ by relatively slow addition (k = 2.1 x 10^{-10} cm^3/s, efficiency = 0.1); its clusters $CH_3CO_2(CH_3CO_2H)_n^-$; n = 1, 2 do not react at all (k < 10^{-13} cm^3/s). An interesting "solvent effect" was encountered with the hydroxide-ammonia cluster, $HO(NH_3)^-$. Here, the metallocarboxylic acid anion, $\underset{\sim}{1}$, is the major product (45%), however the iron tetracarbonyl hydride $HFe(CO)_4^-$ is also produced (30%) by decarboxylation (eq. 3)

(3) $$HO(NH_3)^- + Fe(CO)_5 \longrightarrow \begin{cases} (CO)_4FeCO_2H^- + NH_3 \\ (CO)_4FeH^- + CO_2 + NH_3 \\ (CO)_4\bar{F}eOH + CO + NH_3 \end{cases}$$

In contrast, when the metallocarboxylic acid anion $\underset{\sim}{1}$ is generated independently from $HO(H_2O)_n^-$ reactions with $Fe(CO)_5$, <u>no</u> reaction occurs with added NH_3 or $(CH_3)_2NH$ (eq. 4)

(4) $$(CO)_4\bar{F}eCO_2H + NH_3 \not\longrightarrow (CO)_4FeH^- + CO_2 + NH_3$$

The common intermediate complex in these two reactions $\underset{\sim}{2}$ is formed with differing amounts of energy. In the case of eq. 3 sufficient energy is available to fuel the base catalyzed decarboxylation,

$$\underset{\underset{2}{\sim}}{\left[(CO)_4\bar{F}e-\overset{O}{\overset{\|}{C}}-OH \cdots NH_3\right]}$$

while the complexation energy of $(CO)_4FeCO_2H^-$ with free NH_3 is relatively low.

References

1. Lane, K.L.; Lee, R.E.; Sallans, L.; Squires, R.R.; J. Amer. Chem. Soc., accepted.

2. Foster, M.S.; Beauchamp, J.L.; J. Amer. Chem. Soc. 1975, 97, 4808.

3. Bartmess, J.E.; McIver, R.T. Jr. in "Gas Phase Ion Chemistry" M.T. Bowers, ed. Academic Press 1979, cha 11.

4. Lane, K. L.; Sallans, L.; Squires, R.R.; Inorg. Chem., accepted.

CHAIN LENGTH EFFECTS IN GAS PHASE ORGANOMETALLIC CHEMISTRY. A. Tsarbopoulos, B.D. Radecki, J. Allison, Chemistry Department, Michigan State University, East Lansing, MI 48824

Studies of gas-phase organometallic ion/molecule reactions by various mass spectrometric techniques have provided insights into the mechanisms and thermodynamics by which metal centers interact with organic molecules.

From the studies that have been done to date, gaseous metal ions react in very specific ways with small organic molecules containing one functional group. For example, Co^+ induces the dehydration of alcohols and the dehydrohalogenation of alkyl halides (1). But as the chain length increases, alkane-like reactions occur in addition to reactions characteristic of the functional group.

From studies of a series of straight chain alcohols and alkyl halides containing three to seven carbon chains, insertion into internal C-C bonds occurs leading to formation of metal-alkene complexes, $Co(C_nH_{2n})^+$. In the case of alcohols insertion into C-H bonds has been postulated as well, leading to dehydrogenation products, $Co(C_nH_{2n}O)^+$.

In Table I, the results obtained for the 1-Cl-hexane and 1-hexanol are compared to those obtained for n-hexane.

Table I

REACTIONS OF Co^+ WITH X $-(CH_2)_n-$ Y.

n \ X,Y	H,H		H,Cl		H,OH	
6	$Co(C_6H_{12})^+ + H_2$	(0.22)	$C_3H_7^+$ + "CoC_3H_6Cl"	(0.25)	$Co(H_2O)^+ + C_6H_{12}$	(0.08)
	$Co(C_3H_6)^+ + C_3H_8$	(0.36)	$C_4H_9^+$ + "CoC_2H_4Cl"	(0.34)	$Co(C_3H_6)^+ + C_3H_7OH$	(0.28)
	$Co(C_4H_8)^+ + C_2H_6$	(0.29)	$C_6H_{13}^+ + CoCl$	(0.18)	$Co(C_3H_7OH)^+ + C_3H_6$	(0.13)
	$Co(C_4H_6)^+ + \begin{cases} 2CH_4 \\ C_2H_6 + H_2 \end{cases}$	(0.13)	$Co(C_3H_6)^+ + C_3H_7Cl$	(0.06)	$Co(C_2H_5OH)^+ + C_4H_8$	(0.10)
			$Co(C_4H_8)^+ + C_2H_5Cl$	(0.11)	$Co(C_4H_6)^+ + C_2H_6 + H_2O$	(0.11)
			$Co(C_4H_6)^+ + C_2H_5Cl + H_2$	(0.06)	$Co(C_4H_7OH)^+ + C_2H_6$	(0.12)
					$Co(C_4H_9OH)^+ + C_2H_4$	(0.03)
					$Co(C_6H_{12}O)^+ + H_2$	(0.05)
					$Co(C_6H_{13}OH)^+$	(0.10)

In the case of n-hexane the products observed are formed following insertion of the Co^+ into the internal C-C bonds. Co^+ is highly selective against insertion into the terminal C-C bonds, since these bonds are stronger than the internal bonds by approximately 5 kcal/mol.

The chemistry of Co^+ with 1-Cl-hexane has a number of similarities with that of n-hexane. In both cases the favored pathway is metal insertion into the C_2-C_3 bond leading to formation of fragments containing either four or two carbon atoms. These results indicate that alkyl halides exhibit alkane-like chemistry in addition to the reactions expected for the functional group.

A much richer chemistry has been observed for alcohols. In the case of n-hexanol, every C-C bond is attacked except the C-C bond which is α to the -OH group. (This bond is approximately 4 kcal/mol stronger than the other C-C bonds). The site of attack seems to be limited to the fifth carbon atom away from the -OH group. This may be due to the strong initial Co^+-alcohol interaction which keeps the metal bound to the -OH group and further forms a six-membered ring intermediate via metal interaction with a carbon atom. This intermediate accounts for the majority of the products.

It seems that similar intermediates lead to the products formed for some of the bifunctional molecules studied as in the case of $Cl(CH_2)_5X$ (X = Br, OH).

REACTIONS OF Co^+ WITH $Cl(CH_2)_5X$

Evidence for Formation of Bicyclic Intermediate

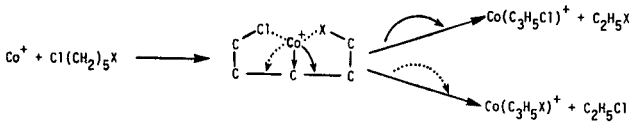

X=Br, OH

A number of bifunctional organic molecules containing three to seven carbon chains are currently under study, in order to determine the change in the reactivity and the preferred site of attack as a function of chain length.

References

1. J. Allison, D.P. Ridge, J. Am. Chem. Soc. 101 (1979) 4998.

ION-MOLECULE REACTIONS OF GROUP VII METAL CARBONYLS

Wilma K. Meckstroth and Douglas P. Ridge
Department of Chemistry, University of Delaware, Newark, DE 19716

and

William D. Reents, Jr.
AT&T Bell Laboratories, Murray Hill, NJ 07974

Using an ion cyclotron resonance spectrometer we have observed ion-molecule reactions in decacarbonyldirhemium which produce clusters with m/z > 2600. Figure 1 shows a high resolution mass spectra of the ion-molecule reaction products obtained with a Nicolet-1000 Fourier Transform mass spectrometer at Bell Laboratories using a 2-inch cubic cell.

In the light of the fact that the Re-Re bond is not cleaved in the dominant pathways of electron impact induced fragmentation of $Re_2(CO)_{10}$, it is interesting that we observed the following reactions between $Re_2(CO)_{10}$ and its cationic fragment, $Re(CO)_7^+$.

$$Re(CO)_7^+ + Re_2(CO)_{10} \rightarrow Re_3(CO)_{12}^+ + Re(CO)_5 \quad (1)$$
$$\rightarrow Re_3(CO)_{15}^+ + Re(CO)_2$$

We have also observed the reaction

$$Re_6(CO)_{15}^+ + Re_2(CO)_{10} \rightarrow Re_8(CO)_{22}^+ + 3\ CO \quad (2)$$

Reactions (1) and (2) were verified by double resonance results using an ion cyclotron resonance spectrometer in our laboratories.

Kinetic data for the clusters shown in Figure 1 were obtained with the Nicolet-1000 mass spectrometer. The kinetics of all the reactions are pseudo first-order, since the neutral concentration is very much larger than the ion concentration. From a plot of the logarithm of intensity versus time, relative rate constants for reactive ions can be determined from the decay portion of the curve. For less reactive ions an upper limit can be derived from the flat or slightly increasing part of the curve. The absolute rate constants for the fastest reactions are ca. 10^{-9} cm^3 $molecule^{-1}$ s^{-1}.

The electron deficiency, D, of a cluster, $Re_n(CO)_m^+$ is given by

$$D = \frac{18n - (7n + 2m + 2b - 1)}{n} \quad (3)$$

where b is the number of metal-metal bonds. Electron deficiency is a numerical representation of the extent to which a cluster is coordinatively unsaturated. If the electron deficiency is two, for example, then each Re atom in the cluster has a vacancy in its coordination shell for one two-electron donor such as CO. It is to be expected that in general clusters with an electron deficiency, D, of two or more will react efficiently. Clusters with an electron deficiency less than two should be less reactive.

Figure 2 shows a plot of the logarithm of the relative rate constants, k, versus electron deficiency, D. Species with electron deficiencies greater than two react most rapidly and at a rate that changes slowly if at all with increasing electron deficiency. Species with electron deficiencies less than two react at rates that decrease smoothly and dramatically with decreasing electron deficiency.

In order to assign electron deficiencies it was necessary to assign the number of metal-metal bonds in each cluster. To do this it was assumed that the electron deficiency was the smallest possible value consistent with the rules for electron counting.[1] For example, Re_4 clusters were assumed to be tetrahedral with six metal-metal bonds, Re_5 clusters were assumed to be trigonal bipyramidal with nine metal-metal bonds, etc. In some instances where electron delocalization makes deviations from the eighteen electron rule possible, Eq. (3) was slightly modified according to the rules given by Teo.[1]

We have also observed ion-molecule reactions in $ReMn(CO)_{10}$ and $Mn_2(CO)_{10}$ and are continuing our studies of the cluster formation for these and other compounds. In addition we have determined the proton affinities for $Re_2(CO)_{10}$, $ReMn(CO)_{10}$, and $Mn_2(CO)_{10}$ which are 192.4 ± 1.3, 189.8 ± 1.5, and 185.1 ± 3.2 kcal/mol, respectively.

References

1. B.K. Teo, Inorg. Chem., 23, 1251 (1984).

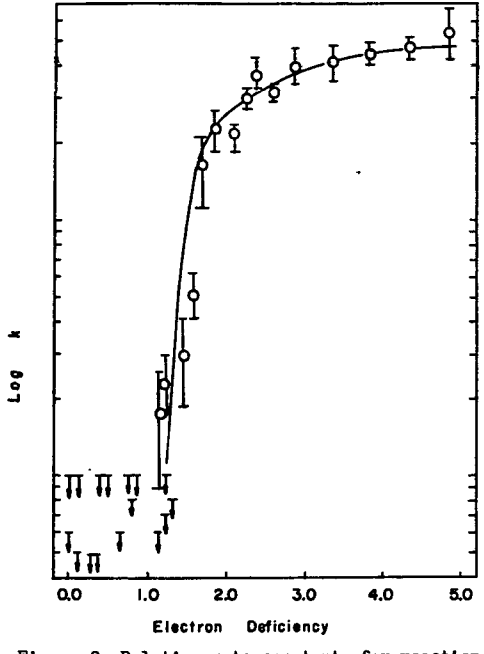

Figure 2. Relative rate constants for reaction or $Re_n(CO)_m^+$ ions with $Re_2(CO)_{10}$ vs. electron deficiency.

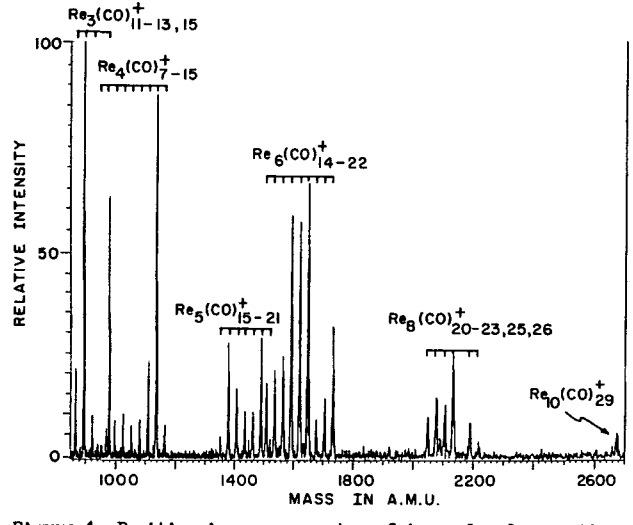

Figure 1. Positive ion mass spectra of ion-molecule reaction products of reactions between $Re_2(CO)_{10}$ and its electron impact produced fragment ions. Trapping time = 500 msec and pressure = 9.5×10^{-8} torr.

STUDIES OF MIXED CLUSTERS VIA HIGH PRESSURE MASS SPECTROMETRY

B. L. Upschulte, F. J. Schelling*, K. I. Peterson+, D. H. Evans, R. G. Keesee, and A. W. Castleman, Jr.

Department of Chemistry
The Pennsylvania State University
University Park, PA 16802, USA

Introduction

Gas phase ion clusters containing two or more different neutral clustering species (henceforth referred to as mixed clusters) are known to play an important role in atmospheric process. In the D-region of the atmosphere, ions of the form $NO^+ \cdot H_2O \cdot X$, where X is CO_2 or N_2, undergo fast switching reactions, converting NO^+ into water clusters (1). It has been suggested that complex clusters like $NO_3^-(H_2O)_x(SO_2)_y(HNO)_z$ are the terminal negative ions of the lower atmosphere (2). Relatively little is known about the stability, structure, reactivity or bonding in mixed clusters. We have studied several mixed cluster systems, including $Na^+ \cdot (CO_2)_x \cdot (H_2O)_y$, $Na^+ \cdot (SO_2)_x \cdot (H_2O)_y$, $Cl^- \cdot (SO_2)_x \cdot (H_2O)_y$, and $Cl^- \cdot (HCl)_x \cdot (H_2O)_y$ with x+y ranging up to a value of four via high pressure mass spectrometry in order to elucidate the thermodynamic properties of these clusters.

Experimental

Initially, positive ions are generated by thermionic emission from an appropriately coated platinum filament, while negative ions are the product of thermalized electron attachment or dissociative electron attachment. Mixed clusters are produced via association reactions of the form:

$$I \cdot A_x \cdot B_n + B \xrightleftharpoons{M} I \cdot A_x \cdot B_{n+1},$$

where I designates a positive or negative ion, A,B are the clustering neutrals and M is the stabilizing third body. The cluster distribution is allowed to equilibrate in a temperature controlled field-free region, before being sampled through a 75 μm orifice. A quadrupole mass spectrometer operating in a pulse-counting mode detects the mixed clusters. The details of the apparatus have been described previously (3,4).

Making common assumptions concerning ideal gas behavior and the proportionality of the chemical activity of an ion cluster to its measured intensity, and taking the standard state to be one atmosphere, it follows that

$$\ln K_{n,n+1} = \ln\left[\frac{I_{n+1}}{I_n P_B}\right] = \frac{-\Delta G^o_{n,n+1}}{RT} = \frac{-\Delta H^o_{n,n+1}}{RT} + \frac{\Delta S^o_{n,n+1}}{R}$$

where I_{n+1} and I_n represent the respective measured ion intensities, and P_B the pressure of the clustering neutral. From the temperature dependence of the equilibrium constant we are able to evaluate the standard free energy, enthalpy and entropy changes.

Results

The measured thermodynamic values are incorporated into the appropriate thermodynamic cycle in order to determine the self-consistency of the data; alternatively the derived values may be used to calculate the missing leg of a cycle (see Figure 1).

A number of interesting findings have been derived from the recent studies. For example, it is found that H_2O bonds initially to Na^+ with an enthalpy change of -24.0 kcal/mol and SO_2 bonds initially with an enthalpy change of -18.9 kcal/mol. But, when adding an H_2O to either $Na^+ \cdot H_2O$ or $Na^+ \cdot SO_2$ the $-\Delta H^o$ is, within experimental error, 20.0 kcal/mol for both. This trend is adhered to in the case of the addition of the more strongly bound species in the other systems studied with the exception of $Cl^-(SO_2)_x(H_2O)_y$. This finding supports previous evidence for a large charge dispersion in the $[Cl\ SO_2]^-$ complex. The enthalpy change for adding SO_2 to $Na^+ \cdot H_2O$ is -14.1 kcal/mol and -16.6

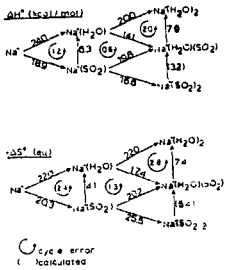

Figure 1

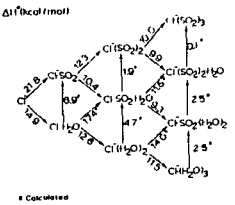

Figure 2

kcal/mol for adding SO_2 to $Na^+ \cdot SO_2$. The previous two examples of thermodynamic cycle data suggest that, when adding the more strongly bound ligand to a cluster containing one ligand, the enthalpy change does not depend on the nature of the previously attached ligand. However, when adding a more weakly bound ligand to a cluster already containing one ligand, the enthalpy change depends on which ligand was previously attached. These observations imply that ligand-ligand interactions may play an important role, not only in the thermodynamic stability, but also in the structure of mixed cluster (see Figures 1 and 2).

Another important result is the cooperative versus hindered bonding effects present in mixed clusters. This has been derived on the basis of plots of total clustering enthalpy changes, $\sum_{n} - \Delta H^{\circ}_{n,n+1}$, versus the mole fraction of the clustering neutrals (see Figures 3 and 4).

Mixed and single ligand clusters behave similarly in some respects. The stepwise bond enthalpy $-\Delta H^{\circ}_{n,n+1}$ for single ligand clusters approaches the $-\Delta H^{\circ}$ vaporization of the ligand for large n. If one starts with an ion complex and then adds n molecules of a different clustering neutral (forming a mixed cluster), the $-\Delta H^{\circ}_{n,n+1}$ value again approaches the $-\Delta H^{\circ}$ vaporization of the clustering neutral for n large. As the number of ligands in the ion complex of the other species increases, one lowers the early stepwise enthalpy changes for the addition of the n clustering neutrals, in accord with simple size considerations; but, this does not change the asymptotic behavior at large n.

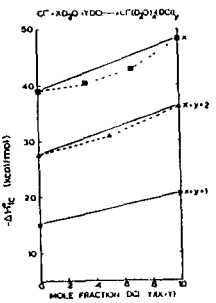

Figure 3

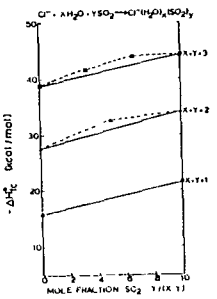

Figure 4

References

1. E. Ferguson, in Gas Phase Ion Chemistry (M. T. Bowers, Ed.), Vol. 1, Chapt. 2, p. 59 (1979).
2. Ibid., p. 76.
3. R. G. Keesee, N. Lee, A. W. Castleman, Jr., J. Am. Chem. Soc. 101, 2599 (1979).
4. A. W. Castleman, Jr., P. M. Holland, D. M. Lindsay, and K. I. Peterson, J. Am. Chem. Soc. 100, 6039 (1978).

Present Address

*Sandia National Laboratory
+Harvard University

ION MOLECULE REACTIONS IN THE NEGATIVE ION
LASER MASS SPECTRA OF NITRO AROMATIC COMPOUNDS

S. K. Viswanadham and D. M. Hercules
Department of Chemistry
University of Pittsburgh
Pittsburgh, PA 15260

Laser mass spectra of organic compounds normally show even-electron quasi molecular ions (M+H, M-H, etc.); formation of odd-electron molecular ions is not common. Compounds containing electron-withdrawing groups like $-NO_2$ are a particularly good example of negative ion formation in NIEI. In order to characterize the fragmentation behavior of the nitro substituted aromatic compounds on laser irradiation, the negative ion laser mass spectra (LMS) of 25 nitro aromatic compounds have been studied using LAMMA-1000 (Leybold-Heraus), equipped with a Nd-YAG laser (frequency quadrupled to 256 nm). The compounds studied include mono-, di- and tri-nitro derivatives of benzene, naphthalene, anthracene, 6- and 8-nitro quinolines, 4-nitro imidazole, 5-nitro 1,10 phenanthroline and 3-nitropyrene.

Interestingly, molecular anion has been observed for most of the nitro aromatic compounds studied when the laser is focused on the sample. Other common peaks noticed in their mass spectra are $\bar{C}N$(m/z 26), $\bar{O}CN$(m/z 42), $N\bar{O}_2$(m/z 46), $C_3\bar{N}$(m/z 50), and $(M-NO)^-$. The formation of molecular anion is found to depend on the position of laser focus with respect to the sample surface. When the focus of the laser is away from the sample surface (~40 microns), the molecular anion is hardly seen and an interesting intense ion could be seen in these compounds at m/z corresponding to $(M+15)^-$, in addition to the other general fragments. Fig. 1 shows the negative ion laser mass spectrum of 1,3,5-trinitrobenzene taken at defocused mode. The ion at m/z 228 corresponds to $(M+15)^-$ and the ion at m/z 183 corresponds to $(M-NO)^-$. The ion at m/z 228 shifted to m/z 230 in the case of 2,4,6-d_3-1,3,5-trinitrobenzene, suggesting the elimination of one of the aromatic hydrogens during the formation of this ion at $(M+15)^-$. The elemental composition of the ion $(M+15)^-$ formed in the case of 3,4-dinitro N,N-dimethylaniline taken on Nicolet FTMS-1000 equipped with CO_2 laser (10·6m) is found to be $C_8H_8N_3O_5$. This ion corresponds to the elimination of one of the aromatic hydrogens with the addition of an oxygen.

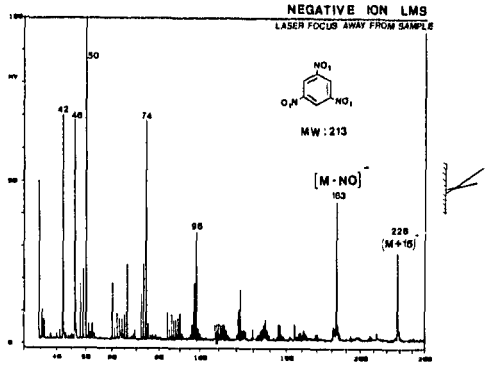

FIG. 1

The formation of the $(M+O-H)^-$ could be accounted by one of three possible mechanisms involving the attack of $\bar{O}$, $\bar{O}_2$, or $N\bar{O}_2$ on the neutral molecules, forming an intermediate, which then eliminates $\dot{H}$, $\dot{O}H$ or HNO respectively. The absence of peaks due to $\bar{O}$ and $\bar{O}_2$ in the spectra of all these compounds and the detection of $(M+NO_2-H)^-$ intermediate ($C_8H_8N_4O_6$) at m/z 256 in the case of 3,4-dinitro N,N-dimethylaniline (FTMS-1000, CO_2 laser), lend support to the mechanism involving $N\bar{O}_2$ as a nucleophilic reagent.

Nitro aromatic compounds with a facile leaving group such as -Cl and $-SO_3Na$ as in 2,6-Dininitrochlorobenzene and sodium salt of 2,4,6-Trinitrobenzene sulphonic acid shows the presence of prominent ions due to $(M+O-X)^-$ (X = -Cl and SO_3Na) rather than due to $(M+O-H)^-$. This observation is in agreement with the nucleophilic substitution mechanism proposed.

This interaction between the ions and molecules resulting in $(M+O-H)^-$ should be occurring in the secondary ionization region (1) which is immediately adjacent to the position of laser irradiation, where the density of the plasma is very high. Gas phase reactions over the surface of the impact region are less likely. Negative ion EI spectra of 2,6-Dinitrochlorobenzene have been recorded on FTMS-1000 in "Self CI" mode at various delay times. Ion corresponding to the formation of $(M+O-Cl)^-$ (m/z 183) could not be seen until a delay of 30 sec (Fig. 2). This observation rules out the possible gas phase reaction for the formation of $(M+O-Cl)^-$ or $(M+O-H)^-$ in the case of laser mass spectra.

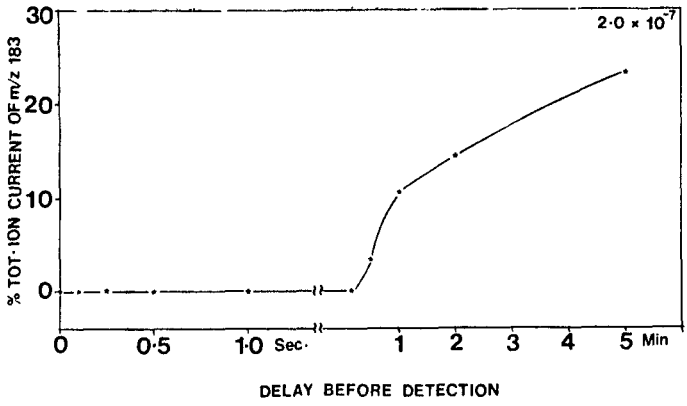

Figure 2: Intensity (as % of total ion current) of the ion at m/z 183 formed from 2,6-Dinitrochlorobenzene as a function of delay time before detection on FTMS-1000.

The number of the nitro groups present in the substrate and the position of the nitro groups in poly nitro-compounds does not seem to have any significant influence on the formation of $(M+O-H)^-$. The presence of functional groups having labile protons (-OH, -COOH, -NH-), in the nitro aromatic compounds lead to the formation of $(M-H)^-$ in the negative ion LMS of these compounds and peaks corresponding to $(M+O-H)^-$ are absent in these cases.

Formation of ions due to this type of ion molecule reactions opens up the possibility of a new kind of chemical ionization source for solid state mass spectrometry. A compound can be mixed with an appropriate nitro compound that will serve as a source of reagent ions for LMS and the LMS of the mixture might then lead to characteristic peaks for the substrate due to ion-molecule reactions.

References:

1. D. M. Hercules, R. J. Day, K. Balasanmugam, T. A. Dang, and C. P. Li, Anal, Chem., 54, 280A (1982).

TEMPERATURE AND SIZE DEPENDENT FRAGMENTATION OF CARBON DIOXIDE CLUSTERS

G. Romanowski and K.-P. Wanczek
Inorganic Chemistry, University of Bremen, 2800 Bremen, FRG

Clusters of carbon dioxide have been generated by supersonic expansion through a nozzle. The cluster beam has been ionized by electron impact and mass analysed by a quadrupole mass filter. Cluster ions $(CO_2)_N^+$ up to N=10 and fragment ions with the compositions $(CO_2)_{N-1}O^+$, $(CO_2)_{N-1}CO^+$, and $(CO_2)_{N-2}O_2^+$ have been observed. The origin of the fragment ions of the latter type has been investigated by measuring the appearance potentials of fragment ions sufficiently abundant. The results show that the ions $(CO_2)_{N-2}O_2^+$ most probably generated by an intracluster ion-molecule reactin:

$$(CO_2)_{N-1}O^+ \longrightarrow (CO_2)_{N-2}O_2^+ + CO \qquad (1)$$

The corresponding reaction between the unclustered species O^+ and CO_2 to produce O_2^+ and CO is known from ICR studies to be rapid and exothermic[1]. The relative abundances of the fragment ions depend on stagnation pressure of the adiabatically expanded gas. Fig. 1 shows the relative intensities of fragment ions formally generated by covalent bond cleavage of the same parent cluster ions as functions of the inlet pressure.

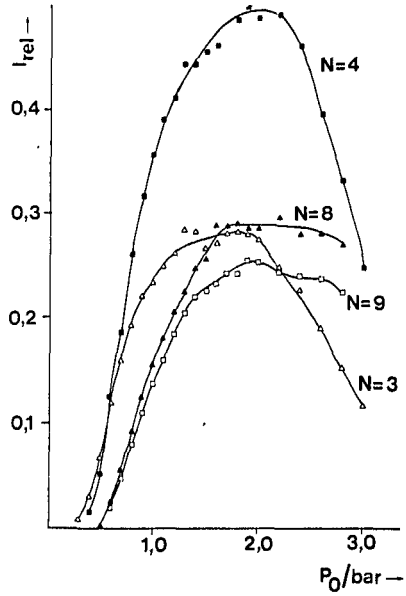

Fig. 1: Relative fragment ion intensities as functions of the inlet pressure p_0.

The curves show the same rapid increases in fragment ion intensities within 1 bar pressure range as has been observed by Stace[2] for $Ar_{16}CH_3OCH_3^+$ clusters. Additionally for smaller clusters a decrease at higher pressures occur. The results can be explained using a kinetic model which considers fragmentation reactions by covalent bond cleavage and evaporation of the clusters. Following the argumentation of Stace[2] and remembering the theoretical treatments of thermodynamic behaviour of clusters[3),4)] the results can be explained in terms of phase transitions within the clusters between solid-like, rigid and liquid-like, nonrigid structures. At low inlet pressure the temperature of the clusters is relatively high. The clusters exist in liquid-like states. The molecule in each cluster which carries the positive charge is highly excited and vibrationally hot. Because of the nonrigid structure of the cluster energy transfer between the ion and the residual cluster is relatively fast. Energy randomization yields evaporation of the cluster before fragmentation has occured. At higher inlet pressures, i.e. lower temperatures, the clusters exist in solid-like, rigid states. Energy randomization is relatively slow due to the less efficient energy transfer. Therefore the degree of fragmentation increases with increasing stagnation pressure.

The relative fragment ion intensities have been observed to depend also on cluster size. Fragment ions $(CO_2)_{3,4}X^+$ (X=O,CO) have been found to appear with extraordinary high intensities due to stable symmetrical structures of these ions. Additionally there is a pronounced decrease of fragment ion intensity for $(CO_2)_{1,2}O^+$ ions. This can be explained with the cluster size dependent tendency of $(CO_2)_nO^+$ ions to undergo the intracluster ion-molecule reaction (1). The CO_2O^+ ion is similar to the transition state of the reaction between O^+ and CO_2 resulting in a fast reaction to produce O_2^+ and CO. Therefore the intensity of CO_2O^+ is small. Succesive solvation of O^+ by CO_2 molecules reduces its reactivity resulting in increasing intensity ratio $(CO_2)_{N-1}O^+/(CO_2)_{N-2}O_2^+$ with inncreasing cluster size N.

References

1) S. Jaffe, F.S. Klein, Int. J. Mass Spectrom. Ion Phys., 14, 458 (1974)
2) A.J. Stace, Chem. Phys. Lett., 99, 47o (1983)
3) R.D. Etters, K.Flurchik, P.P. Dan, V. Chandrasekharan, J. Chem. Phys., 75, 929 (1981)
4) G. Natanson, F. Amar, R.S. Berry, J.Chem. Phys., 78, 399 (1983)

CLUSTER IONS FROM HETEROCYCLIC NITRAMINES

Robert J. Doyle, Jr. and Joseph E. Campana,
Naval Research Laboratory, Chemistry Division,
Washington, D.C. 20375

Large methylenenitramine cluster ions $[(CH_2NNO_2)_nH]^+$ formed by ion/molecule reactions from two different cyclic methylenenitramine oligomers, hexahydro-1,3,5-trinitro-1,3,5-triazine (RDX) and octahydro-1,3,5,7-tetranitro-1,3,5,7-tetrazocine (HMX), have been produced and studied. Solid samples of the RDX or HMX were introduced into a heated high-pressure ion source of a mass spectrometer via a standard solids probe. The sample reacted with itself (self chemical ionization) via ion/molecule reactions under normal chemical ionization conditions (1 Torr and 150-ev electron bombardment), and the mass spectrum was recorded.

Two significant features of the resultant cluster ion distributions for RDX and HMX, shown in Fig. 1, are (i) the observation of *magic numbers* and (ii) their mutual uniqueness. We attribute these features to the molecular structure and to the intermolecular interactions inherent to the condensed phase of the precursors (RDX and HMX).

Magic numbers for the methylenenitramine clusters $[(CH_2NNO_2)_nH]^+$, which are observed at n=6, 9, 12, and 15 for RDX and at n=12, 16, 20,...56 for HMX, are indicative of the respective molecular clusters, $[(RDX)_iH]^+$ (i=2,3,4,5) and $[(HMX)_jH]^+$ (j=3,4,5...14). The prominence of the protonated RDX dimer in the mass spectrum is in direct semblance to crystallographic data that indicates strong intermolecular attractions between RDX molecules resulting in dimers with weak attractive forces between each other [1].

The rapid fall-off in the methylenenitramine cluster ion abundances formed from RDX in contrast to that from the HMX precursor is reminiscent of the intermolecular forces in the respective lattices. The HMX molecules experience much stronger intermolecular forces than RDX in the condensed phase because of numerous intermolecular attractions [2].

We have shown through isotope labeling studies that the protonated dimers of RDX and HMX are formed by ion/molecule reactions of molecular species and not through (i) direct vaporization of a dimeric species from the solid or (ii) ion/molecule reactions of methylenenitramine fragment species [3]. We have not established whether the methylenenitramine cluster ions intermediate from those corresponding to the molecular cluster ions are formed by fast unimolecular dissociations of the molecular cluster ions in the ion source or by ion/molecule reactions of the molecular clusters species with methylenenitramine species.

The unicluster daughter-ion mass spectra of protonated methylenenitramine clusters formed from RDX show that the most abundant decomposition products of clusters with n>6 are formed by the loss of one and three methylenenitramine groups. A dissociative pathway that precludes the loss of two methylenenitramine groups may involve the loss of one methylenenitramine group from a RDX molecule on a cluster followed by the formation of a stable $CH_2N{=}NO_2CH_2NNO_2$ ring with a substituted 1,2,3-oxadiazole-type structure.

The unicluster daughter-ion mass spectra of protonated HMX clusters show abundant decomposition products formed by the loss of one and four methylenenitramine groups. The loss of one methylenenitramine group from an HMX molecule on a cluster apparently results in ring closure to form a stable RDX molecule.

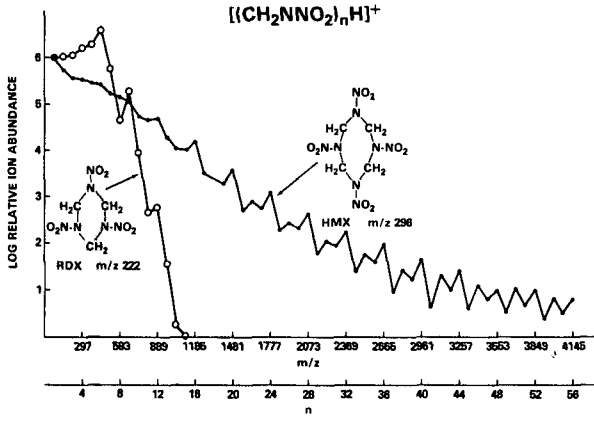

Fig. 1. Logarithm of the relative cluster ion abundance of the $[(CH_2NNO_2)_nH]^+$ series from RDX and HMX.

1. C. S. Choi and E. Prince, Acta Crystallogr., Sect. B., 28, 2857-2862 (1972); R. J. Karpowicz and T. B. Brill, J. Phys. Chem., 87, 2109-2112 (1983).

2. T. B. Brill and R. J. Karpowicz, J. Phys. Chem., 86, 4260-4265 (1982); T. B. Brill and C. O. Reese, J. Phys. Chem. 84, 1376-1380 (1980).

3. R. J. Doyle and J. E. Campana, submitted for publication.

A HIGHLY SENSITIVE PULSED ION BOMBARDMENT TIME-OF-FLIGHT MASS SPECTROMETER

B.T. Chait, F.H. Field, The Rockefeller University, New York, N.Y. 10021

We have recently designed and constructed a mass spectrometer at the Rockefeller University where one of our primary design goals was to render the instrument capable of very high sensitivity measurements of involatile organic compounds. The instrument shown in Fig. 1 is a keV energy pulsed ion bombardment time-of-flight mass spectrometer similar to the instrument constructed by Chait and Standing (ref. 1) at the University of Manitoba but with some differences.

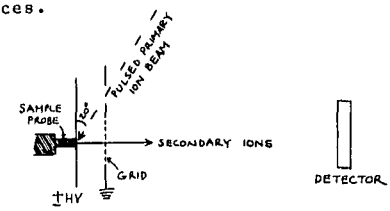

Fig. 1

The primary ion beam is brought to a fine focus on a small surface area probe by a set of pulsed electrostatic deflection plates to effectively produce short duration packets of primary bombarding ions at the target. These bursts of primary ions subsequently give rise to short duration packets of secondary ions which are accelerated into a field-free flight-tube through which they drift to a detector. The time interval between a primary ion burst and the secondaries striking the detector is measured and determines the mass of the secondaries. The design parameters for the device are listed below and where these design goals have not yet been achieved notes are made in parentheses.

1. PRIMARY ION SOURCE: Electrohydrodynamic molten metal e.g. ^{115}In, ^{197}Au, ^{209}Bi (^{115}In).
2. PULSING: Provided by high voltage deflection of the primary ion beam in conjunction with angular bunching - 1ns pulse width (5 ns.).
3. OPTICS designed for:
   (i) 30kV primary ion acceleration
   (ii) 25kV secondary ion acceleration (lower potentials used)
   (iii) 25kV post acceleration (lower potentials used)
4. 70^0 ANGLE OF INCIDENCE.
5. SAMPLE PROBE DETAILS:
   (i) Bombarding ion beam can be tightly focussed and accurately positioned on small probe (100μ beam diameter).
   (ii) Probe diameter: 2mm - 0.2mm
6. Beam Intensity 10^2-10^4 ions/pulse
7. Repetition rate 3 x 10^3/sec.
8. SECONDARY IONS
   (i) positive or negative
   (ii) 2 meter flight-tube with electrostatic particle guide.
   (iii) multichannel plate detector, pulse counting
9. TIME MEASUREMENT made by a TIME-TO-DIGITAL CONVERTER:
   (i) accepting up to 16 events/incident ion bunch
   (ii) 5/8ns resolution
   (iii) 5ns deadtime (longer deadtimes set by discriminator)
10. $m/\Delta m>1000$

The strategy for attaining high sensitivity is outlined below with present conditions given in parentheses:

1. Deposit a monolayer to submomolayer on a small surface area. (Two methods which we have used to date are indicated in fig. 2).
2. Focus the ion beam onto this small surface area sample. (We currently focus and position a 100μ diameter spot on the sample).
3. Fully utilize all the molecules present on the surface. (To date we have been operating the instrument conservatively, so that in a typical

run with a duration of 2 minutes we only utilize about 2% of the sample).

4. Detect virtually all ions produced. (We estimate that the extraction of ions from the source, mass analysis, transport and detection of ions is presently achieved with >10% effeciency).

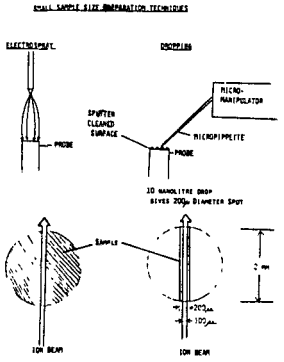

Fig. 2

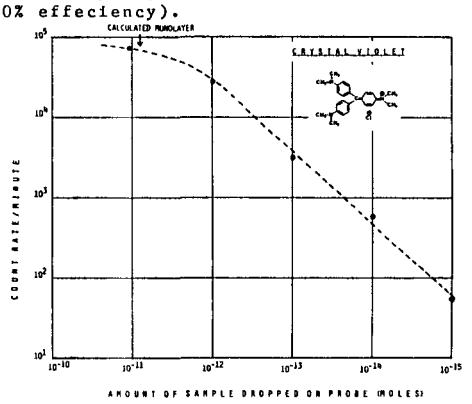

Fig. 3

The response curve showing the count rate in the quasi-molecular ion peak of the catonic dye crystal violet versus the amount of sample inserted into the mass spectrometer is given in fig. 3. In this experiment the sample was deposited on the whole area of a 2mm diameter probe tip but only a stripe representing 6% of the total area deposited was bombarded (see fig. 2). Thus for the point plotted at $1x10^{-15}$ moles we were actually only sampling $6x10^{-17}$ moles or 60 atomoles of material. Thus concentrating the sample onto the area struck by the beam should yield a substantial improvement in sensitivity. Indeed preliminary results with stripe samples produced by the technique shown in fig. 2 did yield sensitivity improvements. Fig. 4 shows a complete time-of-flight mass spectrum taken on 10^{-13} moles of crystal violet where the run time was 2 min and the estimated total ion flux on the sample was $4x10^{8}$ ions.

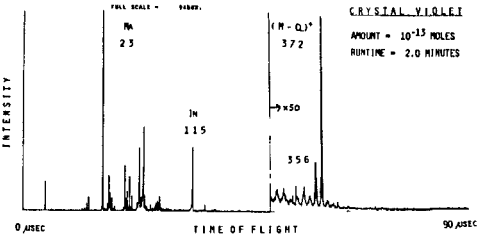

Fig. 4

Preliminary results were also obtained on the neuropeptide leucine - enkephalin which has five amino acid residues and a molecular weight of 555. For these experiments the sample was deposited on the whole area of a 2mm diameter probe by the focussed electrospray process (fig.2). $3x10^{-12}$ moles a leu-enkephalin deposited on the probe yielded a useful QM ion peak in a run with a duration of 2min. Again this result was obtained by bombarding and thus utilizing a stripe representing only 6% of the total sample area deposited. Thus in this case we actually obtained the information on $2x10^{-13}$moles of material.

We conclude that the mass spectrometer described here will probably exhibit a high inherent sensitivity and that the major sensitivity limitations will probably arise in practice from our inability to handle very small amounts of material cleanly.

1. B.T. Chait, K.G. Standing, Int. J. Mass Spectrom. Ion Phys. 40 (1981) 185.

A MULTISTOP TIME DIGITIZER
FOR THE MANITOBA TIME-OF-FLIGHT MASS SPECTROMETER

W. Ens, R. Beavis, D.E. Main, B. Schueler, and K.G. Standing
Physics Department, University of Manitoba
Winnipeg, Canada R3T 2N2

The Manitoba time-of-flight mass spectrometer (1) initially used conventional nuclear timing circuits (a time-to-amplitude converter (TAC) followed by a 4000 channel pulse-height analyser) for data acquisition, since this hardware was readily available and easily implemented. In 1981 we obtained an LSI 11/23 computer and winchester disk to provide permanent storage and more sophisticated analysis of the data.

A better method of time measurement is direct time-to-digital conversion (TDC). Several TDCs have been custom built for data acquisition with fission fragment spectrometers (2,3). Recently a suitable commercial model (LeCroy model 4208 TDC) has become available and we have implemented a new data system based on it. This TDC is a CAMAC module which can accept a common start and up to 8 stops on a single line, with a dead time between stops specified as 3 ns. The unit uses a high stability crystal-controlled 125 MHz clock to digitize in real time, and digital interpolation between pulses to obtain resolution of 1 ns. Time intervals are encoded in 24-bit signed digital words corresponding to a dynamic range of up to 8.3 ms. The data for the 8 events are stored in the unit until read and cleared by the computer. Data are then placed in a 32000 word × 16 bit histogram in the computer memory. The incoming spectrum is displayed on a VT640 terminal (DEC VT100 with Digital Engineering Retro-Graphics) which is also used to control the data acquisition program.

The new system has significantly improved our data handling capability. Since the TDC is a multistop device, the complete mass spectrum can be taken simultaneously at higher beam current without introducing the distortion caused by intense low mass peaks when a single-stop TAC is used (1). The stability of the TDC and the narrow time bins possible with the large histogram gives considerably improved resolution for stable ions. Fig. 1 shows mass resolution of 3200 (FWHM) for a CsBr cluster at m/z ~ 700.

A linear TOF spectrometer has a high efficiency for detecting the products of metastable decay. These give broadened peaks (4), but with sufficiently narrow time bins a sharp component from ions that remain intact may be observed above the broad metastable background. Fig. 2 shows met-enkephalin molecular ion peaks from a spectrum taken with the TAC (4), and a recent spectrum taken with the TDC.

The improved resolution and the linearity of the TDC allow accurate calibrations to be made using peaks stored simultaneously. Fig. 3 shows the complete spectrum of substance P. Even for the predominantly metastable parent ions, a sharp component is observed. Calibration with peaks at m/z 23, 70, and 120 gives accurate mass determination of these sharp peaks.

This system, controlled by our own software, is well suited to measurement of secondary ion multiplicity (the number of secondary ions desorbed for each primary pulse) and correlations between secondary ions. Spectra may be taken in coincidence with a selected line by defining an appropriate time window; only events in which an ion is detected in the window are recorded. Measurements using these features are reported in an accompanying paper (5).

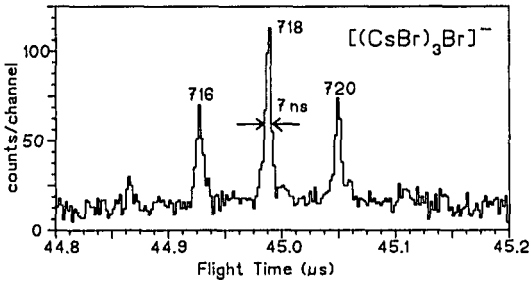

Figure 1 Negative time-of-flight spectrum of CsBr near the 3rd cluster. $t/\Delta t(FWHM) \sim 6400$ so $m/\Delta m(FWHM) \sim 3200$. For a gaussian peak, the equivalent resolution at 1/10 max is 1750.

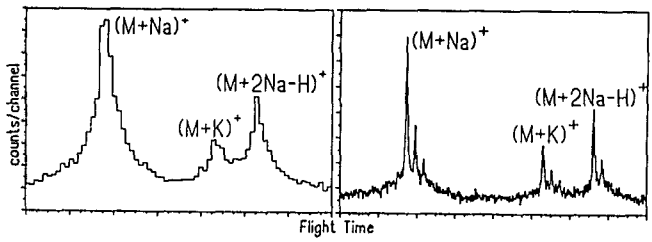

Figure 2 Spectrum of met-enkephalin near the molecular ion taken before (left) and after (right) installation of the TDC.

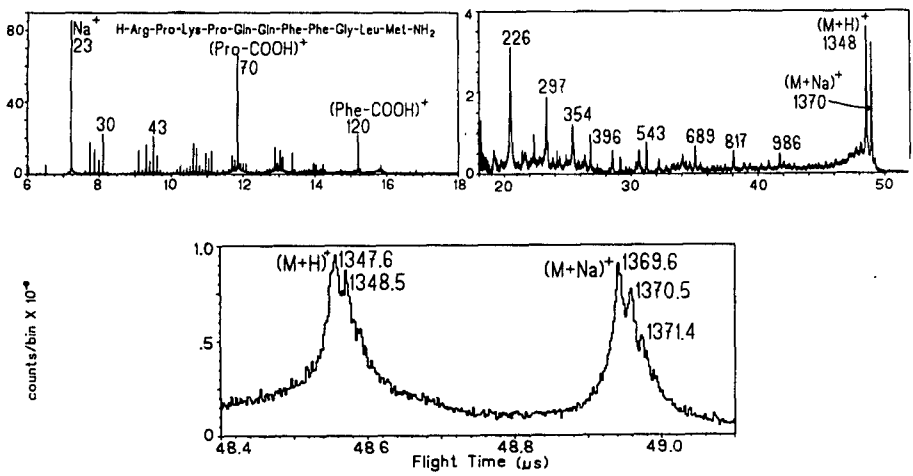

Figure 3 Complete spectrum of substance P (m/z 1346.7) taken with the TDC and stored in a histogram with 2 ns/channel and calibrated with the m/z 23, 70 , and 120 peaks. The upper right trace is displayed in 8 ns bins; 2 ns bins are used for the others. A smooth background has been subtracted above 18 μs. The bottom trace shows the molecular ion region in detail; the isotopic distribution of the C atoms is observed in addition to the broad metastable peak.

References:

1) B.T. Chait and K.G. Standing, Int. J. Mass Spectrom. Ion Phys., 40 (1981) 185.
2) R.F. Bonner, D.V. Bowen, B.T. Chait, A.B. Lipton, F.H. Field, and W.F. Sippach, Anal. Chem. 52 (1980) 1923.
3) B.T. Turko, R.D. Macfarlane and C.J. McNeal, Int. J. Mass Spectrom. Ion Phys. 53 (1981) 353.
4) K.G. Standing, R. Beavis, W. Ens, and B. Schueler, Int. J. Mass Spectrom. Ion Phys. 53 (1983) 125.
5) R. Beavis, W. Ens, D.E. Main, B. Schueler, and K.G. Standing, these proceedings.

VELOCITY COMPACTION FOCUSING IN A TOF MASS SPECTROMETER*

M. Luis Muga

TOFTEC
P.O. Box 12877
Gainesville, Florida 32604
and
Chemistry Department
The University of Florida
Gainesville, Florida 32611

Velocity compaction offers a new focusing principle for attaining improved resolution with the use of time-of-flight mass spectrometers. Computer simulation studies of flight time patterns show the expected improved resolution as a function of ion mass. With higher voltage swings and key changes in relative grid positions which define the post-extraction and velocity compaction acceleration regions, new results suggest that unit resolution at mass 10,000 daltons should be achievable with a simple single stage version as diagrammed in Fig. 1 below.

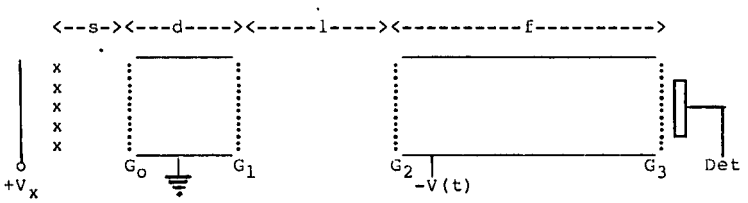

FIGURE 1

A surprising, yet pleasant result is the observation that mass resolution, as defined by $M/\Delta M|_{fwhm}$, increases slightly with mass. However, increased "tailing" or skewness of the mass peaks limits the attainable resolution beyond about 10,000 daltons under the conditions chosen for the current simulation studies.

Arrival times of ion masses follow a simple relation with mass of the form

$$t = k\ M^x$$

where k and x are constants related to the physical dimensions and positioning of the variable acceleration region. This simple form which holds over the 500 to 10,000 mass range should facilitate mass calibration and interpolation procedures in a practical instrument.

As expected, the resolution is a function of the Boltzmann temperature distribution of velocities assumed for the initial ion plasma of finite dimensions, typically .05 cm thickness. Although a temperature of 500°K was used for this study, values as high as 1000°K still indicate that unit resolution at mass 4000 daltons can be obtained.

Because of the high transmission efficiency associated with straight path time-of-flight mass spectrometers, a velocity compaction time-of-flight mass spectrometer should be superior to other types of mass spectrometers for GC/MS and LC/MS applications where fast scanning rates and high sensitivity for heavy mass species are desired.

---

*Supported in part by the Department of Energy through the Small Business Innovative Research (SBIR) program.

PERFORMANCE OF A MICROCHANNEL PLATE DETECTOR IN A TIME-OF-FLIGHT MASS SPECTROMETER: OPERATION AT HIGH DUTY CYCLE AND HIGH ION CURRENTS

Kenneth A. Lincoln
NASA Ames Research Center, Moffett Field, California 94035

In recent years, a number of experimenters have installed microchannel plate detectors (MCPD) in time-of-flight mass spectrometers (TOFMS) for somewhat specialized applications. As far as I can discover, no one has employed MCPD in TOFMS for the more general mass spectrometric applications in which high-duty-cycle, analog mode is typically required. This paper discusses the latter application and the performance of an MCPD using a phosphor screen anode (Varian, model VUW-8998-2-P20-ZS) to provide simultaneous visual and electrical outputs. The TOFMS instrumentation for measuring laser-induced vapor species has been described previously (1); it is worth noting, however, that the neutrals and ions emerge from the target at a high velocity on a path into the ion source that is perpendicular to their subsequent path in the flight tube. Thus the concern arises that this transverse velocity component might be carrying some of the species outside the acceptance area of the original detector. As a means of investigating this effect as a means of monitoring ion beam paths as a function of electrical parameters within the TOFMS, an MCPD with visual output was installed.

A further reason for replacing the original magnetic electron multiplier (MEM) with an MCPD was to increase the quantitative capability of the TOFMS by improving detector repeatability. For example, the MCPD has fewer variables: 1) external magnets eliminated; 2) electrical potentials requiring optimization reduced from about nine to one; and 3) ion collection area increased from 15-mm diameter to 40-mm diameter, ensuring that all ions in the beam are registered by the detector.

Some specifics of the tandem-dual array MCPD are as follows:

Quality	Nonimaging	Open area	60%
Active area	40-mm diameter	Electron gain	10^7
Number of channels	7.9×10^6	Bias angle	5°
Diameter of channels	12 μm	Photosensitive coating	None
Length/diameter	42	Anode phosphor	P-20
Thickness	0.5 mm		

Figure 1 is a schematic of the MCPD and its external circuitry. The gain is controlled by the single adjustment which varies the potential applied across the plates. This voltage is continually measured to monitor the detector gain. The anode is capacitively coupled to a scope and to a waveform digitizer to permit viewing and recording of mass spectra. Simultaneously the anode is either direct-coupled to a +3-kV source to energize the phosphor (for viewing ion beam profiles) or it is direct-coupled to a digital panel meter as a means of conveniently measuring the beam current, which is a summation of all ions in the spectrum.

Unexpectedly, an examination of the beam profiles clearly showed that a significant fraction of the ions were striking wide of the detector active area, despite its 40-mm diameter. This situation was resolved by installing an electrostatic lens upstream in the flight tube. Although the subject of ion trajectories is beyond the scope of this paper, it is apropos to point out that the phosphor screen revealed that ions generated by electron impact from high transverse velocity neutrals arrive at the detector in the same location as those generated from static molecules; however, laser-induced ions entering the ion source (electron beam off) at high transverse velocity arrive at the detector more spread out, and with some apparently missing the detector.

Figure 2 shows the relationship between multiplier gain and the voltage across the dual plates in the typical operating range; the gain doubles in each 65-volt increment. In an effort to determine the linearity range of the MCPD in the analog mode, argon was introduced and the system was driven to produce mass peaks of 6 volts across 93 ohms at the anode. However, to achieve that magnitude it was necessary to reduce the instrument repetition rate from the usual 40 kHz to 0.3 kHz. It was found that the critical factor which limits linearity is the dc component of the output current. Thus with this detector, nonlinearity occurs above 0.8 μA dc (0.06 $\mu A/cm^2$) regardless of the spectral population; however, this can be accommodated easily by reducing the gain of MCPD or the repetition rate of the instrument. In normal operation the mass peaks are less than 100 mV, and the frequency response of the MCPD is sufficiently high so that it is not the limiting factor in mass resolution.

In summary, the nonimaging-quality MCPD performs well in producing both visual and electrical outputs. The trade-off for having both outputs is that the anode is not impedance-matched to a coaxial line and some ringing can occur, but careful adjustments in the external connections nearly eliminated this problem.

Furthermore, this detector has demonstrated good day-to-day stability, and its larger acceptance area has enhanced the sensitivity of the TOFMS. Currently, the long-range sensitivity and durability of the MCPD are unknown.

REFERENCE

1. K. A. Lincoln, Paper presented at the Dynamic Mass Spectrometry Symposium, July 5-7, 1983, at University of Salford, England; accepted for publication in Int. J. Mass Spectrom. Ion Proc.

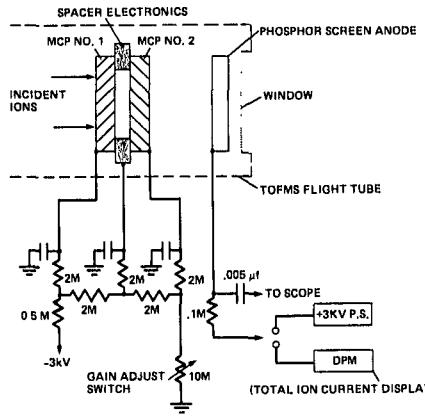

Figure 1. Microchannel plate detector with associated circuitry.

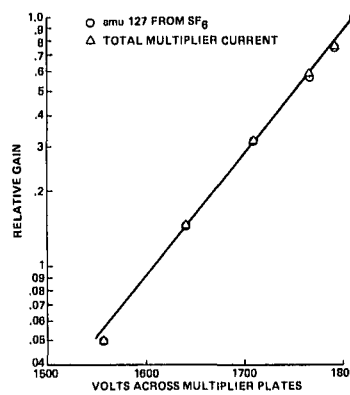

Figure 2. Gain versus voltage applied across the dual microchannel plate detector.

GLYCEROL SOLUTIONS OF SILVER SALTS AS A SOURCE FOR GENERATION OF SILVER-CONTAINING ADDUCT IONS IN FAB-MS. Musselman, B.D. and Watson, J.T., Dept. of Biochemistry, Michigan State University, East Lansing, Michigan 48824.

The addition of silver salts to the glycerol matrix in FAB experiments results in the generation of silver ion adducts of analyte molecules. These silver adduct ions have been identified for all species studied for which conventional FAB spectra contained either $(M+H)^+$, $(M+Na)^+$, or other common $(M+cation)^+$ species. The silver ion adduct species are easily distinguishable from those of the FAB matrix because of the silver isotope peak intensity cluster (52% and 48% from ^{107}Ag and ^{109}Ag). The formation of these adducts at $(M+107)^+$ and $(M+109)^+$ for species which normally produce intense $(M+cation)^+$ ions provides a valuable means of routinely validating the molecular ion-containing species even in the presence of K and/or Na salts which produce adducts that frequently are not readily distinguished from the chemical background.

Silver ion concentration studies were completed in order to determine the concentration of silver ion required for optimal adduct formation between analyte and Ag. The results of this study indicated that a concentration of 1 to 1.5 x 10^{-2}M $AgNO_3$ in glycerol provides enough silver ion to generate the adduct species while minimizing the loss of protonated molecules (Figure 1).

Determination of sensitivity limits indicate that for polyhydroxylated compounds such as carbohydrates, the $(M+Ag)^+$ ion is present in the mass spectrum before $(M+H)^+$ appears (Figure 2). This activity is reversed in the case of peptides (Figure 3), however, this may be due to interaction of specific amino acid side chains with silver ion, as in fluorescence quenching of tyrptophan.

Figure 1.

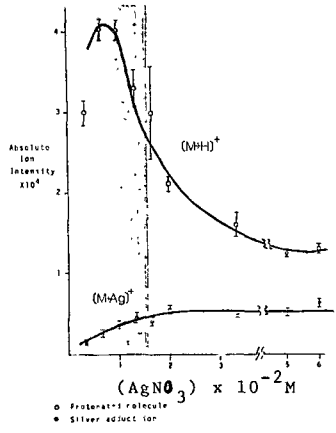

Figure 2.

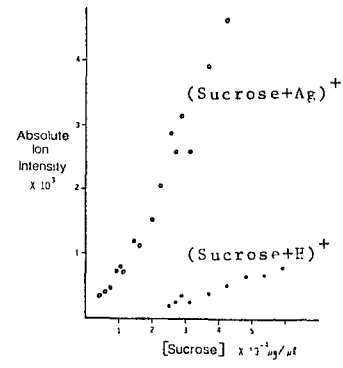

Figure 1. Effects of increasing silver ion concentration in glycerol on the generation of protonated tripeptide and silver tripeptide adduct ions during FAB-MS with 7keV Xenon atoms. Sample size was held constant at 30 nmol for each analysis. The tripeptide was Leu-Gly-Phe.

Figure 2. Absolute ion intensities observed for the silver sucrose adduct ion and protonated sucrose as a function of sucrose concentration in glycerol containing 0.14M $AgNO_3$.

Figure 3. (□) Ion intensity from protonated tripeptide when analyzed in glycerol as a function of tripeptide concentration. (○) Ion intensity from protonated tripeptide when analyzed in glycerol containing 0.14M $AgNO_3$. Decrease in intensity of protonated molecule is observed upon addition of silver nitrate to the glycerol. (●) Ion intensity from silver tripeptide adduct in glycerol containing 0.14M $AgNO_3$. FAB-MS analyses were completed using 7keV Xenon atoms.

The addition of silver ion to FAB matrices can, in general, enhance the reliability and effective sensitivity of the method by enabling the experimenter to distinguish unequivocally the molecular ion-containing species from the background. The partial mass spectra of several compounds illustrate the application of this technique to the determination of molecular weights. Arachidonic acid and organic acids in general yield $(M+H)^+$ as well as $(M-H)^+$ molecular ion species, $(M+Ag)^+$ is the predominant adduct formed even in the presence of large $(M-H)^+$ contributions (Figure 4). The $(M+H)^+$ in the mass spectrum of cholic acid is indistinguishable from background. At first glance the ion at m/z 373 could be designated as the $(M+H)^+$ with loss of water yielding m/z 355. The presence of the silver adduct at m/z 515 results in the correct assignment of molecular weight for this molecule at 515 minus 107 or 408 amu (Figure 5). Other compounds can be analyzed in a similar manner to allow accurate verification of molecular weights of the chemical species being investigated.

As part of this research the effect of adding silica gel to the glycerol matrix was investigated. The results indicate that modest increases in sensitivity of $(M+H)^+$ can be obtained in FAB upon addition of between 2-4% w/w silica gel to glycerol; this phenomenon also holds for FAB experiments with argentated silica gel ($AgNO_3$ impregnated) in which $(M+Ag)^+$ is observed (Figure 6).

Figure 3.

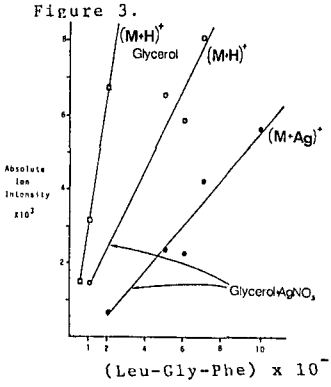

Figure 4.

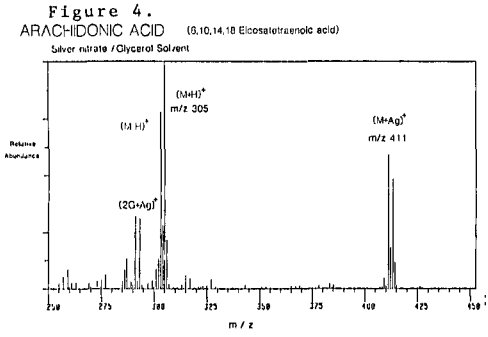

Figure 4. FAB-MS of Arachidonic acid dissolved in glycerol containing 0.14M silver nitrate. Silver adduct ions are apparent in the mass spectrum at m/z 411 and 413.

Figure 5.

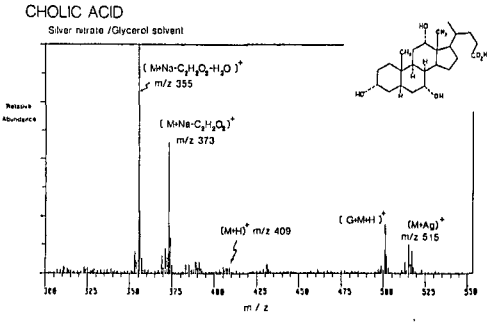

Figure 6.

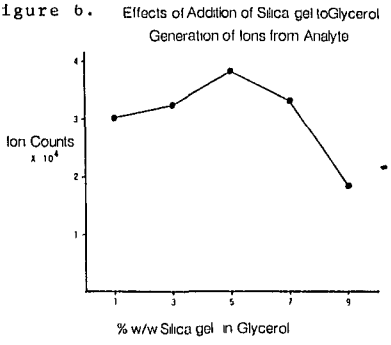

Figure 5. FAB-MS of Cholic acid dissolved in glycerol containing 0.14M silver nitrate.

Figure 6. Effect of silica gel in glycerol on ion current from $(M+H)^+$, when M is $APAP-SO_4$.

MOLECULAR ION ENHANCEMENT USING SOLID MATRICES IN LDMS AND SIMS

E.D. Hardin, T.P. Fan, and M.L. Vestal
Univ. of Houston, Chemistry Dept, Houston, TX 77004

A moving belt LCMS instrument with a laser desorption and ion impact source[1] has been used in our lab to study the effects of diluting a nonvolatile sample in a solid matrix. A solid matrix can be used to increase the desorption efficiency of molecular ions as well as decrease the relative amount of fragmentation in SIMS.[2] In LDMS Erythromycin exhibits a significant reduction in fragmentation as well as a 4-fold enhancement in alkali-attached molecular ion intensity when present in a 12:1 molar inositol matrix. Solvation of the sample by the matrix during desorption with subsequent gas phase desolvation to carry away excess molecular ion internal energy is presumably the mechanism responsible for the observed spectral differences.

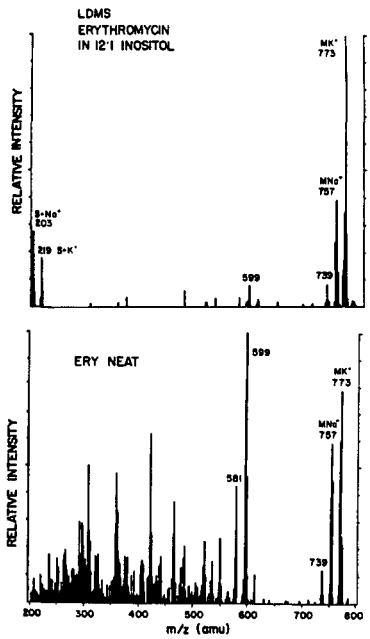

Figure 1. The top spectra shows the relative decrease in fragmentation obtained using a 12:1 molar inositol matrix. Peaks at 203 and 219 amu are from the alkali-attached inositol ions. The bottom spectra is from an equal sample size of erythromycin without the matrix taken under the same conditions.

A tartaric acid solid matrix has been used to both enhance desorption efficiency and change the relative amounts of $(M-H)^-$ and MH^+ preformed ions desorbed from histidine, a basic amino acid. With a constant histidine sample amount and an increasing relative tartaric acid concentration, there is a proportional decrease in the histidine $(M-H)^-$ ion signal and an increase in the MH^+ ion signal, both in LDMS and SIMS. In LDMS there is also a proportional increase in the $(M+alkali)^+$ ion signal with increasing tartaric acid concentration.

1. T.P. Fan, E.D. Hardin, and M.L. Vestal, Anal. Chem, (July 1984) in press
2. Kenneth L. Busch, Bih Hsuing Hsu, Ya-Xiang Xie, and R. Graham Cooks, Anal. Chem, 1983, 55, 1157-1160

GAS PHASE MOLECULAR SIMS*

P. J. Todd, G. S. Groenewold[1] and C. P. Leibmann[2]
Analytical Chemistry Division, Oak Ridge National Laboratory, Oak Ridge, TN 37831

Characteristic secondary ions can be observed if volatile amines are introduced into a secondary ion source in which a glycerol matrix is under ion bombardment. The abundance of these secondary ions relative to the abundance of the protonated glycerol ion has been found to follow the same trends observed for involatile analytes dissolved in glycerol; namely, longer chain amines yield more abundant secondary ions than do shorter chain amines. Therefore, surface activity is an important factor in determining the secondary ion abundance.

The secondary ion abundance from several different primary amines has been compared by admitting the gaseous amines to the mass spectrometer at a constant inlet rate and under conditions of constant ion flux. The ion abundance ratio [amine + H^+]/[93^+] (where 93^+ corresponds to the protonated glycerol molecular ion) for n-primary amines having a chain length of less than six carbons is approximately one-tenth of the corresponding ratio for n-primary amines that contain six or more carbons. A similar effect is observed for secondary amines, except that the increase in secondary ion abundance is observed between dipropyl and dibutylamine. Tertiary amines up to trihexyl amine yield a secondary ion abundance similar to that of the smaller primary and secondary amines. Significantly, neither proton affinities nor $K_B(H_2O)$ values correlated with secondary ion abundances when the amines were compared.

A further observation is that as the abundance of the [amine + H^+] ion increases, the abundance of [93^+] decreases. This effect is consistent with increased coverage of the glycerol surface by the amine, which obscures the glycerol from bombardment. However, introduction of octanoic acid at rates five times greater than the amine introduction rate resulted in a negligible decrease in [93^+] abundance. Introduction of acetic acid to the system resulted in no observable change in [93^+] abundance.

A sharp increase in the [amine + H^+] ion abundances were observed immediately after the gaseous amines were admitted to the secondary ion source. After the initial increase, the [amine + H^+] abundance continues to increase at a slower rate. This slower increase continues for as long as ten minutes after the amine was admitted to the source. A corresponding slow decrease is observed in the [93^+] abundance from glyercol. The rate of increase of the [amine + H^+] abundance is nearly equal to the rate of decrease of the [93^+] abundance (Fig. 1). We attribute this effect to increasing amine concentration in the bulk of the glycerol. Such an increase in the bulk concentration of the amine serves to reduce diffusion of the amine to the bulk from the surface, where ionization presumably occurs.

The kinetic rates of introduction, diffusion and evaporation (including sputtering) may be expected to reach a dynamic equilibrium after some time, which we believe to be approximately twenty minutes after initial analyte introduction in the amine/glycerol systems. The pivotol point of this equilibrium is the concentration of analyte and matrix at the matrix surface. The rate of evaporation is affected by the primary ion current. By interrupting the primary ion beam, new surface equilibrium concentrations are established. When primary ion bombardment is continued, abundant [93^+] and [amine + H^+] ions are immediately observed. However, the [amine + H^+] abundance is greater than it was prior to primary beam interruption (Fig. 2). In contrast, the [93^+] abundance is lower than it was prior to primary beam interruption. Both ions then exponentially return to their previous equilibrium abundances. It appears possible to study the kinetics of analyte-matrix interactions by using this relaxation method.

*Research sponsored by the U. S. Department of Energy, Office of Basic Energy Sciences, under Contract DE-AC05-84OR21400 with Martin Marietta Energy Systems, Inc.; also sponsored in part by the U. S. Army, Aberdeen Proving Grounds.

[1]ORAU Post-doctoral appointment.

[2]Student at University of Tennessee, Knoxville, TN.

By acceptance of this article, the publisher or recipient acknowledges the U.S. Government's right to retain a nonexclusive, royalty-free license in and to any copyright covering the article

Because the behavior of secondary ionization of volatile species parallels that observed for secondary ionization of involatile species, the mechanisms of the two processes are likely to be similar. The use of volatile analytes, however, permits kinetic studies to be performed on the matrix-analyte systems employed in SIMS and FABMS, systems which are clearly not in equilibrium.

Fig. 1

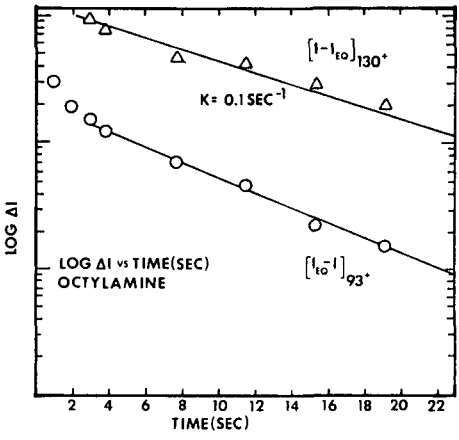

Fig. 2

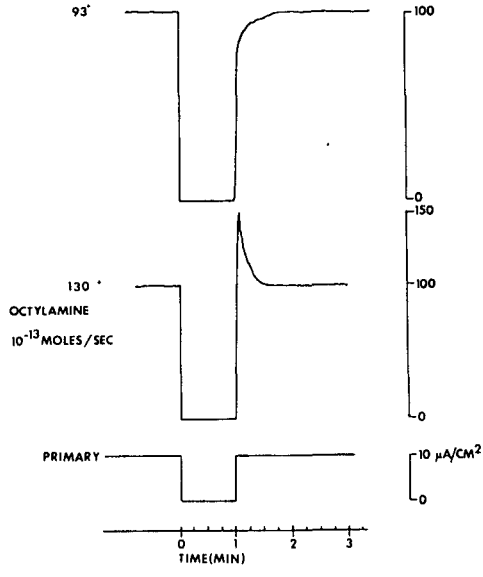

SELECTIVE DETECTION OF MIXTURE COMPONENTS BY SIMS

Mark M. Ross, David A. Kidwell, and Richard J. Colton
Chemistry Division
Naval Research Laboratory
Washington, D.C. 20375

The objective of this work is to develop SIMS for the analysis of low level components of complex mixtures [1]. The approach taken is that of derivatization of target compounds in a matrix to form compounds for which SIMS is a sensitive method of analysis (e.g., quaternary ammonium salts) [2]. The sensitivity of SIMS for precharged organic compounds has been shown to be in the nanogram to subnanogram range [3]. The advantages of this methodology include selectivity and sensitivity as well as direct analysis of the mixture with no prior extraction or sample clean-up steps. Three applications of this analytical method will be discussed.

Carbonyl-containing compounds were reacted in solution with Girard's Reagent P and an aliquot of this solution was deposited on silver for SIMS analysis. The derivative is a hydrazone with a quaternary ammonium group at one end of the molecule. The aldehydes and ketones were detected at low nanogram levels. Low molecular weight aldehydes and ketones such as acetone and benzaldehyde as well as larger compounds such as cortisone, progesterone, and testosterone were derivatized and analyzed. This scheme was applied to the analysis of airborne aldehydes and ketones from paint vapors and compared with a GC/MS analysis (Fig. 1). The derivatization/SIMS technique proved to be a selective method of analysis in that only aldehydes and ketones are observed (as their derivatives) in the SIMS spectrum. In addition, a quantitative analysis procedure based on labelled derivatives was developed.

This analytical scheme was also applied to the study of adsorbates and impregnants on activated charcoals. One example is the analysis of triethylenediamine (TEDA) on charcoal which was exposed to methyl iodide. The TEDA-CH_3I quaternary ammonium salt was formed on the charcoal and desorbed directly from the surface by particle bombardment. Impregnants such as Cu, Ag, and Cr were complexed with various chelating agents and subsequently desorbed from the charcoal as the metal chelate ion.

Finally, drug compounds such as methamphetamine, methadone, quinine, and propoxyphene were derivatized with methyl iodide in basic solution to form quaternary ammonium salts. These drugs were derivatized and analyzed from methanol/water solution and from urine at the picogram level (Fig. 2). The fragmentations of methadone and propoxyphene were studied also.

[1] M.M. Ross, D.A. Kidwell, J.E. Campana, Anal. Chem., in press.
[2] D.A. Kidwell, M.M. Ross, R.J. Colton, J. Am. Chem. Soc., 106, 2219-2220 (1984).
[3] S.E. Unger, T.M. Ryan, R.G. Cooks, Anal. Chim. Acta., 118, 169-174 (1980).

Comparison of GC/MS and SIMS Analyses of Paint Vapors

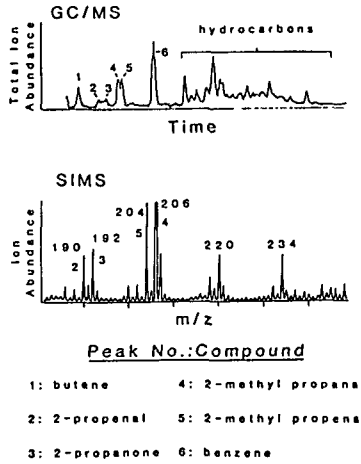

Figure 1

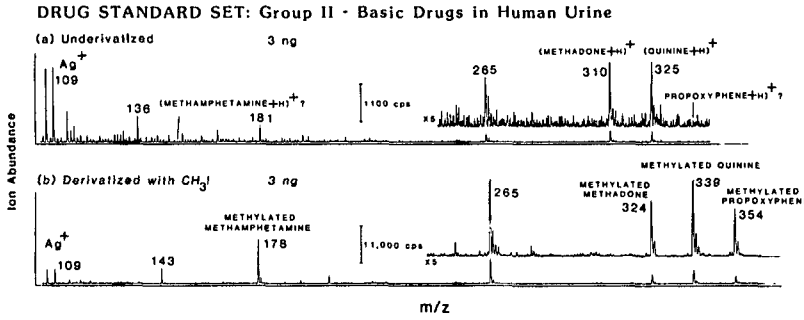

Figure 2

ORGANIC SIMS INVESTIGATIONS OF THERMALLY LABILE ORGANIC MOLECULES ON A SILVER SUPPORT AND IN A GLYCEROL MATRIX

A.Benninghoven, M.Junack and W.Sichtermann
Physikalisches Institut der Universität Münster,
D-4400 Münster, Fed. Rep. of Germany

Secondary ion mass spectroscopy of involatile organic molecules can be performed with a solid or a liquid matrix. SIMS with a liquid matrix is generally referred to as "FAB" (fast atom bombardment). Both, liquid and solid sample SIMS are successfully applied to the detection and structural analysis of large organic molecules.

In comparing the two modes of SIMS-operation some questions may arise:

- Are SIMS and FAB different ionization techniques ?
- Is SIMS a low mass range and FAB a high mass range technique ?
- Are SIMS and FAB spectra in principle different ?
- Are secondary ion yields different for glycerol or noble metal supported molecules ?

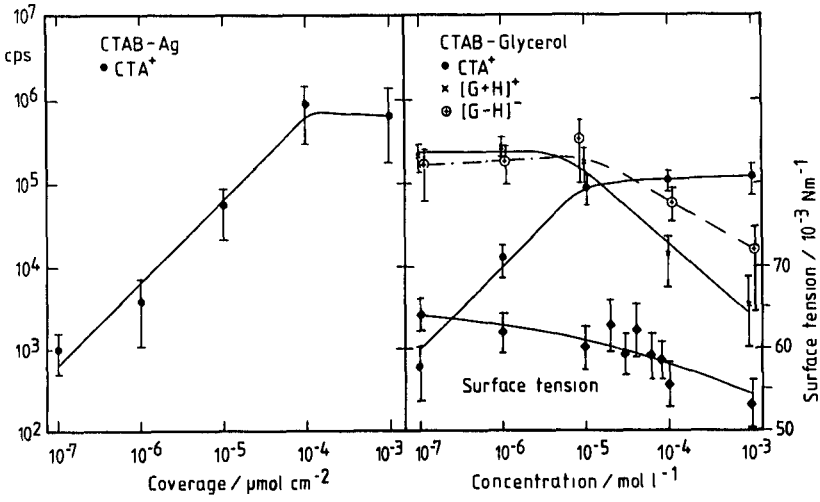

Fig. 1: Secondary ion emission from cetrimoniumbromide (CTAB) deposited on silver and on glycerol. For a silver surface the CTA^+-emission increases up to a surface coverage of 10^{-4} µmol/cm^2, corresponding to a closed monolayer. On the glycerol matrix, a closed monolayer is formed at a bulk concentration of about 10^{-5} mol/l. For higher bulk concentrations, the emission of glycerol specific secondary ions drops sharply, indicating the formation of a closed CTAB-layer.
Static SIMS operation.

By a careful investigation and comparison of glycerol and noble metal supported samples of cetrimoniumbromide, atropine, sucrose and fructose in a quadrupole SIMS-instrument, we found that one gets the same characteristic parent and fragment ions for a silver as well as for a glycerol matrix. The sputtering and the secondary ion yields are the same for both substrates. From these and the corresponding TOF-SIMS experiments with biomolecules such as oligonucleotides, oligosaccharides, and oligopeptides, one can conclude that there is no significant difference in the spectra from both these substrates and that, at least for the low mass range, the ion yields are virtually the same.

For the analytical application of SIMS, these results indicate that if only a small amount (<1 nmol) of sample material is available, its deposition as a stable monolayer on a noble metal substrate in combination with a high transmission mass spectrometer (quadrupol or TOF) is the most sensitive mode of SIMS. For high mass resolution, larger amounts of sample material (>1 nmol) are required which cannot be ionized from a monolayer on a solid but only from a regenerating liquid matrix.

Reference

A.Benninghoven, Int.J.Mass Spectrom.Ion Phys. 53 (1983) 85

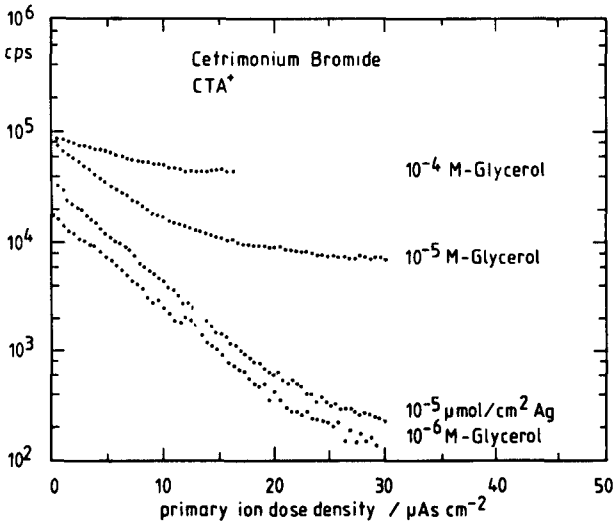

Fig. 2: Removal of cetrimoniumbromide from the uppermost monolayer of a glycerol matrix. For low bulk concentrations of CTAB (10^{-6} M) a complete removal is possible by ion bombardment. At higher bulk concentrations (10^{-4} M and 10^{-5} M) the replacement of the sputtered CTAB-molecules by diffusion from the bulk results in a higher equilibrium surface concentration of the sample molecules.

ENHANCEMENT OF SECONDARY RADICAL CATION EMISSION BY $SbCl_3$*

Gary S. Groenewold and Peter J. Todd
Analytical Chemistry Division, Oak Ridge National Laboratory
Oak Ridge, TN 37831

Two examples of reactions which produce ions in protic matrices are acid-base reactions (equation 1) and ionic dissociation reactions (equation 2). The abundance of gas-phase ions observed in secondary ion mass spectrometry (SIMS) and fast atom bombardment mass spectrometry (FABMS) has been related to the concentration of the solvated ions in the matrix.[1] The enhancement of secondary ion abundances by the matrix is limited by this constraint; if neither reaction (1) nor reaction (2) occurs to an appreciable extent, no enhancement is effected by the matrix.

$$M + AH \rightleftharpoons MH^+ + A^- \quad (1)$$

$$M^+X^- \rightleftharpoons M^+ + X^- \quad (2)$$

We have examined antimony trichloride ($SbCl_3$) as a SIMS matrix[2] to test whether this constraint is valid for the enhancement of secondary molecular ion abundance from aprotic matrices. $SbCl_3$ is a low melting solid (m.p. 73°C) which reacts with a variety of polyaromatic hydrocarbons (PAHs) via a reversible, one electron oxidation reaction.[3] The odd-electron PAH molecular ions produced by these reactions are dissolved in $SbCl_3$ in the same way as protonated analytes are dissolved in protic matrices. If the existence of analyte ions in the matrix has a bearing on the abundances of the corresponding ions in the secondary ion mass spectrum, then the abundances of certain PAH molecular ions should be enhanced by using $SbCl_3$ as a SIMS matrix.

$$1/3\ SbCl_3 + PAH \rightleftharpoons PAH^+ + 1/3\ Sb^\bullet + Cl^- \quad (3)$$

PAH/$SbCl_3$ mixtures (one to four mole percent) were prepared and loaded onto the probe tip under anhydrous conditions. Best results were obtained by using a gold-plated probe tip; other metals reacted with the $SbCl_3$ to produce abundant metal and metal chlorine cluster ions in the secondary ion mass spectrum. In a typical experiment, a small amount of mixture ($\sim$ 10 mg) was loaded onto the probe tip and heated until melting occurred. The probe tip was cooled and then screwed onto the probe. The melting-cooling cycle homogenized the mixture and improved matrix adhesion to the probe tip. The probe was then transferred from the glove box to the mass spectrometer as quickly as possible. The mixture was bombarded with a 5 keV Ar^+ beam (5 $\mu A/cm^2$) and the resulting secondary ions were analyzed by using a tandem mass spectrometer.

Abundant ions corresponding to $SbCl_3^+$, $SbCl_2^+$, $SbCl^+$, Sb^+ and Cl^+ are observed in the secondary ion mass spectrum of $SbCl_3$. The probability of isobaric interference between analyte ions and matrix ions is reduced when using $SbCl_3$ as a matrix because of the low mass spectral background of the matrix. If the analyte and matrix ions do occur at the same nominal mass, the isobars may be identified by using high resolution mass spectrometry or by using MS/MS, because Sb and Cl have large mass defects and Sb_xCl_y ions show very simple MS/MS spectra.

Abundant pyrene molecular ions were observed in the secondary ion mass spectrum of a four mole percent pyrene/$SbCl_3$ mixture at room temperature. The temperature of the source was increased during the experiment because molten (but not necessarily solid) $SbCl_3$ is known to oxidize PAH compounds.[3] The abundance of the molecular ions increased exponentially with increasing temperature until about 40°C. At 60°C the abundance of the pyrene molecular ions was fifty times greater than the abundance recorded at 20°C. Above 60°C the abundance decreased.

Pyrene was sputtered from the bare, gold probe tip (i.e., no matrix) in order to assess the effect of the $SbCl_3$ matrix on the abundance of the secondary molecular ions.

*Research sponsored by the U. S. Department of Energy, Office of Basic Energy Sciences, under Contract DE-AC05-84OR21400 with Martin Marietta Energy Systems, Inc., and by the U. S. Department of Energy Postgraduate Research Training Programs administered by Oak Ridge Associated Universities.

By acceptance of this article, the publisher or recipient acknowledges the U.S Government's right to retain a nonexclusive, royalty free license in and to any copyright covering the article

$SbCl_3$ matrix at room temperature. Heating the bare probe tip enhanced the pyrene molecular ion abundance by a factor of 3.5, but at no temperature was the abundance greater than that observed in the $SbCl_3$ experiment. No molecular ions were observed from a four mole percent mixture of pyrene in glycerol.

Pure, molten $SbCl_3$ is known to spontaneously oxidize PAHs with oxidation potentials ($E_{1/2}$) that are less than or equal to 0.51 V; PAHs with $E_{1/2}$ values greater than 0.51 V are not spontaneously oxidized.[3] Therefore, a series of PAHs that have a range of $E_{1/2}$ values were analyzed to attempt to further relate solution phase oxidation with secondary molecular ion abundance (Table 1). Molecular ions were observed from $SbCl_3$ solutions of phenanthrene and acenaphthene, but the abundances of these ions are not greatly enhanced by heating the sample. In contrast, the abundances of both pyrene and anthracene molecular ions are dramatically enhanced by heating; this behavior may be a consequence of the lower oxidation potentials of these compounds. Surprisingly, no molecular ion was observed from $SbCl_3$ solutions of naphthacene and perylene, despite the fact that these compounds have lower oxidation potentials than pyrene. The failure to observe the molecular ions of these compounds is not fully understood. A likely explanation is that their spontaneous oxidation by $SbCl_3$ produces high concentrations of radical cations in solution, which subsequently induce polymerization prior to SIMS analysis. This explanation is supported by the observation that these PAH/$SbCl_3$ samples appear black following SIMS analysis.

$SbCl_3$ clearly acts to enhance molecular ion abundances for PAH compounds with oxidation potentials between 0.5 and 0.6 V. $SbCl_3$ may formally oxidize only a small fraction of these compounds, producing a low concentration of radical cations in the matrix. This action would enhance molecular ion abundances without initiating polymerizaation. Alternatively, the $SbCl_3$ may merely reduce the energy required for the formation of a gas-phase molecular ion, by forming a charge-transfer complex with the PAH in the matrix. This possibility draws support from the observation that the PAH/$SbCl_3$ solutions are colored (usually bright green).

These observations support the hypothesis that SIMS matrix conditions which favor the formation of ions in the condensed phase also greatly enhance the abundance of the corresponding secondary ions. This conclusion appears to be valid for aprotic and protic matrices.

Table 1. Oxidation Potential, Ionization Potential, and Temperature Enhancement of Secondary Ion Abundance Using $SbCl_3$

PAH	Oxidation Potential (eV)[1]	Enhancement
Naphthacene	0.31	-
Perylene	0.24	-
Anthracene	0.51	190
Pyrene	0.59	63
Acenaphthene	0.64	1.6
Phenanthrene	0.9	2.5

1. Referenced to $Sb^{\circ}/SbCl_3$.

References

1. Caprioli, R. M. Anal. Chem., 1983, 55, 2387-2391.
2. Groenewold, G. S.; Todd, P. J.; Buchanan, M. V. Anal. Chem., in press.
3. Buchanan, A. C., III; Livingston, R.; Dworkin, A. S.; Smith, G. P. J. Phys. Chem., 1980, 84, 423-427.

ISOMER DIFFERENTIATION IN PARTICLE-INDUCED DESORPTION MASS SPECTROMETRY/MASS SPECTROMETRY

Steve E. Unger, The Squibb Institute for Medical Research,
P.O. Box 4000, Princeton, NJ 08540

While particle-induced desorption techniques such as fast atom bombardment (FAB) and secondary ion mass spectrometry (SIMS) have expanded the range of compounds amenable to direct mass spectral investigation, they have also brought forth new challenges to the analyst. Among these are the interpretation of spectral-structural relationships from sampling a condensed phase (solid or solution). This is particularly evident for solution sputtering where matrix effects such as the presence of surfactant or reactive impurities make spectral interpretation difficult. Apart from such adverse effects, deconvolving even simple mixtures by mass spectrometry alone is often impossible. While high resolution and chromatographic analysis is useful, it is often time and labor intensive.

An alternative is the use of mass spectrometry/mass spectrometry (MS/MS) with either FAB or SIMS . This approach minimizes the introduction of unwanted impurities such as surfactants which may mask observation of the analyte when prior chromatographic schemes are employed. It is generally faster and more structurally-informative than high resolution analysis , particluarly for high mass ions. The elimination of solvent background common to FAB often allows fragmentation not evident in the mass spectrum to be defined. Enhancement or control of the extent of fragmentation by collisional-activation may also better define parent/daughter relationships.

Unlike chemical ionization, field ionization, or field desorption, significant fragmentation is often observed in FAB spectra, setting a limit on sample complexity. However, direct analysis of 10-15 component mixtures of structurally-related pharmaceuticals such as monobactams has been accomplished. In combination with forms of chromatography which provide microgram levels of poorly resolved analyte (e.g. thin-layer chromatography) this approach is particularly useful.

For pharmaceutical agents, definition of isomeric forms is critical. While FAB MS/MS does not spatially resolve isomers, it often distinguishes isomeric structures not evident from the mass spectrum. Examples include E- and Z- isomers, enantiomers, and positional isomers of monobactams, peptides, and steroids. Distinguishing features are frequently differences in relatve daughter ion intensities. FAB or SIMS MS/MS spectra may be reproduced to within 5-10% accuracy, allowing such a demanding distinction to be made.

Figure 1 shows MS/MS spectra of the deprotonated molecule of the antibiotic aztreonam. The Z- (top) and E- (bottom) isomers are clearly distinguished (see structure I). The four isomeric forms of dipeptides of isoleucine and leucine are all differentiated from their respective MS/MS spectra of the protonated molecule. Figure 2 shows spectra for LEU-LEU (top) and ILE-ILE (bottom). This distinction has been particularly useful for direct examination of Cathepsin digests by FAB MS/MS.

Differentiation of positional isomers of monobactams and steroids is also possible. Prediction of the best ionic form of the parent for examination by MS/MS must rely upon previous knowledge of fragmentations evident to this class of compounds. The existence of a variety of cationized species in FAB or SIMS adds new possibilities for differentiation yet makes prediction more difficult. Distinguishing features often involve examining fragmentation about the isomeric site relative to a remote site. For monobactams, desulfonation often served as this remote site.

Given the appropriate isomeric compounds, simple mixtures may be deconvolved into their respective isomeric forms and quantified to within 5-10% accuracy. An example is shown in Table I for the E- and Z- isomers of aztreonam.

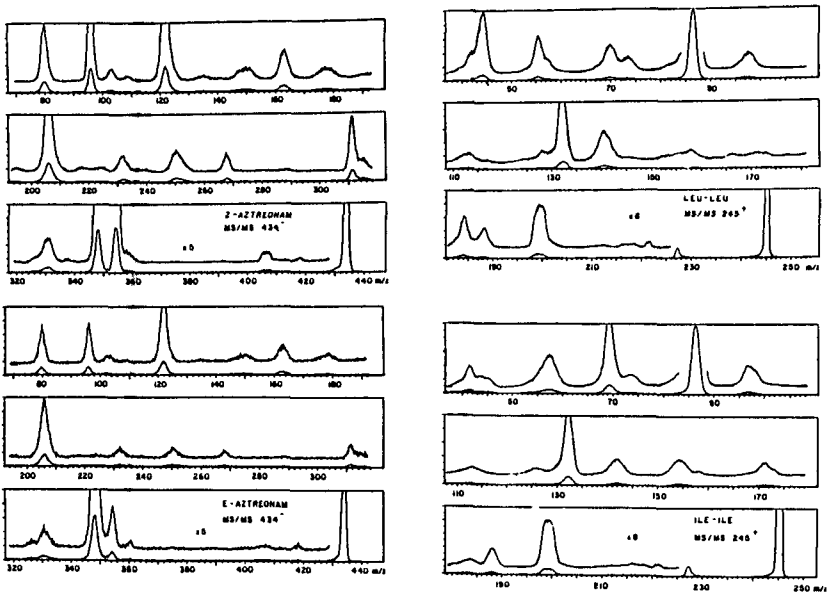

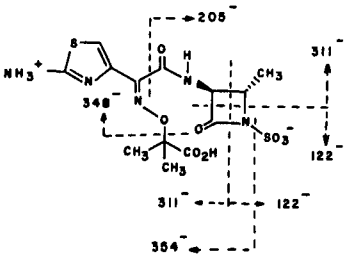

DATA REPRODUCTION OF MIXTURES OF E-/Z-AZTREONAM

USING FACTOR ANALYSIS

%E(meas)	%E(calc)	%Z(meas)	%Z(calc)
100	100	0.0	0.0
90	90	10	12
80	77	20	24
70	73	30	27
60	59	40	41
50	44	50	49
40	35	60	63
30	27	70	70
20	18	80	77
10	7.2	90	86
0	0.0	100	100

two factors, -SO3 and -C4H6O2, are used

INFLUENCE OF THE LASER WAVELENGTH IN LAMMA DESORPTION OR ORGANIC MOLECULES

M. Karas, D. Bachmann, F. Hillenkamp

Institute of Biophysics, University of Frankfurt, 6000 Frankfurt/M. 70
Federal Republic of Germany

Processes resulting in (quasi molecular) ion formation from organic solids in laser desorption (LD) mass spectrometry as well as the experimental parameters affecting it still need further clarification (1). Collective excitation of the solid matrix proposed as a model for LD upon irradiation with high irradiance ns-pulses in the UV, as typically used in LAMMA, would predict only a minor influence of the laser wavelength (2). No systematic investigations have however so far been reported.
In a series of desorption experiments of aromatic and aliphatic amino acids (AA's) with a LAMMA 1000 instrument, using 266 and 355 nm, the role of the wavelength as an important experimental parameter could be demonstrated. Working at 266 nm and irradiances close to ion detection threshold, spectra of all aromatic, i.e. absorbing AA's have reproducibly been obtained. $(M+H)^+$, $(M+H-46)^+$ and the aromatic residue $(R)^+$ are the only signals of appreciable intensities. Signals of neither alkaline ions nor cationized parent molecules are observed. The threshold irradiances E_o for tryptophane (Trp), tyrosine (Tyr) and phenylalanine (Phe) are related as 1:2:5 which qualitatively follows the magnitude of the absorption coefficient at this wavelength. The threshold irradiance for aliphatic AA's is a factor of 12 above that of Trp. Spectra of aliphatic amino acids, always show strong signals of alkaline and alkali attached molecular ions as well as considerable fragmentation. For both, aromatic and aliphatic AA's the ratios $(M+H)^+ / (M+H-46)^+$ and $(M+Alkali)^+/(Alkali)^+$ decrease for increasing irradiance.
A typical series of LD mass spectra is shown in Fig. 1.

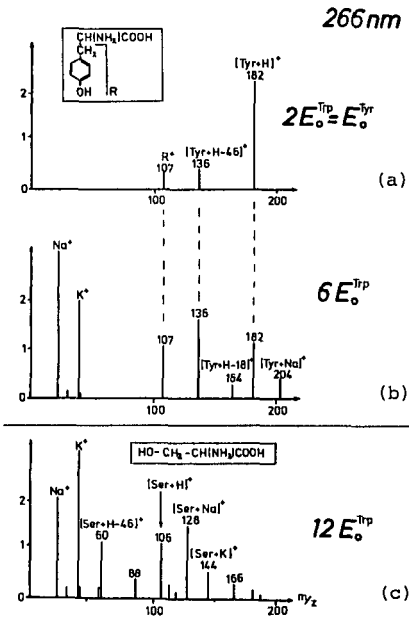

Fig. 1 LDMS of Tyr at threshold irradiance (a), at 3 times above (b) and of Serine (the corresponding aliph. AA) close to threshold irradiance (c).

At 355 nm, where no appreciable absorption for any of the AA's is given all of them showed a nearly equal and high threshold irradiance (50 times that of Trp at 266 nm). Spectra similar to those of the aliphatic AA's at 266 nm above threshold irradiance are obtained, i.e. alkaline and specific fragment ions are most abundant.
Fig. 2 shows the effect of increased irradiance at 266 nm (b) and of the change to 355 nm (c) in the mass spectra of Phe.

Generally, LD works significantly less reproducible at 355 nm and satisfactorily only from thin sample layers. This is indicated by abundant substrate ions. On the other hand ion desorption at 266 nm can reproducibly been induced from bulk samples as well.

These data prove that the laser wavelength is an important experimental parameter in the UV, especially if the single photon energy (4.6 eV at 266 nm) matches sample molecule excitation levels. Under these conditions energy transfer to the sample obviously is most effective and "softest" as indicated by the highest ratio of $(M+H)^+/(M+H-46)^+$. The total absence of alkaline ions and of unspe-

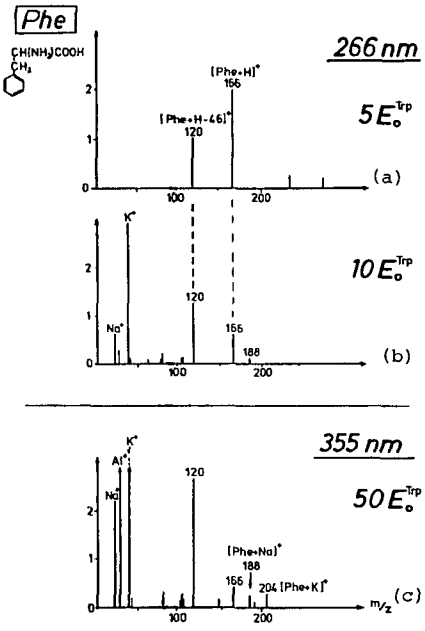

Fig. 2 LDMS of Phe at threshold irradiance (a), twice above (b) at 266 nm, (c) at 355 nm close to threshold

cific low mass fragments rules out desorption models where molecular ion desorption is thought to take place at medium temperatures in the surroundings of a hot laser spot. Ion formation rather seems to take place as a uniform and collective desintegration of the condensed phase initiated by electronically excited sample molecules. The energy primarily stored by excitons is transferred to the solid lattice resulting in vaporization and partial ionization via protonation.
For aliphatic AA's a higher photon flux is needed to initiate ion formation probably via multiphoton absorption.
A less uniform and locally stronger excitation of the sample is manifested by stronger fragmentation.
Conditions like this resulting in reproducible ion formation at 266 nm could not be received for any of the tested AA's at 355 nm. Al^+-ions, always present in the mass spectra, indicate that the dominant effect for sample ionization is the absorption of the laser energy by the substrate metal. Subsequent fast heating of a small sample region may result in melting, vaporization and ionization, but under LAMMA-conditions (10 μm^2 spot) in a far less reproducible fashion.

As a consequence of the model presented an absorbing compound should work as an absorbing matrix inducing "soft" ion formation at relatively low irradiance from a non-absorbing compound. This possibility could easily be varified for alanine (Ala) in a Try matrix. The spectrum of a 1:1 mixture of Ala and Trp close to the threshold irradiance for pure Trp is shown in Fig. 3. This matrix assisted LD can successfully be applied to larger thermally labile compounds, as f.e. for stachyose.

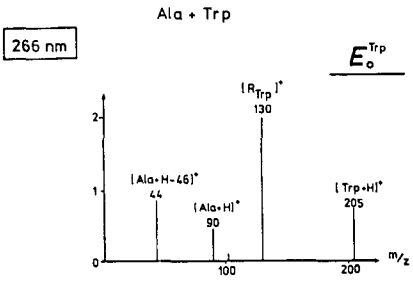

Fig. 3 LDMS of a 1:1 mixture of Ala and Trp at 266 nm and E_o (Trp)

References
(1) F. Hillenkamp, in "Ion Formation from Organic Solids", Ed. A. Benninghoven, Springer Verlag, Berlin, 1983, pp. 190-205.
(2) B. Schueler and F.R. Krueger, Org. Mass Spectrom., 15 (1980) 295

QUALITATIVE AND QUANTITATIVE ANALYSIS OF SYNTHETIC ORGANIC POLLUTANTS IN RIVER WATER BY GC/MS

Andrea M. Dietrich, Young-Hwa Seo, Daniel Cutugno,
David S. Millington
Department of Environmental Science and Engineering
University of North Carolina
Chapel Hill, NC 27541

The growing demand for drinking water in developing areas of the country has resulted in the consideration of unprotected supplies as possible potable water sources. One such example is a new reservoir fed by a North Carolina local river (the Haw River) which meets conventional State criteria for drinking water quality, but as it receives numerous industrial and municipal wastewater effluents and agricultural inputs, is subject to organic pollution. This study (1) was undertaken to characterize synthetic organic pollution in the Haw River. Broad spectrum analytical techniques are required to investigate such pollution in order to identify chemicals indigenous to the river.

A wide range of polar and volatile trace organic pollutants in the river water were concentrated by complementary techniques: methylene chloride liquid-liquid extraction, adsorption onto XAD macroreticular resins, and closed loop stripping (CLSA). After extraction by organic solvents, the extracts were analyzed by capillary column GC/MS (DB1 and DB5 columns). Organic pollutants were identified by EI and CI spectra, accurate mass data obtained at low resolution (VG Analytical 7070F/Datasystem 2035), library search techniques and ultimately, by comparison with authentic reference standards.

Sampling and analysis of the Haw River extended over a two and one half year period. Nearly sixty different trace organic compounds were identified in various river water samples. Among the chemicals repeatedly identified were atrazine, dioxane, o-dichlorobenzene, methyl atraton, naphthalene, tris (chloropropyl) phosphate, tributyl phosphate, triethyl phosphate, N,N-dimethyl p-toluenesulfonamide, toluene and 1,2,4 trichlorobenzene.

For resin adsorption investigations, quantitative measurements of selected organic pollutants were determined by a two tiered internal standard approach. Selection of internal standards was based on analogy to suspected pollutants. 300 ug of primary (1°) internal standards, m-dichlorobenzene, D_8 naphthalene and ametryn, were added directly to 30 liters river water and passed through the XAD resin beds. The resins were sequentially extracted with diethyl ether and methylene chloride. 150 ug secondary (2°) internal standards, o-chlorotoluene, 1-methyl naphthalene, and atraton were added to the combined extracts prior to Kuderna-Danish concentration and chromatographic analysis. Recovery of the 1° internal standards and measurement of the concentrations of indigenous pollutants were determined with respect to the 2° internal standards. The response ratio of characteristic mass spectral peaks (single ion quantification) for each 1°-2° standard pair and pollutant-2° standard pair were compared with a set of calibration curves. Recovery data for the 1° internal standards were (n=4): m-dichlorobenzene- 79±9%; D_8 Naphthalene- 62±6%; Ametryn- 56±9%. The overall recovery was 65±12%. Quantitative results for river water pollutants are presented in Table I.

Table I
Quantitative measurement of Pollutants in the Haw River
(duplicate samples, corrected for % recovery)

SAMPLE	POLLUTANT (ug/L) Atrazine	Tris (chloropropyl) phosphate	Toluene
Site A(1)	1.7	2.1	0.12
Site A(2)	1.6	1.6	0.65
Site B(1)	2.8	1.5	-
Site B(2)	2.7	1.4	-

For CLSA investigations, a 1 liter water sample was purged for 2 hours. 200 ng of C_6, C_8, C_{10}, C_{12}, and C_{18} normal chloroalkanes were added as secondary internal standards to the carbon disulfide extracts prior to chromatographic analysis. Area response ratios were measured for volatile river pollutants with respect to the nearest eluting chloroalkane. Concentrations of pollutants were estimated by comparision to standard curves. The sample river water was then purged for 24 hours, and checked for removal of volatile trace organic pollutants. 50-400 ng of standard compounds (1° standards) of the identified pollutants were equilibrated with the extensively purged river water and the sample again purged for 2 hours. Recoveries for the standard compounds were: p-dioxane- 85±12%; tetrachloroethylene- 99±9%; m-dichlorobenzene- 85±2%; 1,2,4 trichlorobenzene- 76±9%. The overall average recovery was 84±10%. The chloroalkanes were added to the carbon disulfide extract and the recoveries of selected standard compounds were calculated. These recoveries were used to calculate actual concentrations of pollutants in the original river water sample. Quantitative results of volatile pollutants are presented in Table II.

Table II
Quantitative Measurement of Volatile Pollutants in River Water
(duplicate samples, corrected for %recovery)

SAMPLE	POLLUTANT (ng/L) p-dioxane	tetrachloro-ethylene	m-dichloro-benzene	1,2,4 tri-chlorobenzene
Site A(1)	450	984	154	316
Site A(2)	443	1040	165	341
Site B(1)	51	104	30	69
Site B(2)	68	85	32	73

In conclusion, quantitative measurement of specific pollutants in river water can be successfully acheived during broad spectrm analysis by using suitable internal standards added to the sample matrix and to the solvent matrix. The reproducibility of the resin and CLSA methods applied here are very good. Additionally, for the identification of a broad spectrum of organic pollutants in river water, EI, CI and accurate mass measurements are helpful and sometimes necessary for identifying compounds for which library spectra are not available.

Dietrich, A.M., D.S. Millington, R.F. Christman; Specific Identifications of Organic Pollutants in Haw River Water Using Gas Chromatography/Mass Spectrometry (Water Resources Research Institute of North Carolina State University, Report No. 206); University of North Carolina Press, August 1983.

ISOMER SEPARATION OF DIOXINS AND FURANS IN A FLY ASH SAMPLE USING VARIOUS CAPILLARY COLUMNS.

B. P.-Y. Lau, W.-F. Sun, J.J. Ryan, Food Research Division, Health and Welfare Canada, Tunney's Pasture, Ottawa, CANADA, K1A 0L2.

Introduction:

There is an ever-growing concern of the widespread contamination of dibenzofurans (PCDFs) and dibenzodioxins (PCDDs) in the environment. Research in the past was concentrated on the most toxic 2,3,7,8-TCDD isomer. Recently, attention has been extended to other isomers and congeners. Because of the great diversity of toxicity and biological effects among different PCDF and PCDD isomers, the development of an isomer specific analysis is imperative. Proper identification of the tetra- to octa-chlorinated PCDF and PCDD congeners relies heavily on the availability of a complete set of isomeric standards. Unfortunately, synthesis of all pure isomer standards is costly, dangerous, time consuming, and technically difficult. Only a handlful of laboratories around the world will have access to all synthetic isomers. Chlorinated compounds including most PCDF and PCDD isomers are known to be absorbed on fly ash generated from the incineration of municipal waste. This paper describes the characterization of such a fly ash which can be used as a natural isomer mixture and a secondary standard for isomer identification.

Isomer Separation and Identification:

. Identity of all tetra- to octa-congeners of PCDFs and PCDDs (136 possible compounds) in a fly ash sample prepared and supplied by Otto Hutzinger were first confirmed by medium resolution (~5000) MS and the isotopic abundance ratio of 3 ions at the molecular ion clusters on a 50-m chemically bonded CPS-1 column (Quadrex Corp., equivalent to SP-2340, 0.25 mm ID, film thickness = 0.25 u).

. All isomer peaks from
1) O. Hutzinger's fly ash sample (mixture 1);
2) T. Mazer's (Monsanto) PCDF mixture (mixture 2);
3) C. Rappe's PCDD mixture (mixture 3)

on the CPS-1 column were assigned according to published data[1-4] on SP-2340 and Silar 10C columns as well as by comparison to our own individual standards.

. Isomer separation from mixtures 1, 2 and 3 was compared on other fused silica columns with different polarities (all chemically bonded, film thickness = 0.25 u):
a) 30-m DB-225 (J&W), 0.25 mm ID;
b) 10-m DB-5 joined with a 30-m DB-225 by a zero dead volume union;
c) 30-m DB-210, (J&W), 0.25 mm ID;
d) 50-m OV-1701 (SGE), 0.20 mm ID;
e) 60-m DB-5 (J&W), 0.25 mm ID.

. Peak assignments on these columns were based on:
1) Health and Welfare's individual standards (72 of possible 136).
2) Relative intensities of isomers from mixtures 1, 2 and 3.
3) Published data in the literature.

. Since individual isomer standards on hand were limited and several isomers co-eluted on some medium polarity columns, peak identification, especially in the TCDF and PnCDF region, has not been completed.

. As far as the number of GC peaks was concerned, it appeared that the most polar CPS-1 (equivalent to SP-2340) column offered the best isomer separation with the separation power dropping in the order: DB-225, DB-5 + DB-225, OV 1701, DB-210 and DB-5.

. However, some isomers which could not be resolved on one column could be well separated on other columns and vice versa. For example, the toxic 1,2,3,7,8-PnCDF isomer which co-eluted with 1,2,3,4,8-PnCDF only on the CPS-1 column could be separated from 1,2,3,4,8- on the DB-210 column even though it now co-eluted with the 1,2,3,6,7-isomer.

. Among the 6 columns used in this study, no single column was able to separate every single PCDF and PCDD isomer, whereas a combination of several columns, (for example one polar, one medium polarity and one non polar) would readily accomplish the task of separating the most toxic isomers.

References:

1. C. Rappe, Environ. Sci. Technol., 18 (3), 78A-90A (1984).
2. H.R. Buser, C. Rappe, Anal. Chem. 56, 442-448 (1984).
3. T. Mazer, F. Hileman, R.W. Noble, J. Brooks, Anal. Chem. 55 (1), 104 (1983).
4. S.H. Safe, L.M. Safe, J. Agric. Food Chem., 32, 68-71 (1984).

LONG-TERM GC/MS PRECISION AND ACCURACY STUDY FOR ENVIRONMENTAL MONITORING

W. J. Verret, C. M. Hedin, F. C. Garner, and J. R. Donnelly
Lockheed Engineering and Management Services Co., Inc.
P.O. Box 15027, Las Vegas, Nevada 89114

OBJECTIVE: The U.S. Environmental Protection Agency (USEPA) Contract Laboratory Program requires implementation of quality assurance/quality control procedures for environmental analyses performed under USEPA contracts such as IFB WA-83-197/198. Sauter and colleagues have described[1] some of the procedures upon which the contract requirements are based. Long-term precision and accuracy must be achieved in order to reproduce results from day to day and month to month. Another factor that must be considered is linearity of response from low concentrations (5 ng) to high concentrations (400 ng) of each component. The USEPA also defines detection limits[2] which must be consistently less than 10 ng. At present, we have checked three USEPA methods to ensure that USEPA performance requirements can be met on a routine basis. Finally, we will demonstrate data comparability using three USEPA methods over a 5-month time period.

EXPERIMENTAL: We have performed a single laboratory, single instrument long-term (5-month) study of instrument stability, linearity of response vs. amount injected (Figure 1), standard deviation and relative response factors on 93 semivolatile priority pollutants classified as acids, bases, neutrals and surrogates. These compounds were analyzed by three different USEPA GC/MS methods. The December data was obtained using GC and MS conditions as specified under WA 83-A064, February 1983. The March data was obtained by using GC and MS conditions as specified in Method 8270, Solid Matrix Study. The April data was obtained using GC and MS conditions as specified in WA83-197/198. Libraries and response lists were generated using Finnigan Instruments software. Eight concentrations of each pollutant were run (5 ng, 10 ng, 25 ng, 50 ng, 100 ng, 200 ng, 300 ng, and 400ng) and the results of each quantitated run were then appended to their respective response lists. After all 8 concentrations of each priority pollutant were run and appended, a graph was generated plotting area of compound/area of internal standard (y axis) vs. amount of each component (x axis). Using Finnigan software, a line was drawn using linear fit conditions and the Standard Deviation (SD) calculated and $\pm$ 2 SD plotted.

Next, according to USEPA protocols[2], detection limits were determined by three successive runs using a 50 ng standard (Figure 2). The mean, standard deviation (SD) and 3 SD were then calculated. These replicate runs were made using the GC/MS conditions for each of the 3 months as specified earlier.

Data obtained using the conditions described earlier show long-term (5 months) reproducibility of detection limits. Three different methods were used and USEPA performance requirements were then assessed and compared to data generated in a single-laboratory, single-instrument study.

CONCLUSIONS: We have shown in this study that precision and accuracy over a 5-month period are satisfactory for a single instrument and that linearity can be achieved repeatedly and routinely from 5 ng to 400 ng of 93 priority pollutant compounds in standard solutions. Detection limits were consistently within USEPA requirements over a 5-month period using three different GC/MS methods. Finally, data can be readily compared from month to month and method to method.

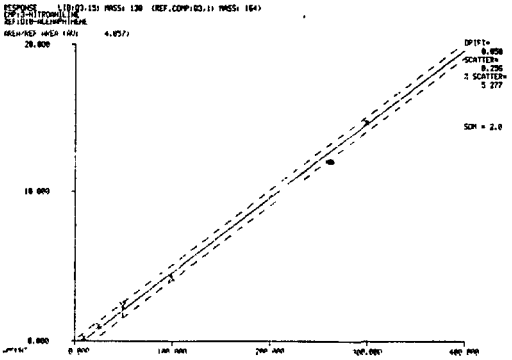

Fig. 1

December

	Compound	Run #1	Run #2	Avg #3	$\bar{x}$	$\hat{\sigma}$	$\hat{\sigma}/\bar{x}$
1	BA-1,4-Dichlorobenzene	50 000	50 000	50.000	--	---	---
2	Phenol	48 653	49 346	52.997	50 199	2 306	4 3
3	2-Chlorophenol	50.022	48 994	49.981	49 639	0 562	1 7
4	N-Nitrosodimethylamine	43 915	43 072	47.315	44 767	2 346	4.7
5	Bis(2-Chloroethyl)ether	51 130	51.843	55 047	53 251	2 012	6 0
6	1,3-Dichlorobenzene	46 848	46 148	45.744	46 247	0 559	1 7
7.	1,4-Dichlorobenzene	48 611	47 886	48.004	48 167	0 319	1.3
8	1,2-Dichlorobenzene	47 372	46 983	43.418	47 591	0 742	2.2
9.	Bis(2-Chloroisopropyl)ether	55.520	50.328	55.318	53 055	2 817	7 6
10	N-Nitrosodi-n-propyl amine	48 206	47 841	46.020	48 022	0 182	0.5
11	Hexachloroethane	51 365	50 973	50.678	50 929	0 474	1.3
12	Benzyl alcohol	54 808	54 578	56.471	54 976	0 697	2 1
13.	o-Cresol	51 632	51 158	55.306	52 699	2 270	6.8
14.	p-Cresol	51 318	49 691	50.527	50 512	0.814	2 4
15	Aniline	55.445	54.247	55.151	54 948	0 624	1 9
16	Bg-Naphthalene	10	10	10	---	---	---
17.	Nitrobenzene	46 623	45 811	49 031	47 155	1 675	5 0
18	Isophorone	47 865	47 162	47 698	47 575	0 367	1.1
19.	Bis(2-Chloroethoxy)methane	46 125	46 798	48 328	47 084	1 129	3 4
20.	Naphthalene	52 044	52 766	54.351	53 047	1 169	3 5
21	1,2,4-Trichlorobenzene	44 852	44 042	44.678	44 807	0 408	1 2
22	Hexachlorobutadiene	48.565	43 970	46 797	48 111	1.154	3 5
23	2-Methylnaphthalene	45.919	45 828	45 907	48 931	0 085	0 2

Fig 1

REFERENCES:

1. A. D. Sauter, L. D. Betowski, T. R. Smith, V. A. Strickler, R. G. Beimer, B. N., Colby and J. E. Wilkinson, J. of High Resol. Chrom and Chrom. Commun. 4, 366(1981).

   A. D. Sauter, P. E. Mills, W. L. Fitch, R. Dyer, J. High Resol. Chrom. and Chrom. Commun. 5, 27(1982).

2. U. S. Environmental Protection Agency, Procurement Section A (PM-214-F), Organics Analysis Invitation for Bid, Contract No. IFB WA-A197/198, April, 1983.

DEVELOPMENT OF ANALYTICAL METHODS FOR RESIDUAL POLYCATIONIC POLYMERS IN DRINKING WATER

Kai-Lo Hsu, Albert R. Trussell
Montgomery Laboratories
Pasadena, CA

James G. Moncur
Lockheed Missiles and Space Co.
Palo Alto, CA

The use of organic polycationic water treatment polymers as coagulant aids has become increasingly popular in the last decade. Dosages of such polymers range from 0.5 to 5 ppm and little information is available on the residual concentrations of such polymers in water treatment plant effluents (1,2). Hence the development of an effective routine analytical method for the determination of polycationic polymers at the sub-parts-per-million level is desirable.

Over the course of the last few years, the authors have reviewed or investigated a number of analytical approaches to the analysis of residual polycationic polymers:

1. Ion pair liquid-liquid extraction/chemically bonded normal phase HPLC with conductivity detection.

2. Colloid titration with colorimetric determination.

3. Evaporation/pyrolysis GC/MS.

4. Size exclusion HPLC with post column derivitization and UV detection.

The authors have focussed on Calgon's Cat-Floc T series of polycationic polymers which are popular in the Western United States. In this research, techniques 2-4 are the most promising to date. Pyrolysis GC/MS results show that the polymer Cat-Floc T-2 yields mass fragments for methylchloride (m/z 50,52) and propylamine (m/z 58,59) distinguishable from natural humic (phenolic and carboxylic moeity) interferences for positive confirmation. The colloid titration technique when coupled with rotary evaporation pretreatment yields excellent results at concentrations as low as 100 parts-per-billion (See Figures 1 and 2).

Results of applications of these techniques to water treatment plant effluents in California will be reported.

REFERENCES

1. Goppers, Velta and Straub, Conrad P., "Polyelectrolyte Persistence in a Municipal Water Supply," JAWWA 68:6; pp 319-320.

2. Baybak, Mary Ann, Calgon Corporation, personal communication, July 1983.

FIGURE 1

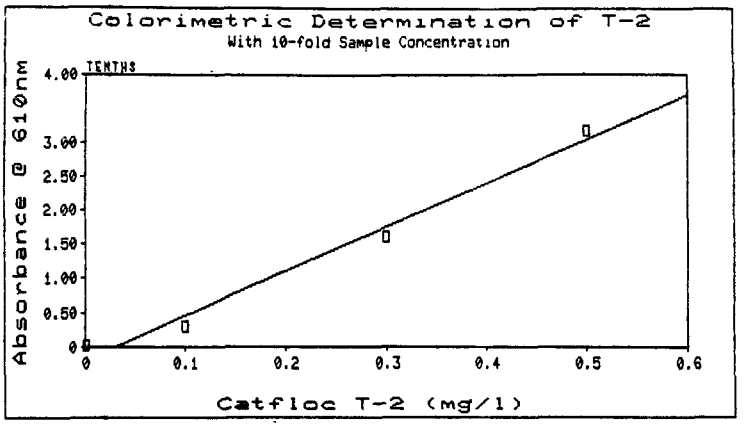

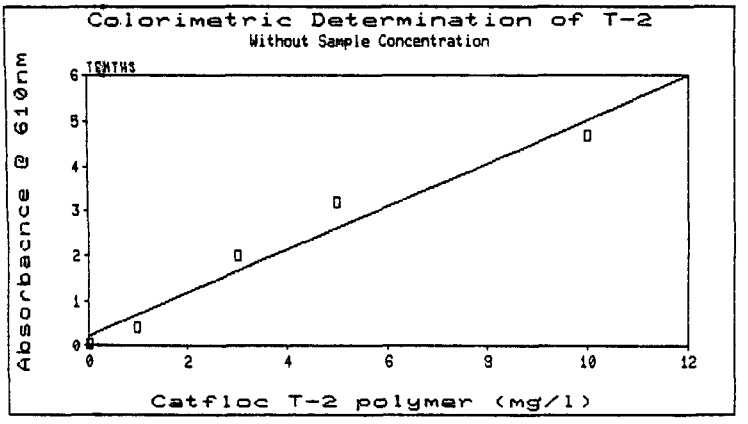

FIGURE 2

ANALYSIS OF A SOLID SLUDGE MATERIAL BY GC/MS

G. D. Byrd and L. R. Hilpert, Center for Analytical Chemistry, National Bureau of Standards, Washington, DC 20234

The migration of hazardous materials from waste dump sites into aquifers and water tables by aqueous leaching is an important environmental problem. Accurate quantitative data on the organics in the waste or its aqueous leachates is vital to any program responsible for the proper management and monitoring of hazardous wastes. The development of standard materials for sludges is difficult due to the complexity of sludge matrices, the number of analytes involved, and the detailed work-up procedure required to produce the aqueous leachate for analysis by GC/MS.

We have prepared and analyzed a quality assurance solid sludge material for the EPA. Our objective is to identify and quantify several organic compounds, most of which are priority pollutants, in an actual composite solid sludge and in aqueous leachates of that material. We also analyzed the components of variability contributed by the sample itself, the work-up procedure, and the GC/MS measurements.

The solid sludge material was prepared by blending two waste samples supplied by the EPA: an API separator sludge and a refinery incinerator ash. Separator sludges often contain high levels of toxic organic as well as inorganic compounds. Incinerator fly ash can also contain a variety of organic species if the combustion process was not complete. An investigation of the separate materials prior to blending showed that the separator sludge was very rich in organics with normal aliphatic hydrocarbons as the predominant species and lesser amounts of polycyclic aromatic hydrocarbons (PAH). Very low levels of organics were found in the ash and its aqueous leachates. Several kilograms of each material were combined in a stainless steel V-blender, mixed for 24 hours, and bottled in 100 gram units.

Aqueous leachates of the composite sludge were prepared according to the EPA EP Toxicity Test Procedure [1]. The methylene chloride extracts of the aqueous leachates were prepared and analyzed according to EPA Test Method 625 [2] for base/neutrals and acids. Quantitative determinations for organics in the extracts were made by capillary column GC/MS using selected ion monitoring and the method of internal standards. A variety of organic pollutants were identified and are listed in Table I. The concentrations of the individual organic species measured in the aqueous leachate were less than 10 μg/L. Since the sludge is to be used as a quality assurance and proficiency testing material, the specific data must be kept blind at this time.

Table I gives the average standard deviations of the mean ($S_{\bar{x}}$) and of a single measurement (S_x) for the targeted analytes. Twenty GC/MS measurements went into each average.

TABLE I

SOLID SLUDGE AQUEOUS LEACHATES

RSD (percent)

	PHENOL	NAPHTHALENE	2-Me-NAPHTHALENE	1-Me-NAPHTHALENE	BIPHENYL	DIPHENYLAMINE	PHENANTHRENE	CARBAZOLE	AVERAGE
S_s	0	0	0	5.0	0	0	0	8.4	--
S_{e+l}	5.8	17.5	12.5	10.1	21.4	12.9	31.2	11.4	15.4
S_r	10.9	13.5	10.3	9.9	18.1	6.8	11.7	10.9	11.1
S_g	2.6	4.5	3.9	4.7	5.7	2.9	7.9	5.9	4.7
S_x	12.3	22.1	16.2	15.4	26.2	14.6	33.3	17.9	19.8

Three components of the standard deviation are also listed in Table I. The between-bottle variability of the sludge samples (S_s) is not statistically significant for any of the analytes. However, the variability of the combined sample work-up step (leaching + extraction + concentration) between samples (S_{l+e}) is statistically significant, relative to the GC/MS measurement variability (S_r) for many of the analytes.

Methylene chloride extracts of the solid sludge were prepared by the Soxhlet method using 10 gram amounts of the sludge material from one bottle. The concentrated extracts were analyzed directly by GC/MS in the same way as was done for the extracts from the aqueous leachates. The same organic analytes were found at considerably higher concentrations.

Table II gives the average $S_{\bar{x}}$ and S_x values for the analytes with each average consisting of ten measurements.

TABLE II

SOLID SLUDGE SOXHLET EXTRACT

RELATIVE STANDARD DEVIATION (percent)

	PHENOL	NAPHTHALENE	2-MEthyl-NAPHTHALENE	1-MEthyl-NAPHTHALENE	BIPHENYL	DIPHENYLAMINE	PHENANTHRENE	CARBAZOLE	AVERAGE
S_s	14.9	6.6	9.8	10.4	8.2	3.9	3.7	13.6	8.9
S_r	3.5	7.5	6.4	5.8	3.4	3.8	4.4	7.5	5.3
S_{l+e}	6.9	3.5	4.8	5.0	3.8	2.1	2.2	6.5	4.4
S_x	21.6	12.0	15.2	15.8	12.1	6.6	7.0	20.6	13.9

One-way analyses of variance were performed. The between-subsample component shown (S_s) corresponds to the combined variability due to extraction imprecision and possible sample heterogeneity. In the current experiment, this latter component cannot be separated. For the smaller (10 grams) subsamples, there is moderately strong statistical evidence of a between-subsample component of about 5-15 percent. The GC/MS imprecision (S_r) is somewhat less for the Soxhlet extracts due, in part, to the higher concentrations of the analytes.

These results show that, for the amounts of sample leached in this study (100 g), the variability of the work-up procedure and GC/MS measurement overshadowed the variability within the sample itself for most of the analytes. However, the smaller sample size, less involved work-up procedure, and higher analyte concentrations in the methylene chloride extracts of the sludge allowed us to detect a small degree of sample heterogeneity.

References

[1] "Test Methods for the Evaluation of Solid Waste, Physical/Chemical Methods," SW-846, U.S. Environmental Protection Agency Office of Solid Waste, Washington, DC 20460.

[2] "Samplers and Sampling Procedures for Hazardous Waste Streams," EPA 600/2-80-018, January 1980.

METHOD FOR THE DETECTION OF BENZOTRIFLUORIDES IN ENVIRONMENTAL SAMPLES

Bertha L. Proctor, University of Texas-Dallas, Richardson, TX, 75080

Benzotrifluorides are important intermediates in the manufacture of crop protection chemical, pharmaceuticals and dyes (1) and are used in large quantities in the United States. Several benzotrifluorides have been found in the Niagara River-Lake Ontario system including water, sediment and fish. Several benzotrifluorides are suspected mutagens (2,3). Given the nature and unknown long term effects of these compounds, necessitates determination of their presence in the environment. This paper outlines a method for the detection of benzotrifluorides in environmental samples. This method has been sucessful in identifying benzotrifluorides in a wide variety of environmental samples including, water, soils, sediments, fish muscle and reproductive tissue and in human adipose tissue. All analyses were done on a *Nermag R-10-10* Mass Spectrometer equipped with a Carlo Erba Gas Chromatograph

Method: Positive Chemical Ionization Mass Spectrometry

Reagent Gas	Methane
Source Pressure	2.5×10^{-1} torr
source Temperature	180C

These conditions produced a strong M-F and often produce strong $M-CF_2$ fragments for the benzotrifluorides. Typical mass Spectra of standards are given in Figure I. Multiple ring benzotrifluorides are less likely to produce the $M-CF_2$ fragment but almost always produce a strong M-F or M-HF fragment. These positive chemical ionization mass spectrometry conditions also help confirm molecular weight of the compound. This procedure has been used to detect over 50 benzotrifluoride derivatives in environmental samples, 28 of these have been positively identified with matching of mass spectra and retention time with standards . Figure 2 gives structures of some of the more unusual benzotrifluorides found in environmental samples. The ** means the compound structure has not been confirmed due to lack of standards. The formation of the $M-CF_2$ fragment can be enhanced by increasing the source pressure but this results in a decrease in sensitivity and a decrease in intensity of the molecular ion (M+, M+1, M+29, depending on compound).

FIGURE I Mass Spectra of Benzotrifluorides A – D

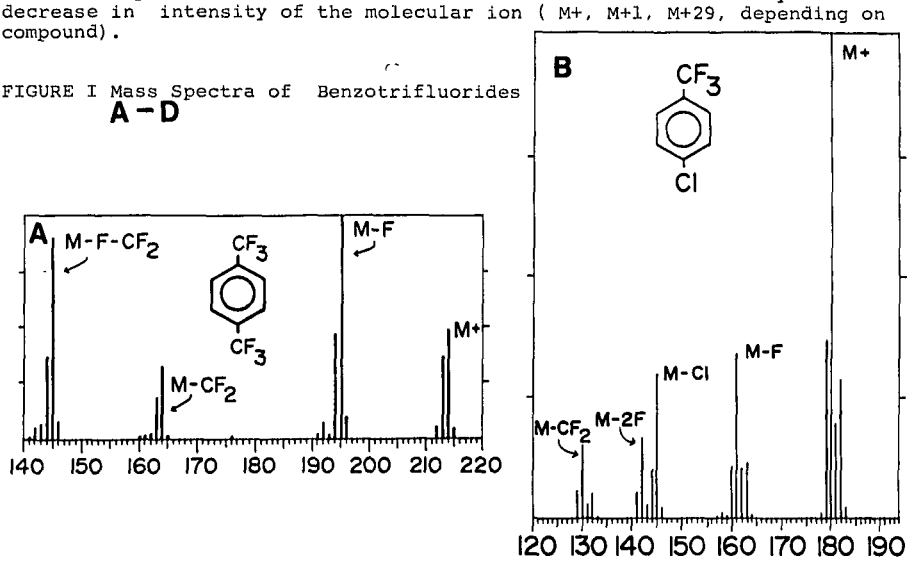

FIGURE II Unusual Benzotrifluoride derivatives

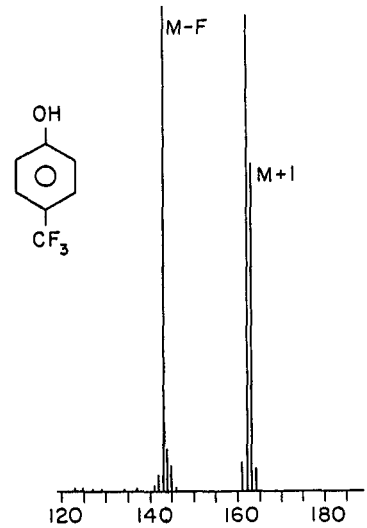

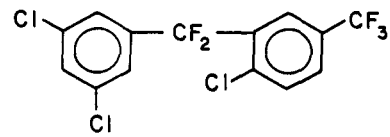

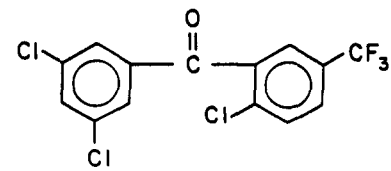

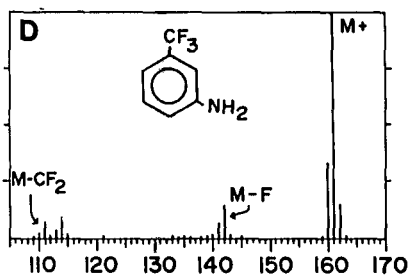

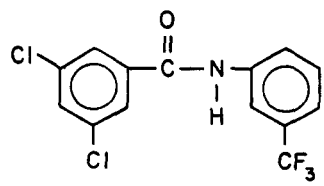

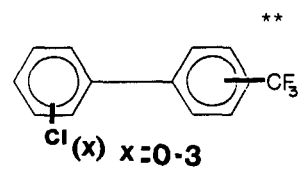

1. Kirk-Othmer Encyclopedia of Chemical Technology 3RD.ED. Wiley & Sons, NY 1978
2. Carere,A et al.1981 Progress in Mutation Research, Vol 2.Elsevier p87-104
3. Gaulden, M.E. 1984 personnal comm. UTHSC

CHARACTERIZATION OF ORGANIC EMISSIONS FROM HAZARDOUS WASTE DISPOSAL SITES BY GC-MS

C.L. Prescott, J.L. Parr, and R.C. Hanisch, Radian Corporation, 8501 MoPac Blvd., Austin, Texas 78759.

Emissions of organic compounds from hazardous waste disposal sites (HWDS) can take place by a variety of routes, including gaseous emissions, liquid runoff, and solid emissions such as dust and fine particles. Analyses of each of these emissions are required to determine the environmental and health related impacts of HWDS. Normally, a wide variety of techniques are used to analyze solid, liquid and gaseous environmental samples. The use of different types of analytical techniques can result in ambiquities when interpreting data, as well as increase costs.

The purpose of this study is to describe a versatile analytical technique capable of analyzing samples of air, water, or soil matrices. This technique is primarily for the determination of emissions of volatile compounds with a boiling point range of -100°C to over 200°C with a single analysis.

This technique basically consists of the following steps:

- separation of volatile organics from the sample matrix;
- water removal if necessary;
- cryogenic concentration and focusing of the organic compounds;
- compound separation using a fused silica capillary analytical column; and
- compound detection and confirmation using a Mass Spectrometer - Data System.

Experimental

A block diagram of the Analytical System is presented in Figure 1. The system will accept air samples either directly from pressurized canisters or from solid sorbent traps. The volatile organics are purged from water or soil samples, or the volatiles can be extracted from solid samples using Tetraglyme with a subsequent water purge. Except for the air samples collected on Tenax®, the gas phase containing the organic analytes is passed through a Perma Pure® dryer or trapped on a solid adsorbent such as Tenax® to remove the moisture. The organics are then concentrated and focused in a cryogenic trap, usually a 1/16" (0.040 ID) nickel tube collected in liquid oxygen (-183°C). After concentration, the sample is flashed on to the fused silica capillary analytical column coupled to the mass spectrometer via an open split interface.

Results

Air samples, collected in evacuated canisters, along with water and soil samples were collected from Hazardous Waste Disposal Sites (HWDS). The samples were analyzed for volatile organic compounds using the same analytic scheme as described above. Figure 2 shows a total ion chromatogram of one of the soil samples from an HWDS. A wide variety of compounds and organic classes were demonstrated in HWDS samples using this technique.

Conclusions

The unique aspect of this technique is the ability to analyze air, water, and soil samples using the same analytical system.

The application of this technique to hazardous waste disposal site samples provided a wide range of information concerning the volatile emissions and greatly simplified the task of data interpretation.

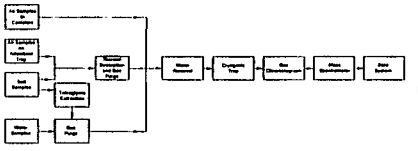

Figure 1. Block Diagram of the Analytical System

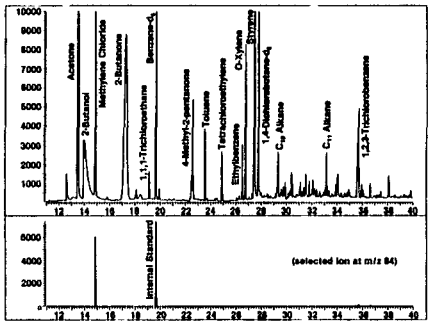

Figure 2. Total Ion Chromatograph of Volatile Organics from HWDS Soil Sample

INDIVIDUAL AND BULK ANALYSIS OF AEROSOLS COLLECTED FROM ATMOSPHERE BY SIMS

by

MARCEL BARIL[+] and ALAIN ADNOT[*]
[+] Département de Physique, CRAM & GRAPS
[*] Département de Génie Chimique
CRAM & GRAPS
Faculté des Sciences et Génie
Université Laval, Ste-Foy, Québec
CANADA, G1K 7P4

Using an impact collector with seven stages similar to the mini-Andersen type, aerosols from atmospheric air are collected and deposited on an aluminum foil. Table I gives the speed of air flowing through holes and mean diameter of the aerosols collected on each stage.

Visual observation of the shape and size of each particulate is made by scanning electron microscopy. Some imaging can also be done by scanning the Ga^+ primary ion beam, which is about 1 micron in diameter, over the area but the quality (resolution) of the images obtained is of course much worse than those from SEM. Some development needs therefore to be done to localize specific particulates chosen from a SEM picture for a chemical analysis with the Ga^+ beam.

Main peaks of the spectrum are typical of the primary ion beam and of the foil on which aerosols are collected such as Ga_n^+, Al_m^+, $Ga_iAl_j^+$ with $1 \leq n \leq 3$; $1 \leq m \leq 5$; $1 \leq i \leq 2$; $1 \leq j \leq 2$. There are also some typical impurities associated with the aluminum foil like Li, Na, K, Ca, etc. Typical spectrum is given in figure 1. But there are many valleys in the spectrum produced from blank aluminum foil so that much information can be obtained from the deposited aerosol. Figure 2 shows a spectrum where peaks from blank aluminum foil have been subtracted.

Peak at 46, 62, 92, 108 can be probably interpreted as various nitric oxides. They are present on spectra obtained from various particulates collected from atmospheric air. If the interpretation is correct, this method may lead to a better understanding of the solid components of the acid precipitation.

TABLE I

1	4.2 ft/s	8.7 μm
2	6.9	6.8
3	11.5	3.9
4	20.4	2.0
5	49.4	1.5
6	90.0	1.0
7	150.	<1.0

FIGURE 1a

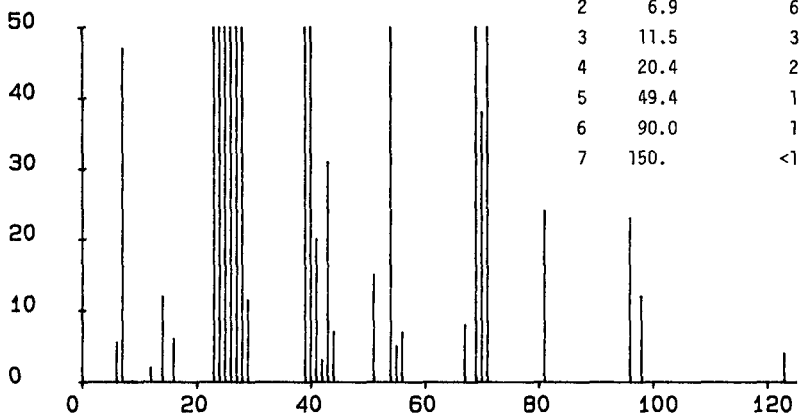

FIGURE 1b

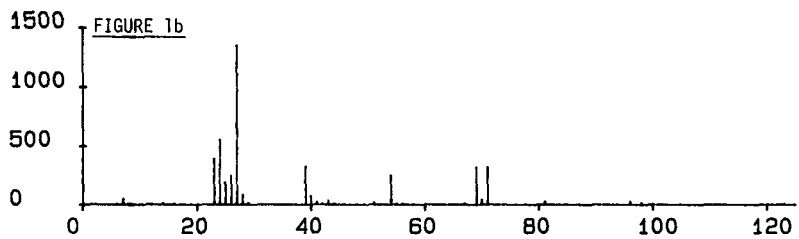

FIGURE 2

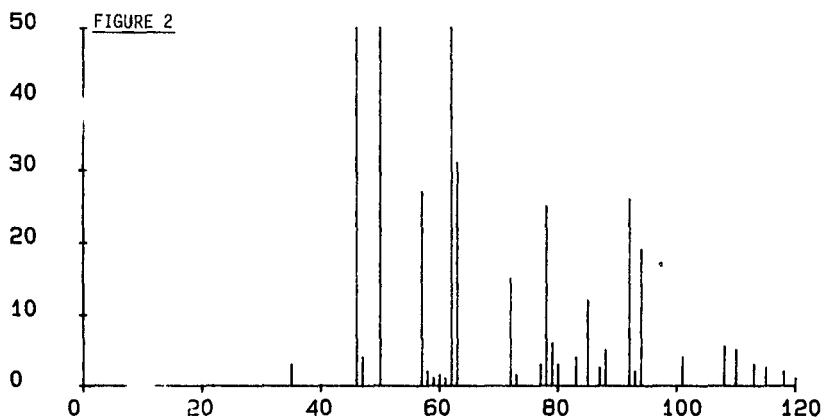

ANALYSIS OF DIESEL SOOT FOR NITRO-PAHS BY GC/MS. Thomas R. Henderson, Ray L. Hanson, James D. Sun and Antonne L. Brooks. Lovelace Inhalation Toxicology Research Institute, Albuquerque, NM.

Analysis for nitropolycyclic aromatic hydrocarbons (nitro-PAH) by GC/MC has been hampered by decomposition and hydrogen exchange in the GC injectors or effluent lines. These difficulties are avoided if samples were injected in dimethylsulfoxide (DMSO). This method was used to show that pyrene or fluoranthene addition to fuels results in increased emissions of the corresponding nitro-PAHs. Also, addition of pyrene or fluoranthene monitro-PAHs to fuels results in increased emissions of nitro-PAHs and increased mutagenicity. These results suggest the stability of pyrene, fluoranthene and their nitro-PAH deriviatives in exhaust streams may be a factor in the formation of thermally stable mutagenicity in exhaust streams.

The direct-acting mutagenicity associated with combustion effluents appears to be due to the formation of mono- and di-nitro-derivatives of polycyclic aromatic hydrocarbons (PAH) (1,2). The predominant nitro-compound detected is often 1-nitropyrene, although it contributes only a few percent to the total mutagenicity (3).

METHODS

A direct-injection single cylinder engine was used to generate diesel soot samples under conditions of constant load. The fuel was technical grade hexadecane with 1% pyrene or 1% fluoranthene added. One set of runs was carried out with saturated 1-nitropyrene in hexadecane (2090 ± 30 PPM) or 3-nitrofluoranthene (2680 ± 60 PPM).

GC/MS analyses were performed with a Finnigan model 4500 instrument with a 30-m fused silica capillary column. The temperature program was 50 to 290°C @ 10°C/min, with a 2-min hold at 50°C.

For nitro-PAH analyses, weighed aliquots of diesel soot extract (50 to 100 mg) was spiked with 0.2 mg of d_9-1-nitropyrene or d_9-3-nitrofluoranthene. The sample was dissolved in 10 ml of hexane and extracted 3 times with 5 ml of dimethylsulfoxide. The DMSO extracts were diluted with 2 volumes of water, and extracted 3 times with hexane. The hexane extracts were evaporated by nitrogen blowdown and dissolved in 0.5 to 2.0 ml of DMSO. A 1-µl aliquot was injected at time 0 into the GC.

Deuterated internal standards were synethesized from 10 mg of d_{10}-pyrene or d_{10}-fluoranthene (>98 at atoms % from Merck & CO., Los Angeles, CA) by direct nitration with HNO_3 in 1:1 v/v methylene chloride:acetic anhydride at 0°C. The linearity of the internal standard curve was determined over a broad range of concentrations of added hydrogen labeled nitro-PAHs, using 247 and 256 molecular ions of the protium and deuterium labeled compounds.

Salmonella typhimurium mutagenicity assays were conducted with strain TA-98 as described previously. Only unfractionated extracts were tested.

RESULTS AND DISCUSSION

Problems were encountered with reproducibility of gas chromatograms containing nitro-PAHs. The reproducibility of the 1-nitropyrene deuterio-molecular ions/protio-molecular ions (256/247) was much more variable when injections were made in toluene. When injected in DMSO, duplicate analyses usually agreed within 5%, but duplicate injections in toluene often showed more than 100% variations between duplicates.

Table 1 shows that pyrene or fluoranthene addition to hexadecane fuel increased the concentration of the corresponding mononitro-PAHs in soot extracts as well as the emissions of these PAHS.

Using deuterated nitro-PAH internal standards, the fuels saturated with 1-nitropyrene and 3-nitrofluoranthene respectively were analyzed. It was found that hexadecane saturated with 1-nitropyrene contained 2090 ± 30 PPM 1-nitropyrene; hexadecane saturated with 3-nitrofluoranthene contained 2680 ± 60 PPM 3-nitrofluoranthene.

Table 1

EFFECTS OF PAH FUEL ADDITIVES ON DIESEL NITRO-PAH EMISSIONS
Nitro-PAH Content in Soot Extracts (PPM)

Fuel	3-Nitrofluoranthene	1-Nitropyrene
Hexadecane	<1	33.1 ± 0.8
Hexadecane with 1% Pyrene	<1	277 ± 7.8
Hexadecane with 1% Fluoranthene	298 ± 3.5	<1

When these fuels were combusted in the single cylinder diesel engine, the nitro-PAH concentrations in soot extracts were found to be increased (Table 2). Neither 1-nitropyrene nor 3-nitrofluoranthene was concentrated in soot extracts over their concentrations in starting fuels (Table 2) as were pyrene and fluoranthene (Table 1).

Table 2

EFFECTS OF FUEL ADDITIVES ON DIESEL NITRO-PAH EMISSIONS

Fuel Additives*	μg/g Extract		Total Recovered (μg/liter Fuel Combusted)	
	1-NP	3-NF	1-NP	3-NF
None	5.0	<0.1	13.4	<0.2
2090 PPM 1-Nitropyrene	414	245	1294	766
2680 PPM 3-Nitrofluoranthene	350	1360	1400	5440

*Hexadecane basic fuel with saturated solutions of nitro-PAH.

The mutagenicity of extracts and total mutagenicity/liter of fuel combusted also were affected by addition of nitrofluoranthene or nitropyrene to fuel, but not by the addition of pyrene or fluoranthene.

The ability to readily measure the concentration of nitro-PAHs in diesel fuel vs. diesel soot extracts provides a useful approach for determining which PAHs in diesel soot extracts are the mutagens of particular concern. In the comparison of 1-nitropyrene and 3-nitrofluoranthene reported here, 3-nitrofluoranthene addition to fuel altered the soot concentration of this nitro-PAH and the mutagenicity of whole extracts more markedly than did 1-nitropyrene.

These results also suggest that dinitro-PAHs may be significant contributors to the mutagenicity of soot extracts, for only about 3% of the 8 reg/μg in 1-nitropyrene combustion products can be accounted for from the specific activity of pure 1-nitropyrene, ca 600 rev/μg (1,2).

REFERENCES

1. Henderson, T. R., et al., "Triple-quadrupole Mass Spectrometry Studies of Nitroaromatic Emissions from Different Diesel Engines," Environ. Sci. Technol. 17, 443-449, 1983.

2. Henderson, T. R., et al., "GC/MS and MS/MS Studies of Diesel Exhausts Mutagenicity and Emissions from Chemically Defined Fuels," Environ. Sci. and Technol. (in press, 1984).

3. Li, A. P., and Dutcher, J. S., "Mutagenicity of Mono-, Di-, and Tri-nitropyrenes in Chinese Hamster Ovary Cells," Mutat. Res. Lett. 119, 387-392, 1983.

ACKNOWLEDGMENTS

Research supported by U. S. Department of Energy Contract DE-AC04-76EV01013.

HPLC-MS Determination of Polycyclic Aromatic Hydrocarbons in Marine Sediments

M.A. Quilliam, R.J.Gergely and M.S. Lant, Department of Chemistry, McMaster University, Hamilton, Ontario, Canada, L8S4M1; W.D. Jamieson, E. Lewis and R.M. Gershey, Marine Analytical Chemistry Standards Program, National Research Council of Canada, Atlantic Research Laboratory, Halifax, Nova Scotia, Canada, B3H3Z1

Polycyclic aromatic hydrocarbons (PAH) occur widely in marine sediments. Since many of these compounds show mutagenic and carcinogenic activity and since the use of marine resources is intensifying, it is of considerable interest to provide accurate analyses of these components. As a consequence, reference materials are required for testing analytical methods. The Marine Analytical Chemistry Standards Program was established to meet present and future needs for marine based standards and reference materials. The objective of this project was to analyze potential marine sediment reference samples for PAH by several complementary techniques. The methods used include capillary column GC with FID and NPD detection, GC-MS, HPLC with UV and fluorescence detection, and combined HPLC-MS. In this paper we examine the effectiveness of HPLC-MS methods for the identification and quantitation of PAH in sediments. A VG7070F mass spectrometer with a moving-belt interface and electron-impact ionization was used in both the scanning and selected ion monitoring (SIM) modes. Our first efforts involved using conventional HPLC columns with a system for spraying the effluent onto the belt. Acetonitrile-water gradients with a flow rate of 1 mL/min were successful, but were limited to 80-100% acetonitrile. Our best success has been with microbore HPLC columns which provided high resolution as well as ease of interfacing due to low flow rates (30 uL/min). Figure 1 illustrates the SIM traces acquired for a standard solution (A) and the PAH fraction from a sediment (B). Good response linearity, reproducibility and detection limits were observed for all of the target PAH (see Table 1).

TABLE 1· Target PAHs in standard solution

Cmpd #	MW	Conc'n (ng/uL)	Compound Name
1	128	11.3	Naphthalene
2	152	9.6	Acenaphthylene
3	154	10.5	Acenaphthene
4	166	2 5	Fluorene
5	178	2 5	Phenanthrene
6	178	1 7	Anthracene
7	202	5.1	Fluoranthene
8	202	4.9	Pyrene
9	228	2.5	Benz[a]anthracene
10	228	2.3	Chrysene
11	252	2.6	Benzo[b]fluoranthene
12	252	2.5	Benzo[k]fluoranthene
13	252	2 7	Benzo[a]pyrene
14	278	1.8	Dibenz[ah]anthracene
15	276	2.0	Benzo[ghi]perylene
16	276	2 0	Indeno[1,2,3-cd]pyrene

FIGURE 1

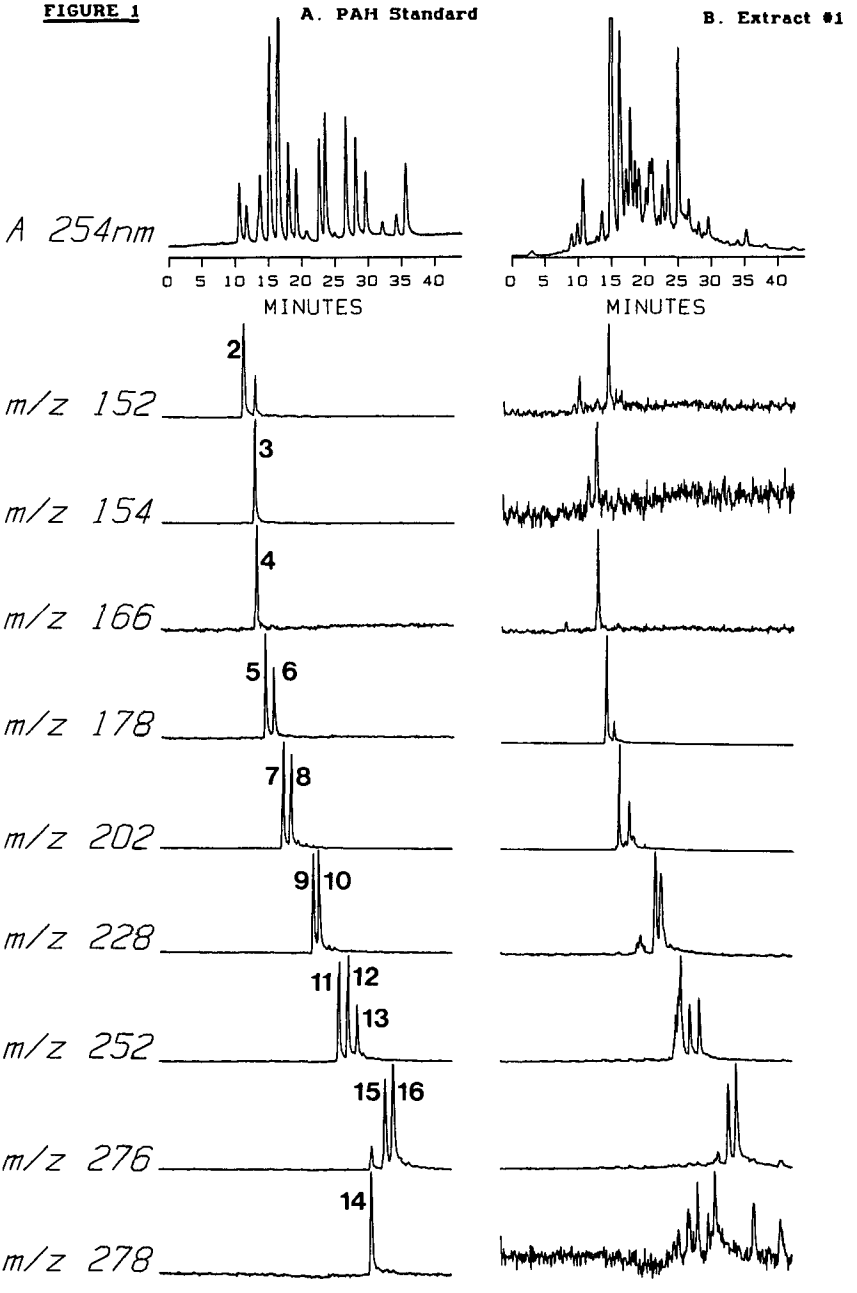
A. PAH Standard
B. Extract #1
A 254nm
0 5 10 15 20 25 30 35 40
MINUTES
m/z 152
m/z 154
m/z 166
m/z 178
m/z 202
m/z 228
m/z 252
m/z 276
m/z 278
2
3
4
5
6
7
8
9
10
11
12
13
14
15
16

Fractionation and Identification of Polycyclic Aromatic Compounds in Mutagenic Extracts of Steel Foundry Particulates

M.A. Quilliam[1], C. Tashiro[1], D.R. McCalla[2], and C. Kaiser-Farrell[2]

[1]Department of Chemistry, McMaster University, Hamilton, Ontario, Canada, L8S4M1; [2]Department of Biochemistry, McMaster University, Hamilton, Ontario, Canada, L8N3Z5

Workers in ferrous foundries show an increased risk of lung cancer. In the steel casting process hot metal is poured into sand moulds solidified with organic binders, producing a plume of smoke containing a variety of organic compounds that exhibit strong mutagenicity in microbial mutagenesis assays. We have collected particulates from the foundry, as well as emissions produced when molten steel is poured into an experimental sand mould solidified with various binder systems. The organic constituents of these samples have been fractionated by a separation scheme using Sephadex LH-20 column chromatography to separate aromatics from aliphatics, followed by chemically bonded normal phase HPLC to separate PAHs and PAH derivatives, and then reverse phase HPLC to separate benzologs and homologs. Mutagenically active fractions have been analyzed by capillary column GC-MS and microbore HPLC-MS. Figure 1 shows the GC-FID trace for the PAH fraction of a foundry particulate sample and Table 1 lists some peak identities established by GC-MS. Many polycyclic aromatic compounds, particularly the alkyl derivatives of aromatic hydrocarbons, have been identified. Some of these compounds are known to be carcinogenic and mutagenic. Microbore LC-MS has also proven to be useful for establishing the retention times of various PAHs and PAH derivatives in the final reverse phase HPLC separation. Figure 2 shows the mass chromatograms for the same sample analyzed in Figure 1.

TABLE 1: Compounds identified in PAH fraction

Peak #	Compound
1	2-Methylnaphthalene
2	1-Methylnaphthalene
3	1,1'-Biphenyl
4-10	C2-Alkyl-naphthalene
11	1,2-Dihydroacenaphthylene
12	3-Methylbiphenyl
13	Dibenzofuran
14-18	C3-Alkyl-naphthalene
19,20	C2-Alkyl-biphenyl
21	C4-Alkyl-naphthalene
22	Methylfluorene
23	Phenanthrene
24	Anthracene
25-27	Methyl-dibenzothiophene/-naphthothiophene
28-32	Methyl-phenanthrene/-anthracene
33,34	C2-Alkyl-phenanthrene/-anthracene
35	Fluoranthene
36	Pyrene
37	C3-Alkyl-phenanthrene/-anthracene
38,41	C4-Alkyl-phenanthrene/-anthracene
39	Benzo(?)fluorene
40	C4-Alkyl-dibenzothiophene/-naphthothiophene
42	Benz(a)anthracene
43	Chrysene
44	Methylbenz(a)anthracene
45	Dialkylphthalate
46,47	Benzo(?)fluoranthene
48	Benzo(a)pyrene

Figure 1

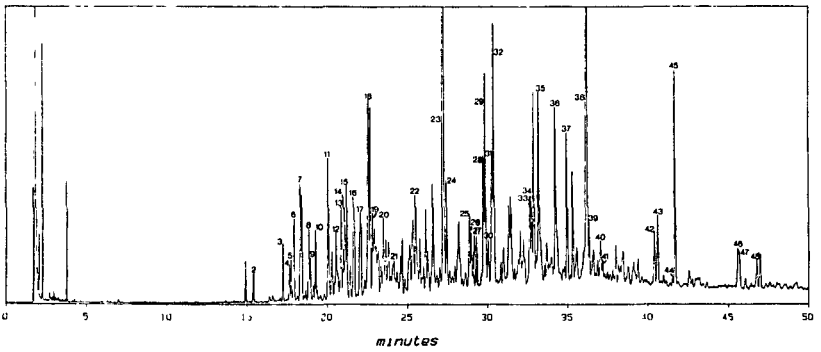

Figure 2

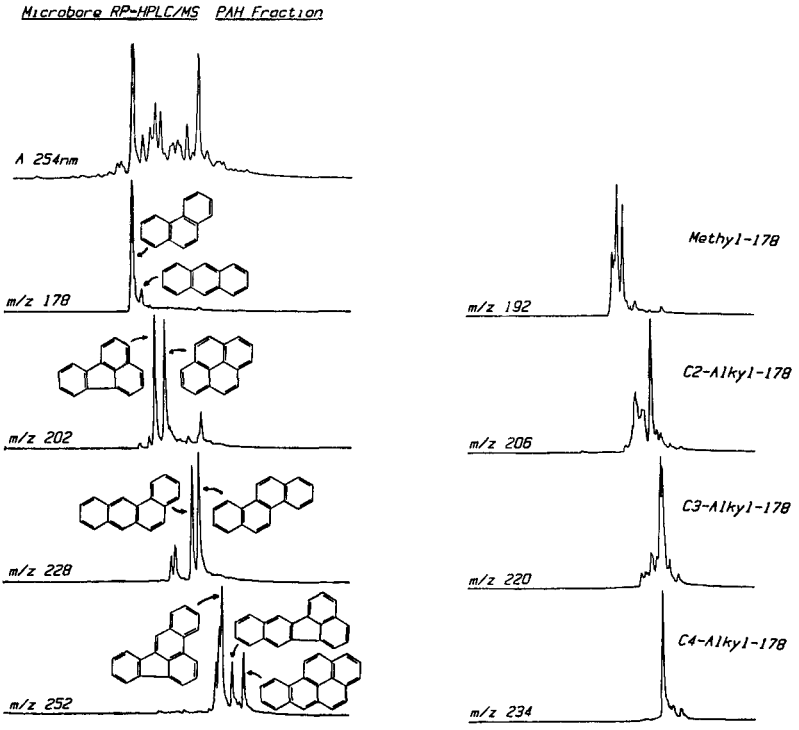

MULTIMEDIA DETERMINATION OF ORGANIC INDOOR AIR POLLUTANTS AT SUB-PART PER BILLION CONCENTRATIONS

C.H. Williams, Jr., Maureen A. McDevitt, and C.L. Prescott, Radian Corporation, Austin, Texas 78759.

A comprehensive study was made to identify and quantify the volatile organic air contaminants in an indoor (office) environment that was thought to be causing respiratory problems in workers. Air samples were collected on Tenax resin and in evacuated stainless steel canisters during two different test periods. Headspace air samples were collected over several building construction materials, including carpet and carpet adhesive. Analysis was performed by high resolution gas chromatography-mass spectroscopy (HRGC-MS), with sample concentration using a cryogenic inlet system.

The sampling strategy involved testing the air in both buildings exhibiting problems and in control (asymptomatic) buildings. A number of chlorinated and oxygenated organic species were detected in the indoor air samples in the range 1-30 ppb v/v, but occurred in both the test and control environments. However, several cyclic diene compounds found in the headspace of the carpet adhesive were detected in the air from the test buildings at concentrations of 0.2-1.0 ppb v/v. Analytical results for cyclopentadiene and styrene detected in canister and tenax air samples collected in test and control buildings, as well as the headspace of carpet and carpet adhesive, are presented in Table 1. Total ion chromatograms of a canister air sample from the test building and headspace of the carpet adhesive with identification of major organics common to both samples are presented in Figures 1 and 2.

TABLE 1. ANALYTICAL RESULTS FOR ODORANT COMPOUNDS FOUND IN AIR AND BULK SAMPLES

Sample Identification	Cyclopentadiene	Styrene
Complaint Building-Canister	0.76	0.94
Complaint Building-Tenax	0.24	ND(<0.4)[1]
Control Building-Canister	ND(<0.1)[2]	0.4 [3]
Control Building-Tenax	ND(<0.4)	ND(<0.4)
Carpet Adhesive-Headspace[4]	0.22	0.27
Carpet Sample-Headspace	ND(<0.1)	ND(<0.1)

[1] Detection limit for Tenax samples is less than 0.4 ppb·v.
[2] Detection limit for Canister samples is less than 0.1 ppb·v.
[3] Upper limit for Styrene due to co-eluting compound.
[4] Results in ng/mg sample.

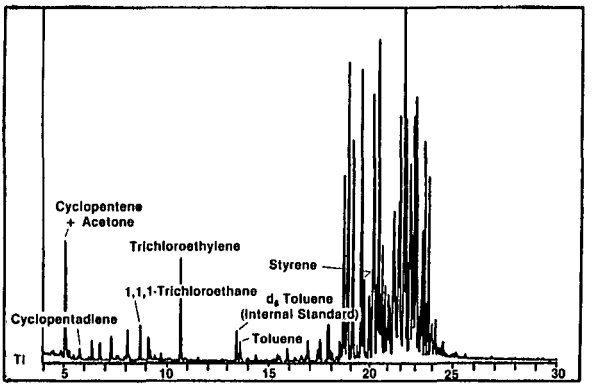

Figure 1. GC-MS Chromatogram of Canister Sample, Test Building

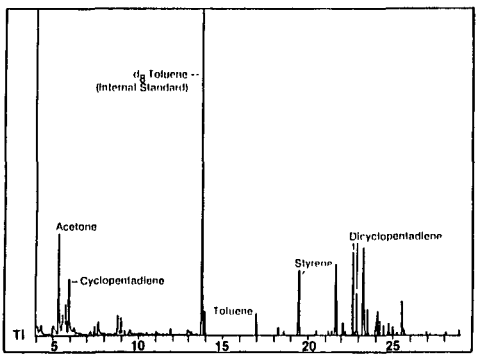

Figure 2. GC-MS Chromatogram of Carpet Adhesive (100 mg)

ANALYSIS OF THE POST DETONATION ENVIRONMENT OF AN EXPLOSIVES TEST FIRING CHAMBER:

Richard O. Yelton, B. M. Hughes and S. M. Mazer; Monsanto Research Corporation, Mound*, Miamisburg, OH 45342

Concerns have arisen relating to the toxicity of combustion and/or detonation products of high explosives. The post detonation environment of a test fire tank has been analyzed by direct probe and capillary gas chromatography and a bio-cytotoxicity assay to determine whether the gases and debris produced during the explosion of a one-pound charge of triaminotrinitrobenzene (TATB) might present any potentially adverse health effects to personnel entering the tank after an explosion. Pyrolysis Gas Chromatography/Mass Spectrometry (PY/GC/MS) was initially employed in the laboratory to simulate an extremely rapid ignition of the high explosive powder. This allowed us to separate and identify the gaseous ignition by-products. The results of these analyses indicated that some potentially harmful gases such as HCN and cyanogen (Figure 1) are produced, along with some heavier organic by-products which include benzene, a reported carcinogen. These experiments, however, were conducted in an inert atmosphere.

The actual test fire tank contains normal atmospheric gases during test explosions, and provided an oxidizing environment. Gas samples taken from the tank immediately after detonation were found to contain approximately 2% carbon dioxide; but, after four minutes of ventilation, the tank atmosphere was found to return to normal.

Samples of explosion debris collected inside the tank following an ambient shot and a sub-ambient shot were Soxhlet extracted and analyzed by capillary GC/MS. Phenol, dimethylbenzene, and several carboxylic acids and phthalates were detected and identified in the sub-ambient residue. The same phenol, carboxylic acids, and phthalates were also detected and identified in the ambient shot debris (see Table 1). All chromatographable compounds detected in both residues were at ppb-ppm levels. Following identification by computer search, these compounds were searched via the Chemical Information Service toxicity data base and all compounds detected were determined to be of low toxicity. Dimethylbenzene and phenol, however, are eye and skin irritants if direct contact is made. The carboxylic acids and phthalates detected are of relatively low vapor pressure and are probably the result of the decomposition of the plastic and polymeric materials used in the construction of the board on which the explosives are detonated.

A direct probe mass spectrometric analysis of the cold shot debris revealed the presence of unexploded TATB which itself is reported to be of low toxicity.[1]

Finally, an in vitro Chinese hampster ovary (CHO) clonal cytotoxicity assay was performed on the debris from the cold shot (worst case). This EPA sanctioned bioassay involves placing varying concentrations of the debris itself in contact with live cells until a 50% kill is observed. The concentration of debris at which this occurred translates into a low toxicity category. The results of the MS and bio-cytotoxicity analyses conducted on the gases and debris produced from the detonation of one pound of TATB do not indicate that any adverse health effects due to toxicity can be anticipated as long as the presently maintained safety practices are adhered to.

[1] B. M. Dobratz, "Properties of Chemical Explosives and Explosive Simulants", UCRL-52997, LLNL Explosives Handbook, Section 19, pg. 137, March 16, 1981.

*Mound is operated by Monsanto Research Corporation for the U. S. Department of Energy under Contract No. DE-AC04-76DP00053.

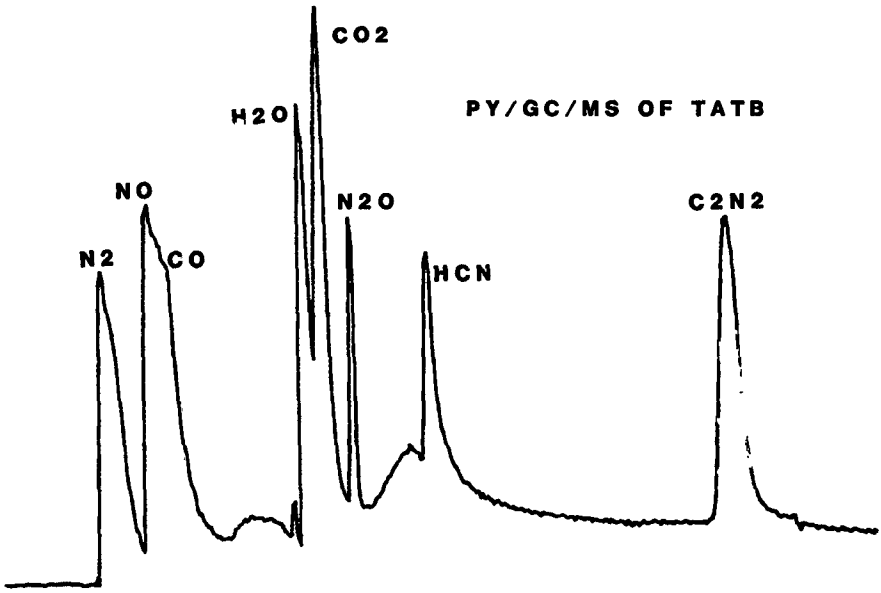

FIGURE 1.

GC/MS OF SOLID DEBRIS

Cold Shot 10/1/82

Peak No.	Retn. Time	Organics Detected	Area	Amount ug/g
1.	3.55	Xylene	16187	170
2.	13.90	Dimethylhexahydroterephthalate	37478	390
3.	16.00	Dimethylphthalate	8808	93
4.	18.30	Tetramethylbutyl Phenol	5436	57
5.	20.40	Hydroxybenzoic Acid, Phenyl Ester		Approx. 25
6.	24.60	Nonanedioic Acid, Dibutyl Ester	5597	59
7.	29.10	Hexanoic Acid, Ethyl Diester with Tetraethylene Glycol	177081	1800
8.	29.70	Phthalates		Approx. 50
9.	30.80	Phthalates		Approx. 50
10.	31.50	Phthalates		Approx 50
11.	33.30	Phthalates		Approx. 50

Ambient Shot 10/21/82

Peak No.	Retn. Time	Organics Detected	Area	Amount ug/g
1.	18.33	Tetramethylbutyl Phenol	6841	140
2.	20.35	Hydroxybenzoic Acid, Phenyl Ester	2777	59
*P	23.30	N-Butyl Isobutyl Phthalate	13426	280
3.	24.55	Nonanedioic Acid, Dibutyl Ester	2679	57
4.	29.03	Hexanoic Acid, Ethyl Diester with with Tetraethylene Glycol	105678	2200

* Peak "P" appears in all runs due to septum bleed.

TABLE 1.

DETERMINATION OF PART PER BILLION LEVELS OF 2,3,7,8-TCDD
IN ENVIRONMENTAL SAMPLES AT HIGH PRECISION AND ACCURACY

Larry D. Garretson, C. Herndon Williams, Jr., and Lloyd P. Provost, Radian Corporation, Austin, Texas 78759

The measurement of 2,3,7,8-TCDD in environmental samples at concentrations to 0.1 ppb w/w with both high precision and accuracy requires the satisfaction of performance criteria for sample preparation, instrument operation, compound identification and quantification. Some of the elements that Radian has used and will be described in this paper are:

- Multipoint calibration;
- Use of two capillary GC columns: DB-5 and SP-2340;
- Spiking of all samples with $^{13}C_{12}$-2,3,7,8-TCDD as an internal standard and $^{37}Cl_4$-2,3,7,8-TCDD as a surrogate standard; and
- Daily instrument performance verification using authentic TCDD isomers.

The application of these and other criteria in the analysis of contaminated soil samples for 2,3,7,8-TCDD will be described, and measures of precisions and accuracy will be presented.

HRGC-MS CHROMATOGRAM OF RADIAN STANDARD OF ALL 22 TCDD ISOMERS

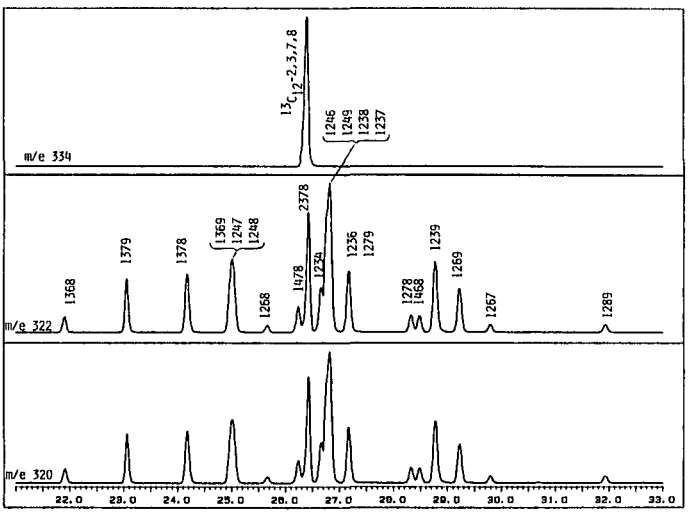

HRGC-MS CHROMATOGRAM OF RADIAN TCDD PERFORMANCE STANDARD

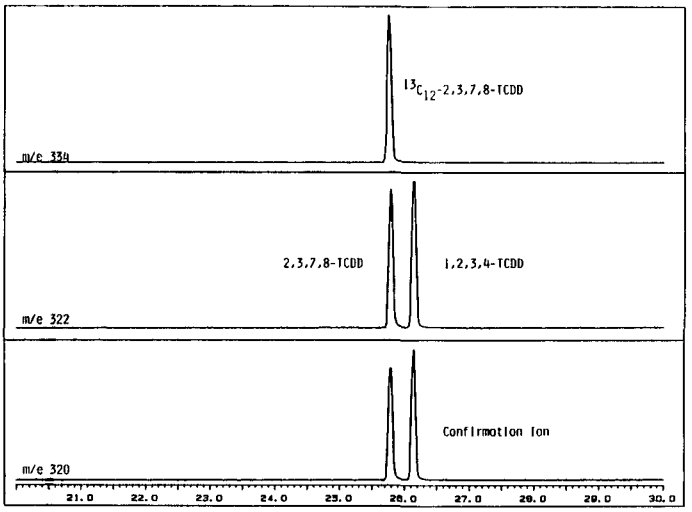

HRGC-MS CHROMATOGRAM OF HAZARDOUS WASTE SITE SOIL

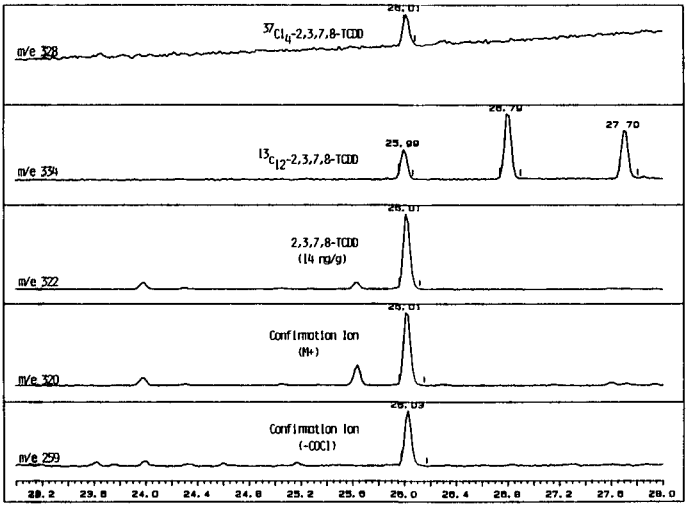

RESPONSE FACTOR STUDIES FOR ANALYSIS OF POLYCHLORINATED DIBENZO-P-DIOXINS BY GAS CHROMATOGRAPHY-ELECTRON IMPACT MASS SPECTROMETRY

R.E. Clement, H.M. Tosine and A. Alfieri

Ontario Ministry of the Environment,
Laboratory Services and Applied Research Branch,
Dioxin Laboratory,
P.O. Box 213, Rexdale, Ont. Canada M9W 5L1

Introduction

In spite of the large body of analytical data reported for the analysis of polychlorinated dibenzo-p-dioxins (PCDD) in environmental sample, studies of optimized response for PCDD using GC-EIMS have not been reported. Also, although there is a lack of commercially available standards of various PCDD congeners, analysis of the entire range of PCDD from tetrachlorinated (T_4CDD) to OCDD congeners has often been reported using only one representative T_4CDD comp. and OCDD, and interpolating the response factors of penta (P_5CDD), hexa (H_6CDD) & heptachlorinated (H_7CDD) congeners from these two. By studying the short and long-term var. of relative response factors (RRF) of standards, the validity of these practices is examined.

Procedures

INSTRUMENT - Finnigan 4500/Incos data system
COLUMN - 25m or 30m DB-1 fused silica WCOT
TUNING - manual tuning daily based on peak shapes and abundances of PFTBA m/z 219 and 502
ANALYSIS MODE - selected ion monitoring/6 ions at a time with dwell times 0.2 sec. each
STANDARD - prepared by direct weighing of pure crystals - concentrations in working solution 30 to 40 pg/microlitre
EFFECT OF ELECTRON ENERGY - instrument tuned per normal procedures/standards run at various values of EE
EFFECT OF EM VOLTAGE - as above for EM
LONG TERM RESPONSE FACTORS - statistical study of 104 standards run over 8 months
SHORT TERM RRF - statistical study of 7 standards run on same day - study repeated 2x
VARIATION IN ISOTOPE RATIOS - statistical study of isotope ratios from above two studies: normalised to largest (theoretical) pk=100

Effect of Electron Energy (EE)

Table 1 summarizes the results of this study. There is a large increase in response from 70 eV to 32 eV. The response drops off rapidly after 32 eV.Although the change in response factors is linear for the five PCDD congeners studied, the slopes of the RF versus EE lines are not the same for all compounds. The relative increase in RF were almost identical for OCDD, H_7CDD and H_6CDD, however, a larger relative increase was obtained for P_5CDD and a much larger relative increase for T_4CDD.

TABLE 1 - RF VARIATIONS DUE TO ELECTRON ENERGY

Congener	32	32[x]	50	50[x]	70	70[x]
tetra	455	361	275	235	144	133
penta	174	152	113	100	56	53
hexa	101	104	70	74	38	32
hepta	102	85	57	65	35	23
octa	82	62	54	53	23	9

[x] duplicate analysis

Effect of Electron Multiplier Voltage(EM)

As expected, the response increased as EM was increased from 1250 to 2500 volts The relative EM gain with 250 volt increments was almost linear between EM 1500 and 2250, and the relative response factors were constant for all five congeners studied. Of course, the absolute responses and linear range depends upon each specific electron multiplier, its age and prior use. If the linear range of relative EM gain and constant RRF was known, however, it should be possible to re-run a sample containing low-level peaks at higher EM, and quantify peaks against an external standard without re-analyzing the external standard at the new EM, if the sample contained an internal standard for which a correction factor could be applied.

Relative Response Factor (RRF) Variations

Table 2 shows the RRF on both a long-term and short-term basis. RRF are reported as area response per picogram injected. Absolute variations in RF are expected to vary considerably but variations in RRF have not been previously reported. Short-term (re: during one day) variations are less than those over an 8-month period, as expected, but can change considerably from one day to the next. Because the RRF depend upon many factors, including the daily tuning of the quadrupole analyser, the RRF cannot be accurately predicted. Therefore, interpolation of RF for P_5CDD, H_6CDD and H_7CDD from only those of T_4CDD and OCDD for purposes of quantitative analysis is inaccurate. However, such RF interpolation is adequate for approximate estimates that should be within a factor of 2 to 5 of the RF obtained by analysing the appropriate P_5CDD, H_6CDD or H_7CDD standard.

Isotope Ratio Variations

Large variations in isotope ratios were observed from the expected theoretical values for some ions. The M/Z 422 ion for H_7CDD, for example, varied from 27% to 45% (std. dev. 7.5), relative to the base peak (M/Z 424), over an 8-month period. Some of the variation is due to the tuning procedures, which were designed to maximise response. Since this ratio was consistently low, however, relative to the theoretical value of 44%, a tight identification criteria based upon isomer ratios may falsely reject H_7CDD which are detected at low levels in samples. It is not known whether the principal cause of these variations is the specific instrument and tuning procedures employed or the fact that the standards analysed are at such low concentrations.

TABLE 2 - RELATIVE RESPONSE FACTOR VARIATIONS

A. LONG TERM RF VARIATIONS

	Congener 4	5	6	7	8
Mean	100	58	13	13	10
SD	-	10	5	7	8
High	-	88	38	59	51
Low	-	31	2	4	1

B. SHORT TERM RRF VARIATIONS

1. Mean	100	31	11	8.3	4.0
SD	-	3.3	1.7	2.0	1.5
2. Mean	100	40	29	29	27
SD	-	1.7	3.2	1.8	2.7

VALIDATION BY HIGH RESOLUTION MASS SPECTROMETRY OF A BIOASSAY FOR "TCDD-LIKE" ACTIVITY,

D.R. Hilker, K.M. Aldous, P.W. O'Keefe, R.M. Smith, J. Gierthy, G. Eadon, J. Jurusik and S.W. Hibbins
Center for Laboratories and Research, New York State Department of Health, Albany, New York 12201

A biological assay for the detection of 2,3,7,8-TCDD has been developed in the Center for Laboratories and Research. A study was conducted to determine the feasibility of applying this assay to various environmental samples. Large numbers of samples can be rapidly and economically screened and those samples appropriate for high resolution chemical analysis chosen. This approach is useful when addressing problems of wide geographic extent or high concentrations. Problems such as these have arisen within New York State and include tetrachlorodioxin contamination in the Great Lakes and in the Love Canal, polychlorodibenzodioxin (PCDD) and polychlorodibenzofuran (PCDF) contamination in the Hudson River and a state office building after a transformer fire.

We currently use an extensive clean-up and analysis procedure for PCDD and PCDF. This procedure includes an exhaustive extraction procedure, a semiautomated liquid chromatographic separation and HRGC/HRMS. Among the capabilities of this analytical scheme are the isolation of planar molecules in the extract, high resolution gas chromatographic separations, high resolution ion monitoring and low parts-per-trillion detection limits. These capabilities compare favorably with HRGC/LRMS which generally has higher detection limits due to the presence of chemical noise. Any screening technique should be capable of the same low ppt detection limits in order to utilize the full advantages of HRGC/HRMS for the accurate and sensitive ultimate quantitation of PCDD and PCDF concentrations.

A 2,3,7,8-TCDD induced alteration in morphological and growth characteristics of a subline of cultured mouse epithelial cells has been investigated for use as a biological screening assay for dioxinlike compounds. This assay is based on the ability of 2,3,7,8-TCDD and related compounds to inhibit cell division in confluent cultures of XBF cells cocultured with irradiated fibroblast feeder cells. This results in these cells acquiring a flat cobblestone-like appearance and a low saturation density. We have designated this alteration the "flat cell effect".[1] The flat cell effect has demonstrated sufficient sensitivity and specificity for the more toxic polychlorinated dioxin congeners and isomers to allow evaluation as an assay. The lowest detectable concentration of this isomer is 10^{-11} M (3×10^{-12} g). The purpose of this study is to validate the flat cell assay to allow priority ranking of large numbers of environmental samples for subsequent isomer specific GC/MS analysis.

HRGC/HRMS was used to validate the bioassay by comparing the results obtained for the same sample extracts and identifying compounds which give a 2,3,7,8-TCDD-like response. Three types of environmental sample were studied, fish, sediment and water. The fish results compared favorably regardless of the extent of extract preparation or the species (see table). The results on the sediment and water samples did not compare as well. Two types of disagreement were apparent, one presumably due to samples containing high concentrations of PAH (polynuclear aromatic hydrocarbons) and the other presumably due to the presence of a compound or compounds other than 2,3,7,8-TCDD which gives a 2,3,7,8-TCDD-like response in the assay. The presence of other dioxin-like compounds was detected in one of the sample extracts by the inspection of the highly resolved ion monitoring chromatogram shown below. We are studying this sample further using high resolution mass spectrometry in order to identify this dioxin-like activity.

1) Gierthy, J.F. and D. Crane. "Reversible Inhibition of In Vitro Epithelial Cell Proliferation by 2,3,7,8-Tetrachlorodibenzo(p)dioxin", Toxicology and Applied Pharmacology, in press.

Comparison of Flat Cell Assay and Mass Spectrometric Analysis for Fish Samples Subjected to Extensive Cleanup Procedures

Sample No.	FCA TCDD eq. (ppt)	Mass Spec 2,3,7,8-TCDD (ppt)
397b	ND (5.3-10.7)	ND (3.0)
398b	3.0-30	10.7
399b	2.7-28	6.8
400b	53-530	127
77	ND (2.7-5.4)	ND (1, 5.3)

Comparison of Flat Cell Assay to Fish Samples Subjected to Minimal Cleanup Procedures

Sample	FCA TCDD eq. (ppt)	Mass Spec 2,3,7,8-TCDD (ppt)
Coho Salmon	ND (2.7-5.4)	ND (1,5.3)
Brown Trout	5.3-53.3	11
Carp	26.7-268	133
Goldfish/Carp	5.3-53.3	32
Goldfish/Carp	1.9-19	7.8
Goldfish/Carp	6-60	50
Goldfish/Carp	2.1-21	4.9
Goldfish/Carp	12-120	113
Goldfish/Carp	ND (3-6)	ND (2)

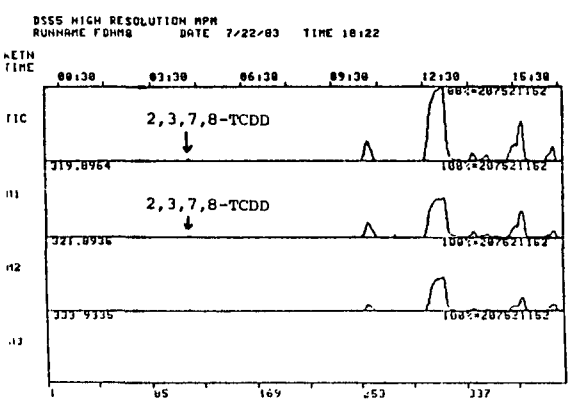

Figure 1. Ion monitored mass chromatograms of sediment sample containing minimal amount of 2,3,7,8-TCDD. This sample elicited a very large response for 2,3,7,8-TCDD in the bio-assay.

GC/MS STUDIES OF SPECIFIC CONGENERS OF POLYCHLORODIBENZOFURANS

Dorcas Fung and R.K. Boyd*,
Chemistry Department, University of Guelph, Guelph, Canada.

B. Chittim,
Wellington Environmental Consultants, Guelph, Canada.

S. Safe,[a]
Department of Pharmacology and Physiology,
College of Veterinary Medicine, Texas A and M University,
College Station, Texas.

Twenty-six specific PCDF congeners, ranging from monochloro through octachloro, have been synthesized and characterized by nmr, etc. The behaviour of these compounds, under capillary GC/low resolution MS conditions, has been investigated. Separation of e.g. tetrachloro isomers, while simultaneously providing good GC conditions for the more fully chlorinated congeners, does not appear to be possible with a single-temperature-ramp program. The EI mass spectra show very little isomer specificity. Positive ion chemical ionization (CH_4 reagent gas) were also obtained, and again offered little hope of isomer specificity. Electron attachment negative ion spectra (CH_4 moderating gas) show mainly M^- and Cl^-, with a ratio very sensitive to temperature and somewhat to pressure. Addition of a trace of O_2 to the CH_4 produces an intense $(M-19)^-$ ion, corresponding to $(M + O - Cl)^-$, (see below). This has been observed previously in the case of chlorinated dibenzofurans. In the present case of the PCDF's, no evidence was found for the ether oxidative cleavage reaction observed previously for the PCDD's under similar conditions (Hunt et al., Chem. Commun. 151 (1975)). Further work to investigate still more of these compounds, under various ionization conditions, is in progress.

[a] Funded by NIH Grant No. ESO-2937.

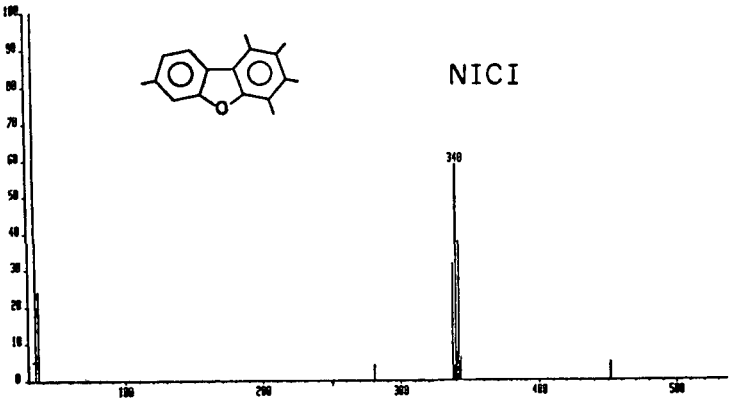
NICI
340

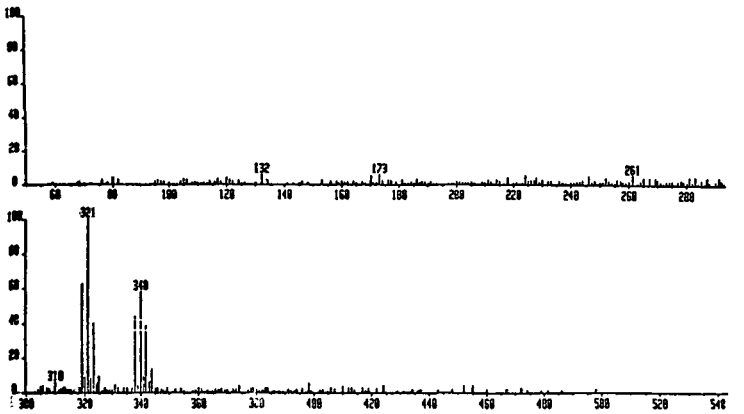
132
173
261
321
340
310

HRGC/HRMS IDENTIFICATION OF CHLORINATED PHENYL AND PHENOXY SUBSTITUTED DIOXINS, FURANS AND DIPHENYL ETHERS IN COMMERCIAL GRADE PENTACHLOROPHENOL

J. Onstot, L. Timmons, and E. Murrill, Midwest Research Institute,
425 Volker Boulevard, Kansas City, Missouri 64110

C.W. Jameson, National Toxicology Program, P.O. Box 12233,
Research Triangle Park, North Carolina 27709

INTRODUCTION

Commercial pentachlorophenol may contain a number of highly chlorinated impurities as by-products of its manufacture. These impurities are potentially much more toxic than the pentachlorophenol itself and thus may significantly affect the outcome of bioassay studies conducted on the material. As part of a bioassay screening analysis program conducted for the National Toxicology Program, pentachlorophenol was analyzed for these chlorinated impurities.

Gas chromatographic analysis of commercial pentachlorophenol using electron capture detection and low resolution GC/MS showed several high molecular weight (> 600 amu) compounds which eluted after octachlorodibenzodioxin. This presentation describes the identification of some of those impurities via HRGC/HRMS.

EXPERIMENTAL

The compounds of interest were removed from the pentachlorophenol using a two-step column chromatography procedure described by Mieure.[1] The first step utilized a basic alumina macro-column to eliminate phenolic components. PCP (1 g) was dissolved in benzene, placed onto the macro-column, and eluted with 150 mL of benzene. The benzene eluent was evaporated to 1 mL. An aliquot (300 µL) of this eluent was loaded onto a micro-column of super activity grade alumina for final cleanup. Two eluent fractions were collected from the micro-column with 10 mL of 2% methylene chloride in hexane, and the second fraction was eluted using 10 mL of 50% methylene chloride in hexane. A 2.0 mL aliquot of each fraction was then reduced in volume to 100 µL, rediluted to 200 µL with tetradecane, and concentrated to a final volume of 100 µL.

Both low resolution and high resolution GC/MS analyses were performed on the two PCP fractions. Preliminary low resolution full scan GC/MS was conducted to obtain fragmentation and isotope information. Subsequent high resolution peak matching GC/MS was used to determine molecular formulas.

Mass spectrometric analysis was performed on a Finnigan MAT 311-A interfaced to a Varian 2700 gas chromatograph modified for capillary use and equipped with a J&W on-column injection system. A J&W DB-5 fused silica capillary column (15 m x 0.25 mm ID) was utilized for the separation of components and also served as the GC/MS interface by routing the exit end of the column directly into the source of the mass spectrometer. A temperature program of 250 to 325°C at 10°C/min with a 2-min initial hold was used. The mass spec source and transfer line region were set at 270°C and 300°C, respectively. Electron energy was 70 eV with a 2.0 mA total emission current, and accelerating voltage was 3,000 V. Resolution was set at 750 for the low resolution analysis and 5,000 (10% valley) for high resolution work. Data collection for the low resolution analysis was performed under computer control using a Finnigan Incos 2400 data system scanning in exponential centroid mode in the 300-800 amu mass range. Data collection for high resolution analysis was performed manually using the Finnigan 311-A peak-matching hardware.

RESULTS AND DISCUSSION

Four classes of compounds were identified from full scan HRGC/LRMS analysis: triphenyl ethers, dibenzodioxin phenyl ethers, phenyldibenzodioxins, and dibenzofuran phenyl ethers. Thirty-two isomers of 11 different homologs were observed, 17 from Fraction 1 and 24 from Fraction 2.

Molecular formulas were confirmed for 7 of the 11 homologs by HRMS. The high resolution data are presented in Table 1. Determination of the exact molecular structure with correct placement of substituted phenyl groups and chlorine atoms was not attempted.

A reconstructed ion current chromatogram for Fraction 2 is shown in Figure 1, and a spectrum representative of those obtained for the isomers is shown in Figure 2.

REFERENCE

1. Mieure, J.P., O. Hicks, R.G. Kaley, and P.R. Michael, "Determination of Trace Amounts of Chlorodibenzo-p-dioxins and Chlorodibenzofurans in Technical Grade Pentachlorophenol," Journal of Chromatographic Science, 15, 275 (1977).

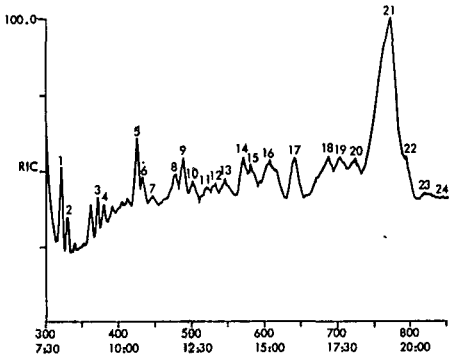

Compound Number	RIC Peak No.	Molecular Weight	Molecular Formula
I	2,4	534	$C_{18}H_6O_2Cl_8$
II	7,10,12	566	$C_{18}H_3O_2Cl_9$
III	1	568	$C_{18}H_5O_2Cl_9$
IV	18	600	$C_{18}H_2O_2Cl_{10}$
V	3,6,10	602	$C_{18}H_4O_2Cl_{10}$
VI	16,22	616	$C_{18}H_2O_3Cl_{10}$
VII	5,8,11,15	636	$C_{18}H_3O_2Cl_{11}$
VIII	20,21,23	650	$C_{18}HO_3Cl_{11}$
IX	9,13,17,19	670	$C_{18}H_2O_2Cl_{12}$
X	24	684	$C_{18}O_3Cl_{12}$
XI	14	704	$C_{18}HO_2Cl_{13}$

Figure 1 - Reconstructed Ion Current Chromatogram for Tetradecane Concentrated Fraction 2

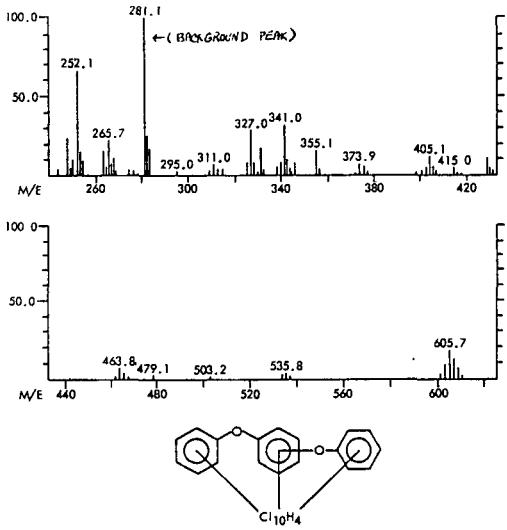

Figure 2 - Mass Spectrum for Decachlorotriphenyl Ether Compound No V

Compound	Molecular Formula	HRMS Data: Peak Monitored	Observed Mass	Theoretical Mass	Δ Mass* (mmu)
Nonachlorotriphenyl ether	$C_{18}H_5O_2Cl_9$	$(m+4)^+$	571.740	571.742	-2
Decachlorotriphenyl ether	$C_{18}H_4O_2Cl_{10}$	$(m+4)^+$	605 701	605.703	-2
Undecachlorotriphenyl ether	$C_{18}H_3O_2Cl_{11}$	$(m+4)^+$	639 667	639.664	+2
Undecachlorodibenzodioxin phenyl ether	$C_{18}HO_3Cl_{11}$	$(m+6)^+$	655.639	655.641	-1
Dodecachlorotriphenyl ether	$C_{18}H_2O_2Cl_{12}$	$(m+6)^+$	675.618	675 622	-4
Dodecachlorodibenzodioxin phenyl ether	$C_{18}O_3Cl_{12}$	$(m+6)^+$	689.598	689.602	-4
Tridecachlorotriphenyl ether	$C_{18}HO_2Cl_{13}$	$(m+6)^+$	709 578	709 583	-5

*Δ Mass = Observed Mass - Theoretical Mass

Table 1 - HRMS Data for High Molecular Weight Compounds Identified in Technical Grade PCP

COMBINED GC/HRMS FOR THE ANALYSIS OF TCDD, TCDF AND PCB IN COMPLEX SAMPLE MATRICES.

N.C.A. Weerasinghe J.L. Meehan and R.L. Harless, Department of Chemistry, University of Nebraska, Lincoln, NE 68588.

Chemical waste is a complex sample matrix which may consist of kerosene, pump oils, chlorobenzene, PCBs (20-30% by weight), and possibly low levels of highly toxic tetrachlorodibenzo-p-dioxins (TCDD) and tetrachlorodibenzofurans (TCDF). In an investigation of the efficacy of incineration for disposal of these compounds, it is necessary to detect the levels of TCDD and TCDF in the matrix prior to its disposal by incineration, since it is known that the dioxins and furans are formed during the combustion due to some inadequacies of the process. The detection of TCDD and TCDF by using HRGC/HRMS after cleanup of the matrix using available methods has not been successful due to the presence of coextractives and coelutants. The new method developed in our laboratory involved liquid partitioning of the matrix followed by column chromatography prior to GC/HRMS analysis. The method is described in Schemes I and II. The analytical method was applied to analyze chemical waste samples for TCDD and TCDF on board the ship Vulcanus -II. The results of an interlaboratory study in which spiked chemical waste samples were analyzed are given in Table 1 and 2. The samples were spiked at the US EPA laboratory at Research Triangle Park and submitted as coded samples to our laboratory for extraction and cleanup. Aliquots of the extracts were also analyzed at the EPA laboratory. The method is capable of detecting TCDD and TCDF in chemical waste (0.5g sample) at detection limits ranging from 100 to 200 ppt. The method is also suitable for the anlysis of penta-octachlorinated dioxins and furans in chemical waste.

Fish and turtle are challenging matrices to analyze for TCDD and TCDF. Although, the TCDD levels in fish from various sites of the US had been determined, not much emphasis has been given to the levels of TCDF in fish despite the fact that the latter is equally as toxic. Two major sources of TCDF contamination of the environment are the incineration and the widespread use of PCBs. PCBs are known to be contaminated with TCDF[1] and due to the ubiquity of its presence in the environment, TCDF is expected to occur more commonly in biota than TCDD. A correlation of TCDF levels in fish to those of PCBs had been already suggested[2]. In the present study, fish tissues from various sites of the US were analyzed for TCDF and PCB by using packed column GC/HRMS under selected ion monitoring mode. For PCB, two molecular ions of penta, hexa and heptachlorobiphenyls were monitored, and the mass profile pattern of different Aroclors was compared with those of the unknowns. The one with similar profile pattern was used for quantitation. Except for two samples of fish, obtained from grocery stores, TCDF was detected in fish from all the sites in ppt to ppb levels, and PCBs in the range of ppb to ppm levels. A turtle sample had the highest concentration of PCB. Low levels of PCBs (10-15 ppb) were also found in the fish from grocery stores. TCDD was detected in one fish sample at a level of 40 ppt and the turtle had 200 ppt of TCDD. The PCB mass profile appeared to be similar to that of Aroclor 1254. The levels of TCDF correlate roughly with those of PCBs.

References:

1. Albro, P.W. and C.E. Parker, J. Chromat., 169, 161, 1980.

2. Dougherty, R.C., M.J. Whitaker, L.M. Smith, D.L. Stalling and D.W. Kuehl, Environ. Health Perspec., 36, 103, 1980.

Scheme 1. Extraction and Cleanup of Chemical Waste

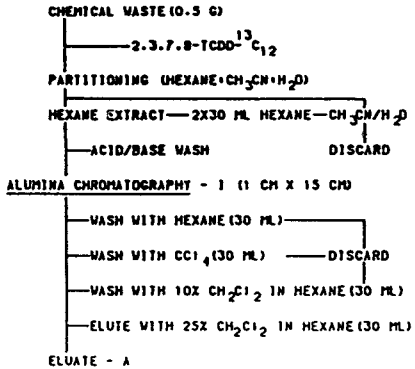

Scheme 2. Cleanup of Chemical Waste

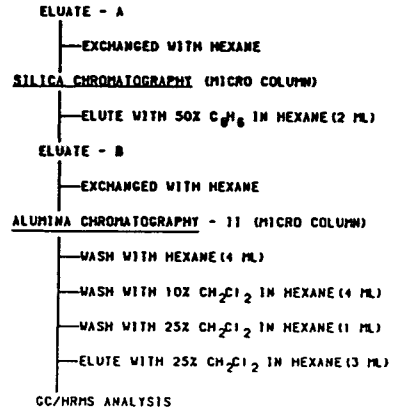

TABLE 1. TCDD SPIKED CHEMICAL WASTE SAMPLES

matrix	Added	Found (UNL)	Found (EPA)
C.WASTE-1	75	75 (5)	90 (5) ppb
C.WASTE-2	95	105 (20)	95 (5)
C.WASTE-1	0	1.2* (0.45)	0.5 (0.15)
C.WASTE-2	0	1.3* (0.70)	0.4 (0.09)

*Background levels of the waste

TABLE 2. TCDF SPIKED CHEMICAL WASTE SAMPLES

Matrix	Added	Found (UNL)	Found (EPA)
C.WASTE-1	130	115 (20)	105 (0.8) ppb
C.WASTE-2	120	165 (20)	85 (5.0)
C.WASTE-1	0	20* (10)	15 (1.0)
C.WASTE-2	0	25* (5))	20 (0.15)

*background levels of the waste

A COMPARISON OF TECHNIQUES FOR THE ANALYSIS OF ETHYLENE DIBROMIDE

A E Ashcroft, M Kearns, R J Greathead, M Almond and K R Compson
Kratos Analytical Instruments, Ramsey, New Jersey, USA

Introduction

Ethylene dibromide (EDB) (1,2-dibromoethane) has been used extensively in agriculture for a number of years as a soil and grain fumigant and for spraying citrus fruits, and has recently gained publicity as a result of its suspected toxicity. The latter has led to the suspension of almost all agricultural uses of EDB by the Environmental Protection Agency, and additionally residue limits have been set for food products which have been in contact with the pesticide at some stage of their manufacture.

The low residue limits set (30 - 900 ppb depending on the type of product) have dictated the necessity for a specific, highly sensitive and rapid method of analysis, for which the mass spectrometer is particularly suitable. Several mass spectral analyses of EDB are described in the following sections and their results discussed.

Results and Discussion

In order to detect low levels of EDB in complex mixtures (for example, food extracts) a chromatographic technique directly coupled to the mass spectrometer is desirable, and gas chromatography is appropriate for this relatively volatile, non-polar compound. The detection of narrow capillary GC peaks dictates the use of a fast scanning mass spectrometer, and the KRATOS MS25RFA was chosen for this reason (see Experimental section for analytical details).

EDB was analyzed initially by electron impact mass spectrometry and the result is shown in figure 1.

The molecular ion region (m/z $186^{+\cdot}$, $188^{+\cdot}$, $190^{+\cdot}$) is clearly visible along with the base peak (m/z 107^{+}, 109^{+}) arising by the loss of bromine from the molecular ion. Electron impact, compared with positive and negative chemical ionization - neither of which produced an ion indicative of sample molecular weight - was found to be the most suitable method of analysis, and in order to establish the limits of detection electron impact Selected Ion Monitoring (SIM) was performed. This powerful technique, which can be carried out either at low or (for increased specificity) high mass resolution, provides a significant increase in sensitivity because only certain chosen ions - in this case the predominant ones, m/z 107^{+} and 109^{+} - are monitored. Figure 2 shows the linear response obtained for the sum of the m/z 107^{+}, 109^{+} peak areas for differing amounts of EDB and illustrates the accuracy and reliability of the method. 1 pg of EDB is easily detected, and the signal detected from the m/z 107^{+} ion only has a signal to noise ratio of approximately 7:1.

Metastable mapping provides an alternative, highly specific mass spectral technique and this is illustrated for the EDB metastable transitions occurring in the first field free region of the mass spectrometer. B/E, B^2/E and Constant Neutral Loss data are all available from this single experiment. The major transition, which occurs at an electrostatic analyser voltage of approximately 48% (figure 3), corresponds to the loss of bromine from the molecular ion. Close inspection of this area reveals two distinct signals, one from the m/z $190^{+\cdot}$, $188^{+\cdot} \rightarrow 109^{+}$ transitions and the other from the m/z $188^{+\cdot}$, $186^{+\cdot} \rightarrow 107^{+}$ transitions. The individual B/E precursor ion spectra of the ions m/z $190^{+\cdot}$, $188^{+\cdot}$ and $186^{+\cdot}$ and their losses Br^{81}, Br^{81} and Br^{79}, and Br^{79} respectively (figure 4) are in good agreement with theoretical predictions. For the highest specificity, these transitions were monitored by Selected Decomposition Monitoring, in which the fragmentation from a chosen precursor to a chosen fragment is monitored.

Experimental

A KRATOS MS25RFA double focussing, forward geometry mass spectrometer equipped with an inhomogeneous field magnet and operated under Autoconsole control was used, with a scan speed of 0.3 seconds per decade of mass, 1000 mass resolution, 70eV, and a source temperature of 200°C. The mass spectrometer was directly coupled with a KRATOS GCMS interface to a CARLO ERBA Mega gas chromatograph. A CHROMPACK CpSil 8CB (25m) capillary column was used at 38°C with helium as the carrier gas.

Summary

The pesticide EDB has been analyzed by a variety of mass spectral techniques including electron impact, positive and negative chemical ionization, Selected Ion Monitoring, Metastable mapping, and Selected Decomposition Monitoring. Electron impact was found to be more sensitive than chemical ionization (by a factor of two), and so electron impact Selected Ion Monitoring was performed to establish the limits of detection. < 1pg (i.e. <1 ppb) was detected and this rapid mode of analysis is ideal for a fast and accurate sample output at highest sensitivity. An increase in specificity, which may be required depending on the precise composition of the mixture to be analyzed, can be achieved by use of high resolution Selected Ion Monitoring, Metastable mapping or for ultimate-specificity, Selected Decomposition Monitoring. This significant increase in specificity as would be expected reduces sensitivity - SIM is more sensitive than SDM by a factor of 10. The adaptability and sensitivity of the double focussing mass spectrometer indicate its suitability for this type of analysis.

Figure 1

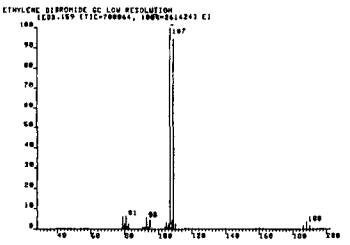

Ethylene dibromide - electron impact spectrum

KRATOS

Figure 2

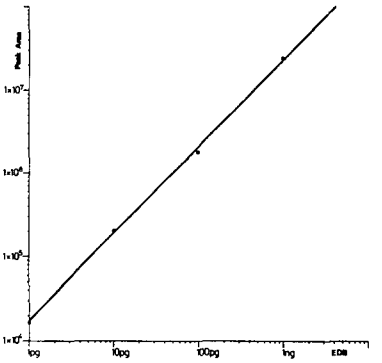

Ethylene dibromide, Selected Ion Monitoring m/z 107, 109 Peak Area v EDB

KRATOS

Figure 3

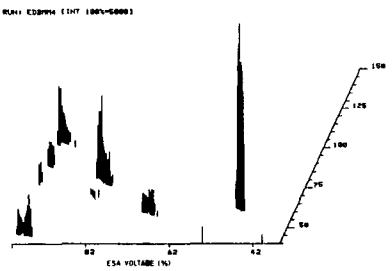

Ethylene dibromide, metastable map

KRATOS

Figure 4

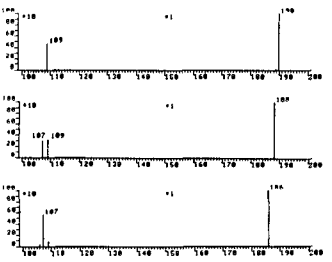

Ethylene dibromide loss of bromine from molecular ion

KRATOS

MASS SPECTRAL EXAMINATION OF CHLORINATED COMPONENTS OF BLEACHED FLOUR

David L. Heikes, Total Diet Research Center
Food and Drug Administration
1009 Cherry Street
Kansas City, MO 64106

The Food and Drug Administration's Total Diet Program surveys table-ready foods for industrial chemicals and pesticides. During the examination of several pastry items an unidentified gas chromatographic / microcoulometric response was observed. Breads, cakes, muffins and soda crackers all contained this compound at various levels. Since these foods have the common ingredient of flour, a survey of various types of flour was conducted. It was found that only bleached flour contained this unidentified chemical.

Capillary column GC/MS indicated that at least four compounds comprised this bleached flour unknown (Figure I). Mass spectra (EI) of the two major components showed a common similarity to the unsaturated pattern exhibited by linoleic acid (i.e. m/z 41, 55, 67, 81, 95, etc.). However, the molecular ion (m/z 280) for linoleic acid was replaced by ions of m/z 278 for these two chemicals. (No ions above m/z 280 were noted in these spectra) (Figures II and III). This observation led to the suspicion that the natural linoleic acid of flour (wheat) was reacting with the bleaching agents to produce a chlorinated derivative of linoleic acid.

Chlorine dioxide, prepared by the method of Lindgren and Svahn, was bubbled through linoleic acid for a period of 24 hours. After gel-permeation cleanup to remove most of the unreacted acid, GC retention data and mass spectra matched that of the compounds found in pastry products.

Negative chemical ionization (methane) spectra suggest the presence of two chlorine atoms, with a molecular weight of 350 daltons. These two compounds are assumed to be formed by the addition of two chlorine atoms at the 9,10 or 12,13 unsaturated positions of linoleic acid, respectively.

Lindgren, B. O., Svahn, C.M. and Widmark, G. Acta Chem. Scand. 19, 7 (1965).

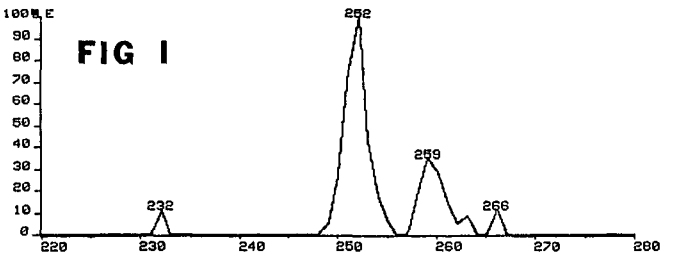

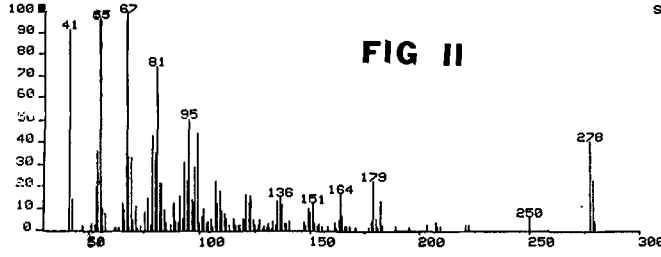
FIG II
S#
100
90
80
70
60
50
40
30
20
10
0
41
55
67
81
95
136
151
164
179
250
278
50
100
150
200
250
300

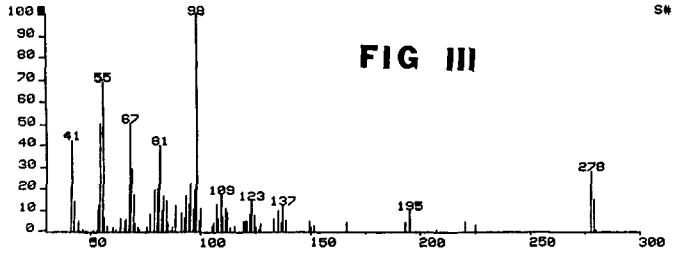
FIG III
S#
100
90
80
70
60
50
40
30
20
10
0
41
55
67
81
98
109
123
137
195
278
50
100
150
200
250
300

MS-MS ANALYSIS OF GEOLOGICAL BIO-MARKER COMPOUNDS.

P.W. Brooks, C.J. Porter, J.C. Bill. VG Analytical Limited, Floats Road, Wythenshawe, Manchester M23 9LE. ENGLAND.

INTRODUCTION.

High resolution GC/high resolution MS[1] and high resolution GC/metastable ion monitoring[2] are the most suitable methods for detecting and quantitating biological marker compounds using a double focusing mass spectrometer. These techniques eliminate the requirement for extensive sample preparation prior to analysis but, in general, require time consuming gas chromatographic separations.

A highly selective and sensitive technique for rapid screening of biological marker distributions is the use of MS-MS. Examples are presented for saturated hydrocarbon fractions isolated from geological samples.

EXPERIMENTAL.

MS-MS studies were performed on a VG 70-70EQ interfaced to a PDP 11 VG 11-250 data system. The 70-70EQ consists of a VG 70-70E double focusing mass spectrometer coupled to a quadrupole collision gas cell followed by a high mass quadrupole analyser. Such a combination of analysers (EBQQ) offers extremely high flexibility since it may be used as a conventional double focusing M.S. or as a double focusing MS-MS system. The conventional mass spectra were obtained at 3s/dec., the parent ion MS-MS spectra at 10s/dec., and the daughter ion MS-MS spectra over 10 s per scan. MS-MS multiple ion detection analyses were performed by transmitting the daughter ion m/z 191 through the quadrupole analyser and, switching the electric sector and accelerating voltages in synchronism to transmit the triterpane molecular ions.

RESULTS.

All geological triterpenoid hydrocarbons have a predominant contribution from m/z191 in their mass spectra. The molecular weights of these compounds range from m/z370 (C_{27}) to greater than m/z700.

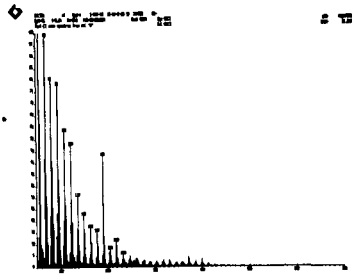

Figure 1

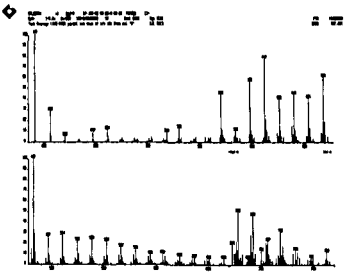

Figure 2

Figure 1 shows the full mass spectrum of a saturated hydrocarbon fraction of oil A. The spectrum is extremely complex and although m/z191 is intense, ions above m/z370 are low in abundance and are present at every mass unit. Figure 2 shows the parent ion spectrum of m/z191 Intense ions are present above m/z350 and correspond to the triterpanes. Ions are also present up to m/z762 indicating pentacyclic triterpanes of C_{55}, not previously seen by conventional GC/MS.

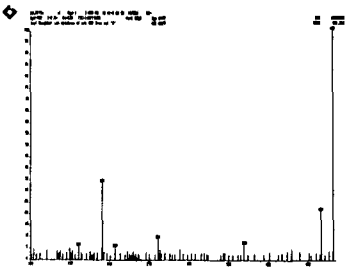

Figure 3

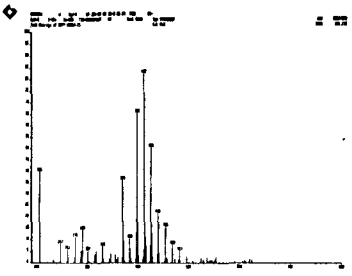

Figure 4

Figure 3 shows a daughter ion spectrum of one of the selected parent ions $^{m}/z482$ from oil A. All the ions present and above background are fully consistant with the proposed structure for a C_{35} triterpane. Figure 4 shows the parent ion spectrum from $^{m}/z191$ present in oil B, acquired in continuum mode and subsequently centroided using a sophisticated peak centroiding algorithm. As for oil A triterpanes are apparent from C_{27} upwards, however, the distribution is dissimilar to that for oil A. GC/MS/MS also provides high selectivity and sensitivity for the determination of the geometrical and stereochemical isomeric distribution of the molecular weight species. The quadrupole is allowed to transmit only $^{m}/z191$ daughter ions and voltage M.I.D. over the parent ions of interest is performed. The distrubution of isomers is readily obtained as shown in Figures 5 and 6 for oil B. Clearly more than one isomer is present for all parent ions. The specificity of such an analysis is very high and leads to unambiguous identification of the triterpanes present. Confidence in quantitative analysis of triterpane ratios for geochemical studies is greatly enhanced.

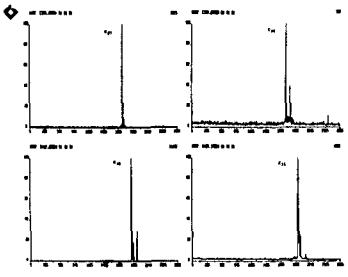

Figure 5

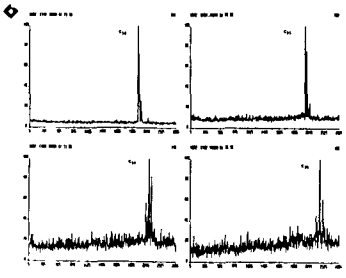

Figure 6

REFERENCES.

1. Bjorey, M., Brooks, P.W., Hall. K, 1981, Advances in Organic Geochemistry , eds John Wiley and Sons.
2. Warburton, G.A., Zumberge J.E., 1983, Anal. Chem., 55, 123-126

FINGERPRINTING OF OIL SAMPLES BY MULTIPLE METASTABLE ION RECORDING

Uwe Rapp, Monika Höhn, Reinhold Pesch and Ron Bonner, Finnigan MAT GmbH, Barkhausenstr.2, D-2800 Bremen, FRG.

Specificity is a key analytical goal with mass spectrometry. Accordingly MS/MS techniques become more and more important. A double focussing magnetic mass spectrometer is a simple approach to MS/MS, whereby the reversed arrangement (the magnet preceding the electric sector) has distinct advantages. The linked scans which allow the recording of the so-called metastable ion transitions in the first or second field free region can be used for these experiments. Since the two fields are scanned according to certain functions such as B/E = const. or B^2/E = const. the "normal" masses are not transmitted, but only "metastable peaks" which are due to preselectable fragmentation processes.

In the analysis of crude oils and sedimentary rock extracts the pattern of steranes and pentacyclic triterpenes can be used as characteristic fingerprint[1,2] The two substance classes have key fragments at m/z 217 (steranes) and m/z 191 (triterpanes) which stem from the molecular ions. These fragmentations have been monitored using linked scans methods.

Cholestane serves as standard for method verification. The B^2/E = const. linked scan shows an intense metastable transition for the process m/z 372 → 217 (figure 1). Figure 2 gives an indication on the sensitivity; 100 pg were injected yielding a good signal/noise ratio.

Several analytical problems can be addressed in this way such as the origin of oil from land or marine matter or the thermal maturity of samples[3]. The technique is extremely specific and removes the alkanes, alkenes etc. background completely, as is demonstrated with a saturates fraction of a North Sea Oil sample (figure 3). Reconstructed mass chromatograms from scan data showing the molecular ions of the C_{27}, C_{28} and C_{29} steranes (m/z 372, 386 and 400) as well as the key fragment m/z 217 are shown in the upper traces. The bottom traces are the metastable ion recordings (B^2/E = const.), where the transitions of the three sterane molecular ion species m/z 372, 386 and 400 to m/z 217 are measured.

When comparing the "normal" scan data and the linked scan metastable ion data it is obvious that a reliable quantification for oil maturity indicator purposes is made possible by the metastable ion data.

Experimental

The measurements were performed with a Finnigan MAT Model 8230 in the GC/MS mode. A 25 m SE 54 fused silica capillary column was used. The splitless injection was achieved at 100° C, programming up to 200° C with 30° C/min, then with 5° C/min up to 290° C as final temperature.

References

(1) A.S. Mackenzie in J. Brooks and D.H. Welte (Ed.): "Advances in Petroleum Geochemistry" Academic Press, New York, Vol. 1, in press.
(2) G.A. Warbuton and J.E. Zumberge, Anal. Chem. 55, 123 (1983).
(3) W.K. Seifert and J.M. Moldowan, Geochim. Cosmochim. Acta 45, 783 (1981).

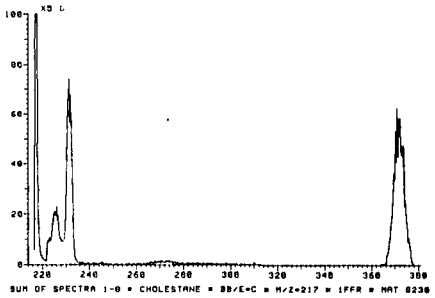

Figure 1. Parent ion linked scan (B^2/E = const. first field free region) for m/z 217 of cholestane.

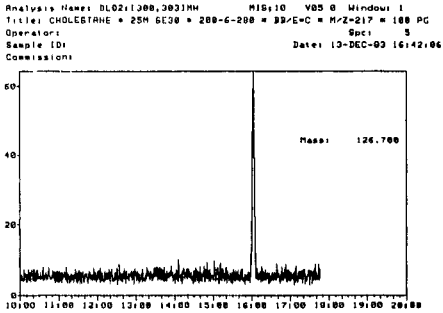

Figure 2. Metastable ion monitoring of the transition 372 → 217 (B^2/E = const.), 100 pg cholestane.

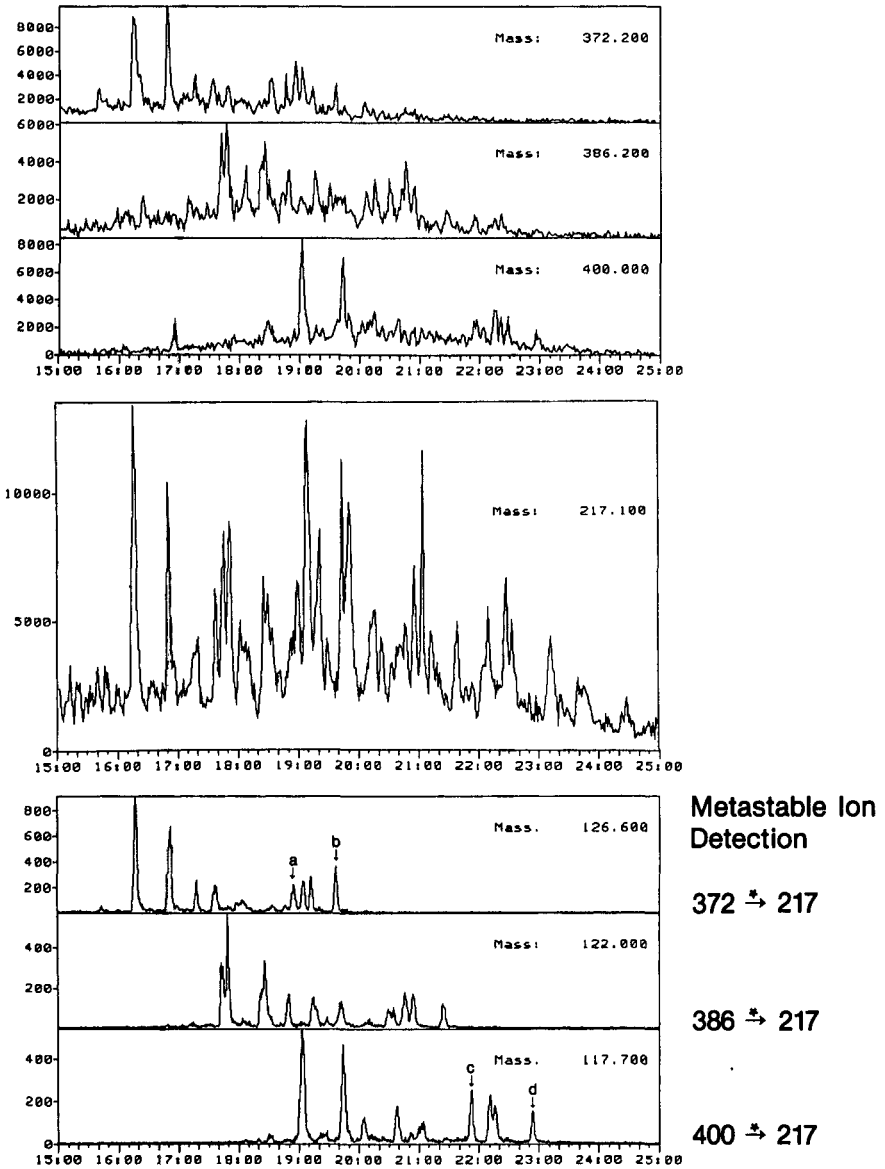

Figure 3. Comparison of mass chromatograms from scan data with metastable ion monitoring data, showing increased specificity for sterane determination in the saturates fraction of a North Sea Oil sample.

Mass Spectral Detection and Characterization of Petroleum Dyes, Tracers and Polar Fractions

T. L. Youngless, J. T. Swansiger, D. A. Danner, and M. Greco
Gulf Research and Development Co. Pittsburgh Pa. 15230

Techniques for the identification of the manufacturer of petroleum products are important for several reasons, including spills, excess lead violations, boot-legged fuels, and contamination problems. Such techniques as GC fingerprinting provide a powerful and simple solution to many problems. Leaded fuels can also be identified on the basis of their alkyl lead compound distribution as determined by electron capture GC, however it is possible for different manufacturers to use the same lead packages. Since leaded fuels are required by Federal law to contain a dye(s) the analysis of the dyes can frequently identify the manufacturer. In many cases, thin layer chromatography of the gasoline dyes and comparison of their Rf values is sufficient to identify a fuel.

Problems occur with the above identification techniques when several fuels have mixed or weathering has changed the hydrocarbon distribution. Analysis of the dyes can be difficult when the fuel has percolated through the soil and become contaminated by other polar components which obscure the dye bands. In addition, while TLC is adequate for resolving different dye colors, the technique lacks the resolution to separate structurally similar dyes varying only in alkyl substitution. Unleaded fuels can present other problems in identification since they do not contain a lead package and are not required to contain dyes. The addition of a unique chemical compound to the fuel which will act as a tracer can be used to unambiguously identify the fuel. Several tracers are available commercially, however many are prohibitively expensive and suffer severe adsorbtion problems when in contact with soils.

This work demonstrates the application of high resolution mass spectrometry (HRMS) to the characterization and identification of petroleum dyes used in leaded fuels and the development of a GC/MS technique for distinguishing unleaded fuels on the basis of their polar compound distributions. The use and GC/MS detection of a tracer which is unique to the fuel, economically feasible, and resistant to soil adsorption is also shown.

The HRMS spectra of many commercially available petroleum dyes were obtained. Separation and concentration from the fuel was achieved through the use of column chromatography and subsequent TLC if applicable. Most of the dyes were found to consist of azo,diazo and anthraquinone parent structures. A few dyes were found to consist of a single pure compound; however, most dyes were mixtures which varied significantly in alkyl substitution. Further, some dyes were also found to be mixtures of various colored dyes and thus different ring structures. Figure 1 shows a specific ion plot of the probe microdistillation data for the molecular ions of the three components of a red dye which vary in alkyl substitution of 1-3 carbons.TLC and subsequent direct-probe HRMS were found to be very useful for characterization of the more complex mixtures although components varying in alkyl substitution were not always resolved.

Preliminary data employing GC/HRMS to characterize the dyes appears promising but suffers from the non-volatility and sensitivity to thermal degradation of the dyes. The molecular weights of the dyes range from 200 to over 700 amu. GC/HRMS with on-column capillary injection has been succesfully used to characterize dyes with molecular weights up to 400 amu. Trade-offs exist therefore between polar columns which give the best resolution for the lower molecular weight dyes and non-polar columns which allow higher MW dyes to be chromatographed. In order to obtain elution of the higher MW dyes, short capillary columns were necessary. The resulting chromatograms provide better and faster separation than TLC/HRMS but further work remains to optimize the chromatography.

Figures 2 and 3 show a comparison of the polar components of unleaded fuels A and B obtained by GC/MS of the polar fractions separated by liquid chromatography. Fuel B is also shown to contain a 1 ppm concentration of an alcohol used as a tracer which is resistant to soil adsorption effects.

In conclusion, the identification of fuels is not always a straight forward problem and various analytical techniques are required for various problems. These techniques were found to be useful in providing additional fuel identification information.

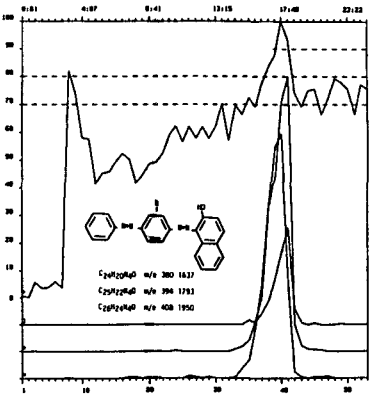

FIGURE 1 - SPECIFIC ION PLOT - RED DYE

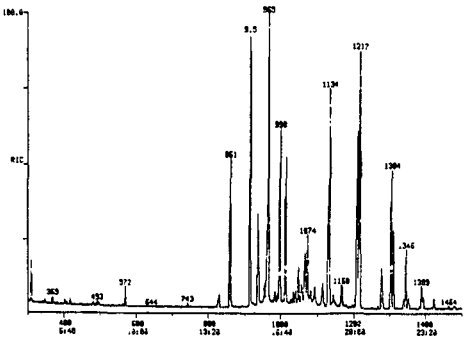

FIGURE 2 - FUEL A GC/MS OF POLARS

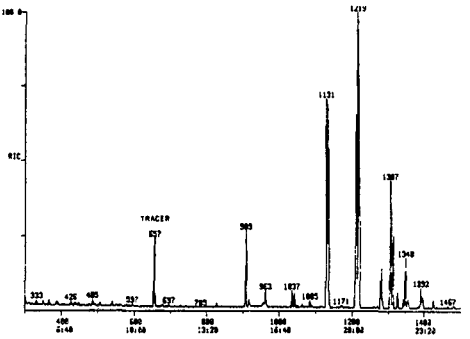

FIGURE 3 - FUEL B GC/MS OF POLARS AND TRACER

MOLECULAR BEAM MASS SPECTROMETRIC STUDIES OF THE OXIDATION OF ORGANIC MOLECULES*

Frank T. Greene and J. Eugene O'Donnell
Midwest Research Institute
Kansas City, Missouri 64110

This research was undertaken to determine the rates and mechanisms of oxidation of organic molecules, with emphasis on aromatic and other compounds relevant to the problems encountered in the incineration of hazardous waste. These studies are being carried out in both premixed laminar flames and a high temperature laminar flow reactor. The concentrations of the various species, including free radicals and other reactive intermediates, are being measured using molecular beam mass spectrometry (MBMS). Temperatures are measured by thermocouple and other techniques as needed.

The MBMS apparatus utilizes two mass spectrometers: a modified EAI quadrupole mass spectrometer and a Nuclide 12-90 large magnetic mass spectrometer. The molecular beam passes sequentially through the ion sources of the two instruments, which can be operated simultaneously. The quadrupole scan is slaved to the molecular beam chopper and can be used to obtain signal (time) averaged spectra with phase sensitive detection. The magnetic mass spectrometer has sufficient resolution to permit the observed ions to be identified from their mass defects.

Both atmospheric and subatmospheric premixed laminar flames have been investigated. To date, the emphasis has been on the reduced pressure flames because of the better spatial resolution available. For these studies a sintered bronze burner has been developed. Liquid fuels are contained in a thermostated reservoir, and introduced into the burner as in saturated N_2 through heated lines. The quartz sampling probes used are similar to those used by Biordi et al.[1] and Bittner and Howard[2] although several variations have been investigated.

Preliminary species measurements have been made in several alaphatic and aromatic hydrocarbons flames. A .05 atm toluene-N_2-O_2 flames has been selected for more extensive study, and detailed profiles for a number of intermediate species ranging from CH to C_6H_6 obtained. The spatial resolution obtained with a 50 μm sampling probe is better than that needed. These results are being compared with alternative oxidation mechanisms.

An isothermal laminar flow reactor has been designed and is now being constructed. This reactor will permit kinetic measurements to be made under well defined conditions, including temperature, thermal history of the reactants, and flow field. These results should therefore be easier to interpret than those for the flame, but will lack some of the complexities present in "real" combustion systems.

* This research was supported in part by the United States Environmental Protection Agency under Assistance Agreement No. R808184-01-0.

1 Biordi, J. C., C. P. Lazzara, and J. F. Papp, Combustion and Flame, 23, 73 (1974).

2 Bittner, J. D., and J. B. Howard, "Eighteenth Symposium (International) on Combustion, p. 1105, The Combustion Institute (1981).

QUANTITATIVE TRACE ANALYSIS BY LC/MS/MS

R. G. Christensen and E. White V
National Bureau of Standards
Center for Analytical Chemistry
Washington, D.C. 20234

Quantitative trace analysis for organic compounds in matrices such as oils often requires time-consuming and laborious sample preparation. Such techniques as extraction, preparative scale liquid chromatography, or conventional column chromatography are often resorted to. These manipulations in addition to being time-consuming, can lead to the introduction of systematic errors.

The combination of liquid chromatography with a mass spectrometric detector (LC/MS) has been used to perform some such analyses without extensive sample preparation (1,2). Many analyses are not amenable to this technique because of interferences which cannot be resolved either by the liquid chromatographic separation, or by the selectivity of the mass spectrometer.

Tandem mass spectrometry (MS/MS) with collision-induced dissociation offers another degree of selectivity. This presentation discusses the use of a triple quadrupole mass spectrometer as a liquid chromatographic detector in an analysis which is not feasible by LC/MS alone.

Samples of a petroleum crude oil (SRM 1582) and a solvent-refined coal liquid (SRC) were analyzed for dibenzothiophene. Oil samples were diluted 1:10 or 1:20, and 20 μL of the solution were injected onto a proprietary polar (amino-cyano-) column. Elution was with hexane containing 1-2% methylene chloride at a flow rate of 1.5 mL/min. The interface between the liquid chromatograph and the mass spectrometer was a preconcentrating device of our own construction (1). The preconcentrator was operated at enrichments of up to 40-fold.

LC/MS chromatograms were recorded, monitoring M+ (m/z 184) and LC/MS/MS chromatograms were recorded passing m/z 184 in the first quadrupole, colliding with N_2 in the second quadrupole, and monitoring m/z 152 (neutral loss of 32) with the third quadrupole. Quantitation was by comparison of peak heights with the peak heights given by an external standard. Typical chromatograms are shown in Figure 1 and 2. Table I compares our analytical results with the results obtained by other methods.

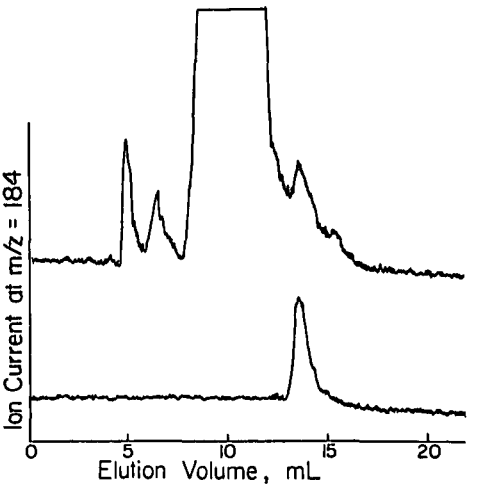

Figure 1. LC/MS Traces from injection of petroleum crude oil (SRM 1582) and standard solution of dibenzothiophene.

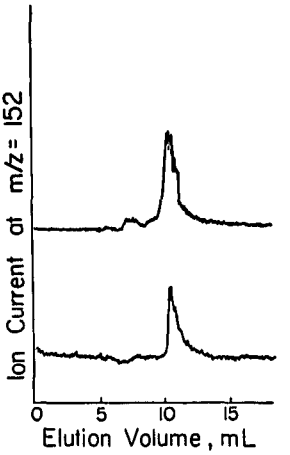

Figure 2. LC/MS/MS traces from injection of petroleum crude and a standard solution of dibenzothiophene

TABLE I

	LC/MS	LC/MS/MS	Other NBS Methods	
SRC	933 ± 57(n=5)	1017 ± 78(n=11)	1020 ± 70	μg/g
SRM 1582	----	41.3 ± 6.7(n=12)	33 ± 2	μg/g

References:

1. R. G. Christensen, H. S. Hertz, S. Meiselman, and E. White V, Anal. Chem., 53 (1981) 171.

2. R. G. Christensen, E. White V, S. Meiselman, and H. S. Hertz, J. Chromatogr., 271 (1983) 61.

APPLICATION OF CAPILLARY GC/MS TO MONITOR THE EFFECTS OF PRETREATMENT CHLORINATION OF NATURAL WATERS FOR THEIR USE IN DESALINATION

Thomas J. Leiker and Judith M. Hohnholt
Bureau of Reclamation
Engineering and Research Center
Denver CO 80225

INTRODUCTION

The Bureau of Reclamation has been responsible for the design and operation of a 460,000 gal/d desalination test facility. This is a pilot study for desalination of a natural inland water system using cellulose acetate reverse osmosis membranes. This water is from the Welton-Mohawk Canal in southwestern Arizona and consists of irrigation runoff and release flows from reservoirs upstream. This water is characterized as having a total dissolved solids of 4,000 mg/L and a dissolved organic carbon of 3.6 mg/L. Prior to desalination, the water is subjected to extensive pretreatment through the use of dual media filter, settling tanks, pH changes, and chlorination throughout pretreatment.

The purpose of this investigation is twofold. First, to characterize the extractable organic context of the water before and after in-house chlorination. Second, to determine if pretreatment chlorination can be reproduced in the laboratory.

EXPERIMENTAL

In-house chlorinations are conducted using NaOCl at a dosage of 1ppm free chlorine and maintained at a pH between 8 to 8.5 by the addition of a sodium borate buffer. The chlorinations are conducted at ambient temperatures for 4 hours. After chlorination, the samples are extracted immediately or stored overnight at 4°C and extracted the following day.

Chlorination at the test facility is conducted by direct injection of chlorine gas at a dosage of 1ppm free chlorine into the pretreatment facility. Depending upon the location within the pretreatment facility, the pH will vary from 5.6 to 10. The residence time of the water in the pretreatment facility is 4 to 5 hours.

EXTRACTION

A 1.3-L sample is placed into a 2-L separatory funnel along with the internal standards (10 ug each of D_5-Benzoic acid, D_8-Naphthalene and D_{10}-Anthracene). The pH of the sample is adjusted to 7 and extracted three times with methylene chloride (1x100 mL, 2x75 mL). The extracts are combined and concentrated by Kudernia-Danish to a volume of 1.0 mL. Next, the sample is adjusted to pH 0.5 with concentrated HCl and extracted and concentrated as before. The final extracts are combined and concentrated, under a gentle stream of nitrogen, to 100 ul and analyzed by GC/MS. After the initial analysis is complete, the sample is methylated using diazomethane and reanalyzed by GC/MS.

The mass spectral analyses were conducted using a VG Micromass 7035 double-focusing mass spectrometer. The mass spectrometer is scanned from 500-25 amu at a resolution of 1000 and a scan rate of 0.5 s/decade (1-second cycle time), electron-multiplier is at 1800 V, accelerating voltage 4000 V, and electron-energy 70 eV. Accurate mass measurement is conducted at a resolution of 5000, set statically, and scanned from 500-25 amu at 1.5 s/decade (cycle time of 2.5 s.). The gas chromatographic analysis is conducted on a HP5731 with the fused silica capillary column directly interfaced to the ion source. Chromatographic separations are performed with 30-m x 0.32-mm i.d. DB-5 fused silica capillary column. The column temperature is programmed from 40°C (held at 40°C for 4 minutes) to 280°C at 4°C/min. The injection port temperature is 250°C; carrier gas is helium with a flow rate of 1 mL/min. The transfer line temperature is 280°C. Injection volumes of 1.0 to 2.0 ul are made in the splitless mode.

RESULTS AND DISCUSSION

Selected compounds that have been detected before or after in-house chlorination are listed in table 1. Semiquantitation of individual compounds is performed by comparing their area counts with that of the internal standard. Figures 1 and 2 are typical total ionization chromatograms before and after in-house chlorination.

The majority of the halogenated compounds produced are brominated. Bromide has been detected in the water before and after chlorination by ion chromatography at concentrations from 0.5 to 18 mg/L. The presence of bromide in the canal is believed to be responsible for the production of brominated material.

CONCLUSION

A noticeable change has been observed in the composition of this water system after chlorination. The most significant finding of this investigation is the production of predominantly brominated compounds during chlorination. Future studies will examine the effect that these compounds and chlorination with water have on the performance and molecular structure of cellulose acetate membranes.

Table 1. - Selected Compounds Identified Before and After In-house Chlorination

Scan No.	Proposed structure	$\bar{x}$ concentration, ug/L Before	After
37	Bromodichloromethane[1,5]	ND	4.8
162	1-Bromo-2-methylpropane[5,6]	ND	2.0
247	Dibromochloromethane[1,5]	ND	21
369	4-Hydroxy-4-methyl-2-pentane[2]	4.08	3.98
417	7-Oxabicyclo [4.1.0] heptane[2]	31.2	18.3
497	Bromoform[1,5]	ND	43
500	2-Cyclohexene-1-ol[2]	11.43	DNQ
568	Dibromoacetonitrile[2,3,5]	ND	1.23
627	2-Cyclohexene-1-one[2]	8.42	DNQ
704 and 1002	Dichlorocyclohexane, 2 isomers[2,5]	ND	DNQ
888	2-Chlorocyclohexanol	7.49	10.5
982	1,2-Cyclohexanediol[2]	ND	13.47
1067	D_5-Benzoic Acid[4]	2.30	2.03
1102	2-Bromocyclohexanol[2,3,5]	ND	41.7
1216	Bromochlorocyclohexane[5,6]	ND	1.26
1303	D_8-Naphthalene[4]		
1369	2,5-Diethyl tetrahydrofuran[2,5]	11.26	DNQ
1428	Dibromocyclohexane[2,5]	ND	DNQ
1477	Chloroiodocyclohexane[6]	4.99	DNQ
2575	D_{10}-Anthracene[4]	19.2	18.1

1 Analyses conducted by Purge and Trap with ms confirmation.
2 Confirmed with standard library spectrum.
3 Confirmed by accurate mass measurement.
4 Internal standard.
5 Detected at the test facility.
6 Tentatively assigned structure.
ND Not detected.
DNQ Detected at less than 1 µg/L but not quantitated.

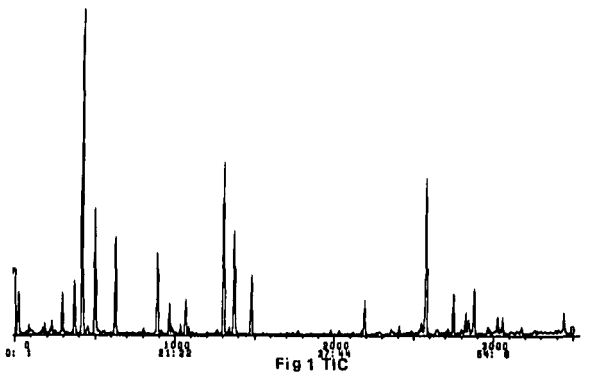

Fig 1 TIC
Before Chlorination

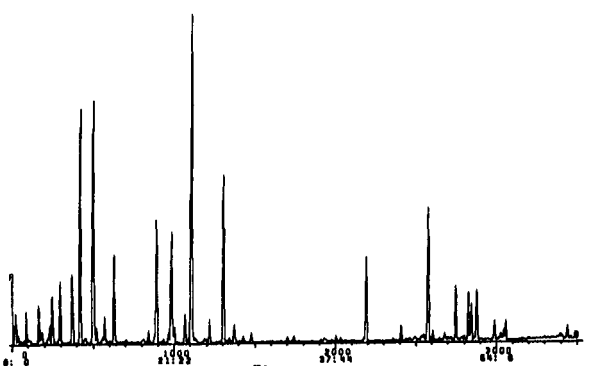

Fig 2 TIC
After Chlorination

SOME ION/MOLECULE REACTIONS REQUIRING TRANSLATIONAL ENERGY INPUT

Earl L. White, Michael T. Kinter, and Maurice M. Bursey*

Laboratory of Molecular Biophysics,
National Institute of Environmental Health Sciences,
P.O. Box 12233, Research Triangle Park, North Carolina 27709

and Department of Chemistry, University of North Carolina at Chapel Hill,
Chapel Hill, North Carolina 27514

Collisionally activated dissociations of organic ions require the conversion of part of the kinetic energy of the ion into internal energy. In our triple quadrupole mass spectrometer (Extranuclear Laboratories, Pittsburgh), the ion kinetic energy can be varied and energy-resolved breakdown curves can be obtained. This kinetic energy can also be used to provide access to ion/molecule reactions that require energy input and, for these reactions, the intensities of the products can be plotted as a function of ion energy as in the collisional activation breakdown curves. These curves can provide information that is useful not only for the differentiation of isomeric ions but also for the study of the thermochemistry of the reactions.

In these experiments the major $C_2H_5O^+$ isomers, $CH_3CH{=}OH^+$ and $CH_3OCH_2^+$, reacted with NH_3. The ion kinetic energy was varied from 5 to 30 eV in the laboratory frame of reference (lab) corresponding to a range of 1 to 8 eV in the center-of-mass frame (com), with the collision cell pressure in the single-collision range. Two features of the results are of interest. First, the spectra of the two isomers differ significantly. Ions observed at m/z 19, 27, and 44 for the $CH_3CH{=}OH^+$ isomer were not observed for the $CH_3OCH_2^+$. Conversely, ions observed at m/z 17, 31, and 32 for the $CH_3OCH_2^+$ isomer were not observed for the $CH_3CH{=}OH^+$ isomer. While not all ions observed result from ion/molecule reactions, these differences could be used to distinguish the isomers. The second feature of these experiments is the onset of some ions at higher kinetic energies. Ions at m/z 15, 19 and 30 from the $CH_3CH{=}OH^+$ isomers and m/z 15, 17, 18 and 31 from the $CH_3OCH_2^+$ isomer all showed onsets at kinetic energies greater than 5 eV (lab). Of these ions, those at m/z 18 and 31 for the $CH_3OCH_2^+$ isomer were studied in greater detail.

Neither the m/z 18 nor the m/z 31 ion was observed when $CH_3OCH_2^+$ collided with N_2. Both ions are therefore the products of ion/molecule reactions with NH_3. Reactions 1 and 2 are proposed for their formation. The ion kinetic energies at which they appear are shown in Figures 1 and 2.

$$\underset{\substack{m/z\ 45\\ +153}}{CH_3OCH_2^+} + \underset{-11}{NH_3} \rightarrow \underset{\substack{m/z\ 18\\ +149}}{NH_4^+} + \underset{\leq -12}{C_2H_4O} \qquad (1)$$

ΔH_f, kcal/mole
$\therefore \Delta H_r \leq -5$ kcal/mole

$$\underset{\substack{m/z\ 45\\ +153}}{CH_3OCH_2^+} + \underset{-11}{NH_3} \rightarrow \underset{\substack{m/z\ 31\\ +172}}{CH_2OH^+} + \underset{-6}{CH_3NH_2} \qquad (2)$$

ΔH_f, kcal/mole
$\therefore \Delta H_r = +24$ kcal/mole

The ion of m/z 31 appeared at about 4 eV (com). Since the reaction enthalpy is about 1 eV, ca. 25% of the ion kinetic energy is converted into internal energy if there is no activation barrier; more is converted if a barrier exists. The ammonium ion, m/z 18, appeared at about 1.5 eV (com). Because this reaction would be exothermic even for the least stable C_2H_4O isomer (ethylene oxide) this reaction must have some barrier <1.5 eV. Such a barrier could be due to a rearrangement of the $CH_3OCH_2^+$ ion, for example to protonated ethylene oxide (ΔH_r = +16 kcal/mol), intrinsic to the overall mechanism.

These energy-resolved experiments provide a means for studying the thermochemistry of ion/molecule reactions. Although the extent of conversion of the ion kinetic energy into internal energy is difficult to determine, the onset energy of an ionic product does set a limit on the thermochemistry of its formation here. Such numbers can in turn be used as an indicator of ion structure.

*on an R. J. Reynolds Industries leave from the University of North Carolina.

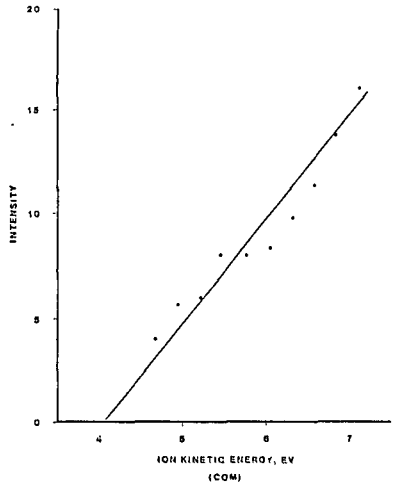

Figure 1. Onset of the observation of m/z 31. Each data point is the average of three determinations.

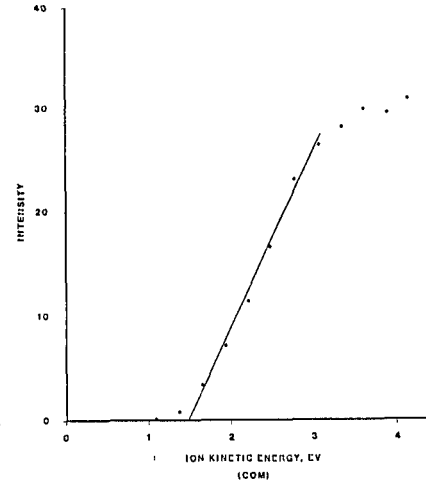

Figure 2. Onset of the observation of m/z 18. Each data point is the average of five determinations

Characteristics of Unimolecular Decompositions via Ion-Neutral Complexes

D.J. McAdoo and C.E. Hudson, Marine Biomedical Institute, The University of Texas Medical Branch, 200 University Blvd., Galveston, Texas 77550.

Ion-neutral complexes have recently received considerable attention as intermediates in unimolecular ionic decompositions in the gas phase.[1,2] We define a complex as an ionic and neutral species held in association by non-covalent attractions. We have concluded that low energy alkane losses from a variety of ions take place via such complexes.[3] These reactions have the following characteristics. 1. They give abundant metastable decompositions,[4-6] indicating that they are among the lowest energy fragmentations of the decomposing ions. 2. Alkane eliminations take place by processes which would be symmetry forbidden if concerted. Decomposition via an intermediate complex would bypass the symmetry imposed barrier.[7] 3. Losses of the corresponding alkyl radicals is very intense at energies higher than the energies at which the losses of alkanes occur.[3] For example, in the decompositions of the acetone ion, the loss

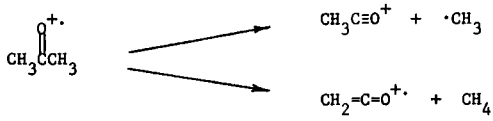

of methane dominates the metastable decompositions,[4,8] but the loss of methyl dominates at much higher energies. Another example is the ethyl isobutyl ether ions which loses ethane at threshold, but ethyl at slightly higher energies.[6] 5. Translational energies released in some of these reactions are very small, e.g., for T_{av} = ca. 1.0 kJ mol^{-1} for the loss of CH_4 from metastable acetone ions.[8] 6. Very large and variable isotope effects are observed in conjunction with metastable alkane eliminations. Primary isotope effects can be very strong, as metastable $CD_3C(=O^{+\cdot})CH_3$ loses CHD_3 70 times as often as CH_3D.[8] However, $(CD_3)_2CHCH_3^{+\cdot}$ loses CH_3D 6.0 times as often as CHD_3 + CD_4,[9] so this decomposition is dominated by a secondary isotope effect. Both primary and secondary isotope effects are strong in the metastable spectrum of $CH_3CD_2CHD_2^{+\cdot}$ ($-CH_4$: $-CH_3D$: $-CH_2D_2$ = 0.87: 0.01: 0.12).[10] The secondary isotope effect, (CH_4 + CH_3D)/CH_2D_2, is 7.3 and the primary isotope effect CH_4/(CH_3D x 0.5) is 174. Strong, highly energy dependent isotope effects on the loss of methane from deuterium-labeled <u>tert</u>-butoxide anions have recently been interpreted as evidence that that decomposition occurs via a radical-anion complex.[11] We conclude that secondary isotope effects will dominate when bond cleavage to form the complex is rate determining, and that primary isotope effects will dominate when hydrogen abstraction in the complex is rate determining. Both effects will be prominent when the two transition states have very close to the same energy. It is hard to devise an alternate decomposition mechanism which accounts for the variable isotope effects observed.

Based on the foregoing, we conclude that complex formation in slow unimolecular ionic decompositions is largely confined to energies between that required for bond cleavage to form the complex and energies sufficient to overcome the non-covalent attractions holding the complex together. (Fig. 1).

Fig. 1.

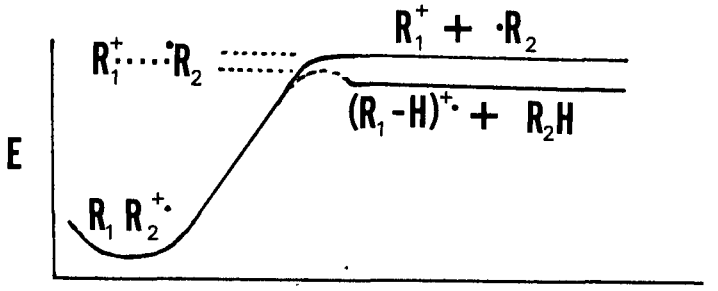

The conclusion that alkane eliminations take place via intermediate complexes is consistent with our view[12] that gas phase ionic fragmentations take place insofar as possible elementary single bond processes. Unimolecular decompositions which proceed via intermediate complexes are potentially useful for investigating low energy interactions between ions and neutral species.

1. R.D. Bowen and D.H. Williams, J. Am. Chem. Soc., 102 (1980) 2752.
2. A. Maccoll, Adv. Phys. Org. Chem., 3 (1965) 91.
3. C.E. Hudson and D.J. McAdoo, Int. J. Mass Spectrom. Ion Proc., in press.
4. D.J. McAdoo and D.N. Witiak, J. Chem. Soc. Perkin II, (1981) 770.
5. D.J. McAdoo, W. Farr and C.E. Hudson, J. Am. Chem. Soc., 102 (1980) 5165.
6. C.E. Hudson and D.J. McAdoo, Org. Mass Spectrom., 14 (1979) 109.
7. J.F. Wendelboe, R.D. Bowen and D.H. Williams, J. Am. Chem. Soc., 103 (1981) 2333.
8. C. Lifshitz and E. Tzidony, Int. J. Mass Spectrom. Ion Phys., 39 (1981) 181.
9. P.T. Mead, K.F. Donchi, J.F. Traeger, J.R. Christie and P.J. Derrick, J. Am. Chem. Soc., 102 (1980) 3364.
10. P.J. Derrick, Current Topics in Mass Spectrometry and Chemical Kinetics, J.H. Beynon and M.L. McGloshan, Eds., Heydon, London, 1982, p. 61.
11. W. Tumas, R.F. Foster, M.J. Pellerite and J.I. Brauman, J. Am. Chem. Soc., 105 (1983) 7464.
12. D.J. McAdoo and C.E. Hudson, Int. J. Mass Spectrom. Ion Proc., submitted.

Reactions of Negative Cluster Ions in a Tandem Quadrupole Mass Spectrometer

F. Dale, J.F. Paulson, and A.A. Viggiano
Air Force Geophysics Laboratory (AFSC), Hanscom AFB, MA 01731

A triple quadrupole mass spectrometer system, previously used for studies on ion photodissociation (1), has been converted to an apparatus for studies on ion-neutral collisions. The reactions occur in a thin (0.38 cm) collision chamber between the first and second quadrupole mass filters. Reactant ions are generated in a tightly enclosed electron impact ion source which is particularly useful for producing cluster ions, such as $OH^-\cdot nH_2O$(n = 1 to 4), $NO_3^-\cdot nHNO_3$ (n = 1,2), $HSO_4^-\cdot nH_2SO_4$(n = 1 to 4), $Cl^-\cdot nHCl$(n = 1,2), and $HSO_4^-\cdot HNO_3$. Typical ion currents of these species are 10^{-9}A after analysis in the first quadrupole mass filter. The ion source is the same type also used in the AFGL Selected Ion Flow Tube (SIFT)(2).

Reactions discussed in this paper are those of $OH^-\cdot nH_2O$ with CO_2, SO_2, CH_3CN, and CH_3Br, i.e.,

$$OH^-\cdot nH_2O + CO_2 \rightarrow HCO_3^-\cdot mH_2O + (n - m)H_2O \quad (1)$$
$$n = 1 \text{ to } 4,\ m = 0,1$$

$$OH^-\cdot nH_2O + SO_2 \rightarrow HSO_3^-\cdot mH_2O + (n = m)H_2O \quad (2)$$
$$n = 1 \text{ to } 4,\ m = 0$$

$$OH^-\cdot nH_2O + CH_3CN \rightarrow CH_2CN^-\cdot mH_2O + (n - m + 1)H_2O \quad (3)$$
$$n = 0 \text{ to } 4,\ m = 0,1,2$$

$$OH^-\cdot nH_2O + CH_3Br \rightarrow Br^-\cdot mH_2O + CH_3OH + (n - m)H_2O \quad (4)$$
$$\rightarrow CH_2Br^-\cdot mH_2O + (n - m + 1)H_2O \quad (5)$$
$$n = 0 \text{ to } 4,\ m = 0,1$$

In addition to reactions (1)-(6), collision induced dissociation of $OH^-\cdot nH_2O$ was observed in all cases for n = 1 to 4. Charge transfer was also observed for collisions of SO_2 with $OH^-\cdot nH_2O$.

Reactions (1) and (2) have been studied previously at thermal energy (3) for n = 2,3,4 and at beam energies (4) for n = 1,2,3. Reaction (4) has been studied at thermal energy for n = 0,1 by several authors (see ref. 5) and for n = 0,1,2 at beam energies (6). Reaction (3) has been studied (7) at thermal energy for n = 0,1,2. The same collision partners have also been proposed (8) to form $CN^-\cdot CH_3OH$.

The performance of the tandem quadrupole apparatus may be evaluated by comparing the results of the present work with previous work at thermal energies (3,5,7,8) and beam energies (4,5,6). The lower energy limit of the present apparatus appears to be about 1 eV (Lab), compared with a limit of about 0.2 eV in our earlier system (9). The very strong energy dependence of reactions (1) and (2) observed previously (4), e.g. reaction cross sections proportional to $(\text{energy})^{-6}$, is also observed here, suggesting a comparable energy spread in the reactant ion beam. However, retarding potential analysis of the reactant ion beam at the collision chamber shows a long low energy tail in the distribution. The beam is only weakly collimated in the present configuration. Products observed at only the lowest attainable energies in the earlier apparatus, e.g., $HCO_3^-\cdot 2H_2O$ for reaction (1) with n = 3, could not be observed in the present apparatus. Cross sections obtained here are generally smaller than those measured earlier. The very high signal levels for cluster ions, easily variable resolution, and high mass capability are significant advantages of the present apparatus.

References

1. T.F. Thomas, F. Dale, and J.F. Paulson, J. Chem. Phys. 79, 4078 (1983).
2. A.A. Viggiano and J.F. Paulson, J. Chem. Phys. 79, 2241 (1983).
3. F.C. Fehsenfeld and E.E. Ferguson, J. Chem. Phys. 61, 3181 (1974).
4. P.M. Hierl and J.F. Paulson, J. Chem. Phys., in press (15 May 1984).
5. M. Henchman, J.F. Paulson, and P.M. Hierl, J. Am. Chem. Soc. 105, 5509 (1983).
6. P.M. Hierl, M. Henchman, and J.F. Paulson, unpublished data.
7. J.F. Paulson and F. Dale, unpublished data.
8. B. Caldwell, M.D. Rozeboom, J.P. Kiplinger, and J.E. Bartmess, J. Am. Chem. Soc. 106, 809 (1984).
9. J.F. Paulson and P.J. Gale, Adv. Mass Spectrom. 7A, 263 (1978).

SOME ION-MOLECULE INTERACTIONS OBSERVED IN A TRIPLE QUADRUPOLE. P.H. DAWSON, National Research Council, Ottawa, K1A 0R6, Canada.

Triple quadrupoles are used for the unambiguous analysis of traces of impurities in the MS/MS technique. The analysis makes use of the low energy collisionally activated dissociation of ions. A well-designed triple quadrupole can itself be used to study the mechanisms of dissociation. However, a wide variety of other ion-molecule interactions can be observed and studied. The primary ion is selected by the first quadrupole. It is interacted with a target gas in the second rf-only quadrupole which cannels primary ions and product ions towards the third quadrupole for mass analysis.

The fundamental parameters that can be varied in the experiment are (a) the target thickness - this controls the number of successive collisions by primary ions or fragments. A kinetic analysis is often possible (b) the energy of the primary ions - this permits threshold energies to be determined and (c) the energy level of the analysing quadrupole with respect to the reaction (second) quadrupole - this permits an energy analysis of the product ions.

The table below summarises some of the ion-molecule interaction processes that have been observed and their typical characteristics. In making quantitative measurements, great care is necessary (a) to avoid fringing field effects at the exits and *entrances of the quadrupoles which may discriminate against very low energy ions*, (b) to operate the third quadrupole without mass discrimination (c) to minimise focussing effects at the exits from each quadrupole.

References

1. D.J. Douglas, J. Phys. Chem. 86 (1982) 185
2. P.H. Dawson and D.J. Douglas, Chapter 6, Tandem Mass Spectrometry, Ed. F.W. McLafferty, Wiley (1983)
3. P.H. Dawson, Int. J. Mass Spectrom. Ion Phys. 43 (1982) 195
4. P.H. Dawson and W-F Sun, Int. J. Mass Spectrom. Ion Phys. 44 (1982) 51
5. P.H. Dawson, Int. J. Mass Spectrom. Ion Phys. 50 (1983) 287
6. W-F Sun and P.H. Dawson, Org. Mass Spectrom. 18 (1983) 396
7. P.H. Dawson, In Press, Int. J. Mass Spectrom. Ion Phys.
8. P.H. Dawson, 31st ASMS Conference (1983)
9. See paper RPC 9
10. See paper WPA 21
11. J.P. Schmit, P.H. Dawson and N. Beaulieu, to be published, Org. Mass Spectrom.
12. P.H. Dawson, to be published

TABLE I

PROCESS	ENERGY DEPENDENCE	PRODUCT ION ENERGIES	EXAMPLES	COMMENTS, REFERENCES
(1) Collisionally Activated Dissociation from ground state)	Depends on centre-of-mass energy Thresholds observed	Low near threshold. Close to parent ion velocity at high energies	$C_6H_5Br^+ \rightarrow C_6H_5^+$ $(H_2O)_nH^+ \rightarrow (H_2O)_{n-1}H^+$ $C_{10}H_{14}^+ \rightarrow$ products	Linear yield dependence on thickness at low thickness Thresholds independent of thickness 1-8
(2) Collisionally Activated Dissociation - electronically excited ions	Threshold energies reduced Cross-sections may be enhanced	"	$O_2^{+*} \rightarrow O^+$ $C_6H_6^{+*} \rightarrow$ products	9
(3) Charge Transfer (exothermic or resonant)	No collision energy dependence	Quasi-thermal	$Ar^+ + Ar$ $Ar^+ + C_3H_8$ $O_2^{*+} + Ar$	May be dissociative 9
(4) Charge Transfer (endothermic)	Threshold energy	Quasi-thermal	$O_2^+ + Ar$	9
(5) Ion-molecule adduct formation	Critical energy dependence Yield maximises at low energy	Need a drawout voltage from collision region	Protonated esters + NH_3 Aromatics + NH_3	10,11
(6) Proton Transfer	Depends on proton affinities	Quasi-thermal	Protonated esters + NH_3	10,11
(7) Reaction-induced Fragmentation	Occurs below normal collision threshold	Low	Protonated esters + NH_3	10,11
(8) Dissociation via intermediate excited state	Threshold energies reduced		$C_6H_6^+ \rightarrow$ products	Thresholds depend on target thickness Non-linear kinetics 12
(9) Ion-molecule reactions	May be in competition with CAD	May indicate a stripping mechanism or intermediate complex formation	$C_6H_6 + CH_4 \rightarrow C_7H_7^+$ $N^+ + O_2 \rightarrow$	12

RATE CONSTANTS FOR QUENCHING THE METASTABLE $^2A_2$ STATE OF SO_2^+ BY ATMOSPHERIC GASES.

T. F. Thomas, Dept. of Chemistry, University of Missouri-Kansas City, Kansas City, MO 64110; Fred Dale and John F. Paulson, Air Force Geophysics Laboratory/LID, Hanscom AFB, MA 01731.

The photodissociation spectrum of SO_2^+ in the range 4400-5120 Å has previously been reported to originate from the vibrationally excited metastable $\tilde{A}\ ^2A_2$ state.[1] Since the cross sections for the photodissociation process,

$$(1) \quad SO_2^+ + h\nu \longrightarrow SO^+ + O$$

were found to decrease with increasing pressure within the electron impact ion source, a systematic study of the pressure dependence was undertaken. Data were obtained for the irradiation wavelengths 4735 Å and 4795 Å, corresponding to the $1_3\ 2_0$ and $1_3\ 2_3$ peaks, respectively, in the $\tilde{A}\ ^2A_1 \longrightarrow \tilde{C}\ ^2B_1$ transition. The added gases N_2O, CO_2, and N_2, as well as pure SO_2, were used.

To obtain the quenching rate constants it was necessary to determine the average residence time (τ) of SO_2^+ ions in the ion source, which was done by two methods. In one method the time delay between a pulse turning on the electron beam and a pulse shutting off the resulting ion beam was varied to obtain the most symmetrical dip in the time-of-flight spectrum of SO_2^+ ions. The result, extrapolated to zero pressure in the ion source, was $\tau = 2.8$ μs. In the second method the reaction cross section was measured in the ion source for the $CH_4^+ + CH_4 \longrightarrow CH_5^+ + CH_3$ reaction, and the result used to obtain a value of $E = 8.08\ V \cdot m^{-1}$ for the electric field within the ion source, from the data of Giardini-Guidoni and Friedman.[2] This value of E was used in the equation of Field, Franklin, and Lampe[3] to calculate $\tau = 2.5$ μs.

The rate constants, calculated from slopes of Stern-Volmer plots and $\tau = 2.6$ μs, are shown in the figure on the next page. The strong dependence on $IP(Q) - IP(SO_2)$ indicates that electronic energy transfer is the major pathway for quenching, at least for $Q = SO_2$ and N_2O. In particular, the k_Q for $Q = N_2O$ is roughly 5 times that predicted for an ion-molecule reaction,[4] indicating the occurrence of

$$(2) \quad SO_2^+ (\tilde{A}, V_1 = 3) + N_2O \longrightarrow SO_2\ (V_1 = 3) + N_2O^+(\tilde{X})$$

in a virtually resonant process. (From available photoelectron data plus our analysis of the photodissociation spectrum of SO_2^+ in the visible region, it is estimated that $\Delta E = 0.02 \pm .04$ ev for reaction (2).) The smaller, but still substantial, rate constants found for CO_2 and N_2, indicate that vibrational energy transfer is a significant contributor to the observed quenching as well.

$SO_2^+(\tilde{A}^*)$ QUENCHING RATE CONSTANTS

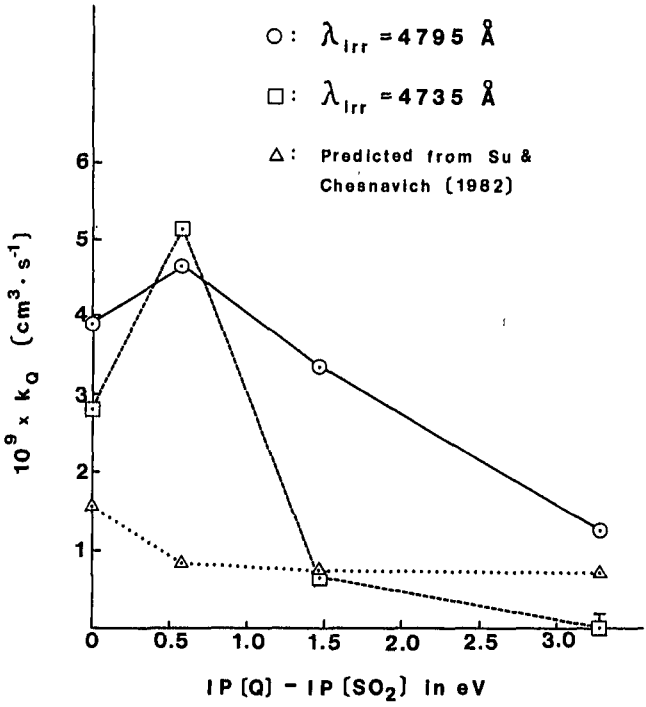

1) T. F. Thomas, F. Dale, and J. F. Paulson, J. Chem. Phys., 79, 4078 (1983).

2) A. Giardini-Guidoni and L. Friedman, J. Chem. Phys., 45, 937 (1966).

3) F. H. Field, J. L. Franklin, and F. W. Lampe, J. Am. Chem. Soc., 79, 2419 (1957).

4) T. Su and W. J. Chesnavich, J. Chem. Phys., 76, 5183 (1982).

LASER DESORPTION: THE THERMAL APPROACH.

Robert J. Cotter, Department of Pharmacology, The Johns Hopkins University, Baltimore MD 21205

The time-dependent temperature behavior of a surface exposed to a high power, short-pulsed laser beam has been described by Ready (1) and Kistemaker et. al. (2):

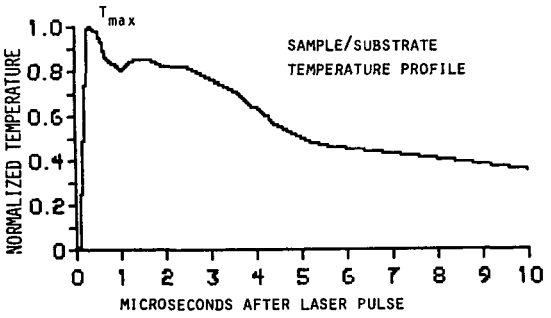

If one assumes that there is some "activation energy" for desorption, then ions (or neutrals) will have a rate of desorption (integrated over the irradiated surface area) given by:

$$dn/dt = k_1 C \exp(-E_d/kT)$$

where:
- n = # ions desorbed
- E_d = desorption activation energy
- k_1 = rate constant for desorption
- C = concentration (amount) of sample

If T_{max} for the temperature profile above is 2,000^0 K, then the desorption profiles of species with activation energies of 0.1, 0.6 and 3.0 e.v. are shown below:

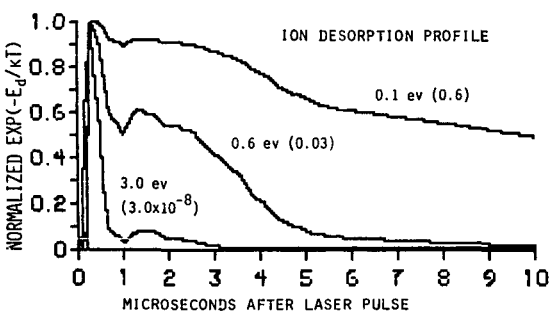

On the time-of-flight mass spectrometer, variation of the delay time between the laser pulse and an ion extraction pulse, provides a unique opportunity to observe the time-

dependent desorption of different ions. The ion intensity is actually observed as the integral (from t_o to $t_{extraction}$) of the equation:

$$dn/dt = k_1 C \exp(-E_d/kT) - k_2 n$$

where k_2 is the rate constant for ion losses in the source due to collision, etc. during the time between the laser and drawout pulses.

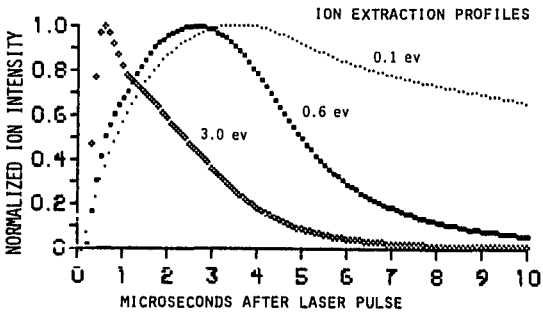

The rate of appearance of maximum intensities of several ions indicate that:

$$E_d(R_4N^+) < E_d(K^+) < E_d(Na^+)$$

which has been correlated previously with lattice energies (3). In addition, since k_2 is a function of the average velocity of the ions formed, or $(2E/m)^{1/2}$, then longer delay times produce spectra where the relative intensities of high mass ions have been improved and where the peak widths, due to kinetic energy spreads, have been decreased. Several thermal mechanisms are considered, with some consideration of the fact that the ions observed are generally not the result of changes in oxidation state.

(1)	$Na \rightleftharpoons Na^+ + e^-(metal)$	Langmuir-Saha	IP, ϕ_e
(2)	$M_{metal} \longrightarrow M^+ + M_{metal}(-)$	Richardson-Smith	ϕ_I
(3)	$NaCl_c \longrightarrow Na^+ + Cl^-$	high flux Na, Cl	IP, EA
(4)	$NaCl_c \longrightarrow Na^+ + Na_nCl^-_{n+1}$	low flux band gap energy	$\frac{1}{2}\Delta H_{lattice}$
(5)	$Na^+(substrate) \longrightarrow Na^+$	desorption	ΔE_{des}

(1) J.F. Ready, Effects of High Power Laser Radiation, Academic Press, New York, 1981

(2) G.J.Q. Van der Peyl, J. Haverkamp, P.G. Kistemaker, Int. J. Mass Spectrom. Ion Phys., 47, 125 (1982).

(3) R.B. van Breemen, M. Snow and R.J. Cotter, Int. J. Mass Spectrom. Ion Phys., 49, 35 (1983).

ISOTOPIC RATIOS IN FAST ATOM BOMBARDMENT MASS SPECTROMETRY

Ronald L. Cerny and Rick L. Lapp,
Midwest Center for Mass Spectrometry, Department of Chemistry,
University of Nebraska, Lincoln, NE 68588

The isotopic distribution pattern of an ion can be important information pertaining to its elemental composition particularly for halogen- or isotopically rich metal-containing species. For low abundance ions, exact mass measurements requiring high mass resolution may be impossible and the isotopic patterns, obtainable at low resolution, may be the only recourse for determining elemental compositions.

This information is often overlooked when fast atom bombardment (FAB) is employed because it is believed that the technique provides poor isotopic patterns due to overlap of M^+, $(M+H)^+$, and $(M-H)^+$ species. It is important to determine when this is a problem and what roles the sample and the liquid matrix play in the process.

To evaluate the accuracy of the isotopic ratios obtained by FAB several classes of compounds were analyzed in both the positive and negative ion modes. The observed ratios were compared to theoretical values calculated using the natural abundances of the atoms in the sample.

The data were acquired using a Kratos MS50-TA mass spectrometer and a Nicolet 1170 signal averager. Resolution was kept at approximately 3000, and 256 one-second scans were obtained in each run.

The $C_{18}F_{32}N_3$ fragment of tris-(perfluoroheptyl)- s-triazine was selected to evaluate FAB's ability to provide correct isotopic ratios as compared to EI, due to its strong signal intensity in both types of spectra. Ten individual acquisition experiments were run by each technique to obtain average values and standard deviations.

TRIAZINE BY EI

MASS	$\bar{x}$	s	THEO.
866	80.54	0.64	80.99
867	17.68	0.32	17.27
868	1.78	0.35	1.74
	Average s =	0.44	

TRIAZINE BY FAB

MASS	$\bar{x}$	s	THEO.
866	80.61	0.86	80.99
867	17.34	0.49	17.27
868	2.05	0.54	1.74
	Average s =	0.63	

The precision of reproducibility in both of these measurements is better than 1%, and the FAB results compare favorably with those obtained using EI.

To determine the accuracy of the ratios obtained using FAB, a sample having no hydrogens available for interaction with the matrix was desired. Rubidium Iodide was selected, using Rb_2I, Rb_3I_2 and Rb_4I_3 in the positive ion mode and RbI_2, Rb_2I_3, and Rb_3I_4 in the negative ion mode. As an example, the spectrum obtained for Rb_3I_2 is shown in Figure 1. For all of these benchmark tests, the accuracy of the determined ratios is within the experimental precision of the measurement.

The isotopic measurements were extended to organometallics, phosphonium salts, and nucleosides. For the charged organometallics the obtained ratios are also in agreement with those expected from the sample's empirical formula. However, in both the phosphonium salts and the nucleosides the abundances of the A+1 and A+2 ions are much too large (for the nucleosides A refers to the M+H species).

The A+1 peak in the spectrum of guanosine was examined at high mass resolution to determine why these abundances are too large; The results are shown in Figure 2. The ions were peak matched to the M+H ion. The formation of $(M+2H)^+$ causes the abundance of the A+1 species to appear too large at low mass resolution. Combining the abundances of the ^{13}C and ^{15}N species, the A+1 abundance is again within experimental error of the expected value.

MASS	THEO.	OBS.	|Δ|
509	37.56	38.04	0.48
511	43.49	43.28	0.21
513	16.79	16.03	0.76
515	2.16	2.65	0.49
		Average |Δ|	0.48

Nominal mass 285 from Guanosine in glycerol
Resolution = 41,500

	Mass	Formula	Error	Assignment
①	285.09670	C10 H14 N4 O5 ^{13}N	.6ppm	$(M+H)^+$ ^{15}N
②	285.10288	C9 H14 N5 O5 ^{13}C	.1ppm	$(M+H)^+$ ^{13}C
③	285.10726	C10 H15 N5 O5	.2ppm	$(M+2H)^+$

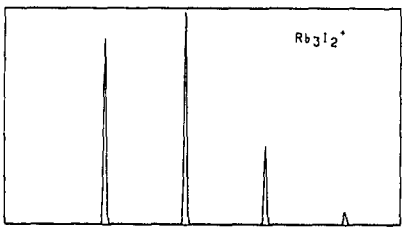

FIGURE 1

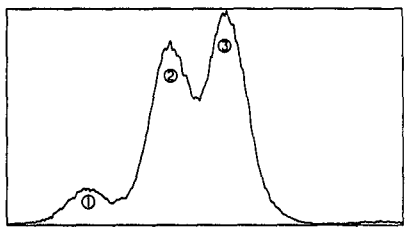

FIGURE 2

A proposed mechanism for the formation of the $(M+2H)^+$ is:

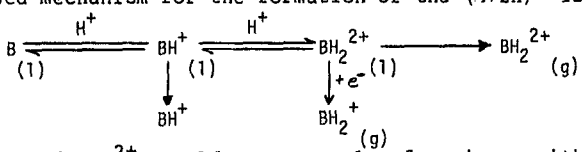

Reduction of BH_2^{2+} would occur only for ions with available low-energy unoccupied molecular orbitals (LUMOs). To test this mechanism the isotopic ratios of compounds with and without available LUMOs were determined and compared. The compounds were an aliphatic amine hexadecylamine, an aliphatic polyamine triethylenetetramine, an aromatic diamine 1,4-phenylenediamine, and the nucleosides guanosine and uridine. As expected the ratios for the aliphatic amines are correct but those for the aromatic diamine and the nucleosides are distorted by enhanced A+1 and A+2 abundances. This fits with the proposed mechanism.

Conclusions

Precise and accurate isotopic ratios can be measured for certain ions desorbed by using FAB. However, the A+1 and A+2 abundances for phosphonium salts, nucleosides, and aromatic polyfunctional compounds are too large, in some cases because of extra proton attachment. The mechanism for the formation of these polyhydrated species must involve the reduction of $(M+2H)^{2+}$.

STUDIES OF THE TRAPPING OF POSITIVE IONS IN THE ELECTRON BEAM OF A SOURCE USING LASER RADIATION AS A PROBE

T.G.Morgan, R.E.March*, A.G.Brenton, F.M.Harris and J.H.Beynon.

Royal Society Research Unit, University College of Swansea, Singleton Park, Swansea SA2 8PP, U.K.

* Dept. of Chemistry, Trent University, Peterborough, Ontario, Canada.

Photodissociation of ions has been studied in this Laboratory by introducing laser radiation into double-focusing mass spectrometers. Most of the work to date has been done by irradiating ions in the field-free regions but, more recently, ions in the source have been photodissociated before they leave the ion chamber.[1,2] The number density of ions in the ion chamber is considerably higher than in the field-free regions thus resulting in higher interaction rates and higher photo fragment-ion yields. In the present work, a ZAB-2F mass spectrometer has been modified in a simple way so that radiation from an argon-ion laser can be introduced into a standard VG Analytical EI/CI source. A window has been fitted to one of the sample inlet ports and radiation, which is introduced into the source block via one of the sample inlet holes, intersects the magnetically-confined ionizing electron beam.

It has been known for some time that positive ions can be trapped in the negative space charge created by a magnetically-confined electron beam within a conventional source.[3] The present work reports experiments in which the photodissocation of m-bromotoluene molecular ions is used to probe the average residence times of ions and the dependence of ion trapping on the conditions within the source.

The molecular current of m-bromotoluene arriving at the detector is depleted when the laser is on, as the ions are induced to fragment following photoexcitation by the laser beam. As all the ions are formed within the electron beam, and thus within the region of the trapping potential and interaction region of the laser, the rate of recovery of the molecular-ion current back to its initial level after the cessation of irradiation is a measure of the residence time of the ions within the trapping region. The ion current reaching the detector, before, during and after pulses of radiation, which varied from 0.1 to several milliseconds in duration, was monitored as a function of source pressure, electron energy and repeller voltage.

Results were obtained which showed that the percentage of photodissociation increased as the source pressure and electron energy are decreased reaching maxima at certain values of these parameters. These effects are shown to be due to increased residence times of ions in the source. Under optimum conditions of these two source parameters and that of the repeller voltage, it was found that over 50% of all molecular ions in the source could be photodissociated the corresponding residence time of the ions under these conditions being 2.5 milliseconds.

The observed temporal variation of ion current due to a pulse of radiation is successfully simulated by a simple kinetic scheme in terms of a sequence of successive and competitive reactions of the form

$$A_1 \xrightarrow{k_1} A_2 \begin{cases} \xrightarrow{k_2} A_3 \\ \xrightarrow{k_3} A_4 \end{cases}$$

k_1 is the rate constant for ionization with an electron current i_e, that is

$$M + e^- \xrightarrow{k_1} M^{+\cdot} + 2e^-$$

In the absence of laser radiation the loss of $M^{+\cdot}$ from the source to the first field free region is represented by

$$\underset{\text{(in the source)}}{M^{+\cdot}} \xrightarrow{k_3} \underset{\text{(outside the source)}}{M^{+\cdot}}$$

$1/k_3$ may be interpreted as the lifetime of the molecular ions within the source.

Laser irradiation causes dissociation of molecular ions and is represented by

$$M^{+\cdot} + h\nu \xrightarrow{k_2} F^{+\cdot} + N$$

k_2 is the photodissociation cross section using a laser beam of flux i_p.

Consider the <u>period of time when the light is on</u> that is after t = o. Let the times during this period be t_L and the concentration of $M^{+\cdot}$ during this period be $[M^{+\cdot}]_{t_L}$. Solution of the differential equations based on the kinetics scheme just described leads to

$$[M^{+\cdot}]_{t_L} = k_1 i_e [M] - (k_1 i_e [M] - (k_2 i_p + k_3)[M_s^{+\cdot}])e^{-(k_2 i_p + k_3)t_L}/(k_2 i_p + k_3) \quad (1)$$

where $[M_s^{+\cdot}]$ is the concentration of molecular ions at t_L = o

Consider the <u>period of time after the laser pulse ends</u> and during which the ion current returns to its original value. Let the times during this period be denoted by t_d and the concentration of $M^{+\cdot}$ be $[M^{+\cdot}]_{t_d}$. Solution of the differential equations gives

$$[M^{+\cdot}]_{t_d} = \frac{k_1 i_e [M]}{k_3}(1 - e^{-k_3 t_d}) + [M_m^{+\cdot}]e^{-k_3 t_d} \quad (2)$$

where $[M_m^{+\cdot}]$ is the concentration of molecular ions at the cessation of irradiation.

Solving equations (1) and (2) yields values of k_3, the reciprocal of which is the residence time of the ions in the trapping region. $1/k_3$ has been investigated as a function of source parameters.

It is apparent from the results obtained that laser-induced photodissociation is a useful technique for probing positive-ion trapping in potential wells. The present experiments show that judicious choice of source parameters increases the average source residence time of ions up to several milliseconds and thus allows the age distribution and hence the internal energy distribution of ions leaving the source to be changed systematically.

<u>References</u>

(1) E.E.Kingston, T.G.Morgan, F.M.Harris and J.H.Beynon, <u>Int.J.Mass Spectrom. and Ion Phys.</u>, <u>43</u> (1982) 261.
(2) M.S.Kim, T.G.Morgan, E.E.Kingston and F.M.Harris, <u>Org.Mass Spectrom.</u>, <u>18</u> (1983) 582.
(3) F.A.Baker and J.B.Hasted, <u>Phil.Trans.Roy.Soc. (London)</u>, <u>261</u> (1966) 33.

PENETRATION CHARACTERISTICS OF LOW ENERGY ELECTRONS.

T.H.T. van Kalleveen and G.G. Meisels, Dept. of Chemistry, University of Nebraska, Lincoln, Nebraska 68588.

The range of electrons is defined as the thickness of an absorber necessary to stop the incident electron completely. Knowledge of the range of low energy electrons is important to design of chemical ionization sources, the optimization of their performance, and to a better understanding of their characteristics.

For the gas phase, the electron range is not measured but the ionization range R, a closely related quantity. R is defined as the distance within which a certain percentage (97% is used here) of the total ionization has occurred. Since the spatial distribution of the primary ions is related to the linear ionization rate, di/dx, the ionization range can be obtained from this distribution (1). Illies and Meisels (2) have developed a method for determining the spatial distribution of mass selected ions formed by a collimated electron beam in a specially designed ion source. Coincidence methods are used to measure residence time distributions from which their points of ion formation are derived using a simple model based on known ion diffusion properties.

In this communication, the effect of electron current, pressure of the target gas, and choice of probe ion on R will be discussed using methane as the target gas.

The ionization ranges of energetic electrons in methane are shown in figure 1. A large discrepancy between the R values is observed at higher electron energies. Since higher electron currents lead to seemingly higher ionization ranges, the effect of electron current on RTD's has been studied in more detail. Figure 2 shows two distributions; RTD 2 is obtained for a higher electron current than RTD 1, which is not affected by lowering the electron current even more and is thus taken to be the correct distribution. The intensity of the electron current is thought not to affect the spatial distribution but only the total number of ions. The effect has been ascribed to an experimental parameter typical for coincidence techniques.

When R is expressed in ug/cm^2, it should not depend on the pressure of the target gas inside the ion source. Figure 3 shows the ionization range of 400 eV electrons in methane as a function of the gas pressure. The observed dependence is related to the discrimination of ions formed off axis in the cylindrical ion source. Since this effect is greatest near the ion exit slit, the increase in R is expected when the pressure is raised.

In almost all cases the primary ion is very reactive and so the probe ion will be the product of a sequence of ion-molecule reactions. For an ion to qualify as the probe ion it must be formed on a time scale short compared to its residence time, be stable and unreactive, and have a high abundance. The $(CH_5)^+$ and $(C_2H_5)^+$ ions formed from methane (3) meet these requirements fairly well. The R values obtained for either ion as probe ion should therefore be identical; table 1 shows that this is indeed the case.

Acknowledgements: We thank the Department of Energy for support under contract number DE-AS02-76-ER02567.

References:

(1) G.G. Meisels and A.J. Illies, Anal. Chem., 53, 2162 (1981).
(2) A.J. Illies and G.G. Meisels, Anal. Chem., 52, 326 (1980).
(3) M.S.B. Munson and F.H. Field, J. Am. Chem. Soc., 88, 2621 (1966).

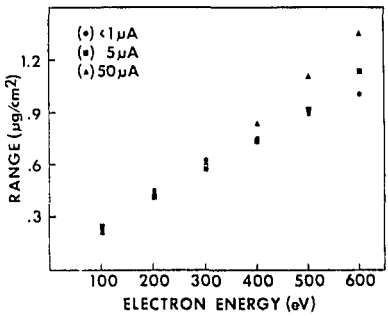

Fig. 1. Ionization ranges in .8 torr CH_4 at different electron currents.

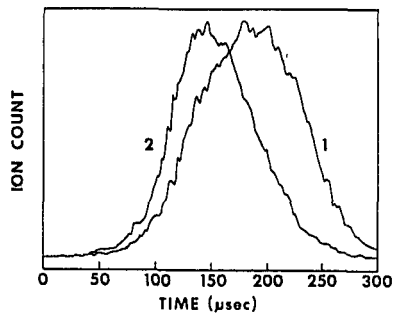

Fig.2. Residence time distributions of CH_5^+ at a low (1) and a high (2) electron current.

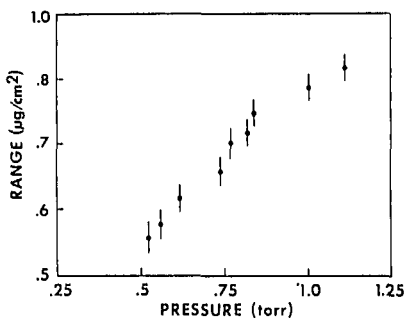

Fig.3. Ionization ranges of 400eV electrons in CH_4 as a function of pressure.

Table 1. Ionization ranges in .8 torr CH_4.

Electron Energy (eV)	Ionization Range ($\mu g/cm^2$)	
	CH_5^+	$C_2H_5^+$
100	.21	.23
200	.45	.46
300	.62	.61
400	.73	.74
500	.89	.85
600	1.00	1.00

BREAKDOWN GRAPH OF DIMETHYL ETHER ION FROM ONSET TO 18 eV USING TPEPICO MASS SPECTROMETRY.

Pradip R. Das, Toshihide Nishimura and G. G. Meisels*, Department of Chemistry, University of Nebraska, Lincoln, Nebraska 68588-0304.

The fragmentation characteristics of dimethyl ether ion, $[CH3-O-CH3]^{+}$ were investigated using threshold photoelectron-photoion coincidence time-of-flight mass spectrometry(1). A previous study (2) indicated that autoionization contributes to ionization and fragmentation of this molecule at higher energies. However, a major fragment ion in the mass spectrum, m/z 29, was not reported in that study.

Four major fragment ions are observed between onset and 18 eV: m/z 45, m/z 31, m/z 29 and m/z 15; their appearance potentials increase in that order. Resolution of our TOF instrument is about 50 (FWHM definition). Masses 45 and 46 were separated by deconvolution on the basis of the gaussian shapes of each peak. Detailed breakdown curves were constructed from the TOF peak areas.

The behavior of two of the ions, m/z 46 and m/z 45 show some "unusual" characteristics. The time-of-flight spectra at higher energies is shown in Fig 1. In the experimental and corrected breakdown curves, Figs. 2 and 3, the parent ion disappears at ca. 11 eV, which is the onset of m/z 45, reappears at 11.6 eV with a maximum intensity of ca. 23% at 12.1 eV, disappears again at 13 eV, and then shows a second substantial increase at 16.3 eV. M/z 45 also shows a substantive increase at about 16.3 eV. This behavior for the reappearance of the parent ion was reported previously by Refaye and Chupka (3) for ethanol. In dimethyl ether, the increase in the parent ion coincides exactly with the second band in the HeI PES (Fig. 4), whereas in ethanol it does not. Both the first and second bands in dimethyl ether have been assigned to non-bonding orbitals of oxygen. The onset of the m/z 45 ion occurs at ~11 eV where the PES intensity is close to zero. Thus it is likely that autoionization contributes substantially to ion formation in this region as suggested by previous workers (2). At higher energies (>13 eV), m/z 45 decreases as m/z 29 and m/z 15 are formed.

Photoionization yields for masses 46 and 45 show an increase in the ion yield for each of these ions at about 16.5 eV which is consistent with the increase in m/z 46 and m/z 45 beginning at about 16.3 eV. The increase coincides with the onset of the fifth band in the PES which has a σ_{CO} + $^{\pi}CH3^{+}$(pseudo) character. We do not as yet have a reasonable interpretation to offer for this behavior.

Kinetic energy release data on the formation of m/z 31 ion indicate that there is nearly complete conversion of the available excess energy in the parent ion to kinetic energy which suggests that the dissociation proceeds on a repulsive surface. This is consistent with the absence of a metastable transition for m/z 31 ion. The thermodynamic onset for the process $CH3OCH3^{+}$ ---> $CH3O^{+}$ CH3 assuming a $CH3O^{+}$ structure is very close to our appearance potential value for m/z 31 indicating that the KER is not a result of reverse activation barrier. If dissociation occurs on a repulsive surface, the m/z 31 ion must have the $CH3O^{+}$ structure (2),(4) since it would not be able to rearrange to the $CH2{=}OH^{+}$ structure.

The BDG of m/z 29 shows two stepwise increases suggesting two pathways for its formation. Metastable studies show that m/z 45 and m/z 31 are each precursors of m/z 29 ion.

On the basis of the present findings, we suggest that dissociation of dimethyl ether molecular ion includes to a significant extent processes which cannot be interpreted by conventional QET Theory.

Further work is being done to substantiate our ideas.

REFERENCES:

1. C. Batten, J. Taylor and G. G. Meisels, J. Chem. Phys. 65, 3316(1976).
2. R. Botter, J. M. Pechine and H. M. Rosenstock, Int. J. Mass Spectrom. Ion Phys., 25, 7(1977).
3. K. M. A. Refaye and W. A. Chupka, J. Chem. Phys. 48, 5205(1968).
4. A. G. Harrison, A. Ivko and D. Van Raalte, Can. J. Chem., 44, 1625(1966).

1

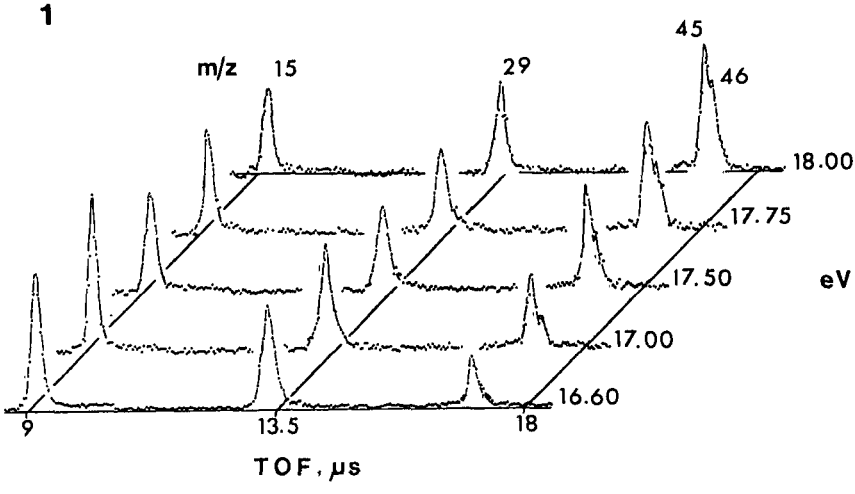

2

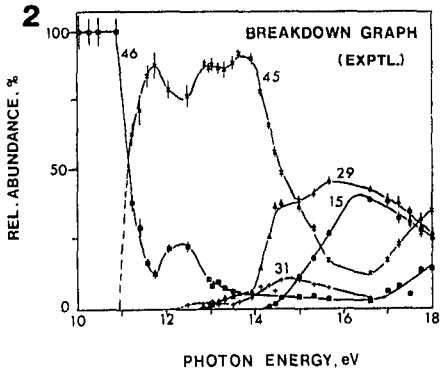

3

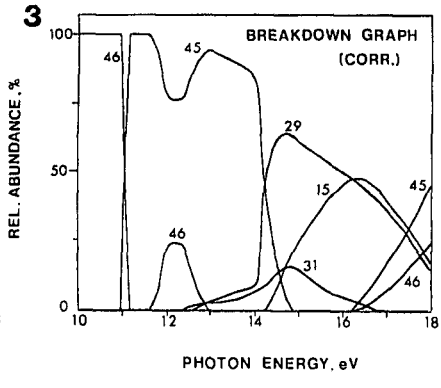

$(CH_3)_2O$ Dimethyl Ether

4

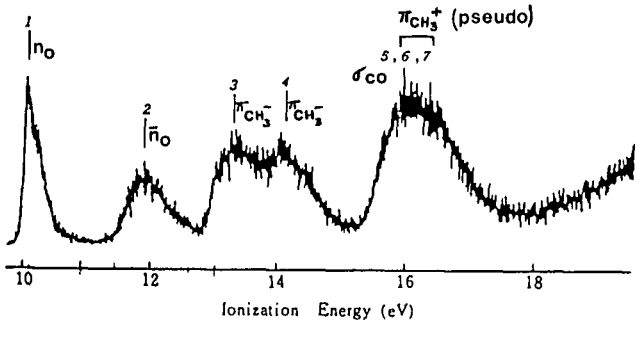

ELECTRON AFFINITIES FROM DISSOCIATIONS OF MIXED NEGATIVE ION DIMERS

Elaine K. Fukuda, David J. Burinsky, and Joseph E. Campana, Naval Research Laboratory, Chemistry Division, Washington, D.C. 20375

We report a new method for the determination of gas-phase electron affinities [1]. The basis of this method is the comparison of the rates of competitive dissociation reactions for mixed negative ion dimers,

$$[M_1M_2]^{-\cdot} \xrightarrow{k_1} [M_1]^{-\cdot} + M_2$$
$$[M_1M_2]^{-\cdot} \xrightarrow{k_2} [M_2]^{-\cdot} + M_1$$

These mixed negative ion dimers are formed in a high-pressure ion source of a VG ZAB-2F reverse-geometry double-focusing mass spectrometer, where they undergo many thermalizing collisions with the neutral bath species. The ensemble of mixed-dimer anions is kinetically sampled and the dissociations of the dimers are observed mass spectrometrically.

Using absolute rate theory, the following equation is derived,

$$\ln (k_1/k_2) = \Delta EA/kT$$

where k_1 and k_2 are the relative dissociation rates, ΔEA is the difference in electron affinity between M_1 and M_2, k is the Boltzmann constant and T is the average effective temperature of the dissociation dimer. This method is analogous to the method of Cooks *et al.* for the determination of relative proton affinities and gas-phase acidities from proton-bound dimers [2].

A mixture of nitrobenzene and p-nitrotoluene gives a negative ion chemical ionization mass spectrum that displays intense signals at m/z 123 and m/z 137 due to the molecular anions ($M^{-\cdot}$), and minor peaks at m/z 246, 260, and 274 corresponding to the three possible negative ion complexes. Figure 1 shows a CID/MIKES (collision-induced dissociation/mass analyzed ion kinetic energy spectrometry) spectrum of the mixed dimer ion of interest

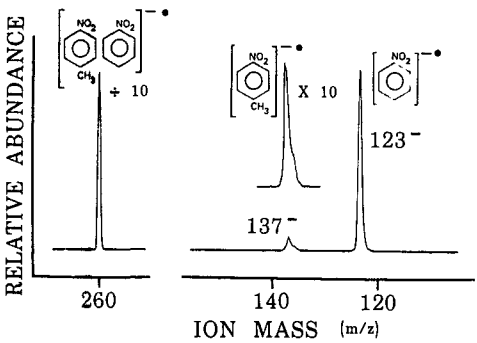

Figure 1

$[(C_6H_5NO_2)(CH_3C_6H_4NO_2)]^{-\cdot}$ at m/z 260. The two competing decomposition reactions correspond to the elimination of one or the other neutral molecule from the complex. From the ratio of the ion abundances we infer that nitrobenzene has a greater electron affinity than p-nitrotoluene. This observation is confirmed by the literature value, reported as a difference of 1.4 kcal/mole [3].

The results of the unimolecular and collision-induced fragmentations for a series of substituted nitrobenzenes are plotted in Fig. 2 and 3, respec-

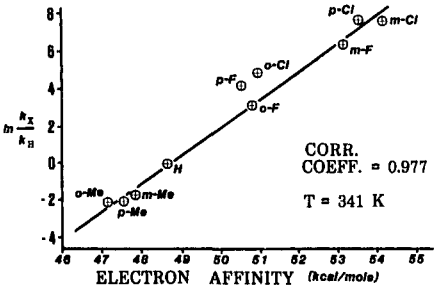

Figure 2

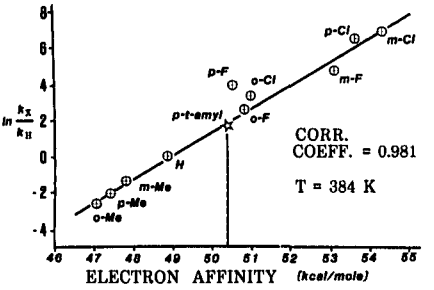

Figure 3

tively. The ratio of the substituted compound ($C_6H_5NO_2$ = H) $(M_X]^{-\cdot}/[M_H]^{-\cdot}$ yields a value $\ln(k_X/k_H)$ for each reaction pair. Compounds with relatively large electron affinity differences cannot be compared directly in a single experiment, because large differences in ion abundances cannot be measured accurately. Consequently, the plot is constructed in a stepwise fashion, as is true for equilibrium methods. A plot of the $\ln(k_X/k_H)$ values vs. the electron affinity of each of the substituted nitrobenzenes gives a straight line with a correlation coefficient of 0.98. The average effective temperature of the dissociating dimer ions is 341 K for those unimolecularly dissociating and 384 K for the collision-induced dissociations, as calculated from the slope of the line ($1/kT$). The higher temperature of the dimer ions that undergo CID is consistent with the fact that the internal energy of the reactant ion is increased upon collision.

The electron affinity of p-*t*-amyl nitrobenzene was determined using the data in Fig. 3 and serves as an illustrative case for the determination of an unknown electron affinity. In the CID/MIKES experiment the ratio of the peak height of the negative ion of p-*t*-amyl nitrobenzene to that of nitrobenzene was 7.23. Therefore, the electron affinity is assigned the value of 50 ± 4 kcal/mole (95% confidence interval), which is consistent with the size and structure of the substituent.

This study indicates that abundant radical negative ion dimers can be formed in a high-pressure ion source of a mass spectrometer, and the dissociations of these mixed negative ion complexes are useful for the determination of the relative gas-phase electron affinities of the monomer components. Previously, this information had been available only by more complex methods. The technique, which appears to yield results of comparable precision to other methods [4], uses an approximate kinetic approach for the determination of a gas-phase thermochemical quantity.

References

1. Burinsky, D. J., Fukuda E. K., and Campana, J. E., J. Am. Chem. Soc. in press.
2. Cooks, R. G., Kruger, T. L., J. Am. Chem. Soc. 99 (1981) 1279-1281; McLuckey, S.A., Cameron, D., Cooks, R. G., J. Am. Chem. Soc., 103 (1981) 1313-1317.
3. Fukuda, E. K., McIver, R. T. Jr., J. Phys. Chem., 87 (1983) 2993-2995.
4. Janousek, B. K., Brauman, J. I., "Gas Phase Ion Chemistry," Bowers, M. T., Ed.; Academic Press: New York, 1979, Ch. 10.

EXPERIMENTAL AND THEORETICAL STUDIES OF PREDISSOCIATION PROCESSES IN DOUBLY-CHARGED DIATOMICS.

J. M. Curtis[a], R. W. Wetmore[a], R. J. Le Roy[b] and R. K. Boyd[a], Guelph-Waterloo Centre for Graduate Work in Chemistry, Ontario, Canada

a University of Guelph, Guelph, Ontario.
b University of Waterloo, Waterloo, Ontario.

A program has been initiated to investigate diatomic di-cations XY^{2+}, for which little information is available. The present experimental approach measures kinetic energy release values T for XY^{2+} dissociating on the microsecond timescale. Existing experimental information include appearance energies, Auger spectra and double-charge-transfer spectra. In order to correlate all of this information, ab initio calculations of potential curves for XY^{2+} species have been undertaken. For the lower states of each symmetry, the computed energies are believed to be accurate to within 0.1 eV but the upper states are appreciably less reliable. Many of these potential curves involve potential wells which support quasi-bound states. This feature arises from mixing of the essentially repulsive (coulombic) states, correlating with $X^+ + Y^+$, with bound diabatic states correlating with X^{2+} +Y. The energies and widths of the rotational-vibrational levels supported by these potential wells have been calculated quantitatively. The processes responsible for the slow (microsecond) dissociations are either such tunnelling predissociation processes, or electronic (curve-crossing) predissociations. Presently, this work on $CO^{2+}$is the most complete, (J. Chem. Phys. 80, 1150(1984) J. Phys. Chem. (in press)). Work on the species N_2^{2+}, O_2^{2+} and NO^{2+}, which are of aeronomic interest, is in progress, and some of the experimental results obtained are shown below. Theoretical treatments of N_2^{2+} are considerably more difficult than those for the isoelectronic species CO^{2+}, since the density of states is much higher. In turn, this is due partly to gerade/ungerade doubling, but also to the density of states in atomic N^+.

Another system of this type, which has been of some interest, is CH^{2+} which has been observed (Ast et al., Chem. Phys. Lett. 78, 439 (1981)) as a product of charge-stripping of CH^+. Previous theoretical treatments (Pople et al., Chem. Phys. Lett. 88, 533 (1983)) concluded that all states of CH^{2+} are purely repulsive, but we (Chem. Phys., in press) have shown the existence of a small well in the ground state potential curve, which could account for the experimental observation.

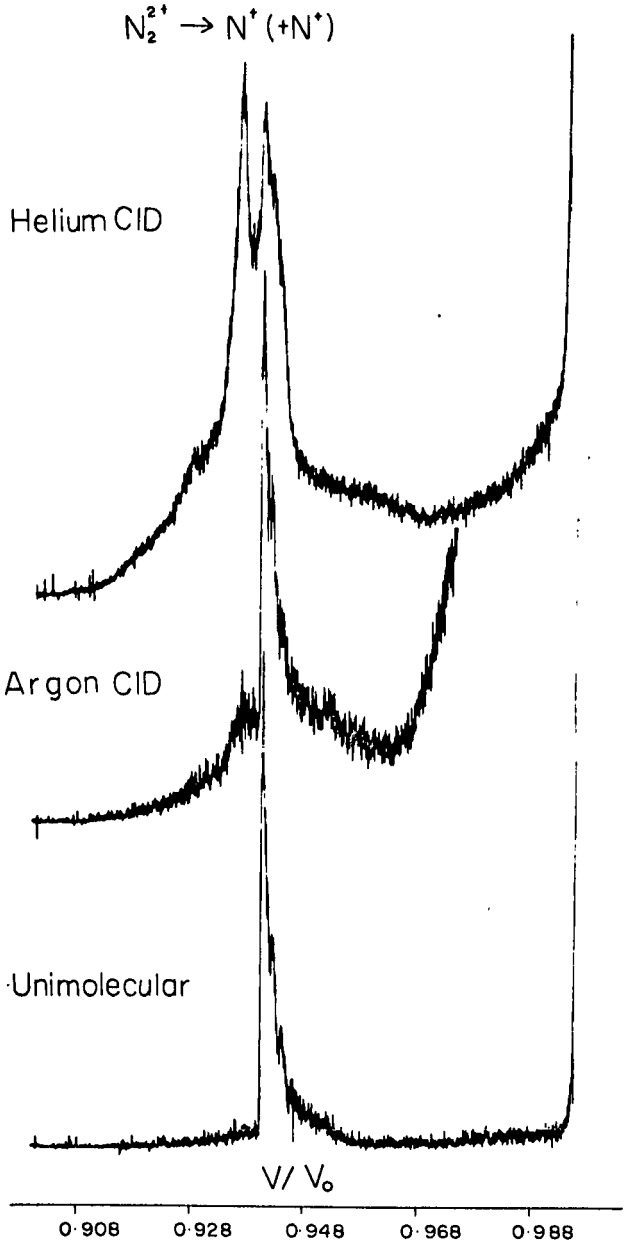
$N_2^{2+} \rightarrow N^+ (+N^+)$
Helium CID
Argon CID
Unimolecular
V/ V₀
0·908
0·928
0·948
0·968
0·988

AROMATIC HYDROCARBONS IN THE MURCHISON METEORITE

B. Basile, B. S. Middleditch and J. Oró
Department of Biochemical and Biophysical Sciences
University of Houston
Houston TX 77004

Early reports of the organic constituents of meteorites generated much controversy and were generally considered spurious. The fall of a meteorite in September, 1969 near Murchison, Australia afforded an opportunity to study the organic composition of a carbonaceous chondrite which had minimal terrestrial contamination. Extraterrestrial origin for the amino acids in the Murchison meteorite is suggested by the presence of almost equal amounts of D and L enantiomers as well as by the presence of several nonportein alpha-dialkyl amino acids which cannot racemize (Cronin and Pizzarella, 1983). It is now generally accepted that the compounds identified in the Murchison meteorite are indigenous.

Preliminary reports indicated that the extractable organic material from the Murchison meteorite contained alkyl-substituted dicyclic and tricyclic aromatic compounds as well as naphthalene and phenanthrene or anthracene (Oro et al., 1971). These results were confirmed by the identification of fourteen polynuclear aromatic hydrocarbons by gas chromatography-mass spectrometry (Pering and Ponnamperuma, 1971). Other investigators have used direct probe analysis with a time-of-flight mass spectrometer (Studier et al., 1972) or vaporization-pyrolysis gas chromatography to identify the volatile compounds in the meteorite (Levy et al., 1973).

We have analyzed benzene/methanol extracts of the Murchison meteorite using fused silica capillary column gas chromatography-mass spectrometry. The data obtained from these analyses have been compared to data obtained from the high temperature treatment of simple organic compounds, and a temperature for the formation of polycyclic aromatic hydrocarbons in the meteorite has been estimated.

It has also been reported that the pretreatment of a meteorite with hydrogen fluoride doubles the amount of meteoritic carbon extracted by releasing carbon from the sites where it is trapped by minerals (Becker and Epstein, 1983). A reconstructed total ion chromatogram of the extractable organic compounds released by hydrogen fluoride treatment was obtained and compared to the profile obtained from the meteorite which had not been treated with hydrogen fluoride.

Five grams of the meteorite (from which the outer crust had been removed) was sieved to an uniform mesh size and soxhlet extracted with benzene/methanol (3/1). Cupper was added to the extraction to remove elemental sulfur. Procedural blanks did not indicate any hydrocarbon contamination from the analytical procedures or reagents employed. Samples and blanks were analyzed with a Finnigan 1020/OWA instrument equipped with a 25 m x 0.25 mm i.d. DB-5 bonded-phase fused silica column. A second 5 g sample of the meteorite was heated with 5% HF for 18 h at 70°C. The sample was extracted as described above and chromatographed with a 45 m x 0.25 mm i.d. DB-5 bonded-phase fused silica column. The column was installed in a Finnigan 1020/OWA.

More than thirty polycyclic hydrocarbons were detected in the solvent extract of the meteorite which had not been acid-treated, including those previously identified by other investigators. Compounds identified included phenanthrene, anthracene, fluoranthene, pyrene, benzofluoranthene, dimethylpyrene, benzanthracene, benzophenanthrene, chrysene, fluoren-9-one, dibenzothiophene, 9(10H)-anthracenone, 9H-carbazole, and benzonaphthothiophene. Structural isomers of several alkylated aromatic hydrocarbons, including methylpyrenes and methylphenanthrenes were chromatographically separated, thus allowing calculations of the amounts of alkyl substituted compounds in the solvent extracts. The ratio of odd-carbon number to even-carbon number aromatic hydrocarbons was found to be approximately 0.1. Based on these data and literature data from model pyrolysis experiments (Oro and Han, 1966; Oro et al., 1967), a temperature of 1000°C is suggested for the formation of polycyclic aromatic compounds in the solar nebula or premeteoritic body. 1000°C is within the range of temperatures

for the condensation of the nebular material from the initial high temperature phases at which chondrules were formed to the lower temperature phases at which chemical and isotopic equilibria were frozen.

Among the aromatic hydrocarbons identified in the meteorite, heterocyclic compounds containing nitrogen, oxygen or sulfur were also identified. The amount of nitrogen-containing heterocyclic compounds is about one order of magnitude lower than the amount of aromatic compounds. This is in agreement with the relative ratios of the elemental abundance of carbon and nitrogen in Cl chondrites. It was not possible to calculate analogous ratios for sulfur- and oxygen-containing heterocyclics due to the presence of elemental sulfur and water in the meteorite.

Previous reports on the distribution of polycyclic aromatic hydrocarbons in the Murchison meteorite had demonstrated the presence of large amounts of lower molecular weight compounds, such as naphthalene, biphenyl, methylnaphthalene, and acenaphthalene. We did not detect these compounds in the solvent extracts of the untreated meteorite; however, we did identify these compounds in the solvent extracts of the hydrogen fluoride treated meteorite. In addition to the low molecular weight compounds released from the mineral matrix, other compounds such as chlorinated hydrocarbons and normal and branched alkanes were identified in the solvent extracts of the treated meteorite. The amount hydrocarbons appeared to increase by an order of magnitude after acid treatment.

REFERENCES

Becker, R. H. and S. Epstein. Geochim. Cosmochim. Acta 46, 97(1983).

Cronin, J. R. and S. Pizzarello. Adv. Space Res. 3, 5(1983).

Levy, R. L., M. A. Grayson, and C. J. Wolf. Geochim. Cosmochim. Acta 37, 467(1973).

Oro, J., J. Gibert, H. Lichtenstein, S. Wickström, and D. A. Flory. Nature 230, 105(1971).

Oro, J. and J. Han. Science 153, 1393(1966).

Oro, J., J. Han, and A. Zlatkis. Anal. Chem. 39, 27(1967).

Pering, K. and C. Ponnamperuma. Science 173, 237(1971).

Studier, M. H., R. Hayatsu, and E. Anders. Geochim. Cosmochim. Acta 36, 189(1972).

A COMPILATION OF ANION THERMOCHEMISTRY; John E. Bartmess, Department of Chemistry, Indiana University, Bloomington IN 47405

An update to the Rosenstock "Gaseous Ion Energetics" compliation is now nearing completion. Entitled "Gas Phase Ion Thermochemistry", it is intended for publication in early 1985 as a supplement to *J. Phys. Chem. Ref. Data* with Sharon Lias, J.L. Holmes, F. Lossing, J. Liebman, and R.D. Levin involved in the cationic part. That will include data from both mass spectral appearance and ionization potentials, and from ion/molecule reactions.

The anionic data involves (ideally) both ΔH^{o}_{f} and electron affinities for over 600 anions, plus ΔH^{o}_{acid} for the conjugate acid. These are compiled in a computerized data base, which will be maintained after the original publication. Current problems are: (1) anchoring the acidity scale. This may be off by 2 kcal/mole, since HF is a principal anchor point due to its well known absolute acidity, but it is very poorly tied to the relative acidity scale. (2) There are numerous compounds with known acidities but no ΔH^{o}_{f} for the acid, preventing calculation of ΔH^{o}_{f} for the anion. (3) Similarly, there are classes of acids where neither $DH^{o}(A\text{-}H)$ nor $EA(A\cdot)$ is know (oximes, imines, NH in amides, nitroalkanes, sulfoxides, sulfones, β-diketo compounds) and knowledge of either would give us the other.

MO calculations are not included in this data base; while considerable improvements have occur recently, the time is not yet here to treat then equally with the experimental data. It is hoped that this compilation will provide the data base for further improvements in the calculations.

Until publication time, preprints are available either as hardcopy (specify), or as dBase II or .TXT files on a requestor-supplied 5-1/4" formated floppy for IBM PC or a number of DD CP/M systems (send two floppies for the latter). Address after 1 August 1984: Department of Chemistry, University of Tennessee, Knoxville TN 37996

PHOTODISSOCIATION OF SMALL PEPTIDE IONS

William D. Bowers, Sherri-Sue Delbert and Robert T. McIver, Jr.*

Department of Chemistry
University of California
Irvine, California 92717

Quadrupole and sector mass spectrometers are not well suited for experiments involving pulsed lasers because they scan a spectrum slowly. Low detection efficiency results because the laser pulse lasts typically for less than a microsecond. Fourier transform mass spectrometry (FT-MS) appears to be the method of choice for many laser applications because ions can be stored in the analyzer cell and a complete mass spectrum can be obtained for each pulse of the laser [1,2].

We have constructed a FT-MS instrument at the University of California, Irvine, and have used it to study the photodissociation of small peptide ions in the gas phase. A block diagram of the instrument is shown in Fig. 1. A NOVA 3 computer provides pulses for firing the laser and the Fourier transform detection electronics. Ion image current signals from the preamplifier are digitized and stored in a fast buffer memory [3]. At the end of the detection cycle, the signals are transfered to the NOVA computer where the fast Fourier transform is calculated to yield a mass spectrum. For these experiments we used a Lambda-Physik UV excimer laser.

Our first experiments have been with di- and tripeptides. Protonated parent ions of the peptides were produced by low pressure chemical ionization [4]. Even with vapor pressures as low as 5×10^{-9} Torr, abundant MH^+ ions of the peptides could be generated using dimethylamine as a reagent gas.

$$(CH_3)_2NH_2^+ + M = MH^+ + (CH_3)_2NH$$

Dimethylamine is a good reagent gas for the peptides because it has such a high proton affinity that only a slight amount of fragmentation is observed [5].

As the protonated peptide ions form over a period of about 3 s, they are stored in the analyzer cell of the FT-MS instrument. Initially only the MH^+ ions are observed, but when the laser light is focused at the center of the analyzer cell, fragment ions are produced,

even with pulse energies as low as 20 mJ. We believe this corresponds to a one-photon process, as in the reaction

$$MH^+ + h\nu \longrightarrow \text{fragment ions}$$

The extent of fragmentation depends on the wavelength of the light and roughly parallels the one-photon, solution UV absorption spectra of the peptides. For example, protonated leucylalanine photodissociates at 193 nm and to a small extent at 249 nm. But photofragment ions were not observed at 350 nm. With most of the peptides investigated thus far, fragmentation occurs preferentially at the C-C bond alpha to the carbonyl. These results will be presented in a separate publication.

References:

[1] Irion, M.P.; Bowers, W.D.; Hunter, R.L.; Rowland, F.S.; McIver, Jr., R.T. Chem. Phys. Lett. 1982, 93, 375.

[2] Carlin, T.J.; Freiser, B.S. Anal. Chem. 1983, 55, 955.

[3] Bowers, W.D.; Hunter, R.L.; McIver, Jr., R.T. Ind. Res. and Dev. 1983, 25, No. 11, 124.

[4] Hunter, R.L.; McIver, Jr., R.T. Anal. Chem. 1979, 51, 699.

[5] Locke, M.J.; McIver, Jr., R.T. J. Am. Chem. Soc. 1983, 105,4226.

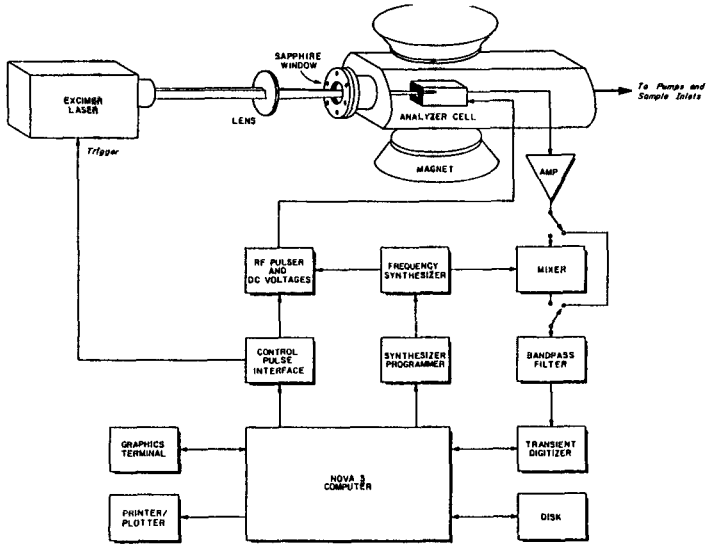

Figure 1. Block diagram of Fourier transform mass spectrometer used for studying laser-induced fragmentation of ions.

FAB MASS SPECTROMETRY OF HUMAN FIBRINOGENS. D. Heller and C. Fenselau: Middle Atlantic Mass Spectrometry Facility, Department of Pharmacology, Johns Hopkins University, Baltimore, MD 21205; R. Townsend and Y. C. Lee: Department of Biology, Johns Hopkins University, Baltimore, MD 21218

Total desialylation of most glycoproteins results in their removal from circulation within minutes by the liver. Asialo triantennary oligosaccharides are implicated as a major determinant of this clearance (i.e., exposure of galactose residues). Human fibrinogen, possessing only biantennary oligosaccharides, is cleared over hours, however. Since isolated fibrinogen is partially desialylated, it becomes important to characterize the sialylation pattern of isolated native fibrinogen, and eventually to determine the clearance rate of fibrinogen possessing a defined array of sialic acid residues.

Towards this end, a method of determining relative proportions of sialic acid-containing oligosaccharides by positive FAB mass spectrometry was investigated, with the goal to relate relative intensity of molecular ion peaks to the relative proportion of each species in a mixture.

Homogeneous asialo, monosialo and disialo glycopeptides were prepared. Their positive FAB spectra show no interferences caused by fragmentation. Stock solutions of each standard were prepared, and their concentrations were determined by carbohydrate analysis. Standard mixtures were prepared with 1:40 through 40:1 ratios of asialo:monosialo and monosialo:disialo glycopeptides. Standard curves were prepared with relative intensity ratios plotted vs. mole fraction ratios.

The ionization of these mixtures was studied in positive FAB mode. The matrix used was thioglycerol, with approximately 10 micrograms of carbohydrate dissolved in 1 microliter of thioglycerol on the probe tip. Molecular ion intensities were found to vary smoothly with time, and to compensate for this, multiple scans of peak profile data were averaged before centroiding and mass assignment. Presence of excess sodium was found to alter the results dramatically from expected values. Spectra which were dominated by MNa+ peaks were not used for quantitation. An average level of chemical background was estimated from an 8 amu region around the cluster and subtracted from each isotope peak if the background was significant.

The standard curves showed linearity, but the slopes were not unity. Rather, the presence of an extra sialic decreased the "relative intensity efficiency" by a factor of between 2 and 3 in each case.

An isolated mixture of glycopeptides was quantitated with the standard curves. Only monosialo and disialo glycopeptides were observed. The intensity values of the disialo species were multiplied by 2.6, the slope of the standard curve (the "relative ionization efficiency" of monosialo over diasialo).

The results indicated 53% disialo and 47% monosialo in the isolated mixture. This yielded a value for average sialic scid content (1.5 per molecule) in agreement with carbohydrate analysis and GC-MS data. Without correction, the FAB-determined value is 1.2 -- too low. Using this method, pure disialo glycopeptide was shown not to lose sialic acid on storage (over 8 months) if lyophilized and frozen. But disialo glycopeptide stored frozen in water solution showed an increase in monosialo content of from 4% to 10% over 6 months.

The results indicate that quantitation by FAB using homologous standards (biopolymers varying by one unit) can be successful if standard curves are prepared. A report of this work has been submitted for publication in Biochemistry.

HUMAN FIBRINOGEN GLYCOPEPTIDES

SIALIC ACID HETEROGENEITY

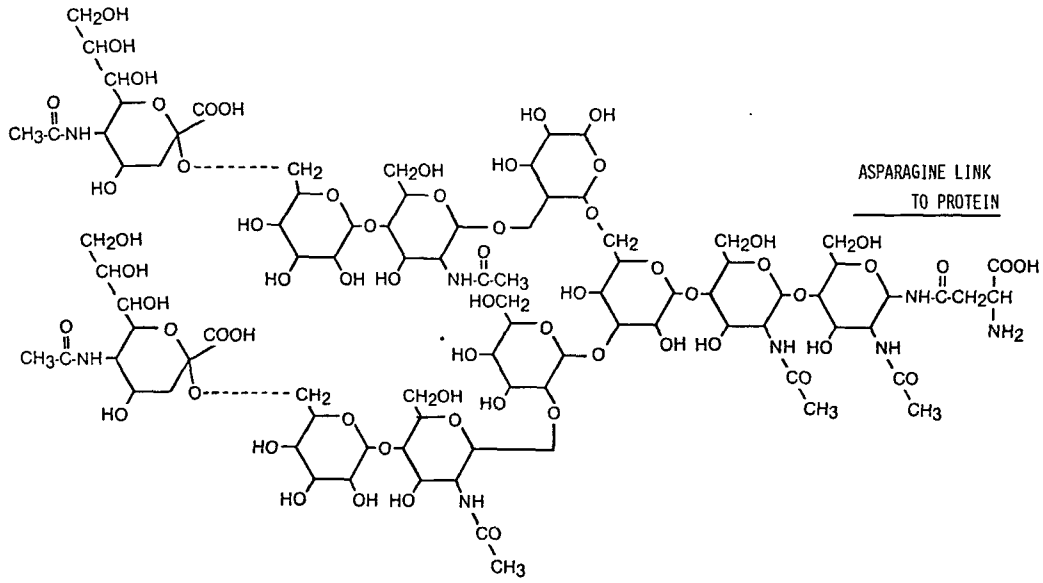

FAST ATOM BOMBARDMENT MASS SPECTROMETRIC CARBOHYDRATE ANALYSIS OF GLYCOPEPTIDE ANTIBIOTICS

G. Roberts, S. Rottschaefer, R. Sitrin and P. Jeffs

Smith Kline & French Laboratories, Philadelphia, PA 19101

A family of glycopeptide antibiotics, commonly referred to as the vancomycin group, are of interest because of their antibiotic activity, which involves interference with the biosynthesis of the bacterial cell wall. Structurally they are composed of a polypeptide aglycone consisting of uncommon amino acids and one or more carbohydrate moieties. Progress in the identification of the molecular structures varies among the different compounds. Extensive work has been conducted on some, such as vancomycin and ristocetin, and their structures are completely characterized. Other less well known members of the group have scarcely been studied at all and very little is known about their structures. Much of the structural work has involved the use of NMR on the intact molecule and physical, chromatographic and chemical techniques on hydrolysis products. Plasma desorption mass spectrometry has proven invaluable in providing molecular weight information on some - usually to within $\pm$ 2 amu - but little else. The molecules are relatively large (molecular weights of 1500-2100 amu) and nonvolatile which precludes studying them with traditional mass spectrometric ionization techniques. Even field desorption can present many difficulties due to the presence of interfering impurities, usually inorganic salts.

Fast Atom Bombardment Mass Spectrometry (FABMS), as might be expected, produces excellent spectra of these glycopeptides. The nominal mass can easily be ascertained from the MH^+ cluster. Though less intense than the pseudomolecular ion, significant peaks resulting from fragmentation of the molecule are quite evident and can provide important structural information, especially with regard to the carbohydrate content.

Seven glycopeptide antibiotics (Table 1) have been examined in our laboratory by FABMS. Six of these seven glycopeptide antibiotics are either fully characterized, or nearly so (1, 2). OA-7653 is the exception. By chemical and physical techniques nine different carbohydrates have been shown to be present (1, 2). In all of the glycopeptides, the carbohydrate units are attached glycosidicly to an oxygen atom that is either benzylic, phenolic or in a non-glycosidic position of another carbohydrate (1). Most of the prominent peaks at the higher mass end of the spectrum are a result of cleaving these glycosidic bonds. Table 1 shows a comparison between the carbohydrates known to the present and those indicated by the FABMS fragmentation data.

The limitations are evident in the use of the technique: 1) It cannot distinguish between isomeric carbohydrate units; and 2) The determination of the carbohydrate unit's position in the molecule is unlikely because the different types of bonds (benzylic, phenolic or carbohydrate-carbohydrate) appear to cleave with essentially equal facility.

Overall, though, FABMS does offer a routine and rapid technique for indicating, substantiating and/or varifying some or all of the carbohydrate units contained in the glycopeptide molecule. The usual mass spectrometry capability of being able to obtain a relatively large amount of information on a minimum amount of sample applies and is, needless to say, an important advantage.

The work was conducted in the FAB mode of operation on a VG ZAB 1F-HF mass spectrometer equipped with a standard FAB ion source. The solid sample was mixed on the stainless steel probe in a thioglycerol-trifluoroacetic acid matrix and examined at R. T. The accelerating voltage was 8kV and 8keV xenon atoms at a discharge current of 1 mA were used to bombard the sample.

Table 1. Glycopeptides Studied

Antibiotic	Carbohydrates Present	Carbohydrates Indicated by FABMS
vancomycin	glucose vancosamine	glucose vancosamine
ristocetin A	glucose mannose rhamnose arabinose ristosamine	glucose and/or mannose rhamnose arabinose
actinoidin A	glucose mannose actinosamine acosamine	glucose and/or mannose actinosamine acosamine
actinoidin B	glucose mannose actinosamine acosamine	glucose and/or mannose actinosamine acosamine
avoparcin	glucose mannose rhamnose ristosamine	glucose and/or mannose rhamnose ristosamine
A-35512-B	glucose mannose fucose rhamnose vancosamine	glucose and/or mannose fucose and/or rhamnose
OA-7653	glucose	glucose

1. D. H. Williams, V. Rajananda, M. P. Williamson and G. Bojesen, Topics in Antibiotic Chem. 5, 119 (1980).
2. A. H. Hunt, J. Am. Chem. Soc. 105, 4463 (1983).

GC/MS CHARACTERIZATION OF DIKETOPIPERAZINES FORMED BY THE ACTION OF DIMETHYLHYDRAZINE ON PEPTIDES

B.D. Bennett, R.A. Day and K. Jayasimulu

Department Of Chemistry
University Of Cincinnati
Cincinnati, Ohio 45221

Exhaustive treatment of peptides with hydrazine is the basis of the Akabori C-terminus identification. Treatment under milder conditions has been shown to yield smaller peptide hydrazides. Treatment of simple peptides with unsym-dimethylhydrazine (DMH) gives relatively high yields of (DKP's). The DKP's, which retain sequence information, were characterized as their trimethylsilylated derivatives

Formation of diketopiperazines from peptides appears to occur by a cyclization process at the N-terminus.

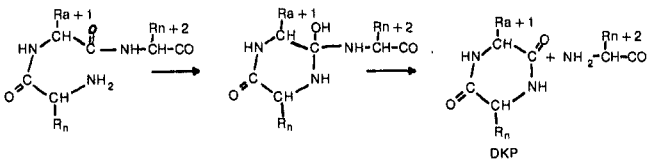

This mechanism is consistent with the following observations:
Partial hydrazinolysis of large peptides yields dipeptide hydrazides arising from interior and C-terminal regions. These hydrazides are stable and apparently do not cyclize to form DKP's. Small peptides give rise to DKP's The hydrazides appear to be more thermodynamically stable than the corresponding amides when the Akabori hydrazinolysis procedure is employed

Trimethylsilylation of DKP's is afforded by the method of Krutsch and Pisano (1978) with minor variations.
For characterization of DKP's, 0.25 mg of various standards were transferred to a Pyrex tube and dried under vacuum at 80° C for 20 minutes. BSTFA and acetonitrile (250 ul each) were added and the Pyrex tube was cooled in dry ice and promptly sealed under vacuum. Reaction conditions can vary, but heating the sample in a glycerol bath at 80° C for 3 hours is adequate for solvation and silylation. For GC/MS analysis the seal is broken and 0.25 to 1.0 ul injected

A 30 meter J&W DB-5 bonded phase capillary column with 0.32 mm I.D. and 0.25 micron film thickness was utilized to separate the trimethylsilylated DKP's generated from DKP standards. Figure 1 shows a typical GC/MS run.

GC CONDITIONS.
Carlo Erba on-column injection
J&W DB-5 30W 0 25 micron film thickness
Flow: 25 cm/sec He at 260° C
Make-up: 15 ml/min
Inject: 30° C
Oven: 30-120° C at 32°/min 120-260° C at 6°/min
Interface Jet separator at 270° C

Figure 1 DS-55 CROSS SCAN REPORT, RUN STD2D
1UL STD2D 30-120 32/MIN 120-260 6/MIN 30M DB-5

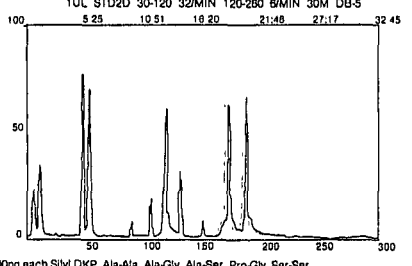

500ng each Silyl DKP Ala-Ala, Ala-Gly, Ala-Ser, Pro-Gly, Ser-Ser, Pro-Pro, Phe-Ser, Gly-Tyr

Trimethylsilylation of dipeptides generated by diaminopeptidases has been studied by Krutsch and Pisano (1978). They reported trimethylsilylation occurs with active protons of the following functional groups: amino, carboxyl, hydroxyl, imidazoyl NH, indole NH, primary amide, and guanidino. They reported that the ring amides of DKP's were also reactive.

The following DKP's were treated with BSTFA and analyzed by GC/MS in this laboratory: Lys-Lys, Phe-Tyr, Ser-Ser, Phe-Ser, Ala-Tyr, Gly-Tyr, Gly-His, Met-Met, Ala-Ser, Phe-Ala, Ala-Ala, Ala-Gly, Pro-Gly, and Pro-Pro DKP. Our results are consistent with what would be predicted from Krutsch and Pisano's trimethylsilylation products.

Trimethylsilylated DKP's were confirmed with exact mass data for molecular and fragment ions.

Confirmaton of each trimethylsilated DKP is easily afforded with molecular ions, the characteristic M-15 of silyl derivatives, and unique fragment ions. Side chain cleavage yields a fragment containing the DKP ring and the complementary amino acid side chain

Table 1 gives a listing of diagnostic ions for silyated DKP standards.

Table 1

Silyl DKP (R_1,R_2)	M +	[M-R_2] +	[M-R_1] +	[R_1] +	[R_2] +
KK	688	472	472	a	a
FY	526	347	435	91	179
SS	462	359	359	103	103
FS	450	347	359	91	103
AY	450	271	435	-	179
GY	436	257	435	-	179
GH	410	257	-	-	153
MM	406	331	331	75	75
AS	374	271	359	-	103
FA	362	347	271	91	-
AA	286	271	271	-	-
AG	272	271	257	-	-
PG	226	-	-	-	-
PP	194	-	-	-	-

a $+CH_2N(Silyl)2$

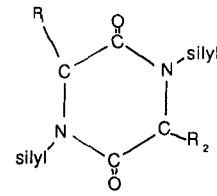

MS Conditions Kratos MS-80 with DS-55 and Preprocessor

Source 200° C
Resolution: 3000
Scan rate 3 sec/dec
Electron energy. 20 eV
Beam current: 50uA

Accelerating voltage. 2667 KV
Bandwidth: 10000 Hz
Sampling period: 30us
Interscan delay 1 sec

Conclusion

We have shown that GC/MS is a viable method of identifiying DKP's generated from partial hydrazinolysis of peptides. Partial hydrazinolysis of small peptides results in DKP formation while larger polypeptides give rise to peptide hydrazides (Day et al ,1984 these proceedings) Small peptide hydrazides and DKP's can be analyzed by GC/MS as their trimethylsilyl derivatives.

H.C. Krutsch and J.J. Pisano, METHODS ENZYMOL. XLVII 391 (1978).

Partial Hydrazinolysis of Peptides and GC/MS and FAB/MS Analysis

R.A. Day, J. Koka, B.D. Bennett, G. Kelso and L. Weber
Department of Chemistry
University of Cincinnati
Cincinnati, Ohio 45221

Mass spectrometric approaches to sequencing naturally occurring peptides has been attended with considerable success. However, determination of entire sequences of proteins has failed to offer significant competition for the Edman degradation based strategies which have afforded the sequence assignments until recently. The advent of dependable recombinant DNA techniques coupled with facile DNA sequencing methods has added a powerful method for protein sequence assignment from the DNA sequence. While this method is rapid once a tract of DNA corresponding to the structural gene has been isolated and amplified, there are inherent problems which can lead to mistaken protein sequence assignments. A GCMS strategy to correct or minimize these errors was described by Biemann et al. (1981). Other strategies were subsequently announced whereby a limited amount of molecular ion measurements could provide corroboration and/or corrective information (Biemann, 1982; Matsuo et al. 1983).

We had shown that partial hydrazinolysis may be readily exploited for generation of molecular weight data and/or of partial sequence information (Day, 1983). Here we report that FABMS analysis of the partial hydrazinolysis reaction products gives such information. GCMS analysis of the resultant silylated peptide hydrazides (PH2) and diketopiperazines (Bennett et al., 1984 these proceedings) provided sequence information after a two step procedure. The first step uses unsym-dimethylhydrazine (75% aqueous, heated 110-140°); the second uses the method of Krutsch and Pisano for silylation. Silylation of the cis-amide bonds of the DKPs occur, while the trans-amide bonds of the peptide are not silylated.

1) Peptide + NH_2NMe_2 ⟶

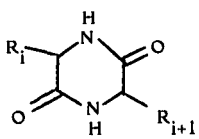

DKP

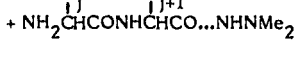

PHZ

2a) DKP $\xrightarrow{BSTFA}$ DKP $(Silyl)_2$

2b) PHZ $\xrightarrow{BSTFA}$ Silyl $NHCH(R_j)CONHC(R_{j+1})$ ...$NHNMe_2$

Partial hydrazinolysis of small peptides gives predominantly DKPs while larger polypeptides give PHZs. It would appear that an N-terminal mechanism analogous to an exo-peptidase could account for the preponderance of DKPs in small peptides. For example, the gastrin peptide, WMDF amide gave as the only products WM and DF. The major components identified from dimethylhydrazinolysis of CM-lysozyme and glucagon were predominantly PHZs.

GCMS of the silylated PHZs was applicable to smaller peptide products. FABMS of the PHZs gave access to the higher molecular weight range. CM-Lysozyme PHZs gave spectra from a single dimethyl hydrazinolysis product corresponded to MH^+ data for peptides representing approximately half of the lysozyme sequence. A partial listing is shown in Table I.

Table I: FABMS Data From Partial Dimethylhydrazinolysis of CM-Lysozyme.‡ Partial Listing of m/z values Corresponding to Peptide Dimethylhydrazide MH^+ of a Given Run. Although not shown, all C-terminal carboxyls are present as $-CONHNMe_2$.

m/z	Possible Assignment
401	LYS^{97}-ILE-VAL
402	VAL^{120}-GLN-ALA
403	ARG^{61}-TRP; THR^{69}-PRO-GLY-SER; TRP^{111}-ARG
404	ASN^{27}-TRP; THR^{40}-GLN-ALA; GLN^{40}-ALA-THR; SER^{91}-VAL-ASN
418	ILE^{58}-ASN-SER
428	ASN^{77}-ILE-PRO
430	LYS^{96}-LYS-ILE
431	ALA^{122}-TRP-ILE
450*	ASN^{93}-CYS-ALA
452	SER^{36}-ASN-PHE
458	ILE^{55}-LEU-GLN; LEU^{56}-GLN-ILE; PRO^{70}-GLY-SER-ARG
472	GLN^{67}-ARG-THR-PRO; ARG^{68}-THR-PRO-GLY
483	HIS^{15}-GLY-LEU-ASP
487	ARG^{73}-ASN-LEU
490	ASN^{39}-THR-GLN; SER^{60}-THR-PRO-GLY
496	ASP^{18}-ASN-TYR
506*	ARG^{114}-CYS-LYS
546	ALA^{42}-THR-ASN-ARG; ASN^{65}-ASP-GLY-ARG
547	ALA^{11}-MET-LYS-ARG; THR^{118}-ASP-VAL-GLN
570	GLY^{102}-ASP-GLY-MET-ASN
587	ASP^{66}-GLY-ARG-THR-PRO
600	TYR^{20}-ARG-GLY-TYR; ALA^{95}-LYS-LYS-ILE-VAL
660	LYS^{97}-ILE-VAL-SER-ARG-GLY

‡ CM = Carboxymethylated

* CYS = Carboxymethyl Cysteine

The data have two immediate uses. First, this procedurally simple procedure affords a data set which may be used to compare with sequence assignments derived from DNA sequencing of structural genes. Second, comparison of pattens from closely homologous proteins afford a means of identifying the non-identical sequence regions. We are currently comparing the serum protein orosomucoid across several species; it is anticipated that a high degree of homology among say the primates will lead to only a few differences in the GCMS patterns and among the MH^+ from FABMS. Identification of these differences combined with the homology of known sequences will aid in the complete sequence assignment.

ACKNOWLEDGEMENT. We thank T. Keough for running the FABMS on the VG-ZAB instrument at MVL.

REFERENCES

K. Biemann, Proc. Seventh Am. Peptide Symp. p. 765 (1981).

K. Biemann, Int. J. Mass Spectrom. Ion Phys. 45 183 (1982).

R.A. Day, C.J. Metral, K. Jayasimhulu, A. Kornel, and D. Vyas THESE PROCEEDINGS, p. 148 (1983).

H.C. Krutsch and J.J. Pisano, Methods Enzymol. XLVII 391 (1978).

T. Matsuo, I. Katakuse and H. Matsuba; THESE PROCEEDINGS (1983), p. 638.

STRUCTURE DETERMINATION OF A NEW CYCLODEPSIPEPTIDE ANTIBIOTIC FROM FUSARIA FUNGI.

S.A. Carr, C.E. Costello and E. Block, Dept. of Chemistry, MIT, Cambridge, MA 02139, and, R.F. Vesonder and H.R. Burmeister, Northern Regional Research Center, USDA, Peoria, IL 61604

Fusaria are plant-infecting fungi that produce a variety of toxins and antibiotics with diverse molecular structures. This report describes the total structure elucidation of a new cyclodepsipeptide (a) isolated from corn media inoculated with Fusarium roseum. This antifungal, antibiotic peptide swells Penicillium digitatum cells to ten times their normal diameter and inhibits germination possibly by disrupting normal membrane permeability.

Mass spectrometric, chemical and chromatographic methods contributed to the elucidation of the structure (a). A nominal molecular weight of 887 was determined by FD and NH_3-DCI, and an elemental composition of $C_{45}H_{73}N_7O_{11}$ was established by high resolution FABMS, (measured MH^+ m/z 888.5459, calculated m/z 888.5446, diff. 1.3 mmu). Data from combustion analysis were consistent with these results. Amino acid analysis indicated the presence of one mole each of Thr, Glx, Leu, Tyr and two moles of Ala. A small amount of Ile is also present and most likely substitutes for Leu in the structure since only a single molecular entity was observed by MS. The types and number of available functional groups in the intact molecule were determined by MS and NMR of selected derivatives. For example, acetylation incremented the apparent M_r by 84u, while NMR of this derivative indicated that the reactive sites correspond to secondary (Thr) and phenolic (Tyr) hydroxyl groups. These data, and the lack of reaction with ninhydrin, confirm that the NH_2-terminus is blocked. Treatment of the peptide with MeOH/HCl under conditions which esterify carboxylates failed to shift the apparent Mr of the peptide, indicating that the COOH-terminus is also blocked (or cyclic with the NH_2-terminus) and that Glx=Gln.

Total acid hydrolysis of the peptide released ether soluble components which were identified by GCMS following trimethylsilylation or diazomethylation as 4-methyl,3-hydroxypentadecanoic acid and its corresponding dehydration product 4-methyl,2-pentadecenoic acid. Liberation of a hydroxyl group upon hydrolysis also supports the conclusion that this group is ester-linked to the COOH-terminus of the peptide.

The sequence of amino acids and the linkage of the hydroxy fatty acid to the peptide were unambiguously established using the GC/MS protein sequencing methodology developed by Biemann and coworkers (1). Numerous overlapping peptides were identified in a single GC/MS experiment on a derivatized partial acid hydrolyzate (Scheme 1). Derivatives of $C_{12}H_{25}CH(OH)CH_2CONH$-Thr and Tyr-Leu-O-$CH(C_{12}H_{25})CO_2H$ were also identified in the GC/MS data, indicating that the peptide is cyclic through the blocking group which is linked via an ester bond to the COOH-terminus and via an amide bond to the NH_2-terminus. These assignments were corroborated by the abundant sequence-related ions in the FAB mass spectra of the partially hydrolyzed peptide. Two series of ions dominate the spectra (Fig. 1) which correspond formally to the protonated molecular ions of released peptides with either a free carboxyl terminus or with the blocking group attached to the COOH-terminus (underlined masses).

The absolute configurations of the amino acids were determined by gas chromatography of the n-pentafluoropropionyl, n-propyl ester derivatives on a chiral phase capillary column (2). One mole each of d-Ala, l-Ala, l-Gln (observed as l-Glu), d-Tyr, l-Leu and a small amount of l-Ile. Surprisingly, no peak was observed at the expected elution position of d- or l-Thr. However, an unknown, later eluting peak had a mass spectrum indistinguishable from that of Thr. The unknown was subsequently identified as d-allo-Thr by comparison with the retention behavior of standards. The remaining question of the relative sequence positions of the d- and l-Ala residues was answered by comparing the relative concentrations of free amino acids present in a partial acid hydrolyzate of the peptide before and after treatment of the hydrolyzate with Carboxypeptidase A. This enzyme will release l-amino acids from the COOH-termini of tri- or larger peptides. Only the peak heights of l-Leu and l-Glu increased relative to the other amino acids; since the hydrolyzate was known to contain Thr-Ala-Ala (Scheme I), the lack of an increase in the l-Ala peak indicates that the probable sequence order is -l-Ala-d-Ala-.

Synergistic application of a variety of MS, chemical and chromatographic methods has enabled total structure elucidation of a new, novel cyclodepsipeptide. The combined use of these complementary techniques constitutes a highly efficient and unambiguous approach for determining the structure of unusual peptides.

1. Carr, S.A., Herlihy, W.H. and Biemann, K.; Biomed. Mass Spectrom., 1981, 8, 51-61.
2. Frank, H., Woiwode, W., Nicholson, G. and Bayer; Liebigs Ann. Chem., 1981, 354-365.

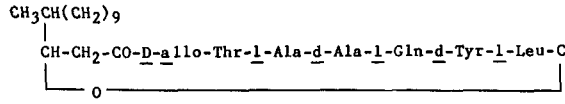

Structure A

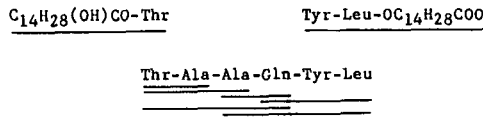

Scheme 1. Peptide sequences identified in a GC/MS experiment on a derivatized partial acid hydrolyzate of the isolate from Fusaria.

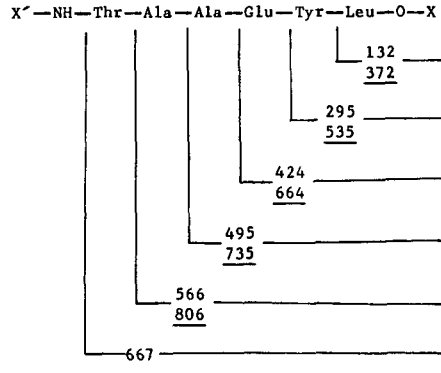

Scheme 2. Origin of the major fragments observed in the FAB mass spectrum of apartial acid hydrolysis of the isolate from Fusaria. Upper mass values correspond to $(M + H)^+$ for the indicated peptide where X = H and X′ = $C_{14}H_{28}(OH)CO$; underlined masses are for X = $C_{14}H_{28}COOH$ and X′ = H.

ALGORITHMS USEFUL FOR THE CONFIRMATION OR CORRECTION OF DNA-DERIVED AMINO ACID SEQUENCES OF PROTEINS

H.A. Scoble and K. Biemann
Dept. of Chemistry, M.I.T., Cambridge, MA 02139

Recent advances in DNA sequencing technology have led to rapid and efficient methodologies for the base sequencing of specific genes encoding large proteins. Since these strategies offer significant advantages as compared to conventional protein sequencing techniques, it is apparent that the establishment of protein structure from the corresponding DNA is the method of choice whenever possible.

The recent advent of refined DNA sequencing techniques has made it possible to sequence a large number genes. These methods require that a number of precautions be followed if an accurate gene sequence is to be determined. For example, to minimize the possibility of sequence errors, both strands are typically sequenced and the experiments performed in replicate. Nevertheless, even under these stringent conditions, errors are still possible and in many cases double-stranded information covering the entire gene is not available. While many investigators provide independent N- and C-terminal sequence information as confirmation of the correct gene sequence, it is well-advised to check the protein structure not only at the protein termini but also throughout the entire translated region.

Recent investigations in our laboratory have been directed toward the confirmation or correction of DNA-derived amino acid sequences of proteins. Briefly, a typical sequencing experiment involves: (1) enzymatic digestion of the protein under study, usually with trypsin, (2) partial fractionation of the resulting digest into groups of approximately 4-6 peptides using reversed-phase high performance liquid chromatography, (3) FABMS analysis of the liquid chromatographic fractions, and (4) comparison of the MH^+ ions experimentally determined with the MH^+ ions predicted based upon the proposed amino acid sequence.

Employing the above strategy one of four possible conditions can result. First, the experimentally determined ions may agree with the ions predicted based upon the proposed amino acid structure. Such a situation provides further evidence that the proposed protein sequence is correct. Second, a few of the experimentally determined ions may match the predicted peptides indicating the DNA may contain many errors or the sequenced DNA region may not code for the protein as expected. Third, most of the experimentally determined ions may agree with the predicted ions in one reading frame, while the remainder fit another reading frame, indicating possible insertion and/or deletion errors. Finally, a majority of the experimentally determined and predicted ions may agree, but others may not fit any reading frame. A result of this type can arise from a number of situations: (a) DNA insertion and/or deletion errors, (b) misidentification of one or more nucleotide bases which changes the codon for one or more amino acids in the proposed structure, (c) a premature stop codon which masks the true size of the protein, (d) posttranslational modification of the protein, (e) nonspecific cleavage of the protein during enzymatic digestion giving rise to unexpected peptides, (f) microheterogeneities in the protein, or (g) peptide impurities in the protein under study.

An integral part of the overall confirmation/correction strategy has been the development of computer algorithms to aid in the verification and correction of DNA-derived protein structures. These algorithms have been divided into three broad categories based upon the specific type of information yielded. Category one programs generate pertinent information concerning the protonated peptides expected after specific cleavage of the proposed amino acid sequence. Category two programs aid in the detection and correction of errors in the proposed DNA sequence as indicated by disagreement between the molecular weights of the peptides predicted from the enzymatic digest of the protein and those experimentally determined. These errors usually involve single base insertions and/or deletions or single base misidentifications. The category three program generates possible sequence ions to be expected from a peptide of known composition when analyzed under positive ion FAB conditions.

The development and application of computer algorithms has proved very beneficial in our laboratory for the identification of possible discrepancies in DNA-derived protein structures. The underlying premise of this strategy involves a comparison of the peptides expected from the proposed structure after specific cleavage with those experimentally determined by fast atom bombardment mass spectrometry. These techniques are particularly well suited for providing phase checks on the translated DNA sequence and therefore independently establish the proper reading frame of the DNA throughout its entire length. In addition, if unmatched peptides are not explained in terms of DNA sequence errors, the

possibility of posttranslational modifications to the protein structure can then be considered. These algorithms have recently led to the correction of a number of DNA-derived protein structures, including Gly-tRNA synthetase (1), Gln-tRNA synthetase (2,3) and Endoglycosidase H (4).

REFERENCES

1. Primary Structures of Both Subunits of Escherichia coli Glycyl-tRNA Synthetase, T.A. Webster, B.W. Gibson, T. Keng, K. Biemann and P. Schimmel, J. Biol. Chem. 258 10637-10641 (1983).

2. Sequencing of Proteins, K. Biemann, J. Mass Spec. Ion Phys., 45 183-194 (1982).

3. Strategy for the Mass Spectrometric Verification and Correction of the Primary Structures of Proteins Deduced from their DNA Sequences, B.W. Gibson and K. Biemann, Proc. Natl. Acad. Sci. USA (in press).

4. Primary Structure of the Streptomyces Enzyme Endoglycosidase H, P.W. Robbins, P.W. Trimble, D.F. Wirth, C. Hering, F. Maley, G. F. Maley, G.F. Das, B.W. Gibson, N.J. Royal and K. Biemann, J. Biol. Chem. (in press).

This work was supported by the National Institutes of Health (GM05472 and RRC00317).

FAST ATOM BOMBARDMENT MASS SPECTROMETRY OF THIOREDOXIN

W. Rodney Mathews and K. Biemann
Dept. of Chemistry, M.I.T., Cambridge, MA 02139

Thioredoxins are relatively small proteins (12K daltons) that are involved as cofactors in a variety of important oxidation-reduction reactions including ribonucleotide reduction, transformation of sulphur containing amino acids and regulation of photosynthesis. This ubiquitous protein has been isolated from a variety of procaryotic as well as several eucaryotic systems. The importance as well as the wide occurrence of these proteins makes them ideal tools for studying the evolutionary process by investigating their primary structures. Thioredoxins from several species have been isolated and are able to substitute for each other in in vitro thioredoxin assays, for example E. coli thioredoxin serves as an efficient hydrogen donor for other bacterial and mammalian ribonucleotide reductases. These findings suggest that thioredoxins from different sources are very similar in structure and that they were derived from a common precursor. Although thioredoxins have been described in a number of systems, only a few have been sequenced. Fast Atom Bombardment Mass Spectrometry (FAB MS) is being used to investigate the structure of thioredoxins in order to provide additional information about the mechanism of action of these proteins in oxidation-reduction reactions as well as information on the evolution of these important proteins.

Thioredoxin from E. coli has been sequenced previously by Dr. A. Holmgren of the Karolinska Institute, Sweden, and was provided by Dr. Holmgren for these studies. Thioredoxin from the photosynthetic bacterium, Chlorobium thiosulfatophilum, was provided by Dr. B. B. Buchanan, University of California Berkeley. Thioredoxins were reduced and alkylated with iodoacetic acid prior to enzymatic digestion. The peptides resulting from the enzymatic digests were dissolved in glycerol/acetic acid and analyzed by FAB MS on a Finnigan MAT 731 mass spectrometer. The MS/MS studies were carried out using a VG ZAB 4F instrument.

Analysis of the peptide mixture resulting from the digestion ofE.coli thioredoxin with trypsin by FAB MS revealed eight molecular ions corresponding to eight of the twelve tryptic peptides predicted for E. coli thioredoxin. The remaining four peptides turned out to be either too small or too large for analysis by FAB MS. The eight peptides that were found covered 56 of the 108 amino acids or 52% of the thioredoxin sequence. When the tryptic digest of Chlorobium thioredoxin were analysed by FAB MS, eight peptides were found out of 11 predicted based on amino acid analysis that represent 55% of the sequence. None of these peptides matched the tryptic peptides from E. coli suggesting that the sequence of Chlorobium thioredoxin is significantly different from that of E. coli thioredoxin.

In order to obtain sequence information for Chlorobium thioredoxin, FAB MS was used in combination with the Edman degradation. Briefly this procedure involves determining the molecular weights of the peptides in a mixture by FAB MS,removing the amino terminal amino acids from the peptides by one cycle of manual Edman degradation and then determining the molecular weights of the newly formed peptides by FAB MS. The amino acids that were removed can be determined by the mass shift seen in the FAB spectra before and after Edman degradation. By eliminating the extraction step in the Edman degradation, as many as eight cycles of FAB MS-Edman degradation have been performed starting with as little as 20 nmols of protein. Table I shows the sequence information obtained using this technique on 20 nmols of Chlorobium thioredoxin following cleavage with trypsin.

Additional sequence information was obtained by analysing the tryptic peptides by MS/MS following collision induced dissociaton (CID) to generate fragment ions (Table I). When partial sequence information was available, the CID MS/MS spectra could be interpreted to reveal the entire sequence, however when no partial sequence information was available, the CID MS/MS spectra could not be interpreted to reveal the sequence.

The amino acid sequence homology between E. coli thioredoxin and the partial sequence information for Chlorobium thioredoxin obtained here is shown in Figure 1. Although the peptide mapping experiment did not reveal any homology between these two thioredoxins these tryptic peptide mapping techniques usually require about 80% homology for detection. The homology shown here between the partial sequence of Chlorobium thioredoxin and E. coli thioredoxin is approximately 60%.

By using FAB MS to analyze tryptic peptides from several thioredoxins, the sequence of thioredoxin from *E. coli* was verified, while thioredoxin from *Chlorobium* appeared to be different. By using FAB MS in combination with the Edman degradation, sequence information for *Chlorobium* thioredoxin was obtained. The use of CID MS/MS also provides sequence information and the combination of these two techniques for determining the amino acid sequences of unknown peptides is especially useful. In this manner sequence homology between *E. coli* and *Chlorobium* thioredoxin has been determined.

TABLE I. SUMMARY OF FAB-EDMAN AND FAB MS/MS DATA

MH^+ OF PEPTIDE	EDMAN	MS/MS	SEQUENCE[1]
1776	NO	YES	?
1446	YES	NO	Xle Asn Val Asp Glu Asn Pro Asn ? Lys
1309	YES	NO	Asn Phe Gln Thr Glu Xle Phe ? ? Lys
1156	YES	YES	Val Val Asp Gln Met Val Gly Ala Xle Ser Lys
1015	YES	YES	Ser Xle Pro Thr Met Xle Xle Xle Lys
811	YES	YES	Gln Xle Asp Glu His Xle Gly
661	YES	NO	Ser Xle Pro ? ?
515	YES	YES	Ala Xle Xle Ala Lys

1. (⟶) Determined by FAB-Edman degradation.

FIGURE 1. HOMOLOGY BETWEEN *E. COLI* AND *CHLOBOBIUM* THIOREDOXINS

```
Ser Asp Lys Ile Ile His Leu Thr Asp Asp Ser [Phe] Asp [Thr] Asp [Leu] Val Lys Ala Asp
                                            Asn [Phe] Gln [Thr] Glu [Xle] Phe  ?   ?   Lys

Gly Ala Ile Leu Val Asp Phe Trp Ala Glu Trp Cys Gly Pro Cys Lys Met Ile Ala Pro

Ile Leu Asp Glu Ile Ala Asp Glu Tyr Gln Gly Lys Leu Thr Val Ala Lys [Leu Asn] Ile
                                                                    [Xle Asn] Val

[Asp] Gln [Asn Pro] Gly Thr Ala Pro Lys Tyr Ile Gly Arg Gly [Ile Pro Thr] Leu [Leu Leu]
[Asp] Glu [Asn Pro] Asn  ?   ?  Lys                     Ser [Xle Pro Thr] Met [Leu Leu]

Phe [Lys] Asn Gly Glu [Val] Ala Ala Thr Lys [Val Gly Ala Leu Ser Lys] Gly Gln Leu Lys
Leu [Lys]             [Val] Val Asp Gln Met [Val Gly Ala Xle Ser Lys]

Glu Phe Leu Asp Ala Asn Leu Ala
```

Acknowledgements: The authors would like to thank Dr. J. R. Hass and Dr. B. N. Green for assistance with the MS/MS experiments and Dr's. Holmgren and Buchanan for providing the thioredoxin samples. This work was supported by a grant from the National Institutes of Health.

PEPTIDE SEQUENCING BY ON-LINE ENZYMATIC HYDROLYSIS AND THERMOSPRAY LC/MS

H.Y. Kim*, D. Pilosof, D.F. Dyckes and M.L. Vestal
Department of Chemistry, University of Houston, Houston, TX 77004

Thermospray LC/MS has been successfully employed to detect pseudomolecular ion species for thermally labile and/or nonvolatile samples such as peptides and nucleosides (1). By coupling with enzymatic hydrolysis using immobilized carboxypeptidase Y (CPY) (2,3) and immobilized trypsin, thermospray LC/MS provides an extremely useful technique for unambiguous sequence determination for peptides. After on-line hydrolysis by immobilized CPY, both amino acids sequentially cleaved from C-terminus of the peptides, and the residual peptides are monitored by thermospray LC/MS. For large peptides or proteines, on-line proteolytic hydrolysis into peptide fragments using immobilized trypsin can be employed along with separation by an LC column, before hydrolysis by immobilized CPY. On-line hydrolysis of peptide samples by immobilized tryspin coupled to separation by an LC column and detection of tryptic digest eluted from the LC column directly by the thermospray mass spectrometer can also provide important information for peptide mapping including assignment of individual fragments. Total amount of sample needed is usually low nanomolar level, although it varies depending on the peptide. For some favorable cases, the detection limit is in the low picomolar range.

Figures 1a and 1b illustrate the results from the 2 nmole samples of angiotensin II (M.W. 1046) injected through the columns containing different amount of immobilized CPY. Five amino acid residues are correctly sequenced by detecting protonated molecular ions for both amino acids PHE, PRO, HIS, Ile and TYR and residual peptides A, B, C, D and E remaining after success cleavage of listed amino acids respectively. The intact molecule and the residual peptide A and B also shows doubly charged molecular ions which can be readily recognized by their sodium and potassium adducts appearing 11 and 19 mass unit higher than their protonated molecular ion peaks. With more favorable hydrolysis condition, the intact molecule is no longer visible (Figure 1b). Instead, the residual peptide peaks for the cleavage of fifth amino acid TYR showed up at m/z 389. MH^+ peak for TYR also showed at m/z 182. For relatively small peptides (with M.W. below 1500) sequencing with immobilized CPY generates the sufficient information to allow almost complete sequence determination with great speed. The sample throughput is usually less than 1 minute although it varies depending on dimensions of enzyme column and flow rates.

Figures 2a and 2b show the results from application of on-line tryptic digestion and HPLC separation and detection by the thermospray mass spectrometer. Tryptic fragments of 1 nmole RCM-RNase were generated in the column containing immobilized trypsin and separated using ultrasil-NH_2 column. As shown in Figure 2a, all the expected fragments were detected as singly charged molecules except the fragments T3, T7, T9 and T13 which have the molecular weights beyond the detection limit of our quadrupole mass analyzer. Even though the separation was not perfect, selective ion recording for the mass ranges of interest permits the deconvolution of unresolved chromatographic peaks of individual fragments. The resolution can be improved by adding an organic modifier to the mobile phase.

Both techniques described above can be combined to generate an on-line sequencing technique with easy sample handling procedures for large peptides, which will rapidly supply sequence information not only for terminal amino acid residues but also for multiple internal sites within the peptide chain. On-line operation using three columns in series (CPY column → HPLC column → Trypsin → Thermospray mass spectrometer) enables efficient sample utilization with great speed. A successful result for this application was recently obtained for α-MSH and will be described elsewhere (4).

References

1. Blakley, C.R.; Vestal, M.L.; Anal. Chem., 1983, 55, 750.
2. Kim, H.Y.; Pilosof, D.; Vestal, M.L.; Dyckes, D.F.; Kitchell, J.P.; Dvorin, E.; Proceedings of the Eighth American Peptide Symposium pp 719-722.
3. Pilosof, D.; Kim, H.Y.; Vestal, M.L.; Dyckes, D.F.; Biomed. Mass Spectrom., in press.
4. Kim, H.Y.; Pilosof, D.; Dyckes, D.F.; Vestal, M.L.; J. Am. Chem. Soc., submitted for publication.

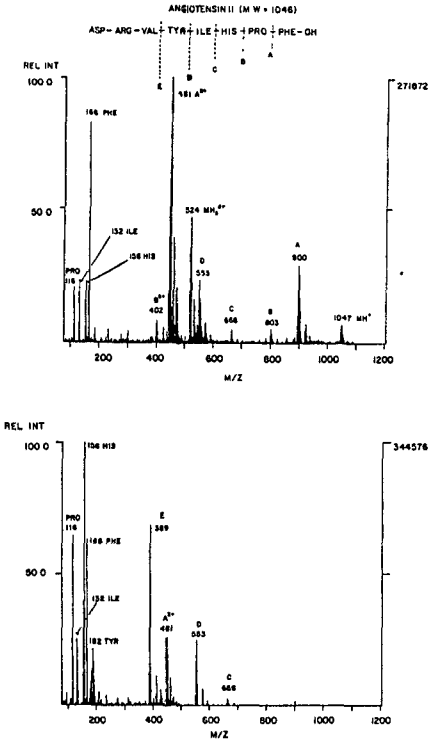

Figure 1: Positive ion mass spectra obtained after hydrolysis with different amount of CPY at pH 5.5, at room temperture; 2.5 x 10^{-8} moles and 1.4 x 10^{-7} moles of CPY for Figure 1a and 1b respectively. A, B, C, D and E in the spectra represent the residual peptides produced by enzymatic hydrolysis at A, B, C, D and E respectively.

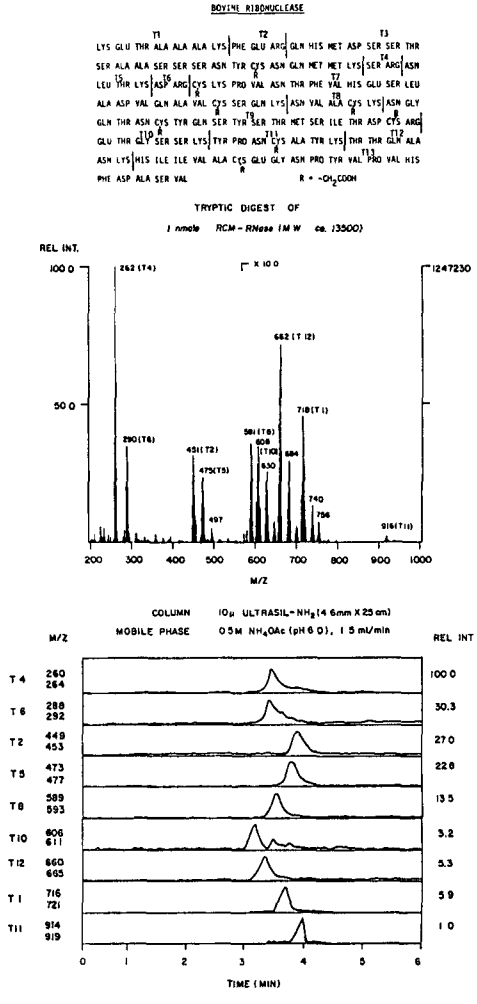

Figure 2: Positive ion mass spectrum obtained by hydrolysis with 4.5 x 10^{-8} moles of immobilized trypsin (Figure 2a). Separation was done using Ultrasil-NH_2 column, NH_4OAc buffer pH 7.0, with the flow rate of 1.5 ml/min (Figure 2b).

MIXTURE ANALYSIS OF PEPTIDES BY FAST ATOM BOMBARDMENT/TANDOM MASS SPECTROMETRY, D.L. Lippstreu, Midwest Center for Mass Spectrometry, Department of Chemistry, University of Nebraska, Lincoln, NE 68588.

Fast atom bombardment (FAB) has proven to be a very powerful tool for determination of peptides because it overcomes limitations of sample volatility and permits the sequencing of amino acid residues. However, spectral data become quite complicated for peptides more than a few residues in length due to nitrogen- and oxygen- directed fragmentation. Also, a high degree of sample purity is essential for accurate identification of the molecular ion; thus, enzymatically cleaved peptides must be isolated prior to mass spectrometric analysis.

We are proposing a possible solution to these difficulties. The strategy will be illustrated by showing its application to a pentapeptide. Tyr-Ala-Gly-Phe-Leu was desorbed by using FAB and a CAD spectrum of the (M+H) was taken (Fig. 1). The principal fragmentation involves cleavage at the CO-NH bond (mechanisms 1 and 2) and the CH-CO bond (mechanism 3). CAD spectra of five other peptides were studied and were found to have the same fragmentation patterns as the pentapeptide.

The pentapeptide was then reduced to the corresponding oligoamino alcohol(1). The product was desorbed using FAB and again, a CAD spectrum of (M+H) was taken (Fig. 2). The protonated oligoamino alcohol fragments primarily toward the formation of carboniom ions (mechanisms 4,5,and 6.

The ultimate goal is to develop a method suitable for analysis of mixtures such as would result from an enzymatic digest. To test the feasibility of analyzing such a digest we prepared a mixture of three peptides: Gly-Gly-Leu Gly-Leu-Tyr, and N-Cbz-Gly-Pro-Gly-Gly-Pro-Ala. The mixture was desorbed using FAB and all three (M+H) ions were observed. CAD spectra of the M+H ions were nearly identical to CAD spectra taken of the pure peptides.

The mixture was then reduced and the reduction product was analyzed. Full scan FAB spectra showed the three predicted (M+H) ions. CAD spectra of these ions were, again, nearly identical to the CAD spectra obtained from individually- reduced peptides. Thus we conclude that diborane-reduced peptides yield sequence information complementary to that of the unreduced peptide and these reduced peptides show potential for mixture analysis.

(1) K. Biemann et al., **Biomed. Mass Spectrom.** 7,51 (1981).

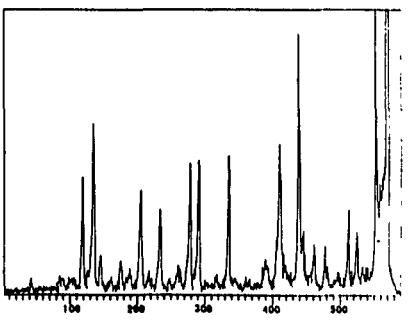

Fig. 1, CAD, m/z 570

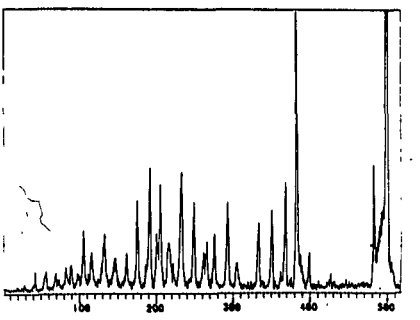

Fig. 2, CAD, m/z 500

Mechanisms:

①

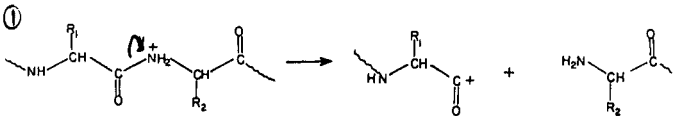

②

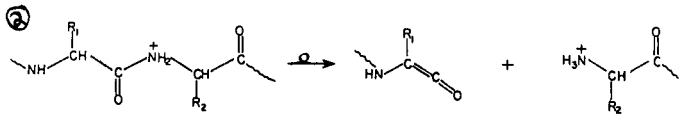

③

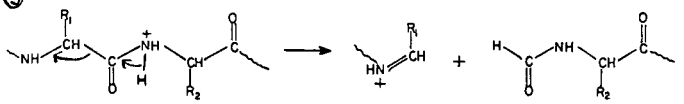

④

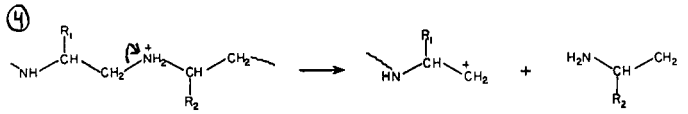

⑤

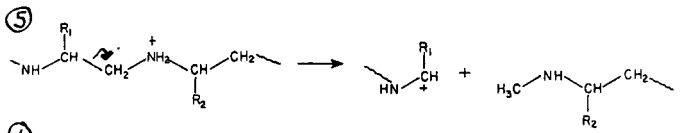

⑥

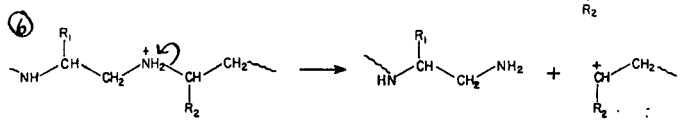

Mechanisms of Antiozonant Protection:
Antiozonant-Rubber Reactions During Ozone Exposure

by
R. P. Lattimer, R. W. Layer, and C. K. Rhee

The BFGoodrich Research and Development Center
9921 Brecksville Road
Brecksville, Ohio 44141

Ozone attack on rubber compounds causes characteristic cracking perpendicular to the direction of an applied stress. This degradation is caused by ozone reaction with the double bonds in the rubber molecules. In order to control the effects of rubber ozonation, chemical antiozonants are added to unsaturated rubbers. The most effective antiozonants are N,N'-derivatives of p-phenylenediamine (PPD).

Several theories have appeared in the literature regarding the mechanism of protection by chemical antiozonants. Most of the evidence to date suggests that the "scavenger" mechanism is the most important one. In this model the antiozonant diffuses to the rubber surface and preferentially reacts with ozone so that the rubber is not attacked until the antiozonant is exhausted. Other theories suggest that there is some chemical interaction between the antiozonant and ozonized rubber.

We have conducted a series of experiments to investigate the possibility of antiozonant-rubber chemical reaction during the exposure of cured (crosslinked) rubbers to ozone. Rubber vulcanizates (cis-polyisoprene and cis-polybutadiene) containing DOPPD antiozonant (N,N'-di-(1-methylheptyl)-p-phenylenediamine) have been aged under ozone, and the soluble constituents have been removed by acetone extraction. Small amounts of nitrogen from the antiozonant remain in the rubber after extraction. The amount of unextractable nitrogen in the rubber before aging is about the same as the amount remaining after ozone aging. This indicates that little, if any, chemical reaction took place between the antiozonant and rubber during ozone exposure.

SCHEME I

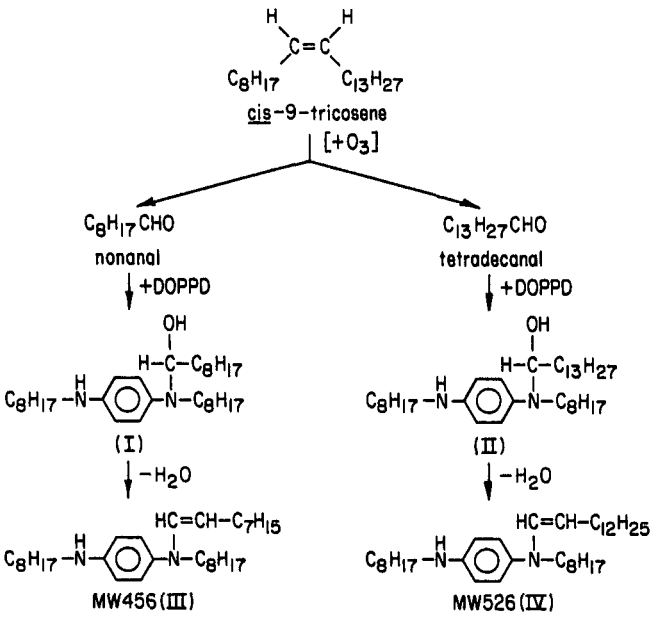

In another approach to this problem, model compound studies were carried out to determine the nature of the products that might be expected from reaction of an antiozonant (DOPPD) with unsaturated rubber during ozone exposure. Using cis-9-tricosene or squalene as models for rubber, we have shown that chemical reactions can take place between the ozonized olefins and DOPPD. Field desorption (FD-MS) proved to be a very convenient method to quickly analyze reaction mixtures. For example, Figure 1 shows the FD mass spectrum of a ozonized tricosene-DOPPD mixture at an early stage of the reaction. Reaction products of MW 456 and 526 can be explained by the sequence of steps shown in Scheme I. Ozonation of the alkene leads to aldehyde intermediates that can then form condensation products with the antiozonant. In later stages of the reaction, other products (not discussed here) are formed.

Other experiments suggest that these types of reactions, though interesting, probably do not occur to any great extent in an actual rubber vulcanizate. That is, these products can form only after the rubber starts to become ozonized, and it has been shown that ozone attack on the rubber does not occur until after the antiozonant is nearly completely consumed. The results of this work are consistent with previous studies in our laboratory that indicate a combined "scavenger-protective film" mechanism is principally responsible for antiozonant protection.

Figure I. FIELD DESORPTION MASS SPECTRUM of OZONIZED cis-9-TRICOSENE/DOPPD MIXTURE (6 Hours After Mixing)

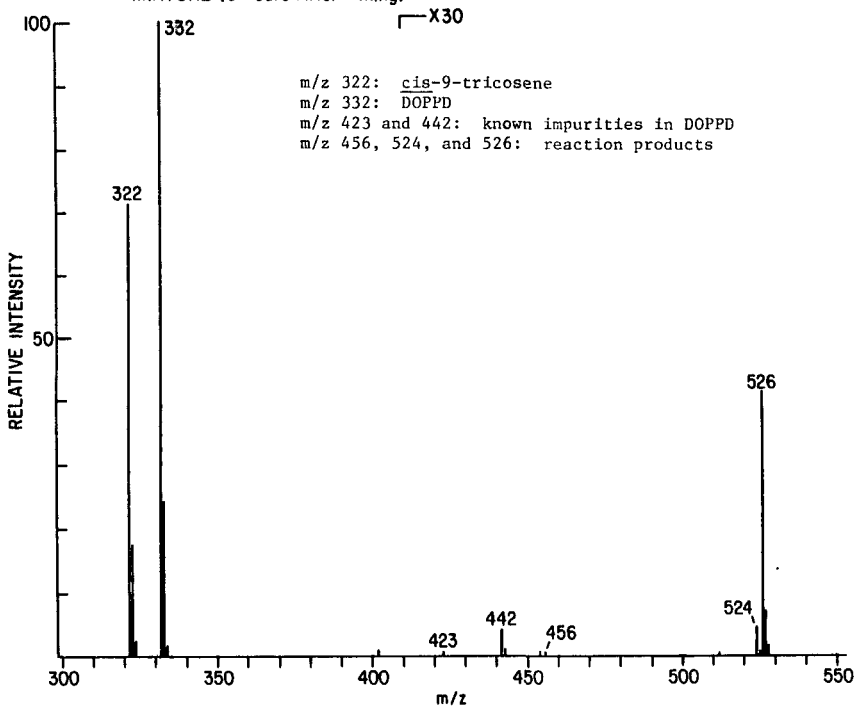

THE USE OF SIGNAL AVERAGING TECHNIQUES FOR THE QUANTITATION AND MASS MEASUREMENT OF HIGH MOLECULAR WEIGHT COMPOUNDS USING FAB MASS SPECTROMETRY

Authors: L GROTJAHN
GBF Mascheroder Weg 1, D-3300 Braunschweig - Stockheim

L C E TAYLOR*
Kratos Analytical Instruments, Urmston, Manchester, UK

Introduction

The technique of Fast Atom Bombardment is capable of providing structurally significant information from a wide range of materials, particularly biomolecules previously not amenable to mass spectrometry.-Many classes of compounds can be directly analysed without the need for modification as demonstrated, for example, by polypeptides. Emperically there is a trend towards lower signal intensities at higher masses, to such an extent that signals at high mass e.g. insulins are weak and transient and only allow a poor recording of the molecular ion region using single scan methods.

Experimental

The mass spectrometer was the Kratos MS50 High Field magnet fitted with a post acceleration detector at GBF with a mass range ca 3000 daltons at 8kV accelerating voltage. The atom gun was a saddle-field source (Ion Tech Ltd) operated at 7-8 kV and a tube current 1mA. Xenon was used to provide the primary particle beam.

Data acquisition and signal averaging was achieved using a Tracor Northern Multichannel Analyser (8192 channels) and data acquired by (i) narrow scanning the accelerating and ESA voltage of the mass spectrometer or (ii) magnetic field scanning. Output of data was to an x-y plotter.

Peptide samples were commercially obtained from Sigma Chemical Co. Poole, Dorset. The oligonucleotide CCTTCTGGAACTG was obtained from the DNA - Synthesis group at the GBF Institute.

Glucagon MH^+ 3481.6

The molecular ion region of Glucagon is devoid of glycerol (matrix) peaks present at lower mass and therefore ions due to sample signal can be accumulated as illustrated by Figs. 1a, b, c for sample loadings of 1 g, 100 ng and 10 ng respectively. This increased sensitivity will also allow higher resolutions to be achieved with an excellent signal to noise ratio Fig. 2. The experimental isotope distribution pattern at approximately 10,000 resolution gives identical agreement with the theoretical result. This has been calculated using a computer program HRISO, developed at GBF which determines the intensity ratios of isotopes at any specified resolution, such that experimental data is readily comparable with calculated results. The stock sample was prepared in glycerol and acidified with 1N HCl.

Bovine Insulin MH^+ 5730.6

The single scan of the molecular ion region Fig. 3a is for a 5 nMol loaded sample. Fig. 3b is the accumulated results of 25 successive scans across the 16 peak window (3000 ppm). The sample was prepared in thioglycerol and 2μl of sample volume loaded onto the probe tip. The isotope ratio calculation is compared with the experimental result in Fig. 3c.

Mass Measurement

A. Vasocative Intestinal Peptide

A sample of VIP (Vasoactive Intestinal Peptide - Sigma Chemical Co) was mass measured without prior knowledge of the molecular weight except that it was in the range 3100 - 3400 daltons. The method used was as follows:

(a) (i) The narrow scan width was set in this case 40,000 ppm and spectra accumulated over the molecular ion region of the VIP sample. In this particular example the unknown was of lower molecular weight than the reference compound glucagon.

(ii) The reference sample was loaded onto the probe and multiple scans accumulated over the molecular ion region of glucagon (reference) with high mass selected on the mass spectrometer. This results in the superimposition of the two accumulated scans as shown in Fig. 4, when a suitable voltage ratio is set using the decade box of the mass spectrometer - Note that it is not important to locate the signal to a specific position.

(iii) The mass difference between the two M+H peaks (for example) can be determined using the multichannel analyser.

(iv) The mass of the unknown which in this case is at low mass is then calculated.

$$\text{Mass unknown} = V_R \ (\text{Ref Mass} - M_{DIFF})$$

So for a measured mass difference (MDIFF) of 53.97, VR = 0.969999 and Ref = 3481.6

Mass VIP protonated = 3324.8

(b) The experiment was then repeated for a 3000 ppm narrow scan using the M + 2 peak. In this case the accumulated scans across the molecular ion region of VIP were stored in the multichannel analyser memory. Subsequently the glucagon sample was run without altering any tuning controls of the mass spectrometer and scans accumulated. The voltage ratio as set by the decade box was adjusted until the apex of the M + 2 peaks on channel two was coincident with the M + 2 peak from the VIP sample and giving the voltage ratio 0.954947.

The accuracy of these two methods was found to be within 15 ppm which is sufficient to reliably assign the nominal mass of an unknown. The accuracy of the result may be used as a confirmation of the mass of a compound at high mass values, but not as a means of determining empirical formulae since the number of possible combinations is prohibitive.

B. Oligonucleotide

The 13-unit oligonucleotide CCTTCTGGAACTG was studied in negative ion mode using Fast Atom Bombardment, This was mass measured using the $(C_3I)I^-$ cluster ion at mass 4024.046 daltons and the mass of the $(M-H)^-$ ion confirmed to be 3922.68 daltons.

When we compare the theoretical and experimental distributions in this case it can be seen that significant discrepancies are present which are due to the partial deprotonation of the molecular ion typical of oligonucleotides and to background contribution.

Conclusion

The use of signal averaging at high mass is advantageous for the recording of weak transient singles and as a means of reducing the minimum detectable sample quantity.

The assignment of accurate mass albeit of less significance than at low mass is both reliable and fast using the accumulation of reference and unknown peaks and is a convenient means of nominal mass assignment.

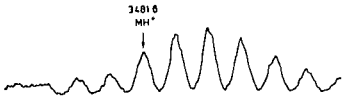

(a) Glucagon 1μg (0.28nM)

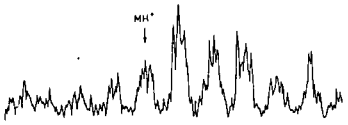

(b) Glucagon 100ng (28pM) 75 scans

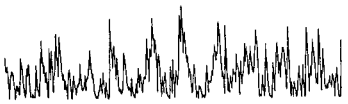

Figure (1) (c) Glucagon 10ng (2.8pM)

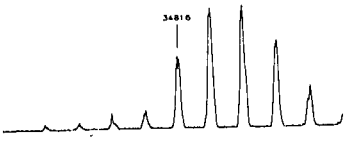

EXPERIMENTAL KRATOS MS 50 Pos FAB MS 4KV
20μg GLUCAGON
100 SCANS ACCUMULATED
RESOLUTION 10 000

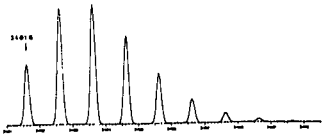

CALCULATED
GBF PROGRAM HR150
FORMULA
$C_{153}H_{226}N_{43}O_{49}S_1$
RESOLUTION 10 000

Figure (2)

PROTONATED MOLECULAR ION ISOTOPE CLUSTER OF BOVINE INSULIN

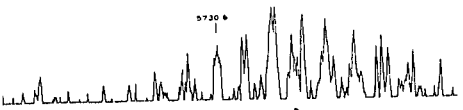

CA 30μg BOVINE INSULIN, SINGLE SCAN (a)

Figure (3)

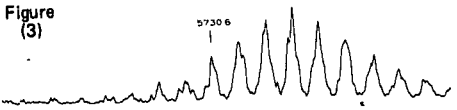

CA 30μg BOVINE INSULIN, 25 SCANS ACCUMULATED (b)

PROTONATED MOLECULAR ION ISOTOPE CLUSTER OF BOVINE INSULIN

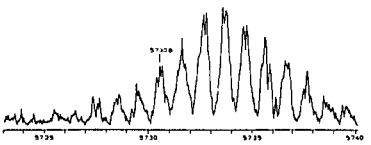

EXPERIMENTAL KRATOS MS50S POS FAB-MS 4KV
TWO INJECTIONS OF 30μg EACH
WITH A TOTAL ACCUMULATION OF 39 SCANS
RESOLUTION 6000

Figure (3) (c)

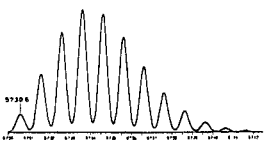

CALCULATED
GBF PROGRAM HR150
FORMULA
$C_{254}H_{378}N_{65}O_{75}S_6$
RESOLUTION 6000

MATCHING FAB-SPECTRA

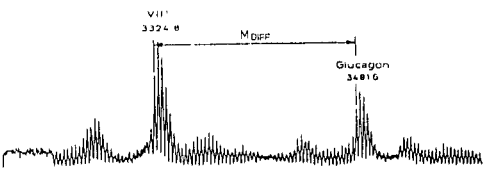

20 Scans VIP accumulated, 10μg
30 Scans Glucagon accumulated, 10μg
MR 0.969999

Figure (4)

SOLUTION INTRODUCTION MASS SPECTROMETRY: A SIMPLE ALTERNATIVE TO DESORPTION TECHNIQUES

Ralph C. Dougherty, John de Kanel and Casey Grimm

Department of Chemistry
Florida State University
Tallahassee, Florida 32306

A number of techniques have recently been developed for obtaining mass spectra from nonvolatile and thermally labile samples. These techniques generally require specialized ion source facilities for specialized sample introduction hardware. Examples of the techniques include field desorption, secondary ion mass spectrometry on liquid matrices, liquid ionization, electrohydrodynamic ionization, laser desorption and plasma desorption mass spectrometry.

The direct introduction of liquid chromatography effluents into mass spectrometer ion sources requires at a minimum a liquid chromatograph and an interface system to the mass spectrometer. The thermospray interface[1] and its variants in the form of liquid ionization[2] or electrohydrodynamic ionization[3] have allowed determination of mass spectra of compounds that would not normally vaporize under direct probe introduction. The key to each of these experiments is introduction of the compound to the mass spectrometer ion source in solution. Overcoming a compound's lattice energy by introducing the compound in solution makes it possible to obtain coherent mass spectral information from compounds that would be destroyed during attempts to evaporate them directly from a solid matrix. The experiments described in this paper were undertaken in an attempt to utilize the advantages of liquid introduction mass spectrometry in an unmodified commercial mass spectrometer.

The mass spectrometer used in these experiments was a Finnigan 4510 GC mass spectrometer equipped with a temperature-controlled direct insertion probe. The instrument was operated in positive or negative chemical ionization mode with 0.4 torr of isobutane as the reagent gas. Primary ionization was accomplished with an 89 eV beam of electrons.

We have investigated three separate methods for direct introduction of solutions of nonvolatile compounds. In each of the methods a 2 mm od pyrex capillary was fashioned to replace the quartz ceramic probe tip that we usually use with this spectrometer. The liquid introduction capillaries are a length of 11 mm. Three approaches were used to fill the capillary volume, namely: (1) the outlet end was sealed to a diameter of approximately 220 μm and the capillary was filled with a 220 μm fused silica needle from a conventional on column capillary GC injection syringe; (2) a hole was left at both ends of the capillary of approximately 10 μm in diameter and the capillaries were filled using vacuum from a squeeze bulb; (3) one end of the capillary was sealed to a hole diameter of 10 μm and the capillary was filled by sealing the other end of the capillary in an oxygen flame followed by dipping the capillary into the solution while the freshly sealed tip was still hot. Samples were then introduced in the conventional manner, using a relatively short pump-down time in the vacuum interlock.

Using this introduction technique with aqueous solutions we have obtained mass spectra of underivatized peptides, carbohydrates and nucleosides. Glucose (2 mM) in a

solution of 0.5 M ammonium carbonate gave the molecule ion at m/z 180 at roughly twice the intensity of the ammonium ion adduct at m/z 198. The negative chemical ionization mass spectrum of adenosine (1 mM) in ammonium thiocyanate (0.5 M) gave the thiocyanate adduct as the dominant high mass ion (m/e 325).

Preliminary experiments indicate that the solution introduction technique described here is applicable for use with non-polar as well as polar solids. We have obtained both protonated molecules and molecule anions from fragile sesquiterpene lactones that have resisted all attempts at direct evaporation. More detailed studies will be necessary before the full analytical utility of this method can be established. Studies along these lines are in progress.

REFERENCES

1. Blakley, C. R., Carmondy, J. J., Destal, M. L., J. Amer. Chem. Soc., 1980, 102, 5931-5933.

2. Tsuchiya, M., Kuwabara, H., Anal. Chem., 1984, 56, 14-19.

3. Evans, C. A. Jr., Hendricks, C. D., Rev. Sci. Instrum., 1972, 43, 1527-1530.

THE HOLLOW CATHODE AS AN ATOM SOURCE FOR RESONANCE IONIZATION MASS SPECTROMETRY, R.K. Marcus and W.W. Harrison, Department of Chemistry, University of Virginia, Charlottesville, Virginia 22901.

The glow discharge with hollow cathode has found a number of uses in analytical chemistry. Recent studies in this laboratory have been oriented towards the use of a hollow cathode as an atom reservoir for resonance ionization mass spectrometry (RIMS). Figure 1 illustrates the two operational modes of the hollow cathode which we have investi-

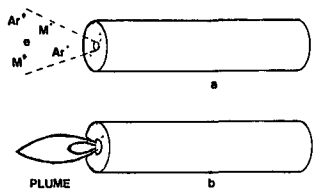

Figure 1. Two modes of hollow cathode ion source operation; a) conventional b) plasma plume.

gated. The first has been previously used as a solids ion source. The hollow cathode plasma plume, which we are developing as an emission source, is depicted in 1b.

Experimental

The hollow cathode source is mounted coaxially to the quadrupole mass filter system in a six-way cross housing. The atomic population exiting the cathode can be probed with the laser through quartz windows perpendicular to the cathode-quadrupole axis. The laser-atom beam intersection and subsequent ion extraction are shown in Figure 2.

Figure 2. Diagrammatic representation of laser-atom beam intersection for RIMS studies.

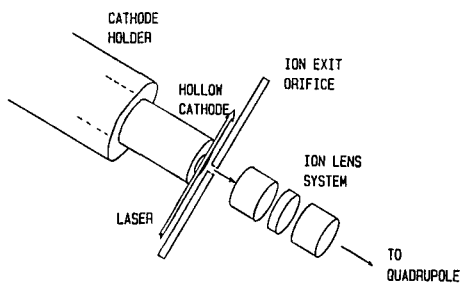

Results and Discussion

A major feature of resonance ionization is its elemental specificity. Figure 3 is a typical mass spectrum of a copper hollow cathode discharge source. The Ar^+ and Ar^{2+} peaks at 40 and 20 amu respectively, as well as other gas species, exist as a constant background ion signal which might impose isobaric interferences. By tuning our excimer pumped dye

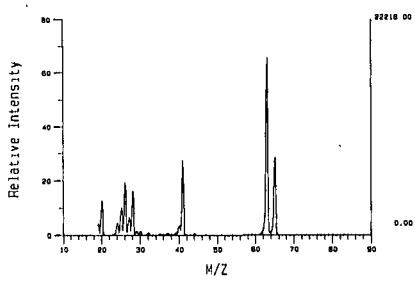

Figure 3. Mass spectrum of copper hollow cathode; 0.5 torr Argon, 100 mA.

laser, with frequency doubler, to a copper atomic transition we can take data using a background correction gate which increases the relative signal to background from 2:1 to 9:1 as in Figure 4. This ratio can be further enhanced by taking a greater number of scans statistically averaging out the glow discharge produced ions from those produced resonantly. Future studies will characterize the plasma plume, particularly with comparison to conventional glow discharge, as an optical and mass spectral source.

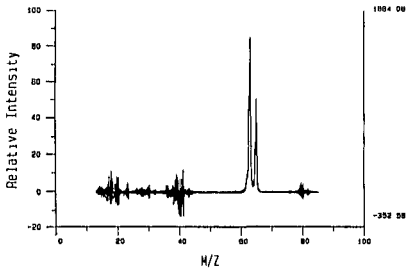

Figure 4. RIMS spectrum of copper hollow cathode; 324.7 nm excitation, 0.5 torr Argon, 100 mA, 20 scans.

Selective Counting of Krypton Atoms Using Resonance Ionization Mass Spectrometry

C. H. Chen, S. D. Kramer, S. L. Allman, and G. S. Hurst

Chemical Physics Section, Oak Ridge National Laboratory
Oak Ridge, Tennessee 37831

The technique of resonance ionization spectroscopy (RIS) is being extended to develop a means for counting individual atoms of a selected isotope of a noble gas. In this method, lasers are used for RIS to obtain atomic species (Z) selectivity, and a small quadrupole mass spectrometer provides isotopic (A) selectivity. After atoms have been Z and A selected, the ions are accelerated to a few kilovolts onto a target where they are implanted. Suitable targets will emit a pulse of several electrons each time that one of the selected ions is implanted. An electron multiplier is used with sufficient gain to count each implanted ion from the electrons emitted by the target.

A four-wave mixing scheme was used to generate a 116.5-nm laser beam with an energy of 500 nJ/pulse. With this wavelength, krypton atoms could be efficiently excited by resonance radiation and subsequently ionized. Finally, an "atom buncher" was needed to enhance the probability that krypton atoms were in the ionization laser beam at the time of the laser pulse. Thus, the major requirements for counting a few isotopically selected atoms include (1) an atom buncher to collect krypton atoms in the ionization laser beam, (2) the appropriate laser beams for achieving excitation and ionization of krypton, (3) a mass spectrometer for isotope selection and as a method for implanting the isotopically selected atoms into a metal target with unit efficiency (4) an electron multiplier with efficiency near 100% for counting the pulses of secondary electrons released during ion implantation, and (5) maintenance of the experimental facility under high vacuum without pumping, low ($<10^5$/min) outgassing rate of krypton from the chamber, and clean surfaces of the chamber to prevent krypton from sticking to the walls of the chamber with a long residence time. The experimental chamber was electropolished to reduce the outgassing rate and to prevent the sticking of rare gases to the walls. Radioactive ^{85}Kr was put into the chamber to determine the loss of krypton. No loss due to sticking to the surface was observed.

In order to keep the chamber surface clean, no pumps containing oil were used. The experimental chamber was pumped to a few microns by a liquid nitrogen cryosorption pump. A compressed helium cryopump was used to achieve ultrahigh vacuum. The chamber was baked and pumped for two days before introducing a sample to reduce the outgassing rate. A titanium-zirconium getter pump was used to getter outgassed molecules without pumping rare gases. The outgas rate of krypton was measured as 10^4 Kr/min.

In the RIS scheme, 116.5 nm radiation excites krypton from the ground state; then photons at 558.1 nm (2 mJ/pulse) further excite to a state that can be ionized with 1.06 μ Nd-Yag radiation. The sum process $2\omega_1 + \omega_2$, with ω_1 corresponding to 252.5 nm for two-photon excitation of xenon and ω_2 corresponding to 1.51 μm, produced 116.5 nm radiation near the 7s level in xenon. With xenon pressure of 40 Torr and argon pressure of 364 Torr to achieve phase matching, the energy per pulse of the VUV laser near 116.5 nm was found to be ~500 nJ. By putting a known amount of krypton into the chamber, the effective detection volume was found to be 1×10^{-4} cm^3. With a laser repetition rate of 10 Hz, 500 h would be required to count all the isotopically selected atoms in a 4-liter chamber.

To reduce the time required to count all of the krypton atoms, an atom buncher was developed. The atom buncher was designed so that rare gas atoms could be trapped on a well-defined cold spot (15 K) on a surface and subsequently released at any desired time by the application of a laser pulse. With the atom buncher, the overall detection probability in one laser pulse was measured to be 3×10^{-5}. Thus, the time to count all the isotopically selected krypton atoms is reduced to about 1 h when the repetition rate of all lasers is 10 Hz. A sample containing 1000 atoms of ^{81}Kr obtained from the National Bureau of Standards was counted with good accuracy.

This method to count krypton atoms can be extended to count ultralow levels of isotopically selected xenon atoms. Provided that about 100 nJ/pulse can be generated for one-photon excitation, isotopically selected argon atoms can also be counted.

This research was sponsored by the Office of Health and Environmental Research, U.S. Department of Energy under contract DE-AC05-84OR21400 with Martin Marietta Energy Systems, Inc.

Analytical Developments in Resonance Ionization Mass Spectrometry

C. M. Miller, N. S. Nogar, and S. W. Downey
Los Alamos National Laboratory
Los Alámos, New Mexico 87545

Resonance ionization mass spectrometry (RIMS) now has obtained the status of an established analytical method. As a technique for isotope ratio measurement, RIMS has the advantages of high elemental selectivity, sensitivity, and dynamic range. Selectivity arises through the use of electronic transitions in the resonance excitation process which are characteristic of the element of interest; isobaric interferences exhibit different transitions and are not ionized. Sensitivity derives from the efficiency of the ionization process, given the laser sources available today, and the reduction of interferences. Significant increases in ionization yields have been demonstrated through the use of continuous wave (cw) lasers, which take advantage of a unity duty cycle to increase sample exposure; this has expanded the dynamic range of feasible isotope ratio measurements. Further increases in dynamic range may also result from isotopically selective ionization, through the reduction of tailing of dominant isotopes into minor isotope channels.

The rare earth element lutetium was used to demonstrate the dynamic range of RIMS isotope ratio measurements. This element may be conveniently ionized using the 452 nm $^2D_{3/2} \rightarrow {}^2D^{\circ}_{3/2}$ transition in a one-color, two-photon scheme. Experiments were performed with a 12", 68° magnetic sector mass spectrometer and broadband cw dye laser. Typical output powers for the latter were 250 mW in a 1.3 cm^{-1} FWHM bandwidth. Samples of lutetium ranged from 60 to 200 ng. Although chemical cleanup of the samples was performed, small amounts of ytterbium were also present; this isobaric interference significantly perturbed thermal isotope ratios, as shown below. Ionization yields for the predominant lutetium isotope, ^{175}Lu, were typically 10^6 to 10^7 ions per second at 1300°C over a period of several hours, for an efficiency of approximately 10^{-4}. Minor isotopes, with ion rates at a few per second, were measured with allowances for scattering from major isotopes and for residual thermal ionization in the source region; corrections were typically thirty percent.

Table 1 shows the results of lutetium isotope ratio measurements for both RIMS and conventional thermal ionization. Internal precision of the RIMS data is 16, 4, and 2 percent, respectively; counting statistics contribute significantly to the uncertainty in the smallest ratio. Confirmation of the ^{173}Lu and ^{174}Lu results was obtained through mass separation and radioactive decay counting, to an agreement of approximately one percent. Note that for ^{173}Lu, the measurement was performed with as few as 10^8 atoms (27 fg). Note also the presence of ytterbium isobaric interferences in the 173 and 174 mass positions in thermal ionization; this effect is eliminated in the RIMS measurement.

Table 1. Isotope Ratio Measurements

173/175	4.4×10^{-7}	3.36×10^{-3}
174/175	3.62×10^{-6}	9.28×10^{-4}
176/175	2.64×10^{-2}	2.63×10^{-2}

Increased dynamic range in isotope ratio measurements is limited in the present system by mass spectrometer resolution. Although additional dispersive stages might suffice, another approach is isotopically selective RIMS. In this method, a narrowband (<1 MHz) laser is used, with discrimination possibly deriving from the differing hyperfine structure of the isotopes of interest. Additional sensitivity and isobaric selectivity may also result, given the better match of laser output to atomic absorption and decreased probability of accidental unwanted overlap.

Preliminary to isotopically selective RIMS, it is necessary to understand in detail the spectroscopy of the isotopes of interest. Experiments to this end have been performed for lutetium, using a single-frequency dye laser and the mass spectrometer to study the optical spectra of the individual isotopes. Note that the dispersion of the mass spectrometer removes the necessity for prior isotope separation; optical spectra for ^{174}Lu have been generated with an abundance of 4×10^{-5} relative to ^{175}Lu. Spectra for ^{173}Lu have also been produced, at a somewhat higher abundance. These data, along with similar results for the stable lutetium isotopes, are currently under analysis to derive nuclear parameters.

Multiwavelength Resonance Ionization of Technetium

S. W. Downey and N. S. Nogar, Chemistry Division
C. M. Miller, Isotope and Nuclear Chemistry Division
Los Alamos National Laboratory
Los Alamos, New Mexico 87545

A two-color, three-photon resonance ionization scheme has been developed for mass spectrometric determinations of technetium. The use of visible light to affect the ionization of Tc has several advantages. First, potential isobaric interferences from Mo are minimized, for free Mo has only ultraviolet resonance ionization pathways. Second, background ionization in the mass spectrometer is less likely as compared to two-photon ultraviolet photoionization. Also, the ultimate utilization of continuous wave (cw) lasers is possible at these wavelengths; cw resonance ionization mass spectrometry (RIMS) has been demonstrated to be extremely sensitive for detecting small numbers ($<10^8$) of atoms and measuring large ($>10^6$) isotope ratios.

The wavelengths used in this work to affect Tc ionization are between 420 and 620 nm. Pulsed lasers and time-of-flight mass spectrometry were used to study the feasibility of the multiple-resonance approach. Twenty-two unique ionization paths originating in the ground state were observed and identified. In addition, transitions out of metastable states ($\sim$3000 cm^{-1}) were observed. The relative populations of these states were found to be in rough agreement with the sample filament temperature. With both lasers operating at wavelengths below 500 nm, a periodic structure in the optical spectrum of Tc was observed. The source of this structure is thought to be a hybrid photodissociation-photoionization of an unidentified

Tc-containing precursor molecule. Although no direct evidence of the parent molecule is available, certain optical and mass spectral data suggest the precursor is a diatomic molecule, the dimer or oxide. The presence of Tc-containing molecules is likely to limit Tc measurement sensitivity, since Tc bound in molecular form is not addressed by the normal atomic photoionization process and constitutes an effective loss of sample. Operation of one laser at 600 nm produced a much lower off-atomic-resonance background and atomic signals with good signal-to-noise. This combination of wavelengths (ca. 420 and 600 nm) greatly facilitates the development of a two-color cw RIMS method for Tc isotope ratio measurements.

In the course of this work, single-color, multiphoton ionization of chromium and tantalum were observed. Most of the Cr (420-430 nm) and Ta peaks (450-460 nm) were identified as three-photon ionization sequences with one resonant intermediate. The observed peaks were at times broad (∿1-5 nm) at rather modest (<2mJ) laser power. These types of ionization sequences may prove to be insidious in the analysis of complicated matrices where RIMS is expected to provide freedom from isobaric interferences. For elements with complicated electronic structure (e.g. Ta), many unpredicted ionization pathways are observed. Fortunately, the problem of multiphoton resonances of concomitant species is much reduced with cw RIMS where low peak powers do not effect high-order processes efficiently.

APPLICATION OF AN ARTIFICIAL INTELLIGENCE EXPERT SYSTEM
FOR OPTIMIZATION OF REAL-TIME DATA FROM PYROLYSIS EXPERIMENTS

Carla M. Wong, Richard W. Crawford, Stanley M. Lanning and Hal R. Brand
Lawrence Livermore National Laboratory, Livermore, CA 94550

ABSTRACT

Tuning of MS/MS instruments is a time consuming process that gives an average spectrum representing the entire mass range of the particular instrument. There are sacrifices in sensitivity and resolution at each end of the spectrum in order to achieve this average spectrum. If the mass spectrum could be optimized in real-time, for all regions of the mass scale, (i.e. continuous tuning), the overall sensitivity and the quantitative capabilities of the instrument would be increased, especially for on-line or dynamic process analyses where components are changing with respect to time (1,2).

To investigate this concept, we have extended the AI expert system that we initially built for tuning the TQMS (3). This extension allows us to do optimization of peak intensity while we are analyzing a sample.

The TQMS Expert System has a knowledge base representing the effects of ∿20 different tuning parameters on peak intensity, shape and resolution. These are implemented in KEE, an object-oriented knowledge representation language with a rule-based reasoning system. This enabled us to build a transparent system where the reasoning behind the decisions to change voltage on a particular lens to increase sensitivity or resolution can be traced. This transparency helps to increase confidence in the decisions made by the system.

An example of the TQMS device representation and a representation of the hierarchy of the parameters important for real-time tuning are kept in the knowledge base as shown in Figure 1.

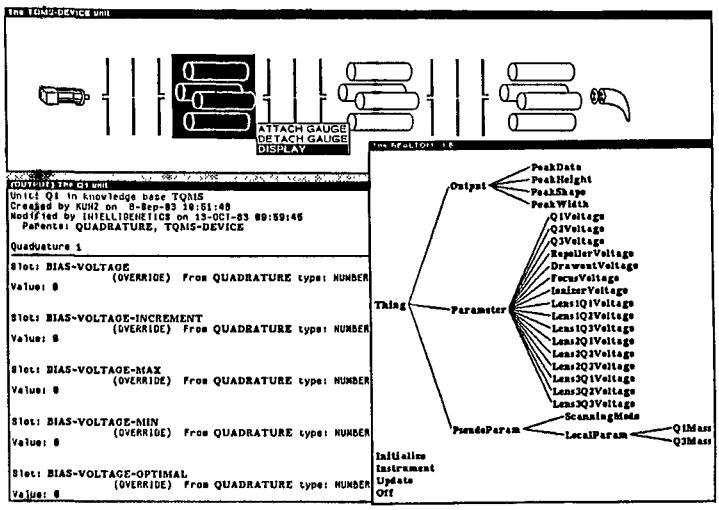

We initially used the calibration compound perfluorotributylamine (PFTBA) in our experiments to show the effects that optimizing the various lens voltages had on increasing the transmission efficiency and therefore the overall sensitivity for various ions formed under normal 70 ev electron impact ionization of this compound. The results in Figure 2 were very encouraging. (Note that the intensities are shown on a logarithmic scale.) The increase in sensitivity of parent mass (502 amu) was particularly impressive.

Our next experiments involved trace sulfur species of the type found in oil shale pyrolysis gas (which is an extremely complex mix), and again we see increases in sensitivity by factors of 2 to 8. Smaller increases in sensitivity for sulfur gases as opposed to PFTBA are due to the fact that the normalized (manual) tuning was done over a small mass range using a sulfur gas standard for tuning; so, AI optimization over this shorter mass range does not give as large of an increase as with the wider mass range represented by PFTBA.

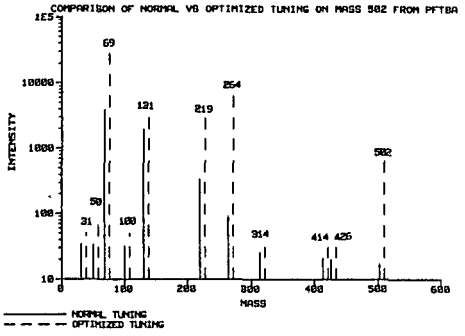

Figure 2

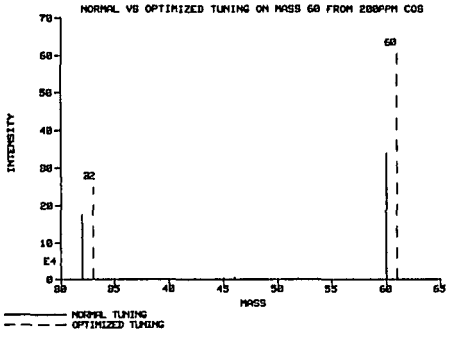

Figure 3

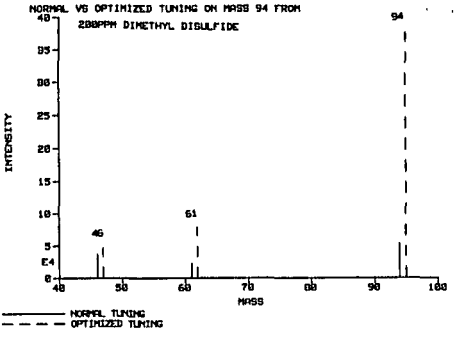

Figure 4

The time required for optimizating on one mass range for the initial tuning files is ~11 minutes and the time for then changing the many operational parameters on-line in a real-time mass scan is 7.7 msec.

These initial excursions into AI and expert systems have helped to make us much more aware of the knowledge we use in day-to-day operation of the TQMS.

REFERENCES

1. C.M. Wong, R.W. Crawford and A.K. Burnham, Anal. Chem., 56, 390-396, (1984).

2. C.M. Wong, R.W. Crawford and A.K. Burnham, Am. Chem. Soc. Petroleum Div., St. Louis, MO., April 8-13, 1984.

3. C.M. Wong, R.W. Crawford, J.C. Kunz and T.P. Kehler, IEEE Transactions on Nuclear Sciences, Vol. NS-31, No. 1, 804-810 (Feb. 1984).

Worked performed under the auspieces of the U.S. Department of Energy by the Lawrence Livermore National Laboratory under contract number W-7405-ENG-48.

DIRECT DETERMINATION OF RELATIVE IONIZATION CROSS SECTIONS BY TRANSPIRATION MASS SPECTROMETRY

D. W. Bonnell and J. W. Hastie
Center for Materials Science
National Bureau of Standards
Washington, DC 20234

The previous development of the coupled transpiration - mass spectrometer technique at NBS, the Transpiration Mass Spectrometer (TMS), and the establishment of its thermodynamic fidelity [1], has provided a unique opportunity for determination of relative ionization cross sections by comparison with well studied gases. The TMS system consists of nearly classical transpiration (saturation flow, [2]) cell design, with the exit orifice being a supersonic nozzle. Gas exhausting from the nozzle into the first stage vacuum system at very high expansion ratios (typically $>10^5$), forms a molecular beam. The beam is skimmed to select the axial portion and, passes through differential pumping orifices before passing through a conventional cross axis mass spectrometer electron impact ion source. The molecular beam itself is collimated before entering the ion source, and scattered gas response is eliminated by modulating the collimated beam. Relative ion currents are the in-phase signal obtained using a vector lock-in amplifier. The electron beam is only mechanically collimated, and not energy selected. Thus, the cross sections which are determined are relative. The electron energy is determined by calibrating the electron energy scale with known appearance potential (AP) gases (e.g. Ar, at 15.76 eV, N_2, 15.6 eV, O_2, 12.06 eV, etc. [3]). Within the error of determining the AP, the scale is linear, and simply offset by the order of 4 volts to apparently higher energy.

The basic technique is simple, as the transpiration sampler operates at pressure ranges convenient for manometric pressure measurement and produces a molecular beam whose number density is proportional to the partial pressure of individual constitutents. Pure carrier gases, mixed with low levels of additional gas species, are passed through the transpiration reactor. Comparison of the mass-flow-mixed gas concentrations with the ion current ratios measured relative to the carrier gas gives the relative cross section directly. This technique is extended to high volatility liquids, such as water vapor, by using saturation mixing techniques to establish composition. In the case of water, confirmation of composition was assured by dew point hygrometry at the relatively high source pressure, before the supersonic expansion.

This technique requires careful attention to molecular beam formation characteristics, which include the prevention of cluster formation, assuring minimal beam mass segregation, and avoiding beam contamination with background gas. Extensive testing with thermodynamically defined systems has shown that such conditions can generally be achieved.

The transpiration process itself allows the extension of the technique to condensed phases. Recognizing that the ion signal, I_c, at temperature T attributed to the carrier gas represents a known pressure $P_c \equiv P$ (the system manometric pressure), the basic mass spectrometer ion current/pressure relationship ($P_c = K_{ms}k_cI_cT$) can be used with carrier gas cross section/mass discrimination data to determine the mass spectrometer constant, K_{ms}. The species dependent constant k_i, for species i, is just $1/\sigma_i,S_i$), where σ_i is the cross section, and S_i is the mass dependent sensitivity factor, which is determined in a separate experiment, typically by using the ion current signals for a gas mixture of inert gases whose cross sections are known. The partial pressures are obtained gravimetrically, by comparing the mass loss over a known time period to the summation of ion currents, using the transpiration equation, $P_i = P(n_i/n_i+n_c)$, which relates moles, n, of material i transported to partial pressure, P_i. n_c is obtained from mass flow measurement of the carrier gas. The ion current summations must be carried out over all ions resulting from the precursor i. Hence a knowledge of the parent ion fragmentation to yield daughter ions is necessary to obtain total ionization cross sections. In typical systems where polymer species are present, additional information is necessary to resolve cross section ratios. This may be assuming monomer to polymer cross sections are additive, or using auxiliary information. One method is to operate in an unsaturated mode, which strongly suppresses polymerization, achieved in the TMS system in a manner similar to the Knudsen Effusion double oven experiment. Another is to perturb the chemistry with external addition of a product gas (e.g. O_2, H_2O, etc.) of known cross section and use thermodynamic equilibrium constants to obtain an independent measurement.

Table 1 gives a relative set of ionization cross sections determined by TMS. These cross sections have been used for deriving partial pressures from Knudsen Effusion experiments in this laboratory as well. Both systems use a similar style of ion source,

quadrupole mass analyzer, channel-type multiplier, and modulated lock-in amplification. Compared to the critical review of Kieffer and Dunn [5], the agreement is consistantly good.

Although a number of workers use some form of the integrated ion intensity calibration (generally to avoid needing cross section information), such studies are relatively few, and molecular ionization cross sections are usually estimated. A common estimation procedure is to use tables of consistant atomic cross sections (e.g. Mann's [6] tables of maximum cross sections) and assume molecular cross sections can be obtained by summing atomic cross sections, the "additivity-of-atomic-cross-sections." Modifications of this assumption, proposing factors other than unity for atomic terms, have been suggested (e.g. Drapcho and Rosenblatt [7] used 0.79, based on a molecular volume argument, i.e. $\sigma(Tl_2Cl_2) = 0.79 \cdot 2 \cdot \sigma(TlCl)$). Table 1 compares our experimental cross sections to those calculated by additivity (unit summation) using Mann's [6] tables. The tendency is to overestimate by 1/0.67, about 50%. The actual errors are often larger, pointing out the limitations of such a simple model, which takes no cognizance of the differences of molecular verses atomic electronic structure, and ignores the major differences in cross section verses energy. Unfortunately, more accurate models are not generally available.

REFERENCES:

1. D. W. Bonnell and J. W. Hastie, in Characterization of High Temperature Vapors and Gases, J. W. Hastie ed., p. 357, NBS SP 561, 1, U. S. Govt. Printing Off. (1979).
2. U. Merten and W. E. Bell, in The Characterization of High Temperature Vapors, J. L. Margrave ed., Chapt. 4, J. Wiley & Sons, Inc. New York (1967).
3. J. L. Franklin, et al., Ionization Potentials, Appearance Potentials, and Heats of Formation of Gaseous Positive Ions, NSRDS-NBS 26, U. S. Govt. Printing Off. (1969).
4. J. W. Hastie and D. W. Bonnell, in Thermochemistry Today and Its Role in the Immediate Future, M.A.V. Ribeiro da Silva ed., Reidel Pub., Boston (1983).
5. L. J. Keiffer and G. H. Dunn, Rev. Mod. Phys. 38, 1 (1966).
6. J. B. Mann, J. Chem. Phys. 46, 1646 (1967).
7. D. L. Drapcho and G. M. Rosenblatt, J. Chem. Thermodyn. 11 335 (1979).

TABLE 1. Total Cross section (σ) values obtained by TMS at 30 eV (units πa_0^2)[a]

Species	Observed(O)[b]	Additivity(A)[c]	O/A
Ar	2.6 (reference)[c]	-	-
N_2	1.48 (1.2)[a]	2.54	0.58
O_2	1.26 (1.12)[a]	2.41	0.52
H_2	0.76 (0.78)[a]	0.43	1.77
HCl	2.3	3.32	0.69
SO_2	1.3	6.17	0.21
H_2O	1.5	1.63	0.92
Na	4.6 (3.92)[c]	-	-
NaCl	1.0	7.03	0.14
KCl	7.4	10.15	0.73
CsCl	3.1	13.63	0.23
$(KCl)_2$	5.5	20.30	0.27
KOH	2.7	8.47	0.32
$(KOH)_2$	3.6	16.93	0.21
As_4O_6	54.	25.12	2.12
		Average =	0.67

[a]See review of Kieffer and Dunn [5].
[b]Typical uncertainity ± 0.2.
[c]See Mann [6]; his Table III maximum cross-sections have been renormalized to the observed reference value in this table.
NOTE: Values may be used to scale ionization efficiency curves if eV dependent corrections of S_i are made.

FAQQQ: THE TANDEM FLOWING AFTERGLOW-TRIPLE QUADRUPOLE. A MARRIAGE OF CONVENIENCE.

Robert R. Squires, Kelley R. Lane, Robert E. Lee
Larry G. Wright, Karl V. Wood, R. Graham Cooks
Department of Chemistry
Purdue University
West Lafayette, IN 47907

We describe here a powerful new instrument for studying gas phase ion chemistry and illustrate its applications to problems of ion structure, reactivity and thermochemistry.[1] The instrument combines a flowing afterglow (FA) apparatus as a chemically versatile ion source and reactor with a triple quadrupole analyzer (QQQ) for characterizing ions through their collision-induced dissociation. The resulting instrument a flowing afterglow-triple quadrupole (FAQQQ) is shown in schematic form in Figure 1. The FAQQQ consists of a Finnigan-MAT Triple Stage Quadrupole assembly housed within the detection chamber of our recently constructed flowing afterglow apparatus. Ions generated by electron impact undergo ion-molecule reactions in a fast flowing He plasma at 0.5 torr. Neutral reactants are introduced into the ion stream at several points along the flow reactor and either positive or negative ions may be sampled through an orifice and focussed into the triple quadrupole analyzer. Ions passing through the analyzer as governed by daughter ion, parent ion or neutral loss scanning modes are subsequently detected by an electron multiplier. The following features of the FAQQQ configuration are discussed: 1) Product ion characterization by tandem mass spectrometry coupled with the unique ion-molecule reaction capabilities of the flowing afterglow, such as access to higher cluster ions than are normally available in conventional ion sources; control over the number of reactive and non-reactive collisions prior to ion sampling and precise definition of reactant energy distribution. For example a complex mixture of polynuclear iron carbonyl cluster cations derives from electron impact on $Fe(CO)_5$ and subsequent condensation reactions at 0.5 torr (Figure 2A). Common structural features among these ions may be identified by combining daughter ion scans for each cluster with parent ion scans for each fragment. Figure 2B represents a parent spectrum of m/z 196 (nominally $Fe(CO)_5^+$). Series of ions are apparent which are separated by intervals of 112 amu to which we have assigned $Fe(CO)_2$ as the common fragment. As another example, the isomeric $C_6H_9O^-$ ions 1 and 2 have been shown to be non-interconverting species by their distinct ion molecule reactions in the FA, despite the favorable

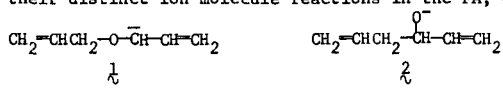

Wittig rearrangement which connects them. This is confirmed by the low total CID cross section for 1 and the facile production of a m/z 43 daughter ion from 2 in the FAQQQ.

Daughter ion spectra from relatively large hydrogen-bonded cluster ions which may be synthesized by association reactions in the flow tube give especially interesting information.[2] For example, addition of a mixture of n-propyl, sec-butyl and n-hexylamines to the FAQQQ ion source region results in alkylammonium ion formation and rapid buildup of proton bound dimers, trimers and tetramers possessing the various possible permutations of alkyl groups. Mass selection of the mixed trimer $[(n\text{-}C_3H_7NH_2)(2\text{-}C_4H_9NH_2)(n\text{-}C_6H_{13}NH_2)\cdot H^+]$ at m/z 234 and subsequent CID gives the daughter ion spectrum shown in Figure 3. The relative abundances of the amine dimer and monomer fragment ion are in excellent accord with the proton affinity ordering of these three bases. Thus, loss of $n\text{-}PrNH_2$ (PA 218.5 kcal/mole) from the parent trimer dominates the spectrum with loss of $n\text{-}C_6H_{13}NH_2$ (PA 220.1 kcal/mole) and $2\text{-}C_4H_9NH_2$ (PA 220.5 kcal/mole) following in order accordingly. More significantly, the alkyl ammonium ion (monomer) fragments are also produced in relative amounts which exactly reflect the proton affinities of the amines. This observation suggests that competitive fragmentations of even larger cluster ions will enable the simultaneous determination of several relative proton affinities at once.

References

1. Squires, R.R.; Lane, K.R.; Lee, R.E.; Wright, L.G.; Wood, K.V.; Cooks, R.G., J. Amer. Chem. Soc., submitted.

2. McLuckey, S.A.; Cameron, D.; Cooks, R.G., J. Amer. Chem. Soc. 1981, 103, 1313.

FIGURE 1

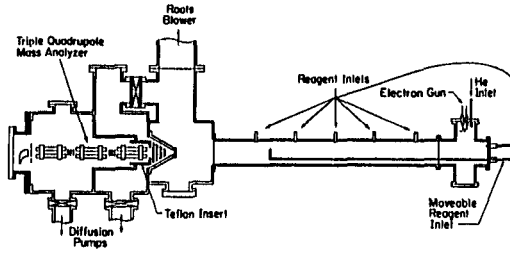

FIGURE 2

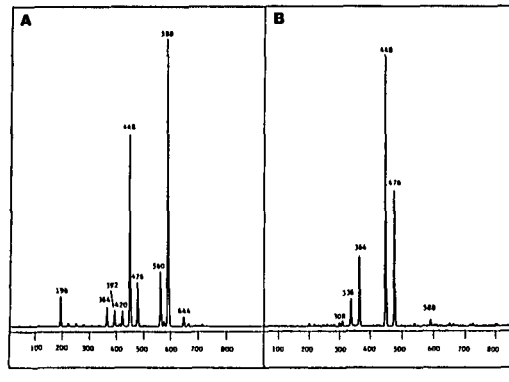

FIGURE 3

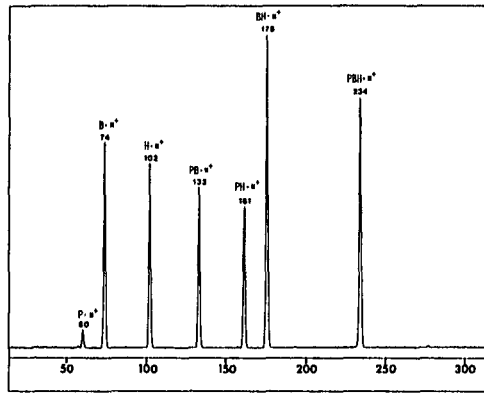

THE BEQQ TANDEM MASS SPECTROMETER

J.D. Ciupek, J.R. O'Lear, R.G. Cooks, Department of Chemistry, Purdue University, West Lafayette, IN 47907; P. Dobberstein, Finnigan MAT, Barkhausenstrabe 2, Postfach 14 40 62.2800 Bremen 14, West Germany; and A.E. Schoen, Finnigan Corporation, 355 River Oaks Parkway, San Jose, California 95134.

The BEQQ mass spectrometer is a versatile high resolution and MS/MS instrument designed to provide access to a range of experiments. These can be used either for in-depth studies of ion chemistry or for demanding analytical measurements. The basic high resolution mass spectrometer is followed by a dual zoom lens deceleration system, an rf-only quadrupole, and a high performance hyperbolic quadrupole. These elements are mounted on an optical rail in a cradle which provides easy access to the components. Modifications to or addition of ion optical elements is accomplished with great ease. The first (FF1) and the third field-free (FF3) regions are fitted with needle collision cells to facilitate collisions at translational energies of up to 3 keV. Fragment ions resulting from collisions taking place in FF1 can be monitored as a function of scattering angle (angle resolved mass spectrometry) by pre-collision electrical deflection of the parent ion beam by means of the Z-plate lenses in the source. The addition of a collision cell to the second field-free region (FF2) facilitates collisions between the two sectors. The third field-free region contains an intermediate detector consisting of a conversion dynode and off-axis electron multiplier. This detector allows the instrument to be operated as a conventional BE mass spectrometer as well as in the BEQQ configuration without the need for hardware modifications. The rf-only quadrupole is encased in a gas tight shroud and serves as a focussing collision device for collisions taking place at ion translational energies typically 1-100 eV but sometimes much more. The instrument is capable of obtaining daughter, parent and neutral loss spectra associated with reactions taking place in each of the four different collision regions of the instrument. In addition to conventional scan types, a variety of unconventional scan modes are possible with the BEQQ configuration. A schematic depicting the many options possible is shown in Figure 1.

An example of one new scan type, E-filter Q-scan, is illustrated in Figure 2 for 3',3",5',5"-tetrabromophenolphthalein (mw=634). The top scan is a portion of a conventional E-scan (MIKE type scan) obtained when m/z 634, formed by electron impact, is mass selected by the magnet and the electrostatic sector scanned to detect metastable ion decompositions taking place between the sectors. The result is a broad peak, the poor mass resolution being due to the kinetic energy spread of the fragment ions. However, by setting the ESA at the potential which corresponds to the maximum peak intensity and then subsequently decelerating the ion beam followed by mass analysis with the analyzer quadrupole (bottom scan in Figure 2), the components of the peak can be resolved. This example demonstrates how an additional stage of quadrupole mass analysis provides increased mass resolution of the broad peaks typically found in MIKE spectra.

The instrument is capable of obtaining MS/MS spectra of higher molecular weight molecules ionized by desorption techniques. The FAB MS/MS spectrum of erythromycin illustrates these capabilities. The MS/MS spectrum shows abundant fragmentation even when no collision gas is employed. Introducing collision gas increases the degree of fragmentation observed. The main reactions are (i) sequential dehydrations from the protonated molecule, (ii) glycosidic cleavage with loss of the nonamino sugar followed by sequential losses of three water molecules and (iii) cleavage of the macrocyclic molecule to give ionized amino sugar with a C_2 unit attached. The capability of obtaining MS/MS spectra of molecules ionized by desorption ionization makes it possible to obtain structural information on thermally labile or involatile molecules which are difficult to ionize by conventional methods.

To evaluate the performance of the BEQQ instrument for low energy MS/MS, data obtained at low collision energies on the hybrid instrument were compared with that obtained on a triple quadrupole mass spectrometer. The hybrid instrument was found to produce nearly identical spectra at similar conditions of collision energy and pressure. Furthermore, low energy MS/MS spectra obtained on the BEQQ as a function of collision energy (energy resolved

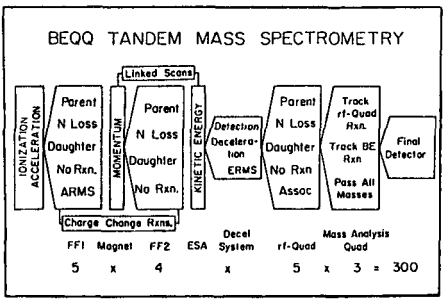

Figure 1

mass spectrometry) for hexafluoropropylene showed that as the collision energy is increased, fragment ions with higher appearance energies are formed. This result indicates increased energy deposition upon increasing collision energy. This point is further substantiated by data obtained from the low energy, ion-molecule reaction of ionized ethylene with neutral ethylene to form the associative products at m/z 39 ($C_3H_3^+$) and m/z 41 ($C_3H_5^+$). At increasing collision energies, the formation of the higher energy product at m/z 39 increases in relative abundance with respect to the ion at m/z 41. The ratio of these association products, as expected, is strongly dependent upon collision energy and can be used to calibrate the collision energy. The fragmentation of n-butylbenzene over the entire collision energy range (10eV-3000 eV) of the hybrid instrument has also been studied. The ratio of fragment ions $91^+/92^{+\cdot}$ increases steadily at collision energies from 10-100 eV. Above a collision energy of 500 eV there is very little change in the relative abundances of these fragment ions. All collisions were performed in the rf-quadrupole with the fragment ions decelerated and mass analyzed by the hyperbolic quadrupole.

Ion structural studies are facilitated by the ease with which consecutive CID reactions can be studied with the BEQQ instrument. In these experiments, ions formed in the source collide in FF1 at a translational energy of 3 keV, the resulting fragment ions are mass selected by the BE section of the instrument using a linked scan and then undergo a second, low energy (<100 eV), collision in the rf-only quadrupole. Using consecutive CID reactions, the heptyl ion formed from collision induced dissociation of n-nonane was found to have a structure indistinguishable from that formed in the source by dissociative electron impact on n-nonane (Figure 3). The potential utility of such consecutive CID reactions for ion structural studies is evident.

The instrument is controlled by the SS-300 data system. A block diagram of the BEQQ control system is shown in Figure 4. Use of multiple microprocessors in a distributed processing scheme simplifies overall system operation by placing the burden of instrument operation upon the instrument itself.

In summary, the BEQQ tandem mass spectrometer combines the performance of sector analyzers with the speed of quadrupoles to produce an instrument with unique capabilities and extreme versatility. High resolution mass spectrometry is available as well as MS/MS information on collision reactions occurring in four different regions of the instrument including consecutive collision experiments.

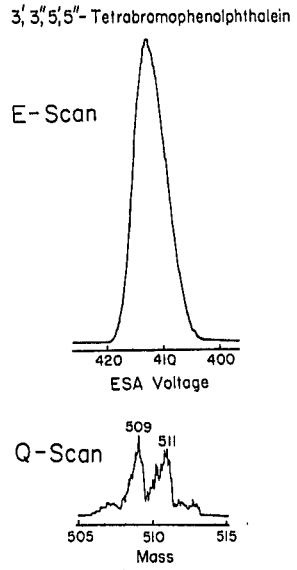

Figure 2

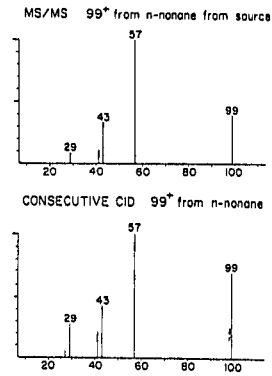

Figure 3

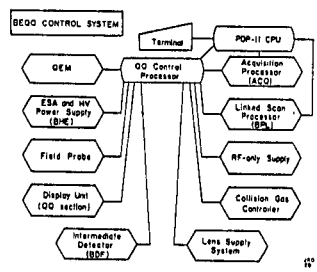

Figure 4

The Design and Performance of a Tandem Double-Focusing Mass Spectrometer.

J.R. Hass, B.N. Green, R.H. Bateman and P.A. Bott. NIEHS, PO Box 12233, Research Triangle Park, NC 27709, and VG-Analytical, Floats Road, Wythenshawe, Manchester M23 9LE, England.

Recent years have seen a number of developments that greatly extend the range of applications of mass spectrometry into areas of biochemical research previously inaccessible to this technique. Perhaps the most important of these is the matrix-assisted ionization of polar compounds by means of energetic particle beams (fast atom bombardment, FAB)[1]. There are two limiting features of this technique that restrict its utilization in the analysis of even favorable compounds. The matrix material contributes a non-specific ion current to the spectrum with the result that the sensitivity is frequently limited by this background ion current rather than amplifier signal:noise. A perhaps more important restriction results from the nature of the sample introduction technique, which is essentially a direct probe. Since the isolation of pure materials from biological origins is uncertain, at best, the possibility of the spectrum being the result of more than one compound is always present.

Tandem mass spectrometry (TMS) has been found useful in a number of instances for the reduction of extraneous ion currents when mixtures are analyzed[2]. The most widely used technique at present for combining FAB and TMS has been mass-analyzed ion kinetic energy spectrometry (MIKES). Although useful data are possible, the technique suffers from poor daughter ion resolution (50-200 being typical) and loss of transmission for parent ions at higher masses, if unit mass resolution is to be retained. One obvious means to overcome both these limitations is the use of a double-focusing mass spectrometer for both parent and daughter ion analysis. Thus a tandem double-focusing mass spectrometer has been designed and constructed.

The more important concerns during the design phase of this instrument were sensitivity at moderate resolutions (5000-20000) for the primary beam, transmission and efficiency of the collision cell, transmission and resolution of daughter ion beams with high energy spread and uniform sensitivity for all daughter ions. Other considerations included the availability of accessories (i.e. ion sources, chromatographic inlets, etc.), maintenance, ease of operation, and versatility to facilate the performance of new experiments.

The requirement that a range of accessories be available and that the instrument be easily maintained mandated the selection of commercially available components as much as possible. The VG-Analytical ZAB/HF was chosen as the most appropriate design for the first mass analyzer (MS-I) on the basis of performance and horizonatal layout. Many design problems could be avoided by using an instrument of similar optics for the second mass analyzer (MS-II). Thus a second ZAB/HF was chosen for this purpose. The second mass analyzer will have ion beams of much greater energy spread to analyze than the first analyzer. Thus the energy acceptance of MS-II is of greater practical concern than its ultimate resolving power. This suggested that it would be desireable to remove any lens elements that would restrict the ion beam in the y dimension between the magnetic and electric sectors of MS-II. One consequence of this modification is an anticipated reduction in the ultimate resolution of MS-II for ion beams with low kinetic energy spread. The configuration of B-E-E-B was selected on the basis of greater experimental versatility and engineering simplicity. The remaining element is the collision cell. Two considerations lead to the conclusion that the collision cell should retard the ion beam prior to collisional excitation. The first is that the magnitude of the energy spread introduced by the kinetic energy release (KER) is proporational to the square-root of the kinetic energy the ions have at the time of fragmentation. The second is that retardation of the beam prior to collisional excitation makes it convenient to include post acceleration to the fragment ion beam. The result is that the minimum kinetic energy of the frasgment ion beam is increased, improving the accuracy with which measured daughter ion intensities can be measured. This retardation-acceleration is conveniently achieved by floating the collision cell relative to ground. A schematic of the design is shown in Figure I.

The achieved performance is listed in the Table. Transmission curves for MS-II as a function of retardation voltage (Figure II) show that the expected improvements in transmission at higher resolutions was achieved. Reasonably intense ion beams at higher resolutions were achieved for the $(M-28)^{+\cdot}$ doublet in dibenzosuberone (Figure III). The daughter ion spectrum of MH^{+} from lysyl-bradykinin (Figure IV) shows intense fragments over a factor of 20 in fragment ion mass as well as uniform resolution over this mass range. A variety of novel gas phase chemical experiments are possible.

---

1. Barber, M., Bordoli, R.S., Sedgwick, R.D. and Tyler, A.N. J. Chem. Soc. Chem. Comm. 1981, 325.

2. For a recent review, see "Tandem Mass Spectrometry"; McLafferty, F.W., Ed., Wiley-Interscience: New York 1983.

MS-I. Full specification of normal ZAB/HF.

MS-II. *Mass Range.* >3000 at 8 keV ion energy.
Ultimate resolution 30000 (parents)
13500 (daughters)
Relative transmission: 75% (0,4, or 6 kV on collision cell)
55% (7.9 kV on collision cell)
Fragmentation efficiency: 11% of $M^{+\cdot}$ from n-decane as collectable daughters.

Table. Performance achieved on ZAB/4F.

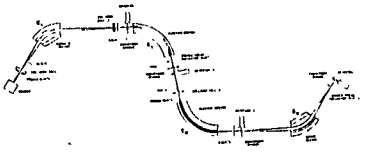

Figure I.

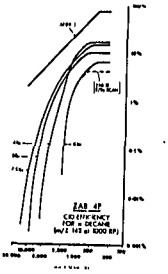

Figure II.

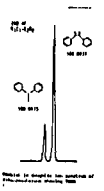

Figure III.

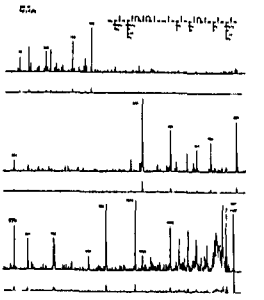

Figure IV.

A DOUBLE FOCUSSING MASS SPECTROMETER FOR THE STUDY OF HIGH MOLECULAR WEIGHT BIO-MOLECULES

J S Cottrell, L C E Taylor, Kratos Analytical Instruments, Urmston, Manchester, UK
and D H Williams, Chemistry Department, Cambridge University, Cambridge UK.

Although Fast Atom Bombardment has provided the means to ionize very high molecular weight bio-molecules, optimum sensitivity will not be achieved if it is necessary to reduce the mass spectrometer accelerating voltage in order to obtain an increased mass range.

There are two principal methods of improving the high mass sensitivity of a mass spectrometer. The first is to maximise ion beam transmission by maintaining a high accelerating potential. The second is to enhance detector efficiency by post acceleration of the ions. The MS50RF is a new double focussing mass spectrometer incorporating both of these improvements. An inhomogeneous field laminated magnet provides a mass range of 10,000u at full accelerating potential without significantly increasing the optical path length over that of the standard MS50. Post acceleration of up to 15kV can be applied to maintain detector efficiency throughout the entire mass range.

Figure 1 shows a single 3 second scan across the molecular ion region of bovine insulin acquired using the MS50RF. Previously, when operating at reduced accelerating voltage, it was necessary to accumulate several scans in order to obtain such a high signal to noise ratio. Because a trace such as figure 1 can now be observed in "real-time" on the instrument oscilloscope, it becomes possible to optimise source tuning and slit widths for maximum signal intensity. Thus, the actual increase in sensitivity obtained from working at full accelerating voltage is amplified into a much larger gain in **apparent** sensitivity. Comparison of figure 1 with recently published spectra acquired at half the accelerating voltage shows an **apparent** sensitivity gain of ~30 (ref. 1).

Figure 2 shows a 2 minute accumulation of these scans. It should be emphasised that these data have not been smoothed in any way other than that inherent in acquiring the data into a finite number of channels (256).

All the spectra shown here have been calibrated against alkali halide reference masses as follows: Spectra were acquired into the DS55 data system over a fixed mass range from one or two loadings of the sample. The sample was then replaced by an evaporated layer of caesium iodide. The peak matching unit was adjusted to bring the nearest caesium iodide cluster peak into the centre of the mass range, so providing an accurate reference point, and further spectra were acquired. Mass measurement accuracy better than 0.1u was readily achieved by this procedure.

Figure 3 shows a low resolution survey scan across the molecular ion region of bovine proinsulin. The very high signal to noise ratio of this spectrum suggested it may be worthwhile to study the molecular ion cluster at higher resolution. Figure 4 shows the molecular ion cluster of bovine proinsulin at a resolution of ca. 8000. Comparison with the simulated isotope distribution reveals two features. Firstly, that the apparant resolution is less than 8000; this may be connected with the underlying "peak at every mass" distribution. The second feature of interest is that the centroid of the cluster is ca. 1 amu lower than the theoretical value. We believe this to be due to the ionisation of a significant proportion of $(M)^+$ ions in addition to the protonated species.

(1) M Barber et al Biomedical Mass Spec. 11 182 (1984) figure 1

Acknowledgements: We thank Dr B H Frank of Eli Lilly & Co. for the sample of bovine proinsulin. We also thank Dr L Grotjahn of GBF Braunschweig for generating the theoretical isotope distributions.

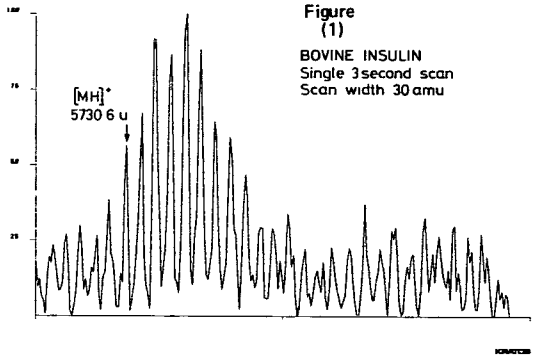

Figure (1)
BOVINE INSULIN
Single 3 second scan
Scan width 30 amu

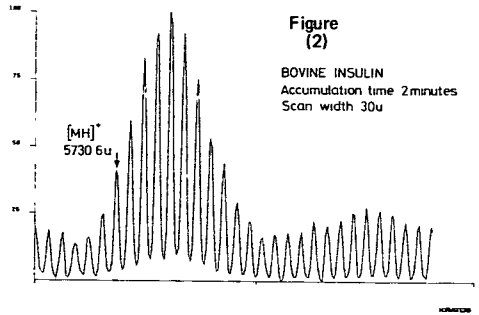

Figure (2)
BOVINE INSULIN
Accumulation time 2 minutes
Scan width 30u

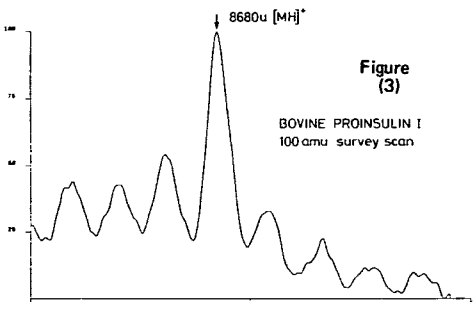

Figure (3)
BOVINE PROINSULIN I
100 amu survey scan

BOVINE PROINSULIN I
Theoretical Isotope Distribution

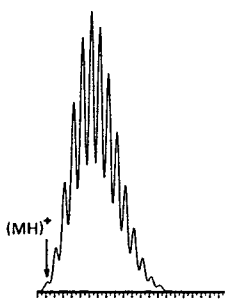

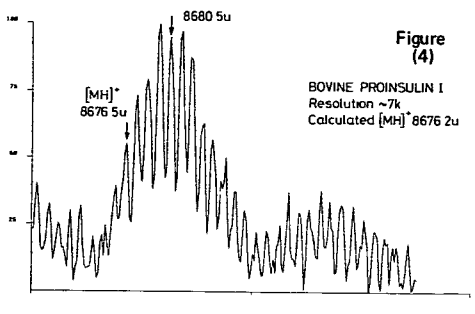

Figure (4)
BOVINE PROINSULIN I
Resolution ~7k
Calculated [MH]+ 8676 2u

Design Aspects in Hybrid Mass Spectrometry

L.C.E. Taylor, R.S. Stradling
Kratos Analytical Instruments, Ramsey, New Jersey, U.S.A
K.L. Busch
Dept of Chemistry, Indiana University, Bloomington, Indiana, U.S.A

Several variants of hybrid mass spectrometers have been constructed as a result of recent interest in direct mixture analysis. The MS80RFAQ uses the MS80RFA double focusing spectrometer as the first MS stage followed by an RF only collision cell and analytical quadrupole to provide the low resolution second MS stage. The use of a high resolution first stage allows a particular species to be selected even if it is present at the same nominal mass as another species. This is illustrated with reference to Fig 1 (a) and 1 (b) for the M^+ species of dimethyl amiline and [the $M-H]^+$ species of methyl anisole which both have a nominal mass of 121 daltons.

The daughter ion spectrum from mass m/z 121 would therefore be a summation of the two individual daughter ion spectra. (Fig 1 (c) however using a primary beam resolution of 7500 it is possible to mass select either species and obtain the individual daughter ion spectra. This is compared to the corresponding spectrum of the pure material.

The two MS stages are interfaced by means of a special lens system which focuses and steers the beam from the MS80RF magnet, and retards the ions from 4kV to low translational energies suitable for transmission through the collision cell and analytical quadrupoles.

The lens assembly is illustrated in Fig 2, showing the focusing deceleration and beam deflection stage, the latter is used in normal scan mode to steer the ion onto an intermediate detector. Additional scan modes are parent ion and constant neutral loss scanning.

MS80RFAQ Daughter ion spectrum at 7500RP of m/z 121·08915 (top) from mixture and daughter ion spectrum of $M^{+\cdot}$ from pure dimethyl aniline (bottom)

Figure (1)a

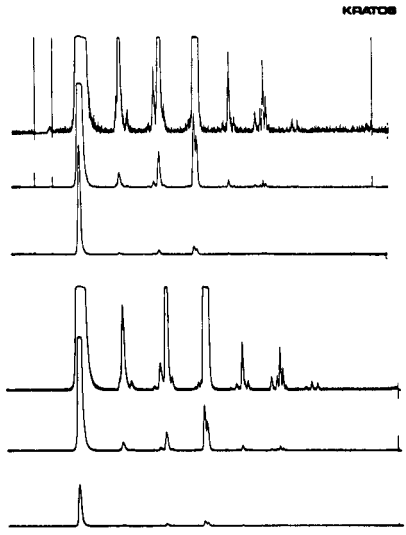

MS80RFAQ Daughter ion spectrum at 7,500RP of m/z 121·06534 (top) from mixture and daughter ion spectrum of $[M-H]^+$ from pure methyl anisole (bottom)

Figure (1)b

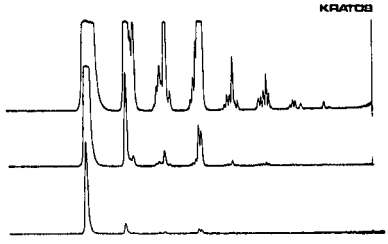

Fig 1c

MS80RFAQ Daughter ion spectrum of m/z 121 (nominal) at 1000RP from mixture of dimethyl aniline and methyl anisole

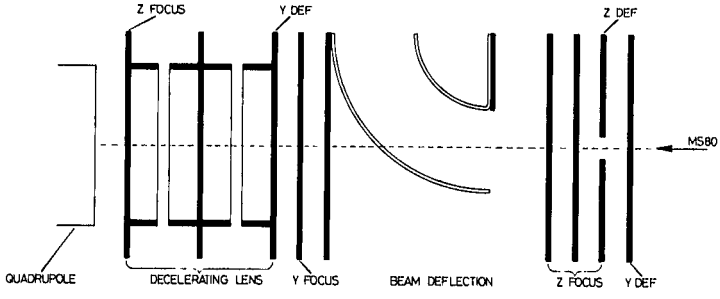

Figure (2) MS80RFQ INTERMEDIATE LENS ASSEMBLY

OLIGOSACCHARIDE SEQUENCING BY FAB, DCIMS, AND MS/MS-CID

V.N. Reinhold, S.A. Carr, Dept. of Nutrition, Harvard School of Public Health, Boston, MA and B.N. Green, V.G. Analytical Ltd, Floats Rd, Wythenshawe, Manchester M23 9LE, England

Biopolymer sequencing by mass spectrometry has gained considerable impetus by the application of "soft" ionization techniques. Peptide sequencing using fast atom bombardment (FAB) ionization has been especially noteworthy. For the lower molecular weight biopolymers, sequence and molecular weight-related ions are readily obtained in the FAB mass spectra, but, as one proceeds to polymers of higher molecular weight there is a gradual diminution of sequence information that is often more pronounced for polysaccharides than for peptides.

In efforts to enhance the amount of structural information obtained from the mass spectra of oligosaccharides we have utilized direct chemical ionization (DCI) with ammonia as the reagent gas. Although DCI of large underivatized polysaccharides provides little structural information, permethylated samples yield excellent sequence and molecular weight detail far beyond the 2000 mass range.

With these considerations in mind, we have compared FAB and DCI for structural detail and sensitivity on numerous linear and branched, neutral and acidic, glycoprotein-derived oligosaccharides. Our findings indicate that ammonia DCI of derivatized material is more sensitive and structurally informative than ionization by FAB of comparable materials that are underivatized.

A probable reason for the enhanced sequence information under ammonia DCI conditions is the presence of gas-phase ammonolysis of glycosidic bonds. This fact has been detected with $^{14}N^{2}H_3$ as the reagent gas for the DCI-MS of permethylated butyl glycoside. A study of the spectra, using $^{14}N^{1}H_3$ as the reagent gas, shows a series of fragments explained by the consecutive loss of methanol. With the deuterated reagent gas, one of these losses is shifted by 1 amu (for the loss, m/z 207----174) which can be explained by covalent nitrogen attachment and loss of CH_3O^2H, (Scheme 1).

In an effort to extract more structural information from FAB ionized oligosaccharides, we have explored the utility of collision induced decomposition (CID) with a neutral gas (1) in a reverse geometry double focusing instrument (VG-ZAB)*. The power of this MS/MS approach is illustrated below for two isomeric (branched and linear) oligosaccharides which failed to yield structural information in the normal FAB mass spectra (+ and - mode), but which gave structurally informative and significantly different CID spectra. The ions of interest (MH^+, m/z 1116) were selected with the magnetic analyzer and brought to focus on a collision chamber and collided with helium at approximately 1 X 10^{-4} torr pressure. The product ions were separated by the electrostatic analyzer, yielding mass analyzed ion kinetic energy spectra, (MIKES). Structural information is markedly enhanced in the CID spectra (Fig. 1 and 2), which exhibit abundant sequence related ions. Furthermore, the differences observed between the CID spectra of these two isomers may be rationalized on the basis of the known structures. For example, the ion of m/z 729, which originates from the non-reducing terminus of the linear structure, can be formed by a simple bond cleavage, but requires multiple bond rupture and/or rearrangement in the case of the branched oligomer. Observed differences in the abundance of other fragments can be rationalized similarly. These preliminary experiments indicate that MS/MS-CID will be a powerful adjunct technique for elucidating the structure of complex carbohydrates.

*We wish to acknowledge the assistance of Dr. Ronald Hass in these endeavors, and Dr. Albert Wu, Texas A & M University for the gift of purified oligosaccharides.

(1.) McLafferty, F.W.; Bente, P.F.; Kornfeld, R.; Tsai, R.-C.; Howe, I., J. Am. Soc. 1973, 95, 2120.

Scheme 1.

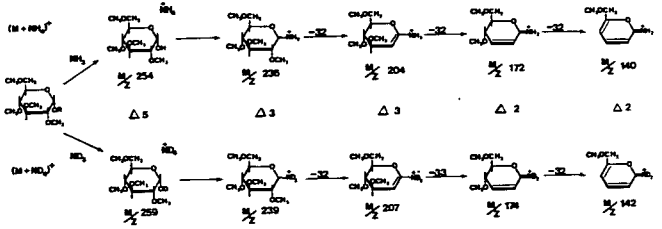

Figure 1.

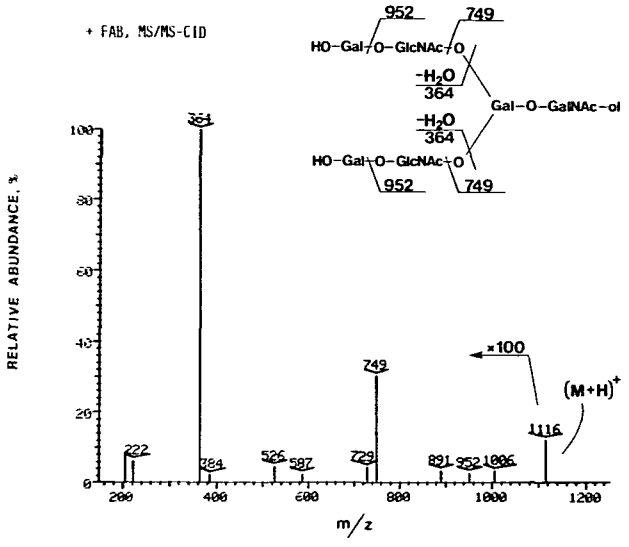

Figure 2.

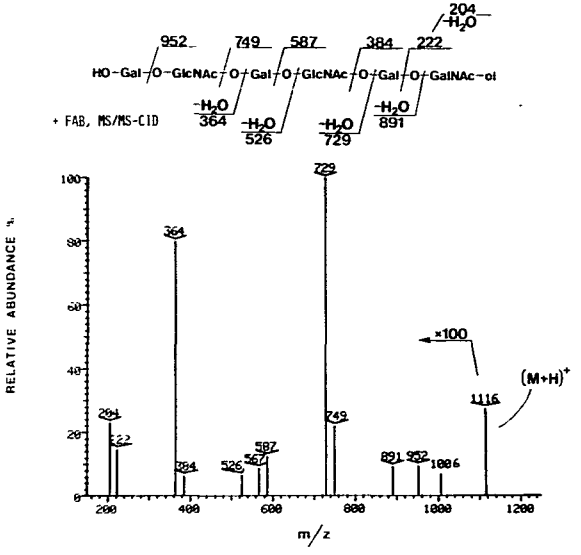

SEQUENCING OF BIOLOGICAL MOLECULES BY SIMS

David A. Kidwell, Mark M. Ross, and Richard J. Colton
Chemistry Division, Naval Research Laboratory
Washington, D.C. 20375

The sensitivity of SIMS for quaternary ammonium salts extends to the subnanogram range (1). Non-charged species are normally observed in SIMS as less intense protonated or cationized ions. The enhanced detection of charged over uncharged compounds forms the basis for a method of sequencing of biomolecules (2).

A peptide is selectively labeled at the N- or C-terminus with a charged group (Figure 1), partially cleaved, esterified and acylated, and the mixture examined by SIMS. Only the charged, labeled components in the mixture are observed. Since the charge is due to the label and the label is at only one end, the sequence of the peptide can be readily reconstructed. The spectra of two peptides sequenced from the N-terminus are show in Figure 2. Only low nanogram levels of each charged species are necessary for detection.

The C-terminus of the peptide was also labeled in one of two ways. The first method relies upon the spontaneous Oxygen to Nitrogen acyl rearrangement of acyl carbodiimides (3). These materials are formed by treating the peptide in aqueous media with charged carbodiimides, for example 1-(3-dimethylaminopropyl)-3-ethyl carbodiimide. The resultant derivatized peptides can be readily observed by SIMS. However, the observation of the complete peptide sequence with this derivative has been unsuccessful to date probably due to concurrent removal of the charged label during the amide backbone cleavage.

The second method of C-terminal derivatization relies upon the production of acyl hyrdazides using Carboxypeptidase Y. This enzyme will selectively add dimethyhydrazine to only the C-terminus of peptide esters (4). The acyl hydrazide then produced can be readily methylated using methyl iodide.

Our method of enhancing the emission of biological molecules by attaching charged groups has also been applied to oligosaccharides. Sugars are normally only observed with difficulty using SIMS (5). However, reducing sugars can be readily labeled in aqueous media with quaternary ammonium acylhydrazides (Girard's reagents). Once labeled, the sugars can be observed at 100 times lower concentrations than the corresponding underivatized materials (Figure 3).

Girard's reagents are preferred over the more commonly used 2-aminopyridines (6-7). The reactions are more facile and can be accomplished in aqueous media with few by-products. Besides the triethyl ammonium grouping shown in Figure 3, the commercially available Girard's Reagent P has also been employed. This reagent contains the pyridinium grouping which allows UV detection of the labeled sugars during isolation and purification.

References

1. S.E. Unger, T.M. Ryan and R.G. Cooks, Anal. Chim. Acta 1980, 118, 169.
2. D.A. Kidwell, M.M. Ross, and R.J. Colton, J. Am. Chem.. Soc. 1984, 106, 2219-20.
3. H.G. Khorna, Chem. Rev. 1953, 53, 145-166.
4. Z. You-Shang, Trends Bio. Sci. 1983, 16.
5. D. Zakett, A.E. Schoen and R.G. Cooks, presented at the 29th Annual Conference on Mass Spectrometry and Allied Topics; Minneapolis, MN, May 24-29, 1981.
6. V.N. Reinhold, E. Coles and S.A. Carr, J. Carbo. Chem. 1983, 2, 1-18.
7. S. Hase, T. Ikeenaka and Y. Matsushima, J. Biochem (Japan), 1981, 90, 407.

Figure 1

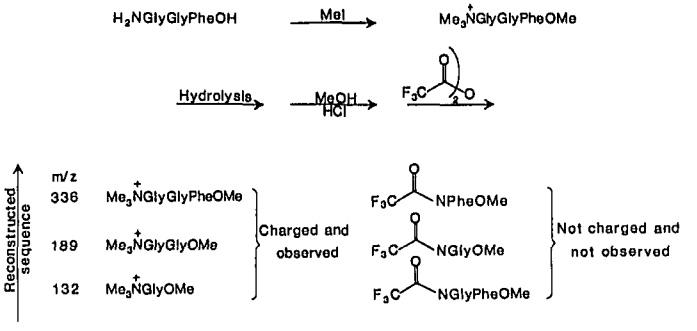

Figure 2

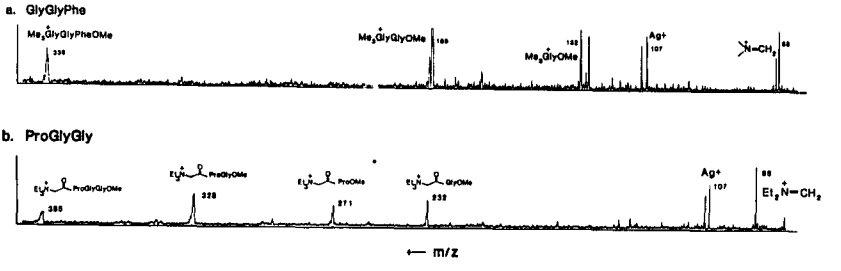

SIMS Spectra of Maltose and Derivatized Maltose

Figure 3

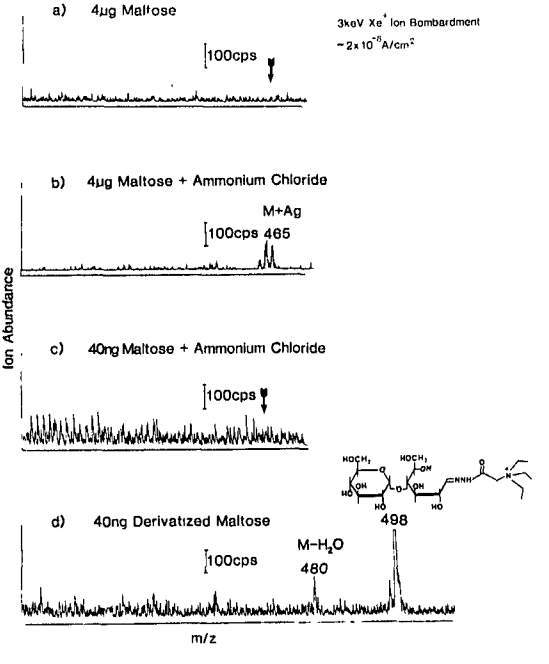

EVALUATION OF CYCLIC DI-t-BUTYLSILYLENE (DTBS) DERIVATIVES FOR GC-MS OF DIOLS AND RELATED COMPOUNDS

C.J.W. Brooks, W.J. Cole, and G.M. Barrett

Chemistry Department, University of Glasgow, Glasgow G12 8QQ, Scotland

The selective conversion of 1,2- and 1,3-diols into cyclic derivatives is of widespread utility in the characterisation of these and related compounds by GC-MS. While cyclic boronates[1] have proved exceptionally versatile in this respect, analogous silicon compounds have not found a comparable range of applications. The dimethylsilylene ("dimethylsiliconide") derivatives introduced by Kelly[2] have useful and distinctive properties in GC-MS, but are inconveniently susceptible to hydrolysis. The more stable tetraisopropyldisiloxane-1,3-diyl group developed by Markiewicz[3] (as a protecting group for nucleosides) confers a mass increment of 242 a.m.u. which would limit its value for GC. The di-t-butylsilylene (DTBS) derivatives introduced by Trost and Caldwell[4] combine the features of stability towards hydrolysis and a moderate mass increment (140 a.m.u.).

We have prepared DTBS derivatives of a range of more than 30 substrates (ca. 0.1-mg amounts) using Trost's conditions (based on di-t-butyldichlorosilane) or modified procedures. In most instances, formation of the cyclic derivatives was complete or nearly so. Diols containing a tertiary hydroxyl group failed to react. [A more powerful reagent, di-t-butylsilyl ditriflate, has been found effective by Corey and Hopkins[5] for some mono- and di-tertiary diols.] Even some disecondary diols exhibited steric effects: for example, methyl erythro-9,10-dihydroxystearate was only partially converted to the DTBS derivative under conditions that gave a quantitative yield from the threo isomer. Satisfactory derivatives were formed from 2- and 3-hydroxy acids.

The DTBS derivatives generally gave excellent gas chromatographic properties (Fig. 1), having retention indices (on OV-1 phase) approximately 300-500 units higher than the methaneboronates. Representative data are given in the Table.

The mass spectra of DTBS derivatives showed several characteristic features, as exemplified in the Table (cf. Fig. 2).

(i) Molecular ions were observed in most instances, but were in relatively low abundance except from some of the aromatic substrates.

(ii) In the absence of other strong fragmentation-directing groups, DTBS derivatives of diols RCH(OH)-CH(OH)R' gave major ions of types A ($[M-C_4H_9]^+$) and B ($[M-C_4H_9-C_3H_6]^+$) as denoted in the Table.

(iii) Ions resulting from alpha-cleavages, though not very abundant, were of diagnostic value in the derivatives of acyclic diols.

(iv) Ions formed by rearrangements involving loss of the elements of water, often from ions A or B as indicated by metastable data, were common features of the spectra.

(v) The catechol DTBS derivatives gave abundant molecular ions and distinctive ions at $[M-C_4H_8]^{+\cdot}$ and $[M-C_4H_8-C_3H_7]^+$.

In summary, the DTBS derivatives are readily obtainable on the analytical scale from unhindered 1,2- and 1,3-diols and from 2- and 3-hydroxy acids. Their GC-MS characteristics are potentially useful, and their known stability towards hydrolysis is advantageous. The use of more powerful reagents such as Corey's di-t-butylsilyl ditriflate would be expected to improve the convenience and generality of application of the DTBS derivatives.

1 C.J.W. Brooks & J. Watson, Chem. Comm. 1967, 952.
2 R.W. Kelly, Steroids 1969, 13, 507.
3 W.T. Markiewicz, J. Chem. Research (S) 1979, 24.
4 B.M. Trost & C.G. Caldwell, Tetrahedron Lett. 1981, 22, 4999.
5 E.J. Corey & P.B. Hopkins, Tetrahedron Lett. 1982, 23, 4871.

Table. Salient data for di-t-butylsilylene derivatives: relative abundances are for ions above m/z 50

Parent compound	I^{OV-1}	$M^{+\cdot}$ (%)	Base peak	Other major ions (%)
n-Dodecane-1,2-diol	2030[a]	342 (2)	A	B (79)*
2-Hydroxydodecanoic acid	2175[a]	356 (9)	C	A (44); D (12)*
Cyclododecane-cis-1,2-diol	2140[a]	340 (2)	A	B (94)*
1,2,3,4-Tetrahydronaphthalene-cis-1,2-diol	1890[b]	304 (10)	A	B (91)*
1,2,3,4-Tetrahydronaphthalene-(cis-2,3),5-triol	2200[a]	320 (3)	B	A (68)
3-Hydroxystearic acid	2800[c]	440 (1)	A	341 (21)*
Hexadecyl 1-glyceryl ether	2815[c]	456 (-)	175	A (34); 119 (22)
Hexadecyl 2-glyceryl ether	2855[c]	456 (-)	117	A (64); 159 (56)
Methyl erythro-9,10-dihydroxystearate	2750[c]	470 (-)	A	D (38)*; E (74)*
Naphthalene-1,2-diol	1915[b]	300 (100)	M	F (34)*; G (21)*

a: 190°; b: 170°; c: 235°
A: $[M-Bu^t]^+$
B: $[M-Bu^t-C_3H_6]^+$
C: $[M-Bu^t-CO_2]^+$
D: $[M-Bu^t-H_2O]^+$
E: $[M-Bu^t-MeOH]^+$
F: $[M-C_4H_8]^{+\cdot}$
G: $[M-C_4H_8-C_3H_7]^+$
*: metastable ions were observed

Figure 1

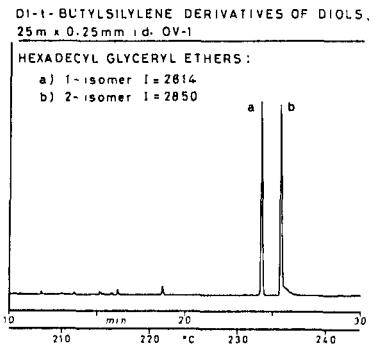

Figure 2

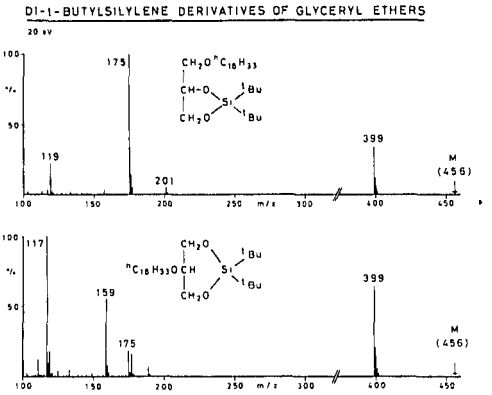

FABMS ANALYSIS OF BACTERIAL ANTIGENIC TREHALOSE-CONTAINING LIPOOLIGOSACCHARIDES

Ian Jardine, Gale Scanlan, Shirley Wu Hunter and Patrick J. Brennan
Dept. Pharmacology, Mayo Clinic, Rochester, MN 55905 and
Dept. Microbiology, Colorado State Univ., Fort Collins, CO 80523

A group of species-specific neutral lipooligosaccharide antigens from the Mycobacterium genus, which includes the pathogens M. tuberculosis and M. leprae, have been isolated. Both the native glycolipids and their inherent oligosaccharides have been purified and the major features of their unique structures determined.[1] They have a common tetraglucose core; β-D-Glcp-(1→3)-β-D-Glcp-(1→4)-α-D-Glcp-(1→1)-α-D-Glcp where Glcp is glucopyranose, distinguished by the presence of an α,α-trehalose substituent. Variable residues of xylose, 3-O-methylrhamnose, fucose and a novel N-acyl aminosugar, are linked to the core and the resulting oligosaccharides are acylated with 2,4-dimethyltetradecanoyl and acetyl functions to present a familial arrangement. A major uncertainty in the structural analysis of the deacylated lipooligosaccharides was in the size and sequence of the oligosaccharide chain. All of the oligosaccharides were therefore subjected to both positive (glycerol matrix) and negative (triethanolamine matrix) FABMS analysis with computer recording of the spectra to m/z 2200 (Kratos MS50/DS55). From the spectra recorded, the structures of the oligosaccharide chains were deduced or confirmed as $Xylose_{1and2}$-3-O-Me-Rhamnose-$Glucose_4$, and Aminosugar-Fucose-$Xylose_{4and6}$-3-O-Me-Rhamnose-$Glucose_4$.

The negative and positive FAB mass spectra of Aminosugar-Fucose-$Xylose_4$-3-O-Me-Rhamnose-$Glucose_4$ are illustrated in Figure 1 and 2, respectively. The negative ion spectrum was recorded from a triethanolamine matrix and the positive ion spectrum was recorded from a glycerol matrix. An intense $(M-H)^-$ ion is evident in the negative ion spectrum along with sequence ions which all contain the trehalose moiety. In contrast the positive ion spectrum contains an $(M+Na)^+$ ion with sequence fragments which retain the aminosugar moiety. That is, in this case, the spectra are neatly complementary.

The negative FAB mass spectrum of the largest oligosaccharide examined (Aminosugar-Fucose-$Xylose_6$-3-O-Me-Rhamnose-$Glucose_4$) obtained from a triethanolamine matrix is illustrated in Figure 3. A $(M-H)^-$ ion is present at m/z 2022 with an intense ^{13}C isotope ion at m/z 2023. Sequence specific fragment ions are indicated. A corresponding positive ion FAB mass spectrum could not be obtained for this molecule, illustrating the utility of the triethanolamine matrix in the negative ion FABMS mode for these underivatized oligosaccharides.

References

1. S. W. Hunter, R. C. Murphy, K. Clay, M. B. Goren and P. J. Brennan, J. Biol. Chem., 258:10481-10487, 1983.

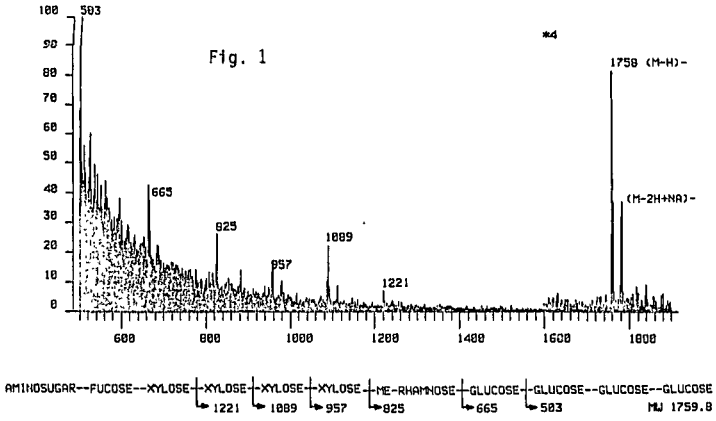
Fig. 1
*4
503
665
825
957
1089
1221
1758 (M-H)-
(M-2H+NA)-
AMINOSUGAR--FUCOSE--XYLOSE--XYLOSE--XYLOSE--XYLOSE--ME-RHAMNOSE--GLUCOSE--GLUCOSE--GLUCOSE--GLUCOSE
1221 1089 957 825 665 503
MW 1759.8

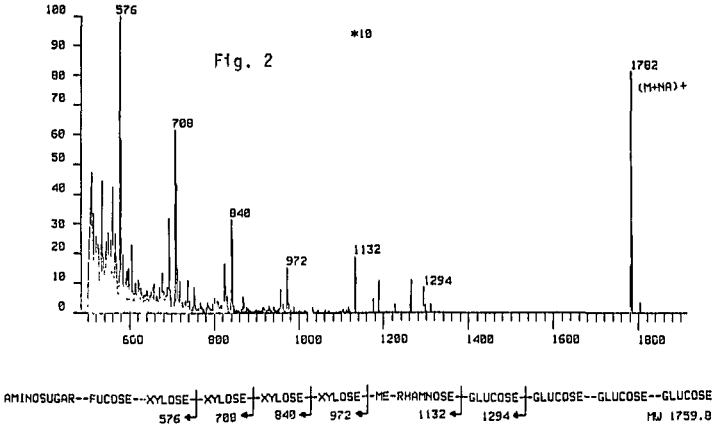
Fig. 2
*10
576
708
840
972
1132
1294
1702
(M+NA)+
AMINOSUGAR--FUCOSE--XYLOSE--XYLOSE--XYLOSE--XYLOSE--ME-RHAMNOSE--GLUCOSE--GLUCOSE--GLUCOSE--GLUCOSE
576 708 840 972 1132 1294
MW 1759.8

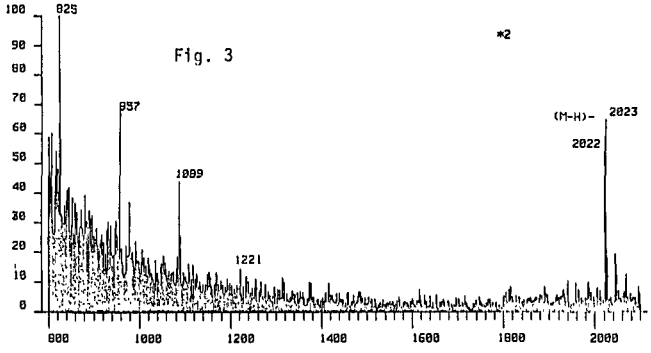
Fig. 3
*2
825
957
1089
1221
(M-H)-
2022
2023
AMINOSUGAR--FUCOSE--XYLOSE--XYLOSE--XYLOSE--XYLOSE--XYLOSE--XYLOSE--ME-RHAMNOSE--GLUCOSE--GLUCOSE--GLUCOSE--GLUCOSE
1221 1089 957 825 665 503
MW 2023.9

SPECIAL TECHNIQUES OF FAST ATOM BOMBARDMENT (FAB) MASS SPECTROMETRY FOR THE STUDY OF OLIGOSACCHARIDE ANTIBIOTICS: STRUCTURE OF KIJANIMICIN AND EVERNINOMICINS.

B.N. Pramanik, A.K. Ganguly, A.K. Mallams and O.Z. Sarre, Schering-Plough Corp., Bloomfield, N.J. 07003.

Kijanimicin and everninomicins are produced by microorganisms; everninomicins B, C, and D are highly active against gram positive bacteria while kijanimicin has antitumor activity and is active against P. acnes. Structural elucidation of these two classes of antibiotics were carried out in our laboratories[1,2] using chemical degradation, NMR and mass spectrometry. Using 252 Californium Plasma Desorption mass spectrometry, molecular ions of N-acetyl everninomicin D and methylkijanimicin were observed; however, the parent compounds everninomicin D and kijanimicin under similar conditions did not yield molecular ions.

Recently we have investigated the use of Fast Atom Bombardment (FAB) mass spectrometry for determining the molecular weights of everninomicin D and kijanimicin, their degradation products and also studied their fragmentation patterns. We wish to report the results of our studies.

In our present investigation we have used a FAB source (Ion Tech. Ltd.) on a Finnigan MAT 312 mass spectrometer employing xenon fast atoms and have noticed that the quality of the spectra depended on the solvents used for dissolving the compounds and also on the liquid used as a matrix. The best spectral data were obtained with a glycerol-thioglycerol mixture as a matrix and dimethyl sulphoxide as a solvent. The methylether (2) of kijanimicin showed an intense ion at m/z 1353 $(M+Na)^+$, while kijanimicin (1) itself displayed a strong ion at m/z 1339 $(M+Na)^+$. In both cases, ions corresponding to $(M+Na-16)^+$, $(M+Na-NO_2)^+$ and $(M+Na-HNO_2)^+$ were observed (see Figure 1). The loss of 16 AMU was found to correspond to the loss of an oxygen atom from the $-NO_2$ group (as determined for compound 3). The FAB spectrum of 17-O-β-D-kijanosylkijanolide (3) showed an intense ion at m/z 783 $(M+H)^+$, with fragment ions at m/z 767 $(M+H-16)^+$, 737, 553, 535, 517 and 499.

We have studied the FAB spectrum of kijanimicin mixed with ammonium chloride. This spectrum showed an $(M+Na)^+$ ion and a much more intense $(M+NH_4)^+$ ion.

We have also developed a simple technique that can provide additional information from FAB spectra of compounds expected to contain exchangeable hydrogens. By using deuterated glycerol as a matrix for recording the FAB spectra, we observed that the spectrum of compound (3) exhibited a series of new ions. Thus the ion at m/z 783 became 787, 767 became 771, 737 became 741, 553 became 557, 535 became 538, 517 became 519 and 499 became 500. This clearly indicated the maximum number of exchangeable hydrogens in both the molecular and fragment ions.

Everninomicins and their degradation products showed adduct ions $(M+H)^+$ and $(M+Na)^+$ of moderate intensity and also exhibited fragmentation patterns which provided valuable structural information. The FAB mass spectrum of (4) displayed ion at m/z 1570 $(M+Na)^+$ and contained two sets of fragment ions (from the cleavage of the center orthoester) which were easy to recognize (see Figure 2). One set (m/z 708, 674, 640 ...) is characterized by chlorine isotopes and the other set (m/z 841, 715, 555 ...) is free of chlorine. We have also noticed that fragment ions corresponding to the successive replacement of halogens by hydrogens are a characteristic of FAB spectra.

Using diethanolamine/triethanolamine as a matrix, we observed intense adduct ions corresponding to $(M+DEAH)^+/(M+TEAH)^+$ but only limited fragment ions.

Thus FAB mass spectrometry, using special techniques such as those described above, can afford molecular weight data as well as provide much useful structural information in highly complex, non-volatile molecules.

References

1. Mallams, A.K.; Puar, M.S.; Rossman, R.R.; McPhail, A.T.; Macfarlane, R.D. J. Am. Chem. Soc., 1981, 103, 3940.

2. Ganguly, A.K.; Sarre, O.Z.; Greeves, D.; Morton, J. J. Am. Chem. Soc., 1975, 97, 1982.

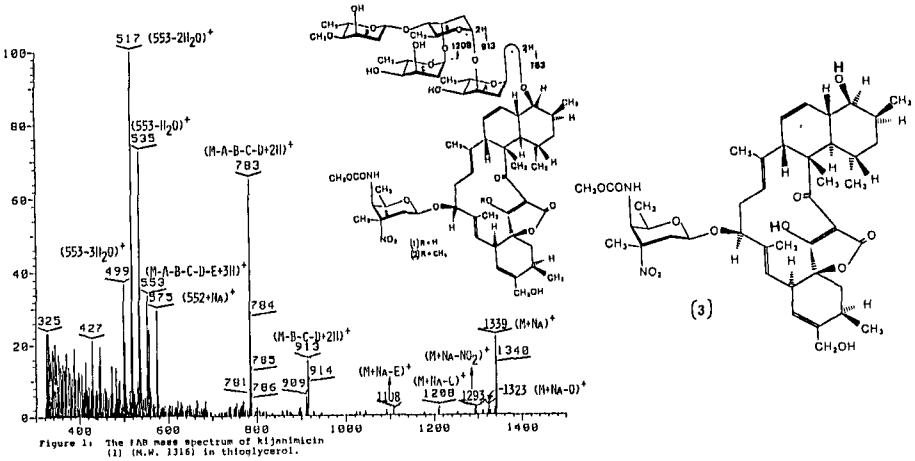

Figure 1: The FAB mass spectrum of kijanimicin (1) (M.W. 1316) in thioglycerol.

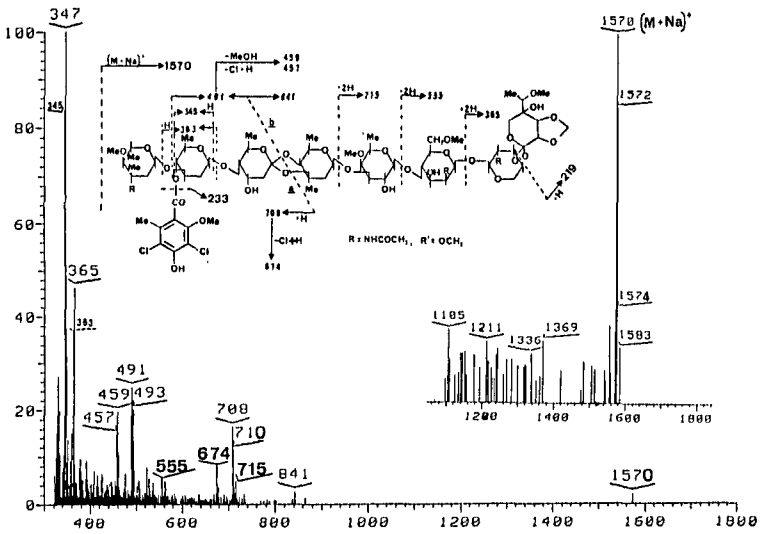

FIGURE 2. FAB Mass Spectrum of (4) N-acetyl everninomicin in glycerol/thioglycerol

MASS SPECTROMETRIC SEQUENCING OF MODIFIED NUCLEOTIDES AND OLIGONUCLEOTIDES

L. GROTJAHN

GBF (Gesellschaft für Biotechnologische Forschung mbH), Mascheroder Weg 1,
D - 3300 Braunschweig (Germany)

ATPαS is a suitable substrate for yeast phe-tRNA synthetase (1) and can therefore be used to determine the stereochemical course of the enzymatic reaction. The same reaction can be used to produce certain ^{18}O-labelled ATPαS compounds (2). Both, α^{18}OATPαS and αβ^{18}OATPαS, can be directly distinguished by negative-ion FAB mass spectroscopy. The negative-ion FAB mass spectra of ATPαS, αβ^{18}OATPαS and α^{18}OATPαS (Fig. 1) show, besides the deprotonated molecular ion at 522 d (unlabelled) and 524 d (^{18}O labelled), characteristic mono-, di- and triphosphate sequence ions. The characteristic sequence ions are accompanied by ions formed by loss of H_2O, $H_2{}^{18}O$ and H_2S, depending on the presence of the appropriate elements. To distinguish between the two ^{18}O labelled ATPαS species the diphosphate sequence ion, arising from the cleavage of P_α-$O_{\alpha,\beta}$ bond is of most interest. The breaking of this bond effectively separates oxygen atoms in the α-non-bridging and the α,β-bridging position.

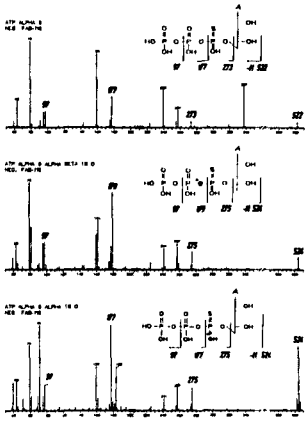

Fig. 1. Negative Ion FAB Mass Spectra of ATPαS, αβ^{18}OATPαS and α^{18}OATPαS.

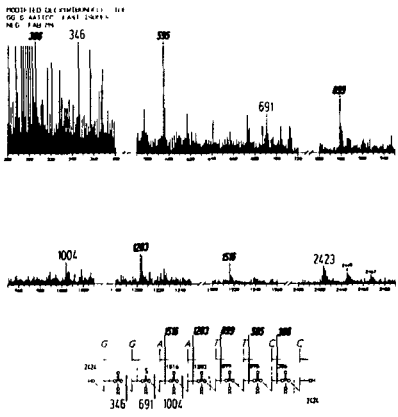

Fig. 2. Relevant Regions of the Negative Ion FAB Mass Spectrum of d(GGsAATTCC).

Nucleotide	Start signal of triphosphate sequence ion	Transition signals	Start signal of diphosphate sequence ion	Transition signals
ATPαS	273 d	255 d ($-H_2O$) 239 d ($-H_2S$)	177 d	159 d ($-H_2O$)
[α,β-^{18}O]ATPαS	275 d	257 d ($-H_2O$) 241 d ($-H_2S$)	179 d	161 d ($-H_2O$) 159 d ($-H_2{}^{18}O$)
[α-^{18}O]ATPαS	275 d	257 d ($-H_2O$) 255 d ($-H_2{}^{18}O$) 241 d ($-H_2S$)	177 d	159 d ($-H_2O$)

Table 1. Results of Linked Scan Mass Spectra of Tri- and Diphosphate Sequence Ions.

The analysis can be further refined by observing the linked scan B/E FAB mass spectra. Table 1. shows, that $\alpha\beta^{18}$OATPαS and α^{18}OATPαS can be unequivocally distinguished by observation of the tri- and diphosphate sequence ions by the linked scan method. $\alpha\beta^{18}$OATPαS loses $H_2{}^{18}O$ from the diphosphate but not from the triphosphate sequence ion, whereas the situation is reversed for α^{18}OATPαS. The linked scan approach needs about 100 nmol of nucleotide, compared with the 10 nmol needed for the normal FAB mass spectrum.

Negative-ion FAB mass spectroscopy was also used to characterise the synthetic octanucleotide, d(GGsAATTCC), containing the recognition sequence of the EcoR1 restriction endonuclease with a phosphorothioate internucleotidic linkage at the cleavage site. The mass spectrum is shown in Fig. 2. The background of the spectrum is higher than those of the unmodified octanucleotide (3,4). Nevertheless, the mass spectrum shows that the fragmentation pattern is fully compatible with the structure of the octamer being d(GGsAATTCC). Of particular importance is overlap for fragmentation from the 3'- and 5'-ends.

This analysis demonstrates, that FAB mass spectrometry can be successfully applied to the analysis of modified olignucleotides, particularly for those, where the phosphate group has been altered and rendered resistant to nucleases, situations where classical sequencing methods have so far failed.

REFERENCES:

(1) F. Eckstein, Angew. Chem. 95, 431 - 447 (1983)

(2) B.A. Conolly, F. Eckstein and L. Grotjahn, Biochem. in press

(3) B.A. Conolly, B.V.L. Potter, F. Eckstein, A. Pingoud and L. Grotjahn, Biochem. in press

(4) L. Grotjahn, R. Frank and H. Blöcker, Nucl. Acids Res. 10, 4671 - 4678 (1982).

CHARACTERIZATION OF COENZYME A AND ITS ACYL DERIVATIVES BY FAB-MS/MS. D.S. MILLINGTON and D.A. Maltby, Box 3028, Duke University Medical Center, Durham, NC 27710.

Many vital steps in intermediary metabolism require coenzyme A as a cofactor. These include the mitochondrial β-oxidation pathway for breakdown of fatty acids and most stages of the degradation of branched-chain amino acids (Leu, Ile, Val). An enzyme deficiency at any of these steps leads to the accumulation of abnormal metabolites that may be excreted as free acids, hence the term "organic aciduria" that has been applied to this group of metabolic disorders. In order to gain a better understanding of these disorders and to investigate new and more effective treatment strategies, methods for the direct analysis of the metabolic intermediates are being developed.

Fast atom bombardment (FAB) was applied to the analysis of coenzyme A and several available acyl derivatives. These included acetyl, propionyl, butyryl, isobutyryl, acetoacetyl, malonyl, succinyl and hydroxymethylglutaryl derivatives, having a molecular weight range from 809-911. Lithium was removed from the aqueous sample preparations using Dowex-50 ion-exchange resin and FAB analysis was performed in glycerol using xenon atoms at 6 KeV for ionization.

Free coenzyme A and all of the acyl derivatives exhibited useful FAB spectra in both the positive and negative modes of ion extraction and analysis. The main characteristics are shown in Figure 1, using propionyl-CoA as an example. The protonated molecular ion and ions due to cleavage at the adenosine diphosphate - pantothenic acid C-O bond are dominant and structurally significant features of the positive ion spectrum. The $(M-H)^-$ ion is the base peak above m/z 200 in the negative ion spectrum, but the fragmentation is more extensive and the overall sensitivity appears to be lower than for positive ions.

To detect and identify acyl-CoA compounds in a biological matrix, auxiliary techniques are required. A useful approach is the use of MS/MS on FAB-generated protonated molecular species. This strategy has been very effective in the analysis of the acylcarnitines[1], another family of polar metabolites of importance in metabolism.

Constant B/E ratio linked-scan spectra of the MH^+ ions from free coenzyme A, and its acetyl and propionyl derivatives are shown in Figure 2. These spectra contain dominant metastable daughter ion peaks corresponding to the same major cleavage ions observed in the normal FAB spectra. The characteristic ion bearing the acyl group is the base peak and has an extraordinarily high abundance relative to the MH^+ ion.

This new capability will facilitate the analysis of acyl-CoA compounds in biological samples and permit the investigation of metabolic pathways, enzyme activities and enzyme-substrate specificities in addition to enzyme kinetic studies previously described[2]. As an example, the transfer of acetyl and propionyl groups from CoA to carnitine has been investigated. Reaction of the acyl-CoA with the enzyme carnitine acetyltransferase in the presence of carnitine and other essential factors was carried out in aqueous glycerol on the FAB sample support. After 10 min at 37°, the acylcarnitine was unequivocally identified by the FAB-MS/MS technique described previously[1].

1. D.S. Millington, D.S. Maltby and C.R. Roe, Biomed Mass Spectrom 11, 236 (1984).
2. L.A. Smith and R.M. Caprioli, Biomed Mass Spectrom 10, 98 (1983).

Figure 1 PROPIONYL-COENZYME-A

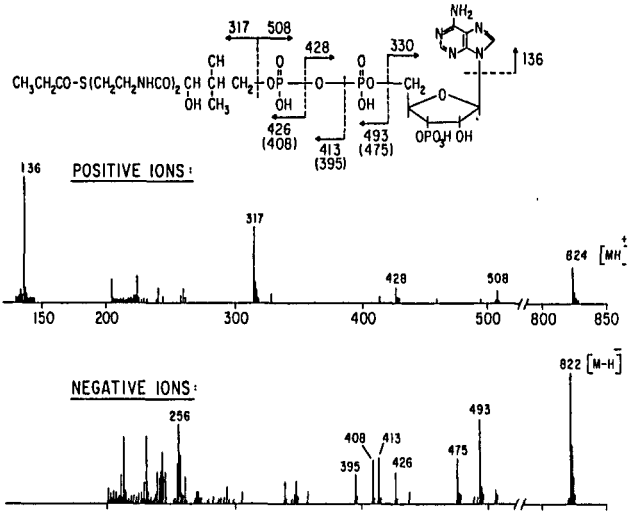

Figure 2 B/E LINKED SCAN SPECTRA OF CO-ENZYME A DERIVATIVES

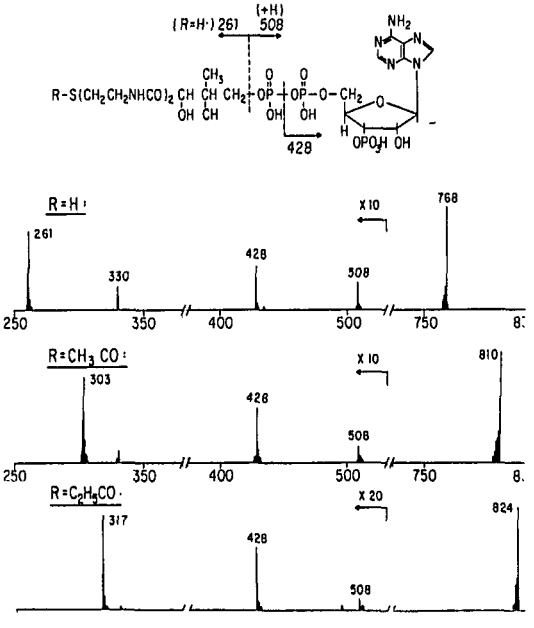

SAMPLE PREPARATION AND CAPILLARY GCMS IDENTIFICATION OF MODIFIED NUCLEOSIDES IN NORMAL HUMAN URINE, Robert G. Teece and Karl H. Schram, University of Arizona, College of Pharmacy, Tucson, AZ 85721

The urinary excretion of modified nucleosides has been found to be increased in certain neoplastic and immunodeficient disease states. Methods used to identify and quantitate these compounds in human urine has been primarily limited to HPLC. In an effort to provide increased specificity and sensitivity we have investigated the use of capillary GCMS for the analysis of modified nucleosides extracted from human urine. To our knowledge, this is the first report of the use of capillary GCMS in this manner.

Two approaches were pursued in preparing the urine sample for GCMS analysis. The first method utilizes a XAD-4 resin column to remove urinary salts and provide a quantitative extraction of nucleosides from urine. Prior to the XAD-4 extraction, the urine sample is prepared in the following manner. Ten milliters of urine is spiked with 5.0 ug of standard(s) and vortexed 1 min. A 1.0 ml aliquot of sample is removed and adjusted to pH 4 with 1.0 N HCOOH to protonate the organic acids. Ten milliters of EtOAc is added to the sample, vortexed 1 min, and then the EtOAc is aspirated from the aqueous layer along with soluable organic acids. The pH of the aqueous phase is readjusted to 8 with 0.25 M $(NH_4)_2CO_3$ and the sample is now applied to the top of a XAD-4 column (50 X 15 mm). The XAD-4 column is washed with 50 ml of distilled H_2O to remove the urinary salts. The column is then washed with 30 ml of MeOH to elute the nucleoside fraction. The MeOH fraction is collected and the organic phase is rotoevaporated leaving approx. 10 ml of residual H_2O in the sample. The desalted urine is lyophilized to dryness and then brought up in 5.0 ml of 0.25 M $(NH_4)_2CO_3$. The sample is now ready for the second approach which utilizes a phenylboronate column to complex cis diol groups and therefore separate base modified from sugar modified nucleosides. The sample is applied to a phenylboronate column (50 X 15 mm) and washed with 30 ml of 0.25 M $(NH_4)_2CO_3$. The $(NH_4)_2CO_3$ fraction is collected since it contains those nucleosides that do not have a free 2' and 3' cis diol group on the sugar moiety. The phenylboronate column is then washed with 0.1 N HCOOH to elute the base modified nucleosides. Both the $(NH_4)_2CO_3$ fraction and the HCOOH fraction are lyophilized to dryness and the TMS derivatives are formed by adding 40 ul BSTFA (1% TMCS) and 10 ul of pyridine. Gas phase analysis is possible after the samples are heated at 100° C for 1 h.

The extracted urine fractions are analyzed by capillary GCMS. An OV-1 WCOT capillary column (20 M) is used for separating the complex mixtures. A split ratio at the injection port of 20:1 is used along with a GC injection port temperature and GCMS interface temperature of 270°C. The column oven temperature is programmed from 120°C to 180°C at 10°/min. Electron impact MS is performed at 70 eV ionization voltage, 3 kV accelerating voltage and a source temperature of 250°C using a Varian Mat 311 A mass spectrometer. Mass spectral data is acquired and processed with a Varian SS200 data system. Acquisition parameters are from 60-700 amu at 2.5 sec/dec and interscan time of 0.5 sec.

At this point of our investigations we have identified 4 base modified nucleosides, namely, pseudouridine (Ψ), N^2-methylguanosine (M^2G), N^2,N^2-dimethylguanosine (M^2_2G), and 1-methylinosine (M^1I), from the XAD-4 fraction of normal human urine. Since no sugar modified nucleosides can be reported at this time from our from our laboratory, we have spiked a urine sample with a standard, 2'-O-methyladenosine (2'-MeA), and a deuterium labeled analog of this compound, 2'-O-methyl(d_3)adenosine (2'-Me(d_3)A), in order that we may demonstrate the utility of these methods. Figure 1 shows the RIC of a XAD-4/MeOH fraction of desalted urine and selected ions indicative of M^1I (M+, m/z 498), M^2G (M+, m/z 585), Ψ (M-15, m/z 589), and M^2_2G (M+, m/z 599). Figure 2 shows the RIC and selected ions of modified nucleosides found in the phenylboranate/$(NH_4)_2CO_3$ fraction. Note that in this fraction no ions are seen for the 2' and 3' cis diol containing compounds but 2'-MeA (M-15, m/z 482) and 2'-Me(d_3)A (M-15, m/z 485) are present. Figure 3 shows an extracted RIC of the phenylboronate/$(NH_4)_2CO_3$ fraction along with the retention time and mass spectrum of the mixture of these compounds. This example demonstrates the potential of using deuterium labeled modified nucleosides as internal standards for determining subnanogram

levels of modified nucleosides in urine if GCMS/MID experiments were performed. Figure 4 shows the RIC and selected ions of modified nucleosides found in the phenylboronate/HCOOH fraction. Note that in this fraction no ions are present for the sugar modified nucleosides but selected ions for ψ and M_2^2G are present. Figures 5 & 6 show the extracted RIC from the phenylboronate/HCOOH fraction and the retention times and mass spectra of ψ and M_2^2G, respectively.

In summary, this report has shown methods developed for the isolation and separation of base modified from sugar modified nucleosides from urine. In addition we have demonstrated the use of capillary chromatography for separating TMS derivatives of modified nucleosides from extracted urine. Finally, we have shown the potential of GCMS as a sensitive and highly specific analyzer that can be used to determine modified nucleosides in urine.

Fig 1.

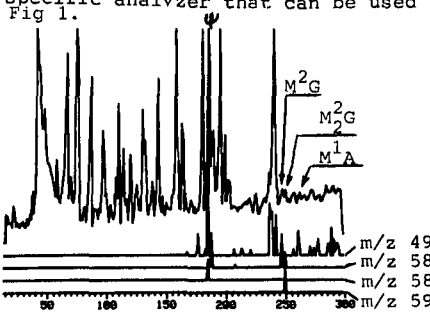

Fig 2.

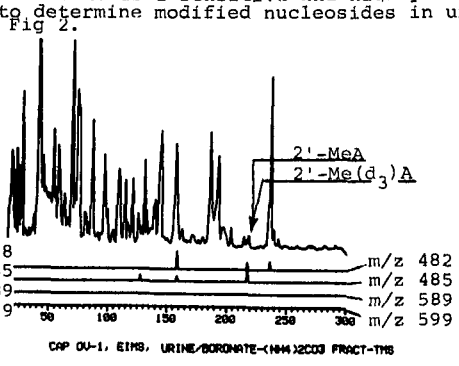

Fig 3.

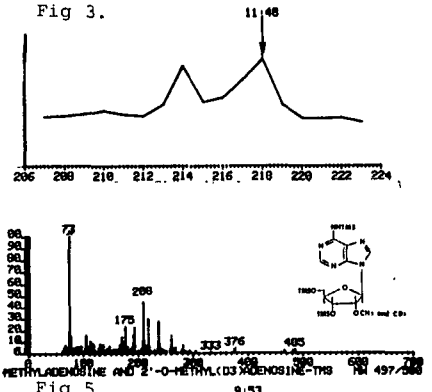

Fig 4.

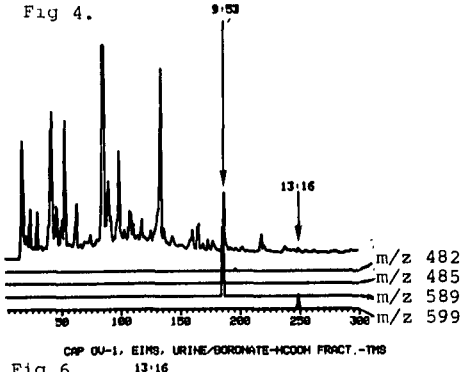

Fig 5.

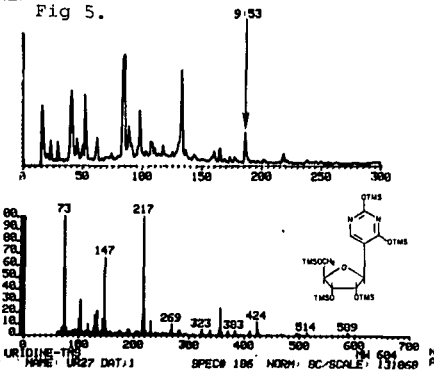

Fig 6.

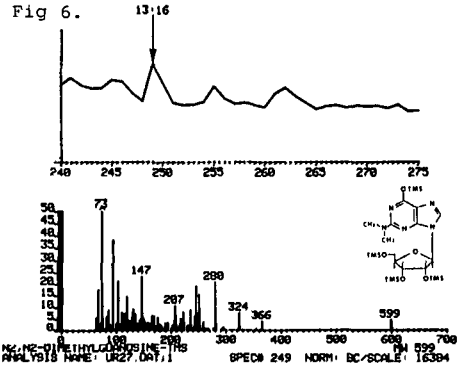

ANALYSIS OF PROTECTED AND UNPROTECTED NUCLEOTIDES BY FABMS

MARK E. HEMLING, J. CARTER COOK, KENNETH L. RINEHART, JR., and RICHARD I. GUMPORT

School of Chemical Sciences, University of Illinois at Urbana-Champaign, Urbana, Illinois 61801

WOLFGANG PFLEIDERER

Fakultät für Chemie, Universität Konstanz, Konstanz, West Germany

The ability to determine rapidly and accurately the structure of polynucleotides is of increasing importance to biochemists and bioengineers: DNA sequencing is an important method for the sequencing of proteins; biochemists synthesize and modify nucleotides for use as probes that will bind specifically to enzymes or regulatory proteins; and gene splicing to incorporate polynucleotides coded to synthesize products such as interferon is of great importance to bioengineers. The nearly exponential growth in the molecular biology and genetic engineering fields has left much room for improvements in the associated analytical techniques necessary to characterize these interesting new biomolecules. While biochemists working with DNA are able to sequence kilobases at a time using established techniques, synthetic biochemists have until recently found difficulty in the analysis of small polynucleotides. Synthetic nucleotides, requiring protection during chemical synthesis need to be deprotected before undergoing traditional chemical and enzymatic sequencing.

Mass spectrometry has made many strides in this area. FABMS has been used to provide bidirectional sequence information for oligodeoxyribonucleotides up to ten nucleotide units in length (1). SIMS has been used to investigate protected oligonucleotides (2). MS/MS has also been combined with FAB to look at the metastable and collisional activation spectra of zwitterionic oligonucleotide quasimolecular ions. Here we have studied protected and unprotected oligonucleotides to ascertain matrix requirements and compare the availability of sequence and structural information from the two groups.

The positive ion spectra of the protected nucleotides are relatively uninformative but do provide molecular weight information. They also show a peak for the monomethyoxytrityl (MMTr) protecting group. Addition of paratoluenesulfonic acid to the thioglycerol increases the intensity of the MMTr ion and the M + H - MMTr, either through chemical decomposition or by facilitating ion formation. Addition of acid provides no further information and in fact decreases sensitivity in the positive ion spectra of those compounds not containing the MMTr protecting group. The negative ion spectra of protected oligonucleotides, which also run best in thioglycerol, are considerably more informative. Ions can be assigned that will sequence the oligonucleotide from each end (e.g., spectrum of 9). Loss of up to three of the nitrophenylethyl protecting groups (pg) are also assigned to ions of diminishing intensity for the consecutive losses. B/E linked scans demonstrate that the main pathway for the formation of these multiple cleavage ions is stepwise from the respective sequence ions. Ions due to simultaneous cleavage from both ends of the molecule, which might confuse sequence assignments, are absent or extremely weak.

The unprotected oligonucleotides, which were analyzed as their triethylammonium salts, showed only extremely weak positive ion spectra in any of the matrices that were used. The negative ion spectra, which ran best in triethylenetetramine, were weaker than those of the protected oligonucleotides. They also show bidirectional sequence ions but, since only dimers have so far been studied, the possibility of nonsequence ions due to simultaneous cleavage from both ends could not be determined.

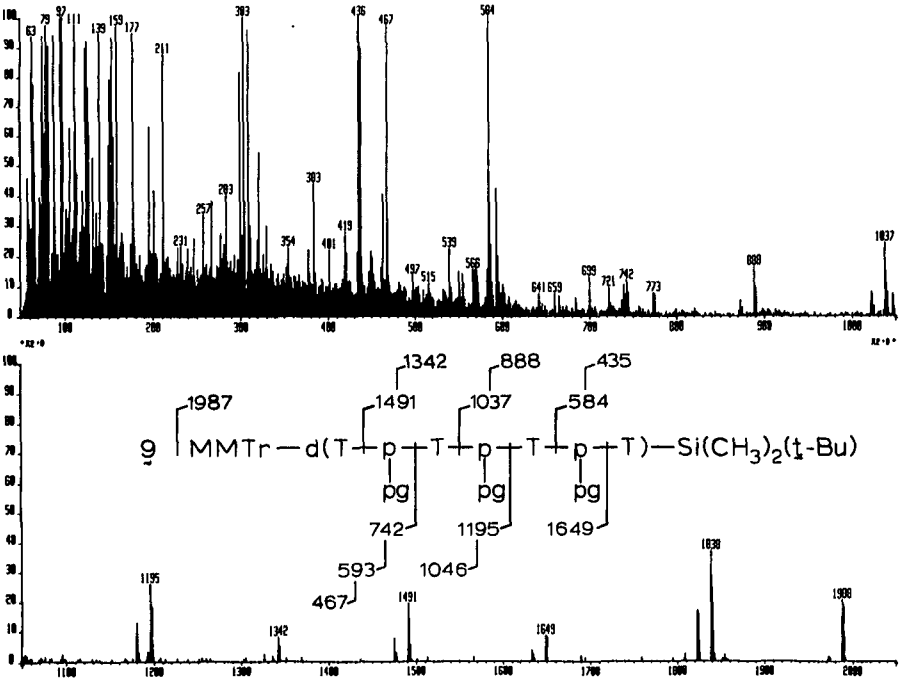

1) Grotjahn, L.; Frank, R.; Blöcker, H. Nucl. Acid Res. 1982, 10, 4671-4678.

2) Beavis, R.; Ens, W.; Nemer, M. J.; Ogilvie, K. K.; Standing, K. G.; Westmore, J. B. Int. J. Mass Spectrom. Ion Phys. 1983, 46, 475-478.

3) Panico, M.; Sindona, G.; Uccella, N. J. Am. Chem. Soc. 1983, 105, 5607-5610.

IN VITRO ALKYLATION OF CALF THYMUS DNA BY ACRYLONITRILE. ISOLATION OF *CYANOETHYL-ADDUCTS OF GUANINE AND THYMINE AND CARBOXYETHYL-ADDUCTS OF ADENINE AND CYTOSINE*

J.J. Solomon, I.L. Cote, K. Decker and A. Segal

Institute of Environmental Medicine, New York University Medical Center, New York, N.Y. 10016

Acrylonitrile (AN, CH_2=CH-C≡N) is used industrially in the manufacture of acrylic resins and fibers (~ 1.5 billion pounds in 1980) and OSHA estimates that about 278,000 workers are exposed. Animal bioassays have established the carcinogenicity of AN in the rat with exposure via inhalation or in the drinking water. In Sprague Dawley rats, tumors occurred at a variety of sites with the brain being the main target. A recent epidemiological study suggested an increased incidence in lung tumors in exposed workers. AN is a weak direct-acting mutagen with *E. coli* WP2 but requires activating enzymes with *S. typhimurium*. Because of its structural similarity to vinyl chloride, metabolism to an epoxide has been suggested as a mechanism for its carcinogenic action. To date the role of metabolism is unclear and attempts to find the epoxide adducts in DNA have been unsuccessful. The objective of this study was to see if AN could react directly with calf thymus DNA at physiological pH and temperature (via Michael addition across the double bond) and to characterize the adducts.

Marker compounds were prepared by reacting a saturated solution of AN (1.4 M) with 2'-deoxynucleosides at pH 7 and 37°C for up to 40 days. Direct cyanoethylation (CNE) was observed with thymidine (dThd) to form 3-CNE-dThd. Figure 1 shows the isobutane desorption chemical ionization (DCI) mass spectra of this adduct. Cyanoethylation of 2'-deoxyguanosine (dGuo) resulted in depurination to form 7-CNE-Gua (Figure 2A and 2B). The depurinated adduct 7-CNE-Gua was further cyanoethylated to form the highly polar betaine-like 7,9-bis-CNE-Gua which was identified by ^{252}Cf fission fragment ionization mass spectrometry, Figure 2D. Imidazole ring opening (IRO) of the bis adduct at pH 11 converted 7,9-bis-CNE-Gua to a less polar species which gave the mass spectra shown in Figure 2C. When AN was reacted with 2'-deoxyadenosine (dAdo) or 2'-deoxycytidine (dCyd) the cyanoethyl adducts were rapidly hydrolyzed to carboxyethyl (CE) adducts. Figure 3 gives the DCI spectra of 1-CE-dAdo (3A) and 3-CE-dCyd (3B) which pyrolyze under DCI conditions to form lactams. Derivatization with BSTFA was necessary to volatilize these species and prevent pyrolysis.

The carboxyethyl adducts resulted from initial cyanoethylation (slow) at a ring nitrogen adjacent to an exocyclic nitrogen followed by rapid hydrolysis of the nitrile moiety to a carboxylic acid. Figure 4 shows a possible cyclic 6-membered intermediate between nitrile carbon and the adjacent nitrogen which autocatalyzes the hydrolysis. Conversion of the adjacent exocyclic nitrogen to an oxygen (e.g. dAdo to 2'-deoxyinosine) resulted in a stable cyanoethyl adduct (1-CNE-dIno) shown in Figure 5.

AN was reacted for 40 days at physiological pH and temperature <u>in vitro</u> with calf thymus DNA. The adducts found after various hydrolysis procedures are given in Figure 6. The adducts 1-CE-Ade, N^6-CE-Ade and 3-CE-Cyt are identical to adducts we previously characterized as products of the <u>in vitro</u> reaction of the carcinogen β-propiolactone with calf thymus DNA. These results demonstrate that AN can directly alkylate calf thymus DNA at physiological pH and temperature by forming a mixed pattern of cyanoethyl and carboxyethyl adducts. Carboxyethylation results from slow cyanoethylation followed by rapid hydrolysis of the nitrile moiety to a carboxylic acid. This occurs with cyanoethylation of a ring nitrogen adjacent to an exocyclic nitrogen.

Supported by USPHS Grants ES 00260, ES 03043 and CA 13343.

Figure 1

CYANOETHYLATION OF THYMIDINE

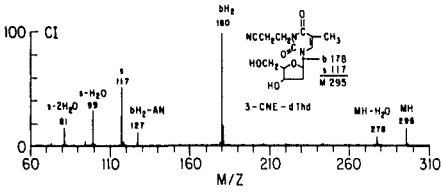

Figure 2

CYANOETHYLATION OF GUANINE

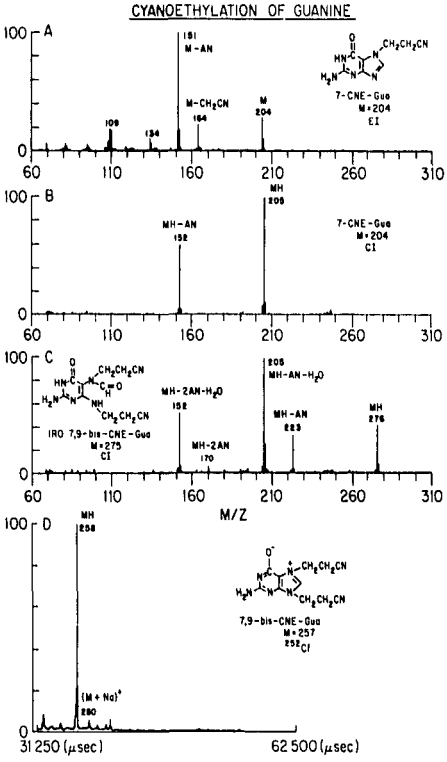

Figure 3

CARBOXYETHYLATION OF 2'-DEOXYADENOSINE AND 2'-DEOXYCYTIDINE DCI

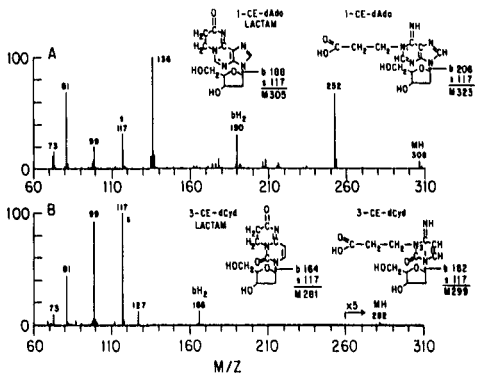

Figure 4

POSSIBLE CYCLIC 6-MEMBERED INTERMEDIATE

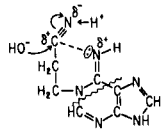

Polarization of nitrile group by electrons on adjacent exocyclic nitrogen autocatalyzes hydrolysis of CN to COOH

Figure 5

REPLACEMENT OF ADJACENT EXOCYCLIC AMINO WITH A CARBOXYL GROUP PREVENTS THE HYDROLYSIS

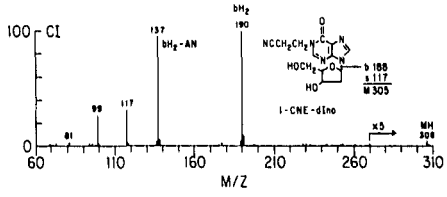

Figure 6

IN VITRO PRODUCTS OF AN WITH CALF THYMUS DNA

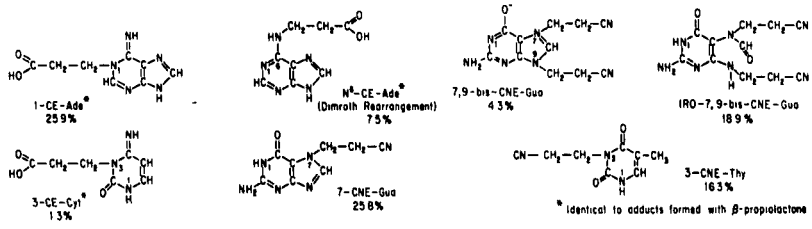

A NEW METHOD FOR ESTIMATING ISOTOPIC RATIOS FROM PULSE-COUNTING MASS SPECTROMETRIC DATA

Charles K. Bayne
Computer Sciences Division

David H. Smith
Analytical Chemistry Division

Oak Ridge National Laboratory,* Oak Ridge, TN 37831

The distribution of counts collected for any given peak in pulse-counting mass spectrometry has a Poisson distribution. A study of the probability distribution of ratios of two such peaks, necessary in isotope ratio mass spectrometry, has revealed that the distribution is not Poisson and cannot be approximated by a normal or any other well-known probability distribution. The probability distribution of the ratio of two Poisson counts is illustrated in Fig. 1 when the expected value of the numerator is five and of the denominator is twenty-five. From Fig 1, we note that the distribution of count ratios is nonsymmetric, skewed, and has non-monotonic probability values. Ratio values that are in the interior of the distribution and have a low probability of occurring are termed "inliers." This means that we can encounter inliers as well as outliers for isotopic ratio estimates. There are no methods presently available to detect inliers. Because of the unconventional characteristics of the probability distribution of count ratios, conventional statistical treatment of isotopic ratios such as calculating averages, standard deviations, and confidence intervals is invalid.

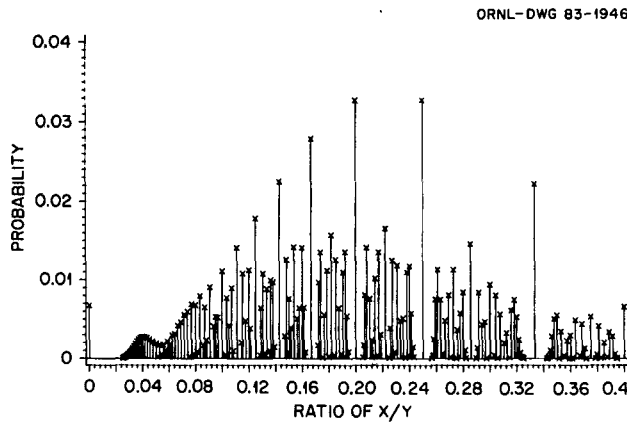

Fig. 1. Probability density function for the ratio of two Poisson variables (X/Y) with expected values of E(X) = 5 and E(Y) = 25.

An alternative method for estimating isotopic ratios is based on mathematical models that account for the sources of pulse-count data. The mathematical models contain parameters that represent the isotopic ratios and are estimated by a weighted nonlinear least squares algorithm. If Y(i) is a pulse-count datum adjusted for dead time and sweep factor in the i-th sample run, its distribution is:

$$Y(i) \sim P[F(\Theta)]$$

where $F(\Theta)$ represents the expected value of the pulse-count data as a function with parameter vector Θ. This expected value has the following form for the counts of the minor isotopes:

$$F(\Theta) = \text{background} + (\text{bias})(\text{run-effect})(\text{isotopic-effect}).$$

*Research sponsored by the U. S. Department of Energy, Office of Basic Energy Sciences, under Contract No. DE-AC05-84OR21400 with the Union Carbide Corporation.

where

background = exp[B(i)], represents background counts.
bias = bias factors.

run-effect = exp[R(i)], represents effects that vary from run to run, such as filament-source geometry, sample-filament chemistry, and filament temperature.

isotopic-effect = exp[I(k)], the effect due to the k-th minor isotope where the major isotope has an effect defined to be 1 and the minor isotopes are normalized to the major isotope. In other words, the minor isotopic effect is quantitatively a fraction of the abundance of the major isotope.

The form of F(Θ) for the background counts would only use the first term (i.e., background) and for major isotopic counts would not include the isotopic-effect term. Once the parameters (B(i)'s, R(i)'s, and I(k)'s) are estimated by iterative nonlinear least squares algorithm, the predicted counts can be calculated from the model.

Two diagnostic tools are available to identify outliers and to judge the suitability of the model. The first tool is the Freeman-Tukey (F-T) residuals (residual = observed - predicted) that are used to identify individual pulse count values as suspected outlier values. The F-T residuals are standardized to have an approximate normal distribution with zero mean and standard deviation of one. The second tool is the chi-square statistic that is used to judge both the appropriateness of the fitted model and removing suspected outliers.

A plot of F-T residuals versus sample run number can indicate suspected outlier counts. The expected values of the F-T residuals should fall between -2 and +2. Those F-T residual values outside these expected values are suspected to be outliers. Calculating the chi-square statistic before and after removing the suspected outliers can indicate a change in the goodness of fit and, therefore, the effect of the suspected data points. The pattern of the F-T residuals can also be used to indicate potential physical problems with the sample. For example, fractionation of a sample occurs when one or more of the isotopes has a higher volatility rate than other isotopes in the sample. F-T residual patterns for a limited number of examples with known fractionation problems have shown residual patterns that are easily identified.

The Poisson regression technique offers a theoretically more defensible method of estimating isotopic ratios than those conventionally used. This method offers additional information about the nature of the count data for background, minor isotopes, and major isotope for each sample run. Refinement of the model offers the possibility of correcting for fractionation and isobaric contaminants.

CHARACTERIZATION OF A PULSED GLOW DISCHARGE AS A SOLIDS IONIZATION SOURCE. P.J. Savickas and W.W. Harrison, Department of Chemistry, University of Virginia, Charlottesville, Virginia 22901.

A number of advantages are observed when pulsing a discharge, compared to dc operation. Higher current and higher voltage conditions existing during the pulse yield greater atomic and ionic populations of a cathode material. In addition, pulsed operation allows a more efficient use of the sample, particularly when coupled with other pulse-dependent methods, such as laser multiphoton ionization. We have examined in this study selected atomic, excited, and ionic states during the pulse and in the interval just after discharge termination in an attempt to explain certain observed phenomena. We have also determined to some extent the analytical utility of the pulsed discharge.

Experimental

Figure 1 shows a block diagram lay-out of the pulsed discharge system. The only significant difference from our dc scheme is the programmable power supply which is controlled by a pulse generator. Voltages to 3.5 KV and peak currents to 10 mA are used at repetition rates of 50 to 200 Hz and duty cycles of 25 -75%. The pulse generator also serves to trigger the ion counter processor for data accumulation.

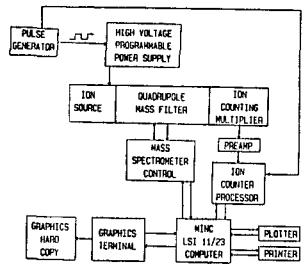

Figure 1. Solids mass spectrometer using a pulsed glow discharge.

Results and Discussion

The pulsed discharge gains a sputter advantage by virtue of the more energetic sputter projectiles (argon ions here) in the discharge. Thus, for the same number of sputter ions, compared with dc operation, a larger sputter yield is observed. Figure 2 shows a typical comparison. The larger atom population also leads logically to a larger ion population for trace element analysis, as shown in Figure 3.

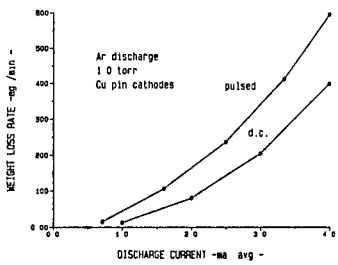

Figure 2. Sputter removal rate, dc vs. pulsed.

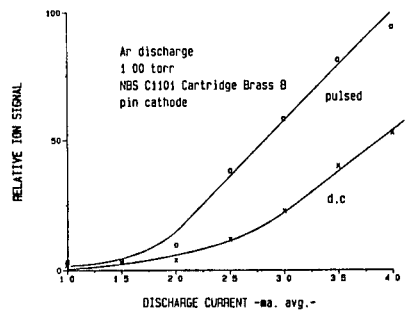

Figure 3. Ion signal, dc vs. pulsed.

We have examined standard reference materials by both dc and pulsed methods. Better sensitivity and enhancement of the sputtered species were found in pulsed operation. Figure 4 shows a low gain mass spectrum of brass to illustrate the copper to argon ratio attainable. Sub-ppm sensitivities were observed.

Figure 4. Pulsed glow discharge mass spectrum of brass. Argon: 1 torr. Current: 3mA.

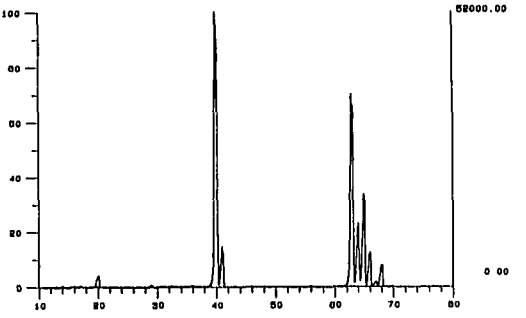

In the period after discharge pulse termination, we have followed the atomic and ionic signal to compare lifetime. Figure 5 demonstrates the much longer lifetime of the sputtered

Figure 5. Ion vs. atom lifetimes as measured after discharge termination.

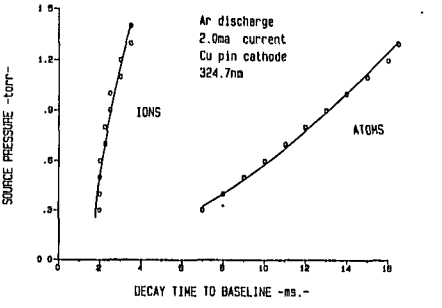

atoms. This has allowed us to carry out laser resonance ionization studies in a post-discharge regime uninfluenced by residual glow discharge ions.

AMERICIUM DETERMINATION USING AN ISOTOPE DILUTION MASS SPECTROMETRY TECHNIQUE

David W. Crawford, Colleen G. Cacic, and Richard D. Peavy* U.S. Department of Energy, New Brunswick Laboratory, 9800 South Cass Avenue, Argonne, IL 60439 *U.S. Department of Energy, Office of Safeguards and Security, Germantown, MD 20545

Americium-241, produced by the β-decay of plutonium-241, represents a significant impurity in plutonium materials, affecting the nuclear properties of the material, as well as measurements such as those for nuclear materials accountability. An isotope dilution mass spectrometry (IDMS) method offers some potential advantages over current methods for the determination of americium, including radiochemistry, nondestructive analysis, and wet chemical techniques. The effectiveness of this technique was demonstrated by comparing IDMS results for americium to the results of these other analytical techniques for americium-bearing samples, and comparing the precision and accuracy obtained by these different methods.

In order to perform IDMS measurements, a ^{243}Am calibrated spike material had to be prepared. IDMS using known quantities of ^{241}Am was used to calibrate an isotopically-pure (99.99%) ^{243}Am spike material. Preparation of americium calibration solutions was not necessary in order to make these measurements since corrections for fractionation need not be applied to ratios obtained when calibrating a spike with an isotope which will later be measured using the spike. (Any correction in the calibration of the spike will be applied reciprocally to the unknown isotope in the sample).

A paper published by Kirby and Sheehan of the Monsanto Research Corporation (Mound Laboratory) in 1983 provided information on the ^{241}Am content of three National Bureau of Standards (NBS) Plutonium Isotopic Standard Reference Materials (SRMs)[1]. The work described the analysis of ^{241}Am by α-spectrometry. These materials, containing large quantities of americium relative to the plutonium content, provided a good ^{241}Am source with well-documented ^{241}Am content data. NBS SRMs 946 and 947 were chosen to be used as the ^{241}Am "spike" for the characterization of two ^{243}Am spike solutions. Table I gives the ^{241}Am value for these two SRM's.

Table I

MOUND LABORATORY MEASURED AMERICIUM-241 CONTENT OF SELECTED NBS STANDARD REFERENCE MATERIALS (NBS SRMs)

NBS SRM	Am-241/Pu-239 (atom ppm)*	Am/Pu (g/g)**
946	23145±77 (0.33%)	0.021472 ±0.00007
947	27549±108 (0.42%)	0.023409 ±0.00010

*as of 09/30/82
**as of 04/05/84

Source: See Reference 1

Aliquots of the ^{241}Am "spikes" (NBS SRM 946 and 947) were mixed with aliquots of ^{243}Am and chemically purified by anion exchange to remove americium from its impurities, most notably the ^{241}Pu isotope, which is isobaric with the ^{241}Am isotope[2]. The purified americium solution was then analyzed by thermal ionization mass spectrometry.

Approximately 3 nanograms of americium was analyzed using a triple-filament assembly mount. The mass spectrometer was a 30-cm radius of curvature 90° magnet sector instrument with an ion current detection system and desktop computer for instrument control and data acquistion. Am^+ currents of 2-3 X 10^{-12} amperes were obtained which allowed for precise ratio measurements (<0.2%) to be made on peak heights of near equal intensities (low dynamic range) representing isotope ratios of near unity. During the analyses, the $^{239}Pu^+$ was monitored to insure that no significant $^{241}Pu^+$ was present to adversely bias the $^{241}Am^+$ measurement. When $^{239}Pu^+$ was identified to be present in the the spectrum, the $^{241}Pu^+$ in the mass-241 peak height (calculated from the $^{241}Pu/^{239}Pu$ ratio in the sample) was subtracted to yield a "plutonium-corrected" 241/243 ratio. This could be done automatically by the computer during data acquisition. Table II gives the results of the calibration of the ^{243}Am spikes using SRMs 946 and 947.

Table II
CALIBRATION OF AMERICIUM-243 SPIKES

Spike	Concentration µg ^{243}Am/g	RSD
A (calibrated using NBS SRM 946)	6.4221	0.068%
B (calibrated using NBS SRM 947)	7.7851	0.114%

Plutonium metal obtained from the Plutonium Metal Sample Exchange Program, a round-robin type analytical exchange program operated by Rockwell International (Rocky Flats), was analyzed by IDMS using Spike A. Since these samples were distributed to various laboratories and analyzed for Am content over a period of several years, a large amount of data on the Am content analyzed using different methods was available for comparison purposes. Table III, contains measurement results for these materials.

Table III
PU METALS EXCHANGE PROGRAM SAMPLES
NBS SRM 946 used for ^{243}Am spike calibration (Spike A)

METHOD -	LAB	"A" METAL Am (ppm)*	"A" METAL RSD	"B" METAL Am (ppm)*	"B" METAL RSD	"C" METAL Am (ppm)*	"C" METAL RSD
IDMS -	NBL	501.0	0.43%	761.8	0.37%	376.6	0.24%
Gamma Spectrometry	- A	494.3	-	780.0	7.9%	374.5	-
Radiochemistry	- B	452.3	6.0%	711.9	5.1%	323.7	2.3%
	- C	507.1	2.9%	764.4	0.9%	366.6	5.8%
	- D	516.0	2.2%	785.6	3.3%	380.2	2.9%
	- E	558.7	1.9%	823.5	1.7%	412.5	0.5%
Alpha Spectrometry	- F	542.6	1.8%	811.6	2.5%	403.9	-
Exchange Average		511.8		779.5		376.9	

*corrected for Am ingrowth and decay to 09/01/83

Another metal, NBS SRM 949f Plutonium Assay Metal, was assayed by IDMS using spike B. The IDMS value was compared to the Los Alamos National Laboratory (LANL) value measured by gamma spectrometry. Table IV contains measurement results for SRM 949f.

Table IV
NBS SRM 949f SAMPLES
NBS SRM 947 Used For ^{243}Am Spike Calibration (Spike B)

METHOD	PURIFIED METAL (purified 10 Jan 83) Am (ppm)*	PURIFIED METAL RSD	UNPURIFIED METAL Am (ppm)*	UNPURIFIED METAL RSD
IDMS - NBL	37.08	0.58%	126.31	0.28%
Gamma Spectrometry - LANL**	36.5	5.76%	125.8	5.76%

*Corrected for americium ingrowth and decay to 15 May 1984
**Calculated from unpurified data supplied by LANL (initial americium content on 1 Oct 1980 = 20.7 ppm)

The data presented demonstrate the highly sensitive and precise americium determination measurement obtained by the IDMS technique using nanogram samples sizes. It is evident that the precision of this technique greatly exceeds the precision of other more conventional methods. The experiment demonstrates that IDMS can provide a viable alternative to other technique for americium determination.

The determination of ^{241}Am by IDMS can also be used for the certification of ^{241}Am non-destructive assay calibration standards where gamma spectrometry is used to estimate the ^{241}Am contribution in calorimetric measurements of ^{239}Pu.

REFERENCES

1. H. W. Kirby, and W. E. Sheehan, "Determination of ^{238}Pu and ^{241}Am in ^{239}Pu by α-Spectrometry," Monsanto Research Corporation (Mound Laboratory), Miamisburg, Ohio (1983).

2. C. E. Pietri, B. P. Freeman, and J. R. Weiss, NBL-298, (1981).

INDUCTIVELY COUPLED PLASMA MASS SPECTROMETRY (ICP-MS): EFFECTS OF EXPERIMENTAL PARAMETERS ON ION ENERGY DISTRIBUTIONS.

José A. Olivares and Robert S. Houk
Ames Laboratory-USDOE and Department of Chemistry
Iowa State University, Ames, Iowa 50011

A study of the ion source in any mass spectrometer should include a thorough knowledge of the kinetic energy distributions of ions from the source. Specifically, the effect of source parameters on the energy distributions of sampled ions will give a better understanding of the effects of these parameters on signal and spectrometer resolution.

In an inductively coupled plasma mass spectrometer (ICP-MS)[1] the inductively coupled plasma (ICP) serves as an atmospheric pressure source of ions. These ions are sampled from the ICP through an orifice in a cone imbedded in the plasma. The ions expand with a supersonic jet into the high vacuum chamber where they are mass analyzed by a quadrupole mass spectrometer and detected. The ICP and ICP-MS interface comprise a complex and unconventional ion source where all the experimental parameters that directly affect the ICP and the ion sampling characteristics have a measurable effect on the ion energy distributions sampled.

Major differences between the above instrument and the one used in this study exist in the ion sampling interface where we now use a nickel sampling cone with a 0.5 mm sampling orifice followed by a stainless steel skimmer with a 1.2 mm diameter orifice. Both the sampler and skimmer were grounded. The area between the sampling cone and the skimmer is pumped (to ~1 Torr) by a mechanical pump. Furthermore for this study the normal ion lens was removed and the ions allowed to expand behind the skimmer, at ~10^{-4} Torr, for 10 cm before reaching the differential pumping plate and orifice that leads into the quadrupole and detector chamber (~10^{-5} Torr). This orifice is also the first ion lens. The entrance to the quadrupole is the second and last ion lens in this experiment.

The stopping energy curve for each ion with each plasma parameter was determined by applying a 0 - 50 V DC ramp to the quadrupole's rod bias. Thus the quadrupole served as a high pass energy filter as well as a mass analyzer. The signal from the electron multiplier was recorded by a signal averager after current-to-frequency conversion. The S-shaped curves obtained were background subtracted and the average ion energy, energy spread and maximum ion energy determined. All three ions studied (H_2O^+, Ar^+ and Co^+) showed similar trends and values for their ion energy distributions with similar changes in operating parameters. Furthermore the ion lenses used showed no apparent effect on ion energy in the negative voltage region where they normally operate.

Overall, a change in an experimental parameter which increased the ion energy distribution caused the signal to decrease. The effect on background was more complicated and not reported here. The effect on resolution was not severe since the ion energies remained below 30 eV in all cases, which was sufficient for unit mass resolution in a typical quadrupole.

The ion energy distributions did not change significantly whether nebulized water was present or absent in the central channel of the ICP. The aerosol gas flow rate had a severe effect on the ion energy causing the average ion energy to increase from 4 - 15 eV in the range of 0.4 - 0.6 L/min. The auxiliary gas flow rate also caused the average ion energy to increase, but slowly, from 4 - 8 eV in the range of 0 - 1.75 L/min. Increasing the plasma's outer gas flow rate and forward power caused the average ion energies to decrease slowly from 12 eV to 6 eV, in the operating range of 13 - 17 L/min and 0.8 - 1.5 kW respectively. Ion energy spreads and maxima also follow these trends.

When Ar^+ ions were sampled from the center of an ICP without aerosol carrier gas (i.e., no central channel), the average ion energy dropped to 2 eV and the energy spread to 2.5 eV. Furthermore, this energy distribution remained constant with increasing outer gas flow rate and forward power.

These results indicate that the introduction of water into the central channel of the ICP has little if any effect on the ion energy distribution from this source. On the other hand, the argon gas which punches the central channel through the ICP has a dramatic effect on the ion energy distribution. Parameters which directly affect the physical properties of this central channel indirectly affect the measured ion energy distributions leading to the results described above.

ACKNOWLEDGEMENT

Ames Laboratory is operated for the U.S. Department of Energy by Iowa State University under Contract No. W-7405-Eng-82. This research was supported by the Director for Energy

Research, Office of Basic Energy Science.

REFERENCES:

1. Houk, R. S.; Fassel, V. A.; Flesch, G. D.; Svec, H. J.; Gray, A. L.; Taylor, C. E. Anal. Chem. 1980, 52, 2283-2289.

ELEMENTAL DETECTION BY COMBINED MICROWAVE PLASMA-GC/MS; R. A. Heppner and D. W. Proctor; Western Research Institute, Box 3395, University Station; Laramie, WY 82071.

Elemental composition information for individual GC peaks can be very useful in the interpretation of complex GC/MS data. Several techniques are available for elemental detection with GC, but each has limited general applicability[1]. In this work a microwave plasma unit has been installed between the GC and the high resolution MS in a GC/MS system. For certain elements, the plasma and the MS function as a quantitative elemental detector system for the GC. The phenomena which make this possible is the nearly complete molecular dissociation which occurs for molecules in the plasma. This is followed by atomic recombination of the dissociated atoms into simple gas species. The species produced in the plasma are determined by the elemental composition of the molecules in the GC effluent (and not their structures) and by the compound used as a buffer gas specie. For example, with a high concentration of hydrogen buffer gas, carbon is primarily converted into CH_4, oxygen is converted into CO, nitrogen into HCN, and sulfur into H_2S and CS_2. Quantitative analysis of these gas species with the mass spectrometer provides elemental characterization of the GC effluent. The analysis was accomplished by measuring molecular ion intensities (and sensitivity coefficients) for each of the gas species listed above. Futher details on the GC/MS-microwave plasma technique may be found in the literature. [2-4]

The microwave plasma-GC/MS technique was applied to several fractions from a coal liquid produced in an underground coal gasification project. Figure 1 shows mass chromatograms at m/z=16.032 (CH_4), 27.011 (HCN), 27.995 (CO), 34 (H_2S), and 76 (CS_2) for the coal liquid base fraction. A comparison of the RIC with that of HCN shows that nearly every chromatographic peak contains nitrogen (except for the ether and acetone solvent peaks). This is expected because the base fraction is mainly composed of alkyl pyridine and alkyl quinoline type compounds. The CO distribution indicates that the principal oxygen containing species are the two solvent compounds. However, there is a low level of CO associated with non-oxygen containing species due to the residual oxygen background. The H_2S and CS_2 distributions indicate that several sulfur containing compounds are present in very low concentrations (the sulfur data was obtained with a factor of 450 sensitivity enhancement). Several of these compounds have been tentatively identified as alkyl benzothiazoles. Table I displays the elemental analysis information for several of the major chromatographic peaks in the base fraction. The measured C/N ratio is in good agreement with the chemical formula for each peak. The measured C/O ratio values are due to oxygen contamination of the buffer and GC carrier gases.

Table II summarizes the elemental analysis results for four fractions from the coal liquid sample. The numbers in parentheses represent measurements made with the GC/MS-microwave plasma technique, the other numbers result from conventional C,H,N and S combustion analysis (oxygen contribution was determined by difference). It is not possible to analyze for hydrogen with the GC/MS microwave plasma system when hydrogen is used as the buffer gas. To compare results from the two techniques, the carbon level measured by the microwave plasma system was set equal to that measured in the combustion analysis. This enables the N, O, and S concentrations to be directly compared (except for the polar aromatic fraction for which only microwave plasma measurements were available). The overall agreement between the two measurement sets is quite reasonable. The only significant discrepancy occurs for oxygen for which the volatile ether solvent caused problems with both techniques.

The GC/MS microwave plasma technique is not limited to use with a high resolution mass spectrometer. Detection of species other than CO is almost unaffected by the change from high to low resolution. In a low resolution instrument, CO and background N_2 are superposed at m/z=28. This results in reduced S/N ratio for oxygen detection (a reduction factor of 2 to 3 for this work).

(1) Farwell, S. O.; Gage, D. R.; Kagel, R. A.; J. Chromatogr. Sci. 1981, 19, 358-376.
(2) Freudenthal, J.; Intern. J. Environ. Anal. Chem. 1978, 5, 311-321.
(3) Heppner, Richard A.; Anal. Chem. 1983, 55, 2170-2174.
(4) Markey, Sanford P.; Abramson, Fred P. Anal. Chem. 1982, 54, 2375-2376.

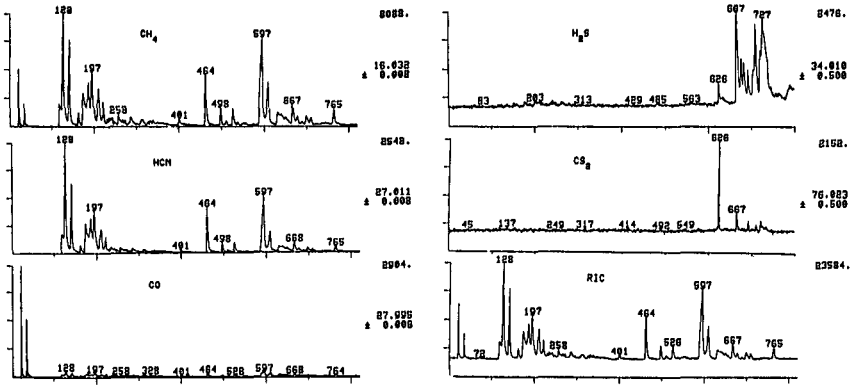

Figure 1. Mass Chromatograms for the Coal Liquid Base Fraction.

Table I.

Coal Liquid Base Fraction

Measured Element Ratios for Major Chromatographic Peaks

Scan No.	Compound	C/O	C/N	C/S
127	C_7H_9N	117	5.8	*
142	$C_8H_{11}N$	70	7.3	*
197	$C_8H_{11}N$	89	8.0	*
211	$C_8H_{11}N$	66	8.1	*
465	$C_6H_5NH_2$	59	6.7	*
593	C_9H_7N	62	8.7	*
610	$C_{10}H_9N$	61	10.9	*

Table II.

Elemental Analysis of Coal Liquid Fractions

(Wt. Percent)

Fraction	C	H	N	O	S
Base	76.4	7.3	11.3 (10.1)	5.0 (2.8)	0.2 (0.1)
Weak Acid	69.9	10.3	0.2 (0.1)	19.6 (16.8)	0.1 (---)
Aromatic	89.3	7.4	0.2 (0.1)	2.6 (3.4)	0.5 (0.9)
Polar Aromatic			(0.4)	(7.1)	(0.1)

GLOW DISCHARGE ATOMIZATION SOURCE FOR RESONANCE IONIZATION MASS SPECTROMETRY, K.R. Hess, P.J. Savickas, and W.W. Harrison, Department of Chemistry, University of Virginia, Charlottesville, VA 22901.

The pin cathode glow discharge is used in our laboratory as an atomization/ionization source for a variety of applications, including solids mass spectrometry. In an effort to improve sensitivity and selectivity, we have coupled the output of a tunable dye laser to the system for use in resonance ionization. Potassium, copper, chromium, and iron have been atomized by the discharge and resonantly ionized to produce mass spectra free from isobaric interferences.

Experimental

Figure 1 shows the glow discharge source with quadrupole mass spectrometer system.

Fig. 1:
- A. Pin Cathode
- B. Glow Region
- C. Lens System
- D. Energy Analyzer
- E. Quadrupole
- F. Gate Valve
- G. Lens Feed Through
- H. Ion Exit Orifice

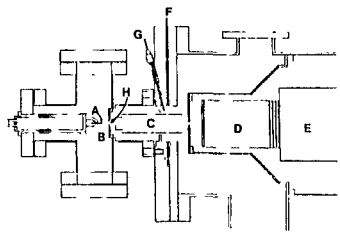

The cathodes were machined from materials of analytical interest to form pins 1.7 mm x 5 mm, except in the case of potassium where potassium chloride was mixed with graphite matrix and pressed into the pin form. The discharge was operated with argon fill gas at pressures of 0.1 - 1.0 torr, 300 - 600 V, and 1 - 5 mA.

A Lumonics TE-860-4 excimer laser with XeCl pumped a Lumonics 330 dye laser which in turn was directed through an Inrad 5 - 12 frequency doubler. The output beam was focused to 1 mm directly in front of the ion exit orifice.

Data were taken with a Princeton Applied Research Model 1112 ion counter/processor operating in its subtracting mode. A data gate was set to cover the signal produced during the laser pulse, consisting of both laser ionization and discharge ionization. The discharge ions, existing as a steady state background, were subtracted out by a second data gate prior to the next laser pulse. A DEC MINC-11 microcomputer controlled the mass scanning, data accumulation, and presentation.

Results and Discussion

Wavelength ionization spectra have been obtained for potassium, copper, chromium, and iron. An example of these spectra is shown in Figure 2.

Fig. 2: ^{56}Fe RIMS Wavelength Spectra

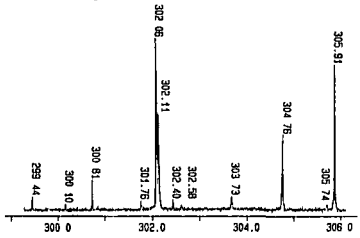

From these spectra it is seen that the atomic population in the discharge exists primarily in ground state or near ground state energy levels. The highest level observed is 0.86 eV above ground, at 305.74 nm. The remainder of the transitions originate from 0.12 eV or below. All lines in this region have been tabulated and correspond to known transitions.

Figures 3 and 4 illustrate the ability of resonance ionization to remove potential isobaric interferences. Figure 3 is a glow discharge mass spectrum of NBS reference material #443. Figure 4 is a laser produced spectrum of this same material generated by tuning the laser to the iron line at 302.06 nm, using the background subtract mode to cancel discharge produced ions. As can be seen, only the iron isotopes remain. Interferences, such as the ^{54}Cr, have been removed from the iron peaks.

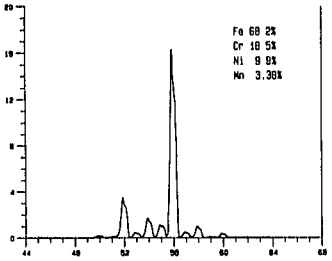

Fig. 3

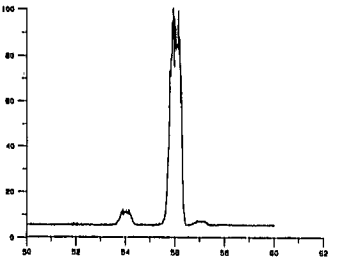

Fig. 4

Investigations continue into maximizing the laser produced signal and novel ways of separating the laser and discharge signals. A pulsed discharge for pulsed atomization is also being investigated in an effort to increase sample utilization and as a method to generate higher sputtered atom populations for the same average current. The combination of glow discharge atomization with laser ionization has been shown to provide a selective method for the direct analysis of solids by mass spectrometry.

"The Production and Provisional Certification of an Equal Atom Plutonium Isotopic Standard"

C. G. Cacic, D. W. Crawford and L. A. Machlan*

U.S. Department of Energy
New Brunswick Laboratory
Argonne, IL 60439

*National Bureau of Standards
Center for Analytical Chemistry
Inorganic Analytical Research Division
Washington, D.C. 20234

The New Brunswick Laboratory (NBL), in joint cooperation with the National Bureau of Standards (NBS), has produced an equal atom $^{239}Pu/^{242}Pu$ isotopic standard, NBL Certified Reference Material (CRM) 128. Provisional certification of the material relative to uranium has been completed. NBL will perform absolute certification of the standard based on mass spectrometric bias measurements determined by the analysis of calibration solutions of accurately known plutonium isotopic ratios. Certification on an absolute basis will allow the nuclear community to measure accurate plutonium isotope ratios relative to plutonium.

Details concerning the CRM 128 certification plan and NBL's work on highly precise mass spectrometric, and chemical assay methods for plutonium have previously been described.[1] Work on the reference material began with dissolution of isotopically pure (99.9%) ^{239}Pu metal and ^{242}Pu oxide. The resulting solutions were analyzed for elemental impurities both before and after anion exchange purification. Total impurities were ~ 300 ppm, consisting mainly of Al, Fe, K, Ni, S and Th. Portions of NBS SRM 947 plutonium isotopic standard were mixed with up to 2.5 times the maximum amount of impurities found in CRM 128. Analysis of these SRM 947 samples by thermal ionization mass spectrometry indicated that impurity levels several times greater than those found in CRM 128 have no significant effect on the measurement precision of the material.

Weighed portions of the separated isotopes were then mixed to yield the CRM 128 equal atom master solution. The master solution was treated with H_2O_2 to achieve isotopic equilibration between the ^{239}Pu and the ^{242}Pu prior to aliquotting the individual units of the CRM. Each of the nearly 1,000 units of CRM 128 contains approximately 1 mg of total Pu, as the dried nitrate, stored in a 30cm^3 Teflon bottle.

NBL performed a study to determine the effects of sample preparation, filament loading and sample burn temperature on CRM 128 isotopic analysis. Sample preparation was studied through dissolution of one unit of CRM 128 in 1 N HNO_3 and isotopic analysis of aliquots (1) with no pretreatment, (2) following ion exchange and (3) following H_2O_2 equilibration and ion exchange. Results indicated no statistically significant difference between any of the three groups of aliquots. Initial filament loading studies attempted to reproduce a value of 100 ng of plutonium per filament. However, due to slight differences in solution concentrations a mean value of 85 ng ±15-20% was actually observed. These variations in sample size caused a significant difference, on the order of ±0.03% at the 95% confidence interval, in the measured $^{242}Pu/^{239}Pu$ ratio. More stringent process controls were used to achieve a mean filament loading of 100 ng ±5% during provisional certification work. Operation at sample burn temperatures of ~ 800°C and ~ 1100°C, as measured using an optical pyrometer, showed no variation in internal precision of the measured ratios, ±0.02% at the 95% confidence interval. Expected lower bias corrections were observed when using the higher temperature analysis method, as indicated by the larger uncorrected ratio, 0.99897, as compared to the lower temperature ratio of 0.99843. Based on this study, selected CRM 128 units were dissolved in 1 N HNO_3 and provisional certification measurements were made using 100 ng filament loadings operating at a sample burn temperature of ~ 1100°C.

The interim certification plan required analysis of 8 units of CRM 128, 3 analyses per unit, with concurrent analysis of 3 units of NBS SRM 947, 9 analyses per unit. Table 1 lists the provisional certification data for CRM 128 as validated by NBS SRM 947.

Table 1 CRM 128 Interim Certification

	Ratio	RSD	95% Confidence Interval	D.F.	N
CRM 128 (Raw $^{242}Pu/^{239}Pu$)	0.998507	0.026%	0.011%	23	24
NBS SRM 947 (Raw $^{240}Pu/^{239}Pu$)	0.241139	0.029%	0.012%	25	26
CRM 128 (Corrected $^{242}Pu/^{239}Pu$)	1.001384	0.091%*	0.033%	30	-

*RSD approximated using the formula:

$$\text{RSD (128-Cor)}^2 = \text{RSD (128-Raw)}^2 + [\text{RSD (947)} \cdot \Delta \text{ Mass (128)}/\Delta \text{ Mass (947)}]^2$$
$$= 0.026^2 + (0.029 \cdot 3.00659/1.00165)^2 = 0.091^2$$

Thus, the certified $^{242}Pu/^{239}Pu$ ratio of CRM 128 as measured relative to uranium is 1.001384 ± 0.091%. NBL recommends dissolution of the CRM in dilute acid (e.g. - 1N HNO_3) with no further treatment prior to mass spectrometric analysis. The calculated ^{241}Am in-growth is 18 ppm/year and total elemental impurities are ~ 300 ppm. The CRM will be available for distribution following completion of the written certificate and cost analysis, currently estimated by the end of FY84.

REFERENCES

1. Cacic, C. G. and Crawford, D. W., Proceeding of 31st Annual Conference on Mass Spectrometry and Allied Topics , Boston, Massachusetts, May 8-13, 1983, p. 846.

SEPARATION AND MASS SPECTROMETRY OF Nd, Pu AND U FROM U AND (U,Pu) FUELS.

L.W. Green and N.L. Elliot, Atomic Energy of Canada Limited Research Company, Chalk River Nuclear Laboratories, Chalk River, Ontario, KOJ 1JO

In the development of nuclear fuels, isotopic and elemental analyses for the actinides and some fission products are frequently required to assess the performance of the fuels. Analysis methods until recently involved time-consuming hot-cell separations, and limited the rate of data collection. The introduction of the resin bead technique over the past ten years offered a substantial simplification and time saving for U and Pu analyses (1-3). This paper describes an extension of the resin bead procedure that is applicable to a wider range of fuels and provides a more complete separation of U and Pu from the fission products. For Nd, a method that uses high performance liquid chromatography (HPLC) on a dynamically coated reversed phase is described.

The bead-disk procedure previously reported (4) for use with $(Th,U)O_2$ fuels was investigated for Pu and U. In this procedure, Pu(IV) and U(VI) are sorbed from the fuel solution into a tributylphosphate (TBP) impregnated resin bead after adjustment of the acid composition to yield a good separation and an appropriate Pu/U ratio. After equilibration, Pu(IV) and U(VI) are back-extracted into a small volume of HNO_3 solution and nanogram quantities are adsorbed onto 1 mm diameter anion-exchange disks.

Distribution coefficients (D) were determined by the radiotracer method for both Pu(IV) and U(VI) on the beads and disks in a range of HNO_3 and HF/HNO_3 solutions to enable selection of appropriate conditions for the equilibrations. Results for the TBP impregnated resin bead are shown in Figures 1 and 2; similar curves were obtained for the anion-exchange disks except that at maximum D_U was only 5.5 whereas D_{Pu} was 200. The large reduction in D_{Pu} observed when HF was added was likely due to strong complexation of Pu(IV) by the fluoride ion.

The conditions chosen for an isotopically natural UO_2 fuel irradiated to ~ 1% fission were as follows: ~ 4 mg/mL fuel in 0.015 M HF/6M HNO_3 for equilibration with a TBP-impregnated bead and 300 µL of 7M HNO_3 for back-extraction and equilibration with an anion-exchange disk. This yielded 1-2 ng of Pu and 20-30 ng of U per disk. One disk was placed on a rhenium ionizing filament and Pu was measured at 1550°C and U at 1700°C.

For equilibration of sample and spike and to ensure reproducible Pu extractions, Pu had to be completely converted to Pu(IV) prior to the bead-disk equilibrations. For this purpose the procedure of Marsh et al. (5) was used. Analyses of a combined Pu-U standard showed that good signals and accurate results (within .2%) were obtained. Work is currently in progress to demonstrate the overall precision for fuel samples.

To separate Nd, an HPLC technique previously used (6) for La determinations was chosen. In this technique a Supelcosil LC-18 column packed with 5 µm diameter reversed phase particles was used as the stationary phase; the particles were dynamically coated with 1-octanesulfonate during the analysis. Uranium and the fission products were eluted with α-hydroxyisobutyric acid on a gradient from 0.1 to 0.4 M over 12 min. As shown in Figure 3, the major lanthanides were well separated from U and other fission products; Nd eluted at ~ 8 min.

Separation of Nd from a fuel sample proceeded as follows: the fuel solution was diluted to ~ 20 µg Nd/g, sample and spike (^{150}Nd) were equilibrated, 100 µL was injected into the HPLC, Nd was collected in a 1 mL fraction, and 5 µL of this fraction was deposited on the side filaments of a triple filament assembly. The effect of the mobile phase on signal quality was examined and a slight enhancement in signal strength and stability was observed relative to loadings from HNO_3 solutions.

Tests were conducted to determine whether there were significant isotopic fractionation and run-to-run cross contamination with the HPLC; results showed negligible effects in both cases. Replicate analysis through the entire procedure demonstrated a precision of 0.2% for Nd determinations by isotope dilution mass spectrometry.

An important feature of the procedure is that Nd, Pu and U can be loaded on the same triple filament assembly; Nd is deposited on the side filaments and then Pu and U on the

centre. Pu and U are measured first, then the centre filament temperature is raised to 1950°C and the side filaments are turned on for Nd measurements. At 1950°C the disk and the Pu and U rapidly burn off and have no effect on Nd signals.

REFERENCES

(1) R.L. Walker, R.E. Eby, C.A. Pritchard, J.A. Carter, Anal. Lett., 7 (8&9), (1974) 563-574.
(2) D.H. Smith, R.L. Walker, J.A. Carter, Anal. Chem., 54, (1982) 827A-832A.
(3) J.D. Fassett and W.R. Kelly, Anal. Chem. 56, (1984) 550-556.
(4) L.W. Green, N.L. Elliot, T.H. Longhurst, Anal. Chem. 55, (1983) 2394-2398.
(5) S.F. Marsh, R.M. Abernathey, J.E. Rein, Anal. Lett., 13, (A17) (1980) 1487-1495.
(6) C.H. Knight, R.M. Cassidy, B.M. Recoskie, L.W. Green, Anal. Chem., 56, (1984) 474-478.

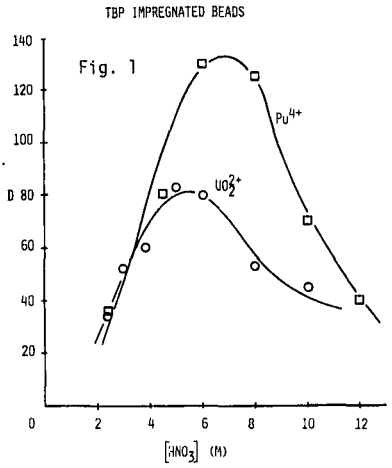

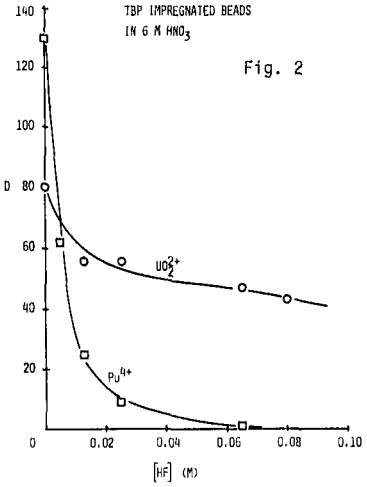

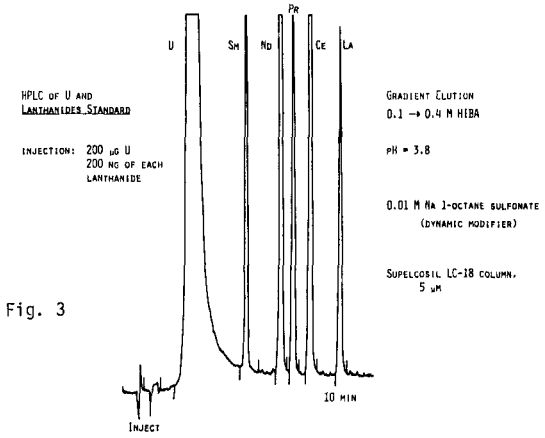

Fig. 3

DETERMINATION OF CONTAMINANTS IN UF_6 - SPECIFIC ANALYTICAL IMPLICATIONS.

W.K. Huber, G. Rettinghaus, BALZERS AG, FL-9496 Balzers, Principality of Liechtenstein

Mass spectrometric measurements with UF_6 call for specific precautions because of the very nature of this material. It is state of the art to introduce UF_6 into the ionizer as a molecular beam avoiding contact between sample and ionizer in order to overcome typical faults: Deterioration of the ionizer due to surface layers, memory, loss of reactive species, occurrence of reaction products. As this is obvious for species like UF_6, the same technique is recommended for less reactive gases if the analytical demands are very stringent, e.g. purity assessment of gases for semiconductor production.

Molecular beam inlet is easy and can be realized in small dimensions if an "ideal" pump is available. This would be a surface with a sticking coefficient of 1 surrounding the ionizer and the beam-defining orifices (Fig. 1). The vapour pressure of UF_6 and of typical impurities as HF and Freon is negligible at LN_2 temperature. Other species as F_2 require lower temperatures attainable with refrigerator cryopumps which are cold enough for practically all cases. The heat dissipation of the ionizer, however, calls for adequate cooling power. Noncondensibles (at LN_2 temperature) can be pumped, however, by an additional pump at lower speed (TMP), provided the species is not reactive (N_2) or has a low concentration. Some species may have an "intermediate" vapour pressure at the given temperature of the cryosurface, high enough to be not negligible and low enough, that deposits may build-up on the surface, resulting in heavy memory (CO_2 at LN_2-temperature). To overcome this the temperature must be reduced (refrigerator instead of LN_2). Condensibles have a density in the ionizer given by the beam expansion. The density of noncondensibles is given by the effective pumping speed. These deviations can be eliminated by calibration and are not a serious drawback of the molecular beam method, whereas the elimination of memory and reactions would not be possible by simple software methods.

The degree to what these effects have been suppressed should be checked, however. The molecular beam is always a little "leaky": Some sample may leave the beam due to scattering, e.g. at the rim of the collimating orifices. Memory on the cryo-surface can be detected or even eliminated by changing the composition or the intensity of the beam (closing the inlet, introduction of "zero" gas, beam shutter or chopper (Fig. 1)). For detection of reaction products a pure sample and the exact knowledge of its mass spectrum for reference are needed. For UF_6 the situation is simple since impurity peaks are easily identified and pure samples - except for HF - are available.

Fig. 2 shows the upper half of a typical UF_6 spectrum at high gain. A lot of peaks in the low ppm range can be seen ("ppm" is used here in terms of the highest peak 333; peak 329 is 55 ppm of 333 (234U/238U abundance ratio)). In the lower mass range (not shown here) impurity peaks much higher have been detected, part of which to be assigned to specific impurities as HF and SiF_4. For most of the impurity peaks the parent species has not been identified. However, the source of these impurities was a not completely conditioned inlet system. The W^+-peaks are due to tungsten evaporation from the filament. The WF_x^+ intensities are clearly below 1 ppm. Thus the reaction of scattered UF_6 with the hot tungsten filament leading to WF_3 can be neglected. Fig. 3 shows the region around the UF_6^+- mass triplet, with 234 UF_6^+ at about 400 ppb of mass 333. Obviously it is not possible to identify all the species associated to the impurity peaks at that low level.

Also in the inlet system reaction and sorption processes may happen. (Here "inlet system" means all the manifold needed to introduce a given sample into the "restriction" in fig. 1). These processes not only produce impurities, they may remove minor constituents as well, in contrast to the molecular beam. A good inlet system should provide for a minimum of sample-to-wall contacts. In other fields this has been approached by the free expansion supersonic beam technique (e.g. for sampling extremely reactive radicals from flames). For UF_6, however, the sample consumption would be too high. Typical systems for UF_6 isotope ratio determination work at a sample consumption as low as 2 mg/h. Typical "memory factors" are here $1 \cdot 10^{-3}$, that means, residual sample from a previous analysis is still present as an impurity in a concentration of that order. For higher demands, the sample consumption must be increased correspondingly. Also for HF, an ubiquitous concomitant of UF_6 with a high adsorption tendency, a realistic background concentration of at least 10^{-3} has to be expected, unless the sample throughput is increased. To check this a sample with a precisely known HF concentration would be necessary.

It turns out that the analytical truth is far from being limited by the sensitivity of the mass spectrometer which has a dynamic range of 20 ppb in terms of peak intensities (fig. 3). In a well conditioned inlet system, with an impurity level as shown in fig. 3, an admixture

of 100 ppb 233U to natural UF_6 would be easily detectable. This is possible because all adsorption sites in the inlet system are saturated. On the other hand, it would be hardly possible to measure an overall UF_6 concentration of a few ppm in a permanent gas unless by the free expansion technique mentioned above.

Reliable calibration gases are essential. For impurity analysis the accuracy requirements are moderate, as long as spectrum overlap does not lead to an unpleasant error propagation. Nevertheless the routine use of such mixtures may be delicate if reactive or unstable species are involved as HF and ClF_3. Occasionally a species may be substituted by another one which, although being easier to handle, is suitable to simulate the original behaviour, for example the specific pumping speed. Notwithstanding that computer operation is a prerequisite for the complex calibration and checking procedures, the human judgement remains indispensable. This, in turn, calls for a flexible and easy-to-handle software support.

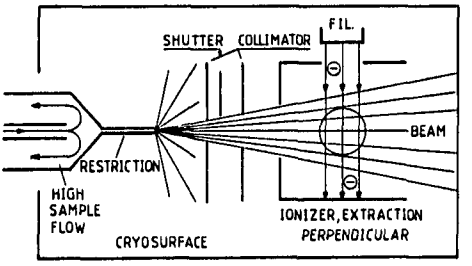

Fig. 1 Molecular beam inlet

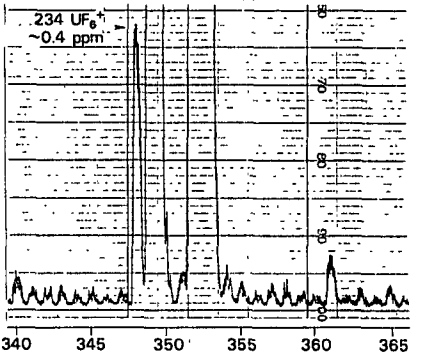

Fig. 3 Detection limit

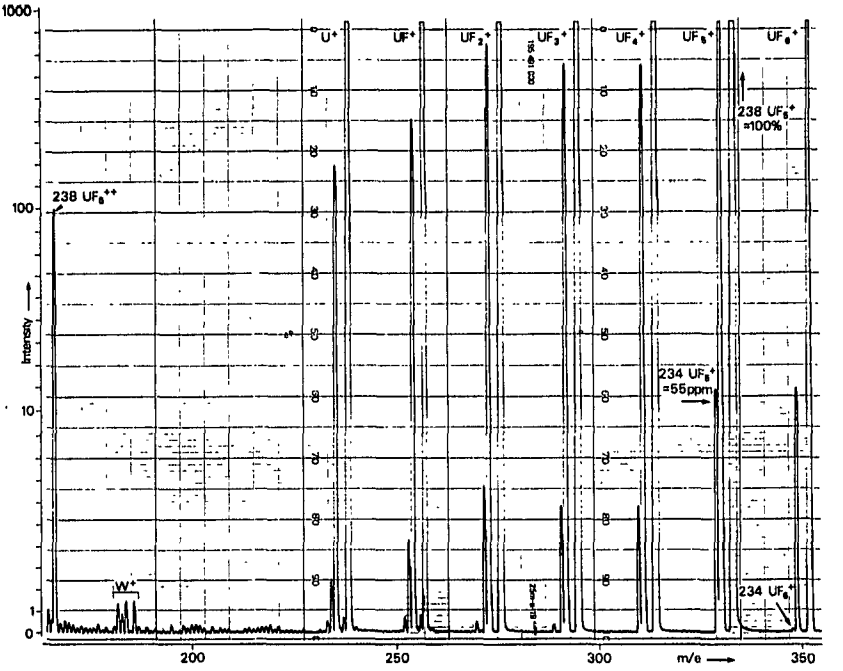

Fig. 2 Mass spectrum of UF_6

MOLECULAR BEAM MASS SPECTROMETRIC STUDIES OF COAL DUST-AIR FLAMES*

Frank T. Greene, Fred W. Brill, John Huang, and J. Eugene O'Donnell
Midwest Research Institute
Kansas City, Missouri 64110

This project was undertaken to determine the chemical form and behavior during coal combustion of the several elements implicated in ash fouling and slagging problems. Techniques for burning premixed, laminar, pulverized coal-air flames, which had previously been developed at MRI, were used to study the relevant combustion processes. The gas phase is analyzed by molecular beam mass spectrometry (MBMS). Gas temperatures are measured by the use of thermocouple techniques. Ash samples, which are coordinated with the vapor phase measurements, are analyzed by SEM, ESCA and other techniques.

The MBMS system, which had been used in earlier studies of coal dust-air flames[1,2] had the quadrupole in the crossed beam mode. In this configuration the coal/ash particles (and the molecular beam) passed through the ion source and were lost in the vacuum system. However, diagnostic studies carried out on this program showed that, with the quadrupole mass spectrometer in the crossed beam mode, that there was serious mass discrimination which varied with gas temperature (beam velocity) and that there was significant loss of sensitivity when high temperature gases were sampled. These effects, which were not detected in the earlier work because measurements were made only over a relatively narrow temperature range, appeared to be the result of poor ion extraction perpendicular to the beam. The quadrupole was therefore placed in the axial mode. This resulted both in improved sensitivity and in greatly reduced mass discrimination. The relatively small variation in 28+/40+ is probably the result of effects other than ion extraction, and would be a second order correction. However, in the axial mode the coal/ash particles can strike the quadrupole structure and produce ions, which resulted in "particulate noise" at a level which sometimes swamped all but the strongest signals. It was therefore necessary to modify the molecular beam sampling system to permit complete trapping of ash and other particulates. This modification included the addition of two additional collimating apertures, physical and electrical modifications of the quadrupole mass spectrometer housing and electron multiplier, the addition of a beam swallowing ion pump, and the design and construction of a precision lateral and angular adjustment mechanism. The modified system, performed satisfactorily. Tests with coal dust flames showed that the particulate noise was reduced to below the normal limit of detection.

Preliminary measurements were made of selected species in lean and rich Decker subbituminous coal flames using the modified system. The production of volatiles and their subsequent reactions were observed. The concentration of sodium species in the burned gas region of the flames were observed to decrease dramatically with temperature, suggesting condensation or reactions with the condensed phases.

Alkali and alkaline earth species were also studied in premixed CH_4-O_2-N_2 flames to obtain data on their thermochemistry and fragmentation behavior. A flat-flame burner system, which permits any water soluble substance to be introduced into premixed gas flames as an aerosol, was constructed for these studies. Preliminary data indicate that, under these conditions, over 60% of NaOH fragments to Na^+ upon ionization with 70 volt electrons.

* This research was supported in part by the U.S. Department of Energy under Contract No. DE-AC18-81FC10287.

1 Milne, T. A., J. E. Beachey, and F. T. Greene, "Direct Mass Spectrometric Sampling of Corrosion Related Gaseous Species from Laboratory Pulverized Coal-Air Flames," Ash Deposits and Corrosion Due to Impurities in Combustion Gases, R. W. Byers (Ed.), Hemisphere (1978).

2 Greene, F. T., J. E. Beachey, and T. A. Milne, "Molecular Beam Mass Spectrometric Sampling of Minor Species from Coal Dust-Air Flames," Proceedings of the 10th Materials Research Symposium, NBS Special Publication 561, U.S. Government Printing Office, Washington, D.C. (1979).

ION/MOLECULE REACTIONS OF SMALL HYDROCARBON IONS: G. Baykut, F.W. Brill and J.R. Eyler, Dept. Chem., Univ. Florida, Gainesville, FL 32611

Small hydrocarbon ions with an H:C ration < 1 have been suggested as important precursors in an ion/molecule pathway initiating soot formation in hydrocarbon flames. Studies with $C_3H_3^+$ formed from propargyl iodide by electron impact show that in addition to stepwise consecutive reactions with neutral acetylene, other reactions with aromatic molecules are possible, which can lead to the formation of polycyclic aromatic ions. We studied the reactions of $C_3H_3^+$ with benzene, toluene, indene, naphthalene, and methylnaphthalenes. The disappearance rate constants for the linear isomer of $C_3H_3^+$ is the highest when reacting with indene, with a value of 2×10^{-9} cm^3s^{-1}. The reactivity of the cyclic isomer is low compared with the linear one. For some neutrals, e.g. benzene, the cyclic isomer shows no reactions. The highest rate constant of the cyclic $C_3H_3^+$ is again measured for its reaction with indene, where a value of 4×10^{-10} cm^3s^{-1} is obtained. Besides particular aromatic ions produced by the reactions of $C_3H_3^+$ with aromatics, charge transfer reactions are also observed, which again lead to aromatic ions in one step instead of a series of consecutive reactions. The rate constants of the reactions with aromatics are high enough to support the rapid ion/molecule soot formation processes.

The $C_5H_5^+$ ions produced by electron impact on norbornadiene undergo slow reactions with acetylene, producing $C_7H_7^+$. However, $C_5H_5^+$ undergoes a much faster hydride transfer reaction with neutral norbornadiene giving $C_7H_7^+$, which, in turn, reacts with diacetylene to produce higher hydrocarbon ions.

We studied the reactions $C_3H_3^+$ with some alcohols. Proton transfer and hydride transfer are the major channels in the reactions of $C_3H_3^+$ with methanol and ethanol. Another type of reactions which is observed in ethanol and butanol is OH^- abstraction from the alcohol molecule. These reactions with alcohols lead to oxygenated ions or hydrocarbon ions with higher H:C ratio, thus providing a quenching mechanism for $C_3H_3^+$, the possible soot precursor.

Screening Middle Distillate Fuels for Selected Species by Triple Quadrupole Mass Spectrometry

A J Schubert and C A Myerholtz
Department of Chemistry
Michigan State University
East Lansing, Michigan 48824

Triple quadrupole mass spectrometry (TQMS), an MS/MS technique, has been examined for use in studies of the composition and stability of middle distillate fuels Tandem mass spectrometry is ideally suited for this type of analysis since the probability of finding a characteristic and unique peak for low-level components or compound classes in a matrix as complex as a fuel is almost negligible. The wide range of instrument conditions and scanning parameters which are readily available with TQMS allow the instrument to take advantage of the particular chemistry of the compound or class of interest and perform a highly selective analysis.

There are two complementary approaches to this type of analysis: compound class detection and specific component analysis. The first case is a rapid screening where the analyst only seeks to determine the presence of a particular compound class at some threshold level. To establish the highly selective screening characteristics to be used for this type of analysis, low energy electron impact ionization was used on several pure components of each compound class studied. From the collisionally activated decomposition (CAD) spectra of these ions, common daughter ions and/or neutral losses were found for the different members of each class. From these data, screening reactions and the corresponding TQMS scans for each compound class studied. To date, screening reactions have been found for anilines, pyridines, indoles, nitrobenzenes, alkylthiols, thiophenes, and alkylbenzenes (see Table I.) The effectiveness of this approach has been verified by using these scans to test for the presence of several species in untreated samples of Jet A aviation fuel, a shale oil derived fuel, and a No. 2 diesel fuel. Thus, once the screening reactions for a compound class are determined, they can be used for the simple and rapid analysis of raw fuel samples introduced through a batch inlet.

A second case in the TQMS study of fuels is a specific component analysis. The addition of a capillary gas chromatograph as an inlet system can frequently simplify this type of problem by dispersing sample components in time. An additional advantage of the chromatographic inlet is that it provides more representative sampling for mixtures with components of wide boiling point range and better reproducibility for quantitation. A more detailed analysis of multiple components in fuel samples is now facilitated by allowing isomeric and isobaric components to be individually analysed and by providing an additional dimension for interpreting experimental results. Chemical ionization has been used with this approach to find highly selective reactions which may be used for the determination of individual compounds of interest while greatly reducing matrix interferences. Additionally, in multiple reaction monitoring (MRM) GC/TQMS experiments, several different components can be simultaneously and independently analysed as they elute from the GC column with much higher sensitivity then would be possible in a full scanning mode. Preliminary results using methane chemical ionization show sub-nanogram sensitivity and excellant selectivity for individual thiophenes

This research was supported in part by a grant from NASA. One of the authors (AJS) has been supported by a NSF Pre-doctoral Fellowship.

Table I. EI Screening Reactions for Compound Classes

NEUTRAL LOSS	COMPOUND CLASS
-17	Anilines
-27	Anilines, Pyridines, Indoles
-30	Nitrobenzenes
-34	Alkylthiols
-45	Thiophenes
-46	Nitrobenzenes
-54	Indoles

DAUGHTER ION	COMPOUND CLASS
65^+	Alkylbenzenes
91^+	Alkylbenzenes
97^+	Thiophenes

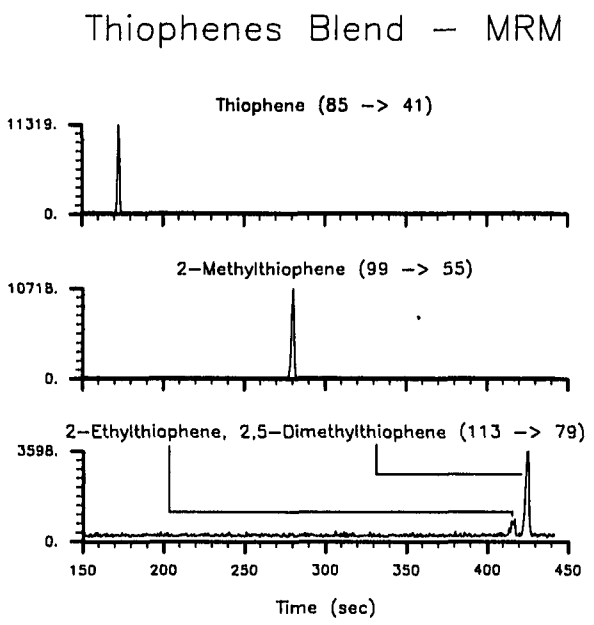

A COMBINATION OF CHEMICAL REDUCTION AND TANDEM MASS SPECTROMETRY FOR THE CHARACTERIZATION OF SULFUR-CONTAINING FUEL CONSTITUENTS. Karl V. Wood, Engine/Fuels Laboratory, Chemistry Building, Purdue University, West Lafayette, IN 47907; James A. Laugal and Robert A. Benkeser, Department of Chemistry, Purdue University, West Lafayette, IN 47907.

The identification of sulfur-containing polynuclear aromatic hydrocarbons (PNAs) in coal and liquids derived from coal (1) is of particular interest because of the environmental effect these constituents have after combustion. However, these compounds have proven difficult to analyze because of their low relative concentration and characteristic mass overlap with hydrocarbon components. Complex separation schemes have been used to address these problems by concentrating sulfur-containing PNAs prior to GC/MS (2). The purpose of this study is to develop a specific chemical reduction scheme which could be applied to complex fuel-related materials for the analysis of selected sulfur-containing PNAs by mass spectrometry/mass spectrometry (MS/MS).

Chemical reduction is by calcium metal in a mixed amine solvent system of ethylenediamine and methylamine. We have previously shown calcium to be an effective metal in reducing aromatic substrates to mono-alkenes (3). In the case of aromatic heterocycles containing a benzothiophene moiety, the thiophene ring is opened by calcium through reductive cleavage of the carbon-sulfur bond to yield thiophenol. In basic media, the latter exists as a thiophenolate anion which resists further reduction because of its negative charge. The unsaturated substituent present after the carbon-sulfur bond cleavage is reduced rapidly to yield the alkylated thiophenol. As an example, benzothiophene yields o-ethylthiophenol upon treatment with the calcium reagent.

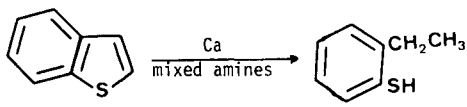

A Finnigan triple quadrupole mass spectrometer was used to characterize these products. Negative ion chemical ionization was employed with isobutane as the reagent gas. Argon was used as the collision gas at a gauge pressure of 2.0 mtorr. The collision energy was set at 20 eV. Figure 1 is the NICI MS/MS spectrum of the conjugate anion, m/z 191, of the reduction product of dibenzothiophene. Of particular interest is the ion at m/z 122, which corresponds to the negative thiatropylium ion, $C_7H_6S^-$. This ion is important because it is also the principal fragment ion in the daughter spectrum of the reduction product of benzothiophene. Therefore, it might be possible to characterize reduction products of both alkyl benzothiophenes and dibenzothiophenes by a parent scan of m/z 122. Figure 2 is a parent scan of m/z 122 which gives evidence for the reduction products of C_0-C_5 alkylbenzothiophenes and dibenzothiophene in a reduced middle distillate fraction of a SRC II coal-derived liquid. This confirms the value of parent spectra combined with Ca reduction in characterizing thiophene derivatives in coal liquids.

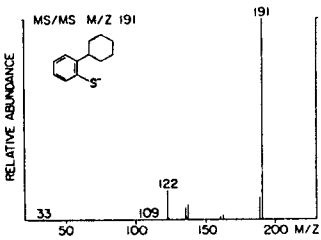

Figure 1

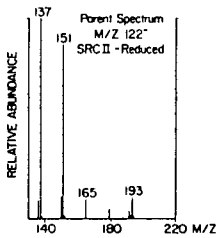

Figure 2

A second parent scan, m/z 176, (the benzo analog of m/z 122) has been used for the tentative identification of C_0-C_3 naphthalothiophenes. Under Ca reduction conditions not only does the C-S bond in thiophene cleave leaving an ethyl substituted thionaphthol but further reduction occurs in the unsubstituted naphthalene ring. The resulting structure 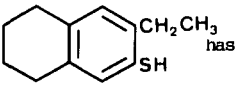

has a molecular weight of 192 daltons, which is the same as the reduction product of dibenzothiophene. However, this reduced naphthalothiophene accounts for the methyl loss observed in the MS/MS spectrum of m/z 191 from the reduced coal-derived liquid. This process does not occur in the MS/MS spectrum of the authentic reduced dibenzothiophene.

Other parent scans can also be used to further characterize these complex mixtures for the presence of sulfur-containing species including HS^-; m/z 33; C_6H_5S; m/z 109; and the dibenzo analog of m/z 122; m/z 230.

1. Czogalla, C.D. and Boberg, F.; Sulfur Reports, ed. A. Senning, 1983 (3).
2. Willey, C., Iwao, M., Castle, R.N., and Lee, M.L., Anal. Chem., 1981 (53), 400-7.
3. Benkeser, R.A., Belmonte, F.G., and Kang, J., J. Org. Chem., 1983 (48), 2796-2802.

Application of Field Desorption Mass Spectrometry to Characterization of Petroleum Products and Identification of Spilled Oils

J. Shen and N.K. Saadeh
Arabian American Oil Company, Dhahran, Saudi Arabia

Recently we have reported the use of selected petroleum biomarkers in the identification of spilled crudes whose gross compositions are similar. (1) Unlike many other methods in use, the reported Gelms method requires no artificial weathering of reference oil samples. This has significantly reduced the overall response time. However, the measurement time is still limited to 70 to 90 minutes per run, or four to six runs per day.

In our search of methods that can bypass gas chromatographic analysis, we have evaluated the use of field desorption mass spectrometry (FDMS) for oil spill identification work.

Experimental

A JEOL DX-300 double focusing mass spectrometer with a combined EI/FI/FD source was used for this work. A JMA-3500 data system was used for instrument control and data acquisition. Carbon emitters used were activated with benzonitrile on 10 micron tungsten wires. Sample loading was accomplished with a microsyringe. Typically 6 KV was applied to cathodic plate, and a heating current of 4 mA/min. was applied to a maximum of 40 mA. PFK was used for field calibration in EI mode and acetone was used for tuning ion source in FI/FD mode. FD spectra were taken at 1 sec. intervals. A typical FD spectrum of an oil sample was obtained by averaging about 200 scans recorded at constant total ion current.

Results and Discussion

A typical averaged FD spectrum of an Arabian Light crude is shown in Fig(1). The saturate (Z=+2) series is predominant. The most intensive mass ion is around C24 (m/e 338). Few mass ions of less than m/e250 were observed.

The gross pattern of the FD spectrum of a weathered crude is similar to that shown in Fig(1). Crudes studied were weathered in open air at Arabian Gulf at a maximum noon temperature of 45 to 50°C for three days. The weathered crudes were further distilled to 280°C to simulate even deeper weathering. The FD spectral pattern of the distilled residue, however, is still similar to Fig(1). The relative amounts of compounds of various Z values have showed little change by visual inspection.

The FD spectra of lube oils are significantly different from those of Arabian crude as lube oils are usually dewaxed. As a result, the dominant compound classes observed in the FD spectrum of a lube oil are naphthenics and aromatics with Z values of 0 or less instead of the Z=+2 series. This makes FDMS a fast and useful screening method to determine if a spilled oil is lube or crude oil. This is important as tanker discharge during cleaning operations has been a major source of undesirable hydrocarbon input into marine environments. While ballast discharge often retains characteristics of a crude, bilge discharge may often be a mixture of lube oils.

In addition, FDMS has been useful in our application to distinguish not only different types of lube oils, but also different lube base stocks. For example, the FD spectrum of a marine engine oil is significantly different from that of a gear lube oil. Different batches of lube oil derived from different feed stocks can be easily recognized through their FDMS spectra.

For spilled oils that have undergone longer term weathering, biodegradation is an important factor to consider. Our study of limiting cases have showed that usual weathering of an Arabian crude would not deplete the saturates, which are the first to be depleted during biodegradation, to the extent that Z=+2 series would become significantly less than other Z serieses as observed in the FD spectrum of a lube oil.

The samples used in the study of limiting cases include (a) a crude sample with n-paraffins removed by 5Å molecular series, and (b) a severely biodegraded oil recovered from a water injuection well. In the absence of long term (>one year) weathering and severe biodegradation, the relative amounts of various Z series can effectively

distinguish an Arabian crude from a lube oil.

Visual comparison of FD spectra of major export crudes from Saudi Arabia has not been successful in distinguishing these crudes whose gross compositions are relatively similar to each other. Pattern recognition techniques, however, have been more useful in detecting subtle differences. Our preliminary results have shown that selected mass ions, especially those corresponding to biomarkers, can be useful in separating even these similar oils. Statistical Analysis System (SAS) from SAS Institute has been used in our evaluation work.

(1) J. Shen, Anal. Chem., 56, 214 (1984)

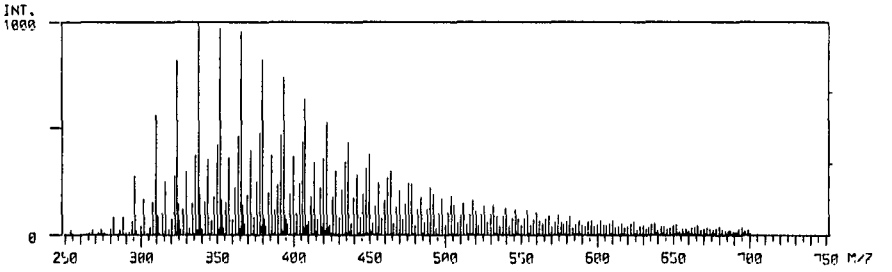

MASS SPECTROMETRIC AND CHROMATOGRAPHIC METHODS APPLIED TO THE ISOLATION AND IDENTIFICATION OF TUMORIGENIC POLYCYCLIC AROMATIC HYDROCARBONS IN COAL LIQUEFACTION DISTILLATES

D. W. Later, E. K. Chess, C. W. Wright, R. B. Lucke, D. D. Mahlum and B. W. Wilson
Pacific Northwest Laboratory
Box 999
Richland, WA 99352

INTRODUCTION

Biodirected analytical approaches have been used to determine the biologically active agents in coal liquefaction materials. Of major concern are constituents in these materials which produce skin tumors. It has been demonstrated that the nonfunctional polycyclic aromatic hydrocarbons (PAH) as a chemical class are the principal dermal tumor initiating components in oncogenic, high-temperature distillates of coal liquefaction materials (1-3). Understanding the effects of alkylation, heteroatomic substitution, and hydroaromaticity on the tumorigenic potency of the PAH has also been of prime interest. Recent investigations have focused on the isolation and identification of specific components from these complex matrices that initiate dermal tumorigenesis. A multiple-step chromatographic method developed for the separation and subfractionation of PAH in complex coal-derived materials was used to generate isolates which were tested for tumor initiating activity. Identification of PAH subfraction components was achieved by mass spectrometric (MS) techniques such as direct probe MS at both high and low ionization voltages, high resolution MS, and capillary column gas chromatographic mass spectrometry (GCMS). Qualitative and quantitative results obtained for PAH isolates by these techniques were correlated with their tumorigenic potency to gain insights into the chemical bases for the observed biological responses.

EXPERIMENTAL

A solvent refined coal (SRC II) liquid distillate, 800-850°F, was used for this study. The PAH were separated from the aliphatic hydrocarbons, nitrogen heterocycles, and hydroxy-PAH by adsorption chromatography (4). The PAH isolate was subsequently fractionated by reverse phase high performance liquid chromatography (HPLC) and subfractions collected for chemical analysis and biological testing (5).

Initiation/Promotion (I/P) mouse skin tumorigenicity assays were conducted by topically applying weight normalized doses of the PAH subfractions on the backs of CD-1 mice. Initiation of the coal liquid subfractions was promoted with twice weekly doses of phorbol myristate acetate (PMA). Details of this assay are described elsewhere (1).

Probe inlet and high resolution MS analyses were performed on a VGZab 1F double-focusing instrument. For the probe work, both 70 and 10-12 eV ionizing electron energies were used. Exact masses of selected PAH subfraction components were determined by peak matching at a static resolving power of 10,000. Capillary column GCMS was achieved on an HP5982A quadropole system equipped with a 15 m x 0.25 mm i.d. DB-5 fused silica capillary column.

RESULTS AND DISCUSSION

A summary of the biological and chemical results are presented in Table 1. Figure 1 is a capillary column gas chromatogram of HPLC subfraction #2, with the 70 eV direct probe mass spectra shown in the insert. In general, the first four HPLC subfractions were composed of a limited number of components within a narrow mass range that were typically isomeric PAH. For example, chrysene and benz[a]anthracene were the two major components in HPLC subfraction #1 and quantitatively accounted for more than 30% of the total mass of the subfraction. Furthermore, constituents identified in these subfractions tended to be parent and methyl PAH. The last four HPLC subfractions had broader mass ranges, were more complex with no single component accounting for more than 4-5% of the overall mass of the subfraction, and were composed primarily of highly alkylated PAH (greater than C_2).

Tumor incidence was greatest in subfractions #2 and #3, with four subfractions producing tumors in more than 80% of their respective test groups. Subfraction #3 produced the highest number of total tumors. The three major components of this HPLC subfraction were C_1-benz[a]anthracene, 3-methylchrysene, and benzo[j or b]fluoranthene and accounted for more than 30% of the subfraction mass. Benzo[a]pyrene was also present in this subfraction at 10±2 parts-per-thousand. The three most tumorigenic subfractions were composed of parent

and methyl PAH. Those subfractions containing the PAH with more than C_2-alkyl substitution were in general less tumorigenic than the parent and methyl PAH containing subfractions.

It is interesting to note that the sum of the tumorigenic potencies for the HPLC subfractions far exceeds the observed potency of the initial PAH isolate. Matrix effects of the complex PAH isolate are felt to be responsible for masking the expression of the tumorigens detected in the HPLC subfractions. Highly alkylated PAH, which are responsible for more than 60% of the mass of the original PAH isolate (see Table 1), are probably the most significant contributors to this masking effect.

REFERENCES

1. D. Mahlum, J. Appl. Toxicol., 3, 31 (1983).
2. D. Later, R. Pelroy, D. Mahlum, C. Wright, M. Lee, W. Weimer, and B. Wilson, In: Polynuclear Aromatic Hydrocarbons: Formation, Metabolism, and Measurement (M. W. Cooke and A. J. Dennis, eds.) Battelle Press, Columbus, Ohio, 1982, p. 771.
3. D. Mahlum, C. Wright, E. Chess, and B. Wilson, Cancer Res. (submitted).
4. D. Later, M. Lee, K. Bartle, R. Kong, and D. Vassilaros, Anal. Chem., 53, 1612 (1981).
5. R. Lucke, D. Later, C. Wright, E. Chess, and W. Weimer, Anal. Chem. (in press).

TABLE 1. Chemical and Biological Results for an SRC II 800-850°F Distillate Fraction

Fraction	Percent Tumor Incidence	Adjusted Number of Tumors	Weight[a] Percent Distribution	Most Abundant[b] Masses (m/z)	Mass[c] Range (m/z)	Most Abundant[d] PAH Compounds in Fraction	Concentration (parts per thousand)
Crude	63	34	---	---	---	---	---
PAH Fraction	88	88	49	242,215/216, 256,252	202-286	6- and/or 4-methylchrysene	35.2 ± 5
PAH Subfractions:							
HPLC #1	57	39	2.9	228,234	226-229	chrysene and/or triphenylene	245 ± 51
						benz[a]anthracene	82 ± 13
HPLC #2	90	76	7.2	242,252	240-252	C_1-benz[a]anthracene	158 ± 2
						benzo[j or b]fluoranthene	91 ± 12
						3-methylchrysene	61 ± 1
HPLC #3	90	84	3.9	254,242,252	242-254	binaphthyls	177 ± 37
						C_1-benz[a]anthracenes	128 ± 30
HPLC #4	85	73	7.1	242	226-242	6- and/or 4-methylchrysene	380 ± 47
HPLC #5	80	59	19.0	256,244,268	244-268	C_2-benz[a]anthracene and/or C_2-chrysenes	128 ± 21
HPLC #6	50	30	23.7	258,270,272	258-284	C_3-benzofluorene and/or C_4-pyrene/fluoranthene	21 ± 2
HPLC #7	23	12	14.4	288,274,298, 310	272-310	C_4-benzofluorene and/or C_5-pyrene/fluoranthene	27 ± 2
HPLC #8	64	21	22.0	288,300,302	276-328	C_5-benzofluorene and/or C_6-pyrene/fluoranthene	6 ± 1

(a) PAH fraction value is the weight percent of crude; values for PAH subfractions are weight percent of PAH isolate.
(b) Masses are listed in order of decreasing abundance.
(c) Mass range is defined as first and last masses ≥20% the intensity of the base peak in the 10-12 eV spectra.
(d) Major components of GC trace identified by retention data and/or GCMS.

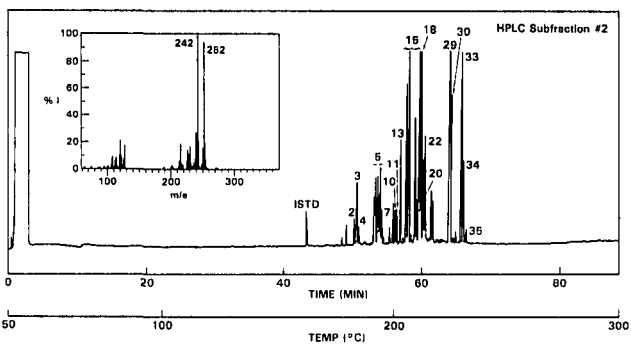

FIGURE 1. Capillary chromatogram and mass spectrum of HPLC subfraction #2.

ANALYSIS OF JET FUELS BY CAPILLARY COLUMN GC/MS

W. E. Blanton, R. A. Heppner, and D. A. Netzel
Western Research Institute
P.O. Box 3395, University Station
Laramie, Wyoming 82071

Jet fuels derived from non-petroleum based sources, such as oil shale, are being considered for use. The shale oil derived fuels, discussed here, have chemical compositions which differ from petroleum based fuels. Current specification testing methods developed for petroleum based fuels may not be applicable for shale oil derived fuels. The intent of this work is to use capillary column GC/MS to analyze these fuels at the individual component level. These GC/MS analyses should assist in development of improved specification tests for these alternative fuels.

A Hewlett-Packard 5985B GC/MS system equipped with a HP 18835C capillary inlet system was used for all GC/MS analyses. A 60m narrow bore fused silica column coated with DB-1, manufactured by J & W Scientific, Inc., was directly inserted into the MS source to maximize chromatographic resolution and MS sensitivity. A HP 5840 GC equipped with an identical column and a flame ionization detector (FID) was used for all gas chromatographic analyses. These instruments were optimized for high sensitivity and resolution using a known mixture and syncrude JP-4.

Under the MS conditions necessary to obtain reliable mass spectra of the less concentrated components in these samples, instrumental saturation occurred for the more concentrated components. This wide concentration range ($>10^4$) necessitated the use of a GC equipped with a FID in order to obtain reliable relative peak area measurements. No correction for FID response factors was made. As many as 430 compounds were either partially or completely separated and identified in a single sample. By matching calculated Kovats[1] indices, GC and mass spectral data were combined to quantify and identify the compound classes in the jet fuel samples. The peak areas for each compound class were summed and expressed as a percentage of the total area. These results were compared with analyses from ^{1}H-NMR, low resolution mass spectral type analyses from the literature[1], and high resolution mass spectrometry to test the feasibility of the GC/MS method.

A comparison of the combined GC and GC/MS results with the ^{1}H-NMR results for the same samples is shown in Figure 1. The agreement between the two methods is especially good for the aromatics. There is an absolute deviation of 3.5% from a 1 to 1 ratio of area percent to mole percent. The agreement between the NMR and the GC/MS analyses for the saturates is less definitive, but much of the discrepancy can be explained.

Table 1 summarizes the comparison of the GC/MS results for sample VN-81-141 with two mass spectral hydrocarbon type analyses. For this sample the GC/MS results for a compound class differ from one or the other of the two type analyses by 10% or less except for the indans/tetralins. Additional comparisons with other fuel samples indicate that results from the GC/MS method are consistently lower for the cycloalkanes and consistently higher for the aromatic compound classes. This is due, at least in part, to not correcting raw peak areas with the FID response factors. There are several other reasons for the observed discrepancies.

The GC/MS results were also compared with those from HRMS to evaluate the effectiveness of the GC/MS method for compound classes containing heteroatoms. This comparison indicates that the two methods are comparable but the threshold of detection is lower for the HRMS method.

The results of these comparisons indicate that capillary column GC/MS in conjunction with FID gas chromatography can be used as an analytical method for the analysis of jet fuels. This method is adequate for comparative or correlative measurements of jet fuel samples. However, if the method is to be developed into a technique for absolute measurement, then the FID response factors will have to be determined and incorporated into the method.

Acknowledgment

This research was sponsored by the Fuels Branch AFWAL/POSF, Fuels and Lubrication Division, Wright Patterson Air Force Base, Ohio, under contract numbers MIPR FY145-82-N0624 and FY1455-82-N0631.

References

[1] F. N. Hodgson, et al., "Analysis of Aircraft Fuels and Related Materials", Air Force Aero Propulsion Laboratory Report AFWAL-TR-82-2082, Wright Patterson Air Force Base, Ohio.

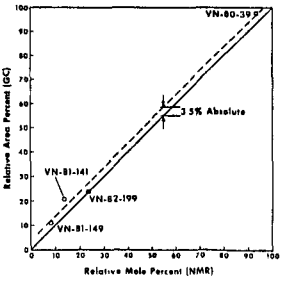

Figure 1. Comparison of NMR and GC/MS Data for Aromatics in Jet Fuels.

Table 1. A Comparison of GC/MS with Classical Type Analyses for VN-81-141

	GC/MS	D2789[1]	Mons.[1]
Saturates			
Alkanes	32.1	41.0	32.0
Cycloalkanes	42.7	45.4	50.2
Total Saturates	74.8	86.4	82.3
Aromatics			
Alkylbenzenes	15.9	10.6	14.9
Indans/Tetralins	4.9	2.4	2.8
Napthalenes	N.D.	0.6	N.D.
Total Aromatics	20.8	13.6	17.7
Unknown	4.4	--	--

MASS SPECTRAL STUDY OF SIMPLE ORGANIC COMPOUNDS FOR COAL STRUCTURE ELUCIDATION

J. H. Zoeller, Jr., A. G. Vindiola, R. A. Zingaro and R. D. Macfarlane

Department of Chemistry, Texas A&M University, College Station, Texas 77843

Mass spectrometry techniques based on high heating rates, such as Pyrolysis-Field Desorption Mass Spectrometry (PFDMS, ref. 1) and Californium-252 Plasma Desorption Mass Spectrometry (CFPDMS, ref. 2) are now finding utility in the study of coal-derived materials. Our use of the CFPDMS technique has been hampered by a lack of understanding on how organic functionalities behave under bombardment with energetic fission fragments. The ensemble of populous functionalities known present in coal is quite limited, including carboxylic acids, aromatic rings, saturated linkages, ethers and hydroxyl groups. Positive and negative ion CFPDMS spectra have been obtained on a suite of pure organic compounds embodying these functionalities. Of the four carboxylic acids, behenic acid (1) and p-octyloxybenzoic acid (3) both exhibit prominent protonated parent ions (M + 1), an acylium ion (M - 17) and a carboxylate anion (M - 1). Compound (3) also shows an oxonium ion (M - 1) by loss of an etheric hydrogen. The spectra of naphthalene acetic acid (2) and omega-phenyloctanoic acid (4) are replete with ions near the molecular mass, and parent ions of either charge could not be identified with certainty. Phenylpentadecane (5) displays numerous ions above and below its molecular mass. In the positive ion spectra of the monoalkylbenzenes (4) and (5) are found a series of heavy cations in the region 900 to 2200 amu whose masses correspond to $C_5(C_6H_2)_n$ +, where n is 12 to 27. Ions of these same masses appear in the PFDMS and CFPDMS spectra of coal-derived fractions. m-Pentadecylphenol (6) shows a sharp phenoxide ion peak (M - 1) and three positive parent ions; the oxonium ion (M + 1), cation radical (M) and benzyl cation (M - 1). Some coal-derived products show broad peaks in their positive ion spectra which correspond in mass to sharp peaks in the negative ion spectra, just as does the pure phenol. Pentacyclic aromatic hydrocarbons pentacene (7) and 1,2,5,6 dibenzanthracene (8) both exhibit a sharp cation radical peak (M) but no anionic parent. Both extrude up to seven methine moieties, forming fragment peaks at (M - 13), (M - 26)...(M - 91). Methine extrusion fragments are found from all the pure compounds posessing a polynuclear aromatic group. Hydroaromatic compounds 1,2,3,6,7,8 hexahydropyrene (9), benz(a)fluorene (10) and 5,6,8,9,tetrahydrobenz(a)anthracen-11(10H)one (11) yield a benzyl cation (M - 1). Ketone (11) in addition shows a protonated parent at (M + 1). Positive fragments in these are due to consecutive loss of methylene and methine groups, and dehydrogenation. Resulting fragment peaks have a periodicity of 13.3 amu. Analogous fragmentation behavior is attributed to benzylic compounds (2), (4) and (5). Similar patterns are seen in the positive ion CFPDMS spectra of coal-derived asphaltenes. Most coal-derived substrates and pure compounds display three types of carbon cluster ions; $H_x(C_2)_n$ - (x = 0,1,2), $H_xC(C_2)_n$ - (x = 0,1,2,3) and H_xC_n + (x = 1,2,3), where degree of polymerization (n) is substrate dependent.

ACKNOWLEDGEMENTS Support from the Gas Research Institute and the Center for Energy and Mineral Resources is gratefully acknowledged.

REFERENCES

1 H - F Schulten "Pyrolysis-Field Desorption Mass Spectrometry of Coal": Fuel 61, 670 (1982)

2 R. A. Zingaro, R. D. Macfarlane and J. H. Zoeller, Jr. : Annual Report to Gas Research Institute, GRI-84/0057, March 1984

Table 1: CFPDMS Parent Ion Patterns and Fragmentation Modes of Simple Organic Compounds

	COMPOUND	M	PARENT IONS ⊕	PARENT IONS ⊖	FRAGMENTATION MODE
1	$CH_3(CH_2)_{20}COOH$	340	M + 1 M - 17	M - 1	Chain Cleavage
2	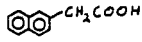	186	M + 1		Methine Extrusion
3		250	M + 1 M M - 1	M - 1	Chain Cleavage
4	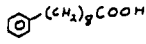	220			Uncertain
5	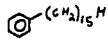	288			Uncertain
6	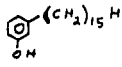	304	M + 1 M M - 1	M - 1	Chain cleavage
7	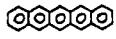	278	M	None	Methine Extrusion
8		278	M	None	Methine Extrusion
9		208	M - 1 M - 3		Elimination of CH , CH_2 , and H_2
10		216	M - 1		Methine Extrusion
11		248	M + 1 M - 1		Elimination of CH , CH_2 , H_2

MASS SPECTRAL COMPARISON OF MUTAGENS EXTRACTED FROM FLUIDIZED-BED AND PULVERIZED COAL COMBUSTION FLY ASHES

E. K. Chess, D. W. Later and B. W. Wilson
Pacific Northwest Laboratory, Biology and Chemistry Department, Richland, WA 99352
W. R. Harris, D. Okamoto and J. F. Remsen
Laboratory for Energy-Releated Health Research, University of California, Davis, CA 95616
Work Supported by the U.S. Department of Energy under Contact No. DE-AC06-76RLO 1830

Fluidized-bed combustion (FBC) of coal is an established technology in several countries and is emerging as an alternative to conventional pulverized coal technology. Several commercial FBC plants are now operating in the U.S. The identification and quantitation of organic compounds found in mutagenically-active coal fly ash extracts are important steps in providing the data needed for determining the potential environmental and biological effects arising from exposure to coal combustion emissions. Results from such studies on PCC fly ash extracts have been reported (Chess et al., 1984; Harris et al., 1984). To provide such data for FBC, pulse-jet baghouse fly ash collected from an experimental atmospheric-pressure fluidized-bed combustion (AFBC) unit at the Grand Forks Energy Technology Center, under test with Beulah, ND lignite, was extracted with 60/40 (W/W) benzene/methanol. This extract was assayed for mutagenic response in the Salmonella typhimurium plate incorporation assay (Ames et al., 1975) using both standard and nitroreductase-deficient variants of TA1538, TA100 and TA98. The crude fly ash extracts were shown to be mutagenic in all six strains, but the activity in the nitroreductase-deficient strains was significantly lower than in the standard strains, indicating the possible presence of nitro-polynuclear aromatic compounds (nitro-PAC; Remsen et al., 1984).

In order to help identify the specific components responsible for the mutagenic activity, the fly ash extract was separated by high performance liquid chromatography using a Varian MicroPak CN-10 column and a binary solvent program with hexane and methylene chloride. Fractions were collected and tested for mutagenic activity using TA98 and TA1538 as tester strains. The HPLC chromatogram and mutagenic responses for each fraction in the standard and nitroreductase-deficient strains of TA98 are shown in Figure 1. Fractions 9-11 exhibited the highest mutagenic activity, and were subsampled to provide six fractions (as shown in Figure 1) which were submitted to further separation using a Varian MCH-10 reverse-phase column. The components corresponding to the largest peak in each fraction (as measured at 390 nm) were collected and submitted to GC/MS and HRMS analyses for further characterization (Chess et al., 1984). The small sample quantities precluded identification of many components in the subfractions. However, the potent mutagen phenalen-1-one, recently identified in combustion products from fossil fuel (Leary et al., 1983), was identified as the major component in subfraction 3 on the basis of its mass spectrum and GC retention index (Lee et al., 1979; Vassilaros, et al., 1982). A compound with the molecular formula $C_{19}H_{10}O$ (as determined by HRMS) was found to be the major component in subfraction 1, and its GC/MS spectrum was readily interpreted as the ketone arising from the oxidation of a $C_{19}H_{12}$ hydrocarbon containing a five-member ring, such as 11H-benz[bc]aceanthrylene, 4H-cyclopenta[def]chrysene, or 4H-cyclopenta[def]triphenylene. The major component in subfraction 4 was determined to have a molecular formula of $C_{17}H_{10}O$ by HRMS measurements. Although the mass spectrum of this $C_{17}H_{10}O$ isomer was very similar to those of benzanthrone, and benzo[a]- and benzo[b]fluoren-11-ones, these three isomers were eliminated as possible identities by the results of retention index measurements. The mass spectra of several components in subfraction 5 displayed losses of 28 amu, followed by losses of 29 amu consistent with the presence of quinone or lactone functionalities. Of the few components characterized by GC/MS which appeared to have odd-massed molecular ions, indicative of nitrogen in the molecules, none could be identified as containing a nitro group. Even though the mutagenicity results indicated the presence of nitro compounds, only one component in the six subfractions examined by GC/MS was unambiguously identified as a nitro compound on the basis of the characteristic nitro group fragmentation scheme (loss of NO and NO_2). GC retention index measurements showed this compound to be the same as a major mono-nitrated product formed by the nitration of carbazole in this laboratory.

Although the small number and quantities of nitro compounds found in the FBC extract are inconsistant with results from the mutagenicity assays, chemical characterization of the extract was not comprehensive, and nitro organic constituents may have been present in the HPLC fractions not examined by GC and GC/MS. The presence of PAH-oxidation products in the mutagenic fractions is of interest in light of recent demonstrations that oxidation

reactions can confer genotoxic activity on certain lower molecular weight PAH (Leary et al., 1983; Salamone et al., 1979; Pitts 1983). Also of interest are the substantial differences in the chemical composition and microbial mutagenicity of the FBC fly ash extracts as compared to those from PCC fly ash studied both here and other laboratories (Harris et al., in press; Wei et al., 1982; Mumford and Lewtas, 1982).

REFERENCES

Ames, B. W., J. McCann and E. Yamasaki, Mutat. Res. 31:347-364 (1975).

Chess, E. K., D. W. Later, B. W. Wilson, W. R. Harris and J. F. Remsen. Pacific Northwest Laboratory Topical Report, DOE/PNL-4983, NTIS, Springfield, VA, 1984.

Harris, W. R., E. K. Chess, D. Okamoto, J. F. Remsen and D. W. Later. Environ. Mutagen. 6:131-144 (1984).

Leary, J. A., A. L. Lafleur, H. L. Liber and K. Biemann. Anal. Chem. 55:758-761 (1983).

Lee, M. L., D. L. Vassilaros, C. M. White and M. Novotny. Anal. Chem. 51:768-774 (1979).

Mumford, J. L., and J. Lewtas. J. Tox. Environ. Health 10:565-586 (1982).

Pitts, J. N., Jr. Environ. Health Perspect. 47:115-140 (1983).

Remsen, J. F., R. Harris and D. R. Sears. "Mutagenicity in Salmonella of Nitro-Organic Compounds in Extracts of Fly Ash from a Lignite-Fired Atmospheric Fluidized-Bed Combustor", submitted to J. Tox. Environ. Health.

Salamone, M. F., J. A. Heddle and M. Katz. Environ. Int. 2:37-43 (1979).

Vassilaros, D. L., R. C. Kong, D. W. Later and M. L. Lee. J. Chromatog. 252:1-20 (1982).

Wei, C. I., O. G. Raabe and L. S. Rosenblatt. Environ. Health 10:565-586 (1982).

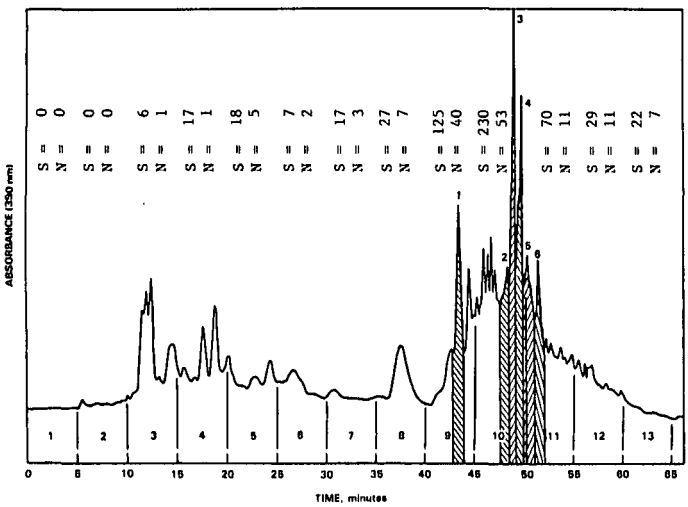

Figure 1. HPLC Chromatogram for the Fractionation of a Benzene/Methanol Extract of FBC Coal Fly Ash Using a Preparative CN-10 Column. Revertants per plate minus spontaneous revertants (SR) for mutagenicity assay of each fraction in TA98 (denoted S) and nitroreductase-deficient TA98nr (denoted N) strains of S. typhimurium are listed above each fraction in chromatogram. SR(TA98) = 12 rev/plate; SR (TA98nr) = 14 rev/plate.

RESOLUTION AND QUANTITATION OF THE ENANTIOMERS OF 6-HYDROXY-1-METHYLTETRAHYDRO-β-CARBOLINE IN URINE OF SEVERAL SPECIES USING CHIRAL CAPILLARY COLUMN NCI GC/MS

Olof Beck, Kym F. Faull and Jack D. Barchas. Nancy Pritzker Laboratory of Behavioral Neurochemistry, Department of Psychiatry and Behavioral Sciences, Stanford University School of Medicine, Stanford, California 94305

Formation of 6-hydroxy-1-methyltetrahydro-β-carboline (6-OH-1-MeTHBC) from the neurotransmitter serotonin and acetaldehyde, in a nonenzymatic Pictet-Spengler reaction, has been implicated in the alcoholic syndrome. Recent work has, however, revealed that 6-OH-1-MeTHBC occurs naturally in mammalian tissues and body fluids. Although a slightly increased urinary excretion of 6-OH-1-MeTHBC is seen among intoxicated alcoholics, it seems unlikely that an in vivo formation from acetaldehyde explains its natural occurrence. Since 6-OH-1-MeTHBC contains a chiral center, it appeared of interest to determine the occurrence of the two enantiomers in order to obtain more information on this compound.

Urine samples were collected from several species in plastic tubes and immediately frozen on dry ice (-70°C). Aliquots (1.0 ml) of urine were pipetted into 15 ml siliconized acid washed (dichromate-sulfuric acid) glass tubes containing 26.2 ng of 6-hydroxy-1-methyl-1,2,3,4-tetrahydro-(3,3,4,4-$^2H_4$)-β-carboline (internal standard) and 380 μg semicarbazide. When enzymatic hydrolyses were performed, 0.5 ml of an 0.2 M citrate buffer (pH 6.0) and 2.5 mg of sulphatase (Sigma type H1) were added and samples were incubated for 16 hrs at 37°C. The hydrolyzed urine was used to determine the total (free + conjugated) amount, the unhydrolyzed urine to determine the free amount, and the conjugated amount was calculated as the difference.

The samples were then shaken with 5 ml of CH_2Cl_2, and the CH_2Cl_2 layers were discarded. After addition of 0.1 ml of 5.8 M K_2CO_3 and 0.4 g NaCl the samples were extracted with 6 ml of CH_2Cl_2. The organic layers were transferred to clean siliconized test-tubes and evaporated to dryness under a stream of nitrogen. The residues were treated with 100 μl of pentafluoropropionic anhydride for 20 min at 60°C. After cooling the excess reagent was evaporated under nitrogen and the residue redissolved in 100 μl of EtOAc.

Aliquots of 1-2 μl of the samples were injected (moving needle) into a 25 m x 0.31 mm I.D. Heliflex Chirasil Val III (Applied Science) capillary column mounted in an HP 5985B GC/MS. Helium was used as a carrier gas and a pressure of 5 psi was applied over the column. The temperature of the oven was programmed from 180°C to 220°C at a rate of 5°C/min. The instrument operated in the negative ion chemical ionization mode with methane as reagent gas (1 torr). Analyses were performed by monitoring m/z 474 and m/z 478 which correspond to the $(M-HF)^-$ ion of 6-OH-1-MeTHBC PFP and the internal standard. Synthetic 6-OH-1-MeTHBC eluted as two base-line separated peaks with retention times of ~9 min. The two enantiomers were designated A and B according to the order in which they eluted.

The analyses of urine revealed that the two enantiomers of 6-OH-1-MeTHBC occur in unequal amounts (Table 1). In the total fraction, rat and cat urine had predominantly the A form, squirrel monkey and mouse had predominantly the B form, and in human and dog urine the two forms occurred in about equal amounts. Furthermore, the results on the proportion of the B form in the free and conjugated fraction, indicated that the two enantiomers are not conjugated at equal rates.

It is concluded from this work that the enantiomers of the endogenous 6-OH-1-MeTHBC occur in urine in unequal amounts. This result suggests that an enzymatic mechanism is involved in its formation in vivo. The natural precursors of 6-OH-1-MeTHBC and the route of formation needs to be established. A formation from serotonin and acetaldehyde cannot be excluded. However, since acetaldehyde occurs only in minute amounts naturally, another carbonyl reactant (e.g., pyruvate) may be considered.

Table 1.

Specie	% B in total	% B in free mean ± S.D.	% B in conj.	n	concentration range ng/ml	% in conj. form mean ± S.D.
Human	52 ± 5	63 ± 4	23 ± 11	9	20 - 570	31 ± 18
Squirrel monkey	63 ± 5	80 ± 8	44 ± 5	6	22 - 120	42 ± 13
Dog	53 ± 9	52 ± 9	---	8	0.5 - 29	n.d.
Cat	17 ± 3	17 ± 2	---	4	7 - 20	n.d.
Rat	18	< 10	22	pools	12 - 21	90
Mouse	56	n.a.	---	pools	7 - 33	---

GC/NCIMS OF N-N-PROPYLNORAPOMORPHINE AND METABOLITES

T.M. Trainor and P. Vouros, Barnett Institute of Chemical Analysis and Department of Chemistry; H. Maksoud and J.L. Neumeyer, Department of Medicinal Chemistry, Northeastern University, Boston, MA 02115.

Introduction

The pharmacology of the dopamine receptor agonists N-n-propylnorapomorphine (NPA, I) and apomorphine (APO, II) has been under study for several years.[1] However, the analytical methods reported to date lack the sensitivity and/or the specificity to monitor therapeutic levels of I or II in physiological fluids. This paper presents a method based on the technique of fused silica capillary gas chromatography/electron capture negative ion chemical ionization mass spectrometry that permits the detection and quantitation of the trifluoroacetyl derivative of NPA at subnanogram per milliliter levels in rat serum.

In addition, gas chromatography/electron impact mass spectrometry has been utilized for the determination of metabolites resulting from the microbial transformation of the dimethyl ethers III and IV.

Results

Under electron capture negative ion chemical ionization conditions (0.30 torr CH_4, 270°C source temperature), the TFA derivative of I produces a mass spectrum with a base peak corresponding to $(M-CF_3CO)^-$ (Figure II). The serum analysis was initially conducted by selected ion monitoring of the $(M-CF_3CO)^-$ ions of derivatized analyte I (m/z 390) and internal standard II (m/z 362). The spiked serum samples were extracted as described previously.[2] A linear calibration plot was obtained by varying the levels of I from 1.0 to 500 ng per ml serum (Figure III). At the 1 ng/ml level, SIM chromatograms exhibiting high S/N are obtained (Figure IV). However, unacceptable precision for multiple measurements of the ratio I_{390}/I_{362} was observed. Significant improvement in this measurement was realized by switching to d_5-NPA as the internal standard (10 ng/ml) and keeping II as carrier (150 ng/ml). Duplicate measurements for three serum samples spiked with I at the 0.50 ng/ml level (Figure V) resulted in a coefficient of variation of 7.9%.

Proposed metabolic pathways for compounds I and II in mammalian systems suggest methylation at the 10- or 11- position to produce the isomeric products V, VI (from I) and VII, VIII (from II). Microbial O-demethylation of the dimethyl ethers III and IV provides a convenient source of the 11-methyl isomers, the more difficult to obtain synthetically.[3] GC/EIMS has permitted the analysis of extracts obtained from cultures of *Cunninghamella elegans* treated with R(-)-III, S(+)-III, R(-)-IV, and S(+)-IV. The TFA monomethyl derivatives can be separated by gas chromatography and have been shown to produce unique fragmentation patterns under EI conditions. Ions corresponding to $(M-R_2)^+$ and not $(M-R_3)^+$ are observed, permitting substitution assignments based on the presence of $(M-CH_3)^+$ or $(M-CF_3CO)^+$ signals. The microbial O-demethylation has been found to proceed with both stereoselectivity and regiospecificity; only the R(-) enantiomers are metabolized, the major products being isomers VI and VIII.

References

1. J.L. Neumeyer, S. Lal and R.J. Baldessarini, in G.L. Gessa and G.U. Corsini (Editors), Apomorphine and other Dopaminomimetics, Vol. 1, Basic Pharmacology, Raven Press, New York, 1981.

2. H.M. Maksoud, S.H. Kuttab, J.L. Neumeyer and P. Vouros, J. Chromatogr., 1983, 274, 149.

3. R.V. Smith and P.J. Davis, Appl. Environ. Microbiology, 1978, 35, 738.

Acknowledgement

The microbial studies were carried out in collaboration with Professor Patrick J. Davis, University of Texas, Austin.

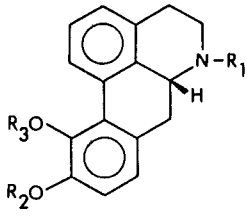

FIGURE I

	R_1	R_2	R_3
I	$n\text{-}C_3H_7$	H	H
II	CH_3	H	H
III	$n\text{-}C_3H_7$	CH_3	CH_3
IV	CH_3	CH_3	CH_3
V	$n\text{-}C_3H_7$	CH_3	H
VI	$n\text{-}C_3H_7$	H	CH_3
VII	CH_3	CH_3	H
VIII	CH_3	H	CH_3

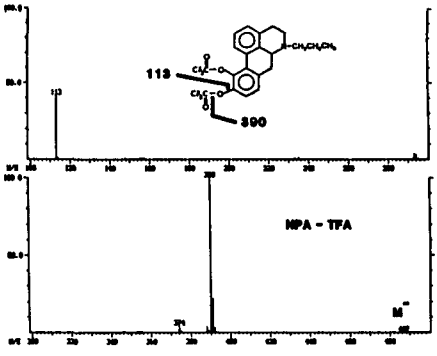

FIGURE II

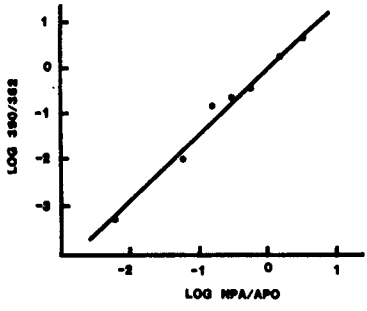

FIGURE III

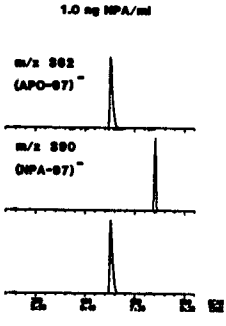

FIGURE IV

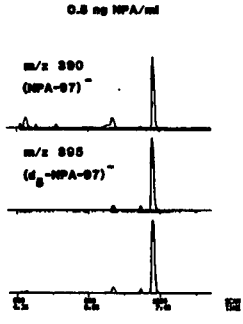

FIGURE V

Fast Atom Bombardment Mass Spectra of Antineoplastic Agents.

Robert Suzuki and John Roboz
Mount Sinai School of Medicine, New York, NY 10029

Fast atom bombardment (FAB) spectra of several clinically important antineoplastic agents were obtained with both quadrupole and double-focusing magnetic mass spectrometers in a simple and inexpensive manner utilizing, without modification, existing chemical ionization sources (with their fast pumping capability) allowing both mass spectrometers to operate routinely with the other inlet systems. On the Finnigan 3300 CI manifold the bottom flange normally used for the heater and thermocouple feedthroughs was used to mount the FAB gun. On the VG ZAB 1F one of the four standard inlet ports was used. The ion gun (Phrasor Scientific, Duarte, CA) was operated with argon at 7KV and an ion current of 40-60 uA.

Nominal masses were obtained at a resolution of 1000 (Finnigan), accurate masses at a resolution of 5000 (ZAB). Mass calibration in the scanning mode was made using equimolar solutions of NaI and CsI in glycerol. The use of this solution resulted in a greater number of salt cluster and salt cluster glycerol adduct ions such that there were few gaps in the spectra in the lower mass range (100-1000) thereby allowing a more accurate mass-to-time table to be generated. In the peak matching mode a chemical analog (1:1 molar ratio) of the compound being analyzed was used; e.g., 4-demethoxy-daunorubicin for the anthracyclines. Samples were dissolved in glycerol.

The FAB spectra obtained with the two instruments gave comparable relative abundances in the molecular ion regions and also comparable fragmentation patterns for all compounds studied. Overall noise and baseline levels, however, were considertably greater in the quadrupole and, as a result, sensitivity was lower than with the magnetic sector instrument. Five to ten individual scans were averaged to obtain representative fragmentation patterns in the FAB mode.

Although the (M+1) ions of the anthracyclines (doxorubicin,daunorubicin, carminomycin, rubidazone, 4'-deoxydoxorubicin, 4'-epidoxorubicin, and detorubicin) were weak (1-4%), accurate masses could still be obtained by peak matching so that molecular compositions could be calculated. Fragmentation of the anthracyclines was characterized by protonated aglycones with subsequent loss of hydroxyl and side chain groups. Pure aglycones yielded weak but measurable (M+1) ions and considerable fragmentation.

The vinca alkaloids (vincristine, vinblastine, vindisine), harringtonine and homoharringtonine all gave mass spectra characterized by highly abundant (70-100%) protonatewd molecular ions with minimum fragmentation. Etoposide gave a small but measurable molecular ion.

The (M+1) and characteristic fragment ions obtained by FAB indicate a potential to detect and quantify these hitherto intractable compounds by high resolution selected ion monitoring. This was accomplished by first tuning in the proper exact mass using either the compound itself or an appropriate standard. With the sample inserted and the FAB gun off, the background signal and gain were adjusted. The gun was then switched on and the signal level was monitored. An immediate increase was noted when the sample contained the compound of interest. The ion current slowly decreased as the concentration of the compound in the glycerol matrix decreased. As an illustration, 185 ng of vincristine was placed on the tip of the probe in 1 ul of a glycerol-methanol mixture (1:1 v/v) and the protonated molecular ion was monitored at m/z = 825.4074 at a resolution of 5000. After the FAB gun was switched on the signal strength increased approximately 10 times followed by a slow decrease lasting for 1.5 min. The initial signal strength as well as the area under the decay curve changed with the amount of compound present, although quantitative relationships have not yet been established.

(Supported by T.J. Martell Foundation for Cancer and Leukemia Research.)

METABOLITE IDENTIFICATION OF CIS - AND TRANS - DECALIN IN KIDNEY AND URINE OF FISCHER RATS BY GC/MS

Kyung O. Yu, Carl T. Olson, and M. P. Serve
Toxic Hazards Division
Air Force Aerospace Medical Research Laboratory
Wright-Patterson AFB, OH 45433

Decalin is commonly used as a solvent and as a component of many Air Force jet fuels. Male Fischer rats exposed to decalin vapors of 5 and 50ppm for 90 days showed the presence of renal tubular degeneration. Other hydrocarbon fuels such as petroleum distillate JP-4 and synthesized JP-10 cause renal tumors following long term exposure. These renal tumors occur only in male rats, not in controls or in females. The mechanism of renal lesion production was hypothesized to be due to metabolites of hydrocarbon fuels.

Decalin, decahydronaphthalene, is an alicyclic hydrocarbon and because of the ring fusion decalin exists in two stereoisometric forms, cis-and trans- decalin. Rats were orally dosed with pure decalin or water (1/2ml) every other day for 14 days. Urine was collected for the first 2 days following initial exposure and pooled. At the end of the exposure, urine and homogenized kidneys were incubated at a pH of 4 with beta-glucuronidase/aryl sulfatace at 37°C for 16 hours. After extraction with CLIN ELUT and methylene chloride, the concentrated organic layer was injected on the Hp GC/MS which was used to identify metabolites. Cis-2-decalone (figure 1) was detected in the kidney extracts of rats treated with cis-decalin, and trans-2-decalone from the kidney extracts of rats exposed to trans-decalin. These ketones were not detected in the kidneys of control rats or female rats. A sex-related difference in the formation of ketone in the kidney was confirmed by the experiments and may be implicated in sex-specific renal lesions in rats. Only male rat kidneys contained ketone.

Major metabolites in the urine samples were identified as hydroxylated decalin. Urine from male and female rats exposed to pure cis-decalin showed the presence of cis, cis-2-decalol (figure 2), cis-1-decalol, and cis,trans- 1-decalol. Urine of rats exposed to trans-decalin contained trans, trans-1- decalol, and trans, cis-2-decalol. TMS-derivatives of hydroxylated decalin and of urine metabolites are shown in figure 2.

In conclusion, there is a sex-related difference in ketone formation in rat kidney. Monohydroxydecalin was the urine metabolite.

Figure 1

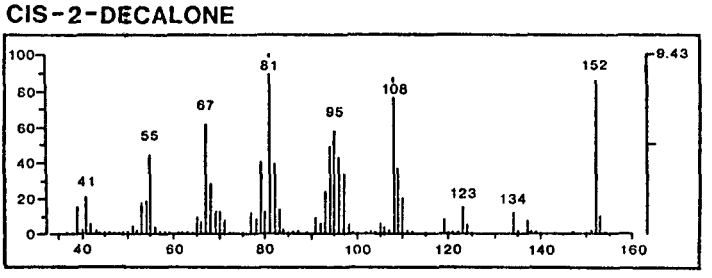

KIDNEY EXTRACT FROM MALE RAT
EXPOSED TO CIS - DECALIN

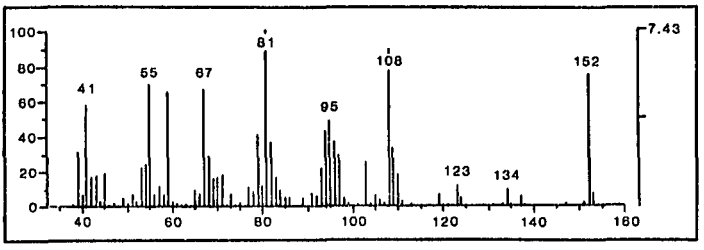

Figure 2

CIS, CIS-2-DECALOL

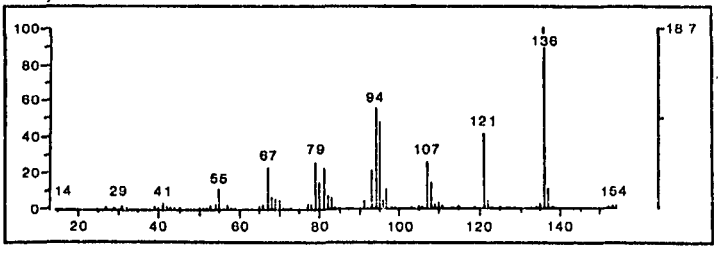

URINE FROM EXPOSED TO CIS-DECALIN

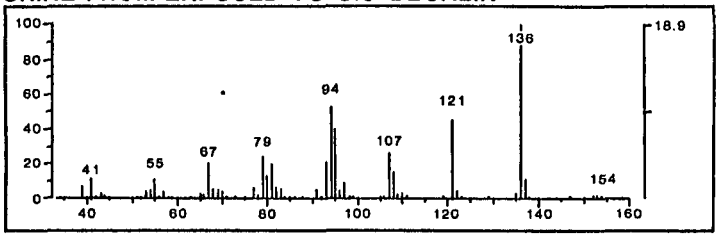

TMS-DERIVATIVE OF RAT URINE (CIS-DECALIN)

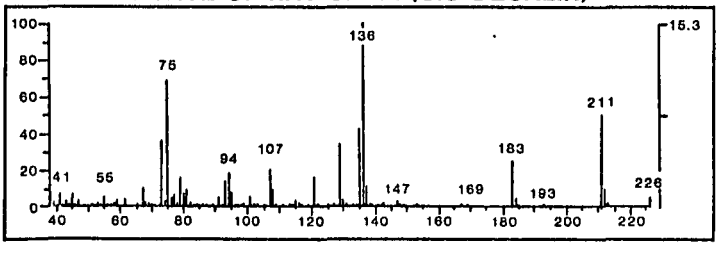

A DLI MICRO LC/MS AND GC/MS PROCEDURE FOR DETERMINATION OF DIETHYLSTILBESTROL AND ITS METABOLITE

T. Covey, J. Crowthers, G. Maylin, and J. Henion, Cornell University, Equine Drug Testing Progra 925 Warren Drive, Ithaca, NY 14850; C.F. Parker, National Institute of Environmental Health Sciences, P.O. Box 12233, Research Triangle, N.C. 27709

DES is a compound of regulatory notoriety. It is a synthetic estrogen that elicits a powerf growth promoting effect in livestock. It has been used to increase production efficiency in meat producing animals. It is also a carncinogen and has been banned for this purpose.

Our Equine Drug Testing and Toxicology Program has we embarked on a two pronged project concerning this drug. First, to develop a rapid, and specific, extraction procedure for capillar GC/MS confirmation and quantitation of DES in animal tissues. Secondly, to screen for and identi the metabolites of DES (and their isomers). We chose to assess the utility of a DLI micro LC/MS procedure to accomplish this task.

Extraction Procedure

Calf liver samples were homogenized, hydrolyzed with β-glucuronidase, and extracted with a strong anion exchange (SAX) polystyrene column was used to cleanup the sample. DES and its isopropanol metabolites were eluted from the column with methanol. Experiments using radiolabele (^{3}H) DES consistently indicated recoveries of 85-90%. Twenty samples could be processed per day.

GC/MS

A capillary GC/MS system was used consisting of a HP5970 MSD with electron impact capabilities and a Grob type splitless injector. Samples were derivatized with HFBA after extraction and run in the selected ion monitoring mode. Three ions from the analyte (660,631,44 and the analogous ions from deuterium labeled internal standard D_8-DES (668,637,455) were used quantitation and to aide in identification. A calibration curve was constructed and the detecti limit was determined to be 50 ppt using the IUPAC definition of 3α above the control. The liver a calf orally administered DES was analyzed by this method and was found to contain 40 ppb DES.

LC/MS

The DLI micro LC/MS system employed the use of a Brownlee dual syringe micro HPLC pump interfaced to a HP5985B mass spectrometer with a DLI micro LC/MS probe (1). The total effluent from the 1 mm microbore column is jetted into the chemical ionization source thrugh a 5 micron orifice in a stainless steel diaphragm. The LC solvent is used as the reagent gas. The positive mode was used.

For the separation of trans DES from α-dienestrol a normal phase system was found to prod the best results. A homepacked irregular silica column utilizing hexane/IPA (93/7) easily achie the separation. On-column detection limits of these compounds using selected ion monitoring of (M+1) was less than 1 ng. Analysis of the same liver sample that was done by GC/MS gave good correlation with respect to the quantitative results (40ppb) again using D_8DES internal standar

A gradient system was used to chromatograph of mixture of DES, α-dienestrol, 3 metabolite 1-OH-DES, 1-OH-Dienestrol, and 3'methoxy DES. Although good separation and reasonable run times could be achieved using the gradient on the microbore silica column, long equilibration times o the silica precluded its practicle use. Microbore reversed phase gradients can be routinely run The major drawback is the lack of capability to separate DES and α-dienestrol on reversed phas systems. The logical solution is the use of a bonded normal phase column such as amino, diol, o cyano. Preliminary results using super critical fluid chromatography on an amino column indicat that the trans DES and dienestrol separation can be readily achieved on this stationary phase Future work will be geared toward the use of LC/MS/MS in order to obtain more structural information.

1. Eckers, C., Skrabalak, D., Henion, J. 1982. Clinical Chemistry, 28, 1882.

Desorption Chemical Ionization and Fast Atom Bombardment Spectra of Dactinomycin.

John Greaves, Malcolm McCamish* and John Roboz
Mount Sinai School of Medicine, New York, NY 10029 and *University of Queensland, Brisbane, 4067 Australia.

Dactinomycin (DACT, Actinomycin D, Cosmogen, NSC-3053) is an antineoplastic antibitotic, used in the treatment of testicular cancer, gestational choriocarcinoma, and Wilm's tumor. It is a natural product produced by Streptomyces antibioticus and Streptomyces v. parvullus. DACT consists of two identical cyclic pentapeptide esters (-L-threonine-D-valine-L-proline-sarcosine-L-methylvaline-O-) linked by the amino group of the threonine to carboxyl groups at the 1 and 9 positions of a phenoxazone ring system. Because of the high molecular weight (MW=1254.628), polar nature, and instability of DACT, mass spectrometric data have not been available. Using desorption chemical ionization (DCI), with ammonia as the reagent gas and fast atom bombardment (FAB), with argon as the bombarding species, we have obtained spectra which contains the molecular ion of DACT.

Instrumentation was a VG ZAB-1F high resolution mass spectrometer with a standard magnet. The accelarating voltage was 7 kV and resolution was 2000. For DCI, scanning was at 2 or 3 s/mass decade. Two mass regions were scanned (m/z 1900-800 and m/z 1100-200) because of the short desorption time of DACT. For the upper mass range Ultramark 1621 (direct probe-ammonia CI) was used to calibrate the mass scale. Ultramark 1621 gave protonated molecular ions for each component of the mixture (i.e., 922, 1022, 1122,...) and fragment ions corresponding to the loss of $(CF_2CF_2)_nCH_2$ groups. For the FAB the atom gun conditions were 8 kV and 70 uA and scanning m/z 1600-300 at 5 s/mass decade (calibration: PFK + heptyl and nonyl triazines in EI mode).

DCI spectra of DACT at the upper mass range showed increasing amounts of fragmentation as the current through the DCI wire increased. As desorption began, the M-1 ion was the base peak with fragments at m/z 1185, 957, and 830, corresponding to progressive losses of proline, methylvaline-sarcosine, and valine, respectively (sometimes with losses of additional oxygens and appropriate proton shifts). The next spectrum obtained (i.e., current for desorption increased) caused losses of methyl groups and water in addition to the proline and methylvaline-sarcosine groups. Other fragments included loss of methylvaline independently and a CH_2NCOCH_3 group. DCI at the lower mass range showed no changes that were dependent upon the amount of current used for the DCI (compound was already highly fragmented). Ions between m/z 830 and 432 showed the breakup of the second pentapeptide with losses of proline-sarcosine-methylvaline and valine. The predominant ions in the spectrum were m/z 432, 350, and 321 which correspond to the progressive loss of fragments of the threonine attached to the chromophore (i.e., 432-C_4H_4NO, followed by 350-CHO).

The FAB spectra contained as the primary ions m/z 1256 $(M+H)^+$, m/z 461 $[\text{chromophore}+(CONHCHCOCHCH_3)_2]^+$ and m/z 482 $(\text{pentapeptide}+H)^+$. The base peak was m/z 461 unless acetic acid was added to the glycerol matrix when the m/z 482 ion became enhanced (approx. X2), presumably due to the availability of additional protons. The m/z 482 ion has no counterpart in the DCI spectrum.

Efforts are underway to use accurate mass measurements to identify DACT and other actinomycins (e.g., 7-amino-DACT, ACT-I, ACT-V, and ACT-C) in the presence of each other in culture media. Some of these compounds have molecular weights that differ by only a few tenths of a mass unit.

(Supported by the T.G. Martell Foundation for Leukemia and Cancer Research).

GC/MS STUDIES ON THE METABOLISM OF TETRAHYDROCANNABINOL HOMOLOGUES

D. J. HARVEY

University Department of Pharmacology
South Parks Road
Oxford OX1 3QT, UK.

Delta-9-tetrahydrocannabinol (delta-9-THC, Ia), the major active constituent of cannabis, is accompanied in many samples of the drug by appreciable concentrations of the propyl homologue (Ib) and small concentrations of methyl-delta-9-THC (Ic). These

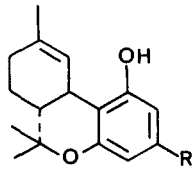

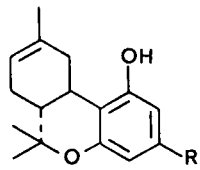

Ia, R = C_5H_{11}
Ib, R = C_3H_7
Ic, R = CH_3
Id, R = C_7H_{15}

IIa, R = C_5H_{11}
IIb, R = CH_3

compounds have a lower psychoactivity than delta-9-THC itself but psychoactivity has been shown to be greater in synthetic homologues having side-chains longer than the pentyl chain in the natural drug. This may reflect an altered metabolism, a different pharmacokinetic profile or both but to date, no metabolic or pharmacokinetic studies appear to have been reported on any of the delta-9-THC homologues. This paper reports some preliminary work on the metabolism by the mouse of delta-9-THC and its propyl and heptyl (Id) homologues together with delta-8-THC (IIa) and its methyl homologue (IIb).

Groups of 3 mice (male, Charles River CD-1, 23-25 g) were treated intraperitoneally with delta-8-THC, delta-9-THC, heptyl-delta-9-THC, methyl-delta-8-THC or cannabis extract containing propyl-delta-9-THC. Each compound was suspended in Tween-80 and isotonic saline at a dose of 100 mg kg^{-1} for each cannabinoid. After 1 hour the animals were killed by cervical dislocation and the livers were removed and frozen (-20°C). The livers were then homogenized in isotonic saline (10 ml) and the metabolites were extracted with ethyl acetate (3 x 8 ml). The combined extracts from each liver were chromatographed on Sephadex LH-20 (5 g packed into a 1 cm diameter column) in chloroform and the fraction eluting between 35 and 70 ml (monohydroxy metabolites) was collected. A further fraction containing polar metabolites was obtained by elution with 10% $MeOH/CHCl_3$ Aliquots of these fractions were converted into TMS, perdeutero-TMS, methyl ester : TMS, methyloxime : TMS or methane boronate : TMS derivatives or were reduced with lithium aluminium deuteride prior to TMS ether formation. Metabolites were identified by GC/MS using a VG Micromass 12B mass spectrometer interfaced to a VG 2050 data system and via a glass jet separator to a Varian 2440 gas chromatograph containing a 2 m x 2 mm glass column packed with 3% SE-30 on 100-120 mesh Gas Chrom Q. The column oven was temperature programmed from 170°C to 310°C at 4°/min. Other operating conditions were: injector, separator and ion source temperatures, 300, 300 and 260°C respectively; carrier gas, helium at 30 ml/min; accelerating voltage, 2.4 kV, electron energy, 25 eV; trap current, 100 μA; scan, 3 sec/decade, exponential.

Because of the very low concentrations of the metabolites present in the livers, identification was based on the GC/MS properties of several derivatives chosen to provide functional group information. Further information was obtained by reduction of metabolite fractions with lithium aluminium hydride. This enabled metabolites containing acid or ketone groups to be reduced to the parent alcohol, usually present as metabolites, thus

enabling correlations to be made between metabolites having functional groups in common positions but in different oxidation states. The origin of the alcohol produced by reduction was reflected by the deuterium incorporation; thus acids and ketones were reduced with the incorporation of two and one atom respectively.

Metabolites of delta-9-THC found in mouse liver have been reported previously (1) and consist mainly of mono-, di- and tri-hydroxylated species and their oxidized (acid or ketone) analogues. The positions substituted were 2', 3', 4', 8(α and β) and 11 with 11-hydroxy-delta-9-THC and delta-9-THC-11-oic acid being the major metabolites. Most other abundant compounds had a carboxylic acid group at C-11 and one or more hydroxy groups at the other positions. The metabolism of delta-8-THC (IIa) was very similar (2) except that hydroxylation at the cyclic allylic-position was at C-7 rather than at C-8.

Although the positions substituted in n-heptyl-delta-9-THC (Id) were the same as those in delta-9-THC itself, the observed profile was very different. Very few of the metabolites contained an acid group but major metabolites were present containing three and four (III) metabolically added hydroxy groups. In each case, two of these were in

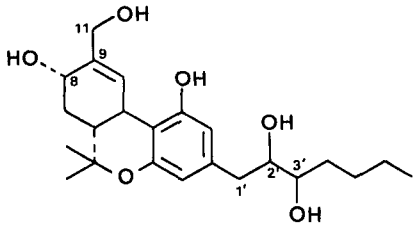

III

the side-chain at positions 2' and 3' as shown by the spectra of TMS and methane boronate : TMS derivatives. The reason for this difference in metabolic profile is thought to reflect the higher lipophilicity of the n-heptyl-homologue which facilitates attack by the membrane-bound cytochrome P-450 oxygenases and inhibits attack by cytosolic alcohol dehydrogenase.

This theory was borne out by the results obtained from the mice treated with lower homologues of THC. Thus the propyl-homologue of delta-9-THC (Ib) present in the crude cannabis extract was metabolized to high relative concentrations of acidic metabolites and no evidence was found for metabolites containing three or four hydroxy groups. Again 11-hydroxylation and oxidation to the acid was the major route of biotransformation. The methyl homologue of delta-9-THC was not available but the studies on the metabolism of methyl-delta-8-THC (IIb) showed the profile to be dominated by methyl-delta-8-THC-11-oic acid with only very small concentrations of metabolites containing additional hydroxylation. Identified metabolites of methyl-delta-8-THC, in addition to the 11-oic acid, included low concentrations of 11-hydroxy-delta-8-THC, 1'-hydroxy-delta-8-THC-11-oic acid, 7,11-dihydroxy-delta-8-THC and a trihydroxy metabolite, possibly 1,7,11-trihydroxy-delta-8-THC.

These results, therefore, show that the metabolism of homologous THC's is strongly influenced by the chain length and thus lipophilicity. The less lipophilic lower homologues are metabolized predominantly to acids whereas the higher homologues are metabolized more extensively by cytochrome P-450 with the production of higher proportions of polyhydroxylated species.

Acknowledgements. This work was supported by grants from the Wellcome Trust and the Medical Research Council.

References

1. D. J. Harvey, B. R. Martin and W. D. M. Paton. J. Pharm. Pharmacol. 1977 29 482.
2. D. J. Harvey and W. D. M. Paton. Drug Metab. Dispos. 1980 8 178.

DEGRADATION PRODUCTS OF 9-ALKYLTHIO-9,10-DIHYDRO-10-HYDROXYPHENANTHRENES

V. J. Feil, J. K. Huwe and J. E. Bakke
Metabolism and Radiation Research Laboratory
State University Station, Fargo, ND 58102

9,10-Phenanthrene oxide was reacted with methanethiol, ethanethiol, phenylmethanethiol, mercaptoacetic acid and cysteine to yield substituted dihydrophenanthrenol which are metabolites or model compounds of the arene oxide-glutathione metabolic process. These compounds decompose slowly on storage in neat form even at 4° C. The benzyl analogue on storage yielded a compound proposed to be 9-benzylthio-10-hydroxyphenanthrene based on its mass spectrum (m/z 316, $M^{+\cdot}$, M - 91, M - 91 and 28).

Storage of these compounds in acidic methylene chloride and methanol generally resulted in the formation of phenanthrene and a disulfide. Commercial methylene chloride was sufficiently acidic to cause a slow rate of decomposition. The benzyl analogue yielded, in addition to phenanthrene and diethyl disulfide, 9-benzylthiophenanthrene and 9-benzylthio-9,10-dihydro-10-methoxyphenanthrene. In neutral methanol the rate of decomposition was slow but more complex. The ethyl analogue yielded phenanthrene, 9-phenanthrenol, 9,10-phenanthraquinone, 9,10-dihydroxyphenanthrene, and two compounds that yield apparent molecular ions at m/z 270. Tentative structures proposed for these oxidized products are 9-ethylsulfonylphenanthrene and 9-ethylsulfonyl-9,10-dihydro-10-hydroxyphenanthrene (one of the compounds is more polar on C_{18} reverse phase HPLC and presumably dehydrates in the mass spectrometer source). In the presence of a large excess of HCl in methylene chloride the benzyl analogue yielded phenanthrene, dibenzyl disulfide, 9-chlorophenanthrene and 9-benzylthio-10-chlorophenanthrene.

A mixture of 9-ethylthio-9,10-dihydro-10-hydroxyphenanthrene and phenylmethanethiol in acidic methanol yielded phenanthrene, ethylbenzyl disulfide and dibenzyl disulfide. Two moles of the cysteine analogue labeled with ^{14}C in both the phenanthryl and cysteinyl groups yielded two moles of phenanthrene and one mole of cystine (quantitation based on ^{14}C). Treatment of either the ethyl or the benzyl analogue with methanolic HCl in the presence of ethyl acrylate yielded phenanthrene, dialkyl disulfides and a compounds whose mass spectra were compatible with ethyl 2-alkylthio-3-chloropropionates suggesting the presence of a sulfenyl chloride during degradation.

The formation of many of the compounds identified in this study can be explained by protonation of the hydroxy group and loss of water to form a cyclic sulfenium ion. Reaction of the sulfenium ion with water would regenerate the starting compound, reaction with methanol would yield the methoxy compound (a compound that was isolated as a degradation product of the benzyl analogue), and reaction with chloride ion would yield the chloro compound. At least the methoxy compound could, via protonation, regenerate the cyclic sulfenium ion. Reaction of the sulfenium ion at sulfur with water, methanol or chloride ion would result in the formation of phenanthrene and a sulfenic acid, methyl ester of a sulfenic acid or a sulfenyl chloride. Coupling of these compounds would yield the disulfide and hydrogen peroxide, dimethyl peroxide or chlorine. In support of this mechanism, positive starch iodine tests were obtained shortly after the reactions were initiated. On long standing the reactions no longer yielded positive starch iodine tests; also on standing the reactions often yielded compounds in which sulfur had been oxidized.

We have used sequential derivatization with diazomethane and Regisil and analysis by GCMS in the purification and identification of the cysteine conjugate isolated from biological sources. We obtained peaks at m/z 178, 280 and 370, but did not obtain $M^{+\cdot}$ or M - 15 ions. Positive ion FABMS in glycerol yielded an M + 1 ion.

We believe that many arene oxide-glutathione type metabolites are unstable resulting in erroneous metabolite identification. This may be particularly true for compounds that undergo several arene oxide-glutathione type metabolism steps. We have preliminary evidence that some sulfur conjugates revert back to parent aryl compounds in vivo, thus subjecting biological systems to greater contact time with some compounds than would be expected.

MASS SPECTRAL CHARACTERIZATION OF GLUTATHIONE CONJUGATES. Sharon L. Pallante, Carol A. Lisek, Deanne Dulik and Catherine Fenselau; Dept. of Pharmacology, The Johns Hopkins University School of Medicine, Baltimore, MD 21205

A major role in the detoxification and excretion of a variety of mutagenic, carcinogenic and pharmacologically active substances is undertaken by the enzyme family known collectively as glutathione S-transferase. These enzymes bind substrates which are at the same time both hydrophobic and electrophilic and catalyze the first step in the formation of mercapturic acids (N-acetylcysteine derivatives). While the effect of the "protective mechanism" is inactivation of the toxic electrophilic center of the substrate compound, it also has the potential for creating a more reactive intermediate. With a few exceptions, little work has been done on the mass spectral characterization of intact glutathione conjugates. Microsomal glutathione S-transferase which has been immobilized on cyanogen bromide activated Sepharose 4B (simultaneously with cytochrome P-450 and glucuronyl transferase) has been employed to synthesize glutathione conjugates of drugs carrying a variety of functional groups -- halides, esters, thiols, epoxides and imines. These products have been characterized by thin layer chromatography, high pressure liquid chromatography and mass spectrometry.

R_X SITE	SUBSTRATE	STRUCTURE	CONJUGATE STRUCTURE	R-SG M.W.
HALIDE	CDNB			473
THIOL	CAPTOPRIL	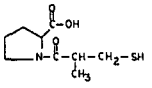	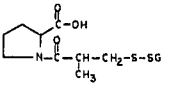	522
EPOXIDE	STYRENE OXIDE	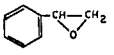	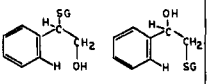	427
IMINE	IMINOCYCLO-PHOSPHAMIDE	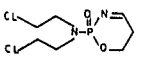	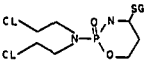	565
MICHAEL ADDITION	ETHACRYNIC ACID	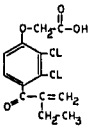	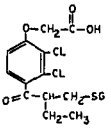	609
ESTER	INDOMETHACIN GLUCURONIDE	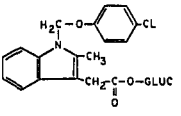	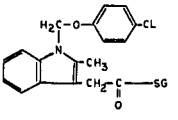	646

A variety of ionization techniques has been evaluated for production of molecular ions and structurally informative fragment ions of both positive and negative sign. As a class, the glutathione conjugates are too thermally labile to be analyzed by EI or CI underivatized. FD has been the method of choice but yields little more information than the MH+ which is the base peak [FD spectrum of conjugate courtesy of Bob Lattimer/B. F. Goodrich]. Positive FAB with thioglycerol as a matrix now seems to be the best complementary mode of ionization, giving ions from the substrate compound, glutathione and the glutathione conjugate, with MH+ frequently as the base

peak. Glycerol appears to be a much poorer matrix for this compound class with lower MH+ formation and often giving rise to side reactions. Negative FAB with glycerol and diethanolamine were also evaluated as giving informative ions but still not surpassing the +FAB/thioglycerol method. A thermospray mass spectrum [courtesy of Barbara Larsen on a magnetic sector MS-50 with Vestec interface] gave positive identification as a glutathione conjugate with [MH]+ and [GSH+H]+ ions; thus leading toward analysis of glutathione conjugates by HPLC/MS. Styrene oxide-SG conjugate spectra are given as a class example of positive and negative FAB with differing matrices.

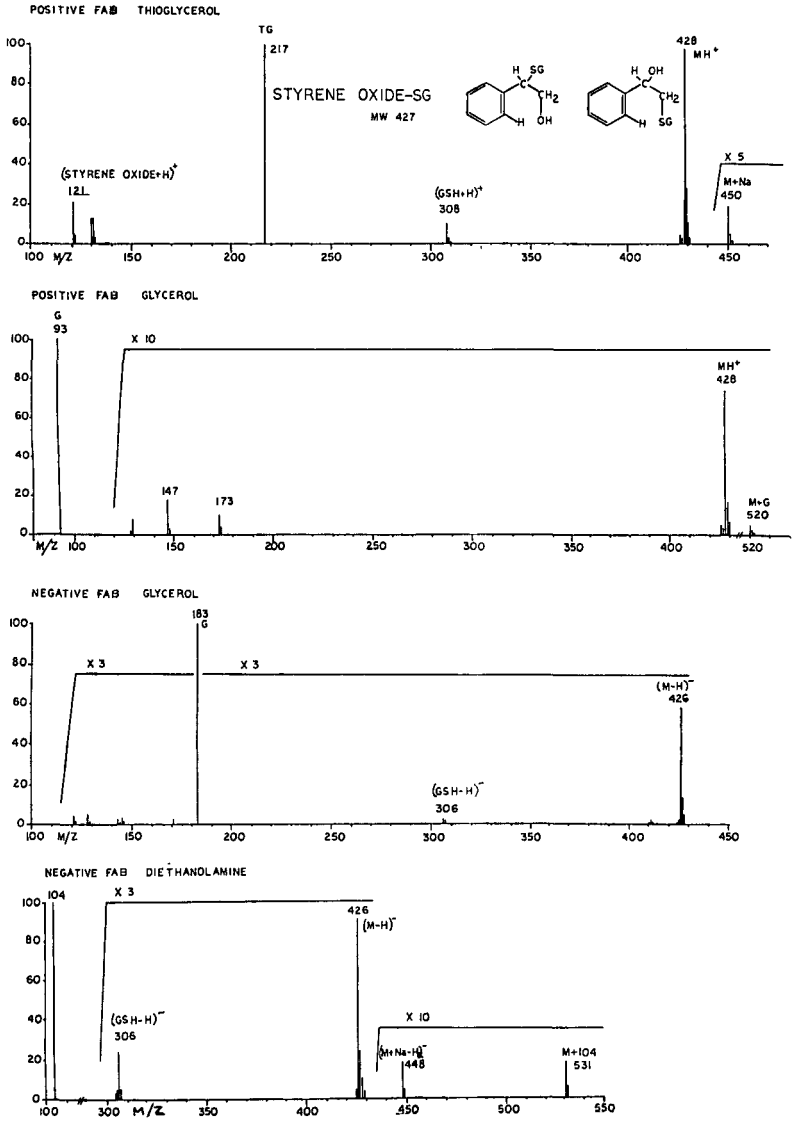

ANALYSIS OF KETIMINES BY FAST ATOM BOMBARDMENT MASS SPECTROMETRY

J.O. Lay, Jr., and T.T. Chang
American Cyanamid, Stamford CT

Fast Atom Bombardment (FAB) mass spectrometry was used to determine the structures of the amine and ketimine cross-linking agents used in new two- and one-component, room temperature cure coatings. (This new cross-linking technology, based on activated carboxylic esters is described elsewhere[1]).

The amine was generated by the reaction of hexamethylene diamine (HMDA) and dimethyl maleate (DMM) and was believed to have the structure, I, shown below. FAB/MS analysis showed the crude reaction products to be a fairly complex mixture. The largest high mass signal was observed at M/Z 429, for $M+H^+$, corresponding to the desired product, (I), from three moles HMDA per mole DMM. The product, at M/Z 313 (II), coming from the incomplete reaction of DMM (at the ester linkage) with only two moles HMDA and the loss of two moles of methanol was also observed. The other possible product, incorporating two HMDA (M/Z 345), with one reacting at the double bond, was not observed. This gives strong evidence that the ester linkages are much more reactive to HMDA than is the carbon-carbon double bond.

The other two straight-forward reaction products were both "dimers". The dimer from Structures I and II, (minus HMDA) gave an ion at M/Z 625 (Structure III), while a dimer from two of Structure I, minus HMDA, gave the second most abundant high mass ion at M/Z 741 (Structure IV).

Several unexpected masses were also observed in the FAB mass spectra. Signals were observed 40 amu higher in mass than Structure I (the predominent "monomer") or Structure IV (the predominent dimer). These unexpected products were believed to be ketimines of acetone at M/Z 469 (I + acetone - H_2O to give V) and M/Z 781 (IV + acetone - H_2O to give VI). In addition, the diketimine of I was also observed at M/Z 509 (Structure VII). These unexpected acetone ketimines were observed as minor components in several lots of the HMDA-DMM products and are attributed to traces of acetone in the reaction mixture.

The corresponding ketimines, important in single component, moisture cure systems, were also studied. Several different ketones were added to the HMDA+DMM products to produce the desired ketimine. The ketones included methyl-ethyl, methyl-i-butyl and methyl-amyl ketone. With all ketones, the di- and tri-ketimines of the major amine product (I) were observed giving Structure VIIIand IX. For Stucture VIII, the diketimine, the masses were 537, 593, or 621; depending on whether the ethyl, isobutyl, or amyl ketone was employed. For Structure IX, the triketimine, the masses were 591, 675 and 717 respectively.

With amyl ketone, there was also observed a series of peaks with correspondingly fewer methylene units. For Structure VIII, peaks were observed at M/Z 621-14XN N=O, 1,2 while for IX, peaks were observed at M/Z 717-14XN N=O, 1,2,3. These were attributed to contamination of the methyl-amyl ketone with methyl-butyl ketone.

Another interesting, and unexpected finding was a peak at M/Z 405 in the HMDA:DMM :Methyl-amyl ketone product. This peak corresponds to ring closure and loss of $H_2N(CH_2)_6N{=}C(C_7H_{14})$ or HMDA from Structures VIII and IX to give Structure X. The observation of this component was attributed to the reaction conditions used to prepare the ketimines containing the higher molecular weight ketones.

In conclusion, we believe that FAB/MS (1) has been shown to be valuable for the analysis of these amine and ketimine mixtures, without prior separation or clean-up, (2) has provided valuable data regarding tje chemical structure of these cross-linking agents, and (3) can be easily used to characterize the major and some minor components in this and otjer complex synthetic mixtures.

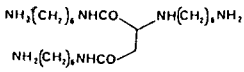

I

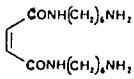

II

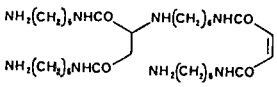

III (or Isomer)

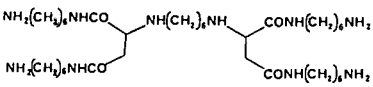

IV (or Isomer)

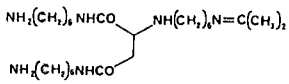

V (or Isomer)

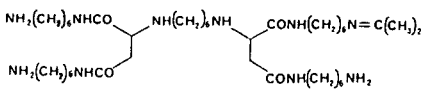

VI (or Isomer)

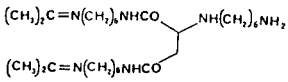

VII (or Isomer)

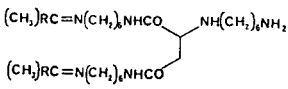

VIII (or Isomer)

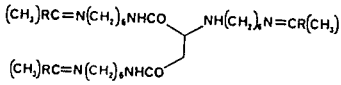

IX

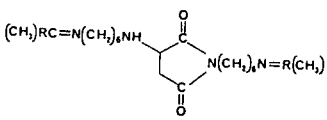

X

HIGH PRESSURE COLLISIONAL ACTIVATION MASS SPECTRA OF SOME SUBSTITUTED BENZENES

Karl F. Blom and Burnaby Munson
Department of Chemistry, University of Delaware, Newark, Delaware 19716

Ions produced under high pressure or chemical ionization (CI) mass spectrometry conditions can be collisionally activated and decomposed within the ion source by applying large electric fields (ca. 100 V/cm) across the source. High pressure collisional activation (HPCA) is a simple and effective method for increasing the fragmentation in CI spectra to obtain some additional structural information. The HPCA mass spectra of some substituted benzenes are presented here to illustrate the major factors controlling the fragmentation under these conditions.

A 2-region high pressure ion source which separates sample ion formation from collisional activation was used in these studies, Fig. 1. This source configuration simplifies the HPCA mass spectrum by minimizing competing bimolecular fragmentation channels such as reactions of collisionally excited reactant ions with the sample:

$$[CH_5^+]^* + M \longrightarrow F_i^+ + N_i + CH_4$$

The high pressure collisional activation process is represented schematically in Fig. 2. Sample ions, P^+, acquire kinetic energy from the electric field in region 2 of the 2-region ion source which is converted to internal modes by inelastic collisions with the high pressure (ca. 1 torr) reagent gas. Ions undergo many collisions within region 2 (ca. 100) and, thus, obtain only a small amount of kinetic energy (ca. <1 eV) between collisions. This results in the "gradual" increase in internal energy shown in Fig. 2. Many collisions are necessary for an ion to accumulate enough internal energy to undergo unimolecular decomposition.

FIGURE 1

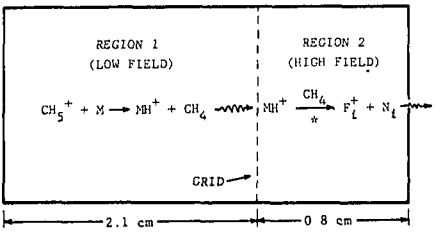

FIGURE 2

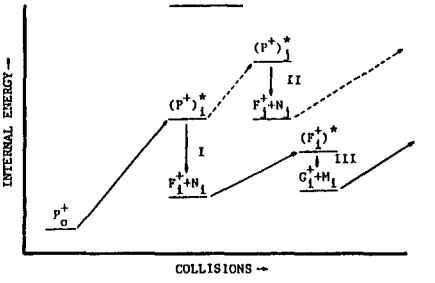

If the lowest energy decomposition (I in Fig. 2) is fast, an excited sample ion may decompose before the additional energy necessary for higher energy decompositions (II) to occur can be accumulated. This is the situation in the HPCA spectrum of chlorobenzene with CH_4 as the reagent gas. The major decomposition of the $(C_6H_5Cl+H)^+$ ion is the lower energy HCl elimination, Table 1. The higher energy decompositions are minor processes.

If the energy difference between competing unimolecular decompositions is small, both processes may be important. This situation occurs in the HPCA spectrum of bromobenzene with CH_4 reagent gas. The decomposition of $(C_6H_5Br+H)^+$ produces abundant $C_6H_5^+$ and $C_6H_6^+$ fragment ions, Table 1. The higher energy decomposition products, $C_6H_5Br^+$ and $C_6H_4Br^+$, are minor products.

If the lowest energy decomposition is slow, the excited parent ion may survive long enough to accumulate the internal energy needed for fast, higher energy decompositions (II in Fig. 2) to occur. This appears to be the case for the HPCA decomposition of smaller alkylbenzenes. The decomposition of protonated toluene, for example, produces an abundant $C_6H_5^+$, Table 1, suggesting that the lower energy decomposition producing $C_7H_7^+$ (presumably benzyl ion) is relatively slow.

Since fragment ions are formed within the ion source they will also be collisionally activated. At high field strengths this can lead to consecutive or step-wise decompositions

Table 1.

Decomposition	Rel. Abund.	D(kcal/mole)
Chlorobenzene/CH_4 (field strength = 135 V/cm)		
$(C_6H_5Cl+H)^+ \rightarrow C_6H_5^+ + HCl$	1.00	54
$(C_6H_5Cl+H)^+ \rightarrow C_6H_6^+ + Cl$	0.10	67
$(C_6H_5Cl+H)^+ \rightarrow C_6H_4Cl^+ + H_2$	<0.01	~76
$(C_6H_5Cl+H)^+ \rightarrow C_6H_5Cl^+ + H$	<0.05	78
Bromobenzene/CH_4 (field strength = 115 V/cm)		
$(C_6H_5Br+H)^+ \rightarrow C_6H_5^+ + HBr$	1.00	56
$(C_6H_5Br+H)^+ \rightarrow C_6H_6^+ + Br$	0.65	54
$(C_6H_5Br+H)^+ \rightarrow C_6H_4Br + H_2$	<0.01	~70
$(C_6H_5Br+H)^+ \rightarrow C_6H_5Br + H$	<0.25	78
Toluene/CH_4 (field strength = 115 V/cm)		
$(C_6H_5CH_3+H)^+ \rightarrow C_7H_7^+ + H_2$	1.00	26
$(C_6H_5CH_3+H)^+ \rightarrow C_6H_5^+ + CH_4$	1.00	63
$(C_6H_5CH_3+H)^+ \rightarrow C_7H_8^+ + H$	<0.10	77
$(C_6H_5CH_3+H)^+ \rightarrow C_6H_6^+ + CH_3$	<0.01	77

(III in Fig. 2). As an example of step-wise decomposition, Fig. 2 shows the variation in the variation in the relative abundances of the major ions in the CH_4 HPCA mass spectrum of ethylbenzene as the field strength in region 2 of the 2-region source is increased. The major decomposition of protonated ethylbenzene is C_2H_4 elimination producing $C_6H_7^+$, presumably protonated benzene. The abundance of $C_6H_7^+$ passes through a maximum as the field strength is increased and an abundant $C_6H_5^+$ is formed. We postulate that the $C_6H_5^+$ results from a step-wise decomposition sequence:

$$C_8H_{11}^+ \xrightarrow{*} C_6H_7^+ + C_2H_4$$
$$C_6H_7^+ \xrightarrow{*} C_6H_5^+ + H_2$$

The postulated decomposition sequence can be tested by comparing the distribution of fragment ions formed during the breakdown of $C_6H_7^+$ in Fig. 3 to that resulting from the decomposition of $C_6H_7^+$ in the CH_4 HPCA spectrum of benzene. The step-wise decomposition of the $C_6H_7^+$ fragment ion should produce the same fragmentation pattern as the direct decomposition of $C_6H_7^+$. Table 2 compares the ionic distributions at the $C_6H_7^+/C_6H_5^+$ cross-over point. The distributions are essentially identical, consistent with the postulated step-wise decomposition sequence.

FIGURE 3

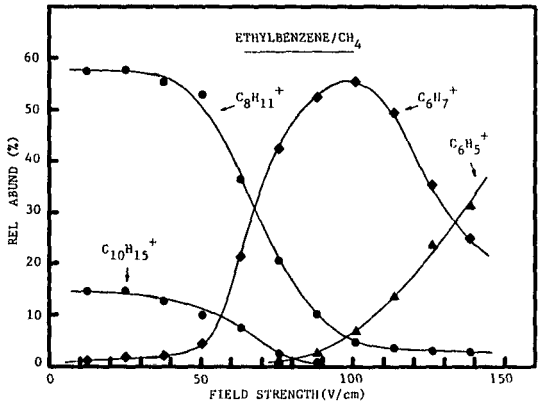

Table 2.

Ion	Rel. Abund. Ethylbenzene	Rel. Abund. Benzene
$C_6H_7^+$	1.0	1.0
$C_6H_5^+$	0.96	0.99
$C_4H_3^+$	0.13	0.12
$C_4H_2^+$	0.01	0.01

NEUTRAL PRODUCT DISTRIBUTIONS FROM DEPROTONATION OF 1-METHYLCYCLOPENTYL CATION

Eric W. Redman and Thomas Hellman Morton

Department of Chemistry, University of California, Riverside, California 92521

The 1-methylcyclopentyl cation represents one of the simplest examples of a Brønsted acid that has two types of chemically nonequivalent acidic protons. As such, its deprotonation in the gas phase has been a focus of interest in our laboratory for several years.[1] This cation is readily generated by electron impact on bromocyclohexane, as reaction 1 shows, and other ions formed concurrently react with the parent neutral to generate more of this cation, as the FTMS spectra in Figure 1 depict. Subsequent reaction of $C_6H_{11}^+$ with base yields two products, as shown in reaction 2. For strong gaseous bases (e.g. NR_3) the ratio is 4/3, the same as the ratio of the methylene to methyl protons, and we have shown that this result is inconsistent with any model for proton transfer than invokes a single intermediate that decomposes directly to the two products.[2]

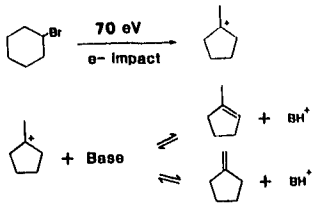

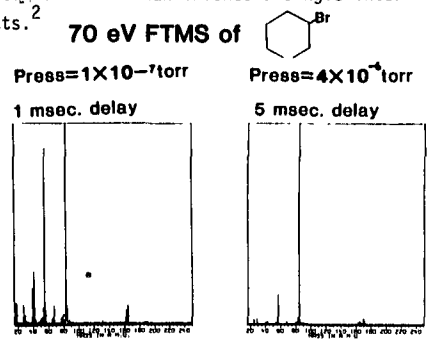

Figure 1

We have studied the distribution of neutral products from deprotonation as a function of base using our EBFlow reactor. The results are summarized in Table 1, with precision as shown by the tabulated standard deviations (σ). When base is absent, the parent neutral does not react with $C_6H_{11}^+$, and the neutral products result from collision of the ion with the walls of the reaction vessel. Under these conditions, the product yield is very much reduced and only the thermodynamically more stable isomer is recovered. As base strength is increased, the abundance of the thermodynamically less stable isomer increases. Of particular note is the comparison between NH_3 and dipentyl ether, which have the same gas phase proton affinities. The product distributions are very much different, much as would be expected from considerations based on density-of-states arguments and the much larger number of degress of freedom of the ether compared to ammonia.

Table 1

Base	Reported Proton Affinity		σ
Trimethylamine	222	.573	0.008
Ammonia	205	.733	0.012
Dipentyl ether (Am_2O)	205	.829	0.006
Dibutyl ether	204	.885	0.038
No Base	(190)	> 985	

We analyze these data in terms of two alternative models, shown to the right. The Eigen model[3] portrays the reaction as proceeding through hydrogen-bonded intermediates. Choice of reaction channel occurs prior to formation of the first intermediate, and the ratio of products is simply the ratio of the efficiencies of two independent channels times a statistical factor (path degeneracy) of 4/3. Using phase space calculations as devised by Chesnavich and Bowers[4] we determine that $\Delta E = 2.0 \pm 0.5$ kcal/mol with $E^{\neq} =$ 5-6 kcal/mol is required to fit our experimental results

An alternative picture, which we call the Lewis model (since a Lewis acid-base complex is the first intermediate), can also be made to fit the experimental data, but ΔE must be less than 1.5 kcal/mol.

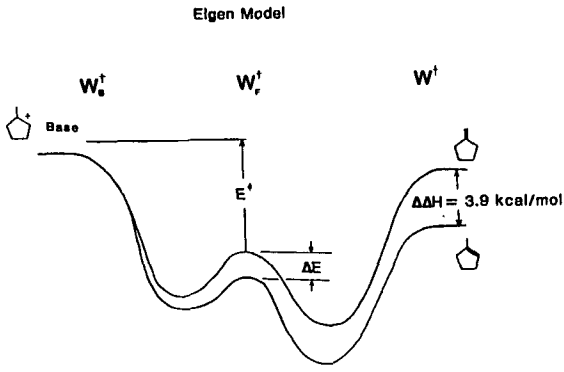

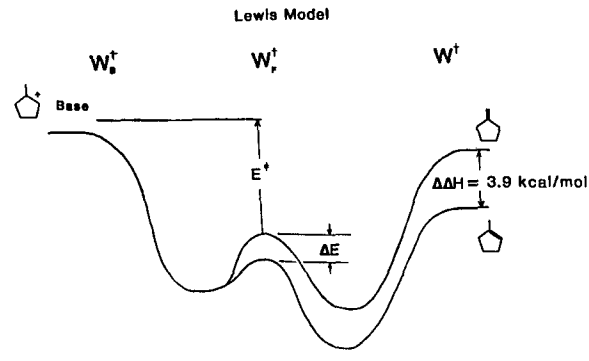

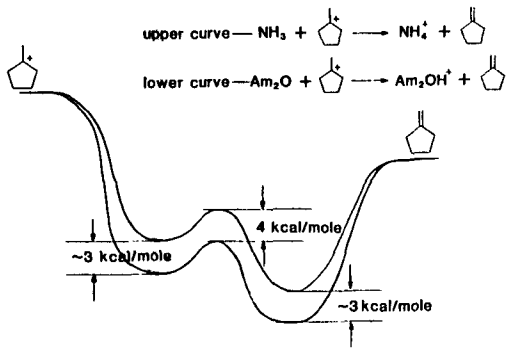

The figure to the left shows the lowering of the potential surface that the Eigen model demands in order to fit the effect of changing base.

Acknowledgment. We are grateful to Dr. M.F. Jarrold and Prof. M.T. Bowers for use of their computer program. This work was supported by NSF grant CHE 83-06081 and ACS-PRF grant 14945-AC4.

1. W.J. Marinelli and T.H. Morton, J. Am. Chem. Soc. 1978, 100, 3536-3539; 1979, 101, 1908.
2. T.H. Morton, Radiat. Phys. Chem. 1982, 20, 29-40.
3. H.Z. Cao, M. Allavena, O. Tapia, and E.M. Evleth, Chem. Phys. Lett. 1983, 96, 458-463.
4. M.F. Jarrold, L.M. Bass, P.R. Kemper, P.A.M. van Koppen, and M.T. Bowers, J. Chem. Phys. 1983, 78, 3756-3766.

SOME COMPARISONS BETWEEN THE ELECTRON IMPACT MASS SPECTRA OF FLUORINE SUBSTITUTED BETA-DIKETONATE AND MONOTHIO-BETA-DIKETONATE COMPLEXES OF METALS. Mark L.J. Reimer and John B. Westmore, Dept. of Chemistry, University of Manitoba, Winnipeg, Manitoba R3T 2N2, Canada; and Manoranjan Das, Dept. of Chemistry, University of Zambia, Lusaka, Zambia .

INTRODUCTION. We have examined the electron-impact mass spectra of volatile neutral metal beta-diketonate and monothio-beta-diketonate complexes of the type shown, in order to assess the influence of sulfur within the chelate ring upon the fragmentation pathways. We have compared the spectra of tris-chelates of Cr(III), Fe(III) and Co(III), and bis-chelates of Ni(II), Cu(II) and Zn(II) to give, in each series, representatives of metals with oxidation states of varying relative stabilities.

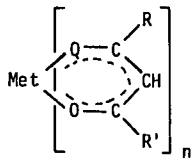

Q = O or S
R = ALKYL or ARYL
R' = CH_3 or CF_3
n = 2 or 3

EXPERIMENTAL. Most of the mass spectra were recorded on a Hitachi RMU-6D single-focussing magnetic sector instrument at 70 eV, using a direct insertion probe. Some spectra were taken from the literature, but were also recorded on magnetic sector mass spectrometers.

RESULTS. In general, both metal-containing and metal-free ions were observed. Here we present a summary of observations on the relative abundances of metal-containing ions.

Copper. Aryl groups such as C_6H_5 or C_4H_3S (thienyl) stabilize the molecular ion. In the absence of an aryl group, sulfur in the chelate ring also appears to stabilize the molecular ion. For thio-ligands with aryl substituents, $Cu(CH{\equiv}CR)^+$ is a prominent ion. Species $LCuH^+$ and $[L_2Cu\text{-}HL]^+$, which are prominent for dioxo-ligands with aryl substituents, are suppressed for thio-ligands.

Zinc. In the absence of an aryl group, the molecular ion is stabilized by a thio-ligand. The spectra of thio complexes are also much simpler. When an aryl group is present, the molecular ions of complexes of dioxo-ligands are more stable than those of the mono-thio ligands. The molecular ions of dioxo-ligands preferentially lose CF_3, while those of thio-ligands preferentially lose a ligand.

Nickel. Molecular ions of both chelate types are very stable. Dioxo-complexes preferentially lose CF_3; thio-complexes preferentially lose ligand.

Chromium. The molecular ions of chelates of both types are stable. In each case, the major decomposition is loss of a ligand. The spectra are quite similar.

Iron and Cobalt. Molecular ions are not observed for complexes of monothio-ligands.

SUMMARY. Since no clear trend is observed in these spectra, it appears that several factors including the specific metal involved and its oxidation state, will influence the effect of sulfur within the chelate ring.

ACKNOWLEDGEMENT. We thank the Natural Sciences and Engineering Research Council of Canada for financial assistance.

STERIOCHEMICAL EFFECTS IN THE ELECTRON IMPACT MASS SPECTRA OF EPIMERIC STEROID KETONES AND DIOLS. John B. Westmore and Mark L.J. Reimer, Dept. of Chemistry, and John F. Templeton and Chung-Ja Choi Jackson, Faculty of Pharmacy, University of Manitoba, Winnipeg, Manitoba, R3T 2N2, Canada.

INTRODUCTION. There has been continuing interest in the problem of identifying steroid epimers by mass spectrometry, with notable successes using techniques such as chemical ionization or linked scanning for example. We have studied the positive ion electron-impact mass spectra of the 3-keto-17-hydroxysteroids {1,2}{a,b} and the 3,17-dihydroxysteroids {3,4}{a-d}. The availability of these complete sets of isomeric steroids presents an opportunity to evaluate the effects of the orientation of the hydroxyl group at C-17 or C-3 and of cis- or trans-fusion at the A/B ring junction. Studies on such a comprehensive set of steroid epimers appear not to have been reported before.

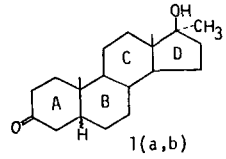

1(a,b)

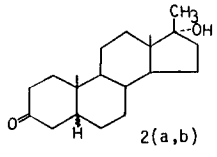

2(a,b)

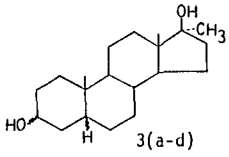

3(a-d)

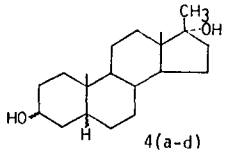

4(a-d)

EXPERIMENTAL. Positive ion electron-impact mass spectra were recorded separately on two mass spectrometers: (i) an Hitachi RMU-6D single focussing magnetic sector instrument at electron energies of 70, 20 and 12 eV (nominal), and (ii) a Finnigan 1015 quadrupole mass filter at an energy of 70 eV. In both cases, samples were introduced via a direct insertion probe. (Results shown are for the Hitachi instrument at 70 eV. The same trends were observed for the other conditions, although the actual peak height ratios differed).

RESULTS. An effective way of observing the influence of structural features is to compare the ratio of the peak height of a fragment ion to that of the molecular ion.

Ketosteroids {1,2}{a,b}

$[M - 18]^{+\cdot}/M^{+\cdot}$ Ratios:

	5α	5β
17α-hydroxy	0.67	0.57
17β-hydroxy	0.54	0.19

Elimination of H_2O from ring D is not sensitive to the configuration at C-17.

$[M - 75]^{+}/M^{+\cdot}$ Ratios:

	5α	5β
17α-hydroxy	0.29	2.17
17β-hydroxy	0.29	2.50

A metastable peak confirms that $[M - 75]^{+}$ is formed by elimination of H_2O from $[M - 57]^{+}$. Hence the O must come from the 3-keto group. This is insensitive to the configuration at C-17, but occurs more readily for the 5β steroids.

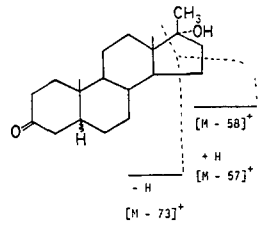

3,17-Diols {3,4}{a-d}

$[M - 18]^{+\cdot}/M^{+\cdot}$ Ratios:

5α	3α-OH	3β-OH	5β	3α-OH	3β-OH
17 α-hydroxy	0.78	0.39	17α-hydroxy	3.08	2.17
17β-hydroxy	0.56	0.35	17β-hydroxy	2.83	2.08

$[M - 36]^{+\cdot}/M^{+\cdot}$ Ratios:

5α	3α-OH	3β-OH	5β	3α-OH	3β-OH
17α-hydroxy	0.41	0.07	17α-hydroxy	2.17	1.13
17β-hydroxy	0.35	0.07	17β-hydroxy	1.67	1.19

Elimination of one or two molecules of H_2O is insensitive to the configuration at C-17, but occurs more readily from 5β steroids, particularly when a 3α-hydroxy group is present

$[M - 76]^{+\cdot}/M^{+\cdot}$ Ratios:

5 α	3α-OH	3β-OH	5β	3α-OH	3β-OH
17α-hydroxy	1.51	0.20	17α-hydroxy	8.33	1.57
17β-hydroxy	1.33	0.24	17β-hydroxy	8.65	1.65

$[M - 91]^{+}/M^{+\cdot}$ Ratios:

5 α	3α-OH	3β-OH	5β	3α-OH	3β-OH
17α-hydroxy	0.92	0.42	17α-hydroxy	4.17	1.17
17β-hydroxy	0.85	0.44	17β-hydroxy	3.83	1.38

Metastable peaks support formation of $[M - 76]^{+\cdot}$ and $[M - 91]^{+}$ by elimination of H_2O from $[M -58]^{+\cdot}$ and $[M - 73]^{+}$, respectively. These fragmentations are insensitive to the configuration at C-17 but occur more readily for 5β steroids, particularly when a 3α-hydroxy group is present.

DISCUSSION. Elimination of H_2O from ring A of 3-ketosteroids occurs more readily from the more strained A/B cis-fused isomers. This reaction probably occurs via ring opening because (a) molecular models indicate that even in the 5β isomer, the closest O to H approach in the intact skeleton is about 2.5A (between O and H-9), which is considerably larger than normal O-H bonding distances (0.96A in H_2O) so that without ring opening, O-H bond formation is unlikely, and (b) on lowering the electron energy to a nominal 12 eV, the relative intensity of the $[M - 75]^{+}$ peak for all ketones decreases significantly compared to most of the other high mass peaks in these spectra, indicating a relatively high activation energy for the process.

Elimination of H_2O from ring A of 3,17-diols is also enhanced for 5β steroids, presumably because of greater ring strain as a result of the cis A/B ring junction. There is a further enhancement in these ratios when the oxygen of the 3-OH group closely approaches a hydrogen in an intact skeleton (to within approximately 1.0A of H-9 in the 3α-hydroxy-5β-steroids when ring A is in the boat conformation). In these cases, O-H bond formation can occur without the requirement of ring fission (thus lower activation energy). In fact, abstraction of H from C-9 in the loss of H_2O from $M^{+\cdot}$ of 5β-cholan-3α-ol has been established by deuterium labelling (H.Klein and C. Djerassi, Chem. Ber. 106, 1897 (1973)).

SUMMARY. The only definitive correlations obtained from the mass spectral data concern the cis or trans fusion of rings A and B. The relative intensities of fragment ions in which loss of H_2O occurs at some stage in their formation are enhanced for 5β steroids. A further enhancement occurs when a 3α-hydroxy group is present, particularly in a 5β steroid.

ACKNOWLEDGEMENTS. We thank the Medical Research Council and the Natural Sciences and Engineering Research Council of Canada for financial assistance.

CIS-AND TRANS - STEROCHEMICAL EFFECTS IN THE NCI/OH^- SPECTRA OF AZA-1 (n,2,0) ALKANE (n=3,4,5) USING MI - AND CAD-MIKE SPECTROMETRY.

J.C. Tabet[1], Y. Tondeur [2], Y. Troin [3], D. Vallee [3], J.C. Gramain [3] and D. Fraisse[4]
(1) Ecole Polytechnique, Palaiseau, France (2) PRI, NCI-FCRF, Frederick, MD. USA
(3) Universite de Clermont II, Aubiere, France (4) CNRS, Vernaison, France.

Large stereochemical effects have been previously reported [1,2] for stereomeric $[M-H]^-$ formed under negative chemical ionization (OH^-) showing the effect of the anchimeric assistance of the alkoxy group upon the elimination of H_2 from trans cyclohexane- 1,4-diol relatively to the cis isomer. In the present study, the stereospecific decomposition reactions of the deprotonated molecule from isomeric (cis and trans) aza-1-bicyclo (n,2,0) alkane derivatives (size of the lactam rings n=3,4,5) generated under NCI/OH^- have been examined using metastable ion and collisionally activated dissociation MIKE spectrometry. There measurements in connection with specifically labelled compounds enabled the determination of the origin of the stereochemical effects.

Experiments undertaken with a reagent gas mixture composed of ND_3 and N_2O, which induced a neutral-neutral H/D exchange reaction in azetidinols 1a and 1b, indicated that the hydroxylic proton constituted the preferential (~90%) site of deprotonation during the ionization. Fragmentations of the deprotonated species (MI-and CAD-MIKE spectra in Fig 1) observed in the second field free region of a reversed geometry instrument are affected by the stereochemistry of the hydroxylic group. As seen on Fig 1, the cis isomer mainly loses H_2O while the trans isomer eliminates a $CH_3^{\bullet}$ with high specificity. Labelling studies indicated that two pathways for the elimination of either H_2O from the cis isomer or $CH_3^{\bullet}$ from the trans isomer are possible as depicted in scheme 1 and scheme 2 respectively. The ring junction hydrogen is involved in both types of eliminations. The major pathway for the elimination of H_2O from the cis isomer also involved the cyclobutane methylene proton and for the $CH_3^{\bullet}$ elimination from the trans isomer, the cyclobutane methylene carbon. These stereochemical effects become less apparent when the size of the lactam ring is increased from a 5 member ring (1a, 1b) to a 6 and 7 member ring.

In conclusion, $[M-H]^-$ ion produced under NCI/OH^- from stereomeric azetidinols decompose in the 2nd FFR according to different specific pathways when the ring is strained enabling the isomeric differentiation of aza-1-bicyclo (3,2,0) alkane derivatives. The ring junction hydrogen from the cis isomer is transfered to the alkoxy group followed by migration of a cyclobutane methylene proton before H_2O elimination. The first step is not possible for the trans isomer and another fragmentation route is observed, i.e. the loss of a methyl radical from the cyclobutane cycle. This work demonstrates the potential of NCI/OH^- for analytical as well as for mechanistic studies.

Research sponsored by the National Cancer Institute under Contract No. N01-CO-23910 with Program Resources, Inc.

scheme 1

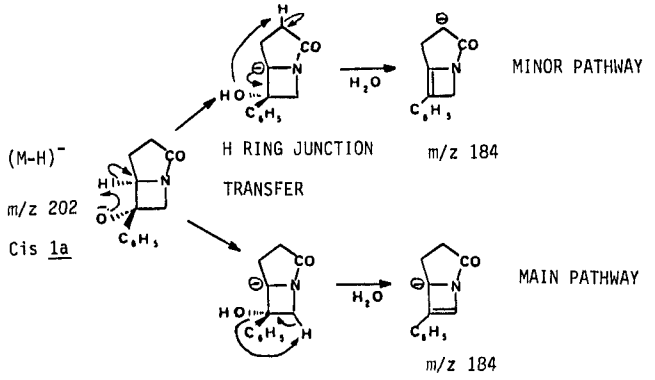

scheme 2

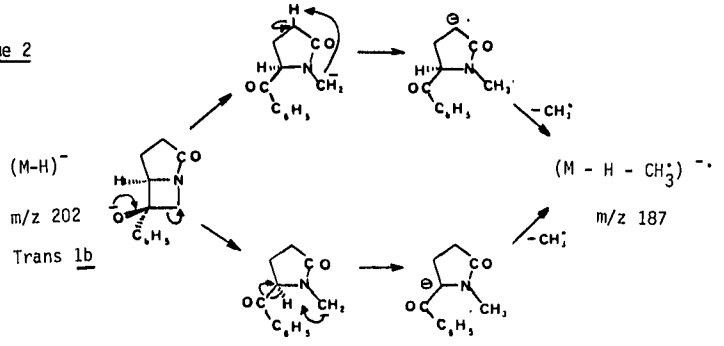

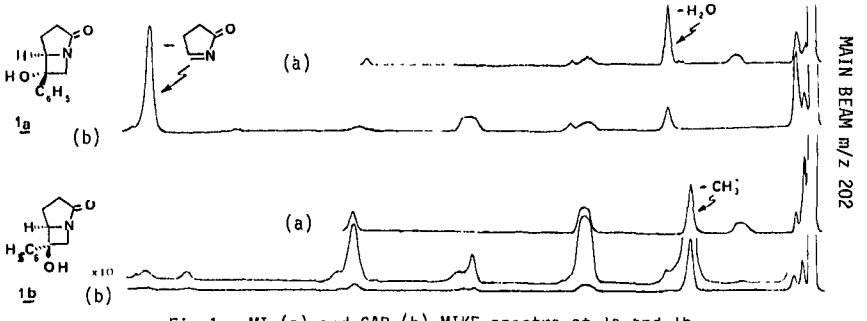

Fig 1 MI-(a) and CAD-(b) MIKE spectra of 1a and 1b

References:

1) T. Gaumann, D. Stahl and J.C. Tabet, Org. Mass Spectrom. 18, 263 (1983).

2) J.C. Beloeil, M. Bertranne, D. Stahl and J.C. Tabet, J. Am. Chem. Soc. 105, 1355 (1983).

STEREOSPECIFIC HYDRIDE TRANSFER IN NEGATIVE CHEMICAL IONIZATION

Jean Claude Tabet*, Issam Hanna and Marcel Fetizon. Laboratoire de Synthese Organique, Ecole Polytechnique, 91128 Palaiseau, France.

Stereospecific intramolecular (1-n) hydride transfer have been reported in solution (1,2,3) as well as in the gas phase under OH^- negative chemical ionization (OH^-/NCI)(4). For instance, such a migration is responsible for the loss of hydrogen molecule from deprotonated molecule $(M-H)^-$ for 1,4 cyclohexane diols, which takes place to a large extent in trans isomer but not in the cis (5). Similar observations have been made in the steroid series(6).

Obviously, in the gas phase the occurence of hydride transfer is difficult to prove, at least directly, in the case of hydroxyketones, since the process is likely to be reversible. However, an indirect evidence of stereospecific internal hydride reduction has been found in the bifunctionnal 9,9 dimethyl bicyclo (3,3,1) nonane series (Figure 1).

These compounds have little conformational flexibility and carbon atoms 3 and 7 are close to each other. Thus, both hydroxyketals 1a and 1b, under OH^-/NCI(7) conditions lead to abundant deprotonated molecule A (m/z 225, $(M-H)^-$) and fragment ion B (m/z 181, $(M-H-C_2H_4O)^-$). These elemental structures checked by high resolution mass spectrometry. However, a loss of water from the latter ion, giving ion C, m/z 163, strongly depends on the stereochemistry of hydroxy group in the starting isomer. The intensity ratio of peaks B and C is about 3 for the exo isomer 1b, and less than 1 for the endo isomer 1a. Hence ion B from 1a (ion Ba) and from 1b (ion Bb) have either different structures, or different internal energy.

Under OD^-/NCI(8) conditions most of the deprotonated molecule is not shifted (about 85 %). Therefore H/D exchange takes place prior deprotonation by a neutral-neutral reaction(5,6) and the fragmentation proceeds essentially through the "alkoxyde" pathway.

Eventually, the differences between the MIKE of ion A for 1a and 1b are much more striking. metastable ion Bb from the exo isomer readily looses one water molecule in the 2nd FFR, whereas there is virtually no such metastable fragmentation of ion Ba (Figure 1). Thus, as previously suggested, ions Ba and Bb should not simply be stereomeric ions.

Since it is known(4,9,10) that alkoxyde ions loose water very readily, our results can be explained on the basis of structures Ba and Bb for the intermediate ions (Figure 2). To check this hypothesis, the collision-induced decompositions spectra (MIKE-CAD) of ion Ba ,from the hydroxyketal 1a, and of the deprotonated molecule $(M-H)^-$,from the hemiketal 2, have been compared. They are identical. In the same way, the MIKE-CAD spectra of ions Bb and of the deprotonated hydroxy ketone 3 are superimposable. The latter two spectra are very different of the former ones.

The conformation of 9,9 dimethyl bicyclo (3,3,1) nonane is rigid, according to force field calculations. Compounds of this serie are valuable models for the study of transannular reactions, either in solution, or in a plasma. This behaviour is obviously due to a permanent close proximity of the both reacting functional groups. No such internal hydride reduction has been observed so far in monocyclic hydroxyketals.

REFERENCES

(1) W. Acklin and V. Prelog, Helv. Chim. Acta, 17 , 1239, 1959.
(2) R. Cernick,G.A. Crase, O.S. Mills and I. Watt, J.C.S. Perkin 2, 361,1982.
(3) N. Numazawa and M. Nagaoka, J.C.S. Chem. Comm., 530, 1982 .
F.H. Field , Plenary Lecture,28th Annual Conference on Mass Spectrometry and Allied Topics, Amer. Soc.of Mass Spectrom., New-York, 1980.
(5) T. Gaumann, D. Stahl and J.C. Tabet, Org. Mass Spectrom., 18 , 263 , 1983.
(6) J.C. Beloeil, M. Bertranne, D.Stahl and J.C. Tabet, J. Amer. Chem. Soc., 105 , 1355, 1983.
(6) F.J. Winkler, D. Stahl, J. Amer. Chem. Soc., 100 , 6779, 1978.
(7) The OH- reagent has been prepared using a gas mixture of N2O and CH4 in a ratio 1/5.
(8)The ND3 gas has been used to perform the neutral-neutral reaction and the OD- ion has been obtained from the gas mixrure.
(9) A.L.C. Smit and F.H. Field, J. Amer. Chem. Soc., 99 , 6471, 1977 .
(10) A.P. Bruins, Anal. Chem., 51 , 967, 1979.

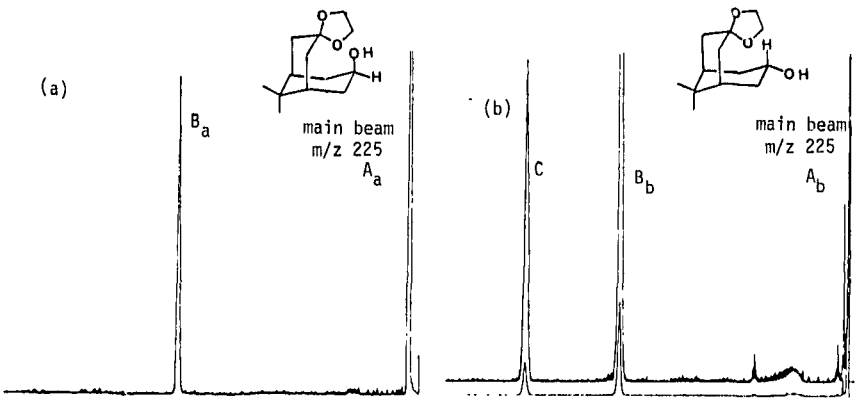

Fig. 1 MIKE spectra of $(M_d\text{-}D)^-$ ions formed under NCI/OD$^-$ Conditions for stereomeric (a) endo 1a and (b) exo 1b hydroxy ketal compounds.

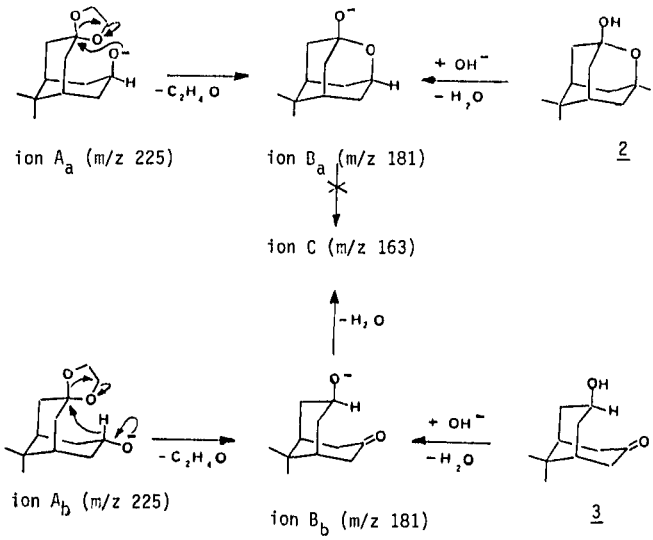

Scheme 2. Origins of the loss of C_2H_4O from stereoisomeric deprotonated molecules $(M\text{-}H)^-$ (structures A_a and A_b).

Nitrogen Trifluoride (NF_3) As A Negative Chemical Ionization Reagent Gas,

L. B. Killmer, Jr., S. Rottschaefer, M. Mentzer, Analytical, Physical, and Structural Chemistry, Smith Kline and French Labs., Philadelphia, PA 19101

The analytical potential of NF_3 as a negative chemical ionization reagent gas was first described by Tiernan, Chang, and Cheng.[1,2] The initial NF_3 investigations were performed on a time of flight mass spectrometer equipped with a modified high pressure ion source. Tiernan and coworkers thoroughly evaluated a variety of small organic compounds (mw<150) in an attempt to determine the types of ion-molecule reactions that NF_3 undergoes. The scope of this presentation is to demonstrate the capabilities and advantages of NF_3 as a negative CI reagent gas on much larger and structurally more intricate compounds than have been previously reported.

All of the NF_3 negative ion CI mass spectra were obtained using a Finnigan Model 3600 GC/MS. To avoid any possible damage to the solenoid valves and flow controllers, which contain Viton rubber O-rings and seals, NF_3 was introduced directly into the ion source by installing a 1/8" Swagelok stainless steel tee in the direct probe CI reagent gas line. The 1/8" stainless steel tee is connected to a fine metering valve via a length of 1/8" OD teflon tubing. The NF_3 source pressure is controlled by this fine metering valve.

NF_3 is an excellent source of the fluoride anion (F^-). Over 90% of the total ion current of NF_3 is due to F^- (m/z 19). The two principal ion-molecule reactions that one observes using NF_3 as a negative ion CI reagent gas are the following:

1. Proton Abstraction - to form the $(M-H)^-$ ion
2. Fluoride Attachment - which yields the $(M+F)^-$ ion via nucleophilic addition and/or hydrogen bonding

The source pressure was measured with a Barocel Model 1400 manometer and the source temperature was monitored using an Omega Model 199 - Iron-Constantin digital thermometer. The optimum source pressure and temperature conditions were found to be:

Optimum Source Pressure - 230-250 microns
Optimum Source Temperature - 110°-120°C

The basicity of the F^- anion is independent of temperature while the nucleophilicity of the F^- anion increases as the source temperature increases. Source temperatures above 200°C should be avoided since rhenium fluorides and oxides are observed at these elevated source temperatures.

The limit of detection using NF_3 as the CI reagent gas was determined by capillary GC/MS using methyl stearate and anthraquinone

Methyl Stearate	- Full Scan (100-450 amu)	5.0 ng* on column
	MID $(M-H)^-$	1.3 ng
Anthraquinone	- Full Scan (100-450 amu)	2.5 ng* on column
	MID $(M+F)^-$	0.6 ng

*signal to noise (3:1)

The following comments can be made about NF_3 as a negative CI regeant gas:

1. CI using NF_3 via fluoride attachment and/or proton abstraction is a very soft ionization process yielding principally quasi-molecular ion species.
2. In the negative ion mode, NF_3 ionizes a larger variety of organic compounds than methane.
3. Capillary GC/MS can be performed using NF_3 as the regeant gas and helium as the carrier gas.
4. NF_3 is presently available only from Air Products Inc., Allentown, PA at a cost of approximately $200.00/lb.

The following mass spectra demonstrate the large variety of organic compounds that can be ionized using NF_3.

1. T.O. Tiernan, C. Chang, and C. C. Cheng, Environmental Health Perspectives 36, 47-62 (1980).

2. C. C. Cheng, C. Chang, and T.O. Tiernan, 27th Annual Conference on Mass Spectrometry and Allied Topics, June 3-8, 1979, Seattle, WA, pp. 722-723.

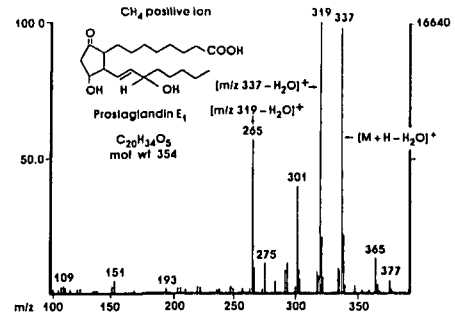
CH4 positive ion
Prostaglandin E1
C20H34O5
mol wt 354
[m/z 337 – H2O]+
[m/z 319 – H2O]+
[M + H – H2O]+
16640

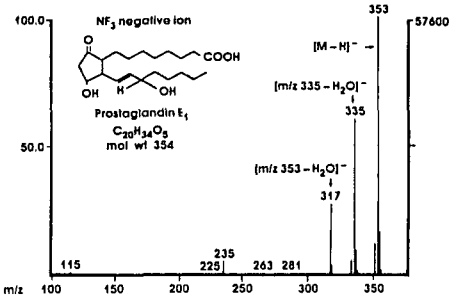
NF3 negative ion
Prostaglandin E1
C20H34O5
mol wt 354
[M – H]–
[m/z 335 – H2O]–
[m/z 353 – H2O]–
57600

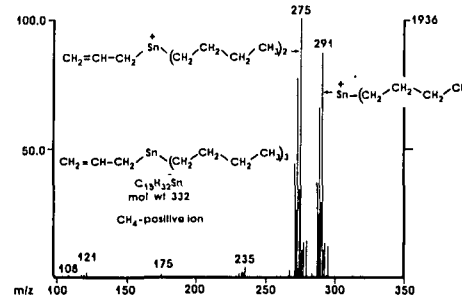
C15H32Sn
mol wt 332
CH4-positive ion
1936

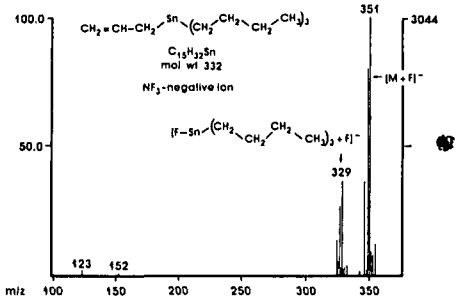
C15H32Sn
mol wt 332
NF3-negative ion
[M + F]–
3044

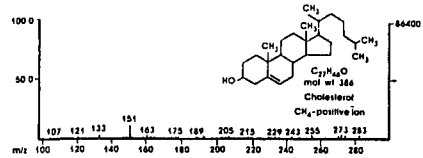
C27H46O
mol wt 386
Cholesterol
CH4-positive ion
86400

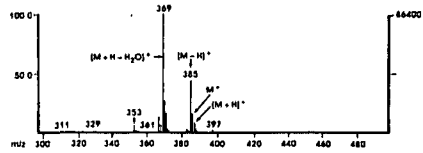
[M + H – H2O]+
[M – H]+
[M + H]+
86400

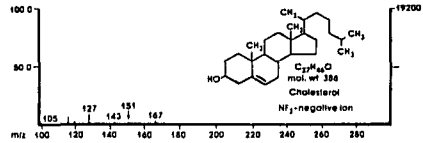
C27H46O
mol wt 386
Cholesterol
NF3-negative ion
19200

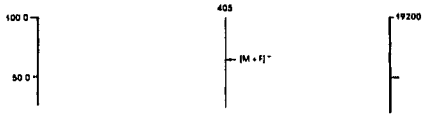
[M + F]–
19200

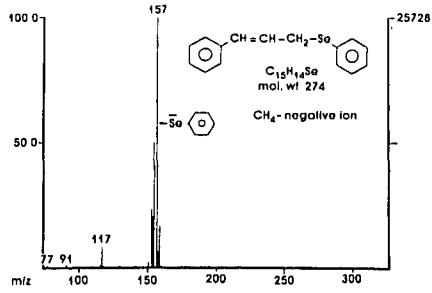
C15H14Se
mol. wt 274
CH4-negative ion
25728

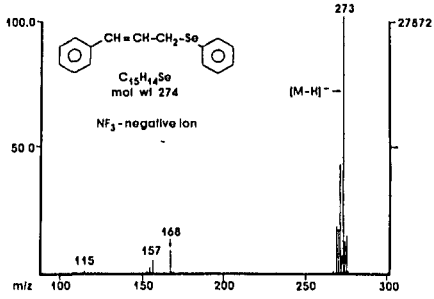
C15H14Se
mol wt 274
NF3-negative ion
[M-H]–
27872

Identification of Submicrogram Quantities of Positional and Geometrical Isomers of Multi-Unsaturated Aliphatic Alcohols Using a Capillary Column GC/MS Method

L.R. Hogge, E.W. Underhill and J.W. Wong
National Research Council, Plant Biotechnology Institute, 110 Gymnasium Road, Saskatoon, Saskatchewan, S7N 0W9, Canada

INTRODUCTION

The determination of the position and geometry of double bonds in long chain aliphatic compounds is often very important, particularly in insect sex pheromone chemistry. Although several useful GC/MS procedures have been reported for locating double bonds, difficulties often occur when using these methods for the analysis of submicrogram quantities of multi-unsaturated compounds.

The method described here, (see Fig. 1) involves partial epoxidation to form an unsaturated monoepoxide corresponding to every double bond position in the starting compound. The double bonds remaining in the unsaturated monoepoxides are then reduced using hydrogen over platinum on neutral alumina catalyst. Subsequently the saturated monoepoxides formed are analysed by GC/MS using high resolution capillary column chromatography. The geometry of each double bond in the original compound is indicated chromatographically by the retention times of the saturated monoepoxide derivatives since the cis and trans epoxides are completely separable. The position of each epoxide group and hence each double bond is determined by examining the mass spectrum of each of the saturated monoepoxides formed. These spectra show diagnostic ions of good intensity for each of the positional isomers due to cleavage alpha to the epoxide function.

Fig. 1

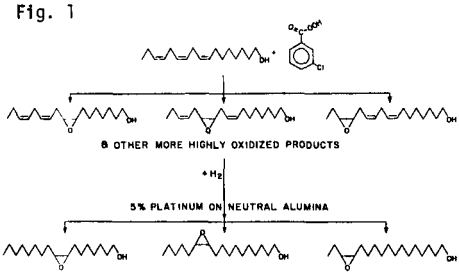

EXPERIMENTAL

The epoxy derivatives of triunsaturated alcohols were prepared by adding 1 µg of m-chloroperbenzoic acid to 500 ng of alcohol in a reacti-vial and bringing the volume up to 50 µl with dichloromethane. This mixture was allowed to stand at room temperature overnight.

Reduction was carried out in the same reacti-vial as the epoxidation. The teflon-rubber laminated cap was pierced twice to provide an inlet and exit for the hydrogen gas. Approximately 0.5 mg of 5% platinum on neutral alumina catalyst was added and hydrogen gas bubbled into the reaction mixture for 20 to 30 minutes with frequent mixing using a vortex mixer. The mixture was then filtered to remove the catalyst and concentrated for GC/MS analysis.

GC/MS data were obtained using a model 4000 Finnigan GC/MS system interfaced to a Finnigan Incos Model 2300 data acquisition system. The gas chromatography was done using a 30 m x 0.25 mm I.D. DB-210 fused silica column connected directly to the ion source. The samples, with heptadecanol added as an internal standard, were injected in the splitless mode at an initial column temperature of 50°. The temperature was immediately raised ballistically to 150° and then programmed at a rate of 4°/min to 240°. Mass spectra were obtained in the electron impact mode at an ionization energy of 70 ev. and were acquired repeatedly every second in the range of 40 to 320 mass units.

RESULTS AND DISCUSSION

(Z,Z,Z)-9,12,15-octadecatrienol was chosen to test the technique. This alcohol was epoxidized using the conditions described above that favor the formation of unsaturated monoepoxides. As the mass spectra of unsaturated epoxides do not show diagnostic cleavage ions and their chromatographic separation is usually difficult, these compounds were reduced to form the saturated monoepoxides. Fig. 2 shows the total ion chromatogram obtained from the GC/MS analysis of saturated monoepoxides found from the above reaction. The retention times of the saturated monoepoxides relative to the internal standard (RRT) were calculated and are shown above the appropriate peaks in Fig. 2. The mass spectra of these peaks showed ions of good intensity at masses indicating cleavages alpha to the epoxide in the 9, 10 position, the 12,13 position and the 15,16 position respectively. Fig. 3 shows the mass spectrum of the peak at RRT 1.80. The ions at mass 155 and 171 are the cleavage ions indicating the 9,10 epoxy derivative.

To confirm the identification of these epoxyoctadecanols and determine their geometry, the cis and trans-isomers of monounsaturated octadecenols with double bonds present in a number of positions including those suspected in the multi-unsaturated alcohol, were epoxidized. These compounds were then analysed by GC/MS using the same conditions as for the previous analysis of the multi-unsaturated alcohol. Their RRT's were calculated and diagnostic ions due to alpha cleavage of the epoxide confirmed. These data are tabulated in Table 1.

Fig. 4a shows the chromatogram of the cis monoepoxide isomers that were prepared and co-injected. Separation of the isomers was sufficient to obtain characteristic spectra for each epoxide. Fig. 4b shows the chromatogram of the corresponding trans isomers. Although not all of the trans-isomers were separated from each other using this column, all were separated from their corresponding cis-isomers. As the mass spectra of the epoxides formed from the octadecatrienol were virtually identical, including the diagnostic cleavage ions, to the mass spectra of epoxides formed from monoenes with double bonds in the 9,12 and 15 positions, these bond positions were confirmed as being present in the starting compound. Confirmation of cis geometry of each bond position was made by comparison of the RRT's of the three monoepoxides from the octadecatrienol with the RRT's of the cis and trans isomers formed from the monoene alcohols.

CONCLUSION

This method is very useful for determining the position and geometry of double bonds in long chain aliphatic compounds. There appears to be two advantages to this method over others reported in the literature. First, it is suitable for determining the geometry as well as the position of double bonds in multi-unsaturated aliphatic compounds and second it is useful for the analysis of submicrogram quantities of material.

Fig. 2

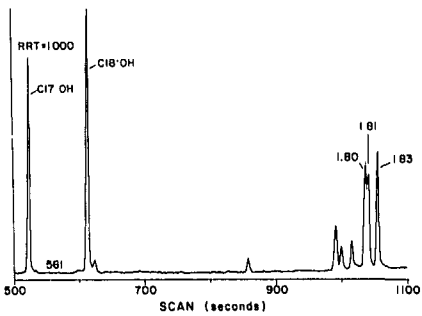

Table 1
Diagnostic Ions and RRT's for monoepoxide isomers

cis-isomers	Diagnostic Ions	RRT	trans-isomers	Diagnostic Ions	RRT
Z3-18:OH	239,87	1.716	E3-18:OH	239,87	1.651
Z6-18:OH	129,197	1.777	E6-18:OH	129,197	1.750
Z9-18:OH	155,171	1.788	E9-18:OH	155,171	1.765
Z12-18:OH	113,213	1.809	E12-18:OH	113,213	1.765
Z15-18:OH	71,255	1.828	E15-18:OH	71,255.	1.761

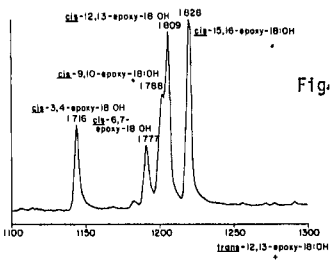

Fig. 4a

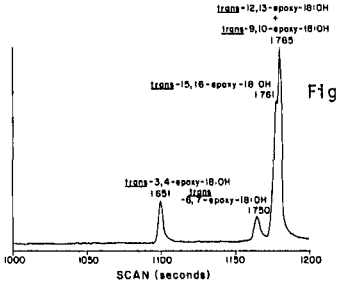

Fig. 4b

Fig. 3

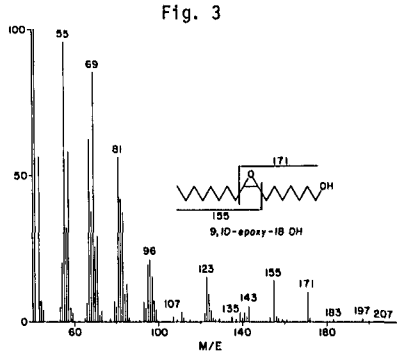

CROSSED-BEAM STUDIES OF THE REACTION OF O^- WITH HYDROGEN AND THE LOWER HYDROCARBONS

Richard L. C. Wu and T. O. Tiernan

Brehm Laboratory and Departments of Engineering and Chemistry
Wright State University, Dayton, Ohio 45435

Introduction Hydrogen-atom abstraction reactions of the type, $O^- + C_xH_y \rightarrow OH^- + C_xH_{y-1}$ (1) where X=0-3, and y=2-4, have previously been studied in our laboratory using a tandem mass spectrometer. The excitation functions for these reactions were generally found to exhibit decreasing reaction cross sections with increasing kinetic energy, dropping to some minimum value, and then rising again as the energy is further increased. This general behavior has also been observed for some of the slower ion-molecule reactions ($K \ll K_C$) which have been studied using the flowing afterglow technique. Ferguson[1] attributed this phenomenon to a change in the reaction mechanism with increasing kinetic energy. An intermediate complex mechanism is thought to be dominant at low energies, whereas a direct reaction mechanism apparently occurs at higher energies. In order to better elucidate the mechanisms and dynamics of such ion-neutral collision processes, a systematic study of reaction (1) for various target molecules was undertaken using a crossed ion-molecular beam apparatus.

Experimental The crossed ion-molecular beam apparatus used here has been described previously.[2] Briefly, the projectile ion, O^-, is produced by electron impact on N_2O, is mass and energy selected, and is then crossed at an angle of 90° by a supersonic nozzle beam. Product ions formed from interaction of these two beams are then mass and energy analyzed by the second stage detector assembly, which includes a retarding potential analyzer, a quadrupole mass filter and a detector, all of which are mounted on an assembly which rotates in the horizontal plane about the scattering center, covering an angular range from -10° to + 60°. In a typical scattering experiment, the angular and energy distributions of the reactant and product ions are measured for each increment of the kinetic energy of the incident beam.

Results and Discussion From the scattering data obtained, a contour diagram is plotted in Cartesian velocity space, where each curve represents a constant product probability, $P(V_x, V_y, V_z)$. For a reaction which involves a long-lived intermediate complex mechanism, the product contour is expected to be roughly centered around the center of mass. The energy disposed, Q, in the reaction is also calculated from the most probable translational energy of the products less the translational energy of the reactants, as a function of the initial energy. The Q values expected for the reaction on the basis of both long-lived complex and spectator stripping models are also calculated for comparison with the experimental results. Results obtained for the several reactions studied here are described below.

A. $O^- + C_3H_4 \rightarrow OH^- + C_3H_3$ This reaction was studied over the relative energy range, 5.7 to 8.9 eV. A typical contour diagram for this reaction at 5.7 eV is shown in Fig. 1. Clearly, the product contour is centered in a region which is forward of the center of mass, indicating that the reaction is direct and occurs on a time scale less than that of a molecular rotation. The spectator stripping model is reasonably consistent with the observed results, as indicated in Fig. 1. This result is in excellent agreement with the data obtained by Karnett and Cross[3], who reported the reaction mechanism to be direct and well-approximated by the spectator-stripping model over the relative energy range, 4.6-10.8 eV.

B. $O^- + H_2 \rightarrow OH^- + H$ This reaction was studied over the relative energy range, 0.9 to 4 eV. The contour plot at 0.9 eV was found to be centered in the energy region between the center of mass and the point predicted by the spectator stripping model, and as the energy was increased, the center of the contour moved toward the stripping model center. Again, these results demonstrated that the reaction mechanism is a direct mechanism. The present results are not consistent with similar data of Johnson et.al.[4], who reported that, at energies below 2.5 eV, the product distribution is centered about the center of mass for the reaction, $O^- + D_2 \rightarrow OD^- + D$.

C. $O^- + CH_4 \rightarrow OH^- + CH_3$ This reaction was studied over the relative energy range, 3.9 to 5.0 eV. The angular distributions of the product OH^- ion were found to be the same as that of the primary ion O^-. A direct reaction mechanism is again indicated.

D. $O^- + C_2H_4 \rightarrow OH^- + C_2H_3$ This reaction was studied over the relative energy range, 1.9 to 7.4 eV. The contour plot at 5.9 eV was observed to be centered around the center of the spectator stripping model, indicating again that the reaction involves a direct stripping mechanism at that energy.

Conclusion The reaction mechanisms for the H-atom abstraction reactions of O^- with H_2 and of O^- with various hydrocarbons were found to involve a direct mechanism in the energy

region examined, and the spectator stripping model reasonably predicts the scattering behavior.

References

1. E. E. Ferguson, Proceedings of the 31st Annual Conference on Mass Spectrometry and Allied Topics, p. 277 (1983).
2. R. L. C. Wu, Y. Ichikawa, C. D. Miller and T. O. Tiernan, Review Scientific Instruments, to be submitted.
3. M. P. Karnett and R. J. Cross, Jr., Chem. Phys. Lett. 84, 501 (1981).
4. S. G. Johnson, L. N. Kremer, C. J. Metral and R. J. Cross, Jr., J. Chem. Phys. 68, 1444 (1978).

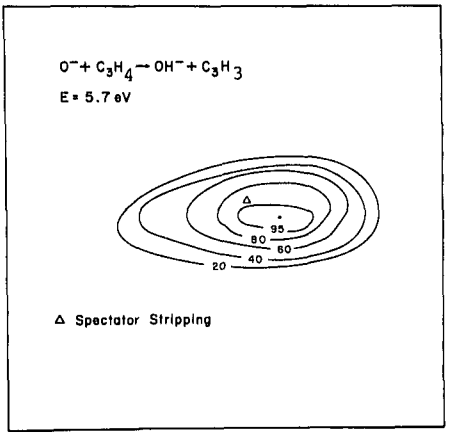

Figure 1. Cartesian Contour Plot of Product Intensity For The Reaction, $O^- + C_3H_4 \rightarrow OH^- + C_3H_3$ At A Relative Energy of 5.7 eV. The Contours are at 20% Intervals. Δ = Position Predicted By The Spectator Stripping Model. The Position Of The Center Of Mass Is To The Far Left.

THE GAS PHASE THERMOCHEMISTRY OF Ph_3C^-, $Ph_3C\cdot$, AND Ph_3C^+; John E. Bartmess, Department of Chemistry, Indiana University, Bloomington IN 47405

Although $Ph_3C\cdot$ was the first stable free radical known, little is known of its thermochemistry, nor of that for the cation or anion. Literature values for $DH(Ph_3C\text{-}H)$ vary from 70 to 82 kcal/mole, none being direct measurements, and $\Delta H^o_f(Ph_3C^+)$ is available from one AP for Ph_3CH.

The gas phase acidity of Ph_3CH was measured using ICR spectrometry, to give ΔH^o_{acid} = 362.8±2.3 kcal/mole. Using the literature $\Delta H^o_f(Ph_3CH)$, a $\Delta H^o_f(Ph_3C^-)$ = 61.9±3.3 kcal/mole is derived. With $DH^o(Ph_3C\text{-}H)$ from below, we get $EA(Ph_3C\cdot)$ = 22.8±8 kcal/mole. The acidity is an increase over that of Ph_2CH_2 by only 1.7 kcal/mole, indicating little resonance stabilization by the third phenyl ring compared to the first (37.2 kcal/mole) or the second (14.9 kcal/mole).

From electron impact on $Ph_3C\text{-}SiMe_3$, the difference in the AP's of Ph_3C^+ and Me_3Si^+ should equal the difference in the radical's IP's; since $IP(Me_3Si\cdot)$ is well known from PIPECO experiments, we derive $IP(Ph_3C\cdot)$ = 7.65±0.1 eV. From the absolute AP's of these fragments and an estimated ΔH^o_f for $Ph_3C\text{-}SiMe_3$ of 18±4 kcal/mole from group additivity, we obtain $\Delta H^o_f(Ph_3C\cdot)$ = 84±7 kcal/mole (corresponding to $DH^o(Ph_3C\text{-}H)$ = 72±8 kcal/mole) and $\Delta H^o_f(Ph_3C^+)$ = 261±7 kcal/mole within experimental error of the one literaure value of 256 kcal/mole.

The IP's for benzyl, benzhydryl, and (here) trityl are 7.20, 7.32, and 7.65 eV, respectively; this is the expected trend for the cationic phenyl-C_α bond being shorter than the radical one. The DH^o values for C-H in $PhCH_3$, Ph_2CH_2, and Ph_3CH are 88, 84, and 72 kcal/mole respectively. We believe that our $Ph_3C\cdot$ value give a slightly low bond strength (75 might be better) but that the Ph_2CH_2 value is too high; it is an extrapolated value from solution phase kinetic data. We are studying futher systems to obtain better values for these data, as well as attempting to measure the IP of $Ph_3C\cdot$ directly from "hexaphenylethane". Structural studies of Ph_3C^+ are also in progress.

Hydrogen Rearrangements in $C_6H_{12}O^{+\cdot}$ Ions with the Oxygen on the Third Carbon.

Lawrence L. Griffin,[a] Charles E. Hudson[b] and David J. McAdoo[b], a. Dept. of Marine Sciences, Texas A&M University at Galveston, Galveston, Texas 77553. b. Marine Biomedical Institute, University of Texas Medical Branch, Galveston, Texas 77550.

The relative rates of hydrogen migrations have long been of interest in mass spectrometry. Previous work from our laboratory has indicated a ring size preference 6>5≅3(α,β)>4.[1] We here refine this order utilizing decompositions of $C_6H_{12}O^{+\cdot}$ ions with the oxygen on the third carbon (Table 1).

Postulated $C_6H_{12}O^{+\cdot}$ Reactions

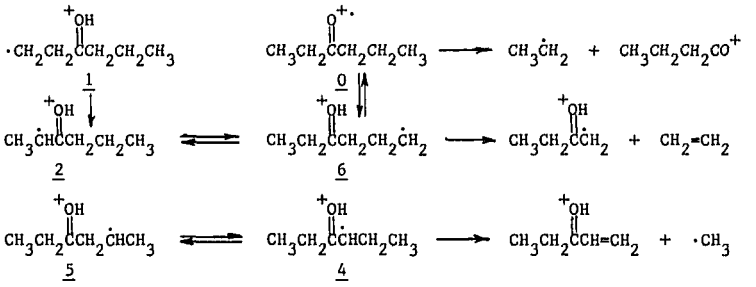

The absence of C_2H_4D loss from 1-0,4,4-d_3 and 1-4,4-d_2 indicates that the five membered ring hydrogen transfers 1 → 0 and 1 → 4 do not occur. Therefore the reactions of 1 are dominantly 1 → 2. The lack of transfer of deuteriums on C-1 to other parts of the ion together with the extensive transfer of deuteriums from C-2 indicates that 2 → 1 does not occur; 2 → 6 appears to dominate the reactions of 2. The β,α-shift 4 → 5 is preferred to the 5-membered ring hydrogen transfer 4 → 1, as negligible C_2H_3D and $C_2H_2D_2$ are lost from 4-1,1,1-d_3. 4 → 5 is presumably followed largely by 5 → 0 (see below). Therefore, the hydrogen transfer preference in reactions involving α-carbons is 6>3>5>4-membered rings. We discuss 3-membered ring isomerizations in more detail in another presentation.[2]

The 5-membered ring hydrogen shift 5 → 0 is preferred to 5 → 2, based on the greater C_2H_3D formation from 5-0-d_1 than from 5-2,2-d_2, even though the latter isomerization is to the more stable product.

The 6-membered ring hydrogen transfer 6 → 0 is less favorable than 6 → 2 based on the greater loss of C_2H_3D from 6-0-d_1 than from 6-2,2-d_2. Thus, in the 6-membered ring hydrogen transfers, the more stable product is formed.

Acknowledgements. Supported by the Robert A. Welch Foundation. We thank Professor Michael Gross and the Midwest Center for Mass Spectrometry at the University of Nebraska for use of the MS 50 TA mass spectrometer to obtain metastable spectra.

1. D.J. McAdoo, F.W. McLafferty, C.E. Hudson and T.E. Parks, Org. Mass Spectrom., in press.
2. C.E. Hudson and D.J. McAdoo, this meeting.

Table 1. $C_6(H,D)_{12}H^{+\cdot}$ Decompositions

Ion	Neutral Lost								
	15	16	17	18	28	29	30	31	32
$\dot{C}H_2CH_2C(=^{+}OH)CH_2CH_2CH_3$ [a]	44				30	22	5		
$\dot{C}H_2CH_2C(=^{+}OH)CD_2CH_2CH_3$ [b]	56	17			15	10	2		
$\dot{C}H_2CH_2C(=^{+}OD)CD_2CH_2CH_3$ [c]	38	31	6		9	13	3	1	
$CH_3\dot{C}HC(=^{+}OH)CH_2CH_2CH_3$ [d]	4				70	20	5		
$CH_3\dot{C}HC(=^{+}OH)CH_2CD_2CH_3$ [e]	4				7	40	48	2	
$CH_3\dot{C}HC(=^{+}OH)CH_2CH_2CD_3$ [f]	0.6	0.6	0.6	0.6	3	27	60	8	
$CH_3CH_2C(=^{+}OH)\dot{C}HCH_2CH_3$ [g]	17				43	37	4		
$CD_3CH_2C(=^{+}OH)\dot{C}HCH_2CH_3$ [h]	19				41			1	39
$CH_3CH_2C(=^{+}OH)CH_2\dot{C}HCH_3$ [i]	31				25	40	4		
$CH_3CH_2C(=^{+}OD)CH_2\dot{C}HCH_3$ [j]	33	3			3	58	2		
$CD_3CH_2C(=^{+}OH)CH_2\dot{C}HCH_3$ [k]	30				24				46
$CH_3CD_2C(=^{+}OH)CH_2\dot{C}HCH_3$ [l]	16	1			12	22	10	35	4
$CH_3CH_2C(=^{+}OH)CH_2CH_2\dot{C}H_2$ [m]	11				59	24	6		
$CH_3CH_2C(=^{+}OD)CH_2CH_2\dot{C}H_2$ [n]	3	4			33	52	7	2	
$CH_3CD_2C(=^{+}OH)CH_2CH_2\dot{C}H_2$ [o]	8	3			10	45	16	19	
$CH_3CH_2C(=O^{+\cdot})CH_2CH_2CH_3$ [p]	4				75	16	5		
$CH_3CD_2C(=O^{+\cdot})CH_2CH_2CH_3$ [q]	5				19	45	17	11	2

Sources of ions were: a. 1-Propylcyclopentanol b. 1-(Propyl-1,1-d_2)-cyclopentanol c. 1-(Propyl-1,1-d_2)-cyclopentanol-O-d_1 d. 5-Methyl-4-octanone e. 5-Methyl-4-octanone-2,2-d_2 f. 5-Methyl-4-octanone-1,1,1-d_3 g. 4-Ethyl-3-hexanone h. 4-Ethyl-3-hexanone-1,1,1-d_3 i. 1-Ethyl-3,4-dimethylcyclopentanol j. 1-Ethyl-3,4-dimethylcyclopentanol-O-d_1 k. 1-(Ethyl-2,2-d_2)-3,4-dimethylcyclopentanol l. 1-(Ethyl-2,2-d_2)-3,4-dimethylcyclopentanol m. 1-Ethylcyclobutanol n. 1-Ethylcyclobutanol-O-d_1 o. 1-(Ethyl-1,1-d_2)-cyclobutanol p. 3-Hexanone q. 3-Hexanone-2,2-d_2

Provitamin D - Vitamin D Interconversions in the Mass Spectrometer. Translational Energy Release and CID MIKE Studies.

Z.V.I. Zaretskii[a], E.E. Kingston[b], J.H. Beynon[b], R. Lauber[c] and U.P. Schlunegger[c].
a-Isotope Dept., The Weizmann Institute of Science, 76100 Rehovot, Israel.
b-Royal Society Research Unit, University College of Swansea, Swansea SA2 8PP, U.K.
c-University of Bern, CH-3012 Bern, Switzerland.

The photochemical and thermal interconversion in solution (Scheme 1) of vitamins D_3(1) and D_2(2), and their respective provitamins, 7-dehydrocholesterol (5) and ergosterol (6), is known to involve the intermediate formation of the respective previtamins (3,4) [1]. Recently we have shown that vitamin D - previtamin D equilibrium occurs also in the gas phase of the mass spectrometer ion source [2,3]. In this study CID MIKE spectrometry and translational energy (T) release measurements have been used to clarify whether the 7-dehydrocholesterol (5), ergosterol (6) $\rightleftarrows$ vitamin D_3(1), vitamin D_2(2) interconversions take place under mass spectrometric conditions, too. It was found that while conventional mass and CID MIKE spectra of the molecular ions of 1,2 and 5,6 are different, the CID MIKE spectra of the respective $(M-H_2O-CH_3)^+$ ions are identical (e.g. see Fig. 1). It can be assumed, therefore, that the 5,6 $\rightleftarrows$ 1,2 interconversion in the gas phase in the ion source occurs on the "fragment ion level" leading to $(M-H_2O-CH_3)^+$ ions of identical structure. The translational energy release study revealed that the $M^{+\cdot} \rightarrow (M-H_2O)^{+\cdot}$ reaction plays the central role in the 5,6 $\rightarrow$ 1,2 isomerization. The T measurements showed that in 7-dehydrocholesterol (5) and ergosterol (6), in contradistinction to vitamin D_3(1) and D_2(2), unusually large amounts of translational energy are released upon the loss of H_2O from the molecular ions (Table 1), suggesting that the elimination of H_2O is preceded by the rate determining rearrangement of the molecular ions (5 and 6). The mechanism of provitamin D - vitamin D interconversion in the gas phase of the mass spectrometer is discussed.

References

1. E. Havinga, Experientia, 29, 1181 (1973).
2. Z.V.I. Zaretskii, Adv. Mass Spectrom. 8, 590 (1980).
3. R. Lauber, U.P. Schlunegger and Z.V.I. Zaretskii, Org. Mass. Spectrom. 18, 315 (1983).

Table 1: Translational energy releases, (meV)[a] and "n" values[b] for the $M^{+\cdot} \rightarrow (M-H_2O)^{+\cdot}$ reaction

Compound	$T_{80\%}$(n)	$T_{50\%}$	$T_{20\%}$(n)	$T_{10\%}$(n)
7-Dehydrocholesterol (5)	28 (1.50)	128	288 (2.10)	388 (2.20)
Vitamin D_3 (1)	19 (1.80)	66	195 (1.55)	302 (1.60)
Vitamin D_2 (2)	23 (1.95)	72	204 (1.65)	316 (1.65)
Ergosterol (6)	49 (1.70)	187	388 (2.30)	509 (2.40)

[a]Mean error ±5%; [b] See J. Holmes, J. Terlouw, Org. Mass Spectrom. 15, 383 (1980).

Scheme 1.

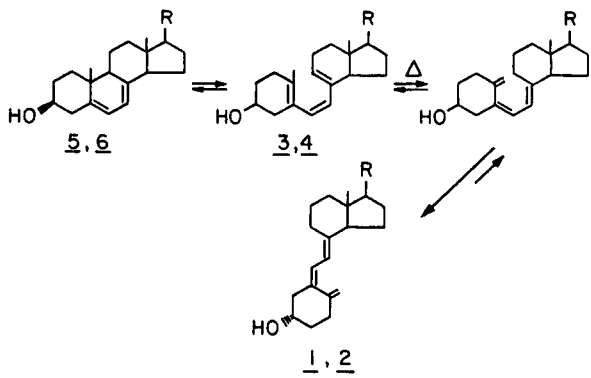

1, 3, 5 R = C_8H_{17}

2, 4, 6 R = C_9H_{17}

Fig. 1.

Ergosterol CID MIKES of m/z 363 $[M-H_2O-CH_3]^+$

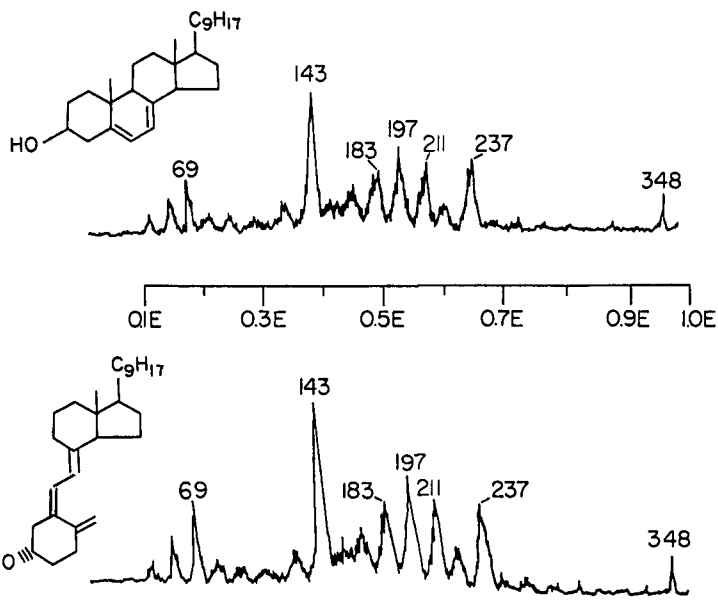

Vitamin D_2 CID MIKES of m/z 363 $[M-H_2O-CH_3]^+$

TANDEM MASS SPECTROMETRY FOR THE ANALYSIS OF TRACE LEVELS OF γ-UNSATURATED SULTONES IN COMPLEX MATRICES.

Devin K. Brain, Procter & Gamble Co., Ivorydale Technical Center, Cincinnati, OH 45217 and John R. B. Slayback and Greg Rahn, Oneida Research Services, New Hartford, N.Y 13413.

Determination of alk-1-ene-1,3-sultones (I) in complex surfactant mixtures by MS/MS provides a perfect example of the power and utility of this technique. These unsaturated sultones or their precursors (II or III) can be produced as trace impurities in sulfation or sulfonation processes.

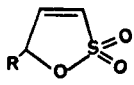

I

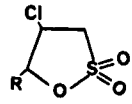

II

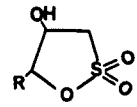

III

In this study, (-)ve ion CI MS/MS in a parent scan mode has been used successfully to identify and quantitate γ-unsaturated- and γ-chlorosultones at ppm levels or less in raw materials, formulated surfactant mixtures and their solutions.

TLC, HPLC, GC and GC/MS have been used to measure the unsaturated sultones with some degree of success. However, these techniques are not only cumbersome for this purpose but also more importantly lack the required sensitivity, specificity and freedom from matrix interference. Since mass spectrometry is especially suited for the analysis of trace substances in complex systems, an evaluation of options including GC/MS and MS/MS in both (+)ve and (-)ve ion modes as well as high resolution GC/MS demonstrated the unique capabilities of (-)ve ion CI MS/MS for this purpose.

With appropriate selection of conditions for the Finnigan Triple Stage Quadrupole MS, the sultone ring fragment, either as the γ-unsaturated (Figure 1) or γ-chloro-sultone (Figure 2) becomes the major ion to which Q_3 is assigned. Scanning Q_1 through the molecular weight range covering the compounds of interest reveals the parents for those sultones present (Figures 3, 4, & 5) free of interference. Quantitation can be best accomplished by direct comparison of the relative intensities of the analyte vs. a suitable internal standard; i.e., a sultone not indigenous to the sample.

To optimize quantitation and sensitivity as well as to avoid source contamination with repeated analyses, sample treatment, as follows, was found to be especially helpful:

1. Pentane extraction (4x) of product or paste samples in a water/ethanol solution can be used to remove the sultones quantitatively from the bulk sample. Solutions can be extracted without dilution as long as sudsing or emulsions are not a problem;
2. Addition of an internal standard to the extract corrects for extraction errors and provides a means to establish absolute sultone concentrations;
3. Insertion of a minimal amount of sample (1-5 μg of pentane-soluble extract which will include mostly matrix in addition to the sultones) into the source by the DCI probe prevents exhaustion of the methane reagent gas and source contamination. Some matrix is desirable, however, to prevent premature or too rapid release of the sultones from the probe. Source temperature was 130°C;
4. Scanning should be rapid (0.25 - 0.125 sec.) and cover only the range of interest. Multiple ion monitoring can be used, of course, to increase sensitivity/detection when looking for specific sultones.

Precision and mean recovery for the γ-sultones has been established at 10% and 85-95%, respectively, over a range from 0.01 to 100 ppm in surfactant raw materials. Performance of this method is equally effective with products or dilute aqueous solutions containing these surfactants.

Figure 1

(-) CI MS/MS Daughter Ions for m/z 274

m^- for C_{14} γ-Unsaturated-sultone Standard

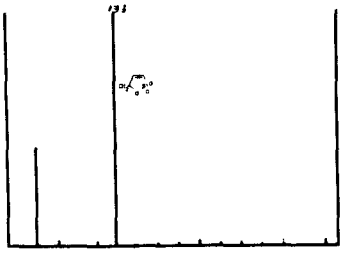

Figure 2

(-) CI MS/MS Daughter Ions for m/z 310

m^- for C_{14} γ-Chloro-sultone Standard

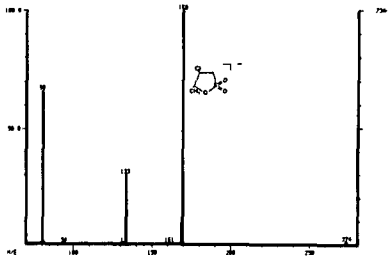

Figure 3

(-) CI MS/MS Parent Scan for m/z 133

Sample - Pentane Extract from AOS spiked with 0.1 ppm C_{14} γ-Unsaturated Sultone plus 1 ppm C_{12} USS Internal Standard

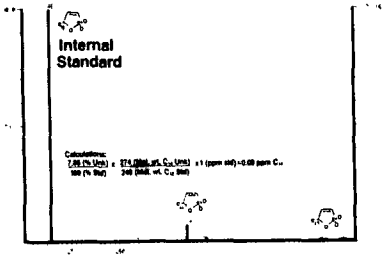

Figure 4

(-) CI MS/MS Parent Scan for m/z 133

Sample - Pentane Extract from AOS spiked with 50 ppm C_{14} γ-Unsaturated Sultone plus 10 ppm C_{12} USS Internal Standard

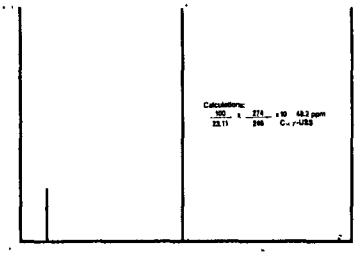

Figure 5

(-) CI MS/MS- Parent Scan for m/z 133 & 169

Sample - Pentane Extract from AOS-containing product solution (0.5%) which had been treated with hypochlorite bleach

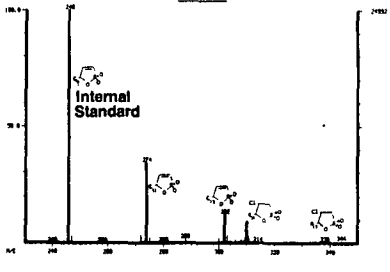

MASS SPECTROMETRIC INVESTIGATION OF 10 AND 11 CARBON ATOM CONTAINING ALPHA-OMEGA DIYNES, R. C. ROBBINS AND N. G. FOSTER, DEPARTMENT OF CHEMISTRY, TEXAS WOMAN'S UNIVERSITY, DENTON, TEXAS 76201

The mass spectral behavior of alkadiynes is well reported in texts and in the literature. Cleavage of the bonds beta to the triple bond was observed to make important contributions to these spectra. Most of this older work did not involve carbon-13 labeling. Deuterium scrambling has been shown to occur to some extent, and therefore was not selected as a definitive means of studying the alpha-omega diynes. The peculiarities of alpha-omega diyne behavior in the mass spectrometer was noted in passing in a program to obtain reference mass spectra for exhaust gas component identifications by the United States Bureau of Mines, (1) Bartlesville, Oklahoma. Subsequently 1,5-hexadiyne has been reported to undergo time dependent conversion to a cyclic form and hence the spectrum exhibits both linear and cyclic fragmentation patterns (2).

Earlier work in our laboratory using carbon-13 labeled molecules of nine carbon atoms (3) showed the extrusion of a methylene group, and an ethylene neutral fragment which led to the formation of a ring, suggested to be the tropylium ion. The C-4,5, and 6 carbon atoms were primarily involved in the losses, and the sp bonded carbon atoms did not take an obvious part in this mechanism. Recognizing that hydrocarbon chains curl (4) this work attempts to determine the minimum functional group that will act as an electron sink, thus leading to true ring formation in a non-branched linear hydrocarbon. Hetero atoms often provide a means for such 4,5,6 centered self-solvating types of reactions to occur (5). The presence of two terminal double bonds (sp^2 hybridization) such as in 1,7-octadiene apparently do not cause ring formation from the molecular ion (6). For chains of 6-9 carbon atoms, the presence of two terminal triple bonds causes some cyclization to occur (2,3). This work examines molecules out to tridecane in addition to considering the high resolution data in detail.

The low resolution mass spectra were obtained on a Consolidated Electrodynamics Corporation (CEC) single focusing mass spectrometer, Model 21-104. The source was operated at 250°C; 10 μA ion current, at 70 eV ionizing volts. Scans were made from m/z 37 to 200 in 6-7 minutes. Sensitivities were varied as required by the desired data. Low ionization data was obtained from 15 eV down to the disappearance of the molecular ion from the spectrum. The voltages were read on a meter capable of reading to .01 volts.

The high resolution mass spectra were obtained from a Kratos MS-50 instrument running at 1/40,000 resolution, at 20 eV ionizing volts. The scan speed was 300 sec/dec. The data is reported as a computer generated formula for each non-reference mass, the deviation in mAMU from the measured mass, the number of points used in the integration, the percent of total ionization (Calibrant, PFK, masses excluded) and the absolute intensity. From 6-10 scans were made on each sample. The reproducibility was excellent. For each spectrum only 2-3 peaks occurred outside of the value of ±0.5 mAMU. A few computer resolved doublets appeared. They are indicated by an asterisk.

In the <u>high resolution</u> mass spectrum of the randomly labeled molecule, the ions from the naturally occurring isotope can be distinguished from the ions of the specie which does not contain a carbon-13 atom. Because peaks under mass 60 were not scanned, the m/z 91 region contains the base peak. In using the data it is assumed that the work of Wagner-Redeker, et. al. (7) is correct; that is: the non-decomposing ions retain their carbon skeletal structure. For the case of just one carbon atom leaving the molecular ion, the data indicate that the molecular ion must have randomized in a ring structure to permit the ejection of any methyl. The almost perfect agreement for the 3,7-di-labeled molecule and very near perfect agreement for the case of the tetra-labeled molecule may be fortuitous. But randomization is indicated. The actual amount of the m/z 109 ion is slightly in favor of the release of an unlabeled methyl group. The low voltage data (3) gave an appearance potential of the ions of the 106 variety of about 2 eV above the molecular ion.

For ions of the 92-91 variety in which two carbon atoms are being lost, the low ionization voltage data showed that these ions had appearance potentials close to that of the molecular ion. Therefore, these processes occur at lower energies. Consideration of the high resolution data for this region shows that a strong skewing in favor of losing none of the carbon-13 atoms is present. Thus with about 75% of the molecular ions losing two carbon-12's simultaneously, a strongly directed process, i.e., ring formation with the extrusion of a C_2H_5 neutral group is indicated. M/z 119 ions cannot be the source of the 92-91 ions since the appearance potential of the 119 ion is well above that of the 92-91 ions.

DATA FOR ONE CARBON ATOM LEAVING

	3,7-Di-LABELED $M^+ = 122$				1,2,8,9-TETRA-LABELED $M^+ = 124$		
m/z	% R.I.	% R.I.	% R.I.	m/z	% R.I.	% R.I.	% R.I.
107	19.14	----		109	17.81	-----	
106	----	5.59		108	-----	12.15	
	24.73				29.96		
Actual	.774	.226			.594	.405	
Theory	.777	.222			.555	.444	
	Therefore Random				Almost Random		

DATA FOR TWO CARBON ATOMS LEAVING TOGETHER

93	100.0	---	----	95	100.0	----	----
92	----	27.1	----	94	----	19.43	----
91	----	----	3.06	93	----	----	12.78
	130.16				132.21		
Actual	.768	.208	.024		.756	.147	.097
Theory	.583	.389	.028		.444	.222	.333

Therefore skewed in favor of losing no carbon-13 atoms.

Once ionization occurs, internal solvation (5) by curling (4) will bring the two sp bonded groups into close proximity and an electrophylic interaction may be expected to take place. The low ionization voltage data did not indicate any direct formation of an m/z 67 ion [presumed to be cyclopentenium] (8) at or near the threshold.

Comparison of the low resolution spectra of the 9, 10, 11, and 13, carbon-containing alpha-omega diynes indicates that changes in the fragmentation paths are occurring. At ten carbon atoms, cleavage Beta to the triple bond may well occur, and other linear fragmentations, gamma, delta, etc., occur to produce ions at m/z 109, 93, 81, and 67, etc., in characteristic of linear processes with the alkynes. Nothing in the data, up to this point, indicates whether or not any other cyclization of these ions is occurring; i.e., the m/z 67 ion may well be the cyclopentenium ion.

In the lower m/z range, ions in the -1 series appear for 5 carbons (69) and 4 carbons (55), further supporting chain fragmentation processes. Only the C-10 molecule shows a small m/z 45.5 ion usually associated with the doubly charged tropylium ion. No other doubly charged ions occur and hence these species do not show the doubly charged ions typical and characteristic of the -6 and -7 series ions from the alkyl benzenes. The seven to nine carbon-containing alpha-omega diynes do show such ions. The nonadiyne showed an ion at m/z 57.5 associated with the doubly charged m/z 115 ion. These ions are not seen, or are of negligible intensity in the spectra of molecules containing ten or more carbon atoms.

1) U.S.B.M. Report of Investigations #6854, R.F. Kendall and B.H. Eccleston, 1966.

2) Lifschitz, C. and Gefen, S., Int. J. Mass. Spectrom. Ion Phys., 35, 31 (1980).

3) Paper MPA-19, "Mass Spectroscopic Fragmentation Pathways of 1,8-Nonadiyne" Robbins, R.C., and Foster, N.G. 30th Annual Conference on Mass Spectrometry and Allied Topics, ASMS, Honolulu, Hawaii, June 1982. Submitted to Org. Mass Spectrom.

4) Winnik, M.A., Chemical Reviews, 81, #5, 491 (1981).

5) Meyerson, S. and Leitch, L.C., J. Am. Chem. Soc., 93, 2244 (1971).

6) ASTM "Uncertified Mass Spectra," #1897.

7) Wagner-Redeker, Winfried, Levsen, K., Schwarz, H., and Zummack, W., Org. Mass Spectrom. 16, #8, 361 (1981).

8) Wolkoff, P., Holmes, J.L., and Lossing, F.P., Can. J. Chem. 58, 251 (1980).

CHEMISTRY AND MASS SPECTROMETRY OF POLYSULFANES: SELECTIVE SULFUR-34 INCORPORATION STUDIES

GEORGE BARANY [1,2], ANDREW W. MOTT, and EDMUND A. LARKA. Department of Chemistry, University of Minnesota, 207 Pleasant Street, S.E., Minneapolis, MN 55455.

An earlier report from this laboratory [3] defined the principal reaction between O-ethyl-N-methylthiocarbamate (1) and chlorocarbonylsulfenyl chloride (2) in the presence of water to give bis(N-ethoxycarbonyl-N-methylcarbamoyl)tetrasulfane (4). Also formed, in lesser amounts, are the corresponding tri-(3), penta-(5), and hexa-(6) sulfanes. The

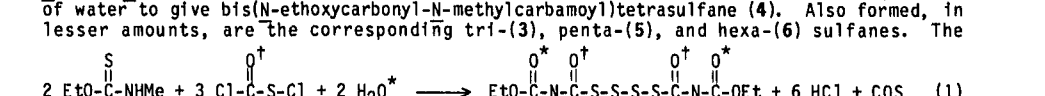

(1)

structures of 3 to 6 were proven by X-ray crystallography, and labelling studies with > 92% isotopically enriched oxygen-18 water (*) or 2 (†) [4] revealed the sources of the oxygen atoms in the products (Equation 1). For the present study, isotopically pure (~ 99%) sulfur-34 carbon disulfide was used as a precursor for the syntheses of each of labelled 1 (Equation 2, 60% overall yield) and 2 (Equation 3, 59% overall yield), and these compounds were used in turn to derive mixtures of labelled polysulfanes.

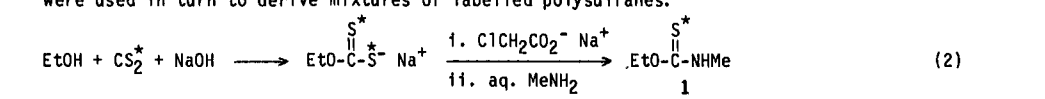

(2)

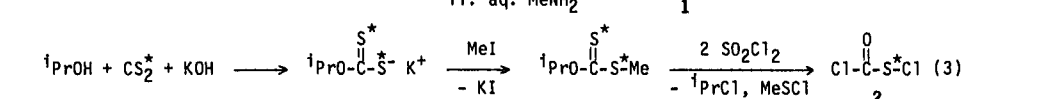

(3)

Pure polysulfanes were obtained by preparative reversed-phase high pressure liquid chromatography (9.4 mm x 25 cm Zorbax-ODS column eluted with MeOH - H_2O = 7:3 at 3.5 mL/min). After crystallization, they were thoroughly characterized by low and high resolution electron impact (70 eV), and positive and negative methane and isobutane chemical ionization, data recorded on a Finnigan 4000 Mass Spectrometer. Alternatively, the separation technique was scaled down: 5 mg of a mixture were applied to an analytical column (4.6 mm x 250 mm Ultrasphere-ODS column eluted with MeCN - H_2O = 11:9 at 0.9 mL/min) and the appropriate fractions were extracted into $CHCl_3$ and concentrated to provide approximately 0.2 mg directly at the bottom of 1.5 x 90 mm capillary tubes. Finally, it was shown that unfractionated polysulfane mixtures could be directly analyzed by the same techniques, since the families of fragmentation ions produced by the individual species overlap.

The positions of sulfurs in the bis(acyl)polysulfane chains are indicated by the following diagrams:

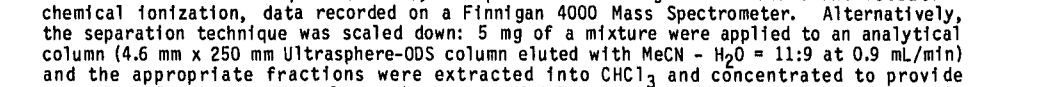

α,α' from 2; β,β' from 1

The carbamoyl sulfurs (α and α') are exclusively derived from 2, as evidenced by isotope incorporations into the base peak in the negative chemical ionization spectra, EtO(C=O)NMe(C=O)S^- (m/z 162 when unlabelled), and strong peaks at this same mass in the positive spectra and upon electron impact (latter assignment confirmed by accurate mass measurement). The positive spectra were not as useful, because both EtO(C=O)NMe(C=O)S^+ and EtO(C=O)NMe(C=O)SH_2^+ formed with more of the latter when isobutane was the reagent gas. Extensions of this analysis allowed the conclusion that those sulfurs (β, β') proximal to the carbamoyl sulfurs are due to thiocarbamate 1. The relevant peaks were at m/z 196 in the negative spectra (>80% incorporation of a single sulfur-34 into EtO(C=O)NMe(C=O)S_2^-, when either labelled 1 or 2 were the precursor to the polysulfanes), and m/z 197 in the electron impact spectra (clean incorporation of a single sulfur-34 into EtO(C=O)NMe(C=O)$S_2H^{+\cdot}$). Supporting these interpretations were the incorporation patterns

into molecular ($M^{+\cdot}$) and quasi-molecular $(M+1)^+$ ions of purified 3 and 4: the trisulfane which has two carbamoyl (α, α') and one central (β) sulfur cleanly incorporated one sulfur-34 from labelled **1** and two from labelled **2**; the tetrasulfane took up two sulfur-34's from either variation of the labelling experiment.

The central sulfurs (γ and/or γ') of **5** or **6** were more difficult to assign. Although the characteristic of the negative spectra was the descending amounts of carbamoyl polysulfanyl ions, $EtO(C{=}O)NMe(C{=}O)S_n^-$, up to n = 6, the well-understood situation of pure labelled **4** revealed that already for n = 3, the ion anticipated for a single cleavage of the linear sequence at the β' sulfur was accompanied by another ion that included two α sulfurs and only one β sulfur. This randomization of labelled sulfurs was even more pronounced for higher n. Fortunately, the isobutane positive chemical ionization spectra were adequate to detect $(M+1)^+$ ions of **5** and **6**, both from mixtures and when purified. The central sulfur (γ) of the pentasulfane evidently originates from either **1** or **2**, in an approximately 3:2 ratio. Similarly, for the hexasulfane, both sulfurs (γ, γ') arise from the same sources in the same approximate ratio.

Knowledge of the exact distribution of labelled sulfurs in the linear polysulfane chains of **3** to **6** makes possible a number of interesting inferences about the details of fragmentation processes of these compounds. For example, the positive chemical ionization spectra are characterized by a series of neutral losses of one or more sulfur atoms and/or carbonyl sulfide (COS) molecules. The labelling patterns show that COS is lost intact (i.e., including the α sulfur) from the sides, and furthermore that sulfur atoms are extruded with good specificity out of the middle [5] of the polysulfane chain (i.e., β and γ sulfurs are lost). Since the central sulfurs are primarily, although not exclusively, originating in thiocarbamate **1**, the observation of an approximately 4:1 ratio of label from **1** to that from **2** in all of the S_n^- ion isotope clusters (n = 2 to 6 but mainly 3 and 4) of the negative spectrum, or in $S_2^{+\cdot}$ of the electron impact spectrum, may be relevant. Finally, the production pathway for the unusual ion **7** (m/z 191 when unlabelled; composition confirmed by high resolution accurate mass measurement) in the electron impact spectrum can be suggested on the basis of the labelling pattern (Equation 4).

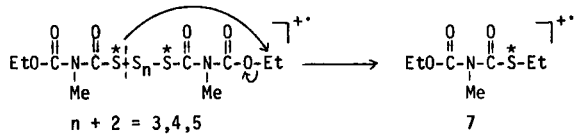

(4)

transition state of 8 to 10 atoms

In conclusion, the results reported herein reveal the power of mass spectrometry for unravelling the complex chemistry of polysulfanes, and should allow suggestions of mechanisms for the formation and disproportionation of bis(N-ethoxycarbonyl-N-methylcarbamoyl)tetrasulfane (**4**).

Acknowledgments. We thank Steven J. Eastep for expert technical assistance, and James H. Gibson and Peter K. Trumper for patient operation of the mass spectrometer.

REFERENCES AND NOTES

[1] Address inquiries to this author. Supported by National Institutes of Health GM 28934 and Searle Scholars Program of the Chicago Community Trust.
[2] Searle Scholar, 1982-1985; NIH Research Career Development Award, 1982-1987.
[3] Barany, G., Słomczyńska, U., and Mott, A.W. ORG 32. American Chemical Society, 187th Annual Meeting, St. Louis, MO, April 8-13, 1984.
[4] Mott, A.W., Eastep, S.J., Słomczyńska, U., and Barany, G. J. Labelled Compounds and Radiopharmaceuticals, 21, 329-336 (1984).
[5] In contrast, the electron impact spectrum of **4** generated when either **1** or **2** had sulfur-34 showed ions at m/z 392, $M^{+\cdot}$ with two sulfur-34; m/z 358 and 360 in equal amounts indicating equal probability for loss of the α or β sulfur; and m/z 326 meaning that exactly one α and one β sulfur remain connected in the resulting $EtO(C{=}O)NMe(C{=}O)SS(C{=}O)NMe(C{=}O)OEt^{+\cdot}$. Pure **5** generated in the same way showed the same ions in the same ratios, meaning that the γ sulfur is the first to be lost either thermally or upon gas-phase ion fragmentation.

QUANTITATIVE GC/MS USING NEGATIVE CHEMICAL IONIZATION WITH OH^- AS THE REACTANT ION; APPLICATION TO FLAVOUR COMPONENTS

A.P. Bruins, E.T. Elema and H. Hendriks, State University, Department of Pharmacy, A. Deusinglaan 2, 9713 AW Groningen, The Netherlands

The majority of publications on quantitative GC/MS with negative chemical ionization report the use of the electron capture process in order to achieve a high sensitivity. Comparatively little use is made of negative ion molecule reactions for quantitative purposes. The OH^- ion is used in an increasing number of papers dealing with identification and structure elucidation (1). Reactions of OH^- with sample molecules are shown schematically in Figure 1.

In our laboratory, OH^-Cl is used for identification of components in essential oils. We have attempted to use OH^- for quantitation. When esters are introduced into the ion source, the OH^- ion not only produces the $(M-H)^-$ ion, but also induces an apparent nucleophilic displacement reaction which cleaves the ester bond. For example, all acetates show the acetate ion at m/z 59, as shown in the spectrum of menthyl acetate (MW = 198) in Figure 2.(2,3)

A total ion current profile of a gas chromatogram (Carbowax glass capillary column) is given in Figure 3. Menthyl acetate can be quantitated with decyl acetate as internal standard. The selected ion current profiles of menthyl acetate and decyl acetate are given in Figure 4. Calibration lines have been constructed using the response ratios of the $(M-H)^-$ ions at m/z 197 and 199, and also by the use of the response of menthyl acetate and decyl acetate on their common m/z 59 ion. The measured concentration of menthyl acetate is:

from peak height	from peak area
m/z 197/199 : 5.4%	m/z 197/199 : 5.4%
59/59 : 5.4%	59/59 : 5.2%

Thus, single ion monitoring of m/z 59 and selected ion monitoring of the $(M-H)^-$ ions give the same result.

Single ion monitoring of m/z 59 can be extended to quantitation of more than one acetate in an essential oil or flavour mixture. Using this procedure, the concentrations of neryl acetate and geranyl acetate in a Californian cold pressed lemon oil have been measured. Response factors were determined relative to decyl acetate which was again used as the internal standard. Peak area and peak height ratios gave the same result:

0.55% neryl acetate and 0.78% geranyl acetate

In conclusion, GC/MS with OH^-CI is a useful method for quantitation. It is as sensitive as positive ion CI, and application is of course not limited to terpene esters in essential oils.

References

1. A.L.C. Smit and F.H. Field, J. Am. Chem. Soc. 99, 6471 (1977)
2. A.P. Bruins, Anal. Chem. 51, 967 (1979)
3. H. Hendriks and A.P. Bruins, Biomed. Mass Spectrom. 10, 377 (1983)

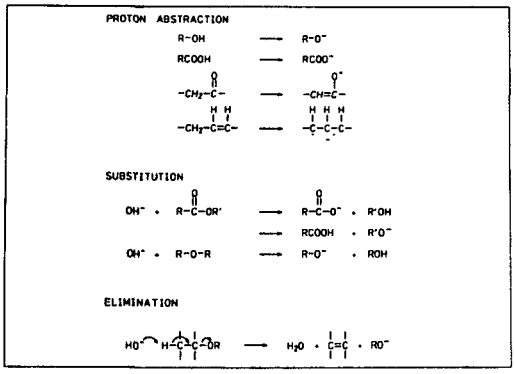

Figure 1
Reactions of OH^- ions

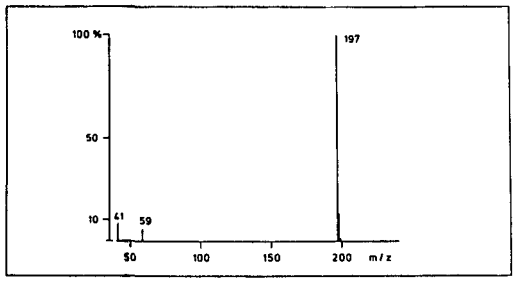

Figure 2
OH^- CI spectrum of
menthyl acetate

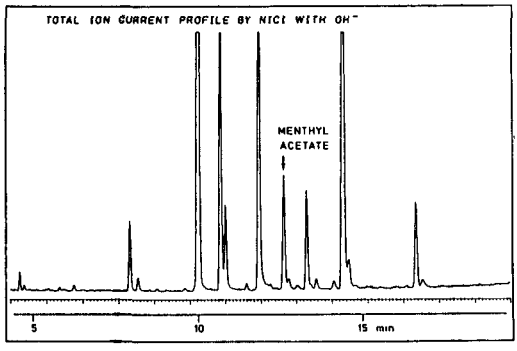

Figure 3
Capillary gas chromatography

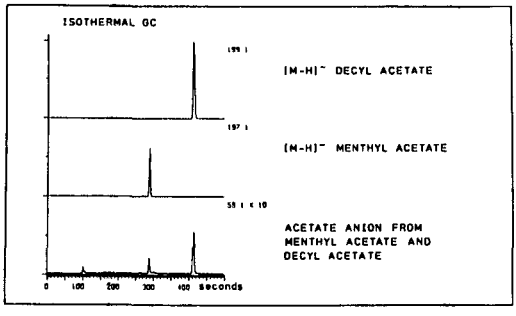

Figure 4
Selected ion monitoring with
decyl acetate as standard

SEQUENTIAL ION-MOLECULE REACTIONS IN A FOURIER TRANSFORM MASS SPECTROMETER FOR ION STRUCTURE DETERMINATIONS

C. Dass, T.M. Sack and M.L. Gross
University of Nebraska-Lincoln
Lincoln, Nebraska 68588

Although Fourier transform mass spectrometry is the method of choice for the study of ion-molecule reactions, the traditional method of sample introduction via standard leak valves can lead to problems:

1. Pressures remain high (10^{-6} torr) throughout the experiment, thus reducing the trapping efficiency and available mass resolution.

2. Ions formed by ion-molecule chemistry cannot be readily studied as reactants for further reactions due to the presence of all the neutral precursors during the entire experiment which can produce confusing side reactions.

The recently introduced pulse valve inlet method (1,2) can alleviate these problems by allowing neutral gases to be introduced as a pulse, so that the cell need not be cluttered with high partial pressures of reagents at all times. This strategy can be taken a step further by using two valves to introduce different reagents in order to carry out reactions of ions which are themselves reaction products. The procedure is to first pulse in a charge exchange (CE) reagent (R), ionize it, and allow it to react with a low pressure of analyte (M). This serves to form $M^{+\cdot}$ with an internal energy defined as the difference in IE(R) and IE(M). After the CE gas has pumped away, double resonance pulses eject all ions except for $M^{+\cdot}$ from the cell. The second neutral reagent (B) is then pulsed into the cell, allowed to react with $M^{+\cdot}$, and the product ions are detected after a suitable reaction period. The pulse sequence is shown in Fig. 1.

This scheme has been applied to the investigation of the

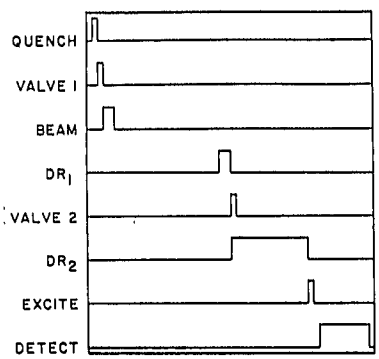

Figure 1

RATIO	PRECURSOR	A	B	C
	1-MCB	0.3	2.5	3.0
I_{94}/I_{93}	ISOPRENE	2.7	5.7	15.0
	3-MCB	0.4	3.7	-
	1,3-PENTADIENE	6.6	56.0	-
I_{85}/I_{94}	1-MCB	5.0	7.9	0.1
	3-MCB	0.8	0.1	-

(A) Static experiment, 9.5 eV electrons
(B) Pulsed experiment, C_6H_6 CE
(C) Pulsed experiment, CS_2 CE

The ionization potentials of 1-MCB and 3-MCB are 8.62 and 9.08 eV, respectively.

Table 1

electrocyclic ring-opening reaction of 1- and 3-methylcyclobutene (1-MCB and 3-MCB) and to the study of the structure of the C_3H_6 radical cations formed by ionization of cyclopropane. It was predicted that the sequential reactions (CE followed by ion-molecule reaction) could be observed with high conversion of the analyte radical cations into products, and minimal cross contamination due to the low average pressure in the cell.

METHYLCYCLOBUTENES

The result from using this scheme to perform the specific ion-molecule reaction of "energy selected" MCB radical cations with methyl vinyl ether (MVE) are shown in Table 1. MVE reacts with the cyclic form of 1- and

3-MCB to form an adduct which loses C_3H_5 to form m/z 85, while the m/z 94 ions arise from the loss of CH_3OH from the adduct of isoprene and MVE.

The data show that 1-MCB appears to isomerize (i.e. exhibit isoprene-like properties) at or about the internal energy imparted by benzene CE (0.68 eV). 3-MCB also has reached its activation barrier by benzene CE, but this only represents an internal energy of 0.22 eV because 3-MCB has a higher IE. Thus we estimate that the activation energies for the electrocyclic ring-opening of 1-MCB and 3-MCB are <14 kcal/mol and <4 kcal/mol, respectively.

CYCLOPROPANE

This scheme was applied to the ion-molecule reactions of "energy selected" C_3H_6 radical ions with both ammonia and propene-d_6 as the diagnostic reagents. The reaction of cyclopropane radical cations with neutral ammonia confirmed the previously determined results (3). That is, cyclopropane ions with 1.1 eV or more internal energy appear to isomerize to a structure which reacts in a similar way to propene.

The reaction with neutral propene-d_6 was chosen to be a structure probe for the propene stucture because of the distinctive reaction of propene radical cations with propene neutral molecules.

The experimental sequence depicted as a set of spectra for the sequential reactions with propene-d_6 are shown in Fig. 2 and Table 2 contains the results. For this second diagnostic reaction, there seems to

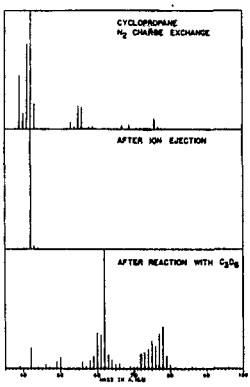

Figure 2

$C_3H_6^+ + C_3D_6$ (PULSED)

IONIZATION METHOD		$\frac{\Sigma I_{58-62}}{\Sigma I_{72-75}}$ △	⩚
electrons	10 eV	3.7	1.0
"	15 eV	6.3	1.6
"	20 eV	6.5	1.8
"	50 eV	6.1	1.9
CS_2 CE		2.7	1.4
COS CE		2.4	1.2
N_2 CE		2.4	1.2

Table 2

be no evidence that cyclopropane radical ions isomerize to the propene stucture, based on the fact that the product distributions do not converge even at high internal energies. Based on these data, we postulate that cyclopropane radical cations ring-open, without hydrogen scrambling, to form the trimethylene radical cation ($\cdot CH_2CH_2CH_2^+$).

In conclusion, the sequential reaction sequence made possible by pulsed valve introduction of reagents enables many new experiments heretofor not readily performed by using conventional ion-molecule chemical techniques in FTMS.

REFERENCES

1. T.J. Carlin and B.S. Freiser, Anal. Chem., 1983, 55, 571.
2. T.M. Sack and M.L. Gross, Anal. Chem., 1983, 55, 2419.
3. S.G. Lias and T.J. Buckley, Int. J. Mass Spectrom. and Ion Proc., 1984, 56, 123.

SELECTIVE SYNTHESIS INSIDE THE COLLISION CELL OF A TANDEM QUADRUPOLE MS / MS

J.P. Schmit and P.H. Dawson; Dept. of Chemistry, Université du Québec à Montréal, H3C 3P8 and National Research Council of Canada, Div. of Physics, Ottawa, K1A 0R6.

In a previous work, a tandem quadrupole MS/MS (TAGA 6000) able to accomodate ions of very low axial kinetic energy with a minimum energy spread has been used to study the formation of adduct ions (1). By using a parent ion center-of-mass axial kinetic energy ranging from 0.001 to 0.008 eV along with an appropriate control of the target thickness, we have been able to get covalently bonded adduct ions resulting from the direct addition of protonated esters onto neutral ammonia.

A similar approach has been successfully followed to study the reaction between aromatic molecular ions and ammonia or methylamine as nucleophilic neutral target.

The parent ions were produced with either an atmospheric pressure chemical ionization source or a conventional EI source without noticing any characteristic difference in the chemical behaviour of the reactants.

As with the ester / ammonia couple, at least three competitive reaction channels were observed: the adduct ion formation, the protonation of the nucleophilic target, and, in a lesser extent, some Reaction Induced Fragmentation (RIF).

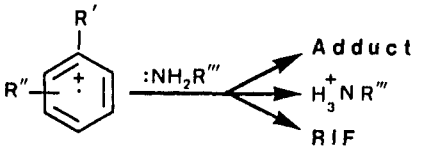

Substitution of ammonia or methylamine by Argon or Nitrogen within the same condition of parent ion axial laboratory kinetic energy and target thickness yields very little if any fragment ions. This latter observation argues in favor of the conclusion that the observed fragment ions result much more from the fragmentation of the adduct ions (RIF) than from a pure Collision Induced Fragmentation (CID).

Depending on the nature of the parent ion, the resulting adduct ion is obtained either through a direct addition mechanism (case of benzene) or via an addition / elimination processus (substituted benzenes). The required center-of-mass axial kinetic energy ranges from 0.05 eV for the reaction between benzene and ammonia up to about 1.2 eV for the reaction between xylenes and methylamine. It is noticeable that such energies are at least one order of magnitude higher than those required for the formation of adduct ions between protonated esters and ammonia.

By using ammonia as neutral nucleophilic target, toluene as well as the various xylenes yield an adduct ion of m/z 125 resulting from the addition of two molecules of ammonia. Yet, toluene adduct formation is accompanied by the loss of a hydrogen radical while the formation of xylene adducts involves the loss of a methyl radical. Moreover, besides the formation of the adduct ion m/z 125, the reaction of toluene molecular ion with ammonia yields a lower mass adduct ion (m/z 108) resulting from the addition of one molecule of ammonia and the concomitant loss of a hydrogen radical.

When using methylamine as neutral nucleophilic target, the whole series of aromatics exhibits two different adduct ions. However, as in the previous case, benzene follows a particular mechanism involving the direct addition of methylamine yielding adduct ions at m/z 109 and 140, while toluene and xylenes exhibit adduct ions at m/z 122 and 152 with a complementary elimination of $H^{\cdot}$ or $CH_3^{\cdot}$ radical.

Finally, by comparison with each other, the different reaction channels were found to be energetically specific allowing one to favor selectively a given channel of reaction by an appropriate setting of the parent ion axial kinetic energy.

(1) 31st ASMS annual meeting, Boston 1983 and submitted for publication.

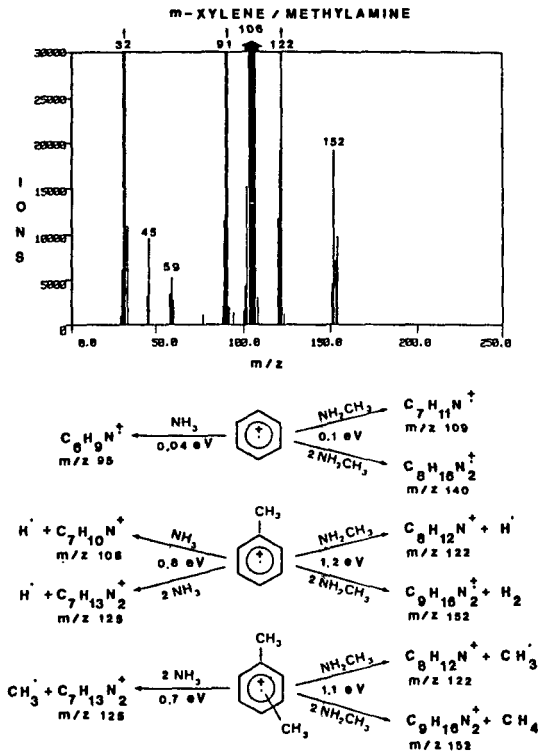

ADDITIVITY OF COLLISIONAL ACTIVATION SPECTRA. A COMPARISON USING RESOLVED ISOBARIC MAIN BEAMS AND CAD PRODUCTS

Donald J. Harvan, Maurice M. Bursey,* and J. Ronald Hass

Laboratory of Molecular Biophysics,
National Institute of Environmental Health Sciences,
P.O. Box 12233, Research Triangle Park, North Carolina 27709

In general, the cross section for fragmentation of an ion differs from those of its isomers and isobars. Similarly, its cross section for scattering by the collision gas also differs from those of its isomers and isobars. These differences must be kept in mind when using tandem mass spectrometry for quantitative analysis of ions of the same mass. We have observed yet another restriction to bear in mind when carrying out such analyses.

The isobaric CH_3CO^+ and $C_3H_7^+$ ions formed by electron ionization of $CH_3COCH(CH_3)_2$ were separated in the first two sectors of a ZAB-4F tandem double focusing instrument (BEEB geometry) and passed through a pressure of He in the collision cell between the second and third sectors sufficient to reduce the intensity of the transmitted major component of the doublet (CH_3CO^+) by 50%. The CAD spectrum of each ion was recorded. Then the resolution of the first two sectors was reduced to its minimum value, about 500, and the ion beams moved back and forth across the slit to transmit varying mixtures of the two ion beams. These mixtures then entered the collision cell under the same pressure of He. The spectrum of the mixture was recorded under conditions of high CAD product resolution and low CAD product resolution.

In no case did the spectrum of the mixture correspond to the sum of the spectra of the individual components weighted by the intensities of the main beams, as might be expected if the ions had the same collision and fragmentation cross sections. Nor did it correspond to a sum corrected for the differences between collision and fragmentation cross sections of the ions. Indeed, an analysis of the intensity ratios of the most intense fragment ions indicated that the spectrum of the mixture was not a linear combination of the spectra of the components.

The reason for this lies in the fact that the two ion beams were not totally transmitted, but instead only partially. Their extremes were cut off. Beynon has shown that the extremes of a collimated beam of ions contains the fraction with not only greater kinetic energy but lower internal energy. Thus the transmitted portion of the ion beams has higher internal energy on average than the full ion beam (which was used for the spectrum of the individual components). The transmitted portion thus has more fragmentations typical of high-energy ions and fewer typical of low-energy ions. For example, the fractional contribution of the loss of H_2 from $C_3H_7^+$ is greatly reduced when the extreme of the peak is removed.

Hence, it is important in quantitative analysis of ion mixtures to transmit the entire width of all primary beams. While the situation with isobaric ions is a bit contrived, the same situation applies to isomeric ions, if the primary beam of at least one of the isomers is broad because of the mechanism of ion formation. Inadvertent exclusion of the extremes of this beam by too high resolution before CAD would produce the same effect noted above — deviation from a linear combination of spectra of pure components and consequent inability to analyze the mixture of ions.

* on an R. J. Reynolds Industries leave from the University of North Carolina at Chapel Hill.

SITE OF GAS-PHASE CATION ATTACHMENT. THE PROTONATION AND ALKYLATION OF BIFUNCTIONAL NUCLEOPHILES

DAVID J. BURINSKY+ AND JOSEPH E. CAMPANA
Naval Research Laboratory, Chemistry Division, Washington, DC 20375

This paper reports the structure elucidation of gaseous ions, which can be used to determine the preferred site of reaction for the protonation and alkylation of several multi-functional nucleophilic compounds. The site of attachment of gaseous positive ions ($[H]^+$, $[CH_3]^+$, and $[C_2H_5]^+$) to morpholine, thiomorpholine, and 1,4-thioxane has been studied using tandem mass spectrometry (MS/MS).

The specific site of reaction (Scheme I) is characterized by the comparison of the CID/MIKES spectra of the gas-phase ion/molecule reaction products to those obtained for authentic model ions [1] generated by fast-atom bombardment (FAB) [2] of appropriate quaternary ammonium salts. In the case of morpholine, correlation of fragment ion spectra for both protonation and methylation reactions was excellent, implying exclusive cation interaction at the nitrogen heteroatom, as predicted by gas-phase proton affinity data [3].

Tables 1, 2, and 3 summarize the results for the dissociation reactions designated most structurally diagnostic (Scheme II). Examination of the data for thiomorpholine reveals two distinct sites of cation attachment, with protonation occuring exclusively at the nitrogen atom and alkylation taking place preferentially at the sulfur atom. This result highlights the intrinsic differences between the properties of basicity and nucleophilicity in gas-phase reactions.

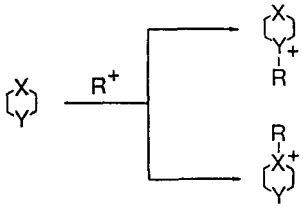

X , Y = S , NH / O , NH / O , S R = H , CH_3, C_2H_5

Scheme I

Despite a lack of authentic model ions, similarities between the data for the protonation and alkylation of 1,4-thioxane and those for the other two substrates allows reasonable assertions to be put forward in favor of sulfur being the preferential site of reaction in this member of the compound class.

References

1. K.V. Wood, D.J. Burinsky, D. Cameron and R.G. Cooks J. Org. Chem. 48, 5236 (1983).
2. M. Barber, R.S. Bordoli, G.J. Elliott, R.D. Sedgwick and A.N. Tyler Anal. Chem. 54, 645A (1982).
3. R. Walder and J.L. Franklin Int. J. Mass Spectrom. Ion Phys. 36, 85 (1980).

+ Present Address: USDA-ERRC, Philadelphia, PA 19118

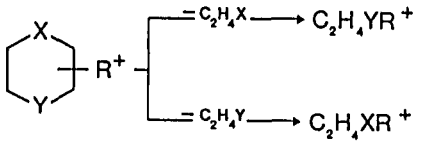

Scheme II

Substrate	Ion Origin	m/z	- C_2H_4X/- C_2H_4Y
Morpholine (X=O, Y=NH)	$C_4H_9NO+H^+$	88	4.5
	$C_4H_{10}NO^+Cl^-$		4.8
	$C_4H_9NO+C_2H_5^+$	116	100
	$C_6H_{14}NO^+I^-$		100
	$C_4H_9NO+CH_3^+$	102	100
	$C_5H_{12}NO^+I^-$		100

Table 1. Summary of Diagnostic Fragmentations of the Cation Attachment Products and Model Systems for the Protonation, Ethylation, and Methylation of Morpholine.

Table 2. Summary of Diagnostic Fragmentations of the Cation Attachment Products and Model Systems for the Protonation, Ethylation, and Methylation of Thiomorpholine.

Substrate	Ion Origin	m/z	- C_2H_4X/- C_2H_4Y
Thiomorpholine (X=S, Y=NH)	$C_4H_9NS+H^+$	104	4.6
	$C_4H_{10}NS^+Cl^-$		7.9
	$C_4H_9NS+C_2H_5^+$	132	0.1
	$C_6H_{14}NS^+I^-$		8.9
	$C_4H_9NS+CH_3^+$	118	0.1
	$C_5H_{12}NS^+I^-$		17.0

Substrate	Ion Origin	m/z	- C_2H_4X/- C_2H_4Y
1,4-Thioxane (X=O, Y=S)	$C_4H_8OS+H^+$	105	2.3
	$C_4H_8OS+C_2H_5^+$	133	3.3
	$C_4H_8OS+CH_3^+$	119	9.1

Table 3. Summary of Diagnostic Fragmentations of the cation Attachment Products and Model Systems for the Protonation, Ethylation, and Methylation of 1,4-Thioxane.

CHARGE STRIPPING MASS SPECROMETRY OF MOLECULAR IONS FROM POLYCYCLIC AROMATIC HYDROCARBONS

D.Stahl and F.Maquin,Institut de Chimie-Physique,Ecole Polytechnique Fédérale de Lausanne,CH-1015 LAUSANNE (Switzerland)

The minimum energy for the reaction $M^{+\cdot} + N \rightarrow M^{2+} + N + e$ has been measured by kinetic energy loss spectrometry for molecular ions in the polyacene and polyphenyl series.The experiments were performed on a ZAB-2F instrument : 70 eV electrons,8 kV accelerating voltage , and O_2 as the collision gas at 10^{-4} Torr.For the determination of the ionization energy of these ions (denoted as Q_{min}),the energy scale was calibrated by admitting toluene as a reference compound for which Q_{min} is known to be 15.7 eV (1).Table 1 presents the Q_{min} values obtained for the five compounds from the polyacene series, along with the single ionization energies IE^{I},double ionization energies IE^{II}calculated as $IE^{II} = IE^{I} + Q_{min}$,$IE^{II}$values from literature when available, and the energy levels m of the highest occupied molecular orbital from HÜckel theory ($E_j = \alpha + m_j \beta$).The results are the average value of 10 to 20 measurements and have a standard deviation of 0.1 eV.

Table 1	Q_{min}(eV)	IE^{I}	$IE^{II} = IE^{I} + Q_{min}$	IE^{II}	m
1 benzene C_6H_6	16.12 16.8[1]	9.20	25.32	26.1[3]	1[a] 0.8[b]
2 naphtalene $C_{10}H_8$ 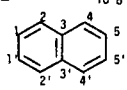	14.61 15.0[1]	8.14	22.74	22.7[2] 22.8[3]	0.6180[a] 0.5353[b]
3 anthracene $C_{14}H_{10}$ 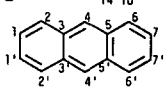	13 56 14 0[1]	7.47	21.07	21.1[2] 21.3[3]	0.4142[a] 0.3753[b]
4 naphthacene $C_{18}H_{12}$ 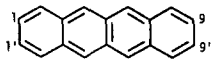	13.14	6.97	20.07	22.14[2]	0.2949[a] 0.2747[b]
5 pentacene $C_{22}H_{14}$ 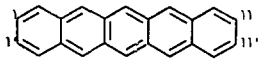	12.81	6.61	19.41	19.6[2]	0.2197[a] 0.2083[b]

a) m from HÜckel MO theory b) m from Extended HÜckel MO theory (EHMO)

1)ref.2 2) ref.3 3)ref.4

A least squares linear regression provides the following results:

HMO $Q_{min} = 11.87(\pm 0.22) + 4.28(\pm 0.38)\ m$ with $r = 0.9988$

EHMO $Q_{min} = 11.56(\pm 0.28) + 5.66(\pm 0.58)\ m$ $r = 0.9984$

These equations allow to predict Q_{min} for higher homologs in the polyacene series.For the next higher homolog , hexacene , for which m_{HOMO}=0.1694 ,one obtains Q_{min} = 12.6 eV.The energy for the process $M^{+} \rightarrow M^{2+}$ is equal to the energy for the removal of the remaining electron in the HOMO plus the energy for the stabilization of the two positive charges.As the size of the polyacene ion becomes larger,it becomes less ans less difficult to accomodate the two positives charges in the dication, and one could expect that the most stable dications are those for which the intercharge distance is the largest(i.e. on atoms 1 and 7 for anthracene). The energy for placing two charges at a distance r is given by $\int_{\infty}^{r} qq/r^2$ which can be reduced to E_{cb}(eV) = 14.4/r(A).It can also be approximated by the Coulomb integrals over $2p_z$orbitals

$$(pp/qq) = \int X_p^*(1)\ X_q^*(2)\ e^2/r_{12}\ X_p(1)\ X_q(2)\ dv$$

The values obtained by these two methods are given in Table 2 for maximum charge separation

Compound	p,q a)	$r_{p,q}$[Å]	(pp/qq) E_{cb} [eV]	Δ(pp/qq) ΔE_{cb}	ΔQ_{min}	m_{HOMO}
4 naphthacene	1,9'	9.73	1.475 1.480			
		—		0.289 0.292	0.33	0.07
5 pentacene	1,11'	12.12	1.186 1.888			

a) see Table 1 for signification of p,q

For large size compounds ,the difference between the Q_{min} values corresponds almost exclusively to the difference in the electrostatic energy.From the analysis of all the data,one can conclude that the structure of the polyacenes dications is the cyclic structure of the corresponding neutrals.The benzene dication is found to have the fulvene dication geometry,in accordance with conclusion of ab initio calculations.

For the polyphenyls the following Q_{min} values were obtained :biphenyl 14.23 eV ;p-terphenyl 13.51 ;o-terphenyl 12.64 ;m-terphenyl 12.86 ;p-quaterphenyl 12.58 ;m-quaterphenyl 12-75 ; m-quinquephenyl 12.70 ; p-hexaphenyl 11.95 .Student's and F statistical tests indicate that the measured Q_{min} values for isomers are significatively different.

Conclusion : This study shows that ionization energies of polyacenes molecular ions can be well discussed in terms of HÜckel molecular orbital theory.The geometries of the stable dications were readily determined from coulombic repulsion energies assuming the maximum intercharge distance in structures of the same geometry as the neutral molecules.The charge stripping experiments are shown to be accurate enough to distinguish between isomers of polyphenyls ,which was not possible by electron impact appearance energy measurements.

(1)F.H.Dorman and J.D.Morrison,J.Chem.Phys. 35 ,575 (1961)
(2)T.Ast,C.J.Porter,C.J.Proctor and J.H.Beynon,Bull.Soc.Chim.Beograd 46 ,135 (1981)
(3)H.M.Rosenstock,K.Draxl,B.W.Steiner,J.T.Herron,J.Phys.Chem.Ref.Data 6,Suppl. 1 (1977)
(4)R.D.Levin and S.G.Lias,"Ionization Potential and Appearance Potential Measurements", 1971-1981, NSRDS-NBS 71,Washington (1982)

THE COLLISONALLY ACTIVATED FRAGMENTATION OF $(M-H)^-$ IONS OF POLYHYDROXY COMPOUNDS PRODUCED UNDER OH^- NICIMS AND APPLICATIONS TO OLIGOMERS OF POLYMERIC FOOD ADDITIVES

W.C. Brumley, D. Andrzejewski, and J.A. Sphon, Division of Chemical Technology, Food and Drug Administration, Washington, DC 20204

Although the fragmentation observed in NICIMS is usually less than that of its positive ion analog, significant fragmentation can be observed in certain polyfunctional molecules. For example, the normal OH^- spectrum of sorbitol (a hexitol) contains well over ten fragment ions whereas the spectrum of a fatty alcohol consists of an $(M-H)^-$ ion and perhaps an $(M-H-H_2)^-$ ion. The transition in behavior from mono- to polyhydroxy compounds must result primarily from the increasing multiplicity of relatively stable fragment ions accessible to the ionized molecule. Thus, a dependence is expected that includes both the number of functional groups and their efficiency in lowering the activation energies needed to reach these fragment ion states.

This study examines fragmentation pathways and fragment ions accessible to collisionally activated $(M-H)^-$ ions of polyhydroxy compounds and certain alcohol/ethers. $(M-H)^-$ ions are produced under OH^- conditions and CID/MIKE spectra obtained. Results are grouped into seven topics that illustrate major findings.

1) Isomeric compounds at m/z 75.—1,2-propanediol, 1,3-propanediol and ethylene glycol monoethyl ether can be distinguished by the CID/MIKE spectra of their $(M-H)^-$ ions. Differences involve both fragment ions and alkoxide ion formation.

2) Various monoethers of ethylene glycol. Fragmentation includes loss of H_2 or alkene elimination as well as production of alkoxide ions.

3) 1,2-;1,3-; 1,4-, and 1,6-diols.—Dependence of fragmentation upon the separation of the hydroxyl groups is found. Variations are observed in the relative abundances of eliminations involving 18 and 32 u.

4) Various substituted 1,3-diols.—The effects of alkyl substituents and structure are found. Results favor 1,2 H_2 eliminations and four center H rearrangements leading to eliminations.

5) Cyclic ethers/alcohols.—Cyclic ethers give one fragment ion but cyclic ether/alcohols afford several fragment ions that depend on structure. Losses of 18, 30, and 32 u as well as multiple bond cleavages are observed.

6) Polyhydroxy compounds.—Fragment ions are obtained for the series from two to six hydroxyl groups. Fragmentation processes frequently involve loss of 18, 32, 62, and 92 u. Carbon-carbon bond cleavage with rearrangement (four center) predominates in polyhydroxy compounds.

7) Polyoxyethylenes (POE) and POE-sorbitans.—POE's fragment by losses of 44 u and multiples thereof. The $(M-H-88)^-$ ion is predominant. POE-sorbitan also fragments by multiple losses of 44 u with the $(M-H-44)^-$ ion predominant. The oligomer nature of these substances, which are food additives, is verified, and the sorbitan unit is indicated by one of the fragment ions.

Our data suggest that in normal OH^- spectra, when four to six hydroxyl groups are present, two or more fragment ions occur. Under CID/MIKES conditions, two functional groups such as a diol or an alcohol/ether can result in substantial fragmentation. Carbon-carbon bond cleavage with H rearrangments predominate over multiple eliminations of water. In some cases, four center transition states are probably involved. Results are consistent with our assumption of the effects of both number and nature of functionality in promoting NI fragmentation. Clearly, polyhydroxy/ether compounds have many accessible fragment ion states via collisional activation. The abundant fragment ions make possible applications of CA spectra to structure determination and analysis.

NEW MS/MS SOFTWARE TOOLS FOR ELUCIDATION OF FRAGMENTATION MECHANISMS IN DI-ACETAMIDES

Susan T. Weintraub
The University of Texas Health Science Center at San Antonio
San Antonio, Texas 78284

Mark Johnston
Finnigan MAT
San Jose, California 95134

The positive ion electron impact mass spectra of a homologous series of N,N'-bis(α-iodoacetyl)diaminoalkanes (di-iodoacetamides) were examined for use in structure proof of these bifunctional protein crosslinking agents in which 2 - 7, 10 or 14 carbons separated the amide groups. Subsequent evaluation of the corresponding di-acetamides revealed that the relative intensity of certain fragments in both series varied with the number of carbons between the amide groups. The intensity of the prominent m/z 30 ion did not depend on the chain length. An ion which was proposed to result from fragmentation at both ends of the molecule was observed at $[M - 102]^+$ for di-acetamides and $[M - 354]^+$ for di-iodoacetamides, with the maximum relative intensity for each found with the 4-carbon homolog. MS/MS evaluation of the di-acetamide series and corresponding deutero-acetyl analogs indicated that a step-wise process involving sequential loss of acetyl, ammonia and ketene groups, as well as concerted pathways for the combined loss of these moieties was operative during fragmentation. Deuterium labelling studies of these compounds confirmed that the ketene loss, both in the formation of the m/z 30 ion, and associated with the $[M - 102]^+$ fragment occurred with transfer of a hydrogen or deuterium to the remaining nitrogen-containing portion of the molecule (1). The $[M - 102]^+$ fragment was not seen in the 2-carbon homolog and was exceedingly small for the 10 and 14-carbon compounds. In the 3-carbon di-acetamide, a different pathway which involves loss of an acetyl group followed by a 1-hydrogen McLafferty rearrangement (2) appears to have occurred. A mechanism has been proposed for the formation of the $[M - 102]^+$ ion which includes a cyclic product, analogous to the one formed after elimination of ammonia from the ethyl ester of lysine (3). Presentation of the MS/MS spectra in a "tree" format greatly aided in postulating fragmentation schemes which were consistent with the observed electron impact results since the TSQ "tree" program is able to display the entire three dimensional MS/MS data field in a convenient and controllable format. The use of a color printer for the "tree" diagrams depicts each subsequent generation of daughter ions in a different color to permit facile mapping of the fragmentation scheme. The MS/MS spectra in the present study were obtained on a Finnigan-MAT TSQ triple stage quadrupole mass spectrometer. Samples were introduced by means of a direct insertion probe. An electron energy of 70 eV was utilized for initial ionization. Argon was employed as the collision gas at a pressure of approximately 1 mTorr and a collision energy of approximately 15 eV.

1. Pelah, Z., Kielczewski, M. A., Wilson, J. M., Ohashi, M., Budzikiewicz, H. and Djerassi, C. J. Am. Chem. Soc. 85:2470 (1963).

2. McLafferty, F. W. and Gohlke, R. S. Anal. Chem. 31:2076 (1959).

3. Biemann, K., Seibl, J. and Gapp, F. J. Am. Chem. Soc. 83:3795 (1961).

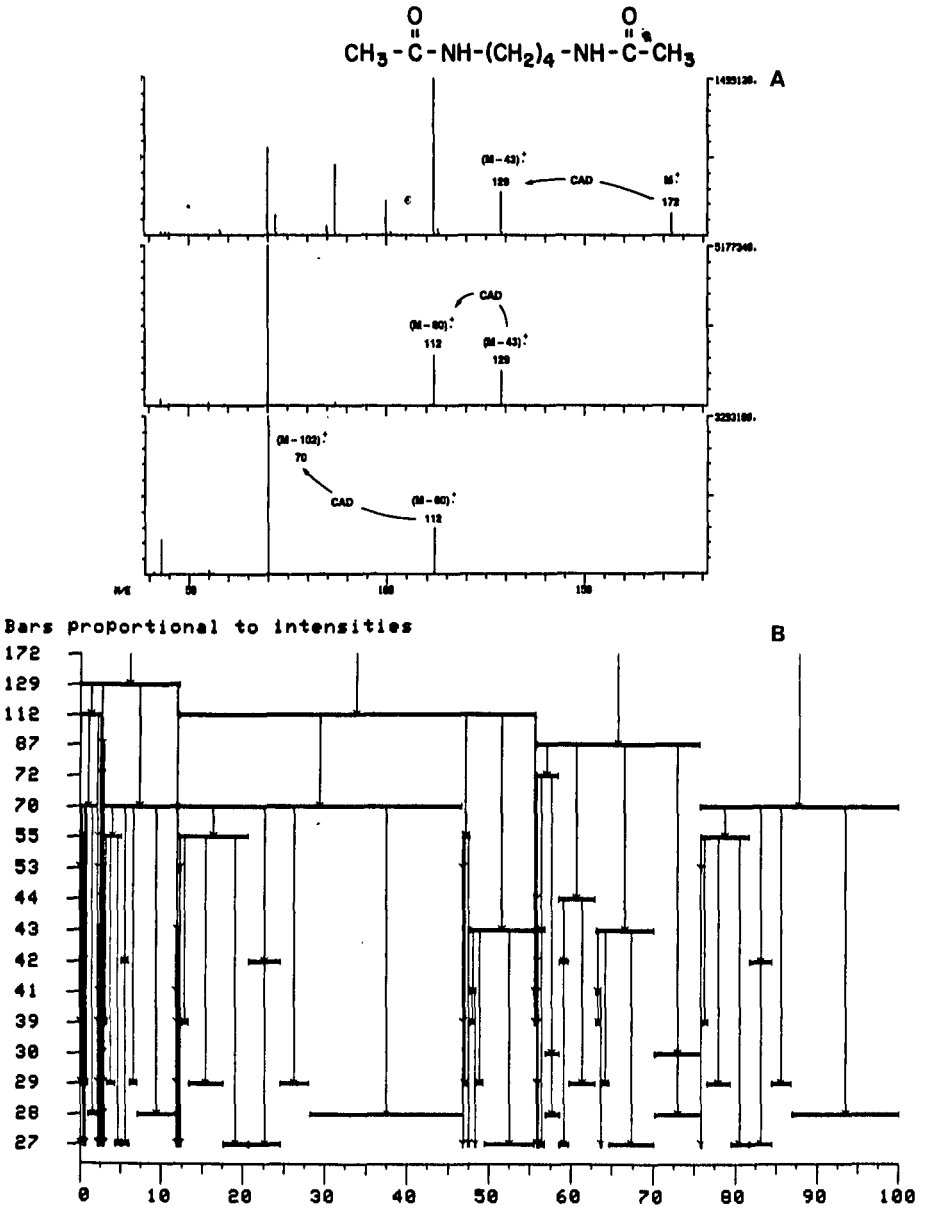

MS/MS spectra of the 4-carbon di-acetamide. A, daughter ion spectra for selected ion source products presented in a traditional histogram display; B, "tree" format representative of the entire three dimensional MS/MS data field.

THE COLLISIONALLY INDUCED DISSOCIATIVE IONISATION OF NEUTRAL SPECIES

P.C.Burgers, Universite Laval, Quebec, Quebec
A.A.Mommers and J.L.Holmes, University of Ottawa, Ottawa,Ontario.
J.K.Terlouw, University of Utrecht, Utrecht, The Netherlands.

When ions fragment in the second field-free region of a ZAB 2F mass spectrometer the resulting ion beamwill consist of unreacted ions (typically ca. 99%), daughter ions (0.5%), and daughter neutrals (0.5%),each having,generally,different kinetic energies.
All those species will enter the collision cell,where they are energised by collision with an inert gas (He,Ar).
By applying a large enough potential to the gas cell only neutral species are permitted to enter the cell.
Thus a beam of fast neutrals may be generated.
These neutrals are collisionally ionised and the resulting ions may undergo fragmentation. The thus formed ions are accelerated by the gas-cell potential upon leaving the colllision cell,and can be energy(mass) analysed in the usual way.
Using this technique (which can be used on any reversed geometry instrument having a collision cell),it can be shown that ionised pyridine loses CNH and not HCN, and that ionised methylacatate loses $CH_2OH^{\cdot}$rather than $CH_3O^{\cdot}$.
The latter observation shows that the mechanism for the loss of "CH_3O" (CH_2OH) from ionised methylacetate,despite thorough research,has not yet been elucidated.
The above technique,whereby the ions are retarded by means of a cell potential suffers from the following disadvantages: a) neutral species originating from negative ions cannot be studied, and b) resolution is rather poor .
To overcome these disadvantages a deflector electrode,situated in front of the collision cell has been installed in the Ottawa ZAB 2F.
Using this electrode to deflect the ion beam away from the cell,it was observed that several polyatomic negative ions(e.g.nitrobenzene$^-$) undergo a common reaction in the microsecond timeframe,being the loss of an electron,resulting in a beam of fast (8Kv) molecules.
Monatomic species do not undergo unimolecular elctron loss,but their neutralisation can be achieved by collision before the electrode.
Thus the two-step charge reversal can be studied,M^- -- M^0 -- M^+, (deflector on) and compared with the one-step charge reversal.(deflector off,now one measures the sum of both processes).
Under conditions of good energy resolution(2 volts at base,8Kv ions) charge reversal in conjunction with ionisation of the collision gas can be observed.
The use of the electrode also permits the study of neutralisation of positive ions: many ions may be neutralised before the electrode,not by charge exchange with the collision gas,but by electron capture(either by free elctrons,or by elctrons carried by a medium other than the collision gas).
Thus H_2O^+; OH^+, and other ions, can be neutralised.
Species such as Ar^+ can be neutralised by resonance charge-exchange,using Ar as collision gas; the resulting energy loss spectrum shows several signals, displaced by multitudes of the ionisation energy of Ar.
These signals correspond to repetitive neutralisation-reionisation sequences taking place before the cell.
We believe that this deflector electrode technique is valuable for elucidating reaction mechanisms,and provides a relatively inexpensive way to study neutral-neutral collisions.

References:

P.C.Burgers,J.L.Holmes,A.A.Mommers andJ.K.Terlouw Chem Phys.Lett. 102,1,1983

P.C.Burgers,J.L.Holmes,A.A.Mommers,J.E.Szulejko,and J.K.Terlouw, Org.Mass Spectrom. 1984, in press

A.A.Mommers and J.L.Holmes, ibid, in press

NEUTRALIZATION-REIONIZATION MASS SPECTROMETRY: P. O. Danis, C. Wesdemiotis, R. Feng, J. Tso, and F. W. McLafferty; Chemistry Department, Cornell University, Ithaca, New York 14853

Neutralization-Reionization Mass Spectrometry (NRMS) is a new technique for the preparation and study of unstable and reactive neutral species, and for the mass spectral formation of fragment ions from sample molecules and from ions through non-ionic dissociation mechanisms.[1] Ions formed and accelerated in a normal mass spectrometer are either neutralized by charge exchange or dissociated to form neutral products. In a tandem mass spectrometer these neutrals are formed from mass-analyzed precursor ions. These fast neutrals and their dissociation products are then ionized by collision with a neutral gas to give a mass spectrum characteristic of their neutral precursors.

A new metal vapor furnace facilitates the study of neutralization using metals with ionization energies from 4 to 11 eV. An electrostatic deflector and in-line detector added just after the reionization region make possible the direct measurement of both neutralization and reionization cross-sec-

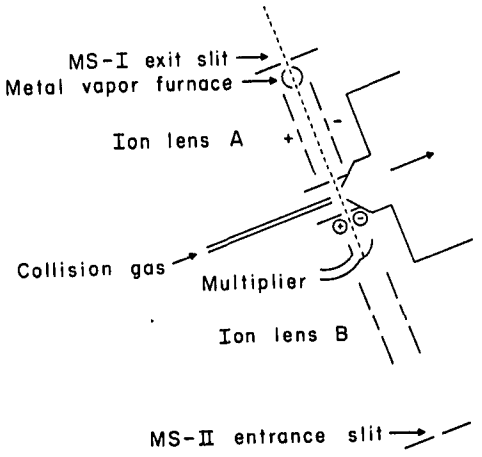

tions. Isomeric ions with different electron affinities (EA, the EI of the corresponding neutral) show different neutralization cross-sections (σ_n). Thus, for ionized methyl chloride, $CH_3Cl^{+\cdot}$ (EA = 11.2 eV), versus the distonic radical ion $H_2{\cdot}CCl^{+}H$ (EA = 5.9 eV),[2] the cross-section ratio $\sigma_n(CH_3Cl^{+\cdot})/\sigma_n(H_2{\cdot}CCl^{+}H)$ is 2.0; it changes to 0.46 when sodium (IE = 5.4 eV) is used for neutralization, consistent with easier neutralization of $H_2{\cdot}CCl^{+}H$ with sodium because of the similar ionization energies of Na and H_2CClH. Similarly, the neutralization cross-section of n-butylamine molecular ions 25 μs after ionization is 5 times greater for Na than it is for Hg, indicating that the molecular ions must have isomerized to the distonic radical ions $CH_3{\cdot}CHCH_2CH_2N^{+}H_3$ before neutralization. The electron affinity of the latter should be similar to $EA(CH_3N^{+}H_3)$ = 4.5 eV,[3] and, thus, closer to the ionization energy of Na.

The dissociation of hypervalent species formed by neutralization of protonated molecular ions can provide useful information about the neutralized ion structure. So, the NRMS spectra of protonated isomeric $C_4H_9NH_2$ molecules (MH^+, m/z 74) show peaks only up to m/z 56. This indicates that the protonated molecular ions 1 have isomerized to the proton bound dimers2 before entering the neutralization chamber (Scheme). The high stability of the proton bound dimer 2 must be related to the similar proton affinities of butenes and ammonia.

Ion	ΔH_f^o, kcal/mol	IE, eV	σ_1/σ_2 Hg	Na	Hg/Na
$CH_3COCH_3^{+\cdot}$	172	9.7	1.5	0.55	2.8
$CH_3C(OH)CH_2^{+\cdot}$	158	8.5			
$CH_3Cl^{+\cdot}$	242	11.2	2.0	0.46	4.4
$H_2\dot{C}-Cl^+H$	252	5.9[2]			
$CH_3NH_2^{+\cdot}$	202	9.0	2.2	0.46	4.8
$CH_3(CH_2)_3NH_2^{+\cdot}$	179	8.7			
$CH_3\dot{C}H(CH_2)_2N^+H_3$		4.3[3]			

Scheme

$$C_4H_9N^+H_3 \longrightarrow C_4H_8\cdots H^+\cdots NH_3 \xrightarrow{+\,e^-} H\cdot + NH_3 + C_4H_8 \xrightarrow{CAD} \text{NR spectrum}$$

(1) Danis, P. O.; Wesdemiotis, C.; McLafferty, F. W. J. Am. Chem. Soc. **1983**, 105, 7454-7456.

(2) Yates, B. F.; Bouma, W. J.; Radom, L. J. Am. Chem. Soc. **1984**, 106, accepted.

(3) Gellene, G. I.; Cleary, D. A.; Porter, R. F. J. Chem. Phys. **1982**, 77, 3471.

FIELD IONIZATION AND FIELD DESORPTION TANDEM MASS SPECTROMETRY

Ronald L. Cerny
Midwest Center for Mass Spectrometry, Department of Chemistry,
University of Nebraska, Lincoln, NE 68588

Although fast atom bombardment (FAB) is often the method of choice for the analysis of nonvolatile, polar, and thermally labile samples, there are many instances where FAB is unable to produce meaningful spectra. FAB and field desorption (FD) have been recognized as complementary techniques in such cases and FD will typically provide molecular ion information. However, the lack of fragment ions for use in structure determination is a disadvantage. FD combined with MS/MS has been shown to provide this kind of information.

Field ionization (FI) is known to produce intense molecular ion species and can be used in conjunction with MS/MS to obtain both molecular weight information and structurally important fragmentation patterns. FI combined with MS/MS may be particularly applicable for analysis of complex hydrocarbon mixtures.

As a test of these ideas a Kratos MS 50 triple analyzer mass spectrometer has been outfitted with a modified FI/FD source. To minimize the instability of the ion current commonly encountered in FD a total ion current-emitter heating controller (model 334, Linden ChroMasSpec) was employed. Carbon emitters were used with needle lengths of approximately 10 microns for FI and 20 to 30 microns for FD. Typical ion currents were $5x10^{-7}$ to $5x10^{-8}$ amps. Heating currents in the FD mode were 10 to 25 milliamps.

Aliphatic hydrocarbons were used to evaluate the performance of the instrumentation for combined FI MS/MS. The CAD spectrum of the FI produced molecular ion of n-tetradecane shown in Figure 1 resembles the EI spectrum of the compound. The CAD spectrum for 8-methyl-pentacosane is quite different. It is displayed in Figure 2. The major peak in the spectrum results from cleavage to provide the most highly substituted carbonium ion. There is evidence that this occurs by both alkyl and alkane losses.

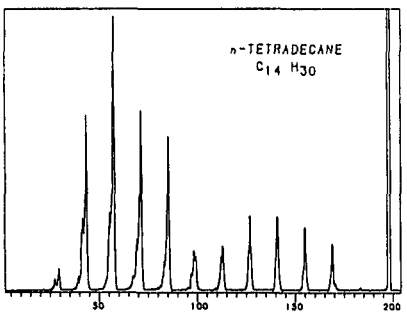

Figure 1

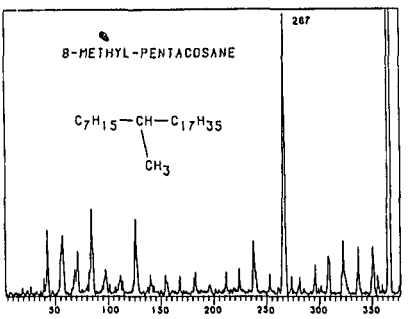

Figure 2

A series of octenes was also examined by FI MS/MS. The CAD spectra of the molecular ions were quite similar making dermination of the double bond position impossible. Even though FI produces molecular ions with little internal energy, isomerization of the double bond presumably occurs upon collisional activation.

The FD MS/MS combination was tested using organometallic cations and disaccharides. Figure 3 is the FD CAD spectrum of m/z 533 from [Ru (2,2'-bipyridine)$_2$ (CO) (benzyl)]$^+$ (PF_6^-). The spectrum displays peaks for successive ligand losses as outlined in Figure 4. By utilization of the emitter heating current controller a main beam intensity of 5 volts was maintained for 20 minutes.

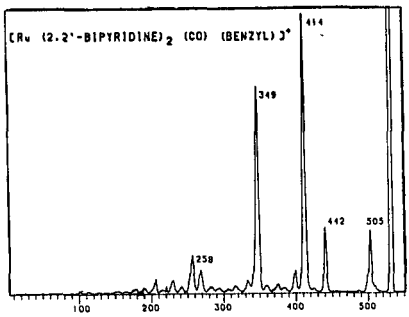

Figure 3

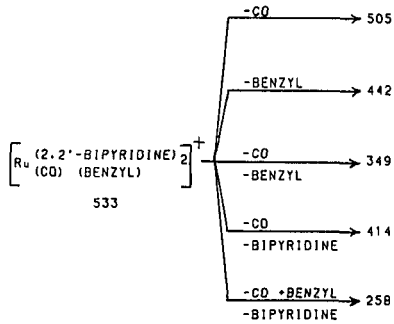

Figure 4

Sucrose was run with the addition of NaCl to desorb $(M+Na)^+$. The CAD spectrum of this ion is shown in Figure 5. Both cleavage of the glycosidic linkage and ring cleavages account for the ions observed. These fragmentations are shown in Figure 6. Again a stable ion current of 3 to 5 volts was maintained allowing several CAD scans to be collected.

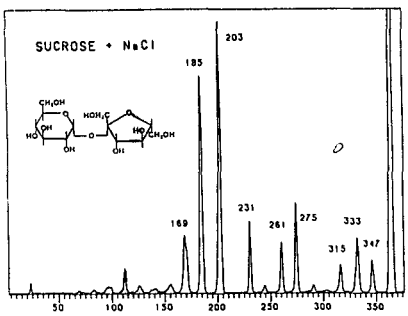

Figure 5

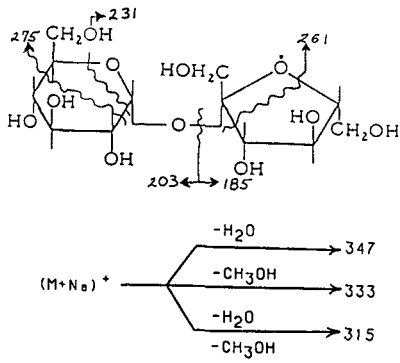

Figure 6

Conclusions

The combination of this instrument with FI and FD to provide CAD spectra has been evaluated and has demonstrated the ability to provide specific structural information for certain compounds. Hydrocarbons fragment to form the most highly substituted carbonium ion. Organometallics are characterized by sequential ligand losses. Disaccharides undergo glycosidic linkage and expected and informative ring cleavages. These raise the possibility for the use of FD MS/MS for sequencing and for determination of structural modifications in oligosaccharides.

TANDEM MASS SPECTROMETRY OF HIGH MOLECULAR WEIGHT COMPOUNDS: I. J. Amster, S. L. Cohen, K. W. Chan, M. F. Ali, J. A. Loo, and F. W. McLafferty; Chemistry Department, Cornell University, Ithaca, New York 14853

Two mass spectrometers connected in tandem (MS/MS) can separate and characterize mixture components as well as supply more detailed structure information on pure compounds. This should be of special value for large, difficultly separated molecules, but these introduce special problems for MS/MS in terms of mass-range, ionization, collisionally activated dissociation (CAD), and detection. The Cornell MS/MS instrument described previously[1] has unique upper mass limits (8 kV ions, m/z 12,500 and 4,900 for MS-I and -II). It is also the first to combine two double-focusing mass spectrometers; the first results from a commercial instrument of this type are described at this meeting by Dr. J. R. Hass and his coworkers.

Fast atom bombardment has broad capabilities for ionization, but glycerol peaks and sample degradation are problems. Results from an alternative method are presented. In this, a dilute solution of the non-volatile sample in a volatile solvent is introduced dropwise into a chemical ionization (CI) source; the drop is flash vaporized by 14 nsec pulses (193 nm) from an excimer laser. With no electron bombardment spectra resembling

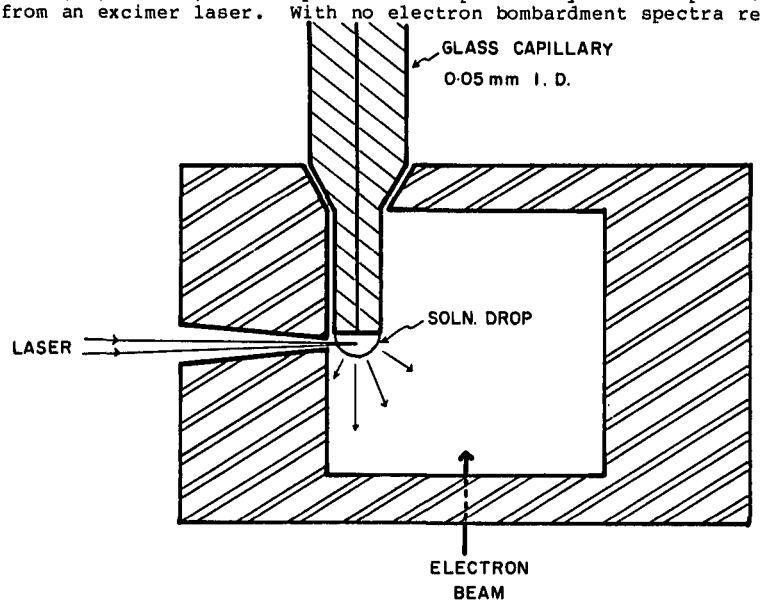

normal CI spectra were obtained, but with sensitivities of only ~10^{-3}. Although a variety of conditions were tried, unfortunately no spectra of intact non-volatile molecules were obtained.

Optimum conditions for CAD change with increasing ion mass; energy requirements for CAD increase while scattering losses decrease. An improved CAD pumping system increases the energy deposited by CAD by increasing the number of collisions an ion undergoes. Increasing ion mass can reduce ion velocity to the point that ion collision with the detector produces insufficient secondary electrons. A "Daly" style detector has been installed to post-accelerate ions by up to 20 keV. This is also important for increasing the detection sensitivity for smaller ionic collision products carrying a small fraction of the precursor ion momentum.

MS/MS also appears promising for compound type characterization of

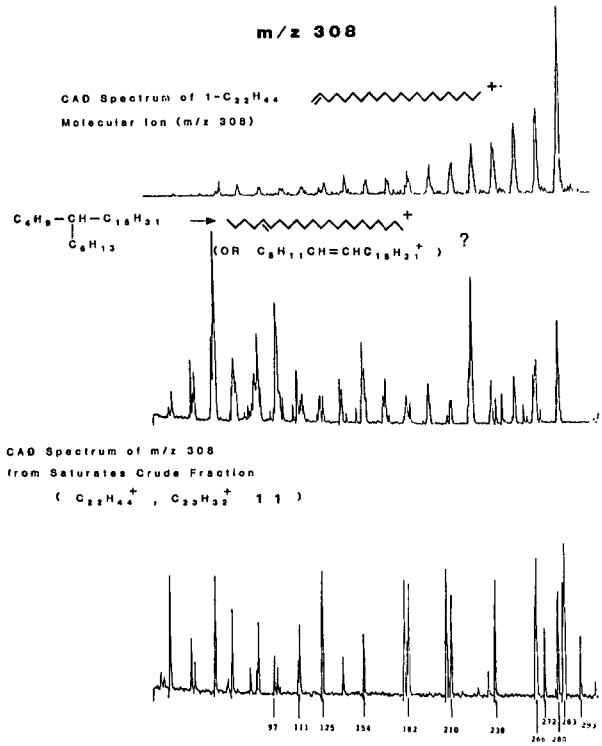

heavier molecules in petroleum oils.[2] An Arabian heavy crude oil was separated by standard extraction and chromatographic techniques. For the saturate fraction, which should contain mainly alkanes, the CAD spectra of 12 of its characteristic $C_nH_{2n}^{+\cdot}$ and $C_nH_{2n+1}^{+}$ ions were obtained and compared to CAD spectra of molecular and fragment ions from reference compounds. An example of CAD spectra of m/z 308 ions is shown above. Anomalous ions in the CAD spectrum from the saturates fraction were explicable when high resolution measurements showed that the m/z peak contained both $C_{22}H_{55}^{+\cdot}$ and $C_{23}H_{32}^{+\cdot}$ ions. The CAD spectra show that even the $C_{22}H_{44}^{+\cdot}$ ions are obviously of complex structure, probably a mixture of structures.

(1) McLafferty, F. W.; Todd, P. J.; McGilvery, D. C.; Baldwin, M. A. J. Am. Chem. Soc. **1980**, 102, 3360-3363.

(2) Kondrat, R. W. in "Tandem Mass Spectrometry;" McLafferty, F. W., Ed.; John Wiley: New York, 1983; Ch. 26.

A THEORETICAL MODEL FOR MASS SELECTIVE INSTABILITY AND HIGH PRESSURE OPERATION OF THE ION TRAP

P.E. Kelley[1], G.C. Stafford,Jr.[1], W.J. Fies,Jr.[1], J.E.P. Syka[1], R.T. McIver,Jr.[2], R.L. Hunter[2], J.F.J. Todd[3], J.J. Bexon[3], (1) Finnigan MAT Corp., 355 River Oaks Parkway, San Jose, CA 95134, (2) University of California, Department of Chemistry, Irvine, CA 92717, (3) Chemical Laboratory, University of Kent, Caterbury, Kent, CT2 7NX UK

INTRODUCTION

From the time of its invention by Paul and Steinwedel, the three dimensional quadrupole ion trap has been primarily used for mass analyzing ions. Prior to the development of the technique described herein, mass analysis of ions with quadrupole ion traps was accomplished by using either one of two techniques-resonance detection or selective mass storage.

The resonance detection technique was the method claimed for performing mass analysis, with the ion trap in Paul's and Steinwedel's original patent, (1) , covering all quadrupole field devices. Paul's and Steinwedel's technique involves appling a small supplementary A.C. voltage between end cap electrodes, in addition to the trapping D.C. and R.F. voltages, U and V $\cos\omega t$, applied between the end cap electrodes and the ring electrode. This resonates any trapped ions that have a mass to charge ratio such that their fundamental frequency of motion in the axial direction, ω_z, is the same as the perturbing field frequency, ω_{ac}. The resonant frequency of the excited ions, along with quadrupole field parameters U, V, r_o and ω , define the mass to charge ratio of the detected ions. These devices were operated with the RF trapping voltage and the supplementary AC voltage having fixed frequencies. The magnitudes of the trapping RF and DC voltages were manipulated so that ions of successive specific masses, would be brought into resonance.

The selective mass storage technique for mass analysis of ions using the ion trap was invented by Dawson and Whetten (2). This technique involves trapping ions, of only one specific mass at a time, and then ejecting the ions from the trap onto the detector. Operation of a quadrupole ion trap in this way, requires that the applied DC and RF trapping voltages are chosen, such that the scan line mapped onto the device's stability diagram, passes through the stability region very close to one of the region's apexes (Figure 1). The range of m/z's trappable in the device is made so narrow, that only ions of the particular m/z of interest are trappable. Ejection and detection of the ions stored in the trap is usually accomplished by applying a supplementary, differential, voltage pulse between the end caps. The trapped ions are driven through perforations in one end cap electrode, onto an electron multiplier. To obtain complete mass intensity data, over a range of specific masses, an experiment must be done for every possible m/z in that range.

A new mode of ion trap operation, mass selective instability and high pressure, has been developed in our laboratory. (3,4) In this new mode, the ion trap is operated with only RF voltages and a background gas pressure of approximately 1×10^{-3} torr of helium or other suitable low molecular weight gas. Since no DC voltages are used, the device is operated along the q-axis only of the stability diagram. Mass selective instability operation consists of ionizing the sample with an electron gun and storing the resultant sample ions at relatively low q's (0.05-0.5). (Fig. 2) The electron gun is then gated off and the RF voltage is scanned. As the sample ions reach the point of theoretical instability, q = 0.91, they exit the device in the axial direction and are detected by an electron multiplier. This results in a mass spectrum.

In addition to mass selective instability, the ion trap is operated at a background pressure of 1×10^{-3} torr of helium or other suitable low molecular weight gas. Sample ions, within the ion trap, collide with the background gas. These collisions remove energy from the sample ions and the sample ions migrate toward the center of the ion trap. (Figs. 3&4) If a low molecular weight gas, such as helium, is used, scattering is minimized. The result of incorporating the use of background gas with mass selective instability operation is improved mass resolution and sensitivity, particularly at high mass.

Stability Diagram for the Ion Trap

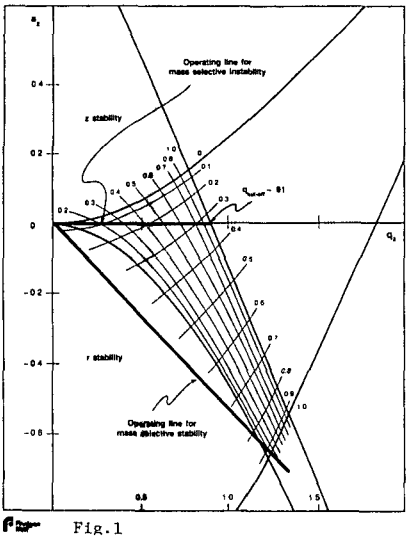

Fig.1

Fig. 2

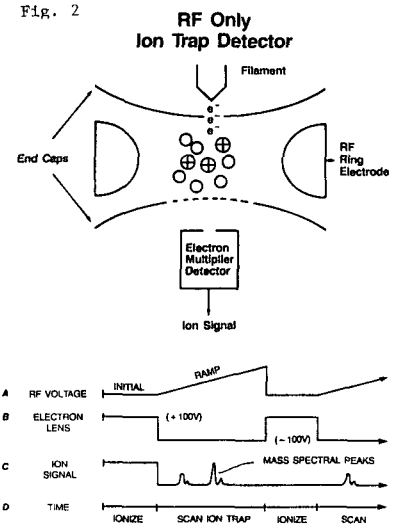

Equation of Motion in the Axial (z) Direction for an Ion in a RF Only Quadrupole Ion Trap.

1) Newtons 3rd Law $F = ma$ Applied in the z Direction Gives

2) $$q \cdot V_{rf} \cos \omega t \left(\frac{2z}{r_0^2}\right) - m\,\xi \frac{dz}{dt} = m \frac{d^2z}{dt^2}$$

Force on Ion Due to Quadrupole Field — Damping Force on Ion Due to Presence of Helium Collision Gas — Acceleration Term

3) $$\xi = 2 \cdot r \cdot q\, n \left(\frac{\alpha (m + m_n)}{m m_n}\right)^{1/2}$$ (ref. 5)

n = Number Density of Damping Gas
α = Polarizability of Damping Gas
V_{rf} = Peak RF Voltage Applied to Ring Electrode
q = Charge on Ion
ω = RF Field Frequency
z = Displacement in z Direction
t = Time
ξ = Reduced Collision Frequency
m = Mass of Ion
m_n = Mass of Damping Gas
r_0 = Characteristic Dimension of Quadrupole Trap Field

Fig. 3

Stabilizing Ion Momentum in the Ion Trap with Inert Gas

Fig. 4

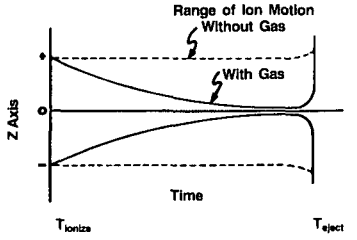

References

1) W. Paul and H. Stienwedel, U.S. Patent, 2,939,952 (1960)
2) P.H. Dawson and N.R. Whetten, U.S. Patent, 2,939,952 (1970)
3) G.C. Stafford, P.E. Kelley, W.R. Reynolds and J.E.P. Syka, 31st Annual Conf. on Mass Spectrom and Allied Topics, Boston, MA (1983) p. 48
4) G.C. Stafford Jr., P.E. Kelley, J.E.P. Syka, W.E. Reynolds and J.F.J. Todd. British Mass Spectrometry Society, 13th meeting, p. 18 (1983)
5) Su, T.; Bowers, M.T. In "Gas Phase Ion Chemistry"; Bowers, M.T., Ed.; Academic Press: New York, 1979; Vol. 1, p. 87.

CONSTRUCTION OF AN INEXPENSIVE POLE BIAS SCANNER FOR QUADRUPOLE MASS SPECTROMETERS OF EARLY DESIGN.

F. Aladar Bencsath, Yiu T. Ng, and Frank H. Field; The Rockefeller University, New York, N.Y. 10021

INTRODUCTION

One of the major setbacks of older quadrupole mass spectrometers is their strong discrimination against high masses. This can be corrected to some extent by increasing the pole bias voltage when the machine is operated in the high mass region. Indeed, newer models are equipped with such automatic adjusting circuits.

OBJECTIVE

Acting upon a suggestion of Marvin Vestal, University of Houston, we constructed a simple device which increases the Pole Bias (=PB) voltage in proportion to the mass scan. It works for both positive and negative ions. We retrofitted our Scientific Research Instruments "BIOSPECT" mass spectrometer a year ago with this scanning device replacing the original "Static" pole bias voltage supply (see figure 1)

Fig. 1.

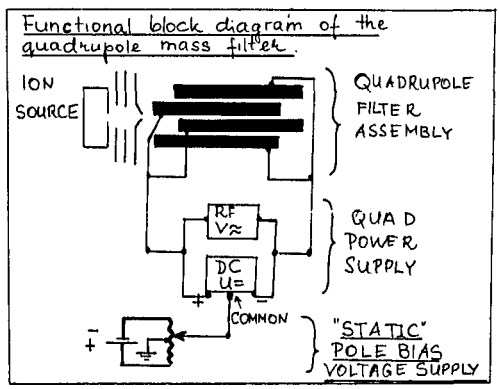

CONSTRUCTION DETAILS

The pole bias scanner requires a dedicated floating +/- 15 V power supply (ACDC Electronics Model 1201), 3 operation amplifiers (OP AMP 741), several resistors, potentiometers and a 4 pole switch for a cost of about $100.

CONCLUSION

The PB-scanner provides good transmission for ions in a wide mass range by reducing the high mass discrimination. It can be fitted to any quadrupole MS that does not have this convenient sensitivity enhancing circuit (see figure 2.) It is easy to tune and requires no maintenance.

PRINCIPLE OF FUNCTION

The scanning pole bias voltage supply (see figure 2. on next page) senses the mass proportional voltage signal at the "RECORDER" connection; amplifies and renders it the required polarity. An adequate portion of it is used as a reference voltage for the quadrupole mass filter. This reference voltage which is the pole bias voltage changes proportionally with the mass, automatically adjusting thus the transmission for any ion.

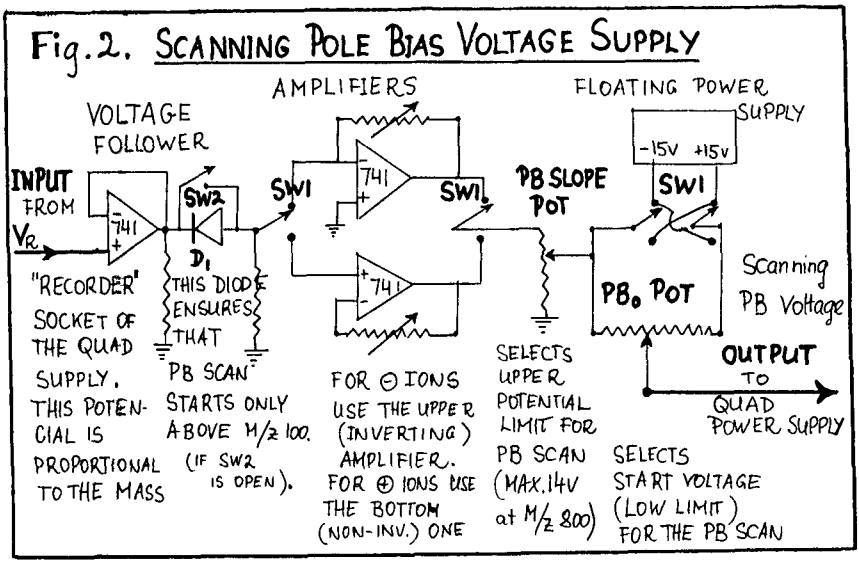

Fig.3.

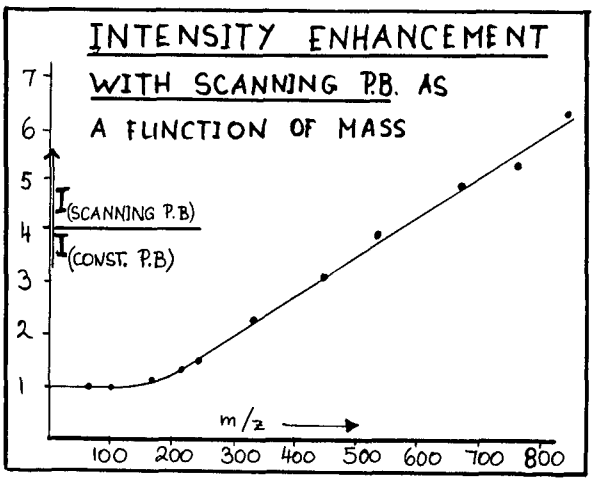

Note: The intensity enhancement values were obtained from a comparison of OH^-/NCI spectra of perfluoro kerosene taken with scanning and with constant pole bias voltage.

QUADRUPOLES OPERATING IN THE SECOND STABILITY REGION: P.H. Dawson and Yu Bingqi, Division of Physics, National Research Council of Canada, Ottawa K1A 0R6, Canada

The quadrupole mass filter can be operated in a stability region near a = 0, q = 7.547 by using higher rf voltages or lower rf frequencies (Region II of fig. 1). Both a theoretical, ion optical examination of operation in this region and an experimental comparison of performance with the normal mode of operation was made. Ion acceptance with and without fringing fields was calculated. Fig. 2 shows effective acceptances in one transverse direction for the operating point a = 0, q = 7.547 with a 0.5 cycle fringing field. The acceptances are for field phases encompassing 25, 50 and 100% of the rf cycle. Fig. 3 gives the variation in ion acceptance in two transverse directions as a function of fringing field length and fig. 4 shows some experimental observations in good agreement. Good resolution is achievable with ions that spend only a few rf cycles in the full field. Fig. 5 demonstrates the separation of a doublet at 131 amu obtained with ions of 300 volts energy which spend only 11 rf cycles in the field. Transmission-resolution measurements for krypton ions at various axial ion energies are shown in fig. 6. Figures 7 and 8 compare the ultimate attainable resolution as a function of the number of cycles spent within the field for normal operation with xenon ions and for second region operation at a frequency of 1.21 MHz.

A length improvement of about 14 times was found (compared to a predicted value of 50) and ultimate resolution was about fifty percent higher. However ion acceptance at moderate resolutions is an order of magnitude lower. Peak shapes are excellent and there may be special applications where operation in this region is useful.

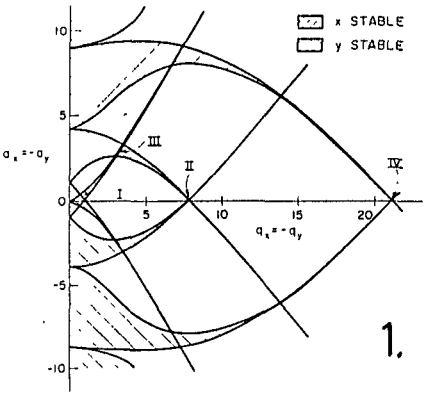

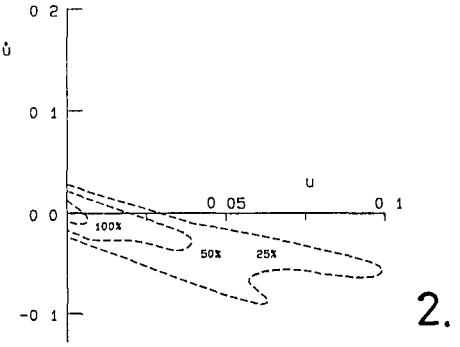

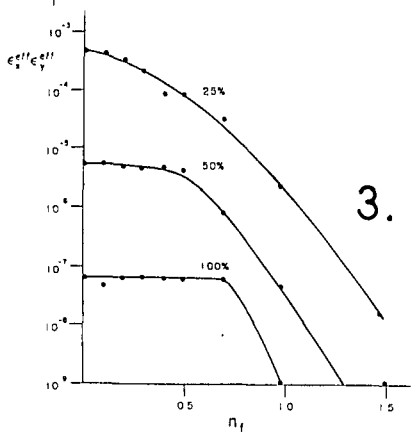

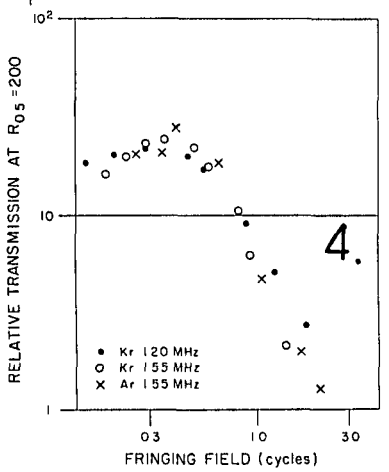

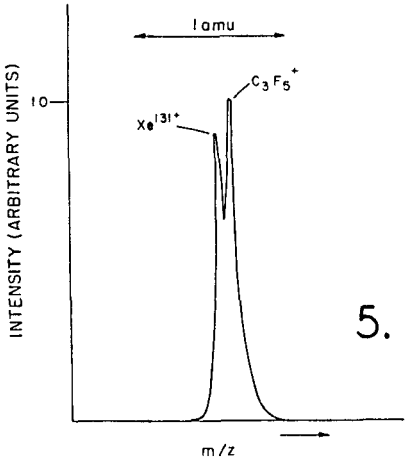
1 amu
INTENSITY (ARBITRARY UNITS)
10
Xe^{131+}
$C_3F_5^+$
m/z
5.

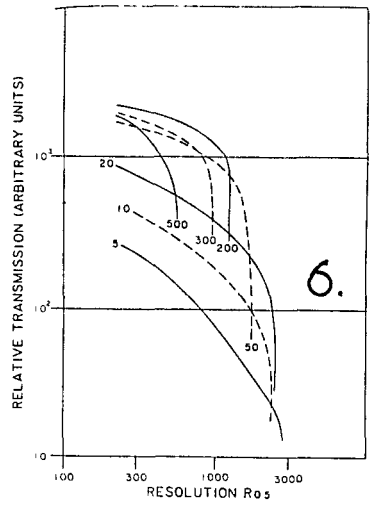
RELATIVE TRANSMISSION (ARBITRARY UNITS)
10^3
10^2
10
20
10
5
500
300
200
50
1
100
300
1000
3000
RESOLUTION R_{05}
6.

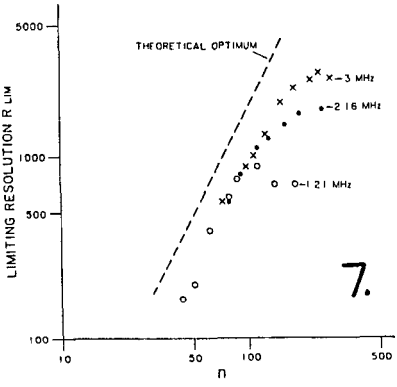
LIMITING RESOLUTION R LIM
5000
1000
500
100
THEORETICAL OPTIMUM
X–3 MHz
•–2 16 MHz
O–1 21 MHz
10
50
100
500
n
7.

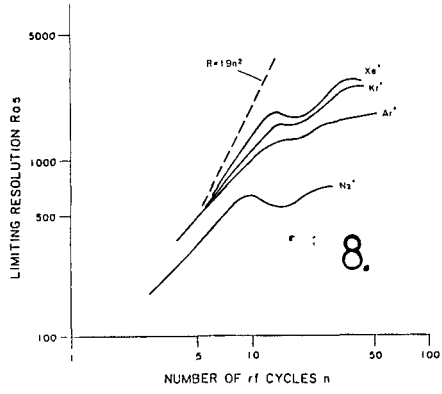
LIMITING RESOLUTION R_{05}
5000
1000
500
100
$R=19n^2$
Xe^+
Kr^+
Ar^+
N_2^+
1
5
10
50
100
NUMBER OF rf CYCLES n
8.

PARALLEL/TANDEM MASS SPECTROMETER

C. Chang and T. O. Tiernan

Brehm Laboratory and Department of Chemistry
Wright State University, Dayton, Ohio 45435

A parallel mass spectrometer (PMS) in the context used here is a mass spectrometer equipped with two or more independent sets of ion extraction plates, mass resolving devices and ion detectors connected in parallel. It allows either two identical or two different ion beams (PIEI, PICI, NICI) characteristic of the sample to be extracted and analyzed simultaneously. A unique feature of PMS is a "real-time TIC (or SIM) - synchronized mass spectrum" mode of operation for GC-PMS sample analysis. It offers numerous advantages over the conventional GC-MS system as discussed in the companion paper (TOA8).

In this presentation, a preliminary report is given on the construction of a novel combined parallel/tandem quadrupole mass spectrometer[1]. The PMS and the tandem mass spectrometer (TMS) are both powerful and complementary tools for chemical analysis. The combination of PMS and TMS into one system allows many instrument components such as quadrupole mass filters, electronic controls, detectors, pumping systems, and computers to be shared between the two mass spectrometers. Considerable cost savings can therefore, be achieved.

Shown in Fig. 1 is a schematic diagram of the present combined parallel/tandem mass spectrometer system. As seen in this figure, both the PMS and TMS assemblies are mounted on a single end flange which is removable from the mass spectrometer vacuum housing. The switching between PMS and TMS is achieved by simply turning a handle (located outside the vacuum housing) which in turn repositions two movable quadrupole mass filters along with an electron multiplier. In the PMS configuration, a PMS ion source assembly (which is removable separately for service) is located between the two quadrupole mass filters. The sample ions are extracted from each end of the ion source, forming two beams which move in opposite directions, and are then mass resolved and detected simultaneously and separately. In the TMS configuration, a RF-only quadrupole sector is sandwiched by the two quadrupole mass filters. This, along with a TMS ion source assembly located on the end, forms the conventional MS-MS configuration.

TABLE 1. PARALLEL/TANDEM MASS SPECTROMETER: INSTRUMENT COMPONENTS

	PMS (or MS/MS)	TMS (or MS-MS)
Ion Source Assembly:	Custom fabricated ion source block with modified Extranuclear lens system	Conventional CI/EI source
Quadrupole Mass Filters:	Two movable Extranuclear quadrupoles (3/8" dia. rod; 20 cm) with modified inlet and outlet lens system	Two movable quadrupoles (same as PMS) and one RF-only quadrupole sector (stationary)
Detectors:	One movable venetian blind electron multiplier and one stationary channeltron with modified housing	Venetian blind electron multiplier
MS Electronics:	All Extranuclear components	Same as for PMS
Sample Inlet:	All glass GC inlet	GC/probe inlet
GC:	Varian 3700 GC	Same as for PMS
Pumping System:	One 6" diffusion pump and two 4" diffusion pumps	Same as for PMS
Application:	Environmental sample analysis	Environmental sample analysis

Table 1 gives a listing of the major instrument components utilized in the present system. At present, construction of this system is nearing completion and the instrument is expected to be functional in the near future.

REFERENCE: 1. C. Chang, U.S. Patent No. 4,377,745

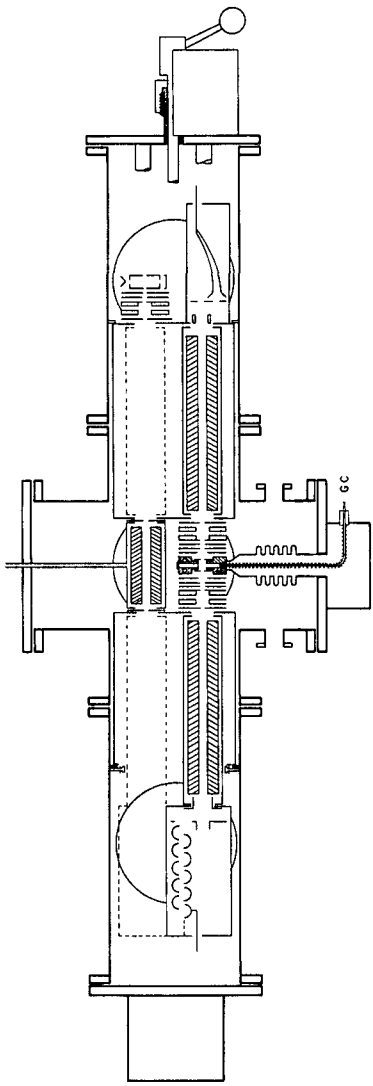

Fig. 1 Schematic diagram of the present parallel/tandem mass spectrometer system

ISOTROPIC COLLISION INDUCED DISSOCIATION STUDIES WITH A NOVEL HYBRID INSTRUMENT:

M. Ho, R.J. Hughes, E. Kazdan, P.J. Matthews, A.B. Young, and R.E. March, Department of Chemistry, Trent University, Peterborough, Ontario, Canada. K9J 7B8

Mass spectra observed conventionally as a result of collision induced dissociation (CID) are highly discriminatory in that fragment ions produced only in glancing dissociative collisions, and retaining an appropriate fraction of parent ion energy are detected and contribute to CID spectra. Recently, studies have been conducted of angle resolved (0.5-1°) spectra [1-3], where detection of high energy processes is favoured; detectable changes in fragmentation patterns compared with those of conventional CID spectra have been observed.

Described here is our attempt to observe collisionally dissociated ions formed over a wide range of scattering angles and decelerated through multiple collisions. A novel hybrid instrument (EBQiQa) has been developed and is composed of an AEI M30 mass spectrometer (EB) to which has been added a QUISTOR (quadrupole ion store, Qi) and a quadrupole mass filter(Qa). While this MS30 is a single beam version of the usual double beam instrument, the detector housing is unchanged and can accommodate two electron multipliers; thus it was possible to position the ion trap, Qi, and the rods of the quadrupole mass filter, Qa, in the housing. In addition, the housing was modified to accommodate a pulsed gas inlet and additional pumping. Part of the endcap electrodes of the QUISTOR were cut away so as to allow the ion beam of the MS30 to pass diagonally through the ion trap. The axis of cylindrical symmetry of the Qa-Qi combination was directed at an angle of 125° to the incoming ion beam, as shown in Fig. 1. The pulsed collision gas valve (General Valve Corporation, Fairfield, N.J.) was triggered creating a pressure pulse as shown in Fig. 2. The amount of collision gas released in each pulse was determined by the trigger pulse duration, backing pressure and trigger frequency. Once the pressure pulse had decayed, an extraction pulse was applied to the bottom endcap of the QUISTOR and stored ions were ejected into the quadrupole mass filter. With a trigger duration of 1ms, a frequency of 100Hz, and a backing pressure to the pulsed valve of some 800mTorr, the optimum signal due to stored ions was obtained.

Ions produced by electron impact were selected sequentially in the MS30 operated at 4keV and directed into the QUISTOR. During the pressure pulse, ions suffer multiple collisions within the QUISTOR provided that the mean free path is << than the diameter ($2r_0$) of the ion trap. The effects of successive collisions on the projectile ion are scattering over a wide range of angles, dissociation, and deceleration resulting in the storage of thermalized projectile ions, isotropic CID fragment ions and ionized target gas.

Fig. 1

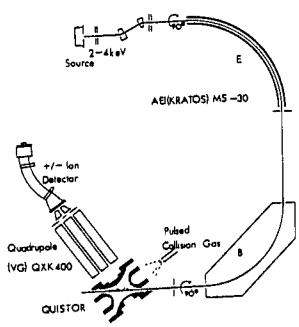

Fig. 2

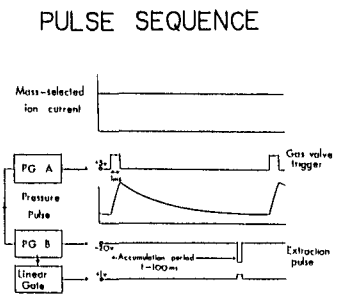

A Monte-Carlo simulation model, used previously to investigate the effect of charge exchange collisions on the motion of ions (single-ion model [4,5] and two-ion model [6]) in a QUISTOR, has been extended to simulate high kinetic energy ion/neutral collisions which may result in ion fragmentation. The study indicated that under normal QUISTOR operating conditions, some 2% of 4keV ions may be stored, i.e. thermalized and intact, after 15 successive collisions and the efficiency of fragment ion trapping, while greater than 4% of fragmenting ions, is dependent on ion mass and collision gas.

There are two modes of operation of the hybrid instrument. In mode I, the magnet of the MS30 was scanned slowly with respect to the extraction frequency applied to the ion trap, and the quadrupole mass filter was operated in the total pressure (RF only) mode. In mode II, the magnet was set to transmit a specific ion continuously, while the mass filter was operated mass selectively. In mode I, decelerated ions, fragment ions, and ionized collision gas were extracted periodically from the QUISTOR, transmitted by the quadrupole in total pressure mode and detected. As there is no mass analysis in this mode, the resulting spectrum reflects directly the electron impact spectrum though with higher sensitivity due to temporal accumulation of ions in the trap. Optimum sensitivity was achieved at an extraction frequency of 10Hz. Mode I may have application in the detection of relatively slow moving heavy ions.

In mode II, successive stages of mass analysis were utilized. A single ion species was selected by the magnet and directed into the QUISTOR where it suffered multiple collisions. The stored ions were ejected periodically and analyzed sequentially with the quadrupole mass filter. When H_2O^+ was selected magnetically and collided with nitrogen collision gas, four peaks were observed: H_2^+ (∿50%), OH^+ (∿20%), H_2O^+ (∿20%) and N_2^+ (∿10%). Thus thermalized projectile ions, CID fragment ions and ionized target molecules were detected. When $C_7H_7^+$(m/z91) was selected magnetically from n-butylbenzene and collided with nitrogen, extensive fragmentation was observed, though with poor resolution by the quadrupole due to high background pressure.

In conclusion, it can be stated that: (i) ions accelerated to 4keV can be decelerated by several successive collisions within the QUISTOR and stored therein; (ii) amplification of the normal e.i. spectrum is achieved when the quadrupole mass filter is operated in the total pressure mode; (iii) extensive fragmentation of mass-selected ions is wrought in isotropic collisions and the fragment ions can be stored for subsequent mass analysis; and (iv) enhanced coupling between the QUISTOR and quadrupole is required in order to increase both sensitivity and mass resolution. This problem is now under investigation.

Acknowledgement:

The authors gratefully acknowledge the assistance of Dr. Harry Ebbs in obtaining the MS-30 mass spectrometer.

References

1. P.H. Hemberger, J.A. Laramée, A.R. Hubik and R.G. Cooks, J. Phys. Chem., 85 (1981) 2335
2. E.E. Kingston, A.G. Brenton, R.K. Boyd and J.H. Beynon, Int. J. Mass Spectrom. Ion Phys., 47 (1983) 117
3. S.A. McLuckey, S. Verma, R.G. Cooks, M.J. Farncombe, R.S. Mason and K.R. Jennings, Int. J. Mass Spectrom. Ion Phys., 48 (1983) 423
4. R.F. Bonner, R.E. March and J. Durup, Int. J. Mass Spectrom. Ion Phys., 22 (1976) 17
5. R.F. Bonner and R.E. March, Int. J. Mass Spectrom. Ion Phys., 25 (1977) 411
6. M.C. Doran, J.E. Fulford, R.J. Hughes, Y. Morita and R.E. March, Int. J. Mass Spectrom. Ion Phys., 33 (1980) 139

A NEW INSTRUMENT FOR HIGH MASS APPLICATIONS.

R.H. Bateman, R.S. Bordoli and B.N. Green. VG Analytical Ltd, Floats Rd, Wythenshawe, Manchester M23 9LE, England , M. Barber, Dept. of Chemistry, UMIST, Sackville St, Manchester M60 1QD, England , A.N.Tyler, K.F.Faull and J.D.Barchas, Dept. of Psychiatry, Stanford University, Stanford, CA.

Introduction

Since the advent of fast atom bombardment (FAB), there has been an increasing need for instrumentation with improved sensitivity at high mass. Previous improvements in magnet technology on commercial instruments have raised the maximum mass to about 3000 daltons at 8 keV ion energy. Above this mass, using magnetic sector radii of no more than 300mm, requires the ion energy to be reduced, with a consequent degradation in performance.

A new instrument, the ZAB-SE, has been developed which, because the magnetic sector radius is more than double the above value, maintains 8 keV ion energy up to 15,000 daltons. This new instrument is an extended mass range development from the ZAB-HF and has been designed primarily to give a substantial increase in sensitivity at high mass, whilst retaining the performance of the ZAB in its more routine areas of application.

Instrument Description

The new instrument has a reversed geometry configuration and is based on the same 381mm radius electrostatic analyser as its predecessor, the ZAB. A 660mm radius homogeneous field magnetic sector, with a maximum field of 2.4 tesla, allows masses up to 12,000 daltons to be selected at the maximum ion energy of 10 keV. The magnet core is fully laminated permitting scan rates down to 0.1s/decade for GC-MS applications.

To ensure that the sensitivity, even at masses approaching 20,000 daltons, is not limited by the conversion efficiency of the detectors, off-axis electron multipliers with conversion dynodes operating at up to 20 keV post acceleration are fitted after both focii.

High Mass Performance

1.Mass Range.

The specified mass range of the instrument is 15,000 daltons at 8 keV (12,000 daltons at 10 keV) ion energy. This is illustrated in Figure 1 which shows the positive ion FAB mass spectrum of cesium iodide above 5500 daltons obtained at an ion energy of 8 keV . The highest mass cesium iodide cluster scanned at this ion energy was $Cs_{60}I_{59}$ at 15,462 daltons. At reduced ion energy, cesium iodide clusters have been observed on this instrument beyond 25,000 daltons.

2.Mass Determination

Although the molecular weight of high mass organic compounds can be measured from the unity mass resolved molecular ion cluster [1], the identification of the monoisotopic peak becomes less certain as the number of peaks in the cluster increases towards high mass. A major reason is that the number of ions collected in each peak decreases as the mass increases, making the isotope pattern statistically imprecise.

An alternative approach is to operate at lower than unity resolution [2], when the number of ions collected dramatically increases and, by using chemical atomic weights to carry out the mass calculations, a chemical molecular weight is obtained.

This approach was used to confirm the molecular weights of Eglin C (MW=8091.0) and a related peptide by scanning the mass range 8260-7900 daltons at 150s/decade with a resolution of 1500. For each sample introduction, about 25 scans, each of 4 seconds duration, were acquired and summed by the 11-250 data system. Calibration data were similarly acquired from a mixture of cesium and rubidium iodides. Typical raw data are shown in Figure 2. Centroids were used to ascertain the peak positions, but chemical atomic weights were used to calculate the masses. Six separate measurements on the peptides gave a mean difference between the measured and calculated masses of -0.28 dalton with a standard deviation of $\pm$0.29 dalton.

Figure 3 illustrates the raw data from a biosynthetic dimer of human insulin (MW = 11597.2) and from the reference mixture. Here two measurements of the molecular weight gave errors of -0.9 and 2.1 daltons.

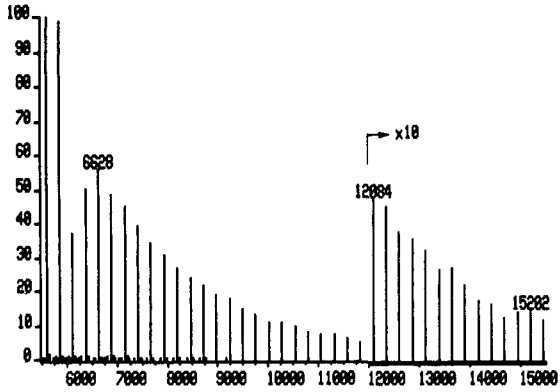

Figure 1. Cesium iodide spectrum above mass 5500 taken at 8 keV ion energy.

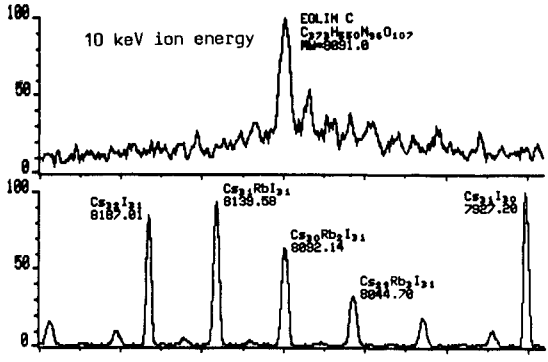

Figure 2. Molecular ion region of Eglin C and cesium-rubidium iodide reference spectrum shown on same time scale.

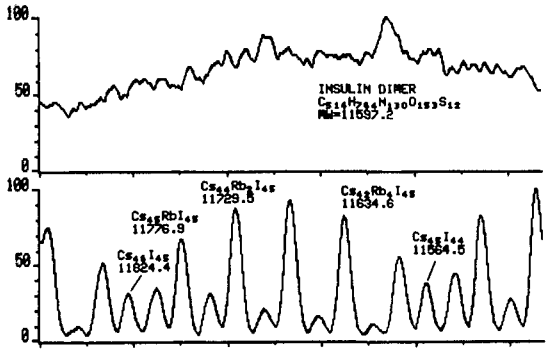

Figure 3. Molecular ion region of insulin dimer and cesium-rubidium iodide reference spectrum shown on same time scale.

Versatile Isochronous Detector for Massive Molecular Ions

John C. Hill, C. J. McNeal and R. D. Macfarlane
Deptartment of Chemistry
Texas A&M University
College Station, Texas 77843

A new detector has been developed with improved efficiency for massive ions baised on the design of Jungclas et al at Marburg University.[1] The new design of the detector utilizes an isochronous secondary electron transport system with microchannel plate (MCP) detection and an ability to change electron conversion surfaces to study electron emission for ions impinging on different surfaces. Isochronous transport of secondary electrons, resulting in no loss of the position/energy relationships of a particle, has been studied by Zebelman et al.[2] At present CsI is used as the electron conversion surface due to its higher electron multiplicity over MCP or metal surfaces, reflecting more favorable electronic surface states in the CsI system.

The detector is shown below. Incomming secondary ions impact onto the CsI surface(A). If the energy of collision is greater than the work function of CsI secondary electrons will be ejected. The secondary electrons are accelerated through 1 KV potential by maintaining the CsI at 1 KV and placing a Ni mesh grid(B), at ground potential, in front of the CsI. The secondary electrons are then isochronously transported towards two tandem MCPs by a uniform magnetic field. Upon reaching the first MCP(C) the secondary electrons enter the microchannels producing an electron cascade. The MCPs are arranged such that the electron cascade from the first MCP is the input to the second MCP(D). A flat stainless steel plate(E) is used to collect the electron output from the second MCP.

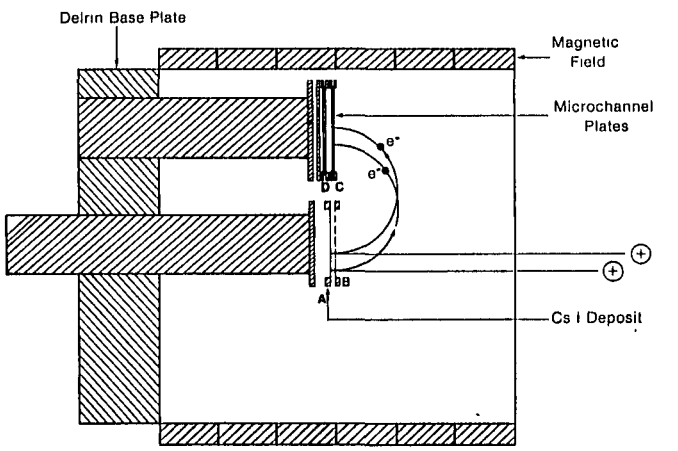

Cross Section of Magnetic Stop Detector Assembly

A plot of integrated intensities as a function of electron voltage for insulin is shown below. This plot compares the integrated intenities obtained from a tandem MCP detector against the data obtained from the CsI detector. The CsI detector showed a slight increase in the integrated intensity over the tandem MCP detector; however, this may be due to attenuation of the target caused by exposure to atmosphere while the detectors were changed. In conclusion no major improvement in the values of the integrated intensity from the detectors has been observed but the CsI detector has a greater potential for further development than the tandem MCP detector.

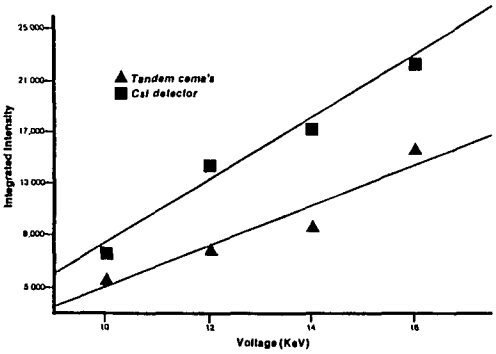

Plot of voltage vs. integrated intensity of 250 Lilly bovine insulin using tandem cemas and CsI detector. M/Z= 5735

References:

1. H. Danigel, H. Jungclas, and L. Schmidt, Inter. J. Mass. Spectrom. Ion Phys. 52, 233 (1983).

2. A. Zebelman, W. Meyer, K. Halbach, A. poskanzer, R. Sextro, G. Gabor and D. Landis, Nucl. Instr. Mteh. 141, 439 (1977).

ION ENERGY EFFECTS IN TIME-RESOLVED ION MOMENTUM SPECTROMETRY (TRIMS)

John T. Stults, Christie G. Enke, Department of Chemistry
John F. Holland, Department of Biochemistry
Michigan State University, East Lansing, MI 48824

Daughter ions formed by metastable or collisionally activated dissociation show larger relative energy distributions than their undissociated parents. This energy spread is due to the release of kinetic energy in the dissociation process (1). In time-resolved ion momentum spectometry (TRIMS) (2), accurate stable and daughter ion mass assignments are made independent of ion energy. However, the energy spread is observed in the momentum-flight time plane as a distribution of ion intensity along a line of constant mass. This energy distribution profile can be analyzed to provide kinetic energy release measurements and to improve the precision of parent mass assignment for daughters.

TRIMS, an MS/MS technique, produces mass analysis by simultaneous momentum and velocity measurements. This is accomplished by pulsing the ion beam and time-resolving the detected signal in a magnetic sector instrument. An ion's mass is determined by the product of the magnetic field ($mv \propto B$) and the flight time ($v \propto 1/T$) at which the ion is observed. All ions of a given mass appear along a line of constant BxT. In addition, daughter ions formed in the field-free region between the source and the magnet essentially maintain the velocity of their parents. The flight time measurement for a daughter thus serves to identify its parent. Ions of different energy but the same mass will still be assigned to the correct mass (BxT) but will appear at different values of B and T. Ions of higher energy will appear at larger magnetic field strengths but shorter arrival times.

The energy of an ion is proportional to the quotient B/T, as given in equation 1.

$$E = B/T(zer1/2) \qquad (1)$$

Measurement of the distribution of field strength/flight time combinations from a particular process can provide the energy distribution for those ions, and if they are daughter ions, helps to identify the parent.

This work was performed on an LKB-9000, magnetic sector mass spectrometer as shown in Figure 1. The ion beam is pulsed with a deflection potential on one of the ion extraction lenses. The flight tube is extended 0.5m past the original detector position to provide a total flight path of 1.5m. The ion optics for magnetic deflection remained unchanged, however, and an increase in the size of the detector compensates for the change in its position. A Galileo FTD-2003 microchannelplate fast timing detector is used. Time-resolved detection is achieved with a gated integrator that measures the signal during a 10ns window at a specified delay time after the ion source trigger pulse. The time delay and magnetic field are under control of a data system that also provides data acquisition, manipulation,display, and storage (3).

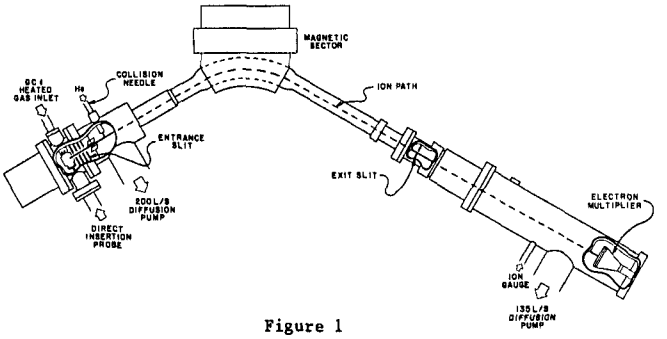

Figure 1

The larger relative kinetic energy spread for daughter ions produces a spread in arrival times that degrades the precision with which the parent is identified. By centroiding the energy peak for a daughter ion, the mean energy and hence mean arrival time can be obtained, increasing the precision for parent mass identification. Figure 2 is a portion of the BT plane for p-chlorotoluene. The points represent the maximum intensity in the time scan for each of a number of magnetic field settings, showing the $(M-Cl)^+$ daughters from metastable dissociation of molecular ions (MW=126, energy=3500eV). There are two sets of points corresponding to the two chlorine isotopes of the parent. The 91^+ daughters of the 126^+ and 128^+ parents fall on the curve of constant BxT for mass 91^+. The energy spread in the daughter ions causes the intensity to be distributed along this curve. By calculating the energy at each point and replotting the data as intensity versus energy, an energy distribution profile is obtained, Figure 3. This is a mass-selected energy distribution for 91^+ ions only. The centroid of each peak gives the mean energy from which the mean arrival time can be calculated and used to improve the precision for parent mass identification.

The energy distribution can also be used to calculate the kinetic energy release for the dissociation process (1). The observed kinetic energy distribution will be a combination of ion thermal energy spread, kinetic energy release, and instrumental parameters such as flight time pulse width and slit width. Present research is centered on understanding and compensating for the instrumental parameters so that the kinetic energy release values will be valid. Though not yet interpretable for kinetic energy release studies, current results indicate that the energy distributions for both stable and daughter ions can be measured, that the daughter ions consistenty show a greater relative magnitude of energy spread, and that they appear as predicted on the appropriate line of constant BxT.

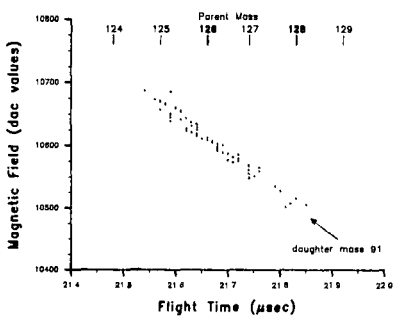

Figure 2

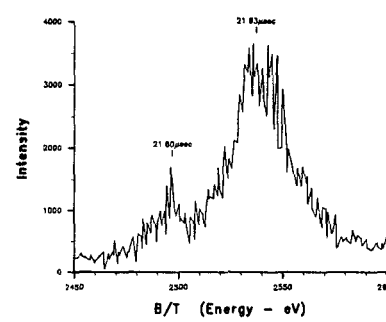

Figure 3

References:

(1) R.G.Cooks, J.H.Beynon, R.M.Caprioli, G.R.Lester, "Metastable Ions". Elsevier:New York, 1973, pp. 57-70.

(2) J.T.Stults, J.F.Holland, C.G.Enke, Anal. Chem., 1983, 55, 1323-1330.

(3) J.T.Stults, B.H.Newcome, C.A.Myerholtz, C.G.Enke, J.F.Holland, presented at the 31st Annual Conference on Mass Spectrometry and Allied Topics, Boston, May 8-13, 1983, bound volume p. 162.

Acknowledgements:

This work was supported by the NIH/MSU Mass Spectrometry Facility though a grant from NIH (RR00480). JTS acknowledges an ACS Division of Analytical Chemistry Graduate Fellowship sponsored by The Procter & Gamble Company.

TANDEM QUADRUPOLE/TIME-OF-FLIGHT INSTRUMENT FOR MS/MS STUDIES*

D. E. Goeringer and G. L. Glish
Analytical Chemistry Division
Oak Ridge National Laboratory, Oak Ridge, TN 37831

We have developed a new type of instrument for MS/MS studies based on the tandem arrangement of quadrupole and time-of-flight mass spectrometers. The simple design provides the potential for MS/MS studies for workers not having access to sophisticated and expensive multiple sector, multiple quadrupole, Fourier transform, or hybrid instruments. The prototype instrument, shown in Fig. 1, consists of a quadrupole mass filter followed by a time-of-flight mass spectrometer. A collision cell is located in the region between the two mass analyzers. Low energy parent ions (< 100 eV) produced by a thermal source are analyzed by the quadrupole and focused by an einzel lens into the collision cell. Daughter ions from collisionally-activated dissociation (CAD), as well as unfragmented parent ions, are accelerated by a four-element lens after exiting the collision cell and then gated into the time-of-flight for mass analysis. Ion detection is performed by a channeltron mounted at the end of the drift region.

Time-of-flight mass analysis is accomplished by using a time-to-amplitude converter in combination with a multichannel analyzer. Figure 2 shows a diagram of the detection and timing scheme used. A free-running pulse generator is used to trigger a delay generator. The output of the delay generator triggers the time-of-flight gating pulse and provides a start pulse for a time-to-pulse height converter (TPHC). The stop input of the TPHC is connected to the channeltron via a fast preamplifier and 100 MHz discriminator. When an ion is detected the TPHC is stopped and the amplitude output to a multichannel analyzer (MCA). The MCA is operated in pulse height analysis mode, so the data are collected as time (mass) versus abundance. In normal operation the pulse generator is run at a rate of 10-30 kHz and the delay generator is operated with no delay. However, the delay generator can be used to delay the start trigger to the TPHC in order to expand certain portions of the spectrum.

The tandem quadrupole time-of-flight instruments has the potential to be a very useful and simple means to perform MS/MS experiments. It has a unique advantage in obtaining daughter ion MS/MS spectra on transient species such as those produced by pulsed laser ionization methods, and it has the potential for fast acquisition of MS/MS spectra which would permit on-line use with chromatographic methods. Figure 3 is an MS/MS spectrum of the tetramethyl ammonium (TMA) cation obtained with the QT in an experiment designed to simulate a pulsed ionization event. The voltage on the sample filament of a thermal source was pulsed from 0 to 32 V for 2.5 μs at a repetition rate of 10 kHz to produce packets of parent ions. Figure 4 is an example of the ability of the QT to rapidly obtain MS/MS spectra on continuous, low-level signals. The spectrum was obtained in one second on a TMA parent ion flux of 3×10^5 ions per second ($\sim 50 \times 10^{-15}$ amps). Conventional mass spectra can also be acquired by scanning the quadrupole without gating the time-of-flight or by operating the quadrupole in rf-only mode and using time-of-flight analysis.

*Research sponsored by the U. S. Department of Energy, Office of Basic Energy Sciences, under Contract DE-AC05-84OR21400 with Martin Marietta Energy Systems, Inc.

By acceptance of this article, the publisher or recipient acknowledges the U S. Government's right to retain a nonexclusive, royalty free license in and to any copyright covering the article.

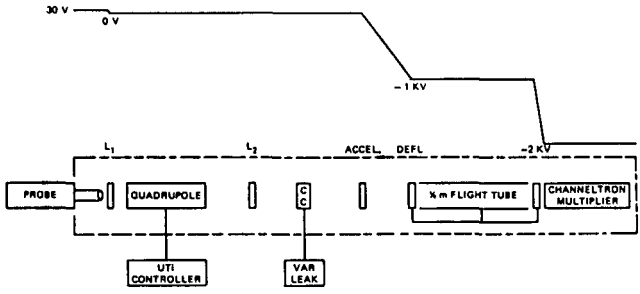

Fig. 1

QT
DATA ACQUISITION SYSTEM

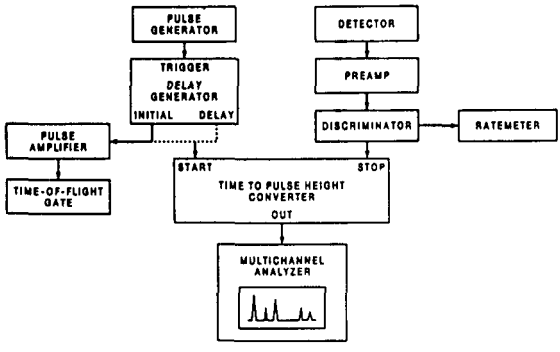

Fig. 2

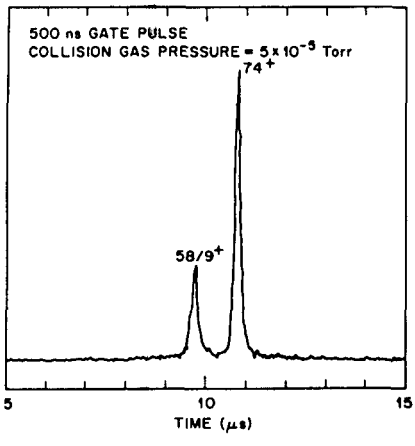

Fig. 3

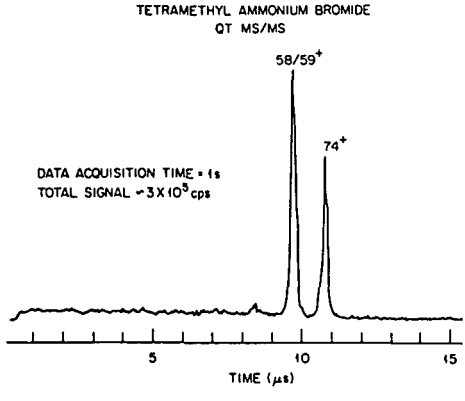

Fig. 4

A NEW TYPE MS/MS WITH A CROSSED ExB FIELD AS THE SECOND MASS ANALYZER

E.Kunihiro, M.Naito, Y.Naito, Y.Kammei and Y.Itagaki
JEOL Ltd., Akishima, Tokyo 196 Japan

It is known that MS/MS has been established as an invaluable method for mixture analysis and for structure elucidation(1). Previously we have also reported the compact MS/MS ion optics and some application results(2). In conventional triple sector tandem mass system such as EBE and BEB, the mass resolution of daughter ion is decreased because of the large translational energy released in the dissociation process(3). In order to improve the resolution, a unique MS/MS system using a crossed ExB field as the second mass analyzer(MSII) was designed. The crossed ExB field(4) consists of the magnetic field and the electric field in the inner part of the magnetic field. Modified crossed field was combined with a JMS-DX300 double focussing mass spectrometer as the second mass analyzer. The ion optics of this MS/MS system is shown in Fig. 1.

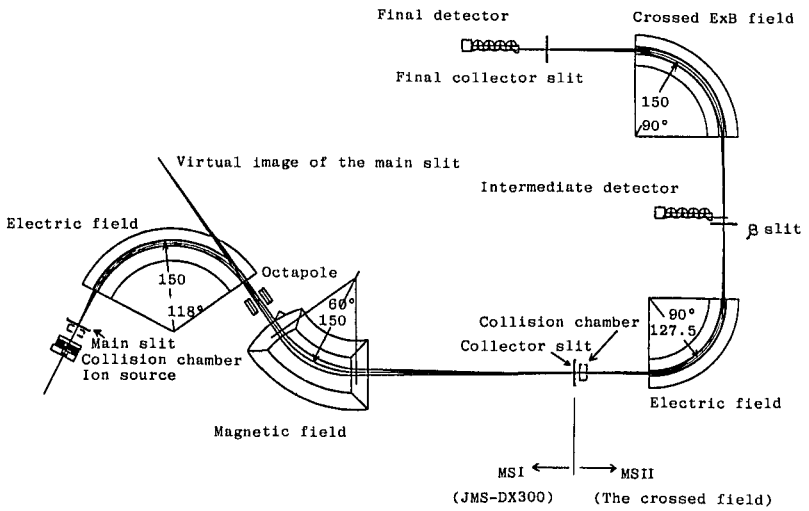

Fig. 1 Ion optical geometry of the MS/MS system with a crossed ExB field.

The unique voltage scanning method of a crossed field was originally developed by H.Matsuda and M.Naito previously(4), and the procedure was to scan the voltage alone, holding the magnetic field strength at constant value. This voltage scanning is applicable to the second mass analyzer by simple alteration of its characteristic curve as follows. The scanning method is based on the equation(1);

$$\frac{Vdx}{Vo} + \left(\frac{Mo}{M}\right)^{\frac{1}{2}} = \frac{Mx}{M} \qquad (1)$$

where M and Mx are the precursor mass and the daughter mass respectively, Vdx is the voltage for the daughter ion and Vo and Mo are constant.

The definitions of Vo and Mo are the same as those in ref.4. This equation shows the simple relation between the daughter mass and the voltage. Because of voltage scanning, this method has rapid scanning, very high reproducibility and simple mass calibration. Furthermore, the unlimited mass range, which is the most important character of the crossed field, can overcome the problem of EBQ system.

In this paper, various characteristics of the second mass analyzer will be shown. The ion transmission was measured and 80% ion transmission in MSII was obtained under the optimum condition. The daughter ion spectrum of n-triacontane using the voltage scanning method is shown in Fig. 2. More than 600 mass resolving power(10% valley) was caluculated from two observed daughter peaks of M/Z392 & M/Z393 in this spectrum. The switching speed in the multiple reaction monitoring(MRM) method was examined using two daughter peaks of M/Z113 & M/Z57 derived from the n-decane molecular peak. As the result, the settling time was in less than 3msec, and therefore rapid MRM method is considered to become practical.

It was proved that the crossed field MS/MS has many advantages over the BEB, EBE and EBQ systems.

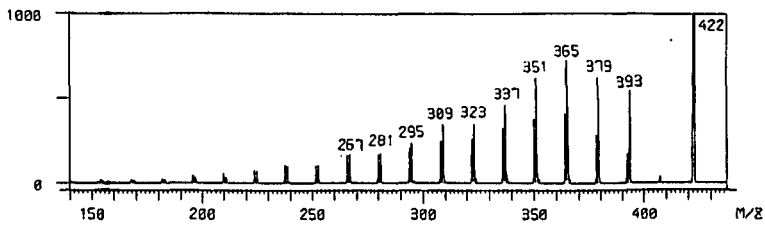

Fig. 2. The daughter ion spectrum of n-triacontane(M.W.422) using the voltage scanning method of the MS/MS system.

Reference;

(1) F.W.McLafferty; Science, 214 280 (1981)

(2) F.Kunihiro, Y.Kammei, M.Naito and Y.Itagaki; Int. J. Mass Spectrom. Ion Phys., 46 151 (1983)

(3) J.H.Beynon, F.M.Harris, B.N.Green and R.H.Bateman; Org. Mass Spectrom., 17 55 (1982)

(4) M.Naito, Y.Naito, M.Takeuchi, H.Matsuda and M.Ishibashi; Adv. Mass Spectrom., 7B 846 (1976)

Tandem Mass Spectrometry with a Hybrid Geometry Instrument

G.C. DiDonato, K.J. Kroha, and K.L. Busch*
Department of Chemistry, Indiana University, Bloomington, IN 47405

A hybrid mass spectrometer of EBQQ geometry has been used for experiments in tandem mass spectrometry. For the prototypical daughter ion MS/MS spectrum, parent ion resolution of up to 25,000 can be achieved, and quadrupole mass analysis provides unit mass resolution up to m/z 1200 for daughter ions. Design criteria for the instrument are discussed in another paper (WOB8); the present discussion centers on capabilities for MS/MS.

Parent ion resolution: Since ion flux drops rapidly with increased resolution, selection of parent ions at high resolution exacts penalties in the amount of time required to obtain an MS/MS spectrum. It would appear that most problems can be solved at resolutions of 10,000 or less. When an isobaric contaminant is due to the solvent as in FAB, it is more feasible to switch solvents that to operate at higher resolution. The present instrument has resolved parent peaks at up to 7,500 resolution in demonstration. A practical example (Figure 1) is the separation of two ions at an integral mass of 279. The protonated molecular ion of sulfamethazine (279.0916) and of dibutylphthalate (279.1596) are separated at $M/\Delta M$ of about 4100 and distinct daughter ion spectra are obtained.

Energy resolved MS/MS: The use of triple quadrupole instruments resulted in the discovery that 10W energy daughter ion MS/MS spectra are dependent on the translational energy of the parent ion. High energy (>2000 eV) MS/MS spectra do not show such a strong dependence. The EBQQ instrument can investigate the energy regime from 10 to approximately 200 eV. This energy is set by varying the potential at which the collision quadrupole is floated relative to the source potential. Daughter ion MS/MS spectra of 2,5-dimethylaniline were investigated and show variations in relative abundance with parent ion translational energy. Cross points are significant in that they represent conditions under which relative abundances of two ions invert. They can be used to calibrate energy resolved MS/MS data against breakdown curves generated by other methods. The abundance curves of 74+ and 75+ from dimethylamiline cross at about 90 eV, with 74+ more abundant at higher parent ion translational energies.

New MS/MS Experiments: MS/MS experiments involve the study of ionic reactions which result in changes in mass, changes in charge, or changes in reactivity. Parent, daughter, and neutral loss spectra involve changes in mass. Redox scans involve changes in charge: examples are charge inversion, stripping, or exchange reactions. Changes in ion reactivity can be best exemplified by survivor ion MS/MS spectra in which a parent ion is modified (either in structure or internal energy) via collision. Although neither its mass nor its charge are changed, the subsequent fragmentation processes are affected. Since the hybrid instrument has both high and low energy collision cells, unique experiments to study these processes can be undertaken (See Figure 2)

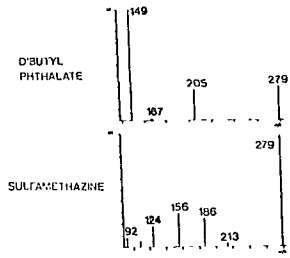

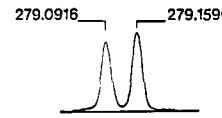

Figure 1: Separation of the parent ions of sulfamethazine (279.0916) and dibutyl phthalate (279.1596) requires about 4100 resolution from EB. The quadrupoles yield daughter ion MS/MS spectra with unit resolution

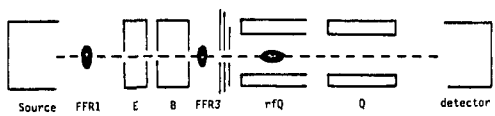

SEQUENCE						PROCESSES
A	M^{2+}			M^{2+}	m_1^{2+}, m_2^{+}	
B	M^{2+}	M^{+}		M^{+}	m_1^{+}, m_2^{+}	exchange
C	M^{2+}			M^{+}	m_1^{+}, m_2^{+}	exchange
D	M^{+}	M^{2+}		M^{2+}	m_1^{2+}, m_2^{+}	stripping
E	M^{+}		M^{2+}	M^{2+}	m_1^{2+}, m_2^{+}	stripping
F	M^{+}	M^{2+}		M^{+}	m_1^{+}, m_2^{+}	stripping exchange
G	M^{2+}	M^{+}	M^{2+}	M^{2+}	m_1^{2+}, m_2^{+}	exchange stripping
H	M^{2+}	M^{+}	M^{2+}	M^{+}	m_1^{+}, m_2^{+}	exchange stripping exchange
I	M^{+}		M^{2+}	M^{+}	m_1^{+}, m_2^{+}	stripping exchange
J	M^{-}	M^{+}		M^{+}	m_1^{+}, m_2^{+}	inversion
K	M^{-}		M^{+}	M^{+}	m_1^{+}, m_2^{+}	inversion
L	M^{-}	M^{+}	M^{2+}	M^{2+}	m_1^{2+}, m_2^{+}	inversion stripping
M	M^{-}	M^{+}	M^{2+}	M^{+}	m_1^{+}, m_2^{+}	inversion stripping exchange
N	M^{-}	M^{+}	$M^{+\cdot}$	$M^{+\cdot}$	m_1^{+}, m_2^{+}	inversion activation
O	M^{+}	$M^{+\cdot}$	$M^{+\cdot}$	$M^{+\cdot}$	m_1^{+}, m_2^{+}	activation
P	M^{+}	M^{+}	$M^{+\cdot}$	$M^{+\cdot}$	m_1^{+}, m_2^{+}	activation

Figure 2: Separable high and low energy collision regions on the hybrid EBQQ mass spectrometer make it possible to study a variety of reactions which involve changes in ionic mass, charge, or reactivity.

APPLICATIONS OF A HYBRID MS/MS INSTRUMENT UTILIZING PARENT IONS SELECTED AT HIGH RESOLUTION

David F. Fraley, Procter & Gamble Co., 5299 Spring Grove Ave., Cincinnati, Ohio 45217

Any MS/MS instrument operates very well as a normal mass spectrometer or as a GC/LC detector. It is the added dimension of flexibility that sets the high resolution hybrid instrument in a class by itself. To demonstrate this flexibility and to show the application of the hybrid MS/MS as a workhorse mass spectrometer, the following performance criteria are considered:

1. Structural Specificity -
   The unprecedented ability to determine ion structures is due to the combination of the following capabilities in a single instrument:
   - MS/MS - determines precursor (parent) and fragment (daughter) ions
   - High resolution - elemental compositions
   - GC-MS or LC-MS - cleans up complex samples and provides retention time data.
   - Ionization modes and +/- ions - enhance the production of selected ions.
2. Advantages of Hybrids over Triple Quadrupoles -
   - Greater mass range with MS-I (to m/z 2600 at 6 kV).
   - Higher resolution with MS-I (25,000) for elemental compositions or high parent resolution
   - Higher collision energies for MS/MS using either the quadrupole or linked scans Charge inversion of negative ions to give + charged fragments.
   - MS/MS/MS utilizing 2 collision cells.
3. Limitations of Hybrids vs. Triple Quadrupoles -
   - Lack of ease of full data system control of the instrument.
   - Cost.
4. Mass Range and Resolution -
   - MS-I: m/z 2600 at 6kV — $\leq$ 25,000 m/Δm
   - MS-II: m/z 1500 — unit mass resolution
5. Scan Techniques -
   Data from MS/MS can be acquired in many forms depending on the information required and instrument configurations available:

• Daughter scans • Parent scans • Constant neutral loss (or gain) • Multiple reaction monitoring	• low and high energy collisions in the CID quadrupole, • unit daughter ion resolution, • no artifacts
• Linked scans-1st Field Free Region • MIKES-2nd Field Free Region only on a BEQQ	• high energy collisions in MS-I, • poor daughter ion resolution, • artifacts may be present

COMPARISON OF MS/MS SPECTRA: A HYBRID VS. TRIPLE QUADRUPOLES

For low energy MS/MS studies (0-30 eV collision energy) a hybrid MS/MS instrument is expected to produce spectra equivalent to a triple quadrupole MS/MS instrument. Extensive reproducibility data for the daughter ions of n-butylbenzene and protonated dimethylphthalate on triple quadrupole instruments is available from P. H. Dawson and W. F. Sun in the Int. J. Mass Spectrom. Ion Physics 55 155-170 (1983/1984). The basis of their international round robin test was to improve the definition of a standardized set of operating conditions (e.g. collision energy, collision pressure) for the generation and interchange of library MS/MS spectra using triple quadrupoles.

The VG 7070EQ-HF produced spectra that have very similar ion ratios for m/z 78, 92, and 105 vs. m/z 91. The intensity ratio of 65/91 is low. Since Dawson and Sun have shown tht m/z 65 is a product of a sequence of several collisions, its low value may be due to an insufficient collision pressure. A similar round robin study will be conducted with various commercial hybrid instruments.

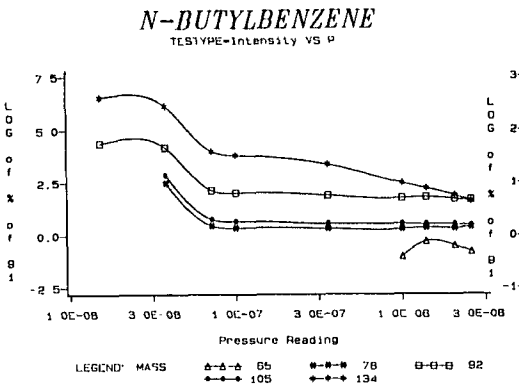

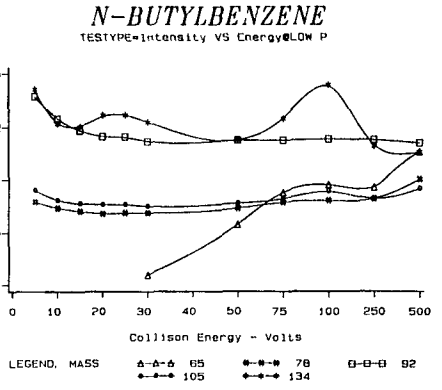

SELECTION OF PARENT IONS AT HIGH RESOLUTION

The capability to select parent ions at high resolution for MS/MS daughter scans is demonstrated by the analysis of a complex perfume mixture consisting of ~40 components. This analysis also utilizes parent scans and elemental compositions determined by high resolution peak matching to provide a more complete analysis which would not be possible under the low resolution MS/MS conditions obtainable on a triple quadrupole instrument.

Instrument - VG 7070EQ-HF controlled by a PDP-11/23 based VG 2350 data system

MS - 70 eV EI, 3 sec/decade scan, sample introduction via septum inlet, 150°C septum inlet, 250°C source temperature, 5000 resolution for high resolution on parent ions and peak matching, 1000 resolution otherwise.

MS/MS - Argon or nitrogen collision gas, 30 & 100 eV collision energy, 10 sec/scan for daughter scans, unit resolution on the mass-analyzing quadrupole.

5000 Resolution on Perfume Mixture

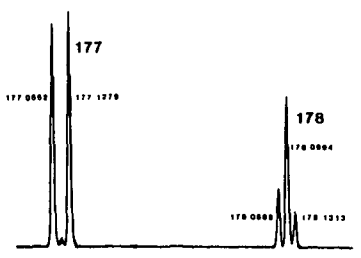

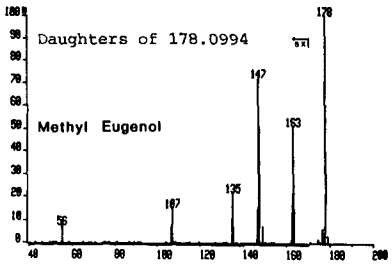

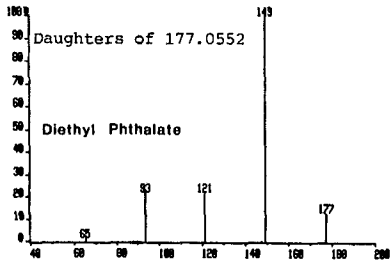

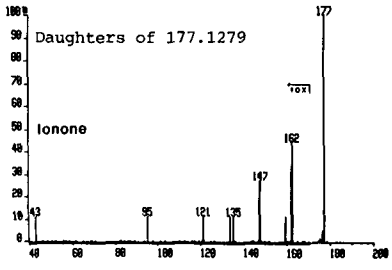

A MODERN CONTROL SCHEME FOR DOUBLE-FOCUSING MASS SPECTROMETERS

W.G. Linn and T.J. Eskew

Nuclide Corporation
State College, PA 16801

In a double-focusing magnetic deflection mass spectrometer, the mass and energy of the ions reaching the collector are determined by the ion-accelerating voltage V, the electric sector field E, and the magnetic sector field B. By either holding two parameters constant while scanning the third or by holding one parameter constant while scanning the other two in various ways (link scanning), much information can be obtained using just one instrument. For example, B scan or V/E scan will generate a spectrum similar to a high resolution single focusing instrument; a V/E^2 or B/E scan will collect all the daughters of a given ion; a B^2/E scan will give a spectrum of all parent ions which decompose to a particular daughter ion and a $B^2(1 - E')/E'^2$ will collect all daughter ions which were formed by the loss of a particular neutral mass.

Unfortunately, because of non-ideal conditions (i.e., the initial energy of the ions, the surface potentials in the electric sector, and non-linearities in the magnet and Hall probe) analog generation of these linked scans were difficult, or expensive requiring at least two external adjustments and at least two "trimmer" adjustments per type of scan, and to achieve all the above mentioned scans on one instrument became excessively awkward and prohibitively expensive.

Now, however, because of advanced technology, generation of any type of scan can be achieved by controlling the V, E, and B parameters separately via three independent D-to-A converters and allowing a desktop computer to compute the scans and make all the necessary corrections in software. This also allows for the easy implementation of any other type of scan which may be found useful in the future.

Nuclide Corporation is presently designing a family of solid-state updates incorporating software linked scan generation for use with the CEC 21-491, 492, 110 and Hitachi RMU-6 double-focusing mass spectrometers.

REFERENCE

K.R. Jennings, "Linked Scans", paper presented at the 31st Annual Conference on Mass Spectrometery, Boston, MA, May 1983

HIGH ACCURACY MASS MEASUREMENT WITH A FOURIER TRANSFORM MASS SPECTROMETER

W. D. Reents, Jr.
AT&T Bell Laboratories
Room 1A-320
600 Mountain Avenue
Murray Hill, New Jersey 07974

Two procedures are described for measuring masses with high accuracy. They are based upon minimizing the ion density and using standardized conditions. As a result calibration masses need not be present simultaneously and the normal pressure dependence of the measurement is greatly reduced.

Conditions for the first procedure: trapping voltage, 0.3 V; heterodyne mode, 8 KHz bandwidth; data points, 8K; zero fill, 4; frequency sweep, 1500 KHz to 0 Hz at 1KHz/μsec; constant excitation power; constant cell temperature; 1-inch cubic cell. The measurement including calibration requires 15-30 minutes. The mass/frequency data was fit to a quadratic equation. A calibration using PFTBA (Table I) was used to measure the mass of $C_2F_5^+$ (Table II). The variation in observed cyclotron frequency for CF_3^+ is 0.3 ppm for an order of magnitude change in pressure (Table III).

The conditions for the second procedure differ from the first one by reducing the ion density until the observed frequency remains unchanged. This is accomplished by reducing the emission current and optimizing the resolution by adjusting the RF excitation energy. This measure is lengthy (requiring hours or days). Using a calibration from m/z 28 to m/z 264 (Table IV), the mass of m/z 466 ($C_{10}F_{16}N_3^+$ from perfluoropropyl-s-triazine) was measured to within 4 ppm (Table V). Calibration from 28 to 466 (Table VI) demonstrates that accuracies of ~1 ppm are obtainable in the absence of calibration gas and that these measurements are stable for greater than one week.

TABLE I

CALIBRATION TABLE

m/z	Freq (Hz) (±a d.)	Mass Error (ppm)
69	512995.401 ± 0.025	0.06
131	270149 844 ± 0 020	-0 5
219	161553.115 ± 0 029	1 8
264	133995 160 ± 0 037	-1.3

TABLE II

MASS MEASUREMENT FOR 119^+

m/z:

118 991356
118.991346
118.991315
118 991350

avg = 118 991350 ± 0 000011

Calculated mass = 118.991468

Error = 0 99 ppm

TABLE III

EFFECT OF PRESSURE ON STANDARD MEASUREMENT

P (Torr)	FREQ (kHz)	
2 5E−8T	512 995622	
		= 0.14 Hz
5 4E−8T	512 995702	Range
		≈ 0.3 ppm
11 3E−8T	512 995764	

TABLE IV

CALIBRATION TABLE

Calc'd m/z	Meas m/z	Error (ppm)
27 99437	27.99436	+0 040
65.97319	65 97324	+0.83
68 99466	68 99457	−1.3
84 97159	84.97155	−0 40
118.99256	118 99273	+1.4
218.98508	218 98520	+0 55
263.98656	263.98627	−1.1

TABLE V

MEASURED MASS OF m/z 466 ($C_{10}F_{16}N_3^+$)

Frequency (kHz)	Measured Mass	Error (ppm)
75 66095	465 98139	−4 9
75 66115	465 98016	−7.6
75.66064	465 98326	−0 95
75 66022	465.98579	+4 5
75 66114	465 98022	−7 5
75 66057	465 98369	−0 02
8 661075	465 98060	−6.7
75 66084	465 98207	−3.5
Average:	465 98215	−3.3
True Mass:	465 98370	

TABLE VI

COMPLETE CALIBRATION TABLE

Calc'd m/z	Meas m/z	Error (ppm)
27.99437	27.99436	+0 03
65.97319	65 97324	+0.92
68.99466	68.99458	−1.2
84 97159	84 97153	−0.61
118 99256	118.99271	+1.2
130.99147	130 99138	−0.17
218.98508	218.98521	+0 61
263.98656	263 98635	−0 78
370.98541	370 98574	+0 90
465 98370	465.98326	−0 95

Accurate Mass Measurement in Fourier Transform Mass Spectrometry

Thomas J. Francl
American Cyanamid Company
Agricultural Research Division
P.O. Box 400
Princeton, NJ 08540

Robert T. McIver,Jr.
Department of Chemistry
University of California
Irvine, CA 92717

In Fourier transform mass spectrometry (FT-MS) the cyclotron frequency can be readily measured to nine significant digits. However, peaks are composed of a distribution of frequencies and high precision measurements are not sufficient to calculate accurate centroids. Therefore, the experimental parameters which affect the cyclotron frequency must be investigated. Aspects related to the instrument and those related to the data system can be considered. Most studies to date have focused on determining a calibration equation which relates the measured cyclotron frequency and the actual mass by taking into account experimental parameters such as plate voltages and number of ions. In this work another approach is taken by examining the effects of acquisition and processing parameters on the measured frequency.

There are essentially two modes of acquisition in FT-MS, broadband and narrowband. High resolution and accurate mass data is obtained by scanning a small region of the spectrum in the narrowband mode. However, to obtain a complete spectrum several succesive experiments must be performed. Preferably, a complete spectrum can be acquired in a single experiment in the broadband mode. However, the discrete nature of the FT-MS experiment limits the accuracy in determining the peak height and centroid.

To date there are three solutions to the limitations imposed by the broadband mode of acquisition:

(1) ZERO-FILLING : Adding a sets of zeroes to the time domain signal decreases the spacing between points in the frequency domain. For example, n zero-fills reduces the spacing by 1/2**n. However, zero-filling rapidly increases the size of the time domain signal. For less than 1 ppm spacing a 1 MW Fourier transform is required.

(2) ANALYTICAL SOLUTION: Comisarow and coworkers utilize an analytical solution to the magnitude Lorenztian lineshape to solve for the "exact" frequency and peak height. This method is computationally fast but is subject to errors for peaks which are close to each other or if there is noise in the spectrum.

(3) ZOOM TRANSFORM: Using this method small regions of the broadband spectrum are chosen. An inverse transform, followed by zerofills and a smaller forward transform are performed. This is much faster than zero-filling and more accurate than the analytical solution. The errors in calculating the centroid for the Zoom transform and the analytical solution are shown below as a function of per cent noise in the spectrum.

A summary of the relative performance of the two methods is given in the table below. In all cases the Zoom transform performs as well or better than the analytical solution.

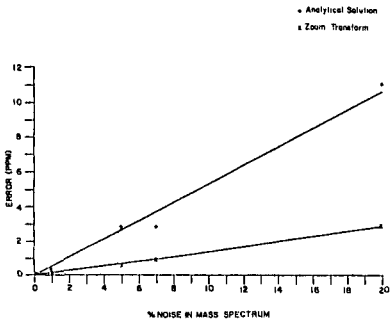

CONDITION.	SINGLE PEAK	TWO PEAKS (amu apart)
NO NOISE	COMPARABLE	ZOOM
WITH NOISE	ZOOM	ZOOM
DIGITIZATION (no noise)	COMPARABLE	ZOOM
DIGITIZATION (with noise)	ZOOM	ZOOM

Table I: Summary of the relative performance of the Zoom transform and the analytical solution.

THE EFFECTS OF DIGITIZATION

FT-MS time domain signals produced by the cycling ions are sampled in both time and amplitude. The number of bits of the analog to digital (A/D) converter will affect how well the sinusoid is defined by the discrete values. As a result of this sampling small errors in peak heights and centroids are introduced. Using the Zoom transform and a parabolic peak fitting routine to calculate the centroids, the relative errors are shown below as a function of the number of bits in the A/D converter, for three computer generated mass spectra:

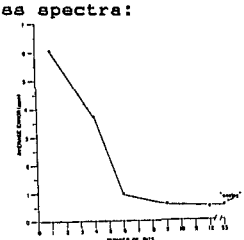

Although the errors for a 1 bit A/D are suprisingly small (less than 6 ppm), the sinewave is now represented by a square wave introducing many harmonics into the spectrum. The frequency spectrum for a single mass (m/z 175) is shown below:

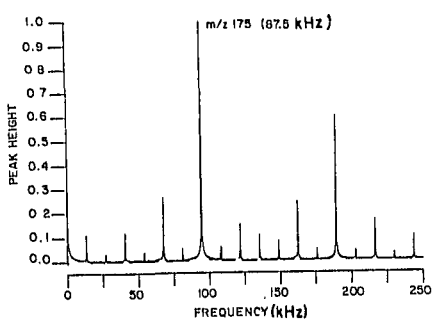

CONCLUSIONS:

The Zoom transform is the preferential method for obtaining accurate mass measurements on broadband data. The discrete nature of the FT-MS exper-iment requires digitization of the time domain signal in time and amplitude. This digitization introduces additional errors in the centroid calculation as well as harmonics in frequency and mass spectrum.

MODIFICATION OF A BENDIX 12-101 TIME-OF-FLIGHT MASS SPECTROMETER FOR IMPROVED MASS RESOLUTION. J.D. Pinkston, J. Allison, J.T. Watson, Departments of Chemistry and Biochemistry, Michigan State University, East Lansing, Michigan 48824.

Increasing chromatographic resolution demands higher scan speeds of mass spectrometers used as chromatographic detectors. To date, time-of-flight (TOF) mass spectrometry (MS) offers the ultimate in scan speed, potentially providing up to 1000 averaged scans per second when used in conjunction with the proposed integrating transient recorder (ITR) (1). However, TOF mass spectrometers suffer from poor mass resolution. Commercially available instruments achieve unit mass resolution (FWHM definition) at the m/z 614 peak for PFTBA (2), but only a very narrow mass range is in focus when this high resolving power is achieved. To obtain the high scan rates offered by the TOF-ITR combination, the entire mass range must be in focus after each pulse of the source. Furthermore, TOF instruments are not compatible with certain alternate modes of ionization, such as chemical ionization (CI), which cannot be pulsed on the time scale required in TOF (3). Therefore, we have undertaken research aimed at both increasing mass resolving power in TOF-MS to at least unit resolution over the entire 1 to 700 dalton range and at allowing non-pulsed sources to be used in TOF-MS.

Three basic phenomena limit mass resolution in conventional TOF: a) Ions are pulsed out of the source from a range of initial positions; b) ions exhibit a range of initial kinetic energies; and c) ions starting in the same plane with the same initial energies but moving in opposite directions will be separated by a "turn-around time". No amount of "space focussing" to compensate for the initial spatial spread or "energy focussing" (with time independent fields) to compensate for the spread in initial energies will reduce the turn-around time (4), which becomes significant at higher m/z.

In our instruments, as illustrated in Figure 1, a beam of ions is continuously extracted from a Dupont 21-491B EI or CI source and energy filtered using an electric sector. After the electric sector, the beam is chopped by beam deflection (5,6) using components of a Tektronix CRT electron gun in conjunction with a 0 to 200V variable amplitude Avtech pulse generator.

The advantages of this arrangement are: 1) Improvement in mass resolving power due to a) the removal of the dependence of time-of-flight on the ion's starting position; b) the reduction of the energy spread of the ions; and c) the elimination of the turn-around time as a resolution limiting phenomenon. 2) Continuous type ion sources such as CI and fast atom bombardment may be used. 3) It may be possible to obtain MS/MS type information by using the electric sector and TOF analysis independently (7).

One major disadvantage of the new design is a reduction in instrumental sensitivity. However, when used with the ITR, the sensitivity should be equivalent to that realized in most magnetic and quadrupole instruments.

An equation has been derived relating mass resolving power R, to various instrumental parameters:

$$R = \frac{m}{\Delta m} = \frac{t}{2\,\Delta t} = \frac{L^2\,V'\,(1-\delta^2)}{2\,S\,D\,V_0\,(1-\delta^2) + 4\,L^2 V'\delta}$$

where m is the nominal mass; t is the time-of-flight, Δm and Δt are the width of the mass peak in mass and time units, respectively; L is the flight tube length; V' is one half the deflection voltage; S is the width of the detector aperture (beam diameter << S); D is the separation of the deflection plates; Vo is the accelerating voltage; and δ is a measure of the energy bandpass of the electric sector such that:

$$\delta = \frac{y - \frac{ax}{\sqrt{2}\,l}\,\sin\sqrt{2}\,\theta - x\cos\sqrt{2}\,\theta}{a\,(1-\cos\sqrt{2}\,\theta)}$$

where y is 1/2 the exit slit width, x is 1/2 the entrance slit width, a is the electric sector radius, θ is the sector angle, and l is the distance from the point source to the entrance of the electric sector.

Figure 2 illustrates the dependence of resolving power on flight tube length and on exit slit width. These plots show that the goals of the research are attainable.

Figure 1.

ENERGY FILTERED BEAM DEFLECTION TIME-OF-FLIGHT MASS SPECTROMETER

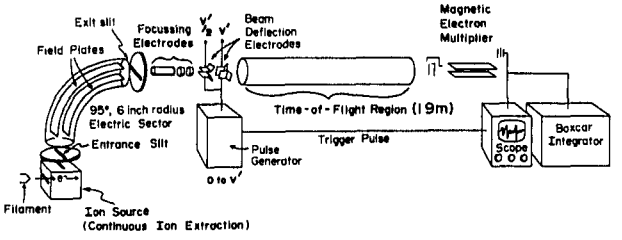

Figure 2. Initial parameters: L=1.9m, V'=100V, V_0=2800V, S=1cm, D=3mm, y=0.002in., x=0.0008in., a=6in., θ=95°, l=8.8cm

RESOLUTION VS. DEFLECTION VOLTAGE

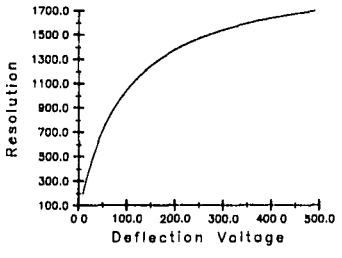

RESOLUTION VS. FLIGHT TUBE LENGTH

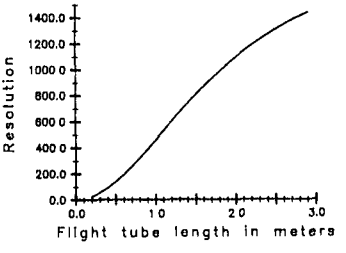

References

1. J.F. Holland, C.G. Enke, J. Allison, J.T. Stults, J.D. Pinkston, B. Newcome, J.T. Watson, Anal. Chem. 1983, 55, 997A.
2. measurement performed in this laboratory
3. C.W. Polley, Jr., A.J. Illies, G.G. Meisels, Anal. Chem. 1980, 52, 1797.
4. R. Stein, Int. J. Mass Spectrom. Ion Phys. 1974, 14, 205.
5. J.M.B. Bakker, J. Phys. E: Sci. Instr. 1973, 6, 785.
6. T.K. Fowler, W.M. Good, Nucl. Instr. Meth. 1960, 7, 245.
7. J.T. Stults, C.G. Enke, J.F. Holland, Anal. Chem. 1983, 55, 1313.

IMPROVEMENT OF MASS RESOLUTION IN THRESHOLD PHOTOELECTRON-PHOTOION COINCIDENCE TOF MASS SPECTROMETER (TPEPICO-MS)

T. Nishimura*, P. Chiarelli and T. van Kalleveen, Department of Chemistry, University of Nebraska, Lincoln, Nebraska 68588-0304.

The main restriction in threshold photoelectron-photoion coincidence experiments is the poor mass resolution of the time-of flight (TOF) spectrometer. The extraction field (Es) applied to the ion source is limited to a small value of about 5-20 V/cm, because high field strength reduces the energy resolution of threshold electrons. Mass resolution is typically about 30 amu. Here we propose a new TOF mass spectrometer for coincidence studies which is characterized by a double field ion source [1] and an ion reflector [2]. This apparatus will give much better mass resolution (>100 amu) at low extraction field and to measure kinetic energy release in fragmentation.

Figure 1 shows the schematic diagram of the new TOF mass spectrometer. Ions produced by ionization are space-focused at the plate P1 so that at this position the spread of their flight time results only from their initial ion kinetic energies. The ion reflector increases the time-of-flight without expanding the initial time spread at the plate P1 and minimizes the ion loss. Since ions at the object plate P1 are energy-focused to the image plate P2, the flight time distribution of the detected ions is directly related to the kinetic energy releases. Trajectory calculations were performed to determine the ion collection efficiencies, mass resolution and sensitivity for slow decomposition.

Coincidence statistics requires a high collection efficiency of ions. Representative transmission functions of ions (m/z 40) were calculated assuming the isotropic fragmentation at the point source. Figure 2 shows the detection probability P as a function of initial ion kinetic energy. These calculated transmission probabilities seem to be comparable with those for normal TOF mass spectrometer although restriction for ion detection becomes more severe for energetic ions. Mass resolution was calculated to be

$$M = 128 \quad \text{for } Es = 20 \text{ V/cm.}$$

Figure 3 represents the simulated TOF distributions for the dissociation process

$$[31]^+ \xrightarrow{\quad} [29]^+$$

as a function of decay rate (k). The arrows 0, I, II, III in the figure denote decompositions in the acceleration fields, the first drift space, the reflector field region and the second drift space, respectively. This figure reveals that the new TOF mass spectrometer has a high sensitivity over the wide range of decay rates. In the usual TOF mass spectrometer detection of slow decompositions is restricted to the region of acceleration fields. Decay rates can be easily estimated from a peak shape analysis. The center position of the peak I depends upon the mass of precursor ion. Therefore, this instrument has the merit of distinguishing between different pathways of ion formation.

From these calculations, we conclude that the proposed TOF mass spectrometer has a high potential for threshold photoelectron-photoion coincidence studies.

Acknowledgements: We are grateful for the Department of Energy for support.

References: [1] W.C. Wiley and I.H. McLaren, Rev. Sci. Instr., 26, 1150 (1953); [2] W. Gohl, R. Kutscher, H.J. Laue and W. Wollnik, Int. J. Mass Spectrom. Ion Phys., 48, 411 (1983); V.I. Karataev, B.A. Mamyrin and D.V. Shmikk, Zhurnal Tekh. Fiz., 41, 1498 (1971). [3] H. Kuhlewind, H.J. Neusser and E.W. Schlag, Int. J. Mass Spectrom. Ion Phys., 51, 255 (1983).

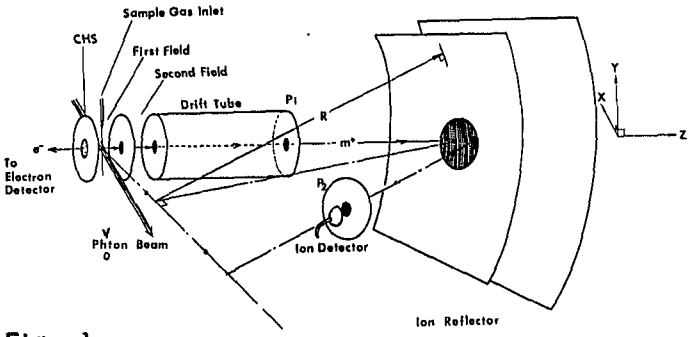

Fig. 1

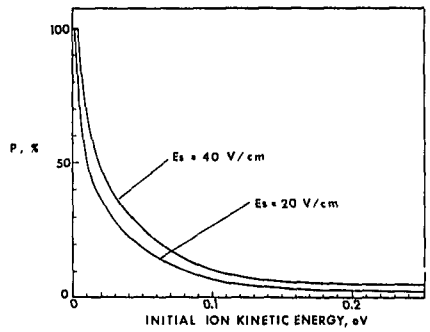

Fig. 2

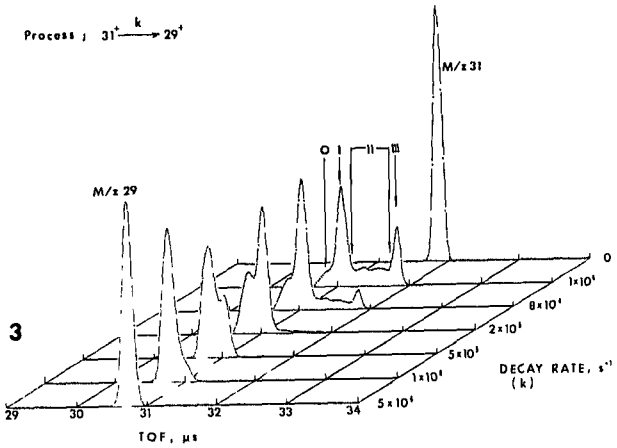

Fig. 3

HIGH FLUX PARTICLE BOMBARDMENT TOF MASS SPECTROMETRY.

Robert J. Cotter, Department of Pharmacology, The Johns Hopkins University, Baltimore MD 21205

A somewhat different approach to the design of a SIMS-TOF mass spectrometer has been investigated. 1. The primary ion beam fluxes are high enough to produce secondary ion currents that are more easily observed as analog signals, rather than single ions. This means that analog-to-digital conversion (waveform recording) and signal averaging techniques are more appropriate than single- or multiple-stop timing. 2. The approach is compatible with a liquid matrix, such as glycerol, which serves the same purposes as in the sector and quadrupole instruments when coupled with FAB sources. An advantage of this approach is therefore the ability to alter the solution chemistry to enhance the formation of molecular ions.

The instrument described here tests the feasibility of this approach. A KRATOS MINI-BEAM I ion gun is interfaced to a CVC-2000 TOF mass spectrometer. There is at this point no special signal processing, although a 100 MHz (analog-to-digital conversion rate), 100 Hz repetition rate real-time signal averaging system is anticipated. The secondary ion currents in this study are strong enough to be observed over several minutes as stable, repetitive (10 KHz) traces on an oscilloscope. They can also be recorded using the gated analog integrating scanner which is part of the CVC instrument. Molecular ion intensities range from 5 to 50/cycle, while total ion currents are greater than 100/cycle.

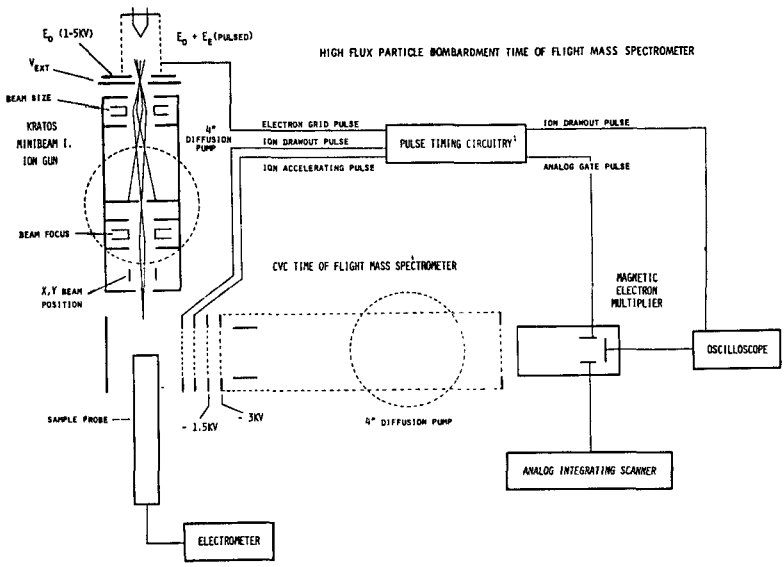

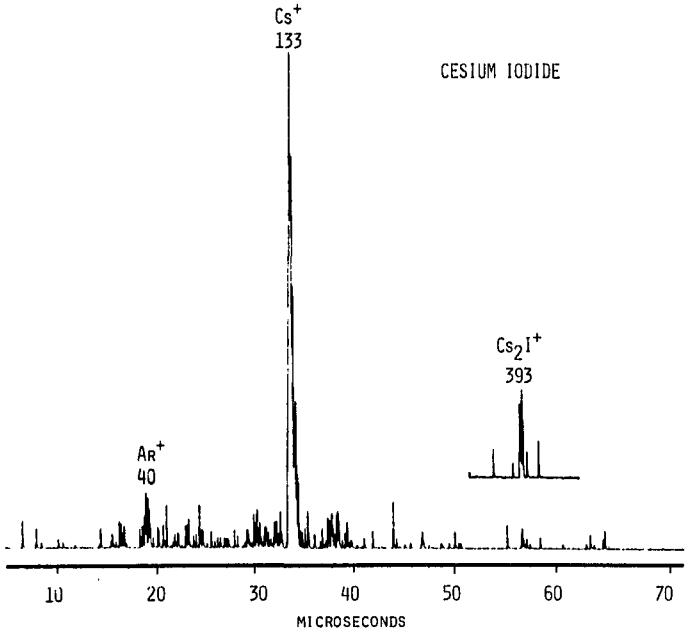
Cs+
133
CESIUM IODIDE
Cs2I+
393
AR+
40
10
20
30
40
50
60
70
MICROSECONDS

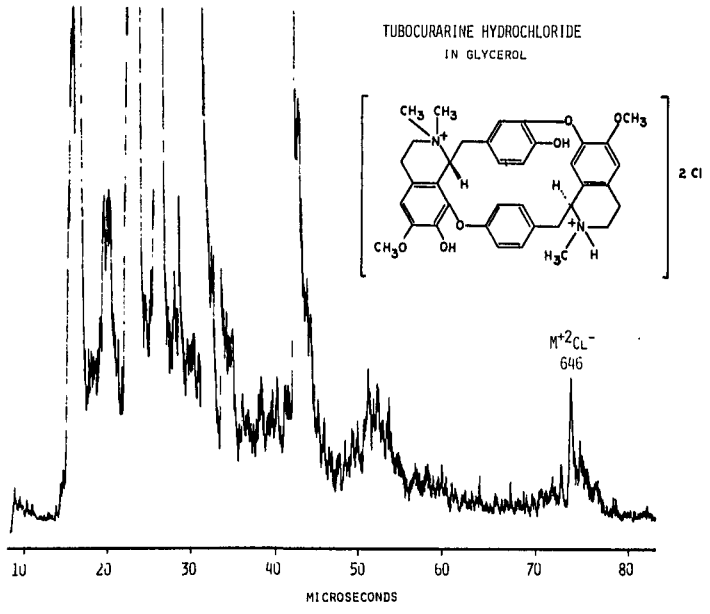
TUBOCURARINE HYDROCHLORIDE
IN GLYCEROL
CH3 CH3
N+
H
O
OH
OCH3
H
O
CH3O
OH
+N
H3C
H
2 Cl −
M+2CL−
646
10
20
30
40
50
60
70
80
MICROSECONDS

QUANTITATIVE DETERMINATION OF RUBBER TRIBLEND COMPONENTS BY CURIE-POINT PYROLYSIS MASS SPECTROMETRY

Henk L.C. Meuzelaar, Alice M. Harper and Willem Windig
Biomaterials Profiling Center, University of Utah
Salt Lake City, Utah 84108

Robert L. Lattimer and Kenneth M. Schur
B.F. Goodrich Research & Development Center
Brecksville, Ohio 44141

Determination of the composition of rubber blends plays an important part in quality, and process control as well as in the analysis of unknown rubber samples. Generally this type of analysis is done with infrared and nuclear magnetic resonance spectroscopy. Due to extensive sample pretreatment procedures, however, these methods can be very time-consuming.

Since pyrolysis mass spectrometry (Py-MS) is a rapid analysis technique with minimal sample pretreatment requirements the feasibility of analyzing rubber triblends by Py-MS was studied. Twenty "vulcanized" (= crosslinked with sulfur) rubber samples composed of different amounts of butadiene rubber (BR), natural rubber (NR) and styrene-butadiene rubber (SBR), were analyzed in triplicate by Curie-point Py-MS [toluene suspensions 1 mg/ml, sample weight 25 μg, end temperature 610°C, temperature-rise time 5 s, total heating time 10 s, electron energy 12 eV (set value), mass range scanned 20-260 amu]. The data were analyzed by a supervised target rotation [1] factor analysis method as well as by a newly developed nonsupervised method [2].

In principle, target rotation constructs in the space in which the data can be described the so called component axes by using the data points of the pure components. Projection of data from the different mixtures on these axes gives the composition in terms of the components [1]. If the pyrolysis mass spectrum of a ternary mixture can be regarded as a linear combination of the spectra of the three individual compounds and if the sum of the three components is normalized to 100%, then the data points representing the different triblends should all plot in a two-dimensional space. However, if significant chemical interaction occurs between the components during the Py-MS procedure then the intrinsic dimensionality of the data space may be expected to be higher than two. Our discriminant analysis results show that 93% of the intercategory variance (one triblend per category) is explained by two discriminant functions, with the third function accounting for only 3%. This provides a strong indication for the absence of significant chemical interactions between the components during the pyrolysis process. Apparently, under the experimental conditions used, the pyrolysis process is characterized by the occurrence of unimolecular decomposition reactions and the virtual absence of recombination reactions.

As a nonsupervised method the newly developed "variance diagram" technique [2] was selected. This is a way to detect and visualize correlations between the mass variables in a data set. A highly correlated behavior of many mass variables indicates a common origin, generally a chemical component [2] (see also abstract by W. Windig and H.L.C. Meuzelaar).

The plot constructed from the first two discriminant functions in Figure 1a clearly shows that the composition of the samples is reflected. There appears to be a systematic difference in the direction of the NR axis. This can be explained by a relatively high yield of this component in the mass spectrometer. Correcting for this "response factor" results in Figure 1b, in which the averaged deviation of the true concentrations is 4%. This level of precision is comparable to that obtainable with infrared or nuclear magnetic resonance spectroscopy. Since the response factor was found to be relatively constant for different mixtures in several data sets this precision level should be the same when predicting the composition of "unknown" samples.

Figure 2a shows the mathematically extracted spectra as obtained by the variance diagram technique, together with the spectra (Figure 2b) of the original constituents. The similarity clearly shows that the variance diagram approach is successful in a qualitative sense. The quantitative results are different from target rotation since this method determines the actual BR content, which has contributions from SBR and BR. When the original data are expressed in the same way, it appears that the precision of the unsupervised method is comparable to that of the target rotation approach.

From the results presented above it appears that Py-MS in combination with computerized multivariate analysis is a rapid method for mixture analysis of rubber blends.

REFERENCES:

1. Windig, W., Meuzelaar, H.L.C., Anal. Chem., 1984 (in press).
2. Malinowski, E.R., McCue, D.G., Anal. Chem., 49 (1977) 248.

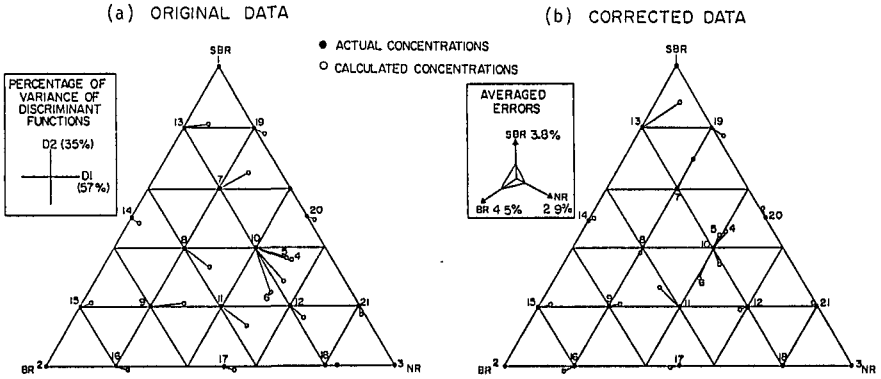

Figure 1. (a) Representation space of the triblend, as obtained with discriminant analysis; (b) correction for "response factor" results in a clearly better representation.

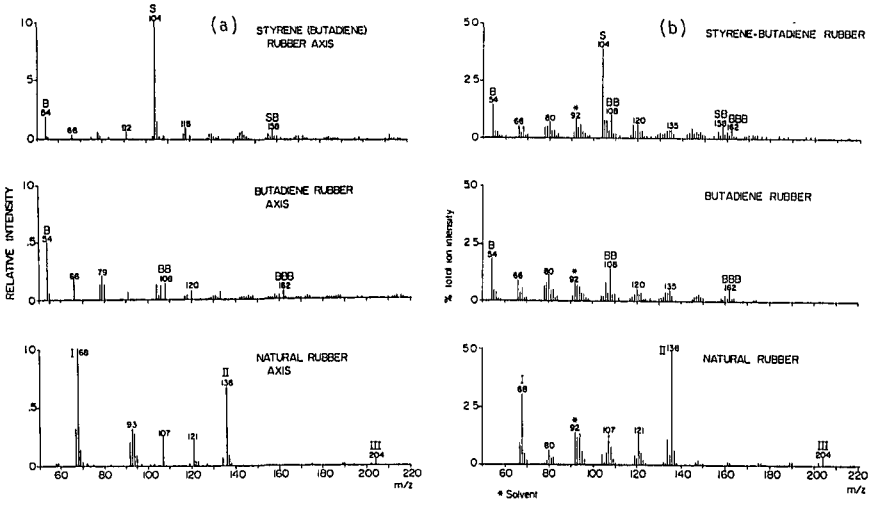

Figure 2. (a) The mathematically extracted pattern, as obtained with the variance diagram; (b) spectra of the original components.

STUDIES OF SUPERCRITICAL FLUID EXTRACTION AND FRACTIONATION PROCESSES FOR POLAR AND MIXED FLUIDS BY DFI-MS[a]

H. R. Udseth and R. D. Smith
Chemical Methods and Kinetics Section
Pacific Northwest Laboratory
Richland, WA 99352

Much of the recent interest in supercritical fluids is related to their application for selective extraction and fractionation processes. By changing the pressure of the fluid the solvent characteristics can be varied from selective (near the critical pressure) to highly solvating at several times the critical pressure. The development of direct fluid injection (DFI)-mass spectrometric techniques now allows the rapid evaluation of extraction processes in terms of product identification and determination of the relative solubility of the various components. These methods may also be utilized to determine optimum extraction conditions during process development.

Consideration of the solubility parameters for the various fluids and fluid mixtures provides a basis for making a qualitative estimate of solubility. However, other factors involving partitioning between other liquid or solid phases can be of major importance for establishing a sufficient supercritical fluid phase concentration. We have found that supercritical CO_2 and CO_2-H_2O mixtures can be used to extract trichothecenes and have obtained relative solubility data as a function of pressure for several fluid systems. Figure 1 gives relative solubility data for three trichothecenes (DAS=diacetoxyscripenol, DON = deoxynivalenol, and T-2 toxin) in supercritical carbon dioxide at 40°C as a function of pressure. These data illustrate the different solubilities as a function of pressure which may be utilized as the basis for the development of new separation methods.

The DFI-MS methods for characterization of supercritical fluid solutions can be employed to aid more rapid and efficient development of new extraction and separation processes for industry. Micro-scale methods coupled with the DFI-MS[1] and other characterization methods, provide rapid and detailed information concerning the effects of pressure and temperature upon fluid composition. A wide range of process variables can be readily explored while detailed information is obtained regarding the composition of the extract, allowing a rapid evaluation of the process and a determination of optimum process parameters.

The application of the various methods to process development applications (including extraction and fractionation) typically requires continuous sampling of a supercritical fluid extraction (SFE) cell and benefits from the DFI-MS detection methods which are selective, sensitive and applicable to all extracted compounds. The extracted products are directly introduced into the mass spectrometer through the DFI interface[2,3]. Once in the ionization region of the mass spectrometer the sample compounds can be handled in a conventional manner using the wide range of available mass spectrometric ionization methods and analysis techniques. The advantage of SFE-MS lies in the small sample flow rate required for analysis (< 1 μl/min) for continuous sampling of an extraction system at high temperatures and pressures, without disturbing the equilibrium established between the various fluid and condensed phases. Thermally labile sample compounds can be extracted when fluids with low critical temperatures (such as CO_2 or ethane) are used. The instrumentation and methodology used for these analyses have been described in detail elsewhere[2,3].

In typical preliminary experiments the pressure of the supercritical fluid is slowly ramped during the extraction process and mass spectra are continuously recorded. This allows changes in the extracted species as a function of pressure to be readily observed. An example of a mass spectrum obtained during the supercritical ammonia extraction of an intractable fuel sediment is shown in Figure 2. These methods have been applied to a wide range of complex natural products, biological samples, and fuel materials to aid process development.

References:

1. Smith, R. D. and H. R. Udseth, Anal. Chem., 55, 2266-2272 (1983).
2. Smith, R. D. and H. R. Udseth, Sep. Sci;. Tech., 18, 245-252 (1983).
3. Smith, R. D. and H. R. Udseth, Fuel, 62, 466-468 (1983).

a. This work was supported by the U.S. Department of Energy, Office of Basic Energy Sciences under Contract No. DE-AC06-76RLO-1830.

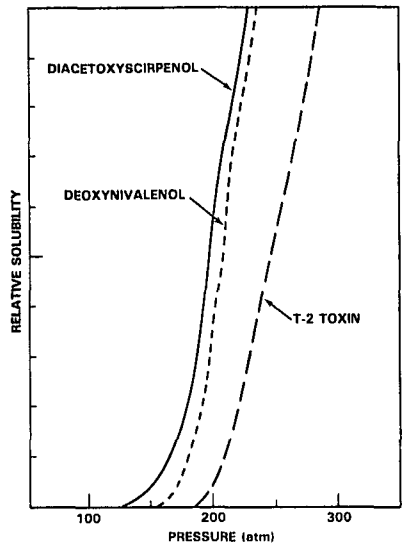

Figure 1. Relative solubilities for three trichothecenes in supercritical carbon dioxide at 40°C. Full scale corresponds to approximately 0.05 mole percent.

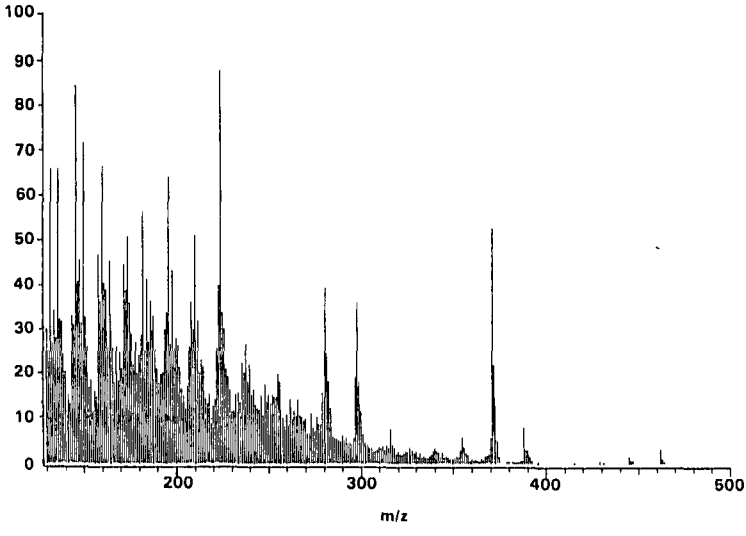

Figure 2. Mass spectrum obtained during the supercritical ammonia extraction of "insoluble" diesel fuel marine fuel sediment at 140°C and 400 atm

A PENNING TRAP MASS SPECTROMETER FOR HIGH PRECISION MASS MEASUREMENTS ON SHORT-LIVED ISOTOPES [1]

P.Dabkiewicz, H.Kalinowski, F.Kern, H.-J.Kluge, L.Schweikhard, H.Schnatz, H.Stürmer, Institut für Physik, Universität Mainz, D-6500 Mainz RFG
and
R.Moore, Foster Radiation Laboratory, Mc Gill University, Montreal, Canada, H3A 2B2

Motivation

- Test, Input for Nuclear Models
- Parameters for Mass Formulae
- Deformation, Pairing and Shell Effects
- Limits of Nuclear Stability Against Spontaneous Particle Emission
- Relationship between Nuclear Binding Energy and Charge Distribution

Principle of Mass Determination

The basic idea of the experiment is to determine the mass of an isotope directly by measuring its cyclotron frequency in a known magnetic field, while it is stored as an ion in a Penning trap. Fig.1 shows the principle and the set up of the experiment. The mass measurement is performed in two stages:

Firstly, the 60 keV ion beam of the ISOLDE facility is stopped on a foil mounted in Penning trap 1 in the pole gap of an electromagnet. The radioactivity is then reevaporated from the foil, cooled by buffer gas collisions and stored in the trap. The efficiency for this procedure, i.e. the ratio of the number of stored ions to that of the incoming ions, has been determined to be 10^{-3} to 10^{-4} for the case of Ba.

In a second step, the ions are transferred by an ejection pulse into Penning trap 2 placed in the very homogeneous and stable field of a superconducting magnet. A rf field is then applied. When in resonance, this field induces larger cyclotron orbits. The ions are then ejected from the trap and allowed to drift to a channel plate detector. In the inhomogeneous part of the magnetic field the radial energy gained from the rf field is transferred into longitudinal energy which is detected as a reduction in time of flight of the ions [2].

Main Features of the Experimental Set Up

- Direct mass determination of an isotope without the knowledge of the mass of neighbouring isotopes.
- Accuracy and resolution better than 10^{-6} ($A=100: \Delta M \gtrsim 100$keV) and, therefore, discrimination between isobars, and between ground and isomeric states of the same isotope.

1) Supported by the Bundesministerium für Forschung und Technologie
2) G.Gräff, H.Kalinowski, and J.Traut: Z.Phys. A 297, 35 (1980)

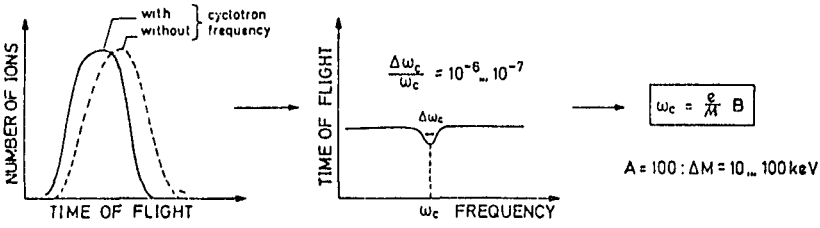
with
without
cyclotron frequency
NUMBER OF IONS
TIME OF FLIGHT
$\frac{\Delta\omega_c}{\omega_c} = 10^{-6} \ldots 10^{-7}$
$\Delta\omega_c$
TIME OF FLIGHT
ω_c FREQUENCY
$\omega_c = \frac{e}{M} B$
A = 100 : ΔM = 10 ... 100 keV

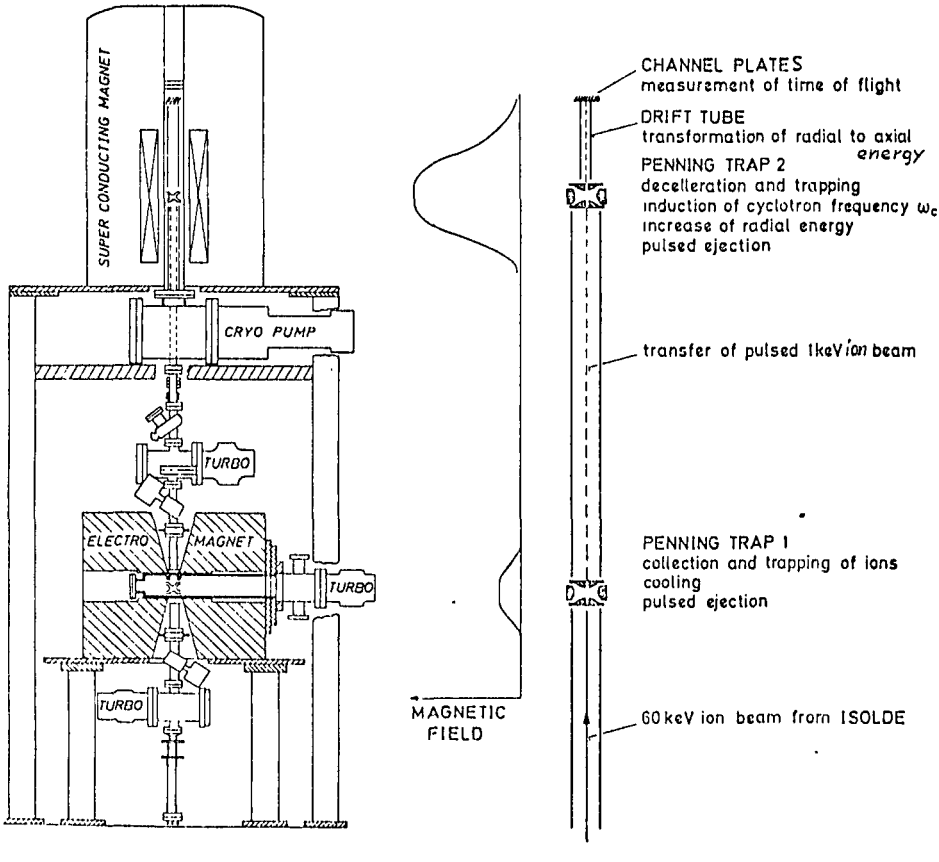
SUPER CONDUCTING MAGNET
CRYO PUMP
TURBO
ELECTRO
MAGNET
TURBO
TURBO
MAGNETIC FIELD
CHANNEL PLATES
measurement of time of flight
DRIFT TUBE
transformation of radial to axial energy
PENNING TRAP 2
deceleration and trapping
induction of cyclotron frequency ω_c
increase of radial energy
pulsed ejection
transfer of pulsed 1keV ion beam
PENNING TRAP 1
collection and trapping of ions
cooling
pulsed ejection
60 keV ion beam from ISOLDE

THE CAUSES OF ION CYCLOTRON FREQUENCY SHIFTS IN FTMS AND THEIR RELEVANCE TO EXACT MASS MEASUREMENT; S.K. HUANG AND D.L. REMPEL, UNIVERSITY OF NEBRASKA, CHEMISTRY DEPT., LINCOLN, NE.

Recently, it has been shown [1] that a mass calibration procedure derived from the space charge theory advanced by Jeffries et. al. [2] works with only partial success. In an attempt to discover the sources of systematic error found in [1], we have identified several mechanisms which contribute to shifts in the measured cyclotron frequencies.

Experimental: The cell used in these experiments is a .0254 meter 304 SS cubic with differential excitation and detection. The cell is operated in a magnet field of 1.2 Tesla, in positive ion EI mode, with a 50 eV electron beam energy, and a 55 volt collector bias. The amplitude of the RF burst waveform applied to the transmitter plates is .77 volts p-p which corresponds to an attenuator setting (AT1) of 30 db in the double resonance experiment (Fig. 3). The frequency data were taken for the M/Z=78 peak of benzene at an indicated pressure of 2×10^{-7} Torr.

X-Y Smearing: This effect appears for all three froms of excitation studied: RF burst, chirp, and ion pulse. The effect is demonstrated in Fig. 1 as the frequency depression at low orbit sizes (RF burst excitation time, TTX, is short). The magnitude of this effect increases with a larger number of ions and with a higher trap voltage. This latter feature occurs because the number of ions retained in the cell after the beam is turned off increases with the trap voltage (VTR) for voltages that are less than approximately 1 volt. From Fig. 2 it is apparent that the frequency shift as a function of the number of ions is markedly influenced by the time of the excitation. From the above facts, one can conclude that the effect is coulombic in nature and that the RF burst is modifying the ion distribution to spread them out in directions perpendicular to the magnetic field (it is unlikely the RF burst is adding energy to the z motion of the ions).

Z Excitation: This effect is evident with excitation waveforms which are short in duration and high in amplitude: very short high amplitude RF bursts, chirp waveforms, and impulse waveforms. In Fig. 3 we show the results of a double resonance experiment which demonstrates the chirp induced z-excitation is strong enough to eject ions. The conditions AT1=2 and VTR=0.44 volts together with a chirp waveform sweeping from 0 to 2 MHz at 2.105 KHz/usec provide good tuning conditions. In the experiment, the chirp is applied as the first excitation 50 msec. after the beam. A 400 usec RF burst is applied 4 seconds after the beam to detect the ions that remain in the cell. The trap voltage is switched from the indicated trap voltage to 4 volts during the sequence to reduce losses in the z direction. In Fig. 3, the complex area [3] of the M/Z=78 peak is plotted to give an indication of the accumulated z loss from beam to trap-switch as a function of the trap-switch time. The drop in the curves in the neighborhood of 50 msec. indicates the loss associated with the chirp excitation.

Dynamical Ion Distribution: The temporal evolution of the trapped ion cloud has been addressed elsewhere [2]. In Fig. 4, it is shown that the frequency is not nearly constant but changes noticably during the time the transient is observable. The frequency shift is computed by comparing the frequency obtained from a transform translated 50 msec. into the transient with the frequency computed in the normal way. At the higher cyclotron orbits where good signals are found, two trends are discernable: increasing the trap voltage makes a positive contribution to the frequency shift while increasing the number of ions makes a negative contributions.

[1] E.B. Ledford, Jr., D.L. Rempel, and M.L. Gross, Analytical Chemistry, submitted.
[2] J.B. Jeffries, S.E. Barlow, and G.H. Dunn, Int. J. Mass Spectrom. Proc., 1983, 54, 169-187.
[3] S.K. Huang, D.L. Rempel, and M.L. Gross, these Proceedings.

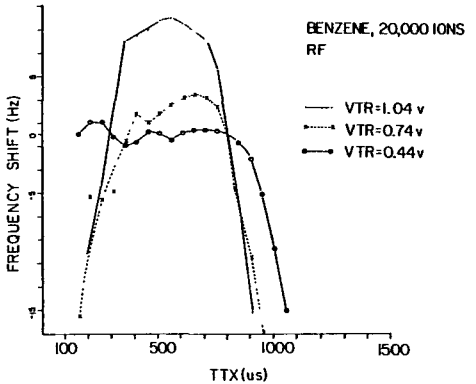

Fig. 1. Frequency shift vs. orbit size.

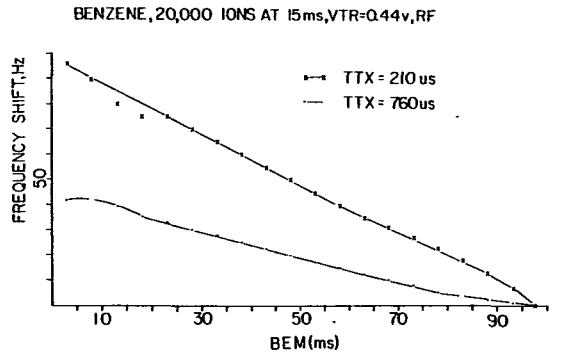

Fig. 2. Frequency shift vs. # of ions.

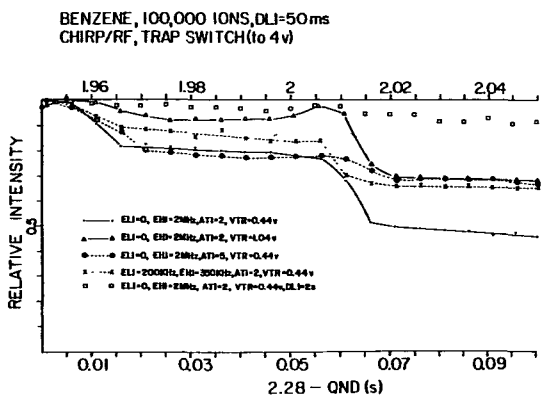

Fig. 3. Z-ejection.

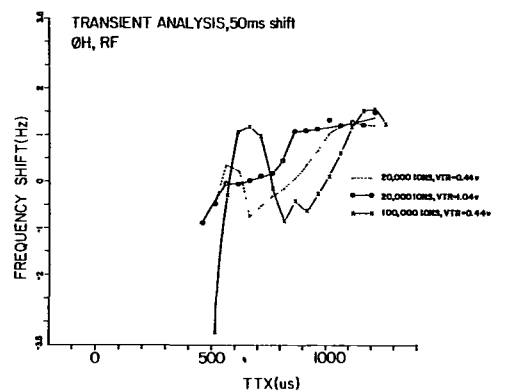

Fig. 4. Frequency shift in transient.

COMPUTER-CONTROLLED PEAK MATCHING

D.E. Giblin and R.L. Lapp
Midwest Center for Mass Spectrometry
University of Nebraska-Lincoln, Lincoln, NE 68588

Exact mass measurement leading to elemental compositions is an important goal of high-resolution mass spectrometry[1-3]. However, there are situations when such measurements are difficult to make in a full magnet scan mode: soft ionization methods such as chemical ionization, high mass and/or very weak peaks, data acquisition by ion counting, and unresolved interfering peaks. To aid in exact mass measurements under such conditions, we have developed a computer-controlled peak matching system.

We have used a custom-built MID with ion counting capabilities which is interfaced to a Data General Nova 4X minicomputer and which controls the ESA and accelerating voltage of a Kratos MS-50. Nevertheless, the principles of operation are applicable for more general cases provided there is, at a minimum, computer control of the mass ratio and signal gain.

The computer program for performing peak matching has several important features. It is interactive allowing full operator control of its various options and operating parameters. Its file-oriented structure and operation fits it into the computer operating system and facilitates input, output, and control functions. Peak centroids are calculated by using a modified algorithm which emphasizes peak tops relative to peak skirts. And the program has peak deconvolution capabilities to separate partially resolved multiplets.

The program uses four files in its operation. The standard mass file contains the masses of the major PFK ions. The configuration file contains the default options and operating parameters such as sweep time and width, filter frequency, and numbers of scans to be averaged for use in the matching steps. The acquired data are stored in the data file and the processed data are spooled in the plot file before being plotted.

Peak centroids are calculated according to the equations: $T = t_i x_i$ where $x_i = A_i^2 / A_i^2$ instead of $x_i = A_i / A_i$ which is the usual algorithm[4] and where t_i and A_i are the time and intensity of the ith sample and the summation is performed across the peak. The advantages of this modification are that it discriminates more effectively against minor interferences, is less sensitive to peak aberrations, and increases effective resolution by a factor of 1.4. A disadvantage is that the estimated standard deviation of the centroid is increased by a factor of about 1.25 for the shot noise limit with dense sampling across the peak. However, this disadvantage can be overcome by collecting data for 45% longer time. (In practice, other sources of error dominate.)

The deconvolution procedure enables the separation of partially resolved multiplets. Peaks are modeled by Gaussian functions by varying the parameters of height, position, and width. Reference peak(s) are assumed to be singlets and are modeled by single Gaussians. Sample peaks are modeled by Gaussians whose widths are the mean of the widths of the reference peaks. The number and initial estimates of the positions of peaks within a multiplet are indicated by using the cross-hairs on the video terminal. Actual deconvolution is accomplished by minimization of the sum of squared residuals between data and modeling functions by using either the Newton-Raphson or Powell directed-search algorithms[5-6].

In normal operation, the operator tunes the instrument on the lowest mass, usually a reference, at unity mass ratio, decreases the magnet current a few ppm, then enters up to five projected masses. The program responds with the nearest higher and lower PFK masses which can be changed to other PFK masses or masses of other standards. Upon the start of aquisition, the program collects sequentially four data sets over the peaks to perform successively the following operations: (1) set gain factors such that peaks are of similar height, (2) make initial mass ratio adjustments to center each peak in its sweep window, (3) make final mass ratio adjustments, and (4) calculate final centroids and masses with results displayed on the video monitor. If necessary, the peak deconvolution routine can be invoked. (This procedure can also be performed offline.)

As an example of the capabilities of the system, the molecular ion region of quadricyclane -C_7H_8-was peak matched. Quadricyclane has a very strong $M\text{-}H^+$ ion and a very weak molecular ion, and the resolution needed to separate the molecular ion from

the ^{13}C isotope of the $M-H^+$ ion is 22K. By using the deconvolution procedure with a resolution of 8K, we were able to determine the masses of molecular ion and the interfering isotope of the $M-H^+$ ion to accuracies of -1.8ppm and 5.1ppm respectively while at a resolution of 18K, we were able to get accuracies of 1.7ppm and 2.0 ppm for the same ions. These results are shown in the figure.

1. F.W. McLafferty, **"Interpretation of Mass Spectra"**, 3rd edition, University Science Books, Mill Valley, CA, 1980, p.94.

2.a. Y. Tondeur, J.R. Hass, D.J. Harvan, and P.W. Albro, Anal. Chem., 56, 373 (1984).
b. D.J. Harvan, J.R. Hass, and D. Wood, Anal. Chem., 54, 332 (1982).

3. K.L.Clay and R.C. Murphy, Int. J. Mass Spectrom. Ion Phys., 53, 327 (1983)

4. J.R. Chapman, **"Computers in Mass Spectrometry"**,Academic Press, New York, 1978, p.34.

5. Y. Bard, **"Nonlinear Parameter Estimation"**, Academic Press, New York, 1974, pp.54, 88.

6. G.R. Walsh, **"Methods of Optimization"**,John Wiley & Sons, New York, 1975, pp.108, 129.

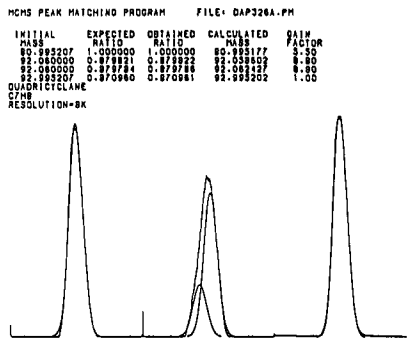

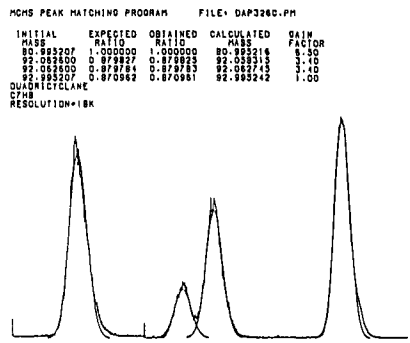

FAB ANALYSES OF POLYMERS BY AN OPTIMIZED QUADRUPOLE MASS SPECTROMETER

M. Youssefi
Union Carbide Corporation
Bound Brook, New Jersey 08805

Fast atom bombardment (FAB) mass spectrometry is a soft ionization technique that has become exceptionally useful for the analysis of nonvolatile and thermally labile molecules. However, most of the applications reported thus far have been with biological and pharmaceutical materials using double focusing mass spectrometers. Briggs[1] investigated polyethylene oxide, polyacrylonitrile, and polystyrene using the FAB technique. Secondary ion mass spectrometry (SIMS) investigations of some polymer surfaces have also provided useful structural information[2].

Useful ions above mass 300 amu have not been reported for most of the polymers studied by either SIMS or FAB. Spectral intensity decay, surface damage, and charging are factors contributing to this problem. Higher mass ions are analytically more useful for microstructural characterization of polymers because they can provide information about stereochemical regularity, chemical defects, and copolymer sequencing.

A quadrupole mass spectrometer was modified to an optimized fast atom bombardment(FAB) ionization instrument, using a spherical energy analyzer, to a mass range of 1-1500 amu. The applicability of FAB for polymers analysis has been demonstrated using this instrument. Useful FAB spectra of phenoxy, polycarbonate, ethylene-vinyl acetate copolymer, polyvinylchloride, polysulfone, and polyethersulfone have been oftained for the first time. These spectra show that FAB can be used to "fingerprint" polymer systems and provide diagnostic fragmentation patterns similar to electron impact and chemical ionization techniques. Most of the polymers studied did not provide useful FAB spectra with the widely used glycerol matrix. Therefore, a critical evaluation of a number of matrices was conducted. Results of this study show that good FAB spectra can be obtained for most synthetic polymers by doping polymer solutions or films with NH_4Cl and dilute HCl to reduce charging and assist ion formation.

Figure 1 shows the FAB spectrum of 500 ng of a solution of polyethersulfone doped with NH_4Cl and HCl. This spectrum illustrates the excellent sensitivity and low and high mass resolution of the modified instrument. The FAB spectrum is very characteristic of the copolymer under investigation. A series of ions separated by m/z 49 (SOH) are observed and the m/z 251 is part of the polymer backbone.

POLYMER BACKBONE

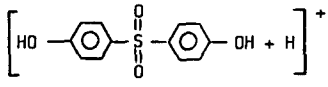

The quadrupole was tuned to favor higher masses. The m/z 1214 corresponds to a pentamer unit. The ion intensity is quite good even above mass 1000 amu.

Recently, we have extended our application of FAB to the direct analysis of additives in polymers. One interesting application of FAB was the identification of an unknown powdery material on the surface of a polymer. EI and CI analyses of the unknown contaminant gave a mass spectrum consistent with that of stearic acid. However, FAB analyses of the unknown gave m/z 630 as the major high mass peak and 339 as the base peak. This is shown in Figure 2. The m/z 606 corresponds to the MW of calcium stearate. Comparison of this spectrum to that of the authentic compound positively identified it as calcium stearate. The m/z 630 is the protenated molecular ion + Na.

References: 1. D. Briggs, Surf. Interface Anal., 1, 151 (1982).
2. J.E. Campana, J.J. DeCorpa, and R.J. Colton, Application Surf. Sci., 8, 337 (1981).

Figure 1: FAB Spectrum Of A Commercial Polyethersulfone

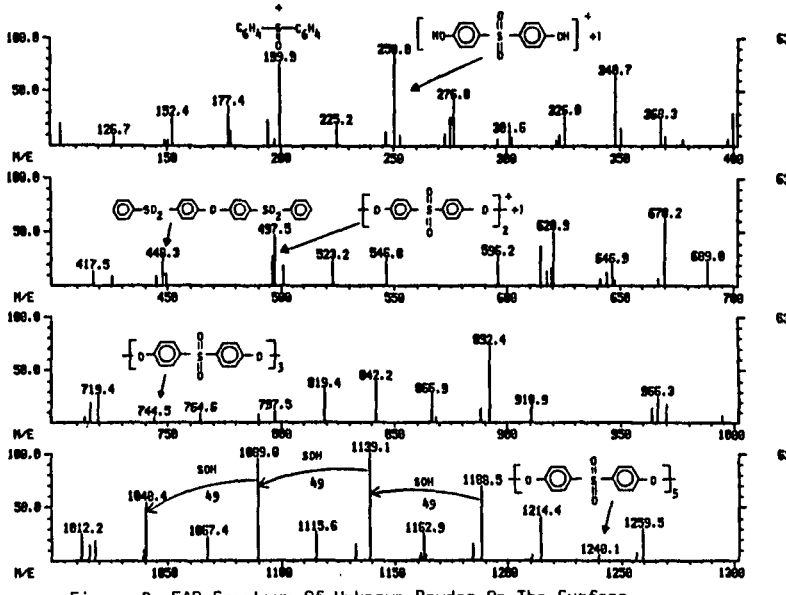

Figure 2: FAB Spectrum Of Unknown Powder On The Surface Of A Polymer

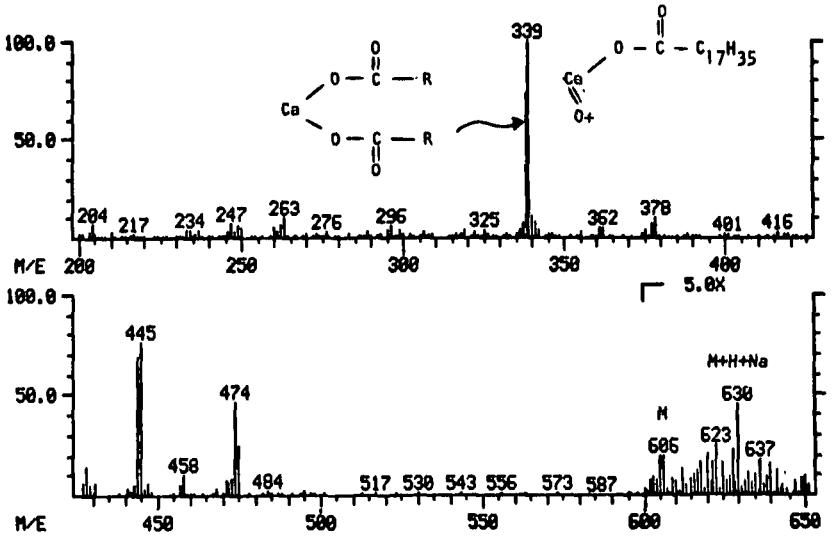

THE EFFECT OF POLYMER-SOLVENT INTERACTIONS ON SAMPLING EFFICIENCY IN ELECTROHYDRODYNAMIC IONIZATION MASS SPECTROMETRY. John H. Callahan and Kelsey D. Cook; Department of Chemistry and Materials Research Lab, University of Illinois, Urbana, IL 61801.

While a variety of mass spectrometric ionization techniques has been employed in the structural characterization of polymers, determination of polymer molecular weight distributions and averages by mass spectrometry has proven to be difficult. The fragmentation that accompanies most ionization techniques, while providing useful structural information, causes variation in the mass spectrometric sensitivity for different oligomers within a polymer sample. As a consequence, techniques which do not cause much fragmentation, such as field desorption (FD) or electrohydrodynamic ionization (EH), have been generally more successful in characterizing polymer molecular weight distributions and averages. In EH, ions are extracted directly from solution by application of an electric field (1). Little excess energy is deposited during ionization. As a result, molecular or quasimolecular ions resulting from ion attachment or electrolytic dissociation are observed with less fragmentation than with techniques such as FAB and SIMS (2). However, solvent-analyte interactions apparently play an important role in the efficiency of the sampling process. For example, ions in which the charge center cannot interact strongly with the solvent (e.g. tris(bipyridyl) complexes of transition metal ions) are more readily sampled than are alkali metal ions (3).

Differences in relative oligomer sampling efficiencies due to solvent-analyte interactions would result in spectra reflecting distortion of the true molecular weight average and distribution of the sample. However, in previous studies in this laboratory with poly(ethylene glycols) (PEG's), evidence for such effects was not found (4,5). Recent work has focused on determining whether this is true for polymers in general, or if the chemical nature of the sample can affect the way in which it is sampled by EH. In poly(ethyleneimine) (PEI), replacement of the oxygen in PEG with nitrogen significantly changes the chemical nature of the polymer. PEI has a far greater sensitivity to acid/base chemistry and ability to complex transition metal ions than does PEG. Additionally, the presence of the amine nitrogen in the polymer backbone provides multiple sites for strong solvent-solute hydrogen bonds and for branching.

As with PEG, sodiated adducts of PEI were observed in the mass spectrum of glycerol solutions of the polymer with sodium nitrate supporting electrolyte. As the polymer chain length increased, double sodium ion attachment to the polymer was also observed. In contrast to PEG, however, an intense series of protonated peaks was observed in the PEI spectrum, and multiply protonated ions could be detected upon the addition of acid. When PEI samples with nominal average molecular weights of 600, 1200, and 1800 were sampled, the number average molecular weights ($\bar{M}_n$) calculated from the spectra were 399, 505, and 584 respectively. The increasing discrepancy between the expected and calculated $\bar{M}_n$ values with increasing molecular weight indicated that sampling efficiency decreased with increasing polymer chain length. Three hypotheses may be proposed to explain this behavior: 1) heavy oligomers were highly charged and ion-dipole interactions between polymer and solvent reduced sampling efficiency; 2) heavy oligomers were uncharged in solution and therefore not sampled; or 3) additively increasing (with increasing molecular weight) polymer-solvent hydrogen bonding interactions produced lower sampling efficiency for heavier oligomers.

Each of these mechanisms would vary differently with solution chemistry, so the various hypotheses were tested by obtaining spectra of a variety of solutions. The addition of base to PEI resulted in simplification of the spectrum by reduction of the intensity of the protonated series, but did not significantly change the relative sampling efficiency for PEI oligomers, suggesting that multiple protonation and resulting high charge (which is reduced by addition of base) was not the source of the sampling bias. Addition of nitric acid to PEI solutions (acid: polymer ratio ~ 1:1) increased the abundance of protonated species in the spectrum and resulted in the formation of doubly protonated and mixed sodiated/protonated adducts. In the case of PEI 1800, triply protonated species (oligomers up to molecular weight 2200) were also observed. These changes were accompanied by increases in $\bar{M}_n$ calculated using all ions in spectra of PEI 1200 ($\bar{M}_n$ increased from 505 to 565) and PEI 1800 ($\bar{M}_n$ increased from 584 to 647). The distribution of singly charged adducts was not changed appreciably; multiple charge attachment evidently improved the relative sampling efficiency for heavier oligomers. This suggests that sampling bias against these oligomers did not arise from their being uncharged in solutions without added acid, but rather from extensive polymer-solvent interactions for molecules with long chains. This effect can be offset to some extent by raising the charge on heavy oligomers (from one to two), thereby increasing

sampling interactions with the extracting field.

The latter hypothesis was tested by continuing to increase the acid/polymer ratio in solution, in order to further promote multiple protonation of oligomers. The number average molecular weight increased with increasing acid/polymer ratios, up to a ratio of 2:1. Above this ratio the molecular weight average began to decrease, and a series of fragment ions appeared in the spectrum indicating degradation of the polymer. The dependence of the degradation on acid concentration suggested that it was a solution process rather than a gas phase or ionization process. Studies with other techniques (e.g. ^{13}C NMR) are currently under way to confirm that the degradation process actually does occur in solution.

Due to this polymer degradation, sampling bias could not be further reduced by increasing acid concentrations. An alternative approach to multiple charge attachment to PEI was tested through the addition of transition metal ions to the polymer solutions. PEI is known to complex a variety of transition metal ions and multiple transition metal ion attachment has been reported. When complexes of PEI with Cu, Ag, Mn, Co, and Zn were sampled by EH, however, no multiple ion attachment was detected. In fact, through a variety of solution processes, only singly charged complexes were sampled from solution. For example, Cu(II) was sampled as the Cu(I)-PEI complex, apparently through the glycerol-induced reduction of Cu(II). Mn(II), Co(II), and Zn(II) were only observed as singly charged ion-paired polymer adducts.

Another approach to improving the sampling efficiency for PEI has been to vary the nature of the solvent. Preliminary results have shown that there are some changes in the sampling efficiency for PEI when mixed glycerol/water solvents are used. The calculated number average molecular weight for PEI 1200 increased from 505 (in glycerol) to 640 when a 70%/30% (v/v) glycerol/water mixture was used. This increase resulted both from an increase in the abundance of doubly protonated adducts and from a shift in the distribution. This suggests that water reduces the sampling bias against heavy oligomers both by increasing solvent acidity and by reducing solvent-polymer interactions. Work aimed at optimizing solvent composition for minimum sampling bias is under way.

References

1. B.P. Stimpson and C.A. Evans, Jr., J. Electrostatics 5, 411-430 (1978).
2. K.D. Cook and K.W.S. Chan, Int. J. Mass Spectrom. Ion Phys. 54, 135-149 (1983).
3. K.W.S. Chan and K.D. Cook, J. Am. Chem. Soc. 104, 5031-5034 (1982).
4. S.-T.F. Lai, K.W. Chan, and K.D. Cook, Macromolecules 13, 953-956 (1980).
5. K.W.S. Chan and K.D. Cook, Org. Mass Spectrom. 18, 423-425 (1983).

Acknowledgement: This work was supported in part by the National Science Foundation (Grant DMR-80-24632, funded jointly by the U.S. Army Research Office). The Materials Research Lab receives support from the National Science Foundation (Grant DMR-80-20250).

CHEMICAL IONIZATION/FAST-ATOM BOMBARDMENT: A NOVEL IONIZATION METHOD

Royal B. Freas and Joseph E. Campana,
Naval Research Laboratory, Chemistry Division,
Washington, D. C. 20375

Fast-atom bombardment (FAB) has proven to be a useful desorption technique for the mass spectrometric analysis of intractable chemical species. These species are sputtered as ions and neutrals from solid surfaces, films, or liquid matrices by an energetic beam of fast atoms. The number of sputtered neutral species should be considerably larger than the number of ionic species, based on typical ion yields from classical surface studies.

A novel high-pressure FAB source has been constructed to study ion/molecule reactions of sputtered ions and neutrals. Pressures in this ion source are typically on the order of 0.1 to 0.5 Torr. A number of studies have been performed with this chemical ionization/-fast-atom bombardment (CI/FAB) source and the MIKES technique.

Collisional stabilization of sputtered ions was affected by different buffer gases, He, Ar, Xe, CO_2, CO, CH_4, i-C_4H_{10}, and NH_3. The unimolecular dissociation of the protonated molecule of pentaerythritol tetrapentanoate (PETP) was observed to decrease in direct proportion to the effective collisional stabilization cross-section of the buffer gas. Figure 1 illustrates the change in the ratio of the abundance of the $[M+H]^+$ species to the abundance of the unimolecular dissociation product ion of PETP versus the pressure of CO_2, CO, and Xe bath gases.

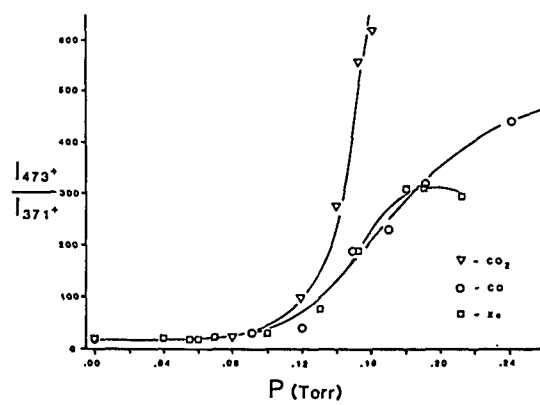

FIGURE 1: The ratio of the molecular ion ($[M+H]^+$, m/z 473) abundance to the unimolecular dissociation product ion (m/z 371) abundance is plotted versus the pressure of three different bath gases, CO_2, CO, and Xe. As the pressure increases beyond 0.1 Torr, the number of collisions occurring becomes large enough to collisionally stabilize effectively the $[M+H]^+$ ion produced by bombardment of fast Xe atoms on a neat sample of PETP. Between 0.1 and 0.2 Torr, the slope of the curves is linear and proportional to the collisional stabilization cross-section of the bath gas. The change in the ratio at higher pressures (> 0.2 Torr) is due to collisional activation by increased pressure in the first field-free region.

Post-desorption ionization (PDI) of sputtered neutrals is accomplished by ion/molecule reactions through the generation of reactant ions in a conventional manner. The PDI of sputtered neutrals has been observed to increase the intensity of the $[M+H]^+$ species of PETP by more than two orders of magnitude. The ratio of the $[M+H]^+$ ion abundance to the metastable ion abundance decreases with increasing ionization potential of the gas used to generate the reactant ions. Table 1 shows this ratio for different bath gases at a pressure of 0.15 Torr. Other processes occurring within the CI plasma include proton transfer, charge exchange, association, and condensation.

TABLE 1.

Gas	I.P. (eV)	I_{473^+}/I_{371^+} (filament on)
He	24.6	24
Ar	15.7	59
CO_2	13.7	109
CH_4	12.6	111
Xe	12.1	90
$i\text{-}C_4H_{10}$	10.7	300

Ion abundances of the $[M+H]^+$ species of PETP and fragment ions change with the addition of a buffer gas to the ion source. Figures 2, 3, and 4 display mass spectra of PETP with different bath gases. The use of NH_3 as a bath gas collisionally stabilizes the molecular ion and results in the formation of an $[M+NH_4]^+$ species. This association reaction has permitted the analysis of the composition of a number of different pentaerythritol tetraester isomers in a commercial lubricant formulation.

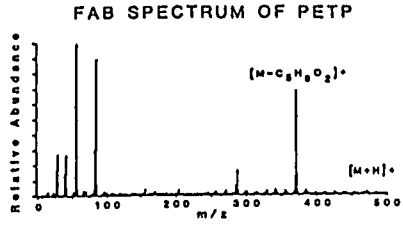

FIGURE 2: Fast-atom bombardment spectrum of neat PETP. The molecular ion ($[M+H]^+$, m/z 473) is less than 0.5% of the base peak.

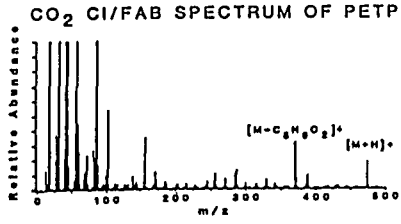

FIGURE 3: A CO_2 chemical ionization/fast-atom bombardment spectrum of neat PETP. The molecular ion ($[M+H]^+$, m/z 473) is fifty times more abundant than in the spectrum shown in Figure 2. The large peaks below m/z 100 (m/z 88 and m/z 44) are due to bath gas ions.

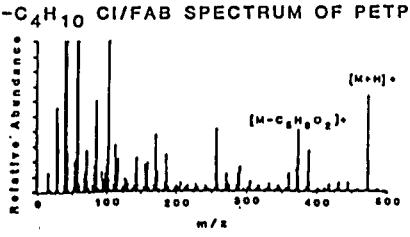

FIGURE 4: An $i\text{-}C_4H_{10}$ chemical ionization/fast-atom bombardment spectrum of neat PETP. The molecular ion ($[M+H]^+$, m/z 473) is over 100 times more abundant than in the spectrum shown in Figure 2. The $[M+H]^+$ species is more abundant than any of the fragment ions of PETP. The large peaks below m/z 200 are due to reactant ions and impurities.

The use of the CI/FAB source has led to the enhancement of the molecular parent ion through several ion/molecule interactions. These include collisional stabilization, charge exchange, proton transfer, association, and condensation. Another advantage of this novel technique has been an increase in the sample lifetime. These studies are currently being extended to include different classes of compounds.

A Simple Approach to "In-Beam" Chemical Ionization. Gene C. Jamieson, Carol Reuter, and William L. Fitch, Zoecon Corporation, 975 California Avenue, Palo Alto, CA 94304.

A simple and inexpensive direct chemical ionization probe is described which is useful for obtaining chemical ionization spectra of thermally labile and low volatility compounds. With this unheated probe design, rapid sample vaporization is achieved using heat inherent in an ion source obviating the need for external probe heating and associated power supply. Rapid sample heating with vaporization from an inert surface in close proximity to the ionization region yields maximum vaporized intact molecules.

This technique involves direct exposure of the sample to a chemical ionization plasma using a chemically inert extended probe of minimal thermal mass and low thermal conductivity (Figure 1). Compounds are coated on the exterior polyimide surface of a flexible fused silica capillary and inserted into the electron beam ionization plume of a chemical ionization source (Figure 2).

The probe has been applied to the analysis of several compound classes including underivatized prostaglandins, amino acids, peptides (up to penta) and metabolic conjugates. Figure 3 is a spectrum of 1 μg of p-nitrophenyl-β-D-glucuronide analyzed with ammonia chemical ionization at a source temperature of 300°C. This compound was used to test several operational parameters and probe designs including source temperature and probe length. The results indicate that the device can successfully operate on any mass spectrometer equipped with a conventional direct inlet probe and a chemical ionization source.

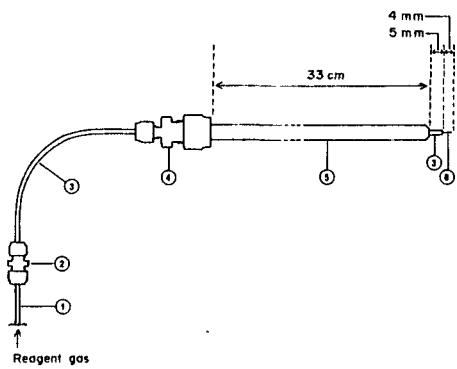

Figure 1. Probe design. (1) 1.5 mm (1/16") o.d. x 0.5 mm i.d. Teflon tubing; (2) 1/16" ss union; (3) 1/16" o.d. x 0.01" i.d. ss tubing; (4) 1/4":1/16" ss reducing union bored to allow feedthrough; (5) 1/4" o.d x 0.075" i.d. ss tubing; (6) 0.22 mm o.d. x 0.005 mm i.d. x >2' length polyimide coated fused silica capillary.

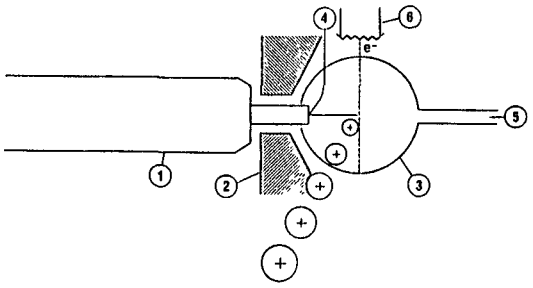

Figure 2. Insertion of probe tip into ionization cell. (1) probe; (2) source body; (3) ionization cell; (4) reagent gas inlet; (5) GC inlet; (6) electron beam filament. Plunger assembly which houses ionization cell bored to accept 1/16" ss tubing.

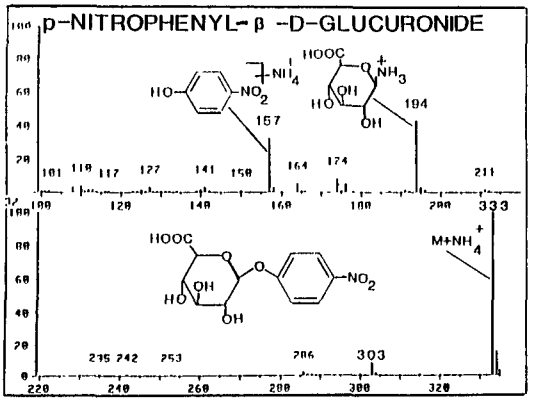

Figure 3. "In-Beam" ammonia chemical ionization. Source temperature = 300°C.

LIQUID IONIZATION MASS SPECTROMETRY OF ORGANOMETALLIC COMPOUNDS

K.Musha, Asahi Denka Co. Ltd.
H.Kuwabara and M.Tsuchiya, Department of Industrial Chemistry, The University of Tokyo, Hongo, Bunkyo-ku, Tokyo 113 Japan

Mass spectrometry has been applied to a few organometallic compounds used as important additives of lubricating oils[1,2]. Thus liquid ionization (LI) mass spectrometry we have developed[3] was applied to several organometallic compounds and a commercial lubricating oil. Since major components of lubricating oils are hydrocarbons and proton affinities of organometallic compounds are higher than those of hydrocarbons, the possibility of analysis without preliminary separation of additives was investigated.

The method (LI) and the instrument used is the same as previously reported[3]. A metal complex is mixed well with a matrix like alkane(s). If the alkane(s) did not give good results, the sample is dissolved in a small amount of solvent before mixing with the alkane(s). Nujol, undecane and decane were examined as a matrix and hexane, benzene and chloroform were examined as a solvent. The temperature of a sample holder has significant effect on ion abundances, an optimum heater current was investigated between 0.8 A (about 80°C) and 1.4 A (about 200°C).

Metal complexes as shown below were examined and most of them gave MH^+ ions and a few fragment ions corresponding well to the structure of the compound. As molybdenum complexes, four types (S_1 - S_4 complexes) were measured. S_1 and S_2 complexes give abundant and stable MH^+ ions as shown in Fig.1 for S_2 complex. If decane and chloroform were used for the molebdenum complexes, more abundant MH^+ ions can be obtained. S_4 and S_3 complexes, however, give less stable MH^+ ions and are easily oxidized with a minute amount of oxygen (H_2O?) at heating, resulting in the formation of S_2 complex. A sample should be well dispersed or dissolved in a matrix and there may be some reagents which stabilize the molecular ions.

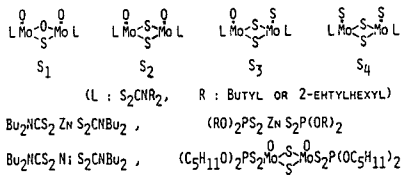

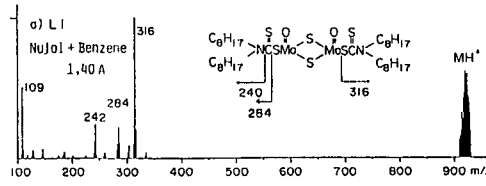

MASS SPECTRA of MOLYBDENUM (V) DI-2-ETHYLHEXYL DITHIOCARBAMATE

Fig.1

A zinc complex, $(RO)_2PS_2ZnS_2P(OR)_2$, commercially available were measured and it was found that decane was good enough (no fragment ions) and heater currents of 1.05 -1.10 A were optimum as shown in Fig.2. Although the complex (ZnDTP) is sold as the hexyl derivative, it was actually produced by reactions between zinc sulfide and a mixture of hexyl alcohol and propyl alcohol with other reagents. If the abundance ratio of hexyl alcohol to propyl alcohol was 5 to 1 and the reactions occur statistically, the abundance ratios of products ($4C_6$-ZnDTP : $3C_61C_3$-ZnDTP : $2C_62C_3$-ZnDTP : $1C_63C_3$-ZnDTP) should be 100 : 80.0 : 24.0 : 3.2. The intensity ratios of the peaks at m/z 659, 617, 575 and 533 obtained by the method (Fig.2) is 100 : 80 : 22 : 3. Since the observed ratios agree well to the calculated ratios, the peak intensities may indicate the abundances of components, although the maker of the ZnDTP did not tell us the correct values.

As known in chemical ionization, proton transfer reactions occur from protonated molecules of a compound having low proton affinity to solute molecules having higher proton affinities. Since the proton affinities of hydrocarbons are lower than those of metal complexes, additives of lubricating oils may be directly analysed without any preliminary separation. An example is shown in Fig.3 for an engine oil commercially available. By depositing about 0.1 µl of

the oil on the sample holder (needle tip) and increasing temperature, several additives in the oil can be observed successively. Also each mass spectrum (Fig.3 a, - d) can be obtained at a constant heater current such as 1.40 A from the beginning. The results are more reproducible by the latter procedure. A molybdenum complex (shown in Fig.1) was added (0.25%) to the engine oil and detected clearly at heater currents of 1.30 - 1.40 A (Fig.3). The group of peaks around m/z 659 coincides the protonated molecules of $4C_6$-ZnDTP. The peak at m/z 425 indicates that there is a compound of molecular weight 424 in the oil. An anti-oxidant often used in lubricating oils, whose molecular weight is 424, is 4, 4'-methylene-bis-di-tertiary butyl phenol as shown in Fig.3 a. This may be correct answer.

The method (LI) is useful to measure organometallic compounds and there is the possibility of mixture analysis even quantitatively. With no preliminary separation, additives in lubricating oils can be detected.

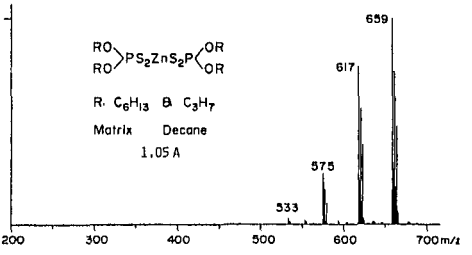

LI MASS SPECTRUM of Zinc (II) DIALKYL DITHIOPHOSPHATES (ZnDTP)

Fig.2

Reference

1) V.Raverdino, G.Natoli and E.Sappa, La Chimica L'Industria, 61 643 (1979)
2) R.P.Morgan, C.A.Gilchrist, K.R. Jennings and I.K.Gregor, Int. J. Mass Spectrom. Ion Phys., 46 309 (1983)
3) M.Tsuchiya and H.Kuwabara, Anal. Chem., 56 14 (1984)

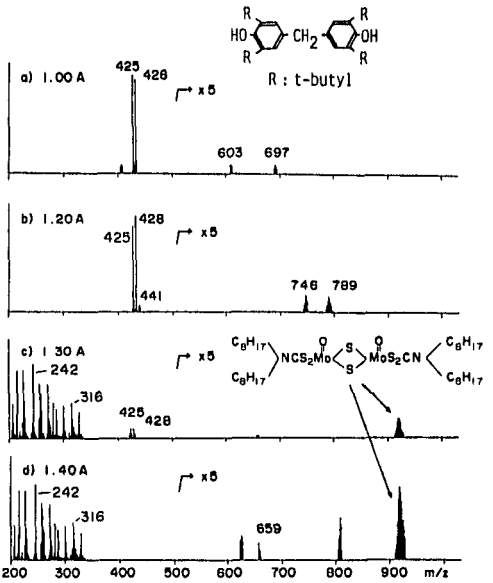

Fig.3 LI MASS SPECTRA of an ENGINE OIL

CHARACTERIZATION OF SUPERCRITICAL FLUIDS USING DIRECT FLUID INJECTION-MASS SPECTROMETRY*

R. D. Smith, H. T. Kalinoski and H. R. Udseth
Chemical Methods and Kinetics Section
Pacific Northwest Laboratory
(Operated by Battelle Memorial Institute)
Richland, WA 99352

Supercritical fluids are being widely explored for a variety of new concepts related to separations, material modification, and analytical instrumentation. The technique of Direct Fluid Injection (DFI) - Mass Spectrometry has provided a new sample introduction technique for mass spectrometry as well as a powerful tool for characterizing supercritical fluid solutions. Our previous work has demonstrated that compounds soluble in the supercritical fluid phase can be efficiently detected by DFI using chemical ionization mass spectrometric techniques.

An improved understanding of the DFI process can be obtained if one considers the expansion of a high pressure jet through a nozzle. This expansion process is represented schematically in Figure 1. The products of the expansion through the nozzle are determined by the fluid pressure, the pressure in the expansion region and other parameters such as the nature of the gas, temperature and orifice design. When the fluid expansion occurs in a chamber with a finite background pressure, the expanding fluid will interact with the background gas producing a shock wave system. This system includes barrel and reflected shock waves along with a shock wave perpendicular to the fluid jet, the Mach disk. The Mach disk is characterized by the destruction of the highly directed jet, resulting in kinetic energy transfer into various vibrational, translational and rotational modes. Therefore, the Mach disk serves to heat and disrupt the solvent clusters formed during the fluid expansion process. Empirical calculations predict that the average cluster formed in the DFI process will be at least 10^6 to 10^9 less massive than the droplets formed in the direct introduction of liquids into a similar low pressure environment. Work in this laboratory has found that the degree of initial clustering of solvent molecules (for CO_2) is much less than predicted. These solvent clusters are rapidly destroyed after the Mach disk and are not observed in the mass spectra. In addition, the dilute solutions typically employed in SFC and DFI-MS lead one to predict that solute-solute clustering will be negligible, which is consistent with our observations. Thus, the net results of the DFI process is to produce a gas spray incorporating the nonvolatile or thermally labile solute molecules. Direct fluid injection-mass spectrometry can be applied to any supercritical fluid solution. The DFI process allows the direct introduction of the solute molecules into the mass spectrometer, which can then be ionized through either conventional electron impact (EI) or chemical ionization (CI) methods.

The advantages of separation or extraction processes using supercritical fluids lie in the physical and chemical properties of the fluid. The ability to precisely change the solvating capabilities of a gas through control of pressure lends a new flexibility in the design of separations or extractions processes. SFC separation efficiencies approaching capillary gas chromatography can now be obtained, allowing the efficient analysis of thermally sensitive compounds. In DFI-MS, the resultant gas spray incorporating the nonvolatile solute molecule facilitates the analysis of a wide range of solute molecules that were previously impossible or very difficult. DFI-MS circumvents some problems inherent in direct liquid introduction or ion desorption from surfaces for analysis of moderately polar materials.

These methods have also found utility in the development of chemical process separations. The combination of the DFI-MS methods with micro-scale high pressure techniques allows the rapid and efficient variation of process variables, and has been found to be of considerable value for more complex systems.

*This work was supported by the U. S. Department of Energy, Office of Basic Energy Sciences, under Contract DE-AC06-76RLO-1830.

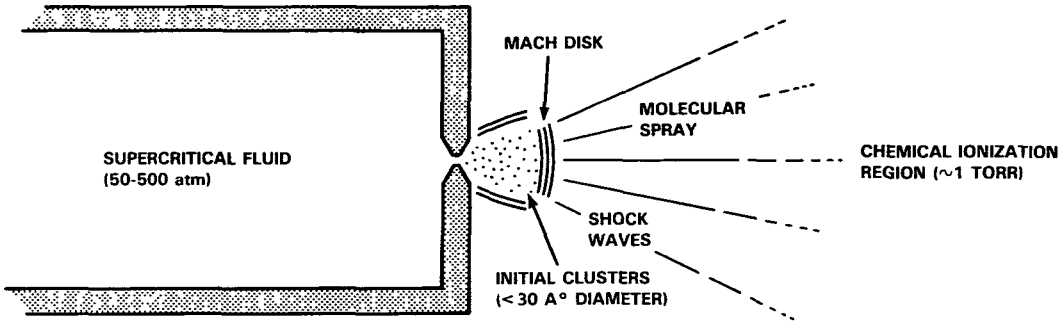

Figure 1. Schematic illustration of the direct fluid injection (DFI) process.

A NEW SOURCE FOR STUDIES OF ANGLE-RESOLVED COLLISION-INDUCED DECOMPOSITIONS OF IONS

K. R. Jennings, J. A. Laramee, R. S. Mason and C. Moore

Department of Chemistry, University of Warwick,
Coventry, CV4 7AL, U.K.

The collision-induced decomposition of ions at high translational energies (4-8 keV) give fragment ions the relative abundances of which have been shown in several laboratories to be a function of the translational energy of the primary ion E_{tr} and the angle θ to the primary ion beam at which products are collected. Most experiments have been carried out by observing ions scattered from the main beam in the xy or xz planes, using mechanical or electrical means of controlling θ. In previous work on the MS50 mass spectrometer, we have employed electrostatic deflection of ions in the xz plane to control θ but although this is a simple and rapid method, θ is difficult to calculate and only qualitative observations can be made.

A new source has been designed for use with the MS50 in which the normal ion source and inlet systems have been pulled back some 30 cm from their usual position and a series of defining slits, deflection plates and an einzel lens have been inserted between the ion source and a newly-designed collision cell. The whole assembly has been mounted on a rigid sub-frame which can be moved through an angle of approximately 3° about the y-axis through the collision cell. The focusing system is designed to give an angular resolution of better than 0.1^{o} in the z-direction for the incident beam. Ions scattered along the normal ion optical path are transmitted and mass analysed in the usual manner with an angular resolution of 0.1^{o} in the z-direction and 0.3^{o} in the y-direction.

Preliminary results obtained for Ar^{+} + Ar using the standard MS50 collision cell compared favourably with those in the literature and differences in relative intensities of the various maxima could be detected for changes of θ of only a few hundredths of a degree. The newly-designed collision cell will be fitted shortly and a full description of the performance of the source will be submitted to IJMSIP later this year.

FIELD DESORPTION MASS SPECTROMETRY OF ortho-, meta-, and para-TRIMETHYLAMMONIOPHENOLATES

Gordon W. Wood, T. Obal, and D. V. Ramana
Department of Chemistry, University of Windsor
Windsor, Ontario, CANADA N9B 3P4

The title compounds and their trimethyl-d_9 analogs were submitted to FDMS as part of our continuing effort to determine the scope and nature of methyl transfers and other artifact-forming reactions accompanying FD. As position isomers this series of compounds provide a more subtle test of structural effects than the homologous aliphatic zwitterions previously studied (1). At the same time, the relation of molecularity of methyl transfer to orientation of adjacent molecules in the condensed phase may be compared to earlier results for trimethylammoniobenzenesulfonates (2).

Depending on the orientation of the two benzene ring substituents, the major ions obtained from FDMS corresponded to one or more of the ions shown in Scheme 1 (C = original cation). Thus, the para compound gave C^+ or $C^+ - CH_3$ as the base peak, depending on the rate of anode heating. The meta compound gave spectra dominated by C^+ with some evidence of tetramethyl species, presumably from replacement of phenolic H by CH_3. Spectra of the ortho compound had $C^+ - H$ as base peak, attributed to transfer of CH_3 to phenolic O and loss of H. A diagram for this process and proposed structures for several high mass ions are shown opposite (Scheme 2).

It should be noted that none of the distinctive FD spectra for these isomers corresponds to the EIMS spectra reported earlier (3).

1. Wood, G.W.; Collacott, R.J. Org. Mass Spectrom. 1983, 18, 42-45.
2. Sukenik, C.N.; Bonapace, J.A.P.; Mandel, N.S.; Lau, P.-Y.; Wood, G.; Bergman, R.G. J. Amer. Chem. Soc. 1977, 99, 851-858.
3. Undheim, K.; Hvistendahl, G. Org. Mass Spectrom. 1970, 3, 1423-32.

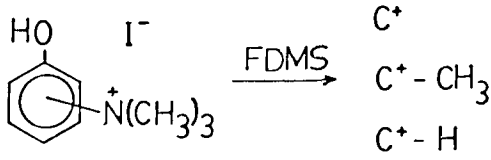

Scheme 1

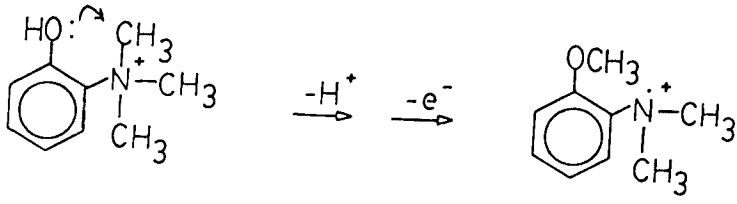

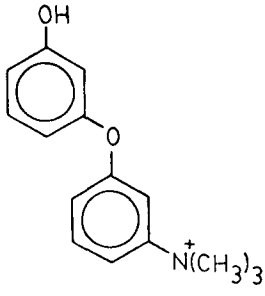

m/z = 244; 253 (d_9)

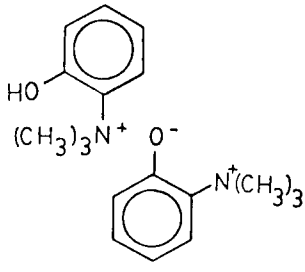

m/z = 303
$(2C - H)^+$

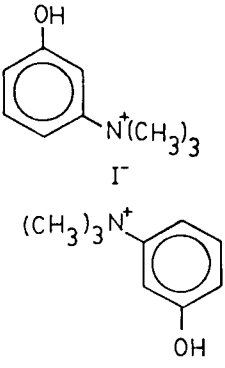

m/z = 431
$(2C + I^-)^+$

Scheme 2

MORE CANDIDATES FOR THE BENZYL/TROPYL PROBLEM: BENZOISOTOLUENE AND DIBENZOISOTOLUENE; John E. Bartmess, Department of Chemistry, Indiana University, Bloomington IN 47405

We have studied the effect of benzo-fused rings on the benzyl/tropyl rearrangement of $C_7H_8^{+\cdot}$, using ICR spectrometry. Based on gas phase acidities (agreeing with MNDO calculations) we find that 2 is 13 kcal/mole higher in energy than 1 and 4 is 6 kcal/mole higher in energy than 3. The (M-1)+ ion from 1 (AP = 13.1 eV by electron impact, 5.1 eV above the IP) behaves similarly to that from toluene, giving a large amount of tropylium near threshold, decreasing to 34% bewteen 20 to 30 eV. The tautomer 2 (AP of $(M-1)^+$ = 8.4 eV, IP = 12.4 eV) behaves similarly. This is in contrast to the monocyclic parent compounds, where the paraisotoluene 5 gives largely benzyl ion at all energies. These populations were probed by measuring the amounts of reactive and non-reacting $(M-1)^+$ ions. For both 1 and 2, these react with their own neutrals to give $(M+13)^+$ ions, presumably via an electrophilic substitution; for 2, these latter ions react further with the neutral to give higher masses involving loss of H_2 or $C_{10}H_8$.

For 3 (IP = 7.2 eV, $AP(M-1)^+$ = 14.1 eV) and 4 (IP = 7.6 eV, $AP(M-1)^+$ = 12.6 eV), no reaction was observed for the $(M-1)^+$ ions either with their own neutrals, or with a wide variety of other nucleophiles. We believe that this does not necessarily represent a pure tropylium population, but rather that the benzyl ion has become so stable that it will not react with these nucleophiles. We are studying other probes for the stuctures.

The radical cations of 1 and 3 did not undergo the autoprotolysis reaction with their own neutrals to give an $(M+1)^+$ ion; the radical cations of 2 and 4 did so, indicating that the neutrals were not tautomerizing on the walls of the vacuum system.

The $(M-F)^+$ ion from perfluorotoluene does not react with a variety of aromatic nucleophiles, but reacts completely away with hexamethyldisilazane to give $C_6F_5CF{=}NHSiMe_3^+$. We will examine the $C_7F_7^+$ structures from perfluorocycloheptatriene, also. MNDO calculations predict that the benzyl isomer is more stable then the tropylium one here by 25 kcal/mole.

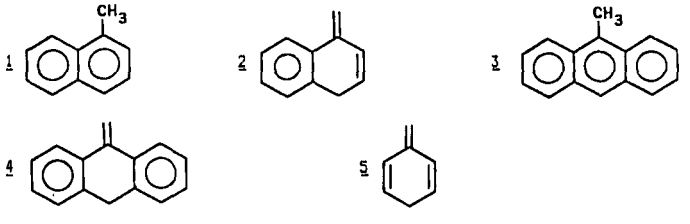

THE NON-RESONANT MULTIPHOTON IONIZATION AND FRAGMENTATION OF SOME SUBSTITUTED BENZENE MOLECULES

William B. Martin and Rebecca M. O'Malley, Chemistry Department,
University of South Florida, Tampa, Florida 33620

In order to study the ionization and fragmentation processes resulting from multiphoton absorption by neutral molecules a Nd:YAG laser has been interfaced with a CVC MA 002 time-of-flight mass spectrometer. Since the mass spectrometer operates normally in the electron beam mode at a frequency of 20 KHz and the laser (Molectron MY 32-10) has a maximum repetition rate of 10 Hz a special system control circuit was built to couple these two pieces of equipment. The circuit utilizes a 10.000 MHz crystal oscillator in conjunction with an array of digital decade counters to produce a 10 Hz 'master pulse' which is used to trigger the laser. A preselected time later (which can be adjusted in 1 μs intervals) a second pulse is produced which triggers the time-of-flight electronics which in turn trigger the ion detection system. Reducing the pulsing frequency of the mass spectrometer from 20 kH to 10 Hz resulted in a drastic reduction in signal intensity. This was compensated for by feeding the signal from the electron multiplier through a fast preamplifier (PAR, Model 115) and into a waveform recorder (Biomation, Model 6500). The captured signals were then down-loaded to a signal averager (PAR, Model 4203). Typically, the data from between 500 and 2000 ionizing events were averaged to obtain a reasonable looking mass spectrum. Hard copy spectra were subsequently obtained using a strip chart recorder. Using the experimental arrangement described spectra can be recorded using a variety of ionizing conditions. In particular, spectra are reproduced here showing the fragmentation patterns observed when ionization is initiated by a) 70 eV electrons b) multiphoton absorption at 532 nm and c) multiphoton absorption at 355 nm.

It is clear that the ionization process initiated by multiphoton absorption is quite different from that initiated by electron impact. Looking at the benzene system, in the electron impact spectrum, a large percentage of the ionization is observed as the molecular ion at m/z = 78 ($C_6H_6^{\cdot+}$). The ions at m/z = 52($C_4H_4^{\cdot+}$), m/z = 51($C_4H_3^+$) and m/e = 50($C_4H_2^{\cdot+}$) correspond to the loss of the neutral species C_2H_2, $C_2H_3\cdot$ and C_2H_4 respectively from the molecular ion. In contrast, the majority of the ionization observed in both the multiphoton absorption initiated spectra corresponds to small fragment ions, the most important ones being $C^{\cdot+}$(m/z = 12), $C_2^{\cdot+}$(m/z = 24), $C_2H_2^{\cdot+}$(m/z = 26) and $C_3H_3^+$(m/z = 39), with smaller amounts of CH^+(m/z = 13), C_2H^+(m/z = 25), $C_3^{\cdot+}$(m/z = 36) C_3H^+(m/z = 37) and $C_3H_2^{\cdot+}$(m/z = 38). The spectra obtained for the phenylacetylene and benzonitrile systems show similar features. In both systems the most intense peak in the electron impact spectrum is due to the molecular ion, and the loss of the neutral C_2H_2 species and the neutral HCN species respectively correspond to the production of the next most intense ions. Again this is not the case in the multiphoton absorption initiated spectra. In both systems and at both wavelengths studied the majority of the ionization arises from the small mass ions, predominantly $C^{\cdot+}$, $C_2^{\cdot+}$, C_2H^+, $C_2H_2^{\cdot+}$, $C_3^{\cdot+}$ and $C_3H_3^+$, as in the benzene system. In the fluorobenzene system under electron impact the most intense ion is again the molecular ion $C_6H_5F^{\cdot+}$ at m/z = 96, with the next most intense ion being $C_4H_3F^{\cdot+}$(m/z = 70) which corresponds to the loss of the neutral species C_2H_2 from the molecular ion. In contrast to the other systems studied the multiphoton initiated spectrum obtained at 532 nm does show an intense molecular ion. The same smaller mass ions as in the other systems are observed; $C^{\cdot+}$, $CH^{\cdot+}$, $C_2^{\cdot+}$, $C_2H_2^{\cdot+}$ and $C_3H_3^{\cdot+}$. The fluorinated ions $CF^{\cdot+}$, $C_2HF^{\cdot+}$ and $C_3H_2F^+$ are also detected. This last observation is probably a direct result of the CF bond strength being greater than the CH bond strength.

The striking differences in fragmentation patterns between the spectra obtained by electron impact and those obtained in the multiphoton ionization process indicates that the mechanisms involved in the two processes are entirely different. In an attempt to investigate the mechanism of the multiphoton ionization process the fragment ion intensities were plotted as a function of laser pulse energy for the benzene, phenylacetylene and benzonitrile systems. All of these plots show some changes in the relative fragment ion intensities in the lower energy range studied. However at higher laser pulse energies the relative fragment ion intensities become essentially constant. These observations indicate that there are two mechanisms operating, one at the lower laser pulse energies and another at the higher laser pulse energies.

Benzene

a)70eV Electron Impact

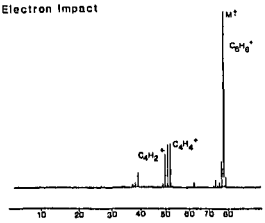

b) 532nm,30mJ

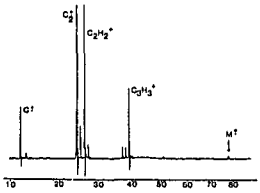

c) 355nm,10mJ

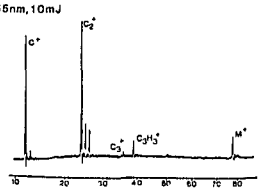

Benzonitrile

a)70eV Electron Impact

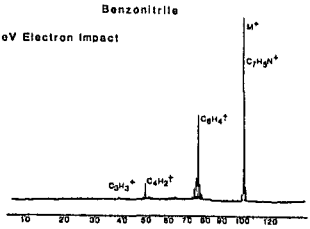

b) 532nm,30mJ

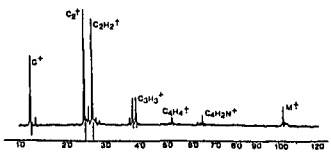

c) 355nm,12mJ

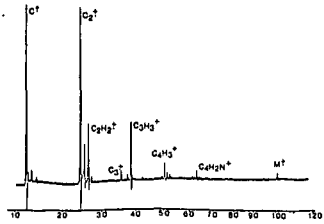

Phenylacetylene

a) 70eV Electron Impact

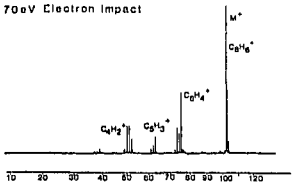

b) 532nm,40mJ

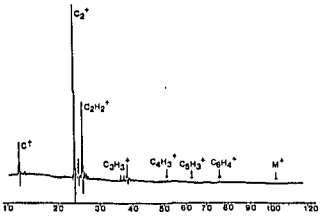

c) 355nm,13.5mJ

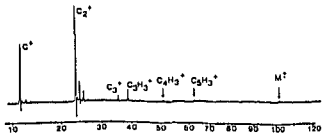

Fluorobenzene

70eV Electron Impact

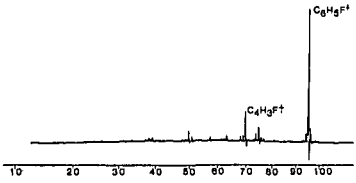

532nm, 55mJ

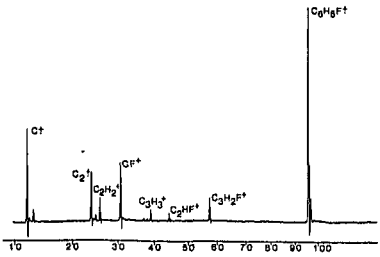

THREE-MEMBERED RING ISOMERIZATIONS IN RADICAL CATIONS: C.E. Hudson and D.J. McAdoo, Marine Biomedical Institute, University of Texas Medical Branch, Galveston, Texas 77550

The butanone enol ion derived from 3-octanone shows metastable peaks for loss of CH_3 and C_2H_5. The mechanism of these decompositions is[1]:

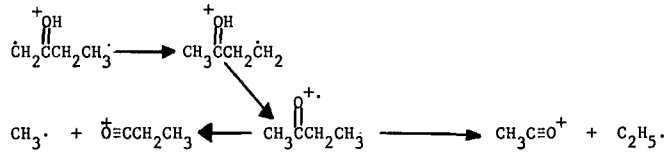

The CA spectra of the $C_2H_3D_2C{\equiv}O^+$ ions derived from labelled precursors are practically identical. $C_2H_5C{\equiv}O^+$ shows a diagnostic CA peak at m/z 42 for loss of CH_3. The peak for loss of CD_3 in $CD_3CH_2C{\equiv}O^+$ is accompanied by peaks for loss of CHD_2 and CH_2D of only 9 and 8% relative intensity respectively. Thus the hydrogen atoms of the propanoyl ion retain their positional identity, and its terminal methyl is lost nearly exclusively. Table 1 shows this region for $C_2H_3D_2CO^+$ derived from metastable $C_4(H,D)_8O^+$ precursors

	Relative Intensity for Loss of		
Precursor	CH_3	CH_2D	CHD_2
$\dot{C}H_2C(=\overset{+}{O}H)CH_2CD_3$	43	100	63
$\dot{C}H_2C(=\overset{+}{O}H)CD_2CH_3$	41	100	57

The most convenient explanation is that $CH_3\overset{+}{C}(OH)CH_2\dot{C}H_2 \rightleftarrows CH_3\overset{+}{C}(OH)CHCH_3$ is faster than formation of ionized 2-butanone. Such 1,2-hydrogen shifts are common in the chemistry of carbonium ions, but rare in free radicals.[2]

1,2-Shifts occur between certain positions of ionized butanoic acid but not others. The MI spectrum of $CD_3CH_2CH_2CO_2H^{+\cdot}$ is:

Group lost	CH_3	CH_2D	CHD_2	CD_3	C_2H_4	C_2H_3D	$C_2H_2D_2$	C_2HD_3
Relative Int.	13	<1	<1.5	100	1	16	51	5

The terminal methyl is lost with very little exchange while the same carbon is lost in the ethylene is highly exchanged. Our present picture of these fragmentations is that the ethylene loss proceeds from $\dot{C}H_2CH_2CH_2CO_2H_2^+$, which is formed reversibly while the methyl losses stem from $CH_3\dot{C}H\underline{CH_2}CO_2H_2^+$. To account for the labelling it is necessary that these intermediates do not interconvert. Nevertheless the CH_3 group which is lost in the above table comes from the underlined hydrogens, so there must be exchange between these positions. ^{13}C-Labelling data show that the methyl is lost from the positions in the indicated proportions[3]

CH_3	CH_2	CH_2	$CO_2H^{+\cdot}$
50%	33%	17%	0%

The simplest mechanism accounting for the two most prominent losses is:

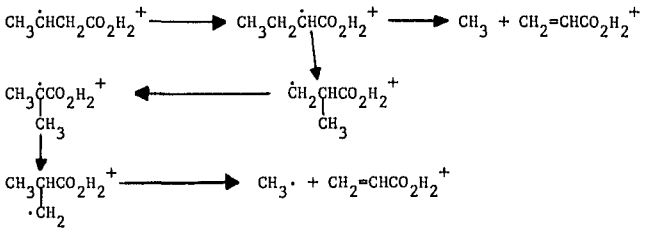

Thus α,β (or β,α) shifts of both hydrogens and carbons occur readily in ionized butanoic acid and its isomers but β,γ shifts do not occur. Such shifts, normally prohibited in radicals because the odd electron occupies an antibonding orbital in the transition state, are greatly facilitated when the radical site is conjugated with a strongly electron withdrawing group such as a protonated carbonyl. The protonated carbonyl withdraws electron density from the antiboding region and grants the transition state some carbonium ion character. Thus the lowest energy reactions of enol radical ions are intermediate in character between those of radicals and those of carbonium ions. This provides further support for the view that gas phase ionic reactions are closely akin to processes observed in conventional chemistry. The ring size preference for hydrogen abstraction in radicals, ions and radical ions is discussed in another presentation.[4]

1. D.J. McAdoo, F.W. McLafferty and T.E. Parks, J. Am. Chem. Soc. 94, 601 (1972).
2. C. Walling "Molecular Rearrangements", P. de Mayo, ed. Interscience: New York, 1963, pp 407-455.
3. D.J. McAdoo, C.E. Hudson, J.J. Zwinselman and N.M.M. Nibbering, submitted.
4. L.L. Griffin, C.E. Hudson and D.J. McAdoo, this conference.

DEPENDENCE OF FRAGMENTATION ON THE METHOD OF ENERGY DEPOSITION. Kenttämaa, H. and Cooks, R.G., Department of Chemistry, Purdue University, West Lafayette, IN 47907.

This work is concerned with the dramatic effects which stepwise excitation has on the fragmentation of some organophosphorus ions. Fragmentation behavior is seen to depend not merely on the total energy added to the ion but on whether excitation occurs promptly or in several steps.

In order to increase the internal energy of the decomposing ion, and thus to produce more structure specific fragmentation, collision induced dissociation (CID) spectra are often acquired under conditions where more than one collision is probable (1). Furthermore, it is sometimes possible to get pseudo-energy-resolved data by varying target pressure (1). Simplified theories, which are based on collision kinetics and CID cross sections at single-collision conditions, have recently been developed to interpret the relative intensities of fragments formed at high target pressures (2-5). They apply reasonably well to simple molecules, such as methane (4,5) and protonated water clusters (2). The present work shows that the relative entropic requirements of competitive reactions will become an important factor in fragmentation of more complex ion structures when multiple excitation steps are used.

Because of unfavourable critical entropies, low-energy rearrangement reactions are usually competitive with simple cleavages only at low internal energies of the parent, but their products may often not have enough energy to fragment further. If a second excitation step occurs, these ions can dissociate, thus forming products which might be absent if only a single excitation step is used. Analogously, an isomerized ion may produce peaks in the MS/MS spectrum which are absent in the mass spectrum of the neutral which corresponds the initial ion structure.

The tautomeric ions dimethyl phosphite (a) and dimethyl phosphonate (b) are differentiated on the basis of their breakdown graphs obtained by varying collision energy in low-energy CID at single collision conditions (Fig. 1). The isomerization barrier for the less stable isomer, dimethyl phosphonate, is estimated to be 0.7 eV - 1.4 eV. Isomerization occurs in competition with fragmentation at low internal energies of the parent. However, when multiple excitation steps are used (high-pressure low-energy CID), dimethyl phosphonate apparently fragments almost exclusively via dimethyl phosphite, and the breakdown graphs obtained for the ions are nearly identical (Fig. 1).

The differences in the electron ionization mass spectrum and single collision high- and low-energy CID spectra of the molecular ion of a bicyclic phosphite (1) (Fig. 2) are explained in routine fashion on the basis of different energy distributions of the fragmenting ions. However, when multiple collision CID is used, entirely new ions are

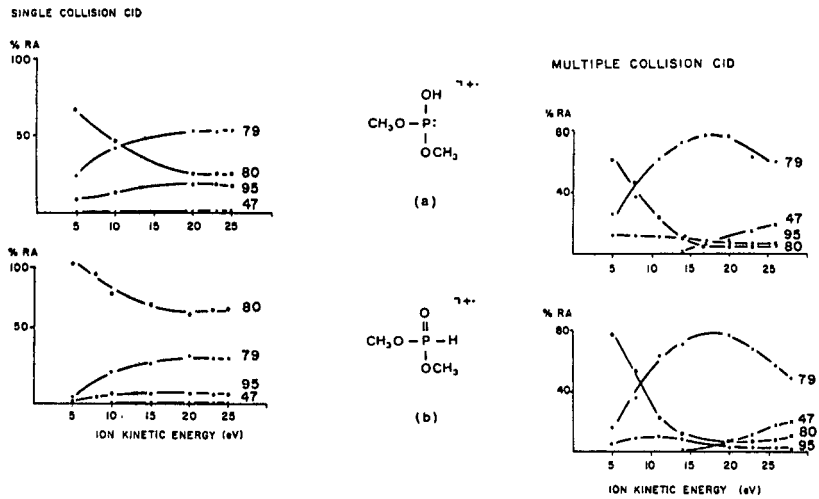

Figure 1.

formed as a result of further fragmentation of rearrangement products. The corresponding phosphate (2) provides an especially striking case of isomerization prior to CID. The fragmentation patterns of the molecular ion obtained with electron ionization (Fig. 3a), single-collision CID (Fig. 3b) and multiple collision CID (Fig. 3c) are all significantly different. In this system, energy barriers for rearrangement of the bicyclic ion to various isomeric monocyclic ions (Fig. 2) are probably lower than fragmentation thresholds (6). The internal energy deposited in the bicyclic molecular ion upon formation is large enough to overcome these barriers. When different excitation methods are used to study the molecular ion, different mixtures of isomeric ions are generated. Under multiple-collision CID, enhanced isomerization and further fragmentation of the isomerized structures produce major peaks which are absent in the spectra obtained with other excitation methods.

In contrast to the commonly encountered assumption that an increase of target pressure results in an increase in structurally characteristic high-energy fragmentations, stepwise excitation can lead to a drastic increase of the abundance of ions which arise via consecutive lowest-energy fragmentation routes. As a result, structural specificity of the ions of interest may be lost rather than enhanced.

Acknowledgements: The support provided by the Academy of Finland is greatfully acknowledged.

References:

1) Tandem Mass Spectrometry, Edited by F.W. McLafferty, John Wiley & Sons, New York, 1983.
2) Dawson, P.H., Int. J. Mass Spectrom. Ion Phys., 43 (1982) 195.
3) Douglas, D.J., J. Phys. Chem., 86 (1982) 185.
4) Kim, M.S., Int. J. Mass Spectrom. Ion Phys., 50 (1983) 189; ibid, 51 (1983) 297.
5) Ouwerkerk, C.E.D., McLuckey, S.A., Kistemaker, P.G., and Boerboom, A.J.H., Int. J. Mass Spectrom. Ion Processes, 56 (1984) 11.
6) The fragmentation characteristics of this ion have been studied earlier; see for example Kenttämaa, H., Int. J. Mass Spectrom. Ion Phys., 47 (1983) 459.

Figure 2.

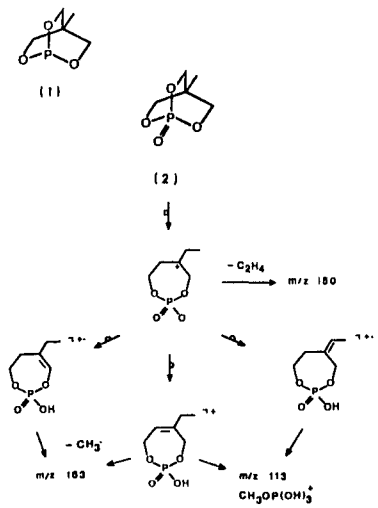

Figure 3.

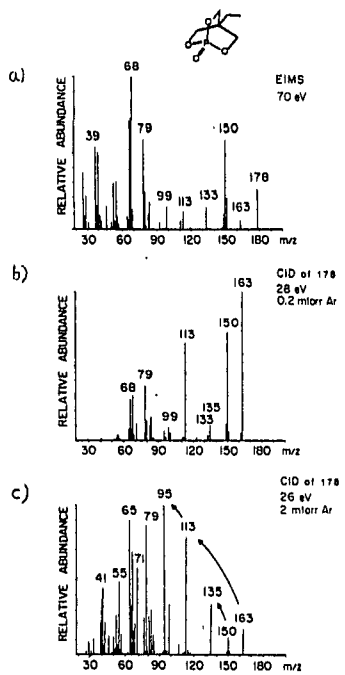

ROTATIONAL PREDISSOCIATION OF $D_2^{+\bullet}$ FORMED FROM CD_4.

A.G.Brenton, M.Guilhaus and J.H.Beynon
Royal Society Research Unit, University College of Swansea,
Singleton Park, Swansea SA2 8PP, U.K.

P.G.Fournier
L.C.A.M., University Paris, Orsay, France.

The spontaneous (unimolecular) fragmentation of ground state $H_2^{+\bullet}$ and $D_2^{+\bullet}$ can only proceed via a predissociative process [1] involving the rovibronic states of the $X^2\Sigma_g^+$ electronic state. Because of the 'simplicity' of these two ions other mechanisms for unimolecular dissociation have been discounted, such as radiationless transitions due to curve crossing. Thus in order to observe the unimolecular process $D_2^{+\bullet} \rightarrow D^+ + D^\bullet$ it is necessary to populate, in sufficient numbers, the higher rovibronic states which lie above the dissociation asymptote; these energy levels are often called quasibound states. It is found experimentally that if $D_2^{+\bullet}$ is formed from the electron impact ionization of deuterium gas, then no detectable unimolecular spectrum is observed. However, if it is formed from a deuterium-containing precursor molecule [2] then it becomes rotationally excited and spontaneous dissociations do occur. Inspection of the unimolecular spectrum shows fine structure to be present, due to predissociations from individual rovibronic states, which have lifetimes in the metastable time window. We have measured the unimolecular spectra, for each precursor molecule, to glean information about which rovibronic states are present and what their relative contributions are to a spectrum. One practical difficulty with this experiment are the very small fragment ion signal intensities, typically 10^{-17} to 10^{-18}A., requiring each spectrum to be signal averaged over long periods of time. As a consequence, in this study we concentrated with the precursor (CD_4) which produced a strong $D_2^{+\bullet}$ ion current. A total of nine quasibound states of $D_2^{+\bullet}$ have been observed and assigned from theoretical calculations [1,3]. The relative lifetimes of the fragmenting states have been investigated by varying the time after formation of the $D_2^{+\bullet}$ ions in which observations of fragmentation are made.

The translational energy spectra of $D_2^{+\bullet} \rightarrow D^+ + D^\bullet$ were recorded using a modified double-focusing mass spectrometer, details of which are given in ref.[2]. To resolve fine structure components in a metastable peak the spectrometer has to be operated at high energy resolution and capable of applying angular collimation to the ion beam.[4] As a consequence of these experimental conditions, the fragment ion signal is reduced considerably. In practice, a compromise has to be made between increasing (or decreasing) the energy/angular resolution and decreasing (or increasing) the signal. To extract the maximum information from the spectrum we divided it into a couple of regions which were individually scanned and signal averaged. This procedure was repeated several times.

When spontaneous fragmentation of $D_2^{+\bullet}$ occurs, from a quasibound state, the excess internal energy (W) above the dissociation limit is released and appears as a translational energy spread of the fragments. In the center of mass frame of reference, ions that dissociate releasing fragments which have velocities in the forward and backward directions give rise to fragment ion signals, in the laboratory frame, with energies E where

$$E = \frac{m_1}{m_2} V \pm \left(\frac{4 m_2 m_3 W V}{m_1^2} \right)^{1/2}$$

and m_1 is the mass of $D_2^{+\bullet}$, m_2 is the mass of the ionic fragment, m_3 the mass of the neutral, and V the accelerating voltage. By measuring the maximum energy spreads (E) of the structural features in the spectrum, we obtained the energy releases (W) which can then be related to the energy levels of the quasibound states of $D_2^{+\bullet}$.

A typical unimolecular spectrum is shown in Fig. 1. This was recorded at a moderate setting of the energy and angular resolution and five structural features are readily identified. The spectrum also shows some evidence of additional structural features even though they are not resolved and appear relatively weak. These weaker features were identified by scanning narrower regions at higher resolution, as shown in Fig.2. By matching the experimental energy releases W for the structural features experimentally measured with the theoretically calculated energy levels [1-3] we have made the following assignment of (v,J) states which are given in Table 1. A condition used in making Table 1 up from the above data, is that the fragmentation rate for a particular state will be large enough to produce a detectable signal in the translational energy spectrum. This

corresponds to states which have lifetimes (τ) between ~10^{-6} and 10^{-4}s. States with shorter or longer lifetimes will not fragment in sufficient numbers to be detected.

As shown in Table 1 we have been able to positively associate seven states, with evidence in some spectra for the existence of two other states, namely (10,39) and (15,30). However, it is not surprising that these are weak features and difficult to see, as the experimental lifetime window sharply limits the number of quasibound states that can be observed by translational spectroscopy for unimolecular decay. It can be shown easily that the sensitivity of detection is directly given by the formula

$$P(\tau,W) = f(W) \times \left[\exp\left(-\frac{t_1}{\tau}\right) - \exp\left(-\frac{t_2}{\tau}\right)\right],$$

where f(W) is an apparatus function, not dependent on the lifetime, t_1 and t_2 are the time-of-flight from the ion source to the beginning and the end of the field-free region. We have measured spectra in the first field free region using the High Voltage scanning method and found the spectral shape to change, which can be adequately predicted from the above relationship. From such data the relative populations ($Io_{\nu,J}$) of these quasibound states, as formed in the source, can be ascertained quantitatively. Values of $Io_{\nu,J}$ are given in Table 1 and show a fairly even population, except for (15,30) and (2,53) which are both weak features and therefore have larger errors associated with their measurements.

When other precursor species were chosen the unimolecular spectra also showed differences, although these were mostly small except for D_2O where the (21,18) state was found to dominate. These differences directly reflect the mechanism by which $D_2^{+\bullet}$ is formed within the ion source and, consequently, the initial population density of the rovibronic states.

TABLE 1 Energy levels, lifetimes and populations of the observed quasibound states of $D_2^{+\bullet}$. ν and J are the vibrational and rotational quantum numbers, W the kinetic energy release, τ the lifetime of that state, $P(\tau,W)$ the probability of detection and $Io_{\nu,J}$ the relative population of the state.

ν,J	W[meV]	τ[μs]	$P(\tau,W)$	$Io_{\nu,J}$
2,53	219.6	2.2	0.14	0.2
3,51	183.3	26.0	0.05	0.7
6,46	129.4	8.3	0.14	0.9
9,41	89.4	2.0	0.21	0.4
10,39	69.6	69.0	0.03	1.1
13,34	48.6	1.4	0.21	1.1
14,32	36.5	22.2	0.13	0.9
15,30	26.6	360.	0.01	3.3
21,18	5.2	3.	1.00	1.
23,13	1.1	170.	0.11	-

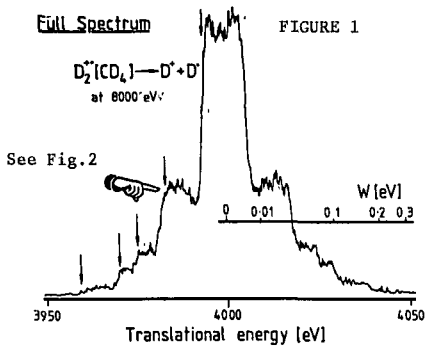

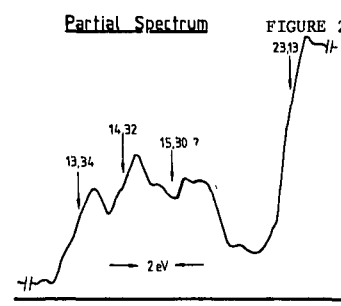

1. Maas,J.G., Van Asselt,N.P.F.B. and Los,J. Chem.Phys. 8 (1975) 37.
2. Brenton,A.G., Richard,E.G., Fournier,P.G. and Beynon,J.H. J.Chem.Phys. 79 (1983) 1834.
3. Kuriyan,M. and Pritchard,H.O. Can.J.Chem. 55 (1977) 3420.
4. Brenton,A.G., Proctor,C.J. and Beynon,J.H. Adv.Mass Spectrom. 8 (1980) 1689.

MECHANISM OF ELECTRON IMPACT INDUCED ALCOHOL ELIMINATION FROM DIALKYL MESACONATES. ANOTHER EXAMPLE OF A HIDDEN HYDROGEN TRANSFER.

A. MANDELBAUM, D. BORNSTEIN AND A. WEISZ
Department of Chemistry, Technion - Israel Institute of Technology
32000 Haifa, Israel

We have been interested for a long time in the mechanism and stereochemistry of the elimination of alcohol molecules from esters under electron impact.[1-5] We have shown that in several cyclic systems hidden hydrogen transfers play an important role in this fragmentation.[2-5] Double bond geometrical isomers seem to be the simplest system for such an investigation.

Dimethyl and diethyl citraconates and mesaconates exhibit a highly stereospecific behavior under electron impact: the mesaconates 1 eliminate an alcohol molecule while the citraconates mainly lose an alkoxyl radical from their molecular ions.

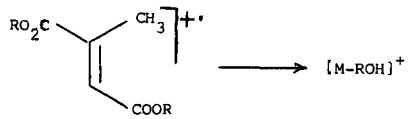

1. R = CH_3 ; C_2H_5

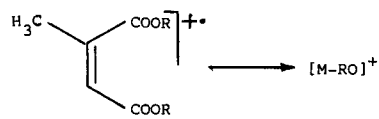

2. R = CH_3 ; C_2H_5

These results show that the geometry of the double bond is retained in the fragmenting molecular ions of 1 and 2 and the proximity of the methyl to the ester group on the other side of the double bond is a condition for the occurrence of the elimination of ROH upon electron impact.

Unsymmetrical methyl ethyl mesaconates 3 and 4 eliminate both methanol and ethanol under electron impact. Similarly the specifically labelled mesaconate 5 gives rise to both $[M-CH_3OH]^{+\cdot}$ and $[M-CD_3OH]^{+\cdot}$ ions. These results exclude the

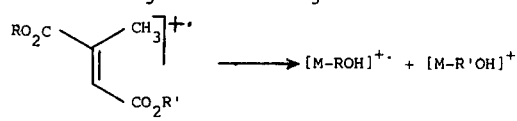

3. R = CH_3 ; R' = C_2H_5
4. R = C_2H_5; R' = CH_3
5. R = CD_3 ; R' = CH_3

simple one-step mechanism for the elimination of a molecule of an alcohol involving a transfer of a hydrogen atom from the methyl group to the alkoxy oxygen atom. Such a mechanism cannot account for the formation of the $[M-ROH]^{+\bullet}$ ions from 3, 4 and 5. The formation of these ions suggests a three-step mechanism: (a) Transfer of a hydrogen atom from the methyl group to the carbonyl oxygen of the ester group on the other side of the double bond resulting in intermediate A. The original configuration is retained prior to this H-transfer. (b) Rotation around the double bond in A. (c) Transfer of the hydrogen atom from the carbonyl group to the R-alkoxyl oxygen resulting in the elimination of ROH.

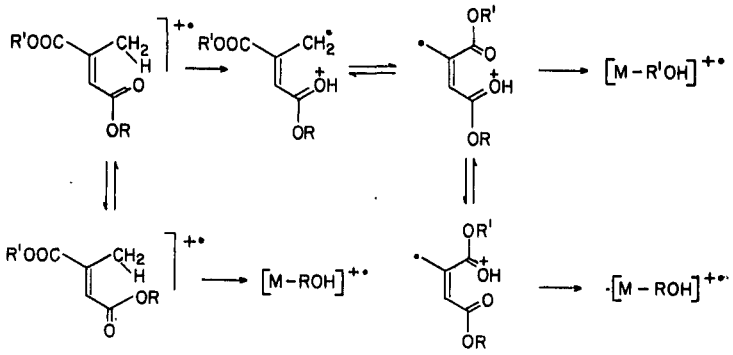

The elimination of R'OH may occur either by the one-step mechanism involving a direct H-transfer from the methyl to the R'-alkoxyl oxygen atom or by the multistep mechanism after an additional hydrogen transfer to the other carbonyl oxygen (intermediate C). The preferential formation of the $[M-R'OH]^{+\bullet}$ ion in 3, 4 and 5 indicates that the one-step process takes place at least in part.

The above results show that intramolecular catalysis plays an important role in the elimination of alcohols from esters[6], but it is not an exclusive pathway.

References

1. J. Deutsch and A. Mandelbaum, J. Am. Chem. Soc., **92**, 4288 (1970).
2. A. Mandelbaum, in "Stereochemistry", H. Kagan ed., Georg Thieme, Stuttgart, 1977, p. 138 and references cited therein.
3. R. Bar-Shai, A. Bortinger, J. Sharvit, and A. Mandelbaum, Israel J. Chem., **20**, 137 (1980), and references cited therein.
4. A. Mandelbaum, Mass Spectrom. Rev., **2**, 223 (1983).
5. I. Merksammer and A. Mandelbaum, Tetrahedron, in press.
6. M.A. Winnik, Org. Mass. Spectrom., **9**, 920 (1974).

HIGH PERFORMANCE CHROMATOGRAPHY AND THE ART OF GC-MS HAVE PRODUCED GC METABOLIC PROFILING. C.C. Sweeley, B. Musselman, M. Martin, J. Holland, Department of Biochemistry, Michigan State University, East Lansing, Michigan 48824.

Metabolic profiling involves the identification and quantitation of compounds obtained from tissues and body fluids. These analyses have been commonly undertaken using GC-MS. Developments in capillary column technology, resulting in increased resolution and reproducibility, have encouraged the development of GC-only profiling analysis. A method is described which utilizes the knowledge gained from automated GC-MS profiling and computer-assisted analysis of GC data.

A situation encountered in the analysis of specific biological fluids is that sample composition is relatively reproducible in qualitative terms. This knowledge can assist in the identification of the components. The major qualitative factor is the retention index. Knowledge of the basic composition of the sample permits use of members of the sample set itself as RI standards. A series of factors are used in a reiterative algorithm to increase confidence in the assignment of the indices, these are as follows: The first factor is concentration-based, f_c, (figure 1). Biological fluids such as urine will normally contain certain concentrations of metabolites which can be utilized in confidence factor calculations. The second factor f_r, incorporates resolution of the peak from its neighbors. The function of the factor is shown in figure 2. The factors are used to designate components that can be identified with the greatest confidence giving a high CF value where $CF = f_{RI} \times f_c \times f_r$. Components with high CF are used as retention index markers in a second reiterative pass through the data, correction of all observed RI values from these reference assignments provides maximum RI accuracy for all components in the sample.

An outline of the approach being taken in these experiments is given in schematic I. The concept of using all of the data available from the GC/integrator is encompassed in this scheme.

In situations where abnormal profiles involve unresolved peaks or assignments with low confidences, additional analyses using different temperature profiles effect changes in RI of individual components. The use of differential temperature programming results in another selective means of using retention characteristics in component determinations. The effects of column temperature on polarity and retention behavior has been documented by Grob and Grob, Chromatographia, 17, 482, (1983). We have utilized this technique to obtain characteristic retention index shifts for each of a series of compounds, these retention shifts (figure 3) can be used for confirmation of peak identity increasing the utility of HR-GC technique.

Fig 1.

CONCENTRATION FACTOR f_c

CONCENTRATION LIMITS ARE DEFINED IN LIBRARY.
COMPARISON OF RAW DATA WITH LIBRARY.

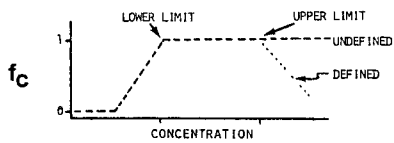

Fig 2.

RESOLUTION FACTOR f_r

COMPONENTS ARE REPRODUCIBLY RESOLVED.
f_r IS ASSIGNED FROM A COMPARISON OF RAW DATA WITH LIBRARY.

		LIBRARY				
		T	BB	BV	VB	VV
	T	1	0	0	0	0
	BB	0	1	8	.8	4
EXPT	BV	.6	7	1	5	7
	VB	.6	7	5	1	.7
	VV	.5	2	6	.6	1

Schematic I

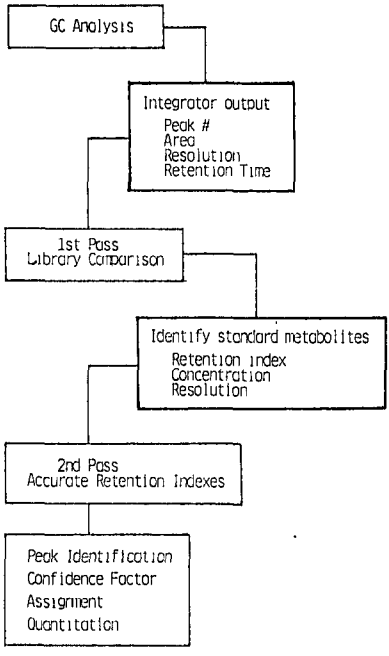

figure 3.

EFFECTS OF TEMPERATURE PROGRAM RATE ON RELATIVE RETENTION INDEX

COMPOUND	RETENTION INDEX		RI Δ
	RATE	3°C/MIN	8°C/MIN	
LACTIC		1063.5	1060	↓
GLUTARIC		1405	1400	↓
MANDELIC		1478	1473.2	o
ANISIC		1504	1503	o
ADIPIC		1508	1510	o
MALIC		1510.5	1502.5	↓
HOMOGENTISIC		1846.5	1845.5	o
SEBACIC		1896	1892	↓
INDOLE-3-ACETIC		1943	1951	↑

Automated Quantitative Routines For Profiling Priority Urinary Organic Acids

Shen-Nan Lin and Richard M. Caprioli

Analytical Chemistry Center, The University of Texas
Medical School, Houston, Texas 77030

Human urine contains hundreds of aliphatic and aromatic acids, many of which are metabolites present only at trace levels. Depending upon the particular metabolic state and dietary intake of the individual, considerable variation in concentration in many of these acids can be observed. Nevertheless, since the levels of these compounds can be profoundly altered in metabolic distress, considerable effort has been made to develop methods for an automated general screening procedure for selected organic acids in urine as a diagnostic aid for metabolic disorders.

Based on the technique of gas chromatography/mass spectrometry (GC/MS) and special quantitation software (AutoQuan, Finnigan-Mat Corp), we have developed an automated procedure for the rapid quantitative analysis of forty different organic acids which are specifically related to known acidurias. This target group of acids represents the most commonly found inborn errors of metabolism or other forms of metabolic distress in patients where screening procedures are indicated. Groups of 12 samples can easily be worked up at one time, taking about 2½ hours for the derivatization and extraction procedure for this group. An additional 40 min. per sample is then used for analysis and data processing.

The analysis requires 1 ml of urine and uses 10 μg of 4-chlorobenzoic acid as an internal standard. The trimethylsilyl (TMS) and ethoxime (EO) derivatives are made in the aqueous phase, and extracted into ethyl acetate. The solvent is removed and the residue is treated with additional silylating agent to ensure complete derivatization. This solution is then analyzed by GC/MS using a Finnigan-Mat 1020 instrument with a Durabond DB-1 fused silica capillary column (30m x 0.32mm id) with polymethyl siloxane as the bonded liquid phase at a film thickness of 1.0 μ. After injection, the oven temperature was held at 100°C for 2 min. and then programmed to 210°C at a rate of 3°C/min. The mass spectrometer was continuously scanned from m/z 160 to 400 in 1 sec.

The special quantitative software package permits automatic identification and quantitation of the target compounds without operator intervention even under conditions where retention times shift up to as much as 60 seconds or more. The mass spectrometric identification of a compound is achieved by matching the mass and intensity data for prominent ions in its mass spectrum with those of the authentic compound in the computer library. This generally consists of 7 to 12 mass and intensity data points for each compound. With a perfect match rated as 1000, the program is set to accept only a fit of 900 or better in order to positively identify a mass spectrum. Calculation of the area of a particular GC peak is achieved by integration of the most intense ion in the mass spectrum of the organic acid within the specified retention time window. The

results of the analysis are presented directly in the form of a reconstructed ion chromatogram and a quantitation list which identifies those compounds found and gives their concentration in μg/mg creatinine. The precision of the measurements are in the ± 10-15% range, considerably better than the biological deviations seen even in the same patient from day to day.

During the last two years, we have screened hundreds of patients' urine for metabolic diseases, including over 60 normals which we ran to establish baseline values. For example, in a recent case, a patient was found to have isovaleric aciduria, with very high levels of 3-hydroxy isovaleric acid, 4-hydroxy isovaleric acid, isovalery glycine, 3-hydroxy butyric acid, and mesaconic acid accumulating in the urine. Isovaleryl glycine was present at greater than 8200 μg/mg creatinine. During therapy with glycine, GC/MS was continuously used to monitor the levels of metabolites in urine to ensure that safe levels were eventually achieved. The same patient's urinary organic acid profile after 8 months of glycine therapy showed normal levels of the hydroxy isovaleric acids, and an isovaleryl glycine level of 1060 μg/mg creatinine. Besides the isovaleryl glycine, the profile looks quite normal and this indeed correlates quite well with the disappearance of the condition of the disease.

This and other examples derived from these patient studies have demonstrated the value of this automated urinary organic acids screening procedure in accomplishing its two primary objectives; 1) to verify or help diagnose organic acidurias, and ii) to follow the treatment of known diseases by following the decrease of toxic metabolites.

THE CONTRIBUTION OF BACTERIAL MICROFLORA IN METABOLIC PROFILING.

M. Stobiecki, S. A. Carr, H-J. Sievert, V. N. Reinhold and P. Goldman. Dept. of Nutrition, Harvard School of Public Health, Boston, MA 02115.

Mammalian urine contains a variety of compounds which provide information about the animal's metabolism and also how it may be influenced by diet. However, in order to correctly interpret the significance of urinary constituents it must be recognized that the nature and amount of these compounds are quite variable, due to differences in body metabolism, variations in diet and the metabolic contribution of bacterial microflora in the gut.

The goal of this study was to design a protocol based upon control of both the diet and the intestinal flora that would enable the true basal metabolic profile of an organism to be established, and to delineate the contribution of the intestinal flora to the metabolism of specific dietary constituents or administered drugs. The present report describes the differences in the urinary acid profiles of germ-free and conventional rats on chemically defined diets, and a diet to which quercetin, a known mutagen, has been added. Organic acids were extracted from urine and converted to the TMS derivatives following the procedure of Sweeley and coworkers (1). Urinary metabolites were identified by capillary column GCMS in both EI and CI modes. Components in the raw urine were also analyzed by HPLC with a scanning UV detector.

The total ion profiles obtained from GCMS experiments on derivatized rat urine extracts obtained from conventional rats fed a chemically defined diet with and without added quercetin, and germ-free rats fed a diet including quercetin are compared in Figure 1; 3-chlorophenylacetic acid (compound 15) was used as an internal standard. The effect of adding quercetin to the diet of conventional animals is readily apparent from the numerous metabolites which were recognized, including: 4-methyl-1-methoxycatechol and 4-methyl-2-methoxycatechol (8 and 10), 4-methylcatechol (12), 3-(3-hydroxyphenyl)propionic acid (24), 3-methoxy-4-hydroxyphenylacetic acid (28), 3,4-dihydroxyphenylacetic acid (34), 3-(3-hydroxyphenyl)-2-propenoic acid (35) and glucuronides of 4-methylcatechol, 4-methyl-1-methoxycatechol, and 4-methyl-2-methoxycatechol (45, 46). The latter two glucuronides and their corresponding aglycones are new, previously unreported metabolites. The phenolic acids and glucuronides of ring cleavage products of quercetin listed above were absent from the urine of germ-free rats fed quercetin (fig. 1c) indicating that these metabolic products are formed exclusively by the intestinal flora.

Although several quercetin-related glucuronides are evident in the GCMS data of the trimethylsilylated urine extract of the quercetin fed conventional rats (fig. 1a), glucuronides of some of the less volatile quercetin-related aglycons would not be expected to have sufficient volatility to chromatograph, even as the TMS derivatives. In the present study two approaches were taken to identify glucuronides: direct analysis of urine by HPLC and GCMS of silylated urine extracts hydrolyzed in methanolic HCl. Urine from conventional and germ-free rats on a defined diet and rats fed a defined diet plus quercetin were analyzed by HPLC by direct injection of urine onto a reversed phase C18 column. A UV diode array detector was used to obtain full scan spectra (190-420nm) and selected wavelength chromatograms. The latter enable components retaining the intact flavanol skeleton to be distinguished from products arising by ring cleavage. Metabolites retaining the flavanol core structure are abundant in the urines of both conventional and germ-free rats fed quercetin. Several of these components have been identified as glucuronides of quercetin and monomethylquercetin by NH3-DCI and FAB MS.

The aglycones of glucuronides present in quercetin-fed conventional rats were also detected by GCMS following methanolysis of the silylated urine extracts with CH_3OH/HCl or CD_3OD/DCl and subsequent resilylation. Under these conditions, the glycosidic bonds of the glucuronides cleave releasing the aglycones and the methyl glycoside of glucuronic acid. No previously unrecognized glucuronides were detected by this method, but 4-methylcatechol and the alpha and beta anomers of dimethylglucuronic acid were greatly elevated.

The differences in metabolic profiles between germ-free and conventional rats demonstrate that bacterial microflora contribute significantly to the degradation of dietary components. These studies clearly define the influence of the bacterial microflora in the metabolism of quercetin in the rat and have aided in establishing the true basal metabolic profile for this organism.

(1) Gates, S. C., Smisko, M. J., Ashendel, C. L., Young, N. D., Holland, J. F. and Sweeley, C. C. Anal. Chem. 50, 433 (1975).

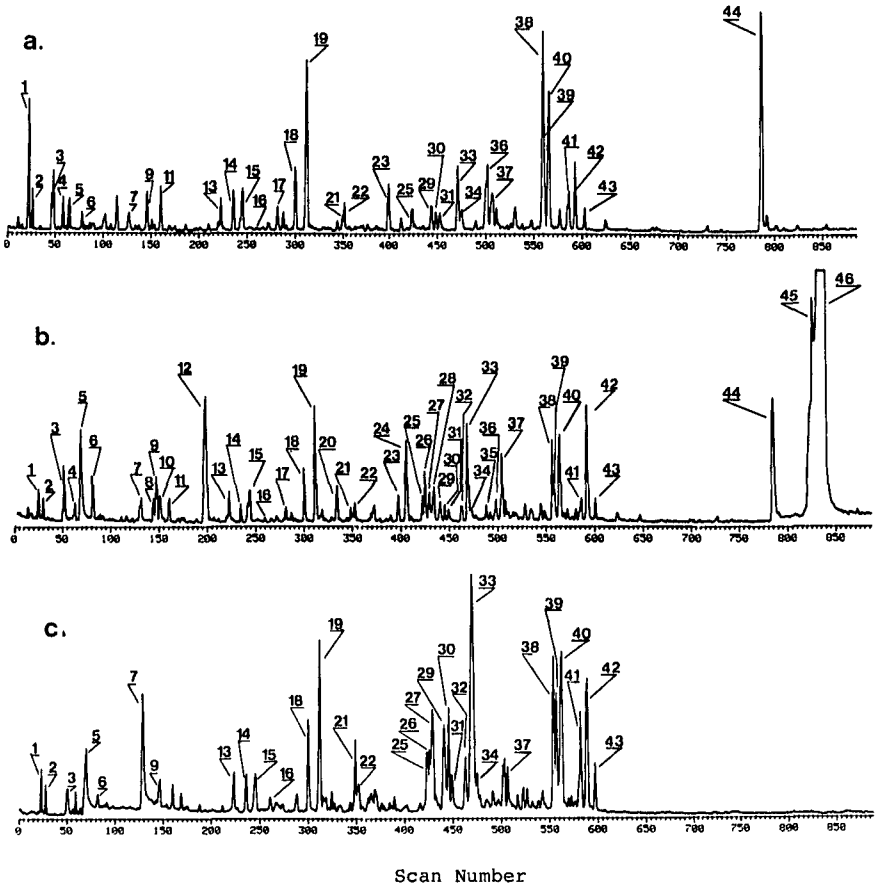

Fig. 1. The total ion profiles of urine extracts from: a) conventional rats fed a diet without quercetin, b) conventional rats fed a diet containing quercetin, and, c) germ-free rats fed a diet with added quercetin.

TRIMETHYLAMINEURIA (FISH ODOR SYNDROME) THE DEVELOPMENT OF A METHOD FOR SCREENING OF THIS INBORN ERROR OF METABOLISM.

S.S. Tjoa and P.V. Fennessey
Department of Pediatrics
University of Colorado School of Medicine
Denver, Colorado, 80262

The medical problems associated with the causes of intense body odor cover a broad spectrum ranging from psychiatric to biochemical. In many cases, the manifestation is episodic and occurs when the patient is under an excessive amount of stress or emotional problems. Often, a clear cause/effect relationship is not clear. We have been surprised over and over again that the intense recurring odor of rotting fish can be dismissed as poor hygene. Recently, a surprisingly large number of patients have been shown to have this problem. In a recent report (1) 18 patients were discussed while in a separate review (2) 6 additional patients were reported. Since January of this year, we have found 2 new cases of this disease.

The biochemistry and genetics of trimethylamineuria (TMA) has been studied in only a few cases. The largest production of TMA appears to be in the intestine where bacteria cleave organic componds containing quarternary amines to TMA and residual organics. The TMA is released into the gut cavity and absorbed into the portal circulation. In healthy individuals, the TMA is either N-oxidized to a non-smelling N-oxide or C-oxidized to form dimethylamine which is either excreted or used as a substrate for further biochemical transformations. If the liver is damaged or if the patient has an enzyme defect, the excess TMA is released in sweat, breath or urine.

We have found that the most difficult task is in the separation of a normal population from those people who suffer mild liver damage; and, further separaration of this second group from those patients that have an inborn error of TMA metabolism.

Our present protocol has combined a series of tests in an attempt to separate our population into at least three groups. The first involves a confirmation that the offending compound is TMA. This involves the gc/ms analysis of urinary head gas to both quantitate and confirm the identifty of TMA. The next test is a choline load test. The patient is given 5 gm of choline bitartrate and urine samples collected for 32 hours in 4 equal time samples. Each sample is then analyzed for TMA and a profile generated. We have found that our normals range from (0.1 - 0.8 mg TMA/mg creatinine) and patients with a defined block in N-oxide capacity range from 1.0 to 10 mg TMA/mg creatinine).

We have recently devised a test to measure the amount of TMA N-oxide in the same urine where we measure the free TMA. This additional test has allowed us to identify that subset of patients who are unable to produce TMA N-oxide. This has made it possible for us to clearly separate our patient population in such a way as to allow us to begin to review the genetics and treatment of each group.

1. E.D. Shelley and W.B. Shelley, JAMA, 251, 253-255 (1984).

2. M.A. Brewster and H. Schedewie, Ann. Clin. & Lab Sci. 13, 20-24 (1983).

GC/MS ANALYSIS OF FREE SHORT CHAIN CARBOXYLIC ACIDS BY ON-COLUMN INJECTION ON A FUSED SILICA CAPILLARY COLUMN. D.A. MALTBY, D.S. MILLINGTON AND C.R. ROE, DIVISION OF GENETICS AND METABOLISM, BOX 3028, DUKE UNIVERSITY MEDICAL CENTER, DURHAM, NC 27710.

The quantitation of free short chain (C_2-C_8) monocarboxylic acids (FFAS) in physiological fluids is difficult. This is due primarily to adsorption of these extremely polar compounds on glassware, GC injector and column surfaces. In GC analysis of these acids, adsorption is evidenced by peak tailing and "ghosting" (reversible adsorption). Most analyses of free acids have been carried out using hot glass and metal injectors and with glass packed columns. These studies have indicated that adsorption occurs primarily in the injector and in the front section of the analytical column. To minimize adsorption, either the acids must be derivatized to reduce their polarity or extensive deactivation of the injector and column is necessary. Furthermore, the polarity of the acids compromises their reproducible extraction from aqueous solutions. Additional losses may occur during concentration prior to analysis.

In an attempt to overcome these difficulties, the following simple method for analysis of FFAS has been developed using recent advances in technology:

1. Quantitation by isotope dilution GC/MS.
2. Simple ether extraction.
3. Use of free fatty acid phase (OV-351).
4. Cold on-column injection.
5. Fused silica capillary column directly coupled to ion source.

Steps 3-5 produce a chromatographic system with minimal adsorption of FFAS, as evidenced by lack of tailing or ghosting of the acid peaks (Figure 1). OV-351 has the additional advantage of producing very clean TIC chromatograms. Monocarboxylic acids, either saturated or unsaturated, run in the time frame shown in Figure 1 (100 scans = 2 minutes). Hydroxyacids, ketoacids, aromatic acids and dicarboxylic acids are not detected. Although the biological isomers isovaleric acid and 2-methylbutyric acid coelute, their EI-spectra contain differentiating fragment ions. This allows their unequivocal identification and quantitation, even when both are present in the same sample.

Isotope dilution analysis allows the use of a rapid and simple ether extraction, since the internal standard/analyte ratio is independent of any losses in recovery. Figure 2 shows a typical standard curve obtained for acetic acid using 50 nanomoles of $^2H_3$-acetic acid as internal standard. Similar curves have been obtained for the other acids. This method has been applied to the analysis of FFAS in urine and serum from patients with various metabolic disorders, including propionic acidemia, methylmalonic aciduria, isovaleric acidemia and Reye's syndrome.

Patients with these metabolic disorders typically excrete elevated amounts of short-chain acylcarnitines. Carnitine (3-hydroxybutyrobetaine) may be assisting the removal of toxic acids that accumulate in these patients. Specific identification of these acylcarnitines has been shown to be much more useful in the diagnosis of these disorders than direct analysis of FFAS. A method using high resolution FAB/MS has been developed[1], but this method cannot distinguish between positional isomers such as isovalerylcarnitine and 2-methylbutyrylcarnitine. In addition, the advanced instrumentation is not available to most hospital research labs. We have applied the new analytical method for FFAS to identify and quantify these acylcarnitines in urine after their partial purification by ion-exchange chromatography. The acyl groups were liberated by mild alkaline hydrolysis, then extracted and analyzed as the free acids. Deuterium-labelled analogues of the acylcarnitines of interest were employed as internal standards. A comparison of quantitative data obtained by this method with isotope dilution FAB and a radioenzymatic assay for total acylcarnitine is given in Table 1.

1. Millington, D.S., Roe, C.R. and Maltby, D.M. Biomed. Mass. Spect. 11, 236 (1984).

Figure 1

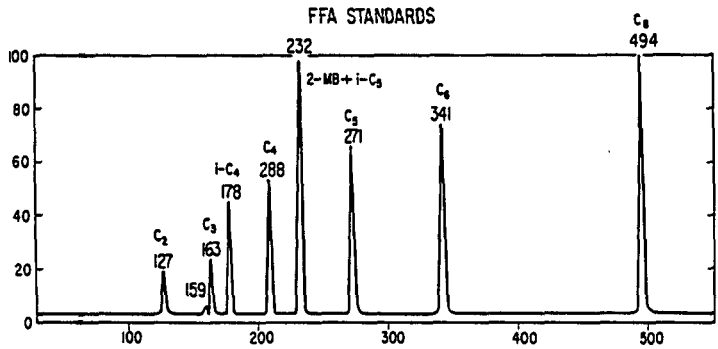

Figure 2

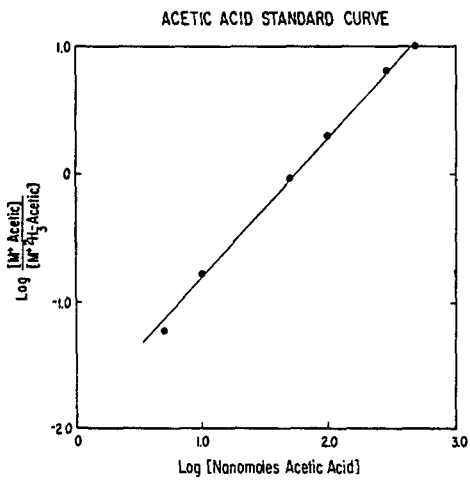

Table 1

ISOVALERYLCARNITINE IN ISOVALERIC ACIDEMIA
(Nanomoles/ml Urine)

Sample	Hydrolysis	FAB	REA
C_4	15721	16380	19000
E_1	3826	3791	3894
F_2	271	284	270

MUSCLE METABOLISM OF BRANCHED CHAIN AMINO ACIDS IN TRAUMA-SEPSIS.

J. H. McReynolds; J. M. Hassett; F. R. Roche; Y. K. Ho; T. D. Paul, M. Anbar & J. R. Border. Departments of Biophysical Science and Surgery, State University of New York at Buffalo; Buffalo, NY 14214.

Metabolic alterations following trauma are an important aspect of patient care. A hypercatabolic state is typical of most illnesses with a 100% increase over basal values common for burns or traumatic injury. Muscle protein catabolism in this state provides the liver with amino acids for acute phase protein synthesis and gluconeogenic substrates for caloric needs of other organs. Some of the branched chain amino acids are oxidized by the muscle as an alternate fuel. This oxidation is believed to limit the liver's synthetic capability resulting in enhanced gluconeogenesis, conversion of the aromatic amino acids into false neurotransmitters, and concurrently liver degradation of normal hepatic proteins to replace branched chain amino acids consumed by muscle. Sepsis or infection may occur as a complication leading to further demands for re-directed hepatic protein synthesis. Normal metabolic control is altered so that insulin resistance occurs, and while glucose utilization decreases, gluconeogenesis remains elevated by continued proteolysis. All of the above factors predispose the patient to eventual multiple organ failure.

Nutritional support mixtures enriched in branched chain amino acids have been utilized based primarily on in vitro and animal model evidence of these amino acids' ability to promote protein synthesis. This type of nutrition has not been shown to increase protein synthesis or to improve outcome in patient studies reported to date. Branched chain nutrition may have benefits other than muscle protein sparing, such as providing muscle energetic needs and maintaining hepatic capacity for stress related protein synthesis.

By measuring amino acid and branched chain keto acid concentration differences across the leg in a group of five closely matched trauma ICU patients, we are able to estimate muscle utilization of branched chain substrates. Amino acids were analyzed by an automated HPLC ion exchange method. The branched chain keto acids were quantitated by GC-CIMS-MID using d_3KIV and d_3KIC as internal standards. The BCKAs were chromatographed as the quinoxalinal-TMS derivatives and the protonated molecular ions monitored on a DuPont 21-491 GC-MS with accelerating voltage MID unit controlled by an INCOS data system. Arterial amino acid concentrations were found to be in the high normal range. Standard caloric and amino acid support (25% BCAA content) was used in this study at levels ranging from 15 - 40 Kcal/kg/dy and 0.5 to 2.6 gms protein/kg/dy. Arteriovenous differences showed, in particular, large releases of alanine and significant releases of phenylalanine and of the branched chain amino acids and keto acids. Branched chain oxidation was estimated by comparing branhced chain substrate release to the branched chain available based on measured phenylalanine release and muscle protein amino acid content.

In this group of patients we found that nutritional support did not result in branched chain uptake by muscle or any apparent reduction in proteolysis. We also found that a significant fraction (25-30%) of the branched chain amino acids are oxidized in muscle with no apparent preference for the oxidation of any single substrate.

This method can estimate muscle branched chain substrate utilization and thus will be useful in evaluating the benefit of various nutritional support therapies. Since indwelling catheters are common for ICU treatment, longitudinal studies are possible with practically no added risk to the patient.

ALTERED METABOLIC PROFILES OF VALPROATE AND ENDOGENEOUS ACIDS IN A PATIENT WITH REYE'S SYNDROME

T. Kuhara, Y. Inoue, T. Shinka, M. Matsumoto and I. Matsumoto

Department of Biochemistry, Institute of Human Genetics, Kanazawa Medical University, Uchinada, Ishikawa, 920-02, Japan

In 1963 Reye and his associate described a syndrome of acute encephalopathy and fatty degeneration of the viscera in infants and children. The real cause of Reye's syndrome is not clearly understood at present. Data supporting the multiple causes (viruses, environmental factors and host genetic factor) for Reye's syndrome are increasing. Recently, an anticonvulsant drug, valproate, has been incriminated as the cause of Reye's syndrome. However, it is unclear whether valproate is really an important factor in the pathogenesis of Reye's syndrome. Even though, the biochemical mechanism has not been clarified yet.

Valproate is a branched medium-chain fatty acid. This drug is effective for the treatment of several types of epilepsy and is accepted to be relatively safe. Only a minute portion of a very large number of patients on VPA therapy exhibited irreversible liver injuries. Genetic or aquired biochemical differences between these cases and those without such serious adverse effects are not clearly understood. Only one report has recently shown biochemical abnormality in the metabolism of valproate in a 7-year-old boy with fatal hepatic failure (Kochen et al. 1983). This paper describes another case with Reye's syndrome, in which the altered metabolic profiles of valproate as well as of endogeneous acids and the case history are different from those already reported.

The major metabolic pathway of valproate in man is the glucuronide conjugation. 2-n-Propyl-3-oxovalerate (β-keto-VPA) is the second major metabolite. The amounts of 2-n-propylglutarate, the end product of ω--oxidation is under 20% of that of β-keto-VPA.

A 6-year-old girl admitted to our hospital was diagnosed as having Reye's syndrome. She had been well until she had a prodrome of mumps. Prior to admission swelling of parotid gland, high fever and delirium were followed by generalized seizures. She was comatose on admission. Serum levels of GOT, GPT and ammonia were elevated. CT scan showed mild brain edema. While mannitol, glycerol, phenobarbital and valproate were administered, her illness rapidly progressed and her respiration was of Cheyne-Stokes type on the 4th hospital day. Electron microscopic examination revealed abundant fat deposits in the muscle fibers compatible with Reye's syndrome. Despite intensive supportive cares, she died on the 24th hospital day. Valproate was administered from the 2nd to 5th

hospital day and the urine sample was collected for organic acid analysis on the 3rd hospital day.

The most striking abnormality in our patient was the complete lack of β-keto-VPA. The same finding was reported by Kochen et al. on a 7-year-old boy with fatal hepatic failure resembling Reye-like syndrome. β-keto-VPA is formed via β-oxidation in mitochondria. The lack of this metabolite in both patients strongly supports that this branched medium-chain-fatty acid can not be metabolized in Reye's syndrome due to mitochondrial disfunction.

Markedly increased excretion of 2-n-propylglutarate was found in our patient. The urinary concentration of this metabolite was 330 μg/mg creatinine. On the contrary, in the patient reported by Kochen et al., the quantity of this metabolite was greatly decreased, but still detectable. ω-Oxidation of fatty acids appears to be enhanced, which occurs in extramitochondria. ω-Hydroxylation of drugs is catalized by the microsomal mixed function oxidase system located in the smooth endoplasmic reticulum of the liver and other tissues. Further dehydrogenation to form corresponding aldehyde, and then the carboxylate takes place in the cytosols. Proliferation of smooth endoplasmic reticulum has been previously reported in Reye's syndrome.

The lactate level was greatly elevated to 18 μmole/mg creatinine (20 times higher than the control). The ketone bodies were not detected. The excretion of adipate was greatly elevated. The quantity of suberate as well as monounsaturated suberate were also increased. This acid pattern was compatible with Reye's syndrome. Any abnormal metabolite indicating the inherited disorder in the metabolism of amino acids or organic acids were not detected by the analyses of organic acids and amino acids.

It was demonstrated that enough glucuronidation took place even in this terminal stage in our patient. Its concentration was 183 μg/mg creatinine. The amount of urinary free VPA was 34.8 μg/mg creatinine. The serum VPA concentration was 82 μg/ml. Glucuronidation occurs extramitochondria. The activity of glucuronyl transferase is found in the microsomes of liver and other tissues. Kochen et al were unable to detect VPA-glucuronide in the urine of their patient and suggested that glucuronidation is impaired due to hepatic failure.

We have confirmed, for the first time, suppressed beta-oxidation of VPA due to mitochondrial failure and markedly enhanced ω-oxidation of VPA in this disease. It seems that these findings are compatible with Reye's syndrome. As our patient had been healthy and never received this drug before, it is difficult to blame VPA for RS. It appears that the altered VPA metabolism was caused as a result of Reye's syndrome, in another words, just the reflection of Reye's syndrome. The possibility, however, can not be ruled out that VPA or its metabolites accerelate pre-existed hepatic mitochondrial damage in RS.

FTMS FOR ANALYSIS OF HIGH MASS AND INVOLATILE MOLECULES:

Carl F. Ijames and Charles L. Wilkins; Department of Chemistry, University of California, Riverside, California 92521-0403.

Mass spectrometric investigation of high mass and involatile molecules is a topic of considerable current interest. Fourier transform mass spectrometry (FTMS), with its demonstrated ultrahigh resolution capabilities is an attractive approach to such research, provided that current "soft" desorption/ionization techniques can be adapted to the low pressure requirements of FTMS. To maximize resolution in FTMS, operating pressures of 10^{-8} torr or lower are required. Also, since FTMS is a pulsed technique, the desorption method chosen ideally would be capable of operating in a pulsed fashion. We are currently pursuing laser desorption (LD) and Cs^+ particle induced desorption (PID) FTMS in our laboratory.

To investigate the performance of LD-FTMS, a CO_2 laser was coupled to a Nicolet FTMS-1000, with samples introduced through the direct insertion probe lock. Initial experiments utilized a glass capillary sample holder with neat samples. Compounds investigated include tetraphenyl porphyrin Fe(III) chloride (TPPFeCl), tetraphenyl porphryin Fe(III) mu-oxo dimer ($(TPPFe)_2O$), vitamin D_3, tetracycline, Gramicidin S, and Gramicidin (Dubos). All but the Gramicidins gave excellent positive ion spectra, yielding cationized molecular weight information as $[M+Na]^+$ and $[M+K]^+$, and also yielding interpretable structural fragments. The highest mass ion observed was the $[M+K]^+$ ion from $(TPPFe)_2O$ at m/z 1391. Also, negative ion spectra of vitamin D_3 and tetracycline were recorded with sensitivity equal to the positive ion spectra. By dissolving the Gramicidins in methanol and doping with either NH_4Cl or KBr, then evaporating to dryness on a stainless steel sample holder, good spectra were obtained. Gramicidin (Dubos) is a mixture of four polypeptides, and an $[M+K]^+$ ion was observed for each component at m/z 1881, 1898, 1921, and 1935. Once more, useful fragment ions were also observed. Finally, unprecedented laser desorption mass resolution of 53,700 for the m/z 668 ion of TPPFeCl was obtained.

To compare LD-FTMS with conventional instrumentation, the same compounds were investigated using a VG ZAB 1 HF double focusing mass spectrometer equipped with a Xe PID source. Spectra of vitamin D_3 and tetracycline dissolved in glycerol gave both positive and negative ion spectra very similar to the LD spectra. In the positive spectra the cationized species were replaced with the equivalent proton attachment products, and a large glycerol background was observed. The major ions of the sample were approximately the same intensity as the major ions of the glycerol, so the interference with weaker fragment ions was severe. Surprisingly, the TPPFeCl yielded only a negative ion spectrum, and then only when dissolved in Triton X100. One concern has been that the different time scales of the two experiments would yield substantially different spectra. The LD-FTMS spectra were recorded by storing the desorbed ions for 10 seconds to allow the large desorbed neutral population to be pumped away, while the time before detection in the ZAB is on the order of microseconds. Our experiments show that qualitatively the results are the same.

FOURIER TRANSFORM ION CYCLOTRON RESONANCE MASS SPECTROMETRY: ANALYTICAL AND CHEMICAL APPLICATIONS

Alan G. Marshall, Tao-Chin Lin Wang, Steven L. Mullen, and Ivan Santos

Departments of Biochemistry and Chemistry
The Ohio State University
140 W. 18th Avenue
Columbus, OH 43210

With the advent of commercial FT-ICR spectrometers in 1981, the advantages of broad-band ICR excitation/detection predicted and demonstrated ten years ago (1) are now generally available to mass spectrometrists, and have recently been reviewed (2). Some representative recent applications are given below.

Thermally sensitive, low-volatility samples (e.g., metal clusters)

Thermally sensitive, high-mass (MW > 1000), low-volatility (< 10^{-7} torr) samples are readily observed by FT/MS using an ordinary solids probe. An FT/MS spectrum of $H_2(\eta^5\text{-}C_5H_5)RhOs_3(CO)_{10}$ (see below) was obtained at a sample pressure of 2 x 10^{-8} torr: i.e., 2-3 orders of magnitude lower than required for a conventional magnetic sector or quadrupole source. Each multiplet exhibits the isotopic pattern characteristic of $RhOs_3$; thus, the metal stoichiometry may be determined from any multiplet. Peaks corresponding to the loss of each of the ten carbonyl groups are clearly visible, further corroborating the molecular formula (3). The lowest-mass peak corresponds to the loss of $Rh(C_5H_5)$.

Although x-ray diffraction can determine metal cluster geometry to high accuracy, it cannot necessarily distinguish (for example) Ru_2Os_2 from $RuOs_3$ in $H_2Ru_xOs_y(CO)_{13}$. However, an FT/MS spectrum at 97°C clearly identifies $H_2RuOs_3(CO)_{13}$ as the correct formula (see below). Other examples have recently been reported (4).

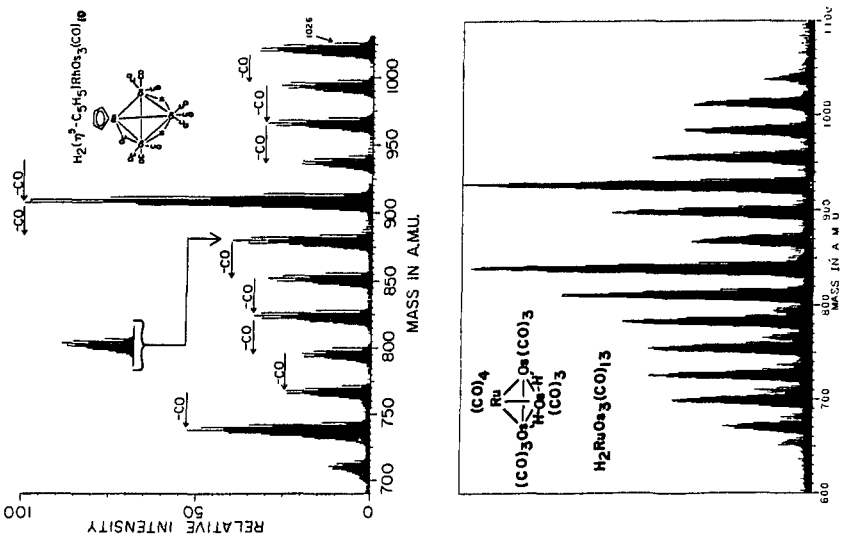

Gas phase basicity

The high sensitivity and mass resolution of FT/MS are well suited to the determination of gas-phase acidities and basicities. A typical basicity determination is shown below for a mixture of cubane with cyclohexanone. At equilibrium (> 1 sec), the peak area for protonated cubane is slightly higher than for protonated cyclohexanone, establishing the gas-phase basicity of cubane as about 197 ± 2 kcal/mole. We are extending such measurements to other unusual and/or biological molecules (e.g., dodecahedrane).

Laser desorption/ionization

Laser desorption/ionization readily yields mass spectra of underivatized involatile compounds. For example, a positive-ion spectrum of daunorubicin (daunomycin) is shown at the right. Daunorubicin is closely related to doxorubicin (adriamycin), one of the most widely used anti-tumor agents.

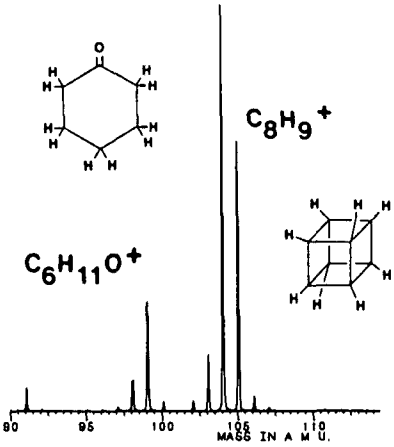

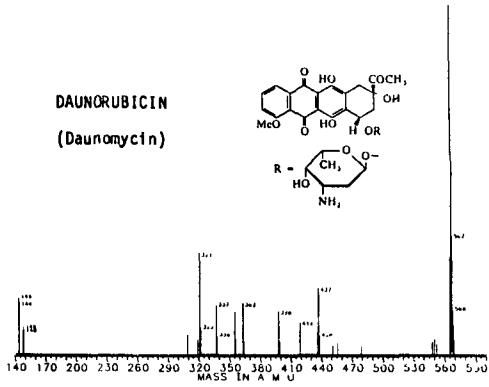

Electron ionization/Chemical ionization

Chemical ionization spectra are readily obtained in FT/MS by self-C.I. In many cases (e.g., phenobarbital, not shown), the parent neutral molecule has a higher proton affinity than its daughter fragment ions. If a short delay period (ca. 1 sec) is introduced between ion formation and ion detection, proton transfer to neutral parent molecules can yield $(M+H)^+$ as the strongest (i.e., "base") peak. Switching from E.I. to self-C.I. thus requires no change in hardware, and can even be done on alternate scans.

[This work was supported by N.I.H. Grant #1 R01 GM31683.]

1. Comisarow, M. B. & Marshall, A. G. (1974) Chem. Phys. Lett. 25, 282-283; 26, 489-490.
2. Johlman, C. J., White, R. L. & Wilkins, C. L. (1983) Mass Spectrometry Reviews 2, 389-415.
3. Shore, S. G., Jan, D.-Y., Hsu, W.-L., Hsu, L.-Y., Kennedy, S., Huffman, J. C., Wang, T.-C. L. & Marshall, A. G. (1984) "A Boroxine Supported Triosmium Oxymethylidyne Cluster System, $[(\mu\text{-}H)_3(CO)_9Os_3CO]_3(B_3O_3)$, its Structure and its Conversion to Halo and Phenyl Methylidyne Complexes," J. Chem. Soc. Chem. Commun. 392-394.
4. Hsu, L.-Y., Hsu, W.-L., Jan, D.-Y., Marshall, A. G. & Shore, S. G. (1984) "Synthesis and Spectra of $(\eta^5\text{-}C_5H_5)RhOs_2(CO)_9$ and $H_2(\eta^5\text{-}C_5H_5)RhOs_3(CO)_{10}$; Crystal Structure of $(\eta^5\text{-}C_5H_5)RhOs_2(CO)_9$," Organometallics 3, 591-595.

GAS CHROMATOGRAPHY/MULTIPHOTON IONIZATION FOURIER TRANSFORM MASS SPECTROMETRY

T.M. Sack, D.A. McCrery, and M.L. Gross
University of Nebraska-Lincoln
Lincoln, Nebraska 68588

Multiphoton ionization(MPI) using ultraviolet laser light has emerged as a promising new technique in mass spectrometry. It is a highly efficient soft ionization method which at higher laser powers is capable of inducing extensive fragmentation analogous to electron ionization. Furthermore, in resonance enhanced MPI, a dramatic increase in selectivity can be realized because the photon energy corresponds to an allowed transition in the absorbing molecule.

In many cases, however, components of real mixtures are similar in their chemical and optical properties; thus, wavelength selectivity is more difficult to achieve. A useful approach to this problem is the coupling of the powerful separation capability of a gas chromatograph with a MPI mass spectrometer (1). The demonstrated characteristics of such a combination using a time-of-flight (TOF) mass spectrometer are selectivity, resulting from the chromatography and the component absorption properties, and very high sensitivity, due to the efficiency of the multiphoton absorption process.

We have coupled a capillary gas chromatography via a pulsed valve interface (2) to a Fourier transform mass spectrometer (FTMS) by utilizing an MPI source. The FTMS is well-suited for this application because, like the TOF, entire spectrum can be acquired with each laser pulse(multiplex advantage); however, unlike the TOF, ions can be monitored at very high resolving powers and accurate mass measurements of stored ions can be provided. Indeed, Irion et al. have shown the capabilities of an MPI-FTMS in a recent publication(3).

The laser utilized in this study was a Nd/Yag, frequency quadrupled to give 266 nm light, with a pulse energy of 5-10 mJ. The laser was pulsed into the cell at 50-100 ms after the GC effluent pulse, and 100-500 ms later the detection was pulsed on.

Figure 1 shows a typical reconstructed chromatogram for a test mixture of polyaromatic hydrocarbons(PAH) ionized both by 15 eV electrons and 266 nm photons. One notes the different relative peak heights for the

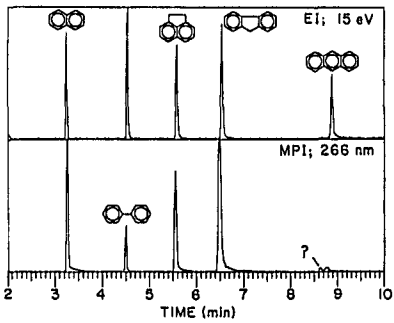

Figure 1

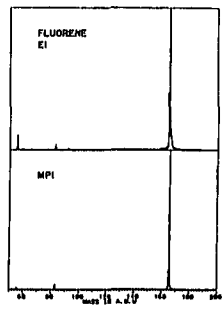

Figure 2

two chromatograms, which suggests that the cross-sections for MPI at 266 nm are quite different than those for electron ionization. Furthermore, a small impurity appeared in the MPI chromatogram that was not present in the EI chromatogram. This peak was found to be due to phenanthrene which was present as an impurity in the anthracene at a level of 2% as determined by using standard addition. This fact reveals that the phenanthrene ionizes approximately 50 times as efficiently as the anthracene using 266 nm MPI.

Representative EI and MPI wide-band spectra of fluorene were acquired in the GC mode (Fig. 1) and are shown in Fig. 2. Very little fragmentation

for these compounds was observed with the unfocussed laser beam. However, with a tightly focussed beam, fragmentation in excess of that induced by 70 eV electrons was observed.

The sensitivity of the GC/MPI-FTMS system is of significant interest if this technique is to be analytically useful. Therefore, both the limit-of-detection and the linear dynamic range were evaluated for naphthalene. Figure 3 shows the measured dynamic range from the detection limit of 10 pg to the point where space-charge effects destroy the linearity of response. At this point, no further increase in S/N is

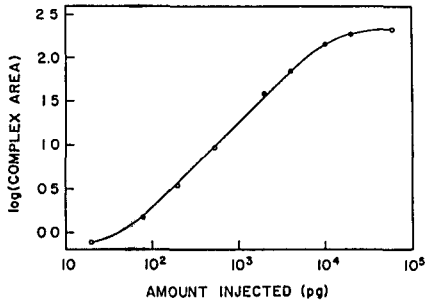

Figure 3

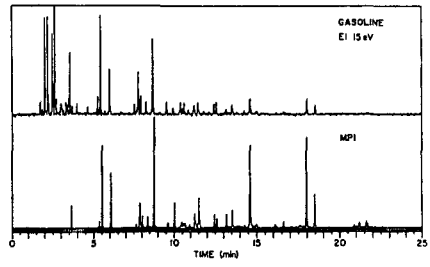

Figure 4

observed with increasing amounts of sample injected. One could expect to lower the detection limits by employing a tunable UV laser which could be tuned to the wavelength of maximum absorption for the sample of interest.

Spectral acquisition in the wide-band mode limited the mass resolution to <2000 (FWHH) for 16k data sets, but higher resolution spectra could be obtained with longer pump-out delays by using narrow band (heterodyne) mode. The sensitivity using either low or high resolution conditions was approximately the same; however, the specificity of an analysis could be greatly enhanced by operating at the high resolving powers provided by the FTMS. In fact, we could easily acquire narrow band spectra of the GC eluants at 20,000-30,000 mass resolution. The highest resolution observed was 87,000 for the m/z 128 molecular ion of naphthalene.

The GC/MPI-FTMS performed equally well with a real mixture consisting of a commercial gasoline sample. Figure 4 shows the comparison of the EI and MPI reconstructed chromatograms for gasoline. Because all the aliphatic components of gasoline have ionization potentials greater than 9.3 eV (corresponding to absorption of two photons of 266 nm light), they do not appear in the MPI trace. Thus, the selectivity due to the I.P.'s could be an extremely useful tool for identification of the aromatic components in complex samples such as fossil fuels, which frequently contain hundreds of compounds. Furthermore, the use of a tunable laser source would greatly enhance the selectivity of this technique by allowing one to choose the optimum wavelength for a particular analysis.

In conclusion, the GC/MPI-FTMS has been shown to provide the selectivity, sensitivity and resolution predicted for the method. The future of this technique possibly lies in the sensitive and highly specific detection of target compounds by high resolution single or multiple-ion-monitoring, such as is required for trace analysis of environmental contaminants.

REFERENCES

(1) G. Rhodes, R.B. Opsal, J.T. Meek, and J.P. Reilly, Anal. Chem., 1983, 55, 280.
(2) T.M. Sack and M.L. Gross, Anal. Chem., 1983, 55, 2419.
(3) M.P. Irion, W.D. Bowers, R.L. Hunter, F.S. Rowland, and R.T. McIver, Jr., Chem. Phys. Lett., 1982, 93, 375.

RECENT DEVELOPMENTS WITH THE TANDEM QUADRUPOLE-FOURIER TRANSFORM MASS SPECTROMETER

Robert T. McIver, Jr.*, Richard L. Hunter and William D. Bowers

Department of Chemistry
University of California
Irvine, California 92717

A year ago we began working with a tandem quadrupole-Fourier transform mass spectrometer (QFT-MS). In QFT-MS, ions produced in a quadrupole mass spectrometer are injected axially into a superconducting electromagnet where they are trapped in an analyzer cell and detected by Fourier transform mass spectrometry (FT-MS). The idea for this instrument arose from the realization that FT-MS is a versatile and sensitive means for detecting ions, but an alternative means was needed for producing the ions and handling the high gas loads associated with GC, LC and FAB.

Figure 1 illustrates the concept of the QFT-MS. Ions extracted from an ion source are injected into a first set of quadrupole rods (Q1). Q1 can be operated in the RF-only or the RF/DC mode to transmit ions in a selected region of the mass spectrum. It functions as a bandpass filter having a variable high mass and low mass cutoff. Unwanted ions are rejected by Q1 while the ions of interest are transmitted.

Next, the ion beam enters a second quadrupole mass filter (Q2) which normally is operated in the RF-only mode. The purpose of Q2 is to guide the ion beam through the intense fringing fields of the superconducting magnet that surrounds the FT-MS analyzer cell. As the ions enter the homogeneous region of the magnetic field, they are decelerated and trapped in the FT-MS analyzer cell. Once the ions are trapped in the analyzer cell, FT-MS detection can be performed in the conventional manner.

The guiding quadrupole mass filter Q2 is a key feature of this design because without it few ions would be able to pass to the FT-MS analyzer cell. The magnetic mirror principle, which is utilized in plasma physics for the containment of ionized gases, predicts that ions leaving the source of the quadrupole mass spectrometer (at a magnetic field strength of about 0.02 T) will be decelerated and reflected backwards as they approach the strong magnetic field (7 T) around the analyzer cell. However, Q2 operated in the RF-only mode overcomes this problem because it focuses the ion beam and directs it precisely down the axis of the solenoidal magnet. The ions are not significantly decelerated by the magnetic mirror effect because they do not encounter the off-axis magnetic lines of force. We have modeled and studied the trajectories of ions in quadrupolar electric fields and inhomogeneous magnetic fields. The results of these calculations will be presented in a separate publication.

QFT-MS signals for the molecular ion region of pyrene are shown in Figs. 2 and 3. Figure 2 is an expanded portion of a single acquisition from m/z 185 to m/z 215 for ions injected from the source of the quadrupole mass spectrometer into the analyzer cell. Notice that the peak at m/z 203, the carbon-13 component of the pyrene molecular ion, has a relative abundance very close to the theoretical value of 17.8%. Even the peak at m/z 204, the molecular ion with two carbon-13's, is very close to its theoretical relative abundance of 3.0%. Figure 3 shows excellent signal-to-noise and mass resolution from a single 20 kHz narrowband scan for the pyrene molecular ion at m/z 202. About 1 μg of pyrene placed on the direct insertion probe of the quadrupole mass spectrometer gave a very stable ion signal for several minutes.

Figure 1 shows that the QFT-MS instrument is conceptually similar to a triple quadrupole mass spectrometer. The main difference is that mass analysis and ion detection are performed in the QFT-MS by a Fourier transform analyzer cell instead of a third quadrupole and an electron multiplier. MS/MS experiments involving low energy collision-induced dissociation of ions are readily performed with triple quad mass spectrometers, and similar experiments can also be done with the QFT-MS instrument. Figure 4 shows an MS/MS experiment performed with collision gas pulsed into the region of Q2. Bromobenzene molecular ions selected by Q1 were collided with N_2 at a pressure of approximately 1×10^{-4} Torr. The collision gas was pulsed into the manifold for 100 ms using an automobile fuel injector valve. Figure 4 shows the QFT-MS signal for the daughter ion m/z 77. The mass resolution, $M/\Delta M$ 110,000, is far greater than can be achieved in daughter ion mass spectra obtained with triple quadrupole and sector MS/MS instruments.

Preliminary results with the QFT-MS are very encouraging. The feasibility of injecting and detecting ions at high resolution has been demonstrated, and it is clear that the quadrupole is capable of passing large ion currents to the FT-MS analyzer cell. All our experiments with the prototype instrument have been done with a needle valve for adding liquid samples and a direct insertion probe for solids. The prototype instrument does not have a sufficient pumping capacity to handle a GC or LC inlet, but appropriate modifications to the manifold will be made during the coming months so that these experiments can be attempted.

Acknowledgements: The equipment for these experiments was provided by the Finnigan Corporation. We are grateful to Dr. R. E. Finnigan, M. S. Story and Prof. J. W. Amy for technical assistance and support.

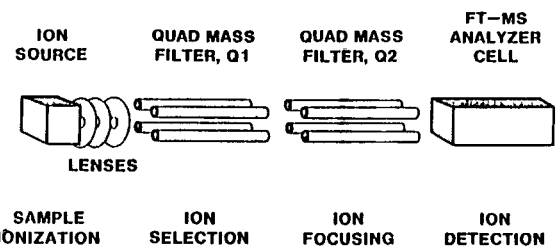

Fig. 1 Block diagram of tandem quadrupole-Fourier transform mass spectrometer (QFT-MS)

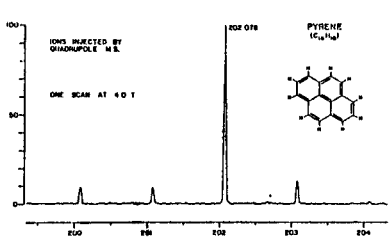

Fig. 2 QFT-MS signals for pyrene ions injected by quad into FT-MS.

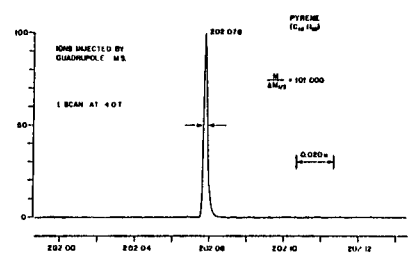

Fig. 3 High resolution QFT-MS signals for molecular ion of pyrene.

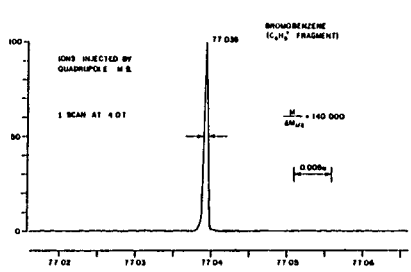

Fig. 4 Demonstration of MS/MS with the QFT-MS instrument. Daughter ions from CID on bromobenzene.

QUANTITATION IN FTMS: R.R. Weller and John R. Eyler, Dept. Chem., Univ. Fla., Gainesville, FL 32611 USA.

Most FTMS development to date has concentrated on qualitative analysis, exact mass determination, and the use of increasingly higher magnetic fields. We have been investigating the quantitative aspects of FTMS: reproducibility of peak height ratios, linearity of response, and the quantitative determination of trace species in the presence of large concentrations of other components which might have quite similar mass. Most of our studies in this area have been concerned with the detection of low levels of CO in the presence of much higher levels of N_2. Our quantitation methodology for such systems has included ejection of the very large quantities of $^{14}N^{14}N^+$ from the analyzer cell, and concurrent production of higher levels of CO^+ using long electron beam pulses and high emission currents. The CO^+ intensity is then compared to that of unejected $^{14}N^{15}N^+$, present at a natural abundance level of 0.74% of the ejected $^{14}N^{14}N^+$ ion intensity. This technique has been successfully demonstrated for CO present in N_2 at 1 - 5% levels, and is currently being extended down to part per thousand levels.

A second aspect of our quantitation studies involves the use of a pulsed valve inlet system with two piezoelectric pulsed valves. Such pulsed valves allow high levels of gas to be present and ionized initially in the FTMS system, and then permit the rapid pumpout of the gas after ions have been formed. Potentially complicating ion/molecule reactions which might deplete CO^+ ion intensities are thus minimized, and ion transient response signals can be collected for a longer period of time, leading to higher resolution spectra. We have successfully modelled the pressure behavior in the various regions of our pulsed valve inlet system by using standard viscous, transition, and molecular flow equations, where appropriate. Such modelling allows optimization of system parameters and achievement of the most rapid system response after pulsed valve opening and closing. The piezoelectric pulsed valves we use have an advantage over solenoidal pulsed valves in that they can be mounted in any position in the fringing fields of the superconducting magnet associated with our FTMS instrument.

PROBLEMS WITH QUANTIFICATION OF ION ABUNDANCE IN FTMS AND A PROPOSED SOLUTION; HUANG, S.K., REMPEL, D.L. AND GROSS, M.L.; UNIV. OF NEBRASKA, CHEMISTRY DEPT., LINCOLN, NE.

In Fourier Transform Mass Spectrometry (FTMS), it is desirable to operate at low pressures to get the best performance for exact mass. The reduction of pressure damping exposes the effect of imhomogeneous electric and magnetic fields in the cubic ion trap. In the investigation of the mechanisms for these effects, which limit mass measurement accuracies, it is useful to have a physically meaningful measure of the intensity of a peak which is insensitive to the varying phase and non-Lorentzian shapes often found when parameters such as trap voltage and excitation are varied from their optimal settings. There are two classes of methods currently in use for measuring intensities of peaks in transform spectra: interpolation methods such as the magnitude-Lorentzian interpolation scheme introduced by Giancaspro and Comisarow [1] and area methods such as the integration of the absorption component of a phase corrected Lorentzian peak [2]. Here we wish to extend this older area method to include non-Lorentzian phase uncorrected peaks.

Extension of area method: To do this we suppose that the transient is a narrow band signal with the essential part of the spectrum confined to a relatively small frequency interval about the "characteristic" frequency of the peak. Employing the discussion in Whalen [3], we can compute the zero time envelope, A, by evaluating

$$|A| = (1/\pi)\left|\int_I f(w)\,dw\right| \qquad (1)$$

where f is the Fourier transform of the transient time function f and I is the small interval of the frequency spectrum on which f is nonzero for the positive half of the frequency spectrum. From (1) we propose an approximation applicable to a discrete spectrum produced by an FFT computation:

$$A \propto \sqrt{(\sum_i R_i)^2 + (\sum_i I_i)^2} \qquad (2)$$

where the sums of the spectral real part, R_i, and spectral imaginary part, I_i, are over the index, i, which is confined to an internal for which the peak of interest contributes to the spectrum.

Physical significance: If the computer acquisition of the transient signal begins with the smallest possible delay after a rapid excitation, we might expect the time zero envelope to be insensitive to those nonlinear effects which cause the non-Lorentzian peak shape: it takes time for the inertial ions to integrate and show the effect of nonlinear component forces which are small compared to the force of the magnetic field. Based on the idealized linear models of the cubic cell, we might hope that the time zero envelope is proportional to the number of ions in the cell and to the ion orbit size. All these features appear to be in evidence as shown in the following experiments.

Experimental Demonstration: The general conditions of the experiment are as follows: 2.5cm 304ss cubic cell, B = 1.2 Tesla, beam excitation delay = 1ms, excitation-detection delay = 400 us, detection bandwidth = 10kHz, number of data points = 32K. The differential RF excitation is measured at one plate as .77 volts p-p. In Figures 1 and 2, the excitation time is 760 us. In spite of the nonideal application of method (use of Rf excitation with a modest length and 400 us delay between excitation and the beginning of detection), the time zero magnitude of the complex envelope exhibits a fair degree of proportionality as we change the number of ions by varying the pressure below 10^{-6} Torr (Figure 1). The 3pt magnitude which gives a good estimate of the peak height is plotted for the same data set for comparison (Figure 2). In Figure 3 the cyclotron orbit size is changed by varying the excitation time with the exhibition of good proportionality. Here the electron beam parameters are 15msec x 35nA

and the pressure is 2 x 10^{-7} Torr. Again in Figure 4 we show the 3pt magnitude to show the method is working for nontrivial examples.

[1] C. Giancaspro and M.B. Comisarow, Applied Spectroscopy, 37, 153-166 (1983).
[2] J.C. Lindon and A.C. Ferrige, Progress in NMR Spectroscopy, 14, 27-66 (1980).
[3] A.D. Whalen, Detection of Signals in Noise, Academic Press, New York, 1971, 56-61.

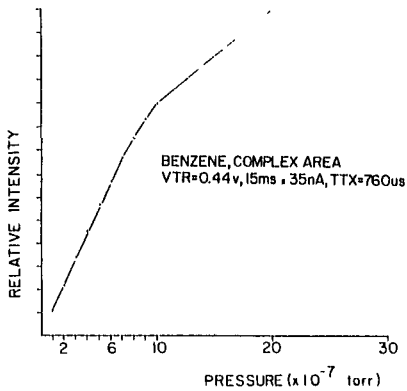

Fig. 1. Zero time envelope vs. # of ions.

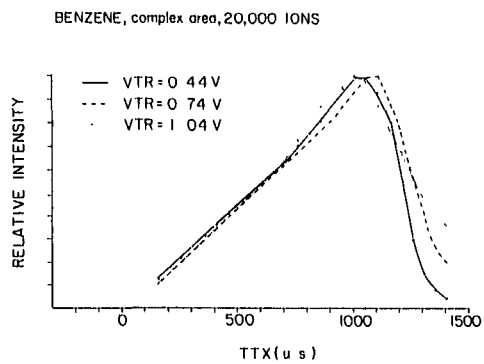

Fig. 3. Zero time envelope vs. orbit size.

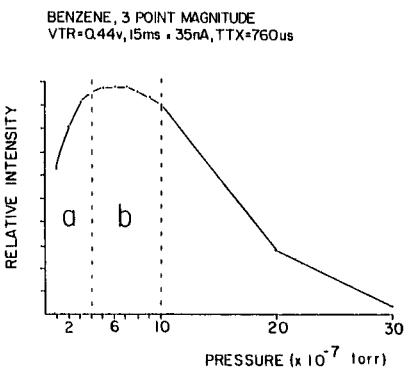

Fig. 2. 3pt magnitude vs. # of ions.

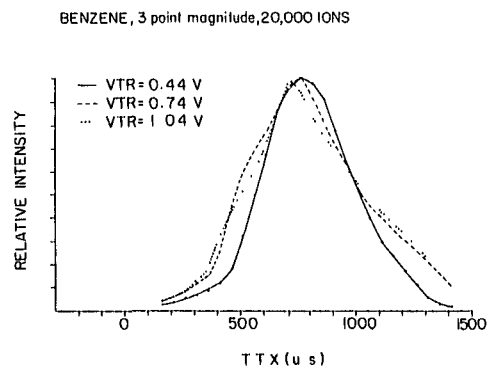

Fig. 4. 3pt magnitude vs. orbit size.

MASS SELECTIVE INSTABILITY HIGH PRESSURE OPERATION OF THE ION TRAP

STAFFORD, G. C., KELLEY, P. E., SYKA, J. E. P., REYNOLDS, W. E., FIES, W. J.
FINNIGAN MAT, SAN JOSE, CA.

TODD, J.F.J.
Chemical Laboratory, University of Kent, Canterbury, Kent, UK.

The quadrupole ion storage trap, first named the 'QUISTOR' by the group at the University of Kent [1], is a three-electrode structure having cylindrical symmetry (Fig. 1). Ions are created within the trap and may be held in stable orbits by a.c. and d.c. applied to the ring electrode. The theory of ion motion within the trap, which has been described in detail elsewhere [2], is essentially analogous to that of the mass filter in that trapping may be mass selective or occur in a 'wide-band' mode over a range of masses. The detection of ions differs, however, in that one may either use resonance energy absorption techniques related to the detailed motion of ions in the trap, or cause the ions to be ejected through holes in one of the end-cap electrodes on to a multiplier.

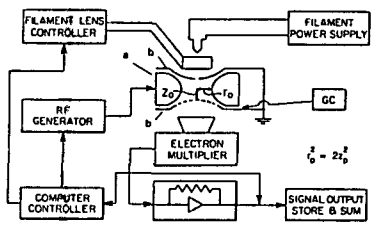

Fig. 1

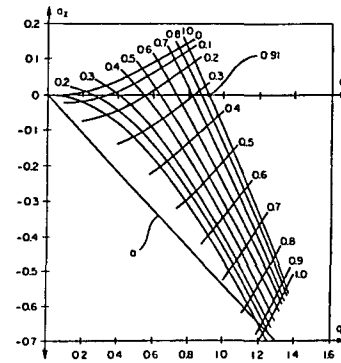

Fig. 2

The range of masses stored simultaneously in the trap depends upon the Mathieu parameters given by $a_z = 4eU/(mr_0^2\Omega^2)$ and $q_z = 2eV/(mr_0^2\Omega^2)$ where e is the charge carried by the ions of mass m, r_0 is the inscribed radius of the ring electrode, U and V are respectively the d.c. and maximum a.c. potentials developed between the ring and end-cap electrodes and Ω is the angular frequency of the a.c. potential. For an ion to be stored the corresponding (a,q) coordinates must lie within the envelope of the 'stability diagram' shown in Fig. 2. When operated with (a_z, q_z) values near the lowest apex ions may be stored mass selectively and ejected by applying a voltage pulse between the end-cap electrodes; as a mass spectrometer the d.c. and a.c. potentials are scanned so that each mass moves along the scan line marked 'a' in Fig. 2 [3].

A new method of operation described below utilises only a.c. potentials so that a range of masses is stored simultaneously equivalent to the limits $0 \leq q_z \leq 0.91$ along the q_z axis of Fig. 2. With the timing sequence shown in Fig. 3 ions are created by admitting a pulse of electrons through an end-cap (or ring) electrode and then sequentially ejected by ramping up the a.c. potential, when for each m/e value at $q_z = 0.91$ the ions become unstable in the axial (z) direction and exit through the end-cap on to the multiplier. This approach is technically simpler than those used previously in that no pulsing of the trap electrodes is required, no d.c. potential is needed (and hence there is no need to maintain a constant U/V ratio) and the value of V required to achieve mass resolution is lower than in the mass selective storage mode, thereby increasing the mass range achievable with a given power supply. In addition the sensitivity and resolution are significantly improved. Further improvement in performance has been achieved by operating the trap with a relatively high pressure (ca. 1×10^{-3} torr) of background gas having low relative mass, e.g. helium:

essentially collisions between the ions and the helium atoms lead to viscous damping of the former [2] and hence the trajectories of the trapped ions collapse closer to the centre of the trap. For example, FWHM resolution of 1700 at m/z 502 from the reference compound perfluorotributylamine (FC-43) has been obtained (Fig. 4).

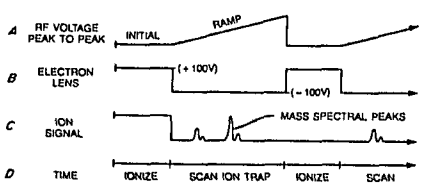

Fig. 3

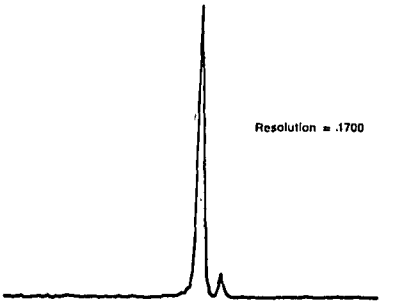

Fig. 4

The miniature size and performance characteristics of the ion trap make for an ideal specific yet universal GC detector capable of operating under computer control and with a sensitivity comparable to that of a flame ionisation detector.[4]

References

1. G. Lawson and JFJ Todd, British Mass Spectroscopy Group Meeting, Bristol 1971, Abstract No. 44.
2. JFJ Todd, G. Lawson and R. F. Bonner, Quadrupole Mass Spectrometry and its Applications (Ed. P. H. Dawson) Chapter VIII, Elsevier, Amsterdam (1976).
3. R. E. Mather, R. M. Waldren and J. F. J. Todd in Dynamic Mass Spectrometry, Vol. 5 (Eds. D. Price and J. F. J. Todd) Heyden, London (1978), p. 71.
4. G. C. Stafford, Jr., P. E. Kelley and D. C. Bradford, American Lab., June 1983.

FOURIER TRANSFORM ION CYCLOTRON RESONANCE MASS SPECTROMETRY: NEW THEORETICAL AND INSTRUMENTAL DEVELOPMENTS

Alan G. Marshall, Tao-Chin L. Wang, and Tom L. Ricca
Departments of Chemistry and Biochemistry
The Ohio State University
140 W. 18th Avenue
Columbus, OH 43210

Tailored excitation: simultaneous multiple-ion-monitoring; MS/MS.

All FT-MS experiments to date have been carried out using pulsed (1) or frequency-sweep (2,3) excitation. The relative merits of pseudo-random noise as a spectral source have been discussed and demonstrated (4). The concept of "de-excitation" of excited ICR motion has been demonstrated (5), and forms the basis for a new "stochastic" excitation/detection scheme which includes all other excitation modes as sub-sets (see below). Stochastic excitation is predicted to produce more selective excitation (as for MS/MS), as well as the first method for truly simultaneous multiple-ion-monitoring. It is based on the correspondence between mass and frequency in ion cyclotron resonance mass spectrometry.

Two-ion monitoring is illustrated in Figure 1. In general, one defines a desired frequency-domain excitation (e.g., Figure 1a), and then constructs its time-domain equivalent by inverse Fourier transformation. The time-domain envelope is then applied as a voltage to the ICR cell plates. For example, the method can be used to produce: (a) essentially flat excitation power over a single frequency range, as for ordinary detection; (b) flat power in the immediate vicinity of any number of selected m/z values, as for multiple-ion monitoring; or a flat power spectrum with sharply defined "windows" for use in ejecting all but previously specified m/z-values, as for MS/MS experiments. A full description of these techniques will be published shortly.

Space charge in FT/MS.

It has long been recognized that when there are too many ions in the excitation/detection "cell", Coulomb repulsion perturbs the motion of the ions, leading to shifts and broadening of the mass spectral signals. We have used simple numerical integration to track the trajectories of a pair of ions of equal m/z, as they are excited and observed in an FT/MS experiment. The trajectories predict that mass resolution should increase with increasing ion orbital radius, as has been confirmed experimentally for benzene ions. Moreover, as the ion orbital radius increases, the Lorentz force becomes strong compared to the Coulomb force, and the apparent ICR frequency increases toward its value in the absence of space charge effects. In other words, both mass resolution and exact-mass determinations are optimized by exciting the ions to the largest possible orbit. The practical limit then becomes the uniformity of the electric field at large ICR orbital radius.

[This work was supported by N.I.H. Grant #1 R01 GM31683.]

1. Comisarow, M. B. & Marshall, A. G. (1974) Chem. Phys. Lett. 25, 282-283.
2. Comisarow, M. B. & Marshall, A. G. (1974) Chem. Phys. Lett. 26, 489-490.
3. Hunter, R. T. & McIver, R. T., Jr. (1977) Chem. Phys. Lett. 49, 577.
4. Marshall, A. G., Wang, T.-C. L. & Ricca, T. L. (1984) Chem. Phys. Lett., accepted and in press.
5. Marshall, A. G., Wang, T.-C. L. & Ricca, T. L. (1984) Chem. Phys. Lett. 105, 233-236.

Figure 1. Simultaneous excitation of two selected m/z values.

The desired frequency-domain excitation is digitized and stored in memory (a). An inverse discrete Fourier transform produces the corresponding digitized theoretical time-domain waveform (b). The time-domain waveform is digital-to-analog converted to a time-domain voltage applied to one pair of transverse plates of a rectangular ICR trapped-ion "cell", and detected simultaneously on the other pair of transverse plates (c). A discrete Fourier transform of the digitized waveform from (c) gives the experimental excitation spectrum shown in (d). The method is demonstrated for perfluorotributylamine: comparison of the "normal" Fourier transform ion cyclotron resonance spectrum excited by a broad-band frequency sweep (e) to the spectrum excited by the two-ion monitoring signal (f) clearly demonstrates simultaneous selective excitation at m/z = 119 and 264.

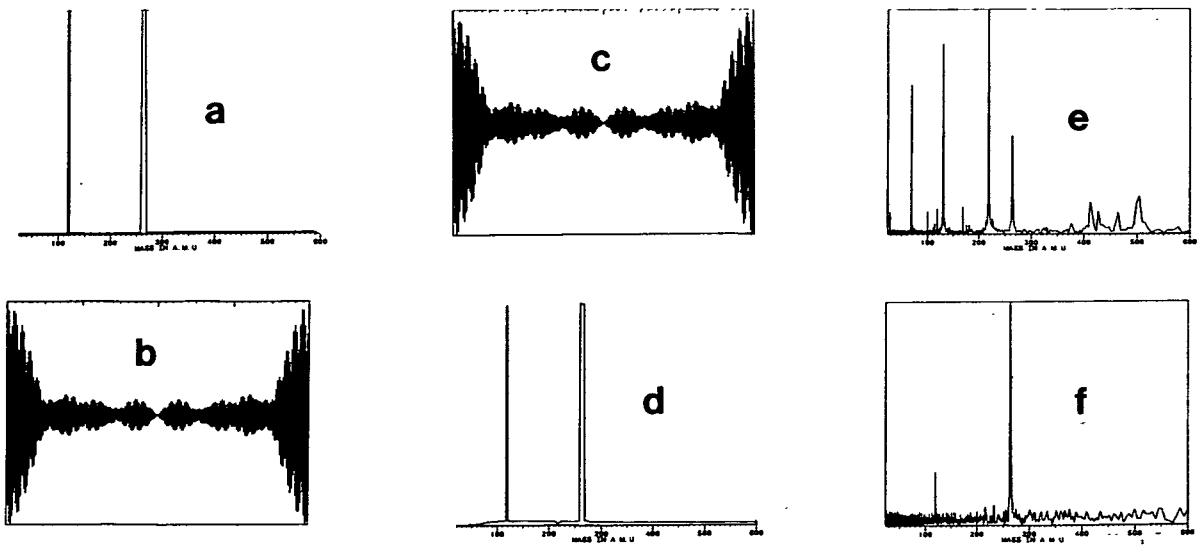

A CESIUM SURFACE IONIZATION SOURCE FOR SIMS

T. Noda and T. Okutani
Toyohashi University of Technology, Tempaku, Toyohashi 440, Japan;
H. Tamura and H. Watanabe
Hitachi Central Research Laboratory, Kokubunji, Tokyo 185, Japan

Secondary ion mass spectrometry (SIMS) is widely employed as a powerful technique for surface analysis. Although SIMS shows a very high sensitivity for many elements when utilizing positive or negative ion ejection from the specimen, its spatial resolution has been limited mainly by the source size of the ion gun with such a type as the duoplasmatron or the surface ionization with a porous W flat emitter. Thus, we developed a new type ion source with a small source size, which can be operated in two modes, either surface ionization or liquid metal ion source (LIMS).

Surface Ionization Source

Figure 1 shows a new type surface ionization source we have developed. It is composed essentially of a reservoir, an emitter tip, a sleeve and a tungsten filament. Electrons from the filament bombard the sleeve enclosing the tip to raise its temperature and melt the source material. The molten material is supplied through the annular gap between the sleeve and the tip, and is surface-ionized at the end of the tip. This mode of operation allows the source size to be very small.

We investigated the characteristics of this gun by using CsCl instead of pure Cs as the source material since the compound is much more stable and easier to handle than the element itself. As shown with a mass spectrum in Fig. 2 taken with the compound, cesium ions are easily obtained with high purity.

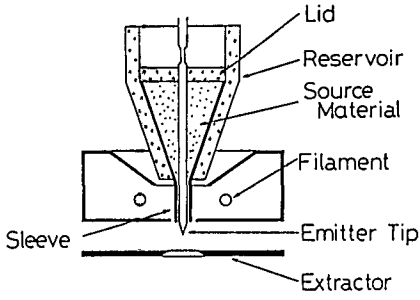

Fig. 1 Construction of the gun.

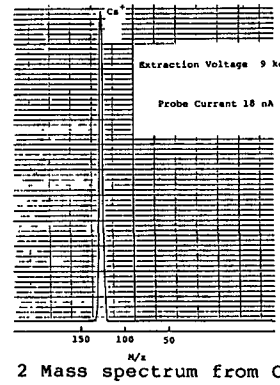

Fig. 2 Mass spectrum from CsCl.

We mounted this ion source on a microprobe SIMS, and compared the secondary ion mass spectrum with that obtained with a conventional duoplasmatron O_2 ion source. Figure 3(a) shows a Ga and As secondary ion mass spectrum from a GaAs sample bombarded by O_2 ions. As is well known, we can see that As, an electronegative element, shows much less intensity of positive secondary ions compared with Ga, an electropositive element, against its stoichiometric concentration. Figure 3(b) shows a negative secondary ion mass spectrum from the same sample bombarded by Cs ions using the present surface ionization source. In contrast with the above O_2^+ ion bombardment, the As ion intensity is much stronger than that of Ga^-, which is below the detection limit. Thus the present ion source demonstrates well known characteristics for negative secondary ion ejection.

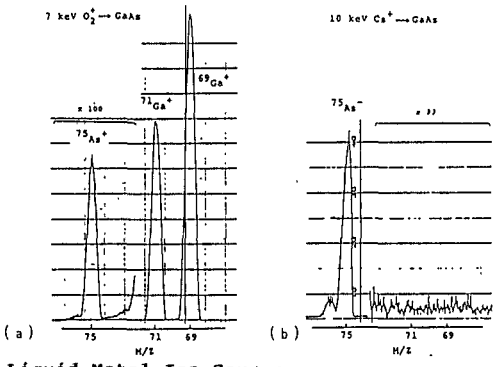

Fig. 3 (a) A positive secondary ion mass spectrum from O_2^+ bombardment,
(b) A negative secondary ion mass spectrum from Cs^+ bombardment.

Liquid Metal Ion Source

Formation of a submicron ion beam has been attracting a great deal of interest due to its potential applications to microprobe surface analysis and microcircuit fabrication. LMIS operates with a high brightness and has been demonstrated to be suitable for the ion probe system. However, conventional LMIS units reported so far have some problems because the operating life time and ion species are limited. The present gun also works as LMIS with the construction shown in Fig. 1. We operated the gun as LMIS using Ga, In, Au and Zn as the source material with a low or high melting point, or a high vapor pressure. The characteristics of the ion current vs extraction voltage showed that this gun easily gave a current density higher than several tens of microamperes per unit solid angle. Figure 4 illustrates the relationship between energy broadening of Ga ion in FWHM and the extracted total ion current using a retarding potential type energy analyzer with the energy resolution of 2 eV. The FWHM value varies with a nearly two-thirds power dependence (solid line) on the ion current as proposed by Knauer. These results show that this gun does operate as LMIS for various source materials.

We applied this LMIS of Ga to a microprobe SIMS for the GaAs sample. As shown in Fig. 5, secondary ions from the sample can be easily obtained as in the case of O_2^+ bombardment illustrated in Fig. 3(a). Because metal ion bombardment is not expected to enhance the secondary ion emission as strongly as O_2^+ bombardment, the fairly strong secondary ion intensity in the present experiment seems to be due to oxygen adsorption onto the sample. By actively using these enhancement phenomena due to oxygen or cesium adsorption, LMIS may allow one to analyze a submicron area of a sample with high sensitivity.

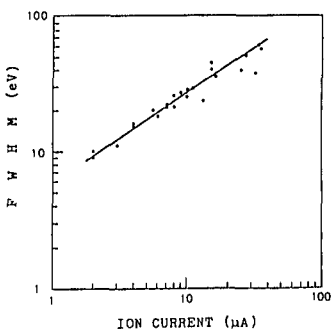

Fig. 4 Variation of FWHM with total current of Ga ions.

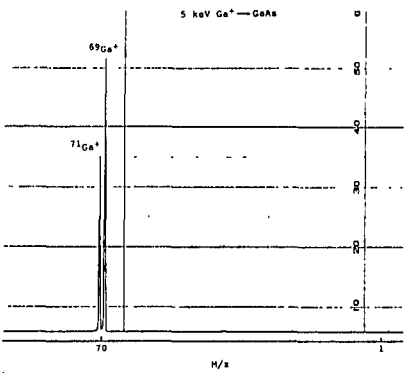

Fig. 5 A secondary ion mass spectrum from GaAs bombarded by Ga ions.

CHARACTERISTICS OF AN IMMERSION LENS Cs^+ SIMS SOURCE QUADRUPOLE MS.

William Aberth

Mass Spectrometry Resource, Dept. of Pharmaceutical Chemistry,
University of California, San Francisco, CA 94143.

An immersion lens liquid SIMS type source utilizing Cs^+ primary beam (1,2) has been incorporated in an Extranuclear Model 4-162-8 QMS instrument. This type of source has been demonstrated on a Kratos MS 50S sector mass spectrometer and has yielded increased signal at reduced primary Cs^+ beam intensity compared with the commonly used 90° geometry type source (3). Figure 1 is a schematic of the QMS source. The 70° incident Cs^+ beam strikes the sample placed on a 3 mm diameter pedestal raised 0.5 mm above the squared-off probe tip surface [1]. An accelerating potential of 20-50 V is placed between electrode 3 containing a 2.5 mm diameter aperture and the probe tip which is in contact with electrode [2]. Electrode [3], [4] and [5] form an aperture einzel lens, operating in an accelerating mode, which focuses the secondary beam through a 1 mm diameter aperture in electrode [7]. Fine beam positioning is accomplished with deflectors in electrode [6]. The aperture in electrode [7] serves to discriminate between the focused ion beam and the background producing excited neutrals (4) which are unfocused. The secondary beam is then focused parallel using [8] and can be energy analyzed by the retarding potential grids of [9].

Best operating conditions for this source are at 8 KeV , (the maximum voltage presently used) and a low current of $1\text{-}2 \times 10^{-8}$ amp. Figure 2 shows a glycerol sample spectrum obtained using 8 KeV and 0.015 μA Cs^+ beam. The $(G4 + H)^+$ glycerol cluster peak is resolved with good S/N. Background signal is roughly proportional to the energy incident on the target (primary beam accel voltage x current). The lower Cs^+ current requirements (which help prolong source and sample lifetimes) coupled with low background levels of this immersion lens source give it distinct advantages over the 90° geometry type sources.

Acknowledgments. This work was supported in part by NIH DRR Grant RR 01614 and NIH GMS Grant GM 32315

References

1. W. Aberth, K.M. Straub, A.L. Burlingame, Anal. Chem., 54, 2029 (1982).
2. Antek, P.O. Box 51311, Palo Alto, CA 94303.
3. W. Aberth, A.L. Burlingame, Proc. 4th Int. Conf. on SIMS, Osaka, Japan, Nov. 13-19, 1983.
4. K.F. Faull, A.N. Tyler, H. Sim, J.D. Barchas, I.J. Massey, C.N. Kenyon, P.C. Goodley, J.F. Mahoney, J. Perel, Anal. Chem. 56, 308 (1984).

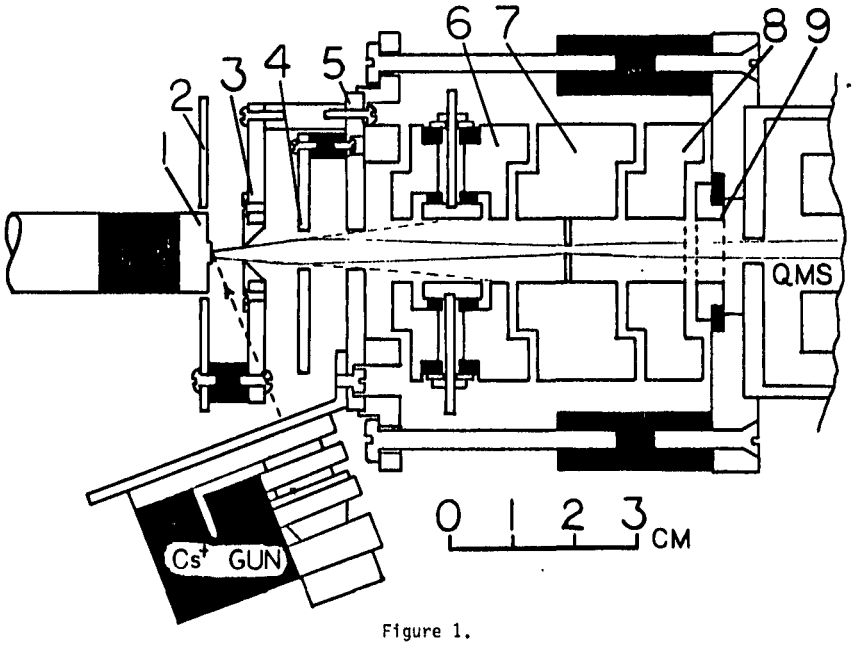

Figure 1.

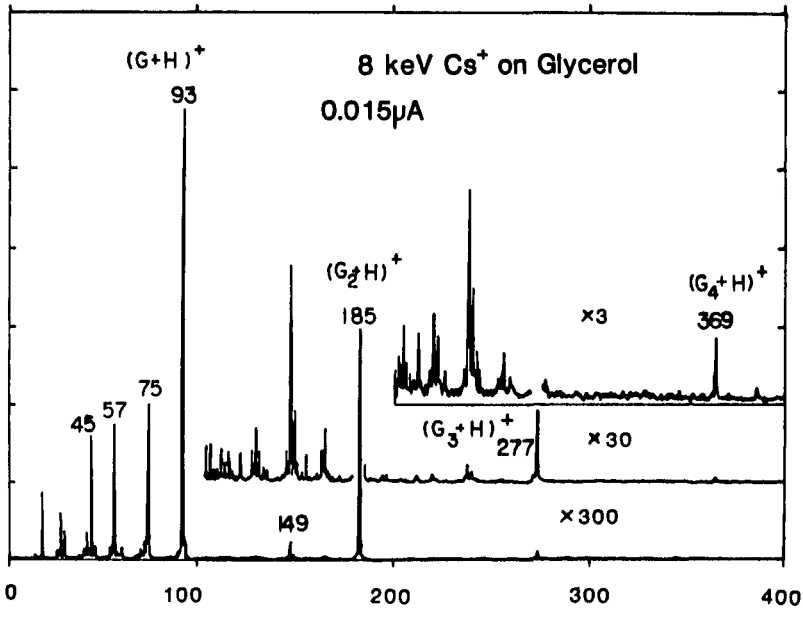

Figure 2.

A COMPARISON OF WIDE APERTURE AND SHORT RESIDENCE TIME ION LENSES

J. E. Delmore

A series of ion lens configurations were computer modeled using the program "SIMION". The salient characteristics of these lenses are: 1) The intermediate inversion point characteristic of ion lenses used in most analytical mass spectrometers is eliminated. The first inversion point is at the focal point of the lens. 2) The potential gradient in the ionization region is increased substantially. This reduces the residence time of an ion in the lens, which is desirable, although it has the undersireable effect of increasing the energy spread of ions produced by electron bombardment. This energy spreading effect does not occur in sources where the ions are made on a surface, such as surface ionization, field desorption, SIMS, FAB, etc. This is determined by the potential difference across the region in which ions are produced.

The importance of ion residence time comes from the kinetic energy of the ion prior to acceleration. This kinetic energy is in random directions, and defocuses the ion beam with increasing ion residence time.

Two of the more promising designs were constructed and tested with rhenium ions generated by positive self surface ionization. The first lens was designed to focus ions from as wide an area as possible, consistant with a reasonable entry angle (0.40°) through the focal slit and a reasonably short residence time. This lens is called the Wide Aperture (WA) lens. The second lens was designed to have as short a residence time as feasible consistant with a reasonable aperture, with a larger entry angle. This lens is called the Short Residence Time (SRT) lens. The overall length of the WA lens is 1.50", and 1.00" for the SRT lens. The distance from the filament shield to the drawout electrode is 0.10", 0.30" to the next electrode, and 0.20" to the next electrode for both lenses. This 1:3:2 spacing gave the best focusing properties with computer simulation. The SRT lens does not have a fourth x-y focusing electrode, while the WA lens has one at 0.40" beyond the third. This extra electrode in the WA lens makes the beam more nearly parallel at the expense of longer flight distances and residence time.

The WA lens was initially tested without z axis compression electrodes, and the optimum focus voltages compared to the voltages predicted by SIMION. Table 1 lists this data. The agreement is sufficiently close to lend credence to the accuracy of SIMION.

Limited time prevents a complete discussion of the properties of these lenses, but Table 2 presents data of the decrease in intensity of the rhenium signal with decreasing accelerating voltage. It is seen that the SRT lens maintains ion transmission at reduced accelerating voltage better than the WA lens, which in turn is better than the standard lens.

These two lenses have interesting properties for certain applications, although that is not the most important point of this presentation. The most important point is that SIMION, and other similar computer programs, can be an invaluable aid in the matching of a source of ions to a mass analyzer. Many such matchings are currently being made, and this type of program is invaluable in providing an optimum focusing system.

TABLE 1. PREDICTED VERSUS MEASURED X-Y ELECTRODE VOLTAGES

Electrode	Predicted	Measured	% Difference
1	5000	5000	----
2	4900	4917	0.35
3	4450	4543	2.05
4	4100	4210	2.61
5	2350	1997	17.70

TABLE 2. RELATIVE ION TRANSMISSION VERSUS ACCELERATING VOLTAGE

KV	SRT	WA	Standard
10	1	1	1
8	.96	.98	.91
6	.92	.92	.81
4	.83	.81	.61
2	.65	.62	.26
1	.41	.28	.08

MICROANALYSIS OF INORGANIC MATERIALS BY LASER IONIZATION MASS SPECTROMETRY (LIMS)

Robert W. Odom, Charles J. Hitzman and S. E. Buttrill, Jr.
Charles Evans & Associates
1670 S. Amphlett Blvd., Suite 120
San Mateo, CA 94402

Laser ionization mass spectrometry (LIMS) is a relatively new surface microanalytical technique which provides a characterization of a materials elemental and molecular composition.[1] The LIMS technique is based on performing a mass and intensity analysis of the ionic components formed during the high power density laser irradiation of a materials surface. The microanalytical character of this technique is achieved by utilizing a finely focused (1.0 to 5.0 microns diameter) laser pulse to initiate the vaporization and ionization of a materials constituents. The combination of this finely focused, high power density (variable between 10^8 to 10^{12} W/cm^2) laser pulse with time-of-flight (TOF) mass analysis techniques provides a complete mass spectrum of the ionization produced during each laser shot.

The LIMS technique promises to augment and complement the microanalytical capabilities of the more established materials analysis techniques which include secondary ion mass spectrometry (SIMS), Auger electron spectrometry (AES) and electron probe microanalysis (EPMA). The most salient advantages the laser microprobe technique offers to materials microanalysis compared with these other microanalytical techniques includes its ability to perform a sensitive, rapid elemental characterization of both insulating and conducting materials and its ability to provide (in favorable cases) a molecular microanalysis of surfaces and thin films. The elemental detection limits of the LIMS technique have been shown to lie in the part per million atomic (ppma) or lower region for a number of elemental species[1] and these detection limits are obtained from sample volumes on the order of 1 cubic micrometer. Although the microanalysis of adsorbed molecular species by laser microscopy is still in its developmental stages, the potential application of this capability are very broad and include such areas as biological materials, organic thin films and inclusions.

Laser ionization mass analysis was originally developed for biological microanalysis[2] and the instrumentation associated with this type of analysis utilized back surface or transmission laser irradiation of the sample material. The transmitted light optics in this instrumental configuration permits achieving analytical areas (or spot size) of 0.5 micrometers in diameter; however, thin sectioned sample materials (less than approximately 1 micrometer) are required for analysis by transmitted light irradiation.

A more recent design of the laser microprobe instrumentation utilizes front surface or reflection laser irradiation which removes the constraint of sample material thickness and allows for the microanalysis of essentially any type of solid sample. A schematic diagram of a reflection mode laser microprobe instrument (manufactured by Cambridge Mass Spectrometry, Cambridge, Eng.) is illustrated in Figure 1.

In our laboratory the laser microprobe technique has been extensively applied to the following types of analyses:

1. bulk analyses of insulating materials,
2. thin film analysis
3. survey microanalysis of unknown contamination, and
4. molecular microanalysis.

Most of the materials analyzed in our laboratory have been related to the semiconductor industry and/or advanced materials development, although we have performed a number of biological materials microanalyses with a reflection mode instrument. An example of the sensitivity of the LIMS technique in the bulk analysis of insulating materials is illustrated in Figure 2. The material in this analysis is $Bi_{12}SiO_{20}$ which contains approximately 5 ppma Cr. This material is one of the most electrically insulating materials known and it is considered an ideal candidate system for future electro optical devices. The spectrum illustrated in Figure 2 is the first known example of the detection of Cr in the microanalysis of this material.

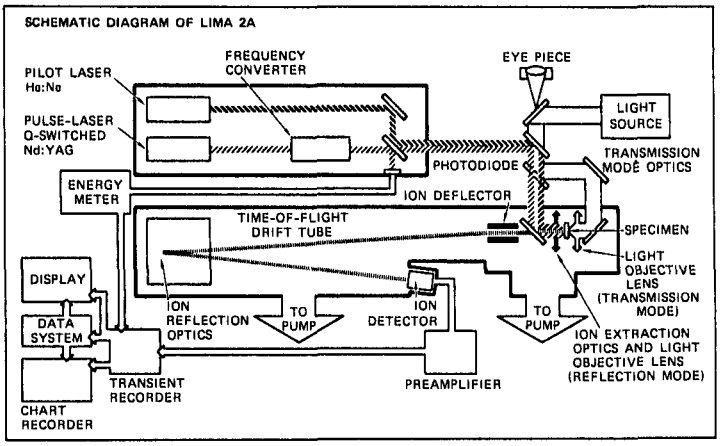

Figure 1.

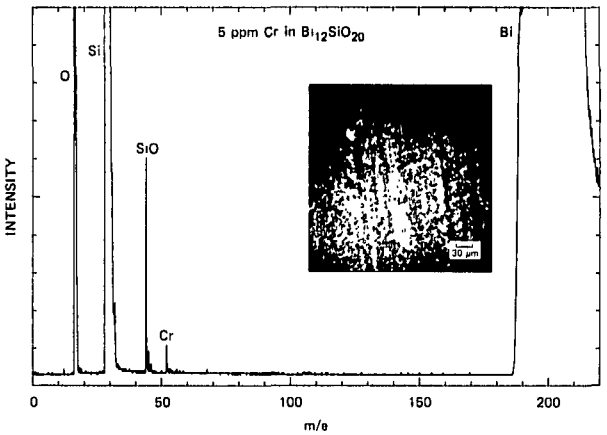

References

1. R. Kaufmann, Microbeam Analysis - 1982, K.F.J. Heinrich San Francisco pp. 341-353 (1982)
2. U. Seydel et.al., Int. J. of Leprosy 50 90 (1982)

Acknowledgements

Partial support for this research was provided by NIH SBIR Grant #1-R43-GM-33123-01

EFFECTS OF LASER FOCUS ON ION PRODUCTION IN THE LASER ION SOURCE FOR ELEMENTAL ANALYSIS

R. J. Conzemius, Shankai Zhao*, R. S. Houk and H. J. Svec
Ames Laboratory-USDOE and Department of Chemistry
Iowa State University, Ames, Iowa 50011

INTRODUCTION

Use of laser ion sources in mass spectrometers for elemental characterization of solid materials has grown significantly in recent years [1,2]. Of the many experimental conditions affecting laser induced ionization processes, the power density of the irradiating laser beam has been shown to be of primary importance. The area of the impacted spot has also been shown to affect ion production processes. Because both the area and the power density will be affected by placement of the specimen in the focal plane of the laser attention must be given to the means used to focus the laser beam as well as to its inherent properties such as pulse energy and temporal and spatial characteristics. Here we show the effects on ion production of alteration of the specimen location relative to the focal point. The most significant observation is that ion signals from doubly charged ions will be highly useful in optimizing laser focusing and in reproducing laser power densities during analyses.

The mass spectrometer and the laser have been described previously [3]. The total ion beam monitor consists of a wire grid situated within the magnetic field shunt and intercepts approximately 15 percent of the ion beam transmitted to the magnetic analyzer. The ion signal on this monitor is labelled the total ion current (TIC) and is directly proportional to the total number of ions accelerated from the ion source. The analyte signal of interest is focused at the image slit by adjusting the magnetic field strength. The ion signal passing the slit is detected with a faraday cup followed by signal amplification with a vibrating reed electrometer (Cary 401).

Specimens were translated in 50 μm steps along the optical axis of the incident laser beam. At each step ion current measurements were made by integrating for 5 to 10 s the high and low energy ion signals, the TIC, and the faraday cup signal. Computer control of the laser, stepping motors and the electrometers permitted optimization of data gathering and minimization of specimen alteration due to cumulative laser erosion. Typically an area of 1 x 1 mm was scanned and approximately 2000 laser shots were used in gathering data for each step.

Plots for the singly charged ions of the matrix element collected at the faraday cup closely match the TIC plots as should be expected because the singly charged ions account for at least 95 percent of all ions produced using these laser power density levels (approximately 1-5 x 10^9 W cm^{-2}).

Production of doubly charged ions is of interest in mass spectrometry because they may overlap singly charged ions of interest or the doubly charged ions may be used for diagnostic or analytical purposes themselves. Plots are shown of TIC and of simultaneously measured doubly charged ion intensity of the matrix element as a function of specimen location.

The response of analyte signals is of most interest. Data is presented showing the ratio of selected isotopic ion signals for analytes Cr (0.80 wt. %), Ni (0.67 wt. %) and Mn (0.96 wt. %) to the TIC as a function of specimen location for an iron specimen, NBS SRM #462.

Operation of the laser ion source is generally considered to be straightforward, i.e., focus the laser at the specimen and turn the laser power up until ions are observed. In fact for low power density operation where molecular ions are of interest this is the normal mode of operation [1]. However in the higher power density regime where elemental characterization is of primary interest the data observed here indicate that some optimization is called for beyond the simple onset of ion current and the visual observation of a bright minimum diameter plasma (BMD location).

At low power densities the ion production is highly dependent upon specimen location as indicated by the triangularly shaped response curves for TIC at 16 A lamp current. However at higher laser powers the TIC response functions show plateaus extending over a range of 300 to 500 μm. The plateau is to some extent due to the long depth of focus of the optical system used in this study. The tendency for the TIC to resolve itself into two distinct maxima at higher power densities was not observed for all specimens and further-

*Present address: Test & Analysis Center, Zhongshan University, Guangchou, PEOPLES REPUBLIC OF CHINA

more the double maximum of the response curve sometimes coalesced into one broad peak.

The TIC response curves tended to be centered approximately 150 μm to the left (i.e., specimen moved 150 μm away from the entering laser beam) of the BMD location. The BMD location was observed to be +300 μm from where the surface was in optical focus. Neither visually focusing on the surface nor visual focusing to the BMD provide optimum centering on the TIC response curve. One of the purposes of this work is to establish means of reproducing local power density levels via measurements on the actual specimen under examination. When the local power density level can be reproduced then the differences in absolute signal levels from different elements can be more legitimately studied.

The plots of the doubly charged ion signals show them to be centered on the general TIC response curve and with the same general shape as the TIC curves at low laser power levels. It is considered likely that the response functions for the doubly charged ions would also develop a plateau region at higher laser power densities than achievable with our apparatus. The doubly charged ion intensities are more sensitive to sample location than the singly charged ions even at the highest power levels. This relationship should have significant analytical usefulness in permitting the automatic calibration of the power density level to preset or desired levels in order to reproduce analytical measurements. This type of calibration would eliminate errors due to laser power fluctuations or inadvertent loss of laser power caused by condensation of materials on any beam transmitting optical components. Thus a standard specimen could be used to set the power density at the specimen required to reproduce a particular desired +2/+1 ratio by automatically adjusting the lamp current during an experiment, from day-to-day, or when major changes in light optics are made such as tuning cavity mirrors or replacing optical components. If it is desirable to diminish the +2 ion signals to minimize interferences, the focusing location could also provide for this. The analyte signals have only small dependencies on focusing when ratioed to the TIC.

CONCLUSION

Ion current production for singly charged ions is observed to plateau over a range of focusing of approximately 300 μm using a 60 mm focal length lens where the computed spot diameter is 12 μm and the depth of focus is 68 μm. In fact the plateau is quite useful in allowing a range of focal positions without greatly affecting the total ion production from which the mass spectrum is obtained. Thus the change of focus as the surface erodes does not greatly offset analytical usefulness for relatively long experiments. Doubly charged ion signals depend sharply on the position of the focal point relative to the specimen. This will permit reproducible setting of the specimen position relative to the focusing plane. The doubly charged ion signal has been observed to be more sensitive to laser power levels than the singly charged ion signals. A linear relationship between the ratio of doubly to singly charged ion signals to the laser power should permit straightforward calibration of the local laser power level for a particular sample matrix. Since both the focusing and the power level are best set by use of the doubly charged ion signals we envision periodic tuning of the mass spectrometer to the doubly charged ion signal from the matrix element, focusing to a maximum on that signal, and then adjusting the laser power level to a predescribed +2/TIC ratio. We plan to incorporate this optimization on actual ionization characteristics of the plasma into the computer control of our scanning laser mass spectrometer system. A more detailed description of these experiments will be published in the International Journal of Mass Spectrometry and Ion Processes.

ACKNOWLEDGEMENT

Ames Laboratory is operated for the U.S. Department of Energy by Iowa State University under Contract No. W-7405-Eng-82. This research was supported by the Director for Energy Research, Office of Basic Energy Science. The authors gratefully acknowledge the help of Clarence Ness who aided in the acquisition of the measurements reported.

REFERENCES

1. R. J. Conzemius and J. M. Capellen, Int. J. Mass Spectrom. Ion Phys., 34 (1980) 197.
2. R. J. Conzemius, D. S. Simons, S. Zhao, and G. D. Byrd, Laser Mass Spectrometry of Solids: A Bibliography 1963-1982, Microbeam Analysis--1983, R. Gooley, Ed., San Francisco Press Inc., San Francisco, CA, 1983, p. 301-332.
3. R. J. Conzemius and H. J. Svec, Anal. Chem., 50 (1978) 1854.

EVALUATION OF GALLIUM DIFFUSION IN GOLD FILMS BY MEANS OF SIMS

H.Yamaguchi, Y.Honma and N.Yasuda
Research and Development Center, Toshiba Ltd. Kawasaki, Japan

1 Introduction

Gold films are generally used as the electrode of compound semiconductor devices. In the device production process, some heat treatments are indispensable. During heat treatment processes substrate atoms diffuse into gold films and sometimes enrich on the surface. Enriched atoms finally form a thin film and causes serious problems in the device production process. In this report, the diffusion and surface enrichment behavior was investigated for a Au/GaP system by means of SIMS.

2 Experimental procedure

A gold film with 1 μm thickness was evaporated by successive evaporations on a mirror polished GaP(111) wafer. The wafer was cut into several pieces. Each specimen was annealed at the temperature of 400°C - 500°C in an argon atmosphere. The diffusion and surface enrichment profiles of substrate atoms were measured by SIMS for each specimen. Then diffusion profiles were adjusted by the theoretical diffusion equations and parameters of the equations are determined. Finally, the numbers of surface enriched atoms were estimated.

3 Diffusion and surface enrichment profiles measured by SIMS

Diffusion profiles measured by SIMS are shown in Fig.1. In SIMS depth profiling, 10KeV Ar^+ ions were used for the primary ions. Ar^+ ions are better in this study because using $O2^+$ ions causes the variation of the sputtering rate. Secondary ions were measured by the beam rastering method with electronic gating. As shown Fig.1, remarkable gallium diffusion into gold films were observed. While phosphor was not detected. Diffused atoms of gallium were more than ten times as many as that of phosphor.

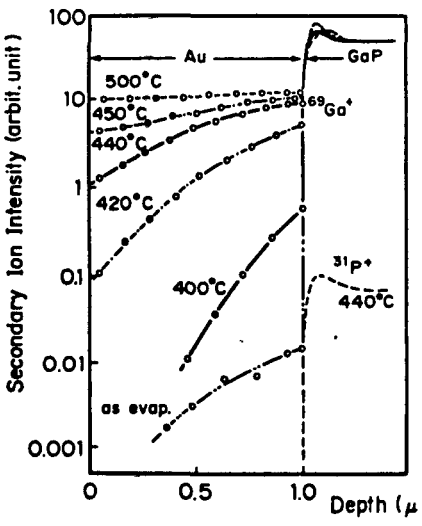

Fig.11 Diffusion profiles of Ga and P in gold films

Profiles of surface enrichment elements measured by SIMS are shown in Fig.2. Low energy primary ions were used for SIMS depth profiling to obtaine high depth resolution. Observed elements were mainly gallium and oxygen. This results indicates the formation of the thin film of gallium oxide on the surface. The quantity of enriched atoms increased rapidly with increasing temperature. The thickness of the film was estimated at several tens angstrom for 450°C annealing.

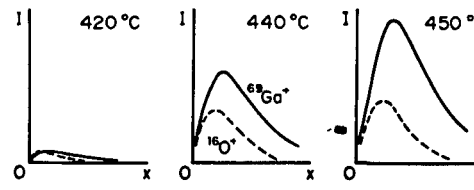

Fig. 2 Profiles of surface enriched elements

4 Diffusion equation and activation energy

Diffusion profiles of gallium measured were compared with classical diffusion equations. In the case of the diffusion from the thick substrate, the diffusion profile is generally represented by a complementary error function.

$$C(x,t) = Cs\,(1 - \mathrm{erf}\,\frac{x}{2\sqrt{Dt}})$$

The fitting results are shown in Fig.3. The longitudinal axis is represented by concentration. Observed values fitted well to complementary error functions shown as real lines.

Arrhenius plots were shown in Fig.4. The activation energy calculated was 60Kcal/mol. The standard diffusion coefficient was $6*10^{6}cm^{2}/sec$.

Surface concentration Cs was determined experimentally. From observed diffusion profiles, Cs was found to approach to a fixed value as increasing temperature. From this tendency, following relation was assumed.

$$\ln(C_0 - \ln Cs(T)) = A + B\left(\frac{1}{T}\right)$$

The relation between the lefthand term of the formula and 1/T is shown in Fig.5 in the case that Co is 4%. Plots were on the straight line and the parameters A and B were easily determined.

5 Estimation of numbers of surface enriched atoms

Numbers of surface enriched atoms were roughly estimated. As the first approximation, the surface enriched atoms are considered to correspond to the integration of the diffusion equation outside the surface. Calcurated values were converted into gallium oxide film thickness, t_s, and plotted versus temperatures for the case of gold films thickness of 0.5, 1.0 and 2.0 micrometers. The results is shown in Fig.6. Calcurated film thickness were agreed with observed values obtained by SIMS in the error of 1 or 2 factors.

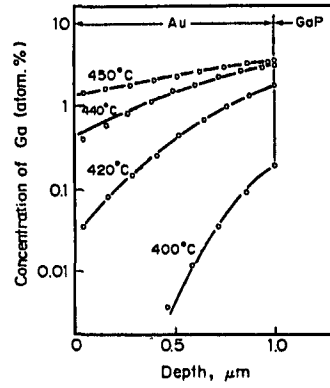

Fig. 3 Results of theoretical curve fitting

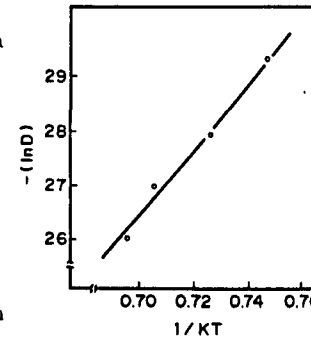

Fig. 4 Arrhenius plots

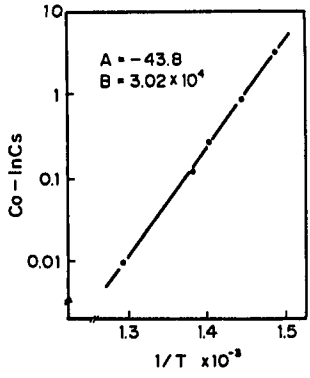

Fig. 5 Relation between Co-lnCs and 1/T

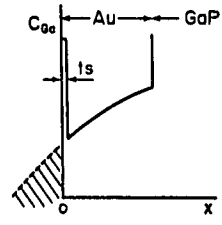

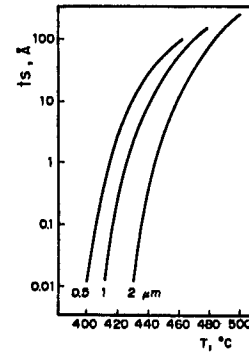

Fig. 6 The surface enriched film thickness as a function of temperature.

SIMS STUDY OF COMPOSITIONAL CHANGES OBSERVED IN A PuO_2 HEAT SOURCE CLADDING ALLOY*

W. H. Christie, [1] D. H. Taylor,[2] R. E. Eby[3] and D. Pavone[4]

[1,3]Analytical Chemistry Division, ORNL, Oak Ridge, TN 37831
[2]Savannah River Laboratory, Aiken, SC 29801
[4]Los Alamos National Laboratory, Los Alamos, NM 87545

Pu-238 oxide is used as a general purpose heat source (GPHS) to power radioisotopic thermoelectric generators for NASA deep space probes, such as the upcoming Galileo mission to Jupiter (launch 1985). After being fabricated into ceramic pellets approximately 2.5 cm long by 2.5 cm in diameter, the PuO_2 is encapsulated in a 700 μm thick iridium shell which is vented on one end to permit escape of the decay helium. The major purpose of the iridium shell, or clad vent set (CVS), is to provide containment of the PuO_2 in the event of a mission failure involving a high velocity impact of the GPHS capsules with the ground. An iridium alloy (DOP 26) consisting of 0.3% tungsten, and nominally 50 wt ppm aluminum and 60 wt ppm thorium was chosen as the cladding material because of its high temperature strength and ductility and chemical inertness, especially to PuO_2. The alloying elements enhance the impact strength and ductility by increasing the coherent strength of the grain boundaries. Perhaps even more importantly these elements, in particular thorium, help maintain ductility during high temperature aging of the iridium by preventing grain growth. Thorium is effective as a grain growth inhibitor because it exists primarily as discrete particles on the grain boundaries.

Although the microstructure and grain boundary chemistry of the iridium have been well characterized for the case where the iridium has been heat treated alone, the effects of high temperature aging in the presence of PuO_2 are unknown. This paper describes the results of using SIMS to investigate some of the effects on iridium DOP 26 alloy of high temperature aging (6 months at 1440°C) under service conditions in the presence of PuO_2. Optical microscopy of polished specimens, prepared from aged sections of this cladding alloy showed a significant increase in average grain size in the near-surface regions exposed to PuO_2. One sample exhibited less grain growth in this region and SIMS was used in an attempt to determine what chemical differences exist between samples exhibiting large grain growth and those exhibiting lesser growth. Prior to fabrication of the cladded heat sources, impurities known to be picked up by the PuO_2 fuel during processing (Al, Ca, Cr, Fe, Ni and Si) were added at various levels (up to 10,000 ppm) to facilitate accelerated testing studies. Sections were cut from three CVS's (A, B, and C) that had been aged for 6 months in vacuum at 1440°C (fuel temperature). These specimens were mechanically abraded and then chemically etched (HF/HNO_3) to remove adhering PuO_2. Transverse cross sections of these decontaminated specimens were then mounted in epoxy and metallurgically polished until a smooth mirror-like finish was obtained. The mounted specimens, which showed no smear removable alpha activity, were then overcoated with 20-30 nm of spectrographic grade carbon, prior to SIMS analysis, so as to render the entire surface conducting.

Mass spectra showed all three samples of the aged cladding alloy (A, B, and C) to have significant Cr, Fe, and to a lesser extent Ni contamination in the inside region. The deepest penetration (up to 150 μm) and highest levels were generally observed in sample C. The PuO_2 fuel in capsule C contained the highest levels of impurity dopants among the three samples studied. Line scans across the 700 μm thickness also showed little Ca and Si and no detectable Pu to have diffused into any of the cladding samples. It was also observed that Al, added as a dopant in the cladding alloy, underwent some depletion from the alloy in regions where Cr and Fe had diffused in. Thorium, also a cladding dopant, was less abundant in the inside surface region as compared to the center of the sample. Line scans across the specimens demonstrated some variability in amount and depth of penetration of Cr and Fe into the alloy. Ion images were then made to further understand these observed variations. These studies showed that Cr and Fe diffused into the alloy primarily along grain boundaries. The amount of Cr or Fe observed in any particular line scan and the depth of penetration depended to some extent on how that line scan intersected grain boundaries; but in general it was shown that for sample C the concentration maxima at the

*Research sponsored by the U. S. Department of Energy, Office of Basic Energy Sciences, under Contract No. DE-AC05-84OR21400 with Martin Marietta Energy Systems, Inc.

By acceptance of this article, the publisher or recipient acknowledges the U S Government s right to retain a nonexclusive, royalty free license in and to any copyright covering the article

inside surface was approximately 0.5 to 1.0 atom % and decreased to background (5-10 ppm atomic) at a depth of about 150 μm. For sample A the maximum concentration of Cr and Fe was about the same as sample C at the surface, but the depth of penetration was significantly less, being only 30-50 μm. The concentration of Cr and Fe at the surface of sample B was also approximately the same as for C and the depth of penetration was midway between A and C.

Ion imaging was used to show that in the interior of all samples Th was segregated to grain boundaries and also existed as discrete precipitates in the interior of grains and on grain boundaries. Earlier studies showed that near surface grain growth is facilitated by loss of Th from the alloy by diffusion along grain boundaries until it reaches the outer surface where it is presumably oxidized to ThO_2. However, in sample C where growth of near surface grains was least pronounced, SIMS revealed a striking correlation between reduced grain growth and the oxidation of Th on grain boundaries by the inward diffusion of oxygen. Two separate regions on the interior edge were studied; both showed ThO_2 precipitates to extend along grain boundaries over 100 μm in depth from the surface exposed to PuO_2. The SIMS study suggests that if the oxygen partial pressure is high enough (as it must have been in capsule C), oxygen can diffuse inward along grain boundaries and oxidize Th in situ. In the locations where Th was seen to exist as ThO_2, minimum grain growth was observed. This suggests that excessive grain growth may be inhibited by oxidation of Th on grain boundaries interior to the sample. The formation of ThO_2 below 10-15 μm in depth was not observed in samples A and B.

Chromium, Fe, and Ni migrate from the PuO_2 fuel to the Ir cladding and alter the chemistry of the near surface grains and grain boundaries. Although the effect of these impurities is not now known, they should probably be excluded from the Ir until their effect is understood. The observation that in situ oxidation of Th on grain boundaries seems to reduce grain growth should be investigated further. Currently no information is available concerning the effect of grain boundary ThO_2 on high temperature impact ductility. This study does suggest that this oxidation phenomena may be a way to stabilize the alloy against exaggerated grain growth and thereby improve its impact resistance.

MOLECULAR BEAM/MS SAMPLING OF SILANE OXIDATION IN A LOW-PRESSURE DISCHARGE-FLOW REACTOR;

G. L. Pellett and B. R. Adams, NASA Langley Research Center, Hampton, VA 23665

This paper presents some unique, newly obtained results from DFR/MB/MS silane oxidation studies at NASA Langley. The research objective has been to obtain direct evidence of molecular and free radical chain intermediates which control initial stages of silane oxidation. These results are being used to gain understanding of, and improve upon, the handling-safety and piloting characteristics of silane and other reactive ignition aids that are being tested and evaluated at Langley for enhanced H_2 ignition and flameholding characteristics in subscale supersonic ramjet combustors.

Experimentally, the reactants used to initiate attack on SiH_4 were Cℓ-atom and O-atom, produced by microwave discharge through dilute (1 %) mixtures of $C\ell_2$ or O_2 in He, at 3.5 torr. Reactants introduced downstream of the microwave included a mixture (in SCCM) of 7 SiH_4, 1416 He and 14 Ar (tracer). During each run, four selected masses, which usually included argon as a reference, were simultaneously monitored at 20 eV (mostly). Repetitive (4000) digital averaging of the four modulated analog outputs, from a quadrupole-MS/-chopped-MB system (Pellett and Adams, Proceedings of 31st Annual Conf. (1983), pp. 46-47), was utilized for both microwave-ON and -OFF conditions. Parameters such as m/z ratio, reactant concentrations (flow rates) and species, reactor length, and/or pressure were varied systematically during several runs (20 to 35) in a typical one-day set of experiments.

As shown in the attached figures, normalized mass spectra of silane and its e-impact fragmentation products, when compared with and without Cℓ-atom attack (microwave ON and OFF), indicate small (1 to 5%), but reproducible and statistically significant, excess concentrations at m/z = 31, and 29. These are attributed to SiH_3 and SiH free radicals. The excesses increase with Cℓ-atom concentration and SiH_4 consumption (calculated from percent reduction of mass 31), and they may represent the first MS observation of these radicals. Masses corresponding primarily to SiH_2 and SiH_5 radicals and SiH_4 parent ion did not exhibit significant excess quantity during Cℓ-atom attack at 20 eV; the same was true for eV's as small as 15 and for O-atom attack (not shown).

The attached figures also show that disilane, Si_2H_6, was formed in relatively large quantity and then destroyed by both Cℓ- and O-atom attack, as SiH_4 consumption increased; disilane maximized at about 25% SiH_4 consumption in each case. Masses 61 and 60, corresponding to Si_2H_5 and Si_2H_4 radicals, increased relative to disilane (mass 62) at high SiH_4 consumption when Cℓ-atom was used, but not for O-atom attack.

The results of the study are now summarized in three major parts. First, the DFMS of silane is complicated by surface processes. Patterns of solid deposition on the pyrex - reactor walls consisted of chlorinated polysilane compounds, and thus represented Cℓ-atom sinks. The patterns were usually stable enough over 2 to 3 hours run time to allow good data reproducibility, including a well defined linear consumption of silane with added $C\ell_2$ or O_2 during each day's set of runs. However the deposition pattern and proportionality varied somewhat from day to day. Thus the results suggest that percent silane consumption, and relative HCℓ production, varied linearly with available gaseous Cℓ-atom concentration.

Second, for reaction of silane with Cℓ-atom: (1) The reaction is very fast, and is probably gas kinetic controlled. (2) SiH chemiluminescence was intense for the first 14 cm of flow reactor (2 ms). (3) Ion current from the parent SiH_4^+ represented only 0.3 percent of the total ion current, with no reaction. (4) Ions from SiH and SiH_3 radicals were detected, and their relative concentrations increased with Cℓ-atom and percent silane consumption. (5) Disilane concentration maximized at about 25 percent SiH_4 consumption. (6) As silane consumption increased from 70 to 90 percent, masses 59, 60, and 61 remained mutually proportional, but increased relative to disilane parent at 62. These excesses represent evidence for Si_2H_5 and Si_2H_4 radicals. (7) Variation of electron voltage from 20 to 15 eV did not enhance quantification of SiH_x radicals.

Third, for reaction of silane with O-atoms: (1) The reaction appears to be considerably (2 to 5 times) slower than with Cℓ-atom, based on the location of downstream wall deposits and intensity of SiH chemiluminescence. (2) Excess ion currents for SiH and SiH_3 at masses 29 and 31 were not as pronounced as they were for Cℓ-atom. (3) Disilane was similarly formed and then destroyed, with increasing O-atom concentration, but no apparent excesses due to Si_2H_{6-x} radicals were found at high silane consumptions. Further investigations of silane oxidation chemistry are being pursued.

DFMS OF SILANE CONSUMPTION BY Cl-ATOM

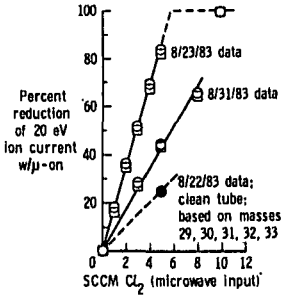

NOTE: linear consumption; interrun variability due to surface reactions.

NOTES:
SCCM: 7 SiH_4; 1416 He; 14 Ar
P = 3 torr, T = 298°K
○ [30] = SiH_2^+
□ [31] = SiH_3^+

HCl PRODUCTION VS SiH_4 CONSUMPTION BY Cl-ATOM

FROM DFMS AT VARIOUS PRESSURES, AND CL_2, SiH_4 CONCENTRATIONS

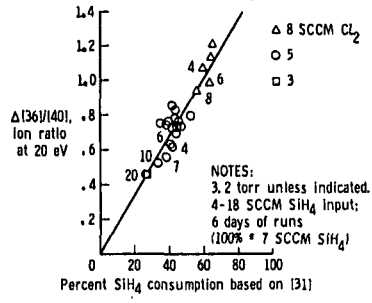

DFMS OF SILANE WITH/WITHOUT Cl-ATOM ATTACK

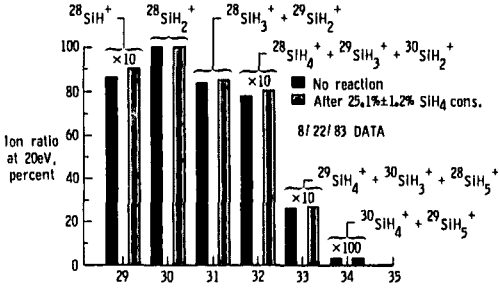

EFFECT OF Cl CONCENTRATION ON SiH_x

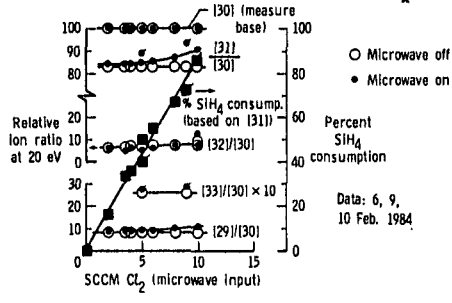

DFMS OF Cl-ATOM REACTION WITH SILANE:

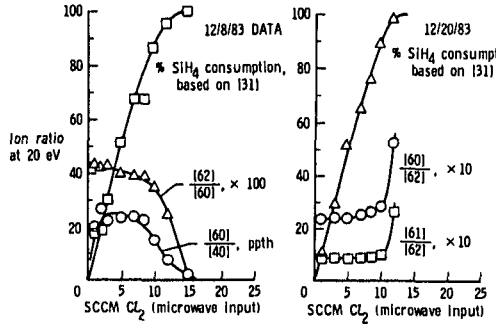

AVERAGED MASS ABUNDANCE OF DISILANE SPECIES
DFMS OF Cl- AND O-ATOM REACTION WITH SiH_4

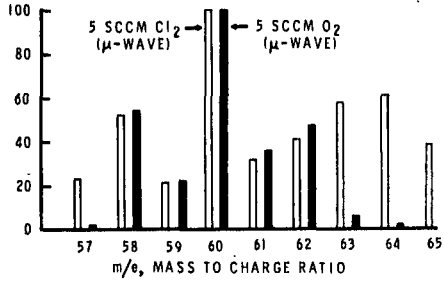

DFMS OF O-ATOM REACTION WITH SILANE, AND FORMATION/DESTRUCTION OF DISILANE SPECIES

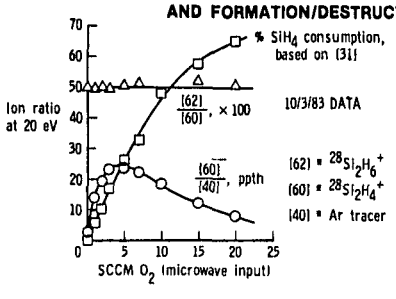

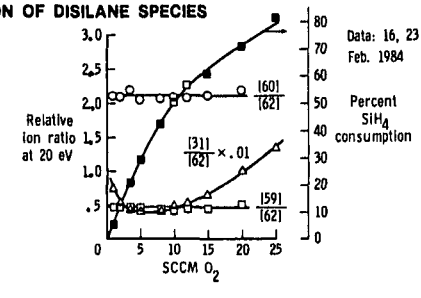

MATRIX EFFECTS ON RELATIVE INTENSITIES OF MOLECULAR IONS, ADDUCTS AND FRAGMENTS IN LSIMS OF BRADYKININ: R. Reginato, W. Chai, F.C. Walls, J.O. Whitney and A.L. Burlingame. Department of Pharmaceutical Chemistry, University of California, San Francisco, CA 94143

Liquid Secondary Ion Mass Spectrometry (LSIMS) complements conventional peptide analysis since molecular weight information, degree of purity and fragmentation data related to amino acid sequence can be obtained on underivatized samples containing "blocked" residues (acylated, phosphorylated, glycosylated, etc.). In studies designed to optimize LSIMS conditions for peptides, we have tested the effect of the additives shown in Table I upon molecular ion intensity and the degree and pattern of fragmentation of a model peptide, Met-Lys-BRADYKININ at the 2 nmole/lul level. A KRATOS MS-50 mass spectrometer equipped with a Cesium ion gun (90° geometry) was operated in positive ion mode with a primary beam flux of ~ 100 uamps/cm^2 at 2000-3000 resolution using a copper probe tip. LSIMS spectra Met-Lys Bradykinin are characterized by the type of fragment ions described in Fig. 1. As can be seen from Table II, the intensities of MH^+ and MH^{2+} as a % of total ionization varied with the type of matrix utilized and was greatest when oxalic acid was added to the matrix. When unadulterated glycerol was used, fragmentations arising from the carboxy terminal end of the molecule dominated the spectrum. Addition of HCl (copper or gold probe tips) or acetic acid did not influence this pattern. Inclusion of oxalic acid in the matrix lowered fragment ions of the C-ALK type. Addition of p-toluene sulphonic acid produced major changes in the nature of the spectrum, including a lowering of ionization arising from C-ALK fragmentation and an enhancement of fragmentation arising from the amino terminal portion of the molecule. These effects can be also demonstrated by plotting the ion intensities of carboxy and amino terminal fragment ions against the intensity of the molecular ion (Table III). The relative amount of fragmentation (C+N terminals) was lowest for oxalic acid, and addition of p-toluene sulphonic acid resulted in greatly enhanced N-terminal sequence ions. Fig. 2 and Fig. 3 show portions of the spectra of bradykinin run in glycerol and glycerol + p-toluene sulphonic acid, respectively. With glycerol, C-terminal sequences (m/z 417, 419, 491, 638, 695, 902, 904) dominate the spectrum. Addition of p-toluene sulphonic acid allowed the N-terminal sequences (m/z 485, 582, 679, 684, 831) to be prominent. Spectra obtained with HCl and acetic acid resembled the glycerol pattern while oxalic acid spectra were intermediate in nature. N-terminal fragment ions could be discerned because of the relatively low intensity of C-ALK ions, but were not as prominent as with p-toluene sulphonic acid.

The ability of p-toluene sulphonic acid to enhance N-terminal sequence ions is probably due to its superior protonating power and to its ability to form an "onium" salt with the peptide $[(NH_3...COOH)^+(CH_3CH_4SO_3]^-)$, stabilizing the positive charge on the cationic portion of the salt. Preliminary results with model amines such as antipyrene have demonstrated a 40-fold increase in MH^+ intensity when p-toluene sulphonic acid was added to the matrix. In addition, pH measurements on matrices made before and after accumulation of spectra (~ 5 minutes) show that pH of the matrix remained lower with p-toluene sulphonic acid (~ 3) than with any of the other additives (~ 5), probably because of its lower volatility. We envision that addition of p-toluene sulphonic acid with concomitant enhancement of N-terminal sequence ions could be of great utility in cases where sequence information obtained by conventional means remained doubtful. (Supported by NIH grant RR01614.)

MATRICES

Glycerol
Glycerol - 0.1N HCl
Glycerol - 0.1N HCl - gold probe tip
Glycerol - 5% Acetic Acid
Glycerol - 10% Oxalic Acid
Glycerol - 0.01N p-toluene Sulphonic Acid

Table I

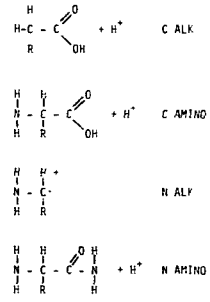

MET-LYS-BRADYKININ

Met-Lys-Arg-Pro-Pro-Gly-Phe-Ser-Pro-Phe-Arg

MH^+ 1319

Fig.1

Intensity as % of Total Ionization

	MH^+	MH^{2+}	C ALK*	C AMINO*	N ALK*	N AMINO*
Glycerol	1.3	0.2	5.3	5.9 (40)+	1.1	0.7
Glycerol HCl	1.4	0.5	3.9	4.8 (39)	1.2	1.2
Glycerol HCl Au Tip	1.3	0.5	4.1	4.4 (40)	1.3	1.7
Acetic Acid	1.7	0.3	4.5	6.7 (53)	1.3	1.0
Oxalic Acid	2.1	1.6	1.0	5.0 (46)	1.1	1.1
P-Toluene Sulphonic Acid	1.4	0.2	1.7	5.2 (40)	2.8	2.8

* Based on total intensity for sequence ions containing 3 to 9 residues

\+ % due to proline terminal residues (m/z 902, 805, 417)

Table II

Ratio of MH^+ to Selected Ions

	$(MH)^{2+}$	C ALK	C AMINO	N ALK	N AMINO	TOTAL
Glycerol	0.1	4.0	4.5	0.8	0.5	9.8
Glycerol HCl	0.1	3.4	4.2	1.1	1.1	9.8
Glycerol HCl Au Tip	0.4	3.1	3.3	1.0	1.2	8.6
Acetic Acid	0.2	2.8	4.1	0.8	0.6	8.3
Oxalic Acid	0.7	0.5	2.4	0.5	0.5	5.0
P-Toluene Sulphonic Acid	0.2	1.2	3.7	1.9	2.0	8.8

Table III

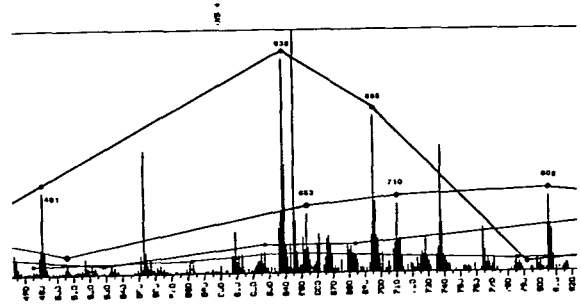

Fig.2

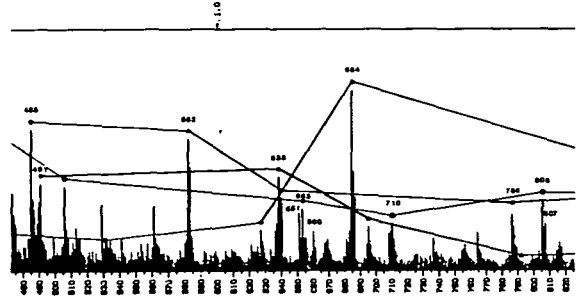

Fig.3

DEHALOGENATION REACTIONS IN FAST ATOM BOMBARDMENT MASS SPECTROMETRY. Satinder K. Sethi, Chad C. Nelson and James A. McCloskey. Departments of Medicinal Chemistry and Biochemistry, University of Utah, Salt Lake City, Utah 84112.

Fast atom bombardment (FAB) mass spectrometry of a variety of halogen-substituted nucleosides and other aromatic compounds leads to reactions, sometimes extensive, involving replacement of halogen by H from the FAB matrix. The extent of dehalogenation observed in positive ion FAB spectra of 5-X-uridines (X = I, Br, Cl, F) was: I, 33%; Br, 21%; Cl, 17%; F, 5.3%. The same order (I > Br > Cl > F) was previously observed from radiolysis and photolysis, and is not readily interpretable in terms of conventional gaseous ion chemistry, whether from EI or soft ionization techniques. Experiments employing both O-deuterated and C-deuterated glycerol matrix showed statistically random incorporation of hydrogen from glycerol into the pyrimidine ring. These results are consistent with the reaction represented in eq. (1), resulting from particle bombardment at the glycerol surface.

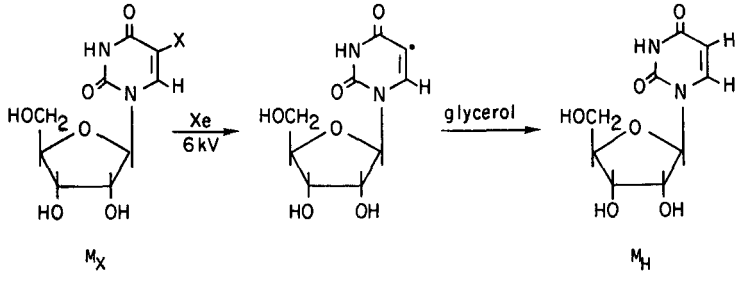

(1)

Ionization of M_X and M_H in the vicinity of particle collision then leads to a distribution of products observed in either the positive or negative ion FAB mass spectrum. The generality of reactions of this type in FAB mass spectrometry is suggested by the finding that the iodinated amino acid thyroxine showed extensive dehalogenation by replacement of both one and two iodine atoms: M_XH^+, m/z 778, 100% relative intensity; M_HH^+, m/z 652, 88%; m/z 526, 34%. It is apparent that reactions of this type, induced by particle bombardment, may be more common than previously thought.

A full length manuscript resulting from this work is in press in Analytical Chemistry.

PHOTOPLATES RECORDING OF FAB MASS SPECTRA TO m/z 3500 C. E. Costello, Dept. of Chemistry, Mass. Inst. of Technology, Cambridge, MA 02139.

The use of photoplates for the recording of complete fast atom bombardment mass spectra in the mass range to m/z 3500 has been explored. Aspects of instrument tuning which have been investigated in order to optimize results for photoplate recording are also relevant to experiments involving electrical detection. Attention to the angular and energy dispersion of the FAB secondary ion beam have been found to be more critical for obtaining adequate sensitivity than is the case for the recording of comparable electron ionization mass spectra.

FAB mass spectra recorded with photoplates at unit resolution are useful for ascertaining molecular weights of unknowns or components of mixtures, since such detection permits the integration of the signal from the whole mass range during the entire observation period. Mass assignment is carried out by overlaying reference spectra or by using distance determinations obtained in separate exposures. For very intense spectra, simple counting of the plotted spectra is also possible. At low mass, lines in the spectrum of the matrix (e.g. glycerol) may be used for extrapolation, but only high resolution spectra are suitable for this type of calibration, because of interferences from sample lines and multiplicity in lines from the matrix itself (1).

The limits of for accuracy in mass assignments at higher resolution are determined by the stability of the total system during sequential exposures of sample and reference, by line width, shape and spacing, and by the parameters of the comparator/densitometer system used for distance determination. Important too is the choice of reference compound and the distance between the lines in the reference spectrum. In cases where the reference spectrum does not contain an adequate number of properly spaced lines to assure sufficient accuracy in mass assignment, it has been possible to generate additional reference lines by accelerating voltage alternation during exposure of the reference compound. The CsI FAB spectrum has been found to be particularly suitable for use in such "peakmatched" exposures.

Acknowledgement. H. Pang and S. Maleknia contributed many hours of careful photoplate measurement to this project. The MIT Mass Spectrometry Facility is supported by the NIH division of Research Resources Grant No. RR00317 (to K. Biemann).

1. C. E. Costello, A. M. van Langenhove, S. A. Martin and K. Biemann, in Ion Formation from Organic Solids (A. Benninghoven, ed.), Springer Series in Chemical Physics, No. 25, Springer-Verlag, New York, 1983, p. 173.

FAST ATOM BOMBARDMENT MASS SPECTROMETRY OF NINE NEUROTOXINS ISOLATED FROM PROTOGONYAULAX

K. D. White, W. C. Brumley, P. A. Dreifuss, J. A. G. Roach, S. W. Page (Division of Chemistry and Physics), S. Hall (Woods Hole Oceanographic Institution, Woods Hole, MA 02543) and J. A. Sphon
Division of Chemical Technology, Food and Drug Administration, Washington, D. C. 20204

Paralytic shellfish poison (PSP) is a group of 12 known neurotoxins that are produced by marine micro-organisms known as dinoflagellates. These 12 toxins are saxitoxin (STX) and 11 analogs of STX. The analogs differ from STX by the addition of functional groups such as hydoxyl, sulfonate, and/or sulfate. These toxins are being investigated because they can enter the food chain and are hazardous to humans. The purpose of this study was to find a rapid means of confirming PSP as well as provide mass spectral information not previously available. STX and 8 of the analogs were isolated from dinoflagellates of the genus Protogonyaulax at Woods Hole Oceanogrpahic Institute and analyzed by FABMS at FDA. FABMS was the technique of choice because of its success in analyzing thermally labile ionic compounds. Experiments were run using an Ion Tech saddle field source attached to a Varian-MAT CH5 double focusing MS operated in a positive ion mode. Samples were mixed with glycerol, applied to a gold-plated target and introduced into a xenon atom beam.

STX and 21-sulfosaxitoxin (B-1) are discussed here because they are representative of the nine toxins that were examined. STX is the most toxic of the group and gives us the basic PSP structure. B-1 has an additional sulfonate group. The positive ion FAB spectra of these toxins afforded [M+H]+ ions and fragment ions corresponding to the loss of water, the loss of specific functional groups and the loss of both water and functional groups. We see a series of ions between 200 and 270 daltons that are characteristic of all the toxins analyzed. These ions are highlighted by asteriks in figures 1 & 2. We also observe ions corresponding to glycerol adducts. These adducts are unique because in almost every case, the adduct is associated with a fragment that has lost water and not with the molecular ion or any other fragment.

In the positive ion FAB spectra of STX in figure 1, we observe the [M+H]+ ion at m/z 300, the loss of water to m/z 282 and the glycerol adduct formed with that fragment at m/z 374. In the positive ion FAB spectrum of B-1 (figure 2) we observe the [M+H]+ ion at m/z 380, the loss of water at m/z 362 and the glycerol adduct with that fragment at m/z 454. The loss of SO_3 yields an ion corresponding to the [M+H]+ ion of STX. All of the ions present in the STX spectrum are also present in the spectrum of B-1 including the glycerol adduct of [STX-H_2O] at m/z 374.

An explanation for the loss of water is that the #12 carbon geminal diol loses water to form a ketone. This is substantiated by experiments using ^{18}O labels. ^{18}O was incorporated at both hydroxyls on the #12 carbon of STX. This shifted the [M+H]+ ion from m/z 300 to 304. Loss of water would then contain ^{18}O and would result in m/z 284. This was observed.

The fact that glycerol forms adducts with the [M-H_2O] species suggests another interaction with the oxygens of the #12 carbon. It has been speculated that the formation of a hemiketal with glycerol is quite feasible. It is known through experiments that we can form the hemiketal of STX with methanol resulting in a shift of the [M+H]+ from m/z 300 to 314.

The series of characteristic PSP ions in the 200 to 270 dalton region are believed to result from cleavages at different sites along the upper side chain. If this is correct, then in the case of STX (figure 1), m/z 255 results from cleavage of the carbamate linkage. M/z 238 results from additional loss of water. M/z 226 corresponds to the loss of the entire side chain. M/z 223 results from the loss of water and cleavage at the alkoxy bond. M/z 207 corresponds to the loss of both water and the entire side chain.

In summary, PSP is easily characterized by FABMS. Characterization includes molecular weight indication; the presence of functional groups such as sulfonate, sulfate and hydroxyl; characteristic adduct formation and a distinct PSP ion series.

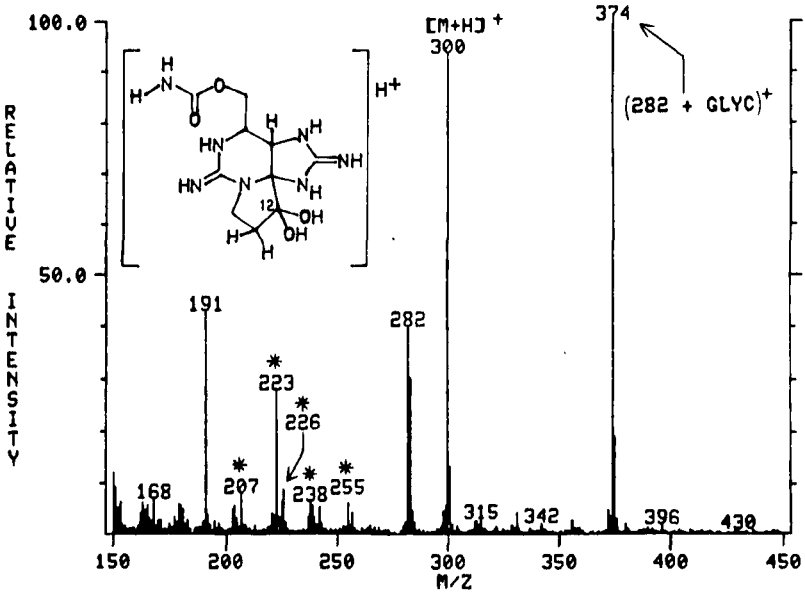

FIGURE 1 STX

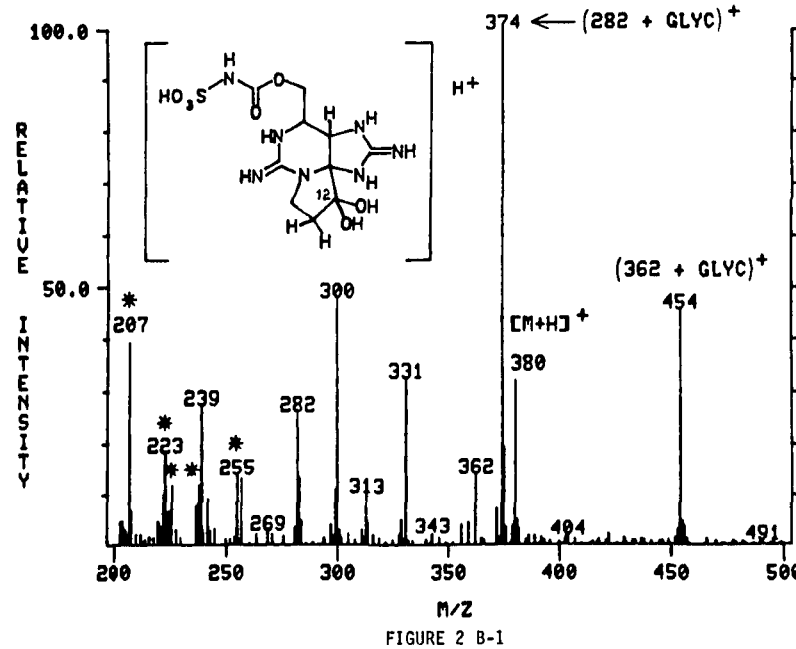

FIGURE 2 B-1

EXACT MASS MEASUREMENT BY FAB MASS SPECTROMETRY WITHOUT REFERENCE COMPOUNDS

Ted T. Chang
Chemical Research Division, American Cyanamid Company
1937 W. Main Street, Stamford, CT 006904

The exact mass measurements of FAB ions are more difficult than was anticipated. Because of selective ionization, use of typical reference materials for EI and CI, such as perfluorokerosene and perfluoropolypropylene oxides, is not feasible with FAB. Successful exact mass measurements, therefore, are dependent upon the availability of known compounds, usually homologs of the unknowns, which exhibit FAB ions alongside those of the unknown compounds. Fortunately, many compounds form cationic adduct ions in the presence of the alkali salts. Taking advantage of this phenomena, we have developed a simple procedure for making exact mass measurements of unknown compounds by peak matching two or more adduct ions, such as MH^+, MK^+, MNa^+, and/or MCs^+. This procedure does not require reference compounds and is applicable to m/z 600 with 10 ppm accuracy. For example, if the exact masses of two unknown adduct ions are given as X and X+C, and the peak matched ratio is given as S, then X can be obtained from the following equations:

$$\frac{X}{X+C} = S \qquad (1)$$

$$X = \frac{C \cdot S}{1-S} \qquad (2)$$

The accuracy, or inherent error, of this measurement is dependent on three major factors: the accuracy of the peak match measurement, expressed as d% of the peak base; the instrumental resolution, R; and the mass difference between the two adduct ions, expressed as X/C. The relationship between the inherent error, E, and these three factors is shown below:

$$E = \frac{1}{R} \cdot \frac{d}{100} \cdot \frac{X}{C} \times 10^6 \text{ppm} \qquad (3)$$

An experienced mass spectrometrist usually can locate a peak center to within ±2% error of the peak base width. At 10K resolution, the base width is 100 ppm of the measured mass. Therefore, ±2% error corresponding to an S value in equation 2 or an inherent error in equation 3 is equivalent to 2 ppm. However, this inherent error is multiplied by the factor of X/C. If C is only 10% of X, the inherent error is as high as 20 ppm. If C is 20% of X, the inherent error is correspondingly reduced to 10 ppm. The mass difference between MNa^+ and MCs^+ is 110 daltons. Exact mass measurement within 10 ppm error is attainable to m/z 550 by peak matching MNa^+ versus MCs^+. On the other hand, the mass difference between MH^+, mass accuracy of less than 10 ppm is attainable only up to m/z 190 and 20 ppm up to m/z 380.

We have found thos procedure simple, and applicable to many compounds. It provides useful exact masses where ±5 mmu is sufficient for structural interpretation up to m/z 500. This procedure is also applicable ofr EI, CI and negative ion FAB.

ANALYSIS OF CATIONIC SURFACTANTS BY MASS SPECTROMETRY/ MASS SPECTROMETRY WITH FAST ATOM BOMBARDMENT

P.A. Lyon, 3M Central Research, 201BS05, St. Paul, MN 55144
F.W. Crow and K.B. Tomer; MCMS, University of Nebraska, Lincoln NE 68588

The analytical utility of tandem mass spectrometry (MS/MS) combined with fast atom bombardment ionization is demonstrated for characterizing cationic surfactants. The cationics have traditionally accounted for only a small fraction of the commercial use but are considered currently one of the fastest growing of the surfactant classes. Most commercial cationic surfactants reflect the mixture nature of their starting materials (amines). The fact that they exist as mixtures and their ionic character have made these surfactants difficult to analyze.

The development of tandem mass spectrometry and fast atom bombardment (FAB) ionization have greatly advanced the capability of mass spectrometry to solve complex analytical problems. The successful use of FAB and FAB combined with tandem mass spectrometry for the study of anionic surfactants has been reported previously.(1) In this work molecular weight information was obtained from FAB ionization of commercial surfactants. Surfactant types successfully studied include amines, amine salts, quaternary amines, amine oxides, polyethoxylated quaternary amines, and amphoteric compounds.

Positive ion spectra were recorded and provided identification of cations, cluster ions and homolog distributions. The amine acetates studied, for example, showed distributions of molecular ions with alkyl chain lengths of 12 to 18 carbons (Table 1). Parent ions generated by FAB were selected and then caused to undergo collision activated dissociation (CAD). The resulting fragment ion (CAD) spectra contained the structural information as to surfactant type, length and number of alkyl chains, presence of isomers, and degree of ethoxylation. The value of CAD with tandem mass spectrometry is clearly demonstrated for dimethyldicocoammonium chloride. The structural identity of ions observed in the positive ion FAB spectrum (Figure 1) can readily be determined from the CAD spectra. The peak at m/z 382 was identified as the dimethyldidodecyl ammonium ion. The confirmation of that assignment can be found in the CAD spectrum of mass 382 (Figure 2a). Loss of neutral decane from the molecular cation results in an intense ion at m/z 212. The most abundant ion in the spectrum is m/z 58, the imminium ion ($C_3H_8N^+$) formed by the loss of both long alkyl chains. The ion at m/z 410 in the positive ion spectrum could be either the di-C_{13} or $C_{12}C_{14}$ structures. From the knowledge that this product is fat derived, we would rule out the presence of a di-C_{13} species. The CAD spectrum of m/z 410 reinforces that conclusion (Figure 2b). Only the losses of a C_{12} group to give m/z 240 and C_{14} to yield m/z 212 are seen.

Negative ion FAB spectra were used to identify the anionic counter ions and the presence of anionic functionalities in the amphoteric species. Mixture analysis and structure identification were performed rapidly and without sample preseparation or derivitization.

(1) Lyon, P.A.; Stebbings, W.L.; Crow, F.W.; Tomer, K.B.; Lippstreu, D.L.; Gross, M.L., Anal. Chem., 56, 8-13 (1984).

Distribution of Molecular Ions Observed in the Positive Ion Spectra of Amine Salts.

	Alkyl Moiety (Relative Abundance)						
Amine Acetate	Stearic m/z 270	Oleic m/z 268	Linoleic m/z 266	Linolenic m/z 264	Palmitic m/z 242	Myristic m/z 214	Lauric m/z 186
Tallowamine	0 94	1 00	0 18		0 92		
Hydrogenated Tallow	0 93	0 32	0 08		1.00	0 06	
Soyamine		1 00	0 51	0 08	0 31	0 04	
Cocoamine	0 12	0 23	0 05		0 62	1 00	0 71
Octadecylamine	1 00	0 23	0 04		0 19		
Hexadecylamine	0 16	0 02			1 00	0 13	
Dodecylamine	0 04	0 02			0 02	0 08	1 00
Oleylamine		1 00	0 22		0 09	0 04	

Table 1

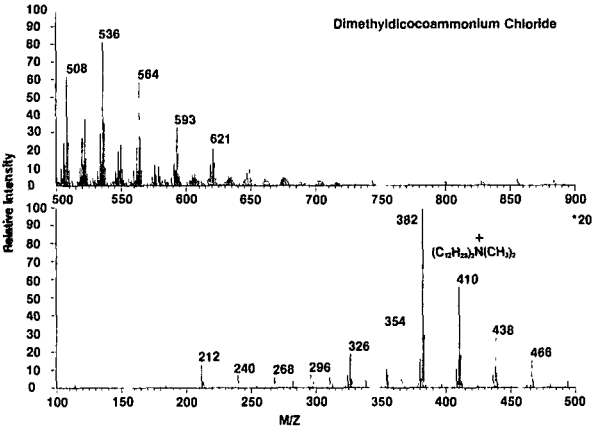

Figure 1

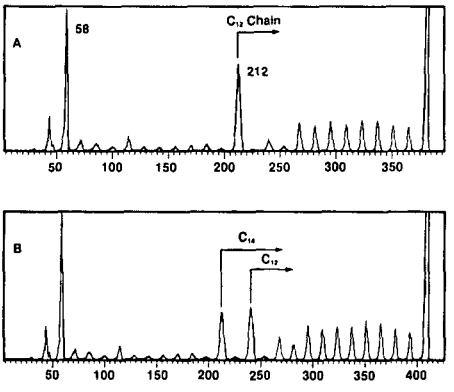

Figure 2

A Study of Alkali Cationization Processes Occurring Under Fast Atom Bombardment Conditions,

T. Keough, The Procter & Gamble Co., Miami Valley Laboratories, P.O. Box 39175, Cincinnati, OH 45247.

Cationization reactions have been previously observed using a variety of ionization techniques including Field Desorption, Laser Desorption, Secondary Ion Mass Spectrometry, Electrohydrodynamic Ionization, and Fast Atom Bombardment. Of the commonly available desorption ionization methods, only FAB utilizes a liquid matrix. The purpose of this work is to help define the role of that matrix in directing cationization reactions.

Based on the previous desorption ionization studies, it is possible that adduct ions observed in FAB arise via several routes, Figure 1. Gas-phase cation attachment (a), which is a dominant mode of cationization in SIMS conducted without the liquid matrix, need not be important under FAB conditions. We infer this from studies in which several analytes were cationized using LiI, NaI, KI, or CsI as the alkali cation donor, Figure 2. The detectable amount of non-solvated metal ion decreases dramatically from CsI ($Cs^+/Gly \cdot Cs^+ \sim 0 \cdot 70$) to LiI ($Li^+/Gly \cdot Li^+ < 0.01$). However, Li^+ ion attachment occurs with an efficiency comparable to or greater than that observed for Na^+, K^+ or Cs^+ ion addition. For the few systems studied here, gas-phase attachment of free alkali cations does not appear to be the dominant mode of cationization.

Since the extent of analyte cationization will depend on how well the analyte competes with the FAB solvent for available alkali cations, we attempted to "get a feel" for the Na^+ ion affinity of glycerol. This was accomplished by studying the gas-phase fragmentation of some unsymmetrical cluster ions, $L_1 \cdot Na^+ \cdot L_2$, where L_1 and L_2 are the species whose relative metal (Na^+) ion affinities were to be determined. Results obtained from the cluster ions produced by glycerol and NaI and produced by NaI and (Gly-H+Na) are shown in Figure 3. These results suggest that (i) the order of Na^+ ion affinities is glycerol < NaI <(Gly-H+Na) and (ii) the Na^+ ion affinity of glycerol is not much less than that of NaI. We would expect that NaI would have a high Na^+ ion affinity because of its large permanent dipole moment ($\sim$9D), which will strongly favor ion-dipole interactions. Most organic molecules, which have considerably lower dipole moments (2-3D), would be expected to have much lower alkali ion affinities. The relatively high alkali ion affinity of glycerol is due to its ability to chelate alkali cations.

We also investigated the Na^+ ion affinities of some potential FAB solvents using the MS/MS approach, Figure 4. The Na^+ ion affinities of the trihydroxy compounds are greater than those of the dihydroxy species. This suggests that the third hydroxyl group is involved, in some way, in stabilizing the resulting adduct ion. Furthermore, the 1,3-diols have a slightly higher gas-phase Na^+ ion affinity than ethylene glycol, indicating that chelation on adjacent hydroxyl groups is not necessarily favored in the gas-phase. Finally, the Na^+ ion affinity of 1-thioglycerol is lower than that of glycerol. Thus, the -SH group is not as effective as the third -OH group in stabilizing the $M \cdot Na^+$ adduct ion.

The occurrence of relatively abundant cluster ions in the FAB spectra of glucose and sucrose obtained from NaCl-doped glycerol solutions provides an opportunity to study, in the gas-phase, the last few stages of the stepwise desolvation of these desorbed cluster ions. Collision-activated MS/MS spectra were obtained on cationized sucrose and glucose ions solvated by up to five glycerol molecules, Figure 5. For sucrose, the relative yield of the completely non-solvated sucrose$\cdot Na^+$ cation decreases smoothly as the size of the precursor cluster ion increases. Notice also that the fragment ion comprised of cationized sucrose bound to a single glycerol molecule shows a similar variation in relative yield with precursor ion size as that exhibited by cationized sucrose. The results obtained on glucose, however, are quite different. The relative yield of cationized glucose drops off more rapidly with precursor ion size than that observed for sucrose and the larger glucose containing cluster ions decompose to yield the mono-solvated species in preference to $Glu \cdot Na^+$.

The mechanism of the cationization process in FAB is quite different from that observed in SIMS. Common FAB solvents have high alkali ion affinities because of their ability to chelate alkali cations. Thus, many organic molecules do not compete effectively with the FAB solvent for available alkali cations. "Pre-charging" may increase a molecule's permanent dipole moment leading to an increased alkali ion affinity. The extent of gas-phase desolvation of desorbed cluster ions is influenced by the nature of the organic molecule and the rate of desolvation may also be influenced by the choice of the FAB solvent.

Origins of Cationized Molecules in Fast Atom Bombardment

I. Gas-phase processes

a. $M + C^+ \xrightarrow{N} M{\cdot}C^+$

b. $M + Gly{\cdot}C^+ \rightarrow M{\cdot}C^+ + Gly$

II. Pre-existing ions in solution

$M{\cdot}C{\cdot}Gly^+_{n(s)} \rightarrow M{\cdot}C{\cdot}Gly^{+*}_{n(g)} \rightarrow M{\cdot}C^+ + nGly$

Figure 1. Origins of cationized molecules in FAB.

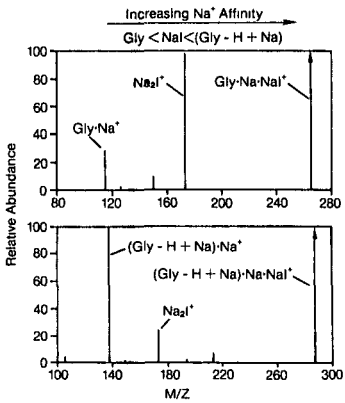

Figure 3. MS/MS spectra of some unsymmetrical cluster ions.

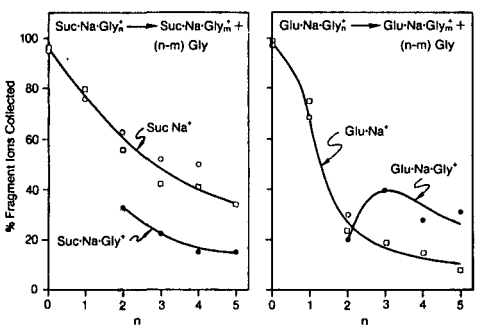

Figure 5. MS/MS study of the last few steps of the gas-phase desolvation of some desorbed cluster ions.

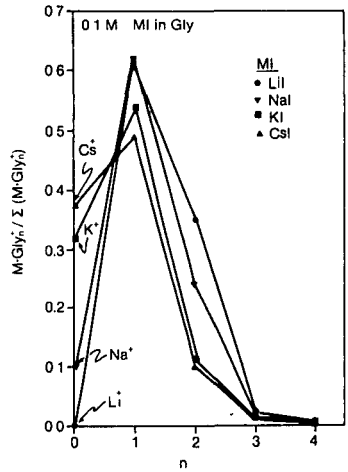

Figure 2. Distribution of cluster ions obtained from FAB of alkali iodides in glycerol.

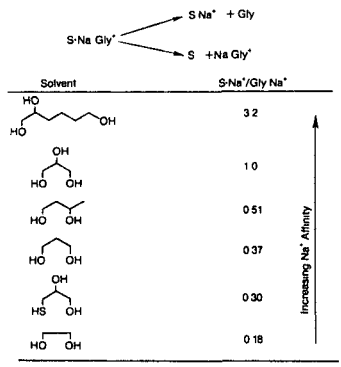

Figure 4. The Na^+ ion affinity order of some potential FAB solvents.

TANDEM MASS SPECTROMETRY STUDIES OF IONS FORMED USING FAST-ATOM BOMBARDMENT IONIZATION

D.L. Bricker, R.E. Krailler, and D.H. Russell

Department of Chemistry
Texas A&M University
College Station, Texas 77843

Tandem mass spectrometry (TMS) or mass spectrometry/mass spectrometry (MS/MS) is now a widely used method for structural characterization and mixture analysis.[1] The method is also potentially valuable for increasing the structural information obtained from mass spectrometry of non-volatile, thermally labile molecules. In particular, fast-atom bombardment (FAB) mass spectrometry has become a standard method for structural characterization of biomolecules. However, this MS method is complicated by the large amounts of chemical noise associated with the liquid matrix used to dissolve the sample and from which ionization occurs. In principle, FAB-MS/MS could be used to discriminate against the chemical noise in the same way as is done for mixture analysis, i.e., one regards the background liquid matrix signals as components arising from any other dirty system. This approach also has advantages in that the FAB ionization produces primarily parent ions, and the TMS spectrum can be used to extract the structurally informative fragment ions. In our laboratory we have used extensively FAB-TMS for structural characterization and to study the fragmentation patterns of large molecules; however, we find two basic problems with these studies: (1) the sensitivity of TMS for large molecules is less than satisfactory, and (2) in many cases the observed fragment ions are not structurally informative.

These observations regarding sensitivity and the structural significance of the observed fragments have motivated us to explore in some detail the collision-induced dissociation (CID) process. In particular, we have examined the CID of molecules such as vitamin B12, vitamin B12 coenzyme, the cyclodextrins, and small peptides (bradykinin and etc.) and were surprized by the limited amount of structural information contained in the CID spectra. A general conclusion that was drawn from these studies was that structural assignment of the compounds would have been extremely difficult had the samples been true unknowns. These considerations raise the question: is the problems associated with CID of large molecules attributed to collision dynamics or dissociation dynamics? That is, is TMS of large molecules limited by the quantity of excitation energy delivered on the collisional activation (CA) step, or does energy randomization occur and preclude the dissociation step? To address this question we have performed CID studies on small model systems using FTMS to model the CA process.

Using model systems such as benzene which are difficult to dissociate using low energy CA, we have concluded that a major limitation of CID is associated with the dynamics of CA. For example, the $C_6H_6^+$ ion (benzene radical cations) only undergoes CID at relatively high collision energy (>500 eV). At low translational energy (<500 eV) the dominant reactions are charge exchange with the collision gas (neutralization of $C_6H_6^+$), and in some cases dissociative ionization of the collision gas. If these reactions also occur for large molecules subjected to CA this could account for the low sensitivity of TMS.

A second factor which leads to low efficiency for the CID of benzene $C_6H_6^+$ is the large appearance energies for fragmentation. In addition, benzene $C_6H_6^+$ has two low lying excited states at energies which lie below the dissociation threshold. Consequently, CA of $C_6H_6^+$ produces $[C_6H_6^+]^*$ with insufficient energy to dissociate. According to Massey's adiabatic criterion[2] the cross-section for formation of these lower lying energy states will be much greater than the cross-section for formation of the higher energy dissociating states. In large molecules the density of low lying, non-dissociating states will be extremely large and could reduce the CID sensitivity and favor dissociation via the lowest energy reaction channels. Again, this prediction is consistent with the CID of large molecule ions, i.e., the CID spectra show the same fragmentation reactions as observed in the metastable specta.

Based on the available experimental results it is clear that one limitation of TMS of large molecules is associated with collision dynamics. The observed CID behavior of large

molecules can be modeled using small systems and energy-resolved CID-FTMS. These studies do not address the question of limitations associated with dissociation dynamics. These questions are now being addressed using laser-ion beam photodissociation experiments. In this experiment, the energy used to activate the molecule is specified (energy of the photon) and direct conclusions can be made regarding the role of dissociation dynamics.

1. Tandem Mass Spectrometry, F.W. McLafferty (Ed.), T. Wiley and Sons, Inc. New York 1983.

2. Collision Spectroscopy, R.G. Cooks (Ed.), pp. 383-384, Plenum Press, New York 1978.

BOMB REDUCTION OF WATER OVER ZINC FOR ISOTOPE RATIO ANALYSIS

D. A. Schoeller, R. Delfino, and C. J. Brown, Department of Medicine, University of Chicago, Chicago, IL 60637

Analysis of deuterium abundance in water samples generally requires reduction of the water to H_2 gas before mass spectrometric analysis. This reduction is typically performed using hot uranium with serial introduction of the water samples (1). This serial procedure is laborious and its accuracy and precision are limited by memory between successive samples.

Recently the use of zinc reduction has re-emerged as an alternative to the uranium reduction (2). We were interested in trying a modification of this method using a single use, sealed bomb, which might be faster and less subject to memory than uranium reduction.

Methods

Samples of 1 μL were sealed in a 25 μL capillary tube and placed under vacuum. The sample was isolated from the 5 l/s Hg vacuum pump, the capillary tube broken, and the water cryogenically (-196°C) distilled into a 15 x 0.6 cm pyrex or quartz tube containing 250 mg of 30 mesh zinc granuals (JT Baker Chemical Co.). Zinc was pretreated by an aqua regia wash and vacuum dried. Zinc granuals should have a shiny surface. Finally, these granuals were sealed in the pyrex or quartz tube under vacuum and heated to 550°C before introducing water.

Reference water samples were reduced over uranium turnings at 700°C. Samples were sealed in capillary tubes as described above and distilled under vacuum before reduction. At least two reference samples were serially reduced to minimize memory. Yields for both reductions were measured in a mercury manometer mounted at the outlet of a Toepler pump.

Isotope ratios were measured on a dual detector, triple inlet (3) 3-60 isotope ratio mass spectrometer (Nuclide Corp., State College, Pa.). Results were expressed as the per mil difference from standard mean ocean water.

$$\delta_{smow} = \frac{(D/H)\ \text{sample} - (D/H)\,\text{smow}}{(D/H)\,\text{smow}} \times 1000$$

Results

Initial reductions at 450° had low yields and were very depleted in deuterium relative to the reference sample (Table 1). Increasing the temperature improved the yield, but the isotope ratios were still depleted relative to the reference sample.

Increasing the time that the samples were kept in the oven caused a further isotopic depletion (Table 2). The gradual isotopic depletion suggested that the sample was exchanging with hydrogen that was relatively depleted in deuterium.

We tested for exchange by reducing water over uranium and sealing the resulting H_2 gas in zinc free reduction tubes. The tubes were then heated at 550°C for 0.5h. Isotopic integrity was lost in all samples (Table 3). Exchange was worst for pyrex tubes and least for annealed quartz. We estimate that pyrex exchanged 8×10^{-6} moles of H_2 and annealed quartz exchanged 2×10^{-6} moles of H_2. The apparent isotope ratio of the exchangeable hydrogen was -240°/oo.

The amount of exchangeable hydrogen was equivalent to over 300 monolayers of water and thus was probably not due to the surface adsorbed water. The exchangeable hydrogen was probably present as chemically bound hydroxyl groups (4).

At present, attempts to reduce the amount of exchange have been largely uneventuful. Preheating the sealed tube containing zinc for 0.5h at 550°C did decrease the exchangeable hydrogen slightly. The preheating had the added advantage of degassing the zinc and thus reducing the nonhydrogen blank to a negligible amount. Preheating, however, did occasionally decrease the activity of the zinc.

Conclusions

Bomb reductions over zinc were faster and more convenient than serial reductions over uranium. Unfortunately, the bomb reduction was limited in our hands by isotope exchange. At this time, the bomb reduction is not useful for analysis of dueterium enriched samples. It may be possible to analyze natural abundance samples because they are isotopically similar to the exchangeable hydrogen.

Table 1. Effect of temperature on reduction of water over zinc

Sample	δ true	Temp °C	Yield[a]	δ measured
TAP	-46°/oo	450	34±12	-420±50°/oo
TAP	-46	550	103±3	-58±2
TAP	-46	650	105±3	-68±8

[a]mean ± SD

Table 2. Effect of heating time over water reduction over zinc

Sample	δ true	Time, h	δ measured
TAP	-46°/oo	0.5	-58±2°/oo
TAP	-46	1	-58±1
TAP	-46	2	-64
TAP	-46	4	-73±8
TAP	-46	8	-93±2

Table 3. Isotope exchange of H_2 gas with bound hydrogen

Sample	δ true	Material	δ measured
H_2-TAP	-46°/oo	pyrex	-62±2°/oo
H_2-SLAP	-428	pyrex	-401±1
H_2-SPIKED	396	pyrex	298±3
H_2-SPIKED	396	quartz	348±20
H_2-SPIKED	396	anneal quartz	366±4

Acknowledgements

We thank R. Slater and P. Taylor for the mass spectrometric analyses.
Supported by NIH grant AM 30031.

References

1. J Bigeleisen, ML Perlman, HC Prosser. Anal Chem 24:1356, 1952.
2. ML Coleman, TJ Shepherd, JJ Durham, JE Rouse, GR Moore. Anal Chem 55:993, 1982.
3. DA Schoeller, DW Peterson, JM Hayes. Anal Chem 55:827, 1983.
4. J Graff, D Rittenberg. Anal Chem 24:878, 1952.

EI AS THE IONIZATION METHOD OF CHOICE FOR MASS SPECTRAL ANALYSIS OF SILOXANE POLYMERS.

W. Bone, J. Marasco, and B.P. Doctor, Walter Reed Army Institute of Research, Division of Applied Biochemistry, Washington, D.C. 20307

Objective: To analyze Siloxane polymers by Mass Spectrometry and be able to classify them according to the side chains on the silicon atoms. Two ionization techniques are evaluated for their ability to accomplish this type of analysis, EI and PID (FAB). Polymers are often mixtures with an average molecular weight outside the mass range of most mass spectrometers. Therefore, fragmentation patterns are used to deduce what the various side chains are in addition to the chain terminus.

Siloxanes: General Properties and Applications

Common feature is the siloxy chain or backbone which may contain several hundred silicon atoms the side chains (R_{1-4}) usually consist of one or two different substituents such as the following: methyl; phenyl, including halogenated phenyl groups; trifluoropropyl; cyanoethyl; alkyl groups up to 3 carbon atoms (more than 3 carbon atoms in an R group do not usually change the properties of the polymers in a positive way; therefore, few siloxane polymers contain chains longer than propyl groups); branched chain polymers are fairly common are are indicated by another siloxy chain in place of an R-group; polymerization is often terminated with a trimethylsilyl ($Si(CH_3)_3$ group; phenyl groups may be substituted for 1 or more of the methyl groups. Another terminal group is the silanol, ($-SiMe_2OH$). Siloxanes have been found useful in such diverse areas as cosmetics and pharmaceuticals, vibration damping, heat transfer fluids, dielectric fluids, lubricants, and even gas chromatography.

Re

Results: The Dimethyl-Polysiloxanes are the simplest of the compounds and can be differentiated from other siloxanes by noting certain ions and ion pairs in the EI Mass Spectra. Intense ions occur at masses 73,147,221 and every 74 amu thereafter up to about mass 517. Also conspicuous are a series of ions beginning at mass 207 and occurring every 74 amu up to mass 503. Together these series of ions appear

as doublets 14 amu apart. The Branched-chain polymers are indicated by an increase in the high mass to low mass ratio (high/low) (high= low + 14) for each doublet in the series. The compositions of the ions are easily rationalized (as repeating $SiO(CH_3)_2$ units) even though their origins may be in doubt.

The Phenyl-substituted Polysiloxanes vary according to the degree of phenyl-substitution and this is reflected in the EI Mass Spectra in the positive ion mode. Phenyl-substituted polysiloxanes are indicated by the presence of intense ions at masses 135 and 197 presumably due to $SiO(CH_e)_2$ and SiO_2CH_3 respectively. An ion at mass 147 and which is present in polysiloxanes with only methyl-substitution can be used in conjunction with peaks at masses 135 and 197 to reflect the degree of phenyl-substitution. The ratio of ion intensities for masses 147 and 197 to 135 vs. the mole% of methyl-phenyl-substitution follow general trends (see plots) which can be used to estimate the degree of phenyl-substitution in other polysiloxanes. Only the Dimethyl-Diphenyl-Polysiloxane did not fall on the plots as expected and this may be due to the silanol chain stopped unit (all others were trimethyl-chain-stopped).

The Dimethyl-MethylCyanoethyl Polysiloxanes are difficult to characterize by their positive ion EI Mass Spectra. The spectra of two polymers of this type yielded significantly different ions which could not easily be assigned. Negative ion mass spectral data may be more indicative of the presence of cyano-groups in polysiloxanes and studies along these lines is called for in the future. To date PI-EI-MS has been unsuccessful in detecting cyanoethyl-substituents in polysiloxanes.

The 3,3,3-Trifluoropropyl-polymethyl Siloxane has not been characterized by the positive ion EI Mass Spectrum. This is due to a lack of appropriate standards more than anything else. Again negative ion mass spectral data might be more promising.

A Tetrachlorophenyltrisiloxy, Dimethyl-Polysiloxane (Trimethyl chain stopped) polymer was available and mass spectral data obtained. In addition this polymer with Iron Octoate added and one with Zinc Dialkylthioposphate were available. Although the mass spectra are different it would be difficult to classify an unknown except by default.

ANALYSIS OF SILANES FOR HYDROGENATED AMORPHOUS SILICON (α-Si:H) PRODUCTION BY GAS CHROMATOGRAPHY/MASS SPECTROMETRY (GC/MS)

P. Jane Gale, Bryan L. Bentz, William L. Harrington,
Charles W. Magee and Herbert A. Weakliem

RCA Laboratories, Princeton, NJ 08540

The presence of impurities in glow discharge systems can cause the inclusion of impurities in thin films grown in the discharge chamber. Among the sources of impurities are the discharge gases themselves, as shown by the data in Table I. Using Secondary Ion Mass Spectrometry (SIMS) to ascertain elemental concentrations in amorphous silicon films, we correlate discharge gas composition with the concentrations of impurities in the films.

TABLE I

Correlation of Impurities in Discharge Gases with Impurities in Amorphous Silicon Thin Films

Gas Cylinder Impurities	Concentration of Element, atomic %				
	Hydrogen	Carbon	Oxygen	Nitrogen	Chlorine
v. clean	16	0.04	0.04	0.0006	0.0002
5% siloxane	18	0.016	0.4	0.018	0.0004
<100ppm "	14	0.01	0.01	0.0018	0.0002
2% methane	12	0.4	0.1	-	0.00014
2% nitrogen	10	0.004	0.08	0.4	0.00008
.07% dichlorosilane	10	0.006	0.006	0.004	0.004

The importance of knowing the composition of the discharge gas before it is used for thin film production is obvious; and, for this reason, we set about establishing a convenient method for handling noxious gases in GC/MS analysis.

Sampling gases for analysis is best accomplished using a flowing system from which aliquots can be extracted. This dynamic sampling method assures uniformity in replicate measurements and minimizes "memory efforts" in the sampling volume. If the gases to be analyzed are poisonous and/or explosive, they must also be exhausted into a closed system, preferably one into which an inert dilution gas can be bled. Shown schematically in Figure 1 is such a system developed at RCA Laboratories for the analysis of silanes. It is coupled to our HP 5985B GC/MS through a Valco 6-port valve, allowing periodic flushing of the 1-cc sample loop onto a CTR Dual Column (Alltech Associates). Using this column, we were able to analyze fixed gases and silane derivatives in one GC injection. Figure 2 contains the Reconstructed Ion Chromatogram (RIC) of a relatively impure tank of silane, showing typical impurities.

DIAGRAM OF SAMPLE FLOW THROUGH GAS HANDLING MANIFOLD

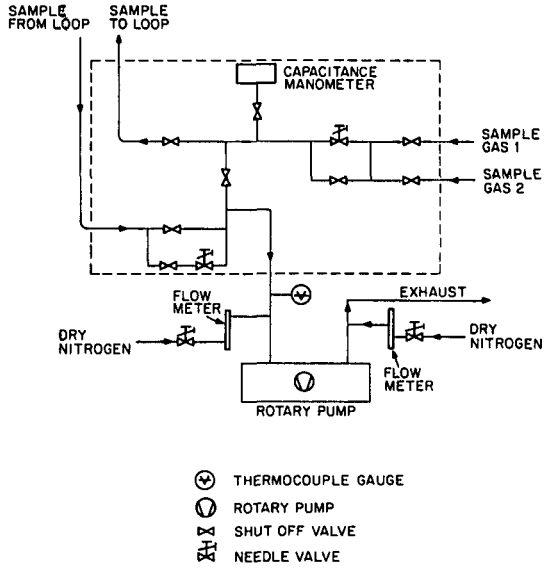

RECONSTRUCTED ION CHROMATOGRAM (RIC) OF A RELATIVELY IMPURE SILANE TANK

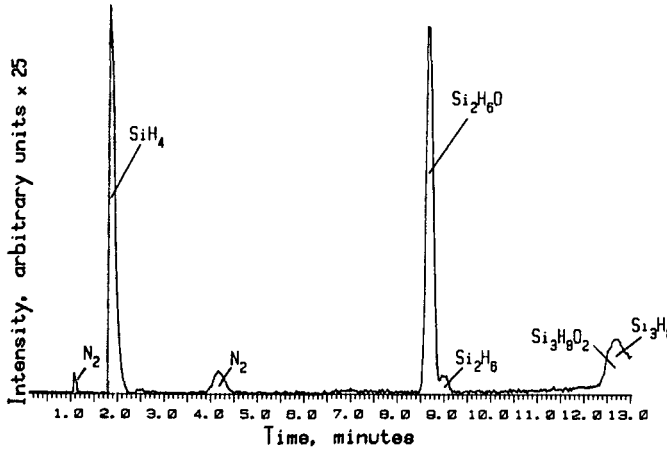

THERMOCHEMICAL STUDIES OF SmO^+ AND SmO_2^+

By

Edmond Murad
(Air Force Geophysics Laboratory, Hanscom AFB, MA, 01731)

Cross sections for the reactions:

$$Sm^+ + O_2 \rightarrow SmO^+ + O \qquad (1)$$

and

$$SmO^+ + O_2 \rightarrow SmO_2 + O \qquad (2)$$

were measured in a double mass spectrometer system in the range E_{CM} = 0.2 to 10 eV. The apparatus has been described before.[1] The primary ions, Sm^+ and SmO^+, were formed by surface ionization using a technique described previously.[2] Reaction (1), which is exothermic by about 0.3 eV, according to thermochemical measurements, exhibited the behavior expected for such reactions, namely rapidly decreasing cross sections with increasing energy. Extrapolation to thermal energy leads to an estimated thermal rate constant of $\sim$ 2 (-10) cc/molecule-sec. The kinetics of the reaction are complicated by the high densities of excited electronic states of Sm^+ and SmO^+. Undoubtedly reaction (2) is likewise complicated. In the case of reaction (2), the cross section curve exhibited a threhold at E_{CM} = 0.6 $\pm$ 0.2 eV. If the correction for the population of excited electronic states in reactions (1) and (2) is the same, then we estimate $D_0(SmO^+-O)$ = 4.3 $\pm$ 0.3 eV.

In an allied experiment the thermochemical properties of SmO_2 were studied in a high temperature mass spectrometer which was used in earlier studies.[3]. These measurements are preliminary and consist of a study of the equilibrium:

$$Sm(g) + SmO_2(g) = 2\ SmO(g) \qquad (3)$$

Third-law heats using estimated free energy functions for SmO_2 yield $D_0(SmO-O)$ = 111 $\pm$ 7 kcal/mol (4.8 $\pm$ 0.4 eV). When this preliminary result is combined with the data derived from reaction (2), $IP(SmO_2)$ is found to 6.1 $\pm$ 0.4 eV.

The work on reaction (1) has been finished and is in press now.[4]

References

1. W. B. Maier, II and E. Murad, J. Chem. Phys., 55, 2307 (1971).
2. E. Murad, J. Chem. Phys., 77, 2057 (1982).
3. E. Murad. J. Chem. Phys., 75, 4080 (1984).
4. E. Murad, Int. J. Mass Spectry. Ion Proc., In Press.

A Mass Spectrometric Investigation of the Vaporization of Germanium-Sulfur Compounds

Toshiaki Kogai* and Edmund J. Rolinski
Chemical Engineering Department
University of Dayton
Dayton, Ohio 45469-0001

1. Introduction

Germanium-sulfur system is being considered for selective optical coatings. However, the vapor pressure of this system has not been investigated extensively. In this study, the mass spectrometer was used to determine the thermodynamic data of GeS and GeS_2. As a result, GeS vaporized according to the reaction $GeS(s) \longrightarrow GeS(g)$ (294-384°C) like most group IV-group VI compounds, while GeS_2 was found to decompose into GeS(g) and $S_2(g)$ under the investigated temperatures (456-578°C).

2. Experimental

The instrument used is a Nuclide Analysis Associates 12-90 HT magnetic sector mass spectrometer. The Knudsen cell used is a tantalum cell which has a Clausing factor of 0.5. Data were taken using nominal 20eV electrons. The GeS and GeS_2 samples were purchased from Alfa Products, Danvers, Massachusetts and listed purities were 99.9 and 99.99%, respectively.

3. Results

3.1 Identification of Neutral Vapor Species

Identification of vapor species was done based on its shutterability, appearance potential and isotopic abundance. The ion species GeS^+ as parent ion and Ge^+ and S^+ as fragment ions were observed in GeS vaporization and $GeS(s) \longrightarrow GeS(g)$ was expected to exist as the most probable reaction in the vaporization of GeS under the investigated temperatures.

Ions observed were GeS^+ and S_2^+ as parent ions and Ge^+ and S^+ as fragment ions in GeS_2 vaporization and from the same Second Law enthalpies of GeS^+, Ge^+ and S_2^+ within experimental errors it was regarded that the most probable reaction existing is $GeS_2(s) \longrightarrow GeS(g) + 1/2\ S_2\ (g)$.

3.2. Thermodynamic Data of GeS and GeS_2

Vapor pressures of GeS are illustrated in Figure as log P vs. 1/T. In the case of present investigation, the calibrations to relate the intensity of a given species as measured by the mass spectrometer to the pressure of the neutral vapor species were carried out by a quantitative vaporizations of a given amount of GeS and GeS_2. The heat of sublimation of GeS at 298 K, ΔH_{298} of 29.7±0.9 (kcal/mole) was calculated using the specific heats of GeS(s) and GeS(g) based on the Σ versus 1/T plots.

Table shows the Second Law enthalpy ΔH_T of the reaction and the partial vapor pressures of GeS(g), P_{GeS} and $S_2(g)$, P_{S_2} in the vaporization of GeS_2.

* On leave from Toshiba Corporation, Tokyo, Japan.

References

1. R.F. Barrow et al., Trans. Faraday Soc., 51, 1480 (1955).
2. V.I. Davydov et al., Zhur. Neorg. Khim., 2, 2003 (1957).
3. E. Shimazaki et al., Bull. Chem. Soc. Japan, 29, 294 (1956).
4. H. Spandau et al., Z. anorg. u. allgem. Chem., 295, 291 (1958).
5. H. Kenworthy et al., U.S. Bureau of Mines Rep. Invest. 5190 (1956).
6. H. Seta et al., Nippon Daigaku Bunrigakubu Shizenkagaku Kenkyusho Kenkyu Kiyo, 4, 61 (1968).

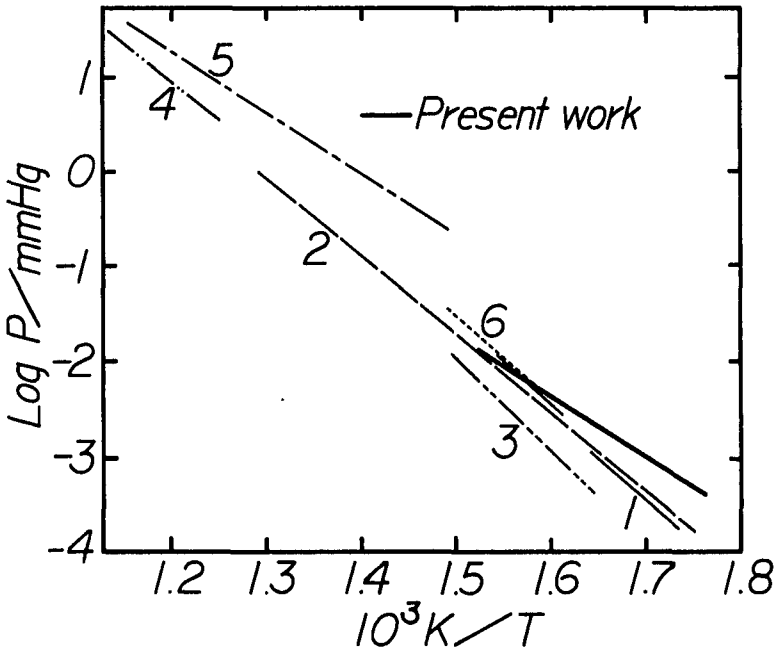

Figure Comparison of GeS Vapor Pressures with Literature

Table Partial Vapor Pressures of Vapor Species of GeS_2 and Second Law Enthalpy of the Reaction :$GeS_2(s) \longrightarrow GeS(g)+1/2S_2(g)$

$\text{Log } P_{GeS/mmHg} = -7281.4/T + 7.57,$

$\text{Log } P_{S_2}/mmHg = -7281.4/T+7.27$ (729—851 K)

$\Delta H_T = 22.2 \pm 0.8$ (kcal/mole)

Californium Plasma Desorption Mass Spectrometry of
Some Metal-Ligand Complexes

L.K. Pannell and H.M. Fales, Laboratory of Chemistry, NHLBI, Bethesda, MD 20205; J.P. Scovill and D.L. Klayman, Division of Experimental Therapeutics, WRAIR, Washington, D.C. 20307; D.X. West, Department of Chemistry, Illinois State University, Normal, IL 61761; and R.L. Tate, DCRT, Computer Systems Laboratory, NIH, Bethesda, MD 20205.

A variety of hexacordinate metal ligand complexes of the general formula $[L_2M]^+[X]^{n-}$ (L was either ligand I or II; M was Fe, Co or Mn; X was the counterion) were studied by californium plasma desorption mass spectrometry on a time-of-flight instrument constructed by Macfarlane and coworkers at Texas A & M.

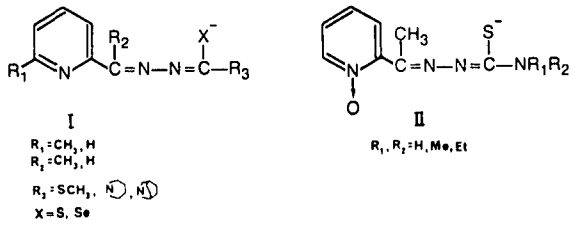

These compounds are under investigation by the army as antimalerial agents. In general, it was found that the positive ions spectra represented the metal-ligand complex and the negative ion spectra the anion. The positive ion spectra showed a strong peak due to the $[L_2M]^+$ species as well as ions resulting from loss of part or all of one ligand. In the lower mass region, peaks due to the metal atom and fragments of the ligand are observed as well as clusters of these fragments with the metal atom. The spectrum below is that for ligand I with R_1 = H, R_2 = Me, X = S and R_3 = 3-azabicyclo[3.2.2]nonane.

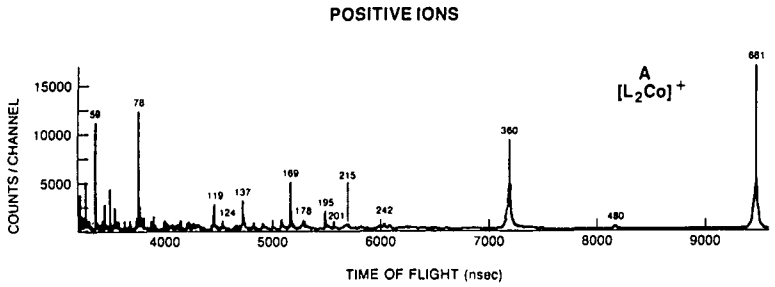

All peaks in the spectra were identified by observing their shifts with varying metal atoms and ligand substituents. The metal atom in the fragment ions had oxidation states which varied from +1 to +3. In the spectrum above, the 4 major peaks are assignable to $[L_2Co^{III}]^+$ (m/e 661), $[LCo^{II}]^+$ (m/e 360), pyridinium ion (m/e 78) and $[Co^I]^+$ (m/e 59). A fragmentation pathway has been found which accounts for the formation of the various species observed.

The negative ion spectra (anion counterion) were more complicated and showed the result of recombinations of the anion and its fragments with the cation metal atom and NCS^-, CN^- and S^{2-} derived from fragmentation of the ligand. For example, $[Co(NCS)NO_3]^-$ was detected in the negative ion spectrum of the above described complex $[L_2Co]^+$ when the counterion was $[NO_3]^-$. In both positive and negative ion spectra, no doubly charged ions were observed, even with the counterion $[CoCl_4]^{2-}$ which instead lost Cl^- and was detected as $[CoCl_3]^-$ and its fragments.

Conclusion. Californium plasma desorption mass spectrometry was found to be a useful tool for characterizing metal-ligand complexes of the type described in positive ion mode. It correctly identified the complex formed from the reaction of ligand I (R_1 = H, R_2 = Me, R_3 = 3-azabicyclo[3.2.2]nonane, X = S) with $FeCl_2$ to be $[L_2Fe]^+[FeCl_4]^-$ and not $[L^-FeCl_2]$ as previously ascribed by Y.K. Bhoon et al. (Transition Met. Chem., 7, 264-266). This result was subsequently confirmed by X-Ray crystallography.

APPLICATION OF ARTIFICIAL INTELLIGENCE PROGRAMMING TECHNIQUES
TO THE DEVELOPMENT OF AN EXPERT SYSTEM
FOR TUNING A TRIPLE QUADRUPOLE MASS SPECTROMETER

Carla M. Wong, Stanley M. Lanning, Richard W. Crawford and Hal R. Brand
Lawrence Livermore National Laboratory, Livermore, CA 94550

ABSTRACT

At Lawrence Livermore National Laboratory (LLNL), a triple quadrupole mass spectrometer (TQMS) has been designed and built which has all operational parameters under computer control using a DEC LSI-11/23 system. The ultimate goal has been to use this system as a prototype for "knowledge-based" instrument control, i.e., an "intelligent" instrument [1].

Triple quadrupole mass spectrometers are ideal candidates for the implementation of self-adaptive, "expert" or "knowledge-based" control for several reasons. Operationally, they are very complex instruments requiring selective tuning or optimization of over 30 control parameters; they produce vast amounts of multidimensional data; and, most importantly, the knowledge required for tuning or optimization can be represented as procedures or rules. Therefore, it is possible to encode a tuning procedure, including heuristics, to describe real-time optimization or tuning of the data acquisition process throughout the entire mass range.

There are three computers used in this system. One DEC LSI-11/23 runs under a single user (RT-11, V4) operating system for instrument control and data acquisition. Another DEC LSI-11/23 runs under a time sharing, multitasking, (RSX-11M) operating system for data processing, manipulation and storage. The third is a Xerox 1100 (Dolphin) LISP processor. Figure 1 shows a detailed view, but complete implementation details are described elsewhere [2].

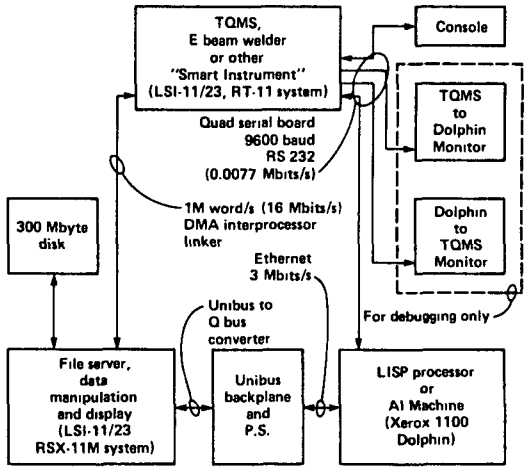

One of the procedures for using the instrument that requires human intervention is the procedure. An artificial intelligence, expert or knowledge-based system has been developed tuning process. Tuning a system as complex as a TQMS is typically a non-algorithmic

Work performed under the auspieces of the U.S. Department of Energy by the Lawrence Livermore National Laboratory under contract number W-7405-ENG-48.

that embodies a set of production rules or heuristics to accomplish this. These rules take the form:

IF <premises> THEN <conclusion>

They are invoked by a "backward chaining" search strategy to automatically tune the TQMS. The AI system resides within a knowledge representation language KEE (Knowledge Engineering Environment) on the Xerox 1100 Dolphin LISP processor.

As illustrated in Figure 2, to tune the TQMS, you load the knowledge base, display the device, attach gauges, initialize the CALIBRATION instructions, and invoke the INTERPRET-INSTRUCTIONS. Initialization proceeds, the rules are invoked and tuning occurs as instructions sent to the device actually vary the voltage on each of the instrument control parameters.

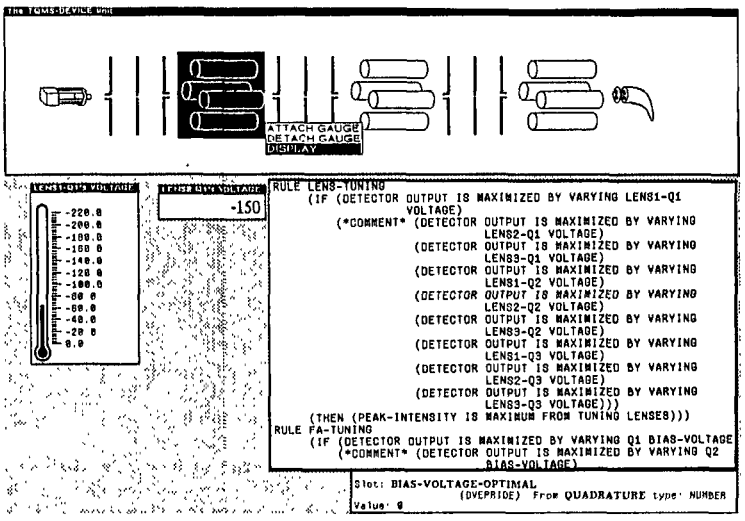

1. C.M. Wong, R.W. Crawford, V.C. Barton, H.R. Brand, K.W. Neufeld, and J.E. Bowman, Rev. Sci. Inst., 54, (8), 996-1004, (Aug. 1983).

2. C.M. Wong, R.W. Crawford, J.C. Kunz and T.P. Kehler, IEEE Transactions on Nuclear Sciences, Vol. NS-31, No. 1, 804-810 (Feb. 1984).

MULTICOMPONENT ANALYSIS OF MS/MS DATA

D.E. Giblin, D.A. Peake, and R.L. Lapp
Midwest Center for Mass Spectrometry
University of Nebraska-Lincoln, Lincoln, NE 68588

Collisionally activated dissociation (CAD) in mass spectrometry has been employed to elucidate ionic structures and to identify components in complex mixtures. However, isomeric and/or isobaric ions give rise to composite spectra which are the superposition of the individual spectra. Often, in such composite spectra there are no unique ions associated with a given component. Therefore we have been developing a method to treat such data for mixtures and also to use as a adjunct for factor analysis to elucidate pure spectra when the pure ions are not available.

A number of objectives have been considered important in the development of a multicomponent analysis technique for MS/MS data. It should not require unique ions but only unique patterns of ion intensities for the various components. It should be easy to use in that it employs already existing data collection and workup routines as its basis and does not requires exotic data collection procedures or involve extensive programming and long execution times[1]. It should give accurate values and be robust; that is, the determined values should not change significantly due to small perturbations of the input parameters. And it should take into account the nature of the data: peak intensities are based on a random counting process with a Poisson distribution[2], peak intensities for the reference ions also have error distributions; and normalization appears to be a necessity[3].

The methodology of the analysis involves several working assumptions. Metastable ion contributions to the CAD spectra are insignificant. No mass vs ion current discrimination occurs after the collision cell. The CAD spectra are constant over the range of collision gas pressures used for analysis and over time. The cross-sections for CAD are the same for the isomeric ions[4]. Ion currents have a Poisson distributions since they are based on a random rate process. The measurements of peak intensities are statistically independent. Also, the effects of peak overlap are considered small on the analysis. And finally, a linear scan law holds for mass assignments of the fragment ions.

In typical operation, scans over the mass range for fragment ions are summed into a buffer to improve the S/N ratio under the control of the data acquisition program.

Normalized peak intensities are determined by using the data workup program. Masses are assigned and the spectrum is displayed on the video terminal from which the operator indicates the locations of baseline intensity. The program then fits a straight line through those points by linear least squares and subtracts the line values from the data to correct for baseline drift. The operator then indicates the locations of all peaks in the spectrum and also selects the peaks which bear significant isomer-specific information. Peak tops are then located searching from the nearest nominal masses. The intensities of the selected peaks are then divided by the sum of the intensities of all peaks in the spectrum to give the normalized intensities which are stored in a file. The workup program then performs the same calculations automatically for all other spectra as instructed by the operator.

The normalized peaks intensities are assembled into files for regression analysis by using an auxiliary program. The operator indicates which files contain reference and which contain sample peak intensities.

Multiple linear least-squares regression is then performed on the files by a standard program that has been modified to include weighting of the residuals by the inverse square-root of the sample peak intensities. The program determines the relative mole fractions along with their respective standard errors and also computes parameters which indicate the significance of the mole fractions and the regression in general.

Mixtures of isomeric octynes were analyzed by forming gas-phase Fe^+ adducts with the various constituents and then obtaining the CAD spectra of the adducts. The data were gathered by using a Kratos MS-50 triple analyzer mass spectrometer. While overall error of determined mole fractions relative to the prepared values was less then 15% for 1:1 mixtures, it degraded to around 60% for the smaller component in 30:1 mixtures. Inspection of the regression parameters and residuals indicates a much higher precision. Examination of the spectra reveals that the limiting factor is probably spectral constancy over time and collision gas pressures.

1. L.M. Karrar, H.L. Gordon, S.M. Rothstein, J.M. Miller, and T.R.B. Jones, Anal. Chem., 55, 1723 (1983).

2. D.W. Peterson and J.M. Hayes, Contemp. Topics in Anal. Clin. Chem., 3, 217 (1978).

3. L.M. Bass and M.T. Bowers, Org. Mass Spectrom., 17, 229 (1982).

4. C.J. Proctor and F.W. McLafferty, Org. Mass Spectrom., 18, 193 (1983).

MS/MS Matching Techniques and Their Dependence on Instrumental Parameters

K.P. Cross and C.G. Enke, Department of Chemistry
Michigan State University, East Lansing, MI 48824

The MS/MS automated search system is a comprehensive, interactive system which allows the user to match an unknown mass spectrum against either primary or CAD spectra in a Reference Data Base. It is a transparent system which employs several matching techniques for flexibility and avoids data compression or dependence on theoretical spectral properties. The system has been used to aid in structure elucidation, as well as in the determination of the effects of instrumental parameters on MS/MS spectral patterns.

The strategy of the search system is to eliminate the vast majority of candidate spectra by pre-screeening data using inverted pointer files (1) Then an intensity-based matching algorithm determines seven match factors to characterize the correspondence between the unknown and each remaining candidate spectrum. Second-order polynomial fits to quotient-spectra may be used to mask some deviations in spectra taken under different conditions (2)

Match Factor Definitions

PT - An overall match factor that indicates how well intensities of all the peaks in the two spectra match

$$PT = \frac{\Sigma \left[Y_{si} + Y_{ri} - 2 \left| Y_{si} - Y_{ri} \right| \right]}{\Sigma Y_{si} + \Sigma Y_{ri}} \times 100$$

$$\text{where } Y_i = \text{Log}_2 (1/TIC) + S$$

where S is a sensitivity factor

PC - A pattern correspondance factor that indicates how well the intensity of the peaks in common match

$$PC = \frac{\Sigma \left[Y_{si} - \left| Y_{ri} - Y_{si} \right| \right]}{\Sigma Y_{si}} \times 100$$

NC - The number of peaks common to both the candidate and unknown spectrum.
NS - The number of peaks remaining unmatched in the sample spectrum.
NR - The number of peaks remaining unmatched in the reference spectrum.
IS - The percent total ion current of the sample spectrum that was unmatched in the comparison due to NS
IR - The percent total ion current of the reference spectrum that was unmatched in the comparison due to NR.
NP - The number of peaks used in the chi-square determination.
X^2 - The reduced chi-square from a second-order polynomial fit to the quotient spectrum

N-Butylbenzene (m/z 134+) daughter spectra taken at various conditions are compared with m/z 134+ daughter spectra of structurally related compounds (Figure 1). These results reveal the ability of the system to correctly identify the sample when reference spectra are obtained under various instrumental conditions It also indicates that collision cell pressure is more critical than collision energy in spectral matching

The matching of Methylbenzoate (m/z 134+) daughter spectra against spectra taken under various experimental conditions (Figure 2) determines the significance of each instrumental parameter and illustrates that similar spectra may be obtained by using different combinations of instrumental parameters

A Methylbenzoate (m/z 134+) daughter spectrum obtained on an Extra-Nuclear EL-400TQ-3 instrument is compared with the same compound run under various conditions on a Finnigan TSQ instrument (Figure 3) (3). The results indicate that the collision cell pressure yielding similar spectra is different for the two instruments. Hence standard conditions for obtaining CAD spectra should determine the collision cell pressure based on the ratio of the parent ion intensity with collision gas present compared to the parent ion intensity when there is no collison gas (P/Po)

This work was supported by National Institutes of Health grant No. 2R01GM28254-04.

(1) P.A Hoffman; Presented at 31st Annual Conference on Mass Spectrometry and Allied Topics; Boston, MA, May 8-13th, 1983.
(2) D. Henneberg, Ibid
(3) Finnigan TSQ data were obtained at Purdue University.

M/Z 134$^+$ DAUGHTER MATCH FACTORS
SAMPLE SPECTRUM (N-BUTYLBENZENE 33 P/P_0, 28 V CE)

PT	PC	NC	NS	NR	IS	IR	NP	Chi-Square	Name	P/P_0	CE(V)
100	100	9	0	0	0	0	6	0 1526D+03	N-BUTYLBENZENE	33	28
96	96	8	1	0	0	0	6	0.7615D+01	N-BUTYLBENZENE	33	33
93	93	7	2	0	0	0	6	0 2337D+02	N-BUTYLBENZENE	33	20
81	82	8	1	2	0	0	6	0 3911D+03	N-BUTYLBENZENE	10	22
69	79	9	0	0	0	0	6	0 1622D+03	N-BUTYLBENZENE	10	27
58	55	8	1	0	24	0	5	0 9602D+02	N-BUTYLBENZENE	.10	17
50	53	8	1	1	43	18	5	0 9690D+02	T-BUTYLBENZENE	10	30
42	45	3	6	0	32	0	2	0 0000D+00	T-BUTYLBENZENE	33	30
42	44	3	6	0	32	0	2	0.0000D+00	TRIETHYLBENZENE	.33	10
39	42	3	6	0	32	0	1	0.0000D+00	DIETHYLBENZENE	.33	20

FIGURE 1

METHYLBENZOATE (m/z 136$^+$ DAUGHTER) MATCH FACTORS
SAMPLE SPECTRUM (5 0 E-5 TORR COLL PRESS, 70 EV, 10 V CE, -10 V DRAWOUT)

PT	PC	NC	NS	NR	IS	IR	NP	Chi-Square	Coll Pres(Torr)	EV	CE(V)	Draw(V)
100	100	8	0	0	0	0	4	0.3052D-03	5 0 E-4	70	10	-10
97	97	7	1	4	0	1	4	0.2467D+01	5.0 E-4	40	10	-20
96	96	6	2	1	1	0	4	0 4652D+02	5 0 E-4	40	10	-10
94	98	6	2	7	1	2	4	0 3277D+01	5 0 E-4	70	10	-20
92	96	6	2	8	1	1	4	0.2612D+00	5 0 E-4	20	10	-20
89	90	4	4	0	2	0	4	0.2171D+03	1 0 E-3	20	50	+10
88	94	6	2	2	1	1	4	0 9262D+02	5 0 E-4	20	20	0
88	88	4	4	0	2	0	4	0 4469D+03	1 0 E-3	20	40	+10
87	95	7	1	5	0	3	4	0 8226D+01	5.0 E-4	20	10	-10

FIGURE 2

METHYLBENZOATE (m/z 136$^+$ DAUGHTER) MATCH FACTORS
EL-400TQ-3 SPECTRUM (10 V CE, 5 0 E-5 TORR COLL PRESS)
COMPARED WITH FINNEGAN TSQ SPECTRA

PT	PC	NC	NS	NR	IS	IR	Reg #	Coll. Pres(Torr)	CE(V)
80	90	7	1	18	0	4	10	9.0 E-4	20
75	88	8	0	30	0	10	17	1 9 E-3	10
74	84	8	0	12	0	6	9	9 0 E-4	10
68	77	8	0	25	0	2	11	9.0 E-4	30
61	64	5	3	6	1	2	2	2.5 E-4	20
60	61	4	4	5	2	1	1	2.5 E-4	10
59	65	5	3	8	1	4	4	2 5 E-4	40
59	64	4	4	8	2	3	3	2.5 E-4	30
51	64	8	0	33	0	7	18	1 9 E-3	20
33	39	8	0	40	0	7	19	1 9 E-3	30

FIGURE 3

ORGANIC STRUCTURE DETERMINATION BY TRIPLE QUADRUPOLE MASS SPECTROMETRY: PROGRESS REPORT

Anne B. Giordani, Hugh R. Gregg, Phillip A. Hoffman, Kevin P. Cross, Carl F. Beckner and Christie Q. Enke

Department of Chemistry, Michigan State University, E. Lansing, MI 48824

Our goals are to evaluate the structural information contained in collisionally activated decomposition (CAD) mass spectra, and to explore the potential of employing this information for organic structure determination. Toward these ends, we are generating a library of reference CAD mass spectra in order to empirically answer the following questions:

* Which features in CAD mass spectra relate unambiguously to particular structural subunits, regardless of the origin of the ions?

* When will the analysis of CAD mass spectra be sufficient to provide positive structural identification?

* When do the CAD mass spectra of the ions in indistinguishable primary mass spectra of isomeric compounds provide the missing structural information?

The outline of our scheme for employing collision activated decomposition (CAD) mass spectral data to identify organic compounds is:

A. Compile a library of reference CAD mass spectra which includes, for each reference compound, the mass spectrum of the ionic decomposition products of all the ions in the conventional mass spectrum

B. For each ion in the primary mass spectrum of an unknown compound, search the data base to get a list of reference compounds, which contain in their mass spectrum, an ion of the same m/z value

C. For each ion in the conventional mass spectrum of an unknown compound, rank the list of reference compounds by the match of the CAD spectrum of the ion in the reference compound to the CAD spectrum of the ion in the unknown compound

D. Note the common structural subunits of the top ranked reference compounds in each list

E. Use the molecular weight and the structural subunits revealed from the data base search to propose possible structures for the unknown compound

Note that our structure determination scheme is totally emperical. We do not assume that structural integrity is maintained in the ionization or fragmentation processes, nor does our scheme require that the ion structures be identified. However, the scheme will test whether CAD spectra which match can reveal one or more common structural subunits in their parent compounds.

We have designed a multi-dimensional data base(1) to aid in selection of standard conditions. It is organized to allow an experimenter to collect the results of all multivariable experiments on a single sample in one data set, and is optimized for quick extraction and presentation of data for any combination of variables. Reference spectra can then be transferred to our archival data base(2). We have

not yet achieved a satisfactory method to standardize CAD mass spectra, and continue to evaluate the effects of instrument parameters on the spectra. The use of quotient specta(3) to determine which instrumental parameters cause skewing of the CAD spectra is being explored.

In our archival data base, all mass-intensity pairs are stored in an unabridged format, along with the operating conditions. Daughter ion spectra are linked to their parent ion in the primary mass spectrum. In order to perform step B in our structure determination scheme, or in order to rapidly access any other type of data in the archival data base, an "inverted" data base(2) has been developed. It is composed of lists of indices into the archival data base which have a particular characteristic. Lists can be combined by logical AND or OR operations, and can be updated without inversion of all archival data. Use of the inverted data base allows us to rapidly reduce the number of candidate spectra for intensity-based matching.

The routine we have developed for intensity-based matching CAD spectra uses all mass-intensity pairs. The match between spectra is characterized through multiple factors, derived from both forward and reverse matching algorithms(4). This routine is used to rank the lists of reference compounds in step C of our structure determination scheme.

At present, step D is performed by inspection. We have created a molecular structure data base which contains connection matrices which represent the structures of the reference conpounds. Automated application of an extended version of the MORGAN algorithm(5) produces unique and unambiguous representations for all structures, and includes stereochemistry(6), all elements and bond types. Future work includes development of algorithms to extract common structural subunits from the ranked lists of indices, development of algorithms to correlate structural subunits with CAD spectra, and exploration of methods to determine possible structures for the unknown compound from the structural subunits.

(1) R. W. Crawford, H. R. Brand, C. M. Wong, H. R. Gregg, P. A. Hoffman and C. G. Enke; presented at the 30th Annual Conference on Mass Spectrometry and Allied Topics; Honolulu, HI; June 6-11, 1982.

(2) P. A. Hoffman and C. G. Enke; presented at the 31st Annual Conference on Mass Spectrometry and Allied Topics; Boston, MA; May 8-13, 1983.

(3) D. Henneberg and B. Weimann; presented at the 31st Annual Conference on Mass Spectrometry and Allied Topics; Boston, MA; May 8-13, 1983.

(4) K. P. Cross and C. G. Enke; presented at the 32nd Annual Conference on Mass Spectrometry and Allied Topics; San Antonio, TX; May 28-June 1, 1984.

(5) H. L. Morgan; J. Chem. Soc., 5, 107-113 (1965).

(6) W. T. Wipke and T. M. Doytt; J. Am. Chem. Soc., 96, 4834-4844 (1974).

This work was supported by National Institutes of Health Grant No. 2R01GM28254-04

A FULLY INTEGRATED COMPUTER-CONTROLLED THERMOGRAVIMETRIC ANALYSER-TANDEM MASS SPECTROMETER (TGA/MS/MS) SYSTEM FOR POLYMER CHARACTERIZATION,

B. Shushan, C. Williamson, and P.H. Buckley, SCIEX®, 55 Glen Cameron Road, Thornhill, Ontario, Canada, L3T 1P2.

INTRODUCTION: Thermogravimetry (TGA) has become a widely used method of quality assurance and degradation-kinetics modeling for the polymer industry by providing weight-loss characteristics of polymers as a function of temperature. Since TGA measures only weight and temperature it must be coupled with ancillary analytical techniques in order to furnish the chemical identification needed to elucidate mechanisms of thermo- (or oxidative-) degradation, and to identify the components of polymer formulations; not surprisingly mass spectrometry has played a prominent role as chemical detector for TGA. Recently TGA has been successfully coupled to a tandem triple quadrupole MS/MS system fitted with an atmospheric pressure chemical ionization (APCI) ion source [1,2]. This ion source technology has obvious advantages when coupled to TGA; ie., both the ion source and TGA are at atmospheric pressure permitting a straightforward coupling and oxidative atmospheres can be used in the TGA since APCI is compatible with air as the carrier/reagent gas. This novel TGA-APCI-MS/MS combination provides complete dynamic headspace analysis of pyrolysate components as they emanate from the TGA, that is, molecular weight information is furnished by APCI/MS and structural identification by MS/MS. Since the introduction of TGA/MS combinations [4,5] there have been a variety of methods for physically linking the two techniques [2,3,6,7] some involving the integration of data acquisition and data analysis capabilities [7]. In the present work we present a unique TGA/MS/MS interface which is not only capable of TGA data acquisition and display from the mass spectrometer's computer terminal, but of programming and controlling the TGA as well. This interface utilizes a second microprocessor which acts as a slave to the main system computer providing a high degree of flexibility which makes possible the following features:

- Compatibility with a variety of TGA instruments.
- Simultaneous integrated operation of the TGA and MS from the same computer terminal.
- Simultaneous real-time display of TGA and MS data.
- Post acquisition TGA data analysis.
- MS/MS identification of unknown compounds evolved from the TGA.

TGA-to-MS/MS INTERFACE: The details of this interface have been presented elsewhere [1,2]. To illustrate the capabilities of TGA/MS a sample of a Styrene-Isoprene-Styrene (SIS) triblock polymer (3.7 mg) was placed on the pan of a Dupont 951 TGA. The TGA was connected to the all-glass heated (ca.220°C) TGA-to-MS transfer line by a ball-and-socket joint permitting easy coupling/decoupling. The polymer was heated under a 100 ml/min stream of N_2 within the TGA from 200 to 600°C at 15°C/min. After passing through a short (2cm) section of wide-bore capillary (0.5 mm ID) an accurately metered portion (1%) of the TGA effluent is carried into the APCI ion source by a high velocity (2 l/min) stream of preheated carrier gas containing a few ppm of C_6H_6 charge transfer reagent. Ionization takes place in a corona discharge by 9.25 eV benzene charge transfer -- a 'soft' ionization process. The ions are focussed through a sampling orifice into the analyzer portion for MS or MS/MS analysis.

TGA-to-COMPUTER INTERFACE: TGA operation and data acquisition through the MS computer terminal is accomplished via the "Slave Microprocessor" (see block diagram). This unit consists of a Z-80 microprocessor connected by an S-100 bus to 64K RAM and two 14 bit ADC channels. In order to activiate this microprocessor a CPM compatible program is downloaded to it from the main computer via an RS-232 serial port. Continuous signal tranfer between the TGA and slave microprocessor, as well as temperature feedback and control takes place in the "Interface" unit (right). These signals are digitize within the slave microprocessor at half-second intervals and sent to the main computer at user-specified intervals.

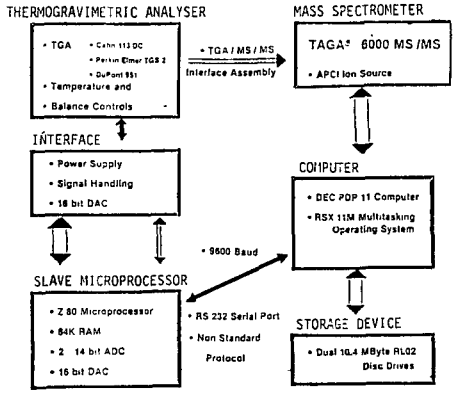

REAL-TIME DISPLAY MODES: During TGA/MS vital paramters may be monitored in real-time including TGA percent-weight and temperature, and APCI reagent-ion intensity (right). It should be noted that there is a depletion of ionizing reagent coincident with the evolution of material from the TGA. The graphics package provided by the MS/MS data system is flexible enough to accommodate several real-time displays of user-specified parameters.

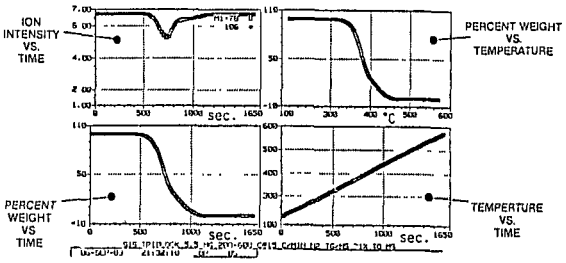

OFF-LINE TGA DATA ANALYSIS: (right) TGA data is stored with the corresponding MS data and the above TGA data displays are available from the MS computer terminal. The ascending the first derivative of weight can be obtained with respect to time or temperature, and for the above sample shows weight-loss maxima at 370°C and ca 425°C.

APCI-MASS SPECTRA: (far right) The background subtracted APCI mass spectra corresponding to the weight loss maxima are shown above. They correspond to the thermodegration of the polyisoprene and polystyrene blocks respectively. This was confirmed by performing MS/MS analysis of the individual ionic components.

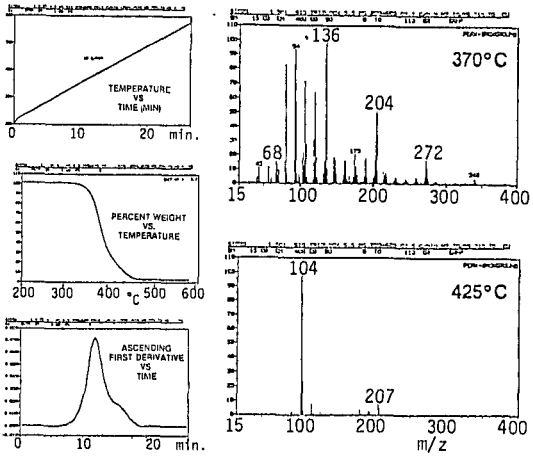

MS/MS IDENTIFICATION: The 136^+ ion was identified as limonene which was formed during the thermodegradation of polyisoprene. Other ions were similarily identified: 68^+, isoprene; 204^+, sesquiterpene(s); 272^+, diterpene(s); and at 425°C, 104^+, styrene and its dimer 207^+. **TOTAL AND MULTIPLE-ION PLOTS** are shown at right from full scan data for Total-Ion, 136^+ (Limonene) and 104^+ (Styrene). The degradation of these two copolymers are clearly separated by plotting ion intensities.

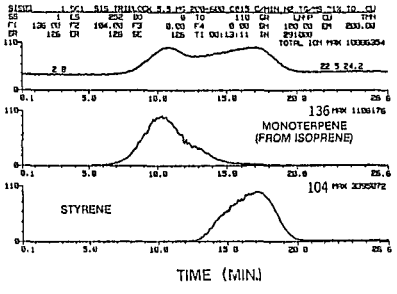

CONCLUSIONS: The integration of TGA with APCI/MS/MS links the bulk thermal properties of polymers with the chemistry involved in thermodegradative processes. This combined technique can be used to characterize polymer composition and identify potentially hazardous pyrolysate products as well as analyse for the various polymer additives.

REFERENCES:

1. B. Shushan and R. B. Prime, ASMS Proceedings (1983) p. 79.
2. B. Shushan, W. R. Davidson and R. B. Prime, Analytical Calorimetry, 5(1984)105.
3. Susan M. Dyszel, Thermochemica Acta, 61(1983)169.
4. F. Zitomer, Anal. Chem., 40(1968)1091.
5. J. Mitchell and J. Chiu, Anal. Chem. Ann. Rev. 45(1973)273R.
6. J. Chiu and A. J. Beattie, Thermochemica Acta, 40(1980)251.
7. H. K. Yuen, G. W. Mappes, and W. A. Grote, Thermochemica Acta, 52(1982)143.

A MICROCOMPUTER-BASED DATA SYSTEM FOR HIGH RESOLUTION MULTIPLE ION MONITORING AND MULTIPLE METASTABLE PEAK MONITORING.

GARETH C. THORNE and SIMON J. GASKELL, Tenovus Institute for Cancer Research, Welsh National School of Medicine, Cardiff CF4 4XX, U.K.

A MAT 731 double-focusing mass spectrometer has been modified to permit high resolution multiple ion monitoring and dual metastable peak monitoring during GC-MS. The latter technique involves synchronous switching of the accelerating voltage and electric sector voltage under hardware or data system control. For the fragmentations,

$$A^+ \rightarrow B^+ + \chi \qquad (1)$$

$$C^+ \rightarrow D^+ + Y \qquad (2)$$

occurring in the first field-free region, the required ratios of accelerating voltages (V) and electric sector voltages (E) are

$$\frac{V_1}{V_2} = \frac{m_A m_D^2}{m_C m_B^2}$$

$$\frac{E_1}{E_2} = \frac{m_D}{m_B}$$

Dual metastable peak monitoring has been applied to the analysis of oestradiol bis-tert-butyldimethylsilyl (TBDMS) ether, using the [$^2H_3$]analogue as internal standard. A detection limit of ca. 5pg was achieved by monitoring the metastable peak corresponding to the $M^{+\cdot} \rightarrow [M-C_4H_9]^+$ fragmentation. During analysis of a plasma extract, the selectivity was superior to that observed during high resolution (m/Δm 8000) selected ion monitoring.

The data system is based on a DEC LSI-11/23 microcomputer. Software has been written, in Forth and Fortran, to allow extensive processing of selected ion monitoring data with a view to maximising the precision of determination of response ratios following GC-MS/SIM with isotope-labelled internal standards. One approach, first suggested by Lawson and coworkers[1], involves linear regression analysis of signal intensities corresponding to the analyte and internal standard. Plots of signal intensities, for the example of the analysis of oestradiol TMS ether and its [$^2H_3$]analogue, are shown in Fig. 1. The elliptical appearance of the plots is attributable to the earlier gas chromatographic elution of the deuterated internal standard. The advantage of response determination using this approach is that the need to define the peak tops and baselines is avoided, with consequent improvements in precision. For replicate analyses of 50pg oestradiol and 80pg [$^2H_3$]oestradiol, as the TMS ethers, determinations of peak height ratios using the display facilities of the data system gave a C.V. of 11%. This was reduced to 2% when response ratios were calculated using the regression analysis approach.

A paper describing part of this work has been accepted for publication in Biomedical Mass Spectrometry.

REFERENCE

1. Lawson, AM, Lim CK, Richmond W, Samson DM, Setchell KDR, Thomas ACS. In: Lawson AM, Lim CK, Richmond W, eds., Current Developments in the Clinical Applications of HPLC, GC and MS. Academic Press, London; 1980. pp125-153.

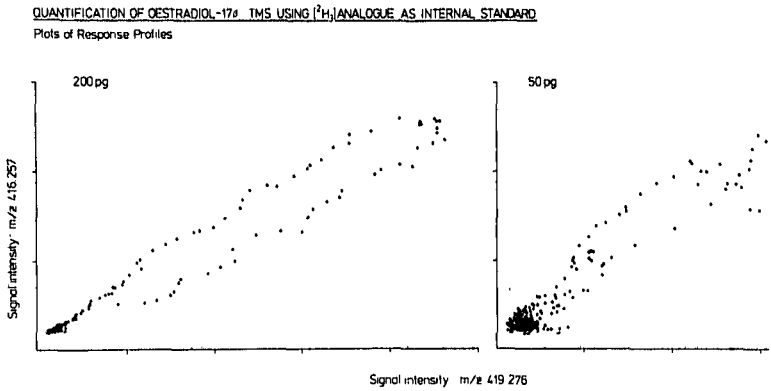

Fig. 1. Plots of signal intensities during GC-MS with SIM of m/z 416.257 ($M^{+\cdot}$ for oestradiol TMS) and m/z 419.276 ($M^{+\cdot}$ for the [$^2H_3$]analogue). Amounts of oestradiol TMS injected are shown; molar ratios of analyte/internal standard were ca. 0.6.

CORRECTION OF MASS SPECTROMETER DRIFT WHILE USING AN INCOS ™ DATA SYSTEM FOR HIGH RESOLUTION SELECTED ION MONITORING

G. J. Collins, Stauffer Chemical Company, Livingstone Avenue, Dobbs Ferry, New York 10522

High resolution selected ion monitoring (HRSIM) is widely used for positive identification of trace level environmental contaminants [1,2]. Advantages of HRSIM are reduction of interferences due to isobaric ions and confirmation of the presence of the analyte by exact mass measurement of the ions detected. Computer controlled peak matching for exact mass determination has also been done by HRSIM[3].

The INCOS ™ data system is limited in its ability to perform these analyses because it was not designed to correct for mass calibration drift which occurs during an analysis. We built a microprocessor based device which, when used with an INCOS, can correct this drift. The drift correction module operates on the "lock mass" principle. A correction voltage is applied to the mass spectrometer (MS) which keeps the measured mass of a reference ion (i.e. a PFK ion) as close as possible to its true mass. Installation of the module required no modification of the data system or the MS (Figure 1). This makes it suitable for use with any MS which is controlled by an INCOS data system.

HMAP/C is an INCOS program which gives a real time plot of the exact mass of an ion, as measured by the data system. The plotting resolution of the HMAP/C display is less than 1 ppm (Figure 2). This real time plot is the heart of the drift correction module.

The Module reads the serial data used to plot the measured mass as it is sent to the display terminal and computes the correction voltage needed to bring the measured mass back to the true exact mass. The microprocessor in the module uses a 12 bit digital to analog converter (DAC) to generate this magnet correction voltage. The voltage span of the DAC is adjustable so that corrections of from 10 ppm per DAC step to <1 ppm per DAC step can be applied. Also, the microprocessor can average 1,2,4,.....,128 measured mass data points to determine the difference between the measured mass and the true exact mass of the reference ion. This averaging reduces the effect of scan to scan mass measurement jitter and allows the module to respond only to actual drift.

Because the module does not interfere with operation of the data system, all display and quantitation programs operate normally using the existing INCOS mass calibration. This design allows the module to be used during SIM or scanning data acquisitions. HMAP/C allows storage of peak profiles. This is useful because peak shape can give added information about possible interferences in HRSIM runs.

The module can correct very large slow drifts and it can also correct offsets of hundreds of ppm within a few scans. Using the module and our INCOS / VG-7070 at 10,000 resolution, HRSIM detection limits are typically in the low picogram range. Figure 3 shows the peak profiles and signal to noise obtained for 50 pg DDE. The system has also been used to determine the exact mass of ions with low ppm accuracy. Figure 4 shows the mass measurement results obtained for hexachlorobutadiene using computer controlled peak matching.

Installation of the device does not involve instrument modification and it could be easily installed on any INCOS / MS system.

[1] De Roos, F.L.; Silvon, L.E. 28th Annual Conference on Mass Spectrometry and Allied Topics, New York, NY 1980; 600-601.

[2] Weiss, M.; Harvan, D.J.; Hass, J.R. 28th Annual Conference on Mass Spectrometry and Allied Topics, New York, NY 1980; 602.

[3] Tondeur, Y.; Hass, J.R.; Harvan, D.J.; Albro, P.W. Anal. Chem. 1984,50, 373-376.

FIGURE 1 Block diagram showing how the drift correction module is installed.

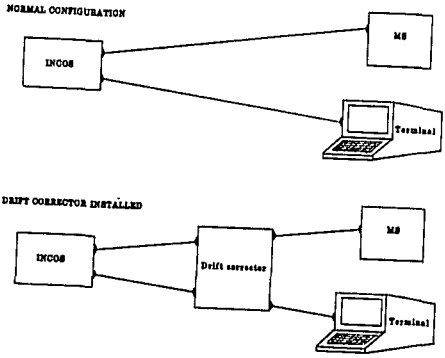

Figure 2 The HMAP/C display showing drift correction.

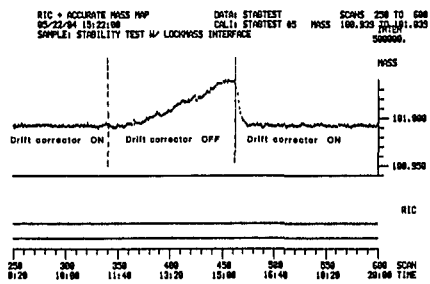

Figure 3 HRSIM (M/ΔM 10,000) total ion chromatogram and peak profiles for M/Z 316, 318, and 320.

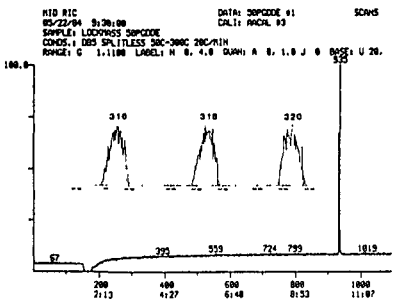

Figure 4 Elemental composition of hexachlorobutadiene.

```
ELEMENTAL COMPOSITION          DATA. HBD #  24          BASE M/E   225
04/30/84 15.08 00 +  2 00      CALI  HBD #  24          RIC·     222976
SAMPLE  HEXACHLOROBUTADIENE
CONDS   LOCKMASS PEAKMATCH
MIN INTEN        0             DEF  30 MMU/100 AMU

MIN   255        0.00      0              -0 5   CL6
MAX   269                  #  0    0.0    5  6 0  C200 H400 C+ CL6
      MASS       % RA    INTEN.   MMU   PPM BONDS FORMULA

 254 9855       12.77     4028
 255 9912        1 08      342
 257 0026        0.81      255.
 257 8136       24.87     7848.   0 4    2  2 0   C4 CL6/0
 258 8174        1.05      330.   0 8    3  2 0   C3/1.CL6/0
 259 8097       49.85    15728   -0.5    2  1 5   C4 CL5/1
 259 9907        0.73      230.
 260.8127        1 71      539   -0 7    3  1.5   C3/1 CL5/1
 260.9946        0.29       90
 261.8076       38.89    12272   0 3     1  1.0   C4.CL4/2
 261 9884        2 02      636
 262.8109        1.43      452.  0 3     1  1.0   C3/1.CL4/2
 262.9933        3.97     1252.
 263 8054       15 47     4880   1 1     4  0 5   C4.CL3/3
 263 9977        0.24       75.
 264.8079        0.55      172   0 2     1  0 5   C3/1.CL3/3
 265 8021        4 61     1456.  0.8     3  0.0   C4 CL2/4
 266 8044        0 18       57  -0.2     1  0.0   C3/1 CL2/4
 266 9841        4 87     1538.
```

GC/MS SPECTRAL DATA ON NITROGEN-CONTAINING COMPOUNDS PUBLISHED AND ARRANGED INTO A CORRELATION INDEX USING COMPUTER TECHNIQUES

M. C. Hamming, H. L. Gearhart, and R. J. Pell
Conoco Inc.
Petroleum Research and Development Department
Ponca City, OK 74603

and

Anna M. Ferguson
The Texas A&M University System
Thermodynamics Research Center
College Station, TX 77843

This paper describes obtaining quadrupole GC/MS spectral data on 85 nitrogen-containing compounds, computer processing of the data for publication, and creating a correlation index. A new reporting format was designed to include GC relative retention data, percent total ionization for detected m/e's arranged in a rectangular array, GC and MS instrumental parameters, and mass spectral peak intensities for a reference compound to ensure reproducible tuning of the quadrupole instrument. A correlation index of fragmentation patterns from the mass spectral data is presented.

The mass spectral data will be published in the Spectral Volumes of the Texas A&M University System under a new "q" series. Several classes of nitrogen-containing compounds make up this publication.

Computer applications of the SAS[1] procedures combined with TSO and PDF make examination of spectral data possible in a wide variety of ways. The procedure for finding frequency is similar to examining spectral data for common modes of fragmentation. An example is given below for the ten most intense peaks of these compounds.

FRAGMENTATION OF MASS SPECTRA	FREQUENCY PROCEDURES OF SAS		FRAGMENTATION OBSERVATIONS
Peak	Frequency	Percentages	Structural Significance
M+	84	99	Molecular ion peak.
M-1	60	71	Elimination of a hydrogen atom.
M-28	42	49	Ejection of hydrogen cyanide and hydrogen.
M-15	32	38	Ejection of a methyl group.
M-27	26	31	Ejection of hydrogen cyanide.
M-42	26	31	Ejection of hydrogen cyanide and a methyl group.

In conclusion, the computer is used to enhance the use of mass spectral data within a given laboratory as well as providing a direct route to publication of the spectra and development of a correlation index.

---

[1] SAS (Statistical Analysis System) is a computer softwave system, SAS Institute Inc., Box 8000, Cary, NC 27511.

THE USE OF ION ABUNDANCE RATIOS FOR THE CHARACTERIZATION OF GC/MS MIXTURES

E. McCarthy
Allied Corp., Morristown, N. J. 07960

Introduction

We have attempted to characterize hydrocarbon mixtures by the use of ion abundance ratios. We pre-select two m/e values that reflect certain structural features and then monitor the change in their ratio as successive components are eluted by the GC/MS. This technique is used to supplement the single ion chromatograms. We have attempted to distinguish alkene/alkane regions of the chromatograms and also to establish the presence of various sulfur-containing components such as methyl thiophenes.

For the alkene/alkane distribution we select 56^+ ($C_4H_8^+$) and 57^+ ($C_4H_9^+$). This is done because in alkene spectra the ratio of $56^+/57^+$ is considerably higher than in that of the alkanes. Consequently, this ratio should maximize as alkenes are eluted from the column. Also the reverse should be true as an alkane elutes. For the thiophene determination we pre-select m/e values corresponding to the respective M^+ and (M^+-H). This choice was suggested by the approximately equal abundances on these ions in thiophene spectra. Thus a ratio of about one for these ions in a mixture spectrum would suggest thiophene elution. The abundant (M^+-H) suggests the following fragmentation.[1]

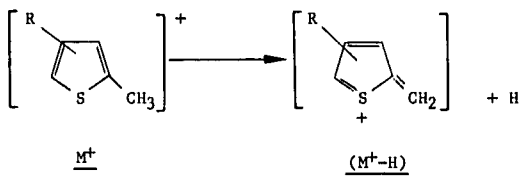

The above ratios are conveniently monitored by using the STAB routine of our Finnigan INCOS data system.

Experimental

Reaction mixtures and synthetic blends were analyzed using a Finnigan 3300 MS (EI mode) employing the following conditions:

Column - 50 m x 0.33 mm, SE-30
Column temp. 50°C $\xrightarrow[10°/\text{min.}]{}$ 250°C

Observations/Results

GC/MS analysis of both C_8-C_{10} alkene/alkane test mixtures and complex mixtures encompassing a C_5-C_{15} range confirms that the STAB routine allows the alkene/alkane distribution to be determined. A $56^+/57^+$ ratio of about 4/1 is observed when an alkene elutes and this allows an alkene assignment to a particular component. The appearance of a value of unity for $\frac{M^+}{M^+-H}$ for thiophene m/e values suggests this type of component. This was confirmed by using hydrocarbon-thiophene synthetic blends. Here we use the following m/e values, $98^+/97^+$; $112^+/111^+$; $126^+/25^+$ to characterize the respective methyl thiophenes.

References

1. Budzikiewicz, H.; Djerassi, C.; Williams, D. H.; "Mass Spectrometry of Organic Compounds", Chapter 7, Holden-Day, Inc., 1967.

Enhanced PBM for Unknown Identification, Robert B. Spencer, Nicolet Analytical Instruments, Madison, Wisconsin, 53711 and Douglas B. Stauffer, Cornell University, Baker Laboratories, Ithaca, N.Y., 14843

Probability-Based Matching (PBM) has been shown to be superior for computer identification of mass spectra. PBM is unique in reporting the probability that a match is due to identity between unknown and reference spectra. The probability is based on the sum of individual contributions for each of the peaks in a reference spectrum which has a corresponding peak in the unknown.

PBM performs its matches between nominal-mass unknown spectra and a library of nominal-mass spectra of reference compounds. Accurate-mass spectra contain more information than do nominal-mass spectra, so that it should be possible to improve PBM results, if the accurate-mass information can be used. Because using accurate-mass spectra is an expansion of PBM beyond the data class (nominal-mass spectra) for which it was developed, the new technique is called Enhanced Probability-Based Matching (EPBM). EPBM is based on the principles of PBM, but accommodates a data class richer in information. Further enhancement of PBM is possible, if library data exists which can be used in the enhancement. EPBM, as represented here, is of particular interest because it uses a library of nominal-mass reference spectra to extract additional information from accurate-mass spectra of unknowns.

As is well-known, exact assignments can often be made for nominal-mass peaks: 77 to phenyl, for example. Neutral fragments lost may also be assigned; loss of 15 is nearly always loss of a methyl. In a spectrum of a known compound, this makes assignment of the peak possible, by subtracting the composition of the neutral loss from the composition of the molecule. Assignments can also be made by an algorithm which considers all possible combinations of atoms, and retaining only those which correspond to the composition of the peak. "Interpretation of Mass Spectra" by McLafferty contains a table of common neutral losses which may be used for assignments; "Mass Spectral Correlations" by McLafferty and Venkataraghavan may be used for assignment of commonly-occurring peaks of lower mass.

Assignment of a reference peak to a composition enables calculation of its exact mass. This may then be compared with the measured mass of the unknown ion. If the unknown ion mass differs by more than the known experimental tolerance from the reference ion mass, the peaks are not compatible (the observed peak is not a peak in the reference spectrum). The reference peak may be "flagged", to indicate it is not present in the unknown spectrum. This same procedure is used in PBM, except that the unknown spectrum must contain no peak at the reference peak nominal mass for flagging to be possible. It is here that the information from the accurate-mass unknown spectrum makes its contribution: an enhanced discrimination between spectra is possible.

Reference peaks are not always uniquely assignable. In such cases, all possible compositions of the reference peak are used to compute exact masses to be compared with the unknown ion mass. If all are incompatible, the peak may be flagged. Accurate-mass reference spectra would allow exact assignments for all reference peaks, providing a further enhancement.

An example of the improved performance of EPBM over PBM is seen in the following, which tabulates returned hits for an FTMS-1000 spectrum of 3,5-dimethyl pyrazole:

Method	Hits	Unique Hits
PBM	20	15
EPBM	12	8

These results show a 40% improvement, based on total hits, or a 45% improvement, based on unique hits (ignoring all duplicate spectra).

Further EPBM developments will include the use of reference peak assignments to compute exact-mass uniqueness values, which can then be used in the PBM calculation.

The guidance and assistance provided for this work by Dr. Fred McLafferty is gratefully acknowledged.

AIDS FOR BUILDING AND MAINTAINING IN-HOUSE SPECIALTY LIBRARIES ON THE SS-200 DATA SYSTEM

Donald F. Magin and Bennie W. Good
Philip Morris Research Center
Box 26583
Richmond, VA 23261

The overall purpose of the work reported here was to develop a package of routines to be used with the MAT SS-200 Mass Spectrometry Data System which would facilitate the building of, and enhance the use of specialty in-house libraries.

The literature is an excellent source for reference mass spectra of compounds, but there are some serious difficulties in efficiently using reference spectra from such sources. First of all is the large number of such spectra which would have to be collected and stored in some easily-indexed form. Also the format of the literature spectra can be a problem. Some spectra are published as tabular mass/intensity values, while others appear as bar plots. The prime objective of this work was to be able to easily, accurately and quickly enter literature reference mass spectra into a library searchable by the SS-200 library routines (BSRCH and BPOKE). In particular, a means was desired to input data from graphical mass spectra without having to measure the intensities and type in mass/intensity pairs.

A graphics tablet (1) was available which could convert graphic information into digital form suitable for entry into a computer. A program (UBUILD) was written which takes the digitized data from the graphics tablet, converts it to meaningful mass/intensity, and writes it to a file in the specialized file format required by the SS-200 data system. The graphics tablet was simply installed as an auxiliary input to an ADM (Lear Siegler) terminal connected to the SS-200 data system (PDP 11/34 computer). No modifications to the terminal, graphics tablet, or computer were necessary.

The concept of a standardized spectrum title was introduced as part of the overall package, in which each spectrum was identified by compound name, molecular weight, molecular formula, and a unique compound number which also coded the source of the spectrum. This kind of standardization enabled the use of sorting routines, whereby lists could be generated, ordering the spectra by molecular weight (LSORT), or by compound number and source (MSORT).

A routine was also written (NEWJOIN) which permits the extraction of individual spectra from normally-acquired analyses, re-titling the spectra with a standardized spectrum title, and joining the newly titled spectrum to others in a data file to be used to build or add to a library.

The data files generated by UBUILD and NEWJOIN look like typical data files to the SS-200 data system, so any of the usual SS-200 routines can be used on them (e.g., FEDIT, SPLOT, SLIST, APLOT, ALIST, etc.).

A slight modification to the standard SS-200 library building routine (BBUILD) permitted totally unattended library building of spectra in these data files, by allowing BBUILD to pick out the molecular weight from each standardized spectrum title, as if the molecular weight had been entered at the keyboard for each compound spectrum. Thus, the library so built can be searched using the normal BPOKE routine for molecular weight. The modification in no way affects the operation of BBUILD on spectra without the standardized spectrum title.

All programs in this package were written to be extremely user friendly, and to allow ample opportunity for verifying the accuracy of the entries. The programs were written in FORTRAN, and run under Version 4 of SS-200 on a PDP 11/34 computer with RSX-11M operating system.

The use of this specialty library package has enabled us to generate a library of ~3000 spectra (so far) of compounds of possible interest to us, the majority of which are not found in commercial mass spec data bases. The time involved to build this library has only involved a few hours per week over a period of about 6 months.

Listings of the source programs (FORTRAN) are available, and arrangements may be made for copying the task files on magnetic tape or hard (Hawk) disks, by contacting one of the authors (DFM).

(1) Summagraphics Bit Pad One, from Summagraphics Corp., Fairfield, CT

ADDING FORWARD-SEARCHING CAPABILITIES TO A REVERSE SEARCH ALGORITHM FOR UNKNOWN MASS SPECTRA: D. B. Stauffer, F. W. McLafferty; Chemistry Department, Cornell University, Ithaca, New York 14853, and R. D. Ellis and D. W. Peterson, Scientific Instrument Division, Hewlett Packard, 1501 California Avenue, Palo Alto, CA 94304

The imperfection of separation techniques still necessitates reverse-searching in mass spectral retrieval algorithms. This lack of use of negative information places them at a severe disadvantage with respect to forward searching algorithms when used on the unknown spectrum of a pure compound. For example, Probability Based Matching (PBM), a reverse search algorithm, retrieved incorrect answers such as 3-octene as a match of 32% reliability for octyl phthalate as an 'unknown' (Table I); the mass spectrum of the latter contains all major peaks of that of octene, but a forward search would find this a poor match from the many unknown peaks not in the octene spectrum.

Table I. PBM Results (Class IV Matches) from Spectra of 2-Ethylhexylphthalate and its 3:1 Mixture with 3-Octene

No.	compound	pure a	pure b	pure c	mixture a	mixture b	mixture c
56290	2-ethylhexylphthalate	47	50	61	56	22	45
78723	isooctylphthalate	42	37	50	35	20	37
67538	2-methyl-1-butene	34	<10	6	43	24	54
2942	(Z)-3-octene	32	14	13	47	27	97
1545	3,4-dimethyl-1-pentene	31	<10	8	<10	<10	<10
78728	2-ethylhexylphthalate	29	44	77	40	24	55
	all octenes	25	14	9	55	24	83
(number of octenes retrieved)		(2)	(1)	(2)	(13)	(10)	(12)
	all C_nH_{2n} compounds	24	14	9	49	23	64
(number of C_nH_{2n} compounds)		(14)	(1)	(3)	(18)	(16)	(17)

[a]current reverse search
[b]with forward search (% contamination) contribution, assuming unknown is of a pure compound
[c]Forward search contribution with multiple subtraction, no knowledge of purity of unknown

In this work PBM has been extended in two ways to give substantially more reliable results through the use of negative information. For the first ("b" of Table I) the user must have separate information, such as the GC peak width, that indicates the spectrum is that of a pure compound. For the second method ("c" of Table II), each of the best matching reference spectra is subtracted from the unknown,[1] and the residual matched against the other references. If the residual from subtracting A matches B better than the unknown matched B, A and B are probably matching separate components of the unknown. For a "pure" spectrum an estimation of its percent contamination is then used to predict the increase or decrease in reliability associated with the match due to the degree of contamination. For mixture spectra the residual matching can also provide substantially more reliable identification of the mixture components (Table I).

To test the resulting reliability on a statistical basis, the spectra of 392 different compounds selected at random from the Wiley/NBS data base[2] were used as "unknowns" representing pure compounds. The spectra were ordered by increasing molecular weight; groups of three were combined in 60:30:10 proportions (total ions) to prepare 130 mixture test spectra. The "recall/reliability"[3] plots show that the addition of forward searching capabilities provides the greatest improvement to PBM since its introduction a decade ago. On average, the number of Class IV wrong answers has been reduced to half of its previous value.

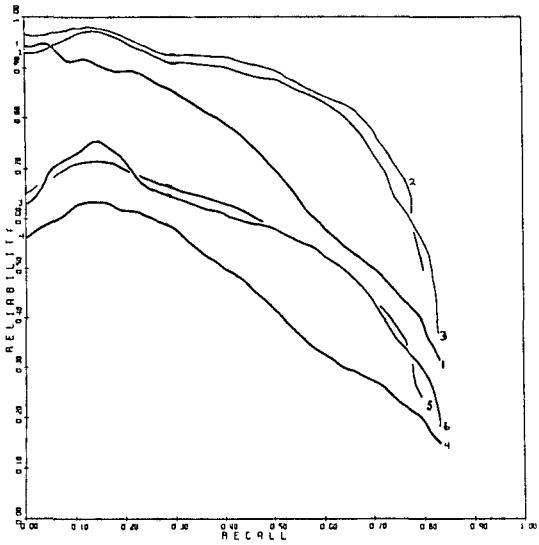

100% Component

	Class	Search
1:	IV	reverse a
2:	IV	forward b
3:	I	forward c
4:	I	reverse a
5:	I	forward b
6:	I	forward c

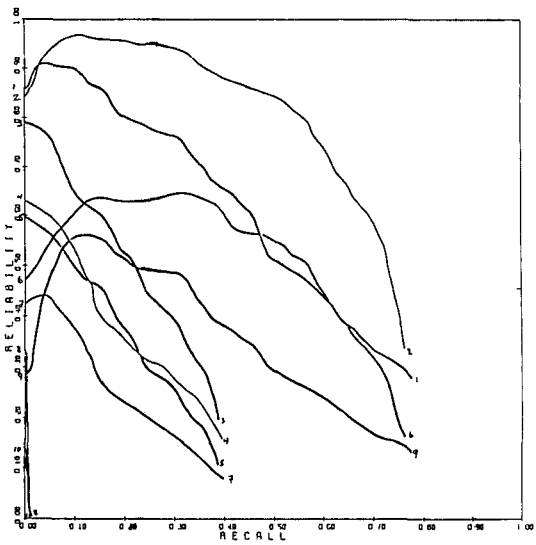

Mixtures

	Class	Conc.	Search
1:	IV	60%	reverse a
2:	IV	60%	forward c
3:	IV	30%	forward c
4:	IV	30%	reverse a
5:	I	30%	forward c
6:	I	60%	forward c
7:	I	30%	reverse a
8:	IV	10%	forward c
9:	I	60%	reverse a
10:	IV	10%	reverse a

(1) Atwater (Fell), B. L.; Venkataraghavan, R.; McLafferty, F. W. Anal. Chem. **1979**, 51, 1945-1949.
(2) McLafferty, F. W.; Stauffer, D. B. Int. J. Mass Spectrom. Ion Proc. **1984**, in press.
(3) McLafferty, F. W. Anal. Chem. **1977**, 49, 1441-1443.

CONSTRUCTION AND USE OF A MASS SPECTRAL LIBRARY OF TRICHOTHECENES TO ASSIST IN THE IDENTIFICATION OF COMPONENTS OF LABORATORY SAMPLES. David Hewetson and C. J. Mirocha, University of Minnesota, St. Paul, MN 55108

Several aspects of computer-assisted interpretation of GC/MS results via library searching are discussed. Among these are Automated library searching, textual searching, considerations in choosing mass spectra, comparisons of electron impact and chemical ionization mass spectra for inclusion in libraries, interpretation of Hewlett Packard's version of Probability Based Matching (PBM)[1] as a search routine, user-generated libraries, and the conversion of tabulations in one format (ANSWER) to mass spectra in another (Real Time Executor RTE) format.

Automated library searching is discussed as a method of decreasing the interactive time necessary to do an initial screening of a collection of sequential mass spectra (as in a GC/MS run). Once the PBM search conditions have been selected and set for a particular run the only interactive step necessary for the user is to enter each scan and perform a library search. This is quite time-consuming however, and may be avoided using the computer. The program PBMULT was developed in this laboratory to enter the initial scan of a GC/MS run, perform a library search, recalculate the scan number as the next higher scan number, perform another library search, and continue until the last scan of interest has been searched. The results of all scans that generated a match with the library(ies) are copied to a printer for later interpretation.

Textual searching is included in addition to library searching since header data, text from specific library entries, and textual abstracts all enter into the interpretation of library search results. While ACSII searching offers few of the challenges of a PBM search, it nonetheless represents another use of the computer to free the researcher's time for research. The computer program introduced here (DPPF) accepts, from the user, any six character string, searches a specific text file for all occurrences of that string, and then prints out on the CRT all occurrences and their line numbers.

Considerations in choosing mass spectra for inclusion in our user-gene-rated libraries represents some of the subtlties we've encountered in our attempts to build a useful library. The comparison of electron impact and chemical ionication mass spectra is again a reflection of our experiences. The use of MW+1 as the molecular weight when building a positive chemical ionization (PCI) library has generated higher reliabilities when PBM searching PCI GC/MS runs.

The interpretation of Hewlett Packard's personal version of PBM is discussed to bring to light some of the strengths and weaknesses of this particular system.

The trichothecene library we are building is an example of a database unlike the standard database used today (i.e. NBS, Wiley, etc.). One of its major advantages is that being small (less than 200 entries to date) the search time necessary is much shorter; however, this also points out its major drawback: interesting compounds that are not similar to trichothecenes are ignored. The molecular weight of derivatized trichothecenes ranges from about 450 amu to 750 amu and this has made chemical ionization an attractive mode for characterization. The reliability of library matching chemical ionization mass spectra has shown itself to be equal to, if not greater than, the matching of electron impact mass spectra for derivatized trichothecenes.

Conversion of ANSWER tabulations to RTE mass spectra represents a third computer program developed in this lab. When we made the switch from ANSWER software to RTE software, we found that our user-developed libraries failed to convert. This program (TSLATE) along with access to a system still using ANSWER, allowed us to recover the library mass spectra. We present TSLATE here to offer anyone else facing a similar situation some possible assistance.

REFERENCE:

1. Pesyna, G. M., Venkataraghaven, R., Dayringer, H. E., and McLafferty, F. W., Probability Based Matching Using a Large Collection of Reference Mass Spectra, Analytical Chemistry, 48, 1362-1368 (1976).

A NEW NON-SUPERVISED NUMERICAL METHOD FOR MIXTURE ANALYSIS OF COMPLEX SPECTRA

Willem Windig and Henk L.C. Meuzelaar

Biomaterials Profiling Center, University of Utah
Salt Lake City, Utah 84108

Pyrolysis mass spectrometry (Py-MS) is an established method for analyzing complex organic materials [1]. Originally, the main emphasis was on "fingerprinting". In many cases, however, a more detailed interpretation of spectra in terms of chemical constituents is an invaluable research tool. Due to the complexity of the pyrolysis process and the samples studied, standard mixture analysis procedures like the more advanced library search routines used in GC-MS are not suited. Over the past few years we have developed special methods capable of extracting chemical information from Py-MS data of complex organic materials, without the necessity of exact reference spectra. A successfull approach proved to be "graphical rotation" [2]. This method "scans" the factor and/or discriminant space derived from the data set. Since this same space can be spanned by axes representing chemical components, the spectral patterns associated with the discriminant functions reveal projections of the "component axes". Projecting the spectral points on the component axes provides a semi-quantitative measure of the concentration of that particular component. Although this method has proven to give valuable and accurate results, a highly experienced researcher is necessary and the method is subjective. Further study of the discriminant space, however, revealed that there is a relative clustering of the mass variables in the directions of the component axes. Plotting the contribution of the mass variables in a two dimensional subspace - the "variance diagram" - indeed shows local maxima in the directions of the component axes [3]. However, the spectrum intensity normalization procedures applied can give rise to complications. In order to correct for differences in sample size, spectra are usually normalized for total ion current. As a result every change in the data set is "compensated" by an opposite change, resulting in local maxima in the variance diagram opposite to the local maxima of the component axes. Fortunately, simple mathematical procedures could be developed which were found to correct for this "normalization effect".

Figure 1 shows the variance diagrams of well known data sets of mixtures of three biopolymers, before (a) and after (b) normalization effect correction. The local maxima clearly point in the directions of the (known) component axes. The rotated discriminant spectrum associated with the component axis of corn starch together with a spectrum of the pure component are shown in Figure 1c and d, respectively. The similarity between the mathematically extracted spectrum and the spectrum of the pure constituent is obvious. It has to be noted that spectra of the pure components were not included in the data set.

Figure 2a shows a typical spectrum of a data set on grass leaves. The variance diagram, after normalization correction, is presented in Figure 2b. Figure 2c shows the spectrum of the component axis at 340 degrees. This pattern is very simple compared to the original spectrum in Figure 2a, which greatly enhances chemical interpretation. From comparison with the polyisoprenoid pattern of natural rubber in Figure 2d it is obvious that the component axis found represents a (poly)isoprenoid compound.

Apart from the results mentioned above, this technique has been applied successfully to pyrolysis MS data from sagebrush wood, wood pulp, lignites, bacteria and technical polymers.

REFERENCES:

1. Meuzelaar, H.L.C., Haverkamp, J., Hileman, F.D., "Pyrolysis Mass Spectrometry of Recent and Fossil Biomaterials; Compendium and Atlas", Elsevier, Amsterdam, 1982.

2. Windig, W., Haverkamp, J., Kistemaker, P.G., Anal. Chem., 55 (1983), 81.

3. Windig, W., Meuzelaar, H.L.C., submitted Anal. Chem., (in press) 1984.

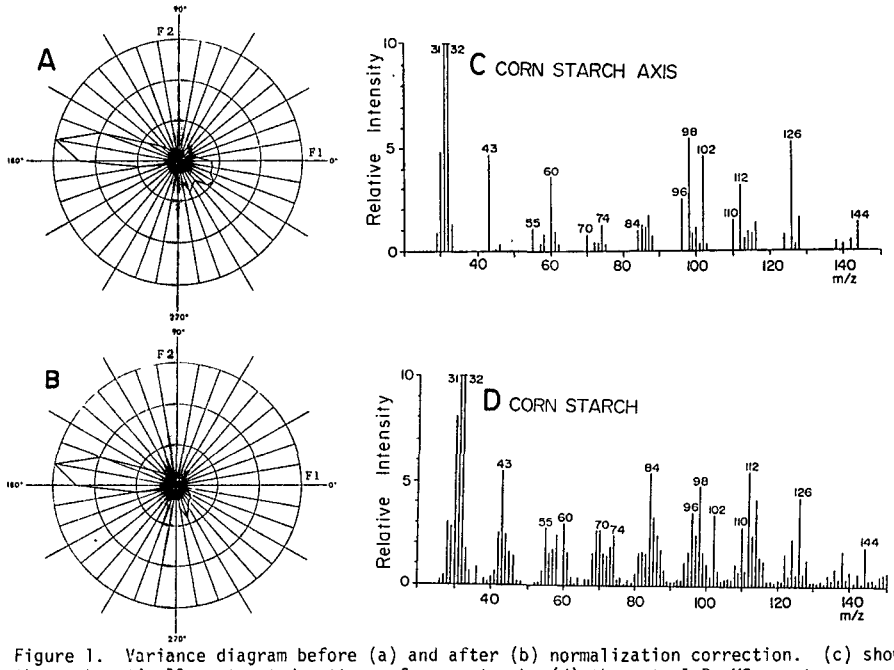

Figure 1. Variance diagram before (a) and after (b) normalization correction. (c) shows the mathematically extracted pattern of corn starch, (d) the actual Py-MS spectrum.

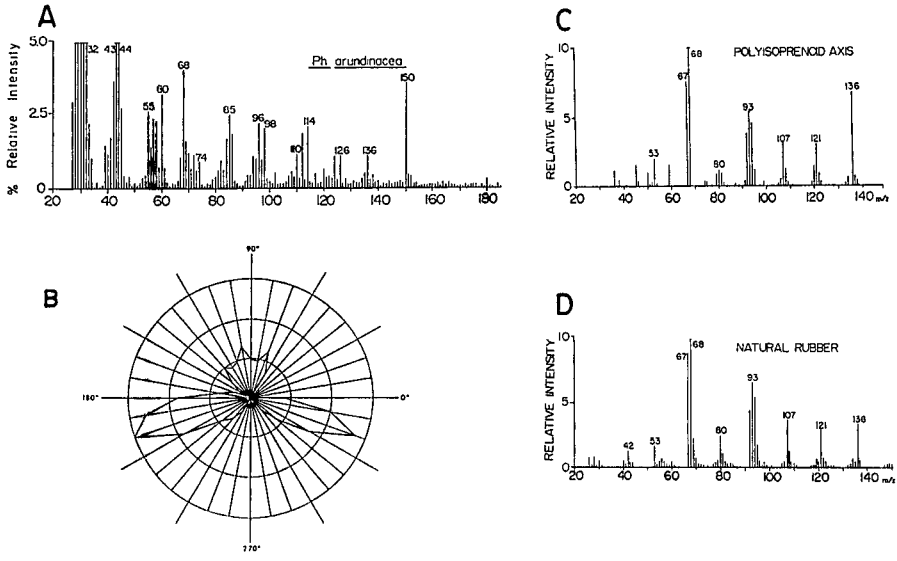

Figure 2. (a) Typical Py-MS spectrum from a set of grass leaf data; (b) variance diagram after normalization correction; (c) spectrum of component axis at 340 degrees; and (d) model spectrum of a polyisoprenoid (natural rubber).

A DATASYSTEM TO COMPLEMENT THE PERFORMANCE OF NEWLY DEVELOPED MASS SPECTROMETERS.

J.C. Bill and N.Lynaugh. VG Analytical Ltd., Floats Road, Wythenshawe, Manchester M23 9LE, England.

INTRODUCTION.

Continuing improvements to the performance capabilities of organic mass spectrometers, and the development of new instrumentation, are imposing ever more stringent requirements on the performance of the computer systems used for the acquisition and processing of mass spectral data.

Significant increases in the rate of scanning, and reset, of magnetic sector instruments now permit data acquisition at rates of up to 5 scans/second. Similarly, major extensions to the available mass range, at full ion energy, now mean that operation at masses in excess of m/z 10,000 must also be accommodated. Successful data acquisition at these high masses is frequently possible only with the use of data capture techniques such as signal averaging or Multi Channel Analysis (MCA).

DIGITIZATION RATE.

For any exponential scan of mass v time, the width of a mass spectral peak is determined only by the scan rate and the instrumental resolution. With a scan rate of 0.1 s/decade and a resolution of 1,000 the peak width will be 43.4 micro-seconds. Using the accepted number of 10 digital samples/peak for the satisfactory determination of a nominal mass centroid, a digitization rate of almost 250kHz is required under these conditions.

For accurate mass assignment, generally at higher resolution, 20 digital samples/peak are needed to give a centroid precision in the low ppm range. Thus, at 5,000 RP and 1 s/decade, a digitization rate of almost 250kHz is again required for optimal operation with a modern magnetic sector mass spectrometer.

Under less demanding scanning conditions, where the required digitization rate is less than 250kHz, System 11-250 continues to operate the A/D converter at 250kHz and automatically averages the appropriate number of A/D conversions, thus enhancing the signal to noise ratio of the overall system.

PEAK ARRIVAL RATE.

Data integrity, which is of paramount importance, can be preserved only if the datasystem and interface can process peaks at least as fast as they arrive.

For an exponential scan:-

$M=M_o e^{(-t/T)}$ Where T is the time constant of the scan.

so, $dM/dt=-M/T$

Or, the rate of change of mass with time (dm/dt) is dependent not only on the scan rate, but also on the instantaneous mass. This means that both of the recent major instrumentation advances, discussed previously, require a considerable increase in the rate of peak processing. For example, the peaks in a molecular ion cluster at m/z 1,000, when scanned at 0.1 s/decade, will arrive at the interface at a rate of over 23,000 peaks/s. conventional systems have previously been limited to rates of 1,000 peaks/s, but System 11-250 has been designed to handle up to 48,000 peaks/s in 'peak burst' mode. The graph in Figure 1 shows the relationship between the required peak processing rate, scan speed, and instantaneous mass when operating at unit mass resolution. Of course, when operating with an instrumental resolution sufficient to separate isobaric ions, similar peak arrival rates may be encountered at considerably slower scan rates.

MULTI TASKING.

A further consequence of faster data acquisition rates is a much increased volume of data; to the extent that conventional data processing and reduction techniques are becoming inadequate. However, with the availablity of low cost CPU memory and powerful operating systems, such as RSX-11M, it has been possible to create an effective multi-tasking environment

In conventional systems, data acquisition is defined as the 'foreground' task, whilst interpretation, using the VDU, is definend as the background task. System 11-250, by virtue of its powerful bit-slice micro processed interface, which performs all the time critical tasks of data acquisition

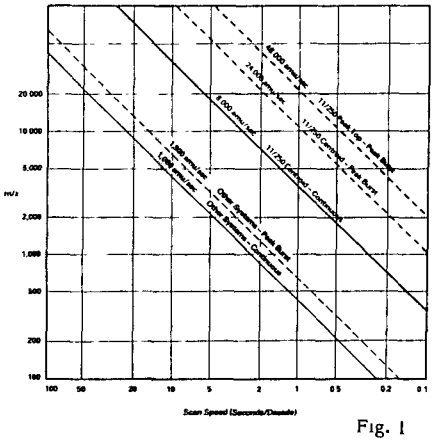

Fig. 1

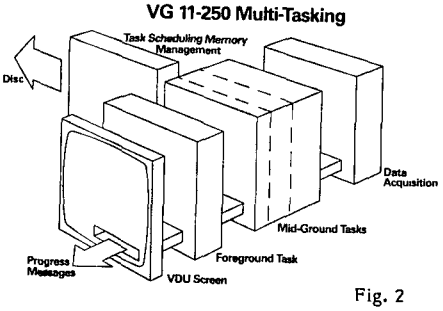

Fig. 2

and uses DMA to transfer data via the host CPU to disc storage, is able to consider data acquisition as the background task. This leaves the foreground available for optimzed interactive data interpretation. Furthermore, additional processing tasks, such as plotting, listing, library searching etc., can simultaneously be running in the CPU memory area defined as the 'midground', as illustrated in Figure 2. The use of a dedicated area of the VDU screen for the presentation of 'progress messages' from the midground tasks ensures that the operator is informed of the current status of operational tasks.

HARDWARE.

System 11-250 has been designed to exploit the concept of distrubuted processing In addition to a 1Mbyte PDP11-24 CPU, 96Mbyte Winchester technology disc drive, high resolution printer/plotter (with a colour option) and DMA colour VDU, the system utilises 2 micro-processed units to perform all the real time tasks of data acquisition and instrument control. The acquisition interface has individually buffered ultra-fast bit-slice micro-processors for peak detection, centroiding, and multiplet separation. A further micro-processor, in communication with the PDP11 controls functions such as ionisation mode (EI/CI), ionisation polarity (+/-), solvent dump valve, GC (and auto-sampler) operation, etc. A second micro-processed unit, with 16 and 18 bit DACs for the magnet and ESA references controls all the instrument scan functions for high and low resolution scanning, SIR, and peak matching It also controls the ESA and magnet scan functions for metastable scanning and SIR.

DYNAMIC RANGE.

GC-MS provides an exceptionally wide range of signal intensities. To measure a 1% peak, in the spectrum of a 1% component, with a precision of 1% whilst keeping 'on scale' the base peak of a 100% component, requires a dynamic range of 10^6 :1. System 11-250 will provide this dynamic range by using a 16 bit ADC and a 4 bit shift which is invoked on detection of a signalwhich would otherwise cause an overflow of the ADC. However, to achieve the maximum dynamic range in practice requires that the amplifier bandwith and electron multiplier gain are optimally adjusted. In normal routine operation this is often not so, and there is a need for some compensation by means of computer control of the amplifier gain factor, which can be adjusted on a scan to scan basis. The interface of System 11-250 can provide this auto-ranging in factors of 1,10 and 100.

Signal to noise ratio, often a limiting factor for dynamic range, can be improved substantially by the use of MCA techniques. System 11-250 has been designed to operate with up to 128,000 channels in this mode.

APPLICATION OF A LOW COST MICROCOMPUTER FOR DIGITAL M/Z READOUT ON A MAGNETIC SECTOR MASS SPECROMETER

J. P. FREEMAN and R. K. MITCHUM

National Center for Toxicological Research, Jefferson, AR 72079

Mass spectrometer manufacturers and independent companies supply digital mass readout and marker devices as options on magnetic mass spectrometers. These devices are expensive but do provide a much needed feature for tuning and manual operation of the instrument. With the wide usage of computerized instrument control and data collection, there is less dependence on mass markers and mass readout devices.

The relationship between the m/z of the focussed ion and the instrumental parameters (ion accelerating voltage and magnetic field strength) can be expressed by the equation (1):

$$m/z = 5000 \times r^2 \times H^2 / A$$

Because 5000 and the magnet radius (r) are constants, the mass to charge ratio is linearly dependent upon the square of the magnetic field (H) and the inverse of the ion accelerating voltage (A). Analog electronic circuits have been constructed from readily available components to perform this calculation (2,3). Nonlinearity of the electronic components and the gaussmeter employed to sense the magnetic field strength results in the need for linearity correction components in the elctronic circuit. Calibration is usually a multistep sequence with repetitive iterations.

Because the most probable source of nonlinearity is the gaussmeter, normal numerical methods for reduction of random errors (linear regression) are of little value in calibration. With the use of a computer to evaluate the mathematical equation for m/z, the capability to apply other statistical methods for calibration becomes available. Interpolation between known data points is a method for dealing with nonrandom error. Neville's algorithm is an iterated interpolation method (4) that can be programed on a small microcomputer (8 Kword RAM).

Using an Analog Devices 12 bit ADC and a Texas Instruments 990 microcomputer in conjunction with the RFL gaussmeter, a digital mass readout device was constructed to operate on a Kratos MS50 mass spectrometer. An evaluation of a Neville fit algorithm written in Basic as a method of calibration was made. Calibrated data was produced over an m/z range of 0 to 900 with an error of less that 1 m/z. Calibration was convenient but somewhat slow. Calibration was seldom necessary because the long term stabiility was greater than 3 months. Changes in the ion sources, modes of ionization (EI & FAB) and modes of ion detection (positive or negative ion) had little effect on the calibration. The ability to read the mass readout directly in peak matching and at reduced IAV modes was very convenient.

References

1. C. Brunnee, Spectra, 9 (2,3), 24, 1983.
2. A. M. Hogg, Abstr. 23rd Conf. on Mass Spectrometry and Allied Topics, Houston, Texas (AMI Soc. Mass Spectrometry) Paper 1.5.
3. J. Bell, et al., J. Phys. E. Sci. Instrum., 12,683-5, 1979.
4. A.C. Norris, Computational Chemistry, John Wiley & Sons, New York, 1981, page 273-6.

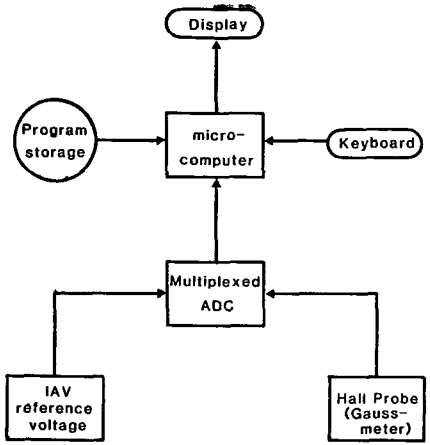
Display
Program storage
micro-computer
Keyboard
Multiplexed ADC
IAV reference voltage
Hall Probe (Gauss-meter)

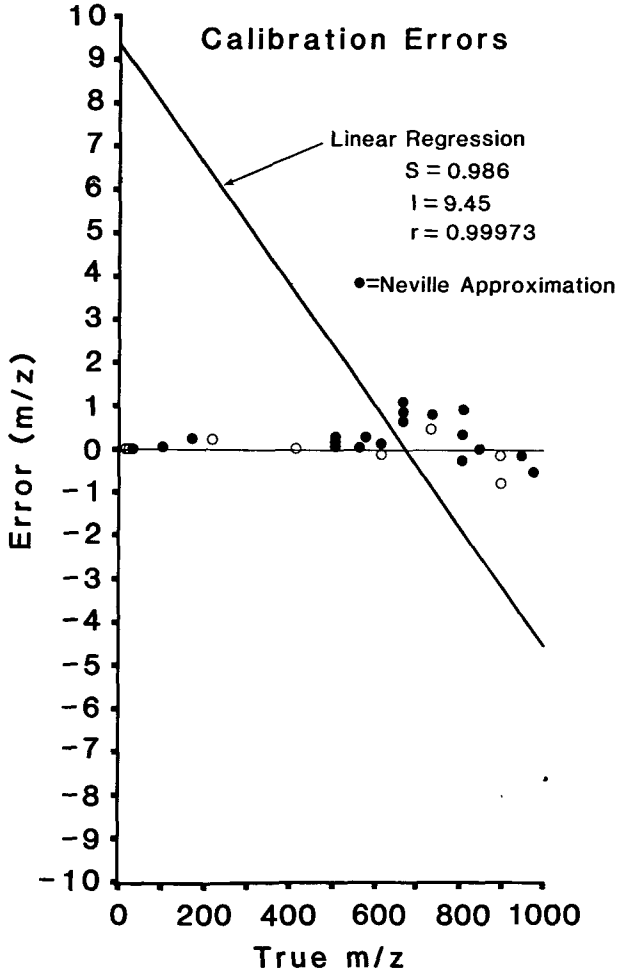
Calibration Errors
Linear Regression
S = 0.986
I = 9.45
r = 0.99973
●=Neville Approximation
Error (m/z)
True m/z
10
9
8
7
6
5
4
3
2
1
0
-1
-2
-3
-4
-5
-6
-7
-8
-9
-10
0
200
400
600
800
1000

USE OF AN 'INCOS' DATA SYSTEM VIA A PERSONAL COMPUTER: AN 'APPLE' PERSPECTIVE*

W.D.Jamieson, R.M.Gershey and R.Guevremont

Marine Analytical Chemistry Standards, Atlantic Research Laboratory
National Research Council of Canada
1411 Oxford Street, Halifax, N.S., Canada, B3H 3Z1

We have enhanced earlier extensions of our INCOS system (1,2) to improve the capability to transfer data between INCOS and other systems or to peripheral devices, linked either by direct wires (300 - 19200 baud) or telephone (300 baud). A major goal was to improve the convenience of transferring INCOS data to 'APPLE II+/IIe' systems so we could conveniently use commercially-available APPLE-resident software for such text or word-processing tasks as report generation or modification of INCOS system source files, and for data base management. Convenient transfers with APPLE systems either at one's home or in the laboratory also allow inspection or interpretation of INCOS data with minimum hard-copy transports, and occasional operation of the INCOS system from a remote APPLE work station.

Provision for these INCOS <--> APPLE data exchanges is an important part of the local network (see Figure) we have developed for our analytical chemistry operation.

Key INCOS-supporting utilities are the 'Phone.SV' and 'Remote.SV' programs (Finnigan MAT) for telephone-linked operations, and 'Line.MS' (1,2) which we developed for direct-wired transfers. We have further enhanced our Line.MS to allow options to meet needs of a non-INCOS system: X-on/X-off control of I/O; delay and/or <LF> after <CR> output; <ctrl-I> conversion. Echo-handshaking is used where possible with direct-wired I/O but is not required.

APPLE-resident utilities we have used include 'Tekterm' (Fountain Computer Products) and 'ASCII Express: Pro' (Southwestern Data Systems). Tekterm incorporates an optional 'Tektronix' emulation mode allowing INCOS graphics to be displayed on an APPLE. Although we have often used 'Applewriter II/IIe' (Apple Computer) for report generation, we plan increased use of 'Gutenberg' (Micromation) since this text processor can 'cut-and-paste' graphics with text.

A typical diskette for the Apple would include I/O utilities, such aids as 'Jtyper' (developed from 'Xtyper' by Beagle Bros.) for creating slides or posters or enhancing graphics, and 'Printpic' for printing graphics or Jtyper products or presenting automatic video 'slide' shows. About 300 sectors (77 Kbytes) would remain for other files.

REFERENCES

1. W.D.Jamieson, E.Lewis and F.G.Mason. Modifications to an INCOS Data System. Int. J. Mass Spectrom. and Ion Phys., Vol. 46, pp. 103-6 (1983). And references therein.

2. R.Guevremont, W.D.Jamieson and E.Lewis. Dialogues Between an INCOS Data System and Other Computers: How and Why. Presented at the 31st Annual Conference on Mass Spectrometry and Allied Topics, Boston, May, 1983, Proc., pp. 560-1.

* NRCC No. 23224

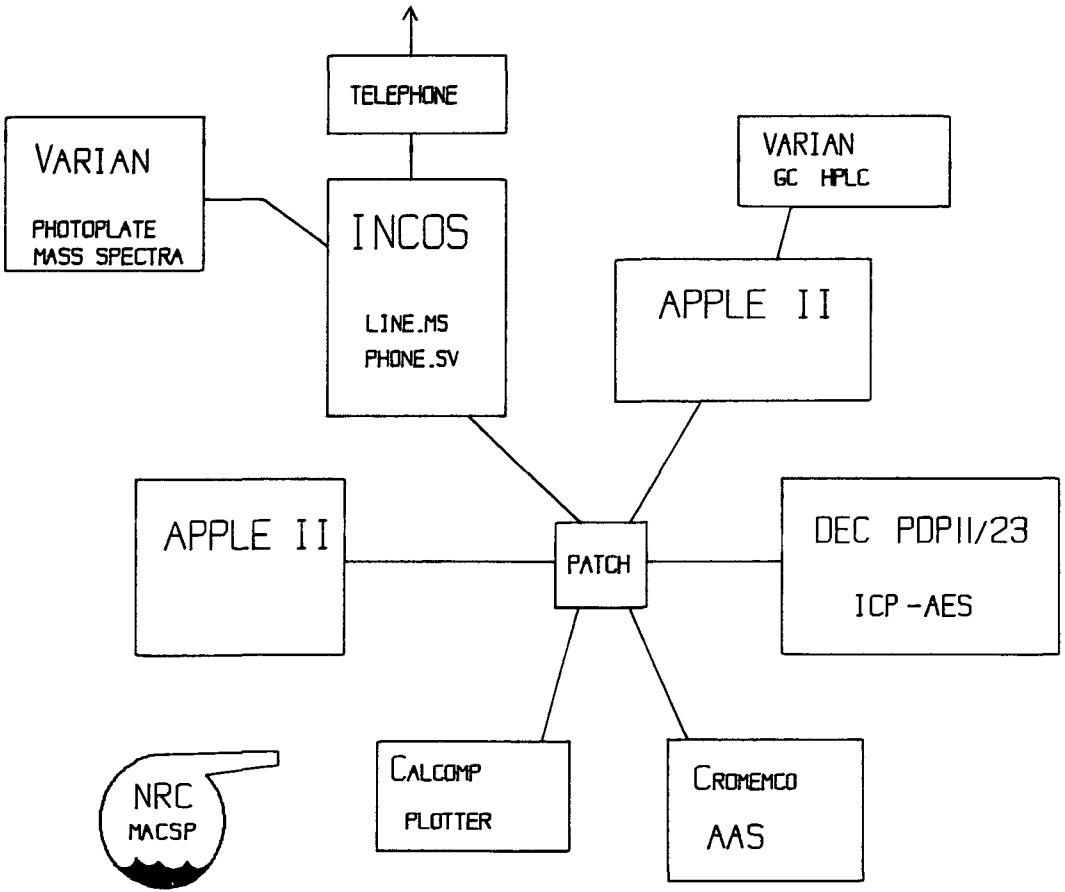
TELEPHONE
VARIAN
PHOTOPLATE
MASS SPECTRA
INCOS
LINE.MS
PHONE.SV
VARIAN
GC HPLC
APPLE II
APPLE II
PATCH
DEC PDP11/23
ICP-AES
NRC
MACSP
CALCOMP
PLOTTER
CROMEMCO
AAS

STRUCTURAL CHARACTERIZATION OF SULFATED GLYCOSAMINOGLYCANS BY FABMS: APPLICATIONS TO HEPARIN AND CHONDROITIN SULFATE. Steven A. Carr and Vernon N. Reinhold. Dept. of Nutrition, Harvard School of Public Health, Boston, MA 02115.

The sulfated glycosaminoglycans (GAG's) constitute a broad class of acidic polysaccharides that includes the chondroitin, dermatan and keratan sulfates. These molecules are widely distributed in connective tissues such as skin, collagen and bone. Heparin, a clinically important member of this family is predominantly found in lung, spleen, liver and muscle tissue. The most important action of heparin is its anticoagulant activity. Heparin inhibits a number of procoagulant proteases mainly by binding to antithrombin-III (AT-III) and enhancing the effects of this inhibitor. These anticoagulant properties appear to be associated with specific structural domains in the heparin chain which are as yet uncharacterized. Thus, detailed knowledge of the sequence, linkage and sites of sulfation of these GAG's is fundamental to understanding their physiological, chemical and physical properties. Another recent finding which underscores this point is the demonstration that a hexasaccharide fraction from heparin, when administered together with cortisone, causes regression of large tumor masses, inhibits angiogenesis and prevents metastases (1). Unfortunately, elucidation of the molecular structures of the sulfated GAG's is remarkably difficult due to the lability of the sulfate residues and to the microheterogeneity which hinders chromatographic separation and purification.

Our goal is to aid in the unraveling of these structures using mass spectrometry. In previous work we demonstrated that polysulfated di-octasaccharides obtained from chondroitin sulfate may be structurally characterized by positive and negative ion FABMS (2). The spectra show intense cationized molecular ions and fragment ions from which sugar sequence and sites of sulfation can be readily determined. In addition, polymers of 4-O-sulfate and 6-O-sulfate positional isomers could be distinguished, and structural homologs of chondroitin sulfate that contain more than one covalently bound sulfate moiety per two sugar residues were identified. We have now extended these preliminary studies to the characterization of the clinically important degradation products of heparin and synthetic sulfated oligosaccharides corresponding to putative structural domains of heparin. The synthetic compounds were provided by the Choay Institute as part of an ongoing collaboration (4). The largest molecule in this series was a synthetic pentasaccharide which corresponds to the minimal sequence required in heparin to bind AT-III and to induce anti-factor Xa activity (see Fig. 2) (3). These studies may ultimately lead to the therapeutic use of heparin fragments with defined specificity and fewer deleterious side effects.

The FAB mass spectra of heparin saccharides exhibit two features that are useful for characterizing structure (Fig. 1, 2). First are the series of molecular weight related ions. Variations in the countercation distribution for these polyanionic molecules are reflected in the clusters of MW-related peaks, separated by 22u (-H,+Na) or 16u (-Na,+K). Second, the presence (and, in some cases, the total number) of sulfate esters may be readily determined from the FAB mass spectra by the losses of 102u which result from facile elimination of sodium sulfite with hydrogen replacement.

In contrast to the FAB mass spectra of chondroitin sulfate oligomers, the spectra of heparin-related oligosaccharides do not exhibit sequence-related fragment ions. The lack of structurally informative fragmentation is probably related, at least in part, to the increased lability of N- versus O-sulfate moieties under the conditions used for FABMS analysis. The (-) FAB spectra of the former exhibit intense ions due to loss of sulfite, whereas these ions are absent from the spectra of the latter. We have attempted to induce glycosidic bond rupture in the heparin-related oligomers during FABMS analysis by collision induced dissociation of selected molecular ions and fragment ions. Unfortunately, MS/MS-CID only enhances elimination of sulfite, and the desired sequence-related fragments are not observed.

FABMS, especially in the negative ion mode, is an extremely sensitive tool for detecting minor structural modifications that may be present in these molecules. For example, the synthetic route used to produce pentasaccharide III (Fig. 2) also results in the formation of a minor amount of the corresponding monomethyl glycoside. The latter can be detected by the satellite peaks

14u above the corresponding molecular ions. This impurity was not detected by NMR.

(1) Folkman, J., Langer, R., Linhardt, R. J., Haudenschild, C. and Taylor, S. Science. 221, 719 (1983).
(2) Carr, S. A. and Reinhold V. N. J. Carbohydr. Chem. 3 (1984), in press.
(3) Choay, J., Petitou, M., Lormeau, J. C., Sinay, P., Casu, B. and Gatti, G. Biochem. Biophys. Res. Commun. 116, 492 (1983).
(4) Reinhold, V. N., Carr, S. A., Green, B., Petitou, M. and Choay, J. J. Carbohydr. Chem. 3 (1984), in press.

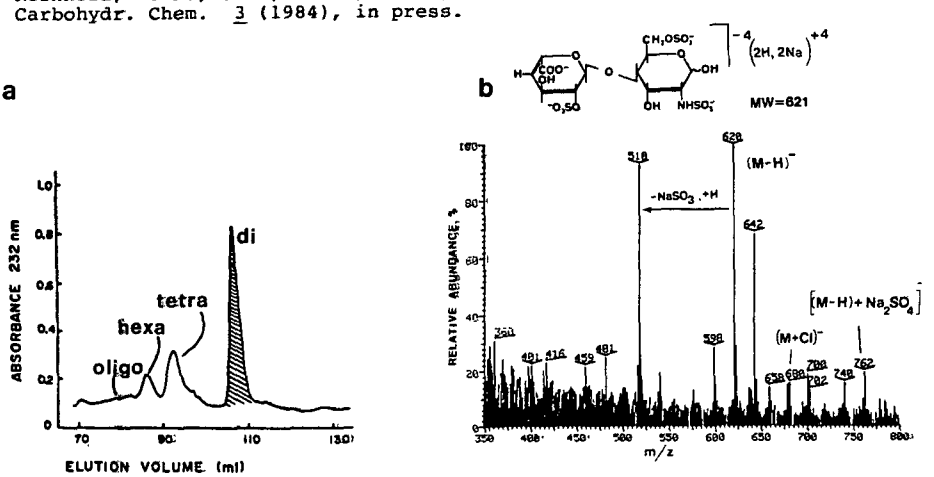

Fig. 1. a) Gel permeation chromatogram of heparin fragments produced by heparinase treatment of heparin, (A. Larsen, Ph.D. Thesis, MIT, 1984). b) Negative ion FAB mass spectrum of the disaccharide fraction from (a), above; thioglycerol matrix.

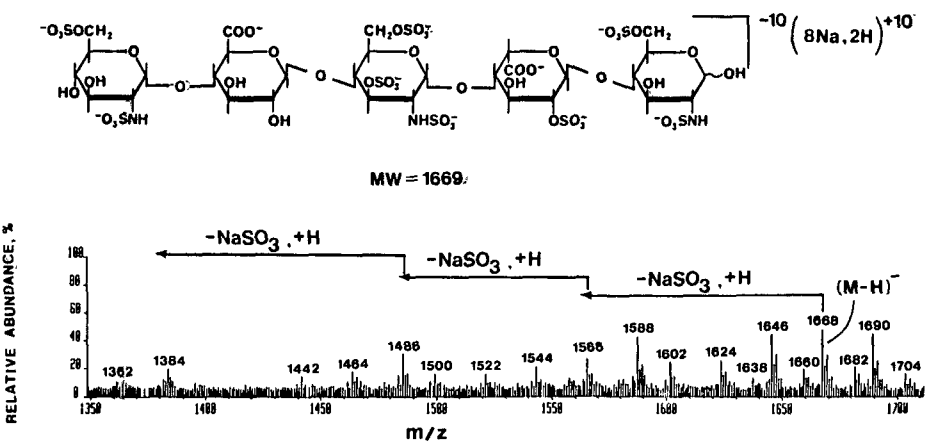

Fig. 2. FAB mass spectrum of a synthetic pentasaccharide which corresponds to the minimal sequence required in heparin for binding to antithrombin-III; (-) ion, thioglycerol.

POLYSACCHARIDE LINKAGE AND BRANCHING INFORMATION; GLYCOSIDIC CLEAVAGE WITH TRIETHYLSILANE AND PRODUCT CHARACTERIZATION BY GC/MS. A. Van Langenhove, V. N. Reinhold. Dept. of Nutrition, Harvard School of Public Health, Boston, MA 02115.

In contrast to the usual linear sequence analysis for other biopolymers, polysaccharides require a determination of branching, linkage point and chirality. These additional complications have classically been approached by sample permethylation, hydrolytic cleavage, reduction and acetylation. The points of acetylation in the resulting methylated alditol acetates are then determined by GC and/or GC-MS. These procedures, however, lack the sensitivity, and, in some cases, the specificity, to approach many current polysaccharide problems. In particular, the losses associated with acid catalyzed hydrolysis and the extensive sample work-up to form alditol acetates does not allow manipulation of small amounts of sample.

We are therefore evaluating a recently introduced alternative to this approach, namely total reductive depolymerization with triethylsilane and boron trifluoride as the catalyst (1, 2). Reductive cleavage, on permethylated oligosaccharides, is a one step procedure during which the glycosidic linkage is reductively cleaved and the original ring form is preserved. The products, 1-deoxy monosaccharides, are acetylated and conveniently analyzed by capillary GC and/or GC-MS as demonstrated in a preliminary report (3).

In order to test the efficacy of this procedure for linkage analysis of oligosaccharides, we have characterized the gas chromatographic retention times and mass spectra of a series of mono-, di-, and unacetylated 1-deoxy monosaccharides using both chemical and electron ionization MS. These products would represent saccharide positions of chain extension, branching and termination, respectively. To generate terminal and extender residues, (monoacetates), for a glucose polymer, we reductively cleaved a series of commercially available disaccharides in which the residues were linked 1-1, 1-2, 1-3, 1-4 and 1-6. Scheme 1 illustrates the technique for obtaining the glucose terminal and 4-O-linked products.

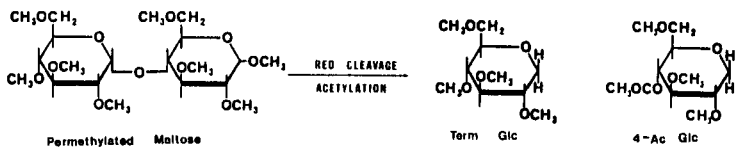

SCHEME 1

With these results we have compiled a collection of EI and CI mass spectra, as well as GC retention times on a fused silica DB-225 capillary column. The EI mass spectra of each of the 1-deoxy monoacetylated, (extender), residues, were significantly different from each other as to allow direct assignment of the acetylation position and hence linkage, Fig. 1-4.

To compile the same physical characteristics for mannose and galactose, we are currently carrying out incomplete permethylation and reductively cleaving and acetylating the products. This approach provides a series of mono-, di-, and unacetylated 1-deoxy monosaccharides. The mixture and degree of acetylation is first characterized by ammonia CIMS followed by EIMS. The characteristics for the diacetylated products would provide information to determining branch points. As anticipated, all 1-deoxy monoacetates, acetylated at the same position, fragment under EI to give identical mass spectra. We found that the method is applicable to keto sugars (e.g., fructose), but under the employed experimental conditions, 2-acetamido sugar linkages are not reductively cleaved. This interesting observation is currently under further investigation. The technique is actively being applied to several unknown oligosaccharide problems.

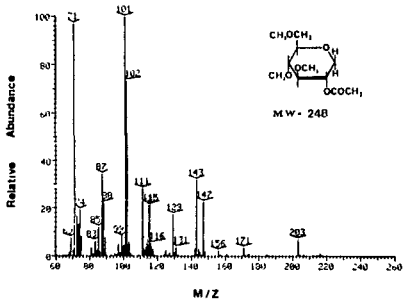

Fig. 1. EI mass spectrum of 1-deoxy-2-O-acetyl-3,4,6-tri-O-methyl-D-glucopyranose

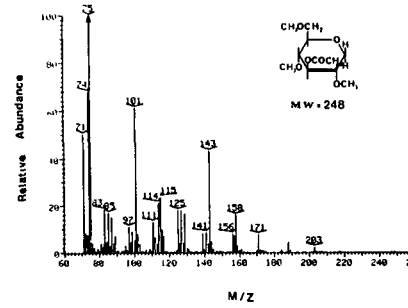

Fig. 2. EI mass spectrum of 1-deoxy 3-O-acetyl-2,4,6-tri-O-methyl-D-glucopyranose

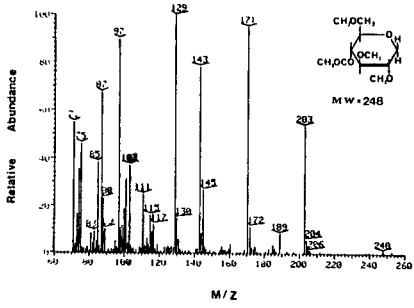

Fig. 3. EI mass spectrum of 1-deoxy-4-O-acetyl-2,3,6-tri-O-methyl-D-glucopyranose

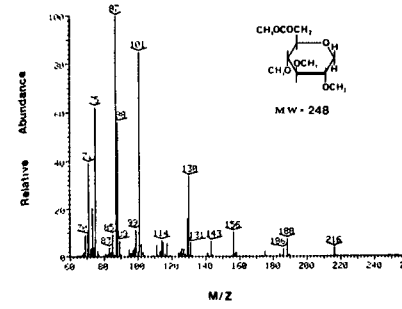

Fig. 4. EI mass spectrum of 1-deoxy-6-O-acetyl-2,3,4-tri-O-methyl-D-glucopyranose

(1) Doyle, M. P., West, C. T., Donnelly, S. J. and McOsker C. C. J. Organometallic Chem., 117, 129 (1976).
(2) Rolf, D. and Gray, G. R. J. Am. Chem. Soc. 104, 3539 (1982).
(3) Reinhold, V. N., Coles, E. and Carr, S. A. J. Carbohydr. Chem. 2, 1 (1983).

ANALYSIS OF CARDIAC GLYCOSIDES BY FAST ATOM BOMBARDMENT MASS SPECTROMETRY

Allmaier G. and Schmid E. R. , Inst. f. Analytical Chemistry , Univ. of Vienna , Waehringerstr. 38 A - 1090 Vienna Austria

The potential and capability of fast atom bombardment (FAB) mass spectrometry for the structural analysis of underivatized steroid glycosides was examined with cardiac glycosides of cardenolid type and their aglycones . Cardiac glycosides have been analysed by EI - MS , but derivatization is usually necessary to obtain useful spectra . FD - MS [1] has been used , producing molecular weight information but accompanied by technical difficulties . Infrared RLD - MS [2] usually produces molecular cations with little fragmentation of low intensity . Recently , negative ion DCI - MS [3] , using $(OH)^-$ as the reactant ion , has been shown to provide good spectra with $(M-H)^-$ ions as well as significant and useful fragments .

At first we have examined the use of FAB for underivatized aglycones - gitoxigenin , digoxigenin and k-strophanthidin . Mass spectra of such substances in glycerol matrix recorded show abundant $(M+H)^+$ ions as well as significant fragments . Fragment ions $(M+H-H_2O)^+$, $(M+H-2H_2O)^+$, $(M+H-3H_2O)^+$, $(M+H-CO)^+$ or $(M+H-CO-nH_2O)^+$ in these spectra are clearly associated with OH - and CHO - groups from the aglycone . In conclusion , it may be stated that the number of OH - or CHO - groups is a measure for the expected fragmentation by loss of H_2O or CO . Addition of alkali metal ions did not suppress fragmentation , but increased the complexity of the spectrum . With the triethanolamine (TEA) / 1,1,3,3 - tetramethylurea (TMU) matrix only $(M+TEA+H)^+$ ions were found . $(M+H)^+$ and fragment ions disappeared completely .

Positive ion FAB - MS spectrum of the underivatized cardiac glycosides lanatosid C - four sugar units - is shown in Fig . 1 . The protonated molecular ion ($^m/z$ 985) of lanatosid C was detected with high intensity using a glycerol matrix . Fragment ions clearly associated with the sugar sequence were found . Ions at $^m/z$ 823 , 651 , 521 and 391 were obtained by sequentially cleavage at glycosidic linkage from the non - reducing terminal . Interesting fragment ions , which were cleaved from the aglycone terminal , were detected additionally . The protonated aglycone ion and the characteristic loss of water molecules was clearly found . The addition of alkali metal ions reduced fragmentation , thereby reflecting the increased stability of the $(M+Na)^+$ ion . When TEA/TMU as matrix is used , a stable molecular adduct ion species , $(M+TEA+H)^+$ ion is formed and no fragment ions are detected . We found that the determination of molecular weight of cardiac glycosides with this matrix is very successfully .

FAB - MS of underivatized cardiac glycosides is an extremely useful technique for determining molecular weights , carbohydrate sequences and structural informations of aglycones .

1. Schulten , H.R. and Games , D.E. , Biomed. Mass Spectrom. 1 , 120 (1974) .
2. Heresch , F. , Schmid , E.R. and Huber , J.F.K. , Anal. Chem. 52 , 1803 (1980) .
3. Bruins , A.P. , Int. J. Mass Spectrom. Ion Phys. 48 , 185 (1983) .

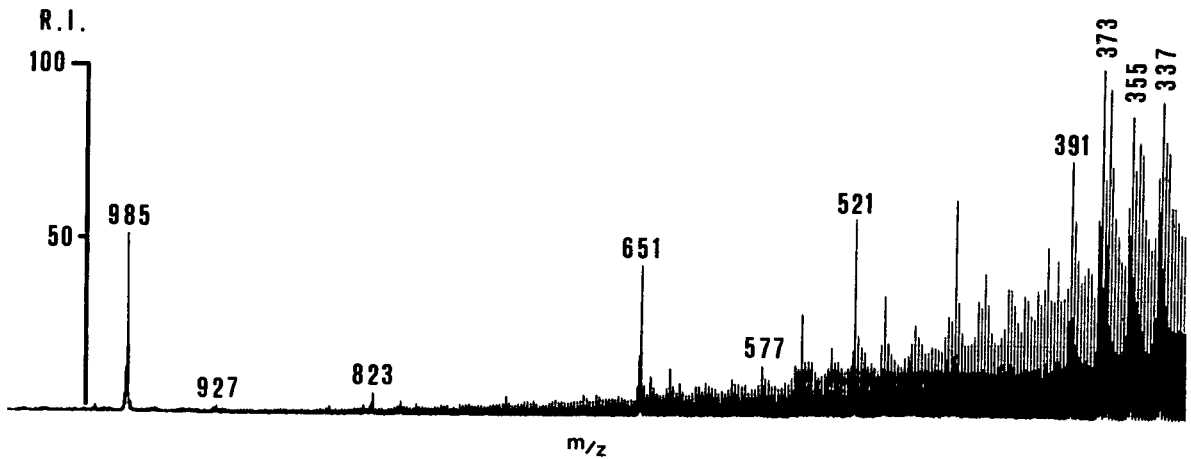

Fig. 1. Positive ion FAB mass spectrum of lanatosid C in glycerol matrix

STRUCTURAL ANALYSIS OF FLAVONOID OLIGOSIDES BY FAST ATOM BOMBARDMENT/TANDEM MASS SPECTROMETRY, F.W. Crow, K.B. Tomer, and J.H. Looker, Midwest Center for Mass Spectrometry, Department of Chemistry, University of Nebraska, Lincoln, NE 68588

PURPOSE: To obtain maximum structural information from FAB spectra containing interferences. Illustrated with a study of glycosidic flavonoids and steroids.

ILLUSTRATION OF THE PROBLEM: FAB spectra can yield few fragment ions and mixture spectra can be ambiguous. Myricitrin required a glycerol/formic acid solvent matrix. Matrix ions include proton bound glycerol oligomers, reaction products for formic acid + glycerol and water loss ions from these ions. The ion at m/z 449 corresponds to an impurity. It is unclear if m/z 319 is a fragment or an impurity.

1. FAB MS/MS TO OBSERVE FRAGMENTS FROM ONE "PARENT" ION: The FAB MS/MS spectra were obtained on a triple sector (EBE) mass spectrometer where the first two sectors (MS-1) are used to select the ion of interest. The ion is collisionally activated (CA) between MS-1 and MS-2 and the CA spectrum taken by scanning MS-2. The spectrum clearly shows that m/z 319 is a fragment of the MH^+ ion from myricitrin. It corresponds to the protonated aglycone portion of the molecule (AH_2^+).

2. SEQUENCE INFORMATION: The polysaccharide chain in glycosidic flavonoids can be sequenced by looking at the positive ion CA spectrum of the MH^+ ion. The CA spectrum of naringin shows fragment ions resulting from sequential loss of sugar residues.

3. GLYCOSIDIC STEROID CA SPECTRA: Digoxin contains three -OH groups on the steroid portion of the molecule. Not only does the CA spectrum of this molecule show the sugar sequence ions but the number of -OH groups can be determined from the fragments coming from the AH_2^+ ion.

4. DIFFERENTIATION OF ISOMERS BY NEGATIVE ION CA: Hesperidin and neohesperidin differ only by the bonding in the saccharide chain. A fragment present in the spectrum of neohesperidin is missing the the spectrum of hesperidin. This common saccharide fragmentation can often aid in determining the point of substitution.

5. DIFFERENTIATION OF ISOMERS BY POSITIVE ION CA: The occurrence of a particular fragment can be dependent on the position of a substituent. The mechanism shown gives a possible explanation for the stability of the indicated fragment.

6. MIXTURE ANALYSIS: The spectrum of xanthorhamnin is complicated by the presence of a major impurity and cation addition products. Assignment of the saccharide sequence is facilitated by isolating the MH^+ ion by MS/MS.

7. RADICAL ANION FORMATION: Although most sample form $(M-H)^-$ ions some molecules which are well suited to stabilize negative charge will form radical anions. Anthraquinoid compounds such as those present in frangulin form this ion. Major fragmentation is similar except that the masses of the ions are shifted. It has also been observed that fragmentation of the $(M-H)^-$ ions produces radical anions corresponding to the aglycone portion of the glycosidic flavonoids.

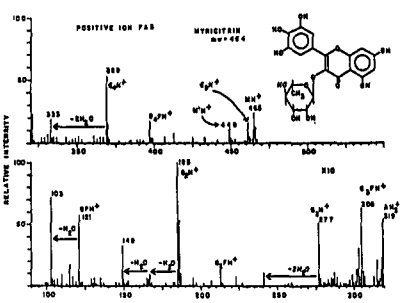

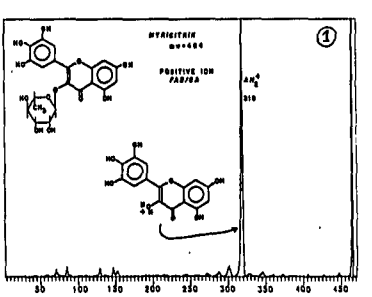

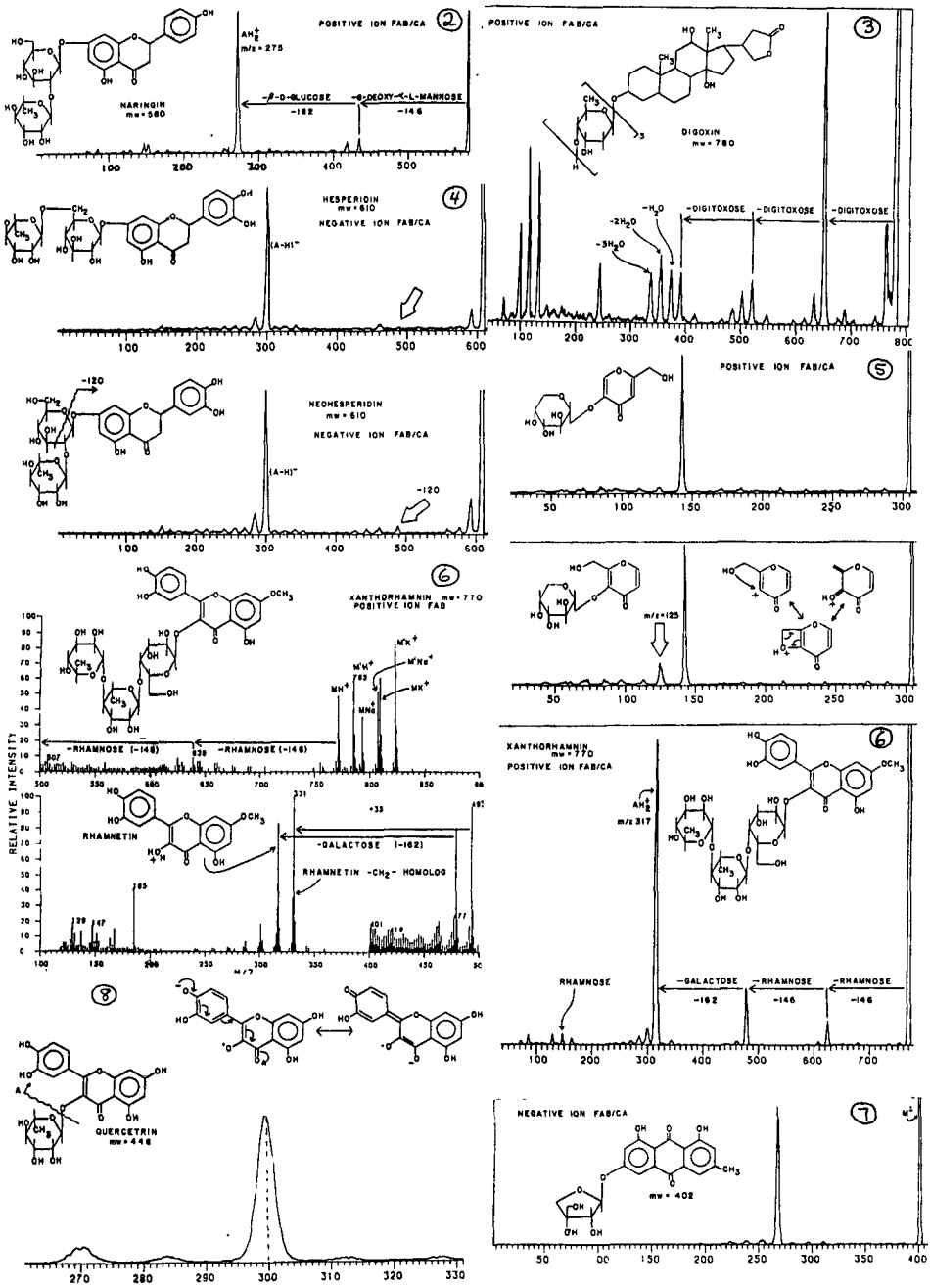
POSITIVE ION FAB/CA
NARINGIN
mw = 580
m/z = 275
-β-D-GLUCOSE
-162
-6-DEOXY-α-L-MANNOSE
-146
HESPERIDIN
mw = 610
NEGATIVE ION FAB/CA
(A-H)⁻
NEOHESPERIDIN
mw = 610
NEGATIVE ION FAB/CA
-120
XANTHORHAMNIN mw = 770
POSITIVE ION FAB
-RHAMNOSE (-146)
RHAMNETIN
-GALACTOSE (-162)
RHAMNETIN -CH2- HOMOLOG
RELATIVE INTENSITY
QUERCETRIN
mw = 448
DIGOXIN
mw = 780
-DIGITOXOSE
m/z = 125
m/z 317
RHAMNOSE
-RHAMNOSE
NEGATIVE ION FAB/CA
mw = 402

APPLICATIONS OF LASER DESORPTION MASS SPECTROMETRY.

Robert J. Cotter, Jean-Claude Tabet and Richard van Breemen,
Department of Pharmacology, The Johns Hopkins University, Baltimore, MD 21205

The laser desorption technique can be used for the mass spectral analysis of non-volatile/thermally labile compounds such as peptides, oligosaccharides, glycolipids, etc. In our laboratory a laser desorption time-of-flight mass spectrometer has been used for structural confirmation of several glucuronic acid conjugates, synthesized by an immobilized-enzyme mediated technique (1). Laser desorption spectra of several small peptides produce both C-terminal and N-terminal fragments (2). The molecular ions are formed by cationization (alkali ion attachment) and the alakali ion is generally found on the C-terminal fragments, suggesting a ionization/fragmentation scheme similar to that observed by chemical ionization. Over mass 1,000 the TOF analyzer, operating at less than "unit" resolution, can be used to determine the number and "branching" of sugar groups in such compounds as the steroidal glycoside digitonin or to characterize components of homologous mixtures (2). The latter point is illustrated using a purified component of lipid A (3) and synthetic trehalose octapalmitate as examples.

(1) J.-C. Tabet, R. van Breemen and R.J. Cotter, Biomed. Mass Spectrom. (in press).

(2) J.-C. Tabet and R.J. Cotter, Anal. Chem. (in press).

(3) N. Qureshi, K Takayama, D. Heller and C. Fenselau, J. Biol. Chem., 258, 12947 (1983).

(JCT) present address: Ecole Polytechnique, Lab. de Synthese Organique, 91128 Palaiseau Cedex, France.

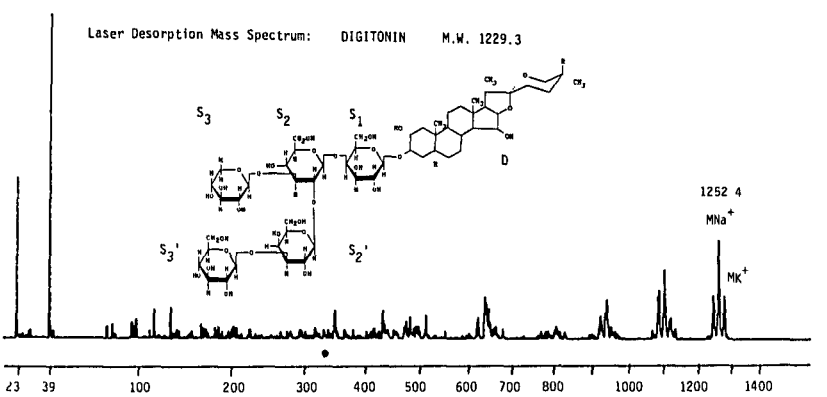

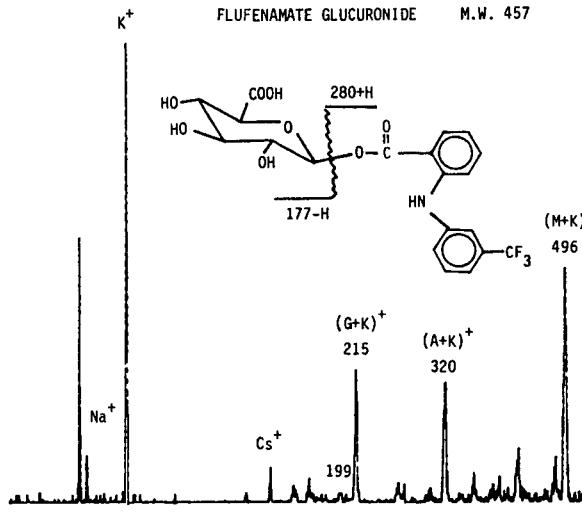
FLUFENAMATE GLUCURONIDE M.W. 457
K+
COOH
280+H
HO
HO
OH
O
O
C
HN
CF3
177-H
(M+K)+
496
(G+K)+
215
(A+K)+
320
Na+
Cs+
199

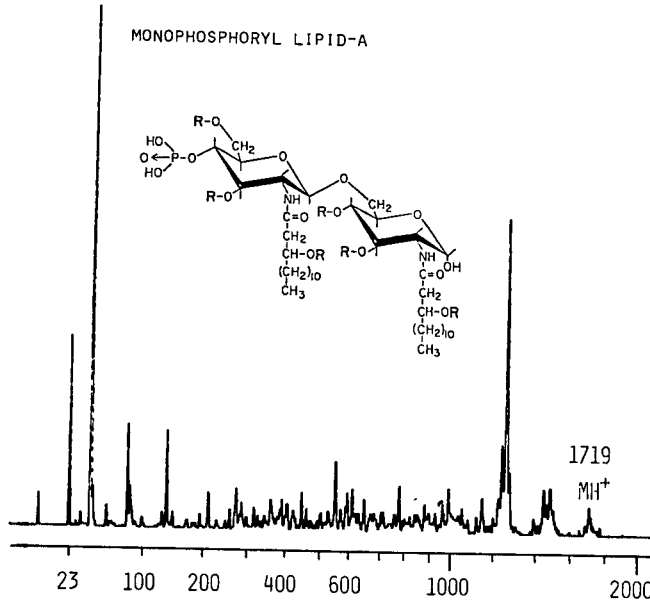
MONOPHOSPHORYL LIPID-A
1719
MH+
23
100
200
400
600
1000
2000

LC/MS ANALYSIS OF UNDERIVATIZED GLYCOSPHINGOLIPIDS FROM TISSUE EXTRACTS

James E. Evans and Robert H. McCluer
E.K. Shriver Center, 200 Trapelo Rd., Waltham, MA 02254

Glycosphingolipids (GSL) are thermally labile, nonvolatile, complex molecules that are present in biological membranes where they play an important role as cell surface recognition factors. They contain both a lipid moiety (ceramide) and a carbohydrate moiety. The ceramide is composed of a fatty acid attached to a long chain amine (sphingosine). Both the fatty acid and sphingosine are heterogenous with respect to carbon chain length, the degree of unsaturation, and the number of hydroxyl groups they contain. The carbohydrate portion varies according to the number and identity of sugar residues present, and their sequence and linkage. In combination these variables create natural mixtures of extreme complexity. The pattern present in these mixtures is highly specific according to type of tissue, species, sex, and many other variables.

Our objective is to develop an online LC/MS method for separation and structural analysis of complex mixtures of glycosphingolipids in biological extracts. The GSLs are to be separated into classes based on their polar functional groups (e.g., carbohydrate moiety, etc.) by normal phase chromatography. Mass spectrometry will be used to provide structural information on both the carbohydrate and lipid moieties of the separated GSL, and to specifically monitor for particular molecular species in complex mixtures. We hope to utilize this methodology for identification, molecular species analysis and measurement of GSLs in biological samples.

Experimental:

A Finnigan 4500 MS equipped with a Finnigan moving belt transport type LC/MS interface was used for these experiments. All spectra were taken under ammonia (0.8 torr) CI conditions with the ion source at 300°C, and the clean-up heater at 270°C. The solvent from the HPLC column was applied to the belt as a fine stream via an orifice drawn from a section of 0.25 min ID fused silica capillary tubing.

HPLC was performed with a Spectra-Physics 8700 gradient solvent delivery system. Two, 2mm x 3 cm columns packed with 5 um sperical silica (Rheodyne Inc.) were used in series. For separation of neutral glycosphingolipid mixtures gradient elution from methylene chloride-methanol-water (93:6.5:0.5) to (65:31:4) was run in 10 min with a flow rate of 0.5 ml/min. Full scan spectra were collected at approximately 6 sec intervals throughout the analysis.

Results:

This method has proven useful for the analysis of ug quantities of glycosphingolipids in biological mixtures. Important information concerning several aspects of such mixtures is obtained. This includes:

1. Separation and detection of various classes (as defined by carbohydrate composition and degree of hydroxylation).
2. MS data concerning composition of the ceramides present.
3. MS data concerning the hexose composition of the carbohydrate moiety (e.g., neutral and/or amino hexose).
4. Identification of sphingosines and fatty acids.
5. The potential for development of procedures for measurement of all the above by the use of areas from specific ion plots.

The chromatogram below shows the total ion current and several specific ion plots from the analysis of 6 ug of a neutral glycosphingolipid extract from mouse kidney. A spectra of the globoside peak is also included below to illustrate the kind of data obtained.

The graph below shows the results obtained when from 0.5 to 16 ug of synthetic 16:0-d18:0-galactosylceramide was applied directly to the transport belt and the area under the m/z 266 ion plot peak for sphingosine was integrated. This data serves to demonstrate the quantitative potential of this method.

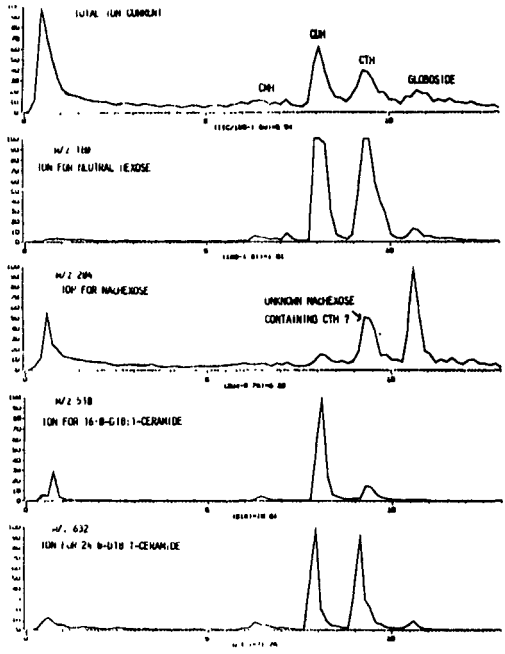
TOTAL ION CURRENT
GlM
CTH
CMH
GLOBOSIDE
M/Z 168
ION FOR FALUTRAL HEXOSE
M/Z 284
ION FOR NACHEXOSE
UNKNOWN NACHEXOSE
CONTAINING CTH ?
M/Z 518
ION FOR 16-B-D18:1-CERAMIDE
M/Z 632
ION FOR 24 B-D18 1-CERAMIDE

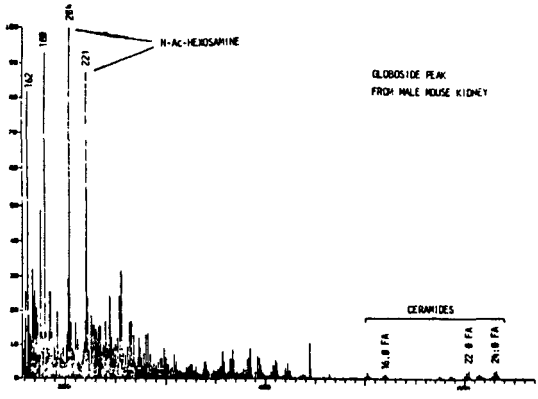
N-Ac-HEXOSAMINE
162
168
284
221
GLOBOSIDE PEAK
FROM MALE MOUSE KIDNEY
CERAMIDES
16:0 FA
22:0 FA
24:0 FA

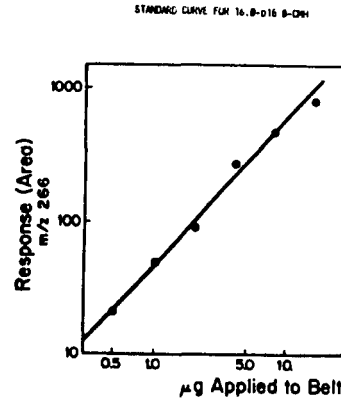
STANDARD CURVE FOR 16:0-D18 B-CMH
Response (Area)
m/z 266
1000
100
10
0.5
1.0
5.0
10
μg Applied to Belt

COMPARATIVE CAPILLARY GC/MS OF STANDARD SOLUTIONS OF CHLORINATED BIPHENYLS*

W.D.Jamieson, R.M.Gershey and R.Buevremont; Marine Analytical Chemistry Standards
Atlantic Research Laboratory, National Research Council of Canada
1411 Oxford Street, Halifax, N.S., Canada, B3H 3Z1

D.Fung, R.K.Boyd and S.Safe; Chemistry Department, University of Guelph
Guelph, Ont., Canada, N1G 2W1

B.G.Chittim; Wellington Environmental Consultants
P.O. Box 1261, Guelph, Ont., Canada, N1G 6N6

As a qualitative and quantitative aid to the determination of individual PCB congeners in complex samples, a set of four standard solutions of PCB congeners in iso-octane has been prepared. Consideration of environmental ubiquity and potential toxicity led to selection of 51 congeners for inclusion in the set. The selected compounds were individually synthesized then purified to >95 % purity. Purity and identity were assessed independently in two of our laboratories by capillary GC/electron-capture detection (ECD), capillary GC/MS and proton magnetic resonance experiments with solutions of single congeners and with candidate solutions of mixtures of congeners. Congeners were only accepted for inclusion in the set of standard solutions after we concluded from our independent experiments that there was good agreement on response factors for GC/MS (electron-impact ionization) and GC/ECD and no reasonable doubt about identity.

The mixtures prepared each contain 14 or 15 PCB congeners selected to avoid ambiguities from inadequate chromatographic resolution. The criterion was complete separation on a 15 m X 0.25 mm quartz capillary column coated with DB-1, OV-1 or SE-54. Where possible the mixtures contain congeners 153 and 209 (IUPAC numbers [1] for 2,2',4,4',5,5'-*hexachlorobiphenyl and decachlorobiphenyl) as references for GC retention* times and ECD sensitivity. Each mixture contains a pair of congeners for which the retention times are so similar that separation of the pair can serve to confirm adequate GC resolution. Concentrations of congeners in each mixture were adjusted in the range 1 to 140 µg/ml to yield similar ECD responses for all congeners.

GC/MS experiments at the University of Guelph are being done using a VG 12/250 system. For those in Halifax, a Finnigan MAT 4500 system is being used. In both laboratories, solutions of single congeners have been analyzed using electron-impact ionization (EI) (70 ev) and negative ion chemical ionization (NCI) (70 ev, isobutane or methane plasmas). Candidate standard solutons have been analyzed in both laboratories by EI.

For selected hexachlorobiphenyl congeners, NCI experiments have been done in both laboratories at two different ion source temperatures and for two or more different intrasource steady-state pressures of reagent gas.

Though the planned series of experiments has not been completed, some conclusions are evident. We are convinced from our parallel, independent experiments with these identical, well characterized samples that both GC/MS systems consistently yield data which can be compared easily.

* NRCC No. 23229

Results to date have confirmed that when EI is used, increased ortho-chlorine substitution increases the probability of primary fragmentation of the molecular ion by loss of a chlorine atom. When NCI is used, results have confirmed that the relative abundance of the molecular anion is greater when the source temperature is lower and that the yield of molecular anions is also enhanced when the flow of reagent gas is controlled so the intrasource steady-state pressure is at the minimum considered acceptable on the basis of other aspects of instrument performance.

Further analyses of these candidate standard solutions are in progress in our and other laboratories. If the results from these confirm the standard solutions will be reliably useful, sets of the solutions sealed in 1 ml all-glass ampoules will be released for distribution by the Marine Analytical Chemistry Standards program, NRCC.

We acknowledge gratefully helpful advice from several colleagues in Europe and North America whose suggestions we considered carefully in selecting congeners to be included in these standard solutions.

REFERENCE

1. K. Ballschmiter and M. Zell. Analysis of Polychlorinated Biphenyls by Glass Capillary Gas Chromatography. Composition of Technical Aroclor and Clophen PCB Mixtures. Fresenius Z. Anal. Chem. 302: pp. 20-31 (1980).

The Elimination of Mass Spectral Interferences for The Determination of Polychlorinated Biphenyls in Transformer Oil and Waste Oil

Vincent P. Nero and Robert D. Hudson
Texaco Research Center-Beacon, N.Y.

PCBs can easily be detected at the low ppb level in clean solvents (Figure 1). However, transformer oils or waste oils will greatly reduce this sensitivity. These oils are composed of a complex mixture of aliphatic, alicyclic and polynuclear aromatic hydrocarbons, all of which have possible alkyl substituents. The compositional analysis of the various classes of hydrocarbons present can be determined by established mass spectrometric methods (1,2), and a typical composition is shown Table I. Some of these compounds have the same masses and boiling ranges as the PCBs and therefore could have interfering mass fragments at a similar GC retention time. An HPLC procedure has been developed which quickly can eliminate these mass spectral interferences from oil matrices. The resulting HPLC fraction is clean enough to be analyzed for PCBs by GC/EIMS down to the low ppb level.

Cleanup Procedure by High Performance Liquid Chromatography

The cleanup procedure was carried out on a liquid chromatograph with UV spectrophotometer detection at 254 nm. A 25 cm long by 4.6 mm i.d. column, packed with Nucleosil 5 NO2, was used with an isoctane/tetrahydrofuran gradient mobile phase.

PCB standards were injected onto the system to initially determine the retention times and were then diluted in various transformer oils to ppb concentrations. EPA carbon-13 PCBs were added as recovery surrogates. The column eluent was collected for the retention time window and was then allowed to evaporate just to dryness using a light nitrogen flow. The PCB residue was taken up with methylene chloride containing 1 ppm dibromobiphenyl as an internal standard.

GC/MS Analysis

The isolated PCB fraction was analyzed on a gas chromatograph by splitless injection. The GC was equipped with a methyl silicone, 25 meter x 0.2 mm fused silica column, inserted directly into the mass spectrometer source. The oven temperature was programmed from 100°C to 300°C at 8°C/min with a 16 minute hold. A VG Analytical 7070 HS mass spectrometer was operated at an initial 4kV accelerating voltage, 1000 resolution (10% valley), 200uA trap current, 70 eV electron energy and source temperature of 250°C. Ion abundances were selectively recorded by voltage using the VG 2000 data system equipped with a digital scanner unit. A 1700 ppm window was scanned for each monitored ion. Ion abundances for 188.04, 194.04, 222.00, 224.00, 255.96, 257.96, 289.92, and 291.92 daltons were continuously measured for 50 msec each during retention times between 6 and 12 minutes. Ion abundances for 289.92, 291.92, 303.96, 311.90, 323.88, 325.88, 325.88, 359.84 and 361.84 daltons were obtained during retention times between 12 and 20 minutes.

RESULTS AND DISCUSSION

Various polar bonded stationary phases have been evaluated for their ability to perform separations of polycyclic aromatic hydrocarbons (PAH) by normal phase HPLC which, unlike reversed phase procedures, uses volatile mobile phases that can be easily removed from fractions collected for further analysis (3,4). The 3-(4-nitrophenyl)-

propyl bonded silica stationary phase has a high affinity for double bonds when used with non-polar mobile phases. Various organic compounds have retention times directly related to their respective number of double bonds (Table II). PCBs eluted in the range appropriate for biphenyls or other PAHs with six double bonds (Figure 2). This column effectively isolated the PCBs from most of the matrix, removing approximately 96% of the oil content with its inherent interferences.

The GC chromatograms, resulting from these HPLC cuts, are not significantly complicated by extraneous peaks (Figure 3). Selected ion chromatograms for 2 ppm Aroclor 1016 into transformer oil clearly reveal characteristic peak profiles free of interferences and have very similar isomer distribution patterns to Aroclor 1016 in hexane. In a second case a mixture of Aroclor 1242 from SRM 1581 was diluted to 2 ppm with the corresponding NBS transformer oil and was then spiked at 250 ppb with (Carbon 13) 3,3'4,4'- tetrachlorobiphenyl as a recovery surrogate. A comparison of the C-13 tetrachlorobiphenyl recovery surrogate chromatogram, m/z 304, with the chromatogram of the tetrachlorobiphenyl in Aroclor 1242, m/z 292 indicates clearly individual isomers at approximately 80 to 150 ppb (Figure 4).

Literature Cited

(1) ASTM Method D-2786, ASTM Standards, Part 24, American Society for Testing and Materials, 1916 Race St., Philadelphia, PA 19103.
(2) ASTM Method D-3279, ASTM Standards, Part 25, American Society for Testing and Materials, 1916 Race St., Philadelphia, PA 19103.
(3) Chmielowiec, J.; George, A. E.: Anal. Chem. 1980, 52, 1154.
(4) Bluemer, G.; Zander, M.; Fres. Z. Anal. Chem., 288, 277 (1977).

AROCLOR 1016 IN HEXANE

FIGURE 1

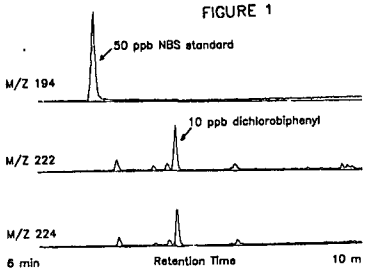

HPLC PROFILES OF a) TRANSFORMER OIL b) AROCLOR 1248

FIGURE 2

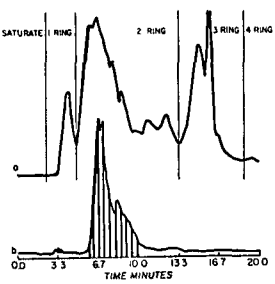

AROCLOR 1016 AT 2PPM IN TRANSFORMER OIL

FIGURE 3

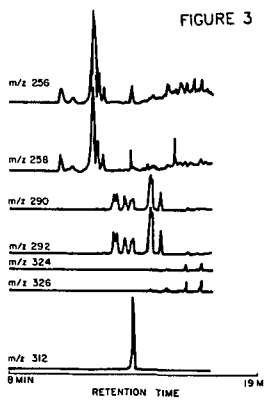

AROCLOR 1242 AT 2PPM IN NBS TRANSFORMER OIL

FIGURE 4

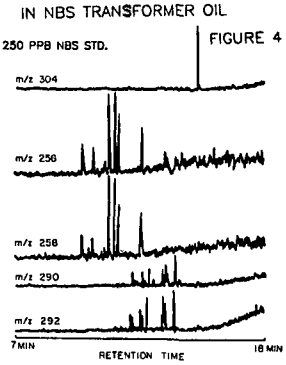

TYPICAL COMPOSITION OF A TRANSFORMER OIL

TABLE I

PARAFFINS	15.6
MONOCYCLOPARAFFINS	20.0
DICYLCOPARAFFINS	12.3
TRICYCLOPARAFFINS	10.3
TETRACYCLOPARAFFINS	8.4
PENTACYCLOPARAFFINS	2.0
ALKYLBENZENES	8.2
ALKYLTETRALINS	9 1
ALKYLNAPHTHALENES	6.3
ALKYLBIPHENYLS	3.7
ALKYLPHENANTHRENES	1.5
ALKYLPYRENES	0.8
ALKYLCHRYSENES	0.8
ALKYLPERYLENES	0.8
	100 0%

TABLE II HPLC RETENTION TIMES

DOUBLE BONDS		RET. TIMES
0	HEXADECANE	3.12 MIN.
3	TOLUENE	4.14
5	NAPHTHALENE	5.51
6	AROCLOR 1248	5.70 to 9.60
7	PHENANTHRENE	13.02
9	FLUORANTHENE	19.90

EFFECT OF CHLORDECONE (KEPONE) ON THE RAT BRAIN CONCENTRATION OF 3-METHOXY-4-HYDROXYPHENYLGLYCOL DETERMINED BY GC/MS/SIM

P. H. Chen, H. A. Tilson, G. D. Marbury, and J. S. Hong

Laboratory of Behavioral and Neurological Toxicology and
Laboratory of Molecular Biophysics
National Institute of Environmental Health Sciences
Research Triangle Park, NC 27709

3-Methoxy-4-hydroxyphenylglycol (MHPG) is the major metabolite of norepinephrine (NE) in the rat brain. Changes in concentrations of MHPG in the brain may provide an index of NE turnover. Thus, an increase in MHPG concentration in the brain may occur as a result of an increase in the turnover of NE in the brain. The most prominent neurological sign observed in the intoxicated workers of the chlordecone (Kepone) production plant in Hopewell, Virginia, was tremor (1). The tremor has also been observed in mice and rats after chlordecone treatment. The purpose of this investigation is to study the possible involvement of the NE system in chlordecone-induced tremor by measuring changes in the concentrations of MHPG in several rat brain regions after chlordecone treatment.

Total MHPG (free and sulfate conjugate) in the brain was determined by GC/MS/SIM with some modification of the method described by Karoum et al. (2). MHPG with the three hydrogen atoms in the side chain replaced by deuterium was added to the supernatant of the brain homogenate as an internal standard. After enzymatic hydrolysis of sulfate, the free MHPG was extracted with ethyl acetate. The extract was concentrated to dryness, converted to its pentafluoropropionic derivative and analyzed by GC/MS/SIM. GC separation was achieved on a 15m x 0.25 mm i.d. J and W Scientific DB-5 fused silica capillary column using on-column injection. The ions at m/z 622 and 625 corresponding to the molecular ions of the pentafluoropropionic derivatives of MHPG and the deuterated MHPG, respectively, were used for monitoring MHPG and the deuterated MHPG. This method allows for the quantitative determination of MHPG in 30-150 mg of brain tissue in the concentration of parts per billion. For NE determination, the supernatant of the brain homogenate was concentrated to dryness, converted to pentafluoropropionic derivative and analyzed by GC/MS/SIM. NE with the three hydrogen atoms in the side chain replaced by deuterium was used as an internal standard. The ions at m/z 590 and 592 were used for monitoring the pentafluoropropionic derivatives of NE and the deuterated NE, respectively.

A single injection of tremorigenic doses of chlordecone to rats resulted in significant increases in MHPG levels in hypothalamus, brain stem, cerebellum, and caudate nucleus (Table 1). The increase in MHPG was accompanied by a decrease in NE in hypothalamus (Table 1), suggesting that chlordecone treatment caused an increase in the turnover of NE in the brain. The data of this study also showed that there was a dose- and time-related correlation between the increases in the levels of MHPG in several brain regions and tremor intensity in rats. The increase in MHPG concentration occurred as early as 1 hr. post-dosing; this preceded the earliest measurable sign of chlordecone-induced tremor. This suggests that alteration in the brain NE system may be involved in the expression of the tremor induced by chlordecone.

REFERENCES

1. Taylor, J. R., Selhorst, J. B., Houff, S. A., and Martinez, A. J. Neurology 28, 626-630 (1978).

2. Karoum, F., Gillin, J. C., and Wyatt, R. J. J. Neurochem. 25, 653-658 (1975).

Table 1

Effects of Chlordecone on the Levels of MHPG and NE in Various Rat Brain Regions

Brain Region	Treatment	MHPG	NE
		mean ± S.E. (nmole/g)	
Hypothalamus	Corn Oil	0.77 ± 0.06	10.0 ± 0.28
	Chlordecone	1.32 ± 0.04*	7.89 ± 0.24*
Brain Stem	Corn Oil	0.97 ± 0.03	3.64 ± 0.15
	Chlordecone	1.56 ± 0.09*	3.31 ± 0.12
Cerebellum	Corn Oil	0.05 ± 0.02	
	Chlordecone	0.77 ± 0.05*	
Caudate Nucleus	Corn Oil	0.42 ± 0.02	
	Chlordecone	0.60 ± 0.04*	

Rats were injected with chlordecone (75 mg/kg, i.p.) or corn oil and were decapitated 24 hrs later. n=5; *$p < 0.001$ (Fisher's LSD t-test) compared to control rats.

MS/MS STUDY OF OXYCHLORDANE AND HEPTACHLOR EPOXIDE

J.M. Ballard,[1] J.R.Donnelly,[1] and G.W. Sovocool[2]

[1]Lockheed Engineering and Management Services Co. Inc.
P.O. Box 15027, Las Vegas, NV 89114
[2]U.S. Environmental Protection Agency, EMSL-LV
P.O. Box 15027, Las Vegas, NV 89114

The mass spectral fragmentation patterns of oxychlordane (I) and heptachlor epoxide (II) are well known.[1-5] Each compound produces a fragment ion (m/z 185 and 151, respectively) under EI conditions which appears to be due to a chlorine migration. To verify the occurrence of the apparent chlorine migration, we used MS/MS to study the fragmentation processes and attempted to identify the parent and daughter ions of the fragment.

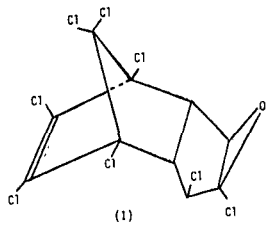

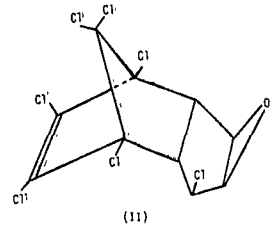

Experimental: Oxychlordane and heptachlor epoxide were obtained from the U.S. EPA Pesticides Repository, Research Triangle Park, North Carolina and spectra were recorded on a Finnigan Triple Stage Quadrupole (TSQ™) mass spectrometer. Samples were introduced via the direct insertion probe and were ionized by 70eV electrons at a source temperature of 150°C. Collision activated dissociation experiments were conducted with a collision energy of 15eV and an argon pressure of 1.3 mtorr.

Results: Collision activated dissociation (CAD) of the fragment ion m/z 185 generated daughter ions at 157 (loss of CO), 149 (loss of HCl), 121 (loss of CO, HCl), 117 (loss of CO, C_3H_4) and 85 (loss of CO, 2HCl), Figure 1. The CAD spectra of the ions at m/z 187, 189 and 191 of oxychlordane were compared with those predicted from the CAD spectrum of m/z 185 for an ion containing three chlorine atoms. Observation of the expected mass shifts together with doublet signals in the correct ratios for losses of ^{35}Cl and ^{37}Cl moieties confirmed the composition of m/z 185 as $C_5H_4\ ^{35}Cl_3O$. We conclude that the m/z 185 fragment ion is formed by a retro-Diels-Alder type rearrangement together with a chlorine migration. Inspection of the relative peak intensities in the range 175-200 amu of the EI mass spectrum of oxychlordane indicated the presence of four overlapping sets of multiplets, of which two provided very minor isotopic contributions to m/z 185. The CAD spectrum of m/z 191 (Figure 2) contained peaks at 156, 141, 131, 121, 107 and 83 in addition to those expected from $C_5H_4\ ^{37}Cl_3O$. Analysis of the CAD spectra of m/z 193 and 195 indicated the presence of $^{35}Cl_2\ ^{37}Cl_1$ and $^{35}Cl_1\ ^{37}Cl_2$, respectively; as shown by the intensity ratio of 2:1 and 1:2 for daughter ions corresponding to losses of ^{35}Cl and ^{37}Cl from the two parent ions. The additional ionic contribution at m/z 191 is therefore due to a second trichloro ($^{35}Cl_3$) containing fragment; absence of daughter ions corresponding to losses of neutral oxygen - containing species (e.g. CO, H_2O, OH), not attributable to $C_5H_4\ ^{37}Cl_3O$, indicated that the parent did not contain oxygen. The composition of the second fragment ion at m/z 191 is therefore $C_7H_2\ ^{35}Cl_3$. Generation of m/z 117 (CCl_3; structural assignment confirmed by singlet peaks at 119, 121 and 123 in the CAD spectra of m/z 187, 189, 191, respectively) by CAD of m/z 185 suggests the presence of a geminal dichloro moiety in the m/z 185 fragment ion. The CAD (parent ion) spectrum of m/z 185 (Figure 3) indicated the presence of several fragmentation pathways, including formation from the [M-Cl]+ ion, m/z 385. This implies that [M-Cl]+ is not formed by loss of chlorine from the cyclopentane ring bearing the epoxide group. CAD parent and daughter experiments performed on the fragment ion m/z 151 of heptachlor epoxide provided results analogous to those obtained with oxychlordane. Daughters of m/z 151 included 123 (loss of CO), 115 (loss of HCl), 87 (loss of CO, HCl), 83 (loss of C_4H_4O) and 51 (loss of CO, 2HCl). The mass shifts and singlet/doublet patterns observed for the corresponding ions in the CAD spectra of m/z 153 and 155 were consistent

with the composition $C_5H_5{}^{35}Cl_2O$ for m/z 151. The parent ion spectrum of m/z 151 was similar to that of m/z 185 of oxychlordane, since several fragmentation pathways are available and the [M-Cl]+ ion was again observed as a parent.

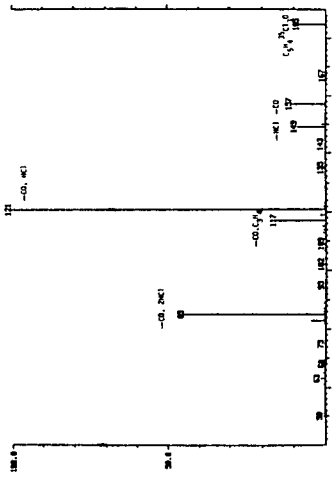

Fig.1. CAD SPECTRUM OF M/Z 185

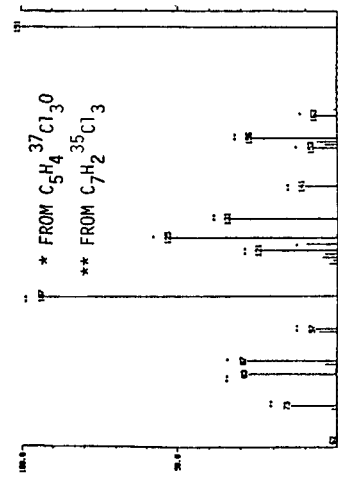

Fig.2. CAD SPECTRUM OF M/Z 191

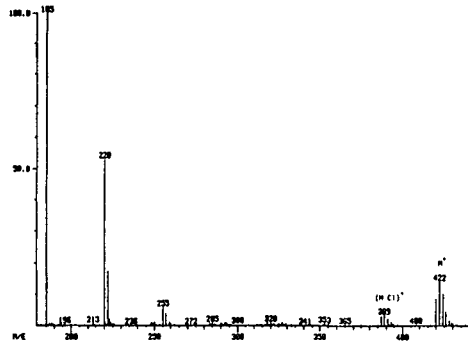

Fig.3. PARENT ION SPECTRUM OF M/Z 185

References

1. S. Safe and O. Hutzinger, Mass Spectrometry of Pesticides and Pollutants, CRC Press, 1973.
2. J. Damico, "Pesticides:" in Biochemical Applications of Mass Spectrometry, G. Waller, Ed. Interscience, 1972.
3. J. Lawrence, R. Barron, J. Chen, P. Lombardo, and W. Benson, J. Assoc. Offic. Anal. Chem. 53, 261 (1970).
4. B. Schwemmer, W. Cochrane, and P. Polen, Science 169, 1087 (1970).
5. F. Biros and H. Enos, Bull. Environ. Contam. Toxicol. 10, 257 (1973).

CHARACTERIZATION OF CARBAMYL MERCAPTURIC ACIDS BY EI AND CI MASS SPECTROMETRY.

James P. Lehman, Environmental Health Center, Stauffer Chemical Company, 400 Farmington Avenue, Farmington, CT 06032.

Thiocarbamates are extensively used as selective herbicides in the production of numerous agricultural commodities. Recently, it has been recognized that the mercapturic acid pathway represents an important route of excretion for these compounds in mammals. Since these carbamyl mercapturic acids are isolated from complex biological matrices, frequently in less than desirable purity, it is important to know the characteristic fragmentation patterns for this class of compounds in order to facilitate their recognition and identification.

We report here the electron ionization (EI), isobutane chemical ionization (C_4H_{10} CI), and ammonia chemical ionization (NH_3 CI) mass spectra of five carbamyl mercapturic acids. The routes of fragmentation and the relative abundances of the molecule and fragment ions are representative of the mass spectra of various mercapturic acids which have been recorded in this laboratory. Figure 1 delineates the source of essentially all the sample-related ions found in the mass spectra of mercapturic acids recorded in this laboratory. These observed molecule and fragment ions contain one of two types of information; either they are "fingerprint" ions characteristic of mercapturic acids as a class of compounds, or they contain some structural information about the variable portion of the molecule, the substituents on the carbamate nitrogen. The ions E and F are fingerprint or class characteristic ions and are indicative that the compound under investigation is a mercapturic acid. The remaining ions, A, B, C, D, G, and M, when present, all contain some information about the nitrogen substituents.

The relative abundances of these ions for the five model mercapturic acids are given in Table 1. Where two relative abundances are given for one class of ion in the ammonia CI spectra, the first relative abundance represents the protonated specie and the second the relative abundance of its corresponding ammonia-adduct ion. Looking first at the fingerprint ions E and F, it is apparent that except for the highly aromatic N,N-diphenylcarbamyl mercapturic acid, these ions are of relatively low abundance in the EI spectra. In contrast, the isobutane and ammonia CI spectra contain at least one of these important fingerprint ions in relatively greater abundance. The ammonia CI spectra are especially noteworthy in that the F ion and its corresponding ammonia-adduct ion are both observed in approximately equal intensity, adding confidence to the interpretation that this ion represents a fingerprint ion in the mass spectrum of an unknown.

Turning to M, the molecule ion or protonated molecule ion, isobutane CI has been found to consistently produce the protonated molecule ion as the base peak of the spectrum. Neither EI nor ammonia CI consistently produce a relatively abundant M. The importance of reliably observing an ionic specie representing the intact molecule cannot be overstated when it comes to determining an unknown structure from mass spectra. Looking at ions A and B, these containing together the most information about the variable portion of a carbamyl mercapturic acid, only EI would appear to yield information about the individual substituents on the carbamate nitrogen as ion A. The presence of $C_2H_5^+$ could not be reliably determined in the reported spectrum of the N,N-diethylcarbamyl mercapturate due to the presence of air and other low mass background ions. The other ions representing the thiocarbamate portion of the mercapturates, B, C, and D, have not been found to be consistently produced by any one ionization mechanism.

In conclusion, it would appear that no one of the ionization methods used in this study would be suitable for the characterization of unknown carbamyl mercapturic acids. Isobutane CI is useful for confirming the molecular weight of a carbamyl mercapturic acid, and both isobutane and ammonia CI appear to reliably produce the important fingerprint ions for this class of compounds, while only EI produces information on the individual substituents on the carbamate nitrogen.

Spectra were recorded with a Finnigan 4000 mass spectrometer. The ion source was at 200°C. Samples were introduced via the direct inlet using SP-2100 coated, silanized, pyrex sample cups and ballistic heating. Ionizing conditions were NH_4^+:$N_2H_7^+$, 5:1, $C_4H_9^+$:$C_3H_7^+$, 20:1, and 70 V electrons.

Figure 1.

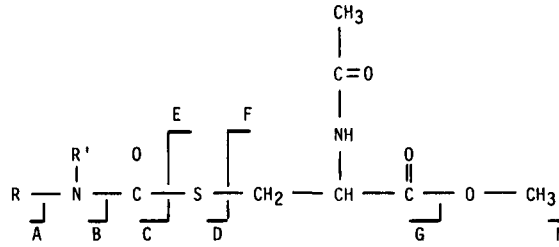

Table 1

	A	B	C	D	E	F	G	M	R	R'
	23	100	63		18	21	7	21	C_6H_5	C_6H_5
		39	100	2	2	7	1	1	C_2H_5	C_2H_5
EI	100	4	62	2	2	4		1	C_6H_{11}	C_2H_5
	--	21	100	4		7		1	$(CH_2)_6$	
	11	21	40		40	100			C_4H_9	H
		42	3		8	48		100	C_6H_5	C_6H_5
		4	4		28	41		100	C_2H_5	C_2H_5
C_4H_{10} CI		11	19	2	15	24		100	C_6H_{11}	C_2H_5
	--	17	8	5	1	1		100	$(CH_2)_6$	
			3		100	20		8	C_4H_9	H
		100, 0	7, 9			35, 40		13, 4	C_6H_5	C_6H_5
		100, 4	95, 95		2, 1	82, 82		47, 0	C_2H_5	C_2H_5
NH_3 CI		18,	33, 15		3, 3	29, 31		100, 2	C_6H_{11}	C_2H_5
	--	98, 3	3, 2	5, 5	4, 4	2, 5		100, 6	$(CH_2)_6$	
		5, 2	10, 2	1, 0	100, 92	60, 68			C_4H_9	H

POST-COLUMN ADDITION OF BUFFER FOR THERMOSPRAY LIQUID CHROMATOGRAPHY/MASS SPECTROMETRY IDENTIFICATION OF PESTICIDES.

Robert D. Voyksner, Joan T. Bursey, and Edo D. Pellizzari, Analytical and Chemical Sciences, Research Triangle Institute, P.O. Box 12194, Research Triangle Park, North Carolina 27709.

Carbamate pesticides have high usage in the United States by virtue of their high effectiveness and low mammalian toxicity (1,2). The ability to separate and identify these pesticides is important because of their increasing presence in the environment, along with their degradation and metabolic products. Analytical procedures for determination of these pesticides are rather limited since the pesticides are thermally labile and cannot be analyzed directly by gas chromatography. Spectrometric methods lack specificity or sensitivity (3-5). Although high performance liquid chromatography (HPLC) is ideally suited for carbamate separation, mass spectromety is most appropriate for their specific detection.

Most LC separations are developed before consideration of the use of mass spectrometry as a detector. This situation poses a problem for Thermospray (TSP)-LC/MS analysis since a separation scheme which has already been developed cannot be used unless ammonium acetate or an equivalent buffer is present for ion formation. If a buffer is added to accommodate the TSP interface, the chromatographic resolution may suffer. Other problems arise in performing gradient elution analysis when many buffers are not soluble in one of the solvents, resulting in a variation of the buffer concentration during the analysis. This variation in buffer concentration can produce changes in sensitivity due to dependence of the operation of the TSP on buffer concentration. These problems would be irrelevant if a method to add the buffer post-column could be developed. Previously established LC conditions then could easily be translated to TSP-LC/MS with no variance in the buffer concentration.

The TSP interface (Finnigan MAT Co., San Jose, CA) was installed on a Finnigan 4500 quadrupole mass spectrometer. This interface did not require any splitting of the LC effluent since the large volume of solvent was pumped out of the source with a liquid nitrogen cold trap prior to a mechanical rough pump. The mass spectrometer was operated with an ion entrance voltage of -15V, extractor voltage of -30V, lens voltage of 0V, and a quadrupole entrance of -48V in the positive ion mode. The instrument was scanned from m/z 150 to m/z 550 at a rate of 2 seconds per scan.

Two methods of post-column buffer addition were examined, involving the use of a right angle tee or a coaxial tee (Fig. 1) respectively. Both tees were located between the UV detector and LC column. A 0.5 M ammonium acetate solution was added through the tee at a rate of 0.4 mL/min resulting in a 0.1 M final concentration (ammonium acetate) when a column flow of 1.2 mL/min was used. Each tee was evaluated in the analysis of four pesticides using isocratic LC conditions. The total ion current traces from the HPLC/MS analysis of these pesticides showed little difference between the two tees (Fig. 2). The coaxial tee appeared to produce less noise, and was ultimately chosen over the right angle tee for post-column buffer addition. Figure 2 also shows the degradation of the established pesticide separation when ammonium acetate was added in a pre-column fashion, demonstrating the necessity of developing a method of post-column buffer addition. The addition of the buffer solution post-column increased MS intensity for the four pesticide compounds compared to pre-column addition of the buffer. Ion intensities were 3 to 5 times greater with the post-column addition technique, primarily due to the increased volume of water.

The post-column addition of buffer through the coaxial tee was optimized to produce the highest possible sensitivity and resolution (peak shape). However, if more water was added post-column to take advantage of this enhanced sensitivity, the sample concentration was decreased. Thus, an optimal column/buffer flow rate was expected to exist with respect to observed sensitivity. The results of an experiment to determine the optimum sensitivity indicated column flow rates of 1.0 to 1.1 mL/min with buffer flow rates of 0.5 to 0.6 mL/min produced the best results.

The thermospray total ion current (TIC) traces for the gradient analysis of a 15 pesticide mixture (100 ng each) with post-column buffer addition is shown in Figure 3. The separation scheme for the carbamates and ureas previously developed was a linear gradient of 50% methanol in water to 70% methanol in water in 15 minutes. No baseline drift or excessive noise was observed due to the gradient analysis or post-column addition methods. Identification of the components of the mixture would have been nearly impossible by UV detection alone because of the number of overlapping peaks. However, overlapping peaks posed no problem for HPLC/MS analysis since the characteristic spectra for the selected pesticides were simple (usually consisting only of $[M+H]^+$ and $[M+NH_4]^+$ ions). This simplicity enabled the determination of the molecular weight and allowed possible identification of these unresolved peaks as well as resolution of the isobaric compounds

based on the ratio of intensities of $[M+H]^+$ to $[M+NH_4]^+$. Detection limits for most of these pesticides were in the 5 to 20 ng range (injected). Estimated detection limits for these compounds are presented in Table 1. The detection limits were found to be dependent upon the chromatographic peak width. Thus, late eluting peaks such as phenmedipham and benzoprop ethyl were wider and showed a lower signal-to-noise ratio. Detection limits were also found to be dependent on the solvent composition where highly retained components eluted in a solvent system containing a lower percentage of water, resulting in a reduction of themospray ionization efficiency. Compared to direct liquid introduction HPLC/MS, moving belt HPLC/MS, or UV/HPLC, thermospray offers greater sensitivity and better specificity for the analysis of these pesticides.

CREDIT

This work was supported by EPA, Office of Research and Development, Environmental Monitoring and Support Laboratory, Cincinnati, Ohio, under Contract No. 68-03-3122.

REFERENCES

1. Kuhr, R. J.; Dorogh, H. W., Carbamate Insecticides: Chemistry, Biochemistry and Toxicology. CRC Press, Cleveland, Ohio, 1976.
2. Dorough, H. W.; Thorstenson, J. H. J. Chromatogr. Sci. 1976, 13, 212-224.
3. Riva, M.; Curisano, A. J. Chromatogr. 1969, 42, 464-469.
4. McDermott, W. H.; DuVall, A. H. JAOAC, 1966, 49, 412-452.
5. Strother, A. J. Gas Chromatog. 1968, 6, 110-113.

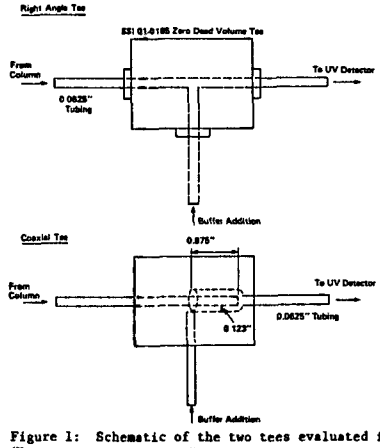

Figure 1: Schematic of the two tees evaluated for post-column addition.

Table 1

Full Scan Detection Limits Using the Base Peak for the Pesticides Analyzed

Compound	Ret. Time (sec)	Detection Limit (ng)
Asulam	126	20-25
Aldicarb	295	3-5
Propoxur	303	4-8
Carbofuran	320	1-4
Propachlor	425	10-15
Fluometuron	445	15-20
BPMC	457	3-5
Carbaryl	468	3-5
Diuron	544	50-80
Alachlor	600	10-20
Linuron	655	4-8
Desmedipham	700	70-100
Phenmedipham	710	5-8
Benzoylprop ethyl	824	60-90

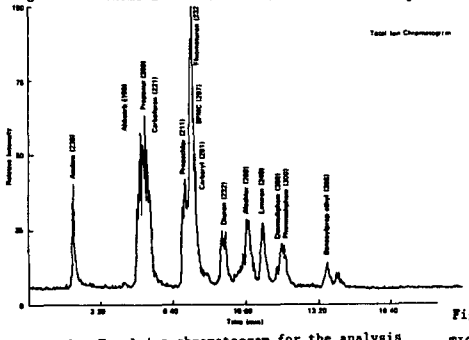

Figure 3: Total ion chromatogram for the analysis of 15 pesticides, 600 ng injected.

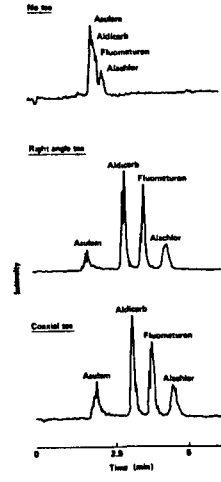

Figure 2: TIC traces for no tee and two different tees at constant conditions of 1.6 mL/min into the mass spectrometer, gain, sample, and column. For the no-tee situation, 0.1 M ammonium acetate was added through column. In the right angle and coaxial tee, buffer added post-column so final concentration is 0.1 M.

QUANTITATION OF 6-KETO-PROSTAGLANDIN-$F_{1\alpha}$ ($6KPGF_{1\alpha}$) AS THE METHOXIME-METHYL ESTER-t-BUTYL-DIMETHYLSILYL (MOMETBDMS) DERIVATIVE USING A RELATIVELY INEXPENSIVE GC-MS-DS. J.J. Vrbanac and D.R. Knapp, Dept. of Pharmacology, Medical University of South Carolina, Charleston, South Carolina 29425.

Introduction: The concentrations of 6-keto-prostaglandin $F_{1\alpha}$ ($6KPGF_{1\alpha}$) in biological fluids and tissues are of research interest since $6KPGF_{1\alpha}$ concentrations are generally believed to be an index of prostacyclin (PGI_2) production. PGI_2, an extremely potent vasodilator, anti-aggretory PG is unstable and is believed to be non-enzymatically hydrolyzed to $6KPGF_{1\alpha}$. Measurement of $6KPGF_{1\alpha}$ in certain biological fluids and tissues represents a challenging analytical problem (Prostaglandins 23, 579, 1983; J. Chromatogr. 239, 71, 1982). The objectives of this study were to examine the utility of the methoxime-methyl ester-t-butyldimethylsilyl (MOMETBDMS) derivative in the determination of $6KPGF_{1\alpha}$ concentrations in plasma and urine and to simplify the extraction and purification procedure over published methods. Another objective was to evaluate the Hewlett-Packard "Mass Selective Detector", which had been placed on loan to the NIH supported Gas Chromatography/ Mass Spectrometry Clinical Research Resource at the Medical University of South Carolina, in performing analyses that are reasonably difficult and of the type encountered in clinical research. We were also concerned with evaluating the relative ease with which the system could be operated and maintained by a clinical investigator who has little or no background in the use of GC/MS.

Methods: $6KPGF_{1\alpha}$ was initially extracted using the method of Powell (Prostaglandins 20, 947, 1980). This procedure was modified during this study and these modifications are explained in the results. The MOMETBDMS derivative of $6KPGF_{1\alpha}$ was prepared as previously described (J. Chromatogr. 236, 201, 1982). The Hewlett-Packard "Mass Selective Detector" (HP 5970A) consists of a GC equipped with a fused silica capillary column which is interfaced with the mass spectrometer by direct insertion of the end of the capillary column into the ion source of the mass spectrometer. The mass spectrometer data system consists of a table-top processor with a cassette tape drive, a thermal printer, and an (optional) 4.8 megabyte fixed disk. The vacuum system consists of a single 40 l/sec turbomolecular pump and mechanical forepump and is designed to handle approximately 1.0 ml He (STP) carrier gas per minute. GC parameters of operation are controlled separately from the mass spectrometer, which is under control of the data system processor. The instrument has electron impact (EI, 70 eV) ionization capabilities only. Data output (parameters of operation, mass spectra, selected ion monitoring plots, peak integration reports, etc.) are via the thermal printer. A 30 m DB-5 bonded phase fused silica capillary column (J & W Scientific, 0.25 mm ID, 0.25 µm film thickness) was used with the following conditions of analysis: injection port temperature, 290°C; splitless injection; injection port purge after 3 minutes; column temperature during injection, 200°C; initial rapid ramp to 270°C then programming at 3°C/min to 310°C; electron impact at 70 eV; monitoring m/z = 698 (protium) and m/z = 702 (deuterium). Two GC peaks (syn- and anti-) for the MOMETBDMS derivative of $6KPGF_{1\alpha}$ eluted between 14.6 and 14.9 minutes using the above conditions (T_o at 270°C).

Results: Figure 1 shows a standard curve obtained with the HP "Mass Selective Detector" by adding various quantities of $6KPGF_{1\alpha}$ and a fixed amount of tetradeutero-$6PGF_{1\alpha}$ to human plasma. The protium/deuterion ratio is plotted vs. ng $6KPGF_{1\alpha}$ per ml plasma. The plasma was extracted as previously described. The insert in Figure 1 shows the mass chromatogram for m/z 698.7 and represents 40 pg injected (dilution of MOMETBDMS-$6KPGF_{1\alpha}$ reference; not extracted). Syn- and anti-stereoisomers were completely separated using the 30 m capillary column. The instrument demonstrated no problem with high mass transmission in that the lower limit of detection of $6KPGF_{1\alpha}$ when monitoring m/z 698 alone was 10 pg (5:1 signal to noise, maximum electron multiplier voltage, "wide-peaks" option, 600 msec dwell time). The HP "Mass Selective Detector" also demonstrated a stable mass axis calibration. Shifts in mass axis calibration from one day to the next were never observed to be greater than 0.5 amu at m/z 698. There was no indication that the instrument need be calibrated more than once each day. In subsequent experiments it was noted that chromatographic interferences occurred when the amount of $6KPGF_{1\alpha}$ added to plasma was decreased to the low ng/ml range. At this point it was decided to determine if a more speciifc elution of $6KPGF_{1\alpha}$ from ODS and silica Sep-Pak® cartridges was of analytical value. It was determined that approximately 80% of the adsorbed $6KPGF_{1\alpha}$ was eluted with 20% ethanol and water (v/v) from the ODS cartridge and that approximately 80% of adsorbed $6KPGF_{1\alpha}$ was eluted with 20% methanol in ethyl acetate (v/v) from the silica cartridge. The $6KPGF_{1\alpha}$ eluted from the ODS cartridge was transferred to the silica cartridge by adding 10 ml H_2O to the 20% ethanol eluate, acidifying with formate, re-extracting with an ODS cartridge, washing with hexane and

eluting with ethyl acetate. This modified procedure thus uses the method of Powell except the $6KPGF_{1\alpha}$ is eluted with 20% aqueous ethanol instead of methyl formate and further purification on silica follows. Using the above procedure no interfering substances were noted down to 100 pg/ml (1-2 ng/ml of the tetradeutero-$6KPGF_{1\alpha}$ also added). Although this concentration is well above baseline plasma concentrations of $6KPGF_{1\alpha}$, which are less than 3 pg/ml (Prostaglandins 23, 579, 1983), this concentration is below reported increases in plasma $6KPGF_{1\alpha}$ in certain pathological conditions (i.e., septic shock). Figure 2 shows mass chromatograms for 698 and 702 in the region where $6KPGF_{1\alpha}$ elutes from the GC. The exact region is shown by the horizontal bar. Part A shows the background noise as determined by a blank injection (2 µl hexane). Part B shows the chromatographic profile obtained for control plasma (normal subject; indomethacin added) purified using the above procedure and represents 0.67 ml injected (2 ml plasma starting material). No interfering peaks are seen in the region where $6KPGF_{1\alpha}$ elutes. Figure 3 shows $6KPGF_{1\alpha}$ spiked plasma (100 PG $6KPGF_{1\alpha}$/ml plasma). Experimental conditions in Figures 2 and 3 are identical.

Summary: Analysis of the MOMETBDMS Derivative of $6KPGF_{1\alpha}$ by HRGC/SIM/MS. The procedure outlined above allows for an interference free chromatogram at the 100 pg/ml concentration when extracting $6KPGF_{1\alpha}$ from plasma and monitoring M^{+}-57 of the MOMETBDMS derivative by HRGC/ SIM/MS. This extraction-purification procedure may not be adequate when other derivatives are employed (i.e., the MOMETMS derivative for example). We have found the method to be inadequate for urine samples; further purification was necessary using Sephadex LH-20 column chromatography to give an interference free mass chromatogram.

HP Mass Selective Detector Evaluation. The overall impression of the HP "Mass Selective Detector" was very positive. High mass sensitivity was good, and there were no major problems in the operation or maintenance of the instrument. Although the instrument was used extensively during the evaluation period and the GC column was continuously connected to the source, there was no need to clean the ion source since instrumental sensitivity did not diminish appreciably during this time. The instrument did have certain undesirable features, although a new data system for the HP 5970B, introduced in March, may have alleviated these deficiencies. Without the disk drive (which adds considerable cost to the price of the unit) the HP mass selective detector was rather slow in data acquisition set-up time and data output time, as well as having very limited data storage capacity. This problem, however, is more an inconvenience than a major deficiency. A more serious fault is the limited buffer storage capacity which became apparent when the instrument was operated in the repetitive scanning mode. The normally routine task of balancing the amount of sample injected, the electron multiplier voltage and the threshold ion intensity for data storage was, at times, difficult when scanning the entire mass range (800 amu). We believe that the instrument should be equipped with a high vacuum gauge (an optional accessory) since small leaks in the vacuum system are not detected by the turbomolecular pump R.P.M. gauge (standard equipment). The relative ease with which the system can be operated by an individual with little or no background in GC/MS is difficult to assess from our limited experience with this type of user, however, our general impression was positive. The HP "Mass Selective Detector" give every appearance of being a relatively inexpensive GC/MS/DS that is able to perform analyses that are reasonably difficult and of the type encountered in clinical research.

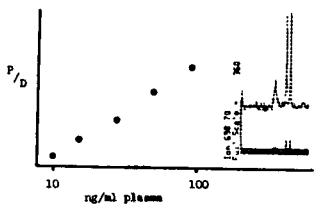

FIGURE 1

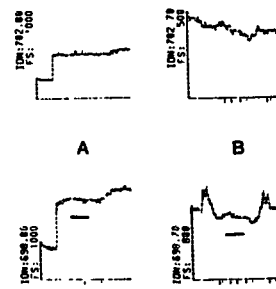

FIGURE 2

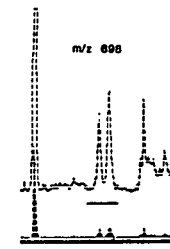

FIGURE 3

BIOCHEMICAL ANALYSES USING AN INSTRUMENT OF EBQ DESIGN.

SIMON J. GASKELL, Tenovus Institute for Cancer Research, Welsh National School of Medicine, Cardiff CF4 4XX.
CHRISTOPHER J. PORTER, PAUL W. BROOKS, VG Analytical Ltd., Floats Road, Wythenshawe, Manchester M23 9LE

Multiple analyser mass spectrometers provide important advantages in two general areas of mixture analysis:
1) During GC-MS, selected fragmentation monitoring may be performed with good resolution of both parent and daughter ion beams. In contrast, the selectivity of metastable peak monitoring using a conventional double-focusing sector instrument is limited by the poor effective resolution of the parent ion beam.
2) Superior resolution of parent and daughter ion beams also improves analyses of mixtures not amenable to combined chromatography-mass spectrometry. Mixture analysis by MIKES, using a reverse-geometry double-focusing instrument, suffers from poor resolution of the daughter ion beam.

Of the various possible configurations for tandem mass spectrometry, particular interest attaches to the double-focusing/quadrupole (EBQ) combination for biochemical work. In addition to the advantages noted above, the capability for high resolution of the parent ion beam provides the possibility for conventional high resolution selected ion monitoring and the double-focusing configuration may also be used for metastable peak monitoring. This paper describes the application of an instrument of EBQ design, the VG 7070EQ, to one problem in biochemical trace analysis.

The bis-tert-butyldimethylsilyl (TBDMS) ether of the steroid hormone, oestradiol, afforded abundant molecular ions (m/z 500) under electron impact. Collision induced dissociation in the quadrupole collision cell (collision energy 35 eV) of the 7070EQ produced a spectrum of daughter ions which was scanned using the quadrupole mass filter. M/z 443 ($[M-C_4H_9]^+$) was present with an abundance of 65%, relative to that of the transmitted molecular ion. By setting the quadrupole to transmit m/z 443, the fragmentation m/z 500 → 443 was monitored during GC-MS of the authentic steroid. 25pg of oestradiol was readily detected with parent ion resolutions of 1000-5000. The selectivity of detection was assessed during the analysis of an extract of blood plasma from a female subject. Conventional selected ion monitoring at low resolution (1000) gave the trace shown in Fig. 1 (top); a peak attributable to oestradiol TBDMS was of low relative abundance in the chromatogram. When the fragmentation, m/z 500 → 443, occurring in the quadrupole collision cell, was monitored, a considerable simplification of the trace was observed (Fig. 1). Two peaks were detected, the first corresponding to oestradiol. Increasing the resolution of the parent ion beam to 5000 eliminated the second peak, indicating that the elemental composition of the parent ion corresponding to this component was different to that of the molecular ion of oestradiol TBDMS.

The results indicate the improved capability for selective analysis provided by multiple analyser mass spectrometry and emphasise the value of enhanced resolution of the parent ion beam.

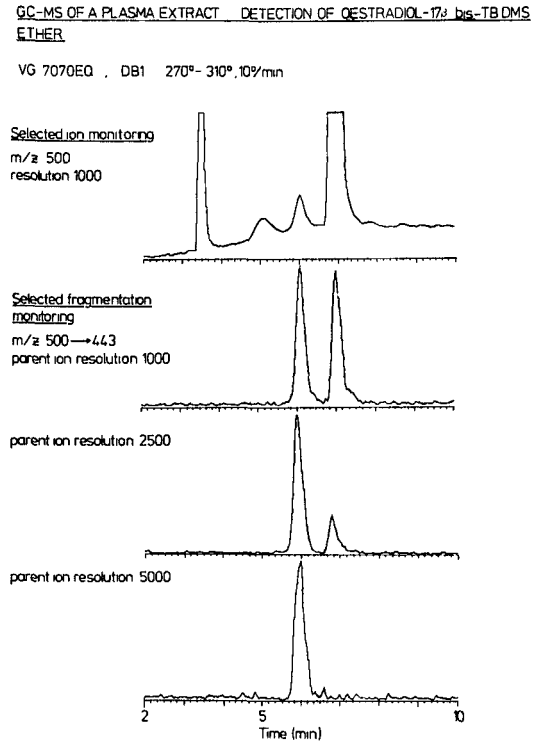

Fig. 1. GC-MS analyses of an extract of blood plasma (4ml), as the TBDMS derivative. 15% Aliquots were injected for each analysis. The plasma concentration of oestradiol was ca. 250pg/ml.

Application of SIM to Determination of Platelet-activating Factor

K. SATOUCHI, M. ODA and K. SAITO

Department of Medical Chemistry
Kansai Medical School, Moriguchi Osaka, 570 JAPAN

The platelet-activating factor (PAF), released in vitro from antigen-stimulated, IgE sensitized rabbit leukocyte containing basophils, was a conglomerate of phosphoglyceride having the chemical structure of 1-hexadecyl/octadecyl-2-acetyl-sn-glyceryl-3-phosphorylcholine (AGEPC) (1). Evidence is now accumulating which indicates that AGEPC is a compound of great biological importance. The synthetic AGEPC has been shown to induce platelet aggregation, chemotaxis and degranulation in neutrophil, an increase of vascular permeability, contraction of smooth muscle and an antihypertensive effect (2). Further, in addition to rabbit basophil, various blood cells including human and rabbit neutrophils, released PAF, which was entirely indistinguishable from the synthetic AGEPC, when appropriately stimulated (3). The amount of PAF was determined biologically by the capacity to activate the washed rabbit platelets, however, the application is limited since biological activity of AGEPC is dependent upon chain length of the alkyl ether substituent (4).

In view of the above circumstance, we used the SIM technique to the simultaneous qualitative and quantitative determination of AGEPC and applied it to PAF generated by human neutrophil on the challenge with ionophore A23187.

The C 16=0 d=3 AGEPC, having deuterium on the acetyl moiety, was used as an internal standard. The tBDMS derivative was used and a selected ion was [M-57], which was informative for determination of the molecular weight (Fig. 1).

Calibration curves were prepared using the various mixtures of C 16=0 AGEPC, C 18=0 AGEPC and internal standard ranging in weight ratios of AGEPCs to internal standard from 3 to 0.25. The lower limit for quantification by this method was a few hundred picograms of AGEPCs (Fig. 2).

As reported in communucation (5), human neutrophils, adjusted to a cell concentration of 6,000 cells/μl Tyrode's solution were challenged with ionophore A23187 at a final concentration at 2.5 μM for 15 min. Then, total lipid including exogenously added internal standard was extracted by the modified procedure of Bligh and Dyer (6). Clean-up procedure contained two column chromatographies (silicic acid and alumina) and two preparative thin layer chromatographies using solvent systems of chroloform:methanol: water, (65:25:4, v/v)and methanol:water, (2:1, v/v). The purified fraction corresponded to AGEPC was dephosphorylated with phospholipase C and the resulting diglyceride was converted to tBDMS derivative. The derivative was further purified by preparative thin layer chromatogrphy with a solvent system of hexane:diethylether, (9:1, v/v).

Representative SIM traces for PAF from human neutrophil after stimulation with ionophore A23187 are shown in Fig. 3. Two types of PAF, 1-hexadecyl (m/z 415) and 1-octadecyl (m/z 443)-2-acetyl-sn-glyceryl-3-phosphorylcholine were detected. Monitoring by [M-57] at m/z 441, corresponded to C 18=1 AGEPC, also formed peak just before the C 18=0 AGEPC, however, the amount was negligible comparing with two other AGEPCs.

Taking into account that PAF is a conglomerate of ether-linked choline phosphoglyceride, the SIM technique is indispensable to PAF determination.

REFERENCES

(1) Hanahan, D. J., Demopoulos, C. A., Liehr, J. & Pinckard, R. N. (1980) J. Biol. Chem. 255, 5514-5516
(2) Pinckard, R. N., McManus, L. M. & Hanahan, D. J. (1981) in Advances in Inflammation Research (Weissman, G., ed) Vol. 4, pp. 147-180, Raven press, New York.
(3) Betz, S. J. & Henson, P. M. (1980) J. Immunol. 125, 2756-2763
(4) Satouchi, K., Pinckard, R. N. & Hanahan, D. J. (1981) Arch. Biochem. Biophys. 211, 683-688
(5) Satouchi, K., Oda, M., Yasunaga, K. & Saito, K. (1983) J. Biochem. 94, 2067-2070
(6) Bligh, E. G. & Dyer, W. J. (1959) Can. J. Biobhem. Physiol. 37, 911-917

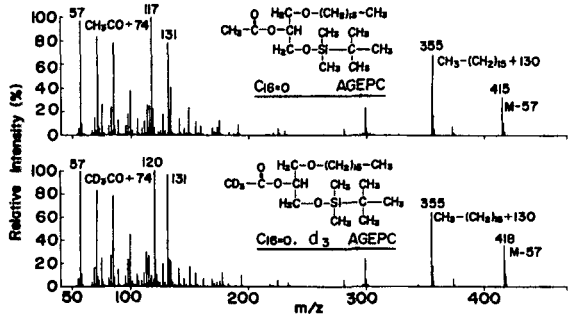

Fig. 1 EI Mass Spectra of the tBDMS Derivatives of C 16=0 AGEPC and C 16=0 d=3 AGEPC

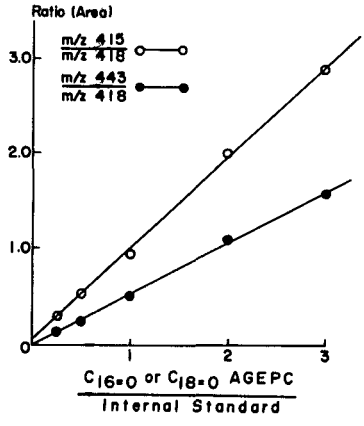

Fig. 2 The Calibration Curves of AGEPC

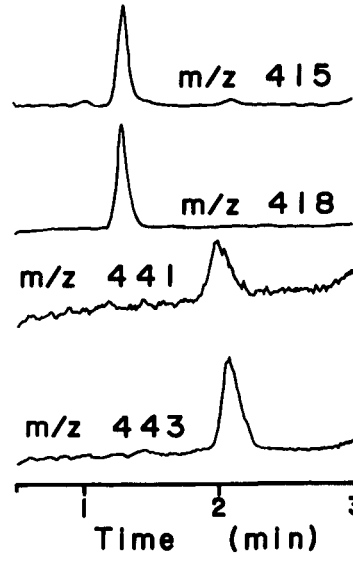

Fig. 3 SIM Traces of PAF from Human Neutrophils

5-HETE QUANTITATION IN THE ISOLATED PERFUSED RAT LUNG BY GC/NCI-MS. R. J. Strife* and R. C. Murphy, Dept. of Pharmacology, University of Colorado School of Medicine, Denver, Colorado 80262

Oxidation of arachidonic acid by various lipoxygenases results in the production of several isomeric hydroperoxyeicosatetraenoic acids (HPETE's). 5-HPETE is of particular interest, because it is the first intermediate for reaction pathways leading to production of 5-hydroxyeicosatetraenoic acid (5-HETE), LTB_4, LTC_4 and LTD_4. 5-HETE, and more significantly LTB_4, are implicated as mediators of the inflammatory response, possessing potent chemotactic and chemokinetic activities for polymorphonuclear leukocytes. LTC_4 and LTD_4 possess activities as slow reacting substances of anaphylaxis, are potent contractors of certain smooth muscle, and are implicated in bronchospasm.

Tissue peroxidases can convert 5-HPETE to 5-HETE. Therefore, we chose to measure 5-HETE as an indicator of the activation of 5-lipoxygenase in the isolated perfused rat lung, in response to injury of the lung tissue. A sensitive, isomer specific, GC/NCI-MS isotope dilution assay was developed for 5-HETE, as the pentafluorobenzyl (PFB) ester, TMS ether derivative (Fig. 1).

5-HETE was isolated from aqueous albumin or plasma perfusate in low ng quantities by extraction or protein precipitation followed by extraction. The intermediate PFB ester derivative was formed using mild conditions[1], and the samples were purified by analytical TLC on silica gel. Following isolation and formation of the TMS ether ($BSTFA/CH_3CN$), the samples were analyzed on a short 5m x .25mm DB-1 column, using a falling needle injector.

By positive ion EI analysis, 5-HETE PFB,TMS showed three <u>isomer specific</u> cleavages at m/z 305 (C_4,C_5), 369 (C_5,C_6) and 421 (C_9, C_{10}). 5-HETE in perfusates was initially confirmed by comparison of peak height ratios observed at t_r = 3 min during GC/MS (SIR), with those of 5ng samples of standard. Good agreement was obtained.

The high mass (> m/z 200) fragment ions observed by +EI were relatively weak, carrying only .5 - 1% of the TIC. Negative chemical ionization (methane) occurred with 20% greater efficiency, and produced the carboxylate anion $RCOO^{\ominus}$ (m/z 391) carrying 50% of the TIC. While all HETE-PFB,TMS isomers co-elute during GC analysis and also produce $RCOO^{\ominus}$ at m/z 391, this assay was selective for 5-HETE, because 5-HETE PFB ester was well separated from the other isomers (i.e. 12,15) during the TLC purification (Table 1). Over a 100-fold increase in absolute sensitivity is obtained (Fig. 2). In assays of biological samples, the more selective NCI process may enhance detection limits further.

The internal standard 1,1-$[^{18}O]_2$-5-HETE produces $RC^{18}O^{18}O^-$ at m/z 395, and contains less than 1% unlabelled material.[2] Calibration lines for a given experiment were constructed with 0-25ng 5-HETE and 5-10ng of the internal standard. A typical calibration line obtained by linear regression (isotope ratio m/z 391:395 vs ng 5-HETE) is represented by y = .110x + .029 and linear correlation coefficients r^2 gave values between .9991 - .9998. For individually prepared samples at the 5ng level (n=7), the coefficient of variation was 3.7%. Back exchange of the labelled internal standard was not observed in control experiments.

5-HETE levels were always elevated when the lungs were subject to injury or stress causing endothelial cell damage (Fig. 3). When the specific inhibitor Piriprost was present, injury was prevented, as determined by morphologic examination. 5-HETE levels returned to control baseline values in this case. Therefore 5-lipoxygenase products may be involved in mechanisms leading to tissue damage.

Acknowledgement: This work was supported in part by NIH grants HL25785 and HL01047. We thank Dr. Norbert Voelkel (Univ. of Colorado, Dept. of Medicine) for perfusate samples and morphologic exam results.

*current address: The Procter & Gamble Company, Miami Valley Laboratories, P.O. Box 39175, Cincinnati, Ohio 45247.

References

1. R. J. Strife and R. C. Murphy, J. Chromatog. <u>305</u>, 3(1984).
2. R. J. Strife and R. C. Murphy, Prosta. Leukotr. and Med. <u>13</u>, 1 (1984).

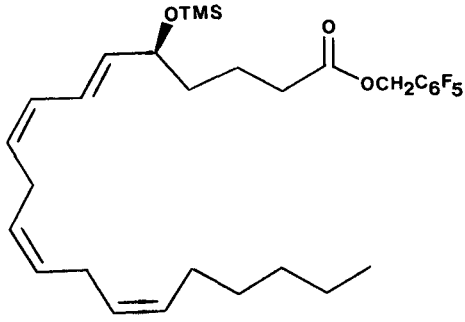

Fig 1. 5-HETE Pentafluorobenzyl Ester, Trimethylsilyl Ether

TABLE 1.

CHROMATOGRAPHIC PROPERTIES OF HETE ISOMERS

Isomer	Rf[1]	ECL[2]	m/z(NCI) $RCOO^{\ominus}$
5	.37	21.0	391
12	.48	21.0	391
15	.48	21.0	391

[1] Separation of HETE-PFB esters on silica gel. Solvent 3/1 Hexane-ethyl acetate.

[2] Migration of HETE-PFB ester, TMS ethers on 5 m DB-1 column. ECL = equivalent chain length to n-chain fatty acid PFB esters.

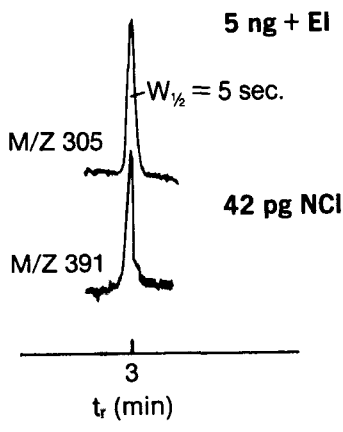

Fig 2. Comparison of GC/MS analyses (selected ion monitoring) of 5 HETE PFB,TMS

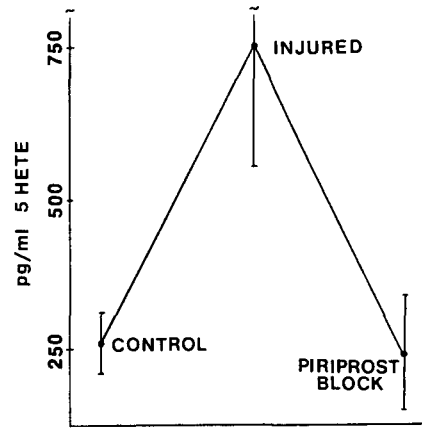

Fig 3. 5 HETE levels in albumin perfusates, $\bar{x} \pm$ std. dev. of the mean, 3 animals

Fast Atom Bombardment (FAB) Mass Spectrometry of
Leukotriene C_4 Decomposition Products

Jay Y. Westcott, K.L. Clay and R.C. Murphy
Department of Pharmacology, University of Colorado Health Sciences Center
Denver, Colorado

Leukotriene (LT) C_4, 5S hydroxy-6R-s-glutathionyl-7,9-trans-11,14 cis-eicosatetraenoic acid is a 5 lipoxygenase metabolite of arachidonic acid (1).[1] LTC_4 is produced in certain cells after appropriate stimulation which causes release of arachidonic acid from membrane phospholipids.[2] This leukotriene is formed in stimulated lung tissue where it is believed to mediate certain of the pathophysiological symptoms associated with immediate hypersensitivity reactions.[3] LTC_4 has been found to be metabolized to other leukotrienes such as LTE_4, LTD_4 and LTC_4 sulfoxide in several different systems.[4,5] The formation of other products from oxidation reactions has not been well studied either in vivo or in vitro, although LTC_4 has been found to be very unstable in acid solutions.[6] Part of the difficulty in analysis of LTC_4 metabolites is due to the presence of the sulfido-peptide group in the molecule which prevents easy volatilization and makes analysis by GC/MS not readily possible. The formation of LTC_4 decomposition products has been examined by using a combination of FAB and HPLC.

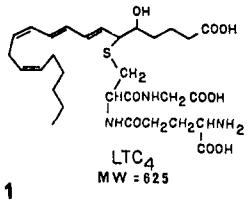

1

To a 3.5 μM solution of ^{3}H-LTC_4 (8 m Ci/mmol) in water or 50% methanol, HCl (0.25 mM, pH 4.0), EDTA (1 mM), or ferrous sulfate (100 μM, pH 5.8) was added and allowed to remain at room temperature (22-24°) for up to 12 hours. LTC_4 degradation was quantitated by monitoring the decrease in UV absorbance at 280 nm or by HPLC using prostaglandin B_2 as an internal standard.[7] Separation of LTC_4 degradation products was performed using a binary HPLC gradient system flowing through a 5 micron octadecylsilyl reserved phase column. Mobile system A (3:7, methanol:water, 0.02% H_3PO_4, adjusted to pH 5.7 with ammonium hydroxide) was pumped through the column for 6 minutes followed by a linear gradient to 100% methanol over 50 min. FAB spectra were obtained using a VG Micromass 7070H double focussing mass spectrometer modified with a saddle-field atom gun. Xenon was used as the particle source with the FAB gun operating with 1 mA emission of 6 KV. The samples to be analyzed were each concentrated to a volume of 10 times (1-5 μg) and added to the 2 micron stainless steel mesh target screen containing the glycerol matrix.

LTC_4 was found to be degraded by HCl on ferrous ion in aqueous solution. This distruction of LTC_4 in acidic medium followed apparent first order kinetics, but the rate of destruction widely differed with different lots of synthetic LTC_4. EDTA (1 mM) prevented the destruction of LTC_4 caused by either HCl of iron. Adding methanol (1 volume) to the solution greatly enhanced the degradation by iron, but protected LTC_4 from acid catalyzed degradation. This suggests some difference in the mechanism of decomposition induced by HCl and ferrous salts. It was also noted that freezing the LTC_4 solution containing ferrous ions (100 μm) caused 98% of the LTC_4 to be destroyed.

FAB was used to analyze the decomposition products of LTC_4 caused by acid or iron. Figure 1 shows the partial FAB spectra of LTC_4 after acid degradation. LTC_4 produces an abundant protonated molecular ion at m/z 626 and also an ion at m/z 308 which arises from the cleavage of the C-(6)-S bond between the eicosanoid chain and peptide moiety with charge retention on the peptide portion. A glycerol cluster ion (G7) is found at m/z 645. Acid degraded LTC_4 revealed decomposition products containing ions at m/z 642 (+O), 644 (+H_2O), 660 (+H_2O_2), 676 (+O + H_2O_2) and 692 (+O_2 + H_2O_2). FAB of LTC_4 degraded by iron showed the formation of products with very similar ions as acid degraded LTC_4.

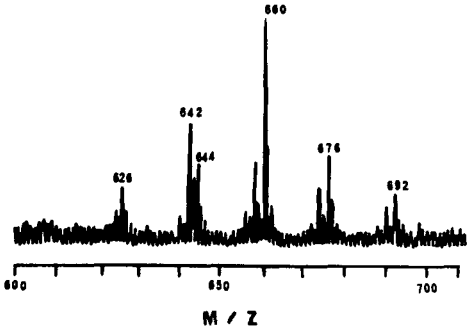

Figure 1. Partial FAB spectra of acid degraded LTC_4

A large sample of synthetic LTC_4 was found by UV to have undergone extensive decomposition after two months storage at -70°. HPLC was used to separate specific decomposition products. These products were further characterized by UV spectroscopy and FAB (Table I). This information allowed the identification of certain metabolites as LTC_4-sulfoxide, 15-hydroxy LTC_4, and 11-trans-LTC_4. There were also two metabolites having the addition of H_2O_2 which could be trihydroxy-LTC_4 compounds. These autodecomposition metabolites were similar to those observed to occur after acid or iron-induced LTC_4 degradation. Structure 2 presents one possible isomer consistent with the FAB-MS data as well as UV properties.

TABLE I Autodecomposition products of LTC_4.[1]

Time of Elution (min)	UV	MH^+	FAB Peptide Ion	Structural Assignment
21	230	660	308	Structure 2[4]
22	230	660	308	Structure 2[4]
26,27	307 (t)[2]	660,642	308	15-OH-LTC_4
36	284 (t)	642	324	LTC-S=O
38	280 (t)	626	308	Structure 1, LTC_4
39	270 (t)	n.d.[3]	n.d.	11-trans-LTC_4

1. Products separated by gradient HPLC and analyzed by UV spectroscopy and FAB-mass spectrometry.
2. Triplet chromophore, max reported.
3. Not determined.
4. Structure 2 or isomeric conjugated diene diol.

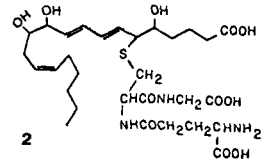

Acknowledgement

This work was supported by grant AA 03527 and fellowhip AA 05193 from the National Institutes of Health.

References

1. R.C. Murphy, S. Hammarstrom and B. Samuelsson, Proc. Natl. Acad. Sci. USA 76, 4276 (1979).
2. J.Y. Westcott and R.C. Murphy, Prostaglandins 26, 223 (1983).
3. N.P. Stimler, M.K. Bach, C.M. Bloor and T.E. Hugli, J. Immunol. 128, 2247 (1982).
4. C.W. Lee, R.A. Lewis, E.J. Corey, A. Barton, H. Oh, A.I. Tauber and K.F. Austen, Proc. Natl. Acad. Sci. USA 79, 4166 (1982).
5. R.M. Clancy and T.E. Hugli, Anal. Biochem. 133, 30 (1983).
6. M.K. Bach, J.R. Brashler and R.R. Gorman, Prostaglandins 14, 21 (1977).
7. W.R. Mathews, J. Rokach and R.C. Murphy, Anal. Biochem. 118, 96 (1981).

THE FT-MS SPECTRA OF CIS-DICHLORODIAMMINE PLATINUM(II) (CIS-PLATIN) AND RELATED ANTINEOPLASTIC DERIVATIVES: Robert R. Weller, Dept. Chem., Univ. of Fla., Gainesville, FL 32611, C.M. Riley, Dept. Pharmaceutics, Univ. of Fla., and L.A. Sternson, Dept. Pharmaceutical Chem., Univ. of Kansas, Lawrence, KS 66044.

Platinum(II) and platinum(IV) compounds of the cis-dichlorodiammine platinum(II) family (cis-platin) have been known for about 15 years to have antineoplastic activity. Presently, cis-platin is the drug of choice for a number of solid tumors of the head, neck, ovaries, and testes. The mechanism of this activity and the identity of the metobolites of these compounds are not well understood due in part to the lack of mass spectral data.

In the past, standard MS techniques, FAB, and SIMS, have proved unsuccessful in providing useful structural information. To date only a CI spectrum of the 2:1 adduct of methionine and Pt(II) has been observed. This lack of mass spectral data is due largely to the low volatility of these compounds and their decomposition at moderate temperatures (200°C).

Through standard FT-MS heated solid sample techniques, the mass spectra of several of these compounds have been obtained. Parent ions and expected daughter ions have been observed for cis-platin and several of its derivatives. The success of this technique arises as a result of the low number of ions required for observation and the possibility of signal averaging.

The mass spectra of cis- and trans-dichlorodiammine platinum(II) show a parent ion cluster of the expected eight lines around mass 300. The relative intensity of these lines is within 10% of that predicted from the natural isotopic abundances. Other clusters observed arise from the sequential loss of ligands. These are mass 283 ($-NH_3$), mass 265 ($-Cl$ or $-2NH_3$), mass 248 ($-Cl$ and $-NH_3$), mass 213 ($-2Cl$ and $-NH_3$), and mass 196 (Pt). The mass spectrum of cis-platin is shown in Figure 1. Also observed were clusters resulting from the addition of one or two chlorines, $Pt(NH_3)_2\ Cl_3^+$ and $Pt(NH_3)_2\ Cl_4^+$. Negative ion spectra were also observed but provided no additional information.

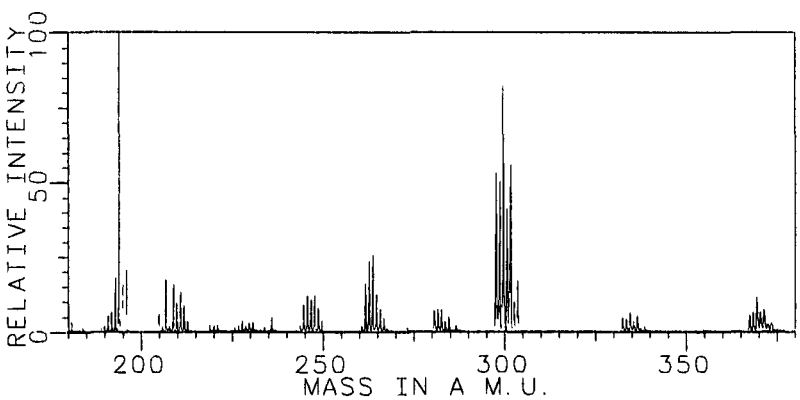

FIGURE 1: FT-MS of cisplatin. See text for details.

Similar spectra were observed for the cis-platin derivatives, cis-dichloro(2-propanamine) platinum(II), cis-dichloro-trans-dihydroxybis(2-propananine) platinum(IV), and cis-dichlorocyclohexyl-1,2-diamine platinum(II) with the exception that no parent ion was observed. The major ion cluster observed was that resulting from the loss of one chlorine atom.

The possibility of observing MS data for these compounds will greatly assist in the structural elucidation of platinum(II) complexes in general. In addition, this technique will be particularly useful in elucidating the structures of the metabolites of cis-platin and other related drugs.

MS/MS STUDIES ON MACROCYCLIC TRICHOTHECENES

THAIYA KRISHNAMURTHY AND EMORY W. SARVER
Chemical Research and Development Center
Aberdeen Proving Ground, MD 21010

Macrocyclic trichothecenes, produced by Myrothecium, Stachybotrys and other species of fungi, have been reported to be the most toxic of all known trichothecenes. However, the ones isolated from plant materials such as Baccharus megabotamica have been found to be biologically active and potential antitumor agents.[1] These macrocyclic trichothecenes are di- or tri- esters of verrucarol or substituted verrucarols. Recently, screening of environmental samples, plant materials, and fermentation products for the presence of toxic and/or biologically active macrocyclic trichothecenes has become extremely important.

Detection of macrocyclic trichothecenes or their derivatives by GC/MS method could not be accomplished due to their non-volatility and the presence of labile macrocyclic ester bridges. The only reported method of analysis for these molecules is by hydrolysis, followed by conversion of the hydrolysates into their HFB esters and analysis by GC/MS-NICI technique[2]. Even though this is an acceptable method of general screening for the presence of all known macrocyclics, it provides the identity of basic verrucarol or substituted verrucarol moiety only and not that of the specific macrocyclic compound.

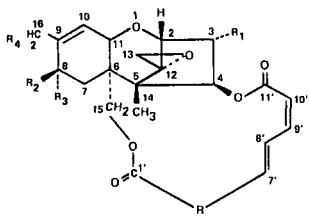

MACROCYCLIC TRICHOTHECENES

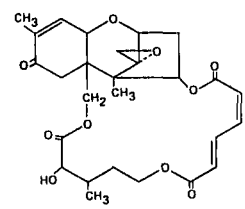

8-KETOVERRUCARIN A (KVA)

Hence, we have investigated and developed a direct, specific, MS/MS method for the analysis of the macrocyclic trichothecenes. These molecules with extended conjugation in the cyclic ester bridges, under CI (CH_4) conditions, produced M^- ions more effectively than the $(M+I)^+$ ions. Presence of CH_2Cl_2 along with CH_4 enhanced the production of negatively charged molecular ions. The mechanism of M^- formation could be either by the dissociation of the $(M+Cl)^-$ adduct or by the charge transfer from Cl- to the molecule or both. The M^- ions thus produced were subjected to collisionally activated dissociation (Ar, 15eV), and the corresponding spectra were recorded. Attempts to obtain CAD spectra of the chloride adducts were unsuccessful. However, the CAD spectra of M^- ions could be obtained with good sensitivity and reproducibility and they are listed below. Minimum detectable limits during these preliminary investigations for Roridin-H, Satratoxin G and Satratoxin H were 1 ng.

The macrocyclic trichothecenes investigated in this study were found to behave similarly under CAD conditions. The CAD ions are formed by the cleavageof the bonds at the cyclic ester groups. This observation is in agreement with the reported results for esters3,4. The diesters, Roridin A and Roridin H form ions with m/e 109 and 153. The triesters, verrucarin J and Verrucarin A and substituted verrucarin A form m/e 97, 141, 147. The satratoxins produce CAD fragments with m/e 137 and 181. This vital information along with neutral losses could be applied to the screening of samples for the presence of macrocyclic trichothecenes.

NEGATIVE ION CAD SPECTRA OF MACROCYCLIC TRICHOTHECENES

Compound	Significant Ions (m/e)
Roridin A	109, 135, 153, 359, 371, 401
Roridin H	109, 125, 137, 153, 403, 512*
Verrucarin A	97, 141, 147, 226, 247, 271 377, 393, 470, 502*
8-Ketoverrucarin A	97, 141, 147, 271, 391, 516*
16-Hydroxyverrucarin A	97, 141, 147, 225, 263, 271 370, 393, 504, 518*
9,10-Epoxyverrucarin A	97, 141, 147, 226, 329, 393, 435, 518*
Verrucarin J	97, 107, 124, 141, 147, 191, 253, 359, 389, 484*
Satratoxin G	73, 85, 113, 137, 141, 157, 181, 415, 430, 499, 529, 544*
Satratoxin H	93, 119, 125, 135, 137, 145, 147, 161, 163, 165, 169, 173, 181, 175, 177, 191, 181, 205, 207, 217, 235, 251, 279, 454, 466, 483, 498, 513, 528*

m/e Base peak.
*molecular ion

Preliminary results of this study indicate that these macrocyclic trichothecenes could be analyzed quantitatively as well by the MS/MS method. Two, semi-synthetic trichothecenes, 8-ketoverrucarin A (KVA) and 16-Hydroxyverrucarin A, were investigated, and the former was found to be a suitable internal standard for the quantitative detection of the macrocyclics. Varied amounts (1-50 ng) of Roridin H, Satratoxin G and H were analyzed using 8-ketoverrucarin A(50 ng) as the internal standard. The relative responses (CAD ions) of these compounds were found to vary linearly with their relative amounts (with respect to internal standard). Optimum conditions for the ionization and CAD need to be determined to improve the detection limits.

References:

1. "Macrocyclic and Other Novel Trichothecenes: Their Structure, Synthesis and Biological Significations", Bruce B. Jarvis and Eugene P. Mazzola, Acc. Chem. Res., 15, 338-395 (1982).

2. "Negative Ion Chemical Ionization Mass Spectrometry: Application to the analysis of Macrocyclic Trichothecenes,," Thaiya Krishnamurthy and Emory W. Sarver, presented at the Gordon Conference on Trichothecenes June 1983, Plymouth, NH.

3. M. Bambagiotti et al., Biomedical Mass Spectrometry, 9 (11), 495-98 (1982)

4. Don Hunt and Dennis L. Shaw, University of Virginia, Proceedings, 31st Annual Conference on Mass Spectrometry and Allied Topics, May 1983, Boston, MA.

IDENTIFICATION OF A CYTOTOXIC METABOLITE OF CIS-DICHLORO-TRANS-DIHYDROXY-BIS-ISO-PROPYLAMINE Pt(IV) [CHIP].

J.W. Cowens[1,2], L. Pendyala[2], B. Paul[1], J. Alderfer[3], S. Dutta[3], G. Chheda[3] and P.J. Creaven[2]. Grace Cancer Drug Center ([1]), Clinical Pharmacology and Therapeutics ([2]) and Biophysics ([3]), Roswell Park Memorial Institute, Buffalo, NY 14263.

Platinum (Pt) containing compounds form a new class of anticancer agents that are effective against certain tumors unresponsive to most other forms of chemotherapy. The clinical utility of cisplatin, the prototype drug of this class, is limited by its severe acute and chronic renal toxicity so that there has been great interest in the development of new Pt-containing compounds that have antitumor activity but are not renal toxic. CHIP is a second generation Pt-containing complex that has shown no renal toxicity either in preclinical toxicology or in a recently completed phase I trial and has shown activity against small cell carcinoma of the lung.

We have studied the pharmacokinetics and metabolism of CHIP in patients with advanced solid tumors receiving doses of 20-350 mg/M^2 by intravenous infusion (1). CHIP was separated from its metabolites in plasma and urine by high performance liquid chromatography with water to methanol gradient elution on a Waters μ Bondapak C18 column. In plasma and urine two classes of Pt-containing metabolites were found: those less polar and those more polar than CHIP. One of the less polar metabolites that elutes at 22 minutes has the same chromatographic properties as a platinum complex formed in vitro by incubating CHIP with the reducing agent ascorbic acid. Therefore, the reduced form of CHIP, cis-dichloro-bis-isopropylamine Pt (II) [CIP], was synthesized. The proton NMR spectrum of the product showed a doublet at 1.2 ppm (CH_3), a septet at 3.1 ppm (CH) and a multiplet at 4.8 ppm (NH_2). The electron ionization (EI) mass spectrum (Figure 1A) obtained from the probe of a Finnigan 4000 GCMS showed a cluster of peaks at m/z 382-388 (molecular ion) whose intensities were in the predicted ratios for a compound containing one Pt and two Cl; the fragmentation pattern showed a peak at m/z 58 [$NHCH(CH_3)_2$] and multiple Pt-containing species at m/z 307-314, 292-297, 250-255, 234-239. These spectra are consistent with the proposed structure of the synthesized product.

When CIP was added to the urine and plasma from patients treated with CHIP, it co-chromatographed with the 22 min. peak. Multiple aliquots of the urine from a patient who had received CHIP (180 mg/M^2) were chromatographed by HPLC and the Pt-containing peak eluting at 22 min. was collected until approximately 5 μg of material was accumulated. The probe EI mass spectrum (Figure 1B) of this material showed the same cluster of peaks at m/z 382-386 and the same fragmentation pattern as that of CIP. Therefore, the platinum containing peak which elutes at 22 minutes is CIP.

While it is clear from in vitro work with cells that DNA seems to be the target for platinum complexes, it is not clear which platinum species is effective in interacting with the DNA. The isolation of a reduced form of CHIP from patients who had received the drug and the antitumor activity of this reduced form (2) of CHIP suggest the possibility that CHIP may be a prodrug and that its active form is CIP. Further studies to elucidate the intracellular metabolism of CHIP are currently being carried out.

REFERENCES

1. Pendyala, L., Cowens, J.W., Madajewicz, S. and Creaven, P.J. Clinical Pharmacokinetics of Cis-dichloro-trans-dihydroxy-bis-isopropylamine platinum IV. In: Platinum Coordination Complexes in Cancer Chemotherapy. M.D. Hacker, E.B. Douple and I.H. Krakoff, eds., Martinus-Nijhoff Publishers, Boston, MA, 1984, p. 114.
2. Cleare, M.J., Hydes, P.C., Hepburn, D.R. and Walerbi, B.W. Antitumor Platinum Complexes: Structure-Activity Relationships. In: Cisplatin. A.W. Prestayko, S.T. Crooke and S.K. Carter, eds., Academic Press, NY, 1980, p. 149.

Cis-Dichloro-Bis-Isopropylamine Platinum (II) - EI

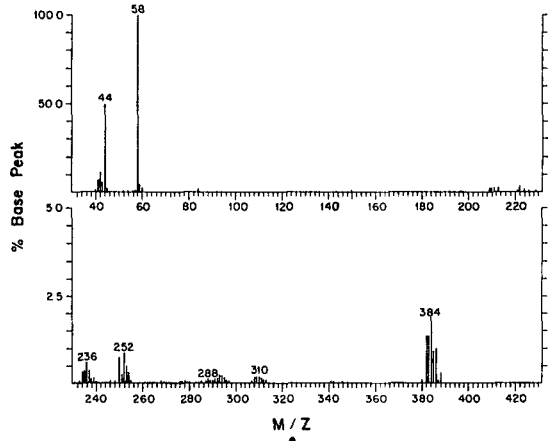

A

CHIP Metabolite (22 min) - E I

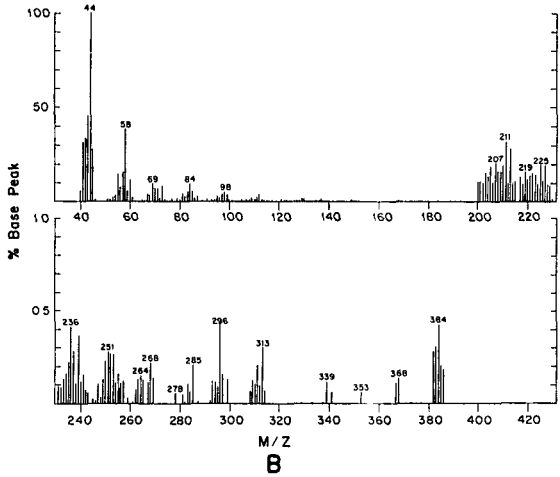

B

FIGURE 1

AN INVESTIGATION OF THE STRUCTURES OF NEUTRAL FRAGMENTS FORMED WHEN IONS DISSOCIATE IN A ZAB-2F SPECTROMETER

T.G.Morgan, R.E.March*, A.G.Brenton, F.M.Harris and J.H.Beynon.

Royal Society Research Unit, University College of Swansea, Singleton Park, Swansea SA2 8PP, U.K.

* Dept. of Chemistry, Trent University, Peterborough, Ontario, Canada.

In a reversed-geometry, double-focusing mass spectrometer such as a VG Analytical ZAB-2F, ions of a given species are selected by the magnetic sector and dissociation reactions in the second field-free region (2FFR) can be studied. The translational energies and thus the masses of the fragment ions resulting from dissociations are determined from energy spectra recorded by scanning the voltages applied to the plates of the electric sector. For each dissociation reaction, the mass of the neutral fragment is obtained from the difference in the masses of the parent and fragment ions. The experimental technique gives no direct evidence of the nature of the neutral fragment. Its structure, in many instances, can be inferred only from a knowledge of the structures of the parent and fragment ions. Recently, however, a ZAB-2F spectrometer has been used [1] to study the structures of triatomic neutral fragments. In the present investigation, the ZAB-2F spectrometer in our Laboratory has been used in a similar way to study neutral fragments from a variety of dissociation reactions.

The experimental procedure is the following. Ions which dissociate between the magnetic sector and the collision-gas cell in the 2FFR give rise to fluxes of ionic and neutral fragments. By electrically biasing the collision cell appropriately, the ions (both parent and fragment) can be prevented from entering it. The neutral fragments can enter the cell, however, and, because they have kilo-electron volts of translational energy, they can be ionized and dissociated in collisions with gas molecules. The ions formed in this way are energy selected by the electric sector to give an ion-kinetic-energy spectrum.

The molecular ion of methane, having 4 keV translational energy, was selected by the magnet sector and an ion-kinetic-energy spectrum recorded with the cell voltage at 5.2 kV. The largest peak corresponded to ions having about 5.2 keV energy. These are ions formed from the collision-gas molecules when the high-energy neutral fragments collide with them. They acquire only small recoil energies in the collisions and thus their translational energies are determined predominantly by the voltage applied to the cell. Other peaks in the spectrum, in order of decreasing height, were due to CH_3^+, $CH_2^{+\cdot}$, CH^+, $C^{+\cdot}$, H^+ and $H_2^{+\cdot}$. Unimolecular dissociation of $CH_4^{+\cdot}$ is known to give CH_3^+ and $H^\cdot$. Since the peak due to ionized $H^\cdot$ in the observed spectrum is small it is concluded that the other peaks are due to neutral fragments formed by collision-induced dissociation outside the cell of either $CH_4^{+\cdot}$ or CH_4 formed by charge transfer. Throughout the experiments, in fact, the cell pressures and pressures in the vicinity of the cell were such that neutral fragments arising from unimolecular dissociations gave peaks which were small in relation to others in the spectra.

The molecular ion of acetone was selected and a spectrum obtained using the procedure described. The acetyl ion, CH_3CO^+, is a major peak in the EI mass spectrum but accounted for only 5% of the total intensity in the spectrum measured. Conversely, CH_3^+ is the major contributor to the ion currents in the present spectrum but is a minor component of the EI mass spectrum.

The perdeuterated molecular ion of dimethyl sulphoxide was studied. Several groups of peaks were observed. In one group, the largest peak was deduced from its position on the energy scale to be due to CD_3^+ or OD^+. In previous work [2], both $CD_3^\cdot$ and $OD^\cdot$ were proposed as the neutral fragments from the unimolecular dissociation of DMSO-d_6.

$C_6D_6^{+\cdot}$ ions were selected for study using the present technique. The ion-kinetic-energy spectrum obtained consisted of groups of peaks each having as a common constituent one of the atoms in the range C_1 - C_6. $C_2D_2^{+\cdot}$ is the largest carbon-containing peak in the spectrum which is not surprising since the loss of acetylene in dissociation

of benzenoid compounds has been proposed frequently. $C_3D_3^+$ is a major component of the EI mass spectrum and, as expected, is of low intensity in the measured spectrum. In the C_6 group, all ions from C_6D^+ to $C_6D_6^{+\cdot}$ are observed. The $C_6D_6^{+\cdot}$ ions are probably formed in the following way. The selected $C_6D_6^{+\cdot}$ ions undergo a charge-transfer reaction between the magnet and the cell to form C_6D_6 molecules which can enter the cell where they are ionized in a collision with target gas molecules. The $C_6D_6^{+\cdot}$ ions on leaving the cell are further accelerated through the potential applied to the cell.

References

1. P.C.Burgers, J.L.Holmes, A.A.Mommers, J.E.Szulejko and J.K.Terlouw, Org. Mass Spectrom. 19, (1984).
2. I.W.Griffiths, I.Howe, R.E.March and J.H.Beynon, Int.J.Mass Spectrom.Ion Phys. 45, 5, (1982).

SCATTERING IN DISSOCIATIVE COLLISIONS OF IONIZED ACETONE WITH HELIUM

W. van der Zande, D. P. de Bruijn, J. Los and P. G. Kistemaker
FOM Institute for Atomic and Molecular Physics, Kruislaan 407,
1098 SJ, Amsterdam, The Netherlands*

and

S. A. McLuckey, Analytical Chemistry Division
Oak Ridge National Laboratory**
Oak Ridge, TN 37831

The angular distribution of fragment ions arising from collision-induced dissociation (CID) using keV collision energies is broadened by the kinetic energy released upon dissociation. This distribution can also be broadened by deflection of the precursor ion center-of-mass (c-o-m) by collision. The extent to which scattering occurs in keV energy collisions involving polyatomic ions has important implications with regard to the mechanism of energy transfer in MIKE/CID spectrometry. This phenomenon is difficult to study directly, however, with conventional mass spectrometers since only the charged fragment of a dissociation is detected. This paper describes a study in which the positions and flight time difference of both the neutral and charged fragments of a CID reaction are measured in coincidence. This allows the position of the precursor ion c-o-m to be determined and hence can provide insight into scatter accompanying dissociation.

The approach is based upon a translational spectroscopy technique described by de Bruijn and Los (1). Briefly, using a time and position sensitive detection system, both fragments of a CID reaction resulting from the passage of a fast ion beam through a gas-filled collision cell are detected in delayed coincidence. By measuring the distance each fragment strikes from the detector center and the flight time difference, the kinetic energy released in the dissociation can be calculated provided the fragment masses are known. In order to study c-o-m scattering, a mask is placed over the 2-dimensional detector which restricts all observed coincidence events to a narrow region of the y-dimension. Scattering in the y-plane can then be followed by translating the detector in this dimension (collecting at each position a range of scatter in the x-direction). Deflection of the ion c-o-m in the x-direction (x_s) is calculable provided each fragment can be correctly identified. Since the fragment masses are not directly measured, however, two values of x_s are possible when for ionized acetone scattering is > 0.2°. Nevertheless, an indication of the extent of scatter in the x-direction can be obtained by comparing experimentally obtained x_s values (arbitrarily assigning the high mass to the particle which strikes nearest to the detector center) with results expected based on an assumed scatter distribution (see below).

The acetone molecular ion was chosen as the model polyatomic ion. By far the major decomposition route for this ion from the onset of fragmentation (~0.6 eV above the ionization potential) to 6 eV above the ionization potential is the loss of methyl radical to give the acetyl cation (2). A laboratory collision energy of 5000 eV was employed with He as the target at a pressure sufficient to attenuate the precursor ion beam by 20%. Figure 1 shows the coincidence count rate as a function of detector displacement in the y-direction. The count rate decreased slowly to 0.8°, the upper limit to the accessible range of angles. The net observed decrease is roughly one order of magnitude over this interval. The solid curve of Figure 2 shows the relative number of coincidences as a function of x_s (calculated from experimental data using the convention noted above). The crosses indicate the results expected from a Maxwell-Boltzmann distribution of energy releases and isotropic scattering over a range of 0.0-0.7°. The close congruence between experimental and calculated values in the latter figure and the slow decline in coincidence count rate in the former indicate that considerable scattering takes place in the CID of

*This work is part of the research program of the Foundation for Fundamental Research on Matter made possible through a grant from the Dutch Organization for the Advancement of Pure Research (ZWO).
**Operated by Martin Marietta Energy Systems, Inc., under Contract DE-AC05-84OR21400 with the U. S. Department of Energy, Office of Basic Energy Sciences.

By acceptance of this article, the publisher or recipient acknowledges the U S Government's right to retain a nonexclusive, royalty free license in and to any copyright covering the article

ionized acetone. The two figures do not match due to differences in detector discrimination associated with the two different methods for following scattering angle. It should not be concluded from these data that scattering is anisotropic. These results do show that momentum transfer collisions can play a major role in the CID of polyatomic ions at keV energies. Direct vibrational excitation is therefore expected to contribute significantly to CID in addition to electronic excitation which is also operative with high velocity projectiles.

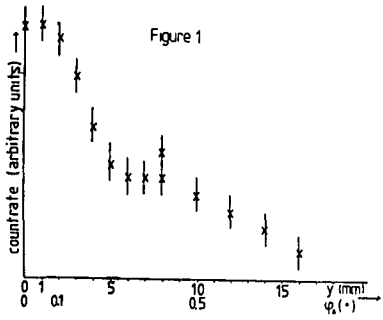

Figure 2

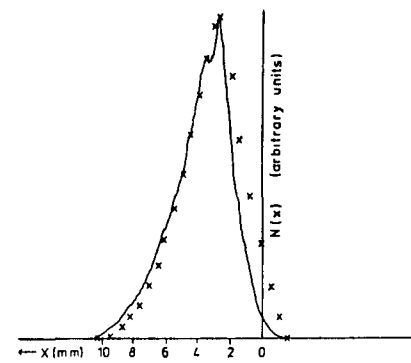

References

1. D. P. de Bruijn and J. Los, Rev. Sci. Instrum., 53, (1982) 1020.

2. I. Powis and C. J. Danby, Int. J. Mass Spectrom. Ion Phys., 32 (1979) 27.

COLLISIONALLY INDUCED FRAGMENTATIONS REMOTE FROM THE SITE OF IONIZATION,

K.B. Tomer, F.W. Crow, N.J. Jensen and M.L. Gross, Midwest Center for Mass Spectrometry, Department of Chemistry, University of Nebraska, Lincoln, NE 68588 and P.A. Lyon, 3M Corporation, St. Paul, MN

During several studies of the collisionally activated decomposition of a variety of compound types, we have observed fragmentation sequences which could formally be described as occurring at sites remote from the site of ionization (1,2).

An example of this phenomenon is illustrated by the CAD spectrum of the $(M-H)^-$ anion of long-chained fatty acids, eg. palmitic acid (Fig. 1). The major fragment ions arise by loss of neutral alkanes. These appear to be occurring from the alkyl end of the molecule, remote from the negatively charged carboxylate moiety. To further delineate the mechanism of this fragmentation mode, the CAD spectra of three isotopically labeled compounds were obtained.

The CAD spectrum of the 16,16,16-d_3-palmitate anion (Fig. 2) does not differ from that of the unlabeled anion (Fig. 1) except for the mass of the parent ion. Thus, the loss of methane occurs with loss of the terminal methyl group. All other neutral alkane losses also include the terminus of the chain.

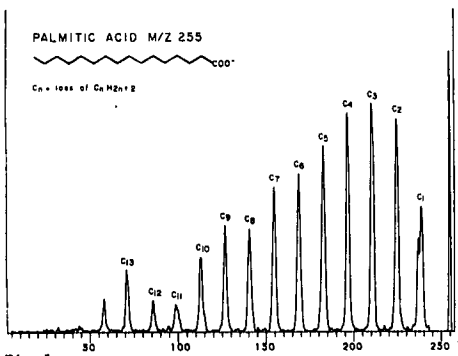

Fig.1

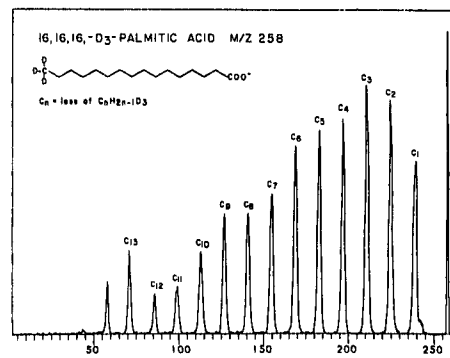

Fig.2

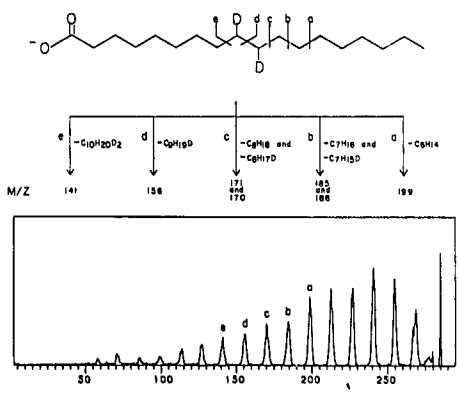

Fig.3

The CAD spectrum of the $(M-H)^-$ anion of 7,7,8,8-d_4-palmitic acid (Fig. 3) shows that a -hydrogen is transferred during the alkane loss in a 1,2-elimination (Fig. 4). The CAD spectrum of 9.10-d_2-stearic acid ((Fig. 5) confirms the mechanism proposed on the basis of the other labeling results. These data also illustrate the potential for locating double bonds in multiply unsaturated fatty acids from the CAD spectra of the reduced acids formed by addition of deuterium across the double bond with N_2D_4 (3).

Although elimination of neutral alkanes upon CAD has been observed (4), in the reported examples the losses occur in close proximity to the charged site. In our examples, alkane elimination is more predominant at sites remote from the charge than from sites close to the charge.

These data are consistent with a mechanism in which the collision process transfers energy into states that are not accessible upon ion formation. Ions in these states then fragment via a mechanism in which the role of the charge is minimal or nonexistent.

Acknowledgement: This work was supported by the Midwest Center for Mass Spectrometry, a National Science Foundation Regional Instrumentation Facility (Grant No. CHE 82-11164).

REFERENCES

1. Tomer, et al. JACS, 105, 5487 (1983).
2. Lyon, et al., Anal. Chem., 56, 8 (1984).
3. Thomas, Deuterium Labeling in Organic Chemistry, Appleton-Cenuty-Crofts, NY, 1971, 324.
4. see eg. Veith, Mass Spectrom. Rev., 2, 419 (84). Sigsby, et al., OMS, 14, 556(79); Holmes, et al., OMS, 17, 127 (82).

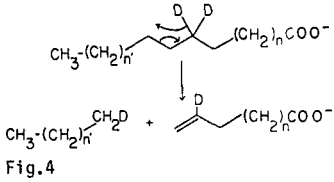

Fig.4

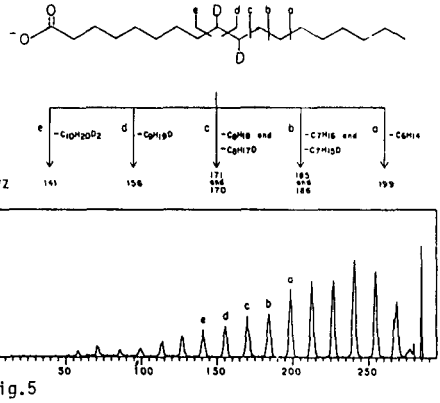

Fig.5

INTERNAL ENERGY EFFECTS IN LOW ENERGY CID*

G.L. Glish, D.E. Goeringer and S.A. McLuckey
Analytical Chemistry Division
Oak Ridge National Laboratory
Oak Ridge, TN 37831

Exploring the effects ion internal energy has on MS/MS spectra has been difficult because it is hard to define the internal energy difference between ions formed by different methods. One way to vary the ion internal energy is to vary the source temperature. The temperature range of conventional sources is rather small, typically a few hundred degrees at most. However, the temperature of a thermal ionization source can be easily varied by more than a thousand degrees, which allows one to investigate, on a crude level, the effect of ion internal energy on MS/MS spectra.

A recently developed tandem quadrupole/time-of-flight instrument was used in this study. This instrument is described elsewhere in these proceedings. Tetramethyl- and tetraethylammonium salts were used as the sample. These species desorb as the intact cation at low filament temperatures (T>600 K) while at high filament temperatures nearby depositions of the salt can be evaporated by radiative heat and then ionized by the hot filament, producing the intact cation. In the experiments in this study, temperatures of approximately 700 K and 2300 K were used to generate the intact cations.

While it is generally accepted that due to the broad energy transfer distribution of keV collisions, ion internal energy has little effect on collision-induced dissociations at these high collision energies, the same cannot be said of the low energy CID process. Figure 1 shows the MS/MS spectra of the tetramethylammonium cations formed at the indicated filament temperatures with a 32 eV laboratory collision energy. Obviously these two spectra are substantially different with the higher temperature spectrum showing increased fragmentation.

Figure 2 shows the MS/MS spectra of the tetraethylammonium cation taken at the indicated temperatures and collision energies. The low temperature spectrum begins to compare with the high temperature spectrum at a laboratory collision energy that is 28.5 eV greater than that used for the high temperature spectrum. This corresponds to a center-of-mass energy difference of 5.1 eV. Using statistical mechanics an average internal energy for each temperature can be calculated. For the tetraethylammonium cation at these two temperatures the maximum difference in average internal energy is 10.0 eV. This suggests that the internal energy difference may contribute significantly to the large difference in collision energy required to get similar MS/MS spectra at the two different temperatures.

Figure 3 shows a plot of the onset of fragmentation for the tetramethylammonium cation. The open squares are the data for 2300 K, the circles the data for 700 K and the filled-in squares correspond to the high temperature data shifted upscale by 4.0 eV. This 4.0 eV shift in laboratory collision energy converts to a 1.1 eV shift in center-of mass energy. For tetramethylammonium cation the maximum average

*Research sponsored by the U. S. Department of Energy, Office of Basic Energy Sciences, under Contract No. DE-AC05-84OR21400 with Martin Marietta Energy Systems, Inc.

By acceptance of this article, the publisher or recipient acknowledges the U.S. Government's right to retain a nonexclusive, royalty free license in and to any copyright covering the article

internal energy difference is 5.6 eV. Thus it is possible that the shift is due to the internal energy difference. The larger difference between these two numbers in contrast to the previous example may be due to the fact that at the onset of fragmentation the tails of the internal energy distributions and not the average internal energies will be the most important factor. We are currently undertaking a more detailed analysis of these data which takes into account the energy distributions.

These results demonstrate that the internal energy of ions can affect the observed MS/MS spectra generated by low energy CID. While extremes were used here, the large differences observed suggest that even moderate changes in internal energy will affect MS/MS spectra. Thus, one area that needs to be approached with considerable caution is the use of energy-resolved mass spectrometry, where ion abundances are plotted versus collision energy to differentiate isomers. Similar curves shifted by some amount may likely be a result of internal energy differences and not structural differences. These results also suggest that low energy CID MS/MS may be a method that can be used to probe internal energy differences in stable ions. We are pursuing this possibility further.

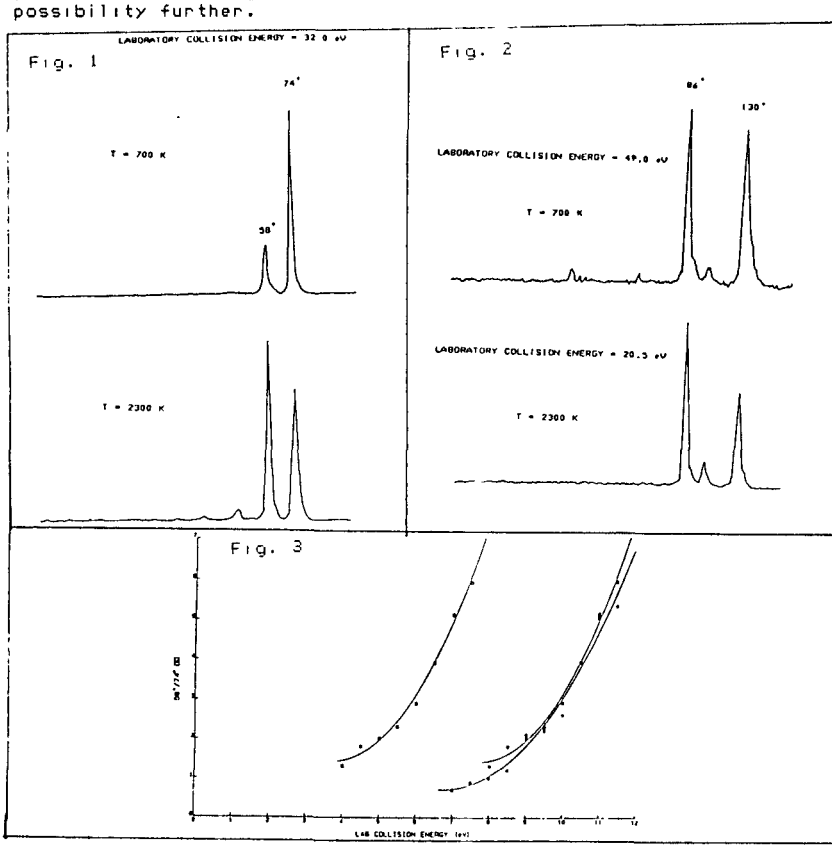

RPC 5. ISOTOPE EFFECTS AS A PROBE OF COLLISION-ACTIVATED DISSOCIATION DYNAMICS

Thomas A. Lehman, Bethel College, No. Newton KS 67117; Kenneth B. Tomer and Frank. W. Crow, Midwest Center for Mass Spectrometry, Lincoln NE 68588

Kinetic isotope effects (KIEs) have yielded much information about reactions, whether in testing a rate theory or in elucidating a mechanism. They appear in both unimolecular and bimolecular processes in gaseous ion chemistry, and were the subject of a previous ASMS poster (1). There it was shown that the collision-activated dissociation (CAD) of an isotopically labeled ion such as CHD^+ produces unequal amounts of CH^+ and CD^+. Such isotope effects are seen in the CAD of both diatomic and triatomic ions.

DEFINITION. Let B and B* represent light and heavy isotopes, respectively. For a general reaction in which ABB^{*+} dissociates to produce either of the ionic products AB^+ or AB^{*+}, we define the KIE as the ratio of product ion peak heights I*/I, where I* refers to the heavier product. Experimental values have ranged from just above unity for relatively heavy isotopes (e.g., ^{35}Cl and ^{37}Cl) to about 5 for HD^+ dissociating to H^+ or D^+.

THEORY. KIEs have been observed over a vast range of reactant energies. They are generally explained in terms of the effect of mass on vibrational and/or rotational energy levels. This is the case for reactions at thermal energies (2) and at energies of a few eV (3). For CAD at ion kinetic energies in the keV range, theoretical work (4) has correlated isotope effects with experimental results in terms of simple ratios of atomic masses. This prediction derives from an analysis of the energy transferred from translation to vibration as a result of interaction with the collision gas.

BACKGROUND. It is essential to determine whether the observed KIEs depend on any of the instrumental variables. The previous poster showed that the z slit width, ion accelerating voltage and collision gas pressure, while contributing to the scatter of the results, are not independent variables in the sense of creating an isotope effect purely as an instrumental artifact. This is particularly important for experiments in which the z slit width was varied, because it establishes that the isotope effects are not simply a function of the ion acceptance angle at the far end of the second electric sector. In extending these studies we find that the multiplier voltage likewise is not the source of these isotope effects. They are influenced by changes in the collision gas and by use of a very low ionizing energy in the source.

INSTRUMENTATION

The triple analyzer (TA) mass spectrometer (5) of the Midwest Center for Mass Spectrometry was used throughout. The collision gas was helium except as noted. The instrument has recently been fitted with a detector that adds 8 keV to ion energies between the second electric sector and the electron multiplier.

RESULTS

We have done the ultimately simple CAD experiment on HD^+ and find that D^+ is favored over H^+ by about 5:1 (see below). The theory mentioned briefly above predicts a ratio of 4:1. In the absence of collision gas no dissociation can be seen when ten scans at high amplification are averaged. Our CAD experiments on this system covered the range from 10 to 65% attentuation of the HD^+ beam and show that both product ions result from two processes, as shown in the figure. The signals at masses 1 and 2 are sums of contributions from a dish-shaped component and a typically sharp one. The former becomes more prominent with increasing attenuation of the main beam as the pressure of the collision gas is increased. Such a change makes more energy available for CAD, so that the dish-shaped signal must be that of a higher-energy process, perhaps the formation of the product atom in an electronically excited state. For H or D, this would require 10.2 eV.

In order to locate the dissociation processes, a retarding potential of 2186 volts was imposed on the collision cell. This caused a nearly complete displacement of both signals, so that both processes occur almost exclusively in the collision cell.

In total, nine CAD experiments were done on HD^+ over the range of 10 to 65% attentuation. The multiplier setting on the TA also varied from one experiment to another. The mean value of the isotope effect for all nine is KIE = $I(D^+)/I(H^+)$ = 4.9 with a standard deviation of 0.9.

COLLISION GAS. We have extended our study of instrumental considerations via experiments with CHD^+ and HDO^+. For the former, a change of collision gas from He to Ar to Xe increases the observed product ion ratio $I(CD^+)/I(CH^+)$ from 3.1 to 3.4 to about 4.0. The heavier collision gases thus increase the extent of formation of the favored product as a fraction of total CAD. This is in accord with

our observation that, in the CAD of $CH_2D_2^+$, the more likely products with He as the collision gas become even more so when Xe takes its place:

Ion	m/z	17	16	15	14	13	12
(Xe/He) rel. intensity		2.1	1.2	0.8	0.7	0.5	0.4

The higher-energy dissociations that form the lighter ions are less likely in the heavy collision gas.

MULTIPLIER VOLTAGE. The voltage on the first plate of the ion multiplier alters the ion kinetic energy just before detection. Because CAD product spectra are produced by an electric sector, which separates ions according to their kinetic energy, we have determined the effect of multiplier voltage on the ratio of products in an isotopic experiment. Let V be proportional to the ion multiplier voltage, and I the height of the product ion signals. We find:

V	2.15	2.65	3.5	4.2	5.0
I_{CD^+}/I_{CH^+}	4.03	3.97	4.00	3.98	3.90

These results lie very easily within the range seen for replicate experiments, so that the multiplier voltage is not influencing the isotope effect. (This series of experiments was carried out before installation of the new detector.)

ELECTRONIC EXCITATION. Is electronic excitation energy retained by the reactant ion from its formation in the source a factor in the ratios of isotopic products? To test this, we varied the ionizing energy (IE) and observed its effect on the CAD of HDO^+ to form DO^+ or HO^+. In order to obtain suitable signals at low ionizing voltages, the multiplier voltage V had to be increased. But this has a negligible effect, as shown above. The slight increase in KIE at the lowest voltage may be significant.

V	2.35	3.1	4.3	6.9
IE (eV)	70	20	16.0	13.0
I_{DO^+}/I_{HO^+}	2.89	2.86	2.70	3.31

We find, not surprisingly, a greater scatter in the product ratios as the value of the ratio itself increases. This is particularly evident in CHD^+ experiments.

DISCUSSION

Three experimental conditions appear to influence the magnitude of the KIE: the ionizing energy, the choice of collision gas, and its pressure. While their effects are not found uniformly in all the systems studied, they are all interpretable in the same manner: whatever reduces the energy available for activation increases the ratio of the product ion peak heights if the heavier ion appears in the numerator. Whatever the exact reasons, the heavier isotope reaches the product ion by a lower-energy path than does the lighter isotope. The time the reactant ion spends within two diameters of a collision gas atom is on the order of 1 fs, which is far too short to permit rotational reorientation of the ion.

Results of experiments (chiefly with HD) after installation of the new detector should lay to rest any fear that such isotope effects are due to unrecognized aspects of detector performance. Experiments done after its installation do not show smaller isotope effects than the earlier experiments.

CONCLUSIONS

These isotope effects are easy to observe. Experiments on four diatomic species and six triatomic ones [Herein and in Ref. (4)] have yielded reasonably consistent ratios that refute the null hypothesis (ratios = 1.00) and that can be correlated by a simple function of the isotopic masses. These effects persist in spite of changes of every experimental condition that we can imagine to be influencing them.

REFERENCES

1. T. A. Lehman, J. R. Hass, F. W. Crow, K. B. Tomer and L. G. Pedersen, 31st Ann. Conf. on Mass Spectrometry and Allied Topics, 1983, p. 719.
2. L. Melander, Isotope Effects on Reaction Rates, Ronald Press, 1960.
3. P. Hierl, J. Chem. Phys. 1977, 67, 4665.
4. See Ref. 1. A full manuscript has been prepared for publication.
5. M. L. Gross, E. K. Chess, P. A. Lyon, F. W. Crow, S. Evans and H. Tudge, Int. Jour. Mass Spectrom. Ion Phys. 1982, 42, 243.

AN UNEXPECTED $(C_3H_5O)^+$ ION: $(CH_2-C(OH)-CH_2)^+$.

Guy BOUCHOUX*, Jean Pierre FLAMENT*, Robert FLAMMANG**, Andre MAQUESTIAU**, Yannik HOPPILLIARD* and Pierre MEYRANT**.
* Laboratoire de Synthese Organique. Ecole Polytechnique.
91128 PALAISEAU-Cedex (France).
** Universite de l'Etat, 19 rue Maistriau. 7000 MONS (Belgium).

ABSTRACT.

The ionized $(CH_3-CH(OH)-CH(OH)-X)^+$ diols successively loss X and H_2O to generate, in FFR an $(C_3H_5O)^+$ ion. The CAD spectrum of this ion exhibits a important peak at m/z=43 never observed with this intensity on the CAD spectra of any previously identified isomeric ions: $(CH_3-CH_2-C{=}O)^+$ 1 ,$(CH_2-CH-CHOH)^+$ 2 or $(CH_3-CO-CH_2)^+$ 3.

The total energy of acetylmethylcarbenium 3, 2-hydroxyallyl 4 and 1-hydroxycyclopropyl 5 cations have been performed by ab initio calculations at the MP2/4-31G level, after geometry optimisation at the 4-31G level

The calculations predict 4 to be more stable than 3 (+34 kcal.mol-1) and 5 (+9.8 kcal.mol-1). Both experimental and theoretical results converge to identify the new structure as the 2-hydroxyallylcation.

EXPERIMENTAL CHARACTERIZATIONS.

The CAD spectra have been measured on the E/B/E triple sectors (modified AEI MS902) mass apectrometer of the Mons University. The $(C_3H_5O)^+$ ions (m/z=57) have been formed in the 1 FFR from metastable precursors. Collision of m/z=57 with helium has been made in the gas cell located in the 3 FFR.

The CAD spectra and the calculated relative stability of eleven isomeric $(C_3H_5O)^+$ ions have been previously studied (1). The two most stable structures are $CH_3-CH_2-\overset{+}{C}{=}O$ 1 and $CH_2-CH-CHOH^+$ 2. They have quite different CAD spectra. 1 is characterized by important peaks at m/z=27, 28 and 42 and the absence of any signal at m/z=30 and 31. The dominant peaks of 2 are: m/z=27, 31, 39 and 55 .

An $(C_3H_5O)^+$ ion has been also produced by collisionally activated charge reversal of the $(C_3H_5O)^-$ anion (2). This anion is obtained by hydrogen loss after dissociative negative ionization of the acetone (scheme 1).

$$(CH_3-CO-CH_3) + e^- \longrightarrow (CH_3-CO-CH_3)^-$$
$$(CH_3-CO-CH_3)^- \longrightarrow (CH_3-CO-CH_2)^- + H.$$
$$(CH_3-CO-CH_2)^- + He \longrightarrow (CH_3-CO-CH_2)^+ + 2e^- + He$$

Scheme 1

The CAD spectrum of the charge reversed ion exhibits peaks of similar intensities at m/z=27, 39, 42 and 43; no signal is detected at m/z=31. These results have been interpreted by the formation of the $(CH_3-CO-CH_2)^+$ cation.

A singular peak at m/z=43 is observed on the CAD spectrum of both $(C_3H_5O)^+$ ions generated from 1,2-propanediol and 2,3-butanediol molecular ions. This particularity survives with $(C_3H_5O)^+$ ions coming from metastable $(C_3H_7O_2)^{*+}$ ions (scheme 2)

$$(CH_3-CHOH-CHOH-X)^+ \longrightarrow (CH_3-CHOH-CHOH)^{*+} + X.$$
$$(X=H, CH_3) \qquad (C_3H_7O_2)^{*+}$$
$$(CH_3-CHOH-CHOH)^{*+} \longrightarrow (C_3H_5O)^+ + H_2O$$
$$(C_3H_5O)^+ \longrightarrow (C_2H_3O)^+ + CH_3.$$

Scheme 2

The overall spectrum supports the ion structure 2 (CH2-CH-CHOH)+ with the exception of the peak at m/z=43. This latter indicates the existence of a second ion structure. The successive losses of water and methyl from the (C3H7O2)+ ions lead to the (C2H3O)+ ion expected to be the acylium ion : (CH3-C=O)+. The geometry of this last ion needs a precursor ion structure with the oxygen atom bonded to a trisubstituded carbon.

Four structures: (CH3-CO-CH2)+ 3, (CH2-C(OH)-CH2)+ 4, CH2-CH2-C-OH 5 and CH2-C(CH3)-O 6 have been investigated to describe this precursor. Assuming the H2O elimination from metastable (C3H7O2)+ ions lead to the most stable final state, the relative stabilities of the 3, 4, 5 and 6 ion structures have been evaluated.

AB INITIO CALCULATIONS.

These calculations have been performed with a double split valence basis set including an electron correlation effect at the second order Moller-Plesset perturbation Theory: MP2/4-31G//4-31G. The geometries have been before optimized at the 4-31G level. Table 1 gives the total and relative energies of the four investigated ions and also those, previously calculated, of the two most stable (C3H5O)+ ions.

Table 1.Calculated total energies E (in a.u.) and relative energies ΔE (in kcal.mol-1) of (C3H5O)+ ions.

Ion structure		E	ΔE
CH3-CH2-C=O	1	-191.20025	-38.5
CH2-CH-CHOH	2	-191.17852	-24.9
CH3-CO-CH2	3	-191.08492	+34.0
CH2-C(OH)-CH2	4	-191.13885	0.0
CH2-CH2-C-OH	5	-191.12307	+9.8
CH2-C(CH3)-O	6	-191.12283	+10.0

The most stable structure describing the unknown ((C3H7O2)+ - H2O)+ ion is the 2-hydroxyallyl cation 4.

In these conditions we have to wonder why the (CH3-CO-CH2)+ ion has been observed. This ion is obtained after charge reversal in 2FFR of a negative ion formed in the source of a mass spectrometer (ZAB 2F). The structure of the (M-H)- initially formed is necessarily (CH3-CO-CH2)- . We have calculated the energy difference between the (CH3-CO-CH2)- and (CH2-C(OH)-CH2)- anion structures. At the 6-31G*//3-21G level the first one is 40 kcal.mol-1 more stable than the second one. Between the source and the second FFR (CH3-CO-CH2)- retains its structure. The charge reversal being a vertical process,the positive ion has the same structure as the precursor anion.

CONCLUSION.

The successive eliminations of X (X=H and CH3) and H2O respectively from the ionized 1,2-propanediol and 2,3-butanediol lead to a mixture of (CH2-CH-CHOH)+ and (CH2-C(OH)-CH2)+ ions following the scheme 3.

```
                        - X                    - H2O
(CH3-CHOH-CHOH-X)+  -->   (CH3-CHOH-CHOH)+ -->  (CH2=CH-CHOH)+
    X= (H, CH3)                 ↓ H1,2      - H2O
                        (CH3-C(OH)-CH2OH)+ -->   (CH2-C(OH)-CH2)+
```

Scheme 3

(1) G. BOUCHOUX, Y. HOPPILLIARD, R.FLAMMANG, A .MAQUESTIAU and P. MEYRANT, Org. Mass Spectrom., 18, 340 (1983).
(2) T.A. LEHMANN, M.M. BURSEY and J.R. HASS, Org. Mass Spectrom., 18, 374 (1983).

HIDDEN REARRANGEMENT OF IONIZED 3-PENTENE,-2ONE BEFORE METHYL ELIMINATION.

Yannik HOPPILLIARD, Guy BOUCHOUX and Pascale JAUDON
Laboratoire de Synthese Organique.Ecole Polytechnique.
91128 PALAISEAU-cedex (France).

ABSTRACT

Methyl elimination from 3-pentene,2-one molecular ion leads to (CH3-CH=CH-C=O)+ (m/z=69). Classical and MIKE spectra of the 1,1,1d3 3-penten,2-one show that the elimination may involve either the α or the terminal methyl. The fragmentation is preceded by a molecular ion isomerization. The potential energy diagramms of the different isomerization processes have been carried out with MO calculations method (MNDO).

INTRODUCTION

The (M-15)+ and (M-X)+ ions generated respectively from ionized 3-penten,2-one and CH3-CH=CH-CO-X (X=Cl, H, OCH3, OC2H5 and OH) carbonyl compounds (1) have been characterized with their MIKE spectra. Whatever the precursor, the (M-X)+ ion loss CO with the same kinetic energy release (T0.5=30 meV). All the (M-X)+ ions have the same structure , identified as the acylium ion (CH3-CH=CH-C=O)+. Competing with the X group elimination,a loss of methyl is also observed on the crotonic acids (X=OH, (2)) and on the transmethylcrotonate (X=OCH3, (3)) spectra.

RESULTS AND DISCUSSION.

The ionized 1,1,1d3 3-penten,2-one molecules eliminate CR3 (R=H, D) in different ways. The relative intensities of these ions, formed in the source or in the 2 FFR of a ZAB-2F mass spectrometer, are compiled on the table 1.

Table 1: (M-CR3)+ ions intensities.

m/z	72	71	70	69
CR3	CH3	CH2D	CD2H	CD3
Source	20.	0.8	0.6	100.
2 FFR	100.	40.	70.	100.

- Source ions:Both (M-CH3)+ and (M-CD)+ ions, formed in the source, eliminate in the 2 FFR a carbon monoxyde molecule with the same distribution of energy release n(T): <T>=89 ± 3 meV or the same T0.5=30 ± 1 meV (figure 1). The (M-CH3)+ and (M-CD3)+ ions have identical structures identified as the conjuguated acylium structure: (CH3-CH=CH-C=O)+.

- Metastable molecular ions: in the 2 FFR, comparing with the (M-CD3)+ ion intensity, the elimination of CH3 increases and important eliminations of CH2D and CHD2 appear.In the source, the molecular ions have no time enough to extensively rearrange; in the metastable time frame, the two terminal methyl groups are interchanged and a H, D exchange occurs to some extend.

Three different mechanisms have been considered to explain the molecular ion isomerizations (scheme 1). The potential energy diagramm of each isomerization process has been calculated, using MO calculations method: MNDO (figure 2).

CONCLUSIONS.

One diagramm (c) seems more compatible with the experimental energy value (212 kcal.mol-1) of the final state and explain very well the intensity differences between the losses of CD3, CH3, CD2H and CH2D.The elimination of CH3 needs a preliminary rearrangement of (CD3-CO-CH=CH-CH3)+ 1 into (CH3-CO-CH=CH-CD3)+ 2 and again the loss of CD2H must be preceded by the isomerization of 2 in (CD2H-CO-CH=CH-CH2D)+ 3; 3 is the intermediate leading to a new isomerization necessary to eliminate CH2D.

Figure 1

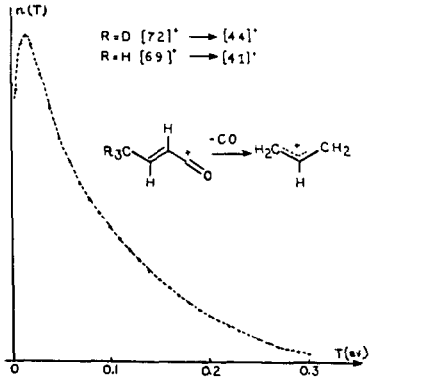

Scheme 1

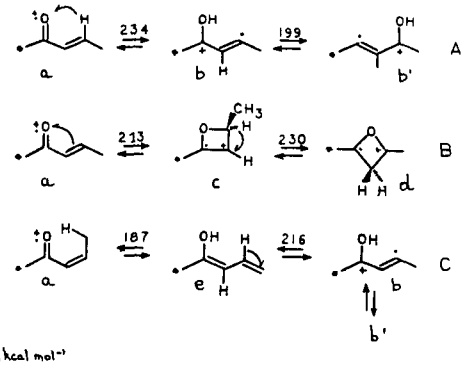

Figure 2

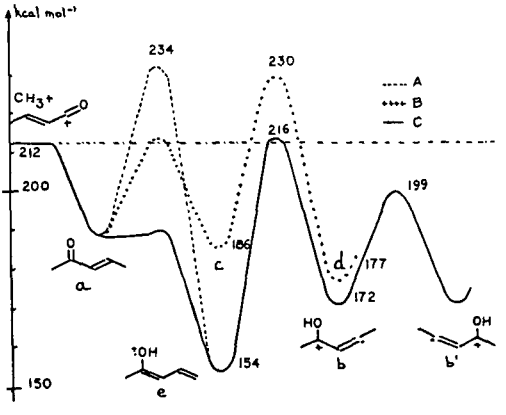

(1) H. HOMMES and J.K. TERLOUW, Org. Mass Spectrom., 14, 51 (1979).
(2) J.L. HOLMES, J.K. TERLOUW, P.C. VIJFHUIZEN and C. A'CAMPO, Org. Mass Spectrom., 14, 204 (1979).
(3) J.K. TERLOUW, P. BURGERS and H. SWARTZ, Org. Mass Spectrom., 15, 599 (1980) and cited references.

STABILITIES OF (C3H3O)+ IONS. AB INITIO CALCULATIONS.

Yannik HOPPILLIARD, Guy BOUCHOUX and Jean Pierre FLAMENT
Laboratoire de Synthese Organique. Ecole Polytechnique.
91128 PALAISEAU-Cedex (France).

ABSTRACT

The relative stability of eleven (C3H3O)+ ion structures have been determinated with different M.O. calculation methods. The vinylcarbonyl cation (CH2=CH-C=O)+ a is calculated to be the most stable structure. Exerimental data agree with the greatest stability of the vinylcarbonyl cation. The other stable structures are:(CH-CH-C-OH)+ b , (CH=C-CHOH)+ c and (CH2=C=C-OH)+ d . Comparing to the total energy of a , their relative energies are respectively: +28, +41 and +52 kcal.mol-1, at the ab intio MP2/4-31G*//3-21G level. The relative stabilities of the ions a, b, c and d have been compared with those of the corresponding isoelectronic (C4H5)+ ions.

INTRODUCTION

Gaseous positive ions of general formula (CnH2n-3O)+ occur as major fragments in the electron impact induced decompositions of the acethylenic and allenylic alcohols or ethers and of the ethylenic carbonyl compounds: aldehydes, ketones, carboxylic acids or methylesters.

As first part of a detailed theoretical study of the (C3H3O)+ ion formation and decomposition mechanisms, we have examinated eleven structures (a-k) expected to be created in a mass spectrometer.

M.O. CALCULATION METHODS

M.O. calculations, at differents levels, have been performed to determine the relative stabilities of the isomeric (C3H3O)+ ions .

- Semi empirical methods: MINDO/3 and MNDO have been used, after a total optimization of the geometric parameters of each structure, to obtain the ion heats of formation ΔHf .

- "ab initio" methods have been carried out to evaluate the total energy of the isomeric ions , in different ways:

1) starting from different geometry optimizations,
2) increasing the basis set size from the 3-21G to the 4-31G* level,
3) including an electron correlation at the level of the second order Moller-Plesset perturbation theory (MP2).

RESULTS

All calculations predict the vinyl carbonyl cation a to be the most stable one. The enthalpy of formation or the total energy of a are choosen as reference energy. The energy differences between a and the others structures are given on the table 1.

Semi empirical calculations I and II (table 1) or single point "ab initio" calculations III and IV using geometry optimizations carried out with semi empirical methods estimate the 3-hydroxy propargyl cation c more stable than the hydroxycyclopropenium ion b.

Ab initio calculations, at any level reverses this order of stability. The cyclic ion is 13 kcal/mole more stable than c and 24 kcal/mole more stable than its allenic isomer d.

COMPARISON WITH THE ISOELECTRONIC (C4H5)+ IONS

The a', b', c' and d' (C4H5)+ ions are respectively isoelectronic of the a , b , c and d (C3H3O)+ ions. Their relative stability are compared on table 2.

Table 2. Comparison between the relative stability of the most stables (C3H3O)+ and (C4H5)+ ions, expressed in kcal/mole.

(C3H3O)+		MP2/4-31G*// 3-21G	(C4H5)+		MP2/3-21G*// 3-21G
CH2=CH-C=O	a	0	CH2=CH-C=CH2	a'	0
CH-CH-C-OH	b	+28.3	CH-CH-C-CH3	b'	-17
HC≡C-CHOH	c	+41.3	HC≡C-CHCH3	c'	+8.6
H2C=C=C-OH	d	+52.0	H2C=C=C-CH3	d'	+12.7

For the (C4H5)+ ions, the structure b' becomes more stable than a'. This inversion has two reasons:

- on the conjuguated ethylenic system "a", the oxygen atom induces a better delocalization of the positive charge than the methylene group.
- on the cyclic "b" form, the hyperconjuguaison or the giving inductif effect of the methyl group increases the stability of the aromatic system; on the contrary, the electron drawning effect of the hydroxy group destabilizes this form.

EXPERIMENTAL RESULTS (1)

- The loss of X from ionized (CH2=CH-CX=O)+ ions leads to (C3H3O)+ ions with both MIKE and CID-MIKE spectra only compatible with the structure a: CH2=CH-C=O.
- The gas phase protonation of propynal leads to an ion having the structure c: HC≡CH-OH. The a and c CID-MIKE specta are quite different.
- The (C3H3O)+ ions generated from acetylenic alcohols molecular ions are expected to give a a and c mixture plus a third ionic species...

CONCLUSION

The cyclopropenium ion b could be a good candidat to explain the metastable decompositions of the ionized acethylenic alcohols. The fragmentations of these alcoholic ions will be better understood after calculations of their isomerization processes .

Table 1.Relative energy of the (C3H3O)+ ions expressed in kcal.mol-1.

Ion structure		I	II	III	IV	V	VI	VII
CH2=CH-C=O	a	0	0	0	0	0	0	0
CH-CH-C-OH	b	34.7	36.1	36.1	34	33	22	28.3
HC≡C-CHOH	c	17.1	15.5	27	33.1	36.9	42	41.3
H2C=C=C-OH	d	21.1	25.8	39.9	38	40	51	52
CH2=C-CHO	e	51.8	55.6	-	-	74	68	-
CH-CH-CH-O	f	43.1	56.7	-	78.9	77	68	-
HC=CH-CHO	g	-	58.6	-	-	71	72	-
CH2=C-CH-O	h	-	63.5	-	94.8	e	-	-
CH3-C=C=O	i	40.4	63.9	-	79	80.5	83	-
CH2-CH-C=O	j	a	77.5	-	100.3	102.7	99	-
CH3-C=C-O	k	39.6	111.2	-	122.8	123.3	102	-

I = MINDO/3, II = MNDO, III = 4-31G//MINDO/3 (1), IV = 3-21G//MNDO, V = 3-21G//3-21G, VI = 4-31G*//3-21G, VII = MP2/4-31G*//3-21G.

REFERENCE

(1) J.L. HOLMES, J.K. TERLOUW and P. BURGERS, Org. Mass Spectrom., 15, 140 (1980).

EXCITED STATES AND COLLISIONALLY ACTIVATED DISSOCIATION AT LOW ENERGIES. P.H. DAWSON, National Research Council of Canada, Ottawa K1A 0R6 Canada.

The simple system O_2^+ + Ar was first studied in a system where the source electron energy used in forming O_2^+ could be varied. Both charge transfer and collisionally activated dissociation were observed. This is a model system with only one long-lived excited state, the $a^4\pi_u$ at 4 eV above ground which has previously been examined in a tandem magnetic sector instrument.[1] Here the experiments were performed in a triple quadrupole[2] which collects ions scattered over a wide range of angles. Figure 1 shows relative yields of Ar^+ at a fixed target thickness for centre-of-mass collision energies of 2, 10.3 and 15.9 eV. Figure 2 shows similar data for the collisionally assisted dissociation to O^+. The importance of the $^4\pi_u$ state of O_2^+ is evident in both cases especially since even at 21.5 eV electron energy the fraction of the excited species is less than 0.2. Figure 3 compares the threshold regions for charge transfer for O_2^+ ions formed with electron energies of 14.5 eV and 21.5 eV. The expected thermochemical thresholds for the ground and excited states are indicated by arrows. Figure 4 shows similar data for the dissociation process. Cross-sections for the excited state are higher than for the ground state.

The second system studied was the dissociation of $C_6H_6^+$. Here a comparison was made of the threshold region for ions produced in an electron impact source which could be in a variety of electronically excited states and ions produced in a chemical ionization source which are expected to be in the ground state. Figure 5 shows the threshold region in the former case for $C_4H_4^+$, $C_3H_3^+$ and $C_2H_2^+$ production. Figure 6 shows measurements for the chemical ionization source for $C_4H_4^+$, $C_3H_3^+$ and $C_5H_3^+$ and Fig. 7 those for $C_4H_2^+$ and $C_2H_2^+$ at a very low target thickness. For the principal ions $C_4H_4^+$ and $C_3H_3^+$, there is a shift in threshold of several volts. The arrow indicates the thermochemical minimum energy for ground state dissociation for these species. For the ground state ions produced in the chemical ionization source, the thresholds were dependent on collision thickness (fig. 8) which has not been the case in our studies of several other chemical systems. A detailed analysis of the reaction kinetics showed the importance of an intermediate step in the dissociation of $C_6H_6^+$, presumably collisional activation to an electronically excited state, followed by its collisionally activated dissociation.

The important role of electronically excited states at low collision energies could influence the choice of standardized conditions for the acquisition and exchange of library spectra and might favour adoption of a higher collision energy.

1. T.O. Tiernan and R.E. Marcotte, J. Chem. Phys. 53 (1970) 2107
2. Sciex Inc. TAGA 6000

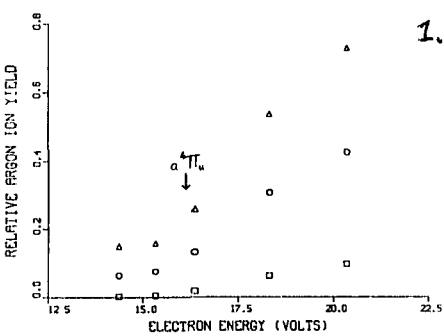

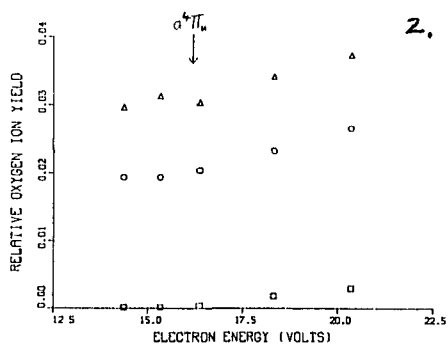

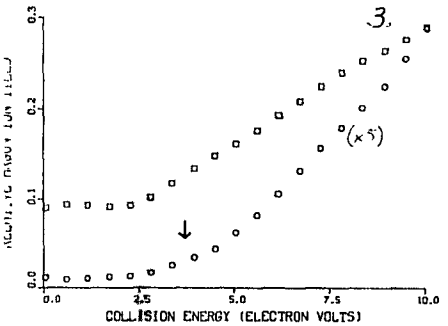
3.
(x5)
COLLISION ENERGY (ELECTRON VOLTS)

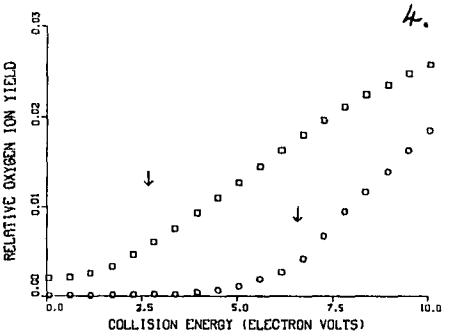
4.
RELATIVE OXYGEN ION YIELD
COLLISION ENERGY (ELECTRON VOLTS)

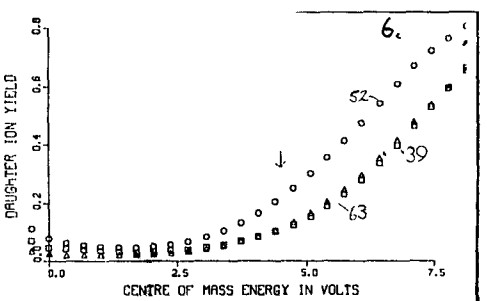
6.
DAUGHTER ION YIELD
52
39
63
CENTRE OF MASS ENERGY IN VOLTS

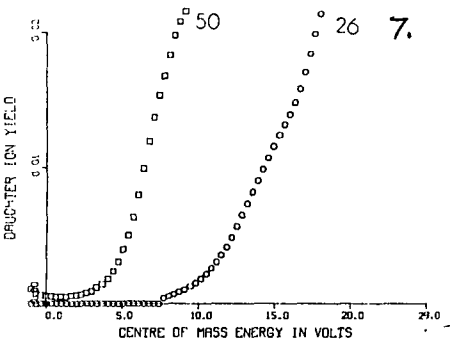
50
26
7.
DAUGHTER ION YIELD
CENTRE OF MASS ENERGY IN VOLTS

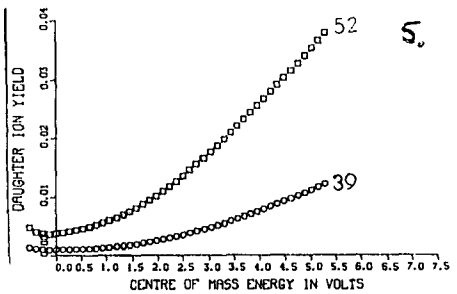
52
5.
39
DAUGHTER ION YIELD
CENTRE OF MASS ENERGY IN VOLTS

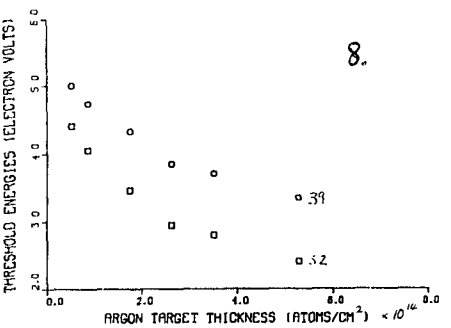
8.
THRESHOLD ENERGIES (ELECTRON VOLTS)
39
52
ARGON TARGET THICKNESS (ATOMS/CM²) × 10¹⁶

RPC 10 FOURIER TRANSFORM MASS SPECTROMETRY AS A PROBE INTO TRANSITION METAL ION CHEMISTRY

DONNAJEAN ANDERSON, DON L. BRICKER, TOM A. ADAMS, JR.

DEPARTMENT OF CHEMISTRY

TEXAS A&M UNIVERSITY

COLLEGE STATION, TEXAS 77843

The characterization of transition metal ions in the gas phase is a rapidly expanding field due to the advent of techniques that allow studies on a molecular level. Such techniques include ion cyclotron resonance spectroscopy (ICR), supersonic beam expansion, cross-beam techniques, and fourier transfrom mass spectrometry (FTMS). A major emphasis of our research program is the use of FTMS as a probe into the positive and negative ion chemistry of transition metal carbonyls by ion-molecule reactions. The objectives of these studies include the study of the reactivities of metal ions with other metal containing species, the synthesis and characterization of metal cluster ions, and utilization of these clusters as catalytic models, e.g. C-H and C-C bond insertion reactions. These studies are further enhanced by the use of ion-ejection methods and pulsed-value sample introduction.

Ion ejection technique can be used to mass-select a particular ion of interest and follow its reaction sequence without interference from other ions. For example, ionization of $Cr(CO)_6$ produces intense signals corresponding to Cr^+, $Cr(CO)^+$ and $Cr(CO)_2^+$ ion. Using ion ejection, the Cr^+ ion can be selected and a suitable delay employed in which the Cr^+ can react with the neutral $Cr(CO)_6$ to form cluster ions. This methodology is used to follow clustering reactions for ions produced by $Cr(CO)_6$, $Fe(CO)_5$, $Co(CO)_3NO$, and $Ni(CO)_4$ in the positive mode.

In all of these systems, one interesting aspect surfaced; the product ions are formed by a particular reaction sequence, i.e. the products formed by M^+ differ from those formed by $M(CO)_x^+$. In particular, the different reactant ions give rise to product ions of different coordination unsaturation; for example the metal-to-ligand ratio (M/L) varies from 0.2-1.0. The $Cr(CO)_6$ and $Fe(CO)_5$ systems produced product ions that are more highly saturated; whereas, the $Co(CO)_3NO$ and $Ni(CO)_4$ system result in product ions that are more highly unsaturated, e.g., the $Co(CO)_2^+$ ion reacts with the neutral $Co(CO)_3(NO)$ to produce cluster ions with a M/L ratio of 1.0. The most unsaturated cluster ions, i.e. those made from Co(CO) NO, were then chosen for further studies.

Ion ejection, coupled with pulsed value sample introduction, was employed in the study of the reaction of $Co_2(CO)_3(NO)^+$ with H_2. The reactivity of the metal ionic systems with the neutral metal carbonyls requires the use of pulsed value sample introduction for the non-metal reactant.

The negative ion chemistry of $Cr(CO)_6$ was studied extensively using the methods described. Upon ionization of $Cr(CO)_6$, the anion $Cr(CO)_5^-$ is formed. This ion reacts with O_2 to produce $Cr(CO)_3O_2^-$ and $Cr(O_3)^-$. The chemistry of $W(CO)_6$ is analogous to $Cr(CO)_6$, i.e. upon ionization the $W(CO)_5^-$ anion is formed and this ion readily reacts with O_2 to produce $W(CO)_3O^-$ and WO_3^-. Due to the apparent high oxidation state of the CrO_3^-, investigations of the oxidizing ability of this compound in the gas phase were undertaken. CrO_3^- showed little tendency for normal oxidation when reacted with numerous organics. However, this ion did show interesting reactions with nitrogen containing aromatics. For instance; the following products were observed when CrO_3^- was reacted with pyrole and pyridine.

$$CrO_3^- + C_5H_5N \rightarrow [CrO_3HCN] + \underset{m/z\ 52}{C_4H_4^-}$$

$$CrO_3^- + C_4H_5N \longrightarrow \begin{cases} CrO_3 + C_4H_4N^- \\ Cr(C_4H_3N)^- + OH + O_2 \\ \quad\downarrow \\ Cr(C_4H_2N)^- + H \end{cases}$$

MASS SPECTROMETRIC INVESTIGATION OF GASEOUS MOLECULES FROM THE VAPORIZATION OF $ZnGa_2Se_4(s)$

Lawrence E. Grimes and Jimmie G. Edwards
Department of Chemistry
University of Toledo
Toledo, Ohio 43606

Use of compounds containing ZnSe and Ga_2Se_3 in solid state devices has aroused interest in the vaporization of the ZnSe-Ga_2Se_3 system. Mass spectrometric investigation of ZnSe[1,2] and Ga_2Se_3[3] report both to vaporize congruently. The goal of this investigation was to identify the gaseous species from the vaporization of $ZnGa_2Se_4$ and determine the mode of vaporization in the temperature range 1050-1170 K.

Experimental

The mass spectrometer was a Nuclide 12-90 HT with a movable shutter to distinguish molecules from the Knudsen cell from the background. The sample was vaporized from a graphite Knudsen cell heated by radiation. Temperatures were measured with an optical pyrometer.

Ions were produced by bombardment with 75 V electrons and identified by their mass, isotopic distribution, and shutter effect. The intensities of the major isotopic ions of each species were investigated at sample temperatures in the range 1050-1170 K. Total intensity of each species was calculated with isotopic fractions.

In a separate experiment, vapor pressures were measured directly by the simultaneous Knudsen-torsion effusion method[4], which gave the average molecular weight of the vapor species as well.

Results

The results of shuttered peak intensity data could be divided into two regions. Gaseous ions were found to be Se_2^+, Zn^+, Se^+, Ga^+, and Ga_2Se^+. The ionic intensities relative to that of Se_2^+ were constant in Region I. They were 1.00, 0.92, 0.32, 0.06, and 0.06, respectively with uncertainty of ± 0.03. In Region II, the relative intensity of Zn^+ decreased continuously with time, while that of Ga^+ and Ga_2Se^+ increased continuously with time.

Total pressures measured in Region I by the Knudsen-torsion effusion method were to calibrate partial pressures from I^+T values. The univariance of pressures in Region I was interpreted in terms of the reaction

$$ZnGa_2Se_4(s) = Ga_2Se_3(ss) + Zn(g) + 1/2\ Se_2(g) \qquad [1]$$

Third-law analysis gave a value of $\Delta H°(298\ K)$ of 385.9 ±0.7 kJ/mol for the reaction. Assuming $Ga_2Se_3(ss)$ an ideal solution, the enthalpy of combination of the binary selenides in $ZnGa_2Se_4(s)$ is -26.5 ±0.9 kJ/mol.

The average molecular weight of the vapor measured in Region I by Knudsen-torsion method was 113.6 ±5.2. The molecular weight calculated from ionic intensities was 130.5. The molecular weights of congruently vaporizing ZnSe, $ZnGa_2Se_4$, and Ga_2Se_3 are 100.9, 155.8, and 189.4, respectively.

Discussion

The ionic species from the vapor over $ZnGa_2Se_4(s)$ were Se_2^+, Zn^+, Se^+, Ga^+, and Ga_2Se^+. Two distinct regions observed in log I^+T vs 1/T plots of the ions revealed that the vaporization is not congruent. The average molecular weight of the vapor from Knudsen-torsion effusion along with the ionic intensity measurements in Region I indicate that Zn(g) and $Se_2(g)$ are the primary vapor species. Continued heating of $ZnGa_2Se_4$ results in vaporization of a solid solution observed in Region II.

References

1. P. Goldfinger, and N. Jeunehomme, Trans. Faraday Soc., 59, (1963) 2851.
2. G. DeMaria, P. Goldfinger, L. Malaspina, and V. Piacente, Trans. Faraday Soc., 61, (1965) 2147.
3. O. M. Uy, D. W. Muenow, F. J. Ficalora, and J. L. Margrave, Trans. Faraday Soc., 64, (1968) 2998.
4. R. Haque, A. S. Gates, and J. G. Edwards, J. Chem. Phys., 73, (1980) 6301.

THERMODYNAMICS OF THE VAPOR PHASE OVER LIQUID InTe AT 1106 ± 2 K

RAMAN S. SRINIVASA and JIMMIE G. EDWARDS

Department of Chemistry
University of Toledo
Toledo, OH 43606

Introduction: The study of indium telluride is of interest because of its applications in solid state devises: nuclear radiation detectors, photoconductors and heterojunction devices. Knowledge of the chemistry and thermodynamics of the gas phase over indium tellurides will be useful in the preparation of such devices by vapor phase growth. In this paper we report our analysis of the vapor phase over InTe(l) at 1106 ± 2 K and thermodynamics of the reaction:

$$2\ In_2Te(g) + Te_2(g) = 2\ In_2Te_2(g) \qquad (1)$$

Colin and Drowart[1] studied the gas phase equilibria among indium tellurides. They reported that the gas phase over liquid In_2Te_3 contained In(g), Te(g), Te_2(g), In_2Te(g) $InTe_2$(g) and In_2Te_2(g) and that their partial pressures varied during the course of evaporation. We carried out a total exhaustion experiment on liquid InTe at 1106 ± 2 K. We analyzed the fragmentation of parent ions and arrived at the gas phase composition.

Experimental: InTe(s) was prepared by heating the elements in evacuated, sealed, Vycor tubes. A nuclide 12-90 HT Knudsen-cell mass spectrometer was used. A movable shutter could be used to focus the molecular beam from the Knudsen-cell into the ionization chamber of the mass spectrometer and to discriminate against the background gases. A sample of 9.39 ± 0.05 mg of InTe(s) in a graphite Knudsen-cell was evaporated completely while the intensities of ions were measured as functions of time. In separate experiments electron multiplier gains and appearance potentials (AP) were measured. The potential scale was calibrated with the appearance potentials of Hg^+, CO_2^+, H_2O^+ and Te_2^+.

Results: In^+, In_2^+, $InTe^+$, In_2Te^+, Te^+, $InTe_2^+$, Te_2^+ and $In_2Te_2^+$ were observed. Their appearance potentials were measured to be 7.3, 9.3, 8.3, 7.9, 9.6, 7.8, 8.4 and 7.2 V, respectively. The uncertainties were estimated to be less than 0.3 V. Comparison of these values with those in literature suggested that In^+, In_2^+, $InTe^+$, $InTe_2^+$ and Te^+ were fragment ions. The ion intensities as functions of time fell in three regions. (Figure 1). In the first region, the intensities sharply increased with the sample temperature. In the second region of constant temperature, (1106 ± 2 K) they continuously dropped to a point of discontinuity, where $In_2Te_2^+$, $InTe_2^+$, Te_2^+, In_2^+, $InTe^+$ and In_2Te^+ dropped below the sensitivity limit of the instrument. At this point, In^+ dropped by a factor of 15, and that of

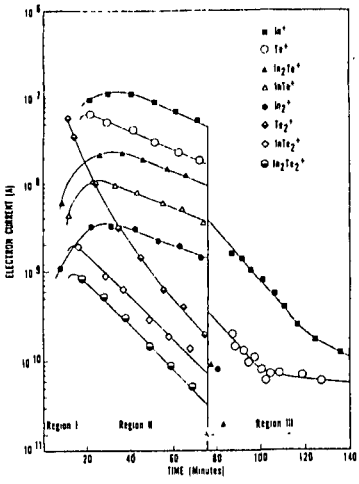

Figure 1: Variation of ion intensities, measured as electron currents at the electron multiplier output, and corrected for the isotopic fractions, with time.

Te^+ by a factor of 60. In the third region at the same sample temperature, the In^+ and Te^+ intensities continuously dropped to a value about a thousandth of their maximum intentsities. At this stage, the variation of ion intensities with the shutter position, suggested that they originated from the radiation shields.

In the second region of the intensity-time plots, curves of In^+, In_2^+, Te^+, $InTe^+$ and In_2Te^+ were parallel and indicated that a single precursor contributed nearly completely to the formation of these ions. The curves of $In_2Te_2^+$ and $InTe_2^+$ were parallel and indicated a common precursor. The curve for Te_2^+ was unique. These observations and the appearance potentials led to the proposition that $In_2Te(g)$, $Te_2(g)$ and $In_2Te_2(g)$ were the major constituents of the vapor phase over molten InTe at the experimental temperature.

Hypothetical equilibrium constants were calculated for various gas phase equilibria with the assumption that all ions were parents. The variation of these hypothetical equilibrium constants with time supported our conclusion previously drawn from intensity-time plots and appearance potentials. The mass spectrometer was calibrated with the integrated ion intensities and fragmentation schemes. Partial pressures of the vapor species were calculated from the ion intensities. The gas phase equilibrium constant for the reaction (1) was found to be $(1.81 \pm 0.10) \times 10^{-3}$ Pa^{-1}. With the free energy functions from Colin and Drowart[1], the standard enthalpy of reaction (1) was found to be -310.9 ± 0.5 kJ against 287 ± 13 kJ reported. The latter difference arises because our work led to a better understanding of the fragmentation schemes in this system.

Reference: 1) R. Colin and J. Drowart, Trans. Farad. Soc. 64, 2611, (1968).

GC/FI/MS AND GC/EI/MS ANALYSIS
OF A MONOAROMATIC FRACTION
FROM KERN RIVER CRUDE

E. J. Gallegos
Chevron Research Company, Richmond, CA 94802-0627

GC/MS in the field ionization and electron impact mode were used to analyze a distillate, liquid chromatograph monoaromatic fraction from Kern River crude. The sample was composed of pentacyclic terpanes, monoaromatized Steranes at varying degrees of unsaturation, and other monoaromatized tetracyclics and/or pentacyclics not related to Steranes.

Field ionization mass spectrometry, FI/MS, is very useful in obtaining the molecules weight profile and Z, C_nH_{2n-z}, category of hydrocarbon components.

This molecular ion information, however, does not distinguish between possible component-type differences within a Z category, even though the separation procedure does give clues to the type of molecule that might be expected with respect to the number of rings or double bonds.

Figure 1 shows the GC/EI/MS map display of the most prominent components in this fraction. These components have been reported previously[1] and are due to monoaromatized petroleum sterates with a structure similar to that shown. The components with a base peak of m/z 253 do not give a parent ion by electron impact, but the parents can be observed in comparable GC/FI/MS runs. This is shown in Figure 2.

A summary of the remaining components is given in Table I.

Figure 1. Map Display of Z = -11, -12 Components of a Kern River Monoaromatic Fraction

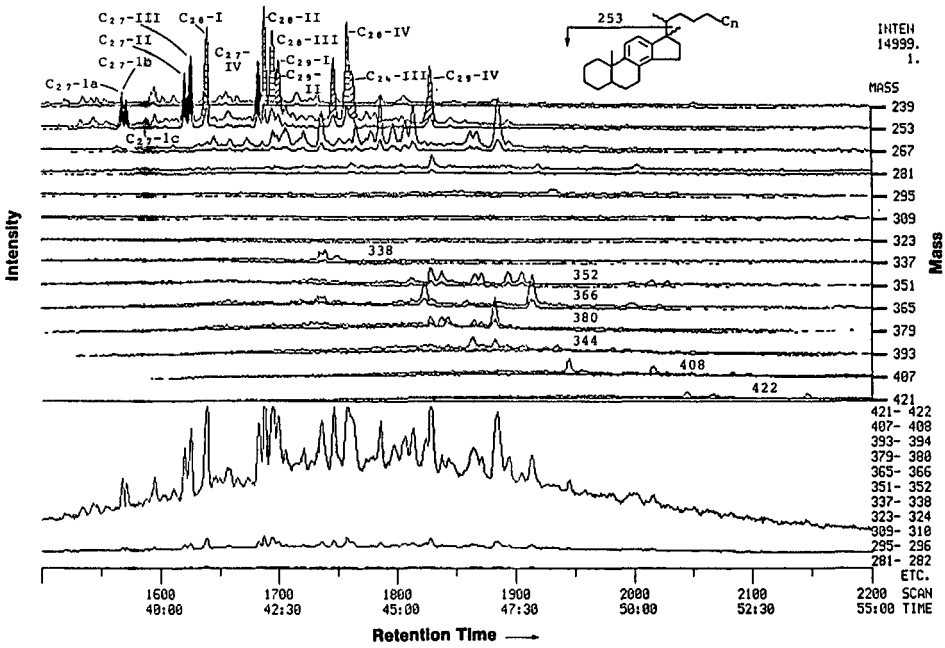

Figure 2. Comparison of the GC/EI/MS Molecular Ion Profile to the GC/EI/MS Fragment Ion Profile for the Z = 12 Components

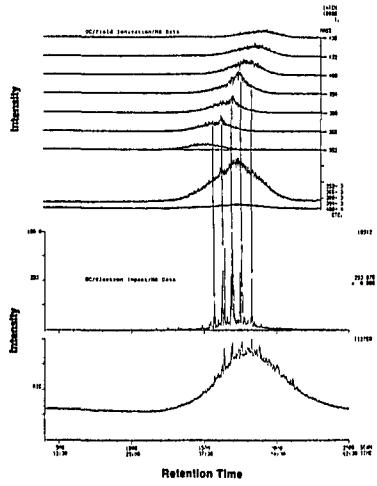

Table I. Quantitation of "Biomarkers" by Type

Monoaromatized Steranes (Base Peak M/Z 253) Z = -12	
C_{27}	11%
C_{28}	19%
C_{29}	7%
Total:	37%
Monoaromatized Steranes (Base Peak M/Z 267) Z = -12	
C_{27}-C_{29}	4%
Monoalkene Monoaromatized Steranes (Base Peak M/Z 251) Z = -14	
C_{27}	2%
C_{28}	4%
C_{29}	2%
Total	8%
Dialkene Monoaromatized Steranes (Base Peak M/Z 255) Z = -10	
C_{27}	3%
C_{28}	5%
C_{29}	2%
Total	10%
Hopanes (Base Peak M/Z 191) Z = -8	
C_{27}	2%
C_{28}	2%
C_{29}	2%
C_{30}	4%
Total	10%
Monoaromatized Tetracyclics (Base Peak 201) Z = -12	
C_{29}-C_{31}	6%
Monoaromatized Tetracyclics (Base Peak at $(M-1)^+$) Z = -12	
C_{25}-C_{29}	4%
Monoaromatized Tetracyclic Alkenes (Base Peak $(M-1)^+$) Z = -14	
C_{25}-C_{28}	5%
Monoaromatized Tetracyclic Alkenes (Base Peak $(M-15)^+$) Z = -14	
C_{20}-C_{27}	5%
Monoaromatized Tetracyclic Dialkene (Base Peak $(M-1)^+$) Z = -10	
C_{27}-C_{29}	2%
Monoaromatized Tetracyclic Dialkenes (Base Peak $(M-15)^+$) Z = -10	
C_{27}-C_{29}	2%

References

1. Siefert, W.K.; Carlson, R.M.K.; and Moldowan, J.M., "Advances in Organic Geochemistry 1981," John Wilson and Sons, Ltd., 1983, pp 710-724.

FD-MS, FAB-MS, and ESR Oxidation Studies of Partially Hindered Amines - 3,3-Dialkyldecahydroquinoxalin-2-ones.

by

R. W. Layer, J. T. Lai, R. P. Lattimer, and J. C. Westfahl

The BFGoodrich Research and Development Center
9921 Brecksville Road
Brecksville, Ohio 44141

Fully hindered amines are known to be excellent UV stabilizers which retard the photodegradation of polyolefins, but they are not very effective thermal stabilizers. Their acivity centers around their ability to form stable nitroxyl radicals which function as chain breaking electron aceptors but not as chain breaking hydrogen atom donors in the free radical oxidative process. Partially hindered amines, those that possess an alpha hydrogen atom, are generally much less effective as UV stabilizers. This has been related to the known instability of their nitroxyl radicals. For example, it has been found that nitroxyl radicals of partially hindered amines are very unstable with life-times of only a few seconds. We have found that a class of partially hindered bicyclic amines, 3,3-dialkyldecahydroquinoxalin-2-ones, are excellent UV stabilizers and, more interestingly, excellent thermal stabilizers for polypropylene.

We used three techniques - FD-MS, FAB-MS, and ESR - to study the oxidation of 3,3-dialkyldecahydroquinoxalin-2-ones with m-chloroperbenzoic acid. These three methods all provide complementary information to help elucidate chemical structures for the free radical products. FD-MS was particularly useful in identifying the molecular weights of components in product mixtures. ESR identified the types of radicals that were present. Our results show that two types of radical species are formed. The initial oxidation produces nitroxyl radicals which are surprisingly stable. These nitroxyl radicals yield six line ESR spectra resulting from the hyperfine splitting of the nitrogen atom and the alpha hydrogen atom (Figure 1, Radical I). An excess of peroxide yields a radical with a three line ESR spectrum (Figure 1, Radical II), indicating a fully hindered amine (i.e., no alpha hydrogen). Mixtures of the two radicals yield complex nine line spectra (Figure 1, Radical I + II).

The appearance of these radicals was also followed by FD- and FAB-MS. Figure 2 is a typical FD mass spectrum in which both radicals are present. The principal ions observed are m/z 312 ($M^{+\cdot}$ for the starting amine), m/z 328 (Radical I + H)$^{+\cdot}$, and m/z 342 (Radical II + H)$^{+\cdot}$. FAB mass spectrometry (thioglycerol matrix) yielded similar results, except that the principal quasimolecular ions are m/z 313 (MH^+ for the amine), m/z 329 (Radical I + 2H)$^+$, and m/z 343 (Radical II + 2H)$^+$.

Plausible structures for the types of radicals observed are shown in Scheme I. Our rsults suggest that this class of compounds may function as antioxidants via their two nitroxyl radicals and as hydrogen atom donors (see Scheme I).

FIGURE 1. ESR SPECTRUM OF AN OXIDIZED 3,3-DIALKYLDECAHYDROQUINOXALIN-2-ONE.

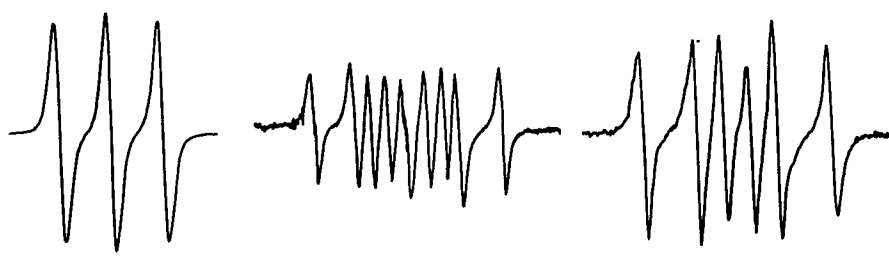

RADICAL II RADICAL I + II RADICAL I

SCHEME I

POSSIBLE MECHANISM for the ANTIOXIDANT and LIGHT STABILIZATION ACTIVITY of 3,3-DIALKYLDECAHYDROQUINOXALIN-2-ONES

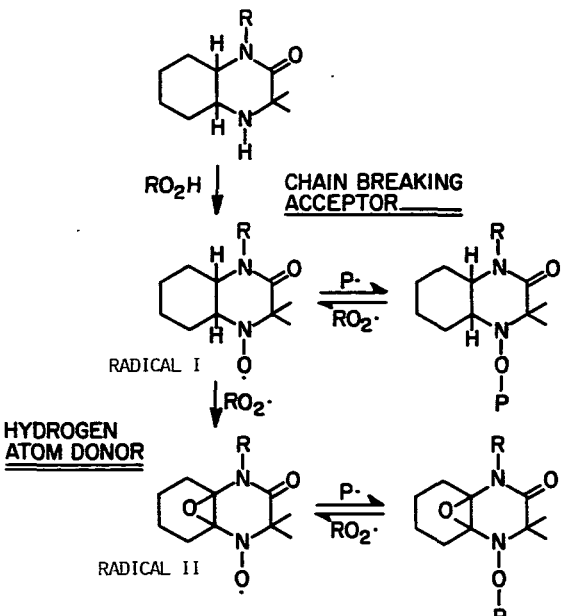

FIGURE 2. FD MASS SPECTRUM OF AN OXIDIZED 3,3-DIALKYLDECAHYDROQUINOXALIN-2-ONE.

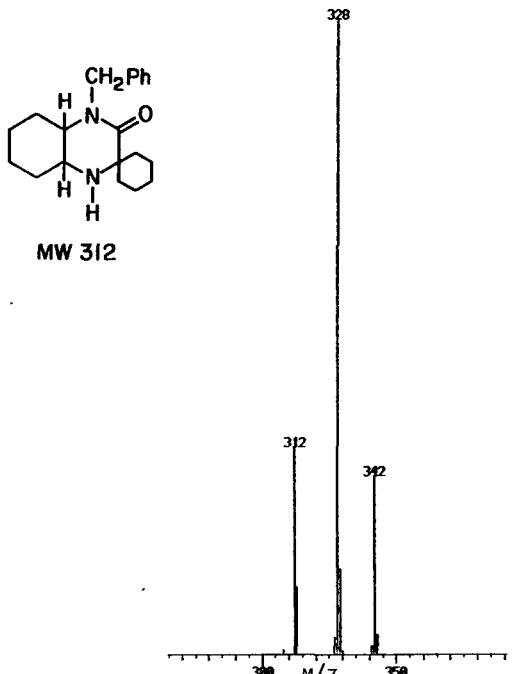

FAB/MS ANALYSIS OF HI-6 AND ITS DEGRADATION PRODUCTS. W. BONE, J. MARASCO, L. KAZYAK, and B.P. DOCTOR, Walter Reed Army Institute of Research, Division of Applied Biochemistry, Washington, D.C. 20307

Severe poisoning by organophosphorus compounds (e.g. insecticides and nerve agents) occurs from the inhibition of cholinesterase activity, resulting in an accumulation of acetylcholine in the effector organs. When the accumulation occurs near the ends of motor nerves to skeletal muscle, the resulting neuromuscular block causes such effects as weakness and fasciculation. The accumulation of acetylcholine is thought to cause the persistent depolarization of the end plate region, and the block appears to last until partial restoration of cholinesterase activity in the muscle occurs. In severe anticholinesterase intoxication, central respiratory paralysis and paralysis of the peripheral respiratory musculature occurs, resulting in death.

One of the more widely used therapeutic antidotes for organophosphate poisoning, atropine, has little or no influence on the above symptoms. Atropine does however treat the muscarine-like effects caused by accumulation of acetylcholine at postganglionic cholinergic nerve endings to smooth and cardiac muscle and secretory glands (symptoms of vomiting, abdominal cramps, sweating, etc.)

Therefore, studies of drugs that reactivate acetylcholinesterase have been undertaken with the assumption that once the enzyme has been reactivated with such an antidote, it will perform its normal function of destroying the accumulated acetylcholine and the syndrome of poisoning should abate.

The present study has focused on one of the most promising new drugs for anticholinesterase poisoning, HI-6. Clearly there is a need to assay not only the activity of HI-6, but also its stability at various temperature and pH values.

The objective of the present study was to obtain a convenient, reliable assay for this class of bispyridinium oximes used as potent therapeutic compounds for organophosphate poisoning.

Reported here are the first mass spectral data on the bispyridinium oxime, HI-6. Due to the ionic nature of the compound, EIMS and CIMS are unsuccessful in obtaining molecular weight and other essential mass data. FABMS was used success-

fully, as shown in the spectra below, to obtain mass information for use as a stability probe in conjunction with HPLC, UV, and NMR analysis. Studies in this laboratory (both completed and in progress) reveal a marked effect of temperature and pH on the degradation of HI-6. Some of these products are shown below.

We conclude that 1) FABMS is an effective probe in the analysis of certain bispyridinium compounds, 2) the stability of HI-6 exhibits a temperature and pH dependence due to the oxime and carboxamide moieties, along with the presence of an ether linkage between the pyridine moieties; this was concluded upon investigation of several analogues of HI-6, 3) FABMS may be used in the analysis of certain polycharged organic compounds, with the apparent reduction in the gas phase giving molecular weight information.

POS. ION FAB OF HI-6 BEFORE AND AFTER HYDROLYSIS

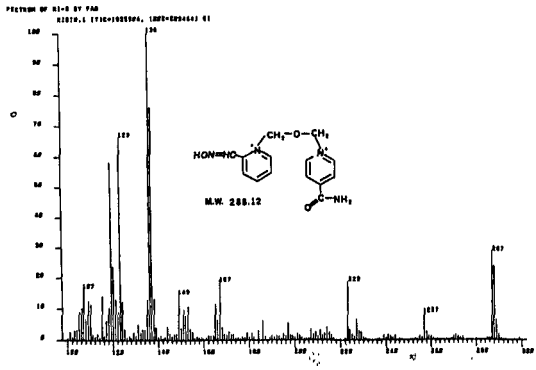

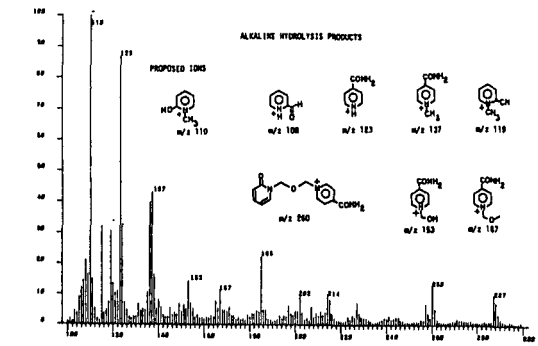

Californium Plasma Desorption Mass Spectrometry of Cationic, Anionic and Neutral Dyes

L.K. Pannell, H.M. Fales and E.A. Sokoloski, Laboratory of Chemistry, NHLBI, Bethesda, MD 20205; and
R.L. Tate, DCRT, Computer Systems Laboratory
NIH, Bethesda, MD 20205

In order to compare Cf^{252} plasma desorption mass spectrometry with SIMS, and to gain insight about the desorption/ionization process, we have investigated a series of dyes (Aldrich) similar to those studied by Cooks et al. (Scheifers, S.M., Verma, S., and Cooks, R.G., Anal. Chem. 1983, 55:2260). These include quaternary amines (Crystal Violet, Methyl Violet 2B, Brilliant Cresyl Blue, Neutral Red, Brilliant Green, Methylene Blue, Pinacyanol Chloride, Rhodamine B Base) sulfonic acid sodium salts (Acid Blue 25, Metanil Yellow, Thymol Blue, Acid Alizaren Violet N, Brillant Sulphaflavine, dications and dianions (Methyl Green, Eosin Y, Lucifer Yellow V/S, Thorin Indicator, Bis-N-Methylacridinium Nitrate, Blue Tetrazolium, Naphthochrome Green) and neutral dyes (Methyl Red, Pyrogallol Red, Methyl Yellow, Malachite Green Base, Acridine Orange Base, Tetrabromophenol Blue, Mordant Brown 24, Eosin Y Free Acid, Fluorescein, Bismark Brown Y, Aluminon).

The simple quaternarys and the dicationic dyes showed spectra strongly resembling SIMS, with somewhat less fragmentation visible. Neutral dye spectra also resembled their SIMS counterparts and the same effect (intensification of M + H) was noted when Methyl Yellow was oversprayed with p-toluensulfonic acid. We conclude that the mev and kev desorption processes are, in this regard at least, basically similar. The quatenary dyes, with the exception of Rhodomine B Base, provided poor spectra when run in the negative ion mode. The sodium sulfonates, however, showed intense M-Na negative ions along with M + Na positive ions (sodiated sodium salts).

No dications or dianions were observed in the corresponding dyes. Instead, addition of hydride ion, loss of a single sodium ion, and loss of singly charged fragments occurred to provide singly charged species related to the original dication and dianion. No useful spectra were obtained with Thorin Indicator or Naphthochrome Green.

Neutral dyes provided the expected intense positive and negative ions by gain or loss of H^+. Aromatic substitution of bromine enhanced the negative ion spectra and reduced the positive ion spectra although loss of up to 6 bromine atoms was easily discerned in the case of Tetrabromophenol Blue. Intense ions at $M-H^+$, $[M-CO_2-H_2-H]$ etc., were all easily correlated with formation of cyclic structures allowing extended conjugation or placement of charge on the appropriate heteroatoms. It is concluded that the Cf^{252} plasma desorption method is especially well suited to corroborating and identifying dye structures.

Identification of Rubber Additives by
Field Desorption and Fast Atom Bombardment Mass Spectrometry.

R. P. Lattimer, R. E. Harris, D. B. Ross, and H. E. Diem
The BFGoodrich Research and Development Center
Brecksville, Ohio 44141

The identification of ingredients in a rubber vulcanizate is a difficult task for the analytical chemist. The compound generally must be separated into various fractions prior to identification using a number of chromatographic and/or spectroscopic methods. In a typical analysis scheme, the rubber is extracted with a solvent to remove organic additives such as plasticizers, processing oil, stabilizers, and curatives. The chemical identification of these additives is most often accomplished by infrared spectroscopy (IR).

We have examined several rubber extracts by two desorption ionization techniques - field desorption (FD-MS) and fast atom bombardment (FAB-MS). As an example, FD (Figure 1) and FAB (Figure 2) mass spectra are included for a particular extract. This sample was from an EPDM rubber hose cover that had been extracted with acetone overnight in a Soxhlet apparatus. IR analysis indicated the presence of a phthalate plasticizer, an aromatic amine antioxidant, and an aliphatic processing oil and/or a paraffin wax. The FD and FAB spectra were able to establish the exact identities of these components. The plasticizer is dioctylphthalate (DOP), as evidenced by $M^{+\cdot}$ 390 and $(M+H)^+$ 391 in both the FD and FAB spectra. The well-known DOP fragment ions at m/z 279, 167, and 149 were prominent in the FAB spectrum. The antioxidant yielded $M^{+\cdot}$ 219 in both FD and FAB, which is due to phenyl-β-naphthylamine (PBNA).

The hydrocarbon component was observed as a series of aliphatic molecular ions in FD between m/z 310 and 380 (MW = C_nH_{2n+2}). These oligomers are no doubt due to a paraffin wax rather than to a processing oil, since typical processing oils do not display this orderly distribution of aliphatic oligomers. Note that wax molecular ions were not observed in the FAB spectrum, since (1) the hydrocarbon oligomers are nonpolar and (2) the oligomers tend to fragment during the FAB process. Some of the lower mass fragment ions in the FAB spectrum undoubtedly arise from wax oligomers.

From our results on this sample and others, it is clear that FD-MS and FAB-MS are very effective analytical methods for the identification of organic additives in extracts from rubber compounds. These desorption ionization techniques supplied molecular weight information that provided a nice complement to IR data obtained on the same samples. In cases where IR could give only a general component identification (i.e., a compound class), the mass spectral data provided a very specific compound identification. Both FD and FAB produced simplified mass spectra compared to that which is obtainable by the traditional electron impact ionization (EI-MS) technique.

FIGURE 1. FIELD DESORPTION MASS SPECTRUM OF RUBBER HOSE COVER EXTRACT.

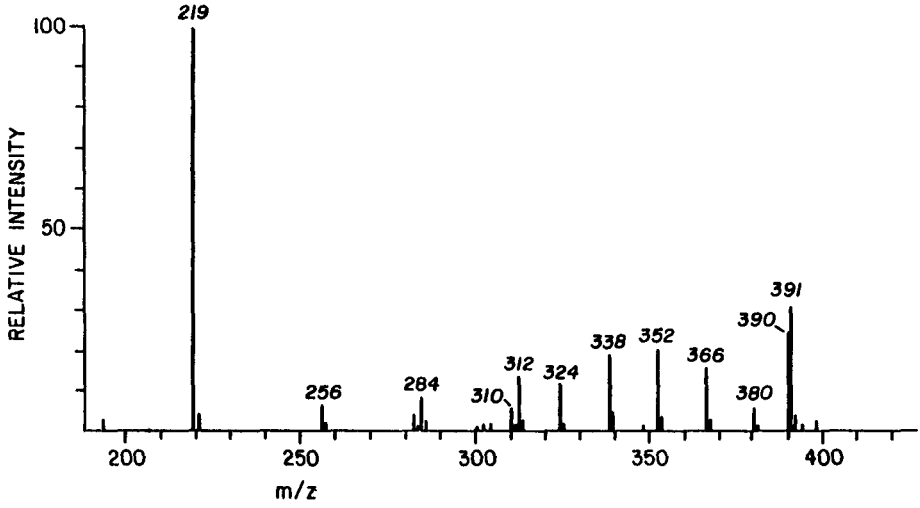

FIGURE 2. FAST ATOM BOMBARDMENT MASS SPECTRUM OF RUBBER HOSE COVER EXTRACT.

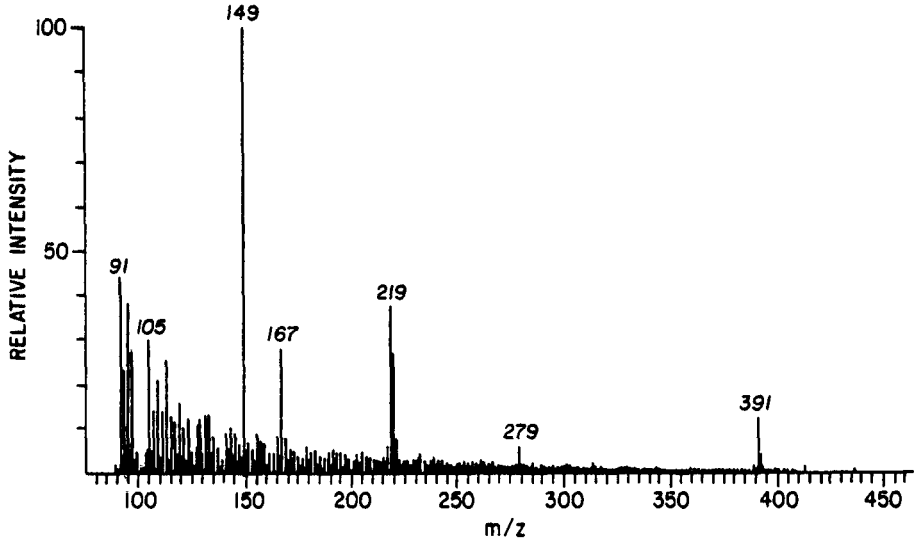

Enhancement of Fast Atom Bombardment Spectra by Charge Transfer Derivatization

K.J. Kroha, G.C. DiDonato, and K.L. Busch*
Department of Chemistry, Indiana University, Bloomington, IN 47405

Reverse derivatization reactions can be of three types: mass transfer, charge transfer, or ion segregation. Proton transfer reactions and the functional group specific reagents described here belong to the first category. In mass transfer derivatization, charge is transferred to the neutral analyte by a reaction which forms a new chemical bond. Charge transfer reactions are of the general type: Donor + Acceptor $\longrightarrow\longrightarrow$ Donor$^{+\cdot}$ + Acceptor$^{-\cdot}$. The spectral effects of the charge transfer reactions are more subtle than the mass transfer reactions, and the effects of the surrounding matrix much more significant. The third category of reverse derivatization processes are those which physically separate the cations and the anions and impose an overall order on the mixture of preformed ions. A good example of a reagent in this class is a crown ether, with well-defined interactions with such cations as sodium and potassium, but also with ammonium cations.

Mass Transfer: Of the three derivatization strategies this has to date been the most successful. Reagents can be chosen such that they react specifically with chosen functional groups. For instance, pyrylium salts react with primary amines to form pyridinium salts observed as intact cations in the FAB spectra. The spectrum of 2,5-dimethylaniline treated with 2,4,6-triphenylpyrylium tetrafluoroborate, for example, contains as its base peak (other than solvent ions) the intact cation at m/z 412. Aldehydes and ketones can be reacted with several reagents to create preformed ions. With pyrrolodinium perchlorate, they react to form ions observed as intact cations at a mass of (M+54) where M is the molecular weight of the neutral. Girard's Reagents (P and T) react with ketones and ketosteroids to produce water-soluble ionic derivatives often used in separating these compounds from non-ketonic matrices. They can be used as reverse derivatization reagents to create preformed ions for FAB analysis. The spectrum of derivatized 5 -androstan-17-one is given in the Figure. This reagent should be useful in the analysis of ketones directly from non-reacting matrices.

Charge Transfer: Another means of separating charges in the condensed phase is the formation of charge transfer compounds between strong electron donors and acceptors and their subsequent ionization. We have studied the FAB spectra of these compounds. Acceptors have included TCNQ and TCNE. Polynuclear aromatic hydrocarbons (PAHs) have been used as donors because of the importance of their analysis in complex matrices such as coal and coal liquids. The enhancements observed in the $M^{+\cdot}$ abundances for the mixture of donor and acceptor over those from the underivatized sample average only about a factor of two. This enhancement is not nearly as large as can be expected from even simple acid/base reaction. The most useful of the charge transfer reagents are likely to be picric acid and 2,4,7-trinitrofluorenone, as both of these compounds form useful charge transfer complexes with the PAHs. Chromatographic separation the PAHs can be based on the reversible formation of charge transfer compounds of this type.

The influence of solvents on charge transfer chemistry is substantial. Most complexes do not involve a formal transfer of charge when dissolved in a solvent of low polarity, and the complexes exist as isolated pairs with an overall neutral charge. In polar solvents, solvation of the radical ions increases the extent of ionization. For instance, ferrocene-TCNE in cyclohexane exists as the paired complex, but in acetonitrile, the separated radical species are present. The degree of ionization in glycerol has not been established, but there is evidence that many of the complexes are not ionized. It is an inherent disadvantage of FAB that the sample must be dissolved in a liquid matrix. Although matrix modifications that increase dissociation of the complex are being studied, more pronounced effects of charge transfer derivatization may be found in those desorption ionization techniques that sample neat rather than matrix diluted samples.

Sample Preparation: Methods of sample preparation in reverse derivatization are fairly important. Not only must the reactions proceed in high yield with a minimum of side reactions, but the products must be formed in a matrix convenient for sampling. Of four support materials [celite, cellulose acetate, powdered activated charcoal, and powdered molecular sieve (5A)], celite performed best in encapsulating reagents and reaction products so that reaction could take place on a small, readily controlled scale. Glycerol is added to the celite after reaction, and the mixture is placed on the FAB platform. The glycerol extracts the derivatives from the celite. The celite itself yields no ions in the FAB specturm. Preloading a support with a derivatizing reagent, such as the pyrylium salts, Girard's reagent, or even charge transfer reagents, allows reaction to occur as volatile samples are passed over the support. The reaction products are non volatile salts, and can be stored for later analysis. The use of charge transfer reagents in this way mimics their use as column packings in the separation of mixtures. The use of ion exchange resins as supports yields new ions in the mass spectra as anions or cations are replaced, and provides a convenient means of creating ions of novel composition *in situ*.

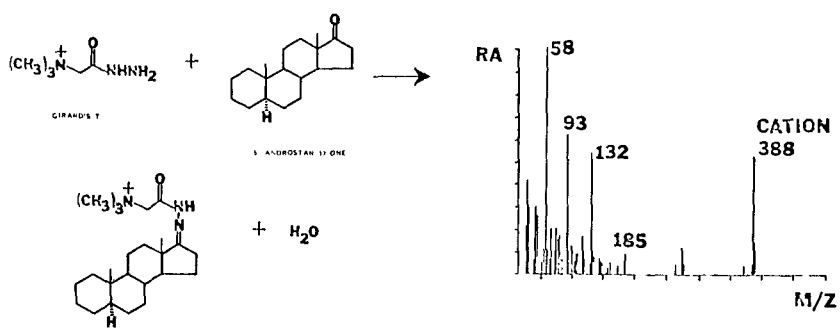

FAB-MS DIRECTLY FROM ELECTROPHORETIC PLATES.
APPLICATIONS TO QUATERNARY ORGANOARSENIC COMPOUNDS

D. F. Barofsky and M. L. Zimmerman
Oregon Graduate Center
19600 N. W. Walker Road
Beaverton, OR 97006

Marine organisms are known to accumulate inorganic arsenic and to biosynthesize stable organoarsenic compounds. Arsenobetaine has been found in high quantities in a number of marine organisms in the higher trophic levels, and strong evidence has been presented for the presence of arsenocholine in shrimps. Most of the organoarsenicals are apparently synthesized in the lower stages of the marine food chain. Since consumption of seafoods may contribute significantly to the total arsenic burden in human beings, confirmation of the structures of organoarsenicals in the marine food chain is an important analytical pursuit.

The identification of components directly from paper chromatograms by SIMS (1) and from thin-layer chromatorgrams by FAB (2) has been demonstrated relatively recently. The use of FAB to aid in the identification of arsenobetaine in various fish has also been reported recently (3). We have combined these techniques and have developed a method for the mass spectrometric analysis of quaternary organoarsenic compounds directly from silica-based electrophoretic plates via fast atom bombardment as an approach to the above mentioned problem. In this paper we describe the salient experimental features of our procedure and the results of its preliminary application to actual marine samples.

The general analytical scheme for the extraction and analysis of organoarsenicals from fish includes lipid extraction, ion pair extraction, two stages of ion exchange, thin layer chromatography on aluminum backed silica gel plates, and identification directly from the plates by FAB-MS. Only the identification step by FAB will be discussed in this paper.

Mass spectra were obtained from a CEC 21-110 mass spectrometer modified for FAB analysis and operated at an accelerating voltage of 8 kV. A small section (0.5 cm x 1.0 cm) containing an eluted sample spot was cut out of a given TLC plate and affixed with vacuum compatible silver paint to the mass spectrometer's sample probe for insertion into the ion source. After attaching the chromatogram segment to the probe, it was wetted first with 1-5 μl of one of the mobile phase solvents and second with a minimal amount (~5 μl) of glycerol. The FAB gun (Ion Tech FAB 11NF) was operated at 6 kV with argon.

Mass spectra of authentic samples of both arsenobetaine and arsenocholine (4) were produced off a regular FAB probe for reference. The arsenobetaine spectum exhibits a relatively intense $(M+1)^+$ peak at m/z 179, but the base peak in the spectrum occurs at m/z 135 and is attributable to the loss of CO_2. Cluster ions of the sort $(nM+H)^+$, $(nM+Na)^+$, and $(nM+CH_3)^+$ are observed in arsenobetaine's spectrum up to n = 9 (m/z 1603 for the protonated molecular species). The limit of detection for arsenobetaine on our instrumentation was determined to be about 100 ng. By comparison the regular FAB spectrum of arsenocholine is very simple exhibiting essentially only the mass peak corresponding to the cation (m/z 165). The detection limit for arsenocholine was also found to be around 100 ng.

Mass spectra produced directly off sections of TLC plates which had either been moistened with solutions of the authentic compounds or contained eluted spots of these compounds, Figure 1, exhibited intense mass peaks corresponding to the molecular ion or cation, as the case may be. Quite notable was the suppression of the glycerol background spectrum by a factor of about 4-5. Mass peaks corresponding to molecular cluster ions and the intense mass peak at m/z 135 due to the loss of CO_2 were conspicuously absent from the TLC mass spectra of arsenobetaine. The appearance of these mass spectra was unaffected by the use of different mobile phase wetting solvents ($CHCl_3$, MeOH, H_2O, or NH_3). The limits of detection of both compounds off the electrophoretic plates were found to be between 0.1 and 1.0 μg, i.e. about the same as off a normal FAB probe.

We produced mass spectra from several TLC spots containing unknown compounds from actual fish samples (5). None of these spectra provided convincing evidence for the presence of either arsenobetaine or arsenocholine. A mass peak at m/z 168 was the only nonglycerol peak present in all of the spectra. The mass spectrum of a spot taken off the chromatogram of unknown material extracted from raw fish meal (5) exhibited a mass peak at m/z 165, Figure 2, which might indicate the presence of arsenocholine. If this were the case, it would be the first direct identification of this compound in marine life forms.

Future efforts will be directed toward refining the technique described herein and applying it to the study of organoarsenicals in fish living in the heavily exposed waters of the Puget Sound near Tacoma, Washington.

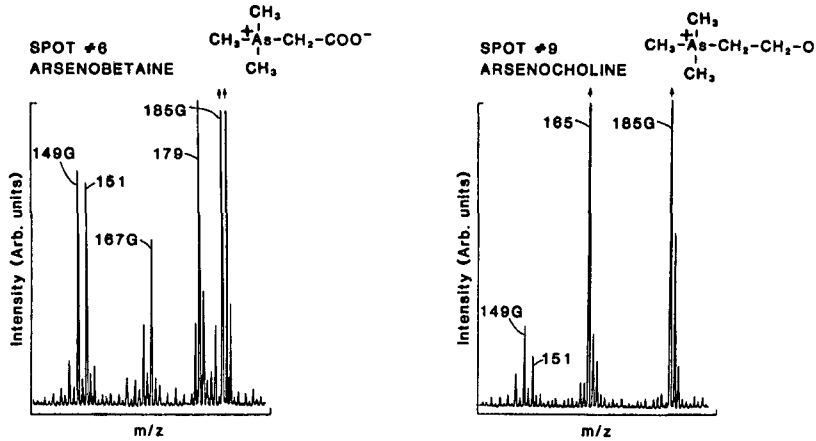

Figure 1

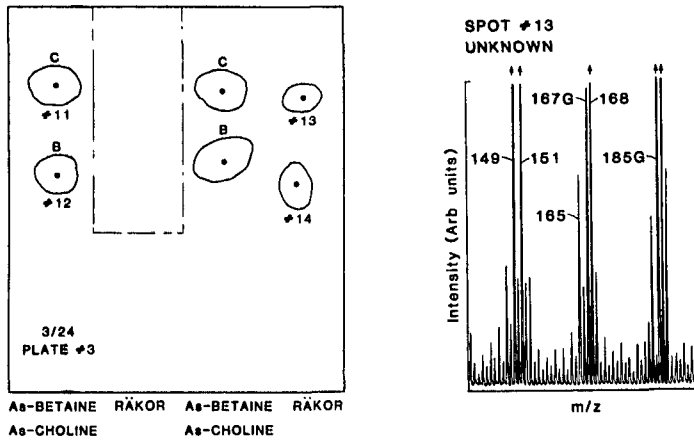

Figure 2

References

1. R. J. Day, S. E. Unger, and R. G. Cooks, Anal. Chem. 1980, 52, 557A.
2. T. T. Chang, J. O. Lay, Jr., and R. J. Francel, Anal. Chem. 1984, 56, 111.
3. J. B. Luten, G. Riekwel-Booy, J. v. d. Greef, and M. C. ten Noever de Brauw, Chemosphere 1983, 12, 131.
4. Compounds supplied courtesy of M. O. Andreae, Department of Oceanography, Florida State University, Tallahassee, FL.
5. Chromatograms supplied courtesy of H. Norin, National Institute of Environmental Medicine, Stockholm, Sweden.

ALKALI HALIDE CLUSTER IONS OBSERVED BY TIME-OF-FLIGHT SIMS

B. Schueler, R. Beavis, W. Ens, D.E. Main, and K.G. Standing
Dept. of Physics, University of Manitoba, Winnipeg, Manitoba, Canada R3T 2N2

1. Dependence of the cluster ion distribution on the energy loss:

Positive and negative secondary ion mass spectra of alkali halides (alk hal) have been measured with the Manitoba time-of-flight mass spectrometer, using a pulsed K^+ or Cs^+ primary ion beam (f.w.h.m. ~3ns) and a time-to-digital converter[1]. As an extension of our previous measurements on CsI [2], we examined targets of various Cs halides and alkali iodides, as well as LiBr. The base peaks were $(alk)^+$ in the positive spectra and $(hal)^-$ in the negative spectra but many cluster ions $[(alk\ hal)_n(alk)^+$ or $(alk\ hal)_n(hal)^-]$ were also observed. As previously reported for organic targets [3], the yield of secondary ions depends strongly on the primary ion species and on the primary ion energy. The yield of a typical alkali halide ion was a factor ~5 larger for a Cs^+ projectile than for K^+; it increased by a factor ~10 as the Cs^+ energy was increased from 3 keV to 14 keV, as shown in fig. 1 for the $(RbI)Rb^+$ cluster.

The ratio between the base peaks (alk^+ or hal^-) and the cluster ions of Cs-halides was found to vary considerably with dE/dx (by a factor ~ 2 for CsI, and up to a factor ~ 1.3 for the other salts). On the other hand, the relative intensities of the various cluster ions from a given compound were observed to be almost independent of the primary ion energy and species, as shown in figure 2 for a typical case. Relative cluster intensities for positive and negative clusters were also found to be almost the same (within 30%) - see fig. 2. Thus the various cluster ions appear with the same relative intensity in the spectrum of a given alkali halide, even when conditions are changed so as to give one or two orders of magnitude change in the yield of each cluster.

These results clearly show that the cluster ion distributions of alkali halides do not depend on the amount of energy initially put into the crystal. An increase in the primary energy loss simply increases the number of clusters ejected, without changing their relative intensity. This disagrees with the predictions of models based on the concept of local thermodynamic equilibrium in the zone of primary ion impact.

2. Parametrization of the cluster ion distributions:

As in experiments on ion emission from alkali halides induced by Q-switched UV-laser irradiation (5), it is found that the cluster ion distributions can be empirically approximated by an Arrhenius form, $\ln((n+1)\cdot y_n/2\cdot y_1) \sim \delta(\Delta H_n)=(\Delta H_n-\Delta H_1)$, where y_n is the yield of a cluster of order n (e.g. y_1: $(RbI)_1Rb^+$ or $(RbI)_1I^-$), ΔH_n is the solid state enthalpy of formation, and $(n+1)^{-1}$ is the statistical weight of the n-cluster (entropy term). Fig. 3 shows the Arrhenius plot for some alkali halide clusters. Positive as well as negative cluster ion distributions can be fitted by the same line, but not the atomic ions. Although a good empirical fit to the cluster ion distributions is provided, a thermal ion emission process can be ruled out, e.g. from the experiments reported above.

3. Dependence of the mass spectra on the primary ion current:

The secondary ion mass spectra of some of the salts were also measured using average primary ion fluxes from ~30 Cs^+/mm^2 to about 3000 Cs^+/mm^2 ions per pulse (~2000 pulses/sec) at various fixed primary ion energies. It was found that all secondary ion yields were proportional to the primary ion flux; no change in the relative ion intensities was observed. The result is in clear disagreement with any ion formation process involving recombination of emitted particles in the gas phase. It indicates that each secondary ion emission is a result of a single primary ion-solid-interaction, consistent with the ejection of a "preformed" ion from the surface.

4. The effect of target irradiation prior to the measurement:

The secondary ion emissions were measured when the target was irradiated prior to the measurement by a continuous beam of Cs^+ or K^+ ions [6]. The overall ion yield was higher after irradiation, as shown in fig. 1 for RbI. Very similar behaviour was found for Cs-halides and alkali iodides. An ion yield increase of about a factor of 2 is typical for irradiation doses $\gtrsim 10^{14}$ cm^{-2}, but in some cases a stronger enhancement was found, depending on target preparation and treatment. The yield enhancement appeared to be independent of the relative energies of the irradiating and the primary ion beam used for analysis.

In RbI, the intensity of the Rb^+ ion increased by a factor ~3 after irradiation. The increase in intensity of the clusters was considerably greater (a factor ~15), but again the relative intensity of the various cluster ions remained constant. The other alkali halides exhibited similar behaviour except for LiI. In this case, the positive spectrum behaved in a similar way, and the I^- ion increased by a factor ~1.5 after irradiation, but the $(LiI)I^-$ cluster decreased to ~30% of its initial intensity.

The above experiments clearly show the strong influence of the condition of the sample prior to the analysis on the mass spectra. In general sample irradiation favours ionic emission from alkali halide targets, particularly for cluster ions. The effect of sample irradiation on the mass spectra appears to be even more pronounced than changes in the primary ion beam properties.

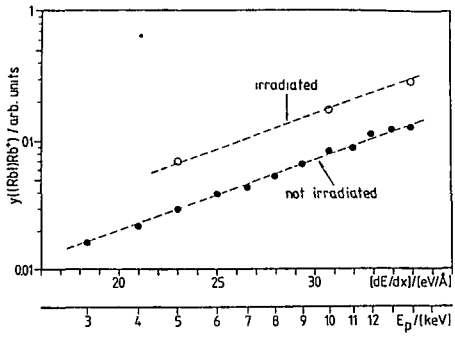

Fig.1: Dependence of the $(RbI)Rb^+$ secondary ion yield from RbI on the energy loss (dE/dx) of the Cs^+ primary ion at the target surface (● unirradiated sample; ○ sample irradiated with about 10^{15} Cs^+/cm^2). (dE/dx) for a given E_p was calculated according to ref. 4.

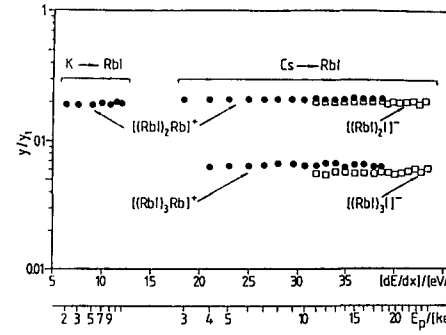

Fig.2: Dependence of the relative cluster ion intensities (y/y_1) on (dE/dx) of K^+ and Cs^+ primary ions. The cluster ion yields (y) are normalized to the yields of the first cluster ions $(RbI)Rb^+$ and $(RbI)I^-$ (y_1) at the given (dE/dx) for positive (●) and negative (□) cluster ions, respectively.

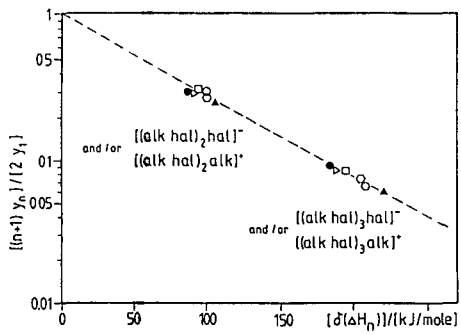

Fig.3: Relative positive and negative cluster ion intensities from some alkali halides vs. difference in enthalpy of formation. The cluster ion yields are normalized to the yields of $(alk\ hal)alk^+$ or $(alk\ hal)hal^-$, respectively. The fitting line does not depend on (dE/dx). (●:CsI, □:RbI, ▷:KI, ○:NaI, ▲:LiI, ○:LiBr)

References:

(1) W. Ens, R. Beavis, D.E. Main, B. Schueler and K.G. Standing, these proceedings.
(2) W. Ens, R. Beavis and K.G. Standing, Phys. Rev. Lett. 50,27(1983); K.G. Standing, W. Ens and R. Beavis in "Ion Formation from Organic Solids", 107, Springer-Verlag(1983).
(3) K.G. Standing, B.T. Chait, W. Ens, G. McIntosh and R. Beavis, Nucl. Instrum. and Meth. 198,33(1982).
(4) W.D. Wilson, L.G. Haggmark, and J.P. Biersack, Phys. Rev. B 5,2458 (1977).
(5) B.Jöst, B. Schueler, and F.R. Krueger, Z. Naturforsch. 37a, 18 (1982).
(6) K.G. Standing, R. Beavis, W. Ens and B. Schueler, Int. J. Mass Spectrom. Ion Phys. 53, 125 (1983).

FAST ATOM BOMBARDMENT INDUCED ADDUCT IONS

H. Pang, C.E. Costello, and K. Biemann; Dept. of Chemistry, M.I.T., Cambridge, MA 02139

INTRODUCTION Barber et.al[1] first demonstrated the use of a glycerol matrix to enhance the ionization of involatile and/or thermally labile compounds by fast atom bombardment. Field[2] in 1982 discussed the effects of the high energy atom beam on the glycerol matrix: in addition to the formation of the protonated molecular ion of glycerol and its association complexes, on prolonged irradiation, new compounds are formed from the glycerol and its decomposition products. The mechanisms for the formation were proposed to involve radicals. The effects of the bombardment on a series of samples dissolved in the glycerol matrix are now reported and discussed.

In the FAB spectrum (Figure 1a) of 1,7,15,21-tetraaza-4,11,18,25-tetra-oxacyclooctacosane (A), in addition to the expected protonated molecular ion, ions of mass 12 and 24 units higher than the protonated ion are also observed. It can be assumed that these ions, $(MH+12n)^+$, do not originate from impurities in the sample because they are not observed in the field desorption spectrum of A (Figure 1b). Hence, these ions are induced by the fast atom bombardment.

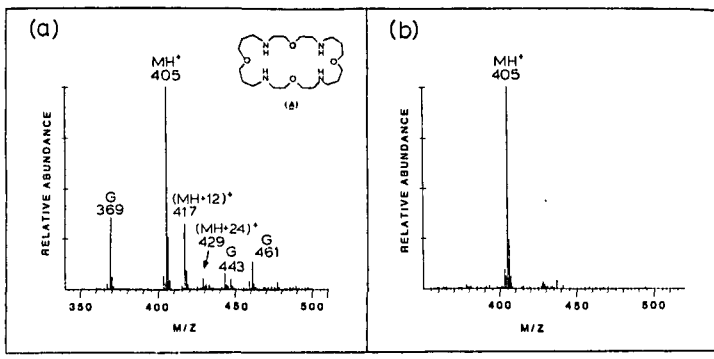

Figure 1

The addition of 12 mass units to the protonated molecular ion corresponds to a carbon atom as determined by exact mass measurement. Comparison of the FAB spectra of compounds dissolved in either glycerol or glycerol-d_5 shows that a CH_2 group of the glycerol skeleton has been added to the compounds with replacement of two hydrogen atoms from the protonated molecular ion. As a result, a net addition of 12 mass units is observed in glycerol-d_0 and 14 mass units in glycerol-d_5.

OCCURRENCE OF ADDUCT IONS The FAB spectra of a series of structurally similar compounds have been obtained to correlate and determine the prerequisites for the formation of these adducts. The results show that $(MH+12n)^+$ adduct ions occur only in the spectra of primary and secondary amines. The relative abundances of the adduct $(MH+12)^+$ to the MH^+ range from about 20% to 175%. That the linkage site of the CH_2 group of the glycerol skeleton to the sample involves the nitrogen atom is shown by the presence of these adduct ions in the nitrogen containing compounds, and their absence in the spectra of non-nitrogen containing analogs. In addition, the absence of the $(MH+12)^+$ ion in the spectra of the alcohols and tertiary amines tested further supported the involvement of the nitrogen. It appears that even though one nitrogen is adequate for the formation of the $(MH+12)^+$ adduct ion, in monoamines the formation seems less predictable. For the cyclic compounds that contain at least two nitrogens, the number of atoms between the two NH groups has no significant effect on the relative abundance of the $(MH+12n)^+$ adduct ions.

We hence proposed the structure of $(MH+12)^+$ adduct ion to be B.

Other adduct ions, $(MH+38)^+$, $(MH+42)^+$, $(MH+54)^+$, and $(MH+72)^+$ are sometimes observed in addition to $(MH+12)^+$. The intensities of these ions, however, are relatively low compared to that of $(MH+12)^+$. For the adduct ions $(MH+42)^+$, $MH+C_2H_2O$, and $(MH+72)^+$, $MH+C_3H_4O_2$, the structures C and D are proposed based on the exact mass measurements and their mass values when glycerol-d_5 was used.

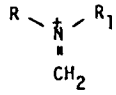

MH+12 (B)

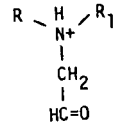

MH+42 (C)

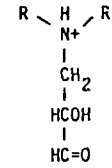

MH+72 (D)

ADDUCT FORMATION IS TIME DEPENDENT, CONCENTRATION DEPENDENT, AND pH INDEPENDENT The relative abundance of these $(MH+12n)^+$ ions increases with the exposure time of the neutral atom beam. For the compounds studied, the rate of increase may vary from compound to compound, but they all show similar behavior. When the fast atom gun was turned off initially for 5 minutes with the sample inside the ion source, then was turned on and the experiment continued, the curves of the relative intensities versus bombardment time are exactly the same. Hence, it can be concluded that the adduct ions are induced by the high energy bombardment.

At a given exposure time of bombardment, the relative ratio of $(MH+12)^+$ to MH^+ increases with the dilution of the sample in glycerol. However, the substantial matrix background at low sample concentration may obscure the significance of this event. Higher mass resolution is required to resolve the $(MH+12)^+$ and MH^+ ions from the matrix ions. The relative ratio of $(MH+12)^+$ to MH^+ for 3,5-dimethylpiperidine, on the contrary, decreases with decreasing concentration. Addition of another nitrogen-containing sample, 1,10-diaza-18-crown-6 (1 ug/ul), to the low concentration 3,5-dimethylpiperidine sample (0.2 ug/ul) can increase the ratio. This phenomenon suggests that the mechanism for formation of $(MH+12)^+$ may involve two nitrogen atoms. While it may not absolutely require the presence of two nitrogens in the same molecule, their proximity will facilitate its formation because the probability of interaction would be greater.

The pH of the glycerol solution has only very minor effect on the $(MH+12)^+$ to MH^+ intensity ratio. The spectra of samples having 1 ul of various concentrations of base (NaOH) or acid (HCl) added to identical solutions of 1,10-diaza-18-crown-6 in glycerol show no significant variation of the $(MH+12)^+$ to MH^+ abundance ratio. The concentration used for NaOH ranges from 10 M to 0.1 mM and that of the acid ranges from 0.1 M to 0.1 mM. The only major difference is that more sodium cationized molecular ion is observed with increasing concentration of NaOH. The pH independence suggests the existing form of the compound (protonated or neutral) in solution plays no role in the formation of $(MH+12)^+$ ion.

OTHER OBSERVATIONS When compound A was dissolved in thioglycerol instead of glycerol, the $(MH+12)^+$ adduct ion was also observed in the FAB spectrum but its relative abundance to MH^+ was reduced by 50%. As predicted, the adduct ion was absent in the spectrum of A in the matrix 2,4-di-*tert*-amylphenol.

Metastable studies using an accelerating voltage scan to find the precursors of the $(MH+12)^+$ ion have so far been unsuccessful. We have not able to observe the $(MH+12)^+$ ion by FD after the sample has been bombarded for 2-3 minutes. (Only those high molecular weight amines could be used for this FD experiment. None of the volatile amines whose FAB spectra show more prominant $(MH+12)^+$ ion could be used because of the volatility.)

CONCLUSION We propose the structure of the $(MH+12)^+$ adduct ion as B, which could originate from $(MH+42)^+$, C, and $(MH+72)^+$, D, by consecutive eliminations of formaldehyde. The formation of this ion by a simple Schiff base reaction between the NH groups and the dehydrogenated glycerol matrix is ruled out because of the incorporation of two glycerol skeleton hydrogens. At present, we are still uncertain whether the $(MH+12)^+$ ion is formed in the gas phase by fragmentation from other precursors or whether it already exists in the liquid matrix and is desorbed into the gas phase during analysis.

REFERENCES (1) M. Barber, R.S. Bordoli, R.D. Sedgwick, and A.N. Tyler, Nature (1981), 293, 270. (2) F.H. Field, J. of Phys. Chem. (1982), 86, 5115.

ACKNOWLEDGMENT We would like to thank Prof. Stephen Lippard of M.I.T. for supplying the compound A. The M.I.T. Mass Spectrometry Facility is supported by the Division of Research Resources, National Institutes of Health.

STABLE ISOTOPE ANALYSIS OF COLLAGEN TURNOVER AND PROLINE RECYCLING IN SCAR TISSUE:

WOLFE, M. H., Molnar, J. A. and Wolfe, R. R.: University of Texas Medical Branch, Shriners Hospital, Galveston, Texas.

Collagen is the most important extracellular protein. It comprises 70-90% of all skin protein, and determining the regulation of its synthesis is important for the understanding of the processes of wound healing and scar formation. Studies of collagen kinetics have not been performed in human subjects.

Several approaches for determining collagen kinetics in vivo have been described, but all utilize radioisotopes, require sample sizes too large to make sampling from human volunteers feasible, and require tedious sample preparation.

The different techniques for determining collagen turnover require the measurement of the isotope enrichment of proline and/or hydroxyproline, two amino acids that are abundant in collagen. Use of labeled proline alone might lead to spurious calculations of synthetic rate, because some of the proline released as a result of the breakdown of collagen can be reincorporated into collagen. During collagen synthesis, some of the proline incorporated into the protein is hydroxylated to form hydroxyproline. In contrast to proline, the hydroxyproline cannot be recycled.

Different techniques for determining collagen synthesis are as follows:

(1) Flood the precursor pool of proline with a large amount of unlabelled proline while simultaneously adding labelled proline, then measure the enrichment of proline and hydroxyproline for the next 3 hours.

(2) Determine the enrichment of the precursor pool of free proline during a constant infusion of labelled proline by measuring the enrichment of hydroxyproline isolated from collagen.

(3) Label the collagen with ^{18}O-hydroxyproline by having the subject breathe $^{18}O_2$ (the O_2 in the hydroxyproline is derived from molecular O_2). When $^{18}O_2$ breathing stops, determine the rate of decay in ^{18}O-hydroxyproline enrichment in collagen.

Although the technique involving the $^{18}O_2$ breathing is the least practical of the above techniques for evential application in human subjects, we have chosen that methodology to adapt to an entirely, stable isotope/gas chromatography mass spectrometry (G.C.M.S.) technique, because the analytical techniques required for this approach are readily applicable to all other approaches for measuring collagen synthetic rates as well. The advantage of substituting the stable isotope deuterium for the radioactive ^{3}H-label on proline is obvious in terms of application to humans. The use of GCMS to analyze the ^{18}O-enrichment of hydroxyproline is preferable to the previously used method in which the hydroxyproline was isolated in pure form prior to combustion and analysis by gas isotope ratio mass spectrometry because of the ease of sample preparation and the small sample size needed for GCMS analysis. We have been able to attain a level of precision of isotopic enrichment well within physiological limits.

TABLE I

COLLAGEN KINETICS CALCULATED WITH DIFFERENT TRACERS

	Ke, Day^{-1}		Half-Life, Days	
	Slope[1] Analysis	Area[2] Analysis	Slope Analysis	Area Analysis
^{18}O-Hydroxyproline	.166±.004	.128±.004	4.16±.104	5.39±.17
d-Hydroxyproline	.139±.009	.103±.010	5.06±.25	6.82±.71
d-Proline	.163±.004	.111±.001	4.23±.05	6.24±.05

Values Mean ± SEM

[1] Calculated from raw data, days 2-7.

[2] Calculated from raw data, days 2-52.

CONCLUSION

It is possible to use stable isotope tracers and GCMS analysis to determine collagen synthesis rates in vivo.

Stable Isotope Ratio Mass Spectrometry Iron Bioavailability Studies

S. Evans, Kratos Analytical Instruments, Ramsey, New Jersey, U.S.A
R. Self, Food Research Institute, Norwich, U.K

Ethical considerations preclude the use of radioisotopes in studies on humans, especially pregnant women and infants, for whom nutrient absorption data are of particular interest. The rate of absorption of iron can be deduced (subtractively) by measuring the much larger proportion excreted in the faeces using neutron activation analysis (NAA), but more interactive methods are sought for work on the total turnover of inorganic nutrients involving low levels of incorporation in blood, saliva, and tissue samples, and for work on other minerals.

The measurement of stable isotope ratios for inorganic elements by mass spectrometry is only new in its routine application to biological samples.

In this rapidly growing area, methods which can be employed for iron include Thermal Ionization, which gives the highest precision and accuracy, but requires complex sample preparation, tends to be slow, and needs expensive special instrumentation. Inductively Coupled Plasma gives poor precision, and also requires expensive specialised equipment. EI and CI also give poor precision, require the preparation of volatile derivatives, and are subject to interference.

An alternative method, already applied to the study of Calcium by Dr. D.L. Smith at the University of Utah, is Fast Atom Bombardment.

This simple, sensitive, technique can be used for rapid, direct analysis of underivatised samples, and is widely available on standard organic mass spectrometers.

We present a preliminary report on the use of FAB on a Kratos MS80 mass spectrometer with DS55 data system for the direct and rapid measurement of the $^{58}Fe/^{56}Fe$ isotope ratio for ashed faecal samples.

Experimental

Fasting human subjects were given a ferrous sulphate solution containing 1.05 mg ^{58}Fe (71.5% enrichment factor, AERE Harwell). Faeces were collected, bulked, freeze dried, ground, then ashed at 480°C for 48 hours. 0.2 g of ash were dissolved in HCl and the iron extracted with diethyl ether. The ether extract was dried, dissolved in HCl, and 1µl aliquots applied to the MS80 FAB probe. The ether extraction procedure effectively eliminates interfering ions, leaving only a small amount of CaO which requires a resolution of 3000 to separate.

The instrument was used in the SIM mode, switching between m/z 56 and m/z 58, using m/z 57 as lock mass, acquiring 75 scans in 2.5 minutes. The isotope ratio of $^{58}Fe/^{56}Fe$ was calculated from 50 of these scans, and typically this experiment was repeated to give 5 sets of data from each sample. Standard iron (1 µg/µl) SpectrosoL grade was used to calibrate the method.

Results

The data from 4 faecal samples is shown, together with the equivalent NAA results. The precision of the method is excellent, and shows a relative standard deviation down to 0.5%. Linearity, demonstrated using a bovine liver matrix spiked with ^{58}Fe, is also good. The method is shown to have the required accuracy and precision for ratio measurements on normal levels of iron excreted and hence, by difference, for normal levels of iron absorbed. Work is continuing to determine whether or not the accuracy and precision are sufficient for direct measurements on blood serum, where much smaller amounts of iron are involved.

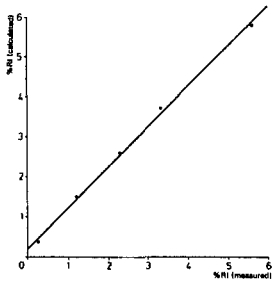

Linearity of response to ^{58}Fe spiked into NBS (bovine liver) SRM1577

KRATOS

Natural abundances (NA) of the stable isotopes of iron

m/z	%NA	atomic mass	%RI
54	6 82	53 9396	6 36
56	91 66	55 9349	100
57	2 19	56 9354	2 39
58	0 33	57 9333	0 36

$^{56}Fe/^{54}Fe$ isotope ratio = 0 0036

KRATOS

Comparison of $^{56}Fe/^{54}Fe$ isotope by NAA and FAB methods

			FAB data		
Sample No	NAA	FAB	n	SD	RSD(%)
8K	1 10	1 45	5	0 007	0 5
5N	2 77	2 12	5	0 013	0 6
1E	1 55	1 62	4	0 01	0 6
10 I	0 80	1 13	6	0 013	1 1

KRATOS

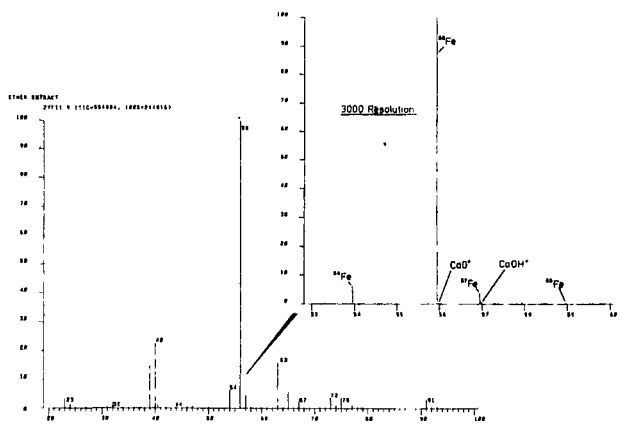

STABLE ISOTOPE ANALYSIS BY FAB

KRATOS

DETERMINATION OF DEUTERIUM CONTENT OF H_2O BY REACTION WITH PHENYLMAGNESIUM BROMIDE AND GC-MS-SIR ANALYSIS OF BENZENE.

Thomas R. Sharp
Dept. of Chemistry, University of Utah, Salt Lake City, UT 84112

One of the most convenient sources for deuterium as a stable isotopic probe in chemical experimentation is water. Analysis of the deuterium content of a given sample of water, however, has been until now a difficult task. A similar challenge presented in measuring the ^{18}O content of water can be met by hydrolyzing a small amount of PCl_5 with the aqueous sample in question, and analyzing the resulting derivatized phosphoric acid by GC-MS-SIR[1]. By analogy, a commercially available, reactive reagent which would quantitatively and irreversibly incorporate the hydrogens of water into an organic molecule amenable to mass spectral analysis would permit a similar means of determining the deuterium content of water. Phenylmagnesium bromide (phenyl Grignard reagent) meets these requirements. Upon treatment of a small amount of reagent with an aqueous solution, the hydrogens from water are incorporated into benzene. Quantification of ion intensities in the molecular ion region of benzene by conventional gc-ms techniques permits calculation of the deuterium content of the original water sample. This very simple procedure gives excellent results over a range of 1 atom% to 99 atom% $[^2H]H_2O$ using standard laboratory techniques, inexpensive commercially available reagents, and conventional mass spectrometric instrumentation. The method will be useful for directly verifying the deuterium content of water in such experiments as solvent deuterium isotope effect determinations, exchange reactions, isotope tracer studies, etc.

Reagents and Procedure. 99.8 atom% $[^2H]H_2O$ was obtained from Merck. An appx. 3 M solution of phenylmagnesium bromide in diethyl ether is commercially available from Aldrich, and is conveniently handled using disposable syringes. Conical-bottom reaction vials (3 or 5 ml capacity) with Teflon-lined screw caps are best suited for sample preparation. A 10 µl aliquot of $[^2H]H_2O$ sample is placed in the bottom of an appropriately cleaned and dried reaction vial. A small aliquot of the phenylmagnesium bromide reagent (0.1 ml or less) is carefully added to the water aliquot and allowed to react. Dry acetone is then added to quench any remaining phenylmagnesium bromide and to dilute the resulting benzene. After allowing the Mg^{2+} salts products to settle, the remaining solution is directly injected onto the chromatographic column.

Gas Chromatography Mass Spectrometry. A VG Micromass 7050 magnetic sector mass spectrometer, coupled to a Hewlett-Packard 5840a gas chromatograph, was used. Analyses were performed by low resolution electron impact (70eV) repetitive scan monitoring of the effluent from a 2 mm i.d. x 1.5 m glass chromatography column packed with Carbopack C/0.1% SP1200, 80/120 mesh (Supelco Laboratories). Benzene elutes in appx. 5 minutes at 100°C and 20 ml/min He carrier gas flow. Repetitive scan analyses were conducted at a scan rate of 1 sec/decade, 1 sec interscan over a 20-320 dalton mass range. Selected ion chromatograms of m/z 78, 79 and 80 were reconstructed, and areas under the peaks determined.

Calculations. Signal intensities measured for m/z 78, 79 and 80 are used to calculate ^2H content of the original water sample, correcting for ^{13}C content according to eq. 1. H_{12} and H_{13} refer to undeuterated benzene containing all ^{12}C and one ^{13}C, respectively. D_{12} and D_{13} are similarly defined for $[^2H_1]$benzene. Assuming ionization efficiencies equal, the intensities observed at m/z 78, 79 and 80 are proportional to the amounts of the various species in the sample, I_{79} being a sum of contributions from H_{13} and D_{12}. The term in parentheses in the numerator represents correction of I_{79} for contributions from H_{13}.

$$\text{Atom\% } ^2H = \frac{(D_{12} + D_{13})}{(H_{12} + H_{13}) + (D_{12} + D_{13})} \times 100 = \frac{(I_{79} - 0.068\, I_{78}) + I_{80}}{I_{78} + I_{79} + I_{80}} \times 100 \qquad \textbf{(eq. 1)}$$

Results and Discussion. Table I lists a typical data set for a dilution series of $[^2H]H_2O$. A plot of expected vs. observed atom% ^2H content using eq. 1 and the data of Table I are shown in Figure 1. These experiments were performed with 10 µl (0.55 µmole) samples of water. An equivalent of the 3 M Grignard reagent would be 0.185 ml. Using only 0.1 ml of Grignard reagent insures that the water is in excess, and that traces of stray water from other sources should not significantly interfere with the determination. The amounts of water sample and Grignard reagent used produce ample benzene for multiple determinations of ^2H content. We routinely dilute the sample to as much as 5 ml total volume, inject 1 µl or less onto the column, and set the mass spectrometer overall gain at its lowest setting and still get excellent results.

Curve a (Fig. 1) represents theoretically expected results. Deviation of curve b from curve a results from the presence of benzene in the commercial Grignard reagent. It is rational to expect that commercial preparation does not include precautions against such presence. Also, the most likely decomposition product is benzene itself, resulting from handling and decomposition on the shelf. Phenylmagnesium bromide prepared in the laboratory using appropriate care can be quenched with 99.8 atom% $[^2H]H_2O$ to produce $[^2H_1]$benzene with the correct atom% labeling. Contamination does not present significant problems. Results can be corrected by running one or two standards along with the experimental samples. We have performed several dilution series over several months and find that our single bottle of reagent has remained unchanged at room temperature. Data from all the experiments lie on the same line - i.e. curve b - within experimental error.

Chromatography need not be performed on the column packing specified above. Many phases, and either packed or capillary columns, could be used equally well. A packed column produces a wider peak, thus improving the quality of the overall determination by permitting more measurements across the peak profile. Isotopic fraction is observed on this chromatographic column. $[^2H]$Benzene elutes from this column with a very slightly faster retention time than unlabeled benzene -- appx. two to four seconds.

Table I:

Expected[a] Atom% $[^2H]$	I_{78}[b]	I_{79}	I_{80}	Calculated Atom% $[^2H]$ (mean ± σ (n))
0.0	939	61	0	0.13±0.13 (4)
10.0	881	117	2	6.38±0.15 (5)
20.0	803	190	7	14.68±0.07 (4)
29.9	731	258	11	22.24±0.09 (4)
39.9	657	327	16	30.19±0.14 (4)
49.9	573	404	23	39.07±0.06 (4)
59.9	492	481	27	47.69±0.12 (4)
69.9	417	550	33	55.25±0.37 (5)
79.8	349	617	34	62.90±0.23 (4)
89.8	263	696	41	72.05±0.04 (3)
99.8	163	789	49	82.60±0.14 (5)

a. Calculated from a dilution series of 99.8 atom% $[^2H]H_2O$.
b. Representative intensities.

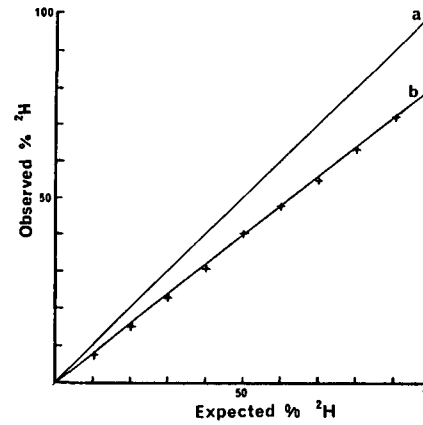

Figure 1:
Observed vs. Expected ^2H content of a $[^2H]H_2O$ dilution series

Summary. Classical methods reduced water to hydrogen, followed by $^2HH/H_2$ isotope ratio measurements,[2,3] and are still required for natural abundance ^2H levels. Continuous sampling of $[^2H]H_2O$ solutions via a directly coupled membrane interface have been successful.[4] The large H_2O flux through the system, high labeling levels, and interest in changes in $[^2H]$ with time and experimental conditions, rather than absolute values, makes the technique very useful. Isotopic equilibration of water with an organic molecule is another approach. Completeness of the equilibration is an important factor. Use of a characteristic metastable decomposition of propanol makes the Schmit and Boulay method[5] very selective, but requires a double focusing instrument. Benesath et al.[6] make use of chemical ionization techniques to determine ^2H content directly on water, using the $^2HH_2O^+/H_3O^+$ ratio. Our method obviates the various difficulties and constraints on performing ^2H analyses on water samples posed by all of these methods, putting a quick, reliable and simple method into the hands of the "occasional" and "casual" $[^2H]H_2O$ user.

---

1. Sharp, T.R., Minard, R.D. (1980). **Anal. Chem.** 52,598.
2. Kishima, N., Sakai, H. (1980). **Anal. Chem.** 52,356.
3. Bigeleisen, J., Perlman, M.L., Prosser, H.C. (1952). **Anal. Chem.** 24,1356.
4. Pungor, E., Klibanov, A.M., Cooney, C.L., Weaver, J.C.(1982). **Biomed. Mass Spectrom.** 9,181.
5. Schmit, J.P., Boulay, G. (1981). **Anal. Chem.** 53,2359.
6. Benesath, F.A., Bradlow, H.L., Field, F.H. (1983). **Biomed. Mass Spectrom.** 10,596.

GC-MS DETERMINATION OF ISOTOPIC ENRICHMENT IN [6-$^{15}NH_2$]-ADENOSINE-5'-MONOPHOSPHATE: APPLICATION TO METABOLIC STUDIES

Sydell Lewis, Marc Yudkoff
Division of Biochemical Development and Molecular Diseases,
Children's Hospital of Phila., Phila., PA 19104

Hyperammonemia is associated with numerous disease states, e.g. Reye's syndrome, urea cycle defects, and liver cirrhosis. The purine nucleotide cycle (PNC) represents a major biochemical pathway for the production of ammonia from amino acids and for the regulation of intermediary metabolism. In order to define the role of the PNC in ammonia production in a given tissue, it is extremely useful to determine isotopic abundance in [6-$^{15}NH_2$]-adenine, a pivotal PNC intermediate from which $^{15}NH_3$ is derived via the adenylate deaminase reaction, following incubation of the tissue with a given ^{15}N precursor.

Isotopic abundance in [6-$^{15}NH_2$]-adenine has been determined by converting enzymatically the 6-$^{15}NH_2$ group to $^{15}NH_3$ and then measuring isotopic enrichment in the latter with isotope ratio-mass spectrometry (IR-MS). This approach has several disadvantages: (a) IR-MS requires a relatively large sample size; (b) IR-MS necessitates the absolute removal of all ammonia from the system other than that liberated enzymatically from AMP, a requirement which is extremely difficult to achieve in a biological system.

We have developed a capillary GC-MS method for the measurement of isotopic abundance in [6-$^{15}NH_2$]-adenine, even in very small biological samples. Samples are deproteinized with perchloric acid (6% final concentration) and neutralized to pH 7 with 15% $KHCO_3$. The adenine nucleotides are first isolated from adenine with solid phase ion-exchange chromatography (Quarternary Amine N^+; 3ml column) (Baker) using 2 ml of 1N HCl as eluant and are then subjected to acid hydrolysis (100°C/1 hr) to convert AMP, ADP and ATP to adenine. The latter is then isolated with reverse phase (C18) chromatography (Baker) and derivatized with N-methyl-N-t-butyl-dimethylsilyl trifluoroacetamide (Regis) and acetonitrile (1:1) by heating for 1 hr at 150°C to form the t-butyl-dimethlysilyl (TBDMS) derivative. The mass spectrum of adenine-TBDMS is shown in figure 1.

Synthetic [$^{15}NH_2$] adenine-TBDMS was prepared from 6-chloropurine and $^{15}NH_4$Acetate. Isotopic abundance in the 6-$^{15}NH_2$ group was determined by selected ion monitoring of m/z 306 and m/z 307, both of which were found to be well separated in biological matrices, as shown in Fig 2. Standard curves of [6-$^{15}NH_2$]-adenine enrichment in the 1.0-50.0 atom % excess range were linear with the injection of 10 nanograms of derivatized adenine. Addition of graded amounts of [6-$^{15}NH_2$]-adenine to rat hepatocytes showed excellent agreement between expected and observed values for isotopic abundance in the 0.5-20.0 atom % excess range with the injection of 10 nanograms of adenine.

The utility of this approach for <u>in vitro</u> studies is underscored by the data illustrated in Figure 3. Rat hepatocytes prepared by the method of Berry and Friend[2] were incubated together with L-[^{15}N]-alanine, 1mM oleic acid and 0.1 mM L-ornithine in Krebs-Ringer bicarbonate buffer (pH 7.4). Samples were taken at the times indicated and analyzed for isotopic enrichment in [6-$^{15}NH_2$]-adenine, which attained a maximal value of 6.5 $\pm$ 0.5 atom % excess by 60 minutes.

Enrichment detected by monitoring of m/z 306 and m/z 307 is not necessarily referable to labelling of the 6-amino group, since the presence of ^{15}N in any nitrogen of the adenine nucleus would result in an increased m/z 307/306 ratio. This should not be a problem for short term experiments in most biologic systems, in which the turnover of ^{15}N at the 6-NH_2 position is much more rapid than that of other nitrogens in adenine. Specific evidence that observed enrichment is referable to 6-$^{15}NH_2$ may be obtained by monitoring of m/z 308 and m/z 307 in hypoxanthine which is the hydrolysis product of inosine-5'-monophosphate and contains all adenine nitrogens except that of the 6-amino group, this moiety having been replaced by a hydroxyl group upon liberation of ammonia in the PNC cycle. With the gas chromatographic method described here, the TBDMS derivatives of hypoxanthine and adenine are well separated from one another (see fig. 2; peak A = hypoxanthine) and the isotopic abundance in either compound can be measured with a single injection into the mass spectrometer.

The current method should prove useful to metabolic studies involving the adenine nucleotides and, possibly, to quantitation of adenine in biologic systems by isotope dilution.

[1]Krebs, H.A., Hems, R., Lund, P., Halliday, D., and Read, W.W.C. (1978) Biochem. J. 176: 733-737.
[2]Berry, M.N. and Friend, D.S. (1969) J. Cell Biol. 43: 506-520.

FIG I

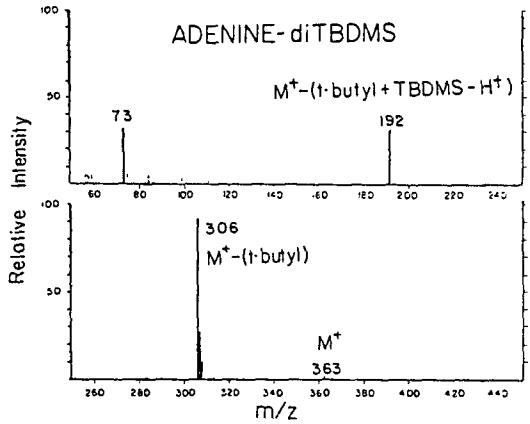

FIG 2

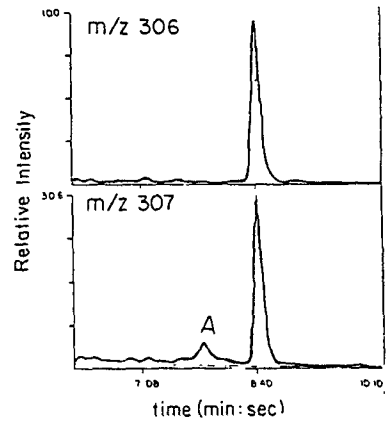

DB5 capillary column (30m x .32mm
Initial T. 200°C
Rate 10°/min
Elution Temp. 284°C

FIG 3

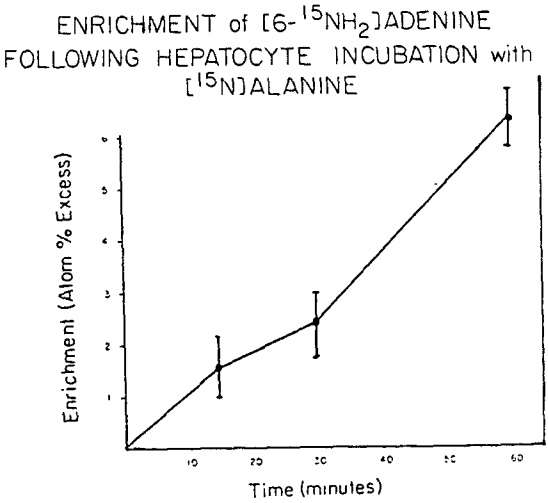

A new approach for the study of glucose metabolism using dual stable isotopic tracer infusions and GC-MS analysis

A. Martineau, L. Lecavalier, J.L. Chiasson, P. Falardeau

Clinical Research Institute of Montreal
Montreal, Canada, H2W 1R7

Introduction

The hazards inherent to the use of radioactive tracers limit their usefulness for studying intermediary metabolism in humans, especially in pregnant women. This led us to elaborate a safe, flexible and reliable method for the determination of various parameters of glucose metabolism (total production, utilization, gluconeogenesis) in a single experiment using dual stable isotopic tracer infusion and GC-MS analysis.

Method

The method is based on the infusion and dilution of two stable isotopic tracers: [2,3,4,6,6-$^{2}H_5$]-glucose and [1,2,3-$^{13}C_3$]-Alanine. The choice of the tracers was done on the basis of a minimal overlap between the ions of interest and those arising from natural isotopic abundances. Both tracers were infused according to a determined protocol and the plasma levels of unlabelled glucose, alanine and lactate as well as those of d_5-glucose, $^{13}C_3$-alanine, $^{13}C_3$-glucose and $^{13}C_3$-lactate were determined by combined gas chromatography mass-spectrometry (GC-MS) under electron impact in the mode of selected ion monitoring (SIM).

Experimental

The plasma samples were purified by the procedure of Kreisberg (1). Briefly, 0.5 ml of plasma is deproteinized by treatment with perchloric acid, centrifugation, neutralization of the supernatant with KOH, followed by a second centrifugation. The supernatant is passed through an AG-1X8 column and then through an AG-50W-X8 column to achieve the separation of lactate, alanine and glucose respectively.

Glucose was analyzed as its 6-acetyl-[1,2:3,5]-bis-butylboronyl-α-D-glucofuranose derivative, alanine and lactate as their bis-t-butyldimethylsilyl derivatives. In each case the (M-butyl)+ ions were monitored: m/z 297, 300 and 302 for glucose, m/z 260 and 263 for alanine and m/z 261 and 264 for lactate (figure 1). Ions related to molecules containing less than three ^{13}C and/or less than five ^{2}H atoms were also monitored, but their level after natural abundance substraction were negligeable or below the limit of confidence.

The isotopic measurements were performed on a Hewlett-Packard 5985b GC-MS having a 10 foot 3% OV-225 packed column. Standard curves for isotopic enrichments between 0.2 and 10 percent were used. A coefficient of variation of less than 2% was estimated from an experiment in which known amounts of labelled glucose and alanine added to a divided pool of plasma were remeasured.

Validation

The method was validated by comparing the results obtained during simultaneous infusions of both stable isotopic and radioactive tracers, the latter being a standard procedure for the study of glucose metabolism (2).

The protocol was planned in order to estimate the various parameters in steady state and non-steady state. Briefly, a bolus of 400 mg of d_5-glucose and 150 μCi of [3-^{3}H]-glucose given at time -90 was followed by a constant infusion of both tracers at a rate of 1.5 mg/min. and 0.5 μCi/min., respectively. Infusion of [1,2,3,-$^{13}C_3$] and [1,2,3-$^{14}C_3$]-alanine started one hour later at a rate of 2 mg/min. and 1 μCi/min., respectively. A mixed meal was then given at time 20. At the end of the experiment, glucagon was infused at increasing doses.

The total production (Ra) and utilization (Rd) of glucose as well as the gluconeogenesis and the turnover rate of alanine were estimated. A good correlation was found between the results obtained with the use of both stable isotopic (SI) and radioactive (RI) tracers (Figure 2).

Conclusion

This new method, based on the simultaneous infusion of two different stable isotopic tracers, provides a unique and reliable approach for the determination of the most significant parameters of glucose metabolism in a single experiment.

References

1) Kreisberg RA, Siegal AM and Crawford Owen W, J. Clin Endocrinol 34:876 (1972).
2) Hetenyi G. Jr., Perez G and Vranic M, Physiological Reviews 63:606 (1983).

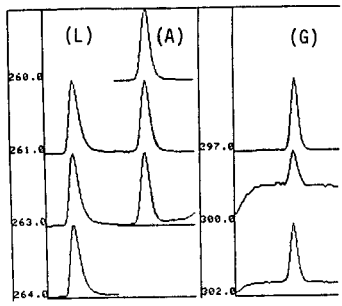

Figure 1: GC-MS trace obtained for lactate (L), alanine (A) and glucose (G).

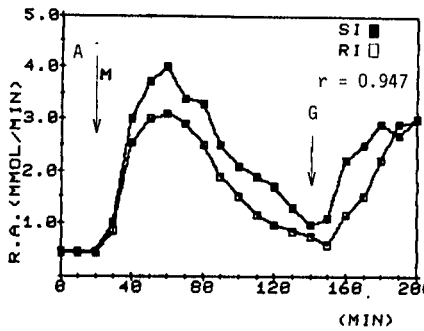

Figure 2: Total production (Ra, Panel A), utilization (Rd, Panel B) of glucose and gluconeogenesis (Panel C) in steady state and non-steady state from stable isotopic (SI) and radioactive (RI) tracer experiments.

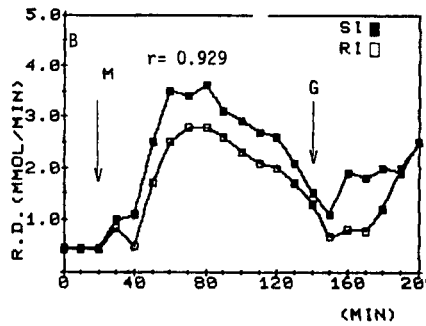

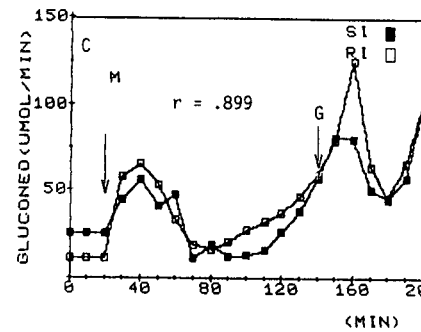

STABLE ISOTOPE EXCHANGE STUDY OF A TRYPTOPHAN TRANSAMINASE ISOLATED FROM STREPTOMYCES FLOCCULUS, DOMENICK VICCHIO, MARILYN K. SPEEDIE AND PATRICK S. CALLERY, UNIVERSITY OF MARYLAND, BALTIMORE 21201.

THE TRANSAMINATION OF L-TRYPTOPHAN BY STREPTOMYCES FLOCCULUS WAS CARRIED OUT IN DEUTERATED BUFFER TO PROVIDE INFORMATION ON THE MECHANISM OF THIS ENZYME CATALYZED REACTION. A NUMBER OF MECHANISMS CAN BE PROPOSED FOR THE TRANSAMINATION REACTION. THE SIMPLEST MECHANISM IS THE CLASSICAL ALDIMINE FORMATION WITH PYRIDOXAL PHOSPHATE, PROTOTROPIC SHIFT OF THE NEW IMINE TO 3-INDOLE PYRUVIC ACID. REAMINATION IS THOUGHT TO BE THE REVERSE PROCESS. MASS SPECTROMETRIC FRAGMENTATION PATTERNS WERE USED TO DETERMINE THE POSITION OF HYDROGEN-DEUTERIUM EXCHANGE, AND THUS WHICH MECHANISTIC PATHWAY THE TRANSAMINATION FOLLOWED.

REAGENTS AND ENZYME WERE EQUILIBRATED IN DEUTERIUM OXIDE FOR 20 MINUTES TO ALLOW DEUTERATION OF EXCHANGEABLE HYDROGENS. TUBES CONTAINING 5mM L-TRYPTOPHAN, 0.03 mM PYRIDOXAL 5'-PHOSPHATE, 3.6 MG PROTEIN (ISOLATED FROM S. FLOCULLUS), IN 50mM, pH 8.0 SODIUM PHOSPHATE BUFFER, FOR A TOTAL VOLUME OF 1.4 ML WERE INCUBATED AT 37°C FOR TIMES RANGING FROM 0 to 90 MINUTES. A PARALLEL REACTION WAS CARRIED OUT WITH TUBES CONTAINING 0.1mM AMINOOXYACETIC ACID IN DEUTERIUM OXIDE. THE REACTION WAS TERMINATED WITH THE ADDITION OF DEUTERIUM CHLORIDE (OR BUTANOL); FOLLOWED BY CENTRIFUGATION AT 5000g FOR 10 MINUTES. THE SUPERNATANT WAS TRANSFERRED TO ANOTHER TEST TUBE AND DRIED UNDER A NITROGEN ATMOSPHERE. THE RESIDUE WAS RECONSTITUTED WITH 200 μl OF WATER, AND EXTRACTED WITH 200μl OF CHLOROFORM. THE AQUEOUS FRACTION WAS DRIED UNDER A NITROGEN ATMOSPHERE, AND THE RESIDUE DERIVATIZED WITH 100μl OF DIMETHYLFORMAMIDE DIETHYL ACETAL (DMF-DEA), ACETONITRILE, ETHANOL (3:2:1). ALIQUOTS OF L-TRYPTOPHAN STANDARD AND SAMPLES WERE THEN ANALYZED ON A CARLO ERBA 4130 GAS CHROMATOGRAPH WITH A 15m (0.25mm I.D.) 0.007 METHYLSILICONE CAPILLARY COLUMN WITH HELIUM AS THE CARRIER GAS. THE COLUMN WAS HEATED FROM 150°C TO 240°C AT 12°/MIN FOLLOWING A 1 MINUTE SOLVENT DELAY. THE CAPILLARY COLUMN WAS DIRECTLY INTERFACED WITH AN EXTRANUCLEAR SIMULSCAN MASS SPECTROMETER OPERATING WITH AN IONIZING VOLTAGE OF 70eV AND UNDER THE CONTROL OF AN EXTRANUCLEAR 1000 DATA SYSTEM SCANNING AT 1000 AMU/SEC OVER A MASS RANGE OF 45-502, OR IN SELECTED ION MONITORING MODE.

THE DATA WERE CONSISTENT WITH A MECHANISM IN WHICH PYRIDOXAL PHOSPHATE CONDENSES WITH THE NITROGEN OF THE AMINO ACID TO FORM AN ALDIMINE. WHEN THE REACTION WAS CARRIED OUT IN DEUTERATED BUFFER, THE TRYPTOPHAN ISOLATED FROM THE INCUBATION MIXTURE HAD DEUTERIUM INCORPORATED ONLY IN THE ALPHA-POSITION. THIS RESULT WAS CONSISTENT WITH THE PROPOSED MECHANISM IN WHICH DEUTERIUM IS INCORPORATED DURING THE PROTOTROPIC SHIFT. FURTHER EVIDENCE FOR THE MECHANISM ARISES FROM THE LACK OF DEUTERIUM EXCHANGE WHEN THE REACTION WAS CARRIED OUT IN THE PRESENCE OF THE CARBONYL TRAPPING AGENT, AMINOOXYACETIC ACID.

TRANSAMINATION MECHANISMS INVOLVING TAUTOMERIZATION OF A KETIMINE INTERMEDIATE TO AN ENAMINE CONJUGATED WITH THE INDOLE

NUCLEUS HAVE BEEN RULED OUT SINCE SUCH MECHANISMS WOULD LEAD TO INCORPORATION OF DEUTERIUM IN THE BETA-POSITION, AND NONE WAS OBSERVED. SIMILARLY, MECHANISMS REQUIRING KETO-ENOL TAUTOMERIZATION OF THE PRODUCT, 3-INDOLEPYRUVIC ACID, WOULD RESULT IN BETA-EXCHANGE WITH DEUTERIUM FROM SOLVENT. THE LACK OF BETA-EXCHANGE SUGGESTED THAT AMINATION OF ANY 3-INDOLEPYRUVIC ACID FORMED WOULD OCCUR AT A FASTER RATE THAN ENOLIZATION.

APPLICATION OF STATISTICAL PHASE SPACE THEORY
TO TERMOLECULAR ASSOCIATION REACTIONS OF CH_3^+ AND CD_3^+

Lewis M. Bass and Keith R. Jennings
Department of Chemistry and Molecular Sciences
University of Warwick, Coventry CV4 7AL, England

Statistical phase space theory has been applied to the reactions

$$CH_3^+ \text{ (or } CD_3^+) + X + He \xrightarrow{k} CH_3X^+ \text{ (or } CD_3X^+) + He$$

where X = H_2 (or D_2), N_2, O_2, CO and CO_2. It is assumed that the reactions proceed according to the mechanism

$$CH_3^+ + X \xrightarrow{k_f} (CH_3X^+)^*$$

$$(CH_3X^+)^* \xrightarrow{k_b} CH_3^+ + X$$

$$(CH_3X^+)^* + He \xrightarrow{k_s} CH_3X^+ + He$$

The results are compared with previous experimental measurements[1] and with the predictions of the modified thermal treatment[2]. The latter, which is an approximate theoretical approach, predicts that

$$k \propto T^{-(r/2+\delta)},$$

where r is the total number of rotational degrees of freedom of the reactant pair (five for the above reactions) and δ is a parameter related to the temperature dependence of the collisional activation step. In a previous study[1] δ was estimated from comparison of experimental results with the modified thermal prediction, yielding values in the range $-0.2 < \delta < +0.9$. This approach assumes that differences between the modified thermal theory and the experimental results are representative of the magnitude of δ. The purpose of the present work is to address the possibility that these differences may be representative of the level of approximation in the modified thermal treatment.

The main assumptions of the modified thermal treatment are: (1)the rate of stabilization is insignificant compared to the rate of dissociation of the complex at all energies and angular momenta, i.e., $k_b(E,J) \ll k_sM$ for all E,J; (2)the effects of the centrifugal barrier and angular momentum conservation can be treated approximately; (3)vibrational modes of the reactants do not contribute substantially to the total reactant density of states; (4)the energy dependence of the vibrational density of states of the ion-molecule complex can be ignored within the range of energies populated by the chemical activation process. The more detailed phase space theory, which accounts explicitly for

angular momentum conservation and all reactant and product degrees of freedom, does not lead to the simple behavior predicted by the modified thermal treatment. Numerical computations show that in the limit of zero pressure the phase space result can be represented as $k \propto T^{-(n+\delta)}$, but that n varies from 2.6 to 3.5 for the above systems, as opposed to the value 2.5 predicted by the modified thermal treatment. At pressures on the order of 1 Torr (the pressure regime of the experimental study) the value of n is shown to decrease by as much as 0.4 for some systems, while for the CO reactions the curvature of a plot of log k vs log T is so large as to render the T^{-n} representation unacceptable.

Comparison of phase space theory with the modified thermal approximation and with experimental data leads to the following conclusions:

(1) Deviation from the behavior $k \propto T^{-n}$ in the limit of zero pressure is caused by the increasing importance of reactant vibrational modes as temperature increases.

(2) At pressures above the low pressure limit deviation from T^{-n} behavior is caused by the increasing importance of the pressure effect as temperature (and hence, k_b) decreases.

(3) Pressures in the range near 1 Torr can be far removed from the low pressure limit for some ion-molecule association reactions. This is most likely for complexes with large bond dissociation energies (well-depths) and many low frequency vibrational and/or internal rotaional degrees of freedom.

(4) The three points above rule out the universal applicability of the modified thermal treatment. Comparison of experimental results with the predictions of this theory cannot be used as the basis for estimating the temperature dependence of collisional stabilization.

(5) For the reactions of CH_3^+ and CD_3^+ discussed here the simplest interpretation is that the experimental results are consistent with the predictions of statistical theory without the need to attribute a significant temperature dependence to the collisional stabilization step.

---

[1] N.G.Adams and D.Smith, Chem. Phys. Lett., 79, 563 (1982).

[2] E.Herbst, J. Chem. Phys., 72, 5284 (1980); D.R.Bates, J. Chem. Phys., 71, 2318 (1979).

Three-Body Ion-Molecule Association Rate Coefficients
As a Function of Temperature and Cluster Size; A.A. Viggiano
and J.F. Paulson; Air Force Geophysics Laboratory, Hanscom AFB, MA

In recent years much effort has been placed on determining the rates of ion-molecule association reactions. These rates are important in the understanding of the chemistry of the earth's atmosphere as well as interstellar clouds. We present here the first results for ion-molecule association rates measured both as a function of temperature and cluster size. The measurements were made in a selected ion flow tube (SIFT). The reactions studied are

$$NO_3^-(HNO_3)_n + HCl \xrightarrow{M} NO_3^-(HNO_3)_n(HCl) \qquad (1)$$

for n=0, 1 and 2 and

$$HSO_4^-(H_2SO_4)_m(HNO_3)_n + HCl \xrightarrow{M} HSO_4^-(H_2SO_4)_m(HNO_3)_n(HCl) \qquad (2)$$

for m=0-3 and n=0 and 1.

Rate coefficients were measured in the temperature range from 153K to room temperature. For some of the reactions, the temperature range was narrower. Three different buffers were used: N_2, H_2 and He. The larger clusters could only be studied in a hydrogen buffer because of excessive collisional dissociation upon injection into the buffer gases. All rates were measured in the low pressure limit as determined by the pressure independence of the three-body rate. All the data could be fitted to power law dependences, and the results of least squares fits to the data are shown in Table 1. Some interesting trends can be seen in the data. The most striking is the increase in the temperature dependence with increasing cluster size. For the series $NO_3^-(HNO_3)_n$ in hydrogen the temperature coefficients are 2.06, 4.17 and 5.59 for n=0, 1 and 2, respectively. The HSO_4^- core ion series shows an even larger increase in the temperature coefficient with cluster size up to a value of 7.00. This increase can be rationalized as follows. Theory predicts the temperature dependence of the low pressure rate coefficient to be inversely proportional to the temperature dependence of the internal partition functions of the reactants plus a small correction factor.[1-5] For unclustered species the temperature dependence is usually determined to be $\ell/2$ where ℓ is the sum of the rotational degrees of freedom of the reactants; vibrational modes are assumed to be inactive at the temperatures considered here. For clustered species this is not a good assumption, and one must then include effects of internal rotation and low energy vibrational modes. Both of these effects will increase the temperature dependences, as is observed.

It is also interesting to note that replacing the NO_3^- core by a HSO_4^- core increases the temperature exponent by about 0.5 This difference even pertains to the clusters $NO_3^-(HNO_3)$ and $HSO_4^-(HNO_3)$. This may indicate that HSO_4^- has a low lying vibrational mode. Replacing the HNO_3 ligand in $HSO_4^-(HNO_3)$ by H_2SO_4 leads to a much larger temperature exponent.

Finally the clustering of NO_3^- to HNO_3 has been studied as a function of pressure at room temperature. The results are shown in Fig. 1. The rate coefficient appears to saturate at a value of 2.6×10^{-10} cm^3 s^{-1} at 0.4 torr. The fact that this reaction saturates was suggested by Davidson et al[6] who noted that the rate coefficient was approximately independent of temperature at a constant pressure. The fact that the rate coefficient saturates significantly below the collision rate has important implications for deriving stratospheric HNO_3 concentrations from in-situ measurements.

References

1. D.R. Bates, J. Phys. B., 12, 4135 (1979).
2. D.R. Bates, J. Chem. Phys., 71, 2318 (1979).
3. E. Herbst, Chem. Phys., 68, 323 (1982).
4. E. Herbst, J. Chem. Phys., 72, 5284 (1980).
5. E. Herbst, J. Chem. Phys., 70, 2201 (1979).
6. J.A. Davidson, F.C. Fehsenfeld and C.J. Howard, Int. J. Chem. Kin. IX, 17 (1977).

Table 1

$k_{300}\ (300/T)^n$ for $X^-\ (HX)_n + HCl \xrightarrow{M} X^-\ (HX)_n\ (HCl)$

	Ligand #						
	0		1		2		Buffer
X^-	k_{300}	n	k_{300}	n	k_{300}	n	
NO_3^-	2.38*	3.52	16.7	3.68			H_e
HSO_4^-	5.65	3.57	0.51	7.00	2.85(T= -120)		
NO_3^-	9.32	2.06	26.5	4.17	5.28	5.59	
HSO_4^-	16.2	2.95	0.88 (H_2SO_4) ligand	6.93			H_2
HSO_4^-			8.6 (HNO_3) ligand	4.61	3.5 (T= -120)		
NO_3^-	5.22	2.62					N_2
HSO_4^-	21.0	3.06					

* 2.38 means 2.38 x 10^{-28} $cm^6\ s^{-1}$

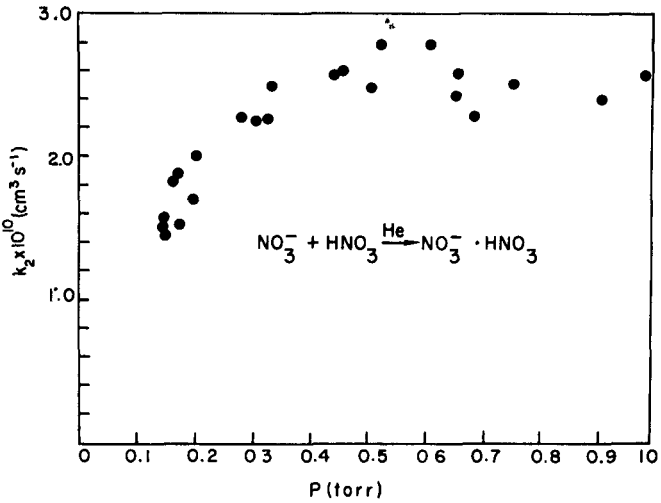

Fig. 1 Effective two-body rate coefficient vs pressure for HNO_3 clustering to NO_3^-

Rate Coefficients at 300K for the Vibrational Energy Transfer Reactions from $N_2(v=1)$ to $O_2^+(v=0)$ and $NO^+(v=0)$.

E.E. Ferguson
Aeronomy Laboratory, NOAA, Boulder, CO 80303
N.G. Adams, D. Smith and E. Alge
Department of Space Research,
University of Birmingham, Birmingham B15 2TT, UK

1. Introduction

Recently, measurements of the vibrational quenching of $O_2^+(v)$ ions[1] and $NO^+(v)$ ions[2] by a variety of neutral molecules have been carried out in flow drift tubes. The values of k_q are generally relatively large, decrease with increasing center-of-mass translational energy of the reactant ion-neutral pair in the drift tube and show a marked correlation with the ion-neutral electrostatic bond energy. These results clearly indicate that the vibrational relaxation is controlled by the long range attractive forces. The ion vibrational relaxation is described rather well by an intermediate complex model[3] in which vibrational predissociation of the complex competes with normal unimolecular decomposition back to reactants.

The reactions studied in the present investigation were,

$$N_2(v=1) + O_2^+(v=0) \rightarrow O_2^+(v=1) + N_2(v=0) + 458\ cm^{-1} \qquad (1)$$

and

$$N_2(v=1) + NO^+(v=0) \rightarrow NO^+(v=1) + N_2(v=0) - 14\ cm^{-1} \qquad (2)$$

To our knowledge these are the first measurements of vibrational transfer from a neutral to an ion at thermal energy.

2. Experimental

The experiments were carried out in a new variable temperature flow tube apparatus which has a Y shaped section upstream of a conventional flow tube. One arm of the Y is a SIFT type ion injection system and the other arm is a glass tube which allows a microwave discharge to be established in a carrier gas. Ground state ions were produced in a high pressure electron impact ion source associated with the SIFT arm of the Y and injected into a helium carrier gas flow. A controlled flow of N_2 was added to the He flow in the other arm of the Y section and vibrationally excited by the external microwave discharge cavity in a familiar procedure[4]. The extent of N_2 vibrational excitation was determined by means of the reaction

$$O^+ + N_2(v) \rightarrow NO^+ + N \qquad (3)$$

for which the rate coefficient is a very steep function of the N_2 vibrational temperature[4]. With O_2 in the ion source it was a simple matter to selectively inject O^+ ions rather than O_2^+ ions and thus utilize reaction (3) to determine T_v. Vibrational excitation of $O_2^+(v=0)$ by reaction (1) was detected using Xe as a monitor gas. The charge-transfer of $O_2^+(v=0)$ with Xe is endothermic and slow whereas the charge-transfer of $O_2^+(v > 0)$ is exothermic and rapid[1]. The Xe was added to the flow tube at either of two positions. The experiment thus involved the determination of the O_2^+ and Xe^+ signals at the downstream detector with and without discharging the N_2 (i.e. in both the presence and absence of $N_2(v > 0)$). These ion signals were used to determine the rate coefficient for reaction (4) in the usual manner. In the case of NO^+, CH_3I was used as a monitor gas[2]. This is a more ideal monitor gas for $NO^+(v > 0)$ than is Xe for $O_2^+(v > 0)$ since CH_3I charge transfers rapidly to $NO^+(v > 0)$ but not detectably to $NO^+(v=0)$.[2]

3. Results

The rate constant for reactant (1) was found to be $k_1 = 1 \times 10^{-12}\ cm^3\ s^{-1}$ within a factor of two. The rate constant for reactant (2) was found to be less than $10^{-13}\ cm^3\ s^{-1}$. Experimental details are in press[5].

4. Discussion

(i) $N_2(v) + O_2^+$

The reaction

$$O_2^+(v=1) + N_2(v=0) \rightarrow O_2^+(v=0) + N_2(v=0) + 1872\ cm^{-1} \qquad (4)$$

has a rate coefficient $k_4 = 1.9 \times 10^{-12}$ cm^3 s^{-1}. Using the intermediate complex vibrational predissociation model[3]

$$O_2^+(v=1) + N_2(v=0) \underset{k_u}{\overset{k_c}{\rightleftharpoons}} [O_2^+(v=1)\cdot N_2] \xrightarrow{k_{vp}} O_2^+(v=0) + N_2(v=0), \quad (5)$$

k_{vp} was found[3] to be 1.4×10^9 s^{-1} and $k_u = 6 \times 10^{11}$ s^{-1}. The value of k_{vp} for

$$[O_2^+(v=0)\cdot N_2(v=1)] \xrightarrow{k_{vp}} O_2^+(v=1) + N_2(v=0) \quad (6)$$

from the present measurements is $\sim 0.7 \times 10^9$ s^{-1} (within ~2).

(ii) $N_2(v) + NO^+$ (reaction 2)

The negative result for this reaction was entirely unexpected. The reaction

$$NO^+(v=1) + N_2(v=0) \rightarrow NO^+(v=0) + N_2 \quad (7)$$

has a rate coefficient[2], $k_7 = 7 \times 10^{-12}$ cm^3 s^{-1}. This is larger than k_4 and is anomalous because in all the other 6 cases of common quenchers for $O_2^+(v=1)$ and $NO^+(v=1)$, the O_2^+ quenching rate coefficient is larger[3], due to the higher NO^+ vibrational frequency (2344 cm^{-1}) compared to that for O_2^+ (1872 cm^{-1}). This anomaly was suggested[2] as being due to a resonant V→V transfer,

$$NO^+(v=1) + N_2(v=0) \rightarrow NO^+(v=0) + N_2(v=1) + 14 \text{ cm}^{-1}. \quad (8)$$

However $k_8 \sim k_2$ from detailed balance, (since 14 cm^{-1} << kT = 200 cm^{-1}). It therefore follows that $k_8 < 1 \times 10^{-13}$ cm^3 s^{-1}. Thus reaction (7) appears to be

$$NO^+(v=1) + N_2(v=0) \rightarrow NO^+(v=0) + N_2(v=0) + 2344 \text{ cm}^{-1} \quad (9)$$

It is clear that reaction (9) will dominate reaction (8) in the vibrational predissociation process from phase space arguments. The $[NO^+(v=1)\cdot N_2(v=0)]$ complex has only a 14 cm^{-1} energy band to vibrationally predissociate into $NO^+(v=0) + N_2(v=1)$, compared to a 2344 cm^{-1} band for $NO^+(v=0) + N_2(v=0)$. From a dynamical point of view, the process of $[NO^+(v=1)\cdot N_2(v=0)]$ complex formation, a prerequisite to vibrational predissociation, involves N_2 and NO^+ rotational excitation. A single rotational excitation of only the N_2 ($\Delta J=2$) by the anisotropic $NO^+ - N_2$ potential would transfer substantially more (~70 cm^{-1}) than 14 cm^{-1} energy from relative translational motion into internal energy of the complex. Thus separation of the complex into $NO^+(v=0) + N_2(v=1)$ is endothermic in the $r\cdot(NO^+ - N_2)$ separation coordinate, whereas most of the 2344 cm^{-1} energy band for vibrational predissociation into $NO^+(v=0) + N_2(v=0)$ is still accessible This model implies that the N_2 and/or NO^+ products of reaction (9) are rotationally excited. The $N_2(v=1) + O_2^+(v=0) \rightarrow N_2(v=0) + O_2^+(v=1)$ reaction has a 458 cm^{-1} energy band available so that such severe phase-space or dynamical constraints do not apply.

REFERENCES

1. H. Böhringer, M. Durup-Ferguson, D. W. Fahey, F.C. Fehsenfeld and E.E. Ferguson, J. Chem. Phys., 79, 4201 (1983).
2. W. Dobler, W. Federer, F. Howorka, W. Lindinger, M. Durup-Ferguson, and E.E. Ferguson, J. Chem. Phys., 79, 1543 (1983).
3. E. E. Ferguson, "Vibrational excitation and deexcitation and charge-transfer of molecular ions in drift tubes", in Swarms of Ions and Electrons in Gases, Editors, W. Lindinger, T.D. Märk and F. Howorka, Springer-Verlag in press, 1984.
4. A.L. Schmeltekopf, E.E. Ferguson and F.C. Fehsenfeld, J. Chem. Phys., 48, 2966, (1968).
5. E.E. Ferguson, N.G. Adams, D. Smith and E. Alge, J. Chem. Phys., 15 June (1984).

STABLE MOLECULAR IONS ABOVE FRAGMENTATION ONSET IN THE BREAKDOWN DIAGRAM OF FURAN

T. Nishimura, P. R. Das and G. G. Meisels*, Department of Chemistry, University of Nebraska 68588-0304.

The dynamics of the dissociation of polyatomic molecular ions can be described as a sequence of three steps:

(1) Ionization, which determines the initial state distribution.
(2) Internal conversion (IC) of an initial electronically excited ionic state to the vibrationally excited ground ionic state.
(3) Vibrational predissociation by which an internal mode reached though the step (2) develops to a reaction coordinate.

The quasi-equilibrium theory (QET) assumes the 100% effective and rapid radiationless transition of the step (2) and the rapid occurrence of step (3) is the basic hypothesis of the RRKM theory. Breakdowns of the step (2) and (3) give the apparent and intrinsic nonstatistical behaviors, respectively.

Lifetime of initial excited state is related to rate of internal conversion for large molecules while for diatomic molecules it may be determined directly by rate of state-specific dissociation. The statistical theory assumes that radiationless transition rate is very fast compared to dissociation rate. Hence, this leads to an interesting point-of-view that there is no reappearance of vibrational structure with increasing energy in the photoelectron spectrum after its initial loss as far as the quasi-equilibrium hypothesis is valid. Since, according to the energy gap law, internal conversion rate decreases with increasing ionization energy, dissociation rate may be disturbed by the slower internal conversion than dissociation rates particularly at higher energies. When internal conversion rate goes below 10-13, that is the typical value of vibrational frequency, vibrational structures will appear in the photoelectron spectrum. This case apparently corresponds to the breakdown of the quasi-equilibrium hypothesis. Furan is one of such interesting molecules because it shows the reappearance of vibrational structure as high as 8 eV above ionization threshold (Fig. 1).

Ionic dissociations of this molecule were studied by means of threshold photoelectron-photoion coincidence mass spectrometry.[1] As seen in Fig. 2, the reappearance of parent ions was observed at the energies corresponding approximately to the photoelectron band where vibrational structure reappears. Fig. 3 is the breakdown curves corrected for the transmission effect of energetic electrons through the threshold electron selector[2]. The breakdown graph obtained confirms the earlier report based on charge exchange measurement[3]. Fig. 4 represents the threshold photoelectron spectrum and photoionization efficiency curves (PIE) of parent and $C3H3^+$ ions. In the PIE curves, the reappearance of parent ion is supported by the increase for the parent ion and the sudden decrease for the $C3H3^+$ ion which is the most abundant ion at these energy regime.

On the other hand, the observed kinetic energy releases of the $C3H3^+$ ion (open circles) exhibits larger values than those calculated by phase space theory (solid line)[4] (Fig. 5). The linearity of kinetic energy release as a function of internal excess energy may indicate some statistical energy partitioning between internal and translational energy. The formation of $C3H3^+$ ion may possibly involve a tight transition state which exists at the late position of reaction coordinate.

We suggest that ionic dissociation of this molecule involves the initial excited states which cannot be completely interconverted to the ground ionic state. However, it seems that a molecular ion undergoing through internal conversion dissociates statistically.

Acknowledgements: We wish to thank the Department of Energy for support.

References:
(1) C. Batten, J. Taylor and G. G. Meisels, J. Chem. Phys., 65, 3316 (1976).
(2) J. P. Gilman, T. Hsieh and G. G. Meisels, Int. J. Mass Spectrom. Ion Phys., 51, 313 (1983).
(3) P. J. Derrick, L. Åsbrink, O. Edqvist, B. -Ö Jonsson and E. Lindholm, Int. J. Mass Spectrom. Ion Phys., 6, 161 (1971).
(4) W. J. Chesnavitch and M. T. Bowers, J. Chem. Phys., 66, 2306 (1977); ibid., 2228 (1981); J. Am. Chem. Soc., 99, 1705 (1977).

C_4H_4O Furan

1.

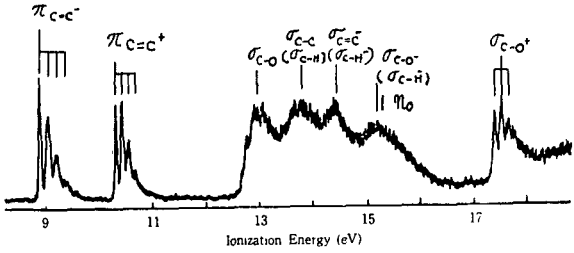

2.

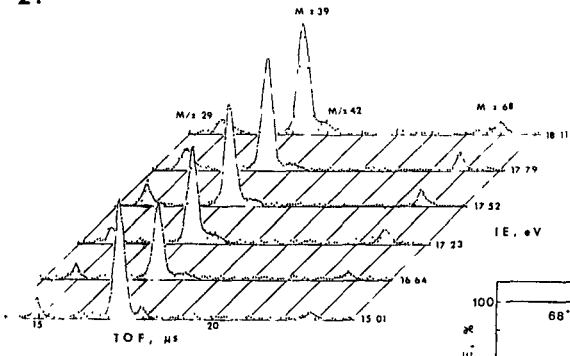

3.

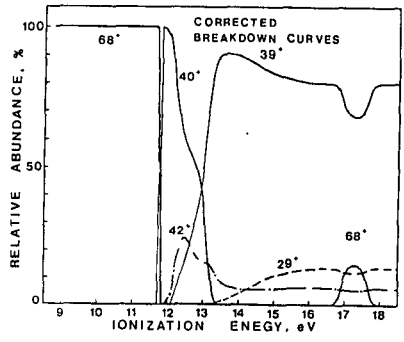

4.

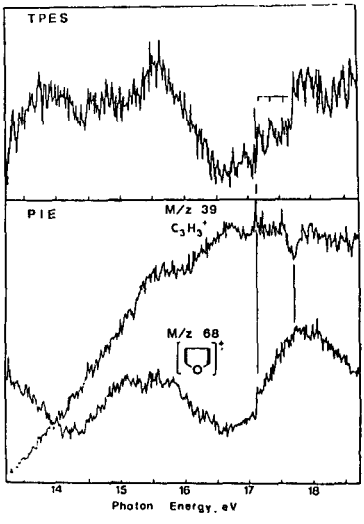

5.

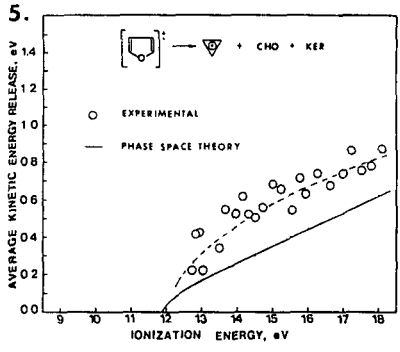

(1 + 2) CYCLOADDITION OF KETENE$^{+\cdot}$ RADICAL CATION AND NEUTRAL ETHYLENE[1]

Chhabil Dass[2]

Department of Chemistry, University of Nebraska, Lincoln, NE 68588

Cycloaddition reactions are of considerable synthetic, mechanistic and theoretical interest. Cycloadditions of neutral reactants have been extensively studied. However, few reports have appeared in the literature that describe cycloadditions involving radical cations, especially the gas-phase ions. We report here on the reaction of ketene$^{+\cdot}$ radical cation and structure of the corresponding adduct ($A^{+\cdot}$).

$$CH_2CO + C_2H_4 \longrightarrow A^{+\cdot}$$

Reactions of neutral ketene and simple olefins are not very facile. Cycloaddition between ketene and ethylene occurs but only under rigorous experimental conditions. However, the reaction occurs with ease only when LUMO-HOMO of the reactants are brought together in energies by substituting ketene with electron withdrawing groups and ethylene with electron donating groups. Compared to cyclodimerization of ethylene, increased propensity of ketene to undergo cycloadditions is attributed to electrophilicity of the central carbon atom and additional interaction of olefin pi-electrons with the vacant p-orbital of the central carbon atom. Ionization lowers energies of the frontier orbitals and should make the central carbon atom of ketene even more electrophilic. This should engender rate enhancement of the reaction of ketene$^{+\cdot}$ and ethylene. This premise was tested by reacting ketene$^{+\cdot}$ with ethylene at high pressure (0.4 torr) in a chemical ionization source of a tandem mass spectrometer (Kratos MS 50 TA).

Ketene (IE 9.6 eV) was ionized by employing $CS_2^{+\cdot}$ (IE of CS_2 10.0 eV) as the charge exchange reagent. This ensured that only ketene$^{+\cdot}$ was present as the ionized spicy (IE of ethylene 10.5 eV). The participation of ketene$^{+\cdot}$ in the cycloaddition was also confirmed by use of Fourier transform MS operating in the ion-ejection mode. The high pressure of the charge exchange gas permitted to stabilize and directly observe the adduct. The structure of the adduct was ascertained by comparison of its CAD and MI spectra with those of the reference compounds and by isotopic labelling. In view of multiformity of reaction mechanisms such as 1,2-cycloadditions across C=C and C=O, 1,3-cycloaddition (involving terminal atoms), $-CH_2$ insertion, and numerous possible acyclic additions, a variety of reference compounds were studied. These included cyclobutanone, cyclopropane carboxaldehyde, butadiene monoxide, methyl vinyl ketone, 3-methoxypropyne, methoxyallene, ethoxyacetylene, crotonaldehyde, methacraldehyde and 2,5-dihydrofuran.

Figure 1 shows CAD spectra of the adduct ($A^{+\cdot}$) and cyclobutanone radical cation, where a perfect match is observed. These spectra are quite distinct from the other reference compounds (Table 1), suggesting that structure of the adduct is that of cyclobutanone radical cation. This was further confirmed by similarities in the unimolecular spectra (Figure 2) and kinetic energy release observed for the loss of 28 amu ($T_{0.5}$ = 6.1 meV). The $T_{0.5}$ for the other reference compounds varied in the range of 35-230 meV.

The final evidence of the structure of $A^{+\cdot}$ was obtained by monitoring CAD spectra of the adducts of the reaction of ketene-$d_2^{+\cdot}$ and ethylene, and ketene$^{+\cdot}$ and ethylene-d_4 (Figure 3). The figure 3b reveals the presence of signals at m/z 58 and 60 but the absence of ion at m/z 59. Similarly, the signals at m/z 43 and 31 are absent, while the signals at m/z 42, 44 (losses of C_2D_4 and $C_2H_2D_2$), 30 and 32 are conspicuous. This is rationalized to mean that H/D scrambling does not occur in the adduct prior to or concurrent with collisional activation. This is only possible if the structure of the adduct is that of cyclobutanone radical cation. The other reference compounds, if isotopically labelled, must undergo H/D scrambling prior to formation of ketene$^{+\cdot}$.

In conclusion, ionization of ketene promotes a facile cycloaddition with neutral ethylene. The 1,2-cycloaddition occurs across C=C double bond and not across C=O double bond consistent with the chemistry of neutral ketene.

1. C. Dass and M.L. Gross, J. Am. Chem. Soc. (in press).
2. Present address: Stout Neuroscience Mass Spectrometry Lab., University of Tennessee Center for the Health Sciences, Memphis, TN 38163.

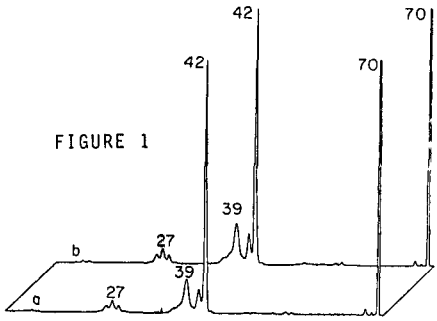

FIGURE 1

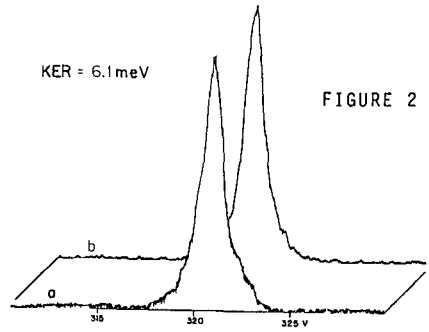

FIGURE 2

a = $A^{+\cdot}$

b = cyclobutanone radical cation

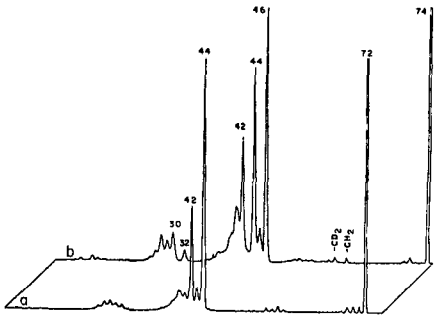

FIGURE 3

a = $CD_2CO^{+\cdot}+C_2H_4$

b = $CH_2CO^{+\cdot}+C_2D_4$

TABLE 1

PARTIAL CAD SPECTRA

COMPOUND	69	55	42	41	40	39	29	27
ADDUCT	1	1	100	10	3	14	<1	5
	1	1	100	12	3	16	<1	6
	158	100	58	41	23	52	11	20
	12	31	99	34	26	100	13	12
$H_2C{=}CH{-}\overset{O}{C}{-}CH_3$	1	100	7	2	-	3	<1	4
$HC{\equiv}C{-}CH_2{-}O{-}CH_3$	66	100	31	9	8	27	13	10
$H_2C{=}C{=}CH{-}O{-}CH_3$	312	33	100	37	34	93	34	31
$HC{\equiv}C{-}O{-}C_2H_5$	5	27	100	8	2	4	21	8
$H_3C{-}CH{=}CH{-}CHO$	659	16	63	80	17	100	22	16
$H_2C(CH_3){-}C{-}CHO$	256	13	63	73	19	100	18	14
	126	2	100	64	24	89	17	12

PROTON AFFINITY AND ENTROPY MEASUREMENTS IN HALOGENOTOLUENE MIXTURES.

M. Tereza Fernandez, Keith R. Jennings, and Rod S. Mason. Chemistry Department, University of Warwick, Coventry, CV4 7AL, England, U.K.

Recently the relative basicities (ΔG_T) of toluenes meta, ortho, and para-substituted with halogen atoms were measured independently and to good agreement at 369[1] and 478[2] degrees K, respectively, by examination of proton transfer equilibria using pulsed high pressure source mass spectrometry (PHPSMS). Relative positions down the Proton Affinity (PA) ladder for each derivative can be qualitatively rationalised, using classical mechanistic arguments in terms of the degree of proton stabilisation at preferred unsubstituted sites on the benzene ring. Both methyl and halogen (X) substituents are regarded as stabilising towards cation attachment at carbon positions on the ring in the order (4)>(2)>>(3), indicated by the open and closed circles in Figure 1.

The combined effect of two ortho, para directing substituents on the ring is also represented in Figure 1 and leads us to expect the order of PAs to be meta-> ortho->para-halotoluene, as observed for ΔG_T[1,2], and in each case a number of distinguishable sites for protonation is possible.

Strictly speaking, the relative PA of two compounds A and B is given by the enthalpy change ΔH in the reaction $AH^+ + B \rightleftharpoons A + BH^+$, where $\Delta H \approx PA(A) - PA(B)$. Measurement of the equilibrium constant K allows an estimate of ΔG as $-RT/\ln K$, where R is the gas constant and T the temperature. Since $\Delta G = \Delta H - T\Delta S$, ΔG values should be corrected for the entropy change ΔS to obtain a true relative PA value. The $T\Delta S$ term is expected, however, to be small with the major contribution coming from changes in rotational symmetry. Hence much of the data collated from the literature is based on single temperature measurements, the correction $\Delta S \approx R \ln (\sigma_{AH^+} \cdot \sigma_B / \sigma_A \cdot \sigma_{BH^+})$ applied, where σ donates rotational symmetry numbers. A further contribution to ΔS can arise, however, due to mixing of isomers if more than one distinguishable site of protonation is possible in one of the species. For n sites of equal energy the correction is R ln n. It was hoped to explore this aspect from carefully measured van't Hoff plots (ln K vs. 1/T).

PHPSMS was again used, in which tertiary mixtures of chloro and fluorotoluenes in a bath/reagent gas of methane were studied at pressures up to 2.5 torr and in the 300-590 degrees K temperature range. The data obtained for 7 systems are summarised in Figures 2 and 3 in the form of relative PA and ΔS ladders. The very surprising feature of these data are the very large values of ΔS, for four of the systems, which could not possibly be accommodated by either external rotational symmetry changes or the entropy of mixing. There also appears to be a high correlation between the magnitudes of ΔS and ΔH. If real, these values could only be accounted for by changes in internal rotation, or more likely a decrease in the number of low frequency vibrations of the more stable protonated species. This concurs with the idea of a more tightly bound proton. The relative PA values are significantly larger than anticipated from the earlier ΔG_T measurements, but still lie in the order expected from the mechanistic interpretation of Figure 1.

References: 1. Mason, R.S., et.al., J. Chem. Soc., Far. Trans. 1, 78 (1982) 1934.
2. Stone, J.A., et.al., Can. J. Chem., 60 (1982) 910.

One of us (MTF) acknowledges the Gulbenkian Foundation for financial support.

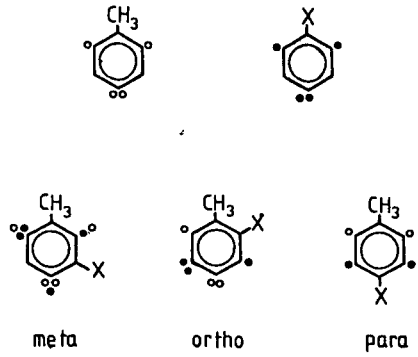

expected sites of protonation

Fig. 1

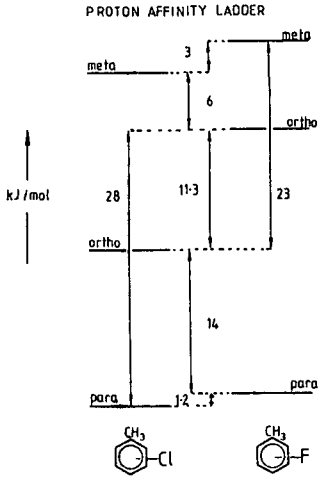

Fig. 2

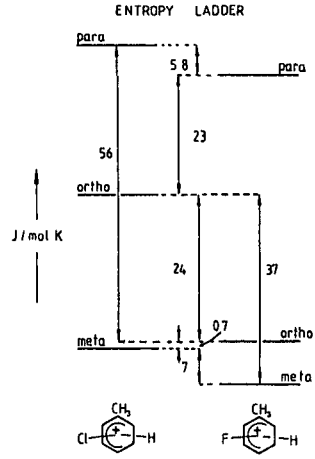

Fig. 3

Fragment-Adduct Ion Formation in Methane Chemical Ionization Mass Spectrometry by

S. Y. Chang* and C. A. Maryanoff, McNeil Pharmaceutical, Spring House, PA 19477

Addition reactions are well documented to form protonated molecular ions and reagent adduct ions, proton bound dimers of amines, dimers and oligomers. Numerous condensation products have been identified for the benzyl acetate system. The alkyl radical species from methane or isobutane reagent gases add to molecules to form M + C_nH_{2n} species. The addition reaction of vinylmethylether to olefinic bonds has been applied to locate double bond positions. Dimers or cluster ions have also been well documented in aldehydes and ketones, alcohols, amines, carboxylic acids, and methyl glucopyranosides. The formation of a benzodioxole in a CI source with catechol and a pentadiene has been shown.

The results of GC-MS analyses of a variety of organic heterocycles resulted in addition to a protonated molecular ion and fragment ions, an ion corresponding to a fragment-molecule adduct ion was observed. Table lists results from a series of saturated and unsaturated 4-diphenylmethylpyridines upon DCI analyses in comparison with hydrocarbon control compounds. In addition to a protonated molecular ion and fragment ions, an ion corresponding to fragment-molecule adduct ion was observed in all cases except controls. In the EI mode, no such ions corresponding to fragment-molecule adduct ions were observed for any of the compounds listed in the Table. It is postulated that the stable fragment ions (usually Lewis acids) form a collisionally stabilized ion with neutral parent molecules. For example, the ion-molecule reactions for compound (I) in the Table may be schematically represented as follows:

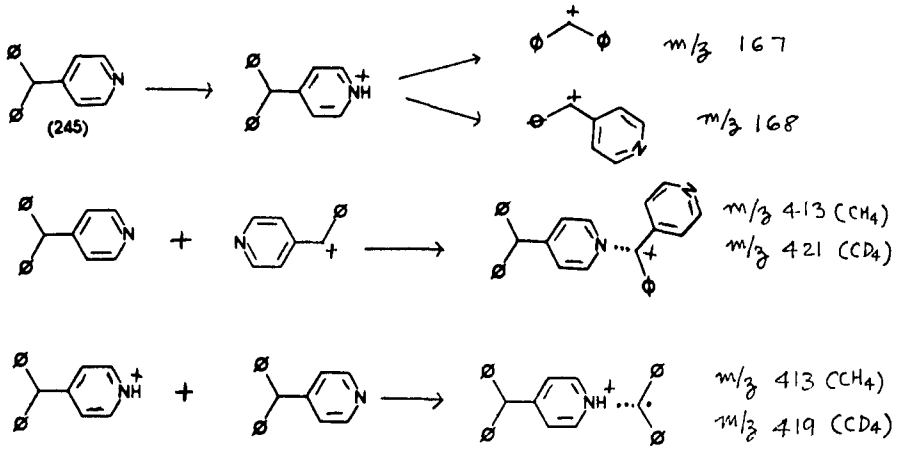

TABLE: THE FRAGMENT-MOLECULE ADDUCT ION FORMATION FROM VARIOUS COMPOUNDS BY DCI ANALYSIS.

Compounds	Molecular Ion Species (Rel. Ab.)	M + Reagent Adduct Ion (Rel. Ab.)	Fragment Ion (Rel. Ab.)	M + Fragment Ion (Rel. Ab.)	Comments
I (245)	246 (100)	M+29 (13) M+41 (3)	168 (91) 167 (5)	M+168 (1)	500 ng
	246 (100)	M+29 (12) M+41 (3)	168 (80) 167 (5)	M+168 (2)	1 μg
	246 (100)	M+29 (11) M+41 (2)	168 (80) 167 (5)	M+168 (1)	2 μg
II (251)	251 (13) 252 (13) 253 (19)	M+29 (0.2)	167 (100)	M+168 (0.3)	1 μg
III 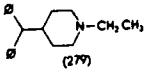 (279)	279 (45) 280 (50) 281 (100) 282 (20)	Not observed	167 (50)	M+168 (0.5)	1 μg
IV 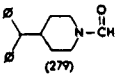 (279)	280 (100)	M+29 (21) M+41 (3)	167 (32)	Not observed	4 μg
V (244)	244 (6)	Not observed	167 (100)	Not observed	4 μg

Previously, dimeric and polymeric species had been observed. The proton bound dimers of amines are well documented. However, this is the first report, to our knowledge, of fragment-molecule adduct phenomena. This report has presented several different examples of molecules which formed fragment-molecule adducts at high sample pressure. The different examples had two common features: they contained basic nitrogen or oxygen atoms and they easily fragmented into stable Lewis acid ions.

BREAKDOWN CURVES FROM ERMS AND ARMS: APPLICATIONS TO ORGANIC ION STRUCTURES.

S. Verma and R.G. Cooks, Purdue University, Chemistry Department, West Lafayette, IN 47907.

Translational energy (E_{cm}) and scattering angle (θ) have recently been recognized as experimental variables that provide much needed internal energy resolution in the collision-activated dissociation (CAD) process. This process is of course widely used for characterizing gas phase ion structures. Because energy resolved mass spectrometry (ERMS) and angle resolved mass spectrometry (ARMS) provide two dimensional spectra resembling breakdown curves, these techniques are expected to have more structural discrimination power than conventional CAD experiments performed at a fixed energy and scattering angle (usually zero). Although both these techniques have been used to obtain breakdown curves in approximate form, neither has seen much application to ion structure problems. We are currently investigating a number of systems for which isomeric ions produce similar or indistinguishable CAD spectra by measuring their breakdown curves by these techniques. Results of these studies on $C_3H_6O^{+\cdot}$ and $C_2H_4O^{+\cdot}$ are described here. Hybrid instruments of BQQ and BBQQ geometry were employed for energy resolved and angle resolved experiments.

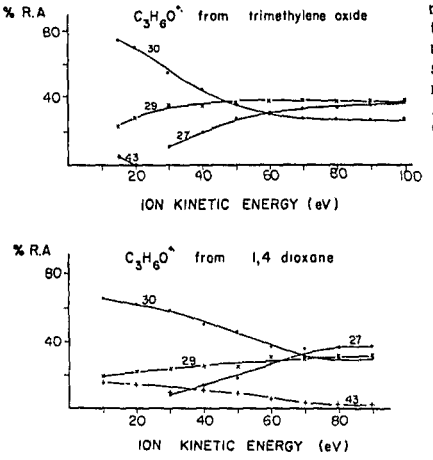

Figure 1

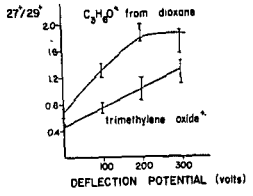

Figure 2

(i) $C_3H_6O^{+\cdot}$ ions - Based on close similarities in their CAD spectra, $C_3H_6O^{+\cdot}$ from 1,4-dioxane was assigned the same cyclic structure, 1, as ionized trimethylene oxide. Because of their sensitivity to internal energy, ions which might have contained contribution from metastable transitions were neglected in making this ion structural distinction. Figure 1 shows ERMS data for $C_3H_6O^{+\cdot}$ ions generated from trimethylene oxide and 1,4-dioxane. Both low activation energy processes (yielding 30^+ and 43^+) and high activation energy processes (giving 27^+ and 29^+) are represented. The relative importance of the two high energy processes as a function of scattering angle (100 volts 0.7°) is shown in Figure 2. One can conclude from the data of Figures 1 and 2:

1. ERMS and ARMS spectra for the two $C_3H_6O^{+\cdot}$ ions, although similar in nature, are quite distinct indicating the presence of twostructures.
2. Both low activation energy processes and high activation energy processes point to this structural difference.
3. Energy deposition in kilovolt collisions (conventional CAD) falls in a region of the break down curves where structural distinctions are most difficult to make.
4. The average energy deposited in keV collisions in these experiments is smaller than that deposited in low energy collisions.

Ion molecule reactions of $C_3H_6O^{+\cdot}$ from labelled 1,4-dioxane found it to have acyclic structure 2 with a life time of at least one millisecond.

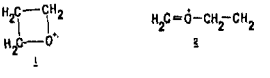

Table 1

Deflection Potential	Source of $C_2H_4O^{+\cdot}$ \ Fragment Ion	29^+	28^+	27^+	16^+	15^+	14^+
0 Volts	Acetaldehyde	87.5	-	2.5	1.5	7	2
	Butyraldehyde	50	-	31	3.5	12.5	2
	1,3-Dioxolane	84	-	-	2.5	12.5	4.5
250 Volts	Acetaldehyde	62	-	13.5	2	16	8
	Butyraldehyde	34	-	37	17	5	6
	1,3-Dioxolane	80	-	-	2	9	9.5
500 Volts	Acetaldehyde	44	-	13	2	18	21
	Butyraldehyde	33	-	25	18	8	15
	1,3-Dioxolane	38	-	-	1	22	40

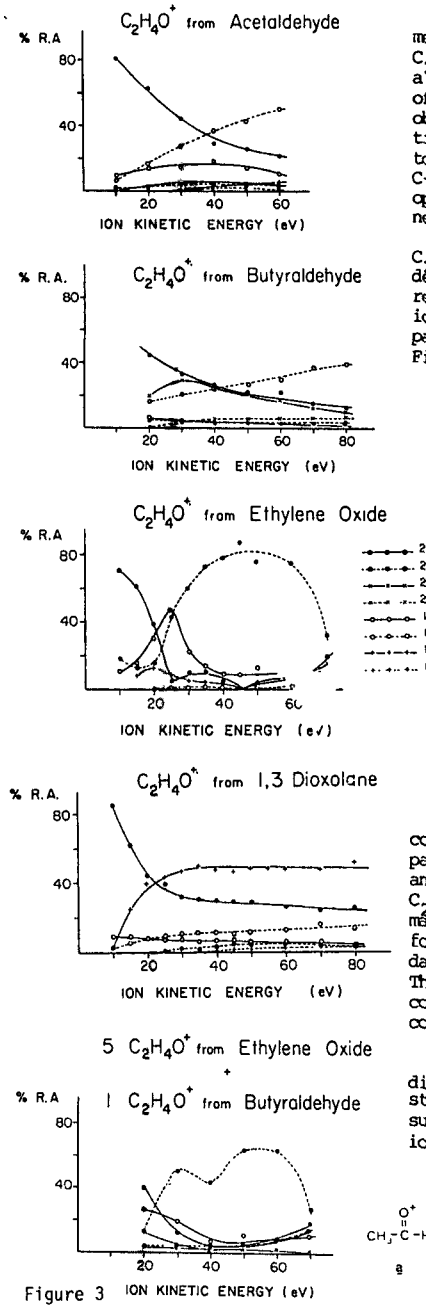

Figure 3

(ii) $C_2H_4O^{+\cdot}$ - A number of mass spectrometric techniques have been applied to $C_2H_4O^{+\cdot}$ isomeric ions in various studies. As a result 11 stable structures have been postulated of which only six (a-f) have been experimentally observed. Ion molecule reactions, photodissociation and isotopic labelling studies have been used to determine whether ethylene oxide ring opens via C—C bond cleavage or C—O bond cleavage. The ring opened ethylene oxide rapidly transfers CH_2 to neutrals in ion-molecule reactions.

Figure 3 shows the ERMS spectra of $C_2H_4O^{+\cdot}$ derived from acetaldehyde, butyraldehyde, ethylene oxide and 1,3-dioxolane. The reconstructed ERMS spectrum of the $C_2H_4O^{+\cdot}$ ions generated from a mixture of ethylene oxide (5 parts) and vinyl alcohol (1 part) is included in Figure 3. Comparison of these data show:

(i) $C_2H_4O^{+\cdot}$ ions from 1,3-dioxolane which reach the collision region are not a mixture of ethylene oxide and vinyl alcohol as suggested earlier in CAD study. Instead the dioxolane spectra indicates it to be a mixture of ions d and g.

(ii) The acetaldehyde-derived ion displays its methyl group in that the major fragmentation at all energies is due to Me^+ or $(M-Me)^+$.

(iii) The butyraldehyde-derived ion, while different to the acetaldehyde-derived ion, has an incipient methyl group (through rearrangement) and it shows abundant ions due to 29^+, 27^+ and 15^+.

(iv) The ethylene oxide-derived ion displays its ether atom function in the domination of its spectrum by $(M-O)^+$.

(iv) Ionized ethylene oxide does not ring open to structure d in the EI source as concluded by photodissociation study although it may open to e.

Corresponding ARMS data (Table 1) supports the conclusions arrived at in the ERMS study. Note, in particular, that acetaldehyde again shows $(M-Me)^+$ and Me^+ as major ions at all angles and that the $C_2H_4O^+$ ion derived from butyraldehyde shows mainly these ions as well as m/z 27. The ARMS data for dioxolane are also broadly similar to the ERMS data, although the energy deposited is smaller. The zero degree 3 keV collision (Table 1) spectra correspond to relative abundances seen in 10 eV collisions in ERMS.

Conclusion: Low energy collisions access dissociations from rather high internal energy states of the parent ion. Both ERMS and ARMS supplement other methods in distinguishing isomeric ion structures.

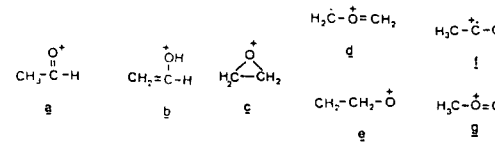

GC/MS AND GC/MS/MS ANALYSIS OF GAMMA-AMINOBUTYRIC ACID IN BIOLOGICAL SPECIMENS. EJ Norman[1], EL Wee[2], HK Berry[3] and EF Zimmerman[4], Department of Medicine (Hematology-Oncology[1]) and Pediatrics, Children's Hospital Research Foundation (Cell Biology [2,4] and Inborn Errors of Metabolism[3]), University of Cincinnati, Cincinnati, OH 45267 and DF Fraley and DL Lawrence, Procter and Gamble Co., Cincinnati, OH 45217

Gamma-aminobutyric acid (GABA) is present in high concentrations in mammalian brain and is believed to be a major inhibitory transmitter.[1] Gaba levels in cerebrospinal fluid (CSF) may reflect altered GABA metabolism in various neurological and psychiatric diseases.[2] High levels of GABA are also present in non-neural tissue of rat pancreatic islets, human insuloma, rat ovary, and rat Fallopian tube. Lower GABA concentrations occur in human blood and peripheral tissues. GABA measurements in body fluids and tissues will help elucidate the metabolic role of GABA and its diagnostic value in detecting disease states. We present a rapid GCMS method for GABA quantitation which has been applied to a wide variety of biological specimens. In addition, GABA quantitation using GC/MS/MS is also demonstrated.

AJ mouse embryos at day 14.5 were dissected and brain, body, and palate (50 pairs) were homogenized in deionized, distilled water. Aliquots were taken for protein determination. The homogenate were then diluted to 80% ethanol and 100 ng GABA-d_2, the internal standard, was added. Samples were centrifuged at 10,000 xg for 30 minutes and the supernatant was transferred to glass vials and evaporated to dryness by a stream of nitrogen. Human plasma (1 ml) and platelets (1 ml) were lyophilized with 100 ng GABA-d_2 and extracted with 80% ethanol prior to centrifugation. CSF (200 ul) and urine (200 ul) were evaporated to dryness directly after adding 100 ng GABA-d_2.

GABA was esterified using 200 ul of 1.5 N HCl in cychohexanol for 15 minutes at 115°C.[3] The cyclohexanol was evaporated to near dryness at 115°C with a stream of nitrogen. To the residue, 200 ul of ethyl acetate and 100 ul of heptafluorobutyryl anhydride were added and allowed to react at 80°C for 15 minutes. The sample was evaporated to dryness at 80°C and dissolved in 100 ul of methanol. One to four ul were injected for GCMS analysis. The HFB-GABA-cyclohexyl derivative is stable in methanol at room temperature for over three years.

GCMS quantitation was accomplished by monitoring the ions at m/z 282 (GABA and m/z 284 (GABA-d_2) with m/z 254, 299 (GABA) and m/z 256, 301 (GABA-d_2) as confirming ions.

Our initial GCMS work was accomplished using a Finnigan 3200 mass spectrometer interfaced to a Finnigan 9500 GC with a packed 3% OV-17 column. The system is equipped with a Teknivent 29 K data system. These analyses of GABA levels were obtained by isothermal injection at 185°C.

To obtain improved accuracy and specificity in quantitating low levels of GABA in complex biological specimens, capillary column separation was next applied using a new Hewlett-Packard 5970A mass selective detector equipped with a 12.5 meter crosslinked dimethyl silicone capillary column. Improved sensitivity and specificity were obtained using the HP 5970 system.

GABA was quantitated in mouse embryonic brain, body, and palate and human fluid specimens of platelets, plasma, cerebrospinal fluid and urine. These samples were injected at 150°C and the column programmed at 15°C/min, with GABA eluting at 188°C. To our knowledge this is the first reported identification of GABA in blood platelets. Because of the possibility of hydrolyzing CSF GABA-conjugates during the derivatization procedure our method should be applied to total CSF GABA analysis.[2]

GABA quantitation by GC/MS/MS was also investigated. This work was conducted using a VG 7070 EQ hybrid tandem mass spectrometer with a VG 2350 data system. The parent scan of the HFB-GABA-cyclohexyl derivative was obtained by monitoring the daughter ion of m/z 226. From the data in this spectra it initially appeared to be feasible to conduct MID parent scan experiments by monitoring m/z 284 and m/z 282 as the parent ions which produce the m/z 226 daughter ion common to both GABA-d_2 and GABA. However, in practice when applying this approach we were unable to get a reliable standard curve. In addition it was discovered that the sensivity was greatly reduced from a superior alternate approach of monitoring the m/z 256 and m/z 254 ions transition to the m/z 226 common daughter ion. Using this much better protocol we were able to get (1) an excellent correlation coefficient for our standard curve, (2) better precision and accuracy, and (3) better sensitivity.

Mouse embryonic brain specimen was analyzed by voltage switching between m/z 256 and m/z 254 on MS-I while monitoring m/z 226 with the quadruple as MS-II. Using this procedure, a standard curve was obtained with a correlation of r^2 = 0.997. Applying this standard curve to the mouse embryonic brain specimen previously shown, we obtained 0.530 nmole GABA/sample. This favorably compared to a value of 0.543 nmole GABA/sample obtained by GC/MS on the same specimen.

We have presented a rapid GCMS method for the quantitation of GABA in a wide variety of biological speciments. This methodology provides researchers and clinicians with a means to study the metabolic role of GABA and to determine the diagnostic importance of GABA in detecting disease states. In addition, we have demonstrated the feasibility of applying GC/MS/MS for GABA quantitation. The additional specificity of GC/MS/MS may prove necessary for GABA quantitation involving complex biological matrices.

References:

1. Colby BN and McCaman MW, Biomed. Mass Spectrom. 5, 215 (1978).

2. Grove J, Palfreyman MG, and Schechter PJ, Clin. Neuropharmacol., 6, 223 (1983).

3. Norman EJ, Berry HK, and Denton MD, Biomed. MAss Spectrom. 6, 546 (1979).

TANDEM MASS SPECTROMETRY FOR THE TRACE DETERMINATION OF TRYPTOLINES IN CRUDE BRAIN EXTRACTS

J.V. Johnson, R.A. Yost, Department of Chemistry, University of Florida, Gainesville, FL 32611; K.F. Faull, Department of Psychiatry and Behavioral Sciences, Stanford University School of Medicine, Stanford, CA 94305

Interest in the physiological significance of the tryptolines (1,2,3,4-tetrahyro-β-carbolines) has arisen due to their known ability to modulate monoamine activity in the central nervous system, the speculation that they may be related to the alcohol-abuse syndrome, and the possibility that they could be endogenous ligands for the benzodiazepine receptors in the brain. However, the natural occurence of tryptolines in mammalian tissue is the subject of controversy (1). This is due to the lack of specificity in the methods used for identification and the possiblity of artifactual formation during sample purification. Tandem mass spectrometry (MS/MS) has been shown to be a powerful tool for mixture analysis due to its high sensitivity and inherent selectivity (2). Here we report a triple quadrupole GC/MS/MS technique for the determination and characterization of the heptafluorobutyryl (HFB) derivatives of the tryptolines in crude extracts of rat brain (3).

A short GC colulmn (38 cm x 0.75 mm I.D., 3 % OV-101 on 80/100 mesh Chromosorb 750, 10 ml/min CH_4, 175 °C isothermal, giving a retention time of ca. 45 secs for tryptoline-HFB) was evaluated as a rapid means of sample introduction. Comparisons were made between positive and negative chemical ionization (PCI and NCI) and between selected ion and selected reaction monitoring (SIM: $(M+H)^+$ and $(M-HF)^{-\cdot}$ and SRM: $(M+H)^+ \rightarrow (M+H-213)^{+\cdot}$ and $(M-HF)^{-\cdot} \rightarrow 179^-$, respectively). Limits of detection of ca. 100 femtograms of injected tryptoline-HFB standards were obtained for both NCI modes (Table 1). However, with the analysis of crude brain extracts, quenching of the negative ion signal by a factor of ca. 6 and enhancement of the positive ion signal by a factor of ca. 23 occurred. In chemical ionization there is a competition between the formation of negative ions by electron capture, and the formation of positive ions by reaction with CH_5^+. In the chemical ionization source, there is a limited pool of thermal electrons available for electron capture by neutral molecules. In the heptafluorobutyryl derivatization of the crude brain extracts, there are many compounds besides the tryptolines which are also derivatized. Because there is little chromatographic separation of these compounds with the short GC column, the coelution of large amounts of electrophilic substances creates a competition for, and a depletion of, the thermal electron population, resulting in a quenching of the NCI signal of the relatively small amounts of tryptoline-HFB. This also results in more neutral molecules becoming available for reaction with CH_5^+ and thus, the enhancing effect of PCI. However, this enhancing effect was not sufficient to lower the limit of detection to the necessary low picogram range.

Thus, in order to take advantage of the sensitivity of NCI-SRM, a DB-5 fused silica capillary column (18 meter, 1 min splitless injection, 64 cm/sec CH_4 (275 °C), 100 °C for 1 min., linearly heated at 15 °C/min to 275 °C, and then held at 275 °C, giving a retention time of 9:41 for tryptoline-HFB) was utilized to provide better chromatographic separation in order to prevent the quenching of the NCI signal of tryptoline-HFB. The limits of detection for tryptoline-HFB with both NCI techniques were again much lower than the PCI techniques (see Table 1) and are readily attributable to the electrophilic nature of the heptafluorobutyryl group. Although NCI-SRM had a sensitivity approximately four times lower than NCI-SIM (due to the ineffeciency of the collisionally activated dissociation of the selected parent ion to the selected daughter and the subsequent mass analysis of this daughter ion), its

limit of detection was approximately two times lower due to the reduction in the chemical noise provided by the two stages of mass analysis. Analysis of a crude brain extract showed there to be a GC peak which corresponded to tryptoline-HFB (Figure 1). Comparison of Figures 1a and 1b illustrates the enhanced selectivity for tryptoline-HFB possible with NCI-SRM as compared to NCI-SIM. With its lower limit of detection and enhanced selectivity, GC/NCI-SRM is the preferred technique for the determination of tryptoline-HFB in crude brain extracts. With this technique, research is currently underway (1) to determine if the tryptolines in the brain extracts are endogenous or artifacts of sample preparation; and if they are endogenous, (2) to quantitatively determine with internal standards the levels present.

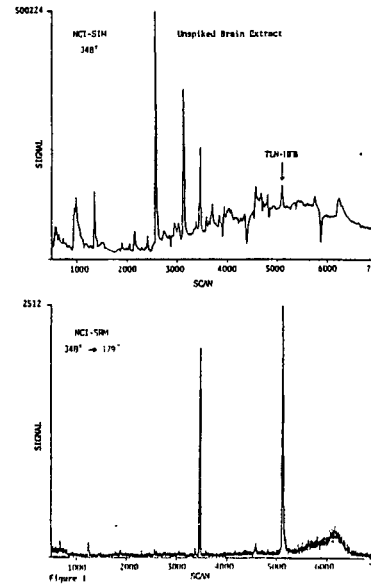

Figure 1

1. Faull, K.F.; Holman, R.B.; Elliott, G.R.; Barchas, J.D. in "Beta Carbolines and Tetrahydroisoquinolines", Alan R. Liss, Inc.: New York, 1982; p. 135.

2. McLafferty, F.W., ed. "Tandem Mass Spectrometry", John Wiley & Sons, Inc.: New York, 1983.

3. Johnson, J.V.; Yost, R.A.; Faull, K.F.; Barchas, J.D. In press, Anal. Chem., 1984.

Table 1. Characteristics of the calibration curves of standard concentrations of tryptoline-HFB.

	Packed Column[a]		Capillary column[b]	
Technique	LOD[c] (picograms)	Sensitivity[d] (counts/pg)	LOD[c] (picograms)	Sensitivity[d] (counts/pg)
Negative CI-SIM	0.07	2×10^6	0.5	3×10^5
Negative CI-SRM	0.11	1×10^5	0.2	7×10^4
Positive CI-SIM	5.5×10^3	9×10^1	19	2×10^4
Positive CI-SRM	4.2×10^3	1×10^2	60	4×10^2

[a]Single 1.0 µl injections of standard tryptoline-HFB solutions onto a short packed 3% OV-101 glass GC column at 175 °C isothermal.

[b]Single 1.0 µl injections of standard tryptoline-HFB solutions onto a 15 meter fused silica capillary. See the text for detail of program rate and CI conditions.

[c]Limit of detection (LOD) calculated as the amount of tryptoline-HFB which would give a peak area approximately three times greater than the peak area of the methanol blank.

[d]Calculated as the slope of the calibration line in the range of linearity.

FAB-MS/MS: Direct Analysis of N-Oxide Metabolites in Biological Samples.

K. Straub and P. Levandoski; Dept. of Drug Metabolism, Smith, Kline & French Laboratories, Philadelphia, PA 19101

Drugs containing alkyl-substituted amine functionalities typically undergo metabolism in vivo by a combination of reactions. These include oxidation at the nitrogen, yielding an N-oxide, or at the carbon alpha to the nitrogen, yielding a carbinolamine which, following hydrolysis, yields a dealkylated amine. Since these pathways are often the major primary reactions responsible for the metabolism of drugs containing amine functionalities, an ability to rapidly identify the relative amounts of desalkyl and N-oxide metabolites would be useful for mapping the biotransformation of candidate drugs. N-oxides in particular are difficult to analyze by conventional ionization techniques, since they readily undergo thermal degradation. We have found that particle-induced desorption techniques such as FAB yield an intense protonated molecular ion (MH^+) for N-oxides, and that collision activated dissociation (CAD) can be used to generate fragments which are characteristic of the N-oxide functionality. In addition, the increased specificity afforded by MS-MS makes it feasible to carry out quantitative analyses for these types of metabolites within a complex biological sample matrix.

A Finnigan-MAT triple stage quadrupole (TSQ) instrument was used in these studies. The instrument was equipped with a 4500 series ion source and an Ion Tech 11NF saddle field (FAB) source using xenon as the primary ionizing beam. Collision spectra were generated within Q2 using argon (1 mtorr) at an energy of -25 eV.

The substituted benzazepine SK&F 86466 (6-chloro-3-methyl-2,3,4,5-tetrahydro-1H-3-benzazepine, figure 1)[1] currently under development as a cardiovascular agent, was employed to demonstrate the utility of FAB-MS/MS for rapidly screening biological samples for amine metabolites. 2 mL of urine obtained after administration of 1 to a male Sprague-Dawley rat (2 mg/kg p.o.) was first applied to a C-18 SepPak cartridge. A methanol extract was concentrated to 50 uL, and 1 uL applied to the FAB probe. The FAB spectrum obtained on this material is shown in figure 1. The signals at m/z 182, 196 and 212 are not observed in control urine, and were further characterized by CAD. Comparison of the collision spectra of m/z 196 with that of SK&F 86466 demonstrated the presence of intact parent drug in the urine extract, and a comparison of the collision spectra of m/z 182 with that of authentic N-desmethyl analog demonstrated the presence of this species as a metabolite. The CAD spectrum of m/z 212 was found to be distinct from that of a monohydroxy analog of SK&F 86466; a comparison with the N-oxide showed that essentially all of the signal at m/z 212 in the urine extract could be accounted for by this metabolite (fig. 2). In contrast to the FAB spectrum, the EI or CI spectra of the N-oxide showed extensive fragmentation and/or thermal degradation, even when rapid heating (direct exposure) techniques were used. Subsequent experiments utilizing ^{14}C-labelled SK&F 86466 confirmed that these three components (parent drug, desmethyl and N-oxide metabolite) accounted for the bulk of drug related material present in urine.

The quantitative applicaton of FAB-MS/MS to measuring metabolite concentrations in complex biological samples was investigated using a stable isotope dilution technique. A $^2H_5$-analog of the N-oxide was added to a 1mL urine sample as an internal standard, and the sample was applied to a C-18 Bond-Elut cartridge (fig. 3). A methanol extract was concentrated and an aliquot applied to the FAB probe. The TSQ instrument was operated in a selected ion monitoring mode, with Q1 set to m/z 212 (MH^+ for the N-oxide) or 217 (MH^+ for its $^2H_5$-analog), and Q3 to m/z 180 (the dominant fragment ion obtained by CAD on m/z 212) or 185. A standard curve was then constructed by plotting the ratios of intensities of m/z 180 to 185 vs. concentration for a set of spiked urine standards. Excellent linearity was observed (correlation coefficient > 0.99) over a range of 1-100 ug/mL. A similar calibration curve was obtained for plasma, and is shown in figure 4. The lower limit of quantification for this assay requires that approximately 50 ng of metabolite be applied to the FAB probe. A comparison of the results obtained using this direct FAB-MS/MS technique with those obtained using a conventional chromatogaphic assay showed excellent agreement between the two methods. Thus the additional specificity afforded by MS/MS permits quantitative analysis of thermally labile materials within a complex sample matrix, provided an appropriate internal standard is used. Isotopically labelled analogs appear to be the best choice for this type of assay.

The in vivo metabolism of a number of amine drugs that form N-oxides have been investigated using FAB-MS/MS. The following generalizations can be made on the basis of the results obtained to date:

1) FAB ionization results in an intense MH^+ for N-oxide metabolites;
2) The CAD spectra of simple aliphatic or alicyclic N-oxides is dominated by loss of 18 amu to form an iminium ion. The CAD spectra of more complex N-oxides are frequently dominated by fragmentation involving other substructural features of the drug. Identification of N-oxide metabolites in urine or plasma extracts can often be made simply by examining the CAD spectra obtained on a mass that is 16 amu higher than MH^+ of the parent drug.
3) Quantification of drugs and their metabolites can be achieved directly in crude mixtures with FAB-MS/MS. The use of stable isotope analogs as internal standards gives the best results, and interferences from matrix components or endogenous substances can be eliminated by the use of CAD with quantification of the resulting daughter ions.

REFERENCES:

1) DeMarinis, R.M., Hieble, J.P. and Matthews, W.D. J. Med. Chem. 26:1213-1214 (1983).

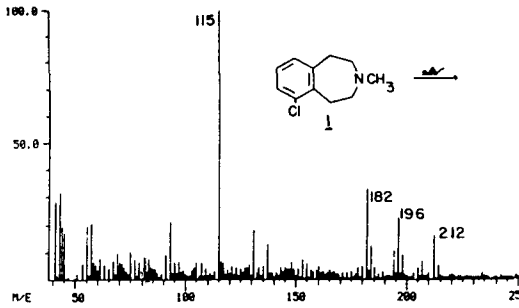

Fig 1: FAB spectrum of urine sample after administration of SK&F 86466.

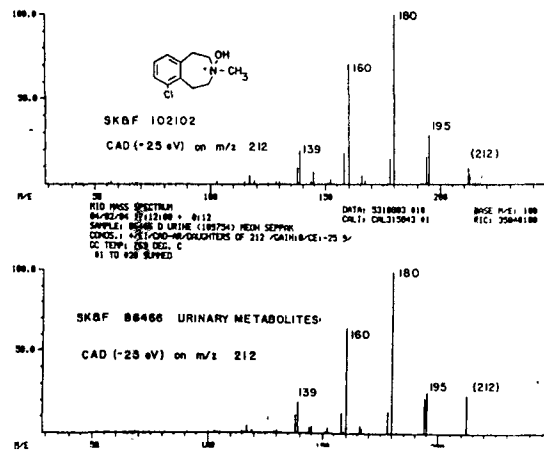

Fig 2: CAD spectra of N-oxide and of m/z 212 from urine sample.

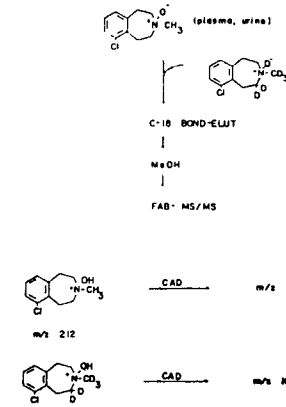

Fig 3: Scheme for FAB-MS/MS quantitation assay of N-oxide in crude extract.

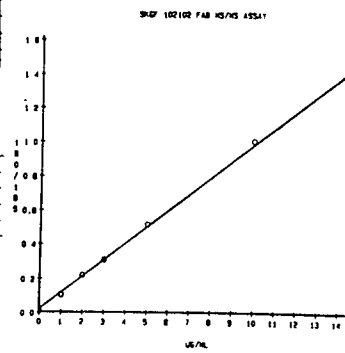

Fig 4: Standard curve obtained for N-oxide assay in plasma.

Measuring Biologically Active Compounds in Crude Plant Extracts by MS/MS

R. D. Plattner, M. D. Grove, and R. G. Powell

Northern Regional Research Center
Agricultural Research Service
U.S. Department of Agriculture
Peoria, IL 61604

MS/MS has generated interest in the past few years as a new technique to reduce the amount of sample work-up needed to analyze target compounds in mixtures. When these compounds are not amenable to GC/MS, the sample cleanup often needed for acceptable detection limits by conventional probe/MS requires that nearly pure components be isolated prior to analysis. In cases where the target compounds are present as traces in a complex sample matrix, sample cleanup requirements put severe limits on the use of MS, an otherwise attractive analytical technique. However, MS/MS yields greatly enhanced detection limits by large improvements in signal-to-noise when compared to conventional MS. Furthermore, even in cases where GC-MS of derivatized samples is possible, MS/MS offers a more rapid analysis without sample derivatization, and often has comparable detection limits.

We routinely apply MS/MS techniques for the characterization and/or quantitation of novel biologically active plant components under study in our laboratory. The following examples are typical of analytical problems that can be solved using MS/MS techniques.

Brassinolide [(22R,23R,24S)-2α,3α,22,23-tetrahydroxy-24-methyl-6,7-seco-5α-cholastano-6,7-lactone], a plant growth-promoting steroid and its probable biogenetic precursor, castasterone [(22R,23R,24S)-2α,3α,22,23-tetrahydroxy-24-methyl-5α-cholestan-6-one), were identified in partially refined extracts of Brassica napus (rape) and Alnus glutinosa (alder) pollens by combinations of probe/MS/MS and GC/MS/MS experiments. Brassinolide was not detected in black locust, oat, or corn pollen extracts. The CI (isobutane) mass spectrum of brassinolide is dominated by an intense protonated molecule (MH^+ = m/z 481). The spectrum also shows the consecutive losses of four water molecules. The daughters (argon CAD at 20 V and 1 mtorr) of m/z 481 show the losses of water as well as intense fragments at m/z 315 and 349 (Fig. 1). Single ion monitoring experiments following daughters of the MH^+ ion (481) at m/z 315 and 349 were run for crude pollen extracts. The alder and rape pollens show m/z 481 daughters at both masses, whereas the other pollens all show none. The response is nearly at the detection limit for these ions, and full daughter scan experiments are too noisy to make a positive confimation of brassinolide (i.e., an identical full daughter spectrum with the authentic standard). After partial purification using both silica and reverse-phase chromatography, the concentration in the sample matrix was increased sufficiently to allow collection of full-scan daughter spectra that are identical to the authentic brassinolide. Alternatively, we formed the methylboronate derivatives and analyzed the crude pollen extracts directly by GC/MS/MS. This allowed us to inject sufficient sample into the GC/MS to get identical full-scan daughter spectra of m/z 529 (MH^+ of the derivative) from the brassinolide methylboronate and the crude pollen extracts (Fig. 2). An authentic sample of castasterone (MH^+ = 465) was not available for MS/MS analysis; however, a homo castasterone (MH^+ = 479) was available. Castasterone was tentatively identified in the partially purified rape and alder pollen fractions, based on the close similarities of the m/z 513 (expected MH^+) daughters of the methylboronate derivative of the pollen fractions and the daughter of m/z 527 (MH^+) of the homo castasterone isomer.

Sesbanimide, an exceptionally potent antitumor compound with a novel tricyclic structure, was isolated originally from Sesbania drummondii seed. We have identified and quantitated sesbanimide at part-per-million levels in several Sesbania species. This was accomplished by MS/MS daughter experiments directly from a simple ethanol extract of the seed. The levels of sesbanimide measured by these MS/MS experiments correlated well with biological assay for the crude seed extracts. Improved detection limits were obtained by simple clean-up of the extract, involving partitioning of the methanol extract between aqueous methanol and hexane. The polar fraction was then partitioned between water and CH_2Cl_2. This simple clean-up removed ~99% of the sample matrix and allowed larger aliquots to be analyzed by MS/MS with resulting lower detection limits.

An important benefit of this simple type of clean-up is that relatively less sample matrix must be put into the mass spectrometer, which results in longer satisfactory performance of the instrument between cleanings.

Using MS/MS, several maytansinoids (novel macrolide esters), which are significantly active in vitro against standard animal tumor systems, have been identified from crude and partially purified extracts of Trewia and Maytenus species plant material and from Nocardia species fermentation broths. In the Nocardia fermentations, the homologous compounds can be identified and measured using a simple parent experiment with an aliquot of an ethyl acetate extract of the fermentation broth. Isomeric macrolide esters from the Trewia and Maytenus fractions, which differ only in the placement of functional groups on the macrolide ring, can be differentiated with daughter experiments. Several new homologs have been identified in these partially purified fractions, and their probable structures have been determined by combinations of MS/MS experiments.

The above examples demonstrate that MS/MS experiments offer a flexible and rapid approach to real analytical problems under study in both identification and quantitation of target compounds and in the finding and determination of structure for new compounds in natural product mixtures.

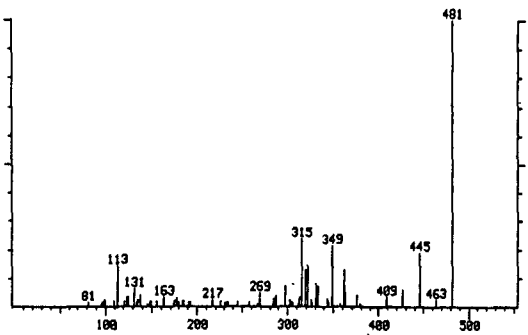

Figure 1. MS/MS (argon CAD) of MH^+ (481) from brassinolide.

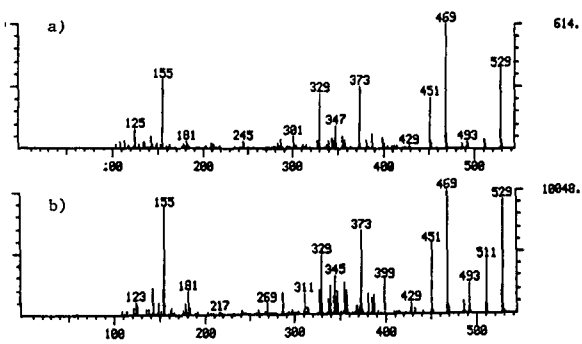

Figure 2. GC/MS/MS (argon CAD) of MH^+ of brassinolide methylboronate from a) pure standard and b) rape pollen extract.

APPLICATION OF GC/CI/MS/MS IN RAPID SCREENING OF EIGHT UNDERIVATIZED TRICHOTHECENES AND ZERALENONE IN GRAINS.

Benjamin P.-Y. Lau, P.M. Scott, Food Research Division, Health and Welfare Canada, Tunney's Pasture, Ottawa, Ontario, CANADA, K1A 0L2 and T. Sakuma, SCIEX Inc., Thornhill, Ontario, CANADA, L3T 1P2.

Current recommended methodology for trichothecene analysis involves column chromatographic clean-up and chemical derivatization followed by gas chromatography with electron capture or mass spectrometry/selected ion monitoring (MS/SIM) used for detection. Most of the methods are focussed on one to three trichothecene toxins and seem to be unsuitable for multi-component and large scale survey studies in various food products.

Using a combination of GC/CI and tandem mass spectrometry, a rapid screening procedure was developed to analyze simultaneously 8 underivatized trichothecenes [monoacetoxyscirpenol (MAS); deoxynivalenol (vomitoxin, DON); 3- or 15-acetyldeoxynivalenol (ADON); diacetoxyscirpenol (DAS); fusarenon-X (FX); neosolaniol (NES); T-2 toxin (T-2) and HT-2 toxin (HT-2)] plus an estrogenic *Fusarium* metabolite, zearalenone (ZEA). All the above *Fusarium* mycotoxins could be gas-chromatographed on a short wide-bore DB-5 fused silica column. Nivalenol tended to decompose at the transfer line temperatures required for late eluting components (e.g. T-2 and HT-2).

Molecular ions of each mycotoxin eluting from the GC column were generated in a Townsend discharge CI source through charge transfer reactions (with $O_2^{+\cdot}$, $N_2^{+\cdot}$ and $NO^{+\cdot}$ etc. from "zero air" reagent gas) and then fragmented by collision induced dissociation (CID) with argon gas. CID mass spectra of each mycotoxin were studied under various CID conditions. A compromised set of optimal operating parameters was chosen for all the components. A characteristic parent/daughter ion pair was selected for the multiple reaction monitoring (MRM) of each mycotoxin during a typical 10-15 min. GC run. Figure 1 shows the relative retention times and the parent/daughter ion masses in MRM for all the mycotoxins under study. The instrumentation detection limits (S/N=3) were 46, 60, 49, 46, 10, 18, 67, 16 and 305 picograms for DON, MAS, ADON, DAS, FX, NES, T-2, ZEA and HT-2 respectively.

The method was evaluated in extensive spiking studies (0, 50, 100, 200, 400, 800, 1000 and 2000 ppb) of these *Fusarium* mycotoxins in extracts from various commodities (Ontario soft wheat, wheat flour, oat flour, dark rye flour, popping corn and barley). Results were comparable whether extracts obtained using a CLIN ELUT™ liquid/liquid extraction column were further cleaned up by silica gel chromatography or not. The responses of each component in the spiked samples also closely matched those from the same amount of standards. In general, no severe matrix effect was observed; however, interference in the FX and NES analyses was encountered. Comparable results were also obtained from GC/CI/MS/MS and conventional GC/MS/SIM (heptafluorobutyrate derivative) analysis of 48 potato rot extracts.

RECONSTRUCTED ION CHROMATOGRAM OF UNDERIVATIZED MYCOTOXINS

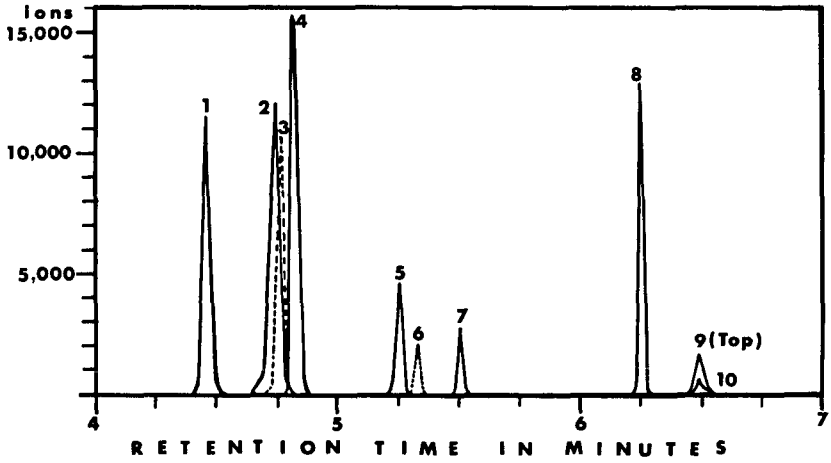

		MP/MD =
1	Deoxynivalenol (DON)	296/248
2	Monoacetoxyscirpenol (MAS)	324/264
3	Deoxynivalenol 3-acetate (3-ADON)	338/296
4	Diacetoxyscirpenol (DAS)	366/153
5	Fusarenon-X (FX)	354/175
6	Nivalenol (NIV)	312/312
7	Neosolaniol (NES)	382/122
8	Zearalenone (ZEA)	318/250
9	T-2 toxin (T-2)	466/121
10	HT-2 toxin (HT-2)	424/ 86

15m x 0.32mm i.d. DB-5 Fused Silica Column by J&W Injector 200°; Splitless mode; N_2 Carrier 7 mls/min; GC Oven held at 140° for 30 sec., then programed to 250° at 20°/min, and held for 2 min; CID Gas Argon 2.2×10^{14} atoms/cm^2

Progress in Rapid Urine Analysis for Drugs by On-Line LC/MS/MS, Jack Henion and Thomas Covey, Equine Drug Testing and Toxicology, Cornell University, 925 Warren Drive Ithaca, NY 14850

Tandem mass spectrometry (MS/MS) has received considerable attention due in part to its ability to "separate" components of a mixture. This capability results from the ability to focus ions characteristic of a given component in a mixture and obtain a CID daughter ion mass spectrum of only that component even though it was ionized in the presence of others (1). Unfortunately, factors such as matrix effects and ion quenching can cause problems with such mixture analysis by MS/MS.

We believe that MS/MS is a potentially powerful technique especially when combined with on-line chromatographic techniques. A simple preliminary sample cleanup by either solid phase or liquid-liquid extraction followed by on-line LC/MS can provide substantial reduction of matrix effects in MS/MS. The resulting LC/MS/MS experiment can provide fast, unequivocal analyte identification in addition to a mild ionization environment for fragile molecules because they are ionized in solution.

EXPERIMENTAL

The potent diuretic, bumetanide, was chosen as a real-world problem because it is not readily suitable for GC/MS confirmation. This drug has at least four active hydrogens which produces non quantitative yields of various derivatives which are required to effect any GC compatibility. GC/MS detection limits are currently only about 100 ng and not adequate for actual levels found in equine urine. HPLC with UV or fluorescence detection easily detects 10 ng and sub nanograms respectively of underivatized bumetanide. MS detection limits in the neighborhood of 20 ng are needed to confirm actual administration levels of bumetanide in equine urine.

A systematic study of various analytical techniques suggested that the heated, gas nebulized LC/MS interface provided by Sciex (Thornhill, Ontario, Canada) was the best way of determining low nanogram levels of bumetanide. The equipment utilized in this work consisted of a Waters Model 6000A pump and Model 440 UV detector set at a fixed wavelength of 254 nm. The chromatographic separation was accomplished on an Alltex three micron C-18 ODS column (4.6 mm x 7.5 cm) operated at a flow rate of 1 mL/min 50/50 acetonitrile/1% acetic acid. Samples were injected via a Model 7410 Rheodyne injector (20 microliter loop) and LC effluent directed to the inlet of the Sciex heated gas nebulizer LC/MS interface.

The interface was introduced into the atmospheric pressure chemical ionization (APCI) source of a Sciex TAGA 6000 E tandem triple quadrupole mass spectrometer. The APCI source was equipped with a corona discharge needle and the Q_2 collision gas was argon. Collision energies in Q_2 were maintained at 80 volts for most of these experiments. LC/MS experiments were conducted with Q_1 in the scanning mode and Q_3 in the RF only mode, while in LC/MS/MS experiments the parent ion was focussed with Q_1 and Q_3 was scanned through the selected mass range. Bumetanide was studied in both the positive ion chemical ionization (PCI) and the negative ion chemical ionization (NCI) modes by simply switching the previously determined optimum voltage settings corresponding to the appropriate ionization mode.

RESULTS AND DISCUSSION

Standard bumetanide was run by LC/MS and LC/MS/MS in both the PCI and NCI modes. The practical full scan detection limit (defined as that amount of standard drug which produced an acceptable full scan mass spectrum) in the LC/MS mode was 20 ng and that for the LC/MS/MS mode was 200 ng injected on column. These results appear in discrepancy from impressive sensitivity gains suggested for MS/MS by others. It is quite true that the chemical noise in the MS/MS mode is significantly reduced over what one normally observes in the single MS mode. This would normally suggest higher sensitivity because a weak ion current signal that ordinarily would be masked by chemical noise could be observed in the absence of such noise. MS/MS does provide a significant reduction in chemical noise, but it also provides a significantly weaker ion current signal through the third quadrupole. This results from focussing losses resulting from ion transmission through the third quadrupole. Since the loss in ion current signal appears to be greater than the gain achieved by reducing the chemical noise, the overall result on MS/MS sensitivity appears to be a ten-fold loss.

In spite of the fact that LC/MS/MS sensitivity was not as good as LC/MS the mixture analysis capability of the former makes it a very worthwhile analytical technique. For example, a one hour bumetanide administration urine extract run in the LC/MS mode gave the (M+1) ion for the drug in the presence of several other ions presumably resulting from coeluting interfering components. However, when the same one hour urine extract was analyzed by LC/MS/MS, a CAD mass spectrum was obtained from the bumetamide (M+1) parent ion which was

identical to that obtained from authentic bumetanide. This mixture analysis capability is made possible by the simple preliminary sample cleanup afforded by liquid-liquid extraction followed by on-line HPLC. Together these techniques provide a rapid, sensitive and very specific analytical technique for the identification of intractable organic coupounds found in biological matrices.

REFERENCES

1. J.D. Henion, B.A. Thomson and P.H. Dawson, Anal. Chem., (1982) 54, 451-456.

LOCATION OF DOUBLE BONDS IN OLEFINS BY MS/MS OF Fe(OLEFIN)$^+$ COMPLEXES.

D. A. Peake and M. L. Gross, Dept. of Chemistry,
University of Nebraska, Lincoln, NE 68588.

Two approaches have been the most successful for locating double bonds in olefinic compounds by using mass spectrometry: chemical derivatization of the double bond prior to analysis or by ion-molecule reactions in a chemical ionization (CI) source. However, weak indicator peaks and complex spectra for substituted or multifunctional olefins have limited the generality of these techniques.

A general method for location of double bonds in isomeric alkenes, alkynes, alkadienes, fatty acids (esters) and alkenyl acetates (often found as pheromones) has been developed. Reaction of olefins with $Fe(CO)^+$, generated by electron impact on $Fe(CO)_5$, in a CI source yields iron-olefin complexes that rearrange by an allylic insertion mechanism[1] (Scheme I). Upon collisional activation, the resulting bis-olefin complex preferentially loses the smaller olefin. Additional information may be derived by examination of the product ion structures. An advantage of this technique is that elemental compositions can be determined by using high resolution mass spectrometry.

The preferential insertion of Fe^+ into allylic C-C bonds is illustrated by the CAD spectra of isomeric decene complexes (Figure 1). For example, Fe(1-decene)$^+$ rearranges to (propene)Fe(heptene)$^+$ which dissociates upon CA to give $FeC_7H_{14}^+$ (m/z 154). The same allylic product is formed from Fe(5-decene)$^+$; however, isomerization to Fe(4-decene)$^+$ (Scheme II) results in the increased abundances of m/z 140 and 168 in the CAD spectrum of the 5-decene complex relative to that of Fe(1-decene)$^+$. Also, the $FeC_7H_{14}^+$ product from Fe(1-decene)$^+$ and Fe(5-decene)$^+$ can be shown to be a 1-heptene or 2-heptene complex, respectively.

The location of triple bonds with Fe^+ is demonstrated by the CAD spectra of Fe(octyne)$^+$ complexes (Figure 2). Fe(1-octyne)$^+$ rearranges via the allylic insertion mechanism to a (propyne)Fe(pentene)$^+$ complex that loses C_3H_4 upon collisional activation. Each isomeric octyne complex rearranges to an alkene-alkyne complex that dissociates to give a unique allylic product ion (m/z 110, 124, 126, 138). Isomeric octadienes are also distinguished from octynes by this method.

The MS/MS spectra of fatty acid esters or alkenyl acetates complexed with Fe^+ yield information about the ester or acetate functionality as well as the position of the double bond. Octadecenoic acid methyl ester complexes dissociate primarily by a series of olefin losses (Figure 3). The loss of olefins following allylic insertion and rearrangement results in two major fragment ions (A and B) between three less abundant ions, a pattern similar to that observed in the CAD spectra of $(M-H)^-$ from FAB ionization of fatty acids[2]. In addition, the loss of methyl radical (C) occurs from the ester functionality of the complex. Complexes of ethyl esters lose ethyl rather than methyl radicals (Figure 4).

The CAD spectra of hexadecenyl acetate complexes (Figure 4) illustrate the differences in reactivity of the ester and acetate functionality with Fe^+. The loss of $COCH_3$ (43) and formation of $FeCO_2CH_3^+$ (m/z 115) indicate that an alkenyl acetate, not a fatty acid, is complexed to the metal.

References
1. D. A. Peake, M. L. Gross and D. P. Ridge, J. Am. Chem. Soc. 1984 106, XXXX.
2. K. B. Tomer, F. W. Crow and M. L. Gross, J. Am. Chem. Soc. 1983, 105, 5487.

SCHEME I

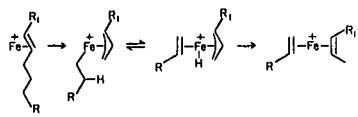

SCHEME II

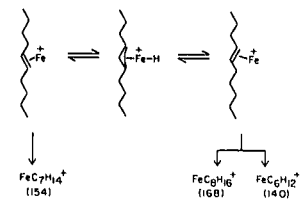

FIGURE 1

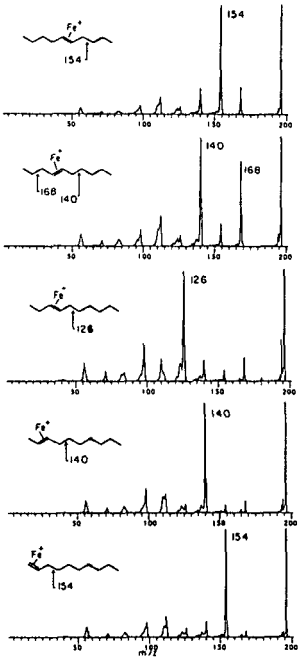

FIGURE 2

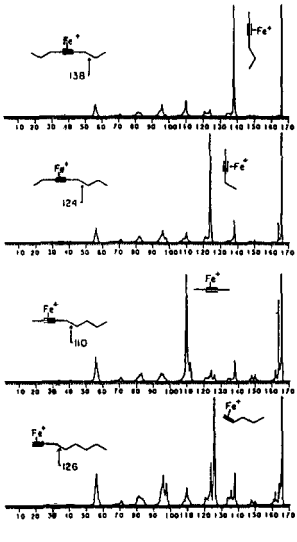

FIGURE 3

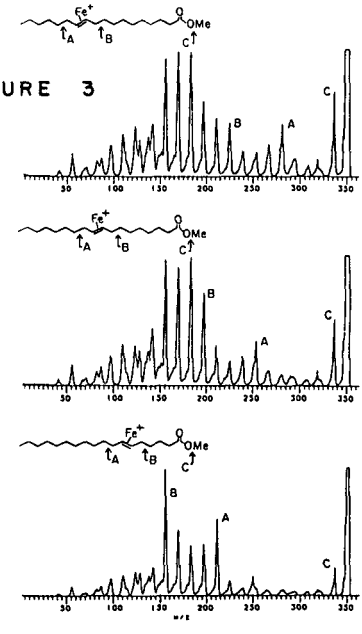

FIGURE 4

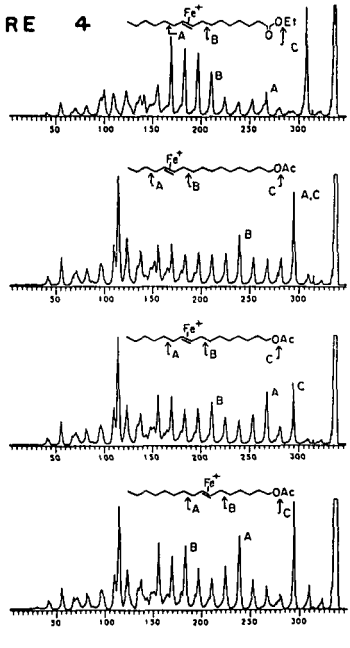

FASTER AND MORE SENSITIVE GC/MS BY REDUCING THE CAPILLARY COLUMN INNER DIAMETER

P.A. Leclercq, C.P.M. Schutjes and C.A. Cramers
Laboratory of Instrumental Analysis, Department of Chemical Engeneering
Eindhoven University of Technology, P.O. Box 513, Eindhoven, the Netherlands

While gas chromatographic retention times can be reduced at will, the possibilities for increasing the speed of analysis for a given separation problem are limited. In order to investigate the separation speed issue, a clear understanding of the relationship between retention time and column resolution (or plate number) is necessary.

The gas chromatographic retention time t_R of a compound is a function of its capacity ratio k, the resolution R with respect to an adjacently eluting solute, the column plate height H, and the average linear gas velocity $\bar{u}$:

$$t_R = f(k)\ R^2\ H/\bar{u} \qquad (1)$$

Combination of equations describing gas chromatographic processes with those describing viscous flow phenomena allows the elaboration of eqn. 1 to yield the dependence of t_R on more basic physical properties. For thin-film capillary columns, operated at the minimum value of $H/\bar{u}$, eqn. 1 reads[1,2]:

$$t_R = g(k)\ R^3\ d^x\ (\eta/D_g)^{1/2} \qquad \text{with } 1 \leq x \leq 2 \qquad (2)$$

Where d is the column inner diameter, η the dynamic viscosity of the carrier gas, and D_g the diffusion coefficient of the solute in the carrier gas (at atmospheric pressure).

If fast chromatographic separations are required, both the mobile gas and liquid stationary phases should be carefully selected. Hydrogen or helium should be employed, since these carrier gases show the lowest values of $(\eta/D_g)^{1/2}$. For a given separation problem, the gas chromatographic process can be accelerated by careful selection of the stationary phase and the separation temperature (program). These should be tuned to yield solute capacity ratios between about one and two, for which both f(k) and g(k) approach minimum values, while maximizing the value of the relative retention $\alpha = k_2/k_1$ of two solutes eluting as adjacent chromatographic peaks.

Once the carrier gas, k, α and R have been selected, the separation speed can only be increased by minimizing $H/\bar{u}$ (eqn. 1). Requiring optimum gas chromatographic operating conditions, one way of minimizing $H_{min}/\bar{u}_{opt}$ is to operate a given open tubular column at vacuum outlet, as reported before[3,4].

This method pays off particularly for (wide-bore and/or short) low-pressure-drop columns with moderate plate numbers. With low-pressure-drop columns, $H/\bar{u}$ can be decreased also by employing linear gas velocities up to three times the optimum value[2].
The other possibility left to shorten analysis times for a given separation problem, is to lower the $H/\bar{u}$ ratio by reducing the column inner diameter d (eqn. 2)[2,5]. Since H is directly proportional to d, the column length can be reduced in proportion to d while maintaining the required resolution. For short, low-plate-number columns working at low pressure drops, the optimum carrier gas velocity is proportional to the column diameter, so that t_R is found to decrease as the square of d. For columns with high plate numbers, and hence with large pressure drops, t_R is directly proportional to d, while $\bar{u}$ approaches a constant value.

In this paper the application of 50 µm i.d. columns in GC/MS was presented. These columns separate mixtures more than five times faster than the conventional 0.25 mm i.d. columns with similar plate numbers. At the same time the identification and detection limits are decreased at least five-fold as well because the GC peaks are narrower and taller. Typically, analysis times with 25 m x 0.25 mm i.d. columns range from 20 - 100 min, and 0.5 - 1 ng per compound is needed to produce interpretable (EI) mass spectra. With 5 m x 50 µm i.d. columns the problem can be solved within 3 - 15 min, while 50 - 200 pg of material suffices.

High scan speeds, up to 20 mass spectra per second, are imperative to match the performance of these columns. Under these conditions high-quality mass spectra could be produced, enabling automatic library searching methods.

Several examples of applications were presented and will be published elsewhere[6].

References:

1. G. Guiochon, Anal. Chem., 50 (1978) 1812.
2. C.P.M. Schutjes, Dissertation, Eindhoven University of Technology, 1983.
3. C.A. Cramers, G.J. Scherpenzeel and P.A. Leclercq, J. Chromatogr., 203 (1981) 207.
4. P.A. Leclercq, G.J. Scherpenzeel, E.A.A. Vermeer and C.A. Cramers, J. Chromatogr., 241 (1982) 61.
5. C.P.M. Schutjes, E.A.A. Vermeer, J.A. Rijks and C.A. Cramers, J. Chromatogr., 253 (1982) 1.
6. P.A. Leclercq, C.P.M. Schutjes and C.A. Cramers, Chromatographia, submitted for publication.

FOC 3 CHARACTERIZATION OF ALKYLAMINE COMPLEXES OF Fe, Cr, AND Mo USING FAB AND MS/MS

GALE A. HOLMES
DOW CHEMICAL U.S.A.
FREEPORT, TX 77541

D.H. RUSSELL
DEPARTMENT OF CHEMISTRY
TEXAS A&M UNIVERSITY
COLLEGE STATION, TX 77843

FAB analyses on the alkylamine complexes of Cr, Fe, Ni and Mo were performed using various matrices. The matrix used include glycerol, thioglycerol, sulfolane and 2-nitrophenyl-octylether. The best overall results were obtained using the glycerol matrix. In most cases the desired $[M + H]^+$ ion was not observed for these complexes.

Using a normal loading (5-10 µg) in glycerol the $Ni(en)_3Cl_2$ complex (mol. wt. 308) formed cluster ions at and above the molecular ion region. To minimize the formation of cluster ions a small loading (<1 µg) of the complex in glycerol was used. However, even under these conditions an ion 4 amu below the expected $[M + H]^+$ ion (m/z 309) was detected, i.e., m/z 305. MS/MS studies on this ion indicated the loss of 92 to form the fragment at m/z 213. These results coupled with the presence of the m/z 245 ion in the normal spectrum supports the following assignment for the m/z 305 ion.

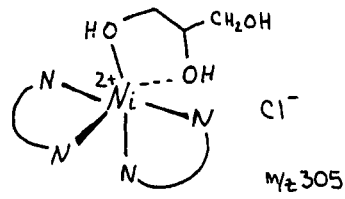

The occurrance of the m/z 305 ion can be rationalized by two different mechanisms: (1) ligand substitution in solution as shown below

$$\underset{\text{(mol. wt. 308)}}{Ni(en)_3Cl_2} \xrightarrow[\text{Substitution}]{\text{Ligand}} \underset{\text{(mol. wt. 340)}}{Ni(en)_2(glycerol)Cl_2}$$

$$\downarrow \text{Bombardment}$$

$$\underset{\text{m/z 305}}{{}^{2+}Ni(en)_2(glycerol)Cl^-}$$

or (2) recombination of the m/z 213 ion with glycerol in the selvedge region above the matrix.

$$Ni(en)_3Cl_2 \xrightarrow{\text{Bombardment}} \underset{\text{m/z 213}}{{}^{2+}Ni(en)_2Cl^-} \xrightarrow{\text{glycerol}} \underset{\text{m/z 305}}{{}^{2+}Ni(en)_2(glycerol)Cl^-}$$

By contrast no evidence of glycerol interaction was observed during analysis of the $Cr(en)_3Cl_3$ complex. Predictable fragments corresponding to the loss of chlorine and chlorine plus HCl were detected at m/z 302 and m/z 266, respectively. The multi-stepped decomposition of these ions was mapped using MS/MS and found to generate common ions at m/z 171 and m/z 142.

The diethylene triamine (DETA) complexes of nickel and iron decomposed by similar mechanisms to form $[M - Cl]^+$ and (M - Cl) - DETA ions. In contrast to the nickel complex, the iron complex formed the $[M + H]^+$ ion. This ion also decomposed by the loss of DETA and $FeCl_2$ to form the protonated DETA ion at m/e 104.

The well-known MoO_3-DETA complex, and uncharacterized $MoO_3(EDA)_x$ complexes were also investigated. Analysis of all complexes indicated the presence of a common species. The positive and negative ion data were interpreted in terms of the fragmentation of $Mo(glycerol)_3$ complex which was formed (presumably) by solution ligand exchange reactions.

Our data shows the difficulties associated with ligand exchange reactions between the liquid matrix and organometallic species. These ligand exchange reactions limit the utility of liquid SIMS for structural characterization of organometallic species; however, these studies do indicate that liquid SIMS may provide a convenient method for measuring (solution phase) relative ligand binding energies.

A MICROCOMPUTER-BASED WORKSTATION FOR THE INTERPRETATION OF MS/MS SPECTRA

Michael P. Barbalas, Department of Pharmacokinetics, Biopharmaceutics and Drug Metabolism, Hoffmann-La Roche, Inc., Nutley, NJ 07110.

The major applications of tandem mass spectrometry (MS/MS) have been mixture analysis and structure elucidation. To date, the majority of applications have been determinations of specific compounds or specific classes of compounds in mixtures. Tandem mass spectrometry should also be generally useful for structure elucidation problems. One obstacle which has hindered this development has been the lack of suitable libraries of reference MS/MS spectra and mechanisms to readily access such libraries.

The major benefit from using tandem mass spectrometry for structure elucidation is the increased amount of information which can be obtained from a sample. The major problem which accompanies this increase in useful information is the increase in the dimensionality of the data. While a normal mass spectrum contains only the two dimensions of mass/charge and abundance, a set of MS/MS spectra contains an additional mass axis. This increase in dimensionality creates problems for the chemist who tries to think in terms of chemical structures but faces data spread out in three dimensional fragmentation plots.

Several groups have proposed the use of computers and graphical displays to help overcome this problem. Two graphical approaches include contour plots and pseudo-three dimensional plots. In either case, while the presentation of the data may be complete, the interpretation is not straightforward. Another technique is fragmentation mapping. Here an inverted tree is constructed with the highest mass (most complex) ions at the top and branching downward to simpler and smaller ions. This approach has also been used for high resolution data and is useful when a series of characteristic losses can be recognized.

This current work provides another approach oriented toward providing substructural information as its major output. A microcomputer workstation was developed to allow a user to interpret MS/MS data in terms of chemically significant substructures without the need to manually inspect two dimensional slices of a three dimensional data set. This approach can be best illustrated by an example. Given an MS/MS data set of an unknown a mass spectrometrist will form and test structural or substructural hypotheses as he develops a coherent interpretation of the data. With the MS/MS workstation the same mass spectrometrist could first retrieve all the ion structures in his unknown data set which match reference spectra in current databases. While this is a relatively minor task for the computer, it would allow the mass spectrometrist to rapidly focus on the truly unknown ions in his data set and to complete the interpretation process much more rapidly. In addition, the system would provide some documentation of structures and spectra which were already contained in the database.

The workstation approach is built around the strengths of both the trained user and the computer. Creative and intuitive functions are left to the user. Retrieval and calculations are done by the computer under the direction and control of the user. The user is free to manipulate his data according to his choice. The workstation merely provides tools to make those manipulations possible and practical. The workstation is capable of displaying multiple graphics windows containing text, spectra, or chemical (sub)structures. The workstation can communicate bidirectionally with other computer systems to allow the user access to corporate or other remote databases.

This workstation was implemented on an IBM-9000 laboratory computer system. There were three attractive features of this micro-computer: 1) relatively high graphics resolution ; 2) large physical memory (500 kB); and 3) multiple communication ports. The first feature in necessary to display several items simultaneously. The second feature permits large development programs to run or for several smaller units to run concurrently. The communication feature was needed to permit communication with other systems.

The workstation software includes a set of tools for the interpretation of MS/MS spectra. These include communication, spectra manipulation, and structure manipulation. Although the workstation currently has almost 1 MB of disk storage the user is not limited to working with local sets of data. The workstation can be used to communicate with an external system in an interactive mode or files of data can be sent to or received from an external system. These external systems could be a corporate computer or an instrument data system.

The spectra handling tools are coupled with the structure display routines. Basic functions for spectra include plotting or tabulation. In addition, spectra can be matched against a database of reference MS/MS spectra. The current searching system uses the ten largest peaks and does a forward search. More sophisticated algorithms can easily be implemented as the quantity and quality of MS/MS reference data increases. At any time the user can display two spectra and, optionally, their difference. When a library search is done both the matching spectra and the associated structures are retrieved. The user can display up to three structures associated with spectra retrieved from the database. This can be quite helpful as a documentation aid and gives the user ouput which is chemically significant. These functions are accessible via a graphics menu or the user can use keyboard commands to direct the system.

Current limitations of the system are the relatively small library of reference spectra (850 spectra) and the general unavailability of connection tables for the ion structures of reference spectra. Despite these limitations the system should be generally useful as a tool to aid the mass spectrometrist in interpretation of MS/MS spectra.

Acknowledgements:

Drs. George Weiss and Alex MacDonald, Animal Science Research, Hoffmann-La Roche, Nutley, NJ for use of IBM-9000 computer.

Dr. In Ki Mun, Lederle Laboratories, Pearl River, NY for structure display.

Dr. William R. Davidson, SCIEX, Thornhill, Ontario, Canada for reference MS/MS spectra.

STRUCTURES AND STABILITIES OF (CnH2n-1O)+ IONS PRODUCED IN LOW ENERGY PROCESSES.

Yannik HOPPILLIARD and Guy BOUCHOUX
Laboratoire de Synthese Organique. Ecole Polytechnique.
91128 PALAISEAU-Cedex (France).

ABSTRACT

The relative stability of isomeric (CnH2n-1O)+ ions, generated from ionized methylketones have been established comparing the experimental evaluations of their enthalpies of formation ΔHf with the corresponding calculated values. The calculations have been performed using both semi empirical and "ab initio" M.O. calculations methods.

INTRODUCTION

The (CnH2n-1O)+ ions are very common daughter ions of a great variety of oxygenated radical cations.

Isomeric ions having the same formula but different geometrical representations are identified with their metastables decompositions, using multiple sectors mass spectrometers. Analytically, the systematic investigation of a serie of isomeric ions becomes later usefull to identify one of these ions generated from an unknown precursor.

Methyl elimination from ionized methylketones leads:

- in high energy processes to an acylium ion (R-C=O)+,
- in low energy processes to the most stable (CnH2n-1O)+ ion. The structure of this ion is depending on its carbon number.

EXPERIMENTS

Precursors and fragments ions, studied in this work, are all metastables ions, formed in the source of a mass spectrometer (ZAB-2F or modified MS902)and decomposed in F.F.R.

The origin of the lossed methyl has been verified using labelled compounds.

The reacting isomeric ions have been differentiated comparing their unimolecular decompositions (MIKES) and the kinetic energy release associated to each decomposition (n(T),T0.5). The non reacting ions have been characterized, with their CID-MIKES.

To the formation of each isomeric ion structure is associated a thermodynamical value: the enthalpy of formation taked as stability criterion.Experimental values of ΔHf have been deduced from ionization and appearance energy determinations (Varian MAT-CH5) and from proton affinity evaluations (Nicolet ICR). The ΔHf of the neutral molecules are known.

CALCULATIONS

Calculated values of ΔHf have been obtained from semi-empirical MO calculation methods (MINDO/3 and MNDO),parametred to give ΔHf.

Ab initio calculations methods, performing only the total energy E of a species, two isomeric ions A+ and B+ are compared evaluating the difference ΔE= E(A+)-E(B+) (relative stability). These calculations have been carried out with a 4-31G basis set and with an electron correlation incorporated at the level of the second order Moller-Plesset (MP2) perturbation theory.

RESULTS

In FFR, ionized acetone and butanone decompose exclusively to acylium ions: respectively (CH3-C=O+, A1 and CH3-CH2-C=O+, A2).

The 2-pentanone molecular ions give a mixture of A3 ($CH_3-CH_2-CH_2-C{=}O^+$, 85%) and B3 ($CH_3-C(OH)-CH-CH_2^+$, 15%). The ionized 3-methyl,2-butanone fragment into 65% of A'3 ($(CH_3)_2-CH-C{=}O^+$) and 35% of B3.

The metastables ions of the four $(C_6H_{12}O)^+$ isomeric ketones: 2-hexanone I, 3-methyl,2-pentanone II, 4-methyl,2-pentanone III and 3,3-dimethyl,2-butanone IV eliminate, quasi exclusively, a methyl from the lateral chain to form B4 ($CH_3-C(OH)-CH-CH_2-CH_3^+$); only II and IV give a weak pourcentage of acylium ions.

Table 1 gives the energy differences between the most stable ($C_nH_{2n-1}O^+$, n=2,3,4,5) ions.

Table 1. Energy difference between the most stable structures of ($C_nH_{2n-1}O^+$) ions. ΔE is expressed in kcal.mol-1.

	KETONIC FORM A		ENOLIC FORM
$C_2H_3O^+$	A1 ($CH_3C{=}O$)+		B1 (CH_2COH)+
Experimental	0		+18
MNDO	0		+27
MP3/6-31G**(1)	0		+44
$C_3H_5O^+$	A2 ($CH_3CH_2C{=}O$)+		B2 ($CH_2CHCHOH$)+
Experimental	0		+11
MINDO/3	0		+14
MP2/4-31G	0		+14
$C_4H_7O^+$	A3	A'3	B3
Experimental	0	-2	0
MNDO	0	-1	-2
$C_5H_9O^+$	The four A4		B4
Experimental	0		-6
MINDO/3	0		-5

CONCLUSION

The relative stability between the enolic and ketonic forms of ($C_nH_{2n-1}O$)+ ions is strongly depending on n. For n=2 or 3 the ketonic form is more stable than the enolic one. For n=4 the acylium and hydroxycarbenium ions have the same stability. For n=5 the conjuguated enolic ion becomes more stable than all the acylim ions (the four acylium ions being very close together in energy). the methyl elimination from ionized ($C_6H_{12}O$)+ (n=3-6) methylketones leads, ever, to the most stable final state.

REFERENCE

(1)R.N. NOBES, W.J. BOUMA and L.RADOM, J. Amer. Chem. Soc.,105, 309 (1983).

THE ANALYSIS OF TRACE QUANTITIES OF THERMALLY LABILE COMPOUNDS BY THERMOSPRAY LIQUID CHROMATOGRAPHY - MASS SPECTROMETRY.

I.A.S. Lewis and D.C. Smith, VG Analytical Limited, Floats Road, Wythenshawe, Manchester, England and M. Veares, The Department of Biochemistry, The University of Liverpool, P.O. Box 147, Liverpool England.

The Thermospray technique[1] has been demonstrated to overcome some of the basic incompatibilities between liquid chromatography and mass spectrometry. In reality, the method comprises, not only an interface designed to permit the continuous introduction of liquid into the mass spectrometer, but also a new ionisation technique.

In practical terms the interface's ionisation efficiency and the flow rate of liquid into it are interdependent. This is because the most acceptable theory for the generation of solute ions from a charged spray teaches[2] that the mass to charge ratio on droplets is the important factor in determination of ionisation efficiency. Thermospray ion analysis is perpendicular to the spray and the charge to mass ratio on droplets generally increases as the distance from spray increases. Given a single set of flow conditions the only variables controlling the droplet charge to mass ratio are the spray temperatures, and the experimenter is required to balance these temperatures to yield drops of the appropriate size, for ion evaporation to take place, at the analysis point (Fig. 1). We have found that insertion of an electrode (Fig. 2) into the spray at a point down stream from the analysis point can excercise repulsion or obstruction to the charged spray, such that a greater abundance of charged drops of 'ion evaporation' size may be made to dwell for a longer period at the analysis orifice. Analysed ion current may be maximised (Fig. 3) and the requirement to establish the best spray temperature, minimised, by the application of electric field to the electrode.
The increase in analysable ion current available by use of this electrode allows the very low level detection of materials by LC-MS. Detection limits at the low nanogram level for steroidal sulphates and penicillins have been demonstrated. An example of the SIR detection for the ^{32}S isotopic parent ion from a diaminoethane is shown (Fig. 4a), together with the response for its ^{34}S isotope parent ion at less than 2pg (Fig. 4b).

An interesting and analytically useful effect resulting from the application of voltage to the downstream electrode is shown in Figs. 5 and 6. As the voltage to the electrode is increased the nature of the thermospray parent ion can be varied. The Thermospray spectra of carbowax 200 in low and high voltage modes are shown in Fig. 5. At low voltages the spectrum is dominated by ammoniated parent species (an ammonium acetate buffer was used), whereas at higher voltage the spectrum is dominated by protonated species. (All other conditions were constant). In certain instances this change is accompanied by a change in the extent of fragmentation observed e.g. the low voltage spectrum of diethypthalate, dominated by parent ions, is accompanied (Fig. 6) by its higher voltage spectrum, dominated by fragment ions (again all other conditions were constant).

The design of this commercially available thermospray interface and source is discussed.

1. C.R. Blakley and M.L. Vestal, Anal. Chem. 1983, 55 750 and references there in.

2. B.A. Thomson and J.V. Iribarne, J. Chem. Phys., 1979, 71, 4451.

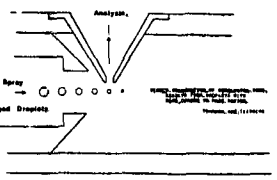

FIG 1

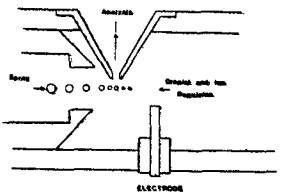

FIG 2

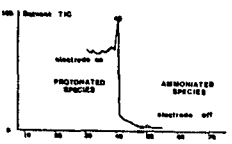

FIG 3

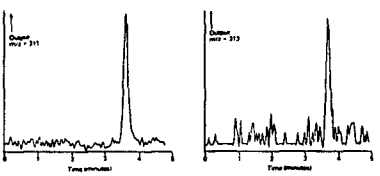

FIG 4

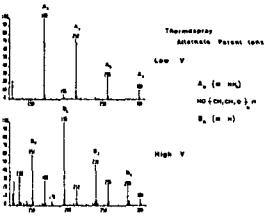

FIG 5

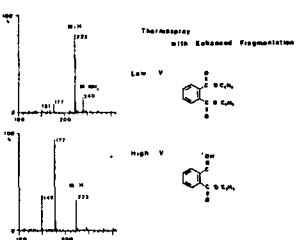

FIG 6

HIGH SENSITIVITY ASSAY FOR PHENOLIC ACID DERIVATIVES WITH OH^- NEGATIVE CHEMICAL IONIZATION.

F. Aladar Bencsath, Jack S. Schweitzer*, Arnold J. Friedhoff* and Frank H. Field; The Rockefeller University, New York, New York 10021, New York University*, School of Medicine New York, New York 10016

Phenolic acids are oxidative metabolite products of catecholamines. Their mass spectrometric determination is usually carried out by GC/MS of the O-perfluoro acyl fluoroalkyl ester derivatives using electron impact ionization and the corresponding deuterated acids as internal standards[1,2]. However, the molecular ion carries less than 1% of the total ionization, and the most abundant fragment ion still adequate for quantification carries 2 to 3%.

Detailed GC/MS studies were performed with homovanillic acid (HVA) derivatives. This acid attracted a special interest of those investigating mental disorders:

its production in the central nervous system seems to be strongly affected by schizophrenia. Because the contribution of the peripheral nervous system can be selectively suppressed by drug treatment (Carbidopa®), the HVA amount produced by the brain can directly be measured by monitoring the blood HVA level.

The normal HVA concentration in the blood is about 10-20 ng/ml and 20-30% of it, i.e. 2-6 ng/ml is generated in the brain. This low concentration calls for a more sensitive detection method than EI/MS.

Different derivatives of HVA were prepared and their mass spectral behavior compared under isobutan +CI and OH^- CI[3] condition. Methanol, trifluoroethanol or heptafluorobutanol were used to esterify the carboxyl end and acetylation, trifluroacetylation or heptafluorobutyrylation was used to esterify the phenolic OH group. The following was found:

1. In the isobutane CI spectra of the acetylated derivatives abundant MH^+ ions appeared, and the spectra of the perfluoro acyl derivatives were dominated by the de-acylated ionization product. Both kinds of ions, carrying 40-60% of the total ionization, are useful for quantitative work.

2. Under OH^- negative CI conditions the senstivity was 40-100 times higher than under i-butane CI. From the acetylated derivatives, mainly (M-H) and $(M-CH_2CO)^-$ ions were generated in about equal amounts. Both are adequate for quantitation. The high response ensures a 2 to 3 order of magnitude higher sensitivity for a HVA assay than that available by the electron impact ionization method. The perfluoro-acylated derivatives provide only analytically useless perfluoro alkyl carboxylate anions with OH^- negative CI.

3. The sensitivity of a GC/MS/selected ion monitoring assay using the acetylated HVA-methyl ester derivative with OH^- negative CI is limited only by the sample loss through the GC column. Using a large amount of the deuterated standard (250 ng d_5-HVA/ml plasma) as GC carrier, a good precision was achieved with a 11.5 ng HVA/ml plasma sample (C.V.=2.0%, N=6).

REFERENCES

1. G.M. Anderson, J. Chrom. 277, 282-286 (1983).
2. E.B.M. DeJon, B.P.M. Horsten and H.M.J. Goldschmidt, J. Chrom. 279, 563-572 (1983).
3. A.L.C. Smit and F.H. Field, JACS 99, 6471-6483 (1977).

Comparison of i-Butane⊕ and OH⊖ CI spectra of HVA derivatives

HVA DERIVATIVE	CI MODE	M/Z (REL INT %)	IDENTITY OF ION	REL. ION YIELD
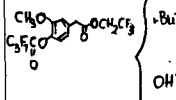	i-Bu+	461 (8) 265 (81) 137 (100)	MH^+ $(M-C_3F_7CO)H_2^+$ $(CH_3O\text{-}C_6H_4\text{-}CH_2)^+$	1
	OH⊖	459 (2) 263 (2.5) 197 (100)	$(M-H)^-$ $(M-C_3F_7O)^-$ $(C_3F_7CO)^-$	42
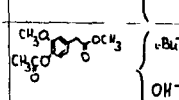	i-Bu+	239 (100) 197 (25)	MH^+ $[MH-(CH_2{=}CO)]^+$	1
	OH⊖	237 (86) 195 (100)	$(M-H)^-$ $(M-CH_2CO)^-$	100

PLASMA HVA DERIVATIZATION PROCEDURE FOR GCMS/OH⊖NCI ASSAY

2 ML **PLASMA**, cooled
↓ set pH to 1 ← add 500 Ng D_5-HVA
← add 2 × 4 ML EtOAc

EXTRACTION
↓ dry EtOAc phase (N_2↑)
← add 200 µl HCl/MeOH

METHYLATION
↓ dry (N_2↑)
← add 50 µl Ac_2O

ACETYLATION keep at 80°, 30 MIN
↓ evaporate Ac_2O nearly to dryness (N_2↑)

FINAL VOLUME ← dissolve residue in 25 µl EtOAc

Inject 5 µl into GC (column: 3% OV 17, 6', temperature program 100-260°, 10°/MIN)
Record ion currents at m/z 237 and 241

GC/MS TRACES OF BLOOD PLASMA EXTRACT (HVA DETERMINATION)

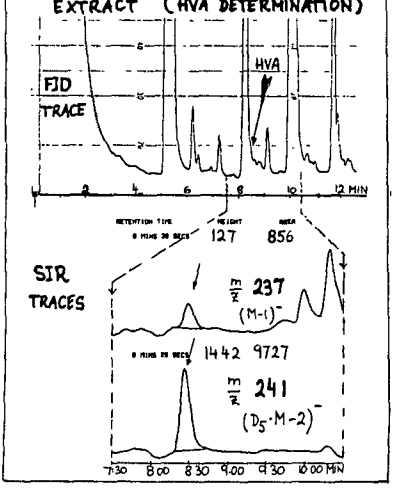

Calculation of HVA concentration in plasma

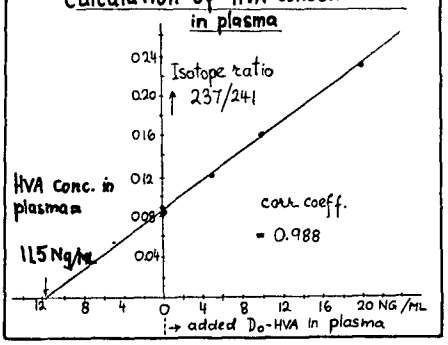

MASS SPECTROMETRY OF FIVE KETENE DIMERS

José A. Olivares, Gerald D. Flesch and Harry J. Svec
Ames Laboratory-USDOE and Department of Chemistry
Iowa State University, Ames, Iowa 50011

The chemistry of the ketenes has been reviewed [1] and it is evident that more knowledge is needed about the mass spectra and fragmentation mechanisms of these compounds [2]. Furthermore, the photochemistry of the ketene dimers has been of interest as a synthetic route to cyclopropanones. Attempts to isolate the cyclopropanones have been unsuccessful. Turro [3] used mass spectrometry to correlate structural information and dissociation paths to the known photochemistry. Such correlations from simple mass spectra do not always hold [4,5], and are not generally used anymore.

Our mass spectrometric study of: diketene(1); 2,2,4,4-tetramethyl-1,3-cyclobutanedione(2); dispiro[3.1.3.1]decane-5,10-dione(3); dispiro[4.1.4.1]dodecane-6,12-dione(4); and dispiro[5.1.5.1]tetradecane-7,14-dione(5); involves the determination of ionization energies, appearance energies, MIKE, parent ion and CAD spectra of particular ions of interest.

The mass spectra of the diones (2-5) have some trends worth noting, i.e., they show a prevalent parent ion peak, a base peak which is always the ketene monomer $(M/2)^{+\bullet}$, a minor monodecarbonylation peak $(M-CO)^{+\bullet}$, a moderate size bidecarbonylation peak $(M-2CO)^{+\bullet}$, and a major peak resulting from the decarbonylation of the ketene monomer $(M/2-CO)^{+\bullet}$. These ions account for 50 - 80% of the total ion currents observed for each compound. Diketene differs, with the monodecarbonylation peak accounting for 16% of the ion current.

Parent ion scans of 2 show the unimolecular dissociation paths in the mass spectrometer. These paths are similar to proposed gas phase photolytic decompositions [3,6,7]. A general ion dissociation scheme for the ketene dimers is therefore proposed to be:

$$M^+ \xrightarrow{-CO} (M-CO)^+ \xrightarrow{-CO} (M-2CO)^+$$

$$\xrightarrow{-2CO} (M-2CO)^+$$

$$\xrightarrow{-M/2} (M/2)^+ \xrightarrow{-CO} (M/2-CO)^+$$

Estimates of the heats of formation of the diones are made by using ancillary thermodynamic data, the last dissociation path, and the equation:

$$\Delta H_f\{2\text{-}5\} = \Delta H_f\{(M/2\text{-}CO)^+_{2\text{-}5}\} + \Delta H_f\{(M/2)_{2\text{-}5}\} + \Delta H_f(CO) - AE\{(M/2\text{-}CO)^+_{2\text{-}5}\}$$

The calculation for 2 yields a value which can be corrected to the known ΔH_f by an additive factor. The same factor added to the calculated values for 3-5 yields ΔH_f's of -16, -74 and -88 kcal/mole, respectively.

The discrepancy between the monodecarbonylation ion peak intensity of the diones (2-5) and the oxetanone (1) reveals possibly different structures for these ions. CAD spectra of the $C_3H_4O^{+\bullet}$ ions of diketene, propionic acid (which forms the methyl ketene ion), acrolein and 2-propyn-1-ol, show that the ion from diketene is structurally different from the other three ions. Figure 1 gives the proposed decarbonylation path of diketene and the possible resonant ionic structure of its monodecarbonylation product.

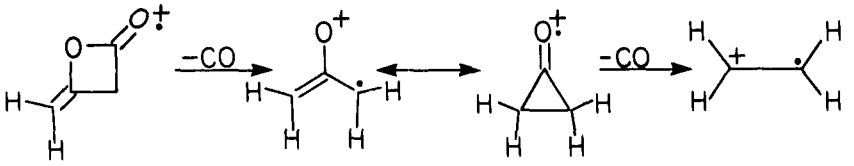

Figure 1. Decarbonylation path of diketene.

ACKNOWLEDGEMENT:

Ames Laboratory is operated for the U.S. Department of Energy by Iowa State University under Contract No. W-7405-Eng-82. This research was supported by the Director for Energy Research, Office of Basic Energy Science.

REFERENCES:

1. S. Patai (Ed.), The Chemistry of Ketenes, Allenes and Related Compounds, Wiley, New York, 1980.
2. H. Schwarz and C. Köppel, in S. Patai (Ed.), The Chemistry of Ketenes, Allenes and Related Compounds, Wiley, New York, 1980, pp. 189-222.
3. N. J. Turro, P. A. Leermakers, H. R. Wilson, D. C. Neckers, G. W. Byers and G. F. Vesley, J. Am. Chem. Soc. 87 (1965) 2613.
4. A. Mandelbaum, S. Weinstein, E. Gil-Av and J. H. Leftin, Org. Mass Spectrom. 10 (1975) 842.
5. C. Wunsche, G. Ege, E. Beisiegel and F. Pasedach, Tetrahedron, 25 (1969) 5869.
6. I. Haller and R. Srinivasan, J. Am. Chem. Soc. 87 (1965) 1144.
7. R. Spafford and M. Vala, J. Photochem. 8 (1978) 61.

Studies in Ammonia Chemical Ionization Mass Spectrometry

Patrick Rudewicz and Burnaby Munson
Department of Chemistry
University of Delaware
Newark, DE 19716

Ammonia has been used as a selective reagent gas in chemical ionization (CI) mass spectrometry for many years.[1,2] Ammonia CI spectra, however, are not highly reproducible from one instrument to another and are very sensitive to experimental parameters. The reagent ions are a set of solvated ammonium ions which are connected, under CI conditions, by a set of reversible (if not equilibrium) reactions:

$$NH_4(NH_3)_x^+ + NH_3 \longrightarrow NH_4(NH_3)_{x+1}^+$$

The relative abundances of these ions are sensitive functions of experimental parameters. Although it is generally assumed that the reactant ion is NH_4^+, the solvated ammonium ions may react, probably with different rate constants. The sample ions themselves may undergo solvation/desolvation reactions with ammonia. Consequently, NH_3 CI spectra unlike CH_4 and i-C_4H_{10} CI spectra will show significant variations with temperature, pressure, and repeller voltage.

At low pressures of NH_3 (0.04 torr NH_3 and 0.06 torr He, from the gas chromatograph), equimolar amounts of aniline, m-toluidine, N-ethylaniline, and N,N-diethylaniline give approximately the same ion currents of $(M+H)^+$ ions. The primary amines give approximately 8% $(M+NH_4)^+$ ions; the secondary amine, significantly less; and the tertiary amine gives essentially no $(M+NH_4)^+$. At 0.4 torr NH_3 (plus 0.06 torr He from the gas chromatograph) the same equimolar mixture gives very different responses for the primary, secondary, and tertiary amines. The relative sensitivities for the primary amines are approximately a factor of ten lower than the sensitivities of the secondary and tertiary amines. The $(M+NH_4)^+$ ions are approximately equal in abundance to the $(M+H)^+$ ions for the primary and secondary amines. The tertiary amine shows essentially no $(M+NH_4)^+$ ions.

Somewhat similar observations are noted if one uses mixtures of NH_3 in CH_4 as the reagent gas. With 1%NH_3 in CH_4 as the reagent gas, the dominant ions for amines are the $(M+H)^+$ ions with small amounts of the $(M+NH_4)^+$ ions: more adduct ions for primary than secondary amines, and essentially no adduct ions for the tertiary amines. The molar sensitivities as $(M+H)^+$ ions for the above set of amines are essentially the same. With 24% NH_3 in CH_4, significantly more $(M+NH_4)^+$ adduct ions are observed for primary and secondary amines, but the molar sensitivities as $(M+H)^+$ and $(M+NH_4)^+$ ions for these compounds are essentially the same. As the partial pressure of NH_3 is increased, the sensitivities for the primary amines decrease rapidly as noted above for the change in total pressure of ammonia.

Temperature effects can be quite pronounced in NH_3 CI spectra. The distribution of reagent ions is sensitive to temperature: at 100°C and 0.5 torr NH_3 in our CI source, $NH_4(NH_3)_2^+ \cong NH_4(NH_3)^+ \gg NH_4^+ \cong NH_4(NH_3)_3^+$, but at 200°, the dominant ion is $NH_4(NH_3)^+$ and $NH_4(NH_3)_2^+ \cong NH_4^+$. At 100°, acetophenone gives a spectrum in which $(M+NH_4+NH_3)^+ \cong (M+NH_4)^+$; and at 200°, $(M+NH_4)^+ \cong 6x(M+NH_4+NH_3)^+$. Increasing the repeller voltage within the CI source gives results which are similar to the results obtained by increasing the temperature. Small repeller voltages significantly decrease the extent of solvation of ammonium ions and also decrease the solvation of the sample ions. At 100°C and 0.4 torr, an increase in the repeller voltage from 0 to 10 v decreases the ratio, $(M+NH_4+NH_3)^+/(M+NH_4)^+$ from about 2 to about 0.3. Although structural information may be obtained from the abundances of the adduct ions in NH_3 CI spectra comparisons must be made under essentially identical conditions.

Dilute mixtures of NH_3 in CH_4 have been used to provide molecular weight information when the CH_4 CI spectra contain very low abundances of $(M+H)^+$ ions.[3] As we have noted above, the abundances of $(M+H)^+$, $(M+NH_4)^+$, and fragment ions will be very sensitive to ammonia partial pressure in the CI reagent gas and also the total pressure. The relative abundances of the

$(M+H)^+$ and $(M+NH_4)^+$ ions for oxygenated compounds depend on the molecular structures through the proton affinities of the samples. The cyclic ether, tetrahydropyran, gives only $(M+NH_4)^+$ ions with 1%NH_3/CH_4 at 0.4 torr, but di-isopropyl ether gives approximately equal abundances of $(M+H)^+$ and $(M+NH_4)^+$ ions under the same conditions. Since the proton affinity of di-isopropyl ether is about 1.5 kcal/mol greater than $PA(NH_3)$ and the proton affinity of tetrahydropyran is about 4.3 kcal/mol less than $PA(NH_3)$, proton transfer followed by solvation is thermochemically allowed for $(C_3H_7)_2O$ and only collisionally-stabilized adduct formation is thermochemically allowed for tetrahydropyran. Phenetole, $C_6H_5OC_2H_5$, under similar conditions has a significantly lower sensitivity than the other two ethers and has a spectrum which contains equal abundances of $(M+H)^+$ and $(M+NH_4)^+$ ions. The proton affinity of phenetole is not readily available, but by analogy with other compounds, it should be less than $PA(NH_3)$. In this case, we assume that NH_4^+ reacts only by adduct formation and that the $(M+H)^+$ ions are formed by reactions with CH_5^+ and $C_2H_5^+$, since $(M+C_2H_5)^+$ and $(M+C_3H_5)^+$ ions are also present in this spectrum. The 1%NH_3/CH_4 spectra of ethylene glycol dimethyl ether and ethylene glycol monobutyl ether both contain only $(M+NH_4)^+$ ions, even though the proton affinity of ethylene glycol dimethyl ether is approximately 0.9 kcal/mol greater than $PA(NH_3)$. In these cases, we presume that the two oxygens both solvate the NH_4^+ ion so that collisionally stabilized adduct formation is favored over proton transfer.

The sensitivities for monofunctional oxygenated compounds decrease significantly with increasing concentration of ammonia in the CI reagent gas at a constant total pressure. The sensitivities of 2-octanone and hexyl acetate (relative to pyridine) decrease by a factor of 2 as the ammonia concentration is increased from 1 to 40% at 0.5 torr. Similar decreases are noted for cyclohexanol and tetrahydropyran. In addition, even with 1%NH_3/CH_4 at 0.5 torr, there are large variations in relative sensitivities for oxygenated compounds: 2-octanone $\cong$ hexyl acetate $\gg$ tetrahydropyran $\cong$ cyclohexanol. In addition, it was observed in GC/CIMS experiments with many oxygenated compounds using 1%NH_3/CH_4 as the reagent gas, that $NH_4(NH_3)^+$ was formed as the compounds pass through the source of the mass spectrometer. This effect is attributed to the reaction sequence of adduct formation followed by a displacement reaction,

$$NH_4^+ + M \rightleftharpoons (M+NH_4)^{+*} \xrightarrow{CH_4} (M+NH_4)^+$$

$$(M+NH_4)^+ + NH_3 \text{ ——— } NH_4(NH_3)^+ + M.$$

Preliminary experiments indicate that these oxygenated compounds give approximately equal molar responses when one includes $(M+H)^+$, $(M+NH_4)^+$, and the increase in $NH_4(NH_3)^+$ ions. We noted that the bifunctional compounds, ethylene glycol dimethyl ether and ethylene glycol monobutyl ether, do not form $NH_4(NH_3)^+$ and that $NH_4(NH_3)^+$ may react with these two compounds. Our observations are consistent with recent data on the thermochemistry of $-NH^+\cdots O$ and $NH^+\cdots N$ bonds.[4]

References:

1. D. F. Hunt, C. N. McEwen, and R. A. Upham, Tetrahedron Lett. 1971, 4539.
2. M. S. Wilson, I. Dzidic, and J. A. McCloskey, Biochim. Biophys. Acta. 1971, 240, 623.
3. D. E. Smith, J. S. Smith, D. Jerolamon, A. F. Weston, D. Richton, and E. J. Brozowski, Presented at 26th Annual Conference on Mass Spectrometry and Allied Topics, St. Louis, MO, May 28 - June 2, 1978.
4. Michael Meot-Ner (Mautner), J. Am. Chem. Soc. 1984, 106, 1257.

CHARACTERIZATION OF GLYCOSPHINGOLIPIDS BY FABMS

MARK E. HEMLING, R. DONALD SEDGWICK,[+] and KENNETH L. RINEHART, JR.
School of Chemical Sciences, University of Illinois at Urbana-Champaign,
Urbana, Illinois 61801

ROBERT K. YU
Department of Neurology, Yale University School of Medicine,
New Haven, CT 06510

The growing interest in the diverse biological functions of cell membrane glycosphingolipids (GSL's) as cell surface antigens, cell-cell recognition sites, and receptors for a variety of signal molecules (1-4) has prompted the constant search for new procedures for their structural analysis. Mass spectrometry, because of its high sensitivity and speed, has always figured prominently in this regard. First applied to GSL's in 1969 by Sweeley and Dawson (5) and by Samuelsson and Samuelsson (6), it has gained rapid recognition as a viable tool in furnishing detailed structural information regarding the carbohydrate composition and sequence and, in some cases, the lipophilic constituents. We provide here a detailed systematic analysis of a number of GSL's of increasing complexity and their ceramides, using FAB mass spectrometry. High resolution measurements and linked scans are used to confirm fragmentations. Matrix requirements and homologous mixture analysis are also discussed.

The positive ion spectra of the glycosphingolipids with neutral sugars were generally more intense than the negative ion spectra but the negative ion spectra were often easier to interpret. Lower background signals and fewer solvent related peaks often caused the signal to background ratio to be higher for the negative ion spectra, which facilitated interpretation. FAB ionization provides enough fragmentations to determine the basic structure of glycosphingolipids. Successive losses of saccharide units, which were often weak in the positive ion spectra but relatively strong in the negative, yield the sequence of the oligosaccharide portion but do not give any information about the configuration at the anomeric (or other) carbons nor about the location of the saccharide linkages. The isomeric hexoses thus cannot be distinguished. Glycosphingolipids with branching in the carbohydrate chain have been examined and branch points can be assigned. The ceramide peak (due to loss of the oligosaccharide) is generally strong in the positive ion spectrum, and sphingosine peaks in the positive and fatty acid amide and related peaks in the negative ion spectra define the nature of those units, allowing unsaturations and homologies to be readily assigned. Information about the position of unsaturations in the lipid chains cannot be extracted from the FAB spectra, however.

FABMS is a good method for obtaining a quick estimate of the relative composition of GSL mixtures since no derivatives need to be made prior to analysis. Although the background peaks inherent in the FAB spectrum limit the ability to determine accurate composition, such information complements that obtained by derivatization and GC and is probably of comparable accuracy. Careful FAB experiments with mixtures of pure compounds still need to be carried out to confirm the present quantitation data. FABMS and GC analysis indicated that several of the commercially available compounds were of less than indicated purity.

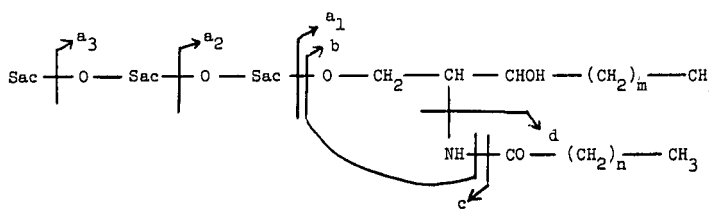

Scheme A. Positive ions

[+]Present address: Allied Corporation, Corporate Research, PO Box 1021R, Morristown, NJ 07960.

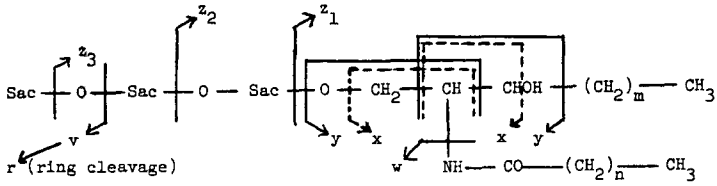

Scheme B. Negative Ions

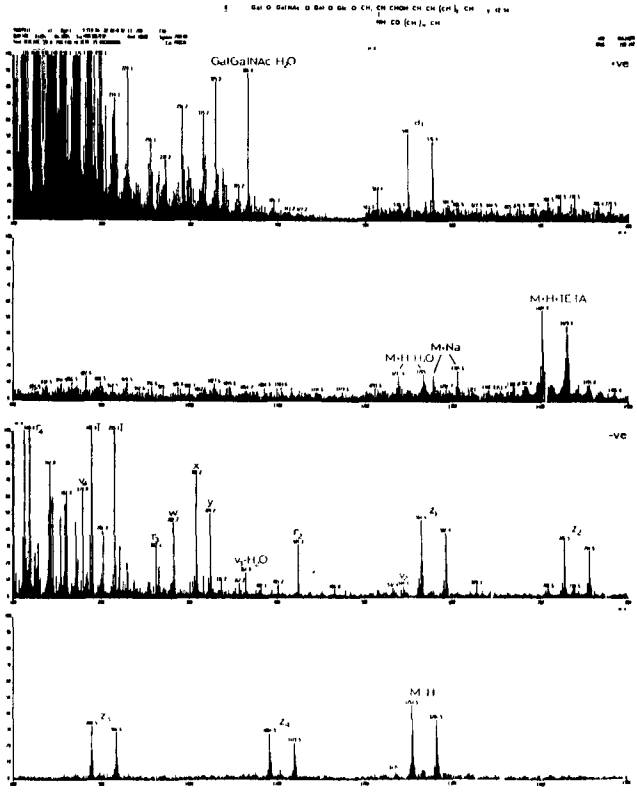

Examples of positive and negative ion FABMS of asialo-G_{M1} in triethylenetetramine matrix

1) Fishman, P. H.; Brady, R. O. Science 1976, 194, 906-915.
2) Yamakawa, T.; Nagai, Y. Trends Biochem. Sci. 1976, 3, 128-131
3) Hakamori, S.-I. Annu. Rev. Biochem. 1981, 50, 733-764.
4) Ledeen, R. W.; Yu, R. K. Methods Enz. 1982, 83, 140-191.
5) Sweeley, C. C.; Dawson, G. Biochem. Biophys. Res. Commun. 1969, 17, 6-14.
6) Samuelsson, K.; Samuelsson, B. Biochem. Biophys. Res. Commun. 1969, 37, 15-21.

FAST ATOM BOMBARDMENT MASS SPECTROMETRY OF PROTECTED OLIGONUCLEOTIDES

D. M. Hindenlang and R. D. Sedgwick, Analytical Sciences Laboratory
C. S. Aaron and P. D. Unger, Molecular and Applied Genetics Laboratory
Corporate Research and Development, Allied Corporation, Morristown, N.J. 07960

Introduction - Fast atom bombardment mass spectrometry is being developed as a valuable analytical tool for the analysis and sequence determination of oligomeric deoxyribonucleotides (DNA). The chemical synthesis of oligonucleotides involves the use of selective protecting agents which are subsequently removed to yield the deprotected product. The fragmentation mechanisms which are important in the FAB-MS analysis of some protected oligonucleotides are reported here.

Experimental - The instrumentation for this examination of oligonucleotides was a VG Analytical ZAB-HF reverse geometry high resolution double focusing mass spectrometer with a FAB source using 7 keV xenon atoms. All spectra were recorded on the VG Analytical 11-250 instrument control and data collection system, with magnetic scanning using field control and an ion energy of 8 keV. Samples were found to give the most intense FAB-MS results when dissolved in thioglycerol. Spectra were generally less intense in glycerol, with more obtrusive solvent oligomer ions. All spectra were calibrated using FAB-MS of sodium iodide, with the ion series $(NaI)_nNa^+$ being used for positive ions and $(NaI)_nI^-$ being used for negative ions.

Protection of Deoxyribonucleotides - A variety of protecting groups are employed in the synthesis of deoxyribonucleotides. Every phosphate group in this study was protected with one p-chlorophenyl group ($Cl-C_6H_4-$) in a phosphate ester linkage. All the free primary amine groups on the nucleotide bases were protected as amides. Adenine was present as N^6-benzoyladenyl, cytosine as N^4-benzoylcytosyl, and guanine as N^2-isobutyrlguanyl. Thymine was not derivatized. The protected oligonucleotides examined by FAB-MS can be divided into three categories: fully protected (5'-dimethoxytrityl, 3'-cyanoethyl chlorophosphate); protected (5'-dimethoxytrityl) with 3'-chlorophenyl phosphate anion termination, as the triethyl ammonium salt; and protected 3'-terminating (5'-hydroxyl, 3'-O-benzoyl termination).

Fully Protected Deoxyribonucleotides - The positive ion FAB-MS gives weak $M+H^+$ and $M+Na^+$ ions and very limited sequence information for these molecules. Both positive and negative ion spectra show ions typical of the (derivatized) bases present. This is also the case for the other two categories of oligonucleotides examined. The characteristic ions are m/z $125^-:127^+$ (thymidyl), $214^-:216^+$ (N^4-benzoylcytosyl), $220^-:222^+$ (N^2-isobutyrlguanyl), and $238^-:240^+$ (N^6-benzoyladenyl).

The negative ion FAB-MS gives weak $M+Cl^-$, very weak $M-H^-$, and strong $(M-CH_2CH_2CN)^-$ ions with good sequence information. The chlorine isotopic patterns are a useful aid to interpretation, defining the number of protected phosphate moeities in the fragments. We see major fragmentation of the C-O bond between a phosphate oxygen and either a 5' or 3' carbon of a deoxyribose to give phosphate anions. Phosphate ion fragments containg the 3'-protecting group (cleavage at 3') are weak except for m/z 260^-, the cyanoethyl chlorophenyl phosphate group itself. Phosphate ion fragments containing the 5'-protecting group are prominent.

For example, the negative ion spectrum of fully protected G-C shows major phosphate terminating ions containing the 5'-protecting group at 1331^- $(M-CH_2CH_2CN)^-$ and 828^- (cleavage at carbon 5' of the C deoxyribose). Both of these anions also lose the 5'-dimethoxytrityl protecting group, with hydrogen transfer to form 5'-hydroxyl terminated phosphate anions at 1029^- and 526^- respectively.

Protected Deoxyribonucleotides with 3'-Chlorophenylphosphate Anion Termination - The preformed anions give excellent sensitivity in the negative ion mode FAB-MS. Phosphate terminated ions predominate, with cleavages at both 3' and 5' carbons. Major ions also show subsequent loss of the 5'-protecting group. While structure determination is not difficult for lower oligomers, the sequence information is complicated by losses of the protecting group.

For example, for the sequence C-T major ions occur at 1256^- (anion) and 822^- (cleavage at 5' of T). Both of these ions also lose the 5'-dimethoxytrityl with hydrogen transfer to form 5'-hydroxyl terminus phosphate anions at 934^- and 520^- respectively. A prominent peak at 625^- arises by elimination of protected dehydroxydeoxycytidine (cleavage at 3').

A substantial 413⁻ peak derives from C-5 cleavage with hydrogen transfer to form dehydrochlorophenylthymidylic acid.

5'-Hydroxyl Protected Deoxyribonucleotides with 3'-O-Benzoyl Termination - These molecules give excellent FAB-MS results in thioglycerol solution. The positive ion spectra show weak $M+H^+$ and $M+Na^+$ species. The negative ion spectra are much more intense, giving $M-H^-$ (also $M+Cl^-$ in some cases) and abundant fragmentation for sequence determination. Phosphate terminated anions are observed for both C-3 and C-5 cleavages. This provides both a series of fragments retaining the 3'-benzoyl terminus and a series of fragments retaining the 5'-hydroxyl terminus. In general those ions retaining the 3'-benzoyl terminus are more intense, especially for lower oligomers.

For example, the sequence C-T shows in addition to $M+Cl^-$ (884⁻) a predominant series of 3'-benzoyl terminus anions at 848⁻(M-H)⁻, 535⁻ (cleavage at 3' of C), and 121⁻ (benzoate). The series retaining the 5'-hydroxyl terminus are weak, with only phosphate anion 520⁻ (cleavage at 5' of T) being of note.

The trimer HO-C-T-G-O-benzoyl shows prominently the phosphate anion series retaining the 3'-benzoyl terminus: 1357⁻(M-H)⁻, 1044⁻ (cleavage at 3' of C), and 630⁻ (cleavage at 3' of T). Similar phosphate ions retaining the 5'-hydroxyl terminus are weaker: 934⁻ (cleavage at 5' of G) and 520⁻ (cleavage at 5' of T). A weak $M+Cl^-$ species is also observed at 1393⁻.

For the tetramer A-T-G-C (M-H 1884⁻) all the phosphate terminated anions include either 5'-hydroxyl or the 3'-benzoyl terminii with the latter being the more intense: 1547⁻ (cleavage at 3' of A), 1133⁻ (cleavage at 3' of T), and 624⁻ (cleavage at 3' of G). The 5'-hydroxyl terminus series of phosphate anions is also quite significant in intensity: 1467⁻ (cleavage at 5' of C), 958⁻ (cleavage at 5' of G), and 544⁻ (cleavage at 5' of T). This compound also evidences a distinct 1780⁻ (M-benzoyl)⁻.

The hexamer HO-G-C-A-T-G-C-O-benzoyl is nearly 3000 molecular weight, illustrating the mass penalty for using derivatized oligonucleotides. As the chain length increases the influence of the 3'-O-benzoyl terminating derivative becomes less evident. The 3'-benzoyl terminated series of phosphate anion fragments occurs at: 624⁻, 1133⁻, 1547⁻, 2075⁻ and 2577⁻. The complimentary 5'-hydroxyl terminated series of phosphate anions occurs at 526⁻, 1029⁻, 1556⁻, 1970⁻, and 2479⁻. Since either series can be used for sequence determination, the total sequence can be obtained by scanning only about half of the total molecular weight range (as shown, with overlap, in the figure below), provided the total mass is also determined. The molecular ion region for this hexamer was recorded separately using averaging with the MCA facilities of the 11-250 Data System. The $M-H^-$ was determined as nominal mass 2897⁻. In these chlorinated derivatives the positive mass defect builds up slowly, i.e., hexamer formula $C_{124}H_{117}N_{23}O_{40}P_5Cl_5$ calculates as 2897.49.

Negative Ion FAB Mass Spectrum of Hexamer HO-G-C-A-T-G-C-O-Benzoyl

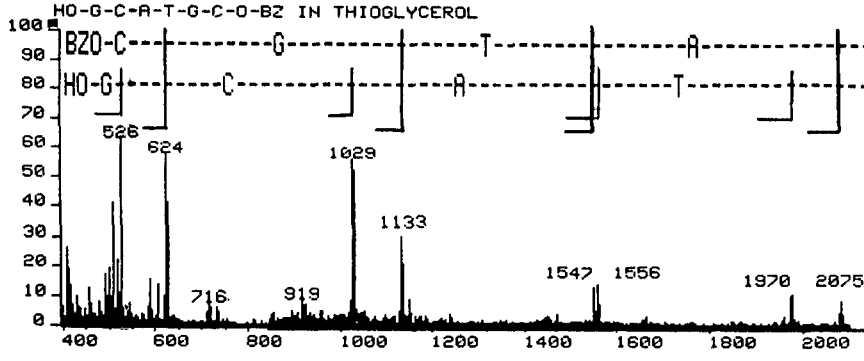

FAST ATOM BOMBARDMENT AND COLLISIONAL ACTIVATION MASS SPECTROMETRY AS PROBES TO IDENTIFY MODEL ISOMERIC CARCINOGEN - NUCLEIC ACID ADDUCTS.

Yves Tondeur[1], R.C. Moschel[2] A. Dipple[2] and S.R. Koepke[2]
(1) Program Resources, Inc. (2) LBI - Basic Research Program; NCI-Frederick Cancer Research Facility, Frederick, MD. 21701.

The mass spectra of a series of 1-, N^2-, O^6-, 7- and 8- (p-Y-benzyl)guanosines (where Y=H, CH_3, OCH_3, Cl and NO_2) (Fig.1) were examined in order to identify spectral characteristics which can distinguish these positional isomers. Field desorption and positive chemical (isobutane) ionization spectra were not diagnostic while a combination of fast atom bombardment (FAB), both positive and negative ion (examples for N^2-benzylguanosines are given in Fig.2), and collisionally activated dissociation (CAD)-MIKE spectra together with measurements of the kinetic energy release ($T_{1/2}$) (Table 1) accompanying the glycosidic bond cleavage (for the metastable reaction $[M-H]^- \rightarrow [B]^-$ where B = base) provided sufficient information to assign the structures in this series of isomers. In our hands a minimum of 5µg of nucleoside was required for successful analysis using conventional magnet scanning techniques whereas sub-microgram amounts could be analyzed by CAD-MIKE analysis of the pseudo-molecular ions.

Abundant $[M+H]^+$ and $[M-H]^-$ ions together with extensive fragmentation are obtained using a glycerol-N,N-dimethylformamide (1:1,v/v) mixture as FAB matrix. Under negative ion FAB conditions, the O^6- derivatives exhibit a relatively weak signal for the de-protonated molecule (i.e.<25% relative abundance in the negative ion current as opposed to 100% for the other isomers). The 1-and N^2-isomers can be distinguished under these conditions by comparing the relative abundance of low kinetic energy ions, i.e. $[B-YBZL]^-$ (representing loss of the p-Y-BZL moiety from the heterocyclic base) and $[S]^-$ (ribose residue). For the case of 7-substituted guanosines having bromide counter ions, signals for the bromide salt of the nucleoside are readily observable. Under positive ion FAB conditions, the 8-substituted isomers exhibit a relatively weak signal for the substituted benzyl cation $[YBZL]^+$ (i.e. <50% relative abundance in the positive ion current as opposed to 100% for the other isomers except for N^2-benzyl guanosine in Fig.2). This is presumably a consequence of the greater energy required to cleave a carbon-carbon rather than carbon-heteroatom bond in the even-electron ion $[M+H]^+$.

Short and long term reproducibilities (±15%) of the relative abundances were similar demonstrating that FAB can be reliably used for isomeric differentiation.

Research sponsored by the National Cancer Institute under Contract No. NO1-CO-23910 with Program Resources, Inc.

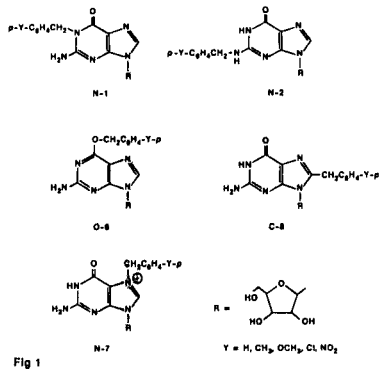

Fig 1

Table 1 KINETIC ENERGY RELEASES ($T_{1/2}$) IN MeV FOR $[M - H]^- \xrightarrow{MI} [B]^-$

ISOMERS (Y = H)	$T_{1/2}$ (MeV)
N-1	37.1
N-2	37.7 ± 3.4 (N = 3)
O-6	18.9 ± 1.2 (N = 3)
C-8	34.4

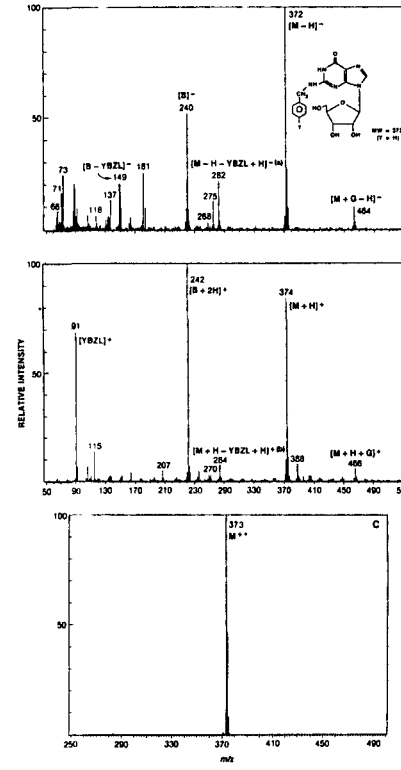

Fig 2. MASS SPECTRA OF N^2-BENZYLGUANOSINE

(A) NEGATIVE ION FAB

(B) POSITIVE ION FAB

(C) FIELD DESORPTION

CONCLUSIONS

- FACILE OBSERVATION OF $[M - H]^-$ AND $[M + H]^+$ TOGETHER WITH EXTENSIVE FRAGMENTATION REACTIONS IN THE FAB SPECTRA OF ISOMERIC (N-1, N-2, O-6, C-8 AND N-7) *p*-Y-BENZYLGUANOSINE DERIVATIVES (Y = H, CH_3, OCH_3, Cl, NO_2) FACILITATE ASSIGNMENT OF SITE OF SUBSTITUTION IN NUCLEIC ACID ADDUCTS.
- POSITIVE AND NEGATIVE ION DETECTIONS ARE ESSENTIAL AND COMPLEMENT EACH OTHER.
- CAD-MIKES AND KINETIC ENERGY RELEASE MEASUREMENTS ($T_{1/2}$ FROM THE METASTABLE REACTION $[M - H]^- \longrightarrow [B]^-$) WERE ALSO FOUND ADVANTAGEOUS IN DISTINGUISHING BETWEEN THESE POSITIONAL ISOMERS.

POSITIVE ION FABMS OF 2-5A TRIMER CORE AND ITS MONOPHOSPHATE

Debra L. Slowikowski and Karl H. Schram
Department of Pharmaceutical Sciences, College of Pharmacy
University of Arizona, Tucson, Arizona 85719
Paul F. Torrence and Jiro Imai
Laboratory of Chemistry, National Institute of Arthritis, Diabetes, and Digestive and Kidney Disease, National Institutes of Health, Bethesda, Maryland 20205

The application of oligonucleotides as potential antitumor and antiviral agents has long been established, and several strategies have been employed in the design of biologically active analogs. The success of the 2',5'-oligoadenylates (2-5A) as interferon inducers and potent antiviral/antimutogenic agents has recently become an area of considerable research interest. The interferon-inducing ability of 2-5A is dependent on the operation of the nuclease pathway or 2-5A system. In this system, 2-5A binds specifically to a latent cellular endoribonuclease which degrades RNA preferentially at UpA or UpU sequences, thus inhibiting protein synthesis. The potental antiviral application of 2-5A and its congeners in intact cells, however, is limited by:(1) a short biological half-life, due to rapid degradation by a 2',5'-phosphodiesterase, and (2) poor penetration into eukaryotic cells, due to its highly polar nature. Several synthetic 2-5A derivatives have been prepared as an approach to solve these problems and to evaluate important structural relationships necessary for enzyme binding and biological activity. However, the mass spectrometry of these compounds had not been examined until now. Positive ion FABMS was applied to 2-5A trimer core 1 and its monophosphate 2.

The positive ion FAB mass spectra of the sodium salts of 1 and 2 show a series of molecular weight related ions of the form $(M + (1-x)H + Na_x)^+$, allowing unambiguous assignment of the molecular weight. The number of sodium cationized ions observed in the $(M + (1-x)H + Na_x)^+$ series is dependent on the number of phosphate hydroxyls and is equal to $P(OH)_x + 1$ when all labile protons have been exchanged with sodium.

Although the positive ion FAB mass spectra are complex due to the formation of various sodium and glycerol adducts, sequence information may be obtained in a manner apparently analogous to that used to sequence oligodeoxynucleotides using negative ion FABMS.[1] Fragmentation pathways leading to a number of significant ions in the mass spectra of 1 and 2 are proposed and the possible identity of these ions for the free compounds is illustrated. These results are based on comparisons with other related analogs, such as 2-5(7-deaza)A trimer monophosphate, which indicated similar fragments with appropriate mass shifts. .

In conclusion, positive ion FABMS may be used to obtain molecular weight and sequence information on oligonucleotides. In particular, 2-5A and its synthetic oligonucleotide derivatives may be successfully characterized by this ionization method.

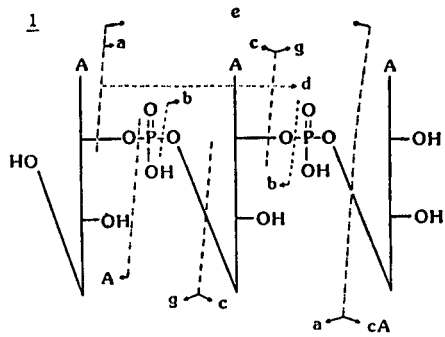

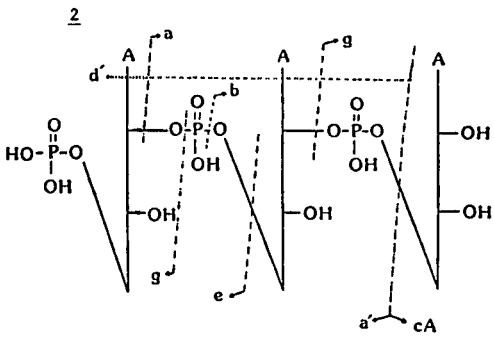

ION	PROPOSED IDENTITY
a	pApA +2H
a'	pApAp +2H
b	ApA +2H
c	b - H_2O
d	pApA +H -134
d'	pApAp+2H-2(134)
e	pAp +2H
f	e - H_2O
g	pA+2H or Ap+2H

Reference:
1. L. Grotjahn, R. Frank and H. Blocker, Nucleic Acids Research 10, 4671 (1982).

TYPE IDENTIFICATION OF INDUSTRIAL SURFACTANTS BY FAB

Ted T. Chang and Jackson O. Lay, Jr.
Chemical Research Division, American Cyanamid Company
1937 W. Main Street, Stamford, CT 06904

Fast Atom Bombardment (FAB) Mass Spectrometry may be used to rapidly determine the class (anionic, cationic, etc.) and molecular weight profile for unknown surfactants. This information is often extremely valuable in industrial applications. Furthermore, this method has the distinct advantage of not requiring an authentic sample for comparison. Finally, it may be used in conjunction with other methods too, such as MS/MS to assist in structure elucidation.

Determination of the molecular weight profile by FAB/MS is generally very straightforward. Because most surfactants give very intense pseudo-molecular ions, the molecular weights are obtained directly from the positive or negative ion mass spectra. To ascertain the surfactant type, however, is less straightforward. We have, however, developed a method to determine surfactant type using FAB/MS by the systematic replacement of the surfactant counter-ions (or adduct ions).

The cationic surfactants, for example the alkyl amine salts, (R_4NCl) show intense molecular ions for the cationic portion of the molecule R_4N^+ in the positive ion mode. The observed mass (for R_4N^+) in the FAB mass spectrum is independent of the changes in the matrix as various salts (NaCl, KCl, CsCl) are added.

Non-ionic surfactants, such as the alkyl ethers of ethylene oxide polymers, $RO(CH_2CH_2O)_nH$, generally show a single cation addition, $RO(CH_2CH_2O)_nH+C^+$ in the presence of a monovalent cation (C^+) salt. Systematic addition of other monovalent salts to the matrix will shift the masses observed in the FAB spectrum according to the mass difference between the monovalent cations. This effect is, of course, readily discernible from addition of salts to cationic sufactants.

Anionic surfactants, such as the alkyl sodium sulfonates RSO_3Na, will show intense pseudo-molecular ions, $(RSO_3Na+Na)^+$ in the FAB spectrum, due to adduct formation with a second counterion, here Na^+. Fortunately, however, these surfactants will show a double exchange of the cation, from $(RSO_3Na+Na)^+$ to $(RSO_3K+K)^+$ for example, upon addition of a large excess of the various monovalent salts.

Similar results are obtained in the negative ion mode, especially when the matrix is changed with salts having a common cation and various anionic moieties (i.e., NaCl, NaBr, NaI).

Finally, this methodology is also useful in other compound classes, for example, the acid functionalities would be counted based on cation replacement and exchange, exchanging up to two cations per acid group for example.

PHOTODISSOCIATION OF IONS GENERATED BY SOFT IONIZATION TECHNIQUES

M. J. Welch, H. S. Hertz, R. L. Sams, and E. White V, Center for Analytical Chemistry, National Bureau of Standards, Washington, DC 20234

Introduction

Interest in the mass spectrometric analysis of large molecules has been the main impetus behind the development of new ionization techniques. Most of the new techniques utilize "soft" ionization processes, i.e., processes that are non-thermal and impart low internal energy to the ions formed. Consequently, the resulting mass spectra are generally predominantly molecular ions or molecular ions plus adducts, with little fragmentation taking place. Collision induced dissociation has been widely applied as a means of obtaining structural information. Photodissociation exhibits promise as an alternative technique for structure determination with the added advantage of greater control over the energy input. Photodissociation has been extensively used in studies of gas phase ion kinetics and structures, but it has only been applied to small molecules. We have now combined photodissociation with field desorption (FD) and field ionization (FI) to investigate the feasibility of obtaining structural information on ions of low internal energy.

Experimental

The instrumentation shown in Figure 1 was designed to allow detection of photon-induced metastable ions formed in the first field-free region (FFFR). The FFFR of a Mattauch-Herzog geometry mass spectrometer was modified to accommodate the addition of a multipass mirror assembly. Light was from a continuous output argon ion laser was equipped with a prism for selection of specific wavelengths of visible light. Ten wavelengths ranging from 457.9 nm to 514.5 nm were available at power outputs of ≥1 watt. In addition, the laser optics could be modified for output of a band of UV light, 351.1 to 363.8 nm, at >1 watt power. Two pathways for introducing laser light to the FFFR were devised. The first, shown in long dashes in Figure 1, involved passage through a quartz window installed in the FD probe port of an FD/FI/EI ion source and then through the ion source and FFFR colinear with the ion beam. Use of this pathway was restricted to the EI mode, but provided good interaction between the laser beam and ion beam. The second pathway, shown in small dashes in Figure 1, was devised to permit photodissociation of ions formed in the ion source by any ionization technique. This arrangement consisted of a window into the FFFR and a five-mirror arrangement in the FFFR to pass the laser light across the ion beam many times. The laser beam-ion beam interaction was poorer with this arrangement, but a colinear arrangement is not possible with FD probe in the ion source.

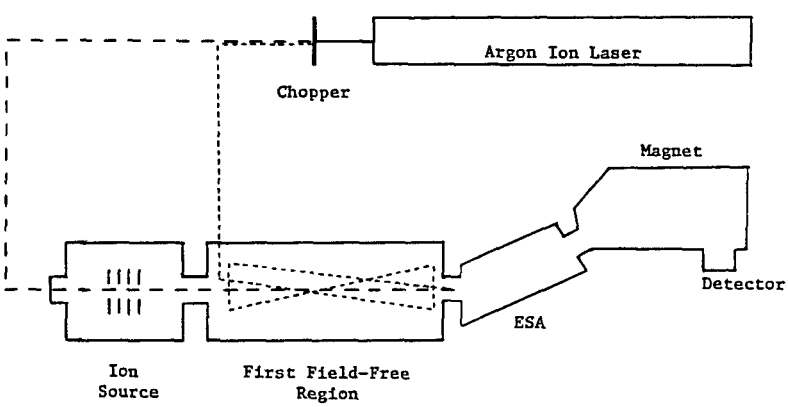

Figure 1. Instrumentation for Photodissociation

A mechanical chopper was placed in the laser path to alternately pass or block light at a preset frequency. Typical operation was at a chop rate of 1 KHz. A lock-in amplifier, not shown in Figure 1, was used to extract the ion intensity signal from the electron multiplier which was in phase with the chopper signal. The output from the lock-in amplifier was thus a measure of the difference between the ion intensity with the light on and off. Metastables formed in the FFFR were detected by one of two modes of operation, linked B/E scans or accelerating voltage scans.

Results and Discussion

Photodissociation has been demonstrated for field ionized and field desorbed ions. The photo-induced metastable transitions observed for field ionized samples include: for n-butylbenzene, m/z 134→92 and 134→91; for nitrobenzene, 123→77; and for 3,5-dinitrobenzoic acid, 212→166. This last metastable was not observed in the absence of laser light. The photo-induced metastable transitions observed for field desorbed samples include: for cresol red, m/z 382→302; for sudan IV, 380→223; and for methyl red, 269→148. All of these metastables were also observed without laser light, but were enhanced by up to 60 percent with laser light. The magnitude of the methyl red transition was wavelength dependent. The parent ion in all cases where photodissociation was observed was $M^{+\cdot}$. Attempts to photodissociate $(M+H)^+$ or $(M+Na)^+$ forms were unsuccessful.

Signal-to-noise is at present a severe limitation on the analytical ability of the technique. Improvements must be made in the magnitude and stability of the ion signals, the degree of laser beam-ion beam interaction, and in signal averaging before the potential analytical applications can be realized.

The fragmentation of n-butylbenzene has been widely studied by a variety of techniques, including photodissociation. In addition to studying the photodissociation of field ionized n-butylbenzene, we have examined the photodissociation of n-butylbenzene generated by electron impact for comparison with earlier published results [1]. Our results for m/z 91/92 ratios versus photon energy ranged from 0.4 at 2.41 eV to 2.0 at 3.47 eV at an ion source temperature of 155°, but were substantially lower than the previous results where ratios increased from 1 to 7 over the same photon energy range. Our results were reproducible regardless of whether we used B/E scans or accelerating voltage scans or which laser path we used and are in reasonable agreement with results from charge exchange mass spectrometry measurements [2]. It is well established that at low internal energies, the formation of 92 is favored and as the energy increases, 91 becomes more favorable. The magnitude of the difference in the results between the two photodissociation studies, however, is not understood, but may relate to different internal energy distributions.

References

[1] E. S. Mukhtar, J. W. Griffiths, F. M. Harris, and J. H. Beynon, Int. J. Mass Spectrom. Ion Phys. 37, 159 (1981).

[2] A. G. Harrison and M. S. Lin, Int. J. Mass Spectrom. Ion Phys. 51, 353 (1983).

A GENERAL NEW SURFACE ANALYSIS TOOL USING SEPARATE SURFACE PROBE AND IONIZATION BEAMS

C. H. Becker, K. T. Gillen, and S. E. Buttrill, Jr.*
Chemical Physics Laboratory, SRI International, Menlo Park, CA 94025

We present a new method for surface analysis by laser ionization (SALI) that has outstanding potential as a general analytical tool with high surface specificity and ultimate detection capabilities in the part per billion and 10^{-18} gram ranges (1,2). In a vacuum system, a small fraction of a monolayer of a suitably-prepared surface sample is removed by a pulsed ion, atom, electron, or photon beam (probe beam). After a small time delay, a focused high intensity pulsed UV laser beam (ionizing beam) crosses the desorbed material a short distance above the surface and ionizes the intersected neutral atoms and molecules with high efficiencies by nonresonant multiphoton ionization. The ions are mass analyzed in a reflecting time-of-flight mass spectrometer (3) (typical resolution $M/\Delta M=500$ at $m/e=200$), with a microchannel plate detector and analog signal recording by a transient digitizer (see the schematic Figure 1). The separation of the desorption process from the ionization step permits separate control over both, allowing a relatively gentle, low fluence, surface irradiation to minimize surface damage and a controllable, quantifiable ionization step (avoiding matrix effects).

Initial SALI experiments utilizing sputtering by a 3 keV Ar^+ probe beam and an excimer laser (248 and 193 nm) ionizing beam have been conducted on several systems including a NBS reference material copper C1252. Figure 2 shows part of the TOF mass spectrum for this sample; elements whose bulk atomic composition values were given by NBS include ^{107}Ag (51 ppm), ^{123}Sb (9 ppm), ^{197}Au (11 ppm), ^{209}Bi (6 ppm), and ^{206}Pb (4 ppm). The raw data values are quite close to the NBS values, indicating small correction factors for many species. The three largest peaks are Cu_2, and peaks at 170, 172, and 174 are CuAg dimers. Pt is a surface impurity deposited on the Cu from an earlier analysis of an adjacent Pt sample. Ta and W are contaminants from the Ar^+ source. Small amounts of other species (Cd, Sn, Ba, Ce, Hg) can be seen. Such spectra demonstrate, at the present stage of development, a detection capability of 1 ppm with removal of ~ 0.01 monolayer over ~ 0.1 cm^2 area. Subsequent heating of this sample shows the usefulness of the SALI method for examining surface segregation and differential evaporation (down to effective partial vapor pressures of $\lesssim 10^{-13}$ torr). Figure 3 shows part of the mass spectrum from the heated NBS sample with and without the use of a probe beam (420 C).

Investigations of signal levels as a function of laser power show saturated ionization (many metals can easily be doubly ionized), which implies that the method will be quantitative, at least for atoms, without needing specially prepared reference standards (unlike SIMS which also routinely needs surface modification to increase sensitivity). Successful experiments have also been conducted on metal and semiconductor samples using a modest intensity Nd:YAG 1.06 μm laser beam as a probe beam to erode submonolayer quantitites per pulse for subsequent analysis.

Erosion for depth profiling and examination of microscopic structures can both be done using suitable probe beams. Many molecular ions have been observed and the SALI technique has potential for analysis of adsorbed or reactive overlayers or prepared biological specimens.

*Presently at: Charles Evans and Assoc., San Mateo, CA 94402

(1) C. H. Becker and K. T. Gillen, Anal. Chem. (in press).
(2) C. H. Becker and K. T. Gillen, Appl. Phys. Lett. (submitted).
(3) B. A. Mamyrin, et al., Sov. Phys.-JETP 37, 45 (1973).

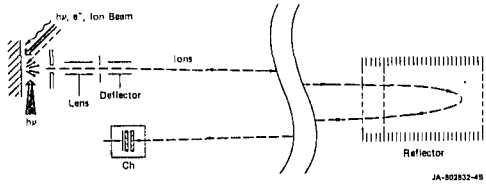

Figure 1

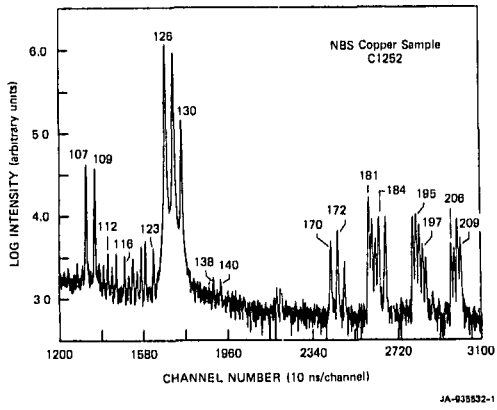

Figure 2

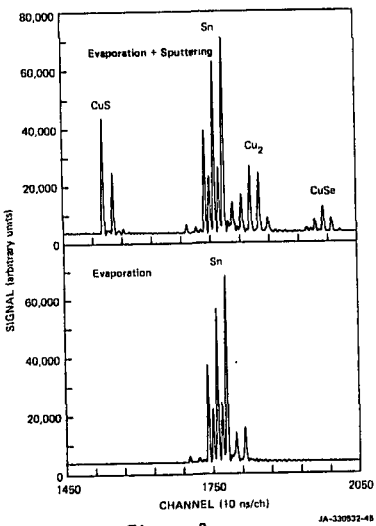

Figure 3a

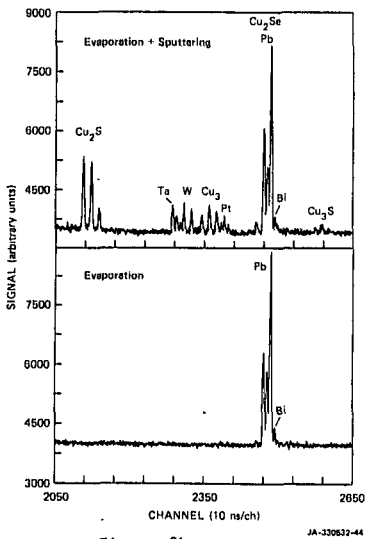

Figure 3b

IN-BEAM IONIZATION BY ALKALI ION ATTACHMENT

G. Schmelzeisen-Redeker, U. Giessmann and F.W. Röllgen

Institute of Physical Chemistry, University of Bonn, D-5300 Bonn, FRG

Alkali ion attachment provides a method for soft ionization of molecules with minimum or no fragmentation. We constructed a simple ion source, similar to that used in previous experiments /1/: A wire covered with sample is placed in a beam of alkali ions produced by electrical heating of a mixture of silicagel and alkali halides (Fig.1). Both the wire probe and the alkali ion emitter were mounted on a pushrod and could easily be replaced for sample loading and renewing the silicagel salt mixture. In order to keep the ion source temperature as low as possible, no inert gas was used for moderating the kinetic energy of the alkali ions. A quadrupole mass spectrometer with a mass range limited to m/z 400 was attached to the ion source.

The ion source was applied for ionization of thermally labile compounds, the analysis of mixtures and for thermochemical measurements. The results are summarized as follows:

1. The mass spectra of most compounds examined did not exhibit fragment ions. The ionization of decomposition products formed at the hot surface of the alkali ion emitter could not be observed. This is probably due to a lower ionization efficiency i.e. lower alkali ion affinity of the decomposition products.
2. Na^+ was found to be superior for the ionization of polar compounds. Although the ionization efficiency for Li^+ and Na^+ is about the same (Fig.2), higher emission currents are more easily produced with Na^+.
3. The analysis of mixtures was facilitated by fractionated desorption. The signal intensities also reflect large variations in alkali ion affinities. The choice of alkali ions such as Cs^+ provides a means to discriminate less polar components of a mixture.
4. For glucose and other saccharides the elimination of water was observed to be induced by the attachment of Li^+ but not of Na^+ ions (Fig.3).
5. Sucrose spectra could not be obtained without abundant fragment ion peaks (Fig.4). The ionization efficiency was probably not high enough for ionization of sucrose at lower thermal stress i.e. at lower vapour pressures.
6. The heat of evaporation of inositol was determined in a preliminary experiment to be about 75 kJ/mol by using the Hertz-Knudsen equation and plotting $I(MLi^+)\cdot\sqrt{T}$ versus 1/T (T = sample temperature). The

method appears promising for measuring the heat of evaporation of thermally labile compounds.

/1/ R. Stoll and F.W. Röllgen, Z. Naturforsch. 37a, 9 (1982).

fig 1

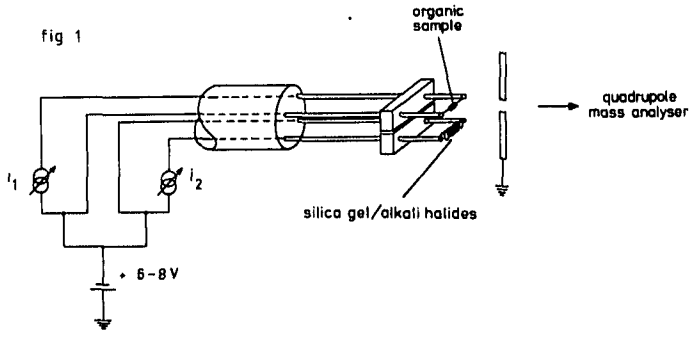

fig. 3a

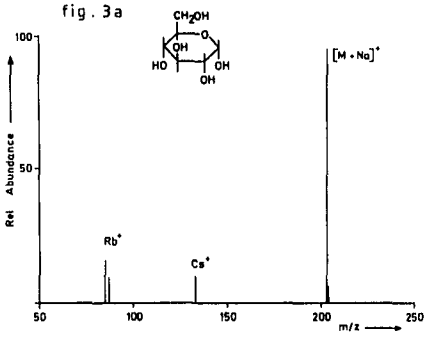

fig. 3b

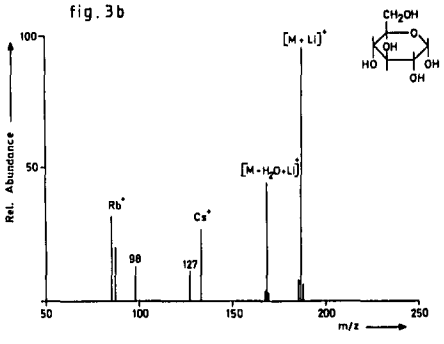

fig. 2

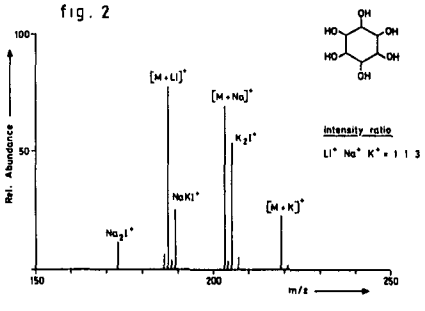

fig. 4

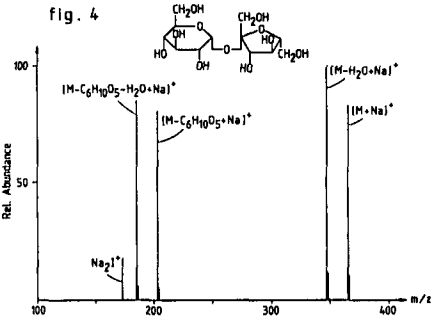

ORGANIC-ALKALI SURFACE IONIZATION SOURCE

S. E. Young, S. E. Buttrill, Jr., and Walter Ogier
SRI International, Chemical Physics Laboratory, Menlo Park, CA 94025.

Thermonic emitters consisting of alkali-doped glasses have been used recently for chemical ionization of organic samples.[1,2] Source pressures in the range of 20 to 700 millitorr are typical, requiring an instrument with differential pumping. It is possible to obtain reasonable ion signals at lower sample pressures with the bead functioning as a surface ionization source.

An organic-alkali surface ionization source (OASIS) has been constructed and evaluated using an alkali glass bead of the type $R_2O:Al_2O_3:SiO_2$ in a 1:1:2 molar ratio[3] mounted on an iridium heater wire with the bead centered on the ion axis (Figure 1). Mass analysis was done on a QB geometry MS/MS previously described.[4] Vapors of the samples in air or N_2 were introduced into the source through a membrane separator kept at 100°C or directly by means of a variable leak. Source pressures varied from 8×10^{-7} torr to 8×10^{-3} torr. When the glass bead is heated to 800° to 1000°C, organic-alkali ions of the formula $[M + X]^+$ are seen in addition to large currents of the alkali itself, where X = Li, Na, K, Rb, or Cs (Figure 2). At higher temperatures, the intensity of the organic-alkali complex drops sharply while the alkali ion intensity increases further, indicating a surface effect rather than chemical ionization. This drop in ion current at higher temperatures has also been observed for surface ionization of simple organics on hot metal wires.[5] However, if an iridium wire without a bead is used, no ions are seen unless it is heated sufficiently to emit electrons, resulting in an EI spectrum.

Polar or polarizable compounds seem to complex most easily with the order: ketones, ethers, alcohols > alkenes > simple aromatics > alkanes. The order for complexing with simple aromatics and alkanes was observed to be Li > Na > K > Rb. For more polar compounds, Na and K glasses work well; pyrex glass also works, giving predominately Na ion adducts.

Some compounds, such as 2-chloro ethyl-ethyl sulfide and benzyl chloride undergo chloride abstraction to form ions with no addition of alkali. Benzyl alcohol produces both a $[M + Na]^+$ at m/z 131 and a loss of OH to produce m/z 91. CID with argon on m/z 131 produces only m/z 23 (Na), while CID on m/z 91 results in a fragmentation spectrum similar to toluene.

For one series of experiments, a sodium glass bead with a thermocouple imbeded in the glass was used to directly read the bead temperature. With this technique it is possible to determine the heat of formation for alkali ions and alkali-organic complexes by using the Arrhenius equation: $\ln k_2 - \ln k_1 = \frac{-\Delta H_f^o}{R}\left(\frac{1}{T_2} - \frac{1}{T_1}\right)$ where T is the temperature in °K, R equals 1.987 cal mol^{-1}, and k is the ion count rate. Table 1 lists the heats of formation for several ions obtained in this manner.

Sensitivity tests were done by introducing the compound of interest through a membrane probe into the source. A vapor generator equipped with a 1-liter dilution flask was used to produced the vapor sample. With a flow rate of 1 liter/min of synthetic air passing through the flask, 1 ml of saturated sample vapor was injected to produce an exponential dilution. The sensitivity for m/z 89 of 2-chloro-ethyl-ethyl sulfide was better than 1 ppb, as shown in Figure 3.

Conclusion It is possible to obtain organic-alkali ions that in many cases yield molecular-weight information at low sample pressures from alkali glass beads. This technique can be applied to older instrumentation that do not have differential pumping.

Table 1

HEATS OF FORMATION FOR VARIOUS IONS USING A SODIUM GLASS BEAD

Ion	kcal mol^{-1}
$^{41}K^+$	71 ± 2
$^{23}Na^+$	94 ± 4
di-isopropylmethyl phosphonate + Na^+	85 ± 3
benzophenone + Na^+	83 ± 8
bis-2-chloro-ethyl ether + Na^+	79 ± 3
m/z 89 of 2-chloro-ethyl-ethyl sulfide	49 ± 2
m/z 91 of benzyl-chloride	47 ± 4.5

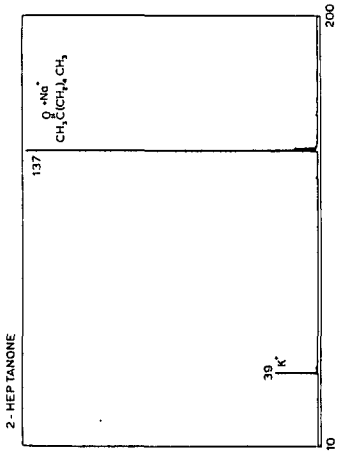

FIGURE 2

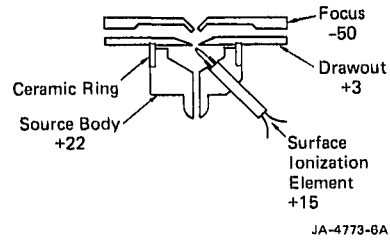

FIGURE 1 ORGANIC-ALKALI SURFACE IONIZATION SOURCE (OASIS)

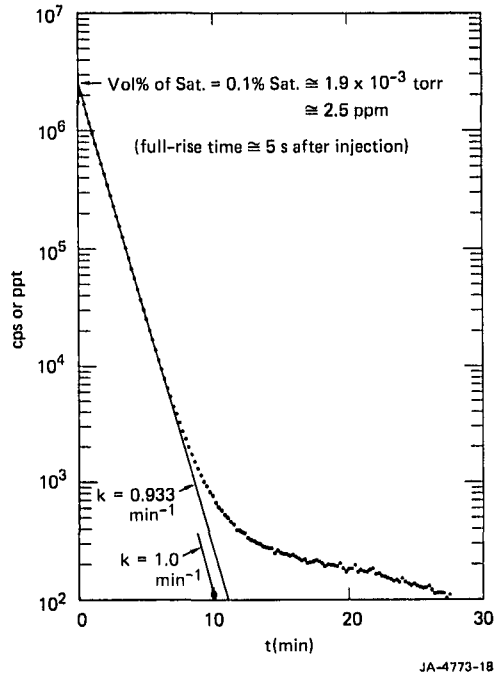

FIGURE 3 DETECTION OF 2 CHLORO ETHYL ETHYL SULFIDE USING A SODIUM GLASS BEAD SURFACE IONIZATION SOURCE

References

1. B. Ackerman et al., Proc. 31st Annual Conference on Mass Spectrometry and Allied Topics, Boston, May 1983; p. 600-601.
2. D. Bombick, J. D. Pinkston, J. Allison, Anal. Chem. 1984, 56, 396-402.
3. J. P. Blewett, E. J. Jones, Phys. Rev. 1936, 50, 464.
4. S. E. Young, S. E. Buttrill, Jr., Proc. 31st Annual Conference on Mass Spectrometry and Allied Topics, Boston, May 1983; p. 197-198.
5. T. Fujii, Proc. 31st Annual Conference on Mass Spectrometry and Allied Topics, Boston, May 1983; p. 526-527.

FAST ATOM BOMBARDMENT STUDIES OF MOLTEN SALTS. A. Tsarbopoulos, R. Rhinebarger, B. Ackermann, J.T. Watson, A.I. Popov, and J. Allison, Departments of Chemistry and Biochemistry, Michigan State University, East Lansing, Michigan 48824.

Molten salts are ionic liquids formed by the combination of AlX_3 with various cationic species. Typical examples include: LiCl, NaCl, KCl, or RCl, where R is commonly an imidizole or pyridinium cation. The component solids combine to create an ionic ion-paired liquid at room or slightly elevated temperatures (vapor pressure ≈0), and have been found to exhibit unique electrochemical properties. Applications of molten salts include: the industrial production of aluminum, use in batteries, electrorefining, and the extraction of metals from ores. While most "melts" are soluble in organic solvents, they are readily oxidized by both oxygen and water. Therefore, they have found extensive use as non-aqueous matrices for the study of specific systems of electrolytes.

Many analytical methods have been used to characterize the various species present in molten salt mixtures. Most commonly, data are obtained from potentiometric determinations (1), as well as NMR (2) and Raman spectroscopies (3). Recently, Knudsen effusion mass spectrometry was used to study the positive ions produced by thermal desorption from $MCl/AlCl_3$ melts (where $M = Na^+$ or K^+) (4).

Investigations in our laboratory have demonstrated the utility of FAB-MS as a convenient analytical probe of the highly studied molten salt system prepared from butylpyridinium chloride (BP^+Cl^-) and aluminum chloride. Direct fast atom bombardment of a series of melts ranging from 45 to 67 mol% $AlCl_3$ produced spectra reflecting the composition of each melt, and confirmed data obtained by other methods concerning equilibria within this system.

Figure 1 displays the positive ion FAB mass spectrum of a melt consisting of 66.591 mol% $AlCl_3$. This spectrum represents the average of 30 scans obtained using a Varian CH5 reversed geometry, double focussing mass spectrometer. Because of the susceptibility of the samples to oxidation, a nitrogen-filled glove bag was attached to the instrument. Each sample was deposited onto a stainless steel probe tip and bombarded with 7.4keV Xenon atoms. Smooth and intense ion currents were produced for the observed ions in excess of 45 minutes by this technique.

7.4 KeV Xe FAB SPECTRUM OF 66.591 MOL% $ALCL_3$ MOLTEN SALT

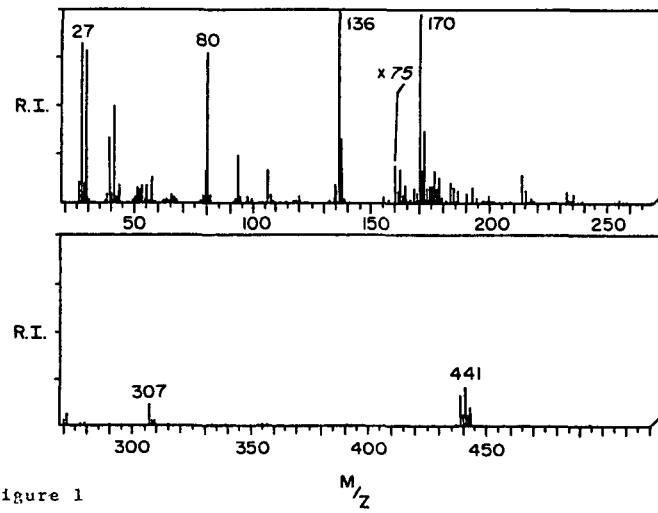

Figure 1

The positive ions observed by FAB-MS are derived almost entirely from BP^+ through fragmentation or through clustering. While the same set of ions was observed over the range of study, the ion abundances vary according to the mol% $AlCl_3$. The ion abundances are also correlated to the extent of ion-pairing of each anionic component to BP^+. The extent of ion-pairing of BP^+ to each of the three anionic species in the melt is summarized in Table 1, along with the positive ions observed in the FAB spectra.

Ion-Pairing to BP^+ and Ions Observed by FAB-MS

Ion-Pair	Ion Observed	
$BP^+ + Cl^- \rightleftharpoons BP^+Cl^-$	$[(BP^+)_2(Cl^-)]^+$	m/z 307
$BP^+ + AlCl_4^- \rightleftharpoons BP^+AlCl_4^-$	$[(BP^+)_2(AlCl_4^-)]^+$	m/z 439
$BP^+ + Al_2Cl_7^- \rightleftharpoons BP^+Al_2Cl_7^-$	$[(BP^+)_2(Al_2Cl_7^-)]^+$	m/z 571 not observed

Table 1

Hence, FAB-MS has displayed potential as a probe of molten salt composition by generating ions characteristic of species present in the melt. Variations in ion intensities as a function of melt composition reflect the "acidity" (mol% $AlCl_3$) of the melt and can be correlated with the equilibria which characterize the system. Additionally, the stable, long-lived signals produced by FAB-MS encourage the use of MS/MS as a method to probe the origin of specific ions in the melt. Finally, the possibility of using FAB-MS to quantitatively study specific equilibria remains to be tested and, certainly, the observation of negative ions could prove useful to this and further endeavors.

1. R.J. Gale and R.A. Osteryoung, Inorg. Chem., 18:1603 (1979).
2. F. Taulelle, A.I. Popov, Polyhedron, 2:889 (1983).
3. R.J. Gale, B. Gilbert, R.A. Osteryoung, Inorg. Chem., 17:2728 (1978).
4. V. Gesenhues, K. Reuhl, H. Wendt, Int. J. Mass Spec. Ion Phys., 47:251 (1983).

Determination of Betaines and Precursor by Stable Isotope Dilution and Fast Atom Bombardment Mass Spectrometry

Gene C. Jamieson, Ann C. Myers, William L. Fitch and David Rhodes; Zoecon Corporation, 975 California Avenue, Palo Alto, CA. 94304

A rapid, sensitive and selective method for the determination of glycine betaine (N,N,N-trimethylglycine) and biosynthetic precursors is described. The method involves derivatization to introduce aliphatic character which has the benefit of increasing surface activity and concommitant sensitivity in fast atom bombardment mass spectrometry (FABMS) as well as imparting a permanent positive charge to glycine betaine.

Derivatization routes seen in Figure 1 allow direct mass spectrometric measurement of these intact quaternary ammonium natural products at each stage of the biosynthetic pathway.

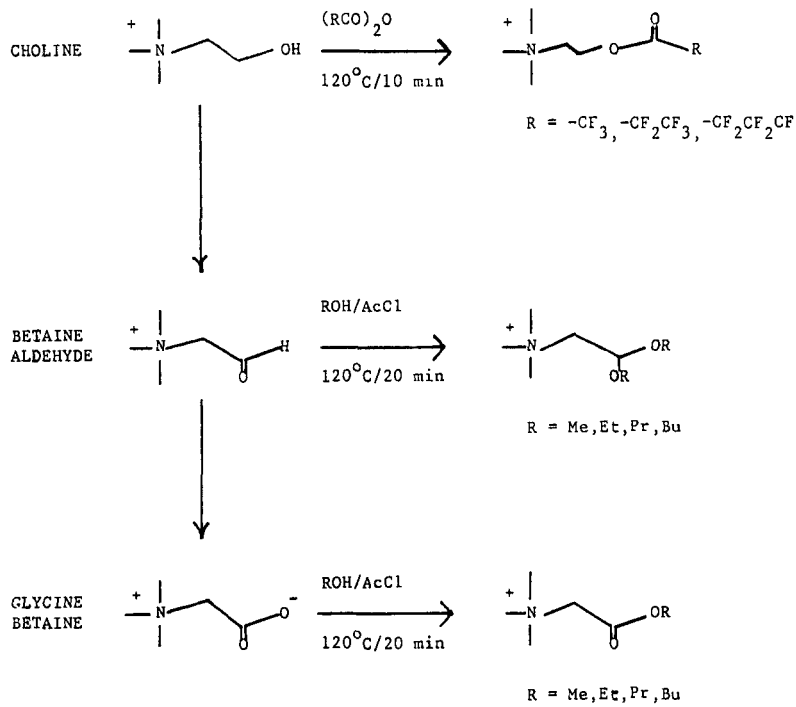

Figure 1. Biosynthetic pathway and derivatization procedures are shown. Derivatization increases surface activity and eliminates glycerol adducts. Methods include acylation, acetal formation and esterification. Significant effects on absolute signal intensity and signal to noise are observed by varying the carbon chain length in the derivative.

Upon fast atom bombardment mass spectrometry stable ion emission combined with rapid scanning around a narrow mass range allows accurate measurement of preformed ions. Aliphatic derivative sensitivity increases with increasing carbon number as shown for betaine aldehyde dialkyl acetals in Figure 2. However, anomalous behavior is noted for choline flourocarbon derivatives. In an equimolar mixture of choline derivatives the pentaflouroproprionate is near 2 times the signal intensity of the heptaflourobutyrate. The dibutyl acetal of betaine aldehyde was observed to be 10 times more sensitive than both the choline pentaflouroproprionate and the butyl ester of glycine betaine. Limit of detection for each derivative is 0.05 nmole/µl glycerol for choline and glycine betaine derivatives and <0.01 nmol/µl glycerol for the dibutyl acetal of betaine aldehyde.

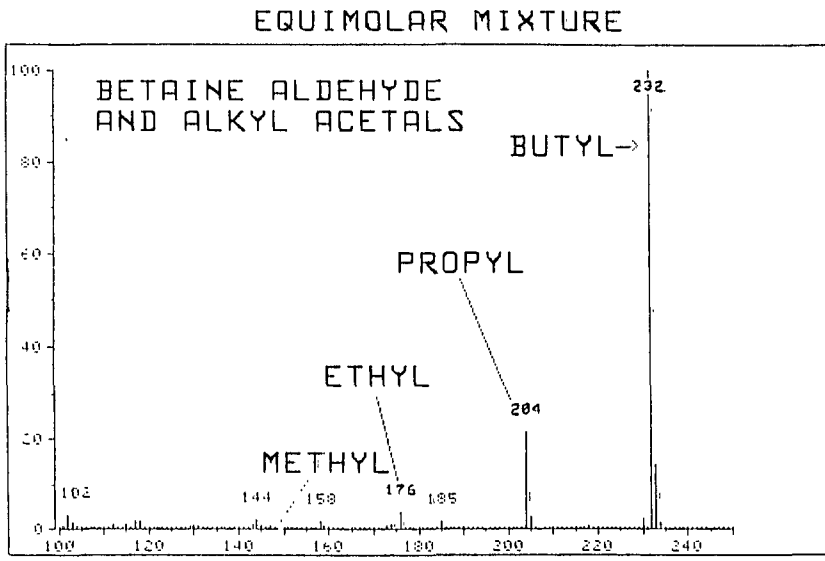

Figure 2. The relationship of carbon number vs. signal intensity is shown for dialkyl acetals of glycine betaine aldehyde. An equimolar mixture at a concentration of 2 nmole/µl of glycerol is analyzed by FABMS.

We illustrate the application of this technique by introduction of N,N,N-tri(CD_3-methyl)glycine betaine as internal standard in the determination of glycine betaine levels in a range of halophytic plant species. In some tissues with abundant levels of glycine betaine (e.g. Cuscuta salina parasitic on Salicornia depressa), glycine betaine ester is the only detectable component in crude methanolic extracts subjected to esterification and FABMS. Further applications of this technique in heavy isotope tracer studies on the pathway of glycine betaine synthesis in spinach leaf discs will be reported. This approach may be useful in rapid screening for genotypic variability in rates of glycine betaine synthesis as a function of salinity or water stress.

COMPARISON OF FAB, FAB AND MS/MS, AND LASER DESORPTION FOR DETERMINATION OF PHOSPHONIUM SALTS.

D. A. McCrery and D. A. Peake; Dept. of Chemistry,

University of Nebraska, Lincoln, NE 68588.

In the preparation of phosphonium salts as synthetic intermediates in Wittig reactions, rearrangements can occur which lead to unexpected products. Thus, a rapid and reliable method, such as mass spectrometry, for the determination of the structure of phosphonium salts is desirable.

The objectives of this research are (1) to examine the facility of obtaining mass spectra of triphenylalkylphosphonium salts by using fast atom bombardment (FAB) and laser desorption (LD), (2) to compare structural information content of FAB and LD ionization mass spectra, and (3) to determine whether collisional activation provides additional structural information. The series consisted of phosphonium salts with alkyl groups which varied from methyl to decyl.

Experimental: The FAB spectra were obtained by using a Kratos MS50 triple analyzer mass spectrometer equipped with an Ion Tech atom gun and a commercial FAB source. Glycerol was used as the matrix in all experiments. CAD spectra were acquired by mass analyzing the ions of interest with the double focussing MS-I, collisionally activating in the third field free region, and scanning the second ESA to obtain the spectrum of the daughter ions. LD spectra were obtained with a home-built FTMS equipped with a Nicolet FTMS1000 data system and a Nd:YAG laser (1060nm and 10-200 MW/cm^2 power density).

Results: The spectra of three isomeric butyl triphenylphosphonium salts are particularly informative. The LD spectra show relatively abundant intact cations and considerable fragmentation. The principal fragments correspond to losses of methane, ethane, propane, butene and butyl.

The FAB spectra are qualitatively the same as the LD spectra, but they indicate that considerably less fragmentation occurs. Although the spectra of n-butyl, s-butyl and i-butyl salts are different and each isomer could be identified if authentic samples were available, the structural information is not complete. Thus, unambiguous structure determination is not possible without comparison with standards.

On the other hand, the CAD spectra of FAB-desorbed ions are more informative. For example, the n-butyl cation shows losses of methane, ethane, propane and butyl wheras the s-butyl does not undergo propane loss and the i-butyl does not lose ethane, in accord with their structures.

Longer chain alkyl triphenylphosphonium cations show enhanced fragmentation proximate to the charge site to produce $Ph_3P\text{-}CH{=}CH_2^+$ (m/z 289) and $Ph_3P{=}CH^+$ (m/z 275). In addition, fragmentation remote from the charge site is observed; i.e. losses of methane, ethane, propane, etc. The remote fragmentation may be another example of a general phenomenon relating to fragmentation of closed shell ions which possess longchain alkyl groups.

TRENDS IN SECONDARY ION EMISSION FROM QUATERNARY SALTS

David A. Kidwell, Mark M. Ross, and Richard J. Colton
Chemistry Division, Naval Research Laboratory
Washington, D.C. 20375

The sensitivity of SIMS for quaternary ammonium salts extends to the nanogram or subnanogram range (1). This enhanced sensitivity forms the basis of a new analytical method to detect components in mixtures. Specifically, a compound in a mixture is selectively derivatized to form a quaternary ammonium salt and the derivative is analyzed using SIMS.

The components are derivatized directly in the mixture without sample extraction or clean-up prior to analysis. To date, we have applied this method to the sequencing of biomolecules (2,3), the analysis of aldehydes and ketones (4), and the analysis of drugs in body fluids (4).

The energy required to desorb an organic cation from a solid-state matrix is primarily proportional to the electrostatic potential, V, between the cation and anion. Since V is inversely proportional to the ionic radius, as the size of the cation or anion increases, it should become easier to desorb the individual ions. Therefore, the secondary ion intensity of organic cations or anions should increase as the size of the cation or anion increases.

In order to determine (and improve) the sensitivity and applicability of our SIMS method, we have measured the relative secondary ion intensities of several quaternary salts as a function of their ionic sizes. Figure 1 shows the SIMS spectrum of an equal molar mixture of several quaternary ammonium, phosphonium, and arsonium salts. As the size of the cation increases, i.e., $Et_4N^+ < Pr_4N^+ < Bu_4N^+ < Pent_4N^+$, the ion intensity of the sputtered cation increases. Therefore, forming large-sized quaternary salts during derivatization should increase the ion yield of the analyte.

We have also observed that, when an equal molar mixture of compounds are derivatized with the same charged group, the ion signal from each *derivative is approximately the same. This implies that the ion yield is* determined by the choice (or size) of the cation and that the size of the analyte portion of the derivative is inconsequential to the emission process.

Since a number of compounds can form dications during derivatization, we have also studied the secondary ion emission of several diquaternary ammonium salts (diquats). The emission of dications in SIMS and FAB is known (5-8), but a question concerning their fragmentation exists because the SIMS spectra of diquats contain many singly-charged ions.

Dications are known to suffer many fates which form singly-charged ions. These include charge separation, one-electron reduction by electron capture, anion attachment, and fragmentation via low-energy pathways. In addition, we find that low-level impurities of monocation species in the diquat salt give intense secondary ion signals, presumed to be due to the dication. Figure 2 shows the SIMS spectrum of dimethyl-triethylenediamine (TEDA) diiodide that contain a 1% impurity of tetrabutylammonium bromide. Note the intense secondary ion signal for Bu_4N^+ compared to the ions from the TEDA salt.

Monocation impurities can be formed during synthesis. For example, the ion species at m/z 141 in Figure 2 (interpretable as $[M-H]^+$ from dimethyl-TEDA) increases in intensity when the dimethyl-TEDA salt is heated with K_2CO_3 in EtOH. The diquaternary salt reacts via a Hofmann elimination reaction to form a monocation impurity with m/z 141. The SIMS spectrum therefore becomes more indicative of the monocation impurity than that of the dication salt.

In summary, this study of mono- and diquaternary ammonium salts has two conclusions: 1) As the size of the cation increases, so does the secondary ion intensity of mono- or dications. 2) The ion yield from diquaternary salts is extremely low compared to trace amounts of monocation impurities formed during synthesis or by fragmentation during sputtering.

References

1. S.E. Unger, T.M. Ryan, and R.G. Cooks, Anal. Chim. Acta 1980, 118, 169.
2. D.A. Kidwell, M.M. Ross, and R.J. Colton, J. Am. Chem. Soc. 1984, 106, 2219-20.
3. D.A. Kidwell, M.M. Ross, and R.J. Colton, "Sequencing of Biological Molecules by SIMS," this volume.
4. M.M. Ross, D.A. Kidwell, and R.J. Colton, "Selective Detection of Mixture Components by SIMS," this volume.
5. T.M. Ryan, R.J. Day, and R.G. Cooks, Anal. Chem. 1980, 52, 2054-7.
6. D.F. Barofsky and U. Geissmann, Int. J. Mass Spectrom. Ion Phys. 1983, 46, 359-62.
7. K.D. Cook and K.W.S. Chan, Int. J. Mass Spectrom. Ion Phys. 1983, 54, 135-49.
8. D.N. Heller, J. Yergey, and R.J. Cotter, Anal. Chem. 1983, 55, 1310-13.

AN EQUIMOLAR MIXTURE OF QUATERNARY AMMONIUM, PHOSPHONIUM, AND ARSONIUM SALTS

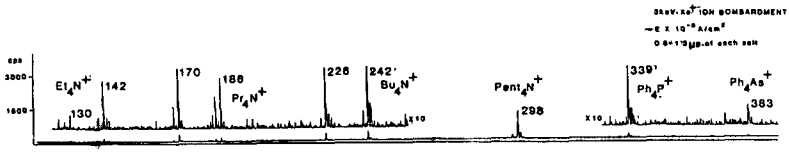

Fig.1

SIMS Spectrum of Dimethyl-TEDA Diiodide and 1% Tetrabutylammonium Bromide

200ng diMe-TEDA$^+$ 2I$^-$

2ng $Bu_4N^+Br^-$

3keV Ar° ~2 X10^{-8} A/cm^2

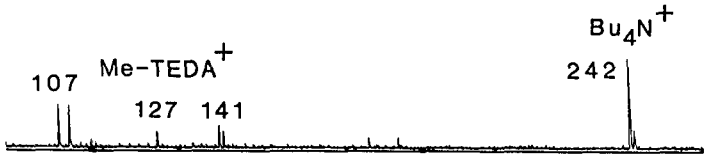

Fig.2 m/z

NEW DEVELOPMENTS IN HIGH RESOLUTION FAB IONIZATION MASS SPECTROMETRY

J.C. Cook, University of Illinois, School of Chemical Sciences, Urbana, Illinois, 61801, and B.N. Green, V.G. Analytical Ltd., Floats Road, Wythenshawe, Manchester, M23 9LE, England

A dual target, alternating position fast atom bombardment sample probe has been developed which permits the technique of high resolution FAB mass spectrometry to be performed routinely and with great ease. The probe operates under command of the peak matching unit or data system. Sample is loaded onto one side of the dual target and reference compound onto the other side. Data can be acquired either by peak matching or by signal averaging employing the continuum or MCA mode of the data system with scans over a limited mass range.

One side of the dual target is loaded with a suitable reference compound and the other with sample. We have found that a mixture of dithiothreitol and dithioerythritol (the so-called "Magic Bullet") to be a useful matrix for high resolution FAB since it is much less volatile than the commonly used thioglycerol. Measurements are performed using the peak matching unit of the mass spectrometer or for weak signals the continuum or MCA signal averaging mode of the VG 11-250 data system with scans over a limited mass range. The data system determines the accurate masses and generates listings of possible elemental compositions.

The current system has been used to perform accurate mass measurements for over 60 different compounds with an average accuracy of 5 to 6 ppm. The next development will be the use of signal averaging in the time domain mode which will permit scans over a wide mass range.

This work supported by a grant from NIH (GM27029)

FPA16: Au^- ION GUN FOR LIQUID SIMS

Charles N. McEwen*, Donald J. Harvan and J. Ronald Hass
Laboratory of Molecule Biophysics
National Institute of Environmental Health Sciences
Research Triangle Park, North Carolina 27709

An ion gun which produces negatively charged gold particles with energies up to about 20 keV is described. As shown in the figure, the negative gold ions are produced by bombarding a gold cone with high energy Cs^+ ions. The Au^- ion intensity slowly increased over a period of an hour or so before becoming stable. This increase is attributed to the time necessary to deposit a steady state concentration of cesium from the Cs^+ ion gun onto the gold surface. Considerably higher Au^- ion current is produced when a method is available for controlling the concentration of cesium on the gold surface.[1] As pictured in the figure, the Au^- ions are focused on the sample probe target by a three element lens.[2] An Au^- primary ion current equivalent to 3-5 uA Cs^+ is obtained from the gold gun as measured by the intensity of sputtered glycerol ions. This ion current is sufficient to produce high quality spectra of compounds such as met-enkephalin.

The perceived advantages of the Au^- ion gun over Xenon or cesium guns is the higher mass of the gold particle[3], and for positive ion liquid SIMS on a high voltage magnetic instrument, the high energy which can be imparted to the negatively charged particle[4]. Neither the higher mass of the Au^- particle nor the higher obtainable energy (up to 20 keV) increased the detection limit for the molecular ion of met-enkephalin relative to a cesium ion gun[5] or a xenon gun[6]. The detection limit for all of the guns were limited to the 10 to 20 ng level by the chemical background. Increasing the primary bombarding particle flux increased the total sputtered ion yield but reduced the signal-to-noise ratio because the chemical background noise increased faster than the sample signal.

While no advantage to the Au^- ion gun was determined at the relatively low mass of the molecular ion of met-enkephalin, at high mass where signal intensity is of more importance than chemical background this gun should be advantageous. Au^- ion guns have been constructed which deliver milliamps of ion current.[1]

The success of this Au^- ion gun depends on having a Cs^+ ion gun which can operate in a stable manner at 20 to 50 μA over relatively long periods of time. The gun is as described previously[5] with the following exceptions. The lead nichrome wires are held in place by a two hole ceramic which fits into a larger one hole ceramic tube. A rhenium ribbon filament is used instead of tungsten wire. The end of the gun is restricted to a 1 mm ion exit hole. The gun is charged with at least 50μl of a saturated cesium chloride solution. The filament is operated at about 2 amps.

1. G. D. Alton and G. C. Blazey, Nucl. Instr. and Meth., 166, 105, (1979).

2. R. Stoll, D. J. Harvan, and J. R. Hass, Anal. Chem., submitted for publication.

3. D. F. Barofsky, U. Giessmann, A. E. Bell, and L. W. Swanson, Anal. Chem., 55, 1381, (1983).

4. R. D. MacFarlane, Acc. Chem. Res., 15, 268, (1982).

5. C. N. McEwen, Anal. Chem., 55, 967. (1983).

6. M. A. Rudat, Anal. Chem., 54, 1917, (1982).

* Present address: E. I. duPont deNemours and Company, Central Research Department, Experimental Station, Wilmington, De. 19808

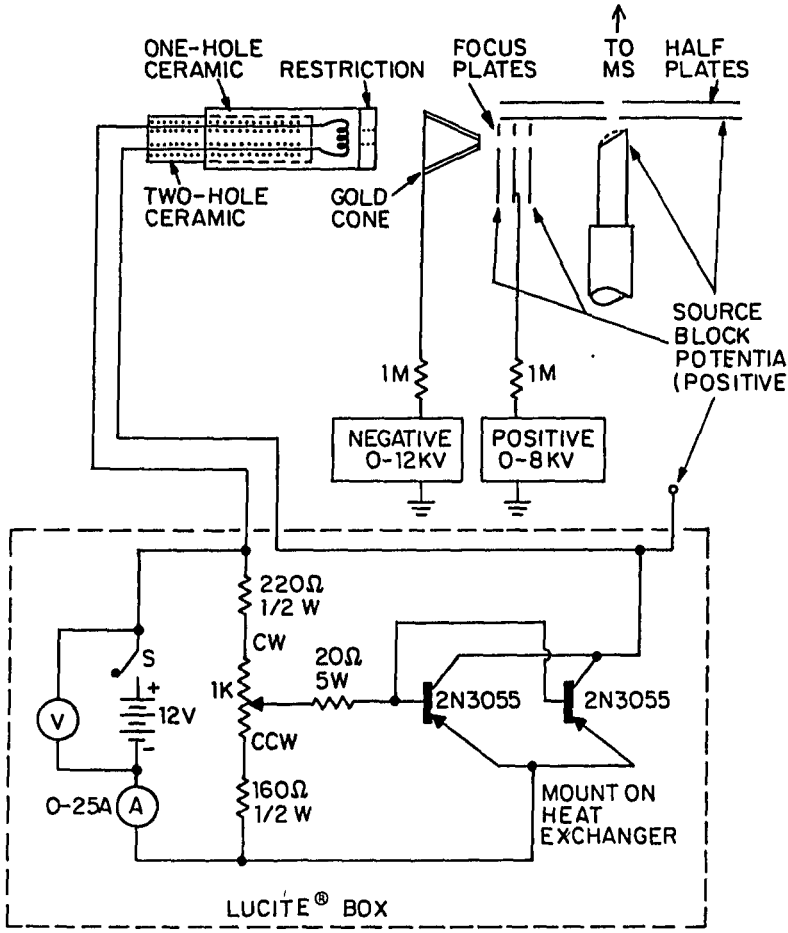

IMAGING SECONDARY ION MASS SPECTROMETRY OF ORGANIC COMPOUNDS

R. G. Stoll, D. J. Harvan, R. B. Cole, J. R. Hass
Laboratory for Molecular Biophysics, National Institute for Environmental Health Sciences, RTP NC 27709

Solid materials are often a complex assembly of chemically different microstructures. A full understanding of such a material can come only from the knowledge of the constitution of its parts and their interaction. Light and electron microscopy have been used in the past extensively to study the topological relation between the component parts of these microsystems. For the same reason it is desirable to perform an in situ chemical analysis of the microstructures confirming their identity or showing the chemical difference between different microparticles. Ion microscopes and microprobes, using several keV energetic ion beams[1] have been used in conjunction with mass spectrometers, to evaluate the elementary composition of microscopic structures.

We report the construction of an ion microprobe, which is able to measure the distribution of organic ions coming from a surface. The ion microprobe utilizes a fine focussed primary ion beam scanning across the sample surface. Secondary ions formed under this beam are mass analyzed with the mass spectrometer. The ion image is reconstructed by relating the ion signal intensity to the primary ion beam position.

The ion microprobe uses a liquid metal field ion (LMI) source (FEI Comp.)[2] to produce the primary ion beam, which can be a primary ion beam of gallium, indium, gold and various other metals. With a total source current of a few microamperes it delivers a current of approximately 1 nA into a spot of less than 0.3 micrometer diameter with kinetic energy of up to 30 keV. This corresponds to a current density of up to 1 A cm-2 and a power density of more than 10 E4 W cm-2.

To keep the optimum acceptance of the mass spectrometer and the spatial resolution of the primary ion source over a large field of view without the need of retuning the instrument, the primary ion beam is not deflected across the sample surface, but the sample is moved under the primary ion beam. The high precision movement in the XY plane defining the field of view is accomplished by two piezoelectric linear motors (TS-101 Burleigh Instruments) which allow a movement of up to 6 X 6 mm with a resolution of 10 nm.

The mass spectrometer used is a high resolution double focusing mass spectrometer (VG ZAB2F). Its mass range at 6 kV acceleration potential is 1-1600 daltons. To accomodate the primary ion source, a CF 100 flange has been added to the source housing. No other ports have been altered, so that the instrument can be reconfigured for conventional ion sources with little downtime.

The data system has to control the data acquisition, store, process and display the data in a convenient form. The data system in its current form consists of two distinct units, a mass spectrometry data system for data acquisition and processing (Finnigan INCOS 2300) and a microcomputer (APPLE II+ with ISAAC interface) to operate the XY stage and the primary ion source.

To test the imaging properties of the system a 500 line Ni-mesh was chosen as a target. Figure 1 shows an area of 100 X 100 micrometer of that mesh covered with fomblin, a perfluoropolyether. The mass spectrometer is monitoring a mass peak at 131 u. The structure of the supporting grid is clearly visible. Low intensity high mass ions can be used to image a surface as well. Figure 2 shows the same grid imaged while monitoring the 1281 ion of fomblin. The signal intensity of the high mass ion is less than one percent of the base peak intensity. The supporting grid wires are actually approximately 10 micrometer wide.

It can be expected that the instrument described above can be used to evaluate the distribution of various other organic compounds on surfaces. To prepare for this, a thorough investigation of the mass spectra obtained with the high intensity primary ion source is planned and the results will be published.

---

1. R. Castings and G. Slodzian, J. Microsc., 1, 395 (1962)

2. J. Orloff, L. W. Swanson, J. Vac. Sci. Technol. 19, 1149 (1981)

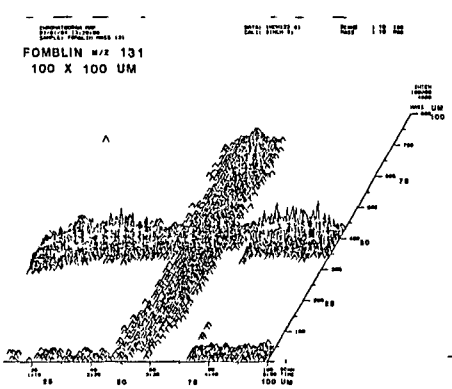

FIG. 1

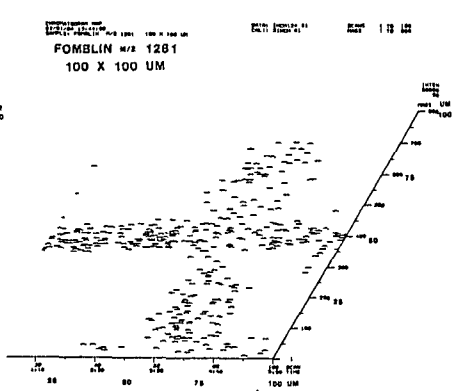

FIG. 2

DIRECT COMPARISON OF SECONDARY ION AND LASER DESORPTION MASS SPECTROMETRY IN A MOVING BELT LC-MS SYSTEM.

T.P.Fan*, E.D.Hardin, M.L.Vestal
Department of Chemistry, University of Houston, Houston, Tx. 77004

An LC-MS instrument, operated in either ion impact or laser desorption mode, has been developed in our laboratory (1). The system employs a thermospray vaporizer to desolvate and spray the sample onto a moving belt under partial vaccum. Samples are carried by the moving belt into the ionization source chamber where they are ionized/desorbed by either an ion beam or a pulsed laser beam. Both ion beam and laser beam are aimed at the target surface at 45 degree angle. Xe^+ accelerated at 3 KV is used as primary ion and is usually operated at a current of 1 uA/cm^2. The Nd:YAG laser employed is typically operated at repetition rate of 100 Hz and power density of 10^8 W/cm^2.

Both secondary ion mass spectra and laser desorption mass spectra can be acquired under otherwise identical conditions. A systematic study has been carried out for the direct comparison of the two soft ionization/desorption techniques using mainly nonvolatile biomolecules as test samples (2). Some characteristic differences have been observed between these two techniques.

Contamination by pump oil and other contaminants on the belt surface is understandable since the system is operated under a "dirty" vaccum about 10^{-6} torr. Pump oil fragment ions are clearly observed in SIMS background mass spectra while it is essentially transparent under laser desorption conditions. Positive ion mass spectra from 14 amino acids and 4 nucleosides are quite complementary between SIMS and LDMS (Fig.1). Laser desorption mass spectra are dominated by alkali (Na^+, K^+) attached ions. By proper adjustment of laser power density, intense quasi-molecular ion signal is usually obtained with minimum fragmentation. Alkali attachment is weak or absent in SIMS mass spectra. It is characterized by protonated molecular ion together with abundant structrual related fragment ions. However, negative ion mass spectra from SIMS and LDMS are very similiar. Mainly deprotonated ions are observed.

A series of belt speed experiments were carried out to investigate the total ion intensity dependence on the energy beam dosage and the surface coverage. LDMS results are straightforward and easily rationized. The total ion intensity reaches optimum at the belt speed where each laser pulse strikes a fresh surface of the belt. At higher or lower belt speeds, incomplete sample desorption or overlapping of adjacent laser pulses occur leads to reduced ion intensities. The response is seen to increase monotonically with surface coverage up to about a monolayer. At higher coverages, the response flattens off and even decreases in some cases most likely due to attenuation of the beam energy by sample light scattering or absorption of laser energy by the sample instead of the substrate. Results from SIMS are less in accord with expectations. It appears that sample react with surface or contaminants may be the interfering factor.

Chromatographic peak shapes, mass spectral reproducibilities, and resolution are much better in SIMS than with LDMS. This is partly because a continuous ionization source is more compatible with the scanning quadruple mass analyzer than with a pulsed source. Fluctuation

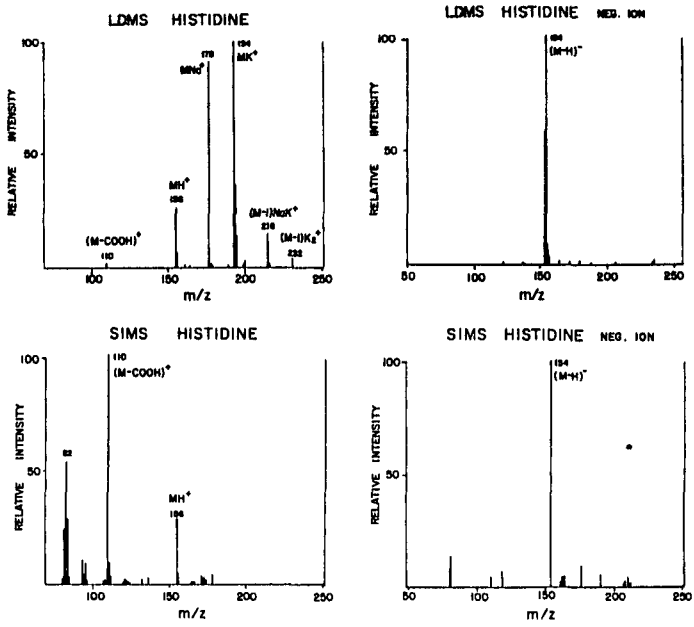

Fig.1

in the LDMS intensities are probably caused mainly by fluctuations in the laser peak to peak pulse energy output. Small changes in laser pulse power density can cause large changes in ion yields.

Using tartaric acid as a matrix for sample analysis has been found to enhance total ion as well as quasi-molecular ion intensities. Low detection limit in both LDMS and SIMS can be enhanced by at least 20 times with this matrix. The matrix effect is most likely a combimation of (1) Enhanced ionization efficiency through solvation of sample in the matrix. (2) Decreased fragmentation through desolvation from desorbed sample-matrix clusters(3). (3) Enhance MH^+ preformed ions by acting as a proton donor.

References

(1)E.D.Hardin, T.P.Fan, M.L.Vestal, Anal. Chem., 1984, 56(1), 2.
(2)T.P.Fan, E.D.Hardin, M.L.Vestal, Anal. Chem., 1984, in press
(3)R.G.Cook, K.L.Busch, Int. J. Mass Spec. Ion Phys., 1983, 53, 111.

EFFECTS OF CS^+ PRIMARY ENERGY AND INTENSITY ON LIQUID SIMS SPECTRA

Y. Morita, W. Aberth and A.L. Burlingame

Mass Spectrometry Resource, Dept. of Pharmaceutical Chemistry,
University of California, San Francisco, CA 94143.

In this laboratory we have begun research to explore the dynamics of sputter ionization from a liquid target by mass spectrometry (LSIMS) in order to develop a better model for this phenomenon. The initial objectives were to explore the effects of primary beam kinetic energy and current on LSIMS spectra and investigate the energy dispersion of secondary ions as a function of primary beam kinetic energy and current, and target state.

The ion optic arrangement schematic is shown in paper ROE 2. It includes an immersion lens for secondary ion extraction and focusing (1) followed by a retarding potential type energy analyzer and a QMS. A Cs^+ ion gun (2,3) is used for the primary beam. Spectra were obtained in the mass range of 1-400 from a liquid glycerol target using a wide range of primary beam ion kinetic energies and currents. Figure 1 shows a typical X-Y plot of a glycerol spectrum. The intensity of glycerol cluster peaks relative to the primary beam current were monitored and compared. Primary energies of 2, 4 and 8 KeV at currents ranging between 5×10^{-9} and 1.1×10^{-6} amp were used. Figure 2 is a plot of glycerol cluster peak intensities normalized to the corresponding primary Cs^+ intensity, for a variety of Cs^+ energies and intensities. General conclusions indicated by the data are: 1. Highest efficiency occurs at highest primary energy and lowest primary current; 2. Relative efficiency of higher cluster production decreases with decreasing primary ion KE and increasing current; 3. In general, secondary efficiency decreases with increasing primary current.

An energy analysis of the secondary ion peaks was obtained by differentiating the retarding potential curve using 2 eV intervals (hence the indicated energy halfwidths are narrower by 2 eV). A comparison of the dimer glycerol peak with that of $(CsI)Cs^+$ obtained from a solid target has about twice the energy half width (Fig. 4) indicating the strong effect of the liquid matrix.

Acknowledgments. This work was supported in part by NIH DRR Grant RR 01614 and NIH Grant GM 32315.

References

1. W. Aberth, A.L. Burlingame, Proc. 4th Int. Conf. on SIMS, Osaka, Japan, Nov. 13-19, 1983.
2. W. Aberth, K.M. Straub, A.L. Burlingame, Anal.Chem. 54, 2029 (1982).
3. Antek P.O. Box 51311, Palo Alto, CA. 94303.

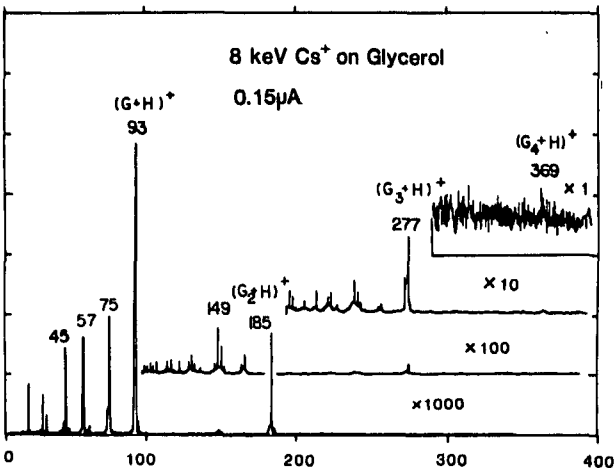

Figure 1.

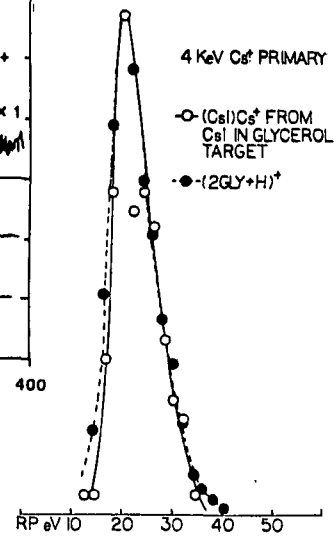

Figure 3.

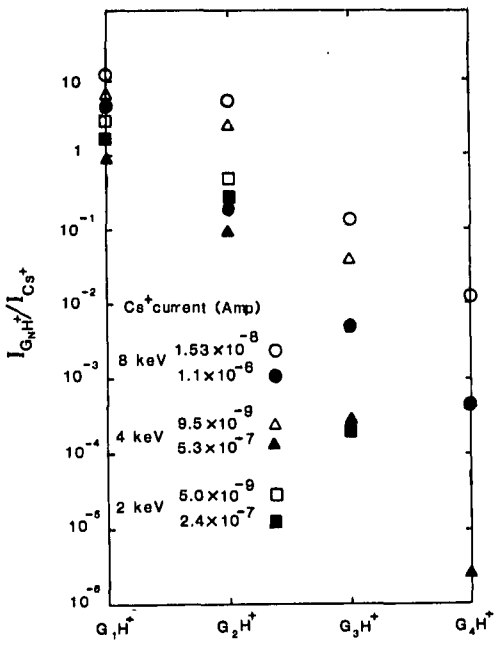

Figure 2.

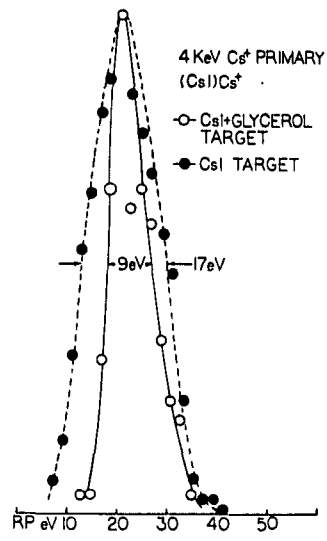

Figure 4.

DETERMINATION OF THE CHARACTERISTICS OF A FAB SOURCE, R. K. Mitchum, J. P. Freeman, B.T. Duhart and J. Hunziker, Department of Health and Human Services, Food and Drug Administration, National Center for Toxicological Research, Jefferson, Arkansas 72079.

Recent developments in mass spectrometry led to the application of energetic ion/neutral bombardment techniques for the analysis of organic compounds. Fast atom bombardment (FAB) has been applied to and the techniques utility lies in the determination of the mass spectra of nonvolatile polar organic compounds. Although many factors have been shown to influence FAB spectra, matrix effects are perhaps the most important and spectra have been enhanced by the addition of inorganic salts and by changing the solution matrix.

Perhaps of more fundamental concern is FAB source design and its effect on beam intensity and the directional characteristics of the beam. This paper describes the determination of the divergence angle of the ion neutral beam emitting from a laboratory constructed saddle field ion/neutral bombardment source.

The ion neutral source is similar in design to that of Hogg[1] except for the annular electrode and electrode isolation design. The FAB source was tested for beam divergence as an indication of alignment and design characteristics. Beam symmetry is an indication of source alignment while beam divergence angle is an indication of performance.

The experimental apparatus consisted of a vacuum stand which could be diffusion pumped to less than 10^{-6} torr. The FAB source was mounted on a test flange offset from the center. A linear motion feedthrough capable of rotation was used to hold the test target. The test target was a circular 3 1/2" X 1/8" aluminum plate mounted on a stainless steel rod. The test targets used consisted of several types of light sensitive paper. The FAB gun was powered by a Spellman high voltage power supply. The supply was operated at 10 milliamperes and 7 kilovolts. Ion beam current profiles were taken with an electrode target capable of rotation. This measurement produced the cross section of the ion beam current profile.

Measurements on photographic type paper produced three distinct concentric exposure patterns. The divergent angles were calculated from the diameter of the exposure pattern and from the distance from the target were taken as the average of the results from seven types of paper at three distances from the source.* The intense central beam had a divergent angle of 2.6° while the second and third exposure patterns resulted in divergent angles of 6.8° and 11.1°.

The results of the second experiment which consisted of measurement of the cross sectional ion beam profile resulted in a divergent angle of 10.3°. The agreement between the divergent angles measured using the diameter of the largest measured exposure pattern and the ion beam current profile is what would be expected. It appears however that there is a central beam area which has a smaller divergent angle with a more intense beam. It has been suggested that the exposure pattern could be due to ions formed with different energies. From the ion beam profile measurements no inconsistencies were observed which would indicate an intense central ion beam of ions but rather a beam with a spread of energies. The measurement of FAB source divergent angles using Kodak linagraph paper produces results comparable to those obtained by measurement of the ion beam current profile which is more difficult.

The comparison of the laboratory constructed FAB source performance with the performance of a commercial design can be made. The Ion Tech neutral beam source is reported to have central beam with a spread of 3.5° which is in good comparison to the measured intense central beam divergent angle of 2.6° with the present source.

In conclusion the saddle field neutral/ion beam source of the general design reported by Hogg perform comparably to commercial sources. It appears however that source alignment may be critical due to the intense central beam in the saddle field source which exhibits a small divergent angle.

1. A.M. Hogg, Int. J. Mass. Spectrom and Ion Phys., 49 (1983) 25-34.

2. R. K. Fitch, S. N. Ghafouri and E. A. Mahmood, Vacuum, 24 (1974) 489-491.

* Measurements were made with targets of linagraph paper, carbonized target, green ditto paper, white bond paper and RC II photosetting paper at 2.5, 5 and 10 cm.

A NEW METHOD FOR THE PREPARATION OF THIN UNIFORM FILMS FOR PARTICLE-INDUCED DESORPTION STUDIES

V. K. Mancill, R. D. Macfarlane, C. J. McNeal
and D. B. Shelton
Department of Chemistry
Texas A&M University
College Station, Texas 77843

One of the problems encountered in the use of thin solid films for mass analysis of involatile biomolecules is the variability of the sample matrix which can have a profound effect on molecular ion yields.[1] The preparation of surfaces containing involatile thermally labile molecules at sub-monolayer coverage cannot be accomplished by the traditional methods of vacuum evaporation. The method described in this paper essentially solves this problem.

When a flat solid surface is slowly (V=0.8mm/s) withdrawn from a solution, a thin film of the solution adheres to the surface and the excess is forced back into the solution forming a liquid prism (Fig. 1). Solute particles at the tip of the

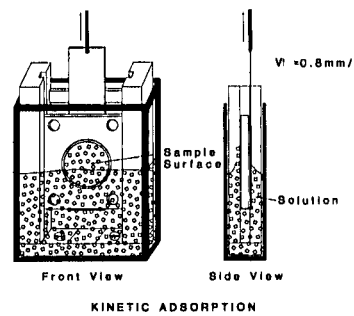

Figure 1. The dipping apparatus.

prism are forced onto the surface as the prism slides back into the bulk solution. The solute particles attach by a kinetic adsorption which is independent of the adsorbate-substrate interaction. The nature of the solute and the relative intermolecular spacing in solution are transferred intact to the surface of the film.[2]

The average spacing between molecules in solution can be measured indirectly using fluorescent dye molecules. The peak wavelength of the fluorescence (λ_p) is influenced by neighboring dye molecules to spacings of ~ 200 Å. Rhodamine 6G has been used to test the method. Measurement of λ_p in the fluorescence of the solution is dependent on solution concentration and intermolecular spacing (Fig. 2). The solution concentration (C) and intermolecular spacing on the film (d) are related by

$$d \sim C^{-1/2}$$

Fluorescence measurements from films prepared by kinetic adsorption show that the intermolecular spacing is preserved.

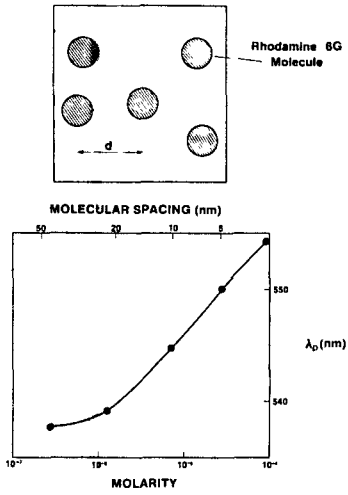

Figure 2. Peak emission wavelength as a function of solution concentration and intermolecular spacing.

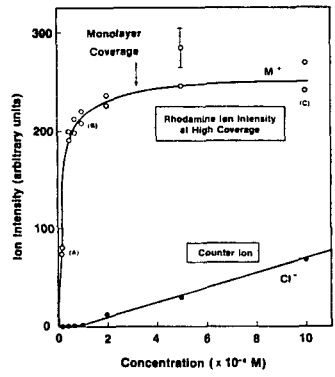

Figure 3. Solution concentration vs. ion intensity.

^{252}Cf-plasma desorption mass spectra of Rhodamine 6G were measured using Mylar substrates containing Rhodamine 6G molecules kinetically adsorbed from different solution concentrations. Molecular ion intensities were measured for films kinetically adsorbed from solutions ranging from 1 x 10^{-6} M to 1 x 10^{-3} M, representing average intermolecular spacings from 200 Å to multilayer coverage.

Over the range from 1 x 10^{-6} M (.003 coverage) to 5 x 10^{-5} M (0.2 coverage) the molecular ion intensity is linear and proportional to solution concentration. At higher coverages, the intensity departs from linearity due to an increased overlay of the excitation track with more than one molecule. The ion intensity maximizes at the concentration expected for monolayer coverage (Fig. 3).

The kinetic adsorption method has been shown to form reproducible uniform layers of solute molecules on surfaces with intermolecular spacings determined by solution concentration. This method is being used to study the role of intermolecular interactions in particle-induced desorption.

1. R. D. Macfarlane, Acct. Chem. Res. 15, 268 (1982).
2. S. Garoff, R. B. Stephens, C. D. Hanson, and G. K. Sorenson, Optics Comm. 41, 257 (1982).

On-Line Accurate Mass Measurement in FABMS; Gilliam, J. M., Landis, P. W., and *Occolowitz, J. L.; Lilly Research Laboratories, Indianapolis, IN 46285

Two methods of on-line, complete spectrum, mass measurement in FABMS were investigated using a ZAB-3F mass spectrometer interfaced to an SS-200 data system.

In the first method, PFK was scanned in the FAB mode using a cooled target, and several minutes later the unknown was scanned, dispersed in glycerol. The time of arrival of m/z 94 in the PFK spectrum was arbitrarily assigned time zero, and the time of arrival of a mass equal to that of m/z 94 in the glycerol spectrum was calculated using the times of arrival of m/z 94 and 100 in the PFK spectrum. The two spectra were then mathematically combined such that the difference in times of arrival of the two peaks at m/z 94 equalled the calculated value.

For calculating unknown masses three methods were used:

i) No allowances were made for differences in dM/dt between the spectrum of PFK and the unknown,

ii) An empirical mass vs. error relationship was found using masses calculated for glycerol cluster ions, and

iii) Experimentally determined exponential scan constants were calculated using peaks in the PFK spectrum and glycerol cluster ions in the spectrum of the unknown, and the ratio of these scan constants used to correct the scan function of the unknown.

When the three methods were compared, it was found that the mean error for 5 scans was between 3-4 ppm for all methods up to m/z 600. However, the standard deviation for methods ii) and iii) was about 8 ppm while for method i) it was 15 ppm.

In the second approach to mass measurement a mixture of polyethylene glycols prepared as a dilute solution in glycerol was used as an internal standard. The glycerol solution was found to be superior to the use of neat glycols insofar as the absolute intensity of the standard peaks in glycerol were between 4 and 10 times more intense in the mass range 600-1000. Using the internal standard method and averaging 6 consecutive scans (10"/decade), we have obtained mass measurement accuracies of 1-3 ppm in a mass range up to m/z 1000 with standard deviations of 3-4 ppm.

(Submitted to Analytical Chemistry)

Determination of Enzyme Kinetic Constants Using FAB

Richard M. Caprioli, Laurence A. Smith and Terry Fan

Analytical Chemistry Center and Department of Biochemistry
University of Texas Medical School, Houston, Texas 77030

FABMS provides an analytical method of great molecular specificity with which to sample complex biological reaction mixtures. We have utilized this technique to study the feasability of measuring enzyme kinetic constants using the proteolytic enzyme trypsin and several polypeptide substrates. Of particular interest were the questions involving the integrity of quantitation of the peptide under FAB conditions and the overall utility of the method compared to classical methods.

A Finnigan-MAT 3300 Incos MS system modified with an Ion Tech B11N neutral atom gun and B50 power supply were used. The atom gun was operated with xenon gas at 0.5 cc/min at 10 psi and an accelerating voltage of 8 KeV giving 40 μamp of ion current.

The rates of hydrolysis of the peptide substrate by trypsin was measured at five peptide concentrations varying between 1 mM and about 24 mM. The reactions were initiated by adding 1-5 μg trypsin/ml of peptide solution containing 40 mM Tris and 10 mM $CaCl_2$ at pH 8.1. An internal standard, G-P-BNA (m/z 298) or Ca taurocholate (m/z 554) was used for quantitation.

The determination of Km and Vmax were made for several peptides. As an example, that for F-R-S-V will be given in some detail. First, a quantitation curve was made for the peptide, using an internal standard. This curve was made throughout the peptide concentration range needed for the study (0.5 - 16 mM). The effects of buffer constituents and peptide concentration on the rate of hydrolysis were determined. The rates of hydrolysis of F-R-S-V at several concentrations at the same enzyme concentration were measured. Finally, from a double-reciprocal plot of these data, ie, 1/[S] vs 1/v, the values for Km and Vmax were calculated. This procedure was repeated for the peptides M-R-F-A and M-R-F-A-NH_2. The kinetic behavior of these peptides with trypsin can be compared by comparing the ratio of kcat/Km, (assuming simple Michaelis-Menton kinetics, kcat = Vmax/[E]).

The methods presented permit the determination of kinetic constants of enzyme/substrate reactions to be determined with ease and accuracy. The molecular specificity, sensitivity, and speed of the procedure makes it ideal for such determinations. Further, the capability of using natural substrates of different sizes and charge distribution, coupled with very simple sample preparation procedures, provides a new approach for the biochemist in the understanding of the mode of action of enzymes.

Determination of Metal-Ligand Binding Constants by Fast Atom Bombardment Mass Spectrometry

William E. Seifert, Jr., Tseng-Ying Fan, and Richard M. Caprioli

Analytical Chemistry Center and Department of Biochemistry and Molecular Biology, The University of Texas Medical School, Houston, Texas 77030

Fast atom bombardment mass spectrometry provides an analytical method by which binding phenomena of molecules and ions in solution can be investigated with a high degree of molecular specificity. This technique has previously been used to determine the acid dissociation constants of weak organic acids in aqueous solutions.[1] In this study, we apply the methodology to investigate the binding of metal ions to organic ligands in aqueous glycerol solutions. Two types of binding phenomena, chelation of the metal and ionic association between the metal and the organic ligand, have been investigated.

The investigations were carried out using a Finnigan-MAT 3300 Incos MS system modified with an Ion Tech B11N neutral atom gun and B50 power supply. The atom gun was operated with xenon gas at 0.5 cc/min at 10 psi and an accelerating voltage of 6-8 KeV yielding 40 μamp of ion current.

Binding constants are determined by measuring the intensity of the quasi-molecular ions corresponding to bound and unbound forms of the ligand, including in the analysis any corresponding glycerol-adduct ions. The binding constant may then be determined by either of two methods; a) using the equation:

$$\text{Kassoc} = \frac{[ML_n]}{[M^{++}]\,[L^-]_n}$$

where $[M^{++}] = [M^{++}]_{initial} - [ML_n]$, or b) using the method of Scatchard.[2] By plotting the fraction of ligand bound to metal vs. the ratio of the fraction of bound ligand to metal ion concentration, the Kassoc can be determined from the Y-intercept. This method is of particular use when investigating the binding of Ca^{++} to the bile acids cholic acid and taurocholic acid, on which $[Na^+]$ has a significant effect.

The methods presented permit the determination of binding constants for metals to organic acids in aqueous-glycerol solutions. The advantages are the simplicity of the analysis and the ability to measure with a high degree of molecular specificity the various ligand and metal-ligand complex components in the mixture.

1 R. M. Caprioli, Anal. Chem., 55, 2387 (1983).

2 G. Scatchard, Ann. N. Y. Acad. Sci., 51, 660 (1949).

MOLECULAR MICROPROBE. L. Kelner, H.M. Fales and S.P. Markey, National Institutes of Health, Bethesda, MD 20205.

Particle-induced desorption mass spectrometry is in the forefront of methods to identify elements and compounds residing on the surfaces of metals, semiconductors and oxides. Recent developments in molecular SIMS/FAB have proven valuable in extending these techniques to biologically important compounds. Currently, molecular SIMS determines the presence of chemicals in bulk specimens: all information is lost concerning the spatial distribution of materials and their relationships to structures visible with light and electron microscopy. With certain precautions, however, the principles of molecular SIMS could be applied to develop a molecular microscope/microprobe. Such a device should allow localization of biologically important chemicals within tissues at submicron resolution and visualization of intracellular distribution and concentration of a variety of organic compounds. We discuss here the design and construction of a prototype molecular microprobe which combines a pinpoint microbeam for particle desorption with mass spectrometric analysis of the resulting molecular or ionic species.

There are four basic areas of the instrument which are addressed below: 1) method of illumination (primary beam parameters); 2) secondary optics including mass analysis: 3) detection system with data processing, and 4) target preparation. Depending on the type of primary beam, two different principles of microscopy could be adapted: a) a molecular microscope - illumination of the surface with a defocused primary beam (.5 to 1 mm in diameter) and subsequent imaging and focusing of the illuminated area into detector, and b)a microprobe - illumination with a pinpoint primary beam of the size of required lateral resolution (.1 to 10 μm) and mass analysis and detection of signals from each picture element or "pixel". The latter method would be much slower, but potentially has higher sensitivity than the microscope principle, although it may take 10-20 min to a few hours (depending on the number of "pixels" required for a given resolution) to record one image picture of a sample. This principle of analysis was adapted for our instrument, since it offers a greater opportunity to detect low concentrations of chemicals in tissues.

With the microprobe scheme we can utilize non-focusing type of mass spectrometers (such as quadrupoles or time-of-flight), which offer higher transmission and thus lower limits of detection of secondary ions than magnetic or double-focusing mass spectrometers.

The detection of ions sputtered from the target is accomplished best by pulse counting. A channel electron multiplier detects each secondary ion and this signal is

transmitted to a computer which stores the raw data, and then reconstructs the image of the bombarded area of interest on the sample. The sample preparation will be one of most critical aspects of successful analysis of organic materials in biological specimens by molecular microscopy. The usual liquid SIMS/FAB arrangement of the target consisting of a sample dissolved in a liquid matrix (glycerol), by its nature, precludes imaging. Similarly with tissue samples, a major problem is diffusion of the organic components of the tissue through the sample. Lyophilization of the sample and performing the analysis of tissues in the frozen stage is the most promising sample preparation technique.

We based our molecular microprobe prototype on the recently developed Secondary Emission Mass Spectrometer [1] with some modifications required to achieve imaging of organic compounds in biological specimens. At present, the ion beam can be focused to about 50-100μm. The addition of focusing lenses will allow beam reduction to 1-10μm. Further reduction of the probe size cannot be achieved with the existing gas discharge ion source, but would require a cesium ion source (probe size about 200 Å) or an electrohydrodynamic ion source. Rastering of the probe is achieved by the addition of two pairs of raster plates which can be controlled by an analog signal internally, or by a data system externally. The size of the raster is variable from .1 to 5 mm. When the data system is used for analysis, the computer, based on an IBM-TX package, will move the beam from "pixel" to "pixel" on the target, and store the mass analyzed signal. The mass analyzer can be used in MS or MS/MS mode (triple quadrupole system). Two modes of primary beam operation will be available: a multi-raster scanning with signal from each "pixel" integrated over the time of analysis, or a single raster scan, where the beam is moving slower and spending much longer time on each "pixel" (the beam in this case can be pulsed at the rate of 10 to 500 nsec).

The system will be tested later this year when all the necessary modifications are completed.

Reference

1. L. Kelner and T. Lundquist, Int. J. Mass Spectrom. Ion Physics, 46 (1983) 27.

FPA 27 CS^+ ION DESORPTION IONIZATION USING FOURIER TRANSFORM MASS SPECTROMETRY

M.E. CASTRO AND D.H. RUSSELL

DEPARTMENT OF CHEMISTRY

TEXAS A&M UNIVERSITY

COLLEGE STATION, TX 77843

It has been roughly ten years since Comisarow and Marshall published the first paper describing the Fourier transform ion cyclotron resonance (FT-ICR) or FTMS experiment (1). In subsequent work several laboratories have reported on other developments in FTMS (2), and more recently there has been growing interest in the development of FTMS for the analysis/characterization of large molecules. The major obstacle which limits the use of desorption ionization techniques with FTMS is the high vacuum requirements of the ICR method. That is, the mass resolution of FTMS is determined by the length of time that the transient signal is observed (equation 1) and the duration of the transient is directly proportional to the analyzer pressure (2). This requirement for ultra-high vacuum

$$\frac{M}{\Delta M} = \frac{BT}{5.769 \times 10^{-5}\ M} \qquad \text{eq. 1}$$

precludes the use of gaseous discharge guns for DI-FTMS and the use of liquid SIMS.

The first successful DI-FTMS experiment utilized laser DI (3) and subsequent work in this area has been quite successful (4). For example, biomolecules with molecular weights in the range 1,000-2,000 a.m.u. and polystyrene (m.w. ≅ 2,500) have been analyzed using this method. In addition, relatively high mass resolution can be achieved using LDI-FTMS.

In our laboratory we have constructed a Cs^+ ion DI source for FTMS and demonstrated its capabilities (5). The emphasis of our present work is: (1) a careful study of the nature of the ions formed by Cs^+ DI-FTMS; and (2) optimization of the experimental parameters, e.g., the effects of changing the Cs^+ ion fluence (integrated beam density) and the incident angle of the Cs^+ ion beam.

Using Cs^+ ion DI, the dominant ions observed in the (FT) mass spectrum correspond to species of the type $[M + Na]^+$ and/or $[M + xNa - (x-1)H]^+$. Also, fragment ion are observed which (we propose) originate from the sodium cationized molecule ion. We have found that the specific ions observed on Cs^+ DI-FTMS, i.e., $[M + H]^+$, $[M + Na]^+$, $[M + xNa - (x-1)H]^+$ or fragment ions is highly sensitive to the Cs^+ beam fluence. For example, at low beam fluence (10-25 nanoamps for ca. 5 ms or 3×10^8 particles/s) the major ion in the FT mass spectrum of β-cyclodextrin is $[M + H]^+$ (m/z 1135); however, at higher beam fluence (100-200 nanoamps or 6×10^{10} particles/s) intense ions are observed which correspond to sodium cationized ions. At even higher beam fluence (250-500 nanoamps or 2×10^{10} particles/s) intense fragment ions are observed, e.g. (M = β-cyclodextrin) $[M + xNa - y(C_6H_{10}O_5)]^+$. Typically, no more than 1-3 sugar units are lost from the sodium cationized molecule ion. These studies clearly illustrate the advantages of static SIMS conditions for studies of biomolecules.

References

1. M.B. Comisarow and A.G. Marshall, Chem. Phys. Lett., 25, 282 (1974).

2. C.L. Wilkins and M.L. Gross, Anal. Chem., 53, 1661A (1981).

3. D.A. McCrery, E.G. Ledford, and M.L. Gross, Anal. Chem., 54, 1437 (1982).

4. R.B. Cody, unpublished results.

5. M.E. Castro and D.H. Russell, Anal. Chem., 56, 578 (1984).

B-CYCLODEXTRIN

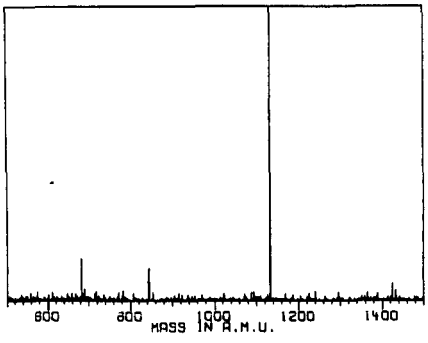

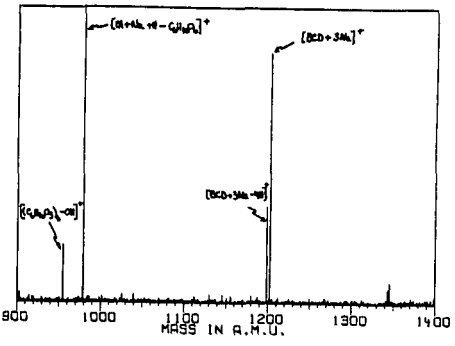

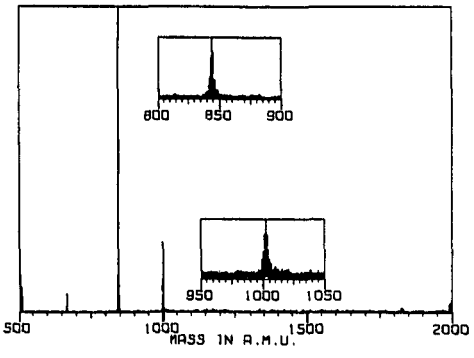

ANALYSIS OF NONVOLATILE COMPOUNDS USING AN ALKALI THERMIONIC EMITTER. D. Bombick, Department of Chemistry, Michigan State University, East Lansing, MI 48824

Alkali thermionic emitters produce alkali metal ions when heated and positively biased. The particular composition for the emitters used in these experiments is a mixture of SiO_2, Al_2O_3 and K_2O that is heated to produce a glass. When this glass is heated and positively biased potassium ions are produced. The possible use of these materials in mass spectrometry for analysis of nonvolatile compounds is presented here.

Peptides. When a solution containing peptide (M) is evaporated onto the potassium glass bead, positively biased and heated quickly, ions representative of the peptide are generated. These ions usually last 10-20 s after the bead is heated, however, in some spectra particular ions may continue to be generated for several minutes. In almost all cases an $(M+K)^+$ ion is formed which is also the highest m/z product found. Low-energy decompositions of the peptides such as loss of H_2O and CO_2, can occur leading to ions with the composition $(M+K-CO_2)^+$ and $(M+K-H_2O)^+$. Products which do not contain potassium are also observed in some spectra. Figure 1 is a representative spectrum of pentaglycine produced in the manner described above. This new ionization technique may be called thermionic desorption mass spectrometry (TDMS).

A simple operating mechanism may be considered as the following: A molecule may thermally decompose to yield several new molecules on the surface of the glass bead. The potassium ions being emitted from the surface can then complex with these species. For example, glycylgycine can decompose as follows:

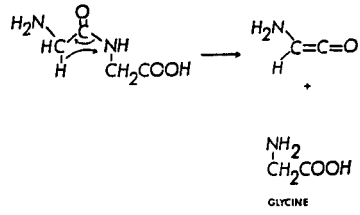

The potassium ions can therefore complex with either one of the decomposition products. Most likely the ions which do not contain potassium are formed via a surface ionization process. These ions are seen arising only from the decomposition products containing the ketene functionality, i.e., the ketene formed from loss of H_2O from the original peptide or the ketene produced as shown in the equation above. Surface ionization of organic compounds is not new and is an active area of research in our laboratory.

Mixture analysis can be done using this new technique. This is shown in Figure 2. The mixture contained the five peptides alanylalanylalanine, phenylalanylglycine, glycylleucylalanine, methionylglycine, and valylglycine which gave $(M+K)^+$ ions at m/z of 270, 261, 298, 245, and 213 respectively. In the spectrum of the mixture no indications of intermolecular reactions are evident.

TDMS can also be extended to other nonvolatile compounds besides peptides. The technique has been proved to work for compounds such as acetaminophen (APAP) and has given promising results for some penicillins (e.g. ampicillin). The benefits of TDMS over other ionization techniques are the absence of any matrix as in FAB and more structural information than can be given by FD.

Our laboratory is actively investigating the mechanism of the thermionic ionization detection used in gas chromatography. The thermionic material used in these detectors are similar to that used in the analysis of nonvolatile compounds. The analysis of nonvolatile compounds may be vastly improved by knowledge obtained from these studies. Currently we are investigating the use of other thermionic emitters and their utility in generating both positive and negative ions in such analyses.

Figure 1

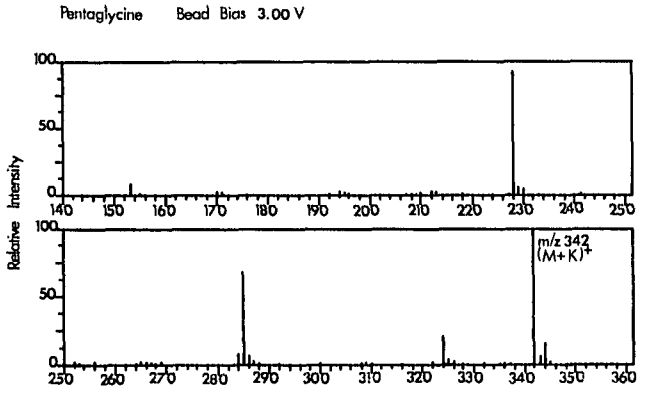

Figure 2

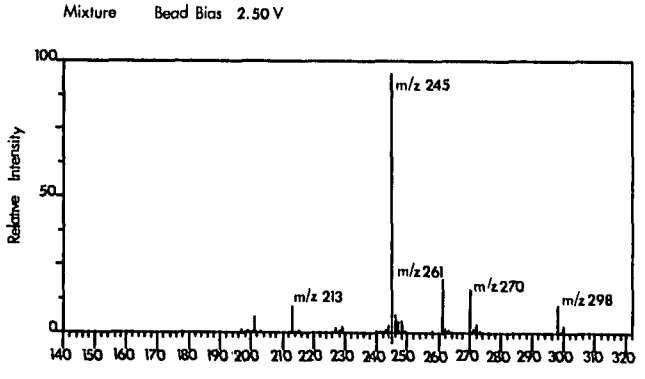

MS/MS ANALYSIS OF NON VOLATILE COMPOUNDS

C. Beaugrand	G. Devant	C. Rolando*
SN Nermag	49 Quai Du Halage	92500 Rueil Malmaison
*ENS	24 Rue Lhomond	75005 Paris

Fragile compounds have always been a challenge to mass spectroscopists. Major progress has been made with the introduction of two complementary "soft ionization techniques" namely D/CI (Desorption Chemical Ionization) and FAB (Fast Atom Bombardment). Unfortunately those methods often give only quasi-molecular ions and very few fragment ions.

In MS/MS the ionization process and the reactions which yield structural information, occur in physically separate regions. Coupling a soft ionization technique to an MS/MS instrument allows a quasi-molecular ion to be fragmented in the CID region and gives access to structural informations not otherwise available.

We ran such experiments using a triple quadruple MS/MS featuring large size rods. Ionization was performed using either D/CI (with ammonia as the reagent gas) or FAB with a M Scan gun utilizing Argon or Xenon to produce 7KeV neutrals. The FAB matrix was Glycerol with additives such as TEA, NAI, KCN and Acetic acid.

Krypton was used as the collision gas in the quadruple CID chamber at a pressure such that the parent ion is reduced to one third its original heighth. Collision energy is defined as the potential difference between the D/CI or FAB probe and the collision chamber axis and was set between 10 and 40 Volts.

An improved signal to noise ratio can be obtained by lowering the chemical noise generated by the ionization process as shown in figure 1 (matrix effects). This is particularly important in low mass FAB experiments. Salt effects are often used in FAB to enhance the protonated ion but can lead to misinterpretation of the data. Operating in the daughter ion mode, MS/MS provides an easy cross check of this potential problem.

D/CI experiments gives information complementary to FAB (and is sometimes the only possible ionization mode). For example in work dealing with sugars, D/CI gives the $(M-H_2O+NH_4)^+$ ion while FAB results in the MH^+ ion, which fragment in different ways.

We have successfully obtained data on different classes of compounds: sugars, antibiotics, peptides and porphyrins, which have traditionally presented great difficulties. This is illustrated in figure 2 and 3 for Vitamin B12 where high mass information has been produced in both the positive and negative mode.

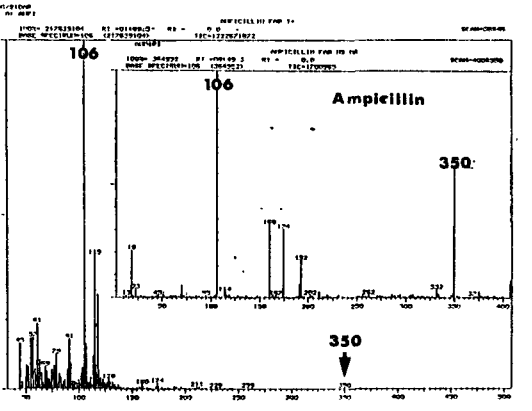

FIG. 1

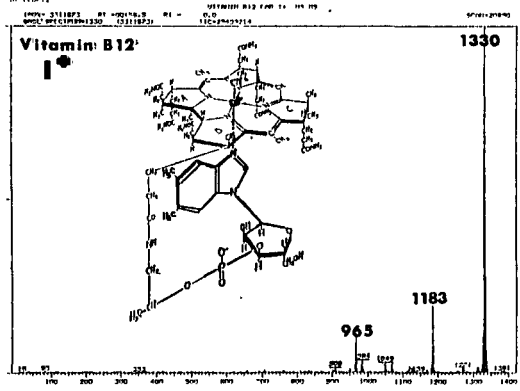

FIG. 2

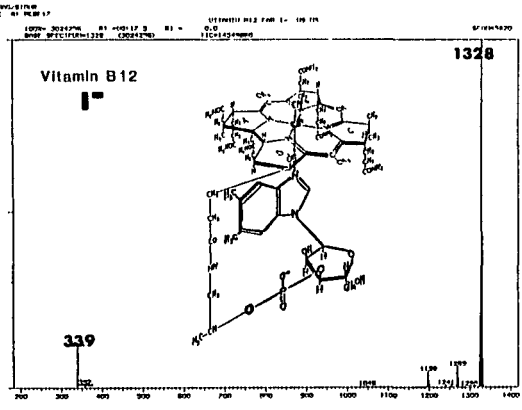

FIG. 3

AS GIVEN

DR. E. E. DAVID, JR.

PRESIDENT, EXXON RESEARCH AND ENGINEERING COMPANY

KEYNOTE ADDRESS

AMERICAN SOCIETY OF MASS SPECTROMETRY

SAN ANTONIO, TEXAS

MAY 29, 1984

HIGH SCIENCE AND HIGH TECHNOLOGY: BALANCING KNOW-WHY WITH KNOW-HOW

HIGH TECHNOLOGY IS THE TALK OF OUR SOCIETY TODAY. DESPITE ALL THE CLICHES, THE TALK HERALDS THE COMING OF A NEW SPIRIT IN POPULAR AND POLITICAL ATTITUDES TOWARD SCIENCE AND TECHNOLOGY. IT ALSO HERALDS THE COMING OF NEW RELATIONSHIPS BETWEEN SCIENCE AND TECHNOLOGY, ESPECIALLY BETWEEN RESEARCHERS IN THE UNIVERSITIES AND INDUSTRY. MUCH OF WHAT I WILL SAY APPLIES TO THIS COUNTRY. BUT THERE IS IN FACT A DRIVE TO MATE HIGH TECHNOLOGY WITH HIGH SCIENCE AROUND THE WORLD; THERE IS A GROWING SENSE THAT ONLY IN THAT WAY WILL INDUSTRY CREATE THE PROGENY OF TECHNOLOGICAL INNOVATION NEEDED TO CREATE JOBS AND RAISE LIVING STANDARDS IN ADVANCED INDUSTRIAL SOCIETIES. I SHOULD SAY HERE THAT BY "HIGH TECHNOLOGY," I MEAN NOT MERELY ELECTRONICS OR COMPUTING BUT THE WHOLE ARRAY OF ADVANCED, SCIENCE-BASED TECHNOLOGIES, INCLUDING INSTRUMENTS. BY "HIGH SCIENCE" I MEAN THE SCIENCE MADE POSSIBLE THROUGH THE DEVELOPMENT OF ADVANCED INSTRUMENTS AND SENSORS IN TANDEM WITH ADVANCED COMPUTING. IT IS THE SCIENCE PRACTICED MAINLY IN OUR UNIVERSITIES AND NATIONAL LABORATORIES, AS WELL AS SOME CORPORATIONS.

AT THIS MEETING, YOUR THEMES ARE THE PAST AND FUTURE--WHERE MASS SPECTROMETRY HAS COME FROM AND WHERE YOU AIM TO TAKE IT. SO, I MAY NOTE THAT MASS SPECTROMETRY HAS BEEN SQUARELY IN THE MIDDLE OF BOTH HIGH SCIENCE AND HIGH TECHNOLOGY SINCE THE FOUNDING OF THE ASMS AND YOUR ALLIED ORGANIZATION, ASTM COMMITTEE E-14. FURTHERMORE, WITH YOUR INDUSTRIAL ROOTS AND

AFFILIATIONS, THE DEVELOPMENT OF MASS SPEC HAS ANTICIPATED MANY OF TODAY'S TRENDS TOWARD INTEGRATING HIGH SCIENCE AND HIGH TECHNOLOGY MORE CLOSELY.

THE TRENDS ARE DRIVEN IN PART BY AN IMPORTANT CHANGE IN PUBLIC ATTITUDE. YOU MAY RECALL THAT IN THE 70'S, THERE WAS A BRIEF PRE-OCCUPATION WITH THE NEED TO ANTICIPATE AND HEAD OFF THE UNWANTED CONSEQUENCES OF NEW TECHNOLOGY. WE HEARD MUCH ABOUT "TECHNOLOGY ASSESSMENT," WHICH SOMETIMES BECAME CONFUSED WITH "TECHNOLOGY ARRESTMENT." BUT, TODAY, THE NATIONAL MOOD HAS TURNED STRONGLY PRO-TECHNOLOGY ... THAT IS, STRONGLY PRO-COMMERCIAL TECHNOLOGY. THE JAPANESE AND OTHER FOREIGN COMPETITORS IN U.S. MARKETS HAVE SHOWN HOW IMPORTANT COMMERCIAL TECHNOLOGY IS. THEY HAVE ALSO SHOWN THAT THE U.S. CAN NO LONGER TAKE THE SYSTEM THAT PRODUCES COMMERCIAL TECHNOLOGY FOR GRANTED.

AS A NATION, WE HAVE UNDERSTOOD MUCH BETTER HOW TO "FORCE" THE TECHNOLOGICAL STATE OF THE ART WHEN PRICE WAS NO OBJECT AND GOVERNMENT THE CUSTOMER. TIME AND AGAIN, THE NATION HAS WITNESSED GREAT LEAPS FORWARD, EITHER FOR MILITARY PURPOSES, FOR COMBATTING DISEASE, OR FOR GREAT NATIONAL PROGRAMS, SUCH AS PROJECT APOLLO. THE LIST OF ACHIEVEMENTS IS LONG AND FAMILIAR--RADAR, COMPUTERS, JET AIRCRAFT, POLIO VACCINES, SPACECRAFT, AND MORE. NOW THE PUBLIC IS ASKING, "IF WE CAN PUT A MAN ON THE MOON, WHY CAN'T AMERICANS MAKE CHEAPER AND BETTER

CALCULATORS, CAMERAS, AND VIDEO CASSETTE RECORDERS?" AND THEY ARE ALSO ASKING, "IF WE CAN WIN ALL THOSE NOBEL PRIZES, WHY CAN'T WE BEAT THE JAPANESE IN AUTOS AND STEEL?"

ORGANIZATION

OF COURSE, THESE QUESTIONS DO BETRAY A CERTAIN NAIVETE ABOUT HOW SCIENCE, TECHNOLOGY, AND ECONOMIC CONDITIONS INTERACT. BUT THEY ARE STILL GOOD QUESTIONS. INDEED, IN MORE SOPHISTICATED FORMS, THEY HAVE BECOME IMPORTANT CONCERNS OF THE PUBLIC AND ITS REPRESENTATIVES. WITNESS ALL THE RECENT TALK ABOUT THE HEALTH OF MATHEMATICS, SCIENCE, AND ENGINEERING EDUCATION AT ALL LEVELS; EFFORTS BY STATE GOVERNMENTS TO ATTRACT INVESTMENTS AND NEW JOBS BASED ON NEW TECHNOLOGY; AND THE HISTORIC INITIATIVES BRINGING INDUSTRY AND UNIVERSITIES TOGETHER FOR JOINT RESEARCH. WHAT IS TOO LITTLE RECOGNIZED IS THAT SCIENCE AND TECHNOLOGY ARE PARTS OF A HIGHLY COMPLEX SYSTEM, INVOLVING GOVERNMENTS, EDUCATION, INDUSTRY, ECONOMIC CONDITIONS, AND SOCIAL ATTITUDES. PEOPLE ARE BEGINNING TO RECOGNIZE A NEED TO OPTIMIZE THE SYSTEM MORE TOWARD COMMERCIAL TECHNOLOGY. THEY ARE BEGINNING TO RECOGNIZE THAT TO DO SO, YOU MUST UNDERSTAND THE SYSTEM, PAYING ATTENTION BOTH TO ITS CONSTITUENT PARTS AND TO THE CONNECTIONS BETWEEN THOSE PARTS.

A FEW YEARS AGO, MANY OF US FELT THAT THE MOST CRITICAL CONNECTION WAS BETWEEN TECHNOLOGY AND MARKETING. TODAY, THE CONNECTION BETWEEN SCIENCE AND BASIC RESEARCH ON ONE SIDE AND COMMERCIAL TECHNOLOGY ON THE OTHER HAS COME TO DOMINATE OUR

THINKING. FURTHERMORE, THAT LINKAGE IS PROBABLY MOST DIFFICULT TO ESTABLISH SINCE MUCH OF SCIENCE AND BASIC RESEARCH IS DONE IN ACADEMIA WHILE COMMERCIAL TECHNOLOGY IS THE DOMAIN OF INDUSTRY.

SO LET ME EXPLORE WITH YOU A FEW CRITICAL ASPECTS OF HOW SCIENCE AND TECHNOLOGY INTERACT IN THE SYSTEM, USING MASS SPECTROMETRY AND EXXON'S OWN R&D AS EXAMPLES. THEN, AFTER NOTING THE SIGNS OF INDUSTRY'S GENERAL AWAKENING TO THE IMPORTANCE OF BASIC RESEARCH, I WILL CONSIDER HOW THE FEDERAL AND STATE GOVERNMENTS ARE TRYING TO PROMOTE CLOSER CONNECTIONS BETWEEN RESEARCHERS IN INDUSTRY AND THE UNIVERSITIES. FINALLY, I'LL TOUCH ON WHAT REMAINS TO BE DONE, ESPECIALLY BY INDUSTRY.

THE INNOVATION PROCESS: INTERACTION OF SCIENCE AND TECHNOLOGY

FIRST, HOW SCIENCE AND TECHNOLOGY HAVE BECOME INTERWOVEN AND HOW THEIR INTERACTION IS CHANGING IN THE NEW ERA. GIVEN YOUR RETROSPECTIVE THEME, WE MAY RECALL THAT SCIENCE AND TECHNOLOGY HAVE ENGAGED IN A DIALECTIC ALMOST FROM THE BEGINNINGS--A DANCE OF KNOWLEDGE AND TECHNIQUE. BUT THE PATTERN HAS BEEN LOOSE AND THE STEPS HAVE NOT BEEN WELL-UNDERSTOOD. I MENTION THIS BECAUSE ONE OF THE PREVALENT MISCONCEPTIONS, ESPECIALLY IN WASHINGTON, D.C., IS THAT THEORETICAL SCIENCE IS BY NATURE THE DOMINANT PARTNER. IN PART, THAT ACCOUNTS FOR DEMANDS FOR QUICK COMMERCIAL PAYOFFS FROM OUR NOBEL PRIZES. OF COURSE, THE TRUTH IS THAT TECHNOLOGY HAS FOR CENTURIES DANCED ALMOST ALONE. TRIAL AND ERROR, EMPIRICISM, HAVE REMAINED A DOMINANT MODE OF PROGRESS IN MANY INDUSTRIES, INCLUDING MY OWN

PETROCHEMICAL INDUSTRY, ALMOST TO THE PRESENT DAY. THE KNOW-HOW OF TECHNOLOGY MANAGED TO GET ALONG WITHOUT THE KNOW-WHY OF SCIENCE.

NO NEED TO TELL THIS AUDIENCE THAT, IF ANYTHING, THE GREAT SCIENTISTS HAVE HISTORICALLY DEPENDED MORE ON THE TECHNOLOGY EMBODIED IN THEIR INSTRUMENTS THAN TECHNOLOGY EVER DEPENDED ON THEM. GALILEO COULD NOT HAVE RE-ORDERED THE UNIVERSE WITHOUT THE TELESCOPE. IN THE SAME VEIN, THE LATE SCIENCE HISTORIAN, DEREK DESOLLA PRICE, POINTED TO THE ODD FACT THAT IN THE 1920'S, NEARLY EVERY PIECE OF PHYSICS RESEARCH EQUIPMENT IN BRITISH LABORATORIES WAS STUCK ALL OVER WITH RED BANK OF ENGLAND SEALING WAX. THE WAX HAPPENED TO BE THE BEST CEMENT AVAILABLE FOR HOLDING A VACUUM. DURING THAT GOLDEN AGE OF EXPERIMENTAL PHYSICS, HE WRITES, ALL PROGRESS SEEMED TO DEPEND ON A BAND OF INGENIOUS CRAFTSMEN, WITH BRAINS IN THEIR FINGERTIPS, WHO KNEW HOW TO EXPLOIT LITTLE-KNOWN PROPERTIES OF MATERIALS AND THE TRICKS OF THE TRADE. THESE TECHNIQUES NOT ONLY DETERMINED WHAT COULD BE DONE IN THE LABORATORY; THEY DETERMINED WHAT COULD BE DISCOVERED. NOTE THAT THE WORDS "TECHNIQUE" AND "TECHNOLOGY" SHARE THE SAME ETYMOLOGICAL ROOT.

FOR DESOLLA PRICE, THE LESSON OF THIS IS THAT OUR SCIENCE POLICIES MUST EMPHASIZE THE BRAINS IN THE FINGERTIPS AS WELL AS THE BRAINS IN THE HEAD. DESOLLA PRICE IS CERTAINLY RIGHT ABOUT HISTORY AND THE IMPORTANCE OF INSTRUMENTS. BUT THE

PATTERNS OF THE PAST ARE BREAKING. MODERN TECHNOLOGY IS BECOMING SO COMPLEX THAT IT CANNOT ADVANCE WITHOUT CONTINUING INFUSIONS OF NEW FUNDAMENTAL UNDERSTANDING.

IN ITS SCIENCE AND INSTRUMENTS, THE HISTORY OF MASS SPECTROMETRY CAN TEACH US MUCH IN THIS REGARD. IN THE 40'S AND 50'S, "MASS SPEC" WAS BEING DEVELOPED MAINLY BY THE PETROLEUM INDUSTRY FOR HIGHLY PRACTICAL PURPOSES ASSOCIATED WITH REFINERY CONTROL. FOR EXAMPLE, AT EXXON'S BAYWAY REFINERY IN NEW JERSEY DURING THIS PERIOD, SOME 20 SCIENTISTS AND SPECIALISTS, WORKING TWO AND THREE SHIFTS EACH DAY, ANALYZED THOUSANDS OF GAS AND PRODUCT SAMPLES EACH YEAR. THE GROUP INCLUDED EIGHT PEOPLE WHO DID NOTHING BUT MAKE CALCULATIONS AND ONE SOUL WHO DID NOTHING BUT MEASURE PEAK HEIGHTS WITH A RULER. HOWEVER, SOME RESEARCHERS IN INDUSTRIAL LABORATORIES SAW THE NEED FOR FUNDAMENTAL STUDIES. LATER IN THIS MEETING, YOU CAN HEAR A FULLER ACCOUNT FROM ONE OF THE GREAT PIONEERS IN THE FIELD, SY MEYERSON. IT IS ENOUGH TO SAY HERE THAT INDUSTRY HAS BEEN RESPONSIBLE FOR BASIC ADVANCES IN SUCH AREAS OF MASS SPEC AS ION/MOLECULE REACTIONS, IONIZATION POTENTIALS, AND THE RELATED THERMODYNAMIC PROPERTIES. THE CHEMICAL IONIZATION TECHNIQUE WAS INVENTED AT EXXON. INDEED, WE ARE PROUD OF THE HONOR ROLE OF "GREATS" WHO HAVE WORKED IN OUR LABORATORIES, INCLUDING EARL LUMPKIN, FRED LAMPE, AND FOUR PAST PRESIDENTS OF THE ASMS: JOE FRANKLIN, FRANK FIELD, JEAN FUTRELL, AND BURNABY MUNSON.

MASS SPEC HAS NOW BURGEONED FAR BEYOND THE CONFINES OF THE PETROCHEMICAL INDUSTRY. THE WIZARDS OF MASS SPEC, WITH BRAINS IN THEIR FINGERTIPS AS WELL AS THEIR HEADS, HAVE OPENED UP WHOLE NEW SCIENTIFIC FIELDS IN BIOLOGY AND CHEMISTRY. THEIR RESEARCH IS IN TURN ENRICHING PETROCHEMICAL TECHNOLOGY. FOR EXAMPLE, WE SEE IMMEDIATE AND IMPORTANT MONEY-SAVING OPPORTUNITIES FOR USING ADVANCED MASS SPECTROMETERS ON-LINE AS A MEANS FOR CONTROLLING AND OPTIMIZING PROCESSES IN EXXON'S REFINERIES AND CHEMICAL PLANTS.

BUT EVEN MORE IMPORTANT FOR THE LONG-RANGE FUTURE IS THE ROLE THAT MASS SPEC IS PLAYING IN BASIC RESEARCH. THUS, IN OUR INDUSTRY, ONE OF THE KEY PROBLEMS IS TO FIND MORE EFFICIENT WAYS TO CONVERT THE HEAVY HYDROCARBONS OF PETROLEUM "RESID" INTO GASOLINE AND OTHER LIGHT TRANSPORTATION FUELS. EVENTUALLY, THE CHALLENGE WILL BE TO PROCESS EVEN HEAVIER MATERIALS--TO CREATE SYNTHETIC FUELS FROM SUCH MATERIALS AS COAL AND OIL SHALE. SYNFUEL TECHNOLOGIES ALREADY EXIST. EVENTS LIKE THE WAR BETWEEN IRAN AND IRAQ MIGHT SUGGEST THAT ALL WE HAVE TO DO IS SIT BACK AND WAIT TO APPLY THEM. HOWEVER, AT EXXON, WE ARE CONVINCED THAT THE CURRENT TECHNOLOGIES ARE SO COSTLY THAT THEY WILL NEVER BE COMPETITIVE. TO ACHIEVE COMPETITIVE TECHNOLOGIES, WE MUST ACHIEVE FUNDAMENTAL PROGRESS IN OUR UNDERSTANDING OF THE STRUCTURE AND CHEMISTRY OF THESE HEAVY HYDROCARBONS.

TOWARD THESE GOALS, WE ARE WORKING IN SEVERAL FRONTIER AREAS OF MASS SPEC. WE ARE TRYING TO FIND WAYS TO USE THE MASS SPECTROMETER TO ANALYZE MIXTURES CONTAINING MATERIALS WITH MASSES IN THE THOUSANDS--THAT IS, MIXTURES DERIVED FROM OIL SHALE, COAL, AND TAR SANDS AS WELL AS FROM PETROLEUM RESIDUES. IN THIS EFFORT, WE ARE USING SUCH IONIZATION TECHNIQUES AS FAST ATOM BOMBARDMENT, FIELD DESORPTION, AND LASER DESORPTION. WE ARE ALSO TRYING TO INCREASE RESOLVING POWER, USING ION CYCLOTRON-MS TO DISTINGUISH AND STUDY DIFFICULT-TO-PROCESS, HIGH MOLECULAR WEIGHT HETEROCOMPOUNDS CONTAINING SUCH CONTAMINANTS AS SULFUR AND OXYGEN. AND WE ARE USING MS-MS TO GIVE US CLUES ABOUT THE FUNDAMENTAL STRUCTURE AND COMPOSITION OF TRACE MATERIALS IN PETROCHEMICAL FEEDSTOCKS AND PRODUCTS.

HEAVY HYDROCARBON SCIENCE IS NOT THE ONLY AREA OF BASIC SCIENCE WHERE EXXON BELIEVES IT MUST BE AT THE CUTTING EDGE. ANOTHER IS CATALYSIS. CATALYSTS ARE TO THE PETROCHEMICAL INDUSTRY WHAT SEMICONDUCTORS ARE TO THE COMPUTING INDUSTRY. INDEED, BOTH ARE STUDIED USING MANY OF THE SAME TECHNIQUES OF SURFACE SCIENCE. ONE OF OUR RESEARCH PROJECTS IN CATALYSIS IS TO STUDY THE BEHAVIOR OF METAL CLUSTERS OF BETWEEN TWO AND A HUNDRED ATOMS IN THE GAS PHASE, USING TIME-OF-FLIGHT-MS AND FOURIER TRANSFORM-MS. OUR SCIENTISTS REASON THAT UNDERSTANDING THESE SYSTEMS WILL HELP THEM UNDERSTAND HOW HIGHLY DISPERSED METALS INTERACT WITH THEIR SUPPORTS IN COMMERCIAL CATALYST SYSTEMS. OF COURSE, THIS IS BUT ONE OF AN ARRAY OF ADVANCED INSTRUMENTS WE ARE MARSHALLING IN OUR PURSUIT OF HIGH SCIENCE. OTHERS INCLUDE

CONTROLLED ATMOSPHERE ELECTRON MICROSCOPY, X-RAY PHOTO-ELECTRON SPECTROSCOPY, AND SYNCHROTRON RADIATION FROM ULTRAVIOLET TO X-RAY.

AT EXXON WE THINK THAT SUCH RESEARCH ACTIVITIES TELL MUCH ABOUT THE PATTERN OF THE EMERGING NEW RELATIONSHIPS BETWEEN HIGH SCIENCE AND HIGH TECHNOLOGY. SCIENCE AND ADVANCED SCIENTIFIC INSTRUMENTS ARE HELPING TO SOLVE REAL PROBLEMS ASSOCIATED WITH THE TECHNOLOGIES WE HAVE AND THAT WE THINK WE MUST HAVE. A KEY FEATURE IS THAT THE UNIVERSITIES ARE HEAVILY INVOLVED. FEW OR NONE OF THE EXXON RESEARCH ACTIVITIES I HAVE JUST DESCRIBED ARE PROCEEDING WITHOUT HELP FROM UNIVERSITY RESEARCHERS. IN SOME CASES, WE DEPEND ON THEM HEAVILY; IN OTHERS WE THINK WE GIVE AS GOOD AS WE GET. BUT IN ALL CASES, WE BELIEVE THAT THERE IS FRUITFUL INTERACTION THAT ADVANCES THE STATE OF BOTH SCIENCE AND TECHNOLOGY.

NEW INDUSTRY ATTENTION TO BASIC RESEARCH

EXXON'S EXPERIENCE IS NOT UNIQUE. BASIC SCIENCE CAN GENERATE ENORMOUS POWER TO DO THINGS--AND SOMETIMES WITH APPARENT SUDDENNESS. GENETIC ENGINEERING IS A RECENT AND SPECTACULAR EXAMPLE. SO ARE OPTICAL FIBERS AND SUPER LATTICES. IT IS TRUE THAT INDUSTRY STILL DOES RELATIVELY LITTLE BASIC RESEARCH OF ITS OWN, ALTHOUGH SOME COMPANIES, SUCH AS IBM, AT&T, AND EXXON, HAVE INTEGRATED BASIC SCIENCE INTO THEIR R&D FOR YEARS. BUT, TODAY, MORE COMPANIES ARE BEGINNING TO PERCEIVE OPPORTUNITIES IN BASIC RESEARCH. THIS IS NOT A REVIVAL OF THE "SCIENCE IS WONDERFUL"

ERA OF THE EARLY 60'S, WHEN CORPORATIONS CREATED "IVORY TOWER" RESEARCH FACILITIES THAT THEY LATER ABANDONED FOR WANT OF RESULTS. THE NEW TREND IS BASED ON A REALIZATION THAT MODERN TECHNOLOGY RESTS ON A SCIENTIFIC BASE, AND SO INDUSTRY CAN AND MUST CONVERT SCIENCE TO EFFECTIVE COMMERCIAL TECHNOLOGY MORE RAPIDLY THAN IN THE PAST.

THAT IS WHY THE NATIONAL SCIENCE FOUNDATION REPORTS THAT WHILE U.S. INDUSTRY IS CURRENTLY INCREASING ITS OVERALL R&D EXPENDITURES AT A RECORD PACE, IT IS INCREASING BASIC RESEARCH EXPENDITURES EVEN MORE RAPIDLY. IN 1984 U.S. INDUSTRY WILL SPEND SOME $52 BILLION ON R&D, MORE THAN THE FEDERAL GOVERNMENT. OF THAT, SOME $2 BILLION WILL SUPPORT BASIC RESEARCH.

THE NSF ALSO TELLS US THAT INDUSTRY SUPPORTED SOME $360 MILLION WORTH OF ACADEMIC R&D IN 1983. COUNTING OTHER SUPPORT NOT INCLUDED IN THIS FIGURE--SUCH AS UNRESTRICTED GRANTS AND COOPERATIVE RESEARCH ARRANGEMENTS--THE AMOUNT EXCEEDED $500 MILLION. THIS IS ONLY A SMALL FRACTION OF FEDERAL SUPPORT, BUT SINCE 1970 INDUSTRY FUNDING HAS BEEN THE FASTEST GROWING SOURCE OF SUPPORT FOR UNIVERSITY RESEARCH, INCREASING BY NEARLY 150 PERCENT SINCE 1970 AND JUMPING BY 7 PERCENT BETWEEN 1982 AND 1983, EVEN AFTER DISCOUNTING THE EFFECTS OF INFLATION. IT IS NOT UNREALISTIC TO EXPECT THAT WITHIN TEN YEARS, INDUSTRY WILL BE SUPPORTING AT LEAST THREE TIMES WHAT IT DOES TODAY.

IT IS SIGNIFICANT THAT FEDERAL, STATE, AND EVEN LOCAL GOVERNMENTS HAVE BECOME ACTIVE IN ENCOURAGING SUCH LINKAGES. PRESIDENTIAL SCIENCE ADVISOR GEORGE KEYWORTH HAS, IN FACT, MADE IT THE OFFICIAL POLICY OF THE U.S. GOVERNMENT TO HELP ESTABLISH RESEARCH CONNECTIONS AMONG INDUSTRY, THE UNIVERSITIES, AND THE NATIONAL LABORATORIES. THIS POLICY EXPLAINS THE ADMINISTRATION'S DECISION TO FOCUS FEDERAL SUPPORT ON BASIC RESEARCH IN THE UNIVERSITIES AT THE EXPENSE OF CIVILIAN DEVELOPMENT PROJECTS. IT EXPLAINS THE FEDERAL GOVERNMENT'S RENEWED FOCUS ON ENGINEERING AND ENGINEERING EDUCATION, BECAUSE ENGINEERS ARE INDISPENSABLE ALLIES IF SCIENCE AND TECHNOLOGY ARE TO REINFORCE EACH OTHER. AND IT EXPLAINS FEDERAL EFFORTS AT LONG LAST TO UPDATE UNIVERSITY RESEARCH INSTRUMENTATION.

THE ISSUE OF THE FEDERAL DEFICIT TENDS TO CAST ALL IN DOUBT. STILL, THE FY 1985 BUDGET INDICATES THAT FEDERAL AGENCIES WILL PROVIDE MORE THAN $400 MILLION FOR RESEARCH INSTRUMENTATION AT THE UNIVERSITIES. CONSIDERING THE HIGHLY FAVORABLE PUBLIC ATTITUDES TOWARD SCIENCE AND TECHNOLOGY, I PREDICT THAT MOST OF THESE FUNDS WILL BE FORTHCOMING. OF COURSE, IT IS VITAL THAT THEY DO. WE ALL KNOW INVESTIGATORS WHO CAN MANIPULATE OLD INSTRUMENTS WITH ALL THE SKILL THAT ITZAHK PERLMAN PLAYS A STRADIVARIUS. BUT SCIENCE IS NOT ART, AND SCIENTIFIC INSTRUMENTS MUST NOT BE ANTIQUES. ON THE OTHER HAND, IT IS UNREALISTIC TO BELIEVE THAT ONE OR TWO BUDGET CYCLES WILL REMEDY YEARS OF NEGLECT. I HOPE THAT THE FEDERAL GOVERNMENT HAS STAYING POWER.

THERE IS NO TIME HERE TO SURVEY THE MANY STATE GOVERNMENT INITIATIVES INTENDED TO PROMOTE CLOSER CONNECTIONS BETWEEN INDUSTRY AND UNIVERSITY SCIENCE. TYPICALLY, THEY INCLUDE INCREASED FUNDING FOR TECHNICAL EDUCATION, "CENTERS OF EXCELLENCE" IN PROMISING FIELDS, TECHNOLOGY EXTENSION SERVICES HOUSED IN SUCH CENTERS, AND INCUBATION QUARTERS FOR START-UP COMPANIES NEAR THE UNIVERSITIES. IN TERMS OF THE EVOLVING U.S. "INNOVATION POLICY," MANY OF THESE STATE INITIATIVES HAVE MORE IMPORTANCE THAN FEDERAL ONES, BECAUSE THEY RESPOND DIRECTLY TO LOCAL INTERESTS, LOCAL NEEDS, AND LOCAL OPPORTUNITIES.

REMAINING TASKS

MUCH STILL REMAINS TO BE DONE. CERTAINLY, THERE IS STILL MUCH MORE ROOM FOR INDUSTRY TO EXPAND ITS SUPPORT FOR BASIC RESEARCH. WHERE POSSIBLE, THIS OUGHT TO INCLUDE IN-HOUSE BASIC RESEARCH. EVEN A COMPANY THAT CANNOT BY ITSELF ASSEMBLE THE CRITICAL MASS OF PEOPLE AND INSTRUMENTS CAN HAVE ACCESS TO PRODUCTIVE RESEARCH. THE ANTI-TRUST LAWS ARE BEING INTERPRETED TO PERMIT THE FORMATION OF JOINT RESEARCH ORGANIZATIONS SUCH AS THE MICROELECTRONICS AND COMPUTER TECHNOLOGY CORPORATION. THIS IS A $70 MILLION-A-YEAR EFFORT INVOLVING SOME 16 COMPANIES IN PURSUIT OF FUNDAMENTAL RESEARCH.

HOWEVER, RESEARCH SUPPORT CANNOT BE APPROACHED AS A NUMBERS GAME. INDUSTRY MUST ENSURE THAT IT RECEIVES VALUE FOR ITS MONEY, BUT IT ALSO MUST ACCEPT SOME RESPONSIBILITY FOR ENSURING THE HEALTH OF THE SYSTEM BY INCREASING ITS DIVERSITY.

FOR EXAMPLE, INDUSTRY SHOULD UTILIZE ITS ABILITY TO RESPOND MORE QUICKLY AND FLEXIBLY TO HIGH-RISK RESEARCH OPPORTUNITIES THAN GOVERNMENT CAN. INDUSTRY CAN MARKEDLY EXPAND ROOM FOR INVESTIGATOR INITIATIVE, WHICH HAS BEEN SHRINKING AS AGENCIES IN GOVERNMENT ADOPT HANDS-ON MANAGEMENT TECHNIQUES.

INDUSTRY ALSO BEARS PRIME RESPONSIBILITY FOR INTEGRATING THE RANGE OF RESEARCH DISCIPLINES THAT UNDERLIE INDUSTRIAL TECHNOLOGIES. AMONG OTHER THINGS, THAT MEANS ENSURING THAT SPECIALISTS IN MASS SPEC AND OTHER INSTRUMENT TECHNOLOGIES ARE PART OF THE RESEARCH TEAM INSTEAD OF PROPRIETORS OF MERE JOB SHOPS. AS GRAHAM COOKS HAS SAID, THE DEVELOPMENT, ELABORATION, AND APPLICATION OF INSTRUMENTS MUST BE AN INTEGRAL PART OF THE SCIENTIFIC PROCESS. RESEARCHERS CANNOT TREAT THEIR INSTRUMENTS LIKE BLACK BOXES; THEY CANNOT PERFORM THEIR TASK UNLESS THEY POSSESS A DEEP UNDERSTANDING OF WHAT THEIR RESULTS MEAN AND HOW THEY WERE OBTAINED. THIS INTEGRATION NEEDS FURTHER ATTENTION.

STILL, WE ARE ALREADY FAR ALONG INTO THE NEW ERA, RE-BALANCING THE ROLES OF KNOW-WHY AND KNOW-HOW. AS YOU, THE MEMBERS OF THE ASMS, LOOK TO YOUR ORIGINS AT THIS MEETING, YOU MAY TAKE PRIDE IN A RECORD OF AWESOME ACHIEVEMENT. BUT AS YOU LOOK TOWARD THE FUTURE, THE NEW RELATIONSHIPS BETWEEN HIGH SCIENCE AND HIGH TECHNOLOGY PROMISE TO OPEN UP EVEN MORE AWESOME OPPORTUNITIES. THE DANCE BETWEEN SCIENCE AND TECHNOLOGY CONTINUES AT AN ACCELERATING PACE. WHAT WAS ONCE A STATELY MINUET

MAY SEEM TO HAVE BECOME TOO MUCH LIKE THE HUSTLE. BUT, WITH SO MANY MORE DISCIPLINES AND SECTORS INVOLVED IN THE INNOVATION SYSTEM, THE TRUTH IS THAT WE MUST CHOREOGRAPH A FAR WIDER RANGE OF INTERACTIONS AMONG A FAR LARGER CAST OF CHARACTERS THAN IN THE PAST, AND ON A FAR VASTER, EVEN WORLDWIDE STAGE. BY TRADITION AND BY TEMPERAMENT, THE MEMBERS OF THIS SOCIETY ARE SUITED TO PLAY A LEADING ROLE IN THE EFFORT TO INTEGRATE HIGH SCIENCE AND HIGH TECHNOLOGY. I URGE YOU TO DO SO, AND TO ACCEPT MY BEST WISHES FOR A MOST SUCCESSFUL MEETING.

AUTHOR INDEX

AARON,C S 813
ABBEY,L E 96
ABERTH,W 604
ABERTH,W 842
ACKERMANN,B 828
ADAMS,B R 616
ADAMS,N G 46
ADAMS,N G 769
ADAMS,T A 209
ADAMS,T A 730
ADNOT,A 273
ALAMERCERY,S 88
ALCOCK,N J 195
ALDERFER,J 711
ALDERFER,J L 135
ALDERWEIRELDT,F C 115
ALDOUS,K M 289
ALFIERI,A 287
ALGE,E 769
ALI,M F 503
ALLISON,J 225
ALLISON,J 534
ALLISON,J 217
ALLISON,J 828
ALLMAIER,G 677
ALLMAN,S L 366
AMSTER,I J 503
ANBAR,M 585
ANDERS,V 30
ANDERSON,D 730
ANDERSON,D J 209
ANDERSON,F A 82
ANDRZEJEWSKI,D 494
ARAKALI,A 135
ARAKAWA,R 162
ARAKAWA,R 42
ARPINO,P J 199
ASHCROFT,A E 297
AYERS,C R 78
AYOTTE,C 137
BADINEC,S 217
BACHMANN,D 257
BADR,M 137
BAER,T 50
BAKKE,J E 450
BALLARD,J M 691
BARANY,G 481
BARBALAS,M P 799
BARBER,M 515
BARCHAS,J D 783
BARCHAS,J D 440
BARIL,M 273
BAROFSKY,D F 747
BAROFSKY,D F 182
BAROFSKY,E 182
BARRETT,G M 390
BARTMESS,J E 336
BARTMESS,J E 472
BARTMESS,J E 565
BASILE,B 334
BASS,L M 50
BASS,L M 765
BATEMAN,R H 380
BATEMAN,R H 515
BAUER,M R 16
BAYKUT,M G 425
BAYNE,C K 406
BEATTIE,I G 195
BEAUGRAND,C 199
BEAUGRAND,C 856
BEAVIS,R 184
BEAVIS,R 239
BEAVIS,R 749
BECK,O 440
BECKER,C H 822
BECKNER,C F 648
BENCSATH,F A 805
BENCSATH,F A 507
BENKESER,R A 428
BENNETT,B D 343
BENNETT,B D 345
BENNINGHOVEN,A 30
BENNINGHOVEN,A 251
BENNINGHOVEN,A 180
BENOIT,F M 143
BENTZ,B L 635
BEXON,J J 505
BEYNON,J H 40
BEYNON,J H 324
BEYNON,J H 572
BEYNON,J H 713
BIEMANN,K 751
BIEMANN,K 351
BIEMANN,K 349
BILL,J C 667
BILL,J C 301
BINGOI,Y 509
BLANCKAERT,N 125
BLANTON,W E 434
BLOCK,E 347
BLOM,K F 455
BOMBICK,D 854
BONE,W 633
BONE,W 740
BONNELL,D W 374
BONNER,R 303
BOORN,A 168
BORDER,J R 585
BORDOLI,R S 515
BORNSTEIN,D 574
BOSTWICK,D E 96
BOTT,P A 380
BOUCHOUX,G 801
BOUCHOUX,G 725
BOUCHOUX,G 723
BOUCHOUX,G 727
BOUTTON,T W 141
BOWERS,W D 337
BOWERS,W D 593
BOYD,R K 332
BOYD,R K 685
BOYD,R K 291
BRAIN,D K 477
BRAND,H 642

BRAND,H R 372
BRENNAN,P J 392
BRENTON,A G 324
BRENTON,A G 572
BRENTON,A G 40
BRENTON,A G 713
BRICKER,D L 219
BRICKER,D L 629
BRICKER,D L 730
BRILL,F W 424
BRILL,F W 425
BROOKS,A L 275
BROOKS,C J W 390
BROOKS,H B 295
BROOKS,P W 699
BROOKS,P W 301
BROWN,C J 631
BROWN,N 740
BROWNER,R F 96
BROWNER,R F 192
BRUINS,A P 111
BRUINS,A P 483
BRUMLEY,W C 622
BRUMLEY,W C 494
BRUNNGE,C 176
BUCHANAN,M V 65
BUCHNER,J 98
BUCKLEY,P H 650
BUDD,M B 80
BUDDE,W L 58
BULLEN,W W 148
BURGERS,P C 48
BURGERS,P C 498
BURINSKY,D J 490
BURINSKY,D J 330
BURLINGAME,A L 842
BURLINGAME,A L 125
BURLINGAME,A L 133
BURLINGAME,A L 618
BURMEISTER,H R 347
BURSEY,J T 197
BURSEY,J T 3
BURSEY,J T 695
BURSEY,J T 117
BURSEY,M M 312
BURSEY,M M 489
BUSCH,K L 525
BUSCH,K L 384
BUSCH,K L 745
BUTTERWORTH,B C 11
BUTTRILL,S E 608
BUTTRILL,S E 826
BUTTRILL,S E 822
BYRD,G D 61
BYRD,G D 267
BYRN,S 28
CACIC,C C 410
CACIC,C G 418
CALLAHAN,J H 552
CALLERY,P S 763
CAMPANA,J E 235
CAMPANA,J E 490
CAMPANA,J E 554
CAMPANA,J E 330
CAMPBELL,J A 59
CAMPBELL,J A 52
CAPRIOLI,R M 578
CAPRIOLI,R M 849
CAPRIOLI,R M 848
CARR,S A 347
CARR,S A 580
CARR,S A 386
CARR,S A 673
CARROLL,D I 131
CARUSO,J L 156
CASSADY,C J 215
CASTLEMAN,A W 229
CASTRO,M E 852
CATLOW,D A 34
CENA,K 143
CERNY,R L 322
CERNY,R L 501
CHABER,J 28
CHAI,W 618
CHAI,W 123
CHAIT,B T 38
CHAIT,B T 237
CHAJ,W 125
CHAN,K W 503
CHAN,W G 152
CHANCE,R 28
CHANG,C 174
CHANG,C 511
CHANG,S Y 777
CHANG,T T 624
CHANG,T T 453
CHANG,T T 819
CHAPMAN,J R 106
CHEN,C H 366
CHEN,P H 689
CHESS,E K 438
CHESS,E K 432
CHHEDA,G 711
CHHEDA,G B 135
CHIARELLI,P 536
CHIASSON,J L 761
CHITTIM,B 291
CHITTIM,B G 685
CHRIST-HAZELHOF,E 67
CHRISTENSEN,R G 308
CHRISTIE,W H 614
CIUPEK,J D 378
CIUPEK,J D 779
CLAEYS,M 67
CLAY,K L 71
CLAY,K L 705
CLEMENT,R E 287
COHEN,A 74
COHEN,S L 503
COLE,R 838
COLE,W J 390
COLLINS,G J 654
COLTON,R 633
COLTON,R J 388

AUTHOR INDEX

COLTON,R J 833
COLTON,R J 249
COMPSON,K R 297
CONZEMIUS,R J 610
COOK,J C 835
COOK,J C 402
COOK,J C 119
COOK,K D 552
COOKS,R G 779
COOKS,R G 570
COOKS,R G 378
COOKS,R G 376
COSTELLO,C E 751
COSTELLO,C E 347
COSTELLO,C E 621
COTE,I L 404
COTTER, R J 681
COTTER,R J 320
COTTER,R J 84
COTTER,R J 538
COTTRELL,J S 382
COUCH,M W 80
COVEY,T 446
COVEY,T 170
COVEY,T 791
COVEY,T 203
COWENS,J W 711
CRAMERS,C A 795
CRAWFORD,D W 418
CRAWFORD,D W 410
CRAWFORD,R 642
CRAWFORD,R W 372
CREAVEN,P J 711
CROSS,K P 646
CROSS,K P 648
CROW,F W 625
CROW,F W 721
CROW,F W 717
CROW,F W 679
CROWTHERS,J 203
CROWTHERS,J 446
CROWTHERS,J 170
CURTIS,J M 332
CUTUGNO,D 259
DADKIEWICZ,P 544
DACUNHA,A R 113
DALE,F 318
DANIS,P O 499
DANIS,P O 22
DANNER,D A 305
DAS,C 773
DAS,M 459
DAS,P R 328
DAS,P R 213
DASS,C 485
DAVIDSON,W R 7
DAWSON,F H 316
DAWSON,P H 729
DAWSON,P H 509
DAWSON,P H 487
DAY,R A 345
DAY,R A 343
DE BRUIJN,D P 715
DE KANEL,J 362
DECKER,K 404
DEINZER,M 52
DELBERT,S S 337
DELFINO,R 631
DELMORE,J E 606
DENNE,D R 297
DESIDERIO,D M 25
DEVANT,G 856
DIEM,H E 743
DIETRICH,A M 259
DIPPLE,A 815
DOBBERSTEIN,P 378
DOLIN,B 538
DONNELLY,J R 263
DONNELLY,J R 691
DOUGHERTY,R C 362
DOUGLAS,D J 168
DOWD,M A 158
DOWNEY,S W 368
DOWNEY,S W 370
DOYLE,R J 235
DREIFUSS,P A 622
DUHART,B I 844
DULAK,J 98
DUTTA,S 711
DYCKES,D F 353
EADON,G 289
EBY,R E 614
EDMONDS,C G 201
EDWARDS,J G 732
EDWARDS,J G 734
EICHELBERGER,J W 58
EINOLF,W N 152
ELEMA,E T 483
ELLIOTT,N L 420

EMMELIN,M 88
ENKE,C G 519
ENKE,C G 16
ENKE,C G 646
ENKE,C G 648
ENS,W 184
ENS,W 239
ENS,W 749
ESKEW,T J 529
ESMANS,E L 115
EVANS,D H 229
EVANS,J E 683
EVANS,J E 102
EVANS,S 755
EVANS,S 106
EYLER,J R 425
EYLER,J R 595
FALARDEAU,P 761
FALES,H F 640
FALES,H M 850
FALES,H M 742
FAN,T P 246
FAN,T P 840
FAN,T-Y 849

FARBER,A 135
FAULL,K F 783
FAULL,K F 440
FEIL,V J 450
FENG,R 499
FENN,J B 92
FENN,J B 188
FENNESSEY,P V 582
FENSELAU,C 84
FENSELAU,C 339
FENSELAU,C 451
FERGUSON,A M 565
FERGUSON,E E 769
FERGUSON,E E 46
FERNANDEZ,M T 774
FETIZON,M 464
FETTEROLF,D D 28
FIELD,F H 237
FIELD,F H 507
FIELD,F H 38
FIELD,F H 805
FIES,W J 505
FIES,W J 598
FITCH,W L 556
FITCH,W L 830
FLAMENT,J P 723
FLAMENT,J P 727
FLAMMANG,R 723
FLESCH,G D 807
FLESCH,G D 24
FOHLMAN,J 32
FOSTER,N G 479
FOURNIER,P G 572
FRAISSE,D 88
FRAISSE,D 462
FRALEY,D F 781
FRALEY,D F 527
FRANCE,T J 532
FREAS,R B 227
FREAS,R B 554
FREEMAN,J P 844
FREEMAN,J P 669
FREEMAN,P 52
FREISER,B S 215
FRIEDHOFF,A J 805
FRIESE,T 180
FUKUDA,E K 330
FULFORD,J 7
FUNG,D 685
FUNG,D 291
GALE,P J 635
GALLEGOS,E J 736
GAMES,D E 195
GAMES,D E 34
GAMMANS,R E 148
GANGULY,A K 394
GARNER,F C 263
GARRETSON,L D 285
GARRETSON,L D 9
GARRETT,J H 5
GASKELL,S J 652
GASKELL,S J 699
GAULDEN,M E 158
GEARHART,H L 565
GEBOES,P 115
GEFEN,S 162
GEFEN,S 42
GELLENE,G I 20
GERGELY,R J 277
GERSHEY,R M 277
GERSHEY,R M 671
GERSHEY,R M 685
GIBLIN,D E 548
GIBLIN,D E 644
GIERTHY,J 289
GIESSMANN,U 824
GIESSMANN,U 186
GILLEN,K T 822
GILLIAM,J M 842
GIORDANI,A B 648
GLISH,G L 521
GLISH,G L 719
GOERINGER,D E 719
GOERINGER,D E 521
GOLDMAN,P 580
GOOD,B W 659
GOODLEY,P C 108
GRACE,L 38
GRAMAIN,J C 462
GREAVES,J 447
GREEN,B N 380
GREEN,B N 515
GREEN,J P 73
GREEN,L W 420
GREENE,F T 424
GREENE,F T 307
GREGG,H R 648
GREIFENDORF,D 180
GRIFFIN,D 52
GRIFFIN,L L 473
GRIMES,L E 732
GRIMSRUD,E P 63
GRIMSRUD,E P 59
GROENEWOLD,G S 247
GROENEWOLD,G S 253
GROENEWOLD,G S 12
GROSS,M L 793
GROSS,M L 717
GROSS,M L 596
GROSS,M L 591
GROTEMEYER,J 22
GROTJAHN,L 396
GROTJAHN,L 359
GROVE,M D 787
GRUNBERGER,D 133
GUENAT,C 172
GUEVREMONT,R 671
GUEVREMONT,R 685
GUILHAUS,M 40
GUILHAUS,M 572
GUMPORT,R I 402
HAKONSON,P 32
HALL,S 622
HAMMING,M C 565

AUTHOR INDEX

HANISCH,R C 271
HANNA,I 464
HANSON,R L 275
HARADA,K -I 150
HARDIN,E D 246
HARDIN,E D 840
HARPER,A M 540
HARRINGTON,W L 635
HARRIS,F M 713
HARRIS,F M 324
HARRIS,R E 743
HARRIS,W R 438
HARRISON,A G 36
HARRISON,J 217
HARRISON,W W 408
HARRISON,W W 364
HARRISON,W W 416
HARVAN,D J 489
HARVAN,D J 838
HARVAN,D J 836
HARVEY,D J 448
HASE,G 42
HASS,J R 838
HASS,J R 380
HASS,J R 836
HASS,J R 489
HASSETT,J M 585
HASTIE,J W 374
HAYES,M J 205
HEDIN,C M 263
HEIKES,D L 299
HELLER,D 339
HELLER,D N 84
HEMLING,M E 402
HEMLING,M E 811
HENDERSON,T R 275
HENDRIKS,H 483
HENION,J 203
HENION,J 791
HENION,J 170
HENION,J 446
HEPPNER,R A 434
HEPPNER,R A 414
HERCULES,D M 231
HEROLD,D A 78
HERTZ,H S 74
HERTZ,H S 820
HESS,K R 416
HEWETSON,D 663
HIBBINS,S W 289
HILKER,D R 289
HILL,J C 517
HILLENKAMP,F 257
HILPERT,L R 267
HILPERT,L R 61
HINDENLANG,D M 813
HINES,J 117
HIRAI,N 150
HIRST,D M 44
HITES,R A 56
HITZMAN,C J 608
HO,M 513
HO,Y K 585
HOFFMAN,P A 648
HOGGE,L R 468
HOHN,M 303
HOHNHOLT,J M 310
HOLLAND,J 576
HOLLAND,J F 519
HOLMES,G A 797
HOLMES,J L 48
HOLMES,J L 498
HONG,J S 689
HONMA,Y 612
HOPPILLIARD,Y 723
HOPPILLIARD,Y 725
HOPPILLIARD,Y 801
HOPPILLIARD,Y 727
HORNING,E C 131
HOUGH,L B 73
HOUK,R S 610
HOUK,R S 412
HSU,C S 166
HSU,K L 265
HUANG,J 424
HUANG,S K 546
HUANG,S K 596
HUBER,W K 422
HUDSON,C E 314
HUDSON,C E 473
HUDSON,C E 568
HUDSON,R D 687
HUGHES,B M 283
HUGHES,H 131
HUGHES,R J 513
HUNT,J E 155
HUNTER,R L 505
HUNTER,R L 593
HUNTER,S W 392
HURST,G S 366
HUWE,J K 450
HWANG,D -G 86
IBRAHIM,K E 80
IJAMES,C F 588
ILIAS,A M 182
IMAI,J 817
INOUE,Y 586
INOUE,Y 139
IRVING,C S 141
ITAGAKI,Y 523
JACKSON,C-J C 460
JACKSON,T C 215
JACOBSON,D B 215
JAMESON,C W 293
JAMIESON,G C 556
JAMIESON,G C 830
JAMIESON,W D 671
JAMIESON,W D 277
JAMIESON,W D 685
JARDINE,I 392
JAUDON,P 725
JAYASIMHULU,J 156
JAYASIMHULU,K 345
JAYASIMHULU,K 343

JEFFS,P 341
JENKINS,E 135
JENNINGS,K R 774
JENNINGS,K R 44
JENNINGS,K R 765
JENNINGS,K R 562
JENSEN,N J 717
JOHNSON,J V 783
JOHNSTON,M 496
JOHRI,K K 160
JORDAN,E A 26
JUNACK,M 251
JUNGHALWALA,F B 102
JURUSIK,J 289
KAISER-FARRELL,C 279
KALINOWSKI,H 544
KAMENSKY,I 32
KAMMEI,Y 523
KARAS,M 257
KARGER,B L 205
KASAI,H 201
KATZ,J J 155
KAZDAN,E 513
KAZYAK,L 740
KEARNS,M 297
KEESEE,R G 229
KELLEY,P E 505
KELLEY,P E 598
KELNER,L 850
KELSO,G 345
KENAN,W R 312
KENTTAMAA,H I 570
KENYON,C N 108
KEOUGH,T 627
KERN,F 544
KERNS,E H 148
KHANDELWAL,J K 73
KIDWELL,D A 388
KIDWELL,D A 249
KIDWELL,D A 833
KILLMER,L B 466
KILLMER,L B 69
KIM,H Y 193
KIM,H Y 353
KINGSTON,E E 475
KINGSTON,E E 127
KINTER,M T 312
KIPLINGER,J P 472
KISTEMAKER,P G 715
KIVITS,G A A 67
KLEIN,P D 141
KLINE,T 73
KLUGE,H -J 544
KNAPP,D R 697
KOGAI,T 638
KOSHIMIZU,K 150
KRAILLER,R E 629
KRAILLER,R E 18
KRAMER,S D 366
KRENZER,E G 144
KRISHNAMURTHY,T 709
KUEHL,D W 11
KUHARA,T 139
KUHARA,T 121
KUHARA,T 586
KUNIHIRO,F 523
KUWABARA,H 558
LAI,J T 738
LANDIS,P W 842
LANE,K 211
LANE,K 223
LANE,K 376
LANNING,S 642
LANNING,S M 372
LANT,M S 277
LAPP,R L 548
LAPP,R L 644
LAPP,R L 322
LARAMEE,J A 44
LARKA,E A 481
LARSEN,B S 84
LASER,B 176
LATER,D W 438
LATER,D W 432
LATTIMER,R P 738
LATTIMER,R P 257
LATTIMER,R P 540
LATTIMER,R P 743
LAU,B P -Y 261
LAU,B P -Y 789
LAUGAL,J A 428
LAWRENCE,D L 781
LAY,J O 819
LAY,J O 453
LAYER,R W 738
LAYER,R W 257
LECAVALIER,L 761
LECLERCQ,P A 795
LEE,R E 376
LEE,R W K 160
LEE,Y C 339
LEHMAN,J P 693
LEHMAN,T A 721
LEIKER,T J 310
LEROY,R J 332
LEVANDOSKI,P 785
LEWIS,E 277
LEWIS,I A S 803
LEWIS,I A S 119
LEWIS,S 759
LIBERATO,D J 90
LIBERATO,D J 76
LIBERATO,D J 129
LIEHR,J G 127
LIFSHITZ,C 162
LIFSHITZ,C 42
LIN,S-N 578
LINCOLN,K A 242
LINN,D 11
LINN,W G 529
LIPPSTREU,D L 355
LISEK,C A 451
LO,H H 98
LOO,J A 503

AUTHOR INDEX

LOOKER,J H 679
LOS,J 715
LUBMAN,D M 164
LUCKE,R B 432
LUCKE,R B 560
LUDOVIC,Y 146
LUYTEN,Y 115
LYNAUGH,N 667
LYON,P A 717
LYON,P A 625
MACFARLANE,R D 436
MACFARLANE,R D 845
MACFARLANE,R D 517
MACHLAN,L A 418
MAGEE,C W 635
MAGIN,D F 659
MAHLUM,D D 432
MAHONEY,J F 94
MAIN,D E 749
MAIN,D E 184
MAIN,D E 239
MAKSOUD,H 441
MALINOVICH,Y 42
MALLAMS,A K 394
MALTBY,D A 583
MALTBY,D A 398
MANCILL,V K 845
MANDELBAUM,A 574
MAQUESTIAU,A 723
MAQUIN,F 492
MAQUIN,F 172
MARASCO,J 633
MARASCO,J 740
MARBURY,G D 689
MARCH,R E 324
MARCH,R E 513
MARCH,R E 713
MARCUS,R K 364
MARKEY,S P 850
MARQUIS,F 78
MARSHALL,A G 589
MARSHALL,A G 600
MARTIN,C R 26
MARTIN,M 576
MARTIN,W B 566
MARTINEAU,A 761
MARYANOFF,C A 777
MASON,R S 774
MASON,R S 562
MASSE,R 137
MATHEWS,W R 351
MATSUMOTO,I 139
MATSUMOTO,I 586
MATSUMOTO,I 121
MATSUMOTO,M 586
MATSUMOTO,M 139
MATTHEWS,H B 110
MATTHEWS,P J 513
MAYLIN,G 446
MAZER,S M 283
MCADOO,D J 568
MCADOO,D J 314
MCADOO,D J 473
MCCALLA,D R 279
MCCAMISH,M 447
MCCARTHY,E R 657

MCCLOSKEY,J A 135
MCCLOSKEY,J A 620
MCCLOSKEY,J A 201
MCCLUER,R H 683
MCCLUER,R H 102
MCCRERY,D A 591
MCCRERY,D A 832
MCDEVITT,M A 281
MCDOWALL,M A 195
MCEWEN,C N 836
MCFADDEN,W H 100
MCFARLANE,R D 26
MCGUIRE,J M 205
MCIVER,R T 337
MCIVER,R T 593
MCIVER,R T 532
MCIVER,R T 505
MCLAFFERTY,F W 503
MCLAFFERTY,F W 499
MCLAFFERTY,F W 22
MCLAFFERTY,F W 661
MCLUCKEY,S A 715
MCNEAL,C J 845
MCNEAL,C J 517
MCNEAL,C J 26
MCREYNOLDS,J H 585
MECKSTROTH,W K 227
MEEHAN,J L 295
MEISELS,G G 771
MEISELS,G G 328
MEISELS,G G 326
MEISELS,G G 213
MENTZER,M 69
MENTZER,M 466
MESSIER,F 137
MEUZELAAR,H L C 540
MEUZELAAR,H L C 665
MEYRANT,P 723
MICHALSKI,T J 155
MIDDLEDITCH,B S 334
MIDGLEY,J M 80
MILLER,C M 370
MILLER,C M 368
MILLER,D 5
MILLINGTON,D S 259
MILLINGTON,D S 76
MILLINGTON,D S 398
MILLINGTON,D S 583
MIROCHA,C J 663
MITCHUM,R K 669
MITCHUM,R K 844
MOLNAR,J A 753
MOMMERS,A A 498
MONCUR,A V 195
MONCUR,J G 265
MOORE,C 562
MORGAN,T G 713

MORGAN,T G 324
MORITA,Y 842
MORTON,T H 160
MORTON,T H 457
MOSCHEL,R C 815
MOSHEN,M 137
MOTT,A W 481
MUGA,M L 241
MUIR,D C F 143
MULLEN,S L 589
MUNSON,B 809
MUNSON,B 178
MUNSON,B 455
MURAD,E 637
MURPHY,J H 182
MURPHY,R C 703
MURPHY,R C 71
MURPHY,R C 82
MURPHY,R C 705
MUSHA,K 558
MUSSELMAN,B 576
MUSSELMAN,B D 244
MYERHOLTZ,C A 426
MYERS,A C 830
NACSON,S 36
NAITO,M 523
NAITO,Y 523
NAVRATIL,P R 141
NELSON,C C 620
NERO,V P 687
NETZEL,D A 434
NEUMEYER,J L 441
NG,K J 74
NG,Y T 507
NGO,A 7
NIEHUIS,E 180
NISHIMURA,S 201
NISHIMURA,T 536
NISHIMURA,T 771
NISHIMURA,T 328
NISHIMURA,T 213
NODA,T 602
NOGAR,N S 370
NOGAR,N S 368
NORMAN,E J 781
NOWLIN,J G 131
NUGTEREN,D H 67
O'DONNELL,J E 307
O'DONNELL,J E 424
O'KEEFE,P W 289
O'LEAR,J R 378
O'MALLEY,R M 566
OBAL,T 563
OCCOLOWITZ,J L 842
ODOM,R W 608
OGIER,W 826
OKOMOTO,D 438
OKUTANI,T 602
OLERICH,G 65
OLIVARES,J A 412
OLIVARES,J A 807
OLSON,C T 444
ONISHI,H 25
ONSTOT,J 293
ORO,J 334
PAGE,S W 622
PALLANTE,S L 451
PANG,H 751
PANNELL,L K 640
PANNELL,L K 742
PARKER,C E 110
PARR,J L 271
PARR,J L 9
PARTHASARATHY,R 135
PAUL,B 711
PAUL,T D 585
PAULSON,J F 767
PAULSON,J F 318
PEAKE,D A 644
PEAKE,D A 832
PEAKE,D A 793
PEAVY,R D 410
PELL,R J 565
PELLETT,G L 616
PELLIZZARI,E 3
PELLIZZARI,E D 695
PENDYALA,L 711
PEREL,J 94
PESCH,R 303
PFEIFFER,R 28
PFLEIDERER,W 402
PILOSOF,D 193
PILOSOF,D 353
PINKSTON,J D 534
PLATTNER,R D 787
POEPPEL,F 98
POPOV,A I 828
PORTER,C J 699
PORTER,C J 301
PORTER,R F 20
POWELL,R G 787
PRAMANIK,B N 394
PRAS,N 111
PRESCOTT,C L 281
PRESCOTT,C L 271
PRICE,H A 54
PROCTOR,B L 269
PROCTOR,B L 158
PROCTOR,D W 414
PROVOST,L P 285
QUALLS,W C 384
QUALLS,W C 745
QUALLS,W C 525
QUAN,E S K 168
QUILLIAM,M A 277
QUILLIAM,M A 279
RAHN,G 477
RAMANA,D V 563
RAMSEY,E D 34
RAMSEY,E D 195
RAPP,U 303
REDEKER,G S 824
REDMAN,E W 160
REDMAN,E W 457

REENTS,W D 530
REGINATO,R 618
REIMER,M L J 460
REIMER,M L J 459
REINHOLD,V N 386
REINHOLD,V N 673
REINHOLD,V N 675
REINHOLD,V N 580
REMPEL,D L 596
REMPEL,D L 546
RETTINGHAUS,G 422
REUTER,C 536
REYNOLDS,W E 598
RHEE,C K 257
RHINEBARGER,R 828
RHODES,D 830
RICCA,T L 600
RIDGE,D P 221
RIDGE,D P 227
RILEY,C N 707
RINEHART,K L 811
RINEHART,K L 119
RINEHART,K L 402
RITCHEY,C R 144
ROACH,J A G 622
ROBBINS,R C 479
ROBERTS,G 341
ROBOZ,J 447
ROBOZ,J 443
ROCCA,J L 88
ROCHE,F R 585
ROE,C R 583
ROEPSTORFF,F 34
ROEPSTORFF,P 32
ROITMAN,E 133
ROLANDO,C 856
ROLINSKI,E J 638
ROLLGEN,F W 824
ROLLGEN,F W 186
ROMANOWSKI,G 233
ROSENTHAL,F 133
ROSS,D B 743
ROSS,M M 833
ROSS,M M 249
ROSS,M M 388
ROSS,R M 78
ROTTSCHAEFER,S 69
ROTTSCHAEFER,S 341
ROTTSCHAEFER,S 466
RUDEWICZ,P 809
RUDEWICZ,P 178
RUSSELL,D H 219
RUSSELL,D H 852
RUSSELL,D H 797
RUSSELL,D H 629
RUSSELL,J R 148
RYAN,J J 261
SAADEH,N K 430
SACK,T M 591
SACK,T M 485
SAFE,S 685
SAFE,S 291
SAITO,K 701
SAKUMA,T 789
SALEM,N 104
SALLANS,L 223
SALLANS,L 211
SAMS,R L 820
SANTOS,I 589
SARRE,O 394
SARVER,E W 709
SATOUCHI,K 701
SAVICKAS,P J 408
SAVORY,J 78
SAYYID,S 106
SCANLAN,G 392
SCHAFFER,R 74
SCHEEL,R H 54
SCHELLING,F J 229
SCHMID,E R 677
SCHMIT,J P 487
SCHNATZ,H 544
SCHOELLER,D A 631
SCHOEN,A E 378
SCHRAM,K H 400
SCHRAM,K H 817
SCHUBERT,A J 426
SCHUELER,B 239
SCHUELER,B 184
SCHUELER,B 749
SCHUR,K M 540
SCHUTJES,C P 795
SCHWARTZ,H E 205
SCHWEIKARD,L 544
SCHWEITZER,J S 805
SCOBLE,H A 349
SCOTT,P M 789
SCOVILL,J P 640
SEARS,L J 59
SEDGWICK,R D 811
SEDGWICK,R D 813
SEGAL,A 404
SEIFERT,W E 849
SELF,R 755
SEO,Y-H 259
SERVE,M P 444
SETHI,S K 201
SETHI,S K 620
SHACKLETON,C 123
SHARP,T R 757
SHELTON,D B 845
SHEN,J 430
SHINKA,T 139
SHINKA,T 586
SHUKLA,A 44
SHUSHAN,B 650
SHUSHAN,B 7
SICHTERMANN,W 251
SIEGEL,M 94
SIEVERT,H -J 580
SIGLER,P 1
SITRIN,R 341
SKETT,P W 195
SLAYBACK,J R B 477

SLOWIKOWSKI,D L 817
SMITH,A 221
SMITH,B J 78
SMITH,C V 131
SMITH,D 46
SMITH,D 769
SMITH,D C 803
SMITH,D H 406
SMITH,L 848
SMITH,R D 560
SMITH,R D 542
SMITH,R D 207
SMITH,R M 289
SMITH,R W 110
SOKOLOSKI,E 742
SOLCH,J G 5
SOLOMON,J J 404
SOVOCOOL,G W 691
SPEEDIE,M K 763
SPENCER,R B 658
SPHON,J A 494
SPHON,J A 622
SQUIRES,R R 223
SQUIRES,R R 376
SQUIRES,R R 211
SRINIVASA,R S 734
STAFFORD,G C 598
STAFFORD,G C 505
STAHL,D 492
STAHL,D 172
STANDING,K G 749
STANDING,K G 184
STANDING,K G 239
STAUFFER,D B 661
STAUFFER,D B 658
STEFFENS,P 180
STEMMLER,E A 56
STERNSON,L A 707
STEWART,P B 9
STOBIECKI,M 580
STOLL,R 838
STOUT,S J 113
STRADLING,R S 384
STRAUB,K 785
STRIFE,R J 703
STROH,J G 119
STUERMER,H 544
STULTS,J T 519
SUN,J D 275
SUN,W -F 261
SUNDQUIST,B 32
SUZUKI,M 150
SUZUKI,R 443
SVEC,H J 24
SVEC,H J 807
SVEC,H J 610
SWANSIGER,J T 305
SWEELEY,C C 576
SYKA,J E P 598
SYKA,J E P 505
TABET,J C 462
TABET,J C 464
TABETT,J-C 681
TAKEDA,N 150
TAKESHITA,H 25
TAMURA,H 602
TANNER,S D 7
TANZER,F S 25
TASHIRO,C 279
TATEMATSU,A 150
TAYLOR,D H 614
TAYLOR,L C E 384
TAYLOR,L C E 359
TAYLOR,L C E 382
TAYLOR,M L 5
TEECE,R G 400
TEMBREULL,R 164
TEMPLETON,J F 460
TERLOUW,J K 48
TERLOUW,J K 498
THOMAS,T F 318
THOMSON,B A 190
THOMSON,B A 7
THORNE,G C 652
THRUSTON,A D 205
TIERNAN,T O 5
TIERNAN,T O 470
TIERNAN,T O 511
TILSON,H A 689
TIMMONS,L 293
TJOA,S S 582
TODD,J F J 598
TODD,J F J 505
TODD,P J 253
TODD,P J 247
TODD,P J 12
TOMER,K B 625
TOMER,K B 679
TOMER,K B 717
TOMER,K B 721
TONDEUR,Y 462
TONDEUR,Y 815
TORRENCE,P F 817
TOSINE,H 287
TOWNSEND,R 339
TRAINOR,T M 441
TREHY,M L 14
TROIN,Y 462
TRUSSELL,A R 265
TSARBOPOULOS,A 225
TSARBOPOULOS,A 828
TSO,J 499
TSUCHIYA,M 558
TUCKER,M G 100
UDSETH,H R 560
UDSETH,H R 542
UDSETH,H R 207
UNDERHILL,E W 468
UNGER,P D 813
UNGER,S E 255
UPSCHULTE,B L 229
VALKENBURG,C A 63
VAN BREEMEN,R 681
VAN DER ZANDE,W 715

VAN KALLEVEEN,T H 326
VAN LANGENHOVE,A 675
VEARES,M 803
VERMA,S 779
VERRET,W J 263
VESONDER,R F 347
VESTAL,M L 246
VESTAL,M L 353
VESTAL,M L 840
VESTAL,M L 193
VESTLING,M M 153
VICCHIO,D 763
VIGGIANO,A A 767
VINDIOLA,A G 436
VISWANADHAM,S K 231
VOUROS,P 205
VOUROS,P 441
VOYKSNER,R D 197
VOYKSNER,R D 117
VOYKSNER,R D 695
VOYKSNER,R D 3
VRBANAC,J J 697
WAGNER,G 176
WALKER,J 25
WALLER,G R 146
WALLER,G R 144
WALLS,F C 618
WANCZEK,K P 233
WANG,T -C L 589
WANG,T-C L 600
WATANABE,H 602
WATSON,J T 534
WATSON,J T 244
WATSON,J T 828
WEAKLIEM,H A 635
WEBER,L 345
WEE,E L 781
WEERASINGHE,N C A 295
WEINTRAUB,S T 129
WEINTRAUB,S T 496
WEISZ,A 574
WELCH,M J 820
WELCH,M J 74
WELCH,R L 54
WELLER,R R 595
WELLER,R R 707
WESDEMIOTIS,C 22
WESDEMIOTIS,C 499
WEST,D X 640
WESTCOTT,J Y 705
WESTFAHL,J C 738
WESTMORE,J B 460
WESTMORE,J B 459
WETMORE,R W 332
WHITE,E 74
WHITE,E 820
WHITE,E 308
WHITE,E L 312
WHITE,K D 622
WHITEHOUSE,C M 92
WHITEHOUSE,C M 188
WHITNEY,J O 133
WHITNEY,J O 125
WHITNEY,J O 618
WILKINS,C L 588
WILLIAMS,C H 9
WILLIAMS,C H 285
WILLIAMS,C H 281
WILLIAMS,C M 80
WILLIAMS,D H 382
WILLIAMSON,C 650
WILLOUGHBY,R C 96
WILLOUGHBY,R C 192
WILLS,M R 78
WILSON,B W 432
WILSON,B W 438
WINDIG,W 540
WINDIG,W 665
WINKLER,P C 96
WOLFE,M H 753
WOLFE,R R 753
WONG,C 642
WONG,C M 372
WONG,J W 468
WONG,S S 186
WOOD,G W 563
WOOD,K V 428
WOOD,K V 376
WOODHALL,B J 34
WRIGHT,B W 207
WRIGHT,C W 432
WRIGHT,L G 376
WU,R L C 470
WYATT,J R 235
YAMAGUCHI,H 612
YAMAGUCHI,K 110
YAMASHITA,M 188
YANG,Y-M 133
YASUDA,S 612
YELTON,R O 283
YERGEY,A L 90
YERGEY,A L 76
YERGEY,A L 129
YERGEY,J 104
YINON,J 86
YOST,R A 783
YOST,R A 14
YOST,R A 80
YOUNG,A B 513
YOUNG,S E 826
YOUNGLESS,T L 305
YOUSSEFI,M 550
YU,K O 444
YU,R K 811
YUDKOFF,M 759
ZARETSKII,Z V I 475
ZHAO,S 610
ZIMMERMAN,E F 781
ZIMMERMAN,M L 747
ZINGARO,R A 436
ZOELLER,J H 436
ZWINSELMAN,J J 36

In Memorium

Harrell Ford

James Gerber

BUSINESS MEETING OF THE AMERICAN SOCIETY FOR MASS SPECTROMETRY
Wednesday, May 30, 1984
5:30 PM
Regency Center Ballroom
Hyatt Regency
San Antonio, Texas

President Fenselau called the meeting to order and introduced Henry Fales as the Parliamentarian for the Business Meeting.

Secretary Harry Hertz presented his report. He asked for a motion to accept the minutes of the Business Meeting of the 31st Annual Conference on Mass Spectrometry and Allied Topics which appeared on pages 936-938 of the proceedings of that meeting. It was so moved, seconded and unanimously approved.

The Secretary then announced the election results and introduced the successful candidates. The election for Vice President for Programs between Gerry G. Meisels and Thomas O. Tiernan, was won by Gerry Meisels. In the election for Treasurer, Jim DeCorpo was unopposed and was elected for a second term. For Board Member-at-Large, Gordon W. Wood defeated Charles H. DePuy. Of the 570 ballots received, 11 were disqualified for inappropriately being submitted or improperly being filled out. The Secretary thanked the Tellers Committee which assisted him in counting the ballots; the Committee was composed of Sanford P. Markey, Brian A. Rogers and Edward White V.

The Secretary next reported on this year's student travel stipend competition. There were many highly qualified applicants for the limited number of student travel stipends available. The successful applicants were John Callahan, Paul Danis, Werner Ens, Lawrence Grimes, Mark Hemling, Jose Olivares, John Pinkston, Thomas Sack, Maciej Stobiecki, Michael Trehy and Chai Wengang. The Secretary concluded his report by reporting on the one death of a Society member, which had been reported to him.

Treasurer James DeCorpo then presented his annual report to the membership. In 1983, ASMS approached the operating reserve which the Society's accountant had advised us to reach. This reserve was $102,000.00 at the end of the year. The major expense during the past year was software development for transfering ASMS membership and fiscal records from a commercial computer system to the microcomputer in the Society's Office in Michigan. The Treasurer summarized conference expenses and income for the past three years. The 31st Annual Conference in Boston was designed with an austere budget and as a result the Society had an $18,500 surplus.

The treasurer next presented a summary of ASMS membership for the years 1978 to 1984. As of May 1984, ASMS has 1744 members. It was moved, seconded and unanimously approved to accept the Treasurer's Report.

Vice President for Programs Graham Cooks presented his report. He reviewed the program suggestions made by ASMS members, which were introduced in this year's program. These suggestions included the retrospective lectures, the discussion periods in oral sessions, lunchtime workshops, and strengthening the Friday program. Vice President Cooks acknowledged the Program Committee for their help in reviewing this year's technical abstracts. The Society members assisting the Vice President were John Allison, Ken Busch, Catherine Fenselau, Jean Futrell, Ron Hites, Tom Keough, and Vern Reinhold. Cooks presented the criteria which were used in the abstract review process. Authors whose abstracts were not considered acceptable were allowed to revise and resubmit the abstracts.

Vice President Cooks next reviewed the history of papers scheduled at the annual conference. In 1984, there were 519 papers scheduled for presentation. Cooks then acknowledged the participants in the historical exhibit preparation and the retrospective lecturers. He announced that a special bound volume would be printed which contains the retrospective lectures and some historical anecdotes. He invited

mass spectrometrists active in the field before 1960 to submit two page anecdotes for inclusion in this bound volume.

Vice President for Arrangements Mike Grayson presented his report next. He announced that the dates for the 1985 annual conference have been shifted to the Memorial Day week, May 26-31, 1985. Grayson reviewed the costs to the Society which resulted in the shift to the less expensive Memorial Day week. In 1986, the meeting will be in Cincinnati, in 1987 in Denver, and in 1988 a west coast site is currently being selected. He informed the membership that for 1989 we are negotiating with several hotels in Toronto, Canada.

Board Member-at-Large Bob Finnigan next reported on this year's annual conference bound volume. He reported that we will print only extended abstracts this year. Workshop organizers and committee chairmen are asked to turn in their reports by June 15. He was happy to report to the membership that there would be no price increase for the production of this year's bound volume.

Member-at-Large Marvin Vestal then reported on this year's short course and fall workshop. The Society had a successful fall workshop in the Bay area on liquid chromatography/mass spectrometry. Vestal reported that attendance was down at the short course at the 32nd Annual Conference. There were 15 attendees. Education Committee Chairman Al Yergey briefly discussed changes which are being planned for next year's short courses. A short course on ion optics is being considered for the 33rd Annual Conference.

President Fenselau then thanked Judith Watson for all her efforts on behalf of ASMS and announced that our contract with her company, Professional Association Management, has been renewed. President Fenselau then announced the members of this year's nominating committee: Chairman Wade Fite, Mike Bowers, Bob Lattimer, Don Hildenbrand and Al Burlingame. President Fenselau thanked the people who helped in the Guadalupe Room during the past week, giving administrative assistance to the annual conference. She also acknowledged the tremendous support given by Sue Weintraub with local arrangements in San Antonio. For her outstanding efforts on behalf of the Society, Sue Weintraub was honored with a plaque recognizing her contributions.

President Fenselau presented certificates of recognition to retiring members of the Board of Directors. They were: Thomas Aczel, Marvin Vestal and Burnaby Munson. She concluded her presentation with the announcement that this year's fall workshop will be on heavy mass ion analysis and that the workshop will be located in the North Jersey area. She acknowledged the support from the North Jersey discussion group in organizing the workshop.

The meeting concluded with Vice President for Programs Graham Cooks thanking Catherine Fenselau for her four years of outstanding and dedicated service to the Society as Vice President for Programs and as President.

President Fenselau adjourned the meeting at 6:20 PM.

Respectfully submitted,

Harry S. Hertz
Secretary

Minutes of the 1984 Meeting of ASTM Committee D-2, Res Div IV, Section M on Mass Spectrometry

The 1984 Meeting of Section M, Res. Div. IV, ASTM D-2, was held in San Antonio, Texas, Monday, May 28, 1984, at the Hyatt-Regency Hotel. As customary, meeting location and time were selected to coincide with the meetings of ASTM Committee E-14 and the Annual Conference of the American Society for Mass Spectrometry.

The meeting was attended by approximately 40 members and non-members (see attached list) and was chaired by the Chairman, Thomas Aczel of Exxon Research and Engineering Company. Ms. Louise Neall, the ASTM staff representative, also participated. The agenda is shown in Table I.

I. The meeting was opened by the Chairman, who reminded all participants of the ASTM policy of conducting meetings in a completely open fashion, satisfying both the letter and spirit of the applicable antitrust statutes. He invited all attendees to participate in the discussions and in any cooperative work sponsored by the Section. He stated that all activities of the Section are open to any interested person, company, or institute, with only the voting rights being reserved to ASTM members. He also reminded participants that membership applications were available, and would be considered favorably.

Ms. Louise Neall strongly concurred with this policy. She gave a status of methods being under the balloting procedure.

III. Gil Greenwood (Phillips Petroleum) (with a slight modification of the agenda, agreed upon by all participants) surveyed the attendees' interest among possible cooperative efforts. The specific efforts, and the number of people interested in working on them, are listed on the next page.

a.	Extension of present type analyses:	3
b.	High resolution, low voltage methods:	9
c.	High resolution, high voltage methods:	6
d.	Field ionization/field desorption:	6
e.	Fast atom bombardment:	2

Items b, c, and d were accepted as of major interest. Dr. Robert Ryba of Amoco proposed to develop a more detailed questionnaire on the above items and on the overall role, scope, and future activities of Section M. This questionnaire will be mailed to members and interested parties in June 1984.

Douglas Cameron (Union Oil) mentioned the need for analysis of samples with significant heteroatom content. This was viewed as a high priority item by the attendees.

IV. Douglas Cameron also discussed issues relevant to on-stream analyzers. A "political" problem was seen in the sense of divided responsibilities for maintenance, method development between analytical experts and in-plant users. Optimum would be a scenario in which users would consult with analytical experts on both a periodic, quality control, and on a "trouble-shooting" basis; this, however, is generally difficult to achieve. Terry Ashe of Exxon Research volunteered to conduct a survey amongst instrument manufacturers on process analyzer availability and applications; to our understanding at present, only Extranuclear and V.G. are involved in this field.

V. Gil Greenwood also reported briefly on the availability of shale oil samples for cooperative method development. Samples will be sent to interested parties (see asterisks near names in enclosed attendance list).

II. Terry Ashe reported on the quantitative studies for evaluation of an instrument to replace the old CEC 103 models. This is an extremely important task, as most of existing D-2 methods involving mass spectrometry were developed on this type of instrument, that is not in production anymore. He reported that samples of saturate fractions were given to Extranuclear, Finnigan-MAT, Hewlett-Packard, Kratos and V.G. Companies in March 1984; data are beginning to be received, but not all are in yet.

A report will be sent to attendees as soon as available. A report on aromatics analysis, coordinated by Terry Ashe, will also be sent to attendees as soon as available.

VI. Application from a new membership candidate, Dr. Hazlett, U.S. Navy, has been received and approved. Ms. Neall will follow upon the administrative procedure.

VII. New business consisted mainly in efforts to revitalize the Section's activities. The questionnaire mentioned above will contain items relevant to the wishes and ideas of the membership and interested parties in this regard.

The meeting was adjourned at 2:00 p.m.

Respectfully submitted,

Thomas Aczel, esq.

THOMAS ACZEL
Chairman

Table I

Agenda of the 1984 Meeting of Section M, Res. Div. IV, ASTM Committee D-2

May 28, 1984
12:30 p.m.
Hyatt-Regency Hotel
San Antonio, Texas

I.	Introduction	Thomas Aczel
II.	Quantitative Studies for Evaluation of Instruments Replacing the CEC 21-103 Model Mass Spectrometers	Terry Ashe
III.	New Hydrocarbon Methods	Gil Greenwood
IV.	On-Stream Analyzers	Gil Greenwood
V.	Shale Oil Samples	Gil Greenwood
VI.	Membership Requests	Thomas Aczel
VII.	New Business	Participants
VIII.	Adjournment	

Attendance List

Name	Affiliation	Phone
Rodney P. Page	ARCO	312-210-3215
Thomas Aczel*	Exxon Research and Eng. Co.	713-425-5131
John Defever	Shrader Labs	313-894-4440
Ben Lass	Engelhard	201-321-5411
Mynard Hamming	Conoco	405-767-3739
Vince Nero	Texaco, Inc.	914-831-3400
Johnie Brown	Niper	918-337-4484
Robert Ryba	Standard Oil Co. (Indiana)	312-420-5966
Chuck Snelling	Exxon R & D Labs	504-359-8361
Bob Brunfeldt	Brunfeldt Co.	918-336-4467
Guenter Wagner*	Finnigan-MAT	049-421-54930
Larry Burchfield	Finnigan-MAT	214-828-3384
Don Remling	Finnigan-MAT	303-973-9703
Doug Cameron	Union Oil Co. (California)	714-528-7201
Mike Almond	Kratos	201-934-9000
Carson Jackson	Brunfeldt Co.	918-336-4467
Stephen Shrader	Shrader Labs	313-894-4440*
Paul C. Samson*	Signal UOP Research Center	312-391-3378
Louise M. Neall	ASTM Staff Manager	215-299-5529
Ray Christopher	Finnigan-MAT	408-946-4848
Steve Reynolds	Exxon Research and Eng. Co.	713-425-5134
C. Sam Hsu*	Exxon Research and Eng. Co.	201-730-2228
Dave Canada	Martin Marietta	615-574-9764
David Battiste	Phillips Petroleum	918-661-3444
Arthur Moore	Marathon Oil Co.	303-794-2601
Ed Emery	Balzers	603-889-6888
Peter Fischer*	Gulf Canada R&D	416-822-6770
Roy W. Vander Haar	Standard Oil Co. (Indiana)	312-420-5240
Ronald D. Grigsby	Masspec, Inc.	405-360-0493
Stuart E. Scheppele	US/DOE	918-337-4414
Seymour Meyerson	Standard Oil Co. (Indiana)	312-420-5231
Jim Litton	Lockheed	408-756-3236
Daniel Phelps	Amoco Production Co.	918-660-3129
Gilbert G. Jones	Standard Oil Co. (Indiana)	312-420-5773
Terry Ashe	Exxon Research & Eng. Co.	201-730-2230
Bob Adams	Kratos	404-255-4817
Gil Greenwood	Phillips Petroleum	918-661-8874
Frank Padrta (Lill Churchill)	Signal-UOP	312-391-3175

Committee: Isotope Ratio Measurements

Workshop: REPORTING OF DATA AND STATISTICS

Speaker: Dr. Keith R. Eberhardt, National Bureau of Standards

This workshop, held on May 30 from 1:15 to 2:30 PM, was attended by about 50 people and consisted of discussion of three topics. The first topic was a comparison of five types of statistical intervals that are useful for describing uncertainty. The second topic topic was the use of propagation of error techniques to derive confidence intervals for measurements of isotope ratios and atom fractions. The confidence intervals described include contributions to uncertainty due to the ratio measurement, the correction factor for isotopic fractionation, and the uncertainty of the standard used to determine the fractionation correction. The third topic was a method for modeling and evaluating two identifiable sources of experimental error in a situation where data from similar, but independent, experiments were used to evaluate one of the error sources. This third topic is reviewed in some detail below.

Components of Variation in Isotope Dilution Measurements

A critical step in evaluating the uncertainty in a data set is correctly identifying all the contributions to the experimental error. A commonly-occuring data analysis situation is illustrated by data obtained during the certification of a Standard Reference Material for Human Serum, SRM 909, at the National Bureau of Standards. In summarizing these data, it is necessary to identify and evaluate two distinct sources of experimental variability.

For SRM 909, isotope dilution mass spectrometry was used to determine the concentrations of cholesterol, creatinine, glucose, urea, and uric acid. When the data came to me for statistical evaluation, I noticed that the chemist had grouped the results of the measurements into "sets". An example is given in Table 1 where the data for urea are displayed.

Table 1. Concentration of Urea Per Gram of Freeze-Dried Serum in Reconstituted Human Serum, SRM 909

Set	Measured Concentration, mmol/(L × g)						Set Mean		Within-Set SD
1	11.376	11.362	11.376	11.367	11.383	11.396	11.376		0.012
2	11.404	11.360	11.378	11.397	11.420	11.398	11.393		0.021
3	11.389	11.378	11.387	11.395	11.397	11.404	11.392		0.009
						Grand Mean	11.387	Pooled Within-Set SD	0.015
						SD of Set Means	0.009		

In the Table, each measurement reported is for an independent sample. The units, "mmol/(L × g)", can be thought of as mmol/L, corrected for the mass (g) of freeze-dried serum beads contained in the particular vial of SRM 909 under analysis.

The grouping of the data into sets is based on the wet chemistry portion of the measurement procedure. For each set, a separate solution of labeled material was prepared and used for spiking samples, which were then carried through the chemistry steps as a group. The chemist expected that some contribution to the total experimental uncertainty would result from the operations shared by each set, so these processes were replicated, producing two or more "sets" per anaylte, so that this contribution to the uncertainty could be evaluated from the data.

Figures 1 and 2 illustrate the set-to-set (and within-set) variability that can be seen in the data for urea and cholesterol. These two examples essentially represent the set-to-set variation found, which ranges from barely discernable (for urea) to clearly significant (for cholesterol). [A statistical analysis of variance showed that the attained significance levels for the hypothesis of no set-to-set variation are $\alpha = .14$, for urea, and $\alpha < .001$, for cholesterol.]

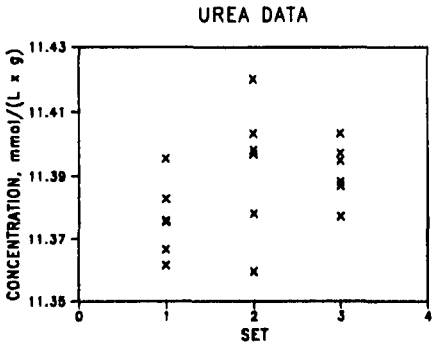

Figure 1.

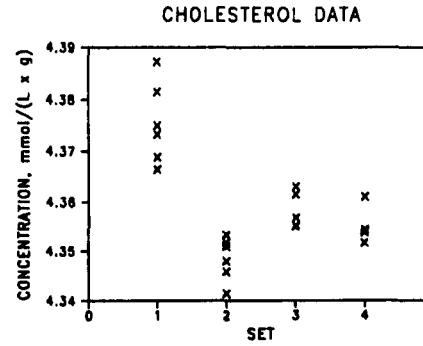

Figure 2.

Once we accept the notion that data from different sets are more variable than data within a set, it is inappropriate to derive confidence intervals based on the simplest statistical model for "n equally precise and independent measurements with no bias." In the present case, a useful model to describe both the within- and between-set variation relaxes the assumption of strictly independent measurements. This statistical model can represented as follows:

$$X_{ij} = \mu + \delta_i + \varepsilon_{ij} , \qquad (1)$$

where,

X_{ij} = measured concentration for sample j of set i
μ = true concentration of the analyte
δ_i = deviation from true concentration caused by experimental error due to set i
ε_{ij} = measurement error for sample j within set i.

In this notation, the index i runs from 1 to k = the number of sets, and j runs from 1 to n_i = the number of samples in set i. For the urea data in Table 1, k = 3 sets and n_i = 6 samples per set. The measurement errors δ_i and ε_{ij} are assumed to have probability distributions that are approximately Gaussian with zero means and standard deviations σ_δ and σ_ε, respectively. Thus, for the urea data, model (1) represents the variability in the data as arising in two stages. First, all 6 samples in set i receive a common "between-set" deviation, δ_i. Then each sample gets its own independent within-set error, ε_{ij}.

Some insight into the way this model represents the data can be gained by closer examination of the urea data in Table 1. The best estimate of the true concentration, μ, is the grand mean, $\bar{x}$ = 11.387 mmol/(L × g). Similarly, the best estimate of δ_1, the measurement deviation shared by all samples in set 1, is the difference between the mean of set 1 and the grand mean, 11.376 - 11.387 = -0.011. Notice that both the grand mean and the mean for set 1 are based on limited data, so the calculated estimate of δ_1, -0.011, is itself subject to measurement error. Similarly, an estimate of $\varepsilon_{1,2}$, the within-set measurement error for the 2nd measurement in set 1, is the difference between the corresponding measurement result and the mean for set 1: 11.362 - 11.376 = -0.014.

In order to evaluate the uncertainty in the grand mean of all measurements, we need to summarize the magnitude of the between-set errors (δ's) and the within-set errors (ε's) as they affect the grand mean. Statistical theory [1] gives the following formula for the standard error of the (unweighted) grand mean, $\bar{x}$, under model (1):

$$\sigma_{\bar{x}} = \left(\frac{\sigma_\delta^2}{k} + \frac{\sigma_\varepsilon^2}{N} \right)^{1/2} \qquad (2)$$

In equation (2), the symbol N represents the total number of measurements made among the k sets, $N = \Sigma n_i$. For the urea data, N = 18 and k = 3. [For data with unequal numbers of measurements per set, equation (2) is an approximation. The exact expression for the general case is obtained by replacing the denominator k with the quantity $(N^2/\Sigma n_i^2)$.]

In a case where the number of sets, k, is sufficiently large (say 9 or more), the between-set and within-set components of uncertainty can be properly accounted-for by the following simple procedure. First, reduce the data to the mean values per set, say $\bar{x}_1$, $\bar{x}_2$, ..., $\bar{x}_k$. Next, compute the mean and standard deviation of the reduced data:

$$\bar{x}' = \Sigma\, \bar{x}_i/k = \text{mean of set means},$$

$$s' = \Sigma\, (\bar{x}_i - \bar{x}')^2/(k-1) = \text{SD of set means}.$$

Then the usual formula, $\bar{x}' \pm ts'/\sqrt{k}$, will produce a confidence interval which remains valid in the presence of a non-negligible set-to-set component of variation, as represented by model (1). In particular, $s'/\sqrt{k}$ estimates the correct standard error of $\bar{x}'$, which is given by equation (2) for the case of equal n_i.

The trouble with the above procedure is that the number of sets is rarely large enough to produce a reliable value for s'. When k is only 3 or 4, s' is statistically quite unstable. In practical terms, the logical basis for treating set-to-set differences as statistical fluctuations--rather than flaws in the measurement method--becomes shaky when k gets too small. The procedure described below overcomes this difficulty by "borrowing" information about set-to-set variability from independent, but similar, measurement situations.

To make practical use of equation (2), we need to estimate the standard deviations σ_δ and σ_ε from the data. The first thing to be aware of is that the usual formula for "standard error of the mean", based on the ungrouped standard deviation of all 18 (generally, N) measurements, is not useful for estimating the correct standard error given by equation (2). In particular, for data that are well-described by model (1), the ungrouped standard deviation, divided by $\sqrt{N}$, underestimates equation (2), as shown in (3):

$$\left(\frac{1}{\sqrt{N}}\right) s_{\text{ungrouped}} \quad \text{estimates} \quad \left(\frac{k-1}{N-1}\,\frac{\sigma_\delta^2}{k} + \frac{\sigma_\varepsilon^2}{N}\right)^{1/2} \tag{3}$$

Since k is often a small fraction of N, the uncertainty implied by expression (3) can be substantially too small compared with (2).

A proper estimate of the standard error can be obtained by considering separately the standard deviations (SD's) within sets and the SD between set means. In Table 1, each of the within-set SD's estimates σ_ε. The best combined estimate of σ_ε is the "pooled" within-set SD given at the bottom of the table. It was obtained as the root-mean-square (rms) average of the three within-set SD's.

The SD among the set means reflects not only the between-set experimental error (represented by σ_δ) but also the within-set measurement error (represented by σ_ε). The statistical technique used to separate these two components, called analysis of variance, can be illustrated quite simply with the urea data. For data with equal numbers of measurements per set (n_i=n), the SD of set means estimates the quantity

$$(\sigma_\delta^2 + \sigma_\varepsilon^2/n)^{1/2} .$$

(For the case of unequal n_i, a slightly more complicated formula is used [1].) Since a separate estimate of σ_ε is available from the pooled within-set SD, it is a simple matter to combine that estimate with the SD of set means to obtain an estimate of σ_δ. For the urea data,

$$\begin{aligned}(\text{estimate of } \sigma_\delta^2) &= [\text{estimate of } (\sigma_\delta^2 + \sigma_\varepsilon^2/n)] - (1/n)(\text{estimate of } \sigma_\varepsilon^2) \\ &= (\text{SD of set means})^2 - (1/n)(\text{pooled within-set SD})^2 \\ &= (0.009)^2 - (1/6)(0.015)^2 = (0.007)^2 .\end{aligned}$$

As previously mentioned, the SD of set means is statistically unstable for k as small as 3 or 4, so it is desirable to "borrow" information about set-to-set variability from other similar data. Table 2 lists the estimates of σ_δ obtained from the other isotope dilution measurements for the human serum material. Since the range of concentrations for various analytes ranges over a factor of 100, the estimates of σ_δ are recorded as relative standard deviations, or (SD/mean), to make them more comparable.

Table 2. Estimates of (σ_δ/Mean), the Set-to-Set Component of Variation, for Various Analytes

	Cholesterol	Creatinine	Glucose	Urea	Uric Acid
Est. of (σ_δ/Mean), in Percent	0.267	0.084	0.123	0.054	0.0
Degrees of Freedom, (k-1)	3	2	3	2	1

Pooled Estimate of (σ_δ/Mean) = 0.159 %

Degrees of Freedom = 11

In Table 2, the pooled estimate of (σ_δ/mean) is computed as a weighted rms average of the values for the five analytes:

$$\text{pooled estimate of } (\sigma_\delta/\text{mean}) = \left(\Sigma f_i s_i^2 / \Sigma f_i \right)^{1/2}$$

where i runs from 1 to 5, s_i = estimate of (σ_δ/mean) for analyte i, and f_i = degrees of freedom for analyte i. The pooled estimate has degrees of freedom equal to the sum, Σf_i.

The technique of borrowing yields a pooled estimate of σ_δ based on 11 degrees of freedom, and therefore, ideally, this pooled estimate is statistically more reliable than any of its individual components. The key assumption underlying the ideal case is that the true values of (σ_δ/mean) are strictly equal for all five analytes. As it happens, the differences among the estimated values of (σ_δ/mean) in Table 2 do not support the assumption of equality as well as one might hope. In general, the technique of borrowing will not produce good results when it amounts to mixing apples and oranges. However, for the human serum data, there were several considerations which led to pushing ahead with borrowing. First, there are chemical reasons to expect comparable set-to-set differences for the five analytes, based on similarities in the laboratory procedures used. Second, the differences in Table 2 were moderated by the chemist's intuition that the apparent set-to-set variation was "too good to be true" for uric acid, but "worse than expected in the long run" for cholesterol. Third, and possibly most telling, the alternative to borrowing was, essentially, to go back to the lab and make measurements on 6 to 8 more sets of samples for each analyte.

Accepting the pooled estimate of σ_δ as the best available for each analyte, equation (2) can be used to construct a realistic estimate of standard error and a corresponding confidence interval.

For the urea example, the analysis is completed as follows. The estimated value of σ_δ is

$$(\text{est. of } \sigma_\delta/\text{mean}) \times (\text{mean}) = (0.00159) \times (11.387) = 0.018 \text{ mmol/(L} \times \text{g)}.$$

Using equation (2), the estimated standard error of the grand mean is

$$\text{Estimate of } \sigma_{\bar{x}} = \left(\frac{(0.018)^2}{3} + \frac{(0.015)^2}{18} \right)^{1/2} = 0.011 \text{ mmol/(L} \times \text{g)}.$$

The statistical stability of this estimate is characterized by at least 11 degrees of freedom. In a table of the t-distribution, the factor t=2.201 is the upper 2.5% point corresponding to 11 degrees of freedom. Thus, a 95% confidence interval for urea concentration is

$$11.387 \pm (2.201) \times (0.011)$$

$$\text{or, } 11.387 \pm 0.024 \text{ mmol/(L} \times \text{g)}.$$

Reference

[1] Box, G.E.P., Hunter, W.G., and Hunter, J.S., (1978). Statistics for Experimenters, John Wiley, New York. pp. 571-583.

Acknowledgements

I am grateful to Michael J. Welch, of NBS, for providing the data used in this discussion, and to Lura J. Powell, also of NBS and chairman of the Isotope Ratio Measurements Committee, for inviting me to speak.

Report submitted by

Keith R. Eberhardt
Statistical Engineering Division
Center for Applied Mathematics
National Bureau of Standards

INTERNAL ENERGY EFFECTS IN COLLISION-INDUCED DECOMPOSITIONS

PART III

This workshop was the third of the series on this topic, initiated in Honolulu in 1982 and continued in Boston in 1983. It continues to attract people from different areas of mass spectrometry and an attendance varying between 50 and 75 attests to this.

Professors McLafferty and Bowers provided the opening remarks and it soon became apparent that feelings were not running quite as high as they had at the two previous sessions. For small ions, eg, 6 atoms or less, for which we frequently know sufficient about the molecule to recognise an internal energy effect when we see one, eg, H_2^+, H_5^+, it now seems to be generally accepted that such effects do exist, especially when there is a fairly large energy barrier between isomeric ions. For larger ions, eg, over 6 atoms, our knowledge of energy levels is very limited and the reproducibility of relative yields of fragments formed in collision-induced decompositions is rarely better than ± 5% so that although it is difficult to exclude internal energy effects in most cases, it is also difficult to demonstrate their existence. Any such effects should be minimised if only high energy processes are used from which to infer structural information and although spectra produced by the collision-induced decomposition of ions will always be a function of internal energy effects and structure, there is no reason at present to assume that large internal energy effects are widespread.

The discussion on angle and energy resolved mass spectrometry was a little disappointing as there were few definitive results reported. The angular dependence of product distributions is determined both by the angle through which the primary ion is scattered and the internal energy released as translational energy of the fragments, but in general, the former is the more likely to be the more important. Work is in progress in several laboratories to determine the relationship between the internal energy deposited in the incident ion and its incident energy and scattering angle but during the discussion, no clear picture emerged.

K R Jennings
University of Warwick
Coventry
UK

Workshop on Spares and Service

Richard M. Caprioli, Moderator

The workshop was held to discuss some long standing problems and current difficulties members have with maintenance of mass spectrometers. This discussion took place with the aid of a panel made up of representatives of five manufacturers; T.Z. Chu (Finnigan-MAT), Keith Compson (Kratos), Gary Beach (Hewlett-Packard), Barry Mulady (VG), and Bob Terio (Nicolet). Overall, the workshop involved a discussion of general aspects of the maintenance and operation of instruments and the attending problems. Most importantly, the session was a trial workshop to see if a forum of this type would be accepted and supported by the membership through their attendance and participation.

The meeting began with a short presentation by T.Z. Chu regarding the 'economics' of manufacturers. In his presentation, Mr. Chu gave averages which he has seen over the years in the industry, (Table I). Mr. Chu finished by stating that customers can influence these economic factors by helping manufacturers in the consideration of trade-offs between certain items such as prices and discount practices, the extent of installation and warranty agreements, funds put into R&D, applications laboratories, field service and tech support, etc. Moreover, manufacturers welcome this customer input.

Table I Manufacturer's Economics - Some General Aspects

SALES		100%
COST OF SALES		(55-65%)
LABOR	5-7%	
MATERIAL	25-50%	
MFG OVERHEAD	25-35%	
(DEPRECIATION OF BUILDING, EQUIPMENT, FREIGHT, CUSTOMS, SCRAP, REWORK, PRICE & PRODUCT VARIANCES)		
INSTALLATION & WARRANTY	5-10%	
GROSS MARGIN		30-45%
OPERATING EXPENSES		(25-35%)
R & D	1-10%	
MARKETING	15-25%	
APP LAB, MANUALS, TRAINING, EDUCATION, FIELD ENGINEERING TECHNICAL SUPPORT ADVERTISEMENT, TRADE SHOWS HOSPITALITY SUITES SALES ENGINEERING		
G & A	4-8%	
ACCT., MIS, HUMAN RESOURCES ADMIN., OTHERS		
CONTRIBUTING MARGIN		(-5) - 10%
INTEREST		0-10%
PRE-TAX PROFIT (LOSS)		(-15) - 10%
TAXES		(-7) - 5%
PROFIT AFTER TAXES		(-8) - 5%

A general discussion followed which covered many considerations of the maintenance and operating costs of instruments. These included estimated costs of ownership of given types of instruments over their lifetimes, completeness and value of operating and service manuals, manufacturers' retrofit policies, warranty costs, manufacturer's training programs, availability of competent tech support via the telephone, spare parts availability and pricing, obsolescence policies, the advisability of approved performance standards, and instrument ordering guidelines. Obviously, these subjects are each worthy of a dedicated workshop and could only be touched on briefly in this 2-hour session.

The workshop was important in setting the stage for future meetings in showing by this heavily attended workshop that this is an appropriate forum for customers and manufacturers to meet, as members of ASMS, and discuss events and policies which mutually effect our professional work and to help direct them more effectively in the future. It is recommended that such workshops be held at least once a year during ASMS meetings where one (or two) well-defined issues can be probed in depth and recommendations made regarding those aspects which we may realistically hope to improve.

BIOMEDICAL APPLICATIONS COMMITTEE WORKSHOP REPORT

OFF-LINE HPLC MASS SPECTROMETRY

This year's workshop considered the application of mass spectrometry to the analysis of biological compounds separated by high performance liquid chromatography and collected prior to analysis. Prior to the meeting several investigators were contacted to participate in the workshop with particular consideration of the techniques used to facilitate off-line analysis, artifacts encountered and ionization techniques employed. Approximately 150 individuals attended the workshop on Monday, May 28, 1984.

Dr. K. Standing presented his experiences with an electrospray deposition technique to load samples on a target for SIMs analysis. An electrostatic lens focused the spray to approximately 2 mm with a flow rate of 1 ul/min from a small bore LC system. Excellent results could then be obtained with Cs^+ ions at 10 kV to desorb small peptides.

Dr. D. Desiderio discussed the use of volatile buffers in HPLC separation. Triethylaminoformate (TEAF), 30 mM at pH 3.0, has been used successfully in the mobile phase to separate neuropeptides by mass spectrometry and analysis (off-line) has been successful to 10 ng. These volatile buffers do not interfere with bio-assays or RIAs.

Dr. J.T. Watson discussed the elution of impurities from Zorbax C18 columns particularly with mobile phases containing 1% acetic acid. These impurities appeared to interfere severely with subsequent FAB analysis of HPLC fractions. A lively discussion followed concerning these interfering substances which have been observed by others. The consensus of opinion (partially based on some NMR data) was that this material might be methyl silicon containing species, perhaps endcapping reagents used for reverse phase columns. The elution of silica itself from HPLC columns may also be a major problem which interferes with FAB analysis.

Dr. R.C. Murphy discussed a potential artifact substance with abundant ions at m/z 515 and 531 by FAB analysis which is extractable from small, conical plastic vials (Eppendorf) with organic solvents.

Dr. L. Baczynskj discussed the analysis of major and minor components eluting from HPLC. Trace alkali metal ions (especially Na_2HPO_4) in the mobile phase appear to affect the analysis of minor components to a larger extent than major components. Ion-pairing reagents for HPLC give good FAB-mass spectra themselves.

Further discussion centered around "HPLC" grade solvents. Dr. Standing pointed out that these are UV transparent but inorganic ions may be present. Dr. M. Horning outlined her methods to purifiy solvents using reverse phase HPLC columns as well as distillation from alkaline $KMnO_4$.

In summary, one should consider non-UV absorbing impurities in "HPLC" grade solvents as artifacts in subsequent off-line analysis.

Suggestions for a possible workshop on Biomedical Applications should be sent to the committee chairman.

Robert C. Murphy
Department of Pharmacology
University of Colorado
Denver, CO 80262

HYBRID MASS SPECTROMETERS

1984 ASMS Workshop San Antonio, Texas

Approximately 200 people attended a midday workshop introducing the topic of hybrid mass spectrometers. Several workers presented a summary of their experience in this relatively new area. Stephen Young from SRI International described his work carried out with a QB instrument equipped with a "volcano" field ionization source. He summarized advantages of the QB configuration over the BQ as follows: the source can be held near ground, and the beam can be better focussed through the interface region. One disadvantage of the QB design is that the flight tube through the magnetic sector must be floated at a high potential. In response to a question, it was emphasized that the collision energy for this instrument ranges from energies of 5-10 eV up to several thousand volts. Thus it can be expected that both low energy associative reactions and higher energy reactions such as charge stripping and charge inversion can be studied.

Chris Porter described the commercial EBQQ instrument available from VG Instruments. For the daughter ion MS/MS experiment, parent ion resolution of up to about 8000 was demonstrated, with unit resolution of the daughter ions up to m/z 1500. Lester Taylor detailed the sector/quadrupole interface of the Kratos EBQQ hybrid mass spectrometer. The defocussing effects of the required deceleration are convoluted with the need to reshape the ion beam profile from that of a slit (as in the sectors) to the circular shape accepted by the quadrupoles. Provision must also be made for the incorporation of an intermediate multiplier so that the hybrid instrument can be operated in the usual double focussing $\overline{EB}$ mode. This is accomplished using an electrical deflection system incorporated into the interface optics. Alan Schoen from Finnigan MAT described that firm's BEQQ hybrid instrument. He emphasized the multiplicity of experiments that can be carried out with such an instrument. As with all hybrid instruments, the availability of separable high and low energy collision cells makes possible new experiments. A "survivor" ion MS/MS experiment was described in which a collision in the first collision cell changes neither the mass nor the charge of a selected ion, but does result in a structural reorganization which is reflected in the daughter ion MS/MS spectrum obtained after a second collision.

Gary Glish of Oak Ridge National Laboratory described a QTOF instrument designed for high sample throughput in MS/MS experiments. The quadrupole can be operated in either a mass-analyzing mode, or in an rf-only mode which passes all ions. After passing through the quadrupole, the ions are focussed into a collision cell, and then pass into a four element acceleration lens into the TOF drift region. A deflector on the last acceleration lens pulses the ions into the TOF with a gated width of about 500 ns. This unique instrument was used to investigate ions formed in thermal desorption of ammonium and phosphonium salts. The QTOF instrument acquires daughter ion MS/MS spectra without scanning of the quadrupole. For a parent ion current of 10^{-11}A, the daughter ion MS/MS spectrum is obtained within a millisecond. Additionally, the quadrupole can be stepped quickly from one mass to the next for sequential parent ion selection.

The relative merits of the various configurations of hybrid mass spectrometers was only briefly discussed during the workshop. Commercial manufacturers have adopted the strategy of adding quadrupoles to existing medium performance instruments. Those constructing "in house" instruments evaluate more carefully expected performance for a specified set of problems. The availability of components makes it likely that additional hybrid instruments will be assembled. The performance of hybrid instruments as compared to that of three and four sector instruments has not yet been adequately evaluated, and might be a suitable topic for a future workshop.

Respectfully submitted,

Kenneth L. Busch
Indiana University

David F. Fraley
Procter and Gamble

"Quality Control and Standardization in Metabolic Profiles of Uinrary Acids"

About 30 persons atended a workshop co-chaired by Yong Lin and Charles Sweeley, titled "Quality Control and Standardization in Metabolic Profiles of Urinary Acids." The purpose of the workshop was to exchange information about the isolation and derivatization of urinary organic acids, to determine the feasibility of standardization of methods, to establish normal in various age groups, and to describe new findings where metabolic profiling analysis is of clinical diagnostic value. Short presentations were made by Yong Lin (Staten Island), Charles Sweeley (E. Lansing), Orville Mamer (Montreal), Isamu Matsumoto (Kanizawa) and T. Niwa (Nagoya).

Extraction and ion exchange are both widely used for the recovery of organic acids from urine but the methods are by no means uniform. Most investigators use the trimethylsilyl derivative, usually with conversion of ketoacids to oximes or methoximes. Packed columns and fused silica capillary columns are being utilized for separations; mass spectrometry and relative retention behavior on GC are both employed to identify abnormal components. Although electron impact ionization is generally used, CI spectra are potentially important. In the discussion period, MS-MS was also described as an approach.

Obscure dietary factors can lead to metabolites that are easily misinterpreted as having clinical significance, and precautions are needed to be certain when unusual substances are introduced via special diets. The abnormal excretion of 3-hydroxy-hexanoic acid was shown to be a characteristic feature of serum samples taken during episodes of diabetic ketoacidosis; this metabolite was not detected in nonketotic diabetics or normals. In Japan, Dr. Matsumoto has diagnosed more than 100 disorders in 6 years of screening of organic acids and has found 87 disorders with the amino acid analyzer. Most common among the organic acidurias were methylmalonic acidemia (27), propionic acidemia (8), and an assortment of lactic acidurias (30).

Respectfully submitted,

Yong Lin
Charles C. Sweeley
Co-Chairmen

Committee Report

Ion Physics and Instrumentation

The committee sponsored a workshop on "Optimization of Sensitivity and Signal/Noise in Particle-Induced Emission", held Wednesday, May 30 at 1:15 P.M. Panel members for the discussion were D. Barofsky (Oregon Graduate Center), A. Benninghoven (Münster), K. Busch (Indiana), B. Chait (Rockefeller), W. Ligon (General Electric), R. Macfarlane (Texas A & M), L. Taylor (Kratos Analytical Instruments) and K. Standing, who served as Chairman.

Topics discussed included choice of instrument, method of processing data, and choice of primary particle, but most of the discussion centered around the preparation of the target. Various recipes for liquid and solid matrices were described, as well as attempts to explain some of the observed phenomena.

About 150 attended the workshop.

Respectfully submitted,

K. G. Standing
University of Manitoba
Chairman

Workshop on Microcomputers in Mass Spectrometry

May 30, 1984 - 1:15 PM

Approximately 120 people attended this workshop. Results were presented from a survey questionnaire sent to 80 labs asking if they had developed or were developing an application using microcomputers. Of the 59 replies received, 39 were doing something with micros. Of the 25 who reported the hardware they were using, 5 were using IBM-PC's; 5 - Dec 11's; 5 - Apples,; 2 - IBM 9000; and one each of Zenith, Hp 150, NEC-APC. Five were building systems based on the Motorola 68000 and one using an Intel 8086. Twelve systems were capable of full data acquisition and control, 12 were subunits of larger systems c.f. intelligent interfaces, sector controller, SIMS target controller, purge and trap controller or mass readout device. Nine were used for information handling c.f. database using Lotus 1-2-3, literature reference file index, peptide sequencing. Six micros were used as Tektronix 4010 emulators, "enhanced" terminals, or intelligent work stations (often using modem communications).

David Jamieson from NRC, Halifax, described one of these TEK emulators which is used with an Apple and the Incos data system. Jose Olivares said he had a number of graphics routines to drive a 4010. Bob Minard described his work on programming the NEC-APC (high resolution color graphics) for enhanced data presentation and described some work by Dave King at USGS in Denver using a Z-80 to set up automated gc-ms (unattended injection of samples) in connection with a KRATOS data system. Ken Dickens of Vacuumetrics and Steve Shrader of Shrader Analytical described their micro-based data acquisition systems which work with both magnetic and quad ms and do essentially all of the primary functions of the much more expensive mini systems (admittedly not as fast for some operations). The BASIC programs are supplied allowing user extension of the system but programs can be compiled to speed up execution time.

Finally, Chris Enke, in a very interesting presentation, described what he's doing at Michigan State in order to use all the computing power available to MS today. Using a multimicroprocessor system, programmed in FORTH for instrument control and data acquisition, data from the interface micros is passed to a file manager minicomputer that has data storage devices, terminals, printers and plotters attached. He told how they have created "soft knobs," a set of digitized analogue pots that allow tuning of the instrument via the computer, but in a way that gives the operator a better feel for instrument tuning since the knobs and CRT feedback yield the immediate continuous response of analogue knobs, meters, and scopes.

The audience requested that a list of names and addresses of individuals willing to share micro information and software be put together and made available. Bob Minard did this within 24 hours and 60 copies of the list shown below were distributed.

ASMS COMMITTEE ON COMPUTER APPLICATIONS

Software references from WORKSHOP ON MICROCOMPUTERS IN MS.

1. Using the APPLE with "TEKTERM" commercial software to emulate a TEKTRONIX 4010 terminal via modem or direct connection.
   Dr. David Jamieson
   National Research Council
   Halifax, N.S. Canada
2. Graphics programs for Tektronix 4010 compatibles (based mainly on DEC PDP-11 systems)
   Dr. Jose A. Olivares
   Ames Lab USDOE
   Iowa State University
   Ames, IA 50011
3. Tektronix 4025 emulator for the IBM PC
   Dr. Rick Lapp
   Midwest Center for Mass Spectrometry
   University of Nebraska
   Lincoln, Nebraska 68588
4. Multicomponent Factor Analysis on the IBM PC tailored to MS/MS data (compiled FORTH)
   Dr. Phil Funk
   E.R. Squibb
   P.O.Box 4000
   Princeton, NJ 08540
5. Peptide Sequencing Program (PEPALG) based on K. Biemann's work at MIT (runs on the IBM PC-XT; FORTRAN)
   Ian Jardine (Brad Erikson)
   Mayo Clinic
   Rochester Minnesota 55905
   507-284-4178
6. Program to calculate M.W. and sequence fragment weights for small peptides (analyzed by FAB; IBM-PC)
   Dr. Blair Fraser
   FDA BOB DBB 8800
   Rockville Pike
   Bethesda, MD 20205
7. Micromputer based digital m/z readout on a magnetic sector MS.
   Dr. J. P. Freeman
   NCTR
   Jefferson, Ark 72079
   501-541-4369
8. A micromputer (uPDP-11/23)-based data system for high resolution multiple ion monitoring and multiple metastable peak monitoring
   Dr. S. J. Gaskell
   Tenovus Institute for Cancer Research
   Welsh National School of Medicine
   Cardiff CF44XX Wales U.K.

If you have any software that you would be willing to share, please contact Bob Minard, Chairman, Computer Applications Committee c/o Dep't of Chemistry, Penn State University, 152 Davey Lab, University Park, PA. 16802 (814-865-2202) If enough interest is shown we may distribute this list via an ASMS mailing

LC/MS Standards Workshop, J.D. Henion, Cornell University, Ithaca, NY 14850, W.Budde, U.S.EPA, EMSL, Cincinnati, OH 45268, D. Games, University College, Cardiff, CF1 1XL, England, P. Goodley, Hewlett Packard Co., Palo Alto, CA 94303, R. Voyksner, Reserach Triangle Institute, Research Triangle Park, NC, 27709, and A. Yergey, NIH, Bethesda , MD 20205.

LC/MS STANDARDS WORKSHOP

The LC/MS standards workshop, was organized around the short presentations of six speakers asked to contribute their thoughts of suitable test compounds for LC/MS. An outline of eleven potential criteria for LC/MS standards was initially presented as a starting point for the ensuing discussion. This summary of the Workshop will present this outline, notes on the presentation of each speaker, and as a summary a short distillation of the key points presented and the discussions which followed.

Jack Henion

CRITERIA FOR LC/MS TEST STANDARDS

1. Soluble in common LC eluents
2. Stable in solution
3. Commerically available in pure form
4. Thermal instability which would allow an assessment of transfer efficiency of the analyte through the ionization stage
5. Sufficient fragmentation to monitor the affects of heat and charge localization on the extent of fragmentation to allow for the comparison of different interfaces with respect to the degree of fragmentation they induce
6. Abundant fragment ions throughout the mass spectrum
7. A molecular weight high enough to verify high mass transmission, mass assignment and tuning of the MS (especially important for quadrupoles) in the mass range of interest
8. A low K' for rapid elution from HPLC columns
9. A three component mixture would allow a look at three different kinds of test analytes plus an evaluation of the chromatographic integrity
10. Inexpensive
11. Non toxic
12. Quantitative assessment and detection limts

The addition of item 12 to this outline was put forth early in the discussion. In essence a presentation of data using a standard should specifically state the quanitity of material used to generate the spectrum and hopefully show the lower limit detection. It was emphacised that the eleven starting suggested criteria were listed in decreasing order of importance and were offered merely to fuel further thought and suggestions.

Bill Budde

Several compounds were suggested by Bill with some suggestions as to why they would be useful. These include Aldicarb (Temik), M.W.=190 which shows no EI or CI molecular ion but thermospray gives a m/z 208 ($M+NH_4$) and a m/z 222 (M+32) ion. Other suggested fragile compounds such as linuron (MW 248) 1,2-diphenylhydrazine (MW 184) and carbendizim (MW 191) were all offered as particularly fragile organic compounds which are known to exhibit decomposition to varying degree when exposed to excessive heat or active surfaces. It was suggested that these types of compounds could favor one type of LC/MS interface over others, and the rather low molecular weights provides no assessment of higher mass LC/MS performance criteria.

Dai Games

Dai presented a list of criteria that he would use to judge an interface and which any standards should be capable of testing. These included: 1) capable of both normal and reversed phase operation, 2) capable of gradient, 3) ability to identify a compound considering both the target and nontargeted case, 4) ability to perform quantitative work, 5) sensitivity (lower detection limit), and 6) range of compound types interface can handle.

Several compound classes were presented for a detailed evaluation: 1) Mixture of aromatic amino acids of varying polarity. Aromatic amino acids can generally be chromatographed by both normal and reversed phase systems. 2) Mixture of poly nuclear aromatics hydrocarbons which can be easily chromatographed by reversed phase systems. 3) Mixture of neucleosides, such as adenosine, guanosine, cytideine, uridine, and 4) Compounds of interest to your laboratory.

Finally Dai proposed that for a rapid evaluation of an LC/MS interface system the following compounds could be either injected into the liquid stream without going through the LC column or simply spotted on the belt depending upon the interface used: glucose, sucrose, raffinose, stachyose nucleoside eg. adenosine, chloic acid, flavoroid glycosides eg. rutin, and cardiac glycosides.

Dai's take-home message was that the user or potential buyer should best choose a suitable test compound(s) similar to the particular problem at hand.

Paul Goodley

Paul stressed that one should not perform LC/MS tests on compounds that are really amenable to GC/MS. He also noted a desparity of consistant LC/MS results on any compounds run on the varitey of LC/MS interfaces available to date. He showed recent thermospray LC/MS results and a plotted mass spectrum out to nearly m/z 2000 of a polypropylene glycol mixture. Although sometimes difficult to dissolve in common solvents, these mixtures provides a wide range of high mass ions at regular intervals for mass calibration and ion transmission evaluation.

Bob Voyksner

Bob brought up the point that we must define the specific purpose of the standard. A clear distinction exists between those compounds for calibration purposes and those used to test the chromatographic performance of the interface. For calibration purposes he used polypropylene glycol AMW 425 by flow injection analysis. Also polyethyleneglycolmethyl ether AMW=750 is useful. Some discussion followed as to whether the components of these mixtures should be separted by HPLC on-line prior to LC/MS.

AL Yergey

Al further clarified the distinctions that need to be made between standards that are to be used for calibration purposes and those used to test the chromatographic, thermal, and ionization properties of an interface. He presented the following outline.

1. Mass calibration. The compound should have an abundance of ion and this is most conveniently and rapidly done by flow injection analysis, the polyethylene and polypropylene glocols are excellent candidates. Another possibility is butane sulfonate disodium salt (MW=183) which forms cluster ions out to 823 daltons.
2. Compounds for chromatographic evalution include: glucuronide conjugates, catecholamines.
3. Compounds to test for thermal degreadation: adenosein, arginene, acetylecholine, small peptides, such as leucine and methionine enkephalin.

Al suggested that erythromycin might be a good LC/MS test standard and several others agreed.

Summary

Calibration standards: It appears the best compounds for LC/MS system calibration are the polyethylene glycol, or polyethylene glycol methylether polymers. Flow injection analysis is the most convenient way of doing this. However, because these compounds are inherantly mixtures of potentially varying composition they may not be a wise choice for comparative purposes. A polymer of a particular AMW may vary enough between labs to generate confusion when trying to compare results presented from different labs.

Finally, it should be stressed that the LC/MS buyer or user and the instrument manufacturer view the subject of test standards differently. It is not reasonable for a potential customer to ask the manufactureer to solve his research or service problem as part of an evaluation demonstration of an interface. On the otherhand, the customer has a right to see convincing evidence that the particular LC/MS interface under purchase consideration may help solve important analytical problems of interest in his or her laboratory. Representative LC/MS test standards (drugs for pharmaceuticals, pesticides for EPA work, industrial synthetic intermediates, etc) should be evaluated in an on-line LC/MS mode.

The properly executed LC/MS experiment on evaluation should be broken down into three sequential, systematic steps: (suggested by Christine Kenyon, Hewlett Packard Co).

1. Tune and calibrate the MS in the appropriate ionization mode and verify that the MS is operating satisfactorily.
2. Set up for introduction of the LC/MS sample standard into the MS, but conduct flow injection analysis (FIA) type experiments wherein a loop injector injects samples after the LC column and into the flowing HPCL effluent stream. This provides no LC separation, rapid indication of whether the interface is working, and some indication of band broadening resulting from the LC/MS interface.
3. Finally, the chosen LC/MS test standards should be injected such that it passes through the HPLC column, the UV detector if appropriate, and on to the LC/MS interface. In this way the effect of band broadening from the overall system be may assessed, and a realistic assessment of the interface can be obtained in a fully operational on-line LC/MS experiment. Particular attention to the resulting total ion current profile in addition to the extracted ion current profiles should be made with respect to ion current stability and signal to noise of the analyte in question. Remember, unless you have MS/MS you problably want the HPLC column to do some chromatographic separation for you so do not evaluate an LC/MS interface without including the HPCL column in the system!

In general, consensus of the Workshop was that there probably is no ideal LC/MS test standard(s), but the concept, properly exercised for a particular user application is valuable for user evaluation and routine assessment of an operating LC/MS system.

REPORT ON THE VICE PRESIDENT'S WORKSHOP

MASS SPECTROMETERS OF YESTERYEAR

In conjunction with the retrospective theme of the meeting, a workshop was held on Tuesday evening to discuss the instruments of the past. Attendance was good (> 100), with a good distribution of young and not-so-young mass spectrometrists. A fair number of the attendees responded that they had been involved in mass spectrometry for over 20 years with a few admitting to being involved in the field for more than twice that long.

There were three invited presentations. The first of these was given by Bob Finnigan and Mike Story of FINNIGAN/MAT. They presented a first-hand account of some more recent history, that which brought the first quadrupole systems, as residual gas analyzers and then GC/MS systems, to the marketplace.

The next speaker was Harry Svec of Iowa State University. He described some of the history of mass spectrometry prior to the availability of commercial instrumentation. Particularly interesting was the accounts of some of the hardware that he had brought for the historical display. This certainly enhanced the appreciation of the people who saw the display for the effort necessary to be a mass spectrometrist in the early days.

The final scheduled speaker was Sid Evans of KRATOS. He made a presentation complete with photographs of the predecessors to the present-day KRATOS mass spectrometers, starting with the MS-1 made by Metropolitan Vickers. After discussing the MS-1, MS-2, and MS-3, he assured the audience that he was not going to go all the way to the MS-80—only through the MS-10. He briefly explained each of the models, providing pertinent facts and recollections (from his predecessors) on the various instruments.

Following this presentation a question was asked as to where on the time scale did CEC fit in. Earl Lumpkin provided a first-hand account of his dealings with both Metropolitan Vickers and CEC to help answer this question. Following this, Charles Judson provided a brief history of CEC.

The workshop ended with a discussion of what role, if any, should the society take in preserving historical documents and hardware. It was almost unanimously agreed that the society should be encouraged to take an active part in collecting and preserving documents and that if space could be found, set up a permanent display of hardware. It is hoped that the retrospective theme of the conference and this workshop will cause people to pause and think of the significance of old items before they are thrown out and that the society can find and support a site where the history of our discipline can be preserved.

Submitted by:

Gary L. Glish
Oak Ridge National Laboratory

Quantitative Organic Analysis Committee

Workshop on Quantitation Using Desorption Techniques

The workshop discussion focused upon quantitative measurements by fast atom bombardment mass spectrometry. Introductory comments were given by representatives from four laboratories which have been active in applying FAB-MS for quantitation.

Dom Desiderio (University of Tennessee) summarized his approach to measurement of brain peptides by FAB-MS, collision activated dissociation, linked scan, selected ion monitoring using ^{18}O labeled internal standards with a MAT 731 instrument. His samples are prepared by HPLC and analyzed in a glycerol matrix. No problem has been encountered with suppression of ionization by other matrix components using this approach. He is able to measure nanograms of peptide per gram of wet tissue. The standard curve for these measurements is linear over 3-4 orders of magnitude. Although significantly lower signal strength of daughter ions vs. parent ions is observed, the increase in signal to noise ratio obtained by monitoring daughters of preselected parents more than compensates yielding a quite adequate sensitivity for the overall method.

Dave Heller (Johns Hopkins University) summarized work on quantitation of phosphatidylcholines and measurements of relative amounts of glycopeptides in human fibrinogen using an MS-50 instrument scanning over the molecular ion region. Both saturated and unsaturated phosphatidylcholines were measured using a d_6-internal standard in a thioglycerol matrix. Differences were observed in ion current from the saturated vs. unsaturated compounds but quantitation was feasible to submicrogram amounts using standard curves. In discussion it was noted that with measurements of betaine esters using a d_6-internal standard, the deuterated ions appear to be more stable resulting in a standard curve with slope not equal to one. The measurements of human fibrinogen glycopeptides involved measurements of relative amounts of compounds in a sample rather than absolute quantitation. Details are given in paper TPC 19 in this volume.

Bob Murphy (University of Colorado) described work from his laboratory on quantitation of platelet activating factor using a d_3-internal standard. This work is done on a VG 70-70 using short scans with a multichannel analyzer. Using 50 ng of internal standard in a glycerol matrix, the standard curve was linear over the 10-200 ng range studied with the lower limit being determined by the glycerol background. It was noted that the signal to noise ratio vs. amount of sample on the probe first increases, then shows a saturation effect, and finally decreases with increasing sample amounts.

Bill Seifert (University of Texas) described work involving a variety of compounds including ATP, maltose, estrone, enkephalins, dansyllysine, triphenylphosphonium propionic acid, and GABA. This work is done in a 50% aqueous glycerol matrix on a Finnigan 3300 with computer acquired scans. Data was shown for d_o-GABA and d_2-GABA illustrating how increasing amounts of the d_o compound suppress the ion current from the d_2 compound. Standard curves were linear, however, over a useable range.

In summary, the examples discussed in the workshop illustrate that quantitation using FAB is practical providing one is cognizant of potential matrix effects upon ionization of the sample and standard. It appears that optimal results are obtained when samples are purified prior to analysis and when isotope labeled internal standards are used.

Daniel R. Knapp
Department of Pharmacology
Medical University of South Carolina

Workshop: Artificial Intelligence in Mass Spectrometry

Panel Members: Carla Wong, Lawrence Livermore National Laboratory, Livermore, CA
Mache Creeger, LMI (LISP Machines Inc.), Los Angeles, CA
John Kunz, IntelliGenetics, Menlo Park, CA
Bo Curry, Hewlett-Packard, Palo Alto, CA
Larry Masinter, Xerox PARC, Palo Alto, CA
Elaine Rich, University of Texas, Dept. of Computer Science, Austin, Texas

Carla Wong introduced the workshop by illustrating how artificial intelligence (AI) techniques were being used at Lawrence Livermore National Laboratory to optimize the tuning procedures of a triple quadrupole mass spectrometer (TQMS) throughout the entire mass range. The difference between "good" tuning and "bad" tuning were shown as a comparison of peak shape when only one tuning parameter, (of the more than 25 available on a TQMS) was out of range. This example was used to introduce the kinds of problems artificial intelligence techniques can address; the kinds of languages and software needed; the difference in AI computers and traditional computers; and, the kinds of problems one must deal with when implementing AI systems.

Mache Creeger described the three types of computing hardware available which were designed specifically to do LISP processing. He also gave detailed information on the memory, speed configurations, product specifications and language available to these processors. These machines are the Xerox Corporation's D-series machine (DORADO, DOLPHIN and DANDELION); the Symbolics Corporation's 3600 machine; and, the LMI LAMBDA machine. In addition to presenting the specification details, comparisons between the machines were given.

John Kunz showed diagrams illustrating the concepts addressed by artificial intelligence and knowledge engineering in determining what kind of knowledge can be integrated and encoded. Separation of the various types of knowledge (declarative, procedural, etc.) from the rules, etc. and then integration of these separate parts into a unified approach at emulating the human expert's reasoning was shown to be a non-trivial, but essential task in the development of expert systems. The knowledge engineering tools (i.e. programming aids) available can simplify trying to develop AI guided, expert systems "from scratch" using LISP.

Bo Curry discussed AI in data interpretation where "independent" domain databases or domain experts in GC, MS (STIRS), IR, or NMR could be used as objects responding to request by a "controller" which has access or is interfaced to a "reasoner" (probably rule based), a molecular assembler (CONGEN) and a human. This would enable more complete evaluation of, testing of and reevaluating of propositions relevant to the determination of the identity and structure of a compound. He also discussed what communication pardigms might be relevant among these autonomous or semi-autonomous "experts" and how conflict resolution between the experts might be resolved by meta-rules or comparison of certainty factors.

Elaine Rich and Larry Masinter both emphasized the point that AI was not the ultimate cure for every problem scientists might have. Elaine very neatly summarized AI as: That attempt by computer scientists to make computers do what we already know that people do better!

She went on to explain the uses of AI as an "aid" to humans; an attempt to take over the more tedious aspects of problem solving to allow humans more time for the very difficult or creative aspects of problem solving. AI or expert systems are also "aids" in the form of an "untiring" teacher or tutor who passes on the codified knowledge of the expert to new students or novices. There was also a caution as illustrated by a "butterfly identification" problem as to how difficult it was to acquire and codify the kind of knowledge that makes reasoning and decision making possible.

Larry Masinter reminded everyone that the "expert systems" area of AI is based on work that was done and was well-understood by AI researchers ten years ago. The really difficult problems of 10 years ago related to reasoning, understanding, learning etc. were not solved then, and are still difficult problems being worked on today!

The workshop was well attended by approximately 200 people. Questions ran to the end of the allotted time whereupon the panel continued to answer questions outside the lecture room for another 1/2 hour.

It was suggested by several people that the workshop had served as a good introduction to: what AI is; what new kinds of computer hardware and software is needed; what problems it can aid in the solution of; and, what problems it cannot solve. It was further suggested that a follow-on workshop next year (San Diego) might have a number of "progress reports" from laboratories other than LLNL and HP who are interested in what AI can do for MS.

Report submitted by:

Carla M. Wong
Analytical Chemistry Section
Lawrence Livermore National Laboratory
Livermore, CA 94550

High Temperature and Inorganic Solids Committee

WORKSHOP on

Electron Impact Ionization Cross Sections

David Bonnell & Edmond Murad, Presiding

The primary discussion was organized into three broad areas, (1) Experimental determinations, past and present, (2) Theorectical calculations, and (3) Current problems in the field. Wade Fite, of Extranuclear Labs, Inc., kindly provided background information on the requirements of experimental determinations, as the difficulties associated with good electron impact ionization cross section measurements are not widely appreciated.

The state of theoretical and semi-empirical calculations was discussed. It was noted that calculations for atomic species, particularly at electron energies much greater than (4 to 20 times) the threshold values, seem to be approaching a consensus, reflecting a relative maturity in the various methods, e.g. the Coulomb-Born method, the scaled hydrogenic method, or the distorted wave Born approximation. The Born and Coulomb-Born methods are not valid near threshold, and require experimental or semi-empirical methods to provide threshold information. The literature reveals continuing research activity in atomic cross section determinations, in response to the needs of high energy physics and astrophysics. However, the situation for molecular species other than simple gases such as atmospheric components, has not apparently improved recently. Conspicuously absent is any widespread effort to promote determination of electron impact cross sections of condensable or high temperature molecules. Mass spectroscopists, particularly in the high temperature community, have come to the realization that general methods for estimating cross sections for pressure measurements are inadequate. A major problem is the need to separate the many individual experimental factors contributing to the overall ionization process. These factors include ionization process factors (discussion included, e.g., excess energy effects on ion extraction efficiency and temperature dependent fragmentation phenomeona), the mass analyzer transmission function, and detector (multiplier) mass dependent gain functions, which need to be determined independently to isolate them from the electron impact cross section. Techniques to separate these effects are generally less well developed than overall system calibration methods.

Techniques for estimating cross sections of molecules have apparently not improved significantly since the publishing of a consistant set of maximum atomic cross section tables by J. B. Mann (J. Chem. Phys., 46) in 1967. The empiricism is still additivity-of-atomic-cross sections. Workshop discussion of the additivity approximation indicated that, although simple summation of atomic cross sections is generally poor, more satisfactory results have been obtained using scale factors other than unity. This is particularly the case for similar types of molecules (e.g. low polymers of inorganic species). General evidence for a factor of the order of 2/3 was mentioned (see WOA 10) and it was noted that this factor is similar to the value obtained by assuming that ionization cross sections are proportional to atomic radius squared or to $V^{2/3}$, where V is atomic volume. Additivity of atomic volumes would then suggest a factor of 0.79. However, as atomic volumes are highly dependent on bonding, additivity empiricisms need to be modified for bonding effects. It was noted that integral total ionization cross sections (ionization gauge sensitivities) have been shown recently (Bartmess & Georgiadias, Vacuum, 33, 1983) to correlate with easily estimated polarizabilities. The use of atomic cross sections at maximum also leads to uncertainties in estimations of molecular cross sections. The peaks in ionization cross section vs. electron energy are not located at uniform "distances" from threshold, nor are the shapes of ionization efficiency curves uniform among species. Hence scaling laws dependent on such assumptions can fail. Recent results of a semi-empirical treatment by Chandra, et al, (Physica 83C, 1976) which takes this into account show promise, but require experimental relative cross section values and maxima locations.

In general, the consensus of opinion of the 35 people present was that more effort should be devoted by mass spectroscopists to converting their instrument sensitivity factors to a relative ionization cross section form, thereby providing a more extensive data base for theoreticians. It was noted by participants that the large compendia of organic mass spectra being collected have both cross section and instrument factors convoluted into them, complicating use for quantitative purposes. Most of the participants agreed that data bases of reliable cross sections with estimating rules would be valuable, but noted the difficulty of supporting such an effort for the diversity of interests represented.

ISOTOPE RATIO MEASUREMENTS USING MULTIPLE COLLECTORS

The Isotope Ratio Committee sponsored this workshop on the specific application of multiple collectors for isotope ratio measurements of elements from hydrogen through uranium. This year's workshop was held on Thursday, May 31, with approximately 60 people in attendance. The emphasis of this workshop was on the experimental uses of multiple detectors as well as some of their general problems and benefits. Four brief presentations were made followed by questions and answers and lively discussions.

The first speaker was Dr. L. K. Herzog, president of Nuclide Corporation. He started his talk by describing the major advantages of using simultaneous detectors, higher sensitivity, the potential for higher sample throughput and the ability to provide useful data with a rapidly varying ion current. He then gave examples of historic machines that had been used with simultaneous detectors in the early 40's in the Manhattan Project. Finally, Dr. Herzog described some of the instruments currently available for simultaneous isotopic analysis.

The second speaker Dr. K. Habfast, a staff scientist working for Finnigan MAT, spoke in detail on the performance of multicollector systems used with thermal ionization sources. His discussion dealt with the accuracy and precision attainable with simultaneous detectors, the sources and propagation of errors and the methods of calibration. With currently available commercial systems and large samples the precision is sufficiently high to make the error limits of available standards a major source of uncertainty.

The third speaker was Dr. Patrick Turner of V. G. Instruments. He pointed out some of the advantages of individually movable multiple collectors. He then showed results using a combination of both Faraday collectors and a Daly type detector used simultaneously. He also presented data that showed the same high levels of precision on solid samples as the previous speaker.

The final speaker was Dr. Justin Halverson of Savannah River Laboratory. As a user he pointed out that detectors and source electronics stability were very important in achieving the precisions the previous speakers said were possible. Relatively small changes in source focusing parameters also could significantly change the isotopic ratios measured.

Simultaneous detectors for mass spectrometers are now commercially available with practical performance for isotopic ratio measurements that make them most desirable for laboratories with the need for high precision and

accuracy,as well as large enough sample sizes to use Faraday collectors. Future developments, it can be hoped, will lead to detector systems with a larger number of individual detectors and higher sensitivity on a path to the goal of an electronic equivalent of the photoplate.

A brief meeting of the Isotope Ratio Committee occurred after the workshop. Potential topics for next years conference were discussed. The desire for improved scheduling to avoid conflicts between instrumentation and isotopic analysis papers was expressed. A vote of thanks was given to Lura Powell, the outgoing chairperson, for her efforts on behalf of the committee over the past two years.

Respectfully submitted,

John D. Stein

COMPUTER APPLICATIONS COMMITTEE REPORT

Wednesday May 30, 2:30 PM

This year's meeting of the computer applications committee consisted of an ad-hoc gathering of about 15 people in the Garden Terrace. Most had attended both of the committee sponsored workshops (Artificial Intelligence on Tuesday, and Microcomputers on Wednesday), and the general feeling was that these two areas were likely to make the greatest impact on data processing in the future. Indeed, many seem to regard traditional mini-computer based data systems as somewhat of a dead issue for the future. Current trends indicate that in a few years all traditional data system type of computing will be microcomputer based, with larger computers being used primarily for Artificial Intelligence type of applications; this was reflected in a reduced number of topics which were mentioned for next year.

Given the upsurge in microcomputers, most people felt that it would be valuable to have a plenary lecture (i.e. an 11:30 type rather than an 8:30 type) on the general topic of "Future Trends in Microcomputers in Mass Spectrometry". There are a number of people who have worked in this area for several years, who should be well qualified to discuss the subject. Such a lecture should complement this years retrospective lecture by Klaus Biemann very nicely.

Bruce Colby (from S-Cubed) volunteered to organize a workshop on Artificial Intelligence, but with the idea of focussing mainly on the applications, rather than the design as was done this year. Several people expressed a greater desire to better understand what current A.I. technology can do to help them, so this should be an interesting topic. Bruce is a newcomer to this committee, so he would appreciate a call from anyone working in this area, or anyone with any ideas on specific topics they would like to see covered (P.O. Box 1620, LaJolla, CA 619-453-0060).

Computer Networks was also mentioned as a possible topic for a workshop, although no volunteers came forward. As data systems shrink in size, and the number of users per system increases, effective networks become more important to overall throughput. If anyone wishes to organize a workshop in this area, contact me; otherwise we will settle for a few posters as part of the regular Computer Applications session.

Last, but certainly not least, Bob Minard of Penn State was elected (nearly unanimously) as the new committee chairman (subject, of course, to board approval). Anyone with any other ideas for next year should contact him.

I will close by thanking both of this year's workshop organizers Carla Wong and Bob Minard, as well as Klaus Biemann and Paul Sigler for two very informative lectures.

Respectfully submitted

D. Thomas Terwilliger

D. Thomas Terwilliger

ASMS EDUCATION COMMITTEE REPORT

The Education Committee once again offered two courses on the weekend preceeding the Annual Conference on Mass Spectrometry and Allied Topics. Due to low registration at the dedline for advanced registration, only the Quantitative Mass Spectrometry course was offered; the advanced registration was 2:1 in favor of this course. Prospective students who desired the Interpretation course were offered the option of taking the Quantitative course or getting their money back. All but one decided to take the course offered. The two lectures on instrumentation that are normally offered were combined, and the rest of the course outline remained the same. The faculty for the two courses is given below, but only Drs. Callery, Strong, White and Yergey taught this year.

Dr. Patrick Callery, University of Maryland at Baltimore, Baltimore, MD.
Dr. Robert Cotter, The Johns Hopkins School of Medicine, Baltimore, MD.
Dr. Peter Dreifuss, Bureau of Foods, F.D.A., Washington, D.C.
Dr. Henry M. Fales, NHLBI, National Institutes of Health, Bethesda, MD.
Dr. James Kelley, NCI, National Institutes of Health, Bethesda, MD.
Dr. John Strong, NCI, National Institutes of Health, Bethesda, MD.
Dr. Edward White V, National Bureau of Standards, Washington, D.C.
Dr. Alfred L. Yergey, NICHD, National Institutes of Health, Bethesda, MD.

Based on course evaluations received from the students, the course was very successful, with most students achieving their goals.

In a committee meeting following the courses, it was decided to recommend to the Board of Diresctors of the Society that both courses be offered next year, but that a concerted effort be made to publicize the courses well before the meeting in places that have not been previously reached by our announcements. It was also suggested, for the second time, that the courses be offered during the year for local groups. After discussing the complexities and expected high expenses of such an effort, it was decided to propose offering the courses in the Washington, DC local area to test the response and to keep expenses to a minimum. Finally it was recommmended that registration be closed earlier than has been done in the past, with an increased tuition for late registration, so that the courses can be directed more effectively toward the specific interests of the students.

Respectfully submitted,

Alfred L. Yergey
Education Chairman

ENVIRONMENTAL COMMITTEE REPORT, 1984

Workshop: The Mass Spectrometrist's Guide to Dioxins

This workshop consisted of three presentations:

"Are dioxins really in mammals"
Prof. M. L. Gross, University of Nebraska

"Where do dioxins come from?"
Dr. J. M. Czuczwa, Indiana University

"Do dioxins have an impact in New York state?"
Dr. D. R. Hilker, New York Department of Health

The workshop was attended by about 150 people. Intellectual stimulation was had by all.

Committee Meeting

The committee meeting resulted in the following suggestions for symposia and/or workshops at the 1985 meeting:

- "Alternate ionization techniques for environmental analysis (NCI, FAB, DCI, etc.)"
- "NCI operating conditions (pressure, temperature, concentration, standardization, etc.)"
- "The use of mass spectrometry for regulation and litigation"
- "Dioxins and furans other than 2378-TCDD"

Submitted by

Ronald A. Hites
Indiana University
Bloomington, IN 47405

GOOD LABORATORY PRACTICES WORKSHOP/COMMITTEE MEETING

The Good Lab Practices (GLP) Workshop was held May 28 at 1:15 and was attended by 45-55 people. A brief history of the committee's work was given, with references to some pertinent documents available (1, 2).

Jim Sphon, of the FDA, presented an outline of mass spectrometric procedures in his lab. The FDA has developed a document (3) on GLP that must be followed in work relating to the Federal Food, Drug, and Cosmetic Act, or Public Health Service Act.

Mike Hoffman, of the USDA at Beltsville, stressed the importance of QA/QC programs to ensure GLP. A great deal of their work involves drug and pesticide residue analyses. Their analysts are tested and qualified at a central location; blind samples are frequently provided to check the sample work. Quality Assurance Officers at each site keep track of the program.

Ron Hass, NIEHS at the Research Triangle Park, led a discussion of some of the problems of low level determinations. He felt that the single strongest analytical evidence for a compound "identification" was an accurate mass measurement/empirical formula. Low concentrations require more proof of structure than is often done. Their lab has found instances of TCDD analyses where GC/metastable decomposition monitoring gave a factor of 3 less 2,3,7,8-TCDD than GC/high resolution MS. The NIEHS lab has established their own QA/QC procedures. During quantitation, every third sample is a reference. All data for publication are kept for 7 years; archived runs are stored on magnetic tape.

Bori Sushan, SCIEX Inc., described some of the fundamental GLP and analytical problems one might encounter during triple quadruple MS/MS work. Since the first step of most MS/MS experiments is chemical ionization, it is important to check that the reagent ions are never depleted during a run. The three quadruples must work properly together to avoid mass discrimination effects during a scan. The Rf on Q2 must be optimized and regulated relative to Q3. The DC rod offset on Q3 should also be carefully measured and optimized. Branching and fragmentation ratios will change with conditions in Q2. These ratios, for some standard, should be used to check and demonstrate system performance.

There were many suggestions for next year's session. A lot of discussion centered around the issue of what constitutes an "identification", particularly when very high confidence levels are necessary. Quentin Thomas mentioned that this has been defined, in one context, by the EPA (4, 5). How many ions and ratios should be monitored during MPM? How can one avoid false positives and negatives during library searches? What are the potential problems in validating a method that will be reviewed by "outsiders"? Can computers be used more effectively to meet and document GLP requirements? Data archiving - how much, how long, what media? What is the cost (time and $) of GLP versus the cost of not doing GLP?

Respectfully submitted,

Phil Price

Philip C. Price

1. 26th Annual Conference on Mass Spectrometry and Allied Topics, St. Louis, MO, May 28 - June 2, 1978. pp. 761-770.
2. 31st Annual Conference on Mass Spectrometry and Allied Topics, Boston, MA, May 8 - 13, 1983. p. 955.
3. "Good Laboratory Practice for Nonclinical Laboratory Studies". Title 21, Code of Federal Regulations, Part 58. Superintendent of Documents, Government Printing Office, Washington, D. C. 20402.
4. Federal Register. Vol. 44, #233, Sect. 14, Dec. 3, 1979, p. 69543. Superintendent of Documents, Government Printing Office, Washington, D. C. 20402.
5. EPA Test Method - Base/Neutrals and Acids, EPA-625/4-82-057, July 1982. USEPA, 26 W. Saint Clair St., Cincinnati, OH 45268.

ISOTOPE RATIO COMMITTEE REPORT

The Committee on Isotope Ratios sponsored sessions on Resonance Ionization and Isotope Ratio Measurements, and workshops on Reporting of Statistical Data and Multiple Collectors at the 1984 ASMS meeting. All sessions were well attended and the topics evoked lively discussions among the participants. Thanks go to Charles Miller for organizing and chairing the Isotope Ratio session, to James Delmore for presiding over the Isotope Ratio contributed session, to Keith Eberhardt for presenting the workshop on Reporting of Statistical Data and to John Stein for organizing and chairing the Workshop on Multiple Collectors.

Several suggestions for next year's program were brought up at the Committee Meeting. Several committee members asked that Isotope Ratio activities be scheduled opposite Organic/Biological Sessions as opposed to sessions such as Instrumentation. The ASMS board has agreed to this scheduling for our group whenever possible. Suggestions for next year's program included a workshop on the emerging technique of ICP-MS for isotope ratio measurements, a continuation of the multiple collector workshop in which users would detail benefits and problems associated with these collectors, and an all day symposium/workshop dedicated to sample preparation for isotope ratio mass spectrometry. This topic has been suggested by a number of participants over the past several years and would include such topics as chemical preparation of a variety of samples, the preparation and use of standards, and filament mounting techniques.

My term as committee chairman expires June 30, and the incoming ASMS President, Graham Cooks, will be choosing my successor. I hope that you will give your new chairman the same level of support and cooperation that you have given me over the past four years.

Respectfully submitted,

Dura J. Powell
Chairman

Qualitative Organic Committee

The annual meeting of the Committee was held at 1:15 p.m. on Wednesday, May 30 with approximately 15 people present. After a brief discussion of the purposes of the committee, there was a free-ranging discussion of possible topics for symposia and workshops for the 1985 Conference. Topics proposed included "Mechanisms of FAB/SIMS Induced Fragmentation", "Negative Ion CI for Structural Studies", "Selection of Ionization Methods for Non-Volatile Molecules" and "Accurate Mass Measurements". Final selection from these topics will be made as a result of consultation between the chairman, the chairman of the Fundamentals Committee, and the Vice-President Programmes.

A.G. Harrison
Chairman

COMMITTEE REPORT

The Committe on High Temperatures and Inorganic Solids held its meeting following following the Workshop on Electron Impact Ionization Cross Sections. About 30 attendees stayed for the Committee Meeting, during which three items were considered:

a. Papers on high temperature topics were scattered throughout the program and that made it difficult for our members to interact with each other.

b. Because of overlapping interests with the Committee on Fundamentals in the area of metal ion thermochemistry and reactions, a suggestion was made that our committee sponsor a joint symposium with the Committee on Fundamentals on topics related to metal ion properties.

c. A suggestion was made to hold a workshop on laser vaporization and ionization of solids.

Edmond Murad
Chairman

ASMS COMMITTEE ON NOMENCLATURE

SAN ANTONIO, 1984

The meeting of the Nomenclature Committee was held on May 26, 1984, and it was attended by 10 people including the Chairman. The Chairman gave a brief history of the actions of the Committee since 1979. The history was deduced from reports of the Committee meetings published in the Bound Volumes from 1979 through 1983. It was particularly pointed out that 370 terms and expressions referring to mass spectrometry have been defined and given in these issues of the Bound Volume, and it may be concluded that the Committee has been very active. It was also deduced from the report of the 1983 meeting of the Committee that action was required at the 1984 meeting on the six terms listed on p. 970 of the 1983 Bound Volume under the heading, "Definitions for Consideration" and on the 58 terms given on pp. 904-909 of the 1982 Bound Volume starting with the terms under the heading "Secondary Ion Mass Spectrometry."

The Committee voted to accept all of the terms under consideration on p. 970 of the 1983 Bound Volume with the exception of the definition of Preformed Ions, which was deleted as being obvious and unnecessary. A small editorial change was made on the definition for Average Mass. The Chairman regrets that the maker and seconder of the motion on these matters was inadvertently not recorded.

It was moved by J. Yergey and seconded by J. Hiller not to accept any of the terms referring to Secondary Ion Mass Spectrometry given on pp. 904-907 of the 1982 Bound Volume. The motion carried. However, in addition it was moved by T. Lehman and seconded by K. Busch that these terms and their definitions be given to the organizers of the conference on secondary ion mass spectrometry going to be held this Fall. The motion carried, and the Chairman asked Dr. Lehman to undertake the action called for by the motion. He agreed to do this.

In the material received by the Chairman from the previous Chairman was a list of 268 terms relating to computers and computer technology. The correspondence examined by the Chairman seemed to imply that these terms should be considered at the 1984 meeting of the Committee. Consequently they were examined with as much care as was possible given the very large number of terms and the relatively limited time of the meeting. It was moved by H. Fales and seconded by J. Yergey that these terms not be accepted by the Committee. The motion passed unanimously.

It was moved by J. Watson and seconded by J. Yergey that the Chairman bring together all of the terms which have appeared in the Bound Volumes through 1983 (and including those approved at this meeting) to make one complete list for easy reference by members of ASMS and mass spectrometrists in general. The Chairman agreed to do this, and the resulting list is included as part of this report.

The Committee discussed the question of what should be the future actions of the Committee. In view of the large number of terms already defined, the sense of the meeting was not to consider any new category of terms for the next year. However, the Committee agreed to meet at the next ASMS meeting to consider further activities.

F.H. Field
Chairman
6 June 1984

COMBINED LIST OF DEFINED TERMS

ANALYZERS

Electrostatic Analyzer. A velocity focusing device composed of means for producing an electrostatic field perpendicular to the direction of ion travel. Effect is to bring to a common focus all ions of a given kinetic energy. Usually used in combination with a magnetic analyzer for mass analysis.

Magnetic Analyzer. A direction focusing device composed of means for producing a magnetic field perpendicular to the direction of ion travel. Effect is to bring to a common focus all ions of a given momentum with the same mass to charge ratio.

Quadrupole Analyzer. A mass filter consisting of means of creating a quadrupole field of a constant component and a varying component in such a manner as to allow transmission of only a selected mass-charge ratio.

Time of Flight Analyzer. A device consisting of a means to measure the flight time of particles with an equivalent kinetic energy over a fixed distance.

Wien Analyzer. A velocity filter composed of means for creating crossed homogeneous electric and magnetic fields such that only ions of a fixed velocity are transmitted.

Mass Resonant Analyzer. A mass analyzer composed of means for mass dependent resonant energy transfer and measurement of the resonance frequency, power or ion current of the resonant ions.

(The following are standard instrumental configurations utilizing one or more of the above techniques.)

Double Focusing Analyzer. The combination of a magnetic analyzer and electrostatic analyzer in either sequence to effect direction and velocity focusing.

Ion Cyclotron Resonance Analyzer. A device to determine the mass of an ion by measuring its resonant frequency.

Ion Trap Analyzer. A mass resonance analyzer composed of means for creating a three dimensional rotationally symmetric quadrupole field capable of storing ions at selected masses.

Mass Spectrometer Configurations. Multianalyzer instruments should be named for the analyzers in the sequence in which they are traversed by the ion beam, where B is for a magnetic analyzer, E for an electrostatic analyzer, Q for a quadrupole analyzer, TOF for time of flight analyzer, and ICR for an ion cyclotron resonance analyzer. For example, we have a BE mass spectrometer ("reversed" geometry double focusing instrument), BQ mass spectrometer (hybrid sector and quadrupole instrument), EBQ (high resolution followed by a quadrupole). Note that a triple quadrupole which has two mass analyzers is a QQ mass spectrometer. Problem: Time of flight, simultaneously or sequentially with other mass analyzers.

DATA SYSTEM

Data Acquisition The process of transforming representations of (spectrometer) signals from their original form into suitable representations, with or without modification, in conjunction with a computer system.

Real Time In data acquisition in Real Time the computer representations are generated within the same time frame as the original experiment.

Off-Line In this method of data acquisition there is some (time) discontinuity in the transfer or transformation of the representations.

Data Logging is a more specific term implying data collection from more than one relatively low frequency source with storage of the collected data for later processing.

Hardware The term used for the physical components of a computer system.

Software This term is used to describe computer programs, whether inside or outside a computer, and whether they are machine readable or normally legible.

Firmware Computer programs stored in a semi permanent form, usually semi conductor memory, and used repeatedly without modification. Firmware can be changed only by exchanging or removing hardware.

Pre-Processor A device in a data acquisition system which performs a significant amount of data reduction, extracting specific information from raw signal representations, in advance of the main processing operation.
A preprocessor may constitute the whole of a data acquisition interface, in which case it must also perform the data acquisition task (spectrometer signal to computer representation conversion), or it may specialise solely in data treatment.

Hard Wired A preprocessor may be hard wired, that is capable of performing only certain defined tasks and no others without major physical modification.

Pre-Programmed A preprocessor may be pre-programmed, that is, it can be a general purpose device incorporating specific but readily alterable instructions to perform a particular task.

Signal Conditioning The process of altering the relationship of a transducer (spectrometer) output with respect to time or other parameters (frequency, voltage or current).

Signal Processing The mechanism of analysing, routing, sampling or changing the representation of a signal.

Operational Amplifier A high gain DC voltage amplifer with high input impedance, low output impedance and the capability of producing a bipolar output from a bipolar input.

Amplifier Complex A number of operational amplifiers configured for a specific function, packaged as a single unit and used as such.

Amplifier Bandwidth The range of signal frequencies over which an amplifier is capable of undistorted or unattenuated transmission. An Operational Amplifier should transmit DC voltage accurately and the upper (bandwidth) limit is defined as the 3 db point (factor of 2 attenuation).
Bandwidth can vary with gain and hence Gain-Bandwidth Product can be a more useful parameter.

Amplifier Noise This can be of two kinds, White Noise which is random signal fluctuations whose power spectrum contains all frequencies equally over a specified bandwidth and Pink Noise where the frequencies diminish in a specified fashion over a specified range.

Differential Amplifier An (operational) amplifier which has two inputs of opposite sense gain polarity with respect to its output. Differential Ouput Amplifiers with two opposite sense outputs, also exist.

Single-ended Amplifier An (operational) amplifier with a single input (or output).

Analogue Signal This is a signal which can be expressed as a continuously variable mathematical function of time.

Digital Signal This is a signal which represents information in a computer-compatible form as a sequence of (binary) numbers which may describe discrete samples of an analogue signal.

IONIZATION NOMENCLATURE

Electron Ionization This is the term used to describe ionization of any species by electrons. The process may, for example, be written

$$M + e^- \rightarrow M^{+\cdot} + 2e^- \quad \text{for atoms or molecules,}$$

and $$M^{\cdot} + e^- \rightarrow M^+ + 2e^- \quad \text{for radicals.}$$

Photo-Ionization This is the term generally used to describe ionization of any species by photons. The process may, for example, be written

$$M + h\nu \rightarrow M^{+\cdot} + e^-$$

[Note: Electrons and photons do not "impact" molecules or atoms. They interact with them in ways that result in various electronic excitations including ionization. For this reason it is recommended that the terms 'Electron impact' and 'Photon impact' be not used].

Field Ionization This term relates to the removal of electrons from any species by interaction with a high electrical field.

Field Desorption This term is used to describe the formation of ions in the gas phase from a material deposited on a solid surface (known as an 'emitter') in the presence of a high electrical field. 'Field desorption' is an ambiguous term because it implies that the electric field desorbs a material as an ion from some kind of emitter on which the material is deposited. There is growing evidence that some of the ions formed are due to thermal ionization, some to field ionization of vapor evaporated from material on the emitter. Because there is little or no ionization unless the emitter is heated by an electric current, 'field desorption' is a misnomer. The term is however firmly implanted in the literature and most users (by no means all) understand what is going on regardless of the implications of the term. In addition, no better simple term has been suggested to take its place and so, reluctantly, it is recommended that it be retained.

Chemi-ionization and chemical ionization are two terms which should not be used inter-changeably.
Chemi-ionization refers to a process whereby gaseous molecules are ionized when they interact with other internally excited gaseous molecules or molecular moieties.
Chemical ionization concerns the process whereby new ionized species are formed when gaseous molecules interact with ions. The process may involve transfer of an electron, proton or other charged species to or between the reactants. When a positive ion results from chemical ionization, the term may be used without qualification. When a negative ion results, the term negative ion chemical ionization should be used.

Surface Ionization takes place when an atom or molecule is ionized when it interacts with a solid surface. Ionization only occurs when the work function of the surface, the temperature of the surface, and the ionization energy of the atom or molecule have an appropriate relationship.

Thermal Ionization takes place when an atom or molecule interacts with a heated surface or is in a gaseous environment at high temperatures. [Examples of the latter may be a capillary arc plasma, a microwave plasma, or an inductively coupled plasma].

Atmospheric Pressure Ionization is an ambiguous term. In essence, it is used to describe chemical ionization at atmospheric pressure. It is recommended that use of the term should be discouraged.

Spark (Source) Ionization occurs when a solid sample is vaporized and partially ionized by an intermittent electric discharge. Further ionization occurs in the discharge when gaseous atoms and small molecular moieties interact with energetic electrons in the intermittent discharge. It is recommended that the word 'source' be dropped from this term.

Auto-ionization occurs when an internally supra excited atom or molecular moiety loses an electron spontaneously without further interaction with an energy source. (The state of the atom or molecular moiety is known as a pre-ionization state).

Associative Ionization occurs when two excited gaseous atoms or molecular moieties interact and the sum of their internal energies is sufficient to produce a single, additive ionic product.

Multi-photon Ionization occurs when an atom or molecule and their concomitant ions have energy states whereby the energy in two or more photons can be absorbed.

Penning Ionization occurs through the interaction of two or more neutral gaseous species at least one of which is internally excited.

Charge Exchange (Charge Transfer) Ionization occurs when an ion/atom or ion/molecule reaction takes place in which the charge on the ion is transferred to the neutral species without any dissociation of either.

Ion-Pair Formation involves an ionization process in which a positive fragment ion and a negative fragment ion are the only products.

Ionization Cross Section This is a measure of the probability that a given ionization process will occur when an atom or molecule interacts with an electron or a photon.

Electron Attachment A resonance process whereby an external electron is incorporated into an atomic or molecular orbital of an atom or molecule.

Ionization Energy This is the minimum energy of excitation of an atom, molecule or molecular moiety required to remove an electron in order to produce a positive ion.

Vertical Ionization This is a process whereby an electron is removed from a molecule in its ground or an excited state so rapidly that a positive ion is produced without change in the positions or momenta of the atoms. The resultant ion is often in an excited state.

Adiabatic Ionization A process whereby an electron is removed from the ground state of an atom or molecule producing an ion in its ground state.

Ionization A process which produces an ion from a neutral atom or molecule.

Dissociative Ionization An ionization process in which a gaseous molecule decomposes to form products, one of which is an ion.

Ionic Dissociation A decomposition of an ion into another ion of lower formula weight and one or more neutral species.

Ionization Efficiency is the ratio of the number of ions formed to the number of electrons or photons used.

An Ionization Efficiency Curve shows the number of ions produced as a function of the energy of the electrons or photons used to produce ionization.

Laser Ionization occurs when a sample is irradiated with a laser beam. In the irradiation of gaseous samples, ionization occurs via a single- or multi-photon process. In the case of solid samples, ionization occurs via a thermal process.

Desorption Ionization (DI). General term to encompass the various procedures (secondary ion mass spectrometry, fast atom bombardment, californium fission fragment desorption, thermal desorption) in which ions are generated directly from a solid sample by energy input.

TYPES OF IONS

Positive Ion This is an atom, radical, molecule or molecular moiety which has lost one or more electrons thereby retaining an electrically positive charge. The use of the term cation as an alternative is not recommended. The use of mass ion is not recommended.

Negative Ion An atom, radical, molecule or molecular moiety in the vapor phase which has gained one or more electrons thereby acquiring an electrically negative charge. The use of the term anion as an alternative is not recommended.

Singly-, Doubly-, Triply- etc. Charged Ion These terms are used to describe an atom, molecule or molecular moiety which has gained or lost one, two, three or more electrons. The term multiply-charged ion is used to refer to ions that have gained or lost more than one electron where the number of electrons lost or gained is not designated.

Parent Ion An electrically charged molecular moiety which may dissociate to form fragments, one or more of which may be electrically charged, and one or more neutral species. A parent ion may be a molecular ion or an electrically charged fragment of a molecular ion.

Fragment Ion An electrically charged dissociation product of an ionic fragmentation. Such an ion may dissociate further to form other electrically charged molecular or atomic moieties of successively lower formula weight. (See also Daughter Ion).

Daughter Ion An electrically charged product of reaction of a particular parent ion. In general such ions have a direct relationship to a particular precursor ion and indeed may relate to a unique state of the precursor ion. The reaction need not necessarily involve fragmentation. It could, for example involve a change in the number of charges carried. Thus, all fragment ions are daughter ions but not all daughter ions are necessarily fragment ions.

Rearrangement Ion An electrically charged dissociation product, involving a molecular or parent ion, in which atoms or groups of atoms have transferred from one portion of a molecule or molecular moiety to another during the fragmentation process.

Stable Ion An ion which is not sufficiently excited to dissociate into a daughter ion and associated neutral fragment(s) or to react further in any other way.

Unstable Ion An ion which is sufficiently excited to dissociate within the ion source.

Metastable Ion An ion which is sufficiently excited to dissociate into a particular daughter ion and neutral species during the flight from the ion source to the detector. The dissociation is most readily observed when it takes place in one of the field-free regions in a mass spectrometer.

Precursor Ion This term is synonymous with Parent Ion.

Product Ion This term is synonymous with Daughter Ion.

Molecular Ion An ion formed by the removal (positive ions) or addition (negative ions) of one or more electrons from a molecule without fragmentation of the molecular structure. The mass of this ion corresponds to the sum of the masses of the most abundant naturally occurring isotopes of the various atoms that make up the molecule (with a correction for the masses of the electrons lost or gained). For example, the mass of the molecular ion of ethyl bromide, C_2H_5Br will be 2x12 plus 5x1.0078246 plus 78.91839 minus the mass of the electron (m_e). This is equal to 107.95751 u - m_e, u being the unit of atomic mass based on the standard that the mass of the isotope ^{12}C = 12u exactly.

Isotopic Molecular Ion A molecular ion containing one or more of the less abundant naturally occurring isotopes of the atoms that make up the molecular structure. Thus, for ethyl bromide there exist molecular isotope ions such as $^{13}CCH_5Br^{+\cdot}$, $C_2H_4D\ Br^{+\cdot}$, $C_2H_5{}^{81}Br^{+\cdot}$, $^{13}C_2H_5{}^{81}Br^{+\cdot}$ etc.

Isotopic Ion Any ion containing one or more of the less abundant naturally occurring isotopes of the elements that make up its structure.

Isotopically Enriched Ions When the abundance of a particular isotope is increased above the level at which it occurs in nature and is incorporated in a molecule the term "isotopically enriched ion" is used to describe any ion containing the enriched isotope.

Dimeric Ion An ion formed either when a chemical species exists in the vapor phase as a dimer and can be detected as such, or when a molecular ion can attach to a neutral molecule within the ion source to form an ion such as $[2M]^{+\cdot}$ where M represents the molecule.

Protonated Molecule An ion formed by interaction of a molecule with a proton abstracted from an ion, as often occurs in Chemical Ionization according to the reaction : $M + XH^+ \rightarrow MH^+ + X$. The symbolism $[M+H]^+$ may also be used to represent the protonated molecule.
[Note : The widely-used term 'protonated molecular ion' to describe the MH^+ ion is not recommended. It suggests an association product of a proton with a molecular ion].

Adduct Ion An ion formed by interaction of two species, usually an ion and a molecule, and often within the ion source, to form an ion containing all the constituent atoms of one species as well as an additional atom or atoms.

Cluster Ion An ion formed by the combination of two or more molecules of a chemical species often in association with a second species. For example, $[(H_2O)_nH]^+$ is a cluster ion.

Radical Ion An ion containing an un-paired electron which is thus both an ion and a free radical. The presence of the odd electron is denoted by placing a dot alongside the symbol for the charge. Thus, $C_2H_6^{+\cdot}$ and $SF_6^{-\cdot}$ are radical ions.

Odd-electron Ion This term is synonymous with Radical Ion.

Even-electron Ion An ion containing no un-paired electrons, for example CH_3^+ in its ground state.

ION/MOLECULE REACTIONS

Ion/Neutral Reaction A process wherein a charged species interacts with a neutral reactant to produce either chemically different species or changes in the internal energy of one or both of the reactants.
(NB. The term ion/neutral reaction is not ideal, simply because the word neutral is not a noun. However, any alternatives such as ion/neutral-species are so clumsy as to seem unlikely to be generally accepted).

Ion/Molecule Reaction An ion/neutral reaction in which the neutral species is a molecule.

Charge Inversion Reaction An ion/neutral reaction wherein the charge on the reactant ion is reversed in sign.

Charge Transfer Reaction An ion/neutral reaction wherein the total charge on the reactant ion is transferred initially to the reactant neutral species so that the reactant ion becomes a neutral entity.

Partial Charge Transfer Reaction An ion/neutral species reaction wherein the charge on a multiply-charged reactant ion is reduced.

Charge Stripping Reaction An ion/neutral reaction wherein the charge on the reactant ion is made more positive.

Charge Permutation Reaction This is a general term to describe an ion/neutral reaction wherein there is a change in the magnitude and/or sign of the charges on the reactants.

[Note : Considering some of the possible reactions of ions M^{2+}, M^+ and M^- with a neutral species N these would be categorised on the basis of the above definitions as follows :

$M^{2+} + N \rightarrow M^+ + N$ (Partial charge transfer)
$M^+ + N \rightarrow M^{2+} + N + e^-$ (Charge stripping)
$M^- + N \rightarrow M^+ + N + 2e^-$ (Charge stripping and charge inversion).

All are ion/neutral reactions and also charge permutation reactions].

Collision-induced Dissociation An ion/neutral process wherein the (fast) projectile ion is dissociated as a result of interaction with a target neutral species. This is brought about by conversion of part of the translational energy of the ion to internal energy in the ion during the collision.

Collisional Activation An ion/neutral process wherein excitation of a (fast) projectile ion is brought about by the same mechanism as in collision-induced dissociation. (The ion may decompose subsequently).

Collisional Excitation An ion/neutral process wherein there is an increase in the (slow) reactant ion's internal energy at the expense of the translational energy of either (or both) of the reacting species. The scattering angle may be large.

[Note : It is recommended that all three of the above terms should be retained].

Elastic Scattering An ion/neutral interaction wherein the direction of motion of the ion is changed, but there is no change in the total translational energy or internal energy of the collision partners.

Inelastic Scattering *An ion/neutral interaction wherein the direction of motion of the ion* is changed, and the total translational energy of the collision partners is reduced.

Elastic Collision A collision resulting in elastic scattering.

Inelastic Collision A collision resulting in inelastic scattering.

Superelastic Collision A collision in which the translational energy of the fast-moving collision partner is increased.

Ionizing Collision An ion/neutral reaction in which an electron or electrons are stripped from the ion and/or the neutral species in the collision. Generally, this term has come to be used to describe collisions of fast moving ions with a neutral species in which the neutral species is ionized with no change in the number of charges carried by the ion. Care should be taken when this term is used to emphasize if charge stripping of the ion has taken place.

Association Reaction (associative combination) The reaction of a (slow moving) ion with a neutral species wherein the reactants combine to form a single ionized species.

Ion/neutral Exchange Reaction In this reaction an Association Reaction is accompanied by the subsequent or simultaneous liberation of a different neutral species as product.

Translational Spectroscopy A technique to investigate the distribution of the velocity of product ions from ion/neutral reactions.

Ion Energy Loss Spectra Spectra that show the loss of translational energy of ions involved in ion/neutral reactions.

Impact Parameter The distance of closest approach of two particles if they had continued in their original direction of motion at their original speeds.

Interaction Distance The furthest distance of approach of two particles at which it is discernible that they will not pass at the impact parameter.

Charge Exchange Reaction *This term is synonymous with Charge Transfer Reaction.*

Partial Charge Exchange Reaction This term is synonymous with Partial Charge Transfer Reaction.

SAMPLE INTRODUCTION

Sample Introduction System. This is a system used to introduce sample to a mass spectrometer ion source. (Sample Introduction System, Introduction System, Sample Inlet System, Inlet System, and Inlet are synonymous terms.)

Reservoir Inlet. This is an Inlet System having an enclosed volume (the reservoir), with provision to evacuate the reservoir, to admit sample to the reservoir, and to allow gas or vapor from the reservoir to flow through a leak to the mass spectrometer ion source. A complete description of the Reservoir Inlet should include a description of the method by which the sample is introduced into the reservoir.

Batch Inlet. This is the historic term for a Reservoir Inlet. Reservoir Inlet is preferred because a Direct Inlet Probe is also a form of Batch Inlet. Batch Gas Inlet or Batch Vapor Inlet is, however, a completely descriptive term.

Dual Viscous-Flow Reservoir Inlet. This is an inlet having two reservoirs, used alternately, each having a leak that provides viscous flow. This inlet is used for making precise comparisons of isotope ratios in two samples.

Continuous Inlet. This is an inlet in which gas or vapor passes continuously into a mass spectrometer ion source, as distinguished from a Reservoir Inlet or a Direct Inlet Probe.

Non-Fractionating Continuous Inlet. This is a Continuous Inlet in which gas flows from a gas stream being analyzed to the mass spectrometer ion source without any change in the conditions of flow through the inlet or by the conditions of flow through the ion source.

Direct-Inlet Probe. This is a rod having a sample holder at one end, which is inserted into the vacuum system of a mass spectrometer through a vacuum lock, placing the sample near to, at the entrance of, or within the ion source, so that the sample can be vaporized after introduction to the vacuum system by heat from the ion source or by heat applied to the probe from an external source. (Direct Inlet Probe, Direct-Introduction Probe or Direct-Insertion Probe are synonymous terms. The use of DIP as an abbreviation for these terms is not recommended.)

Vacuum-Lock Inlet. This is an inlet in which a sample is placed in a chamber, the chamber is pumped out, and a valve is opened so that the sample can then be introduced to the mass spectrometer ion source. A Vacuum-Lock Inlet commonly uses a Direct-Inlet Probe which passes through one or more sliding seals, but other kinds of Vacuum-Lock Inlets are possible.

Extended Direct-Inlet Probe. This probe provides for insertion of a sample on an exposed surface (such as a flat surface or a wire) into (rather than up to the entrance of) the ion source of a mass spectrometer. (This term is synonymous with Direct-Exposure Probe.)

Crucible Direct-Inlet Probe. With this probe, the sample is held in a cup-shaped device (the crucible) rather than on an exposed surface. A Direct-Inlet Probe is assumed to be a crucible type unless otherwise specified.

GC/MS Interface. This is an interface between a gas chromatograph and a mass spectrometer which serves to provide continuous introduction to a mass spectrometer ion source of effluent gas from a gas chromatrograph during the period for which the effluent gas is to be analyzed.

Direct GC/MS. This is an interface in which the entire effluent from the gas chromatograph passes to the mass spectrometer ion source during an analysis, without any splitting of the effluent.

Splitter GC/MS Interface. This is an interface in which the effluent from the gas chromatrograph is divided before admission to the mass spectrometer, without enrichment of sample with respect to carrier gas.

Separator GC/MS Interface. This is an interface in which the effluent from the gas chromatograph is enriched in the ratio of sample to carrier gas. (Separator, Molecular Separator, and Enricher are synonymous terms.) A separator should generally be defined as an Effusion Separator a Jet Separator, or a Membrane Separator.

Effusion Separator (or Effusion Enricher) This is an interface in which carrier gas is preferentially removed from the gas entering the mass spectrometer by effusive flow (e.g. through a porous tube or through a slit).

Jet Separator. This is an interface in which carrier gas is preferentially removed by diffusion out of a gas jet flowing from a nozzle. (Jet Separator, Jet-Orifice Separator, Jet Enricher and Jet-Orifice are synonymous terms.)

Membrane Separator. With this separator, the gas or vapor passes to the mass spectrometer through a semi-permeable membrane (e.g. a silicone membrane) which selectively transmits organic compounds in preference to carrier gas. (Membrane Separator, Membrane Enricher, Semi-Permeable Membrane Separator, and Semi-Permeable Membrane Enricher are synonymous terms.)

Solvent-Divert System. This system is used in conjunction with an interface which permits temporary interruption of the flow from a gas chromatograph to a mass spectrometer by opening a valve to a pumping line, so that an effluent present at a high concentration (usually solvent) does not enter the mass spectrometer ion source at a high concentration.

Liquid Chromatograph/Mass Spectrometer (LC/MS) Interface. This interface is between a liquid chromatograph and a mass spectrometer which serves to provide continuous introduction to a mass spectrometer ion source of the effluent from a liquid chromatograph during the period for which the effluent is to be analyzed.

Moving Belt (Ribbon or Wire) Interface. With this interface, all or a part of the effluent from a liquid chromatograph is continuously applied to a belt (ribbon or wire), which passes through two or more orifices, with differential pumping, into the mass spectrometer vacuum system; after which heat is applied, to remove the solvent, and then to evaporate the solute into the ion source.

Direct Chemical Ionization Interface. With this interface, all or a part of a liquid chromatograph effluent passes continuously to the mass spectrometer, in which the solvent is used as a chemical ionization agent for ionization of the solute.

SCANNING OF SPECTRA

Mass Spectrum A spectrum obtained when a beam of ions is separated according to the mass-to-charge (m/z) ratios of the ionic species contained within it.

[Note : A quadrupole mass spectrometer achieves separation of the various ionic species in this way].

Momentum Spectrum A spectrum obtained when a beam of ions is separated according to the momentum-to-charge ratios of the ionic species contained within it.

[Note : A sector magnetic field achieves separation of the various ionic species in this way. If the ion beam is homogeneous in translational energy, as is the case with sector instruments, separation according to the m/z ratios is also achieved].

Ion Kinetic Energy Spectrum A spectrum obtained when a beam of ions is separated according to the translational energy-to-charge ratios of the ionic species contained within it.

[Note : A radial electric field achieves separation of the various ionic species in this way].

Magnetic Field Scan The usual method of producing a momentum (mass) spectrum in instruments.

Accelerating Voltage (High Voltage) Scan An alternative method of producing a momentum (mass) spectrum in magnetic deflection instruments. This scan can also be used, in conjunction with a fixed radial electric field to produce an ion kinetic energy spectrum.

Linked Scan A scan, in an instrument comprising two or more analysers, in which two or more of the analyser fields are scanned simultaneously so as to preserve a predetermined relationship between parameters characterising these fields. Often, these parameters are the field strengths, but may also be the frequencies in the case of analysers in which alternating fields are employed.

Linked Scan at Constant B/E A linked scan at constant B/E may be performed on a sector instrument incorporating at least one magnetic sector plus one electric sector. It involves scanning the magnetic sector field-strength B and the electric sector field-strength E simultaneously, holding the accelerating voltage V constant, so as to maintain the ratio B/E at a constant value. This constant value is determined by the ratio of the two field strengths which transmit main-beam ions of predetermined mass:charge ratio; these preselected main-beam ions are the precursor ions whose fragment-ion spectrum is required. The fragmentation reactions so observed occur in a field-free region traversed before the two sectors scanned in this way.

[Notes : This term should not be used without prior explanation of the meanings of B and E.

The term "B/E linked scan" is not recommended. It may suggest that the ratio B/E varies during the scan].

Linked Scan at Constant E^2/V A linked scan at constant E^2/V may be performed on a sector instrument incorporating at least one electric sector plus one magnetic sector. It involves scanning the electric sector field E and the accelerating voltage V simultaneously, so as to maintain the ratio E^2/V at a constant value, equal to the value of this ratio which transmits the main beam of ions through the electric sector. The magnetic sector field is set at a fixed value such that main-beam ions of a predetermined mass:charge ratio are transmitted by the magnet; these preselected main-beam ions are the precursor ions whose fragment-ion spectrum is required. The fragmentation reactions so observed occur in a field-free region traversed before the two sectors scanned in this way.

[Notes : This term should not be used without prior explanation of the meanings of E and V.

The term "E^2/V linked scan" is not recommended].

Linked Scan at Constant B^2/V A linked scan at constant B^2/E may be performed on a sector instrument incorporating at least one electric sector plus one magnetic sector. It involves holding the accelerating voltage fixed, and scanning the magnetic field B and the electric field E simultaneously so as to maintain the ratio B^2/E at a constant value. This constant value corresponds to the ratio of the two fields which transmit main-beam ions of predetermined mass:charge ratio; these preselected main-beam ions are the fragment ions whose precursor-ion spectrum is required. The fragmentation reactions thus observed occur in a field-free region traversed before the two sectors scanned in this way.

[Notes : This term should not be used without prior explanation of the meanings of B and E.
The term "B^2/E linked ,can" is not recommended].

Linked Scan at Constant $B[1 - (E/E_0)]^{\frac{1}{2}}/E$ A linked scan at constant $B[1 - (E/E_0)]^{\frac{1}{2}}/E$ may be performed on a sector instrument incorporating at least one electric sector plus one magnetic sector. It involves holding the accelerating voltage fixed, and scanning the magnetic field B and electric field E simultaneously, so as to maintain the quantity $B[1 - (E/E_0)]^{\frac{1}{2}}/E$ at a constant value. This constant value is equal to B_3/E_0, where E_0 and B_3 are respectively the electric sector field and magnetic sector field required to transmit m_3^+ ions in the main ion-beam; m_3 represents the mass $(m_1 - m_2)$ of the selected neutral fragment whose precursor ion spectrum is required. The fragmentation reactions so observed occur in a field-free region traversed before the two sectors scanned in this way.

[Note : This term should not be used without prior explanation of the meanings of B, E and E_0.

The term "$B[1 - (E/E_0)]^{\frac{1}{2}}/E$ linked scan" is not recommended].

The above three definitions are merely examples of the types of linked scan that might be used. Any other linked scans can readily be defined in a similar manner.

Fixed Precursor Ion Scans

1. Mass Selection followed by Ion Kinetic Energy Analysis

If a precursor (parent) ion is selected, for example by a magnetic sector, all product ions formed from it in the field-free region between the magnetic sector and a following electric sector can be identified by scanning an ion kinetic energy spectrum.

2. Linked Scan at Constant B/E or at Constant E^2/V

Both of these linked scans give a spectrum of all product (daughter) ions formed from a preselected precursor (parent) ion.

Fixed Product-Ion Scans

1. High Voltage Scan.

2. Linked Scan at Constant B^2/E.

Both 1. and 2. give a spectrum of all precursor (parent) ions that fragment to yield a pre-selected product (daughter) ion.

Fixed Neutral Fragment Scans

The linked scan at constant $B[1 - (E/E_0)]^{\frac{1}{2}}/E$ gives a spectrum of all product (daughter) ions that have been formed by loss of a pre-selected neutral fragment from any precursor (parent) ions.

[Note : The above definitions have all been given with reference to sector instruments; *linked scans to give similar information have also been devised for instruments* incorporating one or more quadrupoles].

2E Mass Spectrum Processes of the partial charge-transfer type :

$$m^{2+} + N \rightarrow m^{+} + N^{+}$$

occurring in a collision cell (containing a gas, N) located in a field-free region preceding a magnetic and electric sector combination placed in either order, may be detected as follows.

If the instrument slits are wide, and if the electric sector field E is set to twice the value required to transmit the main ion-beam, the only ions to be transmitted will be those with a kinetic energy/charge ratio twice, or almost exactly twice, that of the main ion-beam. The product ions of the process shown fulfill this condition. If the magnetic field B is scanned, a mass spectrum of such singly-charged product ions, and thus of their doubly-charged precursors, is obtained. Such a spectrum is called a 2E mass spectrum.

E/2 Mass Spectrum Processes of the charge-stripping type :

$$m^{+} + N \rightarrow m^{2+} + N + e^{-}$$

occurring in a collision cell (containing a gas N) located in a field-free region preceding a magnetic and electric sector combination placed in either order, may be detected as follows.

If the instrument slits are wide and if the electric sector field E is set to half the value required to transmit the main ion-beam, the only ions to be transmitted will be those with a kinetic energy/charge ratio half, or almost exactly half, that of the main ion-beam. The product ions of the charge-stripping process fulfill this condition. If the magnetic field B is scanned, a mass spectrum of such doubly-charged product ions, and thus of their singly-charged precursors, is obtained. Such a spectrum is called an E/2 mass spectrum.

[Note : Interference from product ions from processes of the type :

$$m_1^+ + N \rightarrow m_2^+ + N + (m_1 - m_2)$$

where $m_2 \approx 0.5\ m_1$, can arise in E/2 mass spectra].

Charge Inversion Mass Spectrum Charge inversion processes of the types :

$$m^+ + N \rightarrow m^- + N^{2+}$$

$$\text{or} \quad m^- + N \rightarrow m^+ + N + 2e^-$$

respectively, occurring in a collision cell (containing a gas, N) located in a field-free region preceding a magnetic and electric sector combination placed in either order, may be detected as follows.

If the instrument slits are wide, and if the connections to the two sectors, appropriate to transmission of either positive or negative main-beam ions, are simply reversed, the negative or positive product ions of the two processes, respectively, will be transmitted. If the magnetic field is scanned, a spectrum of such product ions will be obtained, and this spectrum is called a charge-inversion mass spectrum. These spectra are sometimes referred to as -E and +E spectra, respectively.

[Note : The terms "2E, E/2, -E or +E mass spectrum" should not be used without prior explanation of the meaning of 2E, E, +E or -E].

VACUUM

(The terms in this section have been contributed, almost entirely, by the American Vacuum Society, to whom grateful acknowledgment is made)

Adsorption The process by which gas or vapor is bonded on a solid or liquid surface.

Aperture Impedance The additional resistance encountered by gas flowing through a tube with an abrupt reduction in cross-section. For molecular flow, it is the product of the molecular effusion impedance of an orifice with a cross-sectional area A_2 and the aperture correction factor $(1 - A_2/A_1)$, where A_1 is the cross-sectional area of the larger tube and A_2 that of the smaller tube.

Background Spectrum A mass spectrum of residual gas species in a system. It is usually obtained before a sample of interest is introduced and analyzed in order to deduce by subtraction of spectra the true mass spectrum of the sample.

Backstreaming The flow of charged and/or neutral particles emanating from a pump and moving counter to the flow of the gases being pumped.

Baffle A series of surfaces placed in the line of gas or vapor flow to prevent straight line flow.

Collision Frequency The number of molecules or atoms striking a unit area of surface per unit time; also, the number of collisions between the molecules or atoms in a gas per unit volume and unit time. The collision frequency per molecule is equal to the probability per unit time that a molecule will collide with a surface or another molecule.

Collision Rate The collision probability per unit time for an atom or molecule travelling at a specified speed through a gas.

Conductance The ratio of throughput, under steady-state conservative conditions, to the pressure differential between two specified cross-sections inside a pumping system.

Critical Inlet Pressure The inlet pressure of a vapor pump above which an abrupt decrease in pumping speed occurs.

Cryopump A vacuum pump which operates by the condensation and/or sorption of gas at surfaces maintained at temperatures sufficiently low for the vapor pressures of the condensed gases to be insignificant.

:yosorption Pump A vessel containing an adsorbent which can be refrigerated for the cryosorption pumping of gases.

:yosorption Pumping A technique of producing vacuum by physical adsorption of gases on solid adsorbents cooled to low temperatures.

ıffusion Pump A vapor pump in which the pumped gas flows into a vapor stream under conditions in which molecular flow predominates. Momentum is transferred from the vapor to the gas, carrying it along in the direction of the stream. Pump fluid is heated in vacuum to generate the vapor which is directed through a nozzle. It expands freely in the stream before it reaches a cool wall where it condenses and is returned to the boiler to begin a new cycle.

ıector Pump A vapor pump in which the pumped gas enters the pump and the vapor stream under predominantly viscous flow conditions.

'aporation The conversion of a substance from the liquid state into the gaseous state by absorption of energy.

:haust Port An opening in a vacuum pump or stage from which gases are ejected either to a succeeding stage or to the atmosphere.

:edthrough A device for transmitting electrical current, fluids or mechanical motion through the wall of a vacuum system.

ange A (projecting) rim usually in the form of an annulus intended for fastening and sealing one part of the vacuum system to another.

apper Valve A thin gauge spring steel plate fastened on one end to the pump housing which seals the exhaust port of a mechanical pump from the oil reservoir or atmosphere. During the exhaust cycle, gas pressure is sufficient to deflect the plate away from its seat and gas is discharged from the pump. Syn: flutter reed valve.

ow (Gas) The motion or passage of a gas. A description of gas flow may be characterized by the Knudsen number into three ranges.

ılecular Flow The flow of gas through a channel under conditions such that the mean free path is much greater than the largest dimension of a transverse section of the channel. At these pressures, the flow characteristics are determined by collisions of the gas molecules with the channel surfaces and flow effects from molecular collisions are insignificant.

:ansition Flow The flow of a gas through a channel under conditions that the mean free path is of the same order as the transverse dimensions of the channel. In this pressure range, the flow characteristics are determined by collisions of the gas molecules with surfaces as well as with other gas molecules. Also called Knudsen flow.

scous Flow The flow of a gas through a channel under conditions such that the mean free path is very small in comparison with smallest dimension of a transverse section of the channel. At these pressures the flow characteristics are determined mainly by collisions between the gas molecules, i.e. the viscosity of the gas. The flow may be laminar or turbulent.

ıre Pump A vacuum pump for maintaining the forepressure of another pump below its critical value.

ırepressure The pressure measured downstream from the outlet or foreline of a vacuum pump.

:actionating Pump A diffusion pump whose design allows the more volatile impurities in the pump fluid resulting from decomposition or contamination to be either ejected out of the foreline or trapped within the pump in such a manner as to effectively reduce their chance of escape out of the pump inlet.

ıldıng Time (Pump) The time required for the forepressure of an isolated vapor or diffusion pump to reach the limiting forepressure.

Hot Cathode Ionization Gauge An ionization gauge in which pressure is measured in terms of the current of positive ions produced by electrons emitted from a heated cathode.

Bayard-Alpert Gauge A hot cathode ionization gauge in which a fine wire ion collector is positioned on the axis of a cylindrical grid functioning as anode. The cathode is mounted outside the grid.

Impedance The reciprocal of conductance.

Incidence Rate The number of molecules striking a unit area of surface per unit time.

Inlet Pressure The gas pressure at the entrance to a pump.

Interstage Pressure The gas pressure at any point between the exhaust port of the low-pressure stage and high-pressure or roughing stage of a compound pump.

Ion Pump An electron device in which ionization produces a significant rate of gas removal.

Differential Sputter Pump A sputter-ion pump having two cathodes for which materials and sputtering rates differ.

Diode Pump An ion pump containing two uniquely shaped electrodes, viz. a cathode and anode. Two-electrode ion pumps are also referred to as diode getter and diode sputter ion pumps.

Electrostatic Pump An ion pump having only electrostatic fields rather than both electric and magnetic fields to generate the ionizing discharge. The getter material is sublimed by electron heating or by ohmic heating into the discharge space.

Electrostatic Getter Pump An electrostatic-ion pump in which a getter material is made to sublime.

Evaporation Pump A getter-ion pump in which the getter is evaporated from a molten surface rather than sublimed or sputtered from a solid source.

Getter Pump A pump which combines the pumping mechanisms used in the ion pump and the getter pump. (See sputter-ion pump and electrostatic pump)

Magnetic Pump An ion pump usually with multiple anode cells immersed in a magnetic field parallel to the cell axes with two cathode end plates of reactive material spaced from the ends of the anode cells which terminates the discharge space.

Noble Gas Pump A magnetic-ion pump with novel cathode geometries to enhance the pumping of noble gases.

Sputter Pump A getter-ion pump in which the getter surfaces are continuously renewed by sputtering.

Triode Pump An ion pump usually of the sputter-ion type, containing three uniquely shaped electrodes; an anode, a sputter cathode, and an ion collector electrode.

Triode Getter Pump A triode-ion pump in which gettering is a part of the pumping mechanism.

Knudsen Flow The flow of gas through a pump or system under transition flow conditions which are intermediate between viscous flow and molecular flow.

Knudsen Gauge A vacuum gauge which indicates pressure by responding to the net rate of transfer of momentum by molecules moving between two surfaces maintained at different temperatures and separated by a distance smaller than the mean free path of the gas molecules. Various types of Knudsen gauges differ mainly in the shape and method of suspension of the movable element.

Knudsen Number The ratio of the mean free path of a gas molecule to a characteristic dimension of the channel through which gas is flowing. For a cylindrical tube, the diameter is a characteristic dimension.

Leak A hole or permeable element through which leakage may occur under the action of a pressure difference. This includes a device used to introduce gas into a vacuum system at a controlled rate.

Calibrated Leak A leak which has a known leakage rate for a specific gas under specific conditions.

Capillary Leak A leak having a small cross section dimension and length many times its cross section dimension.

Membrane Leak A leak which permits gas flow by permeation through a thin nonporous wall.

Molecular Leak A leak of such a size that the leakage through it is predominantly molecular flow for a given pressure.

Variable Leak A leak with an adjustable leakage rate which can be controlled.

Virtual Leak An apparent leak because of the presence of contaminants which outgas very slowly within a vacuum system.

Viscous Leak A leak of such a size that the leakage through it is predominantly viscous flow for a given pressure.

Accumulation Leak Detection Technique A leak detection technique in which tracer gas (e.g. helium) enters the part under test and is allowed to accumulate within the part, or within a system containing the part, for a period of time. The part or system is then opened to the leak detector. The system may include the leak detector sensing element.

Backing Space Leak Detection Technique A leak detection technique in which the leak detector is connected to the forevacuum side of a pump attached to the vacuum system or element undergoing leak test. A tracer gas is sampled at a higher pressure after compression by the diffusion pump or other type of pump operating at high speed relative to its backing pump.

Bagging A jargon term for a leak detection technique in which the part under test is enclosed in a bag (or other enclosure) which is filled with a tracer gas to slightly more than atmospheric pressure. A tracer gas is applied to the entire surface of the part to determine the total leakage from all leaks in the part.

Diffusion Leakage A leakage resulting from the temperature dependent diffusion of a specific gas through a membrane. Examples are the diffusion of hydrogen through palladium and helium through glass.

Leakage (leak) Rate The quantity of gas passing through a leak in a given time divided by that time (see throughput).

Limiting Forepressure The pressure at the discharge side of a vacuum pump, at a stated throughput, above which the pumping action of the pump rapidly deteriorates, evidenced by a sudden increase of inlet pressure. Syn: critical backing pressure.

Load (Vapor Pump) The quantity of gas, not including pump fluid vapor, in mass units, flowing through the pump per unit time. It is also called capacity or mass flow.

Manometer An instrument for measuring the pressure of gases and vapors.

Maximum Pressure Ratio (Vacuum Pump) The maximum value of the ratio of forepressure to inlet pressure which a pump can maintain at zero gas flow. In vapor pumps, this term is usually significant only for light gases such as hydrogen and helium.

McLeod Gauge A liquid level manometer in which a known volume of the gas, whose pressure is to be measured, is compressed by the movement of a liquid column and confined in a small measurable volume. Corrections need to be made for any appreciable change in gas pressure in the system caused by the movement of the liquid.

Mean Free Path The average distance a particle travels between successive collisions with the other particles of an ensemble.

Mean Path The mean distance a particle travels between successive collisions with other particles or surfaces. When the pressure is high or the vessel dimensions are large, so that the mean path is small with respect to the vessel dimensions, the mean path and mean free path become numerically identical.

Mechanical Pump (Vacuum) A device with moving parts such as rotating vanes, a piston, or eccentric rotary members used for pumping gas or vapor.

Molecular Effusion The molecular flow of gas from a region at one pressure to one at a lower pressure through an orifice in a wall of negligible thickness and with a diameter much less than the mean free path of the molecules.

Molecular Flux The net number of gas molecules crossing a specified surface in unit time. Those having a velocity component in the same direction as the normal to the surface at the point of crossing are counted as positive and those having a velocity component in the opposite direction are counted as negative.

Molecular Velocity Distribution The average value of the fraction of the molecules in a small volume, $d\underline{r}$, surrounding a given point, located by the radius vector $\underline{r}$ in a fluid medium, which have velocity vectors lying within an infinitesimal volume, $d\underline{v}$, surrounding the point in velocity space. The averaging process is carried out over a time long enough to smooth statistical fluctuations in the molecular populations, but short compared with the time required for significant variations in the macroscopic properties. For a gas in equilibrium at rest, the distribution of the velocity vectors with a given magnitude is uniform over a sphere about the origin in velocity space. The distribution known as Maxwell's law of velocity distribution is $f_v\, dv = 4\pi v^2\, (m/2\pi kT)^{3/2} \exp(-mv^2/2kT)dv$, where m is the mass of a molecule, T is the absolute temperature, k is the Boltzmann constant, and $4\pi v^2\, dv$ is the volume of a spherical shell of radius equal to the magnitude of v and of thickness dv equal to the increment in this magnitude and gives the fraction of molecules having speeds between v and v + dv. The function f_v is the Maxwellian distribution function.

Net Speed (Vacuum Pump) The throughput across a section remote from the pump inlet divided by the pressure as measured at that section. The net speed can be calculated when the pumping speed is known by adding to the sum of all the impedances between the pump inlet and the given cross section, the reciprocal of the measured pumping speed and then taking the reciprocal of the result.

Pascal The basic S.I. unit of pressure recommended for general use in vacuum technology. It is one newton per square meter. (see also : Torr).

Permeability Coefficient The rate of flow of gas through a unit area and a unit thickness of a solid barrier per unit differential pressure at a given temperature.

Permeation The passage of gas through a solid. The process always involves diffusion through the solid and may involve surface phenomena such as sorption, dissociation, migration and desorption.

Physical Adsorption An adsorption process caused by van der Waals forces between adsorbent and adsorbate. Typical binding energies are less than 10 kcal/mole. Syn: physisorption. (See adsorption.)

Positive Displacement Pump A mechanical vacuum pump in which the pumping action is provided by displacement or trapped volume of gases typically by a rotating or reciprocating piston, sliding vane, or intermeshing lobes.

Pressure (Gas) The average normal force per unit area exerted by gas molecules impacting on a surface.

Ultimate Pressure The limiting low pressure approached in a vacuum system after a sufficient pumping time has elapsed to establish that further reductions in pressure will be negligible. Sometimes called the ultimate vacuum, or blank-off pressure, or base pressure when referred to a pump under test.

Ultimate Partial Pressure The part of the ultimate pressure in a vacuum system caused by the partial pressure of a specific gas.

(Saturated) Vapor Pressure The pressure of a vapor in thermodynamic equilibrium with a condensed phase at a fixed temperature. The definition applies to single components as well as to multicomponent systems. In the latter case, it is necessary to distinguish between the total pressure over the condensed phase and the partial pressure of a given component. Syn : saturation pressure.

Pump Fluid A liquid, usually having a low vapor pressure, used as the working fluid in a mechanical or vapor pump.

Pumping Speed The ratio of the throughput of a given gas to the partial pressure of that gas at a specified point near the inlet port of a pump.

Seal (Vacuum) A joint between two elements of a vacuum system which is effective in maintaining leakage at or below a required level.

Bakeable Seal A seal which can be baked at elevated temperatures.

Break Seal A seal consisting of a thin glass membrane separating adjacent sections of a vacuum system. The membrane is broken to connect the two sections.

Demountable Seal A seal between two elements designed for disassembly without resort to cutting, fracturing, or melting, which is effective in maintaining the desired vacuum.

Gasket Seal A demountable seal which employs a closed loop of deformable material pressed between two harder members. It may be reuseable. The gasket may be fabricated from metal washers, wire rings, elastomers or other materials.

O-Ring A demountable, elastomer, gasket seal made with a toroidal gasket of circular cross section.

Pump Speed The volumetric rate of gas flow across a section at the pump inlet. It can be obtained from the ratio of the throughput of a gas to the partial pressure of that gas at a specific point near the inlet port of the pump. (Often called pumping speed.)

Speed Factor The ratio of the speed to the product of the vacuum pump inlet cross section area and the maximum flow rate per unit area as given by the effusion law. It is also called efficiency, or speed efficiency.

Speed of Exhaust The instantaneous rate of reduction of pressure in a system multiplied by its volume and divided by its pressure.

Sticking Coefficient The ratio of the number of molecules which are adsorbed on a surface for a finite period of time to the number of molecules striking that surface.

Sublimation The process of transition directly from the solid vapor phase without passing through the intermediate liquid phase by the absorption of energy. Syn: sublime.

Thermal Conductivity Gauge A vacuum gauge containing two surfaces at different temperatures between which heat can be transported by gas molecules. Changes in the temperatures, or in the heating power required to maintain constant temperature of one of the surfaces can be correlated with the gas pressure. Thermal conductivity gauges differ in the method of indicating the temperature change. (See : thermocouple gauge).

Thermistor Gauge A form of thermal conductivity gauge in which the temperature-sensitive elements are made of semiconducting material instead of metal.

Thermocouple Gauge A thermal conductivity gauge which contains a heated filament and a thermocouple for the measurement of filament temperature as a function of gas pressure.

Throat (Vacuum Component) (a) (Nozzle or Diffuser). The smallest cross section of an expanding nozzle, converging diffuser or converging/diverging nozzle or diffuser. (b) (Vapor Pump). The smallest clearance area between the pump casing and the nozzle nearest the inlet port.

Throughput The quantity of gas in pressure-volume units, at a specified temperature, flowing per unit time across a specified open cross section. Throughput may be referred to a specific constituent of a gas in which case the partial pressure of that constituent and the associated flow rate are the relevant quantities.

Torr A unit of pressure defined as 1/760 of a standard atmosphere. It replaced the term millimeter of mercury (mm of Hg), and has now been replaced by the Pascal as a preferred unit of pressure. (1 mm Hg = 1.000 000 14 Torr = 133.322 386 7 Pascal).

Trap (Vacuum System) A device used in a vacuum pumping line to reduce vapor pressure in a vacuum system or prevent backstreaming and migration of vacuum pump fluids such as mercury and/or oil.

Anti-Migration Trap A trap which includes a chilled surface or other means to prevent surface migration of oil from a source into the vacuum system.

Cold Trap A trap with a refrigerated surface used to condense various vapors present in the vacuum system.

Molecular Sieve Trap A trap containing molecular sieve material that has a high surface area and that adsorbs hydrocarbon and water vapors at or below room temperature.

U-Tube Trap A trap in the form of a U-shaped tube which is immersed in a coolant.

Turbomolecular Pump An axial flow turbine for operation in the molecular flow range consisting of a series of alternate circular rotor and stator disks both of which have inclined blades designed to impart momentum change to gas molecules in a preferential direction from the pump inlet to the outlet.

Vacuum The condition of a gaseous environment in which the gas pressure is below atmospheric pressure.

Low Vacuum A vacuum in which the pressure is less than 10^5 Pa (~750 Torr) and greater than 3.3×10^3 Pa (25 Torr).

Medium Vacuum A vacuum in which the pressure is less than or equal to 3.3×10^3 Pa (25 Torr) and greater than 10^{-1} Pa (7.5×10^{-4} Torr).

High Vacuum A vacuum in which the pressure is less than or equal to 10^{-1} Pa (7.5×10^{-4} Torr) and greater than 10^{-4} Pa (7.5×10^{-7} Torr).

Very High Vacuum A vacuum in which the pressure is less than or equal to 10^{-4} Pa (7.5×10^{-7} Torr) and greater than 10^{-7} Pa (7.5×10^{-10} Torr).

Ultrahigh Vacuum A vacuum in which the pressure is less than or equal to 10^{-7} Pa (7.5×10^{-10} Torr) and more than 10^{-10} Pa (7.5×10^{-13} Torr).

Extreme Ultrahigh Vacuum A vacuum in which the pressure is less than 10^{-10} Pa (7.5×10^{-13} Torr).

Vacuum Valve A mechanical device by which the flow of gas or vapor may be started, stopped, or regulated by a moving part which opens or obstructs a passage.

Angle Valve A valve in which the ports are not in line, as, for example, a right angle valve.

Vacuum Baffle A valve containing a shield which remains in line with the valve port and can thus act as a baffle.

Butterfly Valve A valve which is opened or closed by rotating a disk 90° about an axis through the center of the disk.

Diaphragm Valve A valve in which the valve stem is mounted in a bonnet which is isolated from the rest of the valve by using a diaphragm to divide the space inside the valve body. Either metal, elastomer or plastic is commonly used for the diaphragm. An elastomer or plastic diaphragm sometimes functions also as a gasket. In any case, motion is limited to avoid exceeding the elastic limit of the diaphragm material.

Leak Valve A valve for admitting air or gas at a precisely determined rate into a vacuum system.

Needle Valve A leak valve in which a tapered needle is moved along its axis against a seat which may also be tapered.

Relief Valve A valve which will automatically open when the pressure on the seat side rises above a specific pre-set valve. It is generally regarded as a safety device.

Sealed Bellows Valve A valve usually for high vacuum applications, in which the stem is sealed by a flexible metal bellows. One end of the bellows is attached to the valve body and the other end to the disk part of the valve stem.

Solenoid Valve A valve in which the movable member is actuated electrically by an electromagnet.

Straight Through Valve A valve in which the ports are in line, or coaxial, and for which the internal construction is such that line-of-sight flow occurs when the valve is open.

OTHER TERMS

Mass Analysis A process by which a mixture of ionic or neutral species is identified according to the mass-to-charge (m/z) ratios (ions) or their aggregate atomic masses (neutrals). The analysis may be qualitative and/or quantitative.

Detection of Ions In mass spectrometry this concerns the observation of the arrival of particular ionic species, at a detector under conditions that preclude or minimize ambiguities due to interferences. Ions may be detected by photographic or suitable electrical means.

Scanning Method This term refers to the sequence of control over operating parameters of a mass spectrometer which results in a spectrum of masses, velocities, momenta or energies.

Sample Introduction This refers to the manner in which a material which is to be subject to analysis is placed in the ion source of a mass spectrometer before and/or during such an analysis.

Vacuum System Those components used to lower the pressure within a mass spectrometer are all parts of the vacuum system. This includes not only the various pumping components but also valves, gauges and associated electronic or other control devices, the chamber in which ions are formed and detected and the vacuum envelope.

Data System The components used to record and process information during the analysis of a sample are part of the data system. This includes electronic or other control devices, and recording storage and data manipulation devices.

Data Processing Once information is obtained with an appropriate data system, the information must be interpreted appropriate to the end use. Those steps which lead to this end use are of concern in data processing. Note that data processing does not necessarily include application of modern computer techniques.

Data Reduction The process of transforming the initial digital representation of a spectrometer output into a form which is amenable to interpretation; for example, a bar graph or a table of ion currents.

m/z This abbreviation is used to denote the dimensionless quantity formed by dividing the mass number of an ion by the number of charges carried by the ion. It has long been called the mass-to-charge ratio although m is not the ionic mass nor is z a multiple of the electronic charge, e^-. The abbreviation m/e is, therefore, not recommended. Thus, for example, for the ion $C_7H_7^{2+}$, m/z = 45.5.

Nominal Ion Mass. The mass of an ion with a given empirical formula calculated using the integer masses of the most abundant isotope of each element, e.g. C=12, H=1, O=16.

Monoisotopic Ion Mass. The mass of an ion for a given empirical formula calculated using the exact mass of the most abundant isotope of each element, e.g. C=12.00000, H=1.007825, O=15.9949.

Average Mass. The mass of an ion for a given empirical formula calculated using the atomic mass of each element, e.g., C=12.011, H=1.00797, O=15.999.

Thermal Desorption. The removal of ionic or neutral species from the condensed state by the input of thermal energy into the condensed state. The mechanism of energy input should be specified.

Dynamic Headspace Gas Chromatography/Mass Spectrometry. The distillation of volatile and semivolatile compounds into a continuously flowing stream of carrier gas and onto a gas chromatographic column. This is followed by mass spectrometric analysis of compounds eluting from the gas chromatograph.

1984 CONFERENCE ATTENDEES (U S A)

NAME	A1	A2	A3	CI	STA	ZP
LAWRENCE E ABBEY	GEORGIA TECH	CHEMISTRY DEPT		ATLANTA	GA	30332
R M ABERNATHEY	120 MONTE REY DR N			LOS ALAMOS	NM	87544
WILLIAM H ABERTH	UC SAN FRANCISCO	PHARMACEUTICAL CHEM		SAN FRANCISCO	CA	94143
CRAIG R ABOLIN	SANDOZ INC	ROUTE 10		EAST HANOVER	NJ	07936
BRADLEY L ACKERMANN	BIOCHEM RM 11	MICHIGAN STATE UNIV		EAST LANSING	MI	48824
T ACZEL	EXXON R/E	PO BOX 4255		BAYTOWN	TX	77522
R A ADAMS	3480 TANBARK CT NE			ATLANTA	GA	30319
THOMAS A ADAMS	PO BOX 5795			COLLEGE STATION	TX	77840
ALFRED M AJAMI	TRACER TECHNOLOGIES	225 NEEDHAM ST		NEWTON	MA	02164
KENNETH M ALDOUS	NY STATE HEALTH DEPT	TOXICOLOGY INST	TOWER BLDG	ALBANY	NY	12201
E D ALFORD	BROWN & WILLIAMSON	PO BOX 35090		LOUISVILLE	KY	40232
MOHAMMAD FARHAT ALI	CHEMISTRY DEPT	BAKER LAB 141	CORNELL UNIV	ITHACA	NY	14853
DAVID ALKALAY	CIBA-GEIGY CORP	444 SAWMILL RIVER RD		ARDSLEY	NY	10502
R H ALLEN	R H ALLEN CO	PO BOX 27		BOULDER	CO	80302
J ALLISON	MICHIGAN STATE UNIV	CHEMISTRY DEPT		EAST LANSING	MI	48824
MICHAEL F ALMOND	KRATOS ANALYTICAL	170 WILLIAMS DR		RAMSEY	NJ	07446
JON AMSTER	CORNELL UNIV	BOX 165	BAKER LAB	ITHACA	NY	14853
R J ANDEREGG	UNIV OF MAINE	377 AUBERT HALL		ORONO	ME	04469
GREGG ANDERSON	CVC PRODUCTS	525 LEE ROAD	PO BOX 1886	ROCHESTER	NY	14603
DONNA J ANDERSON	CHEMISTRY DEPT	TEXAS A & M		COLLEGE STATION	TX	77843
VINCENT ANICICH	8036 GRAYSTONE			SUNLAND	CA	91040
CHENG-HWAN AO	6901 RUSTIC LANE	NO 156		HOUSTON	TX	77087
BRUCE K ASAMOTO	SOHIO RESEARCH	4440 WARRENSVILLE		CLEVELAND	OH	44128
TERRENCE R ASHE	EXXON R/E	CLINTON TWNSHP	ROUTE 22 EAST	ANNANDALE	NJ	08801
JOHN W AULD	37748 SUNNYDALE			LIVONIA	MI	48154
PIERRE J AUSLOOS	NAT'L BUR OF STAN	CTR FOR CHEM PHYSICS		WASHINGTON	DC	20234
R J AYERS	1560 E JEFFERSON			DETROIT	MI	48207
LUCIA M BABCOCK	CHEMISTRY DEPT	CHOPPIN HALL	LOUISIANA STATE UNIV	BATON ROUGE	LA	70803
L BACZYNSKYJ	THE UPJOHN CO	301 HENRIETTA		KALAMAZOO	MI	49001
DAVID A BAFUS	4114 CLOVERNOOK LANE			SEABROOK	TX	77586
J T BAILEY	NERMAG INC	136 MOSSWOOD CT		RICHMOND	VA	23236
PETER F BAKER	COLL OF PHARMACY	UNIV OF ARIZONA		TUCSON	AZ	85719
E S BAKER	ROCKWELL HANFORD	200 WEST 234-5		RICHLAND	WA	99352
DEBBE BALBO	EXTRANUCLEAR	PO BOX 11512		PITTSBURGH	PA	15238
J M BALLARD	LOCKHEED EMSCO	PO BOX 15027		LAS VEGAS	NV	89114
KEVIN D BALLARD	MED UNIV OF SC	PHARMACOLOGY DEPT	176 ASHLEY AVENUE	CHARLESTON	SC	29425
MICHAEL P BARBALAS	HOFFMAN LAROCHE	BLDG 86		NUTLEY	NJ	07110
DOUGLAS F BAROFSKY	OREGON GRAD CTR	19600 NW WALKER RD		BEAVERTON	OR	97006
ROBERT P BARRON	FDA-NCDB-OD	HFN-420	200 C ST SW	WASHINGTON	DC	20204
MICHAEL J BARTELS	BAYLOR COLL OF MED	TEXAS MED CTR		HOUSTON	TX	77030
JOHN BARTMESS	INDIANA UNIV	CHEMISTRY DEPT		BLOOMINGTON	IN	47405
BRENDA P BASILE	UNIV OF HOUSTON	18314 ELMDON		HOUSTON	TX	77084
LEWIS M BASS	CHEMISTRY DEPT	UNIV OF N CAROLINA		CHAPEL HILL	NC	27514
C F BATTEN	UNIV OF HOUSTON	CHEMISTRY DEPT		HOUSTON	TX	77004
DAVID R BATTISTE	150 PETROLEUM LAB	PHILLIPS RESEARCH	PHILLIPS PETROLEUM	BARTLESVILLE	OK	74004
MARK R BAUER	MICHIGAN STATE UNIV	CHEMISTRY DEPT		EAST LANSING	MI	48824
CHARLENE W BAYER	GEORGIA INST OF TECH	EES/EDL/EHSD		ATLANTA	GA	30092
M GOKHAN BAYKUT	CHEMISTRY DEPT	UNIV OF FLORIDA		GAINESVILLE	FL	32611
CHARLES K BAYNE	OAK RIDGE NAT'L LAB	PO BOX X BLDG 2029		OAK RIDGE	TN	37830
ALFRED J BEATTIE	E I DUPONT	EXPERIMENTAL STA	PPD BLDG 269	WILMINGTON	DE	19898
DEBRA J BECK	ONEIDA RESEARCH	3 ELLINWOOD CT		NEW HARTFORD	NY	13413
OLAF BECK	PSYCHIATRY DEPT	STANFORD UNIV MED		STANFORD	CA	94305
CHRISTOPHER H BECKER	SRI INTERNATIONAL	M S PS091	CHEMICAL PHYSICS LAB	MENLO PARK	CA	94025
CARL F BECKNER	MICHIGAN STATE UNIV	CHEMISTRY DEPT		EAST LANSING	MI	48824
F A BENCSATH	430 E 63RD ST	APT 3 G		NEW YORK	NY	10021
BRIAN D BENNETT	CHEMISTRY DEPT	UNIV OF CINCINNATI		CINCINNATI	OH	45221

NAME	A1	A2	A3	C1	STA	ZP
BRYAN L BENTZ	RCA LABS	SARNOFF RES CTR		PRINCETON	NJ	08540
WOLFGANG BENZ	HOFFMANN-LAROCHE INC	KINGSLAND ST		NUTLEY	NJ	07110
P S BERGER	TEKNIVENT CORP	10774 TRENTON CORP		ST LOUIS	MO	63132
DOROTHY BERTINO	227 N ROBERSON ST			CHAPEL HILL	NC	27514
LEON D BETOWSKI	EPA-EMSL	QUAL ASSURANCE DIV	PO BOX 15027	LAS VEGAS	NV	89114
MARIA BEUG	CHEMISTRY DEPT	TEXAS A&M UNIV		COLLEGE STATION	TX	77840
K BIEMANN	MIT	CHEMISTRY 56-010		CAMBRIDGE	MA	02139
HEINZ W BIERMANN	CHEMISTRY DEPT	UNIV OF CALIFORNIA		RIVERSIDE	CA	92521
ROBERT C BINIAKEWITZ	ST REGIS PAPER CO	WEST NYACK ROAD		WEST NYACK	NY	10994
GEORGE M BIRD	SUN CHEMICAL CORP	631 CENTRAL AVE		CARLSTADT	NJ	07072
IAN A BLAIR	PHARMACOLOGY DEPT	VANDERBILT UNIV		NASHVILLE	TN	37232
CALVIN R BLAKLEY	UNIV OF HOUSTON	CHEMISTRY DEPT		HOUSTON	TX	77004
WILLIAM E BLANTON	WESTERN RES INST	BOX 3395		LARAMIE	WY	82071
KARL BLOM	6 WENARK DR	APT 12		NEWARK	DE	19713
LYNN J BLUETT	154 BIRCHWOOD DR			ROCHESTER	NY	14622
FRANK M BOCKHOFF	STANDARD OIL CO	4440 WARRENSVILLE CT		CLEVELAND	OH	44128
DANIEL D BOMBICK	2925 BEAUJARDIN	NO 325		LANSING	MI	48910
HENRY A BONDAROVICH	5 CASALE DR			WARREN	NJ	07060
WILLIAM BONE	WRAIR	ATTN BIOCHEMISTRY	WALT REED ARMY MED	WASHINGTON	DC	20307
DAVID W BONNELL	NATL BUR OF STANDARD	A329 223		WASHINGTON	DC	20234
RON BONNER	FINNIGAN MAT INST	11 TRIANGLE PARK DR		CINCINNATI	OH	45042
JIM BORTHWICK	GEOLOGICAL SCIENCES	STHRN METHODIST UNIV		DALLAS	TX	75275
JULIET H BORTHWICK	ARCO OIL & GAS CO	PO BOX 2819	PRC-9128	DALLAS	TX	75221
DAVID BOSTWICK	GEORGIA INST OF TECH	CHEMISTRY DEPT		ATLANTA	GA	30332
WILLIAM J BOULDIN	DOW CHEMICAL	BLDG B-1226		FREEPORT	TX	77541
JAMES A BOURG	3017 HARING ROAD			METAIRIE	LA	70002
M T BOWERS	UNIV OF CALIFORNIA	CHEMISTRY DEPT		SANTA BARBARA	CA	93106
WILLIAM D BOWERS	CHEMISTRY DEPT	UNIV OF CALIFORNIA		IRVINE	CA	92717
D E BRACKEN	GENERAL ELECTRIC CO	BLDG EP3 ROOM 23	PO BOX 4840	SYRACUSE	NY	13221
JOEL C BRADLEY	CAMBRIDGE ISOTOPES	20 COMMERCE WAY		WOBURN	MA	01801
D K BRAIN	PROCTER & GAMBLE	IVORYDALE TECH CENTR		CINCINNATI	OH	45217
HAL R BRAND	MAIL STOP L-308	PO BOX 808		LIVERMORE	CA	94550
VERNON O BRANDT	ETHYL CORP	BOX 341		BATON ROUGE	LA	70821
ALAN BREAU	HARVARD SCH PUB HLTH	665 HUNTINGTON AVE		BOSTON	MA	02115
DAVID BRENT	BURROUGHS WELLCOME	3030 CORNWALLS		RESEARCH TRIANGLE PK	NC	27709
DON BRICKER	TEXAS A&M	CHEMISTRY DEPT		COLLEGE STN	TX	77840
FRED W BRILL	700 N SPENCE ABE	APT B-8		GOLDSBORO	NC	27530
KAREN A BRLETIC	NAT'L BUR OF STAN	BLDG 221 ROOM A21		WASHINGTON	DC	20234
HARRY O BROTHERTON	CHEMISTRY DEPT	NORTHEAST LA UNIV		MONROE	LA	71209
JOHNIE C BROWN	6601 EAST ADAMS			BARTLESVILLE	OK	74006
W M BRUBAKER	1954 HIGHLAND OAKS			ARCADIA	CA	91006
KEITH C BRUCE	LOS ALAMOS NAT'L LAB	PO BOX 1663 MS J980		LOS ALAMOS	NM	87545
ROBERT J BRUNFELDT	R J BRUNFELDT CO	PO BOX 2066		BARTLESVILLE	OK	74005
MICHELLE V BUCHANAN	OAK RIDGE NAT'L LAB	BOX X 4500S E160		OAK RIDGE	TN	37830
JAMES D BUCHNER	EXTRANUCLEAR LABS	PO BOX 11512		PITTSBURGH	PA	15238
W L BUDDE	EPA	26 W ST CLAIR ST		CINCINNATI	OH	45268
L A BURCHFIELD	PO BOX 1089			MIDLOTHIAN	TX	76065
DAVID J BURINSKY	EASTERN REG RES CTR	600 E MERMAID LANE		PHILADELPHIA	PA	19118
A L BURLINGAME	UNIV OF CALIFORNIA	PHARMCEUTICAL CHEM		SAN FRANCISCO	CA	94143
JOAN T BURSEY	RES TRIANGLE INST	PO BOX 12194	CLSD	RES TRI PK	NC	27709
MAURICE M BURSEY	UNIV NORTH CAROLINA	CHEMISTRY DEPT 045A		CHAPEL HILL	NC	27514
KENNETH L BUSCH	CHEMISTRY DEPT	INDIANA UNIV		BLOOMINGTON	IN	47401
GEORGE F BUTLER	554 RED ROCK DR			WADSWORTH	OH	44281
S E BUTTRILL	CHAS EVANS & ASSOC	1670 S AMPHLET BLVD		SAN MATEO	CA	94402
W H BUTTRILL	1616 MEETING HOUSE			ANNAPOLIS	MD	21401
GARY D BYRD	NAT'L BUR OF STAN	A 113 CHEMISTRY		WASHINGTON	DC	20234
COLLEEN G CACIC	US DOE	NEW BRUNSWICK LAB	9800 S CASS AVE	ARGONNE	IL	60439

NAME	A1	A2	A3	CI	STA	ZP
JOHN H CALLAHAN	UNIV OF ILLINOIS	56 ROGER ADAMS LAB	1209 W CALIFORNIA ST	URBANA	IL	61801
JOHN B CALLAGHAN	9224 KNOLL CREST	LOOP		AUSTIN	TX	78759
P S CALLERY	UNIV OF MARYLAND	20 N PINE ST		BALTIMORE	MD	21201
DOUGLAS CAMERON	UNION OIL CO OF CA	SCI & TECH DIV		BREA	CA	92621
JOSEPH E CAMPANA	NAVAL RES LAB	CHEMISTRY DIV	CODE 6110	WASHINGTON	DC	20375
SCOTT CAMPBELL	SHELL DEV CO	PO BOX 4248		MODESTO	CA	95352
THOMAS W CAMPBELL	5611 DELWOOD DR			AUSTIN	TX	78723
DAVID C CANADA	MARTIN MARIETTA CORP	PO BOX P K10048		OAK RIDGE	TN	37830
JOHN E CANTLE	VG INSTRUMENTS	300 BROAD STREET		STAMFORD	CT	06901
RICHARD M CAPRIOLI	UNIV OF TEXAS HSC	PO BOX 20708		HOUSTON	TX	77030
JO CARLIN	MERCK SHARP & DOHME	RESEARCH LABORATORY	PO BOX 2000	RAHWAY	NJ	07065
TIMOTHY J CARLIN	MOBIL RES & DEV CORP	RESEARCH DEPT		PAULSBORO	NJ	08066
STEPHEN F CARLSEN	CIBA-GEIGY	444 SAW MILL RIV RD		ARDSLEY	NY	10502
STEVEN A CARR	DEPT OF NUTRITION	HARVARD SCH PUB HEAL	665 HUNTINGTON AVE	BOSTON	MA	02115
ALLEN M CARY	FINNIGAN MAT	355 RIVER OAKS PKWY		SAN JOSE	CA	95134
BENNETT D CASS	ENGELHARD CORP	MENLO PARK		EDISON	NJ	08818
MAURO E CASTRO	TEXAS A&M	CHEMISTRY DEPT		COLLEGE STN	TX	77843
STEVEN P CEPA	ABBOTT LABS	D 417 AP-9		N CHICAGO	IL	60064
RONALD L CERNY	CHEMISTRY DEPT	MCMS	UNIV OF NEBRASKA	LINCOLN	NE	68588
J W CHAI	TIMBERVIEW APT 1C			ORONO	ME	04473
WENGANG CHAI	PHAR CHEMISTRY	SCH OF PHARMACY	UNIV OF CALIFORNIA	SAN FRANCISCO	CA	94143
B T CHAIT	ROCKEFELLER UNIV	1230 YORK AVE		NEW YORK	NY	10021
JOHN A CHAKEL	GENENTECH INC	460 PT SAN BRUNO		SO SAN FRANCISCO	CA	94080
W S CHAMBERLIN	1001 CEDRO CT			LOS ALAMOS	NM	87544
KELVIN W CHAN	CHEMISTRY DEPT	BAKER LAB BOX 400	CORNELL UNIV	ITHACA	NY	14853
CHERNG CHANG	WRIGHT STATE UNIV	BREHM LAB		DAYTON	OH	45431
S Y CHANG	MCNEIL PHARM	WELSH & MCKEAN RD		SPRING HOUSE	PA	19477
T L CHANG	AMERICAN CYANAMID	1937 W MAIN ST		STAMFORD	CT	06904
RICHARD CHAPMAN	FINNIGAN MAT	355 RIVER OAKS PKWY		SAN JOSE	CA	95134
BONNIE A CHARPENTIER	PROCTER & GAMBLE CO	6071 CENTER HILL RD	FOODS F1B26	CINCINNATI	OH	45224
PHILIPPE CHASTAGNER	E I DUPONT	SAVANNAH RIVER LAB		AIKEN	SC	29808
C H CHEN	OAK RIDGE NAT'L LAB	MARTIN-MARIETTA		OAK RIDGE	TN	37831
EDWARD C M CHEN	4046 DURNESS			HOUSTON	TX	77025
F H CHEN	LBNT NIEHS	PO BOX 12233		RES TRI PK	NC	27709
TUNG-HO CHEN	AMCCOM, ARDC	EMD BLDG 3028		DOVER	NJ	07801
YA-CHI CHEN	2507 CREEK MEADOW DR			HOUSTON	TX	77084
MICHAEL T CHENG	STAUFFER CHEM CO	1200 SOUTH 47TH ST		RICHMOND	CA	94804
EDWARD K CHESS	BATTELLE NWST LABS	PO BOX 999		RICHLAND	WA	99352
G B CHHEDA	ROSWELL PRK INSTITUT	666 ELM STREET		BUFFALO	NY	14263
T C CHIANG	JOHNSON & JOHNSON	RESEARCH CENTER	RT 1	NORTH BRUNSWICK	NJ	08903
MICHAEL P CHIARELLI	2205 S 10TH STREET	NO 107		LINCOLN	NE	68502
JOHN W CHINN	CHEMISTRY DEPT	UNIV OF TEXAS		AUSTIN	TX	78712
DIANE CHO	FINNIGAN MAT	355 RIVER OAKS PKWY		SAN JOSE	CA	95134
R G CHRISTENSEN	NAT'L BUR STANDARDS	RM A-113 CHEMISTRY		WASHINGTON	DC	20234
PETER CHRISTIANSEN	FINNIGAN MAT	355 RIVER OAKS PKWY		SAN JOSE	CA	95134
W H CHRISTIE	OAK RIDGE NAT'L LAB	PO BOX Y BLDG 9735		OAK RIDGE	TN	37830
R K CHRISTOPHER	355 RIVER OAKS PKWY			SAN JOSE	CA	95134
T Z CHU	FINNIGAN CORP	355 RIVER OAKS PKWY		SAN JOSE	CA	95134
HENRY CHUNG	R J REYNOLDS TOBACCO	RESEARCH DEPT	ANALYTICAL DIV	WINSTON-SALEM	NC	27102
LILLIAN CHURCHILL	UOP INC	TEN UOP PLAZA	ALGONQUIN/MT PRSPECT	DES PLAINES	IL	60016
JAMES D CIUPEK	PURDUE UNIVERSITY	CHEMISTRY DEPT	BOX 360	WEST LAFAYETTE	IN	47907
KEITH L CLAY	UNIV OF COLORADO	PHARMACOLOGY DEPT	4200 E 9TH AVE	DENVER	CO	80262
DALE CLYDE	CHEMISTRY DEPT	TRINITY UNIV		SAN ANTONIO	TX	78284
RONALD L COCHRAN	ASHLAND CHEMICAL CO	PO BOX 2219		COLUMBUS	OH	43216
R B CODY	NICOLET INST CO	5225-1 VERONA RD		MADISON	WI	53711
MICHAEL J COGGIOLA	SRI INTERNATIONAL	333 RAVENSWOOD AVE		MENLO PARK	CA	94025
STEVEN L COHEN	CORNELL UNIV	BAKER LAB BOX 35		ITHACA	NY	14853

NAME	A1	A2	A3	CI	STA	ZP
K H COLBERG	AMERICAN CAN CO	TECH SER		BARRINGTON	IL	60010
BRUCE N COLBY	S-CUBED	BOX 1620		LAJOLLA	CA	92038
RICHARD B COLE	CHEMISTRY DEPT	VENABLE HALL 045A	UNIV OF N CAROLINA	CHAPEL HILL	NC	27514
G J COLLINS	STAUFFER CHEM CO			DOBBS FERRY	NY	10522
JOHN J COLLINS	10506 YUCCA DRIVE			AUSTIN	TX	78759
L H COLLINS	708 CANTERBURY HILL			SAN ANTONIO	TX	78209
RICHARD J COLTON	NRL	CODE 6170		WASHINGTON	DC	20375
K R COMPSON	26A FRANKLIN AVE			MONTVALE	NJ	07645
CONRAD CONE	IFF R&D	1515 HIGHWAY 36		UNION BEACH	NJ	07735
JOHN D CONNELL	KRATOS SCIENTIFIC	603 ROSE CT		LISLE	IL	60532
GERALD R CONNER	INFICON LEYBOLD	6500 FLY ROAD		E SYRACUSE	NY	13057
R J CONZEMIUS	1211 GARFIELD AVE			AMES	IA	50010
J CARTER COOK	UNIV OF ILLINOIS	CHEMICAL SCIENCES		URBANA	IL	61801
KELSEY D COOK	CHEMISTRY DEPT	UNIV OF TENNESSEE		KNOXVILLE	TN	37996
R G COOKS	PURDUE UNIVERSITY	CHEMISTRY DEPT		WEST LAFAYETTE	IN	47907
C V COOPER	NIOSH	4676 COLUMBIA PKWY		CINCINNATI	OH	45226
DON A COOPER	DEA SPECIAL TESTING	7704 OLD SPRINGHOUSE		MCLEAN	VA	22101
CATHERINE E COSTELLO	MIT	CHEMISTRY 56-029	77 MASS AVE	CAMBRIDGE	MA	02139
D B COSULICH	LEDERLE LABORATORIES	MIDDLETOWN RD		PEARL RIVER	NY	10965
R J COTTER	JOHNS HOPKINS UNIV	MID ATLANTIC MS LAB	725 N WOLFE ST	BALTIMORE	MD	21205
JOHN COUTANT	MERRELL DOW PHARM	2110 E GALBRAITH RD		CINCINNATI	OH	45215
THOMAS COVEY	EQUINE DRUG TESTING	925 WARREN DR		ITHACA	NY	14850
J WAYNE COWENS	54 IRVING PLACE			BUFFALO	NY	14201
JOHN COWPAR	2880 19TH STREET			BOULDER	CO	80302
STAN CRAFT	2722 DEDMAN			PASADENA	CA	77503
PAMELA F CRAIN	UNIV OF UTAH	310 SKAGGS HALL		SALT LAKE CITY	UT	84112
D W CRAWFORD	US DEPT OF ENERGY	9800 S CASS AVE		ARGONNE	IL	60439
RICHARD W CRAWFORD	LLNL	PO BOX 808	L 310	LIVERMORE	CA	94550
KEVIN P CROSS	CHEMISTRY DEPT	MICHIGAN STATE UNIV		EAST LANSING	MI	48824
F W CROW	UNIV OF NEBRASKA	CHEMISTRY DEPT	MCMS	LINCOLN	NE	68588
FRED CUMMINGS	DUPONT MARSHALL LAB	BLDG 227 ROOM 111	PO BOX 3886	PHILADELPHIA	PA	19146
BOSTICK CURRY	HEWLETT PACKARD	1651 PAGE MILL RD	BLDG 28C	PALO ALTO	CA	94304
ZORAH F CURRY	2650 BENTLEY ROAD			MARIETTA	GA	30067
JEAN CZUCZWA	INDIANA UNIV	CHEMISTRY DEPT		BLOOMINGTON	IN	47405
MARIA-LOURDES DAHL	MONSANTO	800 N LINDBERGH		ST LOUIS	MO	63167
JIM DAHLGRAN	BORG WARNER CHEMICAL	PO BOX 68		WASHINGTON	WV	26181
FRED DALE	LID/AFGL	HANSCOM AFB		BEDFORD	MA	01731
H S DANACEAU	7 BROOKES AVE			GAITHERSBURG	MD	20760
PAUL O DANIS	BAKER LAB	CORNELL UNIV		ITHACA	NY	14853
CHHABIL DASS	STOUT NEUROSCIENCES	MASS SPEC LAB	956 GOURD ST	MEMPHIS	TN	38163
PRADIP R DAS	UNIV OF NEBRASKA	CHEMISTRY DEPT	541 HAMILTON HALL	LINCOLN	NE	68588
JOHN P DAVIES	1016 HAWKINS GRAD	HOUSE		W LAFAYETTE	IN	47906
DEAN V DAVIS	650 TAMARACK AVE	NO 1213		BREA	CA	92621
ROBERT A DAY	UNIV OF CINCINNATI	CHEMISTRY DEPT		CINCINNATI	OH	45221
D E DEAL	11761 E HERNDON AVE			CLOVIS	CA	93612
EMILE C DEAL	3107 GOOD HOPE AVE	NO 216		TEMPLE HILLS	MD	20748
JAMES J DECORPO	NAVAL SEA SYS COMM	CODE 05R32		WASHINGTON	DC	20362
JOHN A DEFEVER	14469 ELLEN DR			LIVONIA	MI	48154
MAX L DEINZER	OREGON STATE UNIV	AGRICUL CHEM DEPT		CORVALLIS	OR	97331
DANA E DEJOHN	WARNER LAMBERT	PO BOX 1047	2800 PLYMOUTH RD	ANN ARBOR	MI	48106
DON C DEJONGH	FINNIGAN CORP	355 RIVER OAKS PKWY		SAN JOSE	CA	95134
JOHN DE KANEL	CHEMISTRY DEPT	FLORIDA STATE UNIV		TALLAHASSEE	FL	32306
SHERRI-SUE DELBERT	C/O W D BOWERS	CHEMISTRY DEPT	UNIV OF CALIFORNIA	IRVINE	CA	92715
DAN DELINGER	RCA SELECTAVISION R7	7900 ROCKVILLE RD		INDIANAPOLIS	IN	46219
JAMES E DELMORE	R #7 BOX 54			IDAHO FALLS	ID	83401
CHARLES H DEPUY	UNIV OF COLORADO	CHEMISTRY DEPT	CAMPUS BX 215	BOULDER	CO	80309
FRED L DEROOS	BATTELLE LABS	505 KING AVE		COLUMBUS	OH	43201

NAME	A1	A2	A3	CI	STA	ZP
DOM DESIDERIO	UNIV OF TENNESSEE	STOUT NEUROSCIENCE	800 MADISON AVE	MEMPHIS	TN	38163
ANTHONY J DESTEFANO	NORWICH EATON PHARM	PO BOX 191		NORWICH	NY	13805
KENNETH J DICKENS	VACUMETRICS INC	2261 PALMA DRIVE		VENTURA	CA	93003
ANDREA M DIETRICH	UNIV OF N CAROLINA	ENVIR SCI & ENGIN	ROSENVA HALL RM 155	CHAPEL HILL	NC	27514
MICHAEL F DIXON	GALILEO ELEC-OPTICS	GALILEO PK		STURBRIDGE	MA	01518
JOSEPH R DONNELLY	734 STRAWBERRY PL			HENDERSON	NV	89015
GEORGE D DOOLEY	NUCLIDE CORP	642 E COLLEGE AVE		STATE COLLEGE	PA	16801
RALPH C DOUGHERTY	FLORIDA STATE UNIV	CHEMISTRY DEPT		TALLAHASSEE	FL	32306
MARY ANN DOWD	UT-DALLAS	PO BOX 688		RICHARDSON	TX	75080
STEVE DOWNEY	LOS ALAMOS NAT'L LAB	MS G738		LOS ALAMOS	NM	87545
ROBERT J DOYLE	NAVAL RESEARCH LAB	CODE 6110	4555 OVERLOOK AVE SW	WASHINGTON	DC	20375
PETER A DREIFUSS	FDA	HFF-459	200 C ST SW	WASHINGTON	DC	20204
GEORGE R DUBAY	BRISTOL-MYERS RES	BLDG 23A-336	PO BOX 4755	SYRACUSE	NY	13221
D L DUGGER	114 LEOLEIS DR			MARLBORO	MA	01752
WAYNE K DUHOLKE	THE UPJOHN CO	7171 PORTAGE RD		KALAMAZOO	MI	49001
RICHARD DUNPHY	MONELL CHEM SEN CTR	3500 MARKET ST		PHILADELPHIA	PA	19103
R C DUTKY	14112 NEW HAMP AVE			COLESVILLE	MD	20904
SHIB PRASAD DUTTA	BIOPHYSICS DEPT	ROSWELL PK MEM INST	666 ELM STREET	BUFFALO	NY	14263
PAUL P DYMERSKI	ANALYTICS LABORATORY	PO BOX 25249		RICHMOND	VA	23235
C G EDMONDS	UNIV OF UTAH	COLLEGE OF PHARMACY	MEDICINAL CHEM DEPT	SALT LAKE CITY	UT	84112
JAMES W EDMONDS	PEI, INC	85 MCKEE DRIVE		MAHWAH	NJ	07430
W NOEL EINOLF	PHILIP MORRIS USA	RESEARCH CENTER	PO BOX 26583	RICHMOND	VA	23261
ROBERT E ELLEFSON	MONSANTO RESEARCH CO	MOUND LAB R171		MIAMISBURG	OH	45342
WILLIAM H ELLIOTT	ST LOUIS UNIV	BIOCHEMISTRY DEPT	1402 S GRAND BLVD	ST LOUIS	MO	63104
ROBERT H ELLIS	HEWLETT PACKARD	SCIEN INSTR DIV	1601 CALIFORNIA AVE	PALO ALTO	CA	94304
EDGAR M EMERY	BALZERS CORP	8 SAGAMORE PK RD		HUDSON	NH	03051
CHRISTIE G ENKE	MICHIGAN STATE UNIV	CHEMISTRY DEPT		EAST LANSING	MI	48824
T J ESKEW	NUCLIDE CORP	642 E COLLEGE AVE		STATE COLLEGE	PA	16801
JAMES S ERSKINE	DOW CHEMICAL	B-1219		FREEPORT	TX	77541
JAMES E EVANS	E KENNEDY SHRIVER CT	200 TRAPELO RD		WALTHAM	MA	02254
JAMES V EVANS	MILES LABORATORIES	BTG R & D	ANALTYICAL RESEARCH	ELKHART	IN	46515
JOHN R EYLER	UNIV OF FLORIDA	CHEMISTRY DEPT		GAINESVILLE	FL	32611
HENRY M FALES	6502 STONEHAM RD			BETHESDA	MD	20817
A M FALICK	UNIV OF CALIFORNIA	CHEMISTRY DEPT		BERKELEY	CA	94720
TSENG-YING FAN	7918 PRESTWOOD #6			HOUSTON	TX	77036
TSENG-PU FAN	UNIV OF HOUSTON	CHEMISTRY DEPT	4800 CALHOUN	HOUTON	TX	77004
K F FAULL	STANFORD UNIVERSITY	PSYCHIATRY DEPT	MEDICAL SCHOOL	STANFORD	CA	94305
VERNON J FEIL	1438 3RD ST N			FARGO	ND	58102
JACK R FELKEY	TMS ANALYTICAL	6264 LAPAS TRAIL		INDIANAPOLIS	IN	46268
JERRY FELSHER	21 A HERITAGE DR			NEW CITY	NY	10956
RONG FENG	CHEMISTRY DEPT	BAKER LAB	CORNELL UNIV	ITHACA	NY	14853
JOHN B FENN	ENGINEERING DEPT	YALE UNIV	PO BOX 2159 YALE STA	NEW HAVEN	CT	06405
P V FENNESSEY	UNIV OF COLORADO	MED CTR C232	4200 E 9TH AVE	DENVER	CO	80262
C C FENSELAU	JOHNS HOPKINS UNIV	PHARMACOLOGY DEPT	725 N WOLFE ST	BALTIMORE	MD	21205
ANNA M FERGUSON	THERMODYNAMICS RES	REED MCDONALD BLDG	TEXAS A&M UNIV	COLLEGE STATION	TX	77843
ELDON FERGUSON	AERONOMY LAB	NOAA BLDG 24	325 BROADWAY	BOULDER	CO	80303
G J FERGUSSON	124 NASSAU PLACE			CLAREMONT	CA	91711
DEAN D FETTEROLF	FBI	FBI ACADEMY		QUANTICO	VA	22135
F H FIELD	ROCKEFELLER UNIV	1230 YORK AVE		NEW YORK	NY	10021
W J FIES	155 CHEROKEE WAY			PORTOLA VALLEY	CA	94025
ROBERT E FINNIGAN	FINNIGAN MAT	355 RIVER OAKS PKWY		SAN JOSE	CA	95134
RAYMOND J FINNEY	MONSANTO RES CORP	MOUND FACILITY R-2		MIAMISBURG	OH	45342
ROBERT W FINNEY	CITY HEALTH DEPT	1115 N MACGREGOR DR		HOUSTON	TX	77030
DERRY L FISHEL	KENT STATE UNIV	CHEMISTRY DEPT		KENT	OH	44242
WADE L FITE	EXTRANUCLEAR LAB	240 ALPHA DR	PO BOX 11512	PIITSBURGH	PA	15238
GERALD D FLESCH	IOWA STATE UNIV	AMES LAB	USDOE	AMES	IA	50011
THEODORE L FOLK	227 WASHINGTON AVE			CUYAHOGA FALLS	OH	44221

NAME	A1	A2	A3	CI	STA	ZP
RODGER L FOLTZ	UNIV OF UTAH	CTR HUMAN TOXICOLOGY	38 SKAGGS HALL	SALT LAKE CITY	UT	84112
NORMAN G FOSTER	2719 ROBINWOOD LANE			DENTON	TX	76201
H G FOUDA	PFIZER INC	DRUG METABOLISM		GROTON	CT	06340
DAVID F FRALEY	903 SARBROOK DR			CINCINNATI	OH	45231
THOMAS J FRANCL	AGRICULTURAL RES DIV	AMERICAN CYANAMID CO	PO BOX 400	PRINCETON	NJ	08540
W FRASURE	326 MARION AVE			ST LOUIS	MO	63119
ROY B FREAS	NAVAL RESEARCH LAB	CHEMISTRY DIV	CODE 6110	WASHINGTON	DC	20375
LEIF FREDIN	RICE UNIV	CHEMISTRY DEPT	PO BOX 1892	HOUSTON	TX	77251
J P FREEMAN	1500 ROCK			PINE BLUFF	AR	71602
BEN S FREISER	PURDUE UNIVERSITY	CHEMISTRY DEPT		WEST LAFAYETTE	IN	47907
NELSON M FREW	WOODS HOLE OCEAN INS	REDFIELD BLDG		WOODS HOLE	MA	02543
CARL FREY	459 GRANITE SPRINGS			YORKTOWN HEIGHTS	NY	10598
EMIL W FU	SANDOZ INC	59 ROUTE 10	BLDG 404 RM 376	E HANOVER	NJ	07936
J D FUHRMAN	MONSANTO	800 N LINDBERGH BLVD		ST LOUIS	MO	63166
H FUJIWARA	MONSANTO CO	800 N LINDBERGH BLVD		ST LOUIS	MO	63166
ELAINE K FUKUDA	NAVAL RESEARCH LAB	CHEMISTRY DIV	CODE 6110	WASHINGTON	DC	20375
PHILLIP T FUNKE	E R SQUIBB	PO BOX 4000		PRINCETON	NJ	08540
RAYMOND L FURNER	NEUROSCIENCES PROG	UNIV OF ALABAMA		BIRMINGHAM	AL	35294
P JANE GALE	RCA	DAVID SARNOFF RES CT		PRINCETON	NJ	08540
KENNETH L GALLAHER	SOHIO	4440 WARRENSVILLE RD		CLEVELAND	OH	44128
EMILIO J GALLEGOS	CHEVRON	PO BOX 1627		RICHMOND	CA	94804
E L GARNER	NAT'L BUR STANDARDS	BLDG 222 RM A349		WASHINGTON	DC	20234
LARRY GARRETSON	RADIAN CORP	PO BOX 9948		AUSTIN	TX	78766
DANIEL GARTEIZ	VESTEC	4815 KNICKERBOCKER		HOUSTON	TX	77035
RICHARD GEDAMKE	AYERST LABS RESEARCH	567 RIDGE ROAD		MONMOUTH JCTN	NJ	
WILLIAM GEIGER	18618 PT LOOKOUT DR			HOUSTON	TX	77058
GREGORY I GELLENE	CORNELL UNIV	BAKER LAB BOX 168		ITHACA	NY	14853
SAHBA GHADERI	NICOLET INST CORP	ANAL BLDG	5225 VERONA RD	MADISON	WI	53771
DARYL GIBLIN	4540 LOWELL			LINCOLN	NE	68506
KEITH T GILLEN	SRI INTERNATIONAL	333 RAVENSWOOD AVE		MENLO PARK	CA	94025
JEROME P GILMAN	803 CASHEW CT APT K			BEL AIR	MD	21014
ANNE B GIORDANI	2480 BOWEN ROAD			HOWELL	MI	48843
GARY G GIRDAUKAS	UNIV OF WISCONSIN	PHARMACY DEPT	425 N CHARTER ST	MADISON	WI	53706
O L GLAESMANN	DOW CHEMICAL	PO BOX BB	ENVIRONMENTAL SERV	FREEPORT	TX	77541
G L GLISH	OAK RIDGE NATL LAB	PO BOX Y	BLDG 9735	OAK RIDGE	TN	37830
DOUG GOERINGER	OAK RIDGE NAT'L LAB	PO BOX Y BLDG 9735		OAK RIDGE	TN	37831
ANN G GOETZ	HOFFMANN-LAROCHE	BLDG 71		NUTLEY	NJ	07110
PAUL C GOODLEY	HEWLETT PACKARD	SCI INST DIV	1601 CALIFORNIA AVE	PALO ALTO	CA	94304
G W GOODLOE	AVON PRODUCTS INC	DIVISION ST		SUFFERN	NY	10901
SETH GOODMAN	NICOLET INSTRUMENTS	5225-1 VERONA RD		MADISON	WI	53711
MICHAEL GOODWIN	BIOCHEMISTRY DEPT	PURDUE UNIV		W LAFAYETTE	IN	47907
GWEN D GORETSAS	STATE LAB OF HYGIENE	465 HENRY MALL		MADISON	WI	53706
LEO A GORMAN	VG INSTRUMENTS	134 JUNEDALE DR		CINCINNATI	OH	45218
K GOTO	JEOL USA	235 BIRCHWOOD AVE		CRANFORD	NJ	07016
H GRADE	GENERAL ELECTRIC CO	R&D CENTER	BLDG K-1 PO BOX 8	SCHENECTADY	NY	12301
WILLIAM L GRADY	5603 OLD GUARD	CRESCENT		VIRGINIA BEACH	VA	23462
PETER W GRAVES	RT 1	PO BOX 118		BROOKFIELD	MA	01506
CHARLES L GRAY	SDS BIOTECH	PO BOX 348		PAINESVILLE	OH	44077
JOHN W GRAY	GALILEO ELEC-OPTICS	GALILEO PARK		STURBRIDGE	MA	01518
MICHAEL GRAYSON	3433 BLUFFVIEW DR			ST CHARLES	MO	63301
JOHN GREAVES	MT SINAI HOSPITAL	11 E 100 ST		NEW YORK	NY	10029
M M GREEN	CHEMISTRY DEPT	POLYTECHNIC INST	OF NEW YORK	BROOKLYN	NY	11201
F T GREENE	MIDWEST RESRCH INST	425 VOLKER BLVD		KANSAS CITY	MO	64110
HUGH GREGG	MICHIGAN STATE UNIV	CHEMISTRY DEPT		EAST LANSING	MI	48824
DONALD A GRIFFIN	OREGON STATE UNIV	AGRICULTURAL CHEM		CORVALLIS	OR	97331
LAWRENCE L GRIFFIN	TEXAS A&M UNIV	PO BOX 1675		GALVESTON	TX	77553
RONALD D GRIGSBY	MASSPEC INC	2500 S BERRY ROAD		NORMAN	OK	73069

NAME	A1	A2	A3	CI	STA	ZP
J KEITH GRIME	PROCTER & GAMBLE	IVORYDALE TECH CTR		CINCINNATI	OH	45217
LAWRENCE E GRIMES	CHEMISTRY DEPT	UNIV OF TOLEDO		TOLEDO	OH	43606
ERIC P GRIMSRUD	CHEMISTRY DEPT	MONTANA STATE UNIV		BOZEMAN	MT	59717
G G GRINDSTAFF	MARTIN MARIETTA	Y-12 PLANT	PO BOX Y BLDG 9995	OAK RIDGE	TN	37831
GARY GROENEWOLD	202 ELMHURST DR	H 12		OAK RIDGE	TN	37830
MICHAEL L GROSS	UNIV OF NEBRASKA	CHEMISTRY DEPT		LINCOLN	NE	68588
MARVIN F GROSTIC	THE UPJOHN CO	DEPT 7820	7000 PORTAGE ROAD	KALAMAZOO	MI	49001
JUERGEN GROTEMEYER	CORNELL UNIV	CHEMISTRY DEPT	BAKER LAB	ITHACA	NY	14853
IAN GROVE	3455 TABLE MESA DR	NO 108 A		BOULDER	CO	80303
ALBERT E GUDAT	HEWLETT PACKARD	W120 CENTURY ROAD		PARAMUS	NJ	07653
CHRISTIAN GUENAT	NIEHS	PO BOX 72233		RES TRI PK	NC	27709
H Y GUH	PFIZER INC	EASTERN POINT RD		GROTON	CT	06340
WILSON M GULICK	MICH TECH UNIV	CHEM & CHEM ENGIN		HOUGHTON	MI	49931
DAVID L HACHEY	BAYLOR COLL OF MED	PEDIATRICS DEPT	1200 MOUR SAND	HOUSTON	TX	77030
W F HADDON	35 WILLOW AVE			LARKSPUR	CA	94939
JOHN L HADFIELD	E I DUPONT	EXPERIMENTAL STATION	E302/112	WILMINGTON	DE	19898
J E HALVERSON	1901 WHITEBARK AVE			NORTH AUGUSTA	SC	29841
MYNARD C HAMMING	CONOCO INC			PONCA CITY	OK	74601
C V HAMPTON	22260 INNSBROOK DR			NORTHVILLE	MI	48167
CAROL A HANEY	204 TRAILS END CT			RALEIGH	NC	27614
LINDA HANN	116 LAKESIDE			BRYAN	TX	77801
ALAN HANNA	NICOLET INST CO	5225-1 VERONA RD		MADISON	WI	53711
ROBERT E HANNAH	2840 NESTLING RD			PHILADELPHIA	PA	19154
GORDON E HANSEN	BOEHRINGER-INGELHEIM	RES & DEV CTR	175 BRIAR RIDGE RD	RIDGEFIELD	CT	06876
SHINJI HARA	JEOL USA	235 BIRCHWOOD AVE		CRANFORD	NJ	07016
E D HARDIN	DEPT OF CHEMISTRY	UNIV OF HOUSTON		HOUSTON	TX	77004
RITA H HARDY	UNIV OF KENTUCKY	3548 LAREDO DR		LEXINGTON	KY	40502
PETER E HAROLDSEN	UNIV COLO SCH MED	4200 E 9TH AVE C236	PHARMACOLOGY DEPT	DENVER	CO	80262
TIMOTHY HARPER	UNIV OF COLORADO	BOX C236	4200 EAST NINTH AVE	DENVER	CO	80220
WILLIAM L HARRINGTON	RCA LABORATORIES	DAVID SARNOFF RES CT		PRINCETON	NJ	08540
JUDITH C HARRIS	15-310 ACORN PARK			CAMBRIDGE	MA	
ROBERT E HARRIS	BOX 41022			BRECKSVILLE	OH	44141
C BRETT HARRISON	PO BOX 11512			PITTSBURGH	PA	15238
W W HARRISON	UNIV OF VIRGINIA	CHEMISTRY DEPT		CHARLOTTESVILLE	VA	22901
NEIL R HARTMAN	MAYO CLINIC	740 GUGGENHEIM BLDG		ROCHESTER	MN	55905
MARK A HARTWIG	HEWLETT PACKARD	5201 TOLLVIEW DR		ROLLING MEADOWS	IL	60008
D J HARVAN	NIEHS	PO BOX 12233		RES TRI PK	NC	27709
J RONALD HASS	NIEHS	PO BOX 12233		RES TRI PK	NC	27709
F W HATCH	BOEHRINGER INGELHEIM	90 EAST RIDGE	PO BOX 368	RIDGEFIELD	CT	06877
SUSAN HATTOX	BOEHRINGER INGELHEIM	175 BRIAR RIDGE RD		RIDGEFIELD	CT	06877
DAVID A HAYES	RADIAN CORP	PO BOX 9948		AUSTIN	TX	78766
MICHAEL J HAYES	CIBA-GEIGY CORP	444 SAW MILL RIVER		ARDSLEY	NY	
EUGENE C HEATH	HARRIS LABS	PO BOX 80837		LINCOLN	NE	68501
D L HEIKES	FDA	1009 CHERRY		KANSAS CITY	MO	64106
RICHARD E HEIN	NICOLET INSTRUMENTS	5225 VERONA RD		MADISON	WI	53711
BRUCE T HEITKE	CRDC	RESEARCH DIV	ANALYTICAL BRANCH	APG	MD	21010
D N HELLER	JOHN HOPKINS UNIV	B-6 BIOHPYSICS DEPT	725 N WOLFE ST	BALTIMORE	MD	21205
MARK E HEMLING	UNIV OF ILLINOIS	456 RAL BOX 76-5	1209 W CALIFORNIA	URBANA	IL	61801
T R HENDERSON	5609 DON FELIPE CT S			ALBUQUERQUE	NM	87105
J D HENION	CORNELL UNIVERSITY	EQUINE DRUG TESTING	925 WARREN ROAD	ITHACA	NY	14850
RICHARD A HEPPNER	WESTERN RES INST	BOX 3395	UNIV STATTION	LARAMIE	WY	82071
GUOR-RONG HER	PO BOX 160	CHEMISTRY DEPT	MICHIGAN STATE UNIV	EAST LANSING	MI	48824
DAVID A HEROLD	UNIV OF VIRGINIA	PATHOLOGY DEPT	MEDICAL CTR	CHARLOTTESVILLE	VA	22908
H S HERTZ	NBS	A309 CHEMISTRY		GAITHERSBURG	MD	20899
L F HERZOG	NUCLIDE CORP	642 E COLLEGE AVE		STATE COLLEGE	PA	16801
KENNETH R HESS	CHEMISTRY DEPT	UNIV OF VIRGINIA		CHARLOTTESVILLE	VA	22901
W B HESS	E I DUPONT	SAVANNAH RIVER LAB	BLDG 232-H	AIKEN	SC	29801

NAME	A1	A2	A3	CI	STA	ZP
DENNIS L HEURING	TMS ANAL SERVICES	6264 LAPAS TRAIL		INDIANAPOLIS	IN	46268
DAVE HEWETSON	STAKMAN HALL	UNIV OF MINNESOTA	1519 GORTNER AVE	ST PAUL	MN	55108
R ANTHONY HICKS	E I DUPONT	BLDG 232 H		AIKEN	SC	29808
BRUCE J HIDY	BATTELLE LABS	505 KING AVE		COLUMBUS	OH	43201
CHARLES E HIGNITE	IBM BLDG 13	DEPT E35	5600 COTTLE RD	SAN JOSE	CA	95120
T HIGUCHI	JEOL USA	235 BIRCHWOOD AVE		CRANFORD	NJ	07016
DAVID R HILKER	17 VAN BUREN AVE			E GREENBUSH	NY	12061
JOHN C HILL	1501 HARVEY ROAD	APT 833		COLLEGE STATION	TX	77843
JOSEPH F HILLER	NALCO CHEMICAL CO	PO BOX 87		HOUSTON	TX	77478
LAURENCE R HILPERT	NAT'L BUR STAN	BLDG 222 RM A-113		WASHINGTON	DC	20234
DAVID M HINDENLANG	ALLIED CORP	PO BOX 1021R		MORRISTOWN	NJ	07960
DAVID S HIRANO	2828 COLLEGE AVE NO			BERKELEY	CA	94705
RONALD A HITES	INDIANA UNIV	SPEA 410 H		BLOOMINGTON	IN	47405
MICHAEL K HOFFMAN	USDA-FSIS-CDLB	BLDG 318 BARC-EAST		BELTSVILLE	MD	20705
CARL HOGBERG	6901 BRYN MAWR DR			AUSTIN	TX	78723
D H HOLKEBOER	231 WINDCREST DR			CAMILLUS	NY	13031
J S HOLLER	CENTER DISEASE CNTRL	TOXI BRANCH C17-1814		ATLANTA	GA	30333
GALE A HOLMES	DOW CHEMICAL CO	BLDG B-1219		FREEPORT	TX	77541
RICHARD E HONIG	RCA LABORATORIES			PRINCETON	NJ	08540
J P HONOVICH	CASE WESTERN RESERVE	CHEMISTRY DEPT	MILLIS SCIENCE CTR	CLEVELAND	OH	44106
ROBIN J HOOD	CHEMISTRY DEPT	75 CHEMISTRY	WAYNE STATE UNIV	DETROIT	MI	48202
JOHN J HOPPE	VACUMETRICS INC	2261-81 PALMA DR		VENTURA	CA	93003
JOSEPH P HOPPESCH	BORG-WARNER RESEARCH	WOLF & ALGONQUIN RDS		DES PLAINES	IL	60018
YANNIK HOPPILLIARD-NGUYEN	UNIV OF N CAROLINA	CHEMISTRY DEPT		CHAPEL HILL	NC	27514
EVAN C HORNING	11610 STARWOOD DR			HOUSTON	TX	77024
MARJORIE G HORNING	BAYLOR COLL MEDICINE	INST LIPID RESEARCH	TEXAS MEDICAL CENTER	HOUSTON	TX	77030
W N HOWALD	UNIV OF WASHINGTON B	331 BAGLEY HALL		SEATTLE	WA	98195
J D HRIBAR	G D SEARLE & CO	4901 SEARLE PKWY		SKOKIE	IL	60077
CHING-HSIU HSIEH	3301 CLEARVIEW DR			AUSTIN	TX	78703
CHRISTINA HSIEH	VESTEC CORP	2524 SUNSET BLVD		HOUSTON	TX	77005
TACHENG HSIEH	VELSICOL CHEM CORP	ANAL RESEARCH	341 E OHIO ST	CHICAGO	IL	60611
THOMAS C HSIEH	BIOCHEMISTRY DEPT	LOUISIANA ST UNIV		BATON ROUGE	LA	70803
C S HSU	EXXON RES & ENGIN	PO BOX 121		LINDEN	NJ	07036
FRANCIS S HSU	PHILIP MORRIS USA	PO BOX 26583		RICHMOND	VA	23261
KAI-LO HSU	861 SAN PABLO WAY			DUARTE	CA	91010
FRANCIS Y HUANG	RABA-KISTNER CONSULT	10526 GULFDALE		SAN ANTONIO	TX	78216
S HUANG	MIDWEST CTR MASS SP	CHEMISTRY DEPT	UNIV OF NEBRASKA	LINCOLN	NE	68588
C E HUDSON	MARINE BIOMEDICAL	200 UNIVERSITY BLVD		GALVESTON	TX	77550
J E HUDSON	ALCON LABORATORIES	PO BOX 1959		FORT WORTH	TX	76101
B M HUGHES	1563 LINDENHURST			DAYTON	OH	45459
DAVID B HUGHES	34 LANGHORNE CR			NEWPORT NEWS	VA	23606
HELEN HUGHES	INST FOR LIPID RES	BAYLOR COLL OF MED	1200 MOURSUND	HOUSTON	TX	77030
MICHAEL HUGHES	UNIV OF TX MED BRNCH	MARINE BIOMED INST	200 UNIVERSITY BLVD	GALVESTON	TX	77550
SUE V HUMMEL	USDA FSIS CDLB	BLDG 318		BELTSVILLE	MD	20705
H L HUNG	CHEMISTRY DEPT	NORTHWESTERN UNIV	2145 SHERIDAN RD	EVANSTON	IL	60201
DONALD F HUNT	UNIV OF VIRGINIA	CHEMISTRY DEPT		CHARLOTTESVILLE	VA	22901
JERRY E HUNT	CHEM DIV 200 C173	ARGONNE NAT'L LAB	9700 S CASS AVE	ARGONNE	IL	60439
R L HUNTER	UNIV OF CALIFORNIA	CHEMISTRY DEPT		IRVINE	CA	92717
PAUL M HYDE	LSUMC	BIOCHEMISTRY DEPT	1901 PERDIDO ST	NEW ORLEANS	LA	70112
KAREN J HYVER	19 E 22ND STREET			BALTIMORE	MD	21218
KAMAL E IBRAHIM	BOX J 374 JHMHC	RADIOLOGY DEPT		GAINESVILLE	FL	32610
ANDREAS J ILLIES	UC-SANTA BARBARA	CHEMISTRY DEPT		SANTA BARBARA	CA	93105
R N INFANTE	CATHOLIC UNIV	CHEMISTRY DEPT		PONCE	PR	00731
RUTH R INNERS	MCNEIL PHARMACEUTIC	CHEMICAL RESEARCH		SPRING HOUSE	PA	19477
CHARLES S IRVING	STABB ISOTOPE LAB	MEDICAL TOWER BLDG	6608 FANNIN	HOUSTON	TX	77030
PHILLIP ISSENBERG	UNIV OF NEBRASKA	EPPLEY INST	MEDICAL CENTER	OMAHA	NE	68105
Y ITAGAKI	JEOL USA	235 BIRCHWOOD AVE		CRANFORD	NJ	07016

NAME	A1	A2	A3	CI	STA	ZP
CARSON JACKSON	R J BRUNFELDT CO	PO BOX 2066		BARTLESVILLE	OK	74005
THOMAS D JACKSON	RT 2 BOX 233L			LEESBURG	VA	22075
T J JACKSON	1614 RICHFOREST			RICHARDSON	TX	75081
DAVID JACOBS	PO BOX 8016			COLLEGE STATION	TX	77844
M LEROY JACOBS	COMMERICAL TESTING	AND ENGINEERING	490 ORCHARD ST	GOLDEN	CO	80401
RUDOLF R JAFFE	INDIANA UNIV	CHEMISTRY DEPT		BLOOMINGTON	IN	47405
GEORGE JAKUBOWSKI	TRAVENOL LABS	6301 LINCOLN AVE		MORTON GROVE	IL	60053
GENE C JAMIESON	ZOECON CORP	975 CALIFORNIA AVE	PO BOX 10975	PALO ALTO	CA	94304
IAN JARDINE	MAYO CLINIC	PHARMACOLOGY DEPT	200 1ST STREET SW	ROCHESTER	MN	55905
K JAYASIMHULU	UNIV OF CINCINNATI	700 MORGAN HALL		CINCINNATI	OH	45219
BARBARA JELUS-TYROR	3656 WOODS RD			WILLIAMSON	NY	14589
NANCY JEAN JENSEN	BOX 725	HAMILTON HALL	UNIV OF NEBRASKA	LINCOLN	NE	68508
ALFRED H JENSON	662 ARBOR VALLEY			CAMPBELL HALL	NY	10916
XIANG-YU JIANG	CHEMISTRY DEPT	PURDUE UNIV		W LAFAYETTE	IN	
JEROME A JOHEMKO	FINNIGAN MAT	355 RIVER OAKS PKWY		SAN JOSE	CA	95134
JODIE V JOHNSON	2124 NE 7 ST			GAINESVILE	FL	32601
RICHARD M JOHNSTON	FINNIGAN CORP	355 RIVER OAKS PKWY		SAN JOSE	CA	95134
GILBERT G JONES	AMOCO RES CTR	PO BOX 400		NAPERVILLE	IL	60566
ERNEST A JORDAN	PO BOX 6959			COLLEGE STATION	TX	77844
CHARLES M JUDSON	UNIV OF KANSAS	CHEMISTRY DEPT		LAWRENCE	KS	66044
GREGOR A JUNK	IOWA STATE UNIV	AMES LAB	USDOE	AMES	IA	50011
LONNIE G JUSTICE	6215 NORTHGATE RD	APT I		COLUMBUS	OH	43229
ROBERT G KALEY	MONSANTO	800 N LINDBERGH		ST LOUIS	MO	63167
GEORGE J KALLOS	DOW CHEMICAL CO	BLDG 574		MIDLAND	MI	48640
KEVIN A KALMBACH	162 GREENBRIDGE D1			NEWARK	DE	19713
TOM KARNS	UNIV OF OKLAHOMA	CHEMISTRY DEPT	620 PARRINGTON OVAL	NORMAN	OK	73019
KENJI KAWAOKA	EASTMAN KODAK	RESEARCH LABS B-82		ROCHESTER	NY	14650
G L KEARNS	58 BUCKINGHAM DR			STAMFORD	CT	06902
RONALD B KEEFE	HARVEY LABS INC	1216 HARRIS ST		CHARLOTTESVILLE	VA	22901
DAVID J KEITH	CELANESE CHEMICAL CO	PO BOX 9077		CORPUS CHRISTI	TX	78469
PAUL R KELLER	PROCTER & GAMBLE	11520 REED HARTMAN		CINCINNATI	OH	45241
J A KELLEY	NIH	NCI DRUG DESIGN	BLDG 37 RM 6D23	BETHESDA	MD	20205
PAUL E KELLEY	FINNIGAN MAT	355 RIVER OAKS PKWY		SAN JOSE	CA	95134
LEONID KELNER	NIH	BLDG 13 RM 3E65		BETHESDA	MD	20205
MARIANNE KEMPFF	650 MERRICH	APT D-26		DETROIT	MI	48202
LLOYD KENT	KRATOS	170 WILLIAMS DR		RAMSEY	NJ	07446
HILKKA KENTTAMAA	PURDUE UNIV	CHEMISTRY DEPT		WEST LAFAYETTE	IN	47907
CHRISTINE N KENYON	HP SCIENTIFIC INSTR	1601 CALIFORNIA AVE		PALO ALTO	CA	94304
T W KEOUGH	8557 CAVALIER DR			CINCINNATI	OH	45231
EDWARD H KERNS	BRISTOL MYERS CO	2404 PENNSYLVANIA AV		EVANSVILLE	IN	47721
J K KHANDELWAL	MT SINAI MED SCHOOL	PHARMACOLOGY DEPT	100 ST AND 5TH AVE	NEW YORK	NY	10029
DAVID KIDWELL	NAVAL RES LAB	CODE 6170		WASHINGTON	DC	20375
LEWIS B KILLMER	325 N EDGMONT ST			MEDIA	PA	19063
HEE-YONG KIM	UNIV OF HOUSTON	CHEMISTRY DEPT	4800 CALHOUN	HOUSTON	TX	77004
BRENDA J KIMBLE	AMPHION ASSO	PO BOX 19406		WASHINGTON	DC	20036
ROY W KING	UNIV OF FLORIDA	CHEMISTRY DEPT		GAINESVILLE	FL	32611
R D KINSER	PHILIP MORRIS USA	RESEARCH CENTER	PO BOX 26583	RICHMOND	VA	23261
JAMES A KINSINGER	NICOLET ANAL INST	5225 VERONA RD	PO BOX 4508	MADISON	WI	53711
MICHAEL KINTER	42 HAMILTON ROAD			CHAPEL HILL	NC	27514
NADIA D KIRZECKY	AMER CYANAMID CO	PO BOX 400		PRINCETON	NJ	08540
ROBERT W KISER	781 GLENDOVER ROAD			LEXINGTON	KY	40502
F G KITSON	3 HARTFORD PLACE			NEWARK	DE	19711
PETER D KLEIN	4608 FANNIN AVE	RM 519		HOUSTON	TX	77030
DANIEL R KNAPP	MED UNIV S CAROLINA	PHARMACOLOGY DEPT		CHARLESTON	SC	29425
TOSHIAKI KOGAI	UNIV OF DAYTON	CHEMICAL ENGINEERING	300 COLLEGE PK AVE	DAYTON	OH	45469
RICHARD W KONDRAT	CHEMISTRY DEPT	UNIV OF CALIFORNIA		RIVERSIDE	CA	92521
RAMONA KRAILLER	CHEMISTRY DEPT	TEXAS A&M		COLL STATION	TX	77843

NAME	A1	A2	A3	CI	STA	ZP
THOMAS KRICK	UNIV OF MINNESOTA	BIOCHEMISTRY DEPT		ST PAUL	MN	55108
T KRISHNAMURTHY	1400 LONGHILL DR			POTOMAC	MD	20854
MICHAEL J KRISTO	CHEMISTRY DEPT	MICHIGAN STATE UNIV		EAST LANSING	MI	48824
TOSHIYA KUBODERA	SHINADZU SCI INSTR	7102 RIVERWOOD DR		COLUMBIA	MD	21046
FRANCIE M KUBIAK	MILES LABORATORIES	1127 MYRTLE ST BOX40		ELKHART	IN	46515
E KUBOTA	JEOL USA	235 BIRCHWOOD AVE		CRANFORD	NJ	07016
JAMES W KUDLESS	HEWLETT PACKARD	60 NEW ENGLAND AVE W		PISCATAWAY	NJ	08854
DOUGLAS W KUEHL	EPA	6201 CONGDON BLVD		DULUTH	MN	55804
F KUNIHIRO	JEOL USA	235 BIRCHWOOD AVE		CRANFORD	NJ	07016
SHARRON LAAS	EI DUPONT	POLYMER PRODUCTS	269 EXPERIMENTAL STA	WILMINGTON	DE	19898
GILLES LABELLE	141 MAGAZINE ST			CAMBRIDGE	MA	02139
WILLIAM M LAGNA	UNIV OF MARYLAND	SCH OF PHARMACY	20 N PINE ST	BALTIMORE	MD	21201
ROGER A LAINE	BIOCHEMISTRY DEPT	LOUISIANA STATE UNIV		BATON ROUGE	LA	70803
DOROTHY C LANE	ENVIRODYNE ENGINEERS	12161 LACKLAND RD		ST LOUIS	MO	63141
LINDA LANE	ARCO PETROLEUM PROD	400 E SIBLEY BLVD		HARVEY	IL	60422
PATRICK LANGVARDT	DOW CHEMICAL CO	1803 BLDG		MIDLAND	MI	48640
VERONICA LANIER	LLNL	PO BOX 808, L-233		LIVERMORE	CA	94550
STAN LANNING	LAWRENCE LIVERMORE	PO BOX 808		LIVERMORE	CA	
RICK LAPP	HAMILTON HALL RM 28	UNIV OF NEBRASKA		LINCOLN	NE	68588
EDMUND A LARKA	6818 WOODHILL TRAIL			EDEN PRAIRIE	MN	55344
BARBARA S LARSEN	2 PINEDALE RD			NEWARK	DE	19711
DEBORAH J LARSEN	ARTHUR D LITTLE	ACORN PARK		CAMBRIDGE	MA	02140
DOUGLAS W LATER	PO BOX 999			RICHLAND	WA	99352
R KAZMER LATVEN	HEWLETT PACKARD	3003 SCOTT BLVD		SANTA CLARA	CA	95050
J O LAY	AMERICAN CYANAMID	1937 W MAIN ST		STAMFORD	CT	06904
EDWARD B LEDFORD	2601 GARFIELD STREET			LINCOLN	NE	68502
TERRY D LEE	CITY OF HOPE	IMMUNOLOGY DEPT	1450 E DUARTE RD	DUARTE	CA	91010
MICHAEL G LEGENDRE	US DEPT OF AG	1100 ROBT E LEE BLVD	PO BOX 19687	NE WORLEANS	LA	19687
A M LEGRAND	886 TRAILMORE CIRCLE			SUMTER	SC	29150
J P LEHMAN	20 8TH STREET			NEWINGTON	CT	06111
THOMAS A LEHMAN	PO BOX 435			N NEWTON	KS	67117
THOMAS LEIKER	BUR OF RECLAMATION	D-1523	PO BOX 25007	DENVER	CO	80225
SYDELL LEWIS	METABOLISM SECTION	CHDN'S HOSP OF PHILA	CIVIC CTR & 34TH ST	PHILADELPHIA	PA	19102
S G LIAS	NBS			WASHINGTON	DC	20234
DAN LIBERATO	NIH	BLDG 6 RM 136		BETHESDA	MD	20205
J G LIEHR	UNIV OF TEXAS	MEDICAL SCHOOL	PO BOX 20708	HOUSTON	TX	77025
W V LIGON	GENERAL ELECTRIC COD	R&D CENTER	BLDG K1 PO BOX 8	SCHENECTADY	NY	12301
DENIS C K LIN	ENVIR TEST & CERT CO	284 RARATAN CTR PKY		EDISON	NJ	08837
S N LIN	UNIV OF TEXAS HSC	ANALYTICAL CHEMISTRY	PO BOX 20708	HOUSTON	TX	77030
YONG Y LIN	INST BASIC RESEARCH	1050 FOREST HILL RD		STATEN ISLAND	NY	10314
K A LINCOLN	2016 STOCKBRIDGE AVE			REDWOOD CITY	CA	94061
JAMES L LINDGREN	TX AIR CONT BD	6330 HWY 290 E		AUSTIN	TX	78723
DIXIE LIPPSTREU	UNIV OF NEBRASKA	CHEMISTRY DEPT		LINCOLN	NE	68588
CAROL A LISEK	PHARMACOLOGY DEPT	JOHNS HOPKINS UNIV	725 N WOLFE ST	BALTIMORE	MD	21205
DAVID T LITTLE	KRATOS ANALYTICAL	2209 QUARTER MASTER		RESTON	VA	22091
DUANE LITTLEJOHN	NICOLET INSTRUMENTS	5225-1 VERONA ROAD		MADISON	WI	53711
JAMES F LITTON	LOCKHEED	0 48-50 B/195B	PO BOX 504	SUNNYVALE	CA	94086
NORMAN W LIU	SEARLE RES LAB	4901 SEARLE PKWY		SKOKIE	IL	60077
SHUYING LIU	CHEMISTRY DEPT	UNIV OF CALIFORNIA		SANTA BARBARA	CA	93106
JOHN R LLOYD	ORTHO PHARMACEUTICAL	RT 202		RARITAN	NJ	08869
HSI H LO	EXTRANUCLEAR LABS	PO BOX 11512		PITTSBURGH	PA	15238
JOSEPH A LOO	CHEMISTRY DEPT	BAKER LAB	CORNELL UNIV	ITHACA	NY	14853
V LOPEZ-AVILA	ACUREX CORP	485 CLYDE AVE		MNTN VIEW	CA	94042
P R LOY	PO BOX 105005			ATLANTA	GA	30348
NORMAN LOW	HEWLETT-PACKARD	1601 CALIFORNIA AVE		PALO ALTO	CA	94304
DAVID M LUBMAN	CHEMISTRY DEPT	UNIV OF MICHIGAN		ANN ARBOR	MI	48109
VOLKER R LUEG	FINNIGAN CORP	355 RIVER OAKS PKWY		SAN JOSE	CA	95134

NAME	A1	A2	A3	CI	STA	ZP
HENRY E LUMPKIN	1600 DEEP WOOD DR			ROUND ROCK	TX	78664
WILLIAM R LUSBY	8028 NEW RIGGS RD			ADELPHI	MD	20783
PHILIP A LYON	3M COMPANY	CENTRAL RESEARCH	201 BS 05	ST PAUL	MN	55144
JAMES L MACDONALD	RALSTON PURINA CO	3RS CHECKERBOARD SQ		ST LOUIS	MO	63164
RONALD D MACFARLANE	TEXAS A&M UNIVERSITY	CHEMISTRY DEPT		COLLEGE STATION	TX	77843
DONALD F MAGIN	PHILIP MORRIS R&D	BOX 26583		RICHMOND	VA	23261
KENNETH O MAHLER	SCI GLASS ENGIN	2007 KRAMER LANE	SUITE 100	AUSTIN	TX	78758
JOHN MAHONEY	PHRASOR SCIENTIFIC	1536 HIGHLAND AVE		DUARTE	CA	91010
DAVID A MALTBY	PEDIATRIC METAB	BOX 3028	DUKE MEDICAL CTR	DURHAM	NC	27710
VANESSA K MANCILL	239 MOBILTOWN DR			BRYAN	TX	77801
JOSEPH M MARASCO	14023 CASTLE BLVD	NO 204		SILVER SPRG	MD	20904
ALVIN B MARCUS	6 BAYARD ROAD	APT 859		PITTSBURGH	PA	15213
MARK MARCUS	CHEMICAL WASTE MGMT	150 W 137TH STREET		RIVERDALE	IL	60627
RICHARD K MARCUS	CHEMISTRY DEPT	UNIV OF VIRGINIA		CHARLOTTESVILLE	VA	22901
SANFORD P MARKEY	NIMH NIH	BLDG 10-3N322	9000 ROCKVILLE PIKE	BETHESDA	MD	20205
TERRY D MARRIOTT	RICE UNIV	CHEMISTRY DEPT	PO BOX 1892	HOUSTON	TX	77251
PHILIP G MARSH	UNION CARBIDE CORP	CEN SCIENTIFIC LAB		TARYYTOWN	NY	10591
ALAN G MARSHALL	CHEMISTRY DEPT	140 W 18TH AVE	OHIO STATE UNIV	COLUMBUS	OH	43210
WILLIAM B MARTIN	1008 E NORFOLK ST			TAMPA	FL	33604
FLOYD C MASELES	UNIV OF TEXAS	2 204A WELCH HALL	CHEMISTRY DEPT	AUSTIN	TX	78712
W RODNEY MATHEWS	MIT	CHEMISTRY DEPT 56-02	77 MASS AVE	CAMBRIDGE	MA	02139
HAJIME MATSUSHIMA	PHARM CHEMISTRY	UNIV OF CALIFORNIA		SAN FRANCISCO	CA	94143
CHARLES J MAZAC	CELANESE CHEMICAL CO	PO BOX 9077		CORPUS CHRISTI	TX	78336
SUEANN MAZER	MONSANTO RESEARCH	BOX 8 STA B		DAYTON	OH	45407
D J MCADOO	62 LE BRUN COURT W			GALVESTON	TX	77551
C A MCCARTHY	RADIAN CORP	PO BOX 9948		AUSTIN	TX	78766
EDWARD R MCCARTHY	ALLIED CORP	PO BOX 1021R		MORRISTOWN	NJ	07960
J A MCCLOSKEY	UNIV OF UTAH	COLLEGE OF PHARMACY	MEDICINAL CHEM DEPT	SALT LAKE CITY	UT	84112
ROBERT H MCCLUER	E K SHRIVER CTR	200 TRAPELO RD		WALTHAM	MA	02254
C R MCCLURE	FINNIGAN MAT	355 RIVER OAKS PWY		SAN JOSE	CA	95134
D A MCCRERY	1201 S 24TH ST			LINCOLN	NE	68502
CLARENCE A MCDANIEL	USDA NMRAL	BOX 3209		GULFPORT	MS	39503
MAUREEN MCDEVITT	RADIAN CORP	PO BOX 9948		AUSTIN	TX	78766
J R MCDONALD	NAVAL RESEARCH LAB	CODE 6110	CHEMISTRY DIV	WASHINGTON	DC	20375
CHARLES MCEWEN		CENTRAL RES DEPT	EXPER STN 228	WILMINGTON	DE	19898
W H MCFADDEN	FINNIGAN MAT	355 RIVER OAKS PKWY		SAN JOSE	CA	95134
DONALD D MCFALL	PPG INDUSTRIES	PO BOX 31		BARBERTON	OH	44203
EDWARD P MCGOVERN	2610 WHISPER LEAVES			SAN ANTONIO	TX	78230
R T MCIVER	UNIV OF CALIFORNIA	CHEMISTRY DEPT		IRVINE	CA	92717
F W MCLAFFERTY	CORNELL UNIVERSITY	CHEMISTRY DEPT	BAKER LABORATORY	ITHACA	NY	14853
S A MCLUCKEY	103 EDINBORO LN	APT 12		OAK RIDGE	TN	37830
RICHARD MCNAUGHT	GENERAL FOODS CORP	TECHNICAL CTR		WHITE PLAINS	NY	10625
CATHERINE J MCNEAL	TEXAS A&M UNIVERSITY	CHEMISTRY DEPT		COLLEGE STATION	TX	77843
J H MCREYNOLDS	SUNY MEDICAL SCHOOL	BIOPHYSICAL SCIENCE	118 CARY HALL	BUFFALO	NY	14214
B D MCVEETY	INDIANA UNIV	ROOM 541	GEOLOGY BLDG	BLOOMINGTON	IN	47405
WILMA K MECKSTROTH	CHEMISTRY DEPT	UNIV OF DELAWARE		NEWARK	DE	19716
JERRY MEEHAN	28 HAMILTON HALL	UNIV OF NEBRASKA		LINCOLN	NE	68588
S MEISELMAN	NBS	CHEMISTRY A113		WASHINGTON	DC	20234
GERRY G MEISELS	UNIV OF NEBRASKA	1223 OLDFATHER HALL		LINCOLN	NE	68588
MARY MENTZER	SMITH KLINE & FRENCH	1500 SPRING GARDEN		PHILADELPHIA	PA	19101
SEYMOUR MEYERSON	STANDARD OIL INDIANA	RESEARCH DEPT	PO BOX 400	NAPERVILLE	IL	60566
RICHARD M MILBERG	UNIV OF ILLINOIS	SCH OF CHEM SCIENCES	505 S MATHEWS	URBANA	IL	61801
BARBARA S MILES	U OF CO HEAL SCI CTR	CI DIV BOX B158	4200 E NINTH AVE	DENVER	CO	80262
WILLIAM G MILLEN	AMERICAN CYANAMID	PO BOX 400		PRINCETON	NJ	08540
CHARLES M MILLER	MS J-514	LOS ALAMOS NATL LAB		LOS ALAMOS	NM	87545
MARTHA MILLER	713A SAN MARIO CT			COLLEGE STATION	TX	77840
DAVID S MILLINGTON	DEPT OF PEDIATRICS	BOX 3028	DUKE UNIV MED CTR	DURHAM	NC	27710

NAME	A1	A2	A3	CI	STA	ZP
R D MINARD	PENN STATE UNIV	152 DAVEY LAB		UNIVERSITY PARK	PA	16802
STEPHEN R MISSLER	9408 FARMINGDALE AVE			WALKERSVILLE	MD	21793
RONALD K MITCHUM	NAT'L CENTER FOR	TOXICOLOGY		JEFFERSON	AR	72079
GORDON J MOL	1662 PUERTO VALLARTO			SAN JOSE	CA	95120
KARIN MONSON-KIRLAND	ICI AMERICAS INC	BMRD L-215	CONCORD PK & MURPHY	WILMINGTON	DE	19897
FREDERICK E MONTGOMERY	VG INSTRUMENTS	5707 WESTWARD #73		HOUSTON	TX	77081
ARTHUR MOORE	MARATHON OIL CO	BOX 269		LITTLETON	CO	80160
DENISE MOORE	R J REYNOLDS TOBACCO	BOWMAN GRAY TECH CTR	PO BOX 2959	WINSTON-SALEM	NC	27102
JOHN A MOORE	DOW CORNING CORP	3901 S SAGINAW RD	BOX 1592 NO 27	MIDLAND	MI	48640
LARRY J MOORE	NBS	A-21 PHYSICS		WASHINGTON	DC	20234
YOSHIMITSU MORITA	2226 DURANT	NO 108		BERKELEY	CA	94704
CURTIS M MORRIS	US EPA	EMSL/RTP, EMD, PAB,	SFMCS (MD-78)	RES TRI PK	NC	27711
FRANK MORRIS	ICI AMERICAS	LAB 120B CRDL		WILMINGTON	DE	19897
GENE MORTENSEN	LOS ALAMOS NAT'L LAB	GROUP M-1 MS C920		LOS ALAMOS	NM	87545
T H MORTON	UNIV OF CALIFORNIA	CHEMISTRY DEPT		RIVERSIDE	CA	92521
M LUIS MUGA	UNIV OF FLORIDA	CHEMISTRY DEPT		GAINESVILLE	FL	32611
P LUIS MUGA	PO BOX 12877			GAINESVILLE	FL	32604
M A MUNROE	HOFFMANN-LAROCHE INC	BLDG 76 PHYS CHEM		NUTLEY	NJ	07110
B MUNSON	UNIV OF DELAWARE	CHEMISTRY DEPT		NEWARK	DE	19711
TOM MUNSON	FBI RESEARCH	FSRTC	FBI ACADEMY	QUANTICO	VA	22135
E MURAD	AF GEOPHYSICS LAB	LID		HANSCOM AFB	MA	01731
SANDRA MURAWSKI	UNIV OF ILLINOIS	50 RAL BOX 97-5	1209 W CALIFORNIA	URBANA	IL	61801
R C MURPHY	UNIV OF COLORADO	MEDICAL CENTER	PHARMCOLOGY DEPT	DENVER	CO	80262
BRIAN D MUSSELMAN	MICH STATE UNIV	BIOCHEMISTRY DEPT	MASS SPEC FACILITY	EAST LANSING	MI	48824
CARL A MYERHOLTZ	HEWLETT PACKARD LABS	1651 PAGE MILL ROAD	28C	PALO ALTO	CA	94304
LESTER MYERS	MASON & HANGER	PO BOX 30020		AMARILLO	TX	79177
JOHN D NAWORAL	PHILIP MORRIS R&D	BOX 26583		RICHMOND	VA	23113
GORDON M NELSON	1432 WATERCREST PL			VIRGINIA BCH	VA	23464
TERRYANN NELSON	UNION CARBIDE	BLDG 9995 MS 001	PO BOX Y	OAK RIDGE	TN	37830
VINCENT P NERO	TEXACO INC	BOX 509		BEACON	NY	12508
A S NEWTON	1665 THOUSAND OAKS			BERKELEY	CA	94707
KWOKEI J NG	NBS	A 113 CHEMISTRY		WASHINGTON	DC	20234
K T NG	CIBA-GEIGY CORP			ARDSLEY	NY	10502
A O NIER	UNIV OF MINNESOTA	PHYSICS/ASTRONOMY		MINNEAPOLIS	MN	55455
J A NIKORA	B F GOODRICH CENTER	CHEMISTRY DIVISION	PO BOX 122	AVON LAKE	OH	44012
T NISHIMURA	UNIV OF NEBRASKA	524 HAMILTON HALL		LINCOLN	NE	68588
C P NULTON	SOUTHWEST RES INST	6220 CULEBRA RD		SAN ANTONIO	TX	78249
J L OCCOLOWITZ	ELI LILLY RES LABS			INDIANAPOLIS	IN	46285
V P O'CONNELL	TEKNIVENT CORP	10774 TRENTON AVE		ST LOUIS	MO	63132
R W ODOM	CHAS EVANS & ASSOC	1670 S AMPHLETT BLVD	NO 120	SAN MATEO	CA	94402
J EUGENE O'DONNELL	MIDWEST RESEARCH INS	425 VOLKER BLVD		KANSAS CITY	MO	64110
SHERRI OGDEN	CHEMISTRY DEPT	UNIV OF CALIFORNIA		BERKELEY	CA	94720
MICHAEL OHARE	RHCG	1 SCARSDALE ROAD		TUCKAHOE	NY	10707
RONALD G OLDHAM	MOTOROLA INC	PO BOX 6000		AUSTIN	TX	78768
JOHN R O'LEAR	CHEMISTRY BLDG	BOX 652	PURDUE UNIV	WEST LAFAYETTE	IN	47906
J A OLIVARES	213 S SHELDON NO 3			AMES	IA	50010
REBECCA M O'MALLEY	UNIV OF S FLORIDA	CHEMISTRY DEPT		TAMPA	FL	33620
JON D ONSTOT	MIDWEST RES CTR	425 VOLKER BLVD		KANSAS CITY	MO	64110
BRYAN ORTMAN	RICE UNIV	CHEMISTRY DEPT	PO BOX 1892	HOUSTON	TX	77025
OLADIPO OYINSAN	16866 GREENFIELD			DETROIT	MI	48235
R P PAGE	ARCO	400 E SIBLEY BLVD		HARVEY	IL	60426
S L PALLANTE	JOHNS HOPKINS UNIV	PHARMACOLOGY DEPT	725 N WOLFE ST	BALTIMORE	MD	21205
HENRIANNA PANG	CHEMISTRY 56-012	M I T	77 MASS AVE	CAMBRIDGE	MA	02139
LEWIS K PANNELL	CO-H M FALES	NIH	BLDG 10 RM 7N322	BETHESDA	MD	20014
GEORGE W PANZER	ALCOLAC INC	3440 FAIRFIELD RD		BALTIMORE	MD	21226
DAVID M PAREES	AIR PRODUCTS & CHEM	PO BOX 538		ALLENTOWN	PA	18105
CAROL E PARKER	PO BOX 232	ROUTE 3		APEX	NC	27502

NAME	A1	A2	A3	CI	STA	ZP
N H PARSONS	GENERAL ELECTRIC CO	PO BOX 11508	N D DEPT	ST PETERSBURG	FL	33733
LESLIE G PARTRIDGE	SYNTEX RESEARCH	3401 HILLVIEW		PALO ALTO	CA	94304
MICHAEL J PASTEL	US STEEL CORP	MS 15	ONE TECH CTR DRIVE	MONROEVILLE	PA	15146
ADAM PATKIN	PERKIN-ELMER	MAIN AVE M/S 90		NORWALK	CT	06856
DONALD G PATTERSON	CTR FOR DISEASE CONT	TOXICOLOGY BRANCH		ATLANTA	GA	30333
RAPHE PAVLICK	201 SAN VINCENTE #12			SANTA MONICA	CA	90402
DAVID A PEAKE	20 HAMILTON HALL	CHEMISTRY DEPT	UNIV OF NEBRASKA	LINCOLN	NE	68588
DAN S PEARCE	HEWLETT PACKARD CO	1601 CALIFORNIA AVE		PALO ALTO	CA	94304
GERALD L PELLETT	NASA LANGLEY RES CTR			HAMPTON	VA	23665
DANIEL PENTEK	YALE UNIV	CHEMICAL INSTR CTR	225 PROSPECT ST	NEW HAVEN	CT	06511
JULIUS PEREL	PHRASOR SCIENTIFIC	1536 HIGHLAND AVE		DUARTE	CA	91010
H A PETERSEN	PO BOX 1380			HOUSTON	TX	77001
DAVID W PETERSON	42900 PALM AVE			FREMONT	CA	94538
ROBERT PFOST	P P G INDUSTRIES	PO BOX 31		BARBERTON	OH	44203
DANIEL PHELPS	AMOCO PRODUCTION CO	PO BOX 591		TULSA	OK	74102
JOHN PHELPS	E I DUPONT	PO BOX 1089		ORANGE	TX	77630
DAVID PILOSOF	UNIV OF HOUSTON	CHEMISTRY DEPT	4800 CALHOUN	HOUSTON	TX	77004
J D PINKSTON	MICH STATE UNIV	CHEMISTRY DEPT	BOX250	EAST LANSING	MI	48824
WILLIAM J PINNICK	MERRELL DOW PHARM	2110 E GALBRAITH RD		CINCINNATI	OH	45237
JAMES W PINSON	AMER LABS & RESEARCH	1008 SOUTHEAST CR		HATTIESBURG	MS	39401
ALBERT J PIRONE	10 KENLEIGH CT			WILMINGTON	DE	19808
DON K REMLING	7622 S JOHNSON ST			LITTLETON	CO	80127
R D PLATTNER	NORTHERN REG LAB	1815 N UNIVERSITY ST		PEORIA	IL	61604
MANFRED O POEPPEL	110 PARKER ROAD			SARVER	PA	16055
TOM POFAHL	801 WAUKEGAN RD			GLENVIEW	IL	60025
STEVEN K POLLACK	AM HOSP SUPPLY CORP	2132 MICHELSON DR		IRVINE	CA	92715
CHARLES W POLLEY	ARCO CHEMICAL CO	3801 W CHESTER PIKE		NEWTOWN SQ	PA	19073
BING T POON	WALTER REED ARMY	INST OF RESEARCH	EXPTL THERAPEUTICS	WASHINGTON	DC	20307
RICHARD F PORTER	CORNELL UNIVERSITY	CHEMISTRY DEPT		ITHACA	NY	14853
LURA J POWELL	NBS	BLDG 221 RM A21		WASHINGTON	DC	20234
B N PRAMANIK	SCHERING CORP	60 ORANGE ST		BLOOMFIELD	NJ	07003
CHARLES L PRESCOTT	12001 SWAN			AUSTIN	TX	78750
G PRETI	MONELL CTR	3500 MARKET ST		PHILADELPHIA	PA	19104
PHIL PRICE	UNION CARBIDE	TECH CTR 770-120	PO BOX 8361	S CHARLESTON	WV	25303
WILLIAM N PRICE	GEORGIA CRIME LAB	PO BOX 1456		ATLANTA	GA	30316
BERTHA L PROCTOR	UNIV OF TEXAS	ENV SCIENCE	BOX 688	RICHARDSON	TX	75080
HARLAN G PULSIPHER	420 EAST 600 NORTH			BRIGHAM CITY	UT	84302
ELLIOT M RACHLIN	MEDICINAL CHEMISTRY	311A SKAGGS HALL	UNIV OF UTAH	SALT LAKE CITY	UT	84112
G RADOLOVICH	11912 HIGH DRIVE			LEAWOOD	KS	66709
LEO RAFTOGIANIS	FINNIGAN MAT	355 RIVER OAKS PKWY		SAN JOSE	CA	95134
GREGORY S RAHN	ONEIDA RES SERVICE	3 ELLINWOOD CT		NEW HARTFORD	NY	13413
HARRI G RAMJIT	MSDRL	DEPT 805	SUMMNEY TPK	WEST POINT	PA	19486
SUDHAKAR G REDDY	PHARMACEUTICAL SCI	UNIV OF ARIZONA		TUCSON	AZ	85721
ERIC REDMAN	CHEMISTRY DEPT	UNIV OF CALIFORNIA		RIVERSIDE	CA	92821
DOUG REED	SEARLE R&D	4901 SEARLE PKWY		SKOKIE	IL	60016
WILLIAM REENTS	BELL LABS	ROOM 1A-320	600 MOUNTAIN AVE	MURRAY HILL	NJ	07974
VERNON N REINHOLD	HARVARD SCH PUBLIC	HEALTH	665 HUNTINGTON AVE	BOSTON	MA	02115
ROBERT W REISER	E I DUPONT	EXPERIMENTAL STATION	BIOCHEM BLDG 402	WILMINGTON	DE	19898
DON L REMPEL	UNIV OF NEBRASKA	CHEMISTRY DEPT		LINCOLN	NE	68588
MICHAEL E RENNEKAMP	4796 CRAZY HORSE LN			WESTERVILLE	OH	43081
STEPHEN REYNOLDS	15719 HAVENHURST DR			HOUSTON	TX	
BRIAN RHEA	GALILEO ELEC-OPTICS	GALILEO PARK		STURBRIDGE	MA	01518
GERRY RHODES	ROHM & HAAS CO	BLDG 8B/RM 104	727 NORRISTOWN RD	SPRING HOUSE	PA	77586
ROBERT M RIDDLE	TEXACO INC	BELLAIRE RES LAB	PO BOX 425	BELLAIRE	TX	77401
DOUGLAS P RIDGE	UNIV OF DELAWARE	CHEMISTRY DEPT		NEWARK	DE	19711
TIM L RILEY	326 E KINGSLEY			ANN ARBOR	MI	48104
KENNETH L RINEHART	UNIV OF ILLINOIS	CHEM 454 ROGER ADAMS	1209 W CALIFORNIA ST	URBANA	IL	61801

NAME	A1	A2	A3	CI	STA	ZP
RUSSELL D RING	BASF WYANDOTTE CORP	1609 BIDDLE AVE		WYANDOTTE	MI	48192
D J RIZZO	GENERAL FOODS CORP	555 SO BROADWAY		TARRYTOWN	NY	10591
BRADEN ROACH	THE UPJOHN CO	7832-259-12	7171 PORTAGE RD	KALAMAZOO	MI	49001
RONNY C ROBBINS	RT 1, BOX 583			CEDAR HILL	TX	75104
G D ROBERTS	636 SCHWENKSVILLE RD			SCHWENKSVILLE	PA	19473
DONALD H ROBERTSON	S.A.T L.	ANAL CHEM GRP	US ARMY NATICK LABS	NATICK	MA	01760
RUSSELL ROBINS	THE UPJOHN CO	7832-259-12	7171 PORTAGE RD	KALAMAZOO	MI	49001
DOUGLAS W ROBINSON	PENNWALT	900 FIRST AVE		KING OF PRUSSIA	PA	19406
RONALD J ROBINSON	DOW CORNING CORP	MAIL 23	3901 S SAGINAW	MIDLAND	MI	48640
JOHN ROBOZ	MT SINAI SCH OF MED	1 GUSTAVE LEVY PL		NEW YORK	NY	10029
DONALD J ROKOP	LAWL	BOX 1663		LOS ALAMOS	NM	87545
PETER ROLLER	NIH	NCI	BLDG 37 RM 1E22	BETHESDA	MD	20205
ROBERT T ROSEN	FMC CORP	PO BOX 8		PRINCETON	NJ	08540
MARK ROSS	CODE 6110	NAVAL RES LAB		WASHINGTON	DC	20375
ROBIN A ROUSH	CHEMISTRY BLDG	BOX 712	PURDUE UNIV	W LAFAYETTE	IN	47907
RAYMOND L ROY	PO BOX K-300			BROOKFIELD	MA	01506
TIM ROY	MOBIL OIL	TOXICOLOGY DIV	PO BOX 1029	PRINCETON	NJ	08540
MELVIN D ROZEBOOM	STAUFFER CHEMICAL CO	EASTERN RESEARCH CTR		DOBBS FERRY	NY	10522
MARTIN A RUDAT	DUPONT	TEXTILE FIBERS	EXP STATION E302	WILMINGTON	DE	19898
PATRICK J RUDEWICZ	UNIV OF DELAWARE	034 BROWN LAB		NEWARK	DE	19711
D H RUSSELL	TEXAS A&M UNIV	CHEMISTRY DEPT		COLLEGE STATION	TX	77843
PHILIP W RYAN	S-CUBED	3398 CARMEL MTN RD		SAN DIEGO	CA	92121
R J RYBA	STANDARD OIL INDIANA	PO BOX 400		NAPERVILLE	IL	60566
THOMAS M SACK	UNIV OF NEBRASKA	CHEMISTRY DEPT		LINCOLN	NE	68588
VINCENT G SALTAMACH	COLUMBIA UNIV	BOX 555 HAVEMEYER	119TH ST & BROADWAY	NEW YORK	NY	10027
MARY E SALYAN	3311-A PINE ROAD			BREMERTON	WA	98310
PAUL C SAMSON	SIGNAL UOP	RESEARCH CTR	TEN UOP PLAZA	DES PLAINES	IL	60016
MADELINE P SAMPSON	12110 HUNTINGTON PK			HOUSTON	TX	77099
R A SANDERS	1900 WILTSHIRE BLVD			FAIRFIELD	OH	45014
ANDREW D SAUTER	2356 AQUA VISTA			HENDERSON	NV	89015
JANICE R SAUCERMAN	MEAD JOHNSON & CO	2404 PENNSYL AVE		EVANSVILLE	IN	47721
P J SAVICKAS	UNIV OF VIRGINIA	CHEMISTRY DEPT		CHARLOTTESVILLE	VA	22901
M D SCAMUFFA	HEWLETT-PACKARD	10535 HARWIN DR		HOUSTON	TX	77036
GALE F SCANLAN	RT # 2	BOX 114A		HAYFIELD	MN	55901
RICHARD H SCHEEL	MICH PUBLIC HEALTH	ENVIRON EPIDEMIOLOGY	PO BOX 30035	LANSING	MI	48909
S E SCHEPPELE	BARTLESVILLE ENERGY	TECHNOLOGY CENTER	PO BOX 1398 DOE	BARTLESVILLE	OK	74003
ANDREW SCHKUTA	CAMBRIDGE ANAL ASSOC	222 ARSENAL STREET		WATERTOWN	MA	02122
CHARLES E SCHMIDT	PETC-DOE	PO BOX 10940		PITTSBURGH	PA	15236
DEBBIE SCHMITZ	PROCTER & GAMBLE	6100 CENTER HILL RD		CINCINNATI	OH	45224
DALE A SCHOELLER	UNIV OF CHICAGO	BOX 400	950 E 59TH ST	CHICAGO	IL	60637
ALAN E SCHOEN	400 N RIVER ROAD	NO 1535		W LAFAYETTE	IN	47906
D M SCHOENGOLD	3655 STORRIE CT			LAS VEGAS	NV	89103
LEONARD SCHRONK	WYETH LABS	ROOM C084	PO BOX 8299	PHILADELPHIA	PA	19101
ADAM J SCHUBERT	CHEMISTRY DEPT	MICHIGAN STATE UNIV		EAST LANSING	MI	48824
WILLIAM G SCHULZE	MILLER BREWING CO	3939 W HIGHLAND BLVD		MILWAUKEE	WI	53208
MARILYN SCHWARTZ	SCH OF PHARMACY	UNIV OF CALIFORNIA		SAN FRANCISCO	CA	94143
HUBERT A SCOBLE	MIT	CHEMISTRY DEPT	ROOM 56-028	CAMBRIDGE	MA	02139
L JOSEPH SEARS	CHEMISTRY DEPT	MONTANA STATE UNIV		BOZEMAN	MT	59717
R D SEDGWICK	ALLIED CORP	CORPORATE TECHNOLOGY	PO BOX 1021R	MORRISTOWN	NJ	07960
WILLIAM E SEIFERT	UNIV OF TX MED SCH	PO BOX 20708		HOUSTON	TX	77025
MUSTAFA I SELIM	4025 BRIARFIELD LN			LAKE CHARLES	LA	70605
SATINDER K SETHI	TRAVENOL LABS	6301 LINCOLN AVE		MORTON GROVE	IL	60053
ROBERT L SETTINE	UNIV OF ALABAMA	GCMS CENTER	222-PHS BLDG UC	BIRMINGHAM	AL	35294
JEFFREY SHABANOWITZ	UNIV OF VIRGINIA	CHEMISTRY DEPT		CHARLOTTESVILLE	VA	22901
CEDRIC H SHACKLETON	OAKLAND CHDN'S HOSP	51ST AND GROVE		OAKLAND	CA	94609
LAMAAT M SHALABY	DUPONT EXPER STA	AGRICHEM DEPT	E402 3018	WILMINGTON	DE	19898
LAWRENCE J SHAMPINE	PR & D DIVISION	BRISTOL MYERS	PO BOX 4755	SYRACUSE	NY	13221

NAME	A1	A2	A3	CI	STA	ZP
A G SHARKEY	PETC	PO BOX 10940		PITTSBURGH	PA	15236
THOMAS R SHARP	UNIV OF UTAH	CHEMISTRY DEPT		SALT LAKE CITY	UT	84112
P W SHEARER	HERCULES INC	RESEARCH CENTER		WILMINGTON	DE	19899
J SHEN	ARAMCO SERVICES	C/O J L JOHNSON	1200 SMITH	HOUSTON	TX	77002
PAUL L SHERMAN	MONSANTO - U1C	800 N LINDBERGH BLVD		ST LOUIS	MO	63167
MIKE SHERMAN	508 VERONA PL			IRVINE	CA	92715
WILLIAM R SHERMAN	WASHINGTON UNIV	SCHOOL OF MEDICINE	PSYCHIATRY DEPT	ST LOUIS	MO	63110
C J SHIMANSKAS	CIBA-GEIGY CORP			ARDSLEY	NY	10502
STEPHEN SHRADER	SHRADER ANAL LAB	3814 VINEWOOD		DETROIT	MI	48208
MARSHALL M SIEGEL	LEDERLE LABS	AMERICAN CYANAMID		PEARL RIVER	NY	10965
DOMINIQUE SILVESTRE	EQUINE DRUG TESTING	925 WARREN DR		ITHACA	NY	14850
NAN SIMON	OCCIDENTAL CHEMICAL	LONG ROAD		GRAND ISLAND	NY	14072
WILLIAM J SIMONICK	INDIANA UNIV	BOX 263	CHEMISTRY DEPT	BLOOMINGTON	IN	47405
MARK R SINE	6303 AUGUSTA LANE			CINCINNATI	OH	45243
KATHLEEN E SINGLETON	PURDUE UNIV	CHEMISTRY DEPT	BOX 742	W LAFAYETTE	IN	47907
EVERETTE SIZEMORE	NERMAC	15423 VANTAGE PKWY		HOUSTON	TX	77032
JOHN SLAYBACK	12 CHEYENNE CRES			WHITEBORO	NY	13492
L E SLIVON	BATTELLE LABS	505 KING AVE		COLUMBUS	OH	43201
REIN A SMIL	8333 PUMALO			ALTA JOMA	CA	91701
DANNE E SMITH	RCA VIDEODISC OPERAT	7900 ROCKVILLE RD	PO BOX 91079	INDIANAPOLIS	IN	46291
DAVID E SMITH	3665 EL GRANDE			SAN JOSE	CA	95132
DAVID LEE SMITH	MEDICINAL CHEMISTRY	PURDUE UNIV		W LAFAYETTE	IN	47907
JAMES S SMITH	7A GRACE'S DRIVE			COATESVILLE	PA	19320
LAURENCE A SMITH	UNIV OF TEXAS AUSTIN	BOTANY DEPT	BIOLOGICAL LAB RM 21	AUSTIN	TX	78712
L L SMITH	UNIV OF TEXAS	MEDICAL BRANCH		GALVESTON	TX	77550
RICHARD D SMITH	BATTELLE-NW	BLDG 329 AREA 300		RICHLAND	WA	99352
RONALD G SMITH	MONSANTO AG PRODUCTS	800 N LINDBERGH	U2C	ST LOUIS	MO	63167
RICHARD W SMITH	NIEHS	PO BOX 12233		RES TRI PK	NC	27709
CHARLES R SNELLING	PO BOX2226	EXXON RES LABS		BATON ROUGE	LA	70821
TIMOTHY A SNOW	CONOCO INC	BOX 1267		PONCA CITY	OK	74603
JOSEPH G SOLCH	8370 HEILMAN DR			NEW CARLISLE	OH	45344
J J SOLOMON	NEW YORK UNIV	ENVIRON MEDICINE	MEDICAL CENTER	TUXEDO PARK	NY	10987
KEN SOUTHARD	1502 WILLOWCREST DR			RICHARDSON	TX	75081
G W SOVOCOOL	3155 HIGHVIEW DR			HENDERSON	NV	89015
WILLIAM SPEED	THE UPJOHN CO	7000 PORTAGE RD	(7881-259-8)	KALAMAZOO	MI	49007
R B SPENCER	5121 FLAMBEAU RD			MADISON	WI	53705
J A SPHON	FDA	HFF-424	200 C ST SW	WASHINGTON	DC	20204
C A SPINDT	SRI INTERNATIONAL	333 RAVENSWOOD AVE		MENLO PARK	CA	94025
RUSSELL C SPREEN	BLDG 33 APT 12	WENARK DR		NEWRAK	DE	19713
ROBERT R SQUIRES	CHEMISTRY DEPT	PURDUE UNIV		W LAFAYETTE	IN	47907
RAMAN S SRINIVASA	CHEMISTRY DEPT	UNIV OF TOLEDO		TOLEDO	OH	43606
GEORGE STAFFORD	FINNIGAN MAT	355 RIVER OAKS PKWY		SAN JOSE	CA	95134
DOUGLAS B STAUFFER	CORNELL UNIV	BAKER LAB	BOX 68	ITHACA	NY	14853
J L STAUFFER	UNIV OF UTAH	311 A SKAGGS HALL		SALT LAKE CITY	UT	84112
EMIL STAVINOHA	5810 SHADOW WAY			SAN ANTONIO	TX	78218
RICHARD STEARNS	M&R ANALYTICAL	700 BARKSDALE RD		NEWARK	DE	84050
J D STEIN	GENERAL ELECTRIC	1334 KATHY CT		LIVERMORE	CA	94550
URS STEINER	FINNIGAN CORP	355 RIVER OAKS PKWY		SAN JOSE	CA	95134
ELIZ A STEMMLER	CHEMISTRY DEPT	INDIANA UNIV		BLOOMINGTON	IN	47406
PAMELA STEWART	RADIAN CORP	PO BOX 9948		AUSTIN	TX	78766
R N STILLWELL	BAYLOR COLL MEDICINE	INST LIPID RESEARCH	TEXAS MEDICAL CENTER	HOUSTON	TX	77030
WANDA G STILLWELL	UT MED SCH AT HOUSTO	PHARMACOLOGY DEPT	PO BOX 20708	HOUSTON	TX	77030
M STOBIECKI	HARVARD SCH PUB HLTH	NUTRUTION DEPT	655 HUNTINGTON AVE	BOSTON	MA	02115
J J STOFFELS	BATTELLE-NW	BLDG 320 AREA 300		RICHLAND	WA	99352
MARTIN STOGNIEW	PO BOX 25			BLOOMING GROVE	NY	10914
REINER G STOLL	NIEHS	PO BOX 12233		RES TRI PK	NC	27703
M S STORY	15745 WOODACRES RD			LOS GATOS	CA	95030

NAME	A1	A2	A3	CI	STA	ZP
STEVEN J STOUT	AMERICAN CYANIMID	AGRICULTURAL DIV	PO BOX 400	PRINCETON	NJ	08540
KENNETH M STRAUB	1500 SPRG GARDEN ST	F60		PHILADELPHIA	PA	19101
GERALD E STREIT	LOS ALAMOS NAT'L LAB	PO BOX 1663 MS G738		LOS ALAMOS	NM	87545
ROBERT J STRIFE	MIAMI VALLEY LABS	PROCTER & GAMBLE	PO BOX 39175	CINCINNATI	OH	45247
JUSTIN G STROH	UNIV OF ILLINOIS	BOX 101-5	1209 W CALIFORNIA	URBANA	IL	61801
J M STRONG	13103 BLUHILL RD			SILVER SPRINGS	MD	20906
SUSAN E STRONG	HEWLETT PACKARD	1601 CALIFORNIA AVE		PALO ALTO	CA	94304
JOHN T STULTS	MICH STATE UNIV	CHEMISTRY DEPT		EAST LANSING	MI	48824
D STULIK	CHEMISTRY DEPT	WASHINGTON STATE U		PULLMAN	WA	99164
JUNKO SUGATANI	BIOCHEMISTRY DEPT	UNIV OF TX HEAL SCI	7703 FLOYD CURL DR	SAN ANTONIO	TX	78284
R L SUMMERS	1062 FALLING LEAF			FRIENDS WOOD	TX	77546
T SUN	USDA-FSQS	PO BOX 6085		ATHENS	GA	30604
AKIRA SUZUKI	FDA	BIOCHEM & BIOPHYSICS	8800 ROCKVILLE PIKE	BETHESDA	MD	20205
H J SVEC	IOWA STATE UNIV	CHEMISTRY DEPT		AMES	IA	50011
ROBERT SWAIM	FINNIGAN MAT	PO BOX 5997		KINGWOOD	TX	77325
CHARLES C SWEELEY	MICHIGAN STATE UNIV	BIOCHEMISTRY DEPT		EAST LANSING	MI	48824
KEVIN M SWEENEY	1412 ALMA DR			AUSTIN	TX	78753
B J SWEETMAN	VANDERBILT UNIV	PHARMACOLOGY DEPT		NASHVILLE	TN	37232
JOHN SYKA	FINNIGAN MAT	355 RIVER OAKS PKWY		SAN JOSE	CA	95134
DANIEL W SZETO	BERLEX LABS	110 E HANOVER AVE		CEDAR KNOLLS	NJ	07927
JAN E SZULEJKO	2-A KINGSWOOD			CHAPEL HILL	NC	27514
BERNARD TAILLIEZ	NICOLET INSTRUMENTS	5225-1 VERONA RD		MADISON	WI	53711
C R PETE TALLEY	E I DUPONT	EXPERIMENTAL STATION	PETRO CHEM BLDG 336	WILMINGTON	DE	19898
Y L TAN	DOE	ENVIRON MEAS LAB	376 HUDSON ST	NEW YORK	NY	10014
CALVIN K TANAKA	CALIF ANALYTICAL LAB	2544 INDUSTRIAL BLVD		W SACRAMENTO	CA	95691
O P TANNER	12664 MARKAIRE			ST LOUIS	MO	63146
PHILLIP TAO	5430 BIRCHWOOD	NO. 320		HOUSTON	TX	77096
PAUL A TAYLOR	2544 INDUSTRIAL BLVD			W SACRAMENTO	CA	95691
RON TECKIENBURG	TEXAS A&M UNIV			COLLEGE STATION	TX	78463
R G TEECE	UNIV OF ARIZONA	COLLEGE OF PHARMACY	PHARMACEUTCL SCIENCE	TUCSON	AZ	85721
JAMES L TEMPLETON	ANALYTICS LABORATORY	PO BOX 25249		RICHMOND	VA	23260
D T TERWILLIGER	29 CHETWYND RD			PAOLI	PA	19301
D W THOMAS	SRI INTERNATIONAL	333 RAVENSWOOD AVE	B-011	MENLO PARK	CA	94025
G V THOMAS	FINNIGAN INSTITUTE	11 TRIANGLE PK DR		CINCINNATI	OH	45246
TIMOTHY THOMAS	CHEMISTRY DEPT	UNIV OF MISSOURI		KANSAS CITY	MO	64110
FREDERICK A THOME	R S REYNOLDS TOBACCO	B GRAY TECH CTR		WINS-SALEM	NC	27103
JOHN J THOMPSON	ALLIED CHEMICAL	20 PEABODY ST		BUFFALO	NY	14210
MICHAEL L THOMSON	AMERICAN CYANIMID	AGRICULTURAL DIV	PO BOX 400	PRINCETON	NJ	08540
R GARY THURMAN	UNION CAMP CORP	PO BOX 412		PRINCETON	NJ	08542
T O TIERNAN	WRIGHT STATE UNIV	BREHM LAB		DAYTON	OH	45431
G W TINDALL	TENNESSEE EASTMAN CO	BLDG 150		KINGSPORT	TN	37662
PETER J TODD	OAK RIDGE NAT'L LAB	PO BOX Y BLDG 9735		OAK RIDGE	TN	37830
L TOKES	SYNTEX RESEARCH	3401 HILLVIEW AVE	STANFORD INDUST PARK	PALO ALTO	CA	94304
ALBERT D TOMASSIAN	PERKIN-ELMER CORP	2771 N GAREY AVENUE		POMONA	CA	91767
KENNETH B TOMER	MIDWEST CTR FOR MASS	CHEMISTRY DEPT	UNIV OF NEBRASKA	LINCOLN	NE	68588
YVES G TONDEUR	1726 DOGWOOD DR			FREDERICK	MD	21701
J C TOU	DOW CHEMICAL CO	ANALYTICAL LAB	B-574	MIDLAND	MI	48640
DAN TRAFICANTE	NAT'L SCIENCE FNDN	CHEMISTRY DIV	1800 G STREET NW	WASHINGTON	DC	20550
THOMAS M TRAINOR	NORTHEASTERN UNIV	CHEMISTRY DEPT	360 HUNTINGTON AVE	BOSTON	MA	02115
V T TRAN	1100 W CHESTER PK	APT C-4		WEST CHESTER	PA	19380
MICHAEL L TREHY	4607 NW 44TH PLACE			GAINESVILLE	FL	32606
FRANKLIN L TRENSCH	PO BOX 11508			ST PETERSBURG	FL	33733
ROBERT L TROTTIER	LOCTITE CORP	705 N MOUNTAIN RD		NEWINGTON	CT	06111
ANTHONY TSARBOPOULOS	MICHIGAN STATE UNIV	CHEMISTRY DEPT	BLDG BOX 267	EAST LANSING	MI	48824
W J TUTING	409 E MCFARLAN ST			DOVER	NJ	07801
ANDREW N TYLER	PSYCHIATRY DEPT	STANFORD MED CTR		STANFORD	CA	94305
GED TYROR	3656 WOODS RD			WILLIAMSON	NY	14589

NAME	A1	A2	A3	CI	STA	ZP
HAROLD R UDSETH	BATTELLE NORTHWEST	PO BOX 999		RICHLAND	WA	99352
STEVE E UNGER	4 BEL AIR DR			YARDLEY	PA	19067
B T UPCHURCH	OLD DOMINION UNIV	CHEMISTRY DEPT		NORFOLK	VA	23508
ROGER UPHAM	TWIN CITY TESTING CO	662 CROMWELL AVE		ST PAUL	MN	55114
BERNARD L UPSHULTE	152 DAVEY LAB			UNIVERSITY PK	PA	16802
ROY W VANDER HAAR	STANDARD OIL INDIANA	PO BOX 400		NAPERVILLE	IL	60566
THEODORUS VAN KALLEVEEN	UNIV OF NEBRASKA	HAMILTON HALL 519		LINCOLN	NE	68588
A M VAN LANGENHOVE	LHRRB ROOM 517	HARVARD MED SCHOOL	45 SHATTUCK ST	BOSTON	MA	02115
FRANK J VAN LENTEN	E I DUPONT	JACKSON LAB		DEEPWATER	NJ	08023
MADAN VERMA	CIBA GEIGY	PO BOX 18300		GREENSBORO	NC	27419
SUNITA VERMA	PURDUE UNIV	CHEMISTRY DEPT	PO BOX 795	WEST LAFAYETTE	IN	47906
WILLIAM J VERRET	5400 S MARYLAND PKY	APT 97		LAS VEGAS	NV	89119
M L VESTAL	UNIV OF HOUSTON	CHEMISTRY DEPT	4800 CALHOUN	HOUSTON	TX	77004
M M VESTLING	SUNY	CHEMISTRY DEPT		BROCKPORT	NY	14420
STEPHEN W VEYSEY	83A GILMAN HALL	IOWA STATE UNIV		AMES	IA	50011
DOM VICCHIO	UNIV OF MARYLAND	SCH OF PHARMACY	20 N PINE ST	BALTIMORE	MD	21201
AL VIGGIANO	91 PALMER ST			ARLINGTON	MA	02174
ARGENTINA G VINDIOLA	2311 YELLOWSTONE			BRYAN	TX	77803
S K VISWANADHAM	CHEMISTRY DEPT	BOX 10	UNIV OF PITTSBURGH	PITTSBURGH	PA	15260
T S VISWANATHAN	8409 WEST 90TH ST			OVERLAND PARK	KS	66212
KENT J VOORHEES	COLORADO SCH MINES	CHEMISTRY DEPT		GOLDEN	CO	80401
R D VOYKSNER	204 TRAIL'S END CT			RALEIGH	NC	27614
JAMES VRBANAC	MED UNIV OF S CARO	PHARMACOLOGY DEPT		CHARLESTON	SC	29425
P A WADSWORTH	SHELL DEVELOPMENT CO	WESTHOLLOW RESEARCH	PO BOX 1380	HOUSTON	TX	77001
DAVID A WAGNER	49 SYMPHONY ROAD	APT 24		BOSTON	MA	02115
AUSTIN L WAHRHAFTIG	UNIV OF UTAH	CHEMISTRY DEPT		SALT LAKE CITY	UT	84112
GEORGE R WALLER	OKLAHOMA STATE UNIV	BIOCHEMISTRY DEPT		STILLWATER	OK	74074
FRED WALLS	PHARM CHEMISTRY	UNIV OF CALIFORNIA		SAN FRANCISCO	CA	94143
DENNIS C WALTERS	WRIGHT STATE UNIV	UNIV RESEARCH CTR	222 ALLYN HALL	DAYTON	OH	45435
JIA-SHEN WANG	CLAIROL INC	2 BLACHLEY RD		STAMFORD	CT	06922
S-I WANG	ABBOTT LABS	D-417 ABBOTT PARK	RTS 137 & 143	N CHICAGO	IL	60064
T HELEN WANG	PENNZOIL PRODUCTS CO	TECHNOLOGY DIV	PO BOX 7569	THE WOODLANDS	TX	77387
V L WARREN	PINE BLUFF ARSENAL	QUALITY ASSURANCE	LABORATORY	PINE BLUFF	AR	71611
CLIFFORD H WATSON	LEIGH HALL BOX 554		UNIV OF FLORIDA	GAINESVILLE	FL	32611
J THROCK WATSON	DEPT BIOCHEMISTRY	MICHIGAN STATE UNIV		EAST LANSING	MI	48824
HUGH M WEBB	31 DEARBORN PL	NO 36		GOLETA	CA	93117
NAKANDALAGE WEERASINGHE	DEPT OF CHEMISTRY	MCMS	UNIV OF NEBRASKA	LINCOLN	NE	68588
ANNEMARIE WEGMANN	STANFORD UNIV	CHEMISTRY DEPT	GC-MS LABS	STANFORD	CA	94305
LEO A WEIBEL	HAZLETON LABS	PO BOX 7545		MADISON	WI	53707
DAVID A WEIL	CHEMISTRY DEPT	PIERCE HALL	UNIV OF CALIFORNIA	RIVERSIDE	CA	92521
R J WEINKAM	ALLERGAN PHARM	2525 DUPONT DR		IRVINE	CA	92713
SUSAN T WEINTRAUB	UT HEALTH SCI CTR	7703 FLOYD CURL DR		SAN ANTONIO	TX	78284
ADRIAN WEISZ	NAT'L INST HEALTH	BLDG 10 ROOM 3N325		BETHESDA	MD	20205
MICHAEL J WELCH	NAT'L BUR OF STAN	RM A-113 BLDG 222		WASHINGTON	DC	20234
ROBERT R WELLER	CHEMISTRY DEPT 595	UNIV OF FLORIDA		GAINESVILLE	FL	32611
CHRYS WESDEMIOTIS	709 TRIPHAMMER RD			ITHACA	NY	14850
JAY Y WESTCOTT	UNIV OF CO HSC	PHARMACOLOGY C-236	4200 E NINTH AVE	DENVER	CO	80262
DAVID G WESTMORELAND	ROHM & HAAS CO	727 NORRISTOWN RD		SPRING HOUSE	PA	19477
ALAN F WESTON	OCCIDENTAL CHEMICAL	RESEARCH CTR	LONG ROAD	GRAND ISLAND	NY	14072
JEFF R WETZLER	WESTINGHOUSE-BETTIS	PO BOX 79		WEST MIFFLIN	PA	15122
ED WHITE	NBS	A113 CHEMISTRY		WASHINGTON	DC	20234
EARL L WHITE	CHEMICAL INDUSTRY	INSTITUTE OF TOXICOL	PO BOX 12137	RES TRI PK	NC	27709
KEVIN D WHITE	FDA	HFF-424	200 C STREET SW	WASHINGTON	DC	20204
MARINELL WHITE	4402 VERONE			BELLAIRE	TX	77401
R H WHITE	VIRGINIA POLYTECH	BIOCHEMISTRY DEPT		BLACKSBURG	VA	24061
CRAIG M WHITEHOUSE	YALE UNIV	ENGIN DEPT MASON LAB	9 HILLHOUSE AVE	NEW HAVEN	CT	06520
JOANNE O WHITNEY	131 TERESITA BLVD			SAN FRANCISCO	CA	94127

NAME	A1	A2	A3	CI	STA	ZP
RICHARD A WIELESEK	UNIV OF OREGON	CHEMISTRY DEPT		EUGENE	OR	97403
P S WILKES	FDA	60 EIGHTH ST NE		ATLANTA	GA	30309
CHARLES L WILKINS	UNIV OF CALIFORNIA	CHEMISTRY DEPARTMENT		RIVERSIDE	CA	92521
C H WILLIAMS	RADIAN CORP	PO BOX 9948		AUSTIN	TX	78766
CLYDE M WILLIAMS	RADIOLOGY DEPT	BOX J-374 JHMHC	UNIV OF FLORIDA	GAINESVILLE	FL	32610
ROSS C WILLOUGHBY	STUART PHARMACEUTIC	DIV ICI AMERICAS		WILMINGTON	DE	19897
LAUREN A WILMESHERR	UNIV OF MISS MED CTR	PHARMACOLOGY DEPT	2500 N STATE ST	JACKSON	MS	39216
B W WILSON	BATTELLE-NW	PO BOX 999		RICHLAND	WA	99352
MARK WILSON	BALZERS	8 SAGAMORE PARK RD		HUDSON	NH	03051
RANDALL L WILSON	BATTELLE COLUMBUS	505 KING AVE		COLUMBUS	OH	43201
WILLEM WINDIG	391 S CHIPETA WAY	SUITE F	RESEARCH PARK	SALT LAKE CITY	UT	84108
D L WINMILL	HERCULES INC	RESEARCH CENTER		WILMINGTON	DE	19899
DALLAS L WINTER	CONOCO INC	RM 314 RDE		PONCA CITY	OK	74602
JOHN S WISHNOK	MIT	NUTRITION & FD SCI	ROOM 56-313	CAMBRIDGE	MA	02139
THOMAS A WITTSTRUCK	NUCLIDE CORP	AGV DIVISION	PO BOX 315	ACTON	MA	01720
MARTA H WOLFE	SHRINERS HOSP	UNIV OF TEXAS	610 TEXAS AVE	GALVESTON	TX	77550
W ALAN WOLSTENHOLME	13840 W OAK GLEN RD			VALLEY CENTER	CA	92082
C M WONG	LLL	PO BOX 808 L-310		LIVERMORE	CA	94550
L K WONG	UNIV OF PITTSBURGH	SCHOOL OF PHARMACY	804 SALK HALL	PITTSBURGH	PA	15261
DAVID WOOD	80-14 MAPLE TREE AVE			STAMFORD	CT	06906
KARL V WOOD	PURDUE UNIV	FUELS ANAL LAB	CHEMISTRY BLDG	WEST LAFAYETTE	IN	47907
NEVILLE WOOD	BASF WYANDOTTE	140 NEW DUTCH LN		FAIRFIELD	NJ	07006
J W WOODS	8 RICHARDS RD			LYNNFIELD	MA	01940
T J WOZNIAK	INDIANA UNIV	CHEMISTRY DEPT		BLOOMINGTON	IN	47401
CHARLES J WRIGHT	1210 MAJESTIC WAY			WEBSTER	NY	14580
NANCY E H WRIGHT	SUN TECH INC	PO BOX 1135		MARCUS HOOK	PA	19061
RICHARD WU	WRIGHT STATE UNIV	BREHM LAB		DAYTON	OH	45435
WU-NAN WU	MCNEIL PHARMACEUTIC	WELSH & MCKEAN ROADS		SPRING HOUSE	PA	19477
J R WYATT	NRL	CODE 6110		WASHINGTON	DC	20375
ROBERT B WYNNE	HEWLETT PACKARD	2750 MONROE BLVD		VALLEY FORGE	PA	19482
K YAMAGUCHI	NIEHS	PO BOX 12233		RES TRI PK	NC	27709
LILY YANG	UNIV OF HOUSTON	CHEMISTRY DEPT	4800 CALHOUN	HOUSTON	TX	77004
LAUREN M YELLE	ARTHUR D LITTLE INC	15 ACORN PARK		CAMBRIDGE	MA	02140
RICHARD O YELTON	116 WALDEN FARM CIR			UNION	OH	45322
ALFRED L YERGEY	NIH	BLDG 6 RM 136		BETHESDA	MD	20205
JAMES A YERGEY	NIH	BLDG 10 RM 3C218		BETHESDA	MD	20205
RICHARD A YOST	UNIV OF FLORIDA	CHEMISTRY DEPT		GAINESVILLE	FL	32611
S E YOUNG	2455 THADDEUS			MOUNTAIN VIEW	CA	94043
TIM L YOUNGLESS	GULF RES & DEV	PO DRAWER 2138		PITTSBURGH	PA	15230
M YOUSSEFI	UNION CARBIDE	670 BOUND BROOK		BOUND BROOK	NJ	08854
KYUNG YU	AFAMRL-THT	AREA B BLDG 79		WRIGHT PATT AFB	OH	45433
A G ZACCHEI	MERCK SHARP & DOHME	RESEARCH LABORATORY		WEST POINT	PA	19486
NABI S ZARR	6330 HIGHWAY 290 E			AUSTIN	TX	78723
MICHAEL ZEMYAN	TECHNICAL OPERATIONS	DLPS		MCCLELLAN AFB	CA	95652
JEROME H ZOELLER	PO BOX 2646			COLLEGE STATION	TX	77841
MARKUS ZOLLINGER	CHEMISTRY DEPT	ROOM 56-012	MIT	CAMBRIDGE	MA	02139
ROSALIE M ZUBYK	230 SUMMIT HOUSE			WEST CHESTER	PA	19380

NAME	A1	A2	A3	CI	ZP
A J ALEXANDER	CHEMISTRY DEPT	UNIV OF ALBERTA		EDMONTON ALBERTA	
GUY P ARSENAULT	RR 2	MIDDLE ROAD		KINGSTON ONTARIO	K7L 5H6
R BADLIEK	12 BAL HARBOUR DR			GRIMSBY ONT	L3M 4P7
MARCEL BARIL	PHYSIQUE DEPT	UNIV LAVAL		STE FOY QUEBEC	G1K7P4
RONALD C BEAVIS	75 HAZELDELL AVE			WINNIPEG MANITOBA	R2K 0P3
F M BENOIT	HEALTH-WELFARE DEPT	ENVIRONMENTAL HEALTH	TUNNEYS PASTURE	OTTAWA ONTARIO	K1A 0L2
M J BERTRAND	UNIV OF MONTREAL	CHEMISTRY DEPT	C P. 6210 SUK A	MONTREAL QUEBEC	H3C 3U1
C BOURDONNAIS	ANALYTECH	100 ALEXIS-NIHON		ST LAURENT PQ	H4M 2P1
ROBERT K BOYD	UNIV OF GUELPH	CHEMISTRY DEPT		GUELPH ONTARIO	N1G 2W1
PAUL BROOKS	I S P G	3303-33 ST	CALGARY NW	CALGARY	
P BURGERS	UNIV LAVAL	FAC DES SCIENCES	CTR RECHERCHE	QUEBEC PQ	G1R 1P7
RAY E CLEMENT	ENVIRONMENT ONTARIO	PO BOX 213	125 RESOURCES RD	REXDALE ONT	
M B COMISAROW	UNIV BRIT COLUMBIA	CHEMISTRY DEPT	2036 MAIN MALL	VANCOUVER BC	V6T 1Y6
P L COULOMBE	ANALYTECH	742 MOONEY'S BAY PL		OTTAWA ONTARIO	
PAUL A D'AGOSTINO	DEFENSE RES ESTAB	SUFFIELD	RALSTON	ALBERTA	T0J 2N0
W R DAVIDSON	SCIEX INC	55 GLENCAMERON RD	SUITE 202	THORNHILL ONTARIO	L3T 1P2
P H DAWSON	NAT RESEARCH COUNCIL	PHYSICS DEPT		OTTAWA ONTARIO	K1A 0R6
DONALD J DOUGLAS	SCIEX	55 GLENCAMERON RD		THORNHILL ONT	L3T 1P2
G K EIGENDORF	UNIV BRIT COLUMBIA	CHEMISTRY DEPT		VANCOUVER BC	V6T 1Y6
WERNER E ENS	UNIV OF MANITOBA	PHYSICS DEPT		WINNIPEG MANITOBA	R3T 2N2
M J EVANS	CHEMISTRY DEPT	UNIV OF MONTREAL	C P G210 SUCC A	MONTREAL QUE	H3C 3U1
H PETER FISCHER	GULF CANADA	RES & DEV DEPT	2489 N SHERIDAN WAY	MISSISSAUGA ONT	L5K 1A8
M G FOSTER	MIN ENVIRONEMNT	OTC	PO BOX 213	REXDALE ONTARIO	M9W 5L1
ROGER A FOXALL	NAT'L RESEARCH COUN	ATLANTIC RES LAB	1411 OXFORD ST	HALIFAX NS	B3H 3Z1
BERNARD F FRANCIS	SHELL RESEARCH CTR	3415 LAKESHORE RD W		OAKVILLE ONTARIO	L7R 2M3
J E FULFORD	SCIEX INC	55 GLENCAMERON RD	SUITE 202	THORNHILL ONTARIO	L3T 1P2
ROBERT GERGELY	636 MOHAWK RD E			HAMILTON ONT	L8V 2K1
D D GODSE	CLARKE INST PSYCHIAT	250 COLLEGE STREET		TORONTO ONTARIO	M5T 1R8
MYRA GORDON	1209 RICHMOND ST	APT 612		LONDON ONT	N6A 3L7
LAWRENCE W GREEN	ATOMIC ENERGY OF CAN	CHALK RIVER NUC LAB		CHALK RIVER ONTARIO	K0J 1J0
ALEX G HARRISON	UNIV OF TORONTO	CHEMISTRY DEPT		TORONTO ONTARIO	M5S 1A1
ROBERT E HILL	PATHOLOGY DEPT	MCMASTER UNIV	1200 MAIN ST WEST	HAMILTON ONTARIO	L8N 3Z5
ALAN M HOGG	UNIV OF ALBERTA	CHEMISTRY DEPT		EDMONTON ALBERTA	T6G 2G2
LAWRENCE R HOGGE	NAT'L RES COUNCIL	110 GYMNASIUM RD		SASKATOON SASK	S7N 0W9
ANDREW HOLMES	HEALTH & WELFARE	HEALTH PROT BRN	2301 MIDLAND AVE	SCARBOROUGH ONT	M1P 4P7
W D JAMIESON	NRC	1411 OXFORD ST		HALIFAX NOVA SCOTIA	B3H 3Z1
M KALLOO	MERCK SHARP & DOHME	PO BOX 899		POINTE CLAIRE QUEBEC	H9R 4P7
J R KRAUSE	UNIV OF OTTAWA	CHEMISTRY DEPT		OTTAWA ONTARIO	K1N 9B4
R C LAO	ENVIRONMENT CANADA	CHEMISTRY DIV	RIVER ROAD CTR	OTTAWA ONT	K1A 1C8
BENJAMIN P LAU	HEALTH & WELFARE CAN	FOOD RESEARCH	TUNNEY'S PASTURE	OTTAWA ONTARIO	K1A 0L2
D B MACLEAN	MCMASTER UNIVERSITY	CHEMISTRY DEPT		HAMILTON ONTARIO	L8S 4M1
DENNIS E MAIN	UNIV OF MANITOBA	PHYSICS DEPT		WINNIPEG MAN	R3T 2N2
ORVAL A MAMER	1130 PINE AVE WEST			MONTREAL QUE	H3A 1A3
R E MARCH	TRENT UNIVERSITY	CHEMISTRY DEPT		PETERBOROUGH ONT	K9J 7B8
TREVOR I MARTIN	XEROX RESEARCH CTR	2660 SPEAKMAN DR		MISSISSAUGA ONT	L5K 2L1
ANDRE MARTINEAU	110 PINE AVE W			MONTREAL QUE	H2W 1R7
ROBERT MASSE	INRS-SANTE	7401 HOCHELAGA		MONTREAL QUEBEC	H1N 3M5
L J MCBURNEY	DCIEM	PO BOX 2000		DOWNSVIEW ONTARIO	M3M 3B9
DOUG MCINTYRE	HEWLETT PACKARD	6877 GOREWAY DR		MISSISSAUGA ONT	L4V 1M8
W F MILES	MASS SPEC LAB	LAB SERVICES DIV	BLDG #22 C E F.	OTTAWA ONTARIO	K1A 0C5
A MOMMERS	305 NICHOLAS ST			OTTAWA ONT	K1W 9B4
RONALD B NEW	CHEMISTRY DEPT	UNIV OF WINDSOR		WINDSOR ONT	N9B 3P4
TARAS W OBAL	CHEMISTRY DEPT	UNIV OF WINDSOR		WINDSOR ONTARIO	N9B 3P4
J B OLTHETEN	2545 DE MINIAC			MONTREAL QUEBEC	H4S 1E5
F I ONUSKA	CCIW-AMRS	PO BOX 5050		BURLINGTON ONTARIO	L7R 4A6
O PELLETIER	HEALTH PROTECTION BR	ROOM 277 HPB BLDG	TUNNEYS PASTURE	OTTAWA ONTARIO	K1A 0L2

NAME	A1	A2	A3	C1	ZP
D W PRIDDLE	UNIV OF TORONTO	CHEMISTRY DEPT		TORONTO ONTARIO	M5S 1A1
M A QUILLIAM	MCMASTER UNIVERSITY	CHEMISTRY DEPT		HAMILTON ONTARIO	L8S 4M1
MARK L J REIMER	56 LOMOND BLVD			WINNIPEG MANITOBA	R2J 1Y2
T SAKUMA	SCIEX INC	55 GLENCAMERON RD	SUITE 202	THORNHILL ONT	L3T 1P2
J P SCHMIT	UNIV OF QUEBEC	CHEMISTRY DEPT	CP 8888 SUCCURSALE A	MONTREAL PQ	H3C 3P8
BRUNO SCHUELER	PHYSICS DEPT	UNIV OF MANITOBA		WINNIPEG MAN	R3T 2N2
D B SERGEANT	DEPT FISH & OCEANS	GLFRB	867 LAKESHORE RD	BURLINGTON ONT	L7R 4A6
BORI I SHUSHAN	SCIEX	55 GLENCAMERON RD		THORNHILL ONT	L3T 1P2
K STANDING	UNIV OF MANITOBA	PHYSICS DEPT		WINNIPEG MANITOBA	R3T 2N2
GENE STRUMILA	NICOLET INSTRUMENT	1-1200 AEROWOOD DR		MISSISSAUGA ONT	L4W 2S7
COLLEEN TASHIRO	CHEMISTRY DEPT	MCMASTER UNIV	1280 MAIN STREET	HAMILTON,ONT	L8S 4M1
PIERRE THIBAULT	10220 PELOQUIN			MONTREAL	H2C 2J0
B THOMSON	SCIEX INC	55 GLENCAMERON RD	SUITE 202	THORNHILL ONTARIO	L3T 1P2
J B WESTMORE	UNIV OF MANITOBA	CHEMISTRY DEPT		WINNIPEG MANITOBA	R3T 2N2
GORDON W WOOD	UNIV OF WINDSOR	GRAD STUDIES & RES		WINDSOR ONTARIO	N9B 3P4
J ZAMECNIK	CAMU	HEALTH & WELFARE CAN	BOX 1035 POST STA B	DOWNSVIEW ONT	M3M 5V5

NAME	A1	A2	A3	CI	CN
M P ALLEMANN	SPECTROSPIN AG	INDUSTRIESTR 26		8117 FALLENDEN	SWITZERLAND
EMIKO AOKI	4-37-27 KUGAYAMA	SUGINAMI-KU		TOKYO 168	JAPAN
R T APLIN	DYSON PERRINS LAB	SOUTH PKS RD		OXFORD	ENGLAND
F J ARPINO	ECOLE POLYTECHNIQUE	LAB CHIM ANAL PHYS	ROUTE DE SACLAY	91128 PALAISEAU	FRANCE
MICHAEL BARBER	U M I S T.	CHEMISTRY DEPT	SACKVILLE STREET	MANCHESTER M601QD	ENGLAND
CLAUDE BEAUGRAND	NERMAG	49 QUAI DU HALAGE		RUEIL MALMAISON	F 92500 FRAN
ALFRED A BENNINGHOVEN	DOMAGKSTRASSE 75			4400 MUNSTER	W GERMANY
JOHN H BEYNON	UNIVERSITY COLLEGE	ROYAL SOC RES UNIT		SWANSEA SA2 8PP	WALES
JOHN C BILL	VG ANALYTICAL LTD	4 TAXMERE CLOSE	SANDBACH	CHESHIRE	ENGLAND
R S BORDOLI	VG ANALYTICAL	FLOATS ROAD	WYTHENSHAWE	MANCHESTER M60 1QD	ENGLAND
P R BOSHOFF	UNIV WITWATERSRAND	CHEMISTRY DEPT	1 JAN SMUTS AVE	JOHANNESBURG 2001	S AFRICA
PETER BOTT	VG ANALYTICAL	FLOATS ROAD	WYTHENSHAWE	MANCHESTER	ENGLAND
WILLI A BRAND	VG INSTRUMENTS	GUSTAV-STRESEMANN	RING 12-16	D-6200 WIESBADEN	F R GERMANY
A G BRENTON	RSRU	UNIV COLL SWANSEA		SWANSEA SA2 8PP	ENGLAND
CHARLES J W BROOKS	UNIV OF GLASGOW	CHEMISTRY DEPT		GLASGOW G12 8QQ	SCOTLAND
A P BRUINS	STATE UNIVERSITY	PHARMACY DEPT	A DEUSINGLN 2	9713-AW GRONINGEN	NETHERLANDS
CURT BRUNNEE	FINNIGAN MAT	BARKHAUSENSTR 2	POSTFACH 14 4062	D-2800 BREMEN 10	WEST GERMANY
MAGDA M CLAEYS	UNIV INSTELL ANTWERP	PHARMACY DEPT	UNIVERSITEITSPLEIN 1	B-2610 WILRIJK	BELGIUM
C CLAUDE	SN NERMAG	49 QUAI DE HALAGE		RUEIL MALMAISON	F 92500 FRAN
E CLAYTON	ICI LTD PHARM DIV	ALDERLEY PARK	MACCLESFIELD	CHESHIRE SK10 4TG	ENGLAND
J S COTTRELL	KRATOS	BARTON DOCK RD	URMSTON	MANCHESTER M31 2LD	ENGLAND
NIGEZ CROSSLEY	VG ISOGAS	ASTON WAY	MIDDLEWICH	CHESHIRE	ENGLAND
PHILIPP DABKIEWICZ	INST F PHYSIK	UNIV MAINZ	POSTFACH 3980	D-6500 MAINZ	WEST GERMANY
T S DAVIS	VG ANALYTICAL	FLOATS ROAD	WYTHENSHAWE	MANCHESTER	ENGLAND
G DEVANT	NERMAG S A	49 QUAI DU HALAGE		92502RUEIL MALMAISON	FRANCE
HANS P EPPLER	BALZERS			BALZERS FL9496	LIECHTENSTEI
E ESMANS	UNIV ANTWERPEN	ORGANISCHE SCHEIKUND	GROENENBORGLN 171	B-2020 ANTWERPEN	BELGIUM
S EVANS	KRATOS SCIEN APP LTD	BARTON DOCK ROAD	URMSTON	MANCHESTER M3I 2LD	ENGLAND
ANA FRAIMAN	15 VITKIN ST	ACHUSA		HAIFA	ISRAEL
DANIEL J FRAISSE	SPEC DE MASSE	SCA-CNRS	BP 22	69390-VERNAISON	FRANCE
DAVID E GAMES	UNIVERSITY COLLEGE	CHEMISTRY DEPT	PO BOX 78	CARDIFF CF1 1XL	WALES
S J GASKELL	TENOVUS INSTITUTE	WELSH NAT'L SCH MED		CARDIFF CF4 4XX	WALES
P J GODDARD	VG ISOTOPES	ION PATH, ROAD 3	WINSFORD	CHESHIRE	U K
ROGER GREATHEAD	KRATOS	BARTON DOCK RD	URMSTON	MANCHESTER	ENGLAND
B N GREEN	VG ANALYTICALD	FLOATS ROAD	WYTHENSHAWE	MANCHESTER M23 9LE	ENGLAND
LUTZ GROTJAHN	GBF	MASCHERODER WEG 1		D-3300 BRAUNSCHWEIG	W GERMANY
ALLMAIER GUNTER	INST F ANAL CHEM	UNIV OF VIENNA		VIENNA A-1090	AUSTRIA
K E HABFAST	FINNIGAN MAT GMBH	BARKHAUSENSTR 2	POSTFACH 14 40 62	D-2800 BREMEN 10	WEST GERMANY
D J HARVEY	OXFORD UNIVERSITY	PHARMACOLOGY DEPT	SOUTH PARKS RD	OXFORD OX1 3QT	ENGLAND
KAZUO HIRAYAMA	AJINAMOTO INC	1-1 SUZUKI-CHO	KAWASAKI-KU	KAWASAKI 210	JAPAN
NAMIKO HIRAYAMA	20-2 TAJIMA CHO	KAWASAKIKU	KAWASAKISHI	KANAGAWA PREF.	JAPAN
W HROSCH	H ALLMERIWEG 13			D 2870 DELMENHORST	W GERMANY
W K HUBER	RAMSCHWAGWEG 336			FL 9496 BALZERS	LIECHTENSTEI
Y I ITAGAKI	JEOL LTD	AKISHIMA	NAKAGAMI CHO 1418	TOKYO 196	JAPAN
MARGITH JANSSON	KAROLINSKA INSTITUTE	MASS SPECTROMETRY LA	BOX 60 400	S-10401 STOCKHOLM	SWEDEN
KEITH R JENNINGS	UNIV OF WARWICK	GIBBET HILL ROAD	SCIENCES DEPT	COVENTRY CV4 7AL	ENGLAND
J D JOLY	SN NERMAG	49 QUAI DE HALAGE		92500RUEIL-MALMAISON	FRANCE
IVAN KAMENSKY	TANDEM ACCEL LAB	UPPSALA UNIV	BOX 533	UPPSALA S-75121	SWEDEN
M KARAS	UNIV OF FRANKFURT	INST OF BIOPHYSICS	T STERN KAI 7	6000 FRANKFURT 70	W GERMANY
E KUBOTA	JEOL MSG	1418 NAKAGAWI	AKISHIMA	TOKYO	JAPAN
TOMIKO KUHARA	INST HUMAN GENETICS	KANAZAWA MED UNIV	UCHINADA KAHOKU-GUN	ISHIKAWA 920-02	JAPAN
FUMIO KUNIHIRO	JEOL LTD	1418 NAKAGAMI	AKISHIMASHI	196 TOKYO	JAPAN
WILLIAM LAUWERS	JANSSEN PHARMACEUTIC	TURNHOUTSE BAAN 30		B-2340 BEERSE	BELGIUM
PIET A LECLERCQ	EINDHOVEN UNIV TECH	PO BOX 513		5600-MB EINDHOVEN	NETHERLANDS
IVOR LEWIS	VG ANALYTICAL	FLOATS ROAD	WYTHENSHAWE	MANCHESTER M23 9LE	U K.
CHAVA LIFSHITZ	HEBREW UNIV	PHYSICAL CHEM DEPT	MAIL CODE 91904	JERUSALEM	ISRAEL

NAME	A1	A2	A3	CI	CN
BERNARD LINDEN	PO BOX 61 03 07			D-2800 BREMEN 61	W GERMANY
ALLAN MACCOLL	UNIVERSITY COLLEGE	CHEMISTRY DEPT	20 GORDON ST	LONDON WC1H 0AJ	ENGLAND
A MANDELBAUM	TECHNION	CHEMISTRY DEPT		HAIFA 32000	ISRAEL
ROD S MASON	UNIV OF WARWICK	CHEMISTRY DEPT		COVENTRY CV4 7AL	ENGLAND
ISAMU MATSUMOTO	INST HUMAN GENETICS	KANAZAWA MED UNIV	UCHINADA KAHOKU-GUN	ISHIKAWA 920-02	JAPAN
BARRY MCKINNON	VG ISOTOPES	ION PATH ROAD 3	WINSFORD	CHESHIRE	U K
E M B MERCKX	IMPERIAL CHEMICAL	POLYURETHANES R&D	EVERSLAAN 45	EVERBERG	BELGIUM
L E MOORE	KRATOS SCIEN APP LTD	BARTON DOCK ROAD	URMSTON	MANCHESTER M31 2LD	ENGLAND
T NIWA	NAGOYA UNIV HOSPITAL	1-1-20 DAIKO-MINAMI	HIGASHI-KU	NAGOYA	JAPAN
TAMOTSU NODA	TOYOHASHI UNIV OF	TECHNOLOGY	TEMPAKU-CHO	TOYOHASHI 440	JAPAN
BERNT OLIN	NESTE OY	RESEARCH CENTRE		SF-06850 KULLOO	FINLAND
V C PARR	VG ANALYTICAL	FLOATS ROAD	WYTHENSHAW	MANCHESTER	ENGLAND
REINHOLD PESCH	FINNIGAN MAT GMBH	BARKHAUSENSTR 2	POSTFACH 14 40 62	2800 BREMEN	WEST GERMANY
CHRIS J PORTER	VG ANALYTICAL	FLOATS ROAD	WYTHENSHAWE	MANCHESTER	ENGLAND
M P PRZYBYLSKI	UNIV MAINZ	INST ORG CHEMIE		D-6500 MAINZ	WEST GERMANY
JOHN A RACE	VG ANALYTICAL LTD	FLOATS ROAD	WYTHENSHAWE	MANCHESTER M23 9LE	ENGLAND
NORMAN RAMSEY	VG ANALYTICAL	FLOATS ROAD	WYTHENSHAWE	MANCHESTER	ENGLAND
PETER ROEPSTORFF	MOLECULAR BIOLOGY	ODENSE UNIV	CAMPUSVEJ 55	DK 5230 ODENSE M	DENMARK
F W ROLLGEN	INST PHYSICAL CHEM	UNIV OF BONN	WEGELERSTR. 12	D-5300 BONN	W GERMANY
P A RYAN	KRATOS SCIEN APP LTD	BARTON DOCK ROAD	URMSTON	MANCHESTER M31 2LD	ENGLAND
KAYOKO SAIKI	KANAZAWA UNIV	HUMAN GENETICS	UCHINADA KAHOKU-GUN	ISHIKAWA 920-02	JAPAN
KIYASHI SATOUCHI	KANSAI MED UNIV	MORIGUCHI		OSAKA 570	JAPAN
U P SCHLUNEGGER	UNIVERSITAT BERN	INSTIT ORGAN CHEMIE	FREIESTRASSE 3	CH-3012 BERN	SWITZERLAND
LONGSHENG SHENG	NANJING COLL OF	PHARMACY		NANJING	PEOPLE REPUB
TOSHIHIRO SHINKA	DEPT OF BIOCHEMISTRY	KANAZAWA MED UNIV	UCHINADA KAHOKU-GUN	ISHIKAWA 920-02	JAPAN
DANIEL STAHL	EPFL-ECUBLENS	INST DE CHIMIE PHYS	ECOLE POLYTECHNIQUE	CH-1015 LAUSANNE	SWITZERLAND
RAFFAELE TABACCHI	UNIV DE NEUCHATEL	INST DE CHIMIE	AV DE BELLEVAUX 51	CH-2000 NEUCHATEL	SWITZERLAND
J C TABET	ECOLE POLYTECHNIQUE	LAB ORGAN SYNTHESIS		PALAISEAU 91	FRANCE
NAOHITO TAKEDA	FAC OF PHARMACY	MEIJO UNIV	TEMPAKU	NAGOYA 468	JAPAN
LESTER TAYLOR	KRATOS LTD	BARTON DOCK ROAD	URMSTON	MANCHESTER	ENGLAND
J P THENOT	LERS	SYNTHELABO	23 AV M SAULNIER	92360 MEUDON FORET	FRANCE
M TSUCHIYA	4 37 27 KUGAYAMA	SUGINIMI KU		TOKYO 168	JAPAN
P J TURNER	VG MICROMASS LTD	ION PATH	ROAD THREE	WINSFORD CHESHIRE	ENGLAND
ADAM VINCZE	ISRAEL INST BIOL RES	PO BOX 19		NESS ZIONA 70450	ISRAEL
GUENTER WAGNER	FINNIGAN MAT	BARKHAUSENSTR 2		2800 BREMEN	W GERMANY
KARL PETER WANCZEK	PARKALLEE 197			D-2800 BREMEN	WEST GERMANY
MARK WEISS	KATTENTURMER	HEERSTR 122		D-2800 BREMEN	W GERMANY
HIROSHI YAMAGUCHI	TOSHIBA LTD	1 KOMUKAITOSHIBA-CHO	SAIWAI-KU	KAWASAKI 210	JAPAN
JIANG YANHAO	CHEMISTRY DEPT	NANJIN UNIVERSITY		NANJIN	P REPUB CHIN
JEHUDA YINON	WEIZMANN INSTITUTE	ISOTOPE RESEARCH		REHOVOT 76100	ISRAEL
ZE'EV V I ZARETSKII	ISOTOPE DEPT	WEIZMANN INSTITUTE		76 100 REHOVOT	ISRAEL
JAN ZWINSELMAN	SPECTROSPIN	INDUSTRIESTRASSE 26		8117 FALLANDEN	SWITZERLAND

VAN KALLEVEEN,T H 326
VAN LANGENHOVE,A 675
VEARES,M 803
VERMA,S 779
VERRET,W J 263
VESONDER,R F 347
VESTAL,M L 246
VESTAL,M L 353
VESTAL,M L 840
VESTAL,M L 193
VESTLING,M M 153
VICCHIO,D 763
VIGGIANO,A A 767
VINDIOLA,A G 436
VISWANADHAM,S K 231
VOUROS,P 205
VOUROS,P 441
VOYKSNER,R D 197
VOYKSNER,R D 117
VOYKSNER,R D 695
VOYKSNER,R D 3
VRBANAC,J J 697
WAGNER,G 176
WALKER,J 25
WALLER,G R 146
WALLER,G R 144
WALLS,F C 618
WANCZEK,K P 233
WANG,T -C L 589
WANG,T-C L 600
WATANABE,H 602
WATSON,J T 534
WATSON,J T 244
WATSON,J T 828
WEAKLIEM,H A 635
WEBER,L 345
WEE,E L 781
WEERASINGHE,N C A 295
WEINTRAUB,S T 129
WEINTRAUB,S T 496
WEISZ,A 574
WELCH,M J 820
WELCH,M J 74
WELCH,R L 54
WELLER,R R 595
WELLER,R R 707
WESDEMIOTIS,C 22
WESDEMIOTIS,C 499
WEST,D X 640
WESTCOTT,J Y 705
WESTFAHL,J C 738
WESTMORE,J B 460
WESTMORE,J B 459
WETMORE,R W 332
WHITE,E 74
WHITE,E 820
WHITE,E 308
WHITE,E L 312
WHITE,K D 622
WHITEHOUSE,C M 92
WHITEHOUSE,C M 188
WHITNEY,J O 133
WHITNEY,J O 125
WHITNEY,J O 618
WILKINS,C L 588
WILLIAMS,C H 9
WILLIAMS,C H 285
WILLIAMS,C H 281
WILLIAMS,C M 80
WILLIAMS,D H 382
WILLIAMSON,C 650
WILLOUGHBY,R C 96
WILLOUGHBY,R C 192
WILLS,M R 78
WILSON,B W 432
WILSON,B W 438
WINDIG,W 540
WINDIG,W 665
WINKLER,P C 96
WOLFE,M H 753
WOLFE,R R 753
WONG,C 642
WONG,C M 372
WONG,J W 468
WONG,S S 186
WOOD,G W 563
WOOD,K V 428
WOOD,K V 376
WOODHALL,B J 34
WRIGHT,B W 207
WRIGHT,C W 432
WRIGHT,L G 376
WU,R L C 470
WYATT,J R 235
YAMAGUCHI,H 612
YAMAGUCHI,K 110
YAMASHITA,M 188
YANG,Y-M 133
YASUDA,S 612
YELTON,R O 283
YERGEY,A L 90
YERGEY,A L 76
YERGEY,A L 129
YERGEY,J 104
YINON,J 86
YOST,R A 783
YOST,R A 14
YOST,R A 80
YOUNG,A B 513
YOUNG,S E 826
YOUNGLESS,T L 305
YOUSSEFI,M 550
YU,K O 444
YU,R K 811
YUDKOFF,M 759
ZARETSKII,Z V I 475
ZHAO,S 610
ZIMMERMAN,E F 781
ZIMMERMAN,M L 747
ZINGARO,R A 436
ZOELLER,J H 436
ZWINSELMAN,J J 36

SLOWIKOWSKI,D L 817
SMITH,A 221
SMITH,B J 78
SMITH,C V 131
SMITH,D 46
SMITH,D 769
SMITH,D C 803
SMITH,D H 406
SMITH,L 848
SMITH,R D 560
SMITH,R D 542
SMITH,R D 207
SMITH,R M 289
SMITH,R W 110
SOKOLOSKI,E 742
SOLCH,J G 5
SOLOMON,J J 404
SOVOCOOL,G W 691
SPEEDIE,M K 763
SPENCER,R B 658
SPHON,J A 494
SPHON,J A 622
SQUIRES,R R 223
SQUIRES,R R 376
SQUIRES,R R 211
SRINIVASA,R S 734
STAFFORD,G C 598
STAFFORD,G C 505
STAHL,D 492
STAHL,D 172
STANDING,K G 749
STANDING,K G 184
STANDING,K G 239
STAUFFER,D B 661
STAUFFER,D B 658
STEFFENS,P 180
STEMMLER,E A 56
STERNSON,L A 707
STEWART,P B 9
STOBIECKI,M 580
STOLL,R 838
STOUT,S J 113
STRADLING,R S 384
STRAUB,K 785
STRIFE,R J 703
STROH,J G 119
STUERMER,H 544
STULTS,J T 519
SUN,J D 275
SUN,W -F 261
SUNDQUIST,B 32
SUZUKI,M 150
SUZUKI,R 443
SVEC,H J 24
SVEC,H J 807
SVEC,H J 610
SWANSIGER,J T 305
SWEELEY,C C 576
SYKA,J E P 598
SYKA,J E P 505
TABET,J C 462
TABET,J C 464
TABETT,J-C 681
TAKEDA,N 150
TAKESHITA,H 25
TAMURA,H 602
TANNER,S D 7
TANZER,F S 25
TASHIRO,C 279
TATEMATSU,A 150
TAYLOR,D H 614
TAYLOR,L C E 384
TAYLOR,L C E 359
TAYLOR,L C E 382
TAYLOR,M L 5
TEECE,R G 400
TEMBREULL,R 164
TEMPLETON,J F 460
TERLOUW,J K 48
TERLOUW,J K 498
THOMAS,T F 318
THOMSON,B A 190
THOMSON,B A 7
THORNE,G C 652
THRUSTON,A D 205
TIERNAN,T O 5
TIERNAN,T O 470
TIERNAN,T O 511
TILSON,H A 689
TIMMONS,L 293
TJOA,S S 582
TODD,J F J 598
TODD,J F J 505
TODD,P J 253
TODD,P J 247
TODD,P J 12
TOMER,K B 625
TOMER,K B 679
TOMER,K B 717
TOMER,K B 721
TONDEUR,Y 462
TONDEUR,Y 815
TORRENCE,P F 817
TOSINE,H 287
TOWNSEND,R 339
TRAINOR,T M 441
TREHY,M L 14
TROIN,Y 462
TRUSSELL,A R 265
TSARBOPOULOS,A 225
TSARBOPOULOS,A 828
TSO,J 499
TSUCHIYA,M 558
TUCKER,M G 100
UDSETH,H R 560
UDSETH,H R 542
UDSETH,H R 207
UNDERHILL,E W 468
UNGER,P D 813
UNGER,S E 255
UPSCHULTE,B L 229
VALKENBURG,C A 63
VAN BREEMEN,R 681
VAN DER ZANDE,W 715

REENTS,W D 530
REGINATO,R 618
REIMER,M L J 460
REIMER,M L J 459
REINHOLD,V N 386
REINHOLD,V N 673
REINHOLD,V N 675
REINHOLD,V N 580
REMPEL,D L 596
REMPEL,D L 546
RETTINGHAUS,G 422
REUTER,C 556
REYNOLDS,W E 598
RHEE,C K 257
RHINEBARGER,R 828
RHODES,D 830
RICCA,T L 600
RIDGE,D P 221
RIDGE,D P 227
RILEY,C N 707
RINEHART,K L 811
RINEHART,K L 119
RINEHART,K L 402
RITCHEY,C R 144
ROACH,J A G 622
ROBBINS,R C 479
ROBERTS,G 341
ROBOZ,J 447
ROBOZ,J 443
ROCCA,J L 88
ROCHE,F R 585
ROE,C R 583
ROEPSTORFF,P 34
ROEPSTORFF,P 32
ROITMAN,E 133
ROLANDO,C 856
ROLINSKI,E J 638
ROLLGEN,F W 824
ROLLGEN,F W 186
ROMANOWSKI,G 233
ROSENTHAL,P 133
ROSS,D B 743
ROSS,M M 833
ROSS,M M 249
ROSS,M M 388
ROSS,R M 78
ROTTSCHAEFER,S 69
ROTTSCHAEFER,S 341
ROTTSCHAEFER,S 466
RUDEWICZ,P 809
RUDEWICZ,P 178
RUSSELL,D H 219
RUSSELL,D H 852
RUSSELL,D H 797
RUSSELL,D H 629
RUSSELL,J R 148
RYAN,J J 261
SAADEH,N K 430
SACK,T M 591
SACK,T M 485
SAFE,S 685
SAFE,S 291
SAITO,K 701
SAKUMA,T 789
SALEM,N 104
SALLANS,L 223
SALLANS,L 211
SAMS,R L 820
SANTOS,I 589
SARRE,O 394
SARVER,E W 709
SATOUCHI,K 701
SAVICKAS,P J 408
SAVORY,J 78
SAYYID,S 106
SCANLAN,G 392
SCHAFFER,R 74
SCHEEL,R H 54
SCHELLING,F J 229
SCHMID,E R 677
SCHMIT,J P 487
SCHNATZ,H 544
SCHOELLER,D A 631
SCHOEN,A E 378
SCHRAM,K H 400
SCHRAM,K H 817
SCHUBERT,A J 426
SCHUELER,B 239
SCHUELER,B 184
SCHUELER,B 749
SCHUR,K M 540
SCHUTJES,C P 795
SCHWARTZ,H E 205
SCHWEIKARD,L 544
SCHWEITZER,J S 805
SCOBLE,H A 349
SCOTT,P M 789
SCOVILL,J P 640
SEARS,L J 59
SEDGWICK,R D 811
SEDGWICK,R D 813
SEGAL,A 404
SEIFERT,W E 849
SELF,R 755
SEO,Y-H 259
SERVE,M P 444
SETHI,S K 201
SETHI,S K 620
SHACKLETON,C 123
SHARP,T R 757
SHELTON,D B 845
SHEN,J 430
SHINKA,T 139
SHINKA,T 586
SHUKLA,A 44
SHUSHAN,B 650
SHUSHAN,B 7
SICHTERMANN,W 251
SIEGEL,M 94
SIEVERT,H -J 580
SIGLER,P 1
SITRIN,R 341
SKETT,P W 195
SLAYBACK,J R B 477

MORGAN,T G 324
MORITA,Y 842
MORTON,T H 160
MORTON,T H 457
MOSCHEL,R C 815
MOSHEN,M 137
MOTT,A W 481
MUGA,M L 241
MUIR,D C F 143
MULLEN,S L 589
MUNSON,B 809
MUNSON,B 178
MUNSON,B 455
MURAD,E 637
MURPHY,J H 182
MURPHY,R C 703
MURPHY,R C 71
MURPHY,R C 82
MURPHY,R C 705
MUSHA,K 558
MUSSELMAN,B 576
MUSSELMAN,B D 244
MYERHOLTZ,C A 426
MYERS,A C 830
NACSON,S 36
NAITO,M 523
NAITO,Y 523
NAVRATIL,P R 141
NELSON,C C 620
NERO,V P 687
NETZEL,D A 434
NEUMEYER,J L 441
NG,K J 74
NG,Y T 507
NGO,A 7
NIEHUIS,E 180
NISHIMURA,S 201
NISHIMURA,T 536
NISHIMURA,T 771
NISHIMURA,T 328
NISHIMURA,T 213
NODA,T 602
NOGAR,N S 370
NOGAR,N S 368
NORMAN,E J 781
NOWLIN,J G 131
NUGTEREN,D H 67
O'DONNELL,J E 307
O'DONNELL,J E 424
O'KEEFE,P W 289
O'LEAR,J R 378
O'MALLEY,R M 566
OBAL,T 563
OCCOLOWITZ,J L 842
ODOM,R W 608
OGIER,W 826
OKOMOTO,D 438
OKUTANI,T 602
OLERICH,G 65
OLIVARES,J A 412
OLIVARES,J A 807
OLSON,C T 444
ONISHI,H 25
ONSTOT,J 293
ONO,J 334
PAGE,S W 622
PALLANTE,S L 451
PANG,H 751
PANNELL,L K 640
PANNELL,L K 742
PARKER,C E 110
PARR,J L 271
PARR,J L 9
PARTHASARATHY,R 135
PAUL,B 711
PAUL,T D 585
PAULSON,J F 767
PAULSON,J F 318
PEAKE,D A 644
PEAKE,D A 832
PEAKE,D A 793
PEAVY,R D 410
PELL,R J 565
PELLETT,G L 616
PELLIZZARI,E 3
PELLIZZARI,E D 695
PENDYALA,L 711
PEREL,J 94
PESCH,R 303
PFEIFFER,R 28
PFLEIDERER,W 402
PILOSOF,D 193
PILOSOF,D 353
PINKSTON,J D 534
PLATTNER,R D 787
POEPPEL,F 98
POPOV,A I 828
PORTER,C J 699
PORTER,C J 301
PORTER,R F 20
POWELL,R G 787
PRAMANIK,B N 394
PRAS,N 111
PRESCOTT,C L 281
PRESCOTT,C L 271
PRICE,H A 54
PROCTOR,B L 269
PROCTOR,B L 158
PROCTOR,D W 414
PROVOST,L P 285
QUALLS,W C 384
QUALLS,W C 745
QUALLS,W C 525
QUAN,E S K 168
QUILLIAM,M A 277
QUILLIAM,M A 279
RAHN,G 477
RAMANA,D V 563
RAMSEY,E D 34
RAMSEY,E D 195
RAPP,U 303
REDEKER,G S 824
REDMAN,E W 160
REDMAN,E W 457

AUTHOR INDEX

LOOKER,J H 679
LOS,J 715
LUBMAN,D M 164
LUCKE,R B 432
LUCKE,R B 560
LUDOVIC,Y 146
LUYTEN,Y 115
LYNAUGH,N 667
LYON,P A 717
LYON,P A 625
MACFARLANE,R D 436
MACFARLANE,R D 845
MACFARLANE,R D 517
MACHLAN,L A 418
MAGEE,C W 635
MAGIN,D F 659
MAHLUM,D D 432
MAHONEY,J F 94
MAIN,D E 749
MAIN,D E 184
MAIN,D E 239
MAKSOUD,H 441
MALINOVICH,Y 42
MALLAMS,A K 394
MALTBY,D A 583
MALTBY,D A 398
MANCILL,V K 845
MANDELBAUM,A 574
MAQUESTIAU,A 723
MAQUIN,F 492
MAQUIN,F 172
MARASCO,J 633
MARASCO,J 740
MARBURY,G D 689
MARCH,R E 324
MARCH,R E 513
MARCH,R E 713
MARCUS,R K 364
MARKEY,S P 850
MARQUIS,F 78
MARSHALL,A G 589
MARSHALL,A G 600
MARTIN,C R 26
MARTIN,M 576
MARTIN,W B 566
MARTINEAU,A 761
MARYANOFF,C A 777
MASON,R S 774
MASON,R S 562
MASSE,R 137
MATHEWS,W R 351
MATSUMOTO,I 139
MATSUMOTO,I 586
MATSUMOTO,I 121
MATSUMOTO,M 586
MATSUMOTO,M 139
MATTHEWS,H B 110
MATTHEWS,P J 513
MAYLIN,G 446
MAZER,S M 283
MCADOO,D J 568
MCADOO,D J 314
MCADOO,D J 473
MCCALLA,D R 279
MCCAMISH,M 447
MCCARTHY,E R 657

MCCLOSKEY,J A 135
MCCLOSKEY,J A 620
MCCLOSKEY,J A 201
MCCLUER,R H 683
MCCLUER,R H 102
MCCRERY,D A 591
MCCRERY,D A 832
MCDEVITT,M A 281
MCDOWALL,M A 195
MCEWEN,C N 836
MCFADDEN,W H 100
MCFARLANE,R D 26
MCGUIRE,J M 205
MCIVER,R T 337
MCIVER,R T 593
MCIVER,R T 532
MCIVER,R T 505
MCLAFFERTY,F W 503
MCLAFFERTY,F W 499
MCLAFFERTY,F W 22
MCLAFFERTY,F W 661
MCLUCKEY,S A 715
MCNEAL,C J 845
MCNEAL,C J 517
MCNEAL,C J 26
MCREYNOLDS,J H 585
MECKSTROTH,W K 227
MEEHAN,J L 295
MEISELS,G G 771
MEISELS,G G 328
MEISELS,G G 326
MEISELS,G G 213
MENTZER,M 69
MENTZER,M 466
MESSIER,F 137
MEUZELAAR,H L C 540
MEUZELAAR,H L C 665
MEYRANT,P 723
MICHALSKI,T J 155
MIDDLEDITCH,B S 334
MIDGLEY,J M 80
MILLER,C M 370
MILLER,C M 368
MILLER,D 5
MILLINGTON,D S 259
MILLINGTON,D S 76
MILLINGTON,D S 398
MILLINGTON,D S 583
MIROCHA,C J 663
MITCHUM,R K 669
MITCHUM,R K 844
MOLNAR,J A 753
MOMMERS,A A 498
MONCUR,A V 195
MONCUR,J G 265
MOORE,C 562
MORGAN,T G 713

JEFFS,P 341
JENKINS,E 135
JENNINGS,K R 774
JENNINGS,K R 44
JENNINGS,K R 765
JENNINGS,K R 562
JENSEN,N J 717
JOHNSON,J V 783
JOHNSTON,M 496
JOHRI,K K 160
JORDAN,E A 26
JUNACK,M 251
JUNGHALWALA,F B 102
JURUSIK,J 289
KAISER-FARRELL,C 279
KALINOWSKI,H 544
KAMENSKY,I 32
KAMMEI,Y 523
KARAS,M 257
KARGER,B L 205
KASAI,H 201
KATZ,J J 155
KAZDAN,E 513
KAZYAK,L 740
KEARNS,M 297
KEESEE,R G 229
KELLEY,P E 505
KELLEY,P E 598
KELNER,L 850
KELSO,G 345
KENAN,W R 312
KENTTAMAA,H I 570
KENYON,C N 108
KEOUGH,T 627
KERN,F 544
KERNS,E H 148
KHANDELWAL,J K 73
KIDWELL,D A 388
KIDWELL,D A 249
KIDWELL,D A 833
KILLMER,L B 466
KILLMER,L B 69
KIM,H Y 193
KIM,H Y 353
KINGSTON,E E 475
KINGSTON,E E 127
KINTER,M T 312
KIPLINGER,J P 472
KISTEMAKER,P G 715
KIVITS,G A A 67
KLEIN,P D 141
KLINE,T 73
KLUGE,H -J 544
KNAPP,D R 697
KOGAI,T 638
KOSHIMIZU,K 150
KRAILLER,R E 629
KRAILLER,R E 18
KRAMER,S D 366
KRENZER,E G 144
KRISHNAMURTHY,T 709
KUEHL,D W 11
KUHARA,T 139
KUHARA,T 121
KUHARA,T 586
KUNIHIRO,F 523
KUWABARA,H 558
LAI,J T 738
LANDIS,P W 842
LANE,K 211
LANE,K 223
LANE,K 376
LANNING,S 642
LANNING,S M 372
LANT,M S 277
LAPP,R L 548
LAPP,R L 644
LAPP,R L 322
LARAMEE,J A 44
LARKA,E A 481
LARSEN,B S 84
LASER,B 176
LATER,D W 438
LATER,D W 432
LATTIMER,R P 738
LATTIMER,R P 257
LATTIMER,R P 540
LATTIMER,R P 743
LAU,B P -Y 261
LAU,B P -Y 789
LAUGAL,J A 428
LAWRENCE,D L 781
LAY,J O 819
LAY,J O 453
LAYER,R W 738
LAYER,R W 257
LECAVALIER,L 761
LECLERCQ,P A 795
LEE,R E 376
LEE,R W K 160
LEE,Y C 339
LEHMAN,J P 693
LEHMAN,T A 721
LEIKER,T J 310
LEROY,R J 332
LEVANDOSKI,P 785
LEWIS,E 277
LEWIS,I A S 803
LEWIS,I A S 119
LEWIS,S 759
LIBERATO,D J 90
LIBERATO,D J 76
LIBERATO,D J 129
LIEHR,J G 127
LIFSHITZ,C 162
LIFSHITZ,C 42
LIN,S-N 578
LINCOLN,K A 242
LINN,D 11
LINN,W G 529
LIPPSTREU,D L 355
LISEK,C A 451
LO,H H 98
LOO,J A 503

AUTHOR INDEX

HANISCH,R C 271
HANNA,I 464
HANSON,R L 275
HARADA,K -I 150
HARDIN,E D 246
HARDIN,E D 840
HARPER,A M 540
HARRINGTON,W L 635
HARRIS,F M 713
HARRIS,F M 324
HARRIS,R E 743
HARRIS,W R 438
HARRISON,A G 36
HARRISON,J 217
HARRISON,W W 408
HARRISON,W W 364
HARRISON,W W 416
HARVAN,D J 489
HARVAN,D J 838
HARVAN,D J 836
HARVEY,D J 448
HASE,G 42
HASS,J R 838
HASS,J R 380
HASS,J R 836
HASS,J R 489
HASSETT,J M 585
HASTIE,J W 374
HAYES,M J 205
HEDIN,C M 263
HEIKES,D L 299
HELLER,D 339
HELLER,D N 84
HEMLING,M E 402
HEMLING,M E 811
HENDERSON,T R 275
HENDRIKS,H 483
HENION,J 203
HENION,J 791
HENION,J 170
HENION,J 446
HEPPNER,R A 434
HEPPNER,R A 414
HERCULES,D M 231
HEROLD,D A 78
HERTZ,H S 74
HERTZ,H S 820
HESS,K R 416
HEWETSON,D 663
HIBBINS,S W 289
HILKER,D R 289
HILL,J C 517
HILLENKAMP,F 257
HILPERT,L R 267
HILPERT,L R 61
HINDENLANG,D M 813
HINES,J 117
HIRAI,N 150
HIRST,D M 44
HITES,R A 56
HITZMAN,C J 608
HO,M 513
HO,Y K 585
HOFFMAN,P A 648
HOGGE,L R 468
HOHN,M 303
HOHNHOLT,J M 310
HOLLAND,J 576
HOLLAND,J F 519
HOLMES,G A 797
HOLMES,J L 48
HOLMES,J L 498
HONG,J S 689
HONMA,Y 612
HOPPILLIARD,Y 723
HOPPILLIARD,Y 725
HOPPILLIARD,Y 801
HOPPILLIARD,Y 727
HORNING,E C 131
HOUGH,L B 73
HOUK,R S 610
HOUK,R S 412
HSU,C S 166
HSU,K L 265
HUANG,J 424
HUANG,S K 546
HUANG,S K 596
HUBER,W K 422
HUDSON,C E 314
HUDSON,C E 473
HUDSON,C E 568
HUDSON,R D 687
HUGHES,B M 283
HUGHES,H 131
HUGHES,R J 513
HUNT,J E 155
HUNTER,R L 505
HUNTER,R L 593
HUNTER,S W 392
HURST,G S 366
HUWE,J K 450
HWANG,D -G 86
IBRAHIM,K E 80
IJAMES,C F 588
ILIAS,A M 182
IMAI,J 817
INOUE,Y 586
INOUE,Y 139
IRVING,C S 141
ITAGAKI,Y 523
JACKSON,C-J C 460
JACKSON,T C 215
JACOBSON,D B 215
JAMESON,C W 293
JAMIESON,G C 556
JAMIESON,G C 830
JAMIESON,W D 671
JAMIESON,W D 277
JAMIESON,W D 685
JARDINE,I 392
JAUDON,P 725
JAYASIMHULU,J 156
JAYASIMHULU,K 345
JAYASIMHULU,K 343

FARBER,A 135
FAULL,K F 783
FAULL,K F 440
FEIL,V J 450
FENG,R 499
FENN,J B 92
FENN,J B 188
FENNESSEY,P V 582
FENSELAU,C 84
FENSELAU,C 339
FENSELAU,C 451
FERGUSON,A M 565
FERGUSON,E E 769
FERGUSON,E E 46
FERNANDEZ,M T 774
FETIZON,M 464
FETTEROLF,D D 28
FIELD,F H 237
FIELD,F H 507
FIELD,F H 38
FIELD,F H 805
FIES,W J 505
FIES,W J 598
FITCH,W L 556
FITCH,W L 830
FLAMENT,J P 723
FLAMENT,J P 727
FLAMMANG,R 723
FLESCH,G D 807
FLESCH,G D 24
FOHLMAN,J 32
FOSTER,N G 479
FOURNIER,P G 572
FRAISSE,D 88
FRAISSE,D 462
FRALEY,D F 781
FRALEY,D F 527
FRANCL,T J 532
FREAS,R B 227
FREAS,R B 554
FREEMAN,J P 844
FREEMAN,J P 669
FREEMAN,P 52
FREISER,B S 215
FRIEDHOFF,A J 805
FRIESE,T 180
FUKUDA,E K 330
FULFORD,J 7
FUNG,D 685
FUNG,D 291
GALE,P J 635
GALLEGOS,E J 736
GAMES,D E 195
GAMES,D E 34
GAMMANS,R E 148
GANGULY,A K 394
GARNER,F C 263
GARRETSON,L D 285
GARRETSON,L D 9
GARRETT,J H 5
GASKELL,S J 652
GASKELL,S J 699
GAULDEN,M E 158
GEARHART,H L 565
GEBOES,P 115
GEFEN,S 162
GEFEN,S 42
GELLENE,G I 20
GERGELY,R J 277
GERSHEY,R M 277
GERSHEY,R M 671
GERSHEY,R M 685
GIBLIN,D E 548
GIBLIN,D E 644
GIERTHY,J 289
GIESSMANN,U 824
GIESSMANN,U 186
GILLEN,K T 822
GILLIAM,J M 842
GIORDANI,A B 648
GLISH,G L 521
GLISH,G L 719
GOERINGER,D E 719
GOERINGER,D E 521
GOLDMAN,P 580
GOOD,B W 659
GOODLEY,P C 108
GRACE,L 38
GRAMAIN,J C 462
GREAVES,J 447
GREEN,B N 380
GREEN,B N 515
GREEN,J P 73
GREEN,L W 420
GREENE,F T 424
GREENE,F T 307
GREGG,H R 648
GREIFENDORF,D 180
GRIFFIN,D 52
GRIFFIN,L L 473
GRIMES,L E 732
GRIMSRUD,E P 63
GRIMSRUD,E P 59
GROENEWOLD,G S 247
GROENEWOLD,G S 253
GROENEWOLD,G S 12
GROSS,M L 793
GROSS,M L 717
GROSS,M L 596
GROSS,M L 591
GROTEMEYER,J 22
GROTJAHN,L 396
GROTJAHN,L 359
GROVE,M D 787
GRUNDERGER,D 133
GUENAT,C 172
GUEVREMONT,R 671
GUEVREMONT,R 685
GUILHAUS,M 40
GUILHAUS,M 572
GUMPORT,R I 402
HAKONSON,P 32
HALL,S 622
HAMMING,M C 565

AUTHOR INDEX

COLTON,R J 833
COLTON,R J 249
COMPSON,K R 297
CONZEMIUS,R J 610
COOK,J C 835
COOK,J C 402
COOK,J C 119
COOK,K D 552
COOKS,R G 779
COOKS,R G 570
COOKS,R G 378
COOKS,R G 376
COSTELLO,C E 751
COSTELLO,C E 347
COSTELLO,C E 621
COTE,I L 404
COTTER, R J 681
COTTER,R J 320
COTTER,R J 84
COTTER,R J 538
COTTRELL,J S 382
COUCH,M W 80
COVEY,T 446
COVEY,T 170
COVEY,T 791
COVEY,T 203
COWENS,J W 711
CRAMERS,C A 795
CRAWFORD,D W 418
CRAWFORD,D W 410
CRAWFORD,R 642
CRAWFORD,R W 372
CREAVEN,P J 711
CROSS,K P 646
CROSS,K P 648
CROW,F W 625
CROW,F W 721
CROW,F W 717
CROW,F W 679
CROWTHERS,J 203
CROWTHERS,J 446
CROWTHERS,J 170
CURTIS,J M 332
CUTUGNO,D 259
DADKIEWICZ,P 544
DACUNHA,A R 113
DALE,F 318
DANIS,P O 499
DANIS,P O 22
DANNER,D A 305
DAS,C 773
DAS,M 459
DAS,P R 328
DAS,P R 213
DASS,C 485
DAVIDSON,W R 7
DAWSON,P H 316
DAWSON,P H 729
DAWSON,P H 509
DAWSON,P H 487
DAY,R A 345
DAY,R A 343
DE BRUIJN,D P 715
DE KANEL,J 362
DECKER,K 404
DEINZER,M 52
DELBERT,S S 337
DELFINO,R 631
DELMORE,J E 606
DENNE,D R 297
DESIDERIO,D M 25
DEVANT,G 856
DIEM,H E 743
DIETRICH,A M 259
DIFFLE,A 815
DOBBERSTEIN,P 378
DOLIN,B 538
DONNELLY,J R 263
DONNELLY,J R 691
DOUGHERTY,R C 362
DOUGLAS,D J 168
DOWD,M A 158
DOWNEY,S W 368
DOWNEY,S W 370
DOYLE,R J 235
DREIFUSS,P A 622
DUHART,B I 844
DULAK,J 98
DUTTA,S 711
DYCKES,D F 353
EADON,G 289
EBY,R E 614
EDMONDS,C G 201
EDWARDS,J G 732
EDWARDS,J G 734
EICHELBERGER,J W 58
EINOLF,W N 152
ELEMA,E T 483
ELLIOTT,N L 420

EMMELIN,M 88
ENKE,C G 519
ENKE,C G 16
ENKE,C G 646
ENKE,C G 648
ENS,W 184
ENS,W 239
ENS,W 749
ESKEW,T J 529
ESMANS,E L 115
EVANS,D H 229
EVANS,J E 683
EVANS,J E 102
EVANS,S 755
EVANS,S 106
EYLER,J R 425
EYLER,J R 595
FALARDEAU,P 761
FALES,H F 640
FALES,H M 850
FALES,H M 742
FAN,T P 246
FAN,T P 840
FAN,T-Y 849

BRAND,H R 372
BRENNAN,P J 392
BRENTON,A G 324
BRENTON,A G 572
BRENTON,A G 40
BRENTON,A G 713
BRICKER,D L 219
BRICKER,D L 629
BRICKER,D L 730
BRILL,F W 424
BRILL,F W 425
BROOKS,A L 275
BROOKS,C J W 390
BROOKS,H B 295
BROOKS,P W 699
BROOKS,P W 301
BROWN,C J 631
BROWN,N 740
BROWNER,R F 96
BROWNER,R F 192
BRUINS,A P 111
BRUINS,A P 483
BRUMLEY,W C 622
BRUMLEY,W C 494
BRUNNEE,C 176
BUCHANAN,M V 65
BUCHNER,J 98
BUCKLEY,P H 650
BUDD,M B 80
BUDDE,W L 58
BULLEN,W W 148
BURGERS,P C 48
BURGERS,P C 498
BURINSKY,D J 490
BURINSKY,D J 330
BURLINGAME,A L 842
BURLINGAME,A L 125
BURLINGAME,A L 133
BURLINGAME,A L 618
BURMEISTER,H R 347
BURSEY,J T 197
BURSEY,J T 3
BURSEY,J T 695
BURSEY,J T 117
BURSEY,M M 312
BURSEY,M M 489
BUSCH,K L 525
BUSCH,K L 384
BUSCH,K L 745
BUTTERWORTH,B C 11
BUTTRILL,S E 608
BUTTRILL,S E 826
BUTTRILL,S E 822
BYRD,G D 61
BYRD,G D 267
BYRN,S 28
CACIC,C C 410
CACIC,C G 418
CALLAHAN,J H 552
CALLERY,P S 763
CAMPANA,J E 235
CAMPANA,J E 490
CAMPANA,J E 554
CAMPANA,J E 330
CAMPBELL,J A 59
CAMPBELL,J A 52
CAPRIOLI,R M 578
CAPRIOLI,R M 849
CAPRIOLI,R M 848
CARR,S A 347
CARR,S A 580
CARR,S A 386
CARR,S A 673
CARROLL,D I 131
CARUSO,J L 156
CASSADY,C J 215
CASTLEMAN,A W 229
CASTRO,M E 852
CATLOW,D A 34
CENA,K 143
CERNY,R L 322
CERNY,R L 501
CHADER,J 28
CHAI,W 618
CHAI,W 123
CHAIT,B T 38
CHAIT,B T 237
CHAJ,W 125
CHAN,K W 503
CHAN,W G 152
CHANCE,R 28
CHANG,C 174
CHANG,C 511
CHANG,S Y 777
CHANG,T T 624
CHANG,T T 453
CHANG,T T 819
CHAPMAN,J R 106
CHEN,C H 366
CHEN,P H 689
CHESS,E K 438
CHESS,E K 432
CHHEDA,G 711
CHHEDA,G B 135
CHIARELLI,P 536
CHIASSON,J L 761
CHITTIM,B 291
CHITTIM,B G 685
CHRIST-HAZELHOF,E 67
CHRISTENSEN,R G 308
CHRISTIE,W H 614
CIUPEK,J D 378
CIUPEK,J D 779
CLAEYS,M 67
CLAY,K L 71
CLAY,K L 705
CLEMENT,R E 287
COHEN,A 74
COHEN,S L 503
COLE,R 838
COLE,W J 390
COLLINS,G J 654
COLTON,R 633
COLTON,R J 388

AUTHOR INDEX

AARON,C S 813
ABBEY,L E 96
ABERTH,W 604
ABERTH,W 842
ACKERMANN,B 828
ADAMS,B R 616
ADAMS,N G 46
ADAMS,N G 769
ADAMS,T A 209
ADAMS,T A 730
ADNOT,A 273
ALAMERCERY,S 88
ALCOCK,N J 195
ALDERFER,J 711
ALDERFER,J L 135
ALDERWEIRELDT,F C 115
ALDOUS,K M 289
ALFIERI,A 287
ALGE,E 769
ALI,M F 503
ALLISON,J 225
ALLISON,J 534
ALLISON,J 217
ALLISON,J 828
ALLMAIER,G 677
ALLMAN,S L 366
AMSTER,I J 503
ANBAR,M 585
ANDERS,V 30
ANDERSON,D 730
ANDERSON,D J 209
ANDERSON,F A 82
ANDRZEJEWSKI,D 494
ARAKALI,A 135
ARAKAWA,R 162
ARAKAWA,R 42
ARPINO,P J 199
ASHCROFT,A E 297
AYERS,C R 78
AYOTTE,C 137
BADINEC,S 217
BACHMANN,D 257
BADR,M 137
BAER,T 50
BAKKE,J E 450
BALLARD,J M 691
BARANY,G 481
BARBALAS,M P 799
BARBER,M 515
BARCHAS,J D 783
BARCHAS,J D 440
BARIL,M 273
BAROFSKY,D F 747
BAROFSKY,D F 182
BAROFSKY,E 182
BARRETT,G M 390
BARTMESS,J E 336
BARTMESS,J E 472
BARTMESS,J E 565
BASILE,B 334
BASS,L M 50
BASS,L M 765
BATEMAN,R H 380
BATEMAN,R H 515
BAUER,M R 16
BAYKUT,M G 425
BAYNE,C K 406
BEATTIE,I G 195
BEAUGRAND,C 199
BEAUGRAND,C 856
BEAVIS,R 184
BEAVIS,R 239
BEAVIS,R 749
BECK,O 440
BECKER,C H 822
BECKNER,C F 648
BENCSATH,F A 805
BENCSATH,F A 507
BENKESER,R A 428
BENNETT,B D 343
BENNETT,B D 345
BENNINGHOVEN,A 30
BENNINGHOVEN,A 251
BENNINGHOVEN,A 180
BENOIT,F M 143
BENTZ,B L 635
BEXON,J J 505
BEYNON,J H 40
BEYNON,J H 324
BEYNON,J H 572
BEYNON,J H 713
BIEMANN,K 751
BIEMANN,K 351
BIEMANN,K 349
BILL,J C 667
BILL,J C 301
BINGOI,Y 509
BLANCKAERT,N 125
BLANTON,W E 434
BLOCK,E 347
BLOM,K F 455
BOMBICK,D 854
BONE,W 633
BONE,W 740
BONNELL,D W 374
BONNER,R 303
BOORN,A 168
BORDER,J R 585
BORDOLI,R S 515
BORNSTEIN,D 574
BOSTWICK,D E 96
BOTT,P A 380
BOUCHOUX,G 801
BOUCHOUX,G 725
BOUCHOUX,G 723
BOUCHOUX,G 727
BOUTTON,T W 141
BOWERS,W D 337
BOWERS,W D 593
BOYD,R K 332
BOYD,R K 685
BOYD,R K 291
BRAIN,D K 477
BRAND,H 642

INDEX OF AUTHORS

Author	Page
Aaserud, David	1086, 1191
Aaserud, David J.	1087
Abbas-Hawks, Christy	669 671, 1201
Abian, Joaquin	1344
Aboleneen, Hoda	1063
Abolin, Craig	1444
Abraham, Vincy	358
Abramson, Fred	1435
Abramson, Fred P.	903 1158, 1435, 1102
Ackermann, Bradley	16 1442
Ackloo, Suzanne Z.	569 1415
Adams, Greg	979, 1373
Adams, Nigel G.	24, 824, 825
Aebersold, Ruedi	436, 613 618, 759
Afonso, Carlos	467
Afzaal, Sunia	515
Agris, Paul	275
Ahuja, Eric S.	120
Ai, Jiu	1497
Aida, Takuzo	1000
Aitken, David J.	864
Akashi, Satoko	988
Alaee, Mehran	738, 739
Alecio , Rob	144, 206
Alexander, Anthony J.	239
Alexander, Michael	1173
Alexander, R.	699
Alexandre, Silvia M. G.	1212
Alianti, John	306
Allen, Michael	302
Allen, Ralph O.	192
Alleyne, Carl	745, 1480
Allington, James W.R.	442
Allison, John	170, 946 994, 1303
Allison, Robert D.	450
Allmaier, Guenter	638
Allman, Steve L.	421, 1101
Almarsson, Örn	568
Almirall, Jose R.	1196
Almo, Steven	973, 1341
Alomary, Ahmed	363, 1396
Altamura, Maria	1482
Alton, Kevin	307, 705
Altwegg, Kathrin	1238
Amado, Francisco M. L.	1410
Amarnath, V.	315
Amirav, Aviv	728, 908 1198, 1470
Amiridze, Nana	316
Amster, I. Jonathan	46, 164 166, 629, 631, 1056, 1192
Amy, J. W.	485
Anacleto, Joseph	288, 1124 1272
Anderegg, Robert	219, 980 1046
Anders, M.W.	1137
Andersen, Jens	525, 978
Andersen, Karin	1083
Andersin, Riitta	721
Anderson, D.C.	1296
Anderson, Gordon A.	49, 477 1270, 1271, 1305
Anderson, Harry	1025
Anderson, Richard M.	958 1220
Anderson, Therese	363
Anderson, Trevor A.	644
Anderson, Vernon E.	213 614
Andren, Per E.	1273, 1314
Andrew, Bowdler	1011
Andrews, Philip	674, 1151
Andrien, Jr., Bruce	39, 889 890
Angelico, Vincent, J.	72
Anil, Shukla	76
Annan, Roland S.	628, 1362
Anspach, Thomas	339
Antonian, Lida	1423
Antonucci, Joseph M.	1076
Antunes, Alexandra M.M.	808
Apffel, Alex	538
Aplin, Robin	1025, 1417
Appelhans, Anthony D.	734
Apuy, Julius L.	611
Arabehety, Gustavo	1376
Arai, Norihisa	1231
Arakawa, Ryuichi	1491, 1492
Arata, Yoji	190
Archer, Renita	731
Arkin, C Richard	506
Armentrout, Peter	408, 465
Arnold, Randy J.	180, 125, 126
Arnott, David	954, 955
Arora, Vinod K.	689, 1448 1449
Artaev, Viatcheslav	915
Artau, Alexander	831
Asam, Michael	471, 983
Asano, Keiji G.	470
Asara, John	946
Asbury, G. Reid	147, 429 652
Ashit, Ganguly	991
Ashley, David	1130
Ashton II, Tommy	1345
Atrih, Abdelmadjid	638
Austin, Daniel	51
Avci, Recep	346, 1065
Avery, M. J.	582, 1458
Babcock, Lucia M.	24, 824 825
Bach, Stephan B.H.	310 748
Bache-Andreassen, L.	829
Bacher, Gerold	638
Bachi, Angela	212, 241, 653
Backus, Sean	738
Bahr, Inke	375, 936
Bahr, Ute	2
Bailer, Josef	772
Bains, Satti	218
Baird, Barbara	587, 645
Bajic, Steve	543, 884
Bajt-Jaeschke, M. L.	1294
Baker, Andrew	600
Baker, Laura A.	419, 1140

INDEX OF AUTHORS

Author	Page
Baker, Martin A.	121 1117, 1121, 1126, 1219
Baker, Peter	532 1220
Baker, Timothy R.	314, 1157 1485
Bakhtiar, Ray	943
Balagopal, Babu	300
Balani, Suresh K.	683, 815
Baldwin, Michael	532, 939 990, 1404
Baldwin, Sam	196
Baldwin, Thomas O.	611
Balk, Steven P.	395
Ball, Haydn	990
Ball, Vincent	162
Balsiger, Hans	1238
Bandy, Alan	371
Banks, J. Fred	39, 1161
Bansal, Surendra	716 1427, 1428, 1429
Barbacci, Damon C.	98, 34
Barbuch, Robert	706
Bardin, Sofiya	320
Barfknecht, Andy	1241
Barinaga, Charles J.	61
Barket, Dennis	340
Barksdale, Charles M.	1300
Barlow, Stephan	451, 1173
Barnett, James, D.	367
Baronas, Elizabeth	1026
Barr, Dana	1130
Barr, John R.	287, 1128 1129
Barr, Robert	191
Barrie, Len	364
Barrish, Andrea	150, 1144
Barros, Cristina M. F.	447 1212, 1410
Barroso, Begona	1276
Barry, Frank	620
Barry, John P.	270
Barshick, C.M.	60, 326
Barshick, Stacy-Ann	60, 666
Bartlet-Jones, Michael	615
Bartlett, Michael G.	107, 311 312, 642, 957, 958, 959
Bartolini, Wilmin	279
Bashir, Sajid	1226, 1364
Basic, Cecilia	1405
Basile, Franco	668, 669 1201
Bateman, Kevin	1033, 1251 1277
Bateman, Mark	817
Bateman, Robert H	42, 220 888, 907, 1062 1281, 1325, 1365
Bates, David	1167
Bauer, Mark D.	158, 203
Baxter, Christina M.	1165
Baxter, Jim	691
Bayer, Charlene W.	1165
Bayer, Robert	1396
Baykut, Gokhan	1397
Bayne, Charles K.	1196
Bean, Mark	1031
Beaudry, Francis	307, 308 317, 703, 1258
Beavis, Ronald	921, 965
Beck, Steve	336
Becker, Christopher H.	415 1200
Becker, Thomas	8
Beckner, Carl	338
Bedman, Tim	1460
Beeson, James G.	398
Beeson, Michelle	1131
Bekele, Haimanot	608
Belisle, Warren	1164
Bell, David	200
Bell, David	774
Bell, Duncan	110
Belov , Mikhail E.	919
Bencsath, F. Aladar	367
Benet, Leslie	1136
Benjamin, Dennis	385
Benner, Steven	1142
Benner, W. Henry	352, 806 1241, 1243
Bennett, Kevin	337, 1465
Bennett, Patrick	117
Benninghoven, Alfred	763
Bennink, Jack R.	395
Benoit, Frank	745
Benson, David R.	945
Benson, Linda M.	381
Benyezzar, Med	1246
Benz, Christopher	1404
Beranova, Sarka	1328
Berberich, David W.	285
Berg, Christian	515
Berg, Fred	1082
Berg, Roberta, G.	367
Bergman, Tomas	221
Bergmann, Carl	394
Bergsma, Derk	1362
Berk, Scott	1042
Berkenkamp, Stefan	7, 796 797, 922, 1004
Berkout, Vadym	345, 1236 1245
Berlin, Kurt	281, 411, 1048 1104, 1105
Berna , Michael	706
Bernemann, Z.	803
Berry-Walker, Yvonne	1194
Bertrand , Marc	13
Bertrand, Michel J.	129, 130 896, 897, 898, 1119 1206, 1207, 1464, 1498
Besada, Vladimir	1368
Bethem, Robert	66
Betowski, Leon	747
Beu, Steve	502
Beutel, Bruce	1050
Beverly, Michael	1201
Beverly, Michael B.	670
Beynon, Robert J.	623
Bhatti, Balwinder	686
Biddlecombe, Robert	1452
Biederman, Kelli	156, 201
Bierbaum, Veronica M.	26 828
Biesiada, Homigol	944

Author	Page
Binder, Ronald G.	374
Binder, Steven	1122
Bishop, Barney	983
Biswas, Kallol M.	590
Biville, Francis	155
Bjoerk, Per	222, 389
Black, Gavin	1435
Black, Roderick S.	1302
Blackburn, Christopher	775
Blackburn, Kevin	219, 980
Blackledge, James A.	239
Blackstock, Walter	218
Blades, Arthur	823
Blair, Ian A.	254, 255, 689
	802, 1132, 1448, 1449
Blair, Sheryl M.	1414
Blair, William R.	1059
Blais, Jean-Claude	155
	920, 921, 1061
Blakney, Greg	507, 910
Blanchard, Steve	1046
Bleibaum, Janice	1332
Blennow, Kaj	768
Blithe, Diana L.	396
Blobel, Gunter	767
Blok-Tip, Leonore	1377
Blom, Karl	1233
Bluhm, Brian	48, 80, 405
Bodganov, Bogdan	444
Bodnar, Wanda	1029, 1139
Boehlein, Susan K.	1352
Boehm, Guenter	1489
	1490, 1500
Bogdanov, Bogdan	464
Boggess, Kathy	358
Bogusz, Maciej J.	1199
Bolanos, B.J.	507
Bolbach, Gérard	155, 920
	921
Bolden, Christina	731
Bolgar, Mark S.	579, 776
Bolton, Judy L.	1143
Bondarenko, Pavel	682
	1107, 1380
Bondesson, Ulf	1273, 1314
Boney, Allison	472
Bonfiglio, Ryan	150
Bonham, Connie	1010
Bonilla, Leo E.	1135
Bonner, Ron	713
Bonnet, Marie Claude	1343
Boon, Jaap J.	45, 1012
Borchers, Christoph	640, 641
Bordini, Ellenia	1312
Bordoli, Robert S	42, 218
	220, 622, 625, 888, 1248
	1314, 1325
Borisenko, Dmitry M.	449
	1211
Borum, Peggy	299
Boschini, Frederic	1218
Bossio, Robert E.	332, 498
	500
Bothner, Brian	1096, 1359
Bottrill, Andrew	1064
Bouchard, Diane	703, 1258
	1456
Boue, Stephen M.	293
Bowers, Larry D.	83, 1302
Bowers, Mike	1057
Bowman, Stephanie C.	265
	269
Bowsher, Ronald	706
Boyd, John	336
Boyd, Robert	66, 116, 1251
Boynton, Raymond	620
Bramble, Frederick	740, 741
Bramhall, Chris	1461
Branco, Paula S.	808
Brand, Tony F.	1040
Braun, Andreas	416
Breau, Alan	320
Breci, Linda	41
Brenna, J. Thomas	648
Brenner, Bernhard	1322
Brenner, Michael, B.	294
Brenton, Gareth	452, 520
	1239
Breton, Patrick	467
Breuker, Kathrin	849
Briche, Céline S.J.	331
Bright, Gene	691
Britt, P.F.	60
Broadus, Katherine	410
	826
Brock, John	1131
Brockman, Adam	295, 440
Brodbelt ,Jennifer S.	475
	476, 533, 841, 842, 843
	1466, 1414
Bromage, Hediye	437
Brookes, Cathy	1057
Brown, Graham V.	398
Brown, Jeffery	220, 1189
	1365
Brown, Nigel K.	317, 703
	1258, 1456
Brown, Olen	316
Brown, Phyllis	777
Brown, Robert S.	167, 929
	1013
Browner, Michelle	1332
Browner, Richard F.	133
	1165
Bruce, James E.	49, 477
	523, 804, 1270, 1271
	1305, 1307, 1394
Brucker, MaryJo	1144
Bruins, Andries P.	137
Brull, Lars	1377, 1378
Brumley, William	742
Brunelle, Alain	917, 1230
Bruno, Alain	896
Brunot, Alain	481, 920, 921
Brushwyler, Kevin	330
Brutkiewicz, Randy R.	395
Bryan, S.	751
Bryant, Duncan	774
Bryant, Matthew	1426
Brynjelsen, Sean	570
Buchanan, M.V.	730
Buchanan, Michelle	518
	1017, 1202
Buckley, Brian T.	756
Buckley, John	1461

INDEX OF AUTHORS

Author	Page
Budde, William L.	1166
Budin, Kenneth	1090
Buettner, Joseph	201, 1045
Bugge, Christopher	322
Buijtenhuijs, Ab	1193
Buko, Alex	85, 982, 1050
	1395
Bukowski, Julie	1041
Bulgarelli, James P.	14, 318
Bullen, William	1434
Bullock, IV, J. S.	132
Bullock, Peter	685, 707, 708
Bundy, Jonathan	1287
Bunger, Andrea	695
Burgoyne, Thomas	329
Burkhart, William	980
Burlina, Alberto	298
Burlingame, A. L.	532, 799
	939, 989, 990
	1136, 1335, 1404
Burnett, Michael	122
Burney, Samar	251
Burton, Jeanie	1256, 1257
Burton, Lyle	1031, 1033
	1034, 1039
Burton, Regina	895
Burton, Richard	982, 1395
Busch, Kenneth L.	311, 749
	957, 958, 959
	1117, 1219
Busch, Kenneth L.	1220
Buschman, Frank L.	1350
Busman, Mark	354, 1133
Butcher, D.J.	730
Butcher, Geoffrey W.	625
Butler, John M.	415, 1200
Butt, Amna	623
Buttrill, S. E. "Bud"	494
Buzy, Armelle	231, 1348
Byrd, Gary	686
Byun, Jaeman	246
Caesar, John	567
Cai, Hong	1380
Cai, Jian	1138
Calaycay, Jimmy	612
Caldwell, William	686
Callahan, John H.	140, 141
	327, 360, 387, 984, 1412
Callejas, Sheryl	1451
Calvey, Elizabeth M.	546
Cameron, Lynn	1041, 1499
Campbell, Clay	895, 1257
Campbell, Dale	719
Campbell, James A.	751, 752
	753
Campbell, Jennifer M.	40, 82
Camphausen, Raymond T.	11
Canas, Benito	615
Cancilla, Mark	402, 773
Canetta, Federico	119
Cantone, Joseph	536
Cantor, Charles	416
Cao, Ping	242, 1279, 1280
Cappiello, Achille	553
Caprioli, Richard	195, 762
	975
Carazzato, Daniel	130, 1464
Carbonell, Ruben G.	134
Cardinall, Cathy	745
Cardoso, Ana M.	1212
Careri, Mariella	553
Cargill, Anne	649
Carlesso, Valérie	865
Carlin, Jo	1432
Carnine, Mechelle	335
Carr, Steven A.	584, 1031
	1362
Carrier, Mark	230, 540
Carroll, James A.	634
Carruthers, Robin	42, 220
	907, 1325
Carson, Mary	355, 701
Carter, Guy T.	557, 576, 1387
Carter, Jeff	1189
Carvalho, Marcia	851
Cassady, Carolyn J.	30, 847
	1023
Cassidy, Ken	687
Castro Perez, Jose Miguel	13
Catana, Florentina	258
Catlin , Don	1455
Caughran, Tashia V.	1163
Cavalcoli, James	1151
Cavaleiro, Ana M. V.	447
Cavey, Gregory S.	1294
Cayen, Mitchell	307, 308
	705
Cazenave, Jean-Pierre	1324
Ceglarek, Uta	339
Cepa, Steven	283
Cerda, Blas A.	101, 404, 783
Cerniglia, Carl	1266
Cerny, Ronald L.	597
Chace, Donald	288
Chai, Wengang	398
Chait, Brian T.	9, 767, 938
	963, 964, 965, 966, 968
	969, 970, 971, 1290
Chakel, John	538, 1095
Chakrabartty, Avijit	976
Chamakura, V. V.	273
Chamberlain, Scott H.	1350
Chan, Kelvin	536, 902
Chan, Kenneth K.	1421
Chan, T.W. Dominic	893
Chance, Mark	972, 973
Chang, Christina	677
Chang, David	1427, 1429
Chang, Lan-Yang	421
Chang, Yoon-Seok	659
Chanoine, Francoise	1434
Charbonnier, Florence	362
	426
Charles, M. Judith	1162
Charlier, Corinne	1127
Charron, Nicole	555
Chaudhary, Ajai K.	254, 255
	1449
Chaudhary, Tanuja	196
Chauret, Nathalie	699, 700
Cheetham, Janet	960
Chelf, Holly	981
Chen, Yen-Hung	1232
Chen, Anthony B.	1066
Chen, C. H. Winston	1101

Author	Page
Chen, Cindy	568, 876
Chen, G.	780
Chen, Huiping	839
Chen, Jinchang	15
Chen, Lixin	764, 930
Chen, Ounan	862
Chen, Pei	1102, 1435
Chen, Qing	20
Chen, Quan	839
Chen, Winston	421
Chen, Xiaohui	213
Chen, Yajuan	531, 677
	1282
Chen, Yet-Ran	1278
Chen, Yonghong	213
Chen, Yu-Luan	82, 1209
Cheng, Changfu	650, 651
	772, 906
Cheng, Michael	811
Cheng, Xueheng	85
	1050, 1395
Cheng, Y.	508
Chernuchevich, Igor	43, 237
	713, 882, 978
Chervet, Jean-Pierre	526
	527, 542
Chess, Edward	570
Chi, Cecilia	1422
Chiabrando, Chiara	653
Chiang, Long Y.	160
Chiarelli, M. Paul	261, 808
Chin, Edward	173
Choi, Bernard K.	1229
Chong, Albert	337
Chong, Bathsheba E.	187
	188
Chorney, Michael	229
Chou, Chau-Wen	933
Choudhary, Gargi	538, 1095
Chow, Art	174, 175
Chow, David T.	178, 960
Chowdhury, Swapan	705
Christian, Noah P.	126, 419
	1140
Christian, Robert E.	947, 949
	950
Christopher, Steven	328
Chun, Donald	707
Chun-Wai, Tsang	1379
Churchwell, Mona I.	259
	1454
Chusuei, Charles	1225
Cicci, Dino	307, 1456
Ciraolo, Justine	792
Claeys, Magda	78, 193, 1228
Clark, Richard A. C.	393
Clark, Susan	1389
Clauser, Karl	532
Clayton, Peter	301
Clement, Robert	308
Clemmer, David	31, 807
Clifton, Carol	818
Coca, Simion	1051
Cochran, Raymond	913, 918
Cockrill, Steve	1107, 682
Coddington, Arthur	1333
Cody, C.	671
Cody, Robert	535, 1245
Coe, Roger	109
Cohen, Lucinda	575
Cohen, Steven L.	963
Colby, Steven M.	903
Cole, Mark	12, 482
Cole, Richard B.	131, 293
	427, 663, 1061, 1094
Colizza, K.	582
Collette, Caroline	1218
Collings, Bruce	40, 82, 99
	1209
Collins, David C.	530
Colombani, Mauro	1482
Colorado, Armando	340
Compton, Robert	108
Comstock, Kate	1332
Conboy, Jim	571, 1254
	1423
Connoirs, Lawreen	159
Constantopoulos, Terri L.	135
	136
Cook, Kelsey	337, 425, 1465
Cook, Lana	942
Cooke, Leonard W.	997
Cooks, R. G.	485, 581, 754
	780, 840, 1176, 1215, 1253
Cools, Paul	1193
Cooper, William	372
Cornell, Richard J.	11
Cornett, Leticia	171, 1058
Cornish, Timothy J.	1261
Cortez, Enriqueta	763
Cortez, Marnie	1167
Costello, Andria	1202
Costello, Catherine E.	159
	236, 392, 1363
Cotter, Robert J.	36, 229
	384, 395, 418, 420
	1261, 1262
Coutu, Michel	1258, 1456
Covey, Thomas	882
Covey, Tom	713, 1247
Covington, Phil	336
Cox, Kathleen A	1426, 1453
Craig, A. G.	1331
Craig, Anthony	580
Craig, Miller	686
Craig, Theodore A.	381
Cramer, Rainer	796, 799
Craven, Kimberly	620
Craze, Andy	452, 520
Creaser, Colin	353, 474
	850, 1246
Creasy, William R.	351
Crellin, Kevin	840, 869
Crenshaw, Michael	744
Crews, Theodore	1429
Critchley, Glenn	220, 1189
	1365
Croley, Timothy R.	488, 1183
Cross, Fred	970
Crowley, Jan R.	1419
Crozier, Patrick	369, 729
Crumley, F. Gene	1163
Cruz, L. J.	1331
Cruze, Charlie A.	314
Cui, Donghui	19, 691, 692
	715, 815
Cui, Yi	347
Cummings, Paul	1405
Cunniff, Jack	12
Cunniff, John	486
Cunningham, Thomas	916
Curcuruto, Ornella	1312
Curtis, Jonathan M.	644
Curtis, Michael	1450
Cusatis, Patrice	813
Cymes, Gisela D.	992
Czerviec, Eva	214
D'Accorso, Norma	1376
D'Agostino, Paul A.	343
D'Antono, Joseph	813
D'Arienzo, Celia	562, 583
Dagan, Shai	728, 908, 1198
	1470
Dahl, Alan R.	5
Dahlin, David	1450
Dai, Yuqin	635
Dain, David R.	590
Daishima, Shigeki	153, 344
Dalcanale, Enrico	846
Dale, Mike	1064
Daley, Donald	1043
Dalsgaard, Lone	522
Dalton, Howard	231, 232
Daly, Edward	685, 707, 708
Dance, Ian	863
Danell, Ryan M.	495
Dang, Richard	341
Dang, Yuhong	316
Daniel, Saucy	1186
Danis, Paul	1190
Darby, Shauna M.	192
Darensbourg, Marcetta Y.	151
Darsey, Jerry	113
Dass, Chhabil	1297, 1306
	1308, 1311
Davenport, Michael	1264
	1265
David, Hercules M.	1229
Davidsson, Pia	1108, 1301
Davis, J. A.	1443
Davis, M. Duff	997
Davis, Margaret R.	19, 683
	715, 815
Davis, Michael T.	284
Davis, Roderick	980, 1046
Davis, Simon J.	1367
Davis, Stephen C.	1118
	1123, 1169
Davis, Tom	1088
Davis, William	368, 1168
Davoli, Enrico	119, 359
Daw, Tracy L.	1461
Day, Stephen	430
De Hoffmann, Edmond	401
De Jond, Ad P.	1356, 1276
De Pauw, Edwin	639, 1218
Dearden, David	51, 844, 845
DeBellis, A.	1008
Dechert, Gary	814
Decker, Brian K.	24
Deforce, Dieter	271
DeGnore, Jon P.	208, 577
	1182
Deinzer, Max L.	228, 345
	1236, 1245
Dejarme, Lindy	376
dela Cruz, R. G.	1331
Delacotte, Jean-Michel	362
Delaney, Jeannine	1383
Delclos, K.B.	1454
Demers, Roger	1437, 1445
Demo, S.	1296
Dempster, Melissa S.	1501
Denault, J. W.	780
Deng, Haiteng	407, 621
	1420
Deng, Yuzhong	601
Denisov, Edward	446, 718
Deprun, Claude	917
DePuy, Charles H.	26
Derrick, Peter J	200, 386
	919, 1064, 1075
	1226, 1364
Desai, Ronak	347
Desaire, Heather R.	473
Desiderio, Dominic M.	172
	962, 1328
Deterding, Leesa	274
Detlefson, David	240
Devasahazam, Mercz	393
Devi, D. Renuka	252
Dharmasiri, Kuruppu	599
	1342
Di Stefano, Emma	1455
Di Virgilio, S.	1372
Dickson, Les	732
DiDonato, Gerald	579
Diehnelt, Chris	1223
Dikler, Sergei	765
Dillon, Stephanie	870
Dilworth, F. Jeffery	697, 698
Dimitrov, Stefan	974
Dimmock, Nigel	232
Dinca, Adriana	1088
Ding, Jianmei	809
Ding, Weixing	1471
DiPerna, James	288
DiPietro, Emily	1128
Dirr, Mary Kay	314
Dobson, Chris	385
Dodonov, Alexander	1232
Dodsworth, David W.	239
Doe, Hidekazu	1491
Doerge, Daniel R.	259, 543
	1454
Doig, Andrew J.	624
Doktycz, Mitchel	1017, 1202
Doles, Chris	1041, 1499
Domingues, Pedro	447
Domon, Bruno	392, 401
Donahue, Robert	184
Donald, L. J.	379
Donnelly, Erin	307
Donoghue, Edward S.	904
Doorn, Steve	56
Doroshenko, Vladimir M.	36
Dorschel, Craig	111
Dotan, Itzhak	23
Dougherty, Ralph C.	870
Douglas, D. J.	995, 996

INDEX OF AUTHORS

Author	Page
Douglas, Don	40, 81, 82, 99, 333, 1209
Dovichi, Norman J.	291, 1266
Downard, Kevin	182, 973, 1341
Drader, Jared J.	499, 505, 886, 910
Drahos, Laszlo	782
Dreifuss, Peter	1475
Dreisewerd, Klaus	922, 956
Dresch, Thomas	1234
Drexler, Dieter	12, 714, 740, 741
Drinkwater, Donald	813, 1474
Droganis, Paul	1437
Drogaris, Paul	1445
Du, Zhaohui	333
Duan, Yixiang	59, 323
Dubois, Frederic	917
Duchateau, Guus	1080
Duchek, John	285
Duchoslav, Eva	684, 1039, 1124
Duckworth, Douglas C.	55, 1196
Duckworth, H.W.	379
Dudding, Travis	658
Duffin, Kevin L.	634
Dufresne, Craig P	992
Duggan, Jeff	548, 723
Dukan, Sam	155
Dunbar, Robert C.	50, 854, 855, 856
Duncan, Mark	1111
Duncan, Wayne	1040
Dunn, John A.	305
Dunn-Meynell, K.	684
Dupont, Dave	1337
Dupuy, Jean-Louis	1124
Durand, Thierry	653
Duretz, Benedicte	1272
Durrant, Edward E.	929
Dutkiewicz, Lukasz	938
Duursma, Marc C.	45
Dwek, Raymond A.	393
Dworschak, Ragnar G.	174, 932
Dworzanski, Jacek	342
Dyer, Ed	116
Dykert, J.	1331
Eades, Donald	1197
Eagle, Gretchen	1197
Eanes, Ritchie C.	875
Easterling, Michael L.	46, 164, 1192
Eberlin, Marcos N.	750, 851, 852, 853
Eckart, Klaus	1360
Eckerskorn, Christoph	924
Eckhardt, S. Gail	303
Edmondson, Ricky	1107
Edom, Richard	117
Efer, Jürgen	339
Egan, Ed	710
Egsgaard, Heige	377, 858
Eguizabal, Hugo	335
Eiden, Gregory C.	61
Eigendorf, Guenter	348
Einhorn, Jacques	867
Ekern, Scott P.	94
Ekman, Rolf	768, 1108, 1291, 1301
El Kourhy, Maroun	1207
Elfarra, Adnan A.	254
Elicone, Christopher	378, 684
Ellington, Andrew J.	419, 1140
Ellis, Joan	712
Elthon, Thomas E.	597
Emmett, Mark R.	44, 1152, 1349, 1352, 1393, 1388
Endo, Ginji	153
Eng, Jimmy K.	121, 617
Eng, Marian	961
Engel, Marc	735, 736
Engel, Tina	647
Engen, John R.	382
Engewald, Werner	339
English, Robert	1221, 1222, 1259
Enke, Christie G.	135, 136, 1263, 1264, 1265
Ens, Werner	37, 174, 175, 379, 794, 932, 937, 1269, 1329
Erickson, Bruce	983
Ericsson, Lowell	1336
Erve, John	315
Esaw, Barbara	688
Eshraghi, Jamshid	1217
Esmans, E.L.	803
Evans, C.	1215
Evans, Mike	1498
Ewing, Nigel	847
Ewing, Robert	1237
Exner, T.	1091
Eyler, John R.	44, 52, 57, 87, 97, 630, 874, 1044, 1142
Eyles, Stephen	380
Ezzell, John	665
Fabris, Dan	3, 1098
Fabris, Daniele	204, 785
Fagerquist, Clifton K.	1118
Fairley, David	868
Fales, Henry M.	1227, 1240
Falick, Arnold M.	168, 169, 637
Falk, Brandon	800
Famiglini, Giorgio	553
Fan, Peter W.	1143
Fan, Xinghua	755, 1164
Fancher, Charles A.	1261
Fanelli, Roberto	359, 653
Farley, John	742
Farmer, Peter B.	1313
Fascio, Mirtha	1376
Faubert, Denis	897, 898, 1498
Faul, Kent C.	1467
Faull, Kym F.	1353, 1254
Favre, Amélie	479
Faye, Thierry	481
Fedora, Jim, W.	1078, 1081

INDEX OF AUTHORS

Author	Page
Felix, Carolyn A.	1132, 1141
Felix, Tonya	1466
Felix, Vitor	1410
Feller, Bruce	914
Fellin, Phil	364
Felmy, Andrew R.	752
Feng, Bingbing	49, 432
Feng, Jinhua	1013
Feng, Wan Yong	227, 469
Fenn, John	146, 424, 708
Fenn, P. Thomas	1448
Fenselau, Catherine	3, 204, 205, 665, 785, 800, 1098, 1287
Fenyö, David	767, 964, 965
Ferguson, William	710
Fernandez, Carmen	712, 1144
Ferrer-Coreia, A. J.	447, 1212, 1410
Ferrige, Anthony	114, 115
Ferro, Myriam	623, 624
Fesik, Stephen	982
Fetterly, Gerald	722
Fey, Stephen J.	586
Ficarro, Scott B.	450, 904
Fiedler, Jessica	656
Fieno, A.M.	158
Fievre, Anne	372
Figeys, Daniel	436, 613
Figueroa, Iddys D.	608, 927
Filby, Royston H.	1411
Finch, Jeffrey W.	41, 752, 1252
Fink, Saul, W.	17
Finke, Bernd	1381, 1382
Fiorentino, M.A.	511
Firestine, Jennifer A.	1346
Fischer, H. David	1294
Fischer, Steven M.	544, 549, 554, 566, 1401
Fisher, Keith	863, 1088
Fisher, Neyoka D.	825
Fishman, Vyacheslav	822
Fitzgerald, Michael C.	993
Fitzgerald, Robert	1122
Fitzgerald, W. Pat	1081
Fitzgibbons, Shawn	1210
Fitzpatrick, D.	1391
Fjeldsted, John	487, 1255
Flammang, Robert	443
Flanagan, Michael	554
Flarakos, Jimmy	685, 707, 708
Flarakos, Themis	685, 707, 708
Fligge, Thilo A.	1327
Flora, Jason W.	234
Flores, Adeliza	820
Floreto, Erick	1396
Floyd, Philip	10
Floyd, Terrance L.	357
Fluharty, Arvan	1354
Fluharty, Claire	1354
Flurer, Rick	547
Flynn, Shannon	188
Fogliatti, Chris	1162
Folk, Brian	895, 1257, 1256
Follansbee, James	1173
Foltz, Rodger	1197
Fong, Godwin W.	249
Fong, Wai Yin, Karen	893
Ford, Charles	300
Forest, Eric	974
Foret, Frantisek	676, 757, 1028
Forssmann, Wolf-Georg	1322
Foster, Simon	638
Fouda, H.G.	709, 1443
Fouda, Hassan	695
Fournier, Françoise	467, 864, 865, 866
Fournier, Isabelle	920, 921
Fowler, Beth	1336
Fowler, Elizabeth	236
Fox, Alvin	264, 361
Fox, Karen	264, 361
Fraley, D. F.	840
Frank, Aaron	460, 461
Frank, Matthias	1241
Frankevich, Vladimir	519
Frazey, Paul	1162
Freckleton, Gordon	881
Freeman, Colin	868
Freeman, James P.	903
Freiser, Ben S.	838, 839
Freitas, Michael A.	32, 53, 499, 870
Frey, Rüdiger	1022
Fridgen, Travis D.	877, 878
Fridriksson, Einar K.	587, 645
Friedman, Robert Mark	763
Fries, D.P.	1391
Frisch, Kristan	771
Frizzell, Scott	741
Fruehan, Peter	338
Fu, Alzhong	300
Fu, Dong-Jing	416
Fu, Emil	289, 1340
Fu, Peter P.	259
Fuché, Christine	481
Fuerstenau, Stephen	916
Fuhrer, Katrin	1232
Fujii, Toshihiro	1216, 1231
Fujimaki, S.	535
Fujita, Tsuyoshi	1006
Fujiwara, Hideji	704
Fujiwara, Makoto	501
Fukuda, Elaine	814
Fukuda, Hiroyuki	1368
Fukuo, Tsuyoshi	1491, 1492
Fukuzawa, Motoko	1495
Fukuzumi, Shunichi	1492
Full, Gerhard	177
Fung, Eliza	680
Furey, John	1168
Furie, Barbara	214
Furie, Bruce	214
Furton, Kenneth G.	1196
Futrell, Jean	73, 74, 75, 76, 446, 857, 901
Gömez, Stephen M.	1353
Gabryelski, Wojciech	96
Gage, Douglas A.	226, 595

Author	Page
Gale, Brenda	1332
Gale, P. Jane	562, 583, 689
Galicia, Tomas	338
Games, Dai	452, 520, 1057
Gangl, Eric T.	690, 809
Gantt, Stephanie	179
Gao, Jun	944
Gao, Lan	85, 1050, 1395
Gao, Quanyin	646
Gao, Vince	571, 1423
Gapeev, Alexei	854
Garcia, David B.	322
Gard, Jim	1496
Garden, Rebecca	10, 591
Gardner, Ben	1264, 1265
Gareyev, Roustam	828
Garner, Carl	1442
Garner, Robert	106
Garr, Cheryl	1041
Gary, Dull	686
Gaskell, Simon J.	106, 622
	623, 624, 625, 633, 1493
Gaspar, Peter P.	906
Gates, Paul J	1364, 1490
	1489
Gatlin, Christine L.	617, 1384
Gauss, Christine	1001
Gautel, Mathias	241
Gaver, Robert C.	689
Ge, Zhaozhu	926, 1170
Gehrig, Peter	1334
Geiger, Robert J.	311
	1117, 1219
Gelpi, Emilio	1344
George, Elizabeth	567
Gerbaux, Pascal	443
Gerber, Nicholas	690
Geromanos, Scott	881, 882
Gesteland, Raymond	413
Getek, Timothy	710, 1430
Geysen, Mario	1029, 1139
Gharahdaghi, Farzin	1336
Ghobarah, Hesham	1455
Giannakopulos, A.	1064
Gianotto, Anita K.	346
	734, 1065
Gibeau, Terri E.	1079, 1501
Giblin, Daryl	610, 860, 873
Gibson, Bradford	399
Gidden, Jennifer	1057
Gier, Lynn	568
Gierasch, Lila	380
Gieray, Rainer A.	1205
Giese, Klaus	1350
Giese, Roger W.	245, 417
Gieske, Hank	1485
Giger, Walter	373
Gilbert, Anthony J.	42, 1325
Gilbert, Jeffrey	21
Gilbert, Tony	907
Giles, G. E.	132
Gill, Lynn A.	485, 1176
Gillespie, Todd	706, 1442
Gillig, Kent J.	48, 513, 801
Gingras, Anne-Claude	759
Giometti, Carol S.	673
Giordani, Anne B.	997
Giordano, Giuseppe	298
	1116
Giorgi, Gianluca	789
Giorgi, Raffaello	1482
Glassman, Jack	742
Gleeson, Juliann	591
Gleitsmann, Eckhard	928
Glish, Gary L.	471, 472, 899
	981, 983, 495, 1175
Glückmann, Matthias	790
	928
Gmeiner, William H.	382
Gobom, Johan	760, 1291
Godswon, Magdalena	389
Godwin, Sue, M.	1169
Goedken, T.	1331
Goeringer, Douglas E.	124
	470, 730, 1208
Goetzinger, Wolfgang	1035
Goldman, Stanley	352
Goldschmidt, Robert	1055
Goldsmith, Sharon	973
Goldstein, David	556
Golovlev, Valeri	421
Gonin, Marc	1232, 1238
Gonnet, Florence	478, 479
Gonyea, George	1217
Gonzales, Steve	1399
Gonzalez, Anne	974
Gooden, Jonathan K.	280
	1072
Goodfellow, Brian	1410
Goodlett, David R.	618, 759
Goodley, Paul C.	487
Goodman, Wayne	1225
Goodner, Kevin	1484
Goolsby, Brian	88
Gordon, Eric	1424
Gordon, W. Perry	1441
Gorman, Christopher	1003
Gorshkov, Michael V.	49
	477, 804, 1394
Gorski, Waldemar	310
Goshe, Michael B.	614
Goto, Yuji	627
Gougnard, Thierry	1127
Gourley, R. Chris	370
Gozzo, Fabio Cesar	851, 853
Grabowski, Joseph	25, 821
	822
Graf, Thomas	905
Graham, Elizabeth	1444
Grange, Andrew H.	349
	350, 742
Grant, Gary	743
Grant, R.A.	158
Grapperhaus, Craig A.	151
Graul, Susan T.	409
Gray, L. J.	132
Grayson, Michael	1120
Green, John	1494
Green, John B.	812
Green, Kirk	604
Green, Martin	907, 1062
Green-Church, Kari B.	247
	1309
Greig, M. J.	248
Greig, Michael	250

INDEX OF AUTHORS

Author	Page
Greis, Kenneth D.	202
Gren, Christian	377
Gresham, Garold L.	346, 734
	1065
Griffey, Richard	248, 250
Griffin, Patrick	612, 1042
Griffin, Timothy J.	1018
Griffith, K.S.	442
Griffiths, William	211, 221
	779, 987, 1134
Grigsby, Ronald D.	812
Grill, V.	1215, 1253
Grimm, Casey	1473
Gritsas, Ari	707
Groenewold, Gary S.	346
	734, 1065, 1167
Groh, Susan	862
Gronert, Scott	26, 227, 469
	820, 1179
Gross, Julia	276
Gross, Michael L.	152, 260
	263, 280, 512, 552, 588
	603, 610, 650, 651, 758
	772, 786560, 873, 906
	1071, 1072, 1120
Grosse, Christine	306
Grosser, Marco	1322
Grossert, J. Stuart	1067
Gruela, Grace	1425
Gu, Chungang	41, 72
Guenther, Richard	275
Guevremont, Roger	58, 430
	468
Guida, Anthony	199
Guilbaud, Rudolf	308, 317
	1456
Guile, Geoffrey G.	1366
Guittard, Joelle	1363
Gulati, Sunita	1374
Gulcicek, Erol E.	39, 891
	1161
Gull, Steve	114
Gunasekera, Angelo	982
Gundersen, Cameron B.	1353
Guo, Baochuan	278, 1074
Gusev, Arkady I.	347, 819
	1153, 1229
Gustafson, Kirk	598
Gustafsson, Jan Åke	1134
Gustafsson, Magnus	987
Gut, Ivo Glynne	281, 411
	1104, 1105
Guttman, Charles M.	1059
	1060, 1076
Gygi, Steven P.	436, 618
	759
Haag, Anthyony M.	1094
Haak, Gerard	225
Häbel, Sophie	1295
Haber, S.	1329
Hack, Christopher A.	352
	806
Hackett, Murray	431, 662
	1336
Haddix, Martin	337
Haddleton, David M.	1075
Haddon, William F.	177, 374
Hadfield, Ted L.	670
Haegele, Klaus D.	1227
Haeil, Park	686
Haemers, Achiel	78
Haff, Lawrnece	414
Hager, James	490
Hahner, Stephanie	277
	1005, 1103
Haiech, Jacques	386
Haigh, Bart	550
Hail, Mark E.	240, 579, 1355
Hakomori, Sen-itiroh	402
Halada, Petr	199-A
Hall, Brad J.	475, 1466
Hall, Laura	414
Hall, Lisa	649
Halls, Timothy	1440
Halm, Kathy	895, 1256
Halmingh, Otto	225
Ham, Amy-J. L.	243
Hama, Koutaro	104
Hamada, Daizo	627
Hamdan, Mahmoud	1312
Hamilton, Brenda	1444
Hamler, Rick L.	489
Hammond, Richard	570
Hampe, Bjoern	214
Hamzavi, Mohammad	302
Hanash, Samir M	677
Hancock, Bill	538
Hancock, Bruce	916
Hancock, James R.	343
Hancock, William	1095
Handa, Kazuko	402
Handa, Shizuo	664
Haney, Carol	156, 201, 275
	1003, 1045
Hanisch, Franz-Georg	1295
Hankin, Joseph	655
Hanley, Luke	70, 71, 1009
Hannen, Richard M.	652
Hanninen, Osmo	726
Hannis, James C.	265, 269
Hansel, Armin	449
Hansen, Eugene B.	543
	1266
Hanson, Stacy R.A.	605
Hanssen, Brenda	16
Hanton, Scott	1055, 1185
Hapiot, Philippe	426
Harada, Atsuhiro	72
Harden, Charles	1237
Harden, Leslie A.	177, 374
Hardy, Mark R.	11
Hare, Michael	410, 827
Harland, Gary B.	1493
Haroldsen, Peter	1431
Harper, C.J.	505, 509
Harrata, Kamel	985, 1150
Harris, Alan S.	11
Harris, Reed	961
Harris, William A.	95
Harrison, Alex. G.	77, 781
Harrison, Kathleen	660
Harrison, W.W.	324, 325
Harsch, Andreas	256, 257
	270
Hart, Kevin	122

INDEX OF AUTHORS

Author	Page
Hartman, Judy	1412
Harvan, Donald	302
Harvey, David J.	393, 1365
	1366, 1367, 1383
Hassfurther, Renee	695
Hatfield, Galen	1187
Hathaway, Gary	1336
Hathout, Yetrib	3
Hauser, Karin	222
Hauser, Michael C.	953
Hauser-Fang, Annette	1298
Havel, James	564, 573, 574
Haverkamp, Johan	1378
	1377
Hawke, David	168, 637
Hayashi, Yuka	1000
Hayes, John	329
Hayes, Johnny	686
Hayes, Michael J.	1460
Hayes, Roger	1434
Haystead, Timothy	949
Hayward, Mark J.	120, 450
	904
He, Fei	1406, 1408
He, Fenglan	69
He, Lin	880
He, Qin	972
He, Tao	289
Head, Lisa L.	38, 69
Head-Gordon, Martin	235
Headley, John	732
Heath, Timothy	1400
Hecht, Stephen S.	1135
Heck, Albert J. R.	383, 386
Hecquet, Emilie	1413
Hedrick, Jerry	397
Hee, Brian	702, 717
Heeren, Ron M.A.	45, 84
	1012
Heerma, Wigger	1377
Heidbrink, Jenny L.	836
Heikkonen, Jukka	112
Heimark, Larry	991
Heine, Curt	1496
Heine, Gabriele	1322
Heinecke, Jay	246
Heinz, Willi	450
Heinze, Tom	194
Heithmar, Edward	747
Held, Andrea	331
Heller, David	355, 701, 1389
Hellerstein, Marc K.	1118
Helmut, Rosenbauer	434
Hemling, Mark E.	584, 1031
Henderson, Jeffrey	246
Hendricker, Alan D.	669
	1201
Hendrickson, C. L.	32, 44
	497, 499, 886, 910, 1087
	1152, 1330, 1349, 1352
	1387, 1393
Hendry, Robert J.	1165
Henion, Jack D.	439, 563
	719, 1274, 1432, 1436
	1438, 1439
Hensel, Russell	792
Henzel, William	955
Hepp, Darlene	338
Her, Guor-Rong	1278
Herberts, Carla A.	1356
Hercules, David M.	347, 678
	819, 1153, 678
Herlert, Alexander	68
Herold, David	1122
Heroux, Karen S.	667, 1203
Herring , Christopher J.	207
	208, 209, 577
Hess , Beat	1462
Hess, Henry	448
Hess, K.R.	326
Hesso, Antti E.	1317
Hester, Marc	1485
Hettich, Robert	108, 422, 518
Higgs, Richard	816
Hildebrandt, John	942
Hill, Brian T.	784, 832
Hill, Herbert H.	147, 148, 429
	652, 887, 1411
Hill, James	914
Hillenkamp, Franz	7, 157
	276, 390, 796, 797
	922, 1004, 1106
Hindsgaul, Ole	1148
Hines, Wade	35, 115, 626
Hinz, Klaus-Peter	375
Hinz, Linda K.	619
Hirabayashi, Atsumu	892
Hirabayashi, Yukiko	565, 892
Hirayama, Kazuo	190
Hiroshi, Nonami	1016
Hiroyuki, Ito	434
Hjelmquist, Lars	221
Ho, Sa V.	746
Ho, Stacy Z.	1165
Ho, Yen-Peng	800
Ho, Yeunghaw	831
Hoaglund, Cherokee	807
Hoberg, Anne-Mette	1075
Hochalter, J. Bradley	1135
Hoeger, C.	1331
Hoes, I.	803
Hoff , Michael	362
Hoff, Edward R.	1066
Hoffman, Tim	1039
Hoffmaster, K.A.	709
Hoffmaster, Keith	695
Hofstadler, Steven A.	477
Hohl, Markus	1238
Höhndorf, Jens	1021
Hoke, II, Steven	647, 1485
Holcomb, Manuel	1119
Holder, C. Lee	1454
Holder, Claude	154, 194
Holderson, Thor	364
Holland, John	1264, 1265
Holland, Ricky	113, 154, 194
Holle, Armin	1021, 1022
Holman, R. W.	860, 873
Holmes, John	79
Holmes, William E.	541
Holowka, David	587, 645
Hoogenboom, L.A.P.	718
Hoops, Alexandra	347
Hop, Cornelis E.C.A.	15, 20
	943, 1145, 1432

INDEX OF AUTHORS

Author	Page
Hopfgartner, Gerard	713
	719, 1462, 1463
Hoppilliard, Yannik	1230
	1413
Horan, M.R.	709
Horn, David	118
Horne, Debbie	705
Horneffer, Verena	796, 923
Horner, Julie	438
Horning, Stevan R.	1114
Hornshaw, Martin	168
Horton, Zoe	774
Houk, R. Sam	57, 62
Houston, Christopher T.	1092
	1321
Howard, Eduardo	1326
Howe, Amy C.	1044
Hoyes, John B.	42, 218
	1043, 12481325
Hronowski, Xiaoping L.	1363
Hsi, Kuo-Liang	1337
Hsieh, Frank	1026, 1027
Hsu, Chang Samuel	814
Hsu, Fong-Fu	1419
Hsu, R.	687
Hu , Ju	784
Hu, Peifeng	570
Huang, Baoming M.	756
Huang, Chaoran	603, 1479
Huang, Jen-Pang	160, 1293
Huang, Kimberley	970
Huang, Lan	532, 989, 1335
Huang, Nelson	186, 998
Huang, Peiqing	531, 677
	1282
Huang, Yulin	245
Huang, Zhi-Heng	226, 595
	951
Hubbard, Simon J.	623
Hubler, T.	751
Huddleston, Michael J.	628
	1362
Huffer, Duane M.	261
Hughes, Christopher J	888
Hughes, Jonathan D.	1118
	1123,
	1169
Hui, Joseph P.M.	539, 561
Huisman, Miranda	1378
Hulse, James	109, 1459
Hung, k	278
Hunt, Donald F.	296, 297
	761, 947, 948, 949, 950
Hunt, Jerry	673
Hunter, Ann P.	1366
Hunter, Joanna M.	415, 1200
Hunter, Kevin	33, 911
Hunter, Rick	931, 1147, 1392
Hunziker, Peter	1334
Hurlbut, Jeffrey A.	1399, 1467
Hurst, Gregory	730, 1017
	1202
Hurst, Harrell E.	1138
Hurst, Julia	340
Hurt, Ed	217
Huskey, Su-Er W.	15
Husser, Christophe	1463
Husson, Henri-Philippe	864
Hutchings, Lian	1062
Huysmans, Lennie	193, 1228
Iden, Charles R.	244, 252
	273
Ijames, Carl F.	584, 1031
Ikezawa, Hidenori	578
Ikonomou, Michael	149, 365
	366, 739
Ilisiu, Patricia	548, 1039
Immler, Dorian	4
Ingendoh, Arnd	534, 1127
	1283, 1320, 1397
Ingram, Jani C.	346, 734
	1167
Inoue, Yoshinori	153
Irimura, Tatsurou	1361
Irvine, Joyce	1036
Ishigai, Masaki	622
Ishizuka, Toshihiro	565
Isiah, Warner	1446
Islam, Sharmin	545
Isola, Narayan	421
Issakova, Olga	1030
Itagaki, Yasuhiro	1006
Ito, Shinya	565
Itoh, Shinobu	1492
Jackman, Joany	665
Jackson, George S.	136
	500, 1393
Jackson, Nicholas	232
Jackson, Tony	1057, 1062
	1189, 1281
Jai-nhuknan, Jaran	1023
Jain, Monish	710
Jain, Rishi K.	1048
Jakubowski, George	570
James, John	336
James, Ken D.	419, 1140
James, Kyranos	1149
Jamin, Marc	639
Janek, Katharina	199-A
Janiszewski, J.	582
Janota, K.	557, 576
Janssens, Willy	1248
Janusz, Richard	1069
Jarrell, Joseph A.	491, 909
Jarvik, Jonathan W.	1155
Jarvis, Jackie	454
Jarvis, Stuart	1043
Jasieczek, Christina B.	1051
	1100
Jäverfalk, Emmy M.	1273
	1314
Jaw, S.S.	709
Jay, Sheffer	798
Jayawardene, Dhammika	
	1308
Jayyosi, Z.	687
Jeannot, Michael	681
Jedrzejewski, Paul T.	953
	967
Jeffreys, William	615
Jella, Prashanthi	1484
Jemal, Mohammed	1438
	1439
Jenkins , H Donald B	1226
Jenkins, Steve	729

Author	Page
Jennifer, Brodbelt	88
Jennings, Keith R.	231, 232
	268
Jensen, Charles	706
Jensen, James	1082
Jensen, O.N.	1091
Jensen, Pamela	1150
Jertz, Roland	1397
Jiang, Xiangyu	109, 1459
Jianhua, Wang	76
Jin, Lei	199
Jin, Xiaoying	531, 677, 1282
Jing, Hongwu	728, 1470
Jing, Wei	985
Jinjun, Li	1141
Jockusch, Rebecca A.	90
	91
Joergensen, Thomas J. d.	
	383
Johansson, Jan	987
Johnson, Andrew	301
Johnson, Charis	657
Johnson, Douglas H.	290
Johnson, Francis	244, 273
Johnson, Jason	1442
Johnson, Jodie	299
Johnson, John E.	285
Johnson, Keith A.	46, 629
Johnson, Kenneth L	1275
Johnson, Kim	692, 693, 694
Johnson, R.	754
Johnson, Richard	589
Johnson, Robert	982
Johnson, Robert E.	938
Johnson, Walter	1031
Johnson, Yevette	264
Johnston, Kenneth H.	1094
Johnston, Murray	142, 279
	519, 604, 926, 1170, 1187
Joliffe, Chuck	1247
Joly, Etienne	625
Jones, A. Daniel	558, 1390
Jones, Anne	1452
Jones, Glenville	697, 698
Jones, Mark A.	1079
Jones, Melissa B.	314
Jones, Richard C.	625
Jonkman, Jan H.G.	572
Jonscher, Karen	657
Josephs, Jonathan L.	579
	776
Joshi, Rajesh K.	594
Joubert, Aidalu A.	1411
Joyce, Karina	1452
Joyce, Sebastian	395
Judkins, Christy M.	285
Juhasz, Peter	35
Julien, Dominique	416
Jungblut, Peter	199-A
Juraschek, Reinhard	138, 145
Jurenitsch, J.	2
Justes, Dina	1222, 1225
Justice, Jay	224, 1242
Juujärvi, Jouni	112
Kachman, Maureen T.	679
	999
Kaczmarek, Michele	201
Kaffashan, Azita	1384, 1385
Kage, David	87, 97
Kahl, Steve	363
Kahn, Esther	181
Kainosho, Masatsune	988
Kaivosaari, Sanna	721
Kalghatgi, Krishna	1037
	1298
Kalkum, Markus	1001
Kalt, W.	566
Kaltashov, Igor	380, 785
Kalume, Dario	214
Kam, Chih-Min	957, 958
	959
Kamath, Burde	731
Kambouris, Sara J.	254, 255
Kamel, Amin	777, 1443
Kanai, Michiko	578, 1319
Kapp, Eugene	218, 220
	1325
Kapron, James	719
Karanam, Bindhu V.	15
Karas, Michael	2, 138, 139
	145, 176, 790, 924
	928, 1381, 1382
Karbach, Volker	941
Karger, Barry L.	757, 953
	676, 1028
Karpinski, M.K.	510
Karty, Jonathan A.	1315
	1316
Kasama, Takeshi	664, 1000
Kasama, Takeshi	1495
Kascheres, Concetta	851
Kashiwagi, Tatsuki	190
Kashiwagi, Yutaka	190
Kass, Steven	410, 826, 827
Kassel, Daniel B.	1032
	1034, 1146
Kast, Juergen	274
Kathleen, Caldwell	798
Kato, Shuji	26
Kato, Yoshiaki	492
Katta, Viswanatham	178
	643, 960
Kaur, Surinder	1350
Ke, Jing	1439
Kearney, Gordon C.	1490
	1489
Kebarle, Paul	407, 621, 823
Keever, Jeff	86
Kehoe, Terry	1190, 1299
Kelleher, N. L.	67, 423
Keller, Bernd O.	636
Kellersberger, Katherine	844
Kelley, James	319
Kelly, Jeffery W.	608, 765
Kelly, John	223
Kempen, Esther	843
Kennedy, Matt	452
Kenneth, Parker	1292
Kenney, Kathryn	305
Kenttämaa, Hilkka I.	833, 834
	835, 836, 837, 1024
Keon, Brigitte H.	967
Keough, T.	158, 1476
Kerns, Edward H.	17, 240
	292, 304, 579

INDEX OF AUTHORS

Author	Page
Kerns, Michael S.	825
Kerwin, James	778
Keshishian, Hasmik	1026
	1027
Keski-Hynnilä, Helena	721
Kesners, Peter	534
Ketcha, M.M.	1476
Ketola, Raimo A.	112, 522
	905
Khalil, Deborah	702
Khan, Noor	748
Khaselev, Nona	660
Khemani, Lakshmi	1460
Khosla, Mike	895, 1257
Khramer, Mark	264
Kiff, Tom	1062
Killeen, Anthony A.	679
Kilpatrick, Peter K.	134
Kim, Byung-Hoon	659
Kim, Hee-Yong	654, 1113
Kim, ManGoo	342
Kim, Moo-Young	228
Kim, Ok-Hee	236
Kim, Sung-Ho	1015
Kim, Yang-Suk	1113
Kim, Yongkyoung	1486
King, Angus	766
King, Fred L.	54, 326, 590
King, Gina M.	1342
King, Martin W.	175
King, Richard	150, 712, 1144
Kingsley, Mark	179
Kinsel, Gary	764, 769, 795
	930
Kinser, Robin	788
Kinsey, Kenneth	1139
Kinter, Michael	632
Kinzler, Kenneth W.	418
Kirpekar, Finn	7, 797, 1004
Kirsch, Jay S.	310
Kiselar, Janna	182, 1341
Kishi, Hiroshi	1216
Kissinger, Peter	581
Kissmehl, Roland	222
Kissmeyer, Ann-Marie	698
Kisternaker, Piet G.	84
Kitchen, Robert	11
Kitrinos Jr., N. P.	545
Kiyonami, Reiko	578, 1319
Klassen, John	403, 848
Klatt, Tracey	1042
Kleemann, Gerd	977
Klein, Richard	1425
Kleintop, Brent L.	240, 776
Kleuss, C.	1091
Klippenstein, Stephen J.	854
	457, 855
Kljavin, Ivar	166
Klohr, Steve, E.	17, 1479
Knapp, Daniel R.	1342
Knight, Paula M.	314
Knippel, Brad	328
Knochenmuss, Richard	849
	917, 941
Knotts, Kirk	1400
Knuth, Dean	302
Kobel, Mike	1041
Koch, K.	754
Kocher, Florence	478
Koczanski, Krystna	364
	1240
Koerner, Roman	638
Koester, Hubert	416
Koichi, Tanaka	1011, 1016
Koike, Nobuko	578
Koizumi, Hideaki	892
Kolakowski, Beata	1067
Kolega, Renato	332
Kolli, V.S. Kumar	1372
Komives, Elizabeth A.	169
Komori, Naoka	181
Konenkov, Nikolai	333
Konermann, Lars	82, 995
	996
Kong, Fangming	1387
Kong, Zhengrong	724
König, Stefan	53, 1181
	1386
Konishi, Yasuo	627
Koomen, John	762
Koons, Robert D.	1196
Koppenaal, David W.	61
Korfmacher, Walter A.	684
	1425, 1453
Kornienko, Oleg V.	1009
	1171
Köster, Claus	1021
Koster, Sander	45
Kostiainen, Risto	720, 721
Kotiaho, Tapio	112, 720
Koupai-Abyazani, M.	688
Kovtoun, Slava V.	1262
Kowalski, Paul	171, 1058
	1060
Kozar, Mike	361
Krahmer, Mark	361
Kramer, Karl	778
Kratzer, Robert	924
Krause, Eberhard	199-A
Kräuter, Karl-Otto	277, 1022
Kretschmer, Matthias	236
Krishnamurthy, Thaiya	284
Krogh, Thomas	978
Krone, Jennifer R.	5, 1155
	1288, 1289, 1323
Krückeberg, Stefan	68, 100
Krüger, Klaus-Dieter	1199
Kruger, N. A.	67
Kruppa, Gary	514, 515
Krutchinsky, A. N.	37, 794
	937, 1269
Krywicki, Ruth H.	303
Kucharzak, Ramön	1104
Kuhlmann, Frank	487
Kuhn, Eric W.	236
Kuhn, John G.	303
Kuiper, Tine	1480
Kulkarni, Trupti	1434
Kuma-Mintah, A.	1480
Kumadaki, Itsumaro	72
Kumar, Rajiv	381
Kuroda, Koichi	153
Kurono, Sadamu	1361
Kurtz, Donald M.	631
Kusai, A.	535

Author	Page
Kusel, Dave	483
Kussmann, Martin	222, 389
Küster, Bernhard	393, 592
	766
Kwei, Gloria Y.	20
Kwok, David	1480, 1036
Laas, William A.	1066
Labov, Simon	1241
Lacey, M. P.	158, 1476
Lachatre, Gerard	1124
Lafitte, Daniel	386
Lagerwerf, Fija M.	572
Lahamer, Amer	108
Lai, Jason	1122
Laiko, Victor	532, 939
Laivenieks, Maris	595
Laken, Steven J.	418
Lall, Santosh P.	644
Lam, Zamas	1137
Lamer, Stephanie	199-A
Lammert, Stephen A.	1172
	1174
Lampe, Frederick	879
Lan, Zhang-Hua	417
Land, Adrian	12, 196, 486
	714
Land, Mark	769, 795
Lane, Leslie C.	607
Lane, Steve	520
Lane, William S.	121
Lang, G. H. Lisa	630
Langridge, James I.	42, 218
	259, 622, 1248, 1314
Lanoue, Bernard	354, 1133
Lanza, François	1324
Lao, Cathy	56
Lapierre, Catherine	362
Lapiguera, Amelia P	1453
Laprade, Bruce	435, 913
	918
Laramee, James	345, 1236
	1245
Larsen, Barbara S.	279, 604
	1049
Larsen, Delmar	448
Larsen, Elfinn	858
Larsen, Martin R.	586
Larsen, Peter M.	586
Lato, Susan	419
Latourte, Laurence	1061
Lattimer, Robert P.	1188
Lau, Tai-Chu	468
Lauber, Wendy M.	634
Laude, David A.	248, 886
	503, 504, 505, 506, 507
	508, 509, 510, 511, 910
Laudicina, Donald	705
Laukien, Frank	514, 515, 883
Lauritsen, Frants R.	112, 522
.	905
Lausecker, Berthold	1462
Lavanant, Hélène	1230, 1413
Lavine, Gary	170
Laviolette, Barbara	688
Law, Say-Jong	270
Lawson, Alexander M.	398
Lawson, Stephen	1014
Lay, Jr., Jackson	113, 154
	194
Layloff, Thomas	1120
Lazar, Iulia M.	530, 1159
Lazzaroni, Raffaello	733
Le Beyec, Yvon	917
Le Blanc, Yves J.C.	703
	1254, 1258
Le Jeune, Ludo	1248
le Maire, Marc	585
Le, John C.	643
Le, X. Chris	291
Leadlay, Peter F.	1489, 1490
	1500
Leary, Julie A.	53, 473, 1180
	1181, 1384, 1385, 1386
Lebedev, Albert	726, 727
Leblanc, Yves	1418
Lebrilla, Carlito B.	227, 397
	402, 469, 773, 1406, 1408
Lecchi, Paolo	1158
Lechner, Doris	411, 1105
Lee, Arthur	731
Lee, Cheng	985, 1150, 1159
Lee, Gab-Yong	821
Lee, Heewon	201, 1045
	1177
Lee, Jean	109, 1459
Lee, Ken	1064
Lee, Michael J.	1477
Lee, Mike	240, 292, 579
Lee, Mike, S.	17
Lee, Milton L.	530, 1159
Lee, Terry D.	284, 529
Lee, Vicky W.-M.	468
Lefebvre, Paul	1036
Lehmann, Edda	1357
Lehn, Jean-Marie	163, 411
Lehrach, Hans	1001, 1104
Leisner, Arne	276, 1295
Leize, Elisabeth	162
Leize, Emmanuelle	162, 163
Leppänen, Jyrki	721
Leppert, Mark	413
Leroy, Martin B.	628
Lesage, Denis	864, 865, 866
Letarte, Simon	897, 1119
Leung, Kwan H.	1145
Levin, Stuart	763
Lewer, Paul	21
Lewis, Cris	54
Lewis, J. Kathleen	1096
	1359
Lewis, Monique	731
Leymarie , Nancy	896
Li, Aijun	205, 785
Li, Chun	699, 1033
Li, Feng	707
Li, Guo-Zhong	491
Li, Jia	415, 1200
Li, Jianjun	223, 1285
Li, Liang	96, 635, 636, 681
	1053, 1054, 1148, 1184
Li, Lijuan	1416
Li, Lily	1035, 1036, 1149
Li, Lingjun	10, 591
Li, Linhui	249
Li, Michael X.	1282, 1479

INDEX OF AUTHORS

Author	Page
Li, Ming	1152
Li, Ping	1379
Li, Ruomei	838
Li, Shihua	1297, 1311
Li, Su-Chen	663
Li, Tiansheng	960
Li, Weiqun	1142, 1152
	1349, 1351
Li, Xing-Fang	291, 1266
	1272
Li, Yang	1440
Li, Yong-Xi	1440
Li, Yu-Teh	663, 664
Li, Yunzhi	931, 1147, 1392
Li, Zhaoyang	1421
Liang, Li	1422
Liang, Xiaoli	673
Liang, Yongjiang	845
Liang, Zhenmin	716
	1427, 1428
Lias, Sharon	818
Libot, Francine	864
Licklider, Larry, J.	529
Lidstrom, Mary	1202
Liguori, Angelo	789
Lilley, Kim A.	1267, 1268
Lim, Chang-Kee	398
Lim, Hanjo	70, 71
Lim, Heng-Keang	536
Lim, Kheng B.	662
Limbach, Patrick A.	105, 247
	262, 412, 793, 810, 933
	934, 1019, 1309, 1494
Limero, Tom	336
Lin, C.C.	684
Lin, Chin-chung	1425
	1426, 1453
Lin, Chuan-Yuan	839
	1305, 1394
Lin, Deng	711
Lin, Hua	415, 1200
Lin, Melanie	596
Lin, Patrick	109, 1459
Lin, Shanhua	384, 418
Lin, Song	685, 708
Lin, T.	1296
Lin, Yang-I	186
Lin, Yuehe	438, 523
Linders, James W.	906
Lindh, Ingemar	221
Lindinger, Werner	449
Lindstrom, Terry	16
Ling, Victor	961
Linhares, Mike	695
Linscheid, Michael	267
Linton, Richard W.	763
Lippert, Andreas	1159
Lippmaa, Endel	517
Litchfield, John	550
Little, Daniel P.	8, 416, 420
Little, James L	1472
Little, Randie	556
Litwiler, Kevin	199
Liu, Beishan	620
Liu, Charles	684, 1033
Liu, Chuanliang	524, 1307
Liu, Chun-Sheng	1266
Liu, Hanghui	1028
Liu, Hui	836
Liu, Lida	1447
Liu, Lin	675, 1002
Liu, Sherry	1197
Liu, Wu-Schyong	1362
Liu, Yan-Hui	991
Liu, Yansheng	31
Liukkonen, Robert	1077
Livi, Stefano	1238
Liyanage, Rohana	408
Llewellyn, Jennifer	372
Lloyd, Steven	1473
Loboda, A. V.	37, 379, 794
Lock, Chris M.	116, 560
Locke, Mary	199
Locke, Steven, J.	1284, 1286
Lockwood, Mark A.	445
Loew, Damarys	1324
Logan, Stuart	301
Logan, Timothy M.	1152
	1351
Lombardi, Paola	553
Longhua, Ma	711
Loo, Joseph A.	805
	1151, 1244
Loo, Rachel O.	1336
Lopata, Ronald J.	120
Loper, Alice	568
Lopez, Linda L.	715
Lorens, J.	1296
Lorenz, Sarah	47, 722
Lottspeich, Friedrich	924
Lowden, Philip	1500
Lowes, Stephen	1439
Lowes, Steve	1432
Loyaux, Denis	1348
Lu, Lin	543
Lu, Rui	1303
Lu, Weiping	203
Lu, Wenzhe	105
Lu, Xiaowen	705
Lubman, David M.	187, 188
	489, 531, 675, 677, 679
	999, 1002, 1282, 1300
Lüdemann, Hans	1004
Ludicky, Robert	1194
Luedemann, H-C	1106
Lumetta, G.	751
Lund, Adrian A.	597
Lund, Anders L.	597
Luo, Jinli	398
Luo, Wendy	1398, 1455
Luo, Yu-Ran	885
Luong, Elise	62
Luross, Jennifer	739
Lützenkirchen, Klaus	100
Luu, Nganha	1137
Luukkanen, Leena	721
Lynn, Jr., Bert C.	488, 541
	1183
Lyons, Curtis D.	396
Ma , Cheng-Yu	1471
Ma, Michael Y.-X.	249
Ma, S.	780
MaaijerGielbert, Janine	84
Macchi, Frank	961
MacCoss, Michael	63, 1115

Author	Page
MacDonald, Linda	743
Macdonald, Robie	365
Macfarlane, Ronald	682, 1107, 1380
Macha, Stephen F.	793, 1494
Macher, Bruce A.	594
Madsen, Gry	522
Maeda, Yoko	578
Maggio, Vince L.	1129
Maggio, Vincent	287
Maghuin-Rogiste, Guy	718
Magnuson, Matthew	356
Maier, Claudia S.	228
Maier, Rolf-Dieter	1199
Majidi, Vahid	56, 59, 323
Majumdar, Tapan	1430
Makarov, Alexander A.	1118, 1123, 1169
Makin, Hugh L.J	697, 698
Malcolm, Bruce	991
Malek, Robert	871
Maleknia, Simin	972, 973
Mallard, Gary	123
Mallet, Anthony	191
Malone, Kevin	42
Maltby, David	989, 1335
MaMahon, Terry	454
Mandell, Jeffrey G.	169
Mandrell, Robert E.	177
Mann, Matthias	43, 212, 216, 217, 237, 238, 241, 592, 593, 766, 978, 1091
Mansoori, Bashir A.	737, 1251
Manura, John	900
Marchand, Alan P.	1414
Marcus, R. Kenneth	328, 875, 1079, 1501
Marietta, M.	687
Marini, Joseph T.	48, 801
Mark, J.	128, 1339
Markey, S. P.	658, 1110, 1093, 1304
Marois, Yves	175
Marquet, Pierre	1124
Márquez, Cristina	583
Marshall, Alan G.	32, 44, 53, 93, 94, 332, 372, 496, 497, 498, 499, 500, 870, 910, 1083, 1087, 1142, 1152, 1330, 1349, 1351, 1352, 1387, 1393, 1388
Marsilio, Renzo	298
Martin, Hornshaw	1292
Martin, Adele	400, 1285
Martin, Charles D.	41, 1252
Martin, John	1362
Martin, Louis	1460
Martin, Millie	336
Martin, Pascal	1464
Martin, Stephen A.	35, 521, 626, 775, 894
Martin, Susan	296, 297, 761, 948
Martin, William	1399
Martin, William B.	1467
Marto, Jarrod A.	296, 297, 761, 948
Marvin, Christopher H.	569, 1415
Marzilli, Lisa A.	257, 270, 256
Masiarz, Frank R.	1350
Masoud, Hussein	400, 1285
Masselon, Christophe	1358
Masuda, Sonoko	697
Maswadeh, Waleed	342
Matassa, Luca C.	1437, 1445
Mathews, W. Rodney	1294
Mathur, Victor	171
Mathurin, Jean-Charles	896, 481
Matney, Marilyn	336
Matson, Dean	523
Matsui, Hiroshi	988
Matsumoto, Hiroyuki	181
Matteson, Karal	421
Matthews, Dwight E.	63, 1115
Matthews, K. S.	379
Matthews, Rowena G.	202
Matuszak, Ken	338, 1395
Matveeva, Lidia	1483
Matyjaszczyk, Matthew	430
Matyjaszewski, K.	1051, 1100
Mayer, James M.	445
Mayer, Manfred	534
Mayer, Sabine	1274
Mayol, Robert F.	689
Mayr, Suzanne	1481
Maziarz, E. Peter	1084
Mazurkiewicz, Paul	1236
McAuliffe, John	307
McCandlish, Carl	1109, 1110
McCarley, Robin L.	793
McCarley, Tracy D.	793
McCarry, Brian E.	569, 1415
McCarthy, M. Cornelius	442
McClellan, Joseph E.	1195
McCloskey, James A.	253, 272
McClure, Cheryl	1128, 1129
McComb, Mark E.	174, 175, 1269
McConnell, Tyra	1475
McCorkle, Dennis	1471
McCraw, Joan	1130
McCue, Bette	1450
McCurry, Michael	1167
McDonald, Jane E.	566
McDowall, Mark	13
McElvany, Stephen W.	327, 360, 984
McEwan, Murray	868
McEwen, Charles N.	1049, 1072
McFee, Bill	1441
McGlinchey, Michael J.	1416
McGraw, Dana	1003
McIntyre, Douglas	344, 817

INDEX OF AUTHORS

Author	Page
McIntyre, Evangeline	954
McIver, Robert	931, 1147, 1392
McKay, Richard G.	1049
McKenna, Rosemary	1294
McKenzie, David E.	746
McLafferty, Fred W.	67, 423, 118, 587, 645, 1380
McLane, David	1485
McLaughlin, Kristine	1400
McLaughlin, Theresa	483
McLean, Matthew A.	5, 1155
McLoughlin, Debra	150, 1144
McLuckey, Scott A.	27, 124, 470, 730, 1089, 1178, 1204, 1208
McMahon, Gillian	1095
McMahon, John	1109
McMahon, Terry	444, 464, 787
McNeil, Leslie K.	673
McNulty, Dean	1362
McQuillen, Daniel P.	1374
McWilliams, Ted B.	812
Mechref, Yehia	1369, 1370
Medzihradszky, Katalin	1097
Meheus, Lydie	271
Mehl, John T.	678
Mehl, Sonja	1103
Mei, Houng-Yau	805
Meiring, Hugo D.	1356
Meisner, Dale	555
Melchert, James	570
Melnyk, Michael C.	957, 958, 959, 1117, 1219
Mendes, Maria Anita	750, 851
Mendes, Maria Anita	853
Meng, Frank	1069
Mentzer, Mary	1031
Menzel, Christoph	796, 797, 922
Mercer, Roger S.	558, 1390
Mercurio-Cason, Marita	1450
Merewether, Lee Anne	643
Merkle, Kara	150, 712
Merrill, Al	661
Merriweather, Roosevelt	1172
Mesmer, Mantai	547
Mets, Berend	1448
Meunier, Cécile	639
Meuzelaar, Henk	342
Meyer, Helmut E.	4
Miceli, Jeff	691
Michael, Steven M.	14, 318, 647
Michalewsky, Joseph	548
Michaud-Soret, Isabelle	974
Michisato, Toyoda	434, 1235
Middleditch, Martin J.	1433
Midey, Jr., Anthony	23
Midgett, Carl	1497
Miesbauer, Laura	85, 1050
Mikaya, Anzor	818, 1488
Mlketova, Petra	304, 671, 1201
Milgram, Eric	57
Milgram, Kenneth	287, 1131
Millar, Alan	231, 232
Miller , Kimberly	330
Miller, Bryan	487
Miller, Christine A.	544, 549, 554, 566, 1040, 1401
Miller, Dwight W.	1486
Miller, Mark L.	192, 1198
Miller-Stein, Cynthia	150
Milligan, Daniel	868
Mimura, Tadao	565
Minarik, Marek	953
Minkoff, Marjorie	775
Minkoff, Marjorie	596, 1299
Mireault, Pascal	1125
Mirgorodskaya, E.	215, 760
Mirza, Urooj	991
Mitchell, Alyson E.	558, 1390
Mitchell, Charles	1151
Mitchell, Dale	493
Mitchell, Glenn	792
Mitra, Sunjay	113
Mittchel, Joel	915
Mize, Todd	1056
Mizuno, Kazuhiko	1491
Mo, Wenjun	1368
Mock, Kuldip	335
Moeller, Peter	354, 1133
Moertz, Ejvind	978, 1090
Mohan, V.	250
Mohanty, Dillip	1071
Mohill, Kristofor	324
Mohill, Matthew	325
Moini, Mehdi	242, 1154, 1279, 1280
Moldover, Brian	1151
Molina, Henrik	978
Molinar, Ricardo	317
Molinaro, Nicholas	902
Molloy, Michael	358
Moloney, Mark	1417
Momplaisir, G.-M.	747
Monarca, Silvano	357
Monasterios, Clevys	723
Monforte, Joseph A.	415, 1200
Mong, Gary M.	179, 753
Monnaie, Didier	603
Monnier, Valérie	864
Moody, D., Branch	294
Moore, Roger, E.	529
Moraes, Luis Alberto B.	852
Morales, Martine	1324
Moras, Dino	1326
Morelli, John J.	771
Morgan, Daniel	545
Morgan, Judy	647
Mori, Brian	745, 1480
Morikaswa, Kosuke	190
Morinello, Eric	243
Morio, Ishihara	434, 1235
Moroz, Tatiana	10, 591
Morris, Mike	301, 888
Mortensen, Peter	1090
Morton, Shelby J.	1196
Moseley, Arthur	590-A, 980
Mosi, Andrew	348

Author	Page
Mosner, Jörn	1103
Mousselmal, Moussa	897
	898
Moxon, Richard	400
Moy, Marie	47
Moyer, Mary	980
Muc, M.	687
Mucchino, Claudio	553
Muddiman, David C.	234
	265, 269, 1424
Mueller, Anja	1072
Muenster, Helmut	1114
	1244
Muhlecker, Walter	294
	1374
Muir, Craig	1026, 1027
Muir, Derek	364, 738
Müller, Dieter	189
Müller, Martin	1001
Mullins, Richard E.	1126
Mulvana, Daniel 1	1439
Munson, Burnaby	777
	861, 1318
Murawski, Sandra	647
Murphy, Anthony	1442
Murphy, C.M.	1304
Murphy, Robert C.	655, 656
	657, 660
Murray, Kermit	798
	880, 1014
Mushtaq, Imran	301
Musie, Ghezai	151
Musser, Steven	143
Myatt, C. Paul	919
Myers, David P.	330
Nagai, Shinji	565
Nagai, Yoshitaka	1361
Naghle, Bassam	983
Nair, Hari	633
Nair, Stree	300
Naito, Yasuhide	501
Nakagawa, Miyuki	1495
Nakajima, Masaharu	802
Nakajima, Terumi	1006
Nakamura, Akiko	1495
Nakanishi, Toyofumi	559
Naoki, Hideo	1006
Napoli, Anna	789
Nardo, C.	684
Narinx, E.P.	158
Naturale, Mauro	298
Naven, Tom	615, 616
Nawrocki, Joseph	598, 1347
Naylor, Edwin	288
Naylor, Stephen	290, 381
	1275
Needham, Larry	287, 1128
Needham, S. R.	1458
Needham, Shane	482
Nelson, Chad	413, 1099
Nelson, Claire V.	1486
Nelson, Eric D.	833, 835
Nelson, Lesa	413, 1099
Nelson, Michael	1219, 1220
Nelson, Randall, W.	5,1155
	1288, 1289, 1323
Nemansky, Martin	396
Nemeth, Jennifer	224, 1242
Nemirovskiy, Olga	610, 786
Nero, Vincent	813, 1474
Nettleton, Ewan	1
Neubauer, Gitte	216
Neubauer, Kenneth	1170
Newby, Craig	191
Newby, Robert	1417
Newton, John	1256, 1257
Ng, Kwokei	1426
Ngoh, Maureen	355
Ngoka, Lambert C. M.	588
	758
Ngu, Maria	1309
Nguyen, Viet	879
Nicholas, Mark	763
Nicholson, Ralph	1010
Nicol, Gordon	142
	861, 1318
Nicola, Anthony	819
Nicolaou, Constantinos	1068
	1069
Nicolas, Jean-Pierre	426
Nicolau, Gabriela	317
Nicolidakis, Helen	745
Nicoll, Jeremy	51
Nicoll-Griffith, Deborah	699
	700
Nielen, Michel	1193
Nielsen, Ole John	858
Nier, Volker	1322
Nierengarten, Helene	163
Nieuwenhuis, Tim	1427
Nikolaev, Eugene N.	41, 446
	857
Nikolaev, Victor	1030
Nikolaeva, Marina	446
Nikolic, Dejan	286
	1047, 1143
Niles, Jacquin	251
Nilsson, Carol	768
	1108, 1301
Nizigiyimana, Libérata	78
Nizzi, Katrina	455
Norberg, T.	1331
Nordblom, Gerald D.	1300
Nordhoff, Eckhard	388
	760, 1005
Noreen, Allen	1077
Norrman, Kim	787
Nousiainen, Marjaana	183
Novotny, Milos	600
	1369, 1370
Nuernberg, B.	1091
Nugent, Kerry	230, 540
Nuutinen, Jari	846
Nuwaysir, Lydia	128
	1337, 1339
O'Connell, Kathy	166
	954, 955
O'Connor, Peter	931, 1147
	1392
O'Donnell, Maryanne J	8
O'Hair, Richard A.J.	28
O'Hara, Koji	1495
O'Malley, Ronan	220, 1391
O'Shea, Thomas	320
Obarewicz, Stephan	1206

INDEX OF AUTHORS

Author	Page
Obarewicz, Stephan	1207
Oda, Yoshiya	970, 1141
	1290
Oe, Tomoyuki	254, 255
Ogawa, Yasuko	559
Ogorzalek Loo, Rachel	674
	1151
Oiestad, Ase Marit Leere	453
Oiestad, Elisabeth Leere	441
Olivera, B. M.	1331
Ojala, Marja	112
Okamoto, Masanori	1491
Oktem, Berk	519
Olah, Timothy	150, 712
	1144
Olejnik, Edyta	1106
Olejnik, Jerzy	1106
Oleschuk, Richard D.	174
	175
Olga, Nemirovskiy	1071
Olivares, Jose	56, 59, 323
Olsen, Gary J.	673
Olsen, Mark	1405
Olumee, Zohra	140, 141
	387, 1008
Ong, Agus	912
Ono, Tetsuyoshi	282
Onstot, Jon	358
Ooms, Bert	225
Oosterkamp, Aaike J.	1344
Ordsmith, Nick	1343
Organ , Andy	200
Orians, Kristin	149, 366
Orlando, Ron	197, 198, 295
	394, 440, 1371, 1372
Orth, Robert. G.	746
Ose, Yoichi	492
Ospina, Maria	1213
Ostovic, Drazen	568
Ostrander, C.M.	505, 509
Ottinger, James	320
	1055, 1185
Oxley, Eric	54
Pabst, Michael J.	1328
Padovan, Julio C.	963, 966
Pagano, Giuseppe	119
Pain, Bedabrata	916
Pakdel, Hooshang	898
Palma, Mario	1006
Palmer, Cynthia	1425
	1426, 1444, 684
Palmer, Peter T.	755, 1164
Pan, Hai	602
Pan, Joseph	370
Pang, Jianmei	1145
Pang, Shaokun	1132
Pannell, Lewis	184, 598
	1347
Papac, Damon	173
Papayannopoulos, I.	233
Pappin, Darryl	615, 616
Parce, J. Wallace	433
Park, Melvin	883, 956
Park, Zee-Yong	611
Parke, Gillian	1139
Parker, Kenneth C.	521, 626
Parnis, J. Mark	877, 878
Parr, Victor	1072
Parrish, Marie	575
Pasa Tolic, Ljiijana	49, 266
	477, 523, 804, 1270, 1271
	1307, 1394
Pascke, Michael	444
Past, Jaan	517
Pastor, Salvador J.	1020
	1085
Patel, Hari	1029
Paterson, Patricia E.	1437
Patkin, Adam	1112, 1469
Patrick, James	307, 705
Patterson, Dale	626
Patterson, Donald G.	287
	1128, 1129
Patteson, Kimberly	262
Paul, Gary J. C.	450
	1160, 1207
Paul, Lefebvre	1149
Pautler, David B.	285
Payan, D.G.	1296
Payne, Anne	981
Pearsall, D.	1296
Pearson, Paul G.	18
Pedder, Randall	1249, 1250
Pedrosa, Julio	1410
Pedrys, Roman	938
Peiris, Dil	316, 1071, 1409
Peltier, JohnM.	521, 775
	894
Pemberton, Jeanne	1167
Penman, Andrew D.	1433
Pennanen, Keijo	720
Pentek, Daniel	117
Peraldi, Olivier	1464
Percey, Shaundel	1197
Pereira, Adrian	1451
Pereira, Antonio	1080
Pérez, James	1024
Perkins, Denis	199
Perlat, Marie-Claude	865
Perreault, Helene	174, 175
	1269, 1375
Peru, Kerry	732
Peschke, Michael	464, 823
Peter-Katalinic, Jasna	1295
Peterman, Scott	80
Petersen, Catherine E.	179
	752
Petersen, Mary	1459
Petrosyan, Valery	726
Petzold, Chris J.	1024
Pfenning, Allen	1399
Pfenninger, Anja	1381, 1382
Philip, John	881, 882
Phillips, Duncan A. S.	1493
Phillips, Eric	345
Phillips, Lawrence R.	1461
Phillips, Richard	580, 1037
Piatek, B.	1008
Picard, Claudine	1343
Pichon, Laurent	229
Piepponen, Sulo	112
Pignot, Marc	267
Pikver, Rein	517
Pinkston, J. David	1157
Pinnaduwage, Lal	1471

Author	Page
Pinson, Jean	426
Pinto, Devanand	1266
Piotrowski, Mary	550
Pipich, Chuck	430
Pirkle, James	287
Pittenauer, Ernst	650, 651, 772
Plante, Genevieve	317
Platt, Francis	393
Plattner, Helmut	222
Pleasance, Stephen	1451, 1452
Plomley, Jeff	369, 548, 1254
Plomteux, G.	1127
Podjarny, Alberto	1326
Podtelejnikov, Alexandre	212, 766
Pohl, Jan	1242
Pohling, John, D.	367
Poiger, Thomas	1163
Poignant, Frederic	895, 1256, 1257
Polce, Michael J.	457, 1188, 1058
Poliakova, Elena	727
Poliakova, Olga	726
Polo, Lenore M.	262, 412, 1019
Pomerantz, Steven C	253
Pommerening, Cynthia	455
Pop, Emil	1457
Pope, R. Marshall	93, 268
Porcelli, Steven, A.	294
Posey, Lynmarie	406
Potier, Noelle	379, 1326
Potter, Nicholas T.	1101
Powell, David	299, 1213, 1483
Powell, Mark L.	1460
Powers, Daniel D.	134
Powers, James C.	957, 958, 959
Prakash, Chandra	691, 692, 693, 694, 1443
Pramanik, Birendra	991
Pratt, John	1318
Preece, Steve	13, 259, 1043
Preisler, Jan	676
Presek, Peter	4
Preston, Andrew	907
Preston, Ken R.	174
Pretty, Jack R.	55, 1156
Price, Duncan	1226
Price, Elvis O.	1007
Price, Philip	65
Price, William	22
Prior, David C.	477
Proctor, Andrew	819
Proefke, Mark	575
Proescholdt, M.	1110
Prokai, Laszlo	1191, 1457
Provost, Lionel R.	343
Prudent, James R.	1018
Prusiner, Stanley	990
Przybylski, Michael	274, 1327
Pucci, Sergio	733
Pugh, Johnathan	1043
Puglielli, Vincent	376
Pulver, Sabine Coates	1439
Purves, Randy	430
Qian, Kuangnan	1187
Qin, James	876
Qin, Jun	207, 208, 209, 210, 313, 577, 767, 964, 1182
Qin, Xue-Zhi	103
Qiu, Yongchang	1136
Quan, Cindy	961
Quarmby, Scott	484
Quilliam, Michael A.	1418
Quinn, Chad	1192
Quinn, Doug	289
Quinn, John, P.	1388
Quinn, Steve	1189
Rading, Derk	763
Radulovic, Louis	1434
Raffaelli, Andrea	733
Rafii, Fatemeh	154, 194
Rafter, Joseph	1134
Ragu, Ramanathan	1071
Rahman, Dinah	615
Raida, Manfred	1322
Rajamani, Uma	979, 1373
Rakov, V. Sergey	446, 857, 901
Ramaley, Louis	1067
Ramanathan, Lata	991
Ramanathan, Ragulan	316, 556, 610, 1120, 1409
Ramirez, Javier	1406
Ramírez-Arizmendi, Luis	837, 1024
Ramjit, Harri	1038, 1333
Ramsey, J. Michael	433, 1171, 1205
Ramsey, Roswitha S.	433
Ramussen, Beth	186
Ranasinghe, Asoka	243
Randall, Linda	1307
Rao, Xin	1162
Rappmund, Andreas	872
Rappsilber, Juri	217, 766
Rashidezadeh, H	1074
Rasmussen, Beth	606
Ray, Jay	334
Ray, Kenneth L.	1175
Ray, Laura	334
Raymackers, Jos	271
Raza, Ashraf	599
Reather, James A.	1490, 1500
Recio, Leslie	254, 255
Reddick, Chris	240
Reddy, G. S.	696
Reddy, S. Madhava	378
Reed, Brian	224
Reed, Dana	410, 827
Regert, Martine	362
Reiber, Duane C.	167
Reich, Claudia I.	673
Reid, Fiona	1499
Reid, Gavin E.	28
Reilly, James P.	95, 125, 126, 180, 419, 1092, 1140, 1315, 1316, 1321

INDEX OF AUTHORS

Author	Page
Reilly, Peter T. A.	1171, 1205
Reimer, Mark	685, 707, 708
Reinecke, Erik	912
Reinhard, Roll	434
Reinhold, Bruce B.	294, 396, 496, 497, 1374
Reinhold, Vernon N.	294, 396, 1374
Reiter, Jeanette	224
Reitzel, Norman	748
Remigi, Carla	755, 1164
Rempel, Don L.	512, 603, 860, 873, 906
Ren, Da	101
Ren, Jinahua	456
Rendle, David	1493
Renouf, Julie P.	303
Renzoni, Aristeo	726
Ress , C.A.	551
Reuschel, Scott	1197
Reuter, Dirk	8
Reyzer, Michelle	476, 842
Riahi, Karim	866
Riba, Isabel	624
Rice, Peter A.	1374
Richards, James	400, 1285
Richards, Nigel G. J.	1352
Richards, Randal	1062
Richardson, Chris	483
Richardson, Dave	87, 52, 874
Richardson, Susan D.	357, 1163
Richert, Clemens	1048
Richter, Wilhelm J.	799
Ricker, Robert D.	566
Ridge, Douglas	74, 142, 788, 862, 1137
Ridley, Will P.	704
Riederer, Donald E.	38, 69
Riediker, Sonja	373
Rieger, Robert A.	244, 252, 273
Riegner, Dawn	1237
Rinaldo, Piero	298, 1116
Rindgen, Diane	802
Rinehart, Kenneth	724
Ringwald, Steven	1167
Risk, James	695
Riter, L. S.	754, 840
Ritter, Michele A.	198
Rivera, Mario	93
Rizzo, Jinee D.	303
Rizzo, N.	1304
Roach, John A.G.	546
Robbins, Ronny	1082
Roberts, Andrew	1042
Robinson, Carol	1, 385
Robinson, J. M.	248
Roboz, John	711, 1451
Rockwood, Alan L.	530, 1159
Rodger, Alison	1226
Rodgers, Griffin	184
Rodgers, Mary	465
Rodgers, Ryan P.	1083
Rodriguez, Alejandra	1407
Rodriguez-Cruz, Sandra E.	91
Roellgen, Franz W.	139
Roepstorff, Peter	214, 215, 222, 383, 388, 389, 586, 638, 760, 1291
Rogers, J. Douglas	1447
Rogniaux, Helene	1326
Rohde, Ellen	290
Rohde, Michael F.	178, 643, 960
Rohrbaugh, Dennis K.	725
Rohrs, Henry W.	906
Rojo, Ricardo	163
Roland, Arlène	653
Rolando, Christian	362, 426
Rosa, Erra-Balsells	1016
Rose, Garry	1243
Rosen, Steven D.	1097
Rosenthal , Stephen E.	1205
Ross, Andrew	149, 366
Ross, Charles	1038, 1086, 1333
Ross, Philip	264, 414
Rossi, Charlie	334
Rossi, David T.	1300
Rossi, Jean-Claude	653
Rossier, Jean	585
Rossky, P.	508
Rostom, Adam	385
Roth, Jeri	319
Roth, Johannes	390
Roth, Kristian M.	1310
Rothschild, Kenneth, J.	1106
Rotstein, Joel	1480
Rourick, Robyn A.	17, 292, 1479
Rouse, Jason C.	11, 391
Rouseff, Russell	1484
Roussel, David	452
Roussis, Stilianos, G.	1078, 1081
Rout, Michael	767
Rouvinen, Juha	183
Rovatti, Luca	1312
Roy, Ray	334
Roybal, Jose	1399
Rozenski, Jef	272
Rozynov, Boris	1077
Rubakhin, Stanislav	10
Rucker, Robert B.	558, 1390
Rudd, Pauline M	1367
Rudewicz, Patrick	308
Rule, Geoffrey	1438
Rumbelow, Steve	1057
Rupp, Heidi	1399
Rusconi, Filippo	585
Russ, Bill	912
Russell, David H.	29, 34, 48, 80, 98, 151, 405, 513, 608, 611, 765, 770, 801, 927, 1107
Russo, Paul S.	947, 949
Ruterbories, Kenneth	16
Ryu, Sung-Ho	659
Ryzhov, Victor	855, 856
Sadagopan, Nalini	951
Sadeghi, Mehrnoosh	387, 791, 925
Saderholm, Matt	983

Author	Page
Sadilek, Martin	445
Saenz, Adam	179
Sakairi, Minoru	565
Sakamoto, Hiroko	1368
Sakoda, Saburo	559
Sakuma, Takeo	321
Sakurada, Norio	1492
Sala, Angelo	657
Salih, Bekir	1358
Salomies , Hannele	720
Salvadori, Piero	733
Salzmann, Jean-Pierre	526, 527, 542
Sampson, Eric	287
Samuel, Maria	1430
Samuelson, Gary L.	41, 1252
Sanborn, Karen	526, 527, 542
Sanchez, Gabriel	1033
Sanchez, Rosa I.	15
Sanders, Mark	240, 579
Sanford, Howard	156, 275, 1003
Sankowski, Paul	564, 890
Santana-Marques, M. G.	447, 1410
Santiago, Vanessa	1224
Santone, Kenneth	1439
Santos, Teresa	1410
Sartwell, Chris	1459
Satterfield-Doe, Mary	841
Satzger, R. Duane	547
Saunders, Connie J.	412
Savickas, Phil	1494
Savory, Patrick	1125
Sawai, Tetsuo	1495
Sawatzki, Guenther	1381, 1382
Sayer, Lawrence M.	213
Scalf, Mark	282
Scammell, Russell	1043
Schaenzer, Wilhelm	1114
Schäfer , Jürgen	176
Schaff, Jason E.	83
Schatz, Courtney	1373
Scheffler, N. Karoline	1097
Scheidemann, Adi	448
Scherer, Stefan	1238
Schey, Kevin	942
Schilling, Alexander B.	286, 989
Schimerlik, Michael I.	228
Schimmelmann, Arndt	329
Schindler, Patrick	189
Schlabach, Timothy	637
Schlager, John J.	1007
Schlenoff, Joseph B.	332
Schlessinger, Sally	763
Schleuder, Detlev	157, 276, 797, 1295
Schmeckpeper, Barbara	420
Schmelz, Eva	661
Schmidt, Andrea	138
Schmidt, E.G.	504
Schmitter, Jean-Marie	585
Schneider, Klaus	1477
Schneider, R. P.	709, 1443
Schneider, Richard	695
Schnier, Paul	89, 92, 403
Schnuchel, Arndt	982
Schoen, Alan	484, 1256
Schoenen, Frank	1139
Schoener, Dale	1405
Schols, Henk	1378
Schram, Karl H.	304
Schraven, Burkhart	238
Schriemer, Dave	1148
Schroeder, Neil J.	697, 698
Schrotz-King, Petra	766
Schubert, Michael	1255, 1283, 1320
Schubert-Z., Manfred	2
Schuerenberg, Martin	796, 1005
Schultz, David G.	70, 71
Schultz, Gary	1432
Schultz, Imke	1322
Schultz, Jocelyn	806
Schultz, Lauri	1041
Schurch, Stefan	1310
Schürenberg, Martin	277, 1103
Schuster, Sheldon M.	1352
Schwartz, Jae C.	484, 485, 740, 869
Schwarz, Jean-Marc	1118
Schwecke, Bill P.	314
Schweikert, Emile	1221, 1222, 1223, 1224, 1225, 1259
Schweikhard, Lutz	68, 100
Scoble, Hubert A.	11, 524
Scott, Brian	738
Scott, Gary	1404
Scott, George	1254, 1398, 1451
Scott, Graham	868
Scott, Jill, R.	935, 1310, 1338
Scott, Mary	307
Scott, Peter	1480
Scott, Rebecca	1452
Scrivens, James H.	1057, 1062, 1075, 1189, 1239, 1281
Searle, Philip	283
Seburg, Randal	784
Sechi, Salvatore	971
Seetharam, Ram	979, 1373
Sehested, Jens	858
Selby, Hugh	1264, 1265
Seldes, Alicia M.	1376
Selenka, Jeffrey	1499
Sellier, Nicole	866
Sells, Todd	270
Selzer, Rebecca R.	254
Sen, Atish	73
Senko, Michael	485, 486
Sepetov, Nikolai	1030
Sergeant, Dave	739
Sergey, Vorobiev	973
Serwe, Maria	1283
Sessions, Alex	329
Settineri, Christine	128, 1339
Settlage, Robert E.	947, 949, 950

INDEX OF AUTHORS

Author	Page
Severs, Joanne	335
Shabanowitz, Jeffrey	296, 297, 761, 947, 948, 949, 950
Shaffer, Scott A.	428
Shahab, Shamsi	1446
Shakey, Quazi Aga	236
Shalaby, Lamaat	199
Shaler, Thomas A.	415, 1200
Shampine, Larry	1139, 1029
Shang, Dayue	365
Shanmugan, Shawn	1497
Sharifi, Mehran	867
Sharma, A. K.	646
Sharrow, Scott	600
Shawver, Laura	1423
Shay, Brian	1080
She, Y. M.	1329
Sheehan, Edward	309
Sheeley, Douglas	980
Sheer, Donald G.	672, 1292
Sheets, Erin D.	645
Sheffer, Jay	1014
Sheldon, Russ J.	314
Shen, Min	1335
Shen, J.	1215
Shen, Jim	476, 533
Shen, Shida	890
Shen, Shiling	748
Shen, Tun-Li	595
Shen, Tunli	226
Shen, Xiaodong	1375, 417
Sheppard, Charles M.	812
Shepson, Paul	340
Sherman, Nicholas	632
Shevchenko, Andrej	*43, 237, 238*
Shevchenko, Anna	238
Shi, Stone D.-H	32, 499, 910, 1087, 1330, 1387
Shida, Yasuo	1495
Shiea, Jentaie	160, 1293
Shields, Sharon J.	29, 405, 770, 801, 34
Shigematsu, Nobuharu	598
Shillinglaw, Wendy	955
Shimamoto, Grant	643
Shimanskas, C.	1008
Shimizu, Akira	559
Shimizu, Naoto	153, 344
Shimizu, Takao	1000
Shimonishi, Yasutsugu	1368
Shin, Chul-Min	1015
Shin-ichirou, Kawabata	1011
Shinichi, Yamaguchi	434
Shipkova, Petia A.	645
Shlaes, David	186
Shoff, Donald	1237
Shou, Wilson	133
Shukla, Anil	73, 74, 75
Shushan, Bori	288, 1124
Shyong, Baojen	961
Siegel, Marshall M.	110, 185, 186, 514, 998, 1387
Siemieniak, David	679, 999
Siems, William F.	147, 148, 429, 652, 887
Siethoff, Christoph	267
Silva, Jose	699, 700
Silver, Alan	1080
Simmons, Tracey A.	412, 934
Simonsick, Willaim	1086, 1056, 1087, 1191
Simpson, Jack	1093
Simpson, Richard J.	28
Sin, Joseph	530, 1159
Sindona, Giovanni	789
Singer, Robert	647
Singh, Gurkeerat	689, 1448
Sinha, Mahadeva	916
Siniossoglou, Symeon	*217*
Sinz, Michael	1434
Sirimanne, Sarath R.	1129
Sisenwine, Samuel	536, 902
Siu, K. W. Michael	430, 468
Siu-Caldera, Mei-Ling	696
Siuzdak, Gary	1096, 1359
Sjövall, Jan	211, 221, 779, 987, 1134
Skelton, Paul C.	1490
Skinner, Martha	159
Slemmon, Randall	1362
Smirnov, Igor	414, 521
Smith, David H.	1196
Smith, David L.	382, 599, 601, 602, 605, 607, 609
Smith, Derek	1088
Smith, Glenn	1384, 1385
Smith, J. Richard	1007
Smith, Jean B.	605, 609
Smith, Lloyd M.	282, 1018
Smith, Misty	322
Smith, Richard D.	49, 266, 428, 432, 438, 477, 523, 804, 1270, 1271, 1305, 1307, 1394
Smith, Richard W.	569, 1415, 1416
Smith, Stuart	1305
Smith, Tom	1096
Smith, Virginia	1307
Smithgall, Thomas E.	382
Smythe, George	1111
Snyder, A. Peter	438, 667, 859, 1203
Snyder, Peter	342
Soerensen, Poul	222, 389
Soli, George	916
Solomon, Harvey M.	1126
Solomon, Keith	738
Solouki, Touradj	363, 1396
Somogyi, Arpad	41, 72, 633, 1252
Sonenberg, Nahum	759
Song, Xinbei	*1166*
Soni, Manish H.	360
Sorg, Clemens	390
Sovocool, G. Wayne	349, 350
Spagnoli, Suzanne	555
Spaltro, John	979
Sparkman, O. David	64, 818
Sparrapan, Regina	851, 853

Author	Page
Spaugh, Art T, Jr.	1472
Spaulding, Reggie	1162
Speder, A.	158
Speir, Paul	514, 515
Spell, J. Christopher	1121
	1126
Spence, Thomas	406
Spengler, Bernhard	375
	936
Spicer, Eddie	830
Spicer, V.	37, 932
Spiess, Joachim	1360
Sproat, Brian S.	249
Squier, Thomas C.	944
Squires, Robert R.	456, 784
	831, 832
Srinivasan, Jannavi R.	679
	999
Srinivasan, Karthik	642
	1121
Srinivasan, N.	156, 275, 1003
Srishailkumar, Hadimani	686
St. Claire, III, R.L.	551
Stacey, Catherine	580, 1037
Stafford, George C.	485
Stahl, Bernd	1381, 1382
Stahl, Douglas C.	284
Stahl-Zeng, Jianru	165
Standing, Kenneth G.	37
	174, 175, 379, 794, 932
	937, 1269, 1329
Stapley, Benjamin J.	624
Starcevic, Borislav	1455
Staunton, James	1489
	1490, 1500
Steadman, Jhobe	8
Steenvoorden, R.J.J.M.	572
Steenwyk, Rick C.	18
Stefacek, Eugene M.	285
Stefanescu, Andrei D.	1072
Stein, Steve	123, 818
Steinbeck, Christoph	1048
Steinborner, Simon	1436
Steiner, Robert	56, 59, 323
	326
Steiner, Valerie	480
Stenflo, Johan	214
Stephenson, Jr., James L.	27
	1089, 1178, 1204
Stern, Gary	364
Sterner, Jennifer	142
Steven, Carr A.	628
Stevens, James	625
Stevens, Richard	1354
Stevens, Stanley	52, 87
Stevenson, E.	508
Stevenson, Tracy	1151
Stewart, James	1121, 1126
Stimson, Elaine	799
Stinson, Sherman F.	1461
Stoeckli, Markus	195
Stoney, Ken	230, 540
Storey, Joseph M.	1467
Stott, Bill	1247, 1254
Stotter, Phillip	748
Strader, Karen	1485
Strader, Thomas	1034
Strahler, John	994, 1303
Strang, Anne-Marie	391
Straub, Kenneth	1332
Straubinger, Robert	722
Stresau, Richard	33, 911
Strittmatter, Eric	89, 235, 403
Strobel, Fred	1242
Stroh, Justin G.	619
Strupat,Kerstin	797, 157
	276, 390, 796, 923, 1295
Stults, John	166, 955, 1336
Stumpf, Chris	1024
Sturgeon, Ralph E.	58
Stygall, James	1246
Subbi, Juhan	517
Subramanian, P.	1402
	1403
Suckau, Detlev	277
	1005, 1022, 1103
Sugui, Janyce	1010
Sukbunthern, J.	1423
Sullards, M. Cameron	661
Sullivan, Anthony	106
Sullivan, Barbara	612
Sullivan, Michael	322
Summerfield, Scott G.	623
	633
Sumner, Lloyd W.	151
Sumpter, Kenneth B.	725
Sun, Wei	769, 795
Sun, Yiping	158, 203
Sunde, Margaret	1
Sunderlin, Lee	455
Sussman, Michael	724
Suter, Marc J.-F.	373
Sutherland, John	154, 194
Suzuki, Chise	190
Svendsen, Henrik	525
Sweedler, Jonathan	10, 591
Sweetman, Gavain M.A.	1313
	1317
Swenberg, James A.	243
Swickard, Scott	1197
Swiderek, Kristine	1336
Swint-Krause, L.	379
Swyden, M.	1443
Sykes, Brian D.	1349
Szczepanski, Jan	94, 97
Szekely, Gabriella	1052
	1070
Szewczuk, Zbigniew	627
Szulejko, Jan	444, 464, 466
Tabani, Ike	1425
Tabei, Keiko	185, 186
Tabet, Jean-Claude	155, 467
	478, 479, 480, 481, 864
	865, 866, 896, 920, 921
	1061
Tabuchi, Ruby	1455
Tackett, Randall L.	312
Taguchi, Vince	729
Tak Wah Dominic	1260
Takach, Edward	775, 894
Takada, Yasuaki	565
Takahashi, Toshie	1000
	1495
Takahashi, Y.	535
Takao, Toshifumi	1368

INDEX OF AUTHORS

Author	Page
Takasu, Daisuke	1000
Takaya, Hiroaki	72
Takayama, Mitsuo	102
Takehana, Yoshi	416
Takekiyo, Matsuo	434, 1235
Taki, Masayasu	1492
Takino, Masahiko	344
Takio, Koji	988
Talley, Jody M.	459
Talrose, Victor	939
Tam, Yuen	1431
Tambara, Yanet	1368
Tambute, André	467
Tan, Melvin	322
Tang, Dazhi	1350
Tang, Kai	8, 416
Tang, Xiaodong	387
Tang, Xue-jun	606
Tanguay, Suzanne	1485
Tani, Travis H.	202
Taniguchi, Hisaaki	1319
Tannenbaum, Steven R.	251
Taranenko, Nelli I.	421, 1101
Tarleton, Rick	295
Tashiro, Takashi	104
Taskinen, Jyrki	720, 721
Tate, Shin-ichi	988
Taylor, Alex	589
Taylor, John	260
Taylor, Lester	1441
Taylor, Lorne	613, 978
Taylor, Mark	52, 87, 874
Taylor, Mike	1057, 1281
Taylor, P. Kristina	631
Taylor, Peter	1025
Taylor, Philip D.P.	331
Taylor, Stephanie N.	1094
Taylor, William P.	830, 1321
Tchekovskoi, Dmitrii	818
Teesch, Lynn M	1402, 1403
Teffera, Yohannes	1431
	1435
Tempst, Paul	437, 881, 882
Ten Hove, G. Jan	1356
Terlouw, Johan K.	569, 1415
Thadeio, Peter F.	619
Thakur, Rohan	483
Theberge, Roger	159
Theodorsson, Elvar	1291
Thibault, Pierre	223, 400
	1285
Thoen, Kami K.	833, 834
	835, 836
Thomas, John	665
Thomas, Nicola	1433
Thomas, P. D.	780
Thomas, Terri L.	1467
Thomas, Timothy	1210
Thomas-Oates, Jane	1377
	1378
Thompson, Cyril	368, 1168
	1174
Thompson, Rukeyser	834
Thompson, Stephen	1072
Thomson, Bruce	43, 713
	1247, 1251
Thomson, Chiquita	1398
Thotakura, N. Rao	396
Thruston, Jr., Alfred D.	357
Thyroff, Matthias	1397
Tichy, Shane	833
Tiller, Philip	714
Timble, Laird	700
Timmermann, Barbara N.	304
Timmons, Richard	764, 930
Tinkle, Mark	451
Tisdale, Michael	1095
To, Trang	1354
Tobias, Trautmann	434
Todd, Peter	518, 1109, 1110
Tollaksen, Sandra L.	673
Tomany, Michael	909
Tomer, Kenneth	274, 640
	641
Tomioka, Masaru	565
Tomlinson, Andy J.	290
	381, 1275
Tomlinson, Medha, J.	935
Tomy, Gregg	364
Tong, H.Y.	1008
Tong, Hui	110
Tonner, Scott	464
Tornaeus, Jarkko A.	1317
Torres, Omar	927
Torres, T.A.	503
Touati, Danielle	155
Townsend, R. Reid	1097
Tracy, McCarley	1446
Trafton, Jill	279
Tretyakova, Natalia	251
Trimble, Laird	699
Triolo, Antonio	1482
Tripathi, Ashish	342
Trotter, Brett	406
Trovao, M. Cristina N.	447
Truong, Long	961
Tsai, Cheng-Yuan	1278
Tsai, Shirling	775
Tsaprailis, George	633
Tseng, Jih-Lie	172, 962
Tseng, Ken	397
Tsuchiya, Fumihiko	190
Tsuchiya, Masahiko	104
Tsuda, Ryoko	578
Tu, Ya-Ping	77, 781
Tubbs, Kemmons	1155
	1288, 1289, 1323, 1155
Tullius, Michael	399
Tung Po Eric, Sze	1260
Tuntland, Tove	702
Tuong , Anne	1343
Turecek, Frantisek	445, 460
	461, 462, 463, 778
Turesky, Robert	809
Turk, John	1419
Turlin, Etienne	155
Turner, Wayman	1128
Turnipseed, Sherri	1399
Tutko, Diane C.	516
Tzanani, Nitzan	908, 1198
Udseth, Gordon A.	477
Udseth, Harold R.	49, 1394
Uggerud, Einar	441, 453
	829
Uljon, Sacha	9, 968

Author	Page
Unanue, Emil	603
Unger, Steve	1422
Upholt, William	236, 1019
Urban, Jan	1214
Ursem, Mario	542
Utkin, Ilya	690
Uzabiaga, Françoise	1343
Van den Eeckhout, E.	271
Vachet, Richard W.	327, 984, 1412
Vainiotalo, Pirjo	183, 846
Vaisar, Tomas	1214
Vala, Martin	94, 97
Valagussa , Anna	653
Valaskovic, Gary	528
Valcic, Susanne	304
Valentine, Nancy	179
Valentine, Stephen	31
Valentine, William	315
Van Berkel, Gary J.	55, 132, 1156, 1420
Van Bockstaele, D.	803
van Breemen, Richard B.	134, 258, 286, 1047, 1143
Van de Ven, Henk	1193
Van den Heuvel, Hilde	78, 1228
van den Steen, Philippe	393
Van der Heeft, Eddy	1356
Van Dongen, William D.	572, 803
Van Dorsselaer, Alain	162, 163, 1324, 1326
Van Els, Cecile A.	1356
Van Heusden, Kees-J.	1377
van Lieshout, Machteld	286
van Oostrum, Jan	189
Van Orden, Steven	514
Van Pelt, Colleen K.	648
van Rooij, Gerard J.	45
van Soest, Remco	526, 527, 542
Van Stipdonk, Michael	1221, 1222, 1223, 1224, 1225, 1259
Van Vyncht, Géry	639, 718, 1218
Van Wijnendaele, Frans	271
VanBogelen, Ruth A.	202, 1151
Vandell, Victor E.	793, 810
Vanhoutte, K.	803
Vass, Arpad	666
Vayer, Philippe	13
Veals, John	1426, 1453
Vedernikova, Irina	78
Veenstra, Timothy D.	381
Vekey, Karoly	782
Velagaleti, Poonam	556
Venesky, John S.	776
Venta, Patrick J.	679, 999
Verentchikov, Anatoli	775, 894
Verkhoturov, Stanislav	1221, 1259
Vermillion, Rachel	347
Vertes, Akos	140, 141, 387, 791, 925, 938, 1008
Vestal, Marvin	35, 626, 775, 894
Vetter, Stefan	1357
Vidavsky, Ilan	552, 603
Viggiano, Albert	23
Vigh, Gyula	1380
Villasenor, Armando	1332
Vince, John	697
Vincent, Bryan	1380
Vincenti, Marco	846
Vining, Bryan A.	498
Vinogradov, Pavel S.	449, 1211
Visentini, Josie	555
Viseux, Nelly	392, 401
Vissers, Hans	542
Vissers, J.P.C.	526
Voegel, Jean-Claude	162
Vogel, Manuel	68
Vogelstein, Bert	418
Vogl, Thomas	390
Volk, Kevin J.	17, 240, 292, 304
Volkmann, Robert A.	619
Volmer, Dietrich A.	539, 560, 561, 1418, 1284, 1286
Volnina, El'vira	1488
Voorbach, Martin	1050
Voorhees, Kent J.	154, 194, 668, 669, 670, 671, 1201
Voragen, Fons	1378
Vorm, Ole	525, 978, 1090
Voshol, Johannes	189
Voss, Lisa	773
Vouros, Paul	256, 257, 270, 690, 696, 809, 1298, 1383
Voyksner, Edward	65
Voyksner, Robert	86, 1177
Vrbanac, J. James	18
Vuica, Andreea	1498
Wachs, Timothy	1274
Waddell, David S.	644
Waddell, Keith	596, 1190, 1299
Wade, Shelly	1030
Wade, Tim	371
Wagner, Brian	861
Wagner, David	1029, 1139
Wagner, John S.	1205
Wahl, Karen L.	179, 752
Waidelich, Dietmar	165
Wainer, Irving	1095
Wainhaus, Samuel B.	908, 1198
Wakefield, Michael	741, 1425
Walker, Angela	764, 930
Walker, Jeremy	1061
Wall, Daniel	188
Wallace, James I	200
Wallace, William E.	1059, 1060, 1076
Wallaert, Arie	1012
Walle, Stefan	1030
Walls, Fred	939
Walsh, E.B.	60
Walter, William	646
Walther, Clemens	68, 100

INDEX OF AUTHORS

Author	Page
Waltman, Lisa	322
Wan, Katty	260, 263, 552
Wanczek, Karl Peter	871, 872
Wang, C.C.	1335
Wang, David	729
Wang, F.	780, 840
Wang, Fang	1349
Wang, Guangdi	131, 731
Wang, Houle	431
Wang, Jia-shen	1487
Wang, Jian	319, 562
Wang, Jianyao	976
Wang, Jinru	30
Wang, June	1447
Wang, Lee Y.	160
Wang, Lintao	607
Wang, Min	184
Wang, PingPing	107, 312, 642, 1126
Wang, Poguang	417
Wang, Rong	9, 968
Wang, Tao	1032, 1034, 1146
Wang, Tao-Chin L.	658
Wang, Xiaoli	1032, 1146
Wang, Xiaomin	321
Wang, Y	278
Wang, Y. Karen	289, 1340
Wang, Yang	1320
Wang, Yanping	776
Wang, Yinsheng	260
Wang, Zhen	20, 1145
Wang-Iverson, David	562
Waraszkiewicz, S. M.	567
Ward, Kenneth	413, 1099
Ward, Malcolm	218
Ward, Susan	647
Waring, Alan	1354
Warrack, Bethanne M.	1355
Warrelow, G.	699
Warren, Maria	197, 440
Warriner, Ruth	520
Watkins, Layle	682, 1107
Watkins, Robert W	1453
Watson, Clifford	52, 57, 87, 97, 630, 874, 1044, 1142
Watson, Jack Throck	6, 226, 951, 952
Watts, Julian	618
Wayne, David	56, 59, 323
Weaver, Kristal	1017, 1202
Weber, Patricia	991
Weeding, Tina L.	84
Wehmeyer, Ken R.	314
Wehofsky, Marco	936
Wei, Dong	1098
Wei, Jian	1249, 1250
Wei, Ru	1036
Weigl, Paul	1427, 1428
Weil, David	510, 1052, 1070
Weinhold, Elmar	267
Weintraub, Susan T.	303
Weiskopf, Andrew S.	696, 1383
Weitman, Steven D.	303
Wellemans, Joelle	979, 1373
Wells, J. Mitchell	485
Wen, Jian Yuan	438
Weng, Naidong	109, 1459
Wenschuh, Holger	199-A
Wensing, Michael W.	667, 859, 1203
Wenthold, Paul	784
Wenzhe, Lu	1446
Wesdemiotis, Chrys	101, 404, 457, 458, 459, 783, 1058, 1188
West, Clive E.	286
West, Paul R.	1478
West, Ray	530, 1159
West, Sarah	474, 850
Westerlund, Douglas	1273
Westmacott, G.	937, 1329
Westman, Ann	768, 1108, 1301
Weston, Daniel	353
Wexler, Anthony	926, 1170
Wheat, Thomas E.	1267, 1268
Wheelan, Pat	655, 656
Wheeler, Susan F.	1367
White, Forest M.	93, 296, 297, 761, 1393
White, Jennifer L	394, 1371
White, Paul	914
Whitehouse, Craig M.	39, 889, 890, 891, 1161
Whitelegge, Julian P.	1353, 1354
Whitney, Jeffrey, L.	17, 292, 304, 1479
Whittal, Randy M.	532, 635, 636, 990, 1404
Whitten, William B.	1171, 1205
Widlanski, Ted S.	1321
Wieling, Jaap	572
Wiesner, Sebastian	1104
Wigger, Maria	1142
Wiggins, Ken	1493
Wight, Helen	168, 637
Wilbert, Sibylle	740
Wilcox, Bruce	1263
Wild, Jennifer	1029
Wileman, Tom	616
Wilgus, Robert	1139
Wilkes, Jon G.	903, 1119, 1486
Wilkins, Charles L.	935, 1020, 1085, 1310, 1338
Wilkins, John	474, 850
Wilkins, Patricia	231
Wilkinson, Bob	739
Willard, Belinda B.	409
Willett, Gary	863, 1088
Williams, Erik	1025
Williams, Evan R.	89, 90, 91, 92, 235, 403
Williams, Jon	452
Williams, Jonathan	452, 1239
Williams, Kathryn	52, 874
Williams, Peter	1345, 1346
Williams, Ted	824
Williams, Todd D.	944, 945

Author	Page
Williamson, Brian L.	1275
Williamson, David A.	945
Williamson, William	370
Willoughby, Ross	65, 309
Wilm, Matthias	241, 593
Wilner, Keith	691
Wilson, Dan	873
Wilson, Terry	570
Wing, David R.	393, 1366
Wingate, Julia	899
Winger, Brian E.	516, 584
Winkler, Martin	1063
Winnik, Witold	747
Winston, Rachel L.	993
Wirth, Urs	172, 962
Wirtz, Sara	632
Wise, Marcus B.	368, 1168
	1172, 1174
Wishnok, John	251
Wislocki, Daniel	1042
Withers, Stephen G.	995
Wojtkowski, Traci	184
Wolf, Barbara P.	151, 1380
Wolf, Dennis	666
Wolken, Jill	463
Wollnik, Hermann	1232
	1238
Wong, Anissa	773
Wong, James T.F.	1468
Wong, Kwong-kwok	1271
Wong, P.	780
Wong, Philip	581
Wood, Karl	1010
Wood, Troy D.	47, 722, 992
	1084
Woods, Amina S.	229, 384
	395, 1261
Woodward, Chris	884
Wooley, Karen L.	1072
Woolfitt, Adrian R.	287, 1129
Worrall, Timothy A.	420
Wright, Emma	1417
Wright, Matt	1422
Wronka, John	514, 883
Wu, Ching	147, 148, 429
	887, 1411
Wu, Danlin	895, 1256, 1257
Wu, Henry	568, 876
Wu, Huaiqin	1063
Wu, Huaping	808
Wu, Jiang	6
Wu, Jianglin	458
Wu, Linda	976
Wu, Shari	1444
Wu, Xiongwu	791
Wu, Yuliang	764, 930
Wu, Zhuchun	161
Wunschel, David S.	266
	432, 804
Wurz, Peter	1238
Wyplosz, Nicolas	1012
Wysocki, Vicki H.	41, 72, 74
	75, 633, 1252
Xia, Yang	749, 1117
Xiao, George	1481
Xie, Fuming	581
Xin, Baomin	1159
Xiong, Henry Y.	258, 286
Xu, Allan	564, 573, 574
Xu, Guozhang	213
Xu, Hongyu	1306
Xu, Keyang	1449
Xu, Linxiao	245
Xu, Ming	668
Xu, Naxing	49, 438, 523, 804
Xu, Nucleus	371
Xu, Rongda	778
Xu, Xiaoying	258, 286
Xu, Yong Hua	1068, 1069
Xuan, Tong	378
Yakushin, Vasilii	1488
Yalcin, Talat	781, 1053, 1054
Yamada, Naoyuki	190
Yamaguchi, Kenji	153, 344
Yamamoto, Kazuo	1361
Yamauchi, Emiko	1319
Yang, Chia-Ning	854, 855
Yang, Houjun	602
Yang, Ill	756
Yang, L. C.	1293
Yang, Lily	336
Yang, Yang	987, 1134
Yang, Yi	439
Yang, Ying	6, 880, 952
Yang, Youjun	186, 606
Yang, Zhiyang	1010
Yao, Jie	1020, 1338
Yao, Yi	1335
Yates III, John R.	121, 617
	977
Yates, Nathan	612, 1042
Ye, Song	396
Yeh, Li-Tain	1423
Yen, Ten-Yang	594
Yergey, Alfred	879
Yergey, James	699, 700
	1033
Yeung, Edward	680
Yewdell, Jonathan W.	395
Yi, Donghui	1111
Yi, Ping	259
Yin, Winnie	1481
Yinon, Jehuda	1195
Yoo, Jong Shin	1015
Yoon, Hye-ran	1116
Yoshida, Kaoru	153
Yoshinari, Kiyomi	492
Yoshioka, Kazuaki	581
Yost, Richard	1195, 1213
	1407
Young, Mary	1338
Yu, Chunli	1116
Yu, Wen	11
Yu, Xiao	19, 683, 715, 815
Yu, Ying-Qing	834, 837, 1024
Yuan, Pau-Miau	1337
Yuko, Fukuyaka	1016
Zacchello, Franco	298
Zagorevski, Dmitri	79
Zaia, Joseph	620
Zaikin, Vladimir	818, 1488
Zand, Robert	1282
Zanger, Murray	1217
Zavitsanos, A.P.	551
Zavitsanos, Paul	738

INDEX OF AUTHORS

Author	Page
Zbaida, Shmuel	705
Zechel, David L.	995
Zeikus, J. G.	595
Zell, Manfred	1463
Zeng, Lu	1032, 1034, 1146
Zenobi, Renato	849, 917
	940, 1357, 1358
Zey, Thomas	534
Zhan, Dongliang	146, 424
Zhan, Qiao	1153
Zhang, Bailin	757
Zhang, D.	780
Zhang, Haiying	975
Zhang, Hongjian	654, 1113
Zhang, Hongwei	563
Zhang, Kanyin E.	717, 702
Zhang, Kate	114, 115, 144
	206
Zhang, Li	440
Zhang, Li-Kang	280
Zhang, Mei-Yi	536
Zhang, Michelle	439
Zhang, Rong	895, 1256
	1257
Zhang, Tianlan	788, 1192
Zhang, Wenzhu	767, 965
	969
Zhang, Xiaolong	208, 209
	210, 313, 1182
Zhang, Xinyi	193
Zhang, Zhong-Yin	1321
	1349
Zhang, Zhongli	609
Zhang, Zhongqi	127, 537
	1351
Zhao, Jamie	1447
Zhao, Jane	291, 1266, 1272
Zhao, Jiang	152
Zhao, Yingming	767
Zharikova, Alevtina	1457
Zheng, Jenny	1421
Zheng, Kefei	1300
Zholdakova, Zoya	727
Zhong, Feng	352, 1241
Zhong, Wenqing	74, 75
Zhou, Shaolian	425
Zhou, Xuedong	76
Zhu, Damo	818
Zhu, Honghui	1054
Zhu, Junhua	427, 663
Zhu, Limin	792
Zhu, Lin	1186
Zhu, Wensheng	1440
Zhu, Xuegong	641
Zhu, Yongdong	675, 677
	1002
Ziberna, Anthony K.	1114
Zidarov, Dimo	129, 130
Ziehl, Valerie	394
Zielinski, Walter	1120
Zirrolli, Joseph	649
Zoller, David	1187
Zook, A.L.	326
Zook, Douglas R.	137
Zubarev, Roman A.	67, 423
	939, 1380

Keyword	Page
Acid-base Equilibria	658, 789
Acids	554, 742, 814, 1226
Acids, Amino	28, 62, 63, 199, 227, 288, 298, 300, 312, 315, 467, 468, 558, 614, 630, 633, 778, 788, 1044, 1093, 1102, 1115, 1154, 1230, 1273, 1293, 1312, 1360, 1413, 1501
Acids, Bile	301, 1407
Acids, Carboxylic	555, 1093, 1162, 1417, 1474, 1488
Acids, Fatty	72, 78, 298, 299, 644, 645, 650, 652, 654, 660, 668, 987, 1116, 1228
Acids, Nucleic	32, 89, 250, 262, 266, 272, 282, 411, 413, 415, 679, 762, 789, 797, 802, 1004, 1099, 1102, 1104, 1200
Acylcarnitines	288, 298, 299, 1116
Adduct	554, 558, 844, 1321, 1390, 1401, 1421, 1481
Adduct, DNA	152, 243, 244, 245, 246, 252, 254, 259, 260, 261, 267, 268, 272, 279, 281, 381, 417, 422, 802, 803, 807, 808, 809
Adduct, Protein	205, 381, 600, 657, 711, 718, 943, 1007, 1136, 1138, 1312, 1317, 1352, 1353, 1354, 1355
Aerosols	139, 375, 519, 880, 926, 1170, 1171, 1205
Affinity, Binding	5, 383, 386, 388, 439, 640, 764, 786, 805, 1026, 1046, 1047, 1047, 1140, 1148, 1155, 1287, 1288, 1289, 1291, 1294, 1295, 1296, 1326, 1348, 1414
Affinity, Cation	227, 422, 465, 588, 780, 786, 823, 1061, 1075, 1293, 1389
Affinity, Electron	442, 453, 780, 784
Affinity, Metal	162, 404, 469, 783, 786, 823, 985, 990, 1290, 1297, 1311, 1357
Affinity, Proton	22, 24, 227, 247, 371, 462, 463, 466, 467, 778, 780, 781, 783, 785, 788, 789, 848, 933, 934, 1318
Alcohols	464, 469, 555, 1130, 1227, 1488
Aldehydes	259, 600, 1162
Alkaloids	344, 1497
Alkanes	822, 861, 868, 727, 1082, 1496, 1498
Amides	469, 658, 1227, 424, 658, 732, 828, 844, 845, 946, 1212, 1487
Anabolic Steroids	885, 1114
Antibiotics	88, 186, 355, 383, 543, 560, 561, 570, 701, 705, 876, 1047, 1389, 1418, 1495
Antibodies	5, 182, 587, 653, 1155, 1294
Aromatics	812
Arrival Time Distribution	31
Artificial Intelligence	113
Automation	8, 19, 110, 117, 118, 120, 128, 144, 206, 277, 317, 338, 344, 515, 516, 521, 526, 527, 579, 583, 617, 626, 683, 684, 685, 707, 708, 715, 766, 775, 815, 819, 947, 954, 965, 1001, 1005, 1017, 1021, 1022, 1027, 1030, 1032, 1034, 1040, 1043, 1096, 1149, 1190, 1233, 1325, 1444, 1452
Azo-dyes	10, 143
Bacteria	125, 154, 164, 177, 179, 180, 187, 188, 194, 284, 342, 361, 375, 400, 438, 662, 666, 667, 669, 670, 671, 674, 675, 897, 1094, 1119, 1201, 1202, 1203, 1204, 1205, 1287, 1315, 1316, 1328, 1374
Benzynes	83, 853
Biodegradation	37, 72, 1202
Biomarkers	125, 154, 177, 180, 194, 258, 259, 261, 284, 342, 649, 665, 666, 667, 668, 669, 670, 671, 808, 1104, 1128, 1135, 1201, 1203, 1291, 1315, 1316
Biomolecules	10, 31, 42, 47, 175, 191, 214, 224, 234, 240, 265, 274, 282, 295, 310, 321, 385, 398, 404, 411, 413, 415, 431, 459, 508, 515, 523, 620, 629, 631, 647, 648, 760, 767, 768, 789, 819, 950, 957, 958, 959, 1090, 1095, 1099, 1104, 1106, 1120, 1200, 1260, 1269, 1294, 1301, 1321, 1326, 1327, 1336, 1378
Biopolymers	184, 239, 382, 527, 601, 676, 757, 1024, 1028, 1336
Biradicals	410, 784, 827, 835
Bond Strengths	87, 408, 456, 862, 874
Bonding, Hydrogen	104, 424, 444, 603, 783, 843
Breakdown Curves	69, 97, 874, 1430
Calculations, Ab Initio	22, 28, 91, 235, 409, 442, 444, 456, 457, 461, 462, 464, 465, 832, 851, 852

INDEX OF KEYWORDS

Keyword	Page
	853, 860, 863, 873, 877, 878, 1082, 1219, 1220
Calculations, Molecular Orbital	11, 40, 469
Calculations, RRKM	409, 461, 782
Calculations, Semi-empirical	111, 250, 449, 1217, 1237
Calculations, Trajectory	41, 494
Carbamates	378
Carbides	863
Carbohydrates	2, 239, 392, 394, 396, 398, 399, 401, 402, 473, 550, 554, 569, 620, 936, 1095, 1096, 1148, 1285, 1287, 1364, 1365, 1366, 1367, 1369, 1370, 1371, 1372, 1373, 1374, 1375, 1376, 1378, 1379, 1380, 1385, 1386, 1415
Carbonyls	74
Carcinogens	256, 259, 261, 803, 808, 809, 1130, 1135, 1313
Carotenoids	286, 1286
Catalysis	878
Cation	29, 833, 860, 919
Charge Exchange	776, 877, 1067, 1078, 1494
Charge Remote	78, 1006, 1228
Charge Stripping	776
Charge Transfer	23, 448, 776, 793, 861, 941, 1494
Charge-State Distribution	45, 639, 642, 806, 995, 996
Chelates	1410
Chemometrics	112, 375, 816, 1119
Chiral Recognition	302, 446, 598, 780, 845, 857, 1093, 1274, 1406
Chlorination	339, 374, 441, 727, 745, 1080
Chromatography	522, 585, 1337, 1499
Chromatography, Affinity	158, 653, 1287, 1298, 1299
Chromatography, Anion Exchange	391, 554, 679
Chromatography, Capillary Liquid	16, 224, 295, 343, 699, 954, 1161, 1275
Chromatography, Fast	342, 531, 907, 908, 1198, 1473
Chromatography, Gas	336, 364, 728, 1123, 1169
Chromatography, Gel Permeation	339, 1158, 1191
Chromatography, Liquid	533, 643, 643, 1159, 1248
Chromatography, Liquid-, Affinity	1300
Chromatography, Liquid-, Anion-Exchange	11
Chromatography, Liquid-, Capillary	152, 202, 431, 505, 509, 526, 528, 540, 541, 542, 553, 590-A, 634, 803, 809, 888, 950, 975, 987, 997, 1319, 1362
Chromatography, Liquid-, High Pressure	44, 47, 173, 181, 188, 296, 297, 307, 308, 309, 351, 397, 437, 538, 552, 558, 567, 577, 581, 605, 679, 695, 697, 698, 732, 747, 814, 1041, 1146, 1199, 1308, 1333, 1353, 1375, 1378, 1390, 1396, 1399, 1437, 1445, 1457
Chromatography, Liquid-, Microcapillary	207, 526, 989
Chromatography, Liquid-, Nanoscale Capillary	525, 526, 779, 344, 388, 393
Chromatography, Supercritical Fluid-	545, 546, 1157
Chromatography, Thin Layer-	347, 678, 1363
Chromophores	1048
Circular Dichroism	945
Cluster Formation	131, 145, 447, 448, 879, 1222, 1223, 1224, 1225, 1227
Cluster Ionization	99, 448, 769, 795
Cluster, Ionic	94, 99, 101, 406, 425, 453
Cluster, Metal	68, 91, 100, 149, 366, 408, 991, 1088, 1334
Cluster, Proton Bound	104, 446, 467, 787, 831, 857
Collision	51
Collision Cell	61, 116, 737, 1247, 1251, 1258
Collision, High Energy	78, 651, 1006, 1064, 1213, 1252
Collision, Low Energy	81, 294, 396, 496, 501, 630, 1213, 1251, 1390
Collision, Reactive	853
Collision, Surface	69, 72, 75, 1215
Collision-Induced Dissociation	26, 35, 37, 41, 74, 75, 76, 78, 79, 81, 82, 84, 85, 86, 88, 99, 101, 102, 103, 104, 106, 107, 121, 131, 185, 221, 227, 231, 250, 268, 269, 270, 311, 315, 343, 397